Vol. 20, No. 3, September, 2021
ISSN (Print): 0972-6268; ISSN (Online) : 2395-3454

Nature Environment & Pollution Technology

A Multidisciplinary, International Journal on Diverse Aspects of Environment

Technoscience Publications
website: www.neptjournal.com

Technoscience Publications
A-504, Bliss Avenue, Balewadi,
Opp. SKP Campus, Pune-411 045
Maharashtra, India

www.neptjournal.com

Nature Environment and Pollution Technology

(An International Quarterly Scientific Research Journal)

EDITORS

Dr. P. K. Goel (Chief Editor)
Former Head, Deptt. of Pollution Studies
Y. C. College of Science, Vidyanagar
Karad-415 124, Maharashtra, India

Dr. K. P. Sharma
Former Professor, Deptt. of Botany
University of Rajasthan
Jaipur-302 004, India

Published by : Mrs. T. P. Goel, B-34, Dev Nagar, Tonk Road, Jaipur-302 018 Rajasthan, India

Managing Office : Technoscience Publications, A-504, Bliss Avenue, Balewadi, Pune-411 045, Maharashtra, India

E-mail : contact@neptjournal.com; journalnept@gmail.com

INSTRUCTIONS TO AUTHORS

Scope of the Journal

The Journal publishes original research/review papers covering almost all aspects of environment like monitoring, control and management of air, water, soil and noise pollution; solid waste management; industrial hygiene and occupational health hazards; biomedical aspects of pollution; conservation and management of resources; environmental laws and legal aspects of pollution; toxicology; radiation and recycling etc. Reports of important events, environmental news, environmental highlights and book reviews are also published in the journal.

Format of Manuscript

- The manuscript (*mss*) should be typed in double space leaving wide margins on both the sides.
- First page of mss should contain only the title of the paper, name(s) of author(s) and name and address of Organization(s) where the work has been carried out along with the affiliation of the authors.

Continued on back inner cover...

Nature Environment and Pollution Technology

Vol. 20, No. (3), September 2021

CONTENTS

1. **X. Tang, J. Luo, L. Wang and X. Li,** Effect of Water Chemistry on the Uptake of Co(II) on Graphene Oxide Investigated by Batch Technique 909-922
2. **Chandi Prasad, Ramesh C. Sharma and Rahul Kumar,** Ethnobotanical Study and Plant Diversity in the Forest of Kedarnath Valley, Garhwal Himalaya, India 923-939
3. **T. Li, G. Li, X. Zhang, S. Xu and H. Ghougassian,** Study on the Electrochemical Anticorrosion Effect of Piezoelectric Materials in the Internal Environment of Water Supply Pipeline 941-953
4. K. M. Hamasha, The Increasing Trend of Black Carbon and Organic Carbon in Jordan During the Period of 2007 to 2018 955-972
5. **K. Saraswathi and K. Selvam,** Procuring Plant Services for Ecological and Human Well Being 973-983
6. **Thi-Kim Chi Do, Sunil Herat, Le Van Khoa and Prasad Kaparaju,** The Current Use and Management of Single-Use Items (SUIs) in the Fast Food Industry in Ho Chi Minh City, Vietnam 985-996
7. **Hao Zhang, Jianping Li, Yi Zhang, Yutao Wang, Juan Zhang, Xu Luo and Ru Zhang,** Soil Organic Carbon Stocks and Its Driving Factors Under Different Land-Use Patterns in Semiarid Grasslands of the Loess Plateau, China 997-1006
8. **Akash, M. Zakir, Navneet and B. S. Bhandari,** Species Diversity, Soil Nutrients Dynamics and Regeneration Status of Sal (*Shorea robusta*) Forests in Western Himalayan Region of India 1007-1019
9. **N. Thakur, D. Parashar, C. Chidambaram and M. Dharwal,** Climate Responsive Strategy Matrix for Designing Buildings in India 1021-1031
10. **B. W. Zhao, Y. Zhao, H. Liu, Y. Q. Li, K. X. Duan and X. Zhang,** Effect of Wheat Straw Biochar on Thermophysical Properties of Loessial Soil 1033-1039
11. **Li Linjin, Men Baohui† and Peng Rui,** Water Quality Evaluation of Wenyu River Based on Single Factor Evaluation and Comprehensive Pollution Index Method 1041-1046
12. **M. P. Adhikari, N. B. Rawal and N. B. Adhikari ,** Real-Time Fine-Scale Measurement of Water Quality Parameters Along the Bagmati River in the Kathmandu Valley 1047-1057
13. **S. Tantry, K. Tharpa, Ajay Kumar, Arun Kumar and B.H.S. Thimmappa,** Reagent Activated Cotton Fiber for Rapid Determination of Aldehydes in Diverse Matrices 1059-1068
14. **R. Rathinam and M. Govindaraj,** Photoelectrocatalytic Oxidation of Textile Industry Wastewater by $RuO_2/IrO_2/TaO_2$ Coated Titanium Electrodes 1069-1076
15. **N. Deepika and R. Jaya Madhuri,** Reliable and Sophisticated Techniques to Evaluate LDPE Degraded Compounds by *Streptomyces werraensis* SDJM 1077-1085
16. **R. Xu, Q. Tian, H. Wan, J. Wen, Q. Zhang and Y. Zhang,** Spatial and Temporal Characteristics of PM Sources and Pollution Events in a Low Industrialized City 1087-1096
17. **G. Rodríguez-Martínez, I. Galaviz-Villa, S. Partida-Sedas, C.A. Sosa-Villalobos, R. de G. Bernal-Ramírez, V. Alcántara-Méndez and A. García-Saldaña,** Water Erosion, its Relationship to Total Suspended Solids and Water Quality in the Lower Basin of the Usumacinta River, Tabasco, Mexico 1097-1106
18. **Y. Li, S. Yi , Y. Lin and S. Liu,** Optimization of the Water and Fertilizer of Rice in the Cold Field and the Biochar Application Amount Based on RAGA Model 1107-1113
19. **H.R. Yu, Y.Z. Wang, Z. Liang and C.K. Min,** The Construction of Regional Ecological Security Pattern Based on a Multi-Factor Comprehensive Model and Circuit Theory 1115-1126
20. **J. Mary Sheela, K. Divya and S. Premina,** Amylase Production by *Aspergillus niger* and *Penicillium* Species by Solid-State and Submerged Cultivation Using Two Food Industrial Wastes 1127-1135
21. **H. Lu, F. Luo, Q. Zhang, J. Li and L. Cai,** The Physicochemical Characteristic of Activated Carbon Based on Sludge and Preparation Method 1137-1145
22. **Qingkong Cai, Erjun Li, Yafei Zhang, Guo Wang and Chao Chen,** Contributions of Land Utilization Differences and Changes in Zhongyuan Urban Agglomeration to Regional Thermal Environment 1147-1156
23. **G. Chelladurai, T.K. Yadav and R.K. Pathak,** Chemical Composition and Nutritional Value of Paddy Straw Milky Mushroom (*Calocybe indica*) 1157-1164
24. **T. Yu, F. Wang, H. Hu, C. Qu and Le Zhang,** Study on Catalytic Oxidation, Flocculation and Sedimentation of Acidizing and Fracturing Wastewater 1165-1171
25. **N.Z. Zabi, W.N. Wan Ibrahim, N.S. Mohammad Hanapi and N. Mat Hadzir,** Removal of Various Contaminants by Highly Porous Activated Carbon Sorbent Derived from Agricultural Waste Produced in Malaysia - A Review 1173-1183

26. **P. Muthupriya and B. Vignesh Kumar,** Experimental Investigation on Concrete with E-waste - A Way to Minimize Solid Waste Deposition 1185-1191
27. **S. Fu, Y. Dong, L. Liang and X. Meng,** Fabrication of Ag/TiO_2 Cotton Fabric to Enhance Photocatalytic Degradation of Anionic Dye 1193-1199
28. **T. S. Subbiah, P. Parthiban, R. Mahesh and A. Das,** Time Series Analysis of Decadal Precipitation Pattern at Selected Cities of Southern India 1201-1208
29. **Zhongchao Hao,** Analysis on Pollution Hazards and Recycling Strategies of Logistics Packaging Wastesof E-Commerce Enterprises 1209-1216
30. **A.M.M. Mawad, H. Albasri and H. A. Temerk,** Biosorption of Malachite Green by Dry Cells of Isolated Free Living Nitrogen Fixing Bacteria 1217-1223
31. **C. Jesu Raj and J. Prema Kumari,** Urban and Rural Airborne Particulate Matter: Seasonal Variation of Alpha Activity in Kanyakumari District 1225-1229
32. **X. Zhao, L. H. Sun and X. Y. Qiu,** Influence of Evaporation on the Hydrogen and Oxygen Stable Isotopes in an Enclosed Water Body: A Case Study 1231-1236
33. **S.R. Krishna Motukuri , D. Vijaya Nagini, J. Nallamothu and S. Karthikeyan**, Insilico Molecular Docking Studies of Volatile Compounds Identified by GC-MS from *Tagetes* Species Against *Mamestra brassicae* (Linnaeus, 1758) 1237-1242
34. **Xianqi Zhang, Zhiwen Zheng and Rulin Ouyang,** Study on Spatiotemporal Evolution Characteristics of Regional Annual Precipitation 1243-1250
35. **T. Arathi, K. P. Rahna, Delse P. Sebastian and Satheesh George,** Assessment of Heavy Metal and Pesticide Contamination in Banana Fields and Development of Phytoremediation System in Kozhikode District, Kerala, India 1251-1256
36. **K. Ruengruehan, R. Junggoth, S. Suttibak, C. Sirikoon and N. Sanphoti,** Contamination of Cadmium, Lead, Mercury and Manganese in Leachate from Open Dump, Controlled Dump and Sanitary Landfill Sites in Rural Thailand: A Case Study in Sakon Nakhon Province 1257-1261
37. **S. Pal, S. Maity, S. Balachandran and S. Chaudhury,** In-vitro Effects of Chlorpyrifos and Monocrotophos on the Activity of Acetylcholinesterase (AChE) in Different Tissues of Apple Snail*Pila globosa* (Swainson, 1822) 1263-1268
38. **M. Riza, M. N. Ehsan and S. Hoque,** Portrayal of Textile Based Pollutants and its Impact on Soil, Plants and Fisheries 1269-1275
39. **Chunwei Han,** Impact of Environmental Subsidies on Environmental Technology Innovation of Polluting Enterprises 1277-1284
40. **D. Nageswara Rao, T. Bhaskara Rao and P.V.S. Machiraju,** Chemical and Pathogen Impacts on Human Health near Aquaculture Areas in West Godavari District of Andhra Pradesh, India 1285-1293
41. **S. Singh, S. Shankar and Shikha,** Evaluation of LDPE Degradation Under Controlled Composting 1295-1300
42. **K.M.P. Mokatse and J.P.H. van Wyk,** Successive Saccharification of Waste Paper as a Resource for Bio-product Development 1301-1308
43. **E. N. Hidayah, O. H. Cahyonugroho, M. Mirwan, R. B. Pachwarya and M. K. Asrori,** Effect of Oxidation on the Formation of Disinfectant By-products of Low Molecular Weight Organic Matter 1309-1313
44. **S. Maheshwari, P. Kriplani, A. S. Jethoo, P. Kumar and M. Khwairakpam,** Study of Change in Physico-Chemical Parameters by Treatment of Sludge from Common Effluent Treatment Plant (CETP) with Earthworms 1315-1321
45. **T. Azhaguthasan, T. Ravimycin and K. Santhi,** Impact of Organic and Inorganic Fertilizers on Morphological and Biochemical Components of *Arachis hypogaea* L. 1323-1329
46. **Shang Li,** Evaluation of Ecological Environmental Pollution in Green Building Construction 1331-1337
47. **B. Paul and D. Paul,** Comparative Analysis of Municipal Solid Waste Management in Kochi and Indore 1339-1345
48. **T. Stalin Subbiah, R. Mahesh, P. Parthiban and A. Das,** Spatio-Temporal Variability of Gamma Radiation Profile Along the Southern-Indian Coastline (Poompuhar to Nagapattinam Stretch) 1347-1351
49. **Zhong Wei Wang and Huan Le Han,** Analysis on Tourism Environmental Pollution and Tourism Economy-Ecological Environmental Coordination Degree: A Case Study from China 1353-1361
50. **I. Galaviz-Villa, C.A. Sosa-Villalobos, N.L. Lagunes-Reyes, C. Landeros-Sánchez, M.A. Castillo-Ferat, A. García-Saldaña, S. Partida Sedas and A. Cabal Prieto,** Nitrate-Nitrogen ($N\text{-}NO_3^-$) in Ground Waters of Agricultural Zones in Tabasco, México; Risks for Aquatic Life and Human Health 1363-1368
51. **Sawkat Ara Pinki, Md. Reazul Karim, Dipankar Dewanjee, Habibur Rahman Bhuiyan, H. M. Abdullah Al Masud and Md. Imranul Hoq,** Microbial Reduction and Detoxification of Chromium from Tannery Effluent by Natural Inhabitants 1369-1380

The Journal is Currently Abstracted and Indexed in:

International Scientific Indexing (UAE) with Impact Factor 2.236 (2018)

NAAS Rating of the Journal (2019) = 3.85

Scopus®, SJR (0.127) 2019

Index Copernicus (2018) = 135.97

EI Compendex of Elsevier

Indian Science Abstracts, New Delhi, India

Chemical Abstracts, U.S.A.

Pollution Abstracts, U.S.A.

Elsevier Bibliographic Databases

Paryavaran Abstract, New Delhi, India

Zoological Records

Indian Citation Index (ICI)

Electronic Social and Science Citation Index (ESSCI)

EBSCO: Environment Index™

Scopus CiteScore (2019) = 0.5

Ulrich's (Refereed) database

CrossRef (DOI)

DOAJ

Zetoc

Google Scholar

ProQuest, U.K.

J-Gate

Environment Abstract, U.S.A.

British Library

Centre for Research Libraries

WorldCat (OCLC)

JournalSeek

Connect Journals (India)

CSA: Environmental Sciences and Pollution Management

Research Bible (Japan)

Indian Science

Geobase

Elektronische Zeitschriftenbibliothek (EZB)

SHERPA/RoMEO

Directory of Science

CNKI Scholar (China National Knowledge Infrastructure)

Access to Global Online Research in Agriculture (AGORA)

AGRIS (UN-FAO)

Present in UGC-CARE List (Group II)

UDL-EDGE (Malaysia) Products like *i*-Journals, *i*-Focus and *i*-Future

www.neptjournal.com

Nature Environment and Pollution Technology

EDITORS

Dr. P. K. Goel (Chief Editor)
Former Head, Deptt. of Pollution Studies
Yashwantrao Chavan College of Science
Vidyanagar, Karad-415 124
Maharashtra, India

Dr. K. P. Sharma
Former Professor, Ecology Lab, Deptt. of Botany
University of Rajasthan
Jaipur-302 004, India
Rajasthan, India

Manager Operations: Mrs. Apurva Goel Garg, C-102, Building No. 12, Swarna CGHS, Beverly Park, Kanakia, Mira Road (E) (Thane) Mumbai-401107, Maharashtra, India **(E-mail: operations@neptjournal.com)**

Business Manager: Mrs. Tara P. Goel, Technoscience Publications, A-504, Bliss Avenue, Balewadi, Pune-411 045, Maharashtra, India **(E-mail: contact@neptjournal.com)**

EDITORIAL ADVISORY BOARD

1. **Dr. Prof. Malay Chaudhury**, Department of Civil Engineer ing, Universiti Teknologi PETRONAS, Malaysia
2. **Dr. Saikat Kumar Basu**, University of Lethbridge, Lethbridge AB, Canada
3. **Dr. Sudip Datta Banik**, Department of Human Ecology Cinvestav-IPN Merida, Yucatan, Mexico
4. **Dr. Elsayed Elsayed Hafez**, Deptt. of of Molecular Plant Pathology, Arid Land Institute, Egypt
5. **Dr. Dilip Nandwani**, College of Agriculture, Human & Natural Sciences, Tennessee State Univ., Nashville, TN, USA
6. **Dr. Ibrahim Umaru,** Department of Economics, Nasarawa State University, Keffi, Nigeria
7. **Dr. Tri Nguyen-Quang,** Department of Engineering Agricultural Campus, Dalhousie University, Canada
8. **Dr. Hoang Anh Tuan,** Deptt. of Science and Technology Ho Chi Minh City University of Transport, Vietnam
9. **Mr. Shun-Chung Lee**, Deptt. of Resources Engineering, National Cheng Kung University, Tainan City, Taiwan
10. **Samir Kumar Khanal**, Deptt. of Molecular Biosciences & Bioengineering,University of Hawaii, Honolulu, Hawaii
11. **Dr. Sang-Bing Tsai,** Zhongshan Institute, University of Electronic Science and Technology, China
12. **Dr. Zawawi Bin Daud,** Faculty of Civil and Environmental Engg., Universiti Tun Hussein Onn Malaysia, Johor, Malaysia
13. **Dr. Srijan Aggarwal**, Civil and Environmental Engg. University of Alaska, Fairbanks, USA
14. **Dr. M. I. Zuberi,** Department of Environmental Science, Ambo University, Ambo, Ethiopia
15. **Dr. Prof. A.B. Gupta,** Dept. of Civil Engineering, MREC, Jaipur, India
16. **Dr. B. Akbar John,** Kulliyyah of Science, International Islamic University, Kuantan, Pahang, Malaysia
17. **Dr. Bing Jie Ni,** Advanced Water Management Centre, The University of Queensland, Australia
18. **Dr. Prof. S. Krishnamoorthy,** National Institute of Technology, Tiruchirapally, India
19. **Dr. Prof. (Mrs.) Madhoolika Agarwal,** Dept. of Botany, B.H.U., Varanasi, India
20. **Dr. Anthony Horton,** Envirocarb Pty Ltd., Australia
21. **Dr. C. Stella,** School of Marine Sciences, Alagappa University, **Thondi -623409**, Tamil Nadu, India
22. **Dr. Ahmed Jalal Khan Chowdhury,** International Islamic University, Kuantan, Pahang Darul Makmur, Malaysia
23. **Dr. Prof. M.P. Sinha,** Dumka University, Dumka, India
24. **Dr. G.R. Pathade**, H.V. Desai College, Pune, India
25. **Dr. Hossam Adel Zaqoot,** Ministry of Environmental Affairs, Ramallah, Palestine
26. **Prof. Riccardo Buccolieri,** Deptt. of Atmospheric Physics, University of Salento-Dipartimento di Scienze e Tecnologie Biologiche ed Ambientali Complesso Ecotekne-Palazzina M S.P. 6 Lecce-Monteroni, Lecce, Italy
27. **Dr. James J. Newton,** Environmental Program Manager 701 S. Walnut St. Milford, DE 19963, USA
28. **Prof. Subhashini Sharma,** Dept. of Zoology, Uiversity of Rajasthan, Jaipur, India
29. **Dr. Murat Eyvaz,** Department of Environmental Engg. Gebze Inst. of Technology, Gebze-Kocaeli, Turkey
30. **Dr. Zhihui Liu,** School of Resources and Environment Science, Xinjiang University, Urumqi , China
31. **Claudio M. Amescua García,** Department of Publications Centro de Ciencias de la Atmósfera, Universidad Nacional Autónoma de, México
32. **Dr. D. R. Khanna,** Gurukul Kangri Vishwavidyalaya, Hardwar, India
33. **Dr. S. Dawood Sharief**, Dept. of Zoology, The New College, Chennai, T. N., India
34. **Dr. Amit Arora,** Department of Chemical Engineering Shaheed Bhagat Singh State Technical Campus Ferozepur -152004, Punjab, India
35. **Dr. Xianyong Meng**, Xinjiang Inst. of Ecology and Geography, Chinese Academy of Sciences, Urumqi , China
36. **Dr. Sandra Gómez-Arroyo**, Centre of Atmospheric Sciences National Autonomous University, Mexico
37. **Dr. Manish Sharma**, Deptt. of Physics, Sharda University, Greater Noida, India
38. **Dr. Wen Zhang,** Deptt. of Civil and Environmental Engineering, New Jersey Institute of Technology, USA

Nature Environment and Pollution Technology
An International Quarterly Scientific Journal

p-ISSN: 0972-6268
(Print copies up to 2016)
e-ISSN: 2395-3454

Vol. 20 | No.3 | pp. 909-922 | 2021

Original Research Paper

https://doi.org/10.46488/NEPT.2021.v20i03.001

Open Access Journal

Effect of Water Chemistry on the Uptake of Co(II) on Graphene Oxide Investigated by Batch Technique

X. Tang*, J. Luo*, L. Wang and X. Li*†**

*College of Yuanpei, Shaoxing University, Shaoxing 312000, P. R. China

**College of Chemistry and Chemical Engineering, Shaoxing University, Shaoxing 312000, P. R. China

†Corresponding authors: Xue Li; lixue@usx.edu.cn

Nat. Env. & Poll. Tech.
Website: www.neptjournal.com

Received: 04-07-2020
Revised: 22-09-2020
Accepted: 09-10-2020

Key Words:
Co(II)
Graphene oxide
Isotherm
Water chemistry

ABSTRACT

The uptake of Co(II) on graphene oxide (GO) by an adsorption process as a function of pH and ionic strength in the absence and presence of humic acid (HA) or fulvic acid (FA) was studied using batch technique. The results indicated that the uptake is strongly dependent on pH but independent of ionic strength. A stimulative effect of HA/FA on Co(II) uptake was found at pH < 7.0, whereas an inhibitory effect was observed at pH > 7.0. Kinetic studies suggest that Co(II) uptake on GO could be described more favorably by the pseudo-second-order kinetic model. The uptake isotherms can be described better by the Langmuir, Freundlich, and D-R models than by the linear model. The thermodynamic data calculated from the temperature-dependent uptake isotherms suggests that the uptake of Co(II) on GO is spontaneous and endothermic. Results of this work are of great importance for the environmental application of GO in the treatment of Co(II) from wastewater and indicated that GO is promising for the natural attenuation of Co(II) and related metal ions from aqueous solution.

INTRODUCTION

Pollution in the natural water due to hazardous and non-biodegradable heavy metal ions such as lead, cuprum, nickel, cadmium, and cobalt, originates from various human industrial activities such as electroplating, mining, fabrication of batteries, and microelectronics (Mobasherpour et al. 2014, Jin et al. 2015, Sun et al. 2015, Arancibia-Miranda et al. 2016, Sheng et al. 2016). It is a potential hazard to living systems; hence, it is essential to develop efficient and inexpensive materials and technologies to remove them from polluted water and recycle them. ^{60}Co(II) is one of the most serious radionuclides that encroach on the environment due to its long half-life ($T_{1/2}$ = 5.27 a). The radionuclides ^{60}Co and ^{58}Co are present in liquid wastes released from pressurized water nuclear power reactors (Zhang et al. 2011). The permissible limits of cobalt in the irrigation water and livestock wastewaters are 0.05 and 1.0 mg·L^{-1} respectively (Shibi et al. 2005). Cobalt poisoning in human beings may cause neuron toxicological disorders, genotoxicity, and cause cancer (Bhatnagar et al. 2010). Until now, various methods are in use to remove and recover heavy metals such as chemical precipitation (Chen et al. 2018), uptake (Ding et al. 2015), ion exchange (Komatsu et al. 2010), and membrane filtration (Almasian et al. 2018) among which uptake is considered an economical and effective strategy (Jin et al. 2014, Ma et al. 2015). Recently, numerous studies have investigated the uptake of Co(II) and related metal ions on a variety of adsorbents such as bentonite/iron oxide (Chen et al. 2011), alumina (Mou et al. 2012), Fe_3O_4@cyclodextrin (Zhang et al. 2014), fungus/attapulgite composites (Cheng et al. 2015), and multiwalled carbon nanotubes/polyacrylamide composites (Yang et al. 2011). However, research seeking novel potential adsorbents for the removal of metal ions with much higher uptake capacities and efficiencies is always necessary.

Graphene (G), a single or several atomic layered graphites, is a fascinating new class of two-dimensional carbon nanostructures and possesses excellent mechanical, thermal, and electrical properties (Zhao et al. 2011, Deng et al. 2013, Luo et al. 2019). Graphene exhibits a huge surface area with a calculated value of 2630 m^2·g^{-1}. It has shown great promise in the application of environmental pollution remediation. However, graphene itself is a hydrophobic substance, preventing it as an adsorbent for directly removing heavy metal ions from an aqueous solution. Graphene oxide (GO), the oxidation product of graphene containing epoxide, carbonyl, carboxyl, and hydroxyl functional groups, is hydrophilic, negatively charged, and readily disperses in an aqueous solution to form a stable suspension (Gao et al. 2011). Therefore, GO has the potential to remove heavy metal ions and organic pollutants in wastewater and has recently attracted significant attention as a high adsorbent in wastewater treatment (Bradder et al. 2011, Zhao et al. 2011). For instance, Wang

et al. (2014) investigated the uptake of polycyclic aromatic hydrocarbons onto G and GO. Pei et al. (2013) used G and GO for the removal of 2-naphthol, 2,4,6-trichlorophenol, 1,2,4-trichlorobenzene, and naphthalene. Zhao et al. (2011) reported that GO showed a strong uptake capacity to Pb(II), Cd(II), and Co(II). Besides, they found that the uptake of heavy metal ions is dependent on the extent of O-containing functional groups. Ramesha et al. (2011) studied the uptake of anionic and cationic dyes on G and GO. They also studied the uptake of Cu(II) and Ni(II) on GO as a function of solution chemistry (Li et al. 2014, 2015). All these investigations indicated G and GO showed an outstanding capability in the removal of a wide range of organic and inorganic contaminants. Nevertheless, to our knowledge, there is little information about the simultaneous uptake of metal ions and organics on GO. And we should realize that metal ions and organics may exist simultaneously in the real environment. For example, the presence of soil humic substances like humic acid (HA) or fulvic acid (FA) obviously influences the uptake of metal ions at the interface (Sheng et al. 2014a, b). So, it is very necessary to study the uptake of metal ions on GO in the presence of organic contaminants and vice versa.

Hence, to extend the practical application of GO in metal ion remediation, Co(II) as a chemical analog of radionuclides was selected in this paper. The objectives of this paper were: (1) to study the uptake kinetics and to simulate the data with a pseudo-second-order equation; (2) to investigate the effect of water chemistries (e.g., reaction time, pH, ionic strength, and temperature) on Co(II) onto GO by batch techniques; (3) to determine the uptake mechanism between Co(II) and GO; (4) The regeneration and reuse of GO in Co(II) uptake were also studied. The highlight of this paper is that the potential application of GO towards the removal of radionuclides from aqueous solutions in environmental remediation strategy.

MATERIALS AND METHODS

Materials and Reagents

GO was prepared using the modified Hummers method; the results of the SEM and TEM characterization of the prepared GO are shown in Fig. 1. From the SEM images (Fig. 1A) we can see that the GO was randomly accumulated by thin nanosheets in a loose state, the surface is smooth, and there was a crimp in the fold oxidation state. More finely, as shown in the TEM image (Fig. 1B), the GO film is transparent and typically wrinkled, sheet-like structures. All reagents used in the experiments were purchased in analytical purity and used without any purification. All solutions were prepared with Milli-Q water. Add 0.8075 g $CoCl_2 \cdot 6H_2O$ analytical reagent into a beaker, add an appropriate amount of deionized water to dissolve, and then pour it into a 1000 mL volumetric flask. Add deionized water to the volumetric flask to the scale line to obtain the Co(II) stock solution in a concentration of 200 $mg \cdot L^{-1}$. The prepared Co(II) stock solution was diluted to the required concentrations in the following experiments. The humic acid (HA) and fulvic acid (FA), which were obtained as a gift from the Institute of Plasma Physics, Chinese Academy of Sciences, were extracted from the soil of Hua-Jia county (Gansu province, China) and had been characterized in detail previously (Tan et al. 2009).

Uptake Procedures

The uptake of Co(II) on GO was investigated by using the batch technique in polyethylene centrifuge tubes under dif-

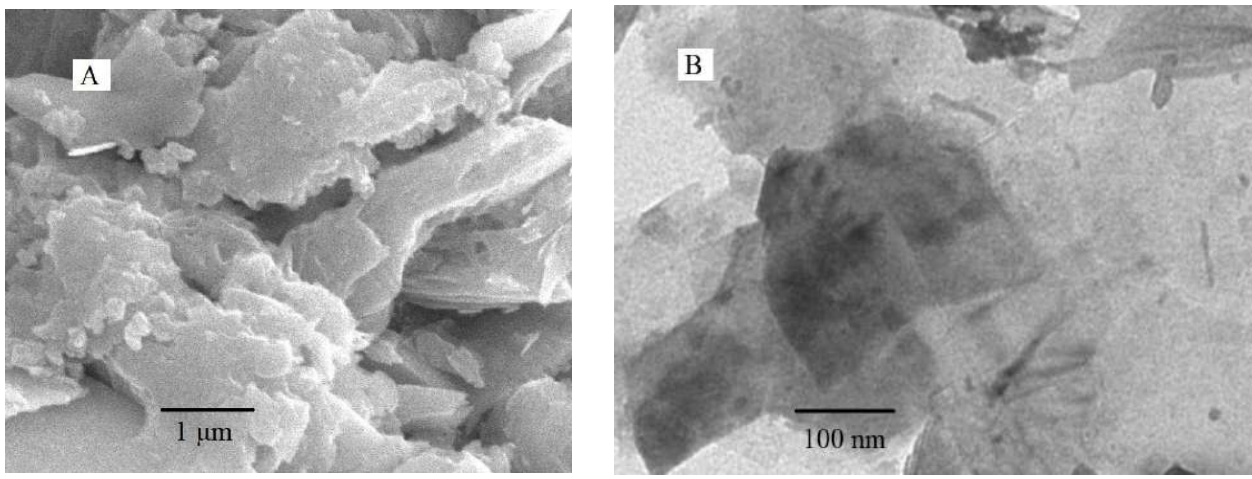

Fig. 1: (A) SEM and (B) TEM of GO.

ferent chemical conditions. The stock suspension of GO and $NaNO_3$ solution was first contacted for two days to achieve the equilibration of GO and $NaNO_3$. Then, Co(II) stock solution and FA or HA stock solution were added to achieve the desired concentrations of different components. The system was adjusted to the desired pH by adding inappreciable volumes of 0.01 mol·L^{-1} HNO_3 or NaOH. After the suspensions were shaken for two days, the solid and liquid phases were separated by centrifugation at 9000 rpm for 60 min at the same temperature control to the uptake experiments. The concentration of ^{60}Co(II) was analyzed by liquid scintillation counting using a Packard 3100 TR/AB Liquid Scintillation Analyzer (PerkinElmer). The scintillation cocktail was ULTIMA GOLD AB^{TM} (Packard) (Chen et al. 2011). The amount of Co(II) absorbed on GO was calculated from the difference between the initial concentration and the equilibrium one.

For reversibility and regeneration study, a typical treatment process was conducted by adding 500 mL of 0.01 mol·L^{-1} $NaNO_3$ and 10 mg·L^{-1} Co(II) into a 1 L beakers containing GO with three different concentrations (i.e., 0.05, 0.1, and 0.2 g·L^{-1}). The pH was adjusted to a certain value. The suspensions were continuously stirred for 24 h by using a mechanical mixer and then separated, and the obtained supernatants were used for the measurement of Co(II) concentration. The solid was washed with 0.001 mol·L^{-1} HNO_3 and high-purity Milli-Q water, until Co(II) could be determined, collected, and dried at 60 ^{o}C. The recovered GO was used for Co(II) uptake a second time. According to this process, the adsorption-desorption process was repeated 6 times.

The uptake of Co(II) was expressed in terms of distribution coefficient (K_d) and uptake percentage (%) was derived from the following equations (Zhang et al. 2014):

$$K_d = \frac{C_0 - C_e}{C_e}\frac{V}{m} \quad \ldots(1)$$

$$\text{uptake percentage (\%)} = \frac{C_0 - C_e}{C_0} \times 100\% \quad \ldots(2)$$

where C_0 is the initial concentration, C_e is the concentration in supernatant after centrifugation, m is the mass of GO, and V is the volume of the suspension.

RESULTS AND DISCUSSION

Impact of Contact Time

To establish the equilibration time for maximum uptake and the uptake capacity of different solid content, and to know the kinetics of the uptake process, Co(II) uptake on the GO of three different concentrations (i.e., 0.05, 0.1, and 0.2 g·L^{-1}) were investigated as a function of contact time and the results are shown in Fig. 2. It can be seen from Fig. 2A that Co(II) uptake on GO increases rapidly at the initial contact time of 1.5 h, and then increases slowly in the following contact time. Specifically, the equilibrium uptake amount decreases from 104.13 to 36.43 mg·g^{-1} with the GO concentration increasing from 0.05 to 0.2 g·L^{-1}. This result indicates that Co(II) uptake on GO is attributed to chemical interaction rather than physical interaction.

To help deduce the uptake mechanisms, the experimental kinetic data of Co(II) on GO are simulated by using the pseudo-second-order models (Zhang et al. 2014):

$$\frac{t}{q_t} = \frac{1}{2kq_e^2} + \frac{t}{q_e} \quad \ldots(3)$$

In the equations, q_t (mg·g^{-1}) is the amount of Co(II) uptake on GO at time t (h), q_e (mg·g^{-1}) is the equilibrium Co(II) capacity, and k (g·mg^{-1}·h^{-1}) is the rate constant of an uptake process. The straight-line plots of t/q_t versus t (Fig. 2B) indicate that the kinetic uptake of Co(II) on GO is well described by the pseudo-second-order rate equation. The values of k and q_e determined from the slopes and intercepts of the kinetic model are listed in Table 1. The correlation coefficients of the pseudo-second-order rate equation for the linear plot are very close to 1, which suggests that the kinetic uptake can be described by the pseudo-second-order rate equation very well.

Effect of Solid Content

Fig. 3 shows the dependence of Co(II) uptake on GO as a function of solid content at T = 293 K and pH = 6.0 ± 0.1. As can be seen that the uptake percentage of Co(II) increases rapidly with increasing GO contents. With increasing solid contents, the number of functional groups at the GO surfaces increases, hence, more exchangeable surface sites are available to form complexes with Co(II) at solid surfaces. As can be seen from Fig. 3, the uptake capacity of Co(II) on GO decreases gradually with the increase of solid content. These phenomena can be attributed to three reasons: (1) The solid surface is composed of sites with a spectrum of binding energies. At low GO content, all kinds of surface sites are entirely exposed for uptake Co(II) and the surface gets to saturation faster, resulting in a higher uptake capacity. But at higher particle concentrations, the availability of higher energy sites decreases with a larger fraction of lower energy sites becoming occupied, leading to a lower uptake capacity (Huang et al. 2008); (2) The higher GO amount enhances the probability of collision between GO particles and therefore creates particle aggregation, causing a decrease in the total surface area and an increase in diffusion path length, both of which contribute to the decrease in the uptake capacity of Co(II) on GO (Li et al. 2011); (3) The increase ratio of

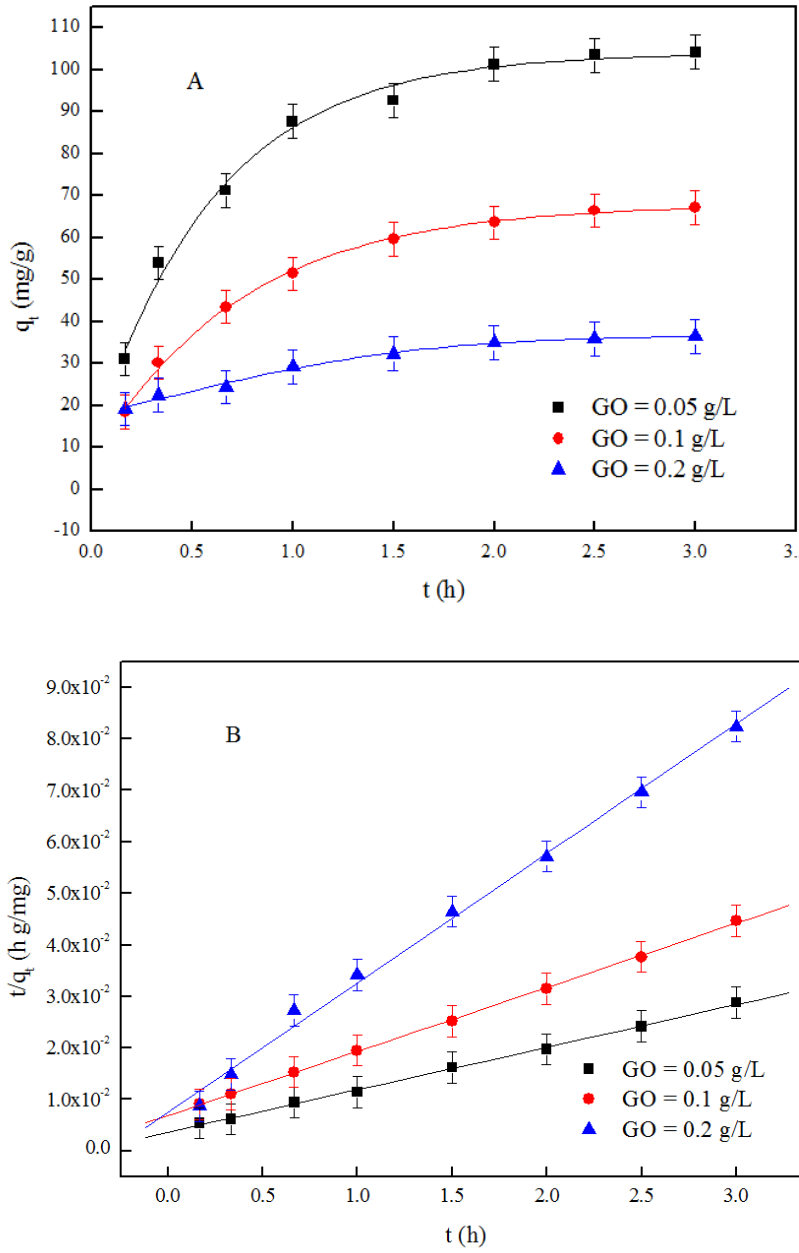

Fig. 2: (A) Uptake of Co(II) on GO as a function of contact time, (B) Plot of t/q_t vs. t for the Pseudo-second-order rate calculation of Co(II) uptake on GO , T = 293 K, pH = 6.0 ± 0.1, $C_{Co(II)initial}$ = 10 mg/L, I = 0.1 mol/L $NaNO_3$.

Table 1: Kinetic parameters of Co(II) uptake on GO.

GO (g/L)	Pseudo-second-order parameters		
	q_e (mg·g^{-1})	k (g·mg^{-1}·h^{-1})	R^2
0.05	120.9190	0.0095	0.9984
0.1	80.5153	0.0112	0.9995
0.2	39.7614	0.0423	0.9949

net uptake quantity of Co(II) on GO surface is lower than that of the solid content, correspondingly decreasing the uptake capacity of Co(II) on GO. This result implies that the augmentation of GO could not unboundedly increase the contact area between metal ions and the solid surface. At the same time, the competition uptake between the sorbent will also reduce the uptake ability of solid particles. Thus, with a view to reducing the cost of pollution treatment in actual application, one should choose a suitable sorbent dosage according to the pollutant concentrations and required removal efficiency.

Impact of pH and Ionic Strength

The pH dependence of Co(II) uptake on GO ranging from 2.0 to 10.0 at three different ionic strengths (i.e., 0.001, 0.01, and 0.1 mol·L^{-1} $NaNO_3$) is shown in Fig. 4. As can be seen, the pH values of the aqueous solution play an important role in the uptake of Co(II) on GO. With the $C_{CO(II)initial}$ of 10 mg·L^{-1}, the uptake of Co(II) on GO increases slowly with pH ranging from 2.0 to 4.0, then increases abruptly with pH 4.0–8.0 and at last maintains the high uptake level with pH increasing at pH > 8.0. About 90% of Co(II) is absorbed on GO at pH > 8.0.

The uptake of metal ions on sorbents is obviously affected by pH values because it not only influences metal ion species in solution but also affects the surface properties of the sorbents according to dissociation of functional groups and surface charge. The increase of Co(II) uptake on GO with increasing solution pH may be attributed to the surface properties of GO in terms of surface charge and dissociation of functional groups. Because of the protonation reaction (i.e., $MOH + H^+ \Leftrightarrow MOH_2^+$), the GO surface contains a large number of binding sites and can become positively charged at low pH. The electrostatic repulsion occurred between Co(II) and the positively charged sites (MOH_2^+) on GO results in the low uptake of Co(II). At high pH, the GO surface becomes negatively charged due to the deprotonation process (i.e., $MOH \Leftrightarrow MO^- + H^+$) and electrostatic repulsion obviously decreases with pH raising, which enhances the uptake of Co(II) on GO through electrostatic force of attraction (Yang et al. 2011, Deng et al. 2013). At the same time, another factor needs to be considered, that is, the increase in pH values may lead to Co(II) precipitation on the GO surface. Previous research has reported that the hydrolysis is constant of $Co(OH)_2$ is $1.58\times10^{-14.80}$ (Chen et al. 2011). In our study, the initial concentration of Co(II) is 10 mg·L^{-1}, so Co(II) begins to form precipitation at a pH of about 8.7. However, at pH 8.0, the Co(II) ions are absorbed on GO completely. Consequently, it is impossible to form precipitation because of the very low concentration of Co(II) that remained in the solution. Hence, the sharp increase of Co(II) uptake on GO at pH 4.0-8.0 is not attributed to the Co(II) precipitation.

Fig. 4 also displays the impact of ionic strength on Co(II) uptake on GO. We can see that ionic strength showed a negligible effect on Co(II) uptake. The uptake is weakly affected by ionic strength at pH 4–8 and no effect is approximately

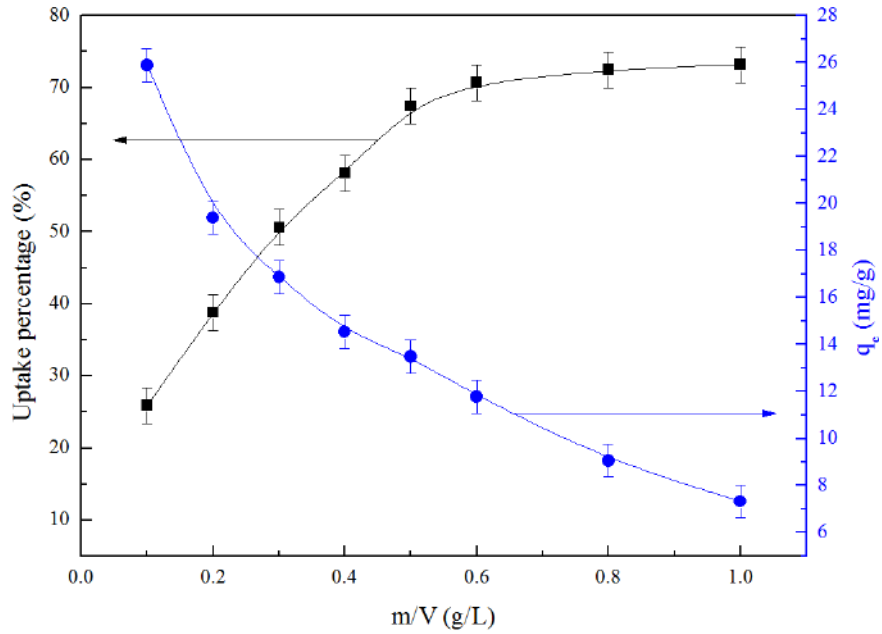

Fig. 3: Uptake of Co(II) on GO as a function of solid content at T = 293 K, pH = 6.0 ± 0.1, $C_{Co(II)initial}$ = 10 mg/L, I = 0.1 mol/L $NaNO_3$.

found at pH < 4.0 or pH > 8.0. The ionic strength may affect the double electrode layer thickness and interface potential, hence, affecting the binding of the adsorbed species. Outer-sphere surface complexes are regarded to be more impressionable to ionic strength variations than inner-sphere complexes as the background electrolyte ions are placed in the same plane for outer-sphere surface complexes (Hayes & Leckie 1987). Based on this theory and the results of these studies, we can deduce that inner-sphere surface complexation is the main mechanism of Co(II) uptake on GO.

Impact of Humic Substances

The humic acid (HA) and fulvic acid (FA), which are ubiquitous in the natural environment, can influence the uptake and transport of metal ions significantly as both of them can form strong complexes with metal ions (Sheng et al. 2014a, b). The uptake of Co(II) on GO in the presence/absence of FA/HA under different pH values is shown in Fig. 5. We can see that the presence of FA or HA enhances the uptake of Co(II) on GO at pH < 7.0, while Co(II) uptake was restrained at high pH > 7.0. The uptake of HA and FA onto GO as a function of pH was determined in previous work (Li et al. 2014), and it was found that 90% of HA/FA can be absorbed on GO at low pH, and then the uptake decreases with pH increasing. It was reported that both HA and FA were negatively charged at pH 3.0–10.0 (Sheng et al. 2012). Hence, at low pH, the negatively-charged HA/FA can be easily absorbed onto the positively-charged GO surface as a result of electrostatic attraction, resulting in the enhancement of Co(II) uptake onto GO due to the strong complexation ability of surface absorbed HA/FA with Co(II). However, at high pH, it is very difficult for the negatively-charged HA/FA to be adsorbed onto the negatively-charged GO surface due to the electrostatic repulsion, therefore, the HA/FA in solution forms HA/FA-Co(II) soluble complexes, and thereby the uptake of Co(II) onto GO was greatly reduced. Similar results found the presence of HA/FA imposing a positive role in Ni(II) adsorption onto GO at low pH, whereas a negative role in the adsorption of Ni(II) onto GO was observed at high pH in previous work (Li et al. 2015).

Uptake Isotherms of Co(II) on GO and Thermodynamic Study

The uptake isotherms for Co(II) on GO at 293, 313, and 333 K are shown in Fig. 6. It is clear from Fig. 6 that the uptake isotherm is the highest at T = 333 K and is the lowest at T = 293 K. The result indicates that high temperature is advantageous for Co(II) uptake on GO. This phenomenon may be attributed to two key factors (Hu et al. 2010, Jin et al. 2014): (1) Increased diffusion rate of Co(II) into GO surface binding sites due to increased temperature that contributes to the observed uptake; (2) The increase in reaction temperature may increase in proportion and activity of Co(II) ions in solution, the affinity of Co(II) ions to GO surface, or the charge and the potential of GO surface. Four different models, viz. Linear, Langmuir, Freundlich, and D-R isotherm equations

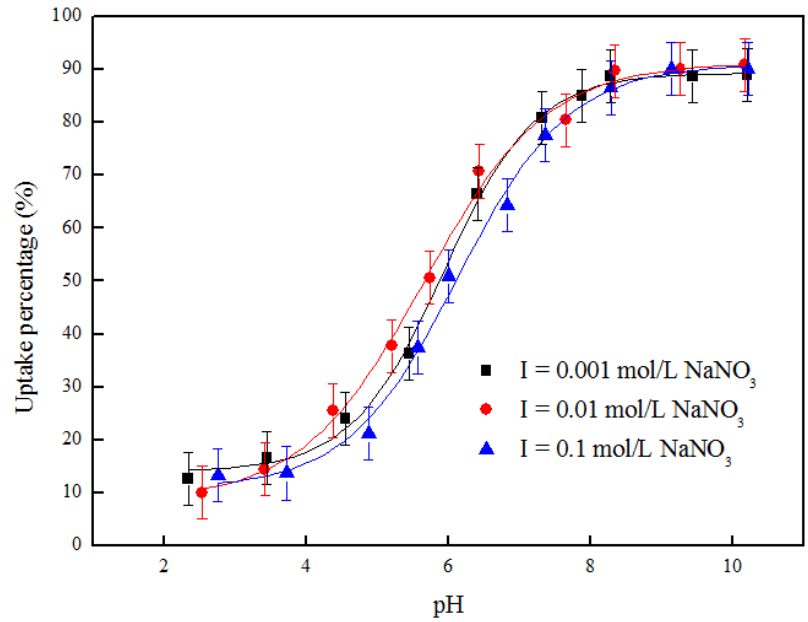

Fig. 4: The role of pH and ionic strength in Co(II) uptake on GO, T = 293 K, $C_{Co(II)initial}$ = 10 mg/L, m/V = 0.1 g/L.

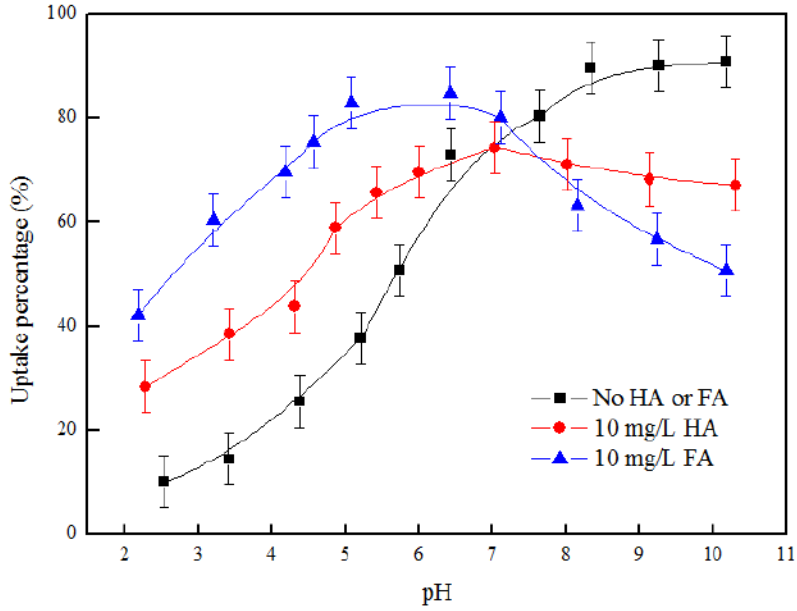

Fig. 5: The role of HA/FA in Co(II) uptake on GO, T = 293 K, $C_{Co(II)initial}$ = 10 mg/L, m/V = 0.1 g/L, I = 0.1 mol/L $NaNO_3$.

are conducted to simulate the uptake isotherms and to establish the relationship between the amount of Co(II) adsorbed on GO and the concentration of Co(II) remained in solution.

The Linear model (Sheng et al. 2012, Li et al. 2015) is as:

$$q_e = AC_e + B \quad \ldots(4)$$

where C_e (mol·L^{-1}) is the equilibrium concentration of Co(II) remained in the solution ; q_e (mol·g^{-1}) is the amount of Co(II) adsorbed on per weight unit of GO after equilibrium.

The Langmuir model assumes that uptake occurs in a monolayer with all uptake sites identical and energetically equivalent (Sheng et al. 2012, Li et al. 2015). Its form can be described by the following equation:

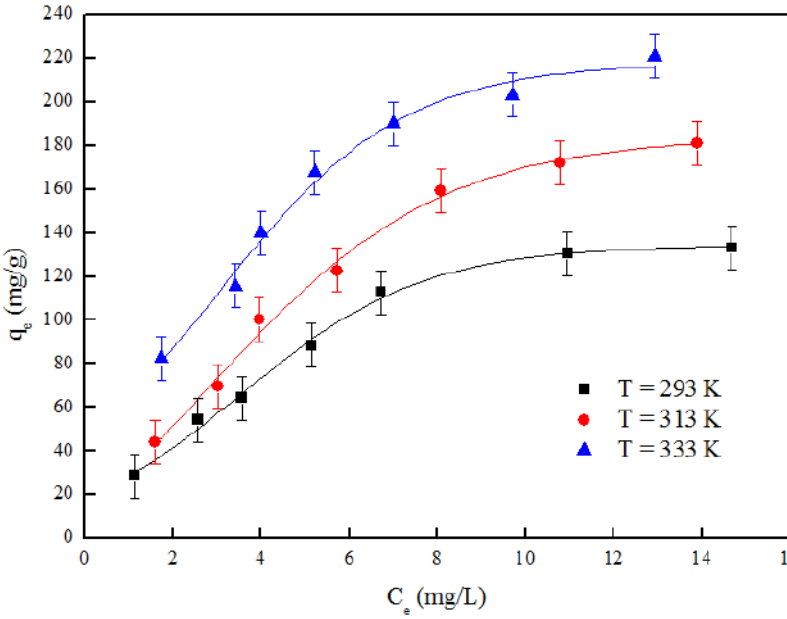

Fig. 6: Uptake isotherms of Co(II) uptake on GO at three different temperatures, pH = 6.0 ± 0.1, m/V = 0.1 g/L, I = 0.1 mol/L $NaNO_3$.

$$q_e = \frac{bq_{max}C_e}{1+bC_e} \quad \ldots(5)$$

which can be represented in the linear form:

$$\frac{C_e}{q_e} = \frac{1}{bq_{max}} + \frac{C_e}{q_{max}} \quad \ldots(6)$$

where q_{max} (the maximum uptake capacity, mol·g^{-1}) is the amount of sorbate at complete monolayer coverage, and b (L·mol^{-1}) is a constant that relates to the heat of uptake.

The Freundlich expression is an exponential equation with the assumption that as the sorbate concentration increases so too does the concentration of sorbate on the heterogeneous sorbent surface (Sheng et al. 2012). The equation is represented by the following equation:

$$q_e = k_F C_e^n \quad \ldots(7)$$

which can be expressed in linear form,

$$\log q_e = \log k_F + n \log C_e \quad \ldots(8)$$

where k_F (mol^{1-n}·L^n·g^{-1}) represents the uptake capacity when Co(II) equilibrium concentration equals 1, and n represents the degree of dependence of uptake with equilibrium concentration.

The D-R isotherm model is more general than the Langmuir isotherm since it does not have the restriction of surface properties or constant uptake potential (Sheng et al. 2012, Li et al. 2015). It has a general expression as follows:

$$q_e = q_{max} \exp\left(-\beta\varepsilon^2\right) \quad \ldots(9)$$

$$\ln q_e = \ln q_{max} - \beta\varepsilon^2 \quad \ldots(10)$$

where β (mol^2·kJ^{-2}) is the activity coefficient related to mean uptake energy, and ε is the Polanyi potential, which is equal to:

$$\varepsilon = RT \ln\left(1+\frac{1}{C_e}\right) \quad \ldots(11)$$

where R (8.3145 J·mol^{-1}·K^{-1}) is ideal gas constant , and T (K) is the absolute temperature in Kelvin.

E (kJ·mol^{-1}) is defined as the free energy change, which requires to transfer 1 mol of Co(II) from solution to the GO surfaces. Its value can be calculated from the following equation:

$$E = \frac{1}{\sqrt{2\beta}} \quad \ldots(12)$$

The experimental data of Co(II) uptake on GO are regressively simulated with the Linear, Langmuir, Freundlich, and D-R models, and the results are given in Fig. 7. The relative values calculated from the four models are listed in Table 2. As can be seen from Fig. 7 and Table 2, the Langmuir, Freundlich, and D-R isotherm equations simulate the experimental data of the uptake isotherms of Co(II) on GO more significantly than the Linear model, which is supported by the good correlation coefficients in Table 2. There is no apparent distinction between the fitting curves of the three

Table 2: The parameters for Linear, Langmuir, Freundlich, and D–R isotherms of Co(II) uptake on GO at different temperatures.

Linear model	A	B	R^2
T = 293 K	6.5062 × ^{1}0-4	7.6581	0.8583
T = 313 K	7.7276 × 10^{-4}	11.2466	0.8966
T = 333 K	1.4400 × 10^{-4}	11.8902	0.8711
Langmuir model	q_{max} (mol·g^{-1})	b (L·mol^{-1})	R^2
T = 293 K	0.0034	8667.4731	0.9709
T = 313 K	0.0054	6164.5186	0.9501
T = 333 K	0.0052	12256.5000	0.9862
Freundlich model	K_F (mol^{1-n}·L^n·g^{-1})	n	R^2
T = 293 K	0.4806	0.6263	0.9629
T = 313 K	1.0403	0.6808	0.9630
T = 333 K	0.2914	0.5067	0.9558
D-R model	q_{max} (mol·g^{-1})	β (mol^2·kJ^{-2})	E (kJ·mol^{-1})	R^2
T = 293 K	0.0251	5.5520 × ^{10}-3	9.4899	0.9744
T = 313 K	0.0437	5.3642 × 10^{-3}	9.6546	0.9727
T = 333 K	0.0275	3.5286 × 10^{-3}	11.9037	0.9654

models as can be seen from Fig. 7 and the R^2 values of Langmuir, Freundlich, and D-R models (see Table 2). The result indicates that the whole surface of GO has identical uptake activity and therefore the adsorbed Co(II) ions do not interact or compete with each other, and they are adsorbed by forming an almost complete monolayer coverage of the GO particles, thus, the chemosorption is the principal uptake mechanism in uptake process.

The thermodynamic parameters (ΔG^0, ΔS^0 and ΔH^0) for Co(II) uptake on GO can be determined from the temperature dependence. Free energy change (ΔG^0) is calculated from the relationship (Sheng et al. 2012, Li et al. 2015):

$$\Delta G^0 = -RT \ln K^0 \quad \ldots(13)$$

where K^0 is the uptake equilibrium constant. Values of $\ln K^0$ are obtained by plotting $\ln K_d$ versus C_e for uptake of Co(II)

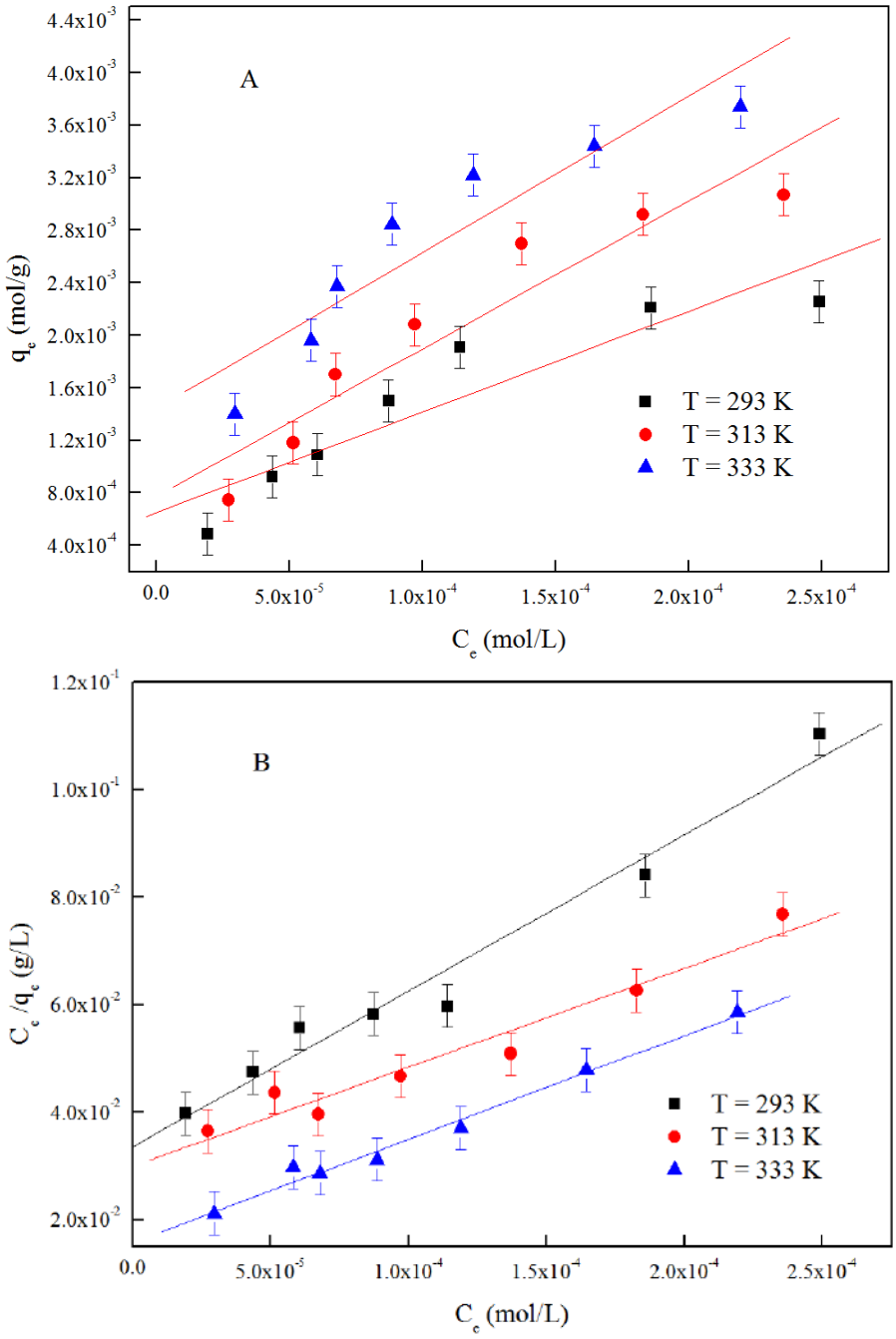

Fig. Cont....

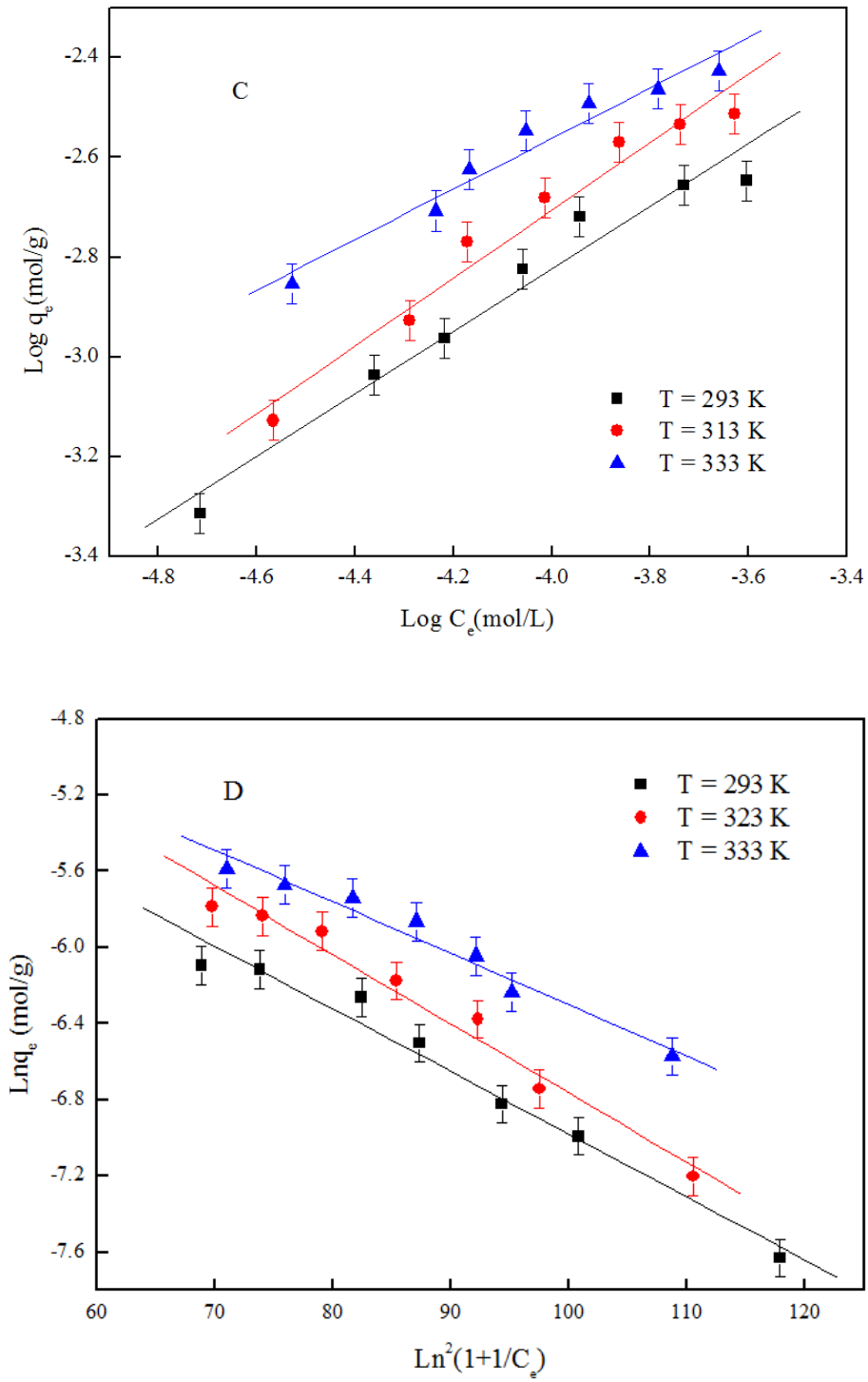

Fig. 7: Fitting results of (A) Linear, (B) Langmuir, (C) Freundlich and (D) D-R adsorption isotherms of Co(II) uptake on GO at three different temperatures, pH = 6.0 ± 0.1, m/V = 0.1 g/L, I = 0.1 mol/L $NaNO_3$.

on GO (Fig. 8A) and extrapolating C_e to zero are 10.14 (T = 293 K), 10.31 (T = 313 K) and 10.82 (T = 333 K), respectively. Standard entropy change (ΔS^0) evaluated from the slope which linear plot of ΔG^0 versus T is achieved according to the equation (Fig. 8B):

$$\left(\frac{\partial \Delta G^0}{\partial T}\right)_p = -\Delta S^0 \quad \ldots(14)$$

The average standard enthalpy change (ΔH^0) is then calculated from the expression:

$$\Delta H^0 = \Delta G^0 + T\Delta S^0 \quad \ldots(15)$$

The values obtained from Eqs. (14) to (15) are tabulated in Table 3. A positive value of the ΔH^0 suggest that the uptake of Co(II) on GO is endothermic. One possible explanation for this positive ΔH^0 is that Co(II) is solved well in water, and the hydration sheath of Co(II) has to be destroyed before its uptake on GO. This dehydration process needs energy, and it is favored at high temperatures. The Gibbs free energy change (ΔG^0) is negative as expected for a spontaneous process under the conditions applied. The value of ΔG^0 becomes more negative with the increase of temperature, which indicates that the reaction is more favorable at higher temperatures. At high temperatures, cations are readily desolvated and hence its sorption becomes more favorable. The positive value of entropy change (ΔS^0) implies some structural changes in Co(II) and GO during the uptake process, which leads to an increase in the disorderliness of the GO-solution interfacial system during the uptake of Co(II) on GO. The thermodynamic analysis derived from temperature-dependent uptake isotherms suggests that the uptake process of Co(II) on GO is spontaneous and endothermic.

Regeneration and Reuse

For the environmental sustainability of GO, it is essential to describe regeneration aspects of the process to improve its cost-effectiveness by recycling the GO for reuse in multiple cycles. Fig. 9 displays that the uptake of Co(II) on the GO with three different concentrations (i.e., 0.05, 0.1, and 0.2 g/L) after 6 times of uptake and desorption process at pH = 6.0 and T = 293 K. As shown in Fig. 9, after six cycles, the uptake efficiency decreased from 53% to 49% (GO = 0.05 $g{\cdot}L^{-1}$), 69% to 64% (GO = 0.1 $g{\cdot}L^{-1}$), 74% to 69% (GO = 0.2 $g{\cdot}L^{-1}$), respectively. The results suggested that the GO after 6 times usage could be efficiently regenerated and reused

Table 3: Values of thermodynamic parameters for Co(II) uptake on GO.

T(K)	ΔG^0 (kJ·mol^{-1})	ΔS^0 (J·mol^{-1}·K^{-1})	ΔH^0 (kJ·mol^{-1})
293	-24.7096	130.9828	13.6683
313	-26.8193		14.1783
333	-29.9489		13.6684

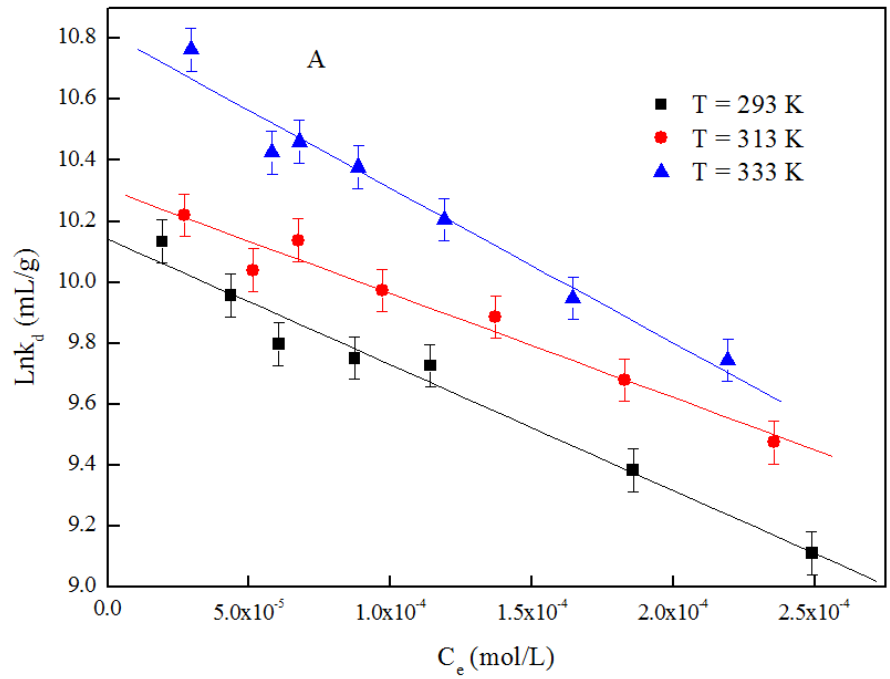

Fig. Cont....

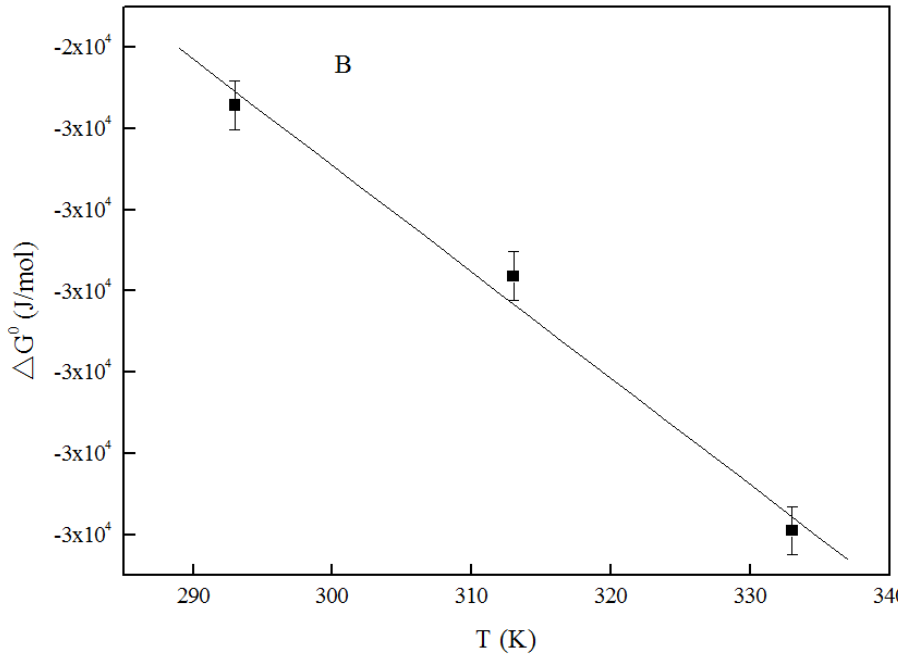

Fig. 8: The linear plot of (A) LnK_d versus C_e at three different temperatures and (B) ΔG^0 versus T for Co(II) uptake on GO, pH = 6.0 ± 0.1, m/V = 0.1 g/L.

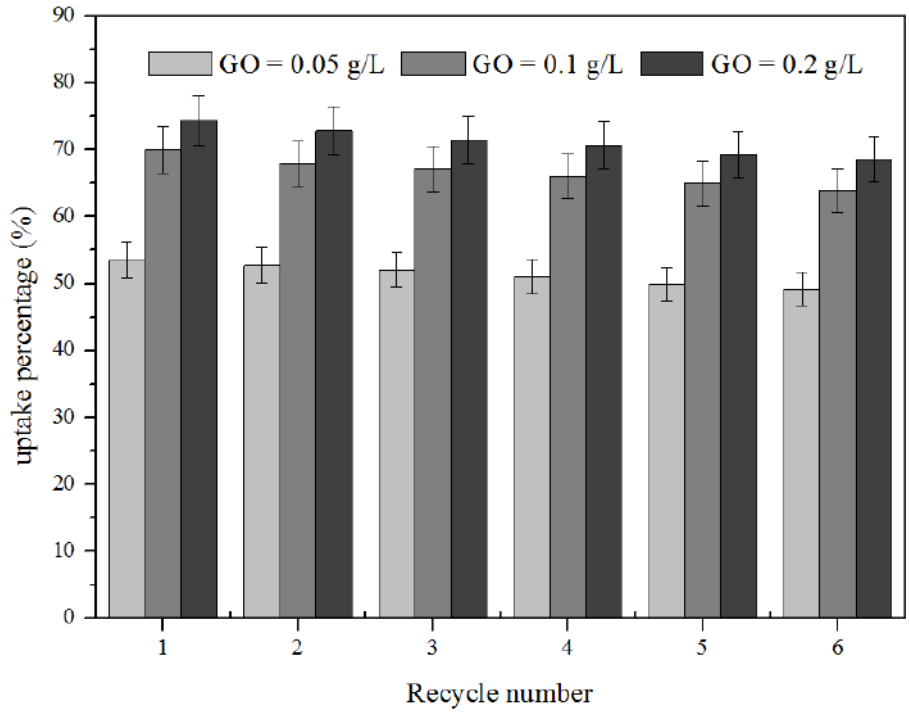

Fig. 9: Recycling for Co(II) uptake on GO of three different concentrations, T = 293 K, pH = 6.0 ± 0.1, $C_{Co(II)initial}$ = 10 mg/L, I = 0.1 mol/L $NaNO_3$.

with a slight decrease in uptake efficiency, which may enhance the economy of the adsorption process. The excellent repeatability of GO indicated that GO is promising for the natural attenuation of Co(II) and related metal ions from an aqueous solution.

CONCLUSIONS

In this study, the batch technique was adopted to investigate the uptake of Co(II) on GO as a function of various water chemistries such as contact time, pH, ionic strength, and temperature under ambient conditions. From the results of Co(II) uptake on GO under our experimental conditions, the following conclusions can be obtained:

(1) Kinetic studies suggest that Co(II) uptake on GO could be described more favorably by the pseudo-second-order kinetic model.

(2) The uptake of Co(II) on GO is strongly dependent on pH values. The uptake increases with pH increasing at pH < 8.0, and then the uptake maintains a high level at pH > 8.0.

(3) The uptake of Co(II) on GO is independent of ionic strength in the wide pH range and thus inner-sphere surface complexation is the main mechanism responsible for the uptake of Co(II) on GO.

(4) The uptake of Co(II) is influenced by HA/FA significantly, and the effect of HA/FA on Co(II) uptake is dependent on pH values. The presence of HA/FA enhances the uptake of Ni(II) on GO at low pH, while reduces Co(II) uptake on GO at high pH.

(5) The Langmuir, Freundlich, and D-R isotherm equations simulate the experimental data of the uptake isotherms of Co(II) on GO more significantly than the Linear model, and there is no apparent distinction among the fitting curves of the three models of Langmuir, Freundlich, and D-R models.

(6) The thermodynamic analysis from the temperature-dependent uptake isotherms suggests that the uptake of Co(II) on GO is spontaneous and endothermic.

ACKNOWLEDGEMENTS

This work was supported by the Science Foundation of the Ministry of Education of China (201802227004).

REFERENCES

Almasian, A., Giyahi, M. H., Dehdast, S.A. and Maleknia, L. 2018 Removal of heavy metal ions by modified pan/pani-nylon core-shell nanofibers membrane: filtration performance, antifouling, and regeneration behavior. Chem. Eng. J., 351(1): 1166-1178.

Arancibia-Miranda, N., Baltazar, S.E., García, A., Munoz-Lira, D., Sepúlveda, P., Rubio, M.A. and Altbir, D. 2016. Nanoscale zero valent iron supported by zeolite and montmorillonite: Template effect of the removal of lead ion from an aqueous solution. J. Hazard. Mater., 301: 371-380.

Bhatnagar, A., Minocha, A.K. and Sillanpää, M. 2010. Adsorptive removal of cobalt from aqueous solution by utilizing lemon peel as biosorbent. Biochem. Eng. J., 48(2): 181-186.

Bradder, P., Ling, S., Wang, S. and Liu, S. 2011. Dye adsorption on layered graphite oxide. J. Chem. Eng. Data., 56(1): 138-141.

Chen, L., Huang, Y., Huang, L., Liu, B., Wang, G. and Yu. S. 2011. Characterization of Co(II) removal from aqueous solution using bentonite/iron oxide magnetic composites. J. Radioanal. Nucl. Chem., 290(3): 675-684.

Chen, Q., Yao, Y., Li, X., Lu, J., Zhou, J. and Huang, Z. 2018. Comparison of heavy metal removals from aqueous solutions by chemical precipitation and characteristics of precipitates. J. Water Process Eng., 26: 289-300.

Cheng, W., Ding, C., Sun, Y. and Wang, X. 2015. Fabrication of fungus/attapulgite composites and their removal of U(VI) from aqueous solution. Chem. Eng. J., 269: 1-8.

Deng, J., Zhang, X., Zeng, G., Gong, J., Niu, Q. and Liang, J. 2013. Simultaneous removal of Cd(II) and ionic dyes from aqueous solution using magnetic graphene oxide nanocomposite as an adsorbent. Chem. Eng. J., 226(8): 189-200.

Ding, C., Cheng, W., Sun, Y. and Wang, X. 2015. Effect of Bacillus subtilis on the reduction of U(VI) by nano-Fe. Geochim. Cosmochim. Acta., 165: 86-107.

Gao, W., Majumder, M., Alemany, L., Narayanan, T., Ibarra, M., Pradhan, B. and Ajayan, P. 2011. Engineered graphite oxide materials for application in water purification. ACS. Appl. Mater. Interfaces, 3(6): 1821-1826.

Hayes, K. and Leckie, J. 1987. Modeling ionic strength effects on cation adsorption at hydrous oxide/solution interfaces. J. Colloid. Interf. Sci. ,115(2): 564-572.

Hu, B., Cheng, W., Zhang, H. and Sheng, G. 2010. Sorption of radionickel to goethite: effect of water quality parameters and temperature. J. Radioanal. Nucl. Ch. 285(2): 389-398.

Huang, J., Liu, Y. and Wang, X. 2008. Selective sorption of tannin from flavonoids by organically modified attapulgite clay. J. Hazard. Mater., 160(2-3): 382-387.

Jin, Z., Sheng, J. and Sun, Y. 2014. Characterization of radioactive cobalt on graphene oxide by macroscopic and spectroscopic techniques. J. Radioanal. Nucl. Chem., 299(3): 1979-1986.

Jin, Z., Wang, X., Sun, Y., Ai, Y. and Wang, X. 2015. Adsorption of 4-n-nonylphenol and bisphenol-A on magnetic reduced graphene oxides: A combined experimental and theoretical studies. Environ. Sci. Technol., 49(15): 9168-9175.

Komatsu, Y. 2010. Research for ion-exchange separation of metal ions. J. Ion. Exch., 10(1): 8-14.

Li, J., Chen, S., Sheng, G., Hu, J., Tan, X. and Wang, X. 2011. Effect of surfactants on Pb(II) adsorption from aqueous solutions using oxidized multiwall carbon nanotubes. Chem. Eng. J., 166(2): 551-558.

Li, X., Fang, Y. and Tang, X. 2014. Using graphene oxide as a superior adsorbent for the highly efficient immobilization of Cu(II) from aqueous solution. J. Mol. Liq., 199: 237-243.

Li, X., Yu, M., Lv, Q. and Tan, Y. 2015. Sequestration of Ni(II) onto graphene oxide from synthetic wastewater as affected by coexisting constituents. Desalin. Water. Treat. DOI:10.1080/19443994.2015.1110841.

Luo, J., Zhao, D., Wang, L., Asiri, A.M. and Alamry, K.A., 2019. Simultaneous Removal of Cu (II) and 1-Naphthol in Wastewater by Magnetic Nanoparticle-Graphene Oxide Composites. Nat. Environ. Pollut. Technol., 18(3): 777-787

Ma, M., Gao, H., Sun, Y. and Huang, M. 2015. The adsorption and desorption of Ni(II) on Al substituted goethite. J. Mol. Liq., 201: 30-35.

Mobasherpour, I., Salahi, E. and Ebrahimi, M. 2014. Thermodynamics and kinetics of adsorption of Cu(II) from aqueous solutions onto multi-walled carbon nanotubes. J. Saudi. Chem. Soc., 18(6): 792-801.

Mou, J., Li, C., Wang, G. and Shi, W. 2012. Complexation and sorption studies of Co(II) with γ-alumina-bound fulvic acid: effect of pH, ionic strength, fulvic acid, and alumina concentration. J. Radioanal. Nucl. Chem., 292(3): 1099-1104.

Pei, Z., Li, L., Sun, L., Zhang, S., Shan, X., Yang, S. and Wen, B. 2013. Adsorption characteristics of 1,2,4-trichlorobenzene, 2,4,6-trichlorophenol, 2-naphthol, and naphthalene on graphene and graphene oxide. Carbon, 51(1): 156-163.

Ramesha, G., Vijaya, Kumara. A., Muralidhara, H. and Sampath, S. 2011. Graphene and graphene oxide as effective adsorbents toward anionic and cationic dyes. J. Colloid. Interf. Sci., 361(1): 270-277.

Sheng, G., Dong, H. and Li, Y. 2012. Characterization of diatomite and its application for the retention of radiocobalt: role of environmental parameters. J. Environ. Radioact., 113: 108-115.

Sheng, G., Yang, Q., Peng, F., Li, H., Gao, X. and Huang, Y. 2014a. Determination of colloidal pyrolusite, Eu(III) and humic substance interaction: A combined batch and EXAFS approach. Chem. Eng. J., 245(4): 10-16.

Sheng, G., Ye, L., Li, Y., Dong, H., Li, H., Gao, X. and Huang, Y. 2014b. EXAFS study of the interfacial interaction of nickel(II) on titanate nanotubes: Role of contact time, pH, and humic substances. Chem. Eng. J., 248(1): 71-78.

Sheng, G., Alsaedi, A., Shammakh, W., Monaquel, S., Sheng, J., Wang, X., Li, H. and Huang, Y. 2016. Enhanced sequestration of selenite in water by nanoscale zero-valent iron immobilization on carbon nanotubes by a combined batch, XPS, and XAFS investigation. Carbon, 99: 123-130.

Shibi, I.G. and Anirudhan, T.S. 2005. Adsorption of Co(II) by a carboxylate- functionalized polyacrylamide grafted lignocellulosic. Chemosphere, 58(8): 1117-1126.

Sun, Y., Yang, S., Chen, Y., Ding, C., Cheng, W. and Wang, X. 2015. Adsorption and desorption of U(VI) on functionalized graphene oxides: A combined experimental and theoretical study. Environ. Sci. Technol., 49(7): 4255-4262.

Tan, X., Fan, Q., Wang, X. and Grambow, B. 2009. Eu(III) sorption to TiO_2 (anatase and rutile): batch, XPS, and EXAFS studies. Environ. Sci. Technol., 43(9): 3115-3121.

Wang, J., Chen, Z. and Chen, B. 2014. Adsorption of polycyclic aromatic hydrocarbons by graphene and graphene oxide nanosheets. Environ. Sci. Technol., 48(9): 4817-4825.

Yang, S., Hu, J., Chen, C., Shao, D. and Wang, X. 2011. Mutual effects of Pb(II) and humic acid adsorptions on multiwalled carbon nanotubes/polyacrylamide composites from aqueous solutions. Environ. Sci. Technol., 45(8): 3621-3627.

Zhao, G., Li, J., Ren, X., Chen, C. and Wang, X. 2011. Few-layered graphene oxide nanosheets as superior sorbents for heavy metal ion pollution management. Environ. Sci. Technol., 45(24): 10454-10462.

Zhang, S., Guo, Z., Xu, J., Niu, H., Chen, Z. and Xu, J. 2011. Effect of environmental conditions on the sorption of radiocobalt from aqueous solution to a treated eggshell as biosorbent. J. Radioanal. Nucl. Chem., 288(1): 121-130.

Zhang, X., Wang, Y. and Yang, S. 2014. Simultaneous removal of Co(II) and 1-naphthol by core-shell structured Fe_3O_4@cyclodextrin magnetic nanoparticles. Carbohydrate. Polymers, 114: 521-529.

Nature Environment and Pollution Technology
An International Quarterly Scientific Journal

p-ISSN: 0972-6268
(Print copies up to 2016)
e-ISSN: 2395-3454

Vol. 20 | No.3 | pp. 923-939 | 2021

Original Research Paper

https://doi.org/10.46488/NEPT.2021.v20i03.002

Open Access Journal

Ethnobotanical Study and Plant Diversity in the Forest of Kedarnath Valley, Garhwal Himalaya, India

Chandi Prasad†, Ramesh C. Sharma and Rahul Kumar

Department of Environmental Sciences, H.N.B. Garhwal University (Central University), Srinagar, Garhwal-246174, Uttarakhand, India

†Corresponding author: Chandi Prasad; cpsemwal2@gmail.com

Nat. Env. & Poll. Tech.
Website: www.neptjournal.com

Received: 28-07-2020
Revised: 14-09-2021
Accepted: 15-10-2020

Key Words:
Forest resources
Kedarnath valley
Dominant species
Total basal area

ABSTRACT

The present study was carried out in the forest of Kedarnath valley in Garhwal Himalaya. The aim of the study was to access the diversity status and ecological status. The study was conducted following the stratified sampling techniques by placing quadrates (1m×1m) for herbs, (5m×5m) for shrubs, and (10m×10m) size for trees in the forest area. A total number of 221 plant species were recorded during the floristic survey in the project area. Plant diversity of the project area encompasses 49 species of trees, 28 species of shrubs, and 144 species of herbs. Important value index, the Shannon diversity index, and total basal area species were recorded. The tree density in the present study was highest in the Kedarnath valley which ranged from 0.3 to 8.5 no./ha. Shrub density in the present study varied from 0.4 to 13.5 no./ha, whereas herb density ranged between 0.2 to 22.4 no.ha^{-1}. Total basal cover (TBC) for trees showed a range of 9.542 to 0.075 m^2.ha^{-1}, and the Shannon diversity index ($\overline{H}$) for tree species was recorded from a minimum of 0.976 to a maximum of 3.048. The horrific disaster in the Kedarnath valley in 2013 caused a lot of damage to the bugyals (High altitude grass) and forests of the valley. About 500 species of vesicular medicinal plants, fodder plants, and other important plant species were washed away (Botanical Survey of India 2015). The current study is a pioneer in the aspect and can be helpful in making district forest plans, protocols, and implementation of forest policy to protect the forest by local people.

INTRODUCTION

Forest plays a vital role in the sustenance of the Himalayan ecosystem. The mountain people are directly dependent on forest resources for food, firewood, fodder, and timber. Mountain forests are rich in biodiversity and are distributed according to different elevations and slopes. Forest also plays an important role in providing habitat for wildlife. The Kedarnath valley is an important upper stretch of the Ganga River system in the Uttarakhand Himalaya. Characterized by rugged, rough, and precipitous slopes, the entire valley is very prone to landslides, mass wasting, landslips, and slope failures.

The climate and vegetation of Uttarakhand vary greatly with different altitudes, from a glacier at a high altitude of 7,817 m asl. to a subtropical forest at lower altitudes. The high altitude region is covered by ice and bare rock. The annual rainfall is 1,550 mm and the average annual temperature ranges between -8°C to 25°C. The human population density of the state is 189 persons per km^2, which is lower than the national average of 382 persons per km^2 (Census 2011). According to the 19th Livestock Census (2012), 4.79 million livestock population has been reported in Uttarakhand. The climate is subtropical in the south and temperate in the north. The climate remains cool in the middle zone of the state (Srivastava & Singh 2005). The state represents one of the four high diversity states of the Indian Himalayan region with about 4,248 species of Angiosperms and 18 species in Gymnosperms (Srivastava & Singh 2005).

The Uttarakhand area has been a major site plant exploration since 1796 when Thomas Hardwicke collected plants from the Alaknanda Valley of Garhwal Himalaya. By the beginning of the 21st century, a large number of plant collectors have explored the area and a great deal of information was available about the flowering plants of this area. Based on these collections, floristic reports, and their own collections, Uniyal et al. (2007) compiled a checklist of flowering plants of Uttarakhand as baseline data for writing the flora of Uttarakhand. This valuable document suggests the presence of nearly 4,700 species of flowering plants, including 32 species of Gymnosperms and a few cultivated species. Kimothi et al. (1989) studied some medicinal plants of the Gopeshwar-Tungnath region of Uttar Pradesh. Negi et al. (2008) worked on the inventory of species richness of Panchayat forests and adjoining reserve forests in three dis-

tricts of Garhwal Himalaya, India. Kumar (2009) identified major religious plants of Rudraprayag district (Garhwal), Uttarakhand (India). Semwal et al. (2010) studied medicinal plants used by local Vaidyas in Ukhimath block, Uttarakhand, India. Ballabha et al. (2013) studied community structure and plant diversity of community-based religious conserved forest of Garhwal Himalaya, India. Pala et al. (2016) worked on community structure and plant diversity of community-based religious conserved forest of Garhwal Himalaya, India. Nautiyal et al. (2017) studied the exploration of some important fodder plants of the Joshimath area of the Chamoli district of Garhwal, Uttarakhand. Singh et al. (2017) studied ethnomedicinal plants used by local inhabitants of Jakholi block, Rudraprayag district, western Himalaya, India. Prasad and Sharma (2018) studied wild edible plant resources of Kedarnath valley, Garhwal Himalaya, Uttarakhand.

The state of Uttarakhand is an important part of the Himalayas. Uttarakhand covers an area of 1.63% of the geographical area of India. The forest cover of Uttarakhand is 24, 295 km^2 which is 45.43% of the state's geographical area. In the term of forest canopy density classes, the state has 4,969 km^2 under very dense forest, 12,884 km^2 under moderately dense forest; and 6, 442 km^2 under open forest (FSI 2017). The forest in Uttarakhand is divided into sixteen types (FSI 2017), which are characterized by Northern Tropical Dry Deciduous Forests (Dry Sal-bearing Forest and Dry Plain Forest), Himalayan Sub-tropical Pine Forests (Himalayan Chir-pine and Sub-tropical Scrubs and Euphorbia Scrub), Himalayan Moist Temperate Forests (Lower Western Himalayan Temperate and Upper West Himalayan Temperate Forests), Himalayan Dry Temperate Forest (Dry Temperate Coniferous and West Himalayan Dry Juniper Forest), Sub-alpine Forests (West Himalayan Birch/Fir Forest and Pastures) and Moist and Dry Alpine Scrub Forests.

MATERIALS AND METHODS

Study Area

The Kedarnath valley is located between the coordinates of latitude 300'25°" to 300'45°" N and longitude 780'55°" to 790'20°" E of Ukhimath tehsil in the Rudraprayag district of Garhwal Himalaya, Uttarakhand. The survey was done from a lower altitude of 864 m above m.s.l to the alpine meadow of Kedarnath-Tunganath (3,680-4,000 m above m.s.l). This study was carried out in nine study sites of Kedarnath valley of Ukhimath tehsil (Fig. 1), their locations, geographical coordinates, and elevations have been presented in Table 1. The Kedarnath valley is in the district of Rudraprayag with an area of 1,248 km^2 including 248 villages with a total population of 87,024 including 42,614 males and 44,410 females (Census of India 2011).

Data Collection

Information regarding the plant biodiversity, economically important plants, fruits and fodder plants and medicinal plants were collected. Field visits were made for the collection of plants and also to collect information on the biodiversity of the area. Plants were identified by the villagers, and scientific validation of these plants was made by the Himalayan Herbarium, Department of Botany and High Altitude Plant Physiology Research Center (HAPPRC), H.N.B. Garhwal University (A Central University), Srinagar-Garhwal. Relevant uses of these plants were also collected from different literature.

Plant biodiversity analysis was carried out during the study period when the majority of the plants were at the peak of their growth. In every study site, 10 transects of 10 m × 10 m (100 sq m) size was randomly laid to study tree species and 10 quadrates of 5m × 5m (25sq m) size were randomly laid to study shrub species. The herbaceous species was studied by laying 10 quadrats of 1m × 1m (1sq m) size randomly in each study site.

Quantitative Analysis

The important quantitative analysis such as density, frequency, and abundance of tree species, shrubs and herbs species were determined as per Gates (1949), Curtis and Mc-Intosh (1950), Misra and Puri (1954), Curtis (1951), Phillips (1959), Misra (1969), Mullar-Dombois and Ellenberg (1974).

Density:

$$\text{Density} = \frac{\text{Total number of individuals of a species in all quadrats}}{\text{Total number of quadrats studied}}$$

(b) Frequency (%):

$$\text{Frequency (\%)} = \frac{\text{Number of quadrats in which the species occurred} \times 100}{\text{Total number of quadrats studied}}$$

(c) Abundance:

$$\text{Abundance} = \frac{\text{Total number of individuals of a species in all quadrats}}{\text{Total number of quadrats in which the species occurred}}$$

Basal Area

The basal area is the area of a given section of land that is occupied by the cross-section of tree trunks and stems at the base. The basal area per tree is the cross-sectional area of a tree at breast height. The term is used in forest manage-

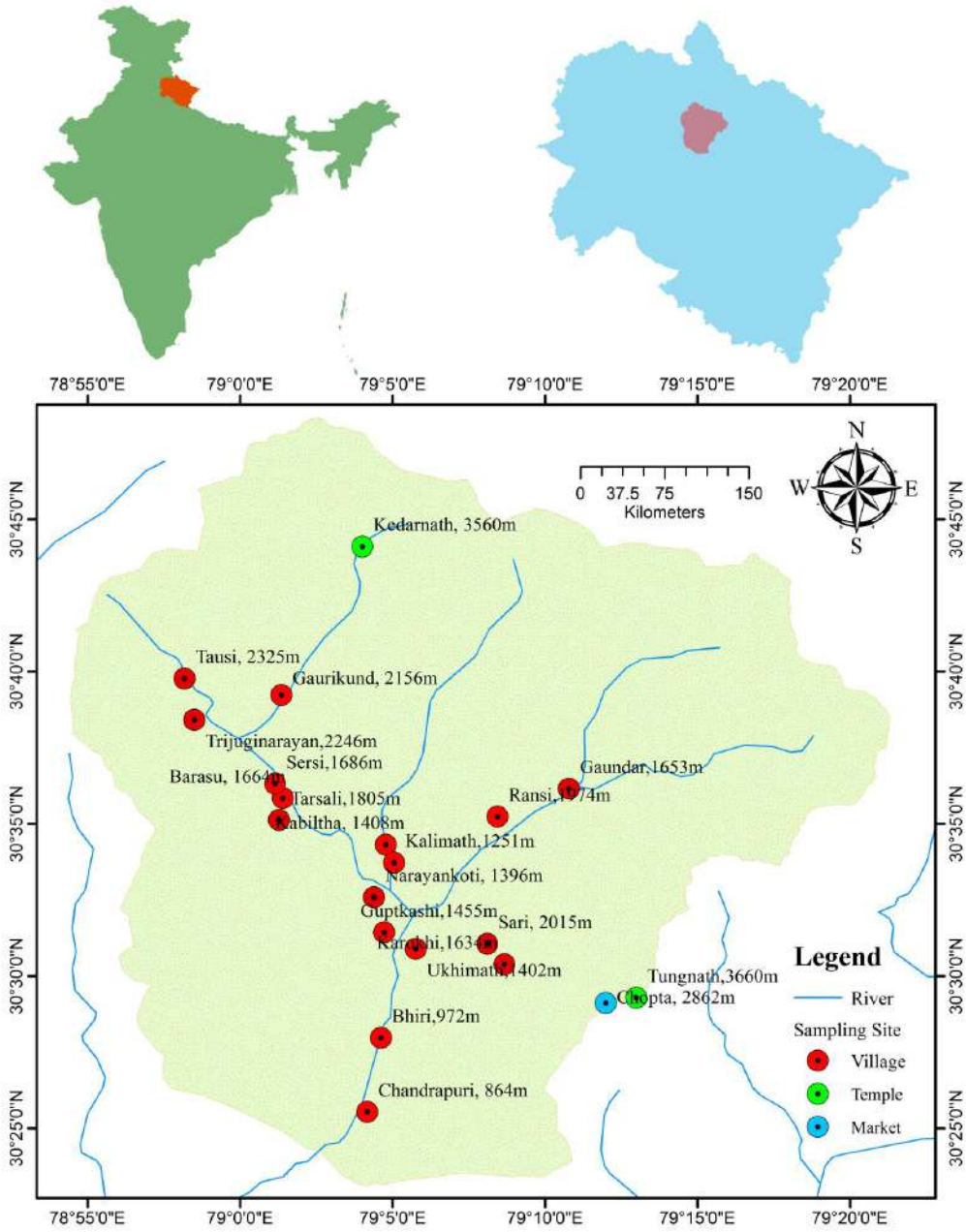

Fig. 1: Location map of the study area: The Kedarnath valley.

ment and forest ecology (Phillips 1959) as:

$$\text{Mean of the circumference (c)} = \frac{\text{Sum of all cbh (circumference)}}{\text{Total number of species}}$$

$$\text{Mean Basal area} = \frac{C^2}{4\pi}$$

$$\text{Total Basal area} = \text{Mean Basal area} \times \text{Density}$$

Where, cbh = Circumference at breast height, C = sum of cbh value of all individuals of a tree species within each plot and $\pi = 3.14$.

Importance Value Index

This index is used to determine the overall importance of

each species in the community structure. In calculating this index, the percentage values of the relative frequency, relative density, and relative dominance are summed up together and this value is designated as the Importance Value Index or IVI of the species (Curtis 1959).

(a) Relative density:

$$\text{Relative Density} = \frac{\text{Number of individual of the species} \times 100}{\text{Number of individual of all the species}}$$

(b) Relative frequency:

$$\text{Relative Frequency} = \frac{\text{Number of occurrence of the species} \times 100}{\text{Number of occurrence of all the species}}$$

(c) Relative dominance:

$$\text{Relative Dominance} = \frac{\text{Total basal area of the species} \times 100}{\text{Total basal area of all the species}}$$

The total basal area was calculated from the sum of the total diameter of immerging stems. In trees, poles, and saplings, the basal area was measured at breast height (1.5m) and by using the formula πr^2; but in the case of herbaceous vegetation it was measured on the ground level by using calipers.

Species diversity indices (Shannon Wiener Index) of general diversity ($\overline{H}$) was computed using the following formula:

$$\text{Shannon Wiener Diversity Index } (\overline{H}) = -\sum_{l-1}^{s}\left(\frac{n_i}{N}\right)\log_2\left(\frac{n_i}{N}\right)$$

Where, $\overline{H}$ = Shannon Wiener index of diversity; n_i = total no. of individuals of a species; and N= total no of individuals of all species.

RESULTS

The Kedarnath valley is very rich in terms of forest resources. Kedarnath valley is a highly elevated alpine meadow (*bugyal*) with a rich diversity of herbs, shrubs, and trees. Pine forest is common in mid-altitude, while in the upper reaches, temperate conifers forest, mainly Oak, *Rhododendron*, Devadar, Kafal are abundant. Many plant species of fodders, medicinal and fruit-bearing plants are common in this Valley. This study on the forest resources was carried out in nine sites of Kedarnath valley (Table 1).

The Kedarnath valley is blessed with the Himalayan Dry Temperate Forests, Dry Temperate Coniferous Forest and West Himalayan Birch/Fir Forests, Sub-Alpine Pasture, Himalayan Chir-Pine Forest, Himalayan Moist Temperate Forest, West Himalayan Sub-Alpine Birch/Fire Forest, and Alpine Forest.

The Forest cover of the study area has been presented in Table 2, and Karokhi has the largest forest cover area wise followed by Sari, Ransi, Ukhimath, Kabiltha, and Tungnath and Barasu have the lowest forest cover (Revenue report of the Village, Tehsil Ukhimath, R-57, 2016-17).

PLANT BIODIVERSITY

The terrestrial ecological survey for various aspects of the Kedarnath valley was conducted for a period of three years (2015 to 2018). The altitude in the villages of Kedarnath valley ranged from 864 m to 4,260 m asl. The major forest type of the valley was a mountain forest. A total number of 221 plant species were collected during the present study in the Kedarnath valley. Plant diversity in the valley encompasses 49 tree species, 28 shrub species, and 144 herb species. An

Table 1: Study sites, their location, geographical coordinates, and elevations of the study area.

Study Site	Location	Latitude	Longitude	Altitude (m above m.s.l.)
S_1	Chandrapuri	30°25'29.72''N	79° 04'17.68''E	864
S_2	Kalimath	30°33'43.66''N	79°05'03.29''E	1,251
S_3	Gaundar	30°36'09.76''N	79° 10'47.29''E	1,653
S_4	Tarsali	30°35'07.94''N	79°01'16.97''E	1,805
S_5	Sari	30°31'03.75''N	79°08'06.71''E	2,015
S_6	Gaurikund	30°39'13.42''N	79°01'26.82''E	2,156
S_7	Trijuginarayan	30°38'25.55''N	78°58'30.01''E	2,246
S_8	Kedarnath	30°44'07.38''N	79°04'00.57''E	3,560
S_9	Tungnath	30°29'17.54''N	79°12'59.84''E	3,660

inventory of plant species, their local names, family, and ethnobotanical uses have been presented in Table 3.

Study Site S_1

The study site S_1 was Chandrapuri village at the left bank of Mandakini River (864 m above m.s.l). This site has some scattered trees with few shrubs and plenty of herbs. The density, frequency, abundance, and Importance Value Index (IVI) of the trees, shrubs, and herbs at S_1 have been presented in Table 4 and Table 5. Ecological analysis revealed the dominant tree species were *Grewia optiva* (IVI: 20.700), *Banhinia variegata* (IVI: 19.286), *Pinus roxburghii* (IVI: 16.921), and *Toona ciliata* (IVI: 16.303) at S_1. The dominant shrub species were *Girardnia diversifolia* (IVI: 30.774), *Adhaoda zeylanica* (IVI: 27.831), *Lantana camara* (IVI: 27.631), and *Urtica dioica* (IVI: 23.440). The dominant herb species were *Galinsoga parviflora* (IVI: 14.549), *Euphurbia chamaesyce* (IVI: 12.127), *Reinwardtia indica* (IVI: 11.902), and *Ganatanthus pumilus* (IVI: 11.798).

Study Site S_2

The study site S_2 was Kalimath (1,251 m asl.) at the right bank of the Kali Ganga and left bank of the Mandakini River. The density, frequency, abundance, and Importance Value Index (IVI) of the trees, shrubs, and herbs have been presented in Table 4 and Table 5. Ecological analysis revealed the dominant tree species were *Quercus liucotrichophora* (IVI: 26.805), *Alnus nepalensis* (IVI: 24.373), *Pyrus pashia* (IVI: 20.456), and *Pinus roxburghii* (IVI: 17.741). However, the dominant shrub species were *Solanum viarum* (IVI: 31.703), *Girardnia diversifolia* (IVI: 28.478), and *Berberis aristata* (IVI: 24.146). The dominant herb species were *Pilea umbrosa* (IVI: 10.690), *Laportea ovalifolia* (IVI: 9.412) and *Eulaliopsis binata* (IVI: 9.311).

Study Site S_3

The study site S_3 (1,653 m asl.) was the Gaundar village at the right bank of the Madmaheswar Ganga. The density, frequency, abundance, and importance value index (IVI) of the trees, shrubs, and herbs have been presented in Table 4 and Table 5. Ecological analysis revealed the dominant tree species were *Quercus liucotrichophora* (IVI: 40.799), *Alnus nepalensis* (IVI: 30.639), and *Myrica esculenta* (IVI: 24.402). However, the dominant shrub species were *Sarcococca saligna* (IVI: 30.712), *Adhatoda vasica* (IVI: 30.402),

Table 2: Forest cover of Ukhiamth Tehsil in 2016-17 (Area in ha).

S.No.	Name of villages	Altitude (m. above m.s.l.)	Geographical area (ha)	Forest Cover (ha)
	Chandrapuri	864	20.157	4.655
	Bhiri	972	63.282	13.419
	Kalimath	1,251	98.389	39.329
	Narayankoti	1,396	29.408	9.876
	Ukhimath	1,402	214.977	85.989
	Kabiltha	1,408	49.105	22.404
	Guptakashi	1,455	195.875	80.207
	Karokhi	1,634	386.831	304.698
	Gaundar	1,653	60.215	7.966
	Sersi	1,686	85.96	16.86
	Barasu	1,664	129.003	0.09
	Tarsali	1,805	25.71	6.04
	Ransi	1,974	253.634	118.833
	Sari	2,015	286	254.702
	Gaurikund	2,156	55.119	25.8
	Trijuginarayan	2,246	419.426	29.66
	Tausi	2,325	50.044	2.64
	Chopta	2,862	3.62	2.845
	Kedarnath	3,568	14.36	-
	Tungnath	3,660	1.636	1.045

Sources: Revenue Report of villages, Tehsil Ukhimath, R-57, 2016-17

and *Girardnia diversifolia* (IVI: 28.320). The dominant herb species were *Bidens pilosa* (IVI: 14.015), *Agrimonia pilusa* (IVI: 12.262), and *Euphurbia chamaesyce* (IVI: 11.681).

Study Site S_4

The study site S_4 (1,805 m a.s.l) was the Tarsali village, located at the right bank of the Mandakini River. The density, frequency, abundance, and Importance Value Index (IVI) of the trees, shrubs, and herbs have been presented in Table 4 and Table 5. Ecological analysis revealed the dominant tree species were *Quercus liucotrichophora* (IVI: 43.294), *Rhododendron arboreum* (IVI: 28.921), and *Neolitsea sericea* (IVI: 19.164). However, the dominant shrub species were *Sarcococca saligna* (IVI: 51.337), *Girardnia diversifolia*

Table 3: Inventory of plant species, their local names, and ethnobotanical uses in the study area of Kedarnath valley

S.No.	Name of Species	Local Name	Family	Ethnobotanical Uses
Trees				
1.	*Abies spectabilis* (D.Don) Spach		Pinaceae	Timber, Fuel
2.	Aesculus indica (Wall.ex Camb.) Hook	Pangar	Sapindaceae	Medicinal, Wild edible, Fuel
3.	*Alnus nepalensis* D.Don	Utis	Betulaceae	Timber, Fuel
4.	*Banhinia variegata* L.	Kachnar	Caesalpinaceae	Medicinal, Wild edible, Fuel
5.	*Betula alnoides* Buch. -Ham.ex D.Don	Saur, sore	Betulaceae	Timber, Fuel, Fodder
6.	*Cedrus deodara* (Roxb.) G.Don	Deodara	Pinaceae	Timber, Fuel
7.	*Celtis australis* L.	Khadik	Cannabaceae	Fodder, Fuel
8.	*Cinnamomum Spp.* Schaeff.		Lauraceae	Fodder, edible, Fuel
9.	*Cotoneaster affinis* Lindl.	Ruins	Rosaceae	Fuel, Agriculture tool
10.	*Debregeasia longifolia* (Burm.F.) Wedd.	Syanru	Urticaceae	Fodder, edible, Fuel
11.	*Emblica officinalis* Gaertn.	Aonla	Euphorbiaceae	Medicinal, edible, Fuel
12.	*Ficus auriculata* Lour.	Timla	Moraceae	Fodder, fruit edible
13.	*Ficus palmata* Forsk.	Bedu	Moraceae	Fodder, fruit edible, medicinal
14.	*Ficus religiosa* L.	Peepal	Moraceae	Medicinal, Fuel
15.	*Ficus semicordata* Bunch.-ham.ex J. E.Smith	Khannu	Moraceae	Medicinal, Wild edible, Fuel
16.	*Fraxinus americana* L.	Anga	Oleaceae	Fuel, Timber
17.	*Grewia optiva* Drummond ex Burrt	Bhimal	Tiliaceae	Fuel, Fodder
18.	*Hippophae salicifolia* D.Don		Elaeagnaceae	Medicinal, Wild edible, Fuel
19.	Holmskiodia sanguinea	Khagsoo	Verbinaceae	Fuel, Fodder
20.	*Juglans regia* L.	*Akhrot*	Juglandaceae	Medicinal, Wild edible, Fish poison, Fuel
21.	*Lyonia ovalifolia* (Wall.) Prude	Anyar	Ericaceae	Fuel, Fish Poison, Medicinal, Fodder
22.	*Mangifera indica* L.	Aam	Anacardiaceae	Fruit edible, woodwork
23.	*Morus alba* L.	Sahtoot	Moraceae	Fruit edible woodwork, sericulture
24.	*Myrica esculenta* Buch. -Ham.ex D.Don	Kafal	Myricaceae	Medicinal, Wild edible, Fish poison, Fuel
25.	*Neolitesa serobiculata* (Meisn.) Gamble	Gadmweda	Lauraceae	Fuel
26.	*Neolitsea sericea* (Blume) Koidz.	(Mweda, chirad)	Lauraceae	Fuel
27.	*Neolitsea Spp.* (Bent. & Hook.F.) Merr.	Lampatiya	Lauraceae	Fuel, Timber
28.	*Phoenix humilis* Royle.	Khajoor	Arecaceae	Medicinal, Wild edible, Fuel
29.	*Pinus roxburghii* Sarjent	Kulain	Pinaceae	Wood for construction, resin, medicinal, timber
30.	*Prunus cerasoides* D.Don	Panya	Rosaceae	Medicinal, Wild edible, Fuel, Timber
31.	*Prunus cornuta* (Wall. ex Royle)	Himalayan bird cherry, padus	Rosaceae	Medicinal, Wild edible, Fuel, Timber

Table cont....

S.No.	Name of Species	Local Name	Family	Ethnobotanical Uses
32.	*Pyrus pashia* Buch. -Ham.ex D.Don	Mol	Rosaceae	Fodder, Fuel, Medicinal, Wild edible
33.	*Quercus floribunda* Lindley.ex Rehder	Moru	Fabuceae	Fodder, Fuel
34.	*Quercus liucotrichophora* A.Camus	Banj	Fagaceae	Fodder, Fuel
35.	*Quercus semecarpifolia* Sm.	Karsu	Fagaceae	Fodder, Fuel
36.	*Quercus Spp.* L.	Harinj, Green oke	Fagaceae	Fodder, Fuel
37.	*Rhododendron arboreum* Sm.	Burans	Ericaceae	Medicinal, Wild edible, Fuel, Timber
38.	*Rhododendron barbatum* W*allich ex G. Don*		Ericaceae	Medicinal, Wild edible, Fuel, Timber
39.	*Rhus sandwicensis* A.Gray	Titret	Anacardiaceae	Fuel, Fodder
40.	*Rosa sericea* Lindl.		Rosaceae	Medicinal, Fuel
41.	*Sapindus mukorossi* Gaertner	Reetha	Sapindaceae	Medicinal, Fuel, Timber
42.	*Symplocos panniculata (*Thunb.) Miq	Lodha	Symplocaceae	Fodder. Fuel
43.	*Syzygium cumiini* (L.) Skeels	Jamun	Myrataceae	Medicinal, Wild edible, Fuel, Timber
44.	*Taxcus baccata* L.	Thuner	Taxaceae	Medicinal, Timber, fuel
45.	*Taxus wallichiana* Zucc.		Taxaceae	Medicinal, Timber, fuel
46.	*Toona ciliata* Roem.	Toon	Meliaceae	Timber and wood work, social forestry
47.	*Ulmus wallichiana* Planch.	Pamani,mairu	Urticaceae	Fodder, Fuel
48.	*Viburmum mullaha* Buch. -Ham.ex D.Don	Malyo	Caprifoliaceae	Fodder, Fuel, Medicinal, Wild edible
49.	Zanthoxylum armatum DC	Timaru	Rutaceae	Fodder, Fuel, Medicinal
Shrubs				
1.	*Ageratina adenophora* (Spreng.) King & H.Rob.	Basinga	Acanthaceae	Medicinal
2.	Arismia tortosum			Medicinal
3.	*Berberis aristata* Roxb.ex.DC.	Kirmor	Berberidaceae	Wild edible, Medicinal, Fuel
4.	*Berberis jaeschkeana* DC.		Berberidaceae	Wild edible, Medicinal, Fuel
5.	*Boehmeria platyphylla* D.Don	Khagsa	Urticaceae	Fodder, Fuel
6.	*Caesalipinia decapetala* (Roth) Alston	Kingari,kunju	Caesalpiniaceae	Fodder, Medicinal, Fuel
7.	*Cannabis sativa* Linn.	Bhang	Cannabinaceae	Bark fibers for ropes, sacs, and rough clothes, seeds as condiment, intoxicating
8.	*Cotoneaster microphyllus* Wall. ex Lindl.		Malaceae	Wild edible, Medicinal, Fuel
9.	*Desmodium concimum* DC.	Sakina	Fabaceae	Fodder, Fuel
10.	*Desmodium elegans* DC.	Chamlai	Fabaceae, Papilion-aceae	Fodder, Fuel
11.	Echinops cornigenus	Kandara	Asterceae	Medicinal, Edible
12.	*Elueagnus parvifolia* Wall.ex Royal	Giwain	Elueagnaceae	Wild edible, Medicinal, Fuel
13.	*Girardnia diversifolia* (Link) Friis	Jhir kandali	Urticaceae	Fodder, Medicinal
14.	*Lantana camara* L.	Gajar ghass	Verbenaceae	Fuel, furniture, Medicinal, Weed
15.	*Lonicera x bella* Zabel	Ghugti	Carprifoliaceae	Fuel
16.	*Prisepia utilis* Royle	Bhenkul	Rosaceae	Medicinal, Fuel
17.	*Pyracantha crenulata* (D.Don) M.Roem.	Ghingaru	Rosaceae	Soil binder, fruit edible, Medicinal, Fuel
18.	*Rhododendron barbatum* W*allich ex G. Don*		Ericaceae	Medicinal, Wild edible, Fuel, Timber
19.	*Rhododendron campanulatum* D.Don	Burans	Ericaceae	Medicinal, Wild edible, Fuel, Timber
20.	*Rosa spp.* L.		Rosaceae	Medicinal, Fuel

Table cont....

S.No.	Name of Species	Local Name	Family	Ethnobotanical Uses
21.	*Rubus ellipticus* Sm.	Hinsalu	Rosaceae	Fruit edible
22.	*Rubus niveus* Thunb.	Kali hisar	Rosaceae	Fruit edible
23.	*Sarcococca saligna* (D.Don)	Geru, paliyala	Buxaceae	Medicinal, Fuel
24.	*Sinarumdinaria anceps* (Mittf.) Chao & Renvoize.Sqn.	Ringal	Poaceae	Fuel
25.	*Smilax aspera* L.	Kukardara	Smilacaceae	Medicinal
26.	*Solanum viarum* Dunal		Solanaceae	Medicinal
27.	*Urtica dioica* L.	Kandali	Urticaceae	Edible, Medicinal
28.	*Viburnum spp.* L.		Adoxaceae	Medicinal
Herbs				
1.	*Abies pindrow* (Royle ex D.Don) Royle		Pinaceae	Medicinal, Edible
2.	Abrus precatorius L.	Ratti	Fabaceae	Medicinal
3.	*Acomastylis elata* (Wall.ex G.Don) F.Bolle		Rosaceae	Medicinal
4.	Agrimonia pilusa Ledebour	Lisukuri	Rosaceae	Fodder
5.	*Ampelocissus latifolia* Planch.		Araliaceae	Fodder, Medicinal
6.	*Anaphalis beddomei* Hook.F.		Asteraceae	Medicinal
7.	*Anaphalis contorta* (D.Don) Hook.f.		Asteraceae	Medicinal
8.	*Anaphalis royleana* DC		Asteraceae	Medicinal
9.	*Anaphalis spp.* DC.		Asteraceae	Medicinal
10.	*Anaphalis spp.*DC.		Asteraceae	Medicinal
11.	*Androsace lanuginosa* Wall.		Primulaceae	Medicinal
12.	*Anemone obtusiloba* D.Don, Prode. Fl.		Ranunculaceae	Medicinal
13.	*Anemone patens* L.		Rosaceae	Medicinal
14.	*Anemone spp* L.		Ranunculaceae	Medicinal
15.	*Anemone vitifolia* Buch.-Ham. ex DC.		Ranuculaceae	Medicinal
16.	*Animone obtusiloba* D.Don		Renunculaceae	Medicinal
17.	*Arisaema flavam* (Foessk.) Schott		Araceae	Medicinal
18.	*Arisaema intermedium* BL.	Akash laguli	Convolvulaceae	Medicinal
19.	*Arisaemia tortosum* (Wall.) Schott		Araceae	Medicinal
20.	Arisuema totuosum (Wall.) Schot	Bell type	Vitaceae	Medicinal
21.	*Aster spp*. L.		Asteraceae	Medicinal
22.	*Bauhinia vahlii* Wight & Arn.	Bagmungari	Araceae	Medicinal
23.	*Bergenia ciliata* (Haworth) Stern.	Silpara	Saxifragaceae	Medicinal
24.	*Bidens pilosa* L.	Kumar	Astoraceae	Medicinal, Fodder
25.	*Bistorta macrophylla* (D.Don) Sojak		Polygonaceae	Medicinal
26.	*Bistorta vaccinifolia* Wall. ex Meisn.)		Polygonaceae	Medicinal
27.	*Boehmeria grandis(*Hook. & Arn.) A. Heller	Foortya	Urticaceae	Fodder
28.	*Boehmeria nivea* (L.) Gaudich.		Urticaceae	Medicinal
29.	Boenninghausenia albiflora	Upniya ghass	Rutaceae	Fodder, Medicinal
30.	*Bupleurum fruticosum* L.		Apiaceae	Fodder
31.	*Carax hirta* L.		Cyperaceae	Fodder
32.	*Carex spp.* L.		Cyperaceae	Fodder

Table cont....

S.No.	Name of Species	Local Name	Family	Ethnobotanical Uses
33.	*Centella asiatica* L.	Brahmi	Apiaceae	Medicinal
34.	*Chenopodium album* L.	Bathua	Chenopodiaceae	Edible, Fodder, Medicinal
35.	*Citrullus colocynthis* (L.) Schrader		Rutaceae	Medicinal
36.	*Clematis montana* Buch.-Ham. ex DC.		Ranunculaceae	Medicinal
37.	*Corydalis cornuta* Royal		Papaveraceae	Medicinal
38.	*Crepidium acminatum* (D.Don) Szlach.	Jeevak	Orchidaceae	Medicinal
39.	*Cuscuta reflexa* Roxb.	Dudhi	Euphorbiaceae	Medicinal
40.	*Cyananthus lobatus* Wall. ex Benth		Campanulaceae	Medicinal
41.	*Cyathula tomentosa* (Roth) Moq.	Lichkura	Amarnathaceae	Fodder, Medicinal
42.	*Cymbopogon citratus* (DC.) Stapf	Lemongrass	Poaceae	Fodder, Medicinal
43.	*Cynodon dactylon* (L.) Pers.	Doob	Poaceae	Medicinal, Fodder
44.	*Cynoglossum zeylanicum* L.		Boraginaceae	Medicinal
45.	*Cyperus odoratus* L.	Ghass	Cyperaceae, Poaceae	Fodder
46.	*Danthonia cachmiriana* L.		Poaceae	Fodder
47.	*Danthonia spp.* DC.		Poaceae	Fodder
48.	*Daphne papyracea* Wall.	Kandara	Asteraceae	Fodder
49.	*Digitaria ciliaris (Retz.)* Koeler	Menaru	Poaceae	Fodder
50.	*Dioscorea belophylla* (Prain) Haines Syn.	Tedu	Deoscoreaceae	Edible, Medicinal
51.	*Dioscorea Spp.* L.		Dioscoreaceae	Edible
52.	*Diplazium caudatum* (Cav.) Jermy	Farn	Athyriacae	Medicinal
53.	*Diplazium esculentum* (Retz.) SW.	Lingra	Dryopteridaceae, Athyriaceae	Edible, Medicinal
54.	*Diplazium melanochlamys* (Hook.) T.Moore	Una, fern	Athyriacae	Fodder, Medicinal
55.	*Diplazium splendens* Ching	Meen	Araceae	Medicinal
56.	Diplazium spp.	Bis lingara	Dryopteridaceae, Athyriaceae	Medicinal
57.	*Dryopteris filixmas* (L.) Schott	Fern	Dryopteridaceae	Medicinal, Fodder
58.	*Dryopteris filix* -mas		Dryopteridaceae	Medicinal
59.	*Dubyaea hispida* (D.Don) DC.		Asteraceae	Medicinal
60.	*Duchesnea indica* (Andrcos) Th.Wolf	Bhina kafal	Rosaceae	Edible, Medicinal
61.	*Echinops cornigenus* Roxb.	Meda	Asparagaceae	Medicinal
62.	*Epilobium hirsutum* L.		Onagraceae	Medicinal
63.	*Eulaliopsis binata* (Retz.) C.E. Hubb.	Ban pindalu	Araceae	Medicinal. Edible
64.	*Euphorbia spp.*L.		Euphorbiaceae	Medicinal
65.	*Euphurbia chamaesyce* L.	Ban-haldi	Zingiberaceae	Fodder, Medicinal
66.	*Evolvulus alsinoides* (L.) L.	Sankpushpi	Convolvulaceae	Medicinal
67.	*Fagopyrum esculentum* (L.) Moench.	Konlya, ougal	Polygonaceae	Fodder, Medicinal, Edible
68.	*Festuca spp.* L.	Grass	Poaceae	Fodder
69.	*Fragaria rubicola* L.		Rosaceae	Medicinal
70.	*Fumaria indica* (haussk.) Pugsl.	Pit-papra	Liliaceae	Medicinal
71.	*Galinsoga parviflora* Cav.	Khor type	Poaceae	Fodder
72.	*Ganatanthus pumilus* (D.Don) Engl. & Krause	Badelu grass	Asteraceae	Fodder, Medicinal

Table cont....

S.No.	Name of Species	Local Name	Family	Ethnobotanical Uses
73.	*Gaultheria trichophylla* Royle		Ericaceae	Medicinal
74.	*Geum elatum* Wall. Ex G.Don		Rosaceae	Medicinal
75.	*Gleichenia spp.* Sm.		Gleicheniaceae	Medicinal
76.	*Hedra nepalensis* K.Koch	Ivi	Polygonaceae	Medicinal
77.	*Hedychium spicatum* Buch.-Ham.	Phiyunli	Liliaceae	Medicinal
78.	*Heracleum maximum* Bartr.		Asteraceae	Medicinal
79.	*Impatiens scabrida* DC.		Balsaminaceae	Medicinal
80.	*Impatiens sulcata* Wall.	Majuro	Balsaminaceae	Medicinal
81.	*Ischaemum rugosum* Salisb.		Poaceae	Medicinal, Fodder
82.	*Juniperus squamata* Buch.-Ham. ex D.Don		Cupressaceae	Medicinal
83.	*Laportea ovalifolia* Schum. (Thonn.) Chew	Malcharu	Nasselxaxter	Fodder
84.	*Lathyrus spp.* L.	Kurfalya	fabaceae	Edible, Fodder, Medicinal
85.	*Lonicera obovata* Royle		Carprifolvaxter	Medicinal
86.	*Oplismenus hirtellus* (L.) P.Beauv.	Menaru, basket grass	Poaceae	Fodder
87.	*Oxalis corniculata* L.	Bhilmori	Oxalidaceae	Edible, Fodder, Medicinal
88.	*Oxora coccinea* L.		Rubiaceae	Medicinal
89.	*Oxyria digyna* (L) Hill		Polygonaceae	Medicinal
90.	*Paeonia emodi* Royal	Dhanduru	Paeoniaceae	Edible, Medicinal
91.	*Parthenocissus semicordata* (Wall) Planch.		Vitaceae	Medicinal
92.	*Persicaria amplexicaulis* (D. Don) Ronse Decraene		Polygonaceae	Medicinal
93.	*Pilea umbrosa* Wall.ex Bl.	Chaolu	Urticaceae	Fodder
94.	*Plantago brachyphylla* Edgew. ex Decne		Plantaginaceae	Medicinal
95.	*Plantago deprassa* Willd.	Luhurya, symlya	Planttaginaceae	Medicinal
96.	*Plantago spp.* L.		Plantaginaceae	Medicinal
97.	*Podophyllum hexandrum* Royle	Ban kakdi	Podophyllaceae	Edible, Medicinal, Fodder
98.	*Polygonatum verticillatam* (L.) All.	Malu	Caesalpiniaceae	Medicinal
99.	*Polygonum capitatum* (Buch.-Ham. Ex D.Don) H.Gross		Renunculaceae	Medicinal
100.	*Polygonum filicaule* Wall. ex Meissn		Polygonaceae	Medicinal
101.	*Polygonum spp.* L.		Polygonaceae	Medicinal
102.	*Polygonum polystachyum* Wall. ex Meissn		Polygonaceae	Medicinal
103.	*Poteatilla spp.* L.		Rosaceae	Medicinal
104.	*Potentilla atrosangunea* G.LOOD.ex D.Don		Rosaceae	Medicinal
105.	*Potentilla fulgens* L.		Rosaceae	Medicinal
106.	*Potentilla fulgens* Wall. Ex HK.F.	Bajaradanti	Rosaceae	Medicinal
107.	*Potentilla spp.* L.		Rosaceae	Medicinal
108.	*Potentilla polyphylla* Wall. ex Lehm.		Rosaceae	Medicinal
109.	*Potentilla polyphylla* Wall. ex Lehm		Rosaceae	Medicinal
110.	*Primula spp* L.		Primulaceae	Medicinal
111.	*Prunella vulgaris* L.		Lamiaceae	Medicinal

Table cont....

S.No.	Name of Species	Local Name	Family	Ethnobotanical Uses
112.	*Ranunculus hirtellus* Royle		Ranunculaceae	Medicinal
113.	*Ranunculus repens* L.		Apiaceae	Medicinal
114.	*Reinwardtia indica* Dum.	Bugla	Asterceae	Medicinal
115.	*Rhododendron anthopogon* D.Don	Burans	Ericaceae	Medicinal, Wild edible, Fuel, Timber
116.	*Rubia manjith* Roxb.ex Fleming	Lichkuri, indian madder	Rubiaceaae	Medicinal, Fodder
117.	*Rumex hastatus* D.Don	Almora	Polygonaceae	Edible, Fodder, Medicinal
118.	*Rumex nepalensis* Speeng.		Polygonaceae	Medicinal
119.	*Saccharum officinarum* L.		Poaceae	Medicinal
120.	*Salix lindleyana* Wallich ex Ander.		Salicaceae	Medicinal
121.	*Salix spp* L.		Salicaceae	Medicinal
122.	*Salvia nubicola* Wall. ex Sweet		Lamiaceae	Medicinal
123.	*Saxifraga parnassifolia* D.Don		Saxifragaceae	Medicinal
124.	*Scrophularia californica* Cham. & Schldl.		Scrophulariaceae	Medicinal
125.	*Sedum spp* L.		Crassulaceae	Medicinal
126.	*Selenium cuneifokiaa* DC.		Asteraceae	Medicinal
127.	*Senecio spp* L.		Asteraceae	Medicinal
128.	*Sibbaldia cuneata* Hornem.ex Kuntze		Rosaceae	Medicinal
129.	*Smilax aspera* L.		Smilacaceae	Medicinal
130.	*Solanum nigrum* L.		Solanaceae	Fodder, Medicinal
131.	*Sweritia chirayia* (Roxb. Ex Fleming) Karsten	Chiraita	Gentianaceae	Medicinal
132.	*Tanacetum longifolium* Wall. ex DC.		Asteraceae	Medicinal
133.	*Taraxacum officinale* (L.) Weber ex F.H. Wigg		Asteraceae	Medicinal
134.	*Taraxacum officinale* (L.) Weber ex F.H.Wigg		Asteraceae	Medicinal
135.	*Tetratigma spp.* Merr.& Chun	Bell-type	Vitaceae	Edible, Medicinal
136.	Tetratigma pubinerve		Thymelaeaceae	Medicinal
137.	*Tetratigma serrulatum* (Roxb.) Planch.		Vitaceae	Medicinal
138.	*Teucrium quadnfarium* Buch -Ham.		Lamiaceae	Medicinal
139.	*Trichosanthes tricuspidata* Lour.	Ilaru	Cucurbiaceae	Medicinal
140.	Trychidium royle			Medicinal
141.	*Urtica dioica* L.		Urticaceae	Fodder
142.	*Valeriana herdwikaii* Wall.		Caprifoliaceae	Medicinal
143.	Viburnum grandiflorum Wall.		Adoxaceae	Medicinal
144.	*Viola biflora* L.	Bana-ksha	Violaceae	Medicinal

(IVI: 35.807), and *Berberis aristata* (IVI: 22.769). The dominant herb species were *Oplismenus hirtellus* (IVI: 21.957), *Cyperus odoratus* (IVI: 18.375), and *Ischaemum rugosum* (IVI: 15.377).

Study Site S_5

The study site S_5 (2,015m a.s.l) was the Sari village, located at the left bank of the Mandakini River. The density, frequency, abundance, and Importance Value Index (IVI) of the trees, shrubs, and herbs have been presented in Table 4 and Table 5. Ecological analysis revealed the dominant tree species were *Quercus liucotrichophora* (IVI: 25.677), *Alnus nepalensis* (IVI: 21.965), and *Aesculus indica* (IVI: 21.701). However, the dominant shrub species were *Girardnia diversifolia* (IVI: 40.998), *Sarcococca saligna* (IVI: 27.752), and *Urtica dioica* (IVI: 25.216). The dominant herb species were *Pilea umbrosa* (IVI: 20.192), *Cymbopogon citratus* (IVI: 16.016), and *Cymbopogon citratus* (IVI: 16.016).

Table 4: Dominance of tree, shrub, and herb species and Total Basal Area (TBA) of plant species in the study area of Kedarnath valley

S.N.	Village Name	Dominance of tree species	Dominance of shrub species	Dominance of herb tree species	TBA
1.	Chandrapuri	*Grewia optiva*	*Girardnia diversifolia*	*Galinsoga parviflora*	*Banhinia variegata*
2.	Kalimath	*Quercus liucotrichophora*	*Solanum viarum*	*Pilea umbrosa*	*Quercus leucotrichophora*
3.	Gaundar	*Quercus liucotrichophora*	*Sarcococca saligna*	*Bidens pilosa*	*Quercus leucotrichophora*
4.	Tarsali	*Quercus liucotrichophora*	*Sarcococca saligna*	*Oplismenus hirtellus*	*Quercus leucotrichophora*
5.	Sari	*Quercus liucotrichophora*	*Girardnia diversifolia*	*Pilea umbrosa*	*Quercus leucotrichophora*
6.	Gaurikund	*Quercus liucotrichophora*	*Echinops cornigenus*	*Oplismenus hirtellus*	*Quercus leucotrichophora*
7.	Trijuginarayan	*Quercus liucotrichophora*	*Sarcococca saligna*	*Agrimonia pilusa*	*Quercus leucotrichophora*
8.	Kedarnath	*Taxus wallichiana*	*Berberis jaeschkeana*	*Trychidium royle*	*Taxus wallichiana*
9.	Tungnath	*Abies spectabilis*	*Rhododendron campanulatum*	*Carax hirta*	*Rhododendron barbatum*

Study Site S_6

The study site S_6 (2,156 m a.s.l) was the Gaurikund village, located at the right bank of the Mandakini River. The density, frequency, abundance, and Importance Value Index (IVI) of the trees, shrubs, and herbs have been presented in Table 4 and Table 5. Ecological analysis revealed the dominant tree species were *Quercus liucotrichophora* (IVI: 38.35), *Neolitsea sericea* (IVI: 35.87), and *Betula alnoides* (IVI: 24.25). However, the dominant shrub species were *Echinops cornigenus* (IVI: 52.24), *Girardnia diversifolia* (IVI: 35.31), and *Sarcococca saligna* (IVI: 26.49). The dominant herb species were *Oplismenus hirtellus* (IVI: 18.55), *Cymbopogon citratus* (IVI: 17.25), and *Diplazium esculentum* (IVI: 16.59).

Study Site S_7

The study site S7 (2,246 m a.s.l) was the Trijuginarayan village, located at the right bank of the Mandakini River. The density, frequency, abundance, and Importance Value Index (IVI) of the trees, shrubs, and herbs have been presented in Table 4 and Table 5. Ecological analysis revealed the dominant tree species were *Quercus liucotrichophora* (IVI: 48.10), *Rhododendron arboreum* (IVI: 28.37), and *Neolitsea sericea* (IVI: 25.40). However, the dominant shrub species were *Sarcococca saligna* (IVI: 33.43), *Girardnia diversifolia* (IVI: 24.12), and *Cannabis sativa* (IVI: 18.25). The dominant herb species were *Agrimonia pilusa* (IVI: 22.48), *Bidens pilosa* (IVI: 14.48), and *Diplazium esculentum* (IVI: 14.27).

Table 5: Different ecological and diversity parameters in the study area of Kedarnath valley.

Parameters	Chandrapuri	Kalimath	Gaundar	Tarsali	Sari	Gaurikund	Trijuginarayan	Kedarnath	Tungnath
Tree density (ind.100 m^{-2})	38.4	100.7	37.9	81	46	54.3	49.4	6.8	15.5
Shrub density (ind.25 m^{-2})	81.5	95	122.9	46.8	65	36.9	49.1	15	11.8
Herb density (ind.m^{-2})	200	323.4	248.7	202.8	198.9	197.6	125.5	229.7	147
TBC (m^2ha^{-1})	21.828	57.364	20.417	33.606	34.086	43.704	38.28	21.475	-
Tree IVI	300.001	299.995	300.002	299.989	300.004	299.83	299.99	300	299.98
Shrub IVI	299.998	300.002	299.999	300.006	299.999	300.01	231.55	300.01	300
Herb IVI	300.002	300.001	300.001	300	299.997	299.99	300.01	299.99	300.02
Shannon Index (Tree) ($\overline{H}$)	3.028	3.048	2.901	3.001	2.918	2.753	2.636	1.737	-
Shannon Index (Shrub) ($\overline{H}$)	2.788	2.696	2.629	2.492	2.594	2.404	2.047	0.192	-
Shannon Index (Herb) ($\overline{H}$)	3.613	3.787	3.531	3.305	3.156	3.367	3.317	3.712	3.115

IVI=Importance Value Index; TBA=Total Basal Area; $\overline{H}$=Diversity Index

Study Site S_8

The study site S_8 (3,568m a.s.l) was the Kedarnath, located at the right bank of the Mandakini River. The density, frequency, abundance, and Importance Value Index (IVI) of the trees, shrubs, and herbs have been presented in Table 4 and Table 5. Ecological analysis revealed the dominant herb species were *Trychidium royle* (IVI: 17.38), *Danthonia spp.* (IVI: 12.00) and *Anaphalis spp.* (IVI: 11.16). However, the dominant shrub species were *Berberis jaeschkeana* (IVI: 35.81), *Rosa spp.* (IVI: 21.38), and *Arismia tortosum* (IVI: 15.39). The dominant tree species were *Taxus wallichiana* (IVI: 66.82), *Abies spectabilis* (IVI: 63.44), and *Rhododendron barbatum* (IVI: 50.12).

Study site S_9

The study site S_9 (3,660 m a.s.l) was the Tungnath, located at the left bank of the Mandakini River. The density, frequency, abundance, and Importance Value Index (IVI) of the trees, shrubs, and herbs have been presented in Table 4 and Table 5. Ecological analysis revealed the dominant herb species were *Carax hirta* (IVI: 26.23), *Potentilla fulgens* (IVI: 20.98), and *Rhododendron anthopogon* (IVI: 19.27). However, the dominant shrub species were *Rhododendron campanulatum.* The dominant tree species were *Abies spectabilis.*

Total basal area (TBA)

In the Chandrapuri forest area, the total basal area was higher for *Banhinia variegata* (1.978 m^2ha^{-1}), possibly due to a higher density of trees (Table 4 and Table 5). In the Kalimath forest area, the total basal area was higher for *Quercus liucotrichophora* (7.688 m^2ha^{-1}), possibly due to a higher density of trees (Table 4 and Table 5). In the Gaundar forest area, the total basal area was higher for *Quercus liucotrichophora* (4.864 m^2ha^{-1}), possibly due to a higher density of trees (Table 4 and Table 5). In the Tarsali forest area, the total basal area was higher for *Quercus liucotrichophora* (9.542 m^2ha^{-1}), possibly due to a higher density of trees (Table 4 and Table 5). In the Sari forest area, the total basal area was higher for *Quercus liucotrichophora* (4.242 m^2ha^{-1}), possibly due to a higher density of trees (Table 4 and Table 5). In the Gaurikhund forest area, the total basal area was higher for *Quercus liucotrichophora* (7.319 $m^2.ha^{-1}$), possibly due to a higher density of trees (Table 4 and Table 5). In the Trijuginarayan forest area, the total basal area was higher for *Quercus liucotrichophora* (8.89 $m^2.ha^{-1}$), possibly due to a higher density of trees (Table 4 and Table 5). In the Kedarnath forest area, the total basal area was higher for *Taxus wallichiana* (4.654 $m^2.ha^{-1}$), possibly due to a higher density of trees (Table 4 and Table 5). In the Tungnath forest area, the total basal area was higher for *Rhododendron barbatum* (20.59 $m^2.ha^{-1}$), possibly due to a higher density of trees (Table 4 and Table 5).

Diversity Index

The species diversity index (Shannon-Wiener) can be regarded as a measure of environmental quality and points to the well-being of any ecosystem. The plant species diversity indices for site S1 to S9 have been presented in Table 5. For site S_1, it was 3.028 for trees, 2.788 for shrubs, and 3.613 for herbs. However, for site S_2, it was found to be 3.048 for trees, 2.696 for shrubs, and 3.787 for herbs. For site S_3, it was 2.901 for trees, 2.629 for shrubs, and 3.531 for herbs. For site S_4, it was 3.001 for trees, 2.492 for shrubs, and 3.305 for herbs. For site S_5, it was 2.918 for trees, 2.594 for shrubs, and 3.1564 for herbs. For site S_6, it was 2.753 for trees, 2.404 for shrubs, and 3.367 for herbs. For site S_7, it was 2.636 for trees, 2.047 for shrubs, and 3.317 for herbs. For site S_8, it was 1.737 for trees, 0.192 for shrubs, and 3.712 for herbs. For site S_9 it was 3.115 for herbs. This pointed out the dominance of herbs and trees at sites S_1, S_2, and S_4, and the dominance of herbs at sites S_3, S_5, S_7, S_8, and S_9. The dominance of both herbs and shrubs is only at site S_6. The dominant tree species was *Abies* spectabilis, whereas, the dominant shrub species was *Rhododendron campanulatum.*

IMPACTS OF ECODISASTER 2013 ON FOREST AREA OF KEDARNATH VALLEY

During the study, it was discovered that during the Kedarnath eco-disaster in Kedarnath valley in June 2013, there was a lot of damage to the forest in the riverbank of the Mandakini River due to flash floods and landslides. The flood plain of the Mandakini River was totally destroyed in which several important medicinal plants flowering plants and ornamental plant species were washed. In this disaster, about 500 valuable plant communities were affected. Even in the lower areas of Kedarnath, the nearby forest area of Mandakini River was damaged. Most of the forest was damaged in Jangalchhati, Rambara, Bhimbali, Gaurikund, Sonprayag, and Sitapur, in which medicinal plants, fodder plants, and wild edible plants were completely destroyed. In this disaster, landslides and flash floods that occurred in Kali gad, Madhmaheswar gad, and Kakara gad destroyed forest, in which, many fuel and fodder plants forest area was damaged.

Rawat et al. (2016) studied the biomass estimation during 2012 by sampling at ten random plots laid at open and dense forest sites. The biomass obtained from that study had shown that 242.24 $ton.ha^{-1}$ to 322.97 $ton.ha^{-1}$ for the Mixed Forest. The total washed-out area from the forest was nearly an average of 92.44 (Open and Dense Forest). This showed that nearly 22392.66 to 29855.35 tons of biomass from the total

area was lost. The disturbance in dense mixed forest (33.16 ha) and open mixed forest (59.28 ha) was recorded by Rawat et al. (2016) (Fig. 2). Over 500 plant species have suffered losses varying from minor to significant. Considering heavy riverbank cutting, multiple landslides event, and deposition of sediments in the Kedarnath pastoral area, the impact on vegetation is comparatively higher in meadows (BSI 2015).

It will take many thousands of years for regeneration in natural conditions for vegetation growth and productivity. To an ecosystem, the biomass and thus carbon sequestration process are directly linked. Loss in biomass from the available species extinction is a greater loss for the ecological cycle from the present area.

Ethnobotanical Plants and Their Use

Kedarnath valley is very rich in terms of the presence of medicinal plants, Edible plants, Fodder plants, Timber trees and fuelwood, and economically important plants. Local people of the Kedarnath valley use these plants for the cure of several diseases, as fodder, timber, and fuelwood (Table 3). A large number of these species are harvested in the wild, particularly for food, medicinal purposes, and for sale (Prasad & Sharma 2018).

DISCUSSION

Species richness in a forest depends on climatic, edaphic, and biotic factors (Ayappan & Parthasarathy 2001). A total of 221 plant species were recorded in Kedarnath valley. The species diversity of Kedarnath valley was found in the following order Herbs (144)> Trees (49) >Shrubs (28). Semwal et al. (1999) reported a total of 81 plant species including 20 tree species, 24 shrubs species, and 37 herbs species in the forests of Jardhar in Garhwal Himalaya. Kharkwal et al. (2005) carried out a study in the pine forest at different altitudes of Central Himalaya and reported a total of 56 species comprising 51 genera and 28 families, which is lower than the present study. The tree density in the present study was highest in the Kedarnath valley which ranged from 0.3 to 8.5no./ha. Sinha and Maikhuri (1998) also reported almost the same density in core and interactive zones of the Haryali sacred forest of Garhwal Himalaya. Chandrashekara & Sankar (1998) reported a stem density of the iringole sacred grove in Kerala. These values were within the values reported by Saxena and Singh (1982), Bargali et al. (1988), Pangtey et al. (1989), and Bhandari et al. (1997) for various forests of Garhwal Himalaya. Shrub density in the present study varied from 0.4 to 13.5no./ha, whereas herb density ranged between 0.2 to 22.4no./ha. These values are comparable to the reported values of Kumar et al. (2009), Uniyal et al. (2010) for a forest in Garhwal Himalaya. A/F ratio is used to interpret the distribution pattern of species. Odum (1971) stated that clumped (contagious) distribution is the commonest pattern in nature, and random distribution is found only in a uniform environment and the regular distribution occurs where severe competition between the individuals exists (Panchal & Pandey 2004). Pala et al. (2011) have reported trees, shrubs, and herbs density of 6.88 trees 100 m^{-2}, 12.8 shrubs 25 $m^{-2,}$ and 16.34 herbs m^{-2} respectively in Chanderbadni sacred forest of Garhwal Himalaya.

Total basal cover (TBC) for trees showed a range of 9.542 to 0.075 $m^2.ha^{-1}$ from the Kedarnath valley forest. The variations in the TBC in different study sites may be due to variations in the number and size of tree species in different sites. The present study values are supported by Pande et al. (2001), who observed TBC ranged from between 56.42-126 $m^2.ha^{-1}$ in a forest in Garhwal Himalaya. Vidyasagaran et al. (2005) reported the average TBC value of 25.79 $m^2.ha^{-1}$ in sacred groves of the Thrissur district of Kerala. Sinha and Maikhuri (1998) also reported TBC values of 47.59 to 26.87 $m^2.ha^{-1}$ in the core and interactive zones of the Hariyali sacred forest from Garhwal Himalaya. Sacred forests mostly show reduced forest loss than unprotected areas and higher plant species richness, canopy heights, and stem diameters (Campbell 2004). Rawat (2005) also reported TBC values between 3.74-80.36 m^2/ha for temperate forests in Garhwal Himalaya. Tripathi and Singh (2009) reported that basal area is an important indicator of tree stocking, which reflects stand volume or biomass and recorded 24.84 $m^2.ha^{-1}$ basal areas of trees in a riverine forest of Katernia ghat Wildlife Sanctuary.

Shannon diversity index ($\overline{H}$) for tree species was recorded from a minimum of 0.976 to a maximum of 3.048 in Kedarnath valley. The values of the present study were higher than the values (1.44-2.27) calculated by Looy et al. (2003) on the effect of river embankment and forest fragmentation on plant species and composition of flood plain forests in the Meuse valley, Belgium. The values of the present study were higher than the values (0.8-1.4) reported by Pala et al. (2011) in the forests along the river Ganga in the Himalayas. Shannon Wiener diversity index ($\overline{H}$) for shrub species was recorded from lowest (0.192) to highest (2.788) in the Kedarnath valley. Ram et al. (2004) reported shrub diversity from 2.6 to 3.8 for different forest types in Kumaun Himalaya. Shannon Wiener's diversity index ($\overline{H}$) for herb species was recorded from minimum (3.115) to maximum (3.787) in Kedarnath valley. The values of the present study were within the values reported for different forests by many workers (Singh & Singh, 1986, Pande et al. 2002). The values of the present study are also within the reported values (3.24 to 4.03) given by Kharkwal et al. (2005).

Several workers (Greig-Smith 1957, Singh & Yadav 1974) have reported contagious distribution in natural veg-

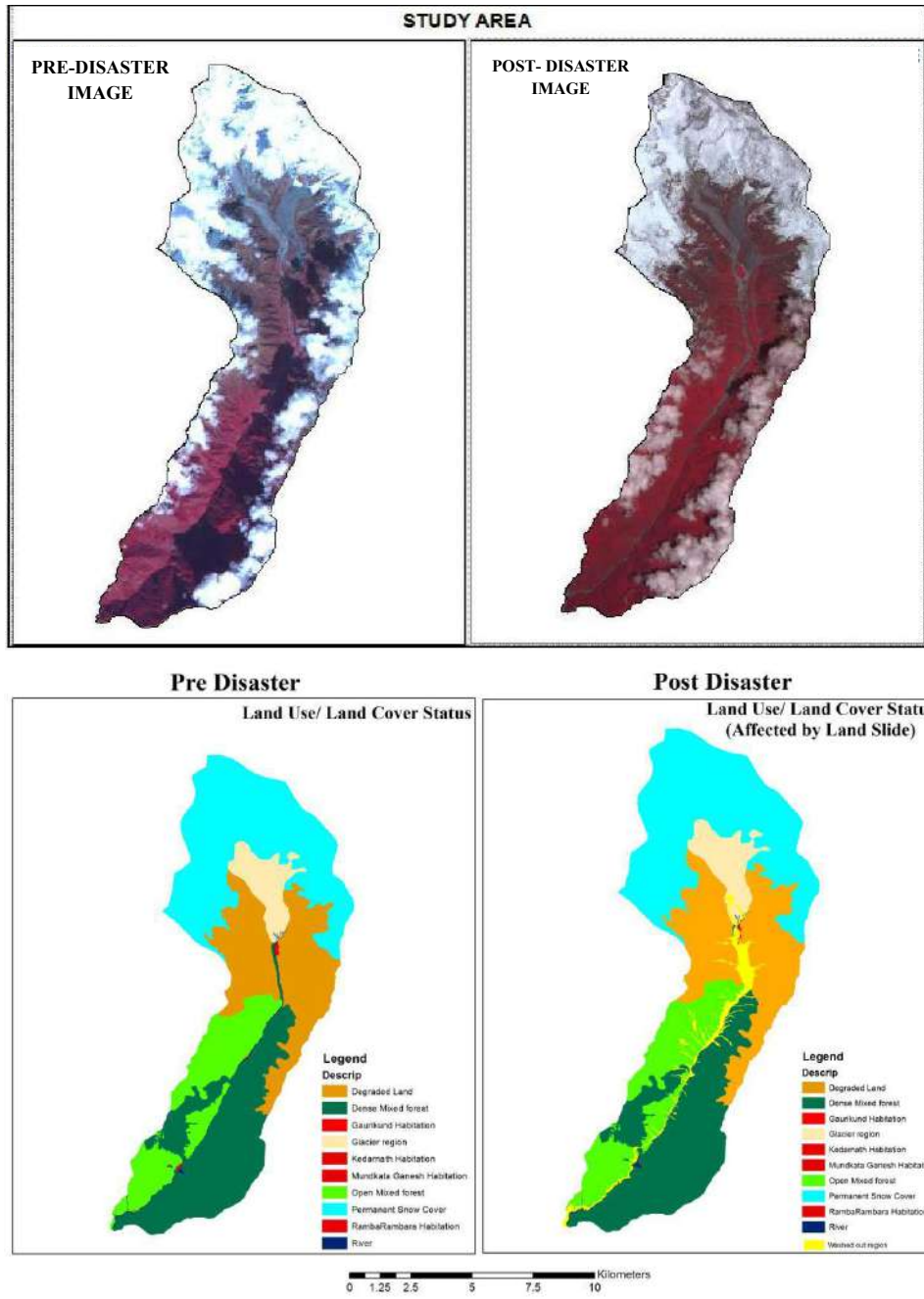

Fig. 2: Satellite imageries: Landuse landcover status of the study area pre and post-disaster of Kedarnath valley.

etation. However, shrubs and herbs were found distributed contagiously in all study sites. The regular distribution pattern was entirely absent. Mishra and Laloo (2005) and Upadhaya et al. (2004) also reported a contagious pattern of distribution for subtropical forests of North-east India. Other studies conducted within Garhwal Himalaya (Bhandari et al. 1998, Pande et al. 2002) have also shown a contagious pattern of Vegetational distribution in different forest types. Rawat et al. (2018) studied tree species richness, dominance, and regeneration status in western Ramganga valley. Bhatt et al. (2020) worked on God's tree: A culturally coded strategy for conservation in Chamoli District. Tiwari et al. (2020) also worked on weed floristic composition and diversity in paddy fields of Mandakini valley.

CONCLUSION

The current study documented that the Kedarnath valley is blessed with mainly eight types of forests that include the Himalayan Dry Temperate Forests, Dry Temperate Coniferous Forest, West Himalayan Birch/Fir Forests, Sub-alpine Pasture, Himalayan Chir-Pine Forest, Himalayan Moist Temperate Forest, West Himalayan Sub-Alpine Birch/Fire Forest, and Alpine Forest. The largest forest cover was found in Karokhi followed by Sari, Ransi, Ukhimath, Kabiltha, whereas, the lowest forest cover was recorded in Tungnath and Barasu. A total number of 221 plant species were collected and documented from the Kedarnath valley. Plant diversity in the valley encompasses 49 species of trees, 28 species of shrubs, and 144 species of herbs. The tree density in the current study was recorded highest in the Kedarnath valley which ranged from 0.3 to 8.5 no.ha^{-1}Shrub density in the present study varied from 0.4 to 13.5 no.ha^{-1}, whereas herb density ranged between 0.2 to 22.4 no.ha^{-1}. Total basal cover (TBC) for trees showed a range from 9.542 to 0.075 m^2/ha, Total basal cover (TBC) for trees showed a range of 9.542 to 0.075 m^2.ha^{-1}, and the Shannon diversity index ($\overline{H}$) for tree species was recorded from a minimum of 0.976 to a maximum of 3.048.

The Kedarnath valley consisted of patchy vegetation including many economically important plants such as medicinal herbs, timber trees wild edible plants, fodder, and fuelwood. During the Kedarnath eco-disaster that occurred in June 2013, huge damage to the forest in the riverbank of the Mandakini River was recorded due to flash floods and landslides. It was estimated that nearly 500 valuable plant species were affected by this eco-disaster.

ACKNOWLEDGEMENTS

The authors are thankful to the local people of the Kedarnath valley and VDO of tehsil Ukhimath to share their valuable knowledge, data and help in data collection. One of the authors (Chandi Prasad) thankfully acknowledges the H.N.B. Garhwal University (A Central University) for providing support during the research.

REFERENCES

Ayyappan, N. and Parthasarathy, N. 2001. Patterns of tree diversity within a large-scale permanent plot of tropical evergreen forest Western Ghats, India. Ecotropica, 5: 197-211.

Ballabha, R., Rawat, D.S., Tiwari, J.K., Tiwari, P. and Gairola, A. 2013. Wild edible plant resources of the Lohba Range of Kedarnath Forest Division (KFD), Garhwal Himalaya, India. Int. Res. J. Biol. Sci., 2(11): 65-73.

Bargali, K., Usman and Joshi, M. 1998. Effect of forest covers on certain site and soil characteristics in Kumaun Himalayas. Indian J. For., 21(3): 224-227.

Bhandari, B.S., Mehta, J.P., Nautiyal, B.P. and Tiwari, S.C. 1997. Structure of a chir pine (Pinus roxburghii Sarg.) community along an altitudinal gradient in Garhwal Himalaya. Int. J. Ecol. Enviro. Sci., 23(1): 67-74.

Bhandari, B.S., Mehta, J.P. and Tiwari, S.C. 1998. Woody vegetation structure along an altitudinal gradient in a part of Garhwal Himalaya. J. Hill Res., 11: 26-31.

Botanical Survey of India. 2015. Kedarnath natural disaster impact on flora. MoEFCC, pp. 1-40.

Bhatt, V.P. and Rawat, D.S. 2020. God's Tree: A Culturally Coded Strategy for Conservation (A Case Study of Gairsain Ecoregion of District Chamoli, Uttarakhand). In: Khasim, S.M., Long, C., Thammasiri, K. and Lutken, H. (eds.) Medicinal Plants: Biodiversity, Sustainable Utilization, and Conservation, Springer, New York, pp. 237-247.

Campbell, M. O. 2004. Traditional forest protection and woodlots in the coastal savannah of Ghana. Environ. Conserv., 31: 225-232.

Census of India. 2011. District Census Handbook Rudraprayag. Directorate of Census Operation, Uttarakhand, pp. 1-156.

Chandrashekara, U. M. and Sankar, S. 1998. Ecology and management of sacred groves in Kerala. For. Ecol. Manag., 112: 165-177.

Curtis, J.T. 1951. An upland forest continuum in the prairie forest border region of Wisconsin. Ecology, 32: 476-496.

Curtis, J.T. 1959. The Vegetation of Wisconsin. An Ordination of Plant Communities. University Wisconsin Press, Wisconsin.

Curtis, J.T. and Mc-Intosh, R.P. 1950. The interrelations of certain analytic and synthetic phtyosociological characters. Ecology, 32: 434-455.

FSI, 2017. Forest Survey of India. India State of Forest Report. Ministry of Environment and Forests, Dehradun, pp. 308-313.

Gates, F. C. 1949. Field Manual of Plant Ecology. Mc Graw Hill, New York.

Greig-Smith, P. 1957. Quantitative Plant Ecology. Butterworths, London.

Kharkwal, G., Mehrotra, P. and Pangtey, Y.P.S. 2005. Comparative studies on species richness, diversity, and composition of oak forests in Nainital district, Uttaranchal. Curr. Sci., 89(4): 668-676.

Kimothi, G.P. and Shah, B.C.L. 1989. Some medicinal plants of Gopeshwar-Tungnath region of Uttar Pradesh**.** Anc. Sci. of Life, 8(3,4): 283-292.

Kumar, B. 2009. Major religious plants of Rudraprayag District (Garhwal), Uttarakhand (India), Ethnobot. Leaflets, 13:1476-1484.

Looy, K.V., Honnay, O., Bossuyt, B. and Hermy, M. 2003. The effects of river embankment and forest fragmentation on the plant species richness and composition of floodplain forests in the Meuse Valley. Belgium. Belg. J. Bot., 136 (2): 97-108.

19th Livestock Census. 2012. All India report. Ministry of Agriculture Department of Animal Husbandry, Dairying & Fisheries Krishi Bhawan, New Delhi, pp. 1-120.

Mishra, B.P. and Laloo, R.C. 2005. Effect of fragmentation on plant diversity and community characters of the sacred grove of Meghalaya. In: National Conference on Current Trends of Research in Science and Technology 50th Annual Technical Session of Assam. Science Society Deka PC, Jha DK Assam Science Society Guwahati.

Misra, R. 1969. Ecology Workbook. Oxford and IBH, Calcutta, p. 244.

Misra, R. and Puri, G.S. 1954. Indian Manual of Plant Ecology. English Book Depot, Dehradun.

Mullar-Dombois, D. and Ellenberg, H. 1974. Aims and Methods of Plant Ecology. John Wiley and Sons, New York.

Nautiyal, M. and Tiwati, J.K., Rawat, D.S. 2017. Exploration of some important fodder plants of Joshimath area of Chamoli district of Garhwal, Uttarakhand. Curr Bot., 8: 144-149.

Negi, B.S., Chauhan, D.S. and Todariya, N.P. 2008. Inventory of species richness of panchayat forests and adjoining reserve forests in three districts of Garhwal Himalaya, India. Int. Soc. Trop. Ecol., 49(2): 121-129.

Odum, E.P. 1971. Analysis of vegetation of Rampara forest in Saurashtra region of Gujarat state of India. J. Trop. Ecol., 45(2), 223-231.

Pala, N.A., Negi, A.K., Gokhale, Y. and Todaria, N.P. 2011. Species composition and phytosociological status of Chanderbadni sacred forest in Garhwal Himalaya Uttarakhand India. NeBIO, 2: 52-59.

Pala, N.A., Negi, A.K., Gokhale, Y.S. and Kumar, M. 2016. Community structure and plant diversity of community-based religious conserved forest of Garhwal Himalaya, India. J. Earth. Sci. Clim Change, 7(2): 334.

Panchal, N. and Pandey, A. N. 2004. Analysis of vegetation of Rampara forest in Saurashtra region of Gujarat state of India. Trop. Ecol., 2)45): 223-231.

Pande, P. K., Negi, J. D. S. and Sharma, S. C. 2001. Plant species diversity and vegetation analysis in moist temperate Himalayan forest. Indian Journal of Forestry, 24: 456-470.

Pande, P. K., Negi, J. D. S. and Sharma, S. C. 2002. Plant species diversity, composition, gradient analysis, and regeneration behavior of some tree species in a moist temperate western Himalayan forest ecosystem. Indian Forester, 128: 869-889.

Pangtey, Y. P. S., Samant, S. S., Bankoti, N. S. and Rawal, R. S. 1989. Soil and vegetation analysis of Pindari area. Second Annual report submitted to Department of Environment, New Delhi, pp. 167.

Kumar, M., Singh, B., Joshi, M. 2009. Effect of aspect on distribution pattern of Anogeissus latifolia Wall ex Bedd. in subtropical belt of Garhwal Himalaya, India. Tanzania J. For. Nat. Conserv., 78(1): 21-27.

Phillips, E. A. 1959. Methods of Vegetation Study. Henry Holt. & Co., Inc., New York.

Prasad, C. and Sharma, R.C. 2018. Wild edible resources of Kedarnath valley, Garhwal Himalaya, India. Indian J. Ecol., 45(3): 433-444.

Ram, J., Kumar, A. and Bhatt, J. 2004. Plant diversity in six forest types of Uttaranchal, Central Himalaya, India. Curr. Sci., 86(7): 975-978.

Rawat, N., Thapliyal, A., Purohit, S., Negi, G.S., Dangwal, S., Rawat, S., Aswal, A. and Kimothi, M.M. 2016. Vegetation loss and ecosystem disturbances on Kedargad Mandakini subwatershed in Rudraprayag district of Uttarakhand due to torrential rainfall during June 2013. Int. J. Adv. Remote Sens. GIS, 5(4): 1662-1669.

Rawat, R.S. 2005. Studies on the interrelationship of woody vegetation density and soil characteristics along an altitudinal gradient in a montane forest of Garhwal Himalayas. Indian For., 131: 990-994.

Rawat, D.S., Tiwari, J.K., Tiwari, P., Nautiyal, M., Praveen, N. and Singh, N. 2018. Tree species richness, dominance, and regeneration status in western Ramganga Valley, Uttarakhand Himalaya, India. FRI, Dehradun, 144(7): 595-603.

Revenue Report of Villages. 2017. Revenue Report of Villages Tehsil Ukhimath: 2016-17 R-57. Ukhimath Tehsil, Rudraprayag district, Uttarakhand, pp. 1-12.

Saxena, A.K. and Singh, J.S. 1982. A phytosociological analysis of woody species in forest communities of a part of Kumaun Himalaya. Vegetatio, 50: 3-22.

Semwal, D.P., Saradhi, P.P., Kala, C.P. and Sajwan, B.S. 2010. Medicinal plants used by local Vaidyas in Ukhimath block, Uttarakhand. Indian J. Tradit. Knowl., 9(3): 480-485.

Semwal, R.L., Nautiyal, S., Rao, K.S., Maikhuri, R.K. and Bhandari, B.S. 1999. Structure of Forests under community conservation: A preliminary study of Jardhar village initiative in Garhwal Himalaya. Envis, 7(2): 20-31.

Singh, A., Nautiyal, M.C., Kunwar, R.M. and Bussmann, R.W. 2017. Ethnomedicinal plants used by local inhabitants of Jakholi block, Rudraprayag district, western Himalaya, Indian J. of Ethnobiol. Ethnomed., 13: 1-29.

Singh, J.S. and Yadav, P.S. 1974. Seasonal variation in composition plant biomass and net primary productivity of tropical grassland at Kurukshetra, India. Ecol. Monogr., 44: 351-376.

Singh, S.P. and Singh, J.S. 1986. Structure and function of Central Himalayan oak forest. Proc. Indian Acad. Sci.: Plant Sci., 96: 159-189.

Sinha, B. and Maikhuri, R.K. 1998. Conservation through socio-cultural religious practice in Garhwal Himalaya: A case study of Hariyali sacred site. In:Ramakrishnan, P.S., Saxena, K.G. and Chandrashekara U.M. (eds.). Conserving the Sacred for Biodiversity Management. UNESCO and Oxford-IBH Publishing, New Delhi, pp. 289-299.

Srivastava, S. K. and Singh, D. K. 2005. Glimpses of the Plant Wealth of Uttaranchal. Bishen Singh Mahendra Pal Singh, Dehradun, pp. 158

Tiwari, P., Bharti, Rawat, D. S. and Singh, N. 2020. Weed floristic composition and diversity in paddy fields of Mandakini Valley, Uttarakhand, India. Int. J.Bot. Stud., 5(3): 334-341.

Tripathi, K.P. and Singh, B. 2009. Species diversity and vegetation structure across various strata in natural and plantation forests in Katerniaghat wildlife sanctuary, North India. Trop. Ecol., 50(1):191-200.

Uniyal, B.P., Sharma, J.R., Chaudhari, U. and Singh, D.K. 2007. Flowering Plants of Uttarakhand: A Checklist. Bishan Singh Mahendra Pal. Singh, Dehradun, pp. 404-1.

Uniyal, P., Pokhriyal, P., Dasgupta, S., Bhatt, D. and Todaria, N.P. 2010. Plant diversity in two forest types along the disturbance gradient in Dewalgarh watershed, Garhwal Himalaya. Curr. Sci., 98 (7): 938-943.

Upadhaya, K., Pandey, H.N., Law, P.S. and Tripathi, R.S. 2004. Diversity and population characteristics of woody species in sub-tropical humid forests exposed to culture disturbances in Meghalaya NE India. Trop. Ecol., 45: 303-314.

Vidyasagaran, K., Abhilash, D. and Babu, L.C. 2005. Plant diversity and conservation of Kalasamala sacred grove of Thrissur District Kerala. In: Kunihikannan, C. and Singh, B.G. (eds.). Strategy for conservation of sacred groves. Institute of Forest Genetics and Tree Breeding, Coimbatore, pp. 77-81.

Nature Environment and Pollution Technology
An International Quarterly Scientific Journal

p-ISSN: 0972-6268
(Print copies up to 2016)
e-ISSN: 2395-3454

Vol. 20 | No.3 | pp. 941-953 | 2021

Original Research Paper

https://doi.org/10.46488/NEPT.2021.v20i03.003

Open Access Journal

Study on the Electrochemical Anticorrosion Effect of Piezoelectric Materials in the Internal Environment of Water Supply Pipeline

T. Li*(**), G. Li*(**)†, X. Zhang*, S. Xu*(**) and H. Ghougassian*(**)**

*School of Energy and Environmental Engineering, University of Science and Technology, Beijing, 100083, P. R. China
**Beijing Key Laboratory of Resource-oriented Treatment of Industrial Pollutants, Beijing, 100083, P. R China
***Chinese Academy of Environmental Planning, Beijing, 100012, P. R. China
†Corresponding author: Ge Li; 1102868992@qq.com

Nat. Env. & Poll. Tech.
Website: www.neptjournal.com

Received: 08-08-2020
Revised: 20-09-2020
Accepted: 01-11-2020

Key Words:
Piezoelectric material
Corrosion rate
Electrochemical anticorrosion
Pipeline anticorrosion

ABSTRACT

The problem of corrosion in water supply pipelines not only poses a considerable threat to the safety of drinking water but also causes a large amount of water wastage due to the leakage of the pipeline network, which can be a chronic problem for a municipal water supply system, as observed in Beijing and other cities in China. In this study, a new piezoelectric PVDF fiber membrane was prepared by electrospinning process, and a piezoelectric anticorrosive film was fabricated based on the internal environment of the pipeline. In the simulated water supply pipeline environment, based on the principle of the piezoelectric effect and the principle of cathodic protection, the electrochemical corrosion protection effect of piezoelectric materials in the water supply pipeline environment, under different water quality conditions, was investigated by a single factor experiment. The results show that piezoelectric anti-corrosion tablets have an obvious inhibitory effect on pipeline corrosion under different pH values, ammonium nitrate concentrations, chloride ion concentrations, and sulfate ion concentrations. Furthermore, under the conditions of pH neutral, alkaline, and high ion concentration, the piezoelectric anti-corrosion sheet can protect the pipeline by 100%. Additionally, since the piezoelectric material can convert mechanical energy into electrical energy and does not cause pollution during the experiment, it has good environmental and economic benefits. The use of piezoelectric materials for preventing corrosion of pipelines is a frontier exploration. We believe that the improvement and development of material properties, and the combination of these new materials and traditional techniques, will provide new ideas and methods for pipeline anti-corrosion technology.

INTRODUCTION

With the continuous development of water treatment technology and process, the quality of pipeline feed water meets the standard. However, pipeline corrosion will cause significant degradation of the drinking water quality through the intrusion of pollutants into the pipes, which will have an impact on human health, and bring massive economic losses. Therefore, there is a need to explore new high-efficiency, energy-saving, and environmentally friendly solutions. Pipeline corrosion is a very complicated process with various influencing factors. In addition to the physical conditions of the pipe itself, the characteristics of the water in the pipe are also the main contributing factor to pipe corrosion. This includes pH, alkalinity, hardness, dissolved oxygen, chloride ion, sulfate, nitrate, temperature, bacterial community, etc. (Hu et al. 2018, McNeill & Edwards 2002, Sarin et al. 2004, Slaimana & Hasan 2010, Sun et al. 2014, Wang & Ma 2009, Zhang et al. 2018). At present, pipeline anti-corrosion technology generally includes pipe lining technology (Li et al. 2016), pipe coating technology (Zhu et al. 2018), and cathodic protection technology (Loto et al. 2019). To solve the problems of high cost, poor performance, and secondary pollution in these methods, this paper combines piezoelectric materials with anti-corrosion technology to achieve energy conservation and an environmentally sound approach.

In recent years, the development and usage of piezoelectric materials have witnessed a widespread resurgence. Piezoelectric materials were widely used during the First World War, and at that time, quartz was used as a resonator for the ultrasonic source in SONAR, and submarine detection was achieved by echolocation (Dineva et al. 2014). Piezoelectric materials are currently used in high-tech fields, such as information technology, laser technology, navigation technology, and biology (Duan & Xing 2015), a wide range of applications in transducer technology (Joseph et al. 2018, Kim et al. 2011), sensors (Wang & Chen 2016), filters (Li 2009), etc. Piezoelectric catalytic technology applied to environmental restoration in recent years is also closely related to piezoelectric materials (Zhang et al. 2019), and their piezoelectric effect and sensing effect can be used to apply them in a wider range of fields

(Butt et al. 2016, Chen et al. 2019, Ramatlo et al. 2018, Tang et al. 2019, Xu et al. 2018).

Based on the vibration mechanism of piezoelectric materials and the corrosion mechanism of pipes, the principle of piezoelectric materials and electrochemical corrosion protection is applied in pipeline anti-corrosion technology. This paper explores whether the continuously provided electrons by the piezoelectric material can inhibit corrosion and protect the pipeline under different conditions. Not only is this an attempt in the application of new materials, but it is rather a new way of thinking in pipeline anti-corrosion technology, which will further promote the development of electrochemical anti-corrosion technology.

MATERIALS AND METHODS

Piezoelectric Anticorrosive Sheet Making Process

The manufacturing process of the piezoelectric anticorrosive sheet is divided into two steps: preparation of the electrospun fiber membrane, and preparation of the electrospun piezoelectric anticorrosive sheet.

Preparation of electrospun fiber membrane: The electrospinning nanofibers were received by a dual-motor-controlled, rotatable, and reciprocating cylinder receiving device. First, a certain amount of PVDF powder was weighed and mixed in a DMF/acetone (60:40) mixed solvent. The doping amount of $FeCl_3 \bullet 6H_2O$ was 50 $\mu mol.g^{-1}$ PVDF, thereby obtaining a PVDF spinning solution having a PVDF concentration of 10%. Then, an appropriate amount of PVDF spinning solution was transferred to a syringe, and the syringe was placed on the syringe pump. The positive electrode of the high-voltage DC power source was connected to the needle, and the negative electrode was connected to the receiving roller. The piezoelectric material was prepared under the conditions of a spinning voltage of 16 kV, a spinning speed of 1.0 $mL.h^{-1}$, and a spinning distance of 15 cm (Ribeiro et al. 2010, Zhao et al. 2005). When the amount of spinning solution reached 2 mL, the high-voltage DC power supply and the syringe pump were turned off, and the aluminum plate was carefully removed. The sample was marked, placed in an oven, dried at 50°C for 30 minutes, and stored for later use. The electrospinning process was carried out at room temperature and relative humidity of 40% to 50%. Fig. 1 represents an SEM image of an electrospun piezoelectric material. The electrospun fiber had a relatively flat surface, a clear shape, a uniform texture, and a relatively uniform fiber diameter distribution.

Preparation of Electrospun Piezoelectric Anticorrosive Sheet: The PVDF piezoelectric material thus produced was subjected to four processes of film cutting, edge treatment,

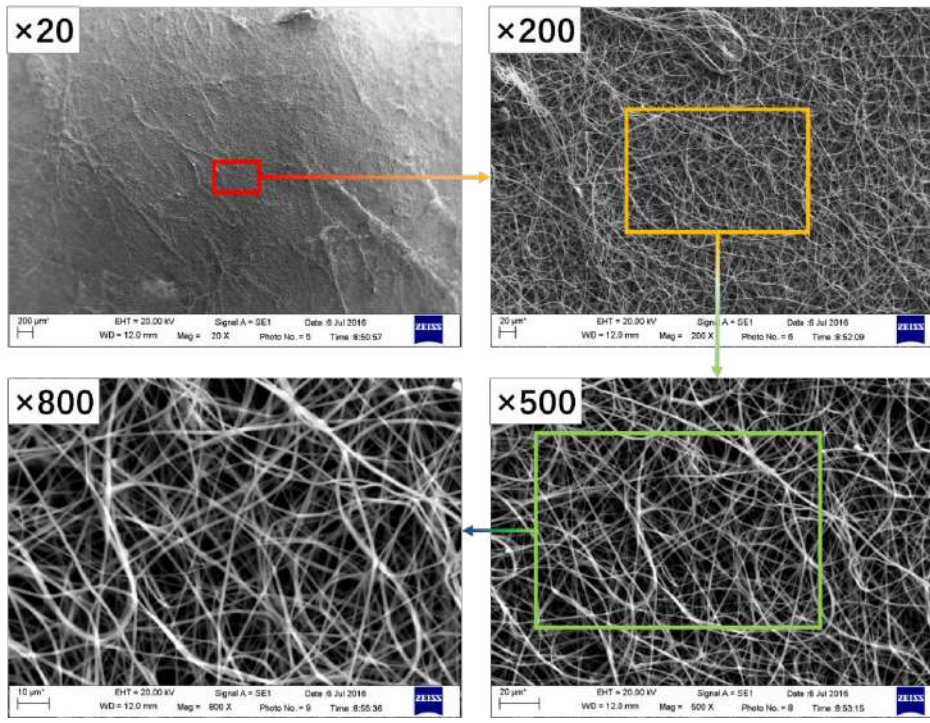

Fig. 1: SEM image of electrospun piezoelectric material.

electrode extraction, and adding of a protective layer to prepare a piezoelectric anticorrosive sheet for experiments (Fig. 2).

Film cutting: An area of the prepared electrospun PVDF fiber membrane, slightly larger than the required area, was marked and then cut with sharp scissors, and its edge was marked. In this paper, the fiber membrane is cut to a size of 2.0 cm × 2.0 cm.

Edge treatment: The edges of the cut fiber film were covered with a layer of insulating tape to prevent the upper and lower copper foil electrodes from short-circuiting due to collision. This also had a certain protective effect on the fiber film in use.

Electrode extraction: The conductive copper foil tape was cut to the desired shape and then carefully attached to the cut fiber membrane. The conductive copper foil tape acts as an electrode, which improves the operability of the preparation process, and makes the preparation process simple and convenient.

Adding of protective layer: Since the conductive copper foil electrode was directly attached to both sides of the fiber membrane, it was exposed to the outer environment and could have easily been damaged during use, affecting the experimental process. Therefore, it was necessary to add a protective layer on the outside and use insulating tape as a protective layer, which served both as protection and insulation.

Anti-Corrosion Experiment Process

First, to ensure the same corrosion area of cast iron during the experiment, a 1cm×2cm corrosion zone was reserved on the cast iron sheet, and other parts were covered with silicone rubber to isolate the corrosion solution. The height of the corrosive solution was controlled slightly above the corrosion zone and was in contact with the silicone rubber sheet, thus ensuring that all the corrosion zones of the cast-iron sheets were corroded and the corrosion area was consistent throughout the experiment.

Second, this study simulated cast iron corrosion in a beaker environment. In practice, only piezoelectric sheets are built into pipes in this method, not the entire device is put into pipes. The piezoelectric power generation device in Fig. 3 was composed of a vibration experiment platform (ESS-050-120 DongLing Technologies), a piezoelectric sheet, a signal generator, and an oscilloscope. The vibration experiment platform was controlled by a signal generator to provide cyclic bending-releasing external force. Then an external force was applied to the piezoelectric sheet to make the piezoelectric sheet generate electrical energy. At this

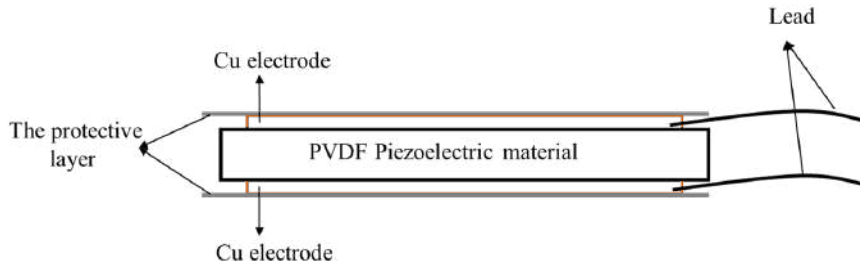

Fig. 2: Schematic diagram of electrospun piezoelectric anti-corrosion sheet.

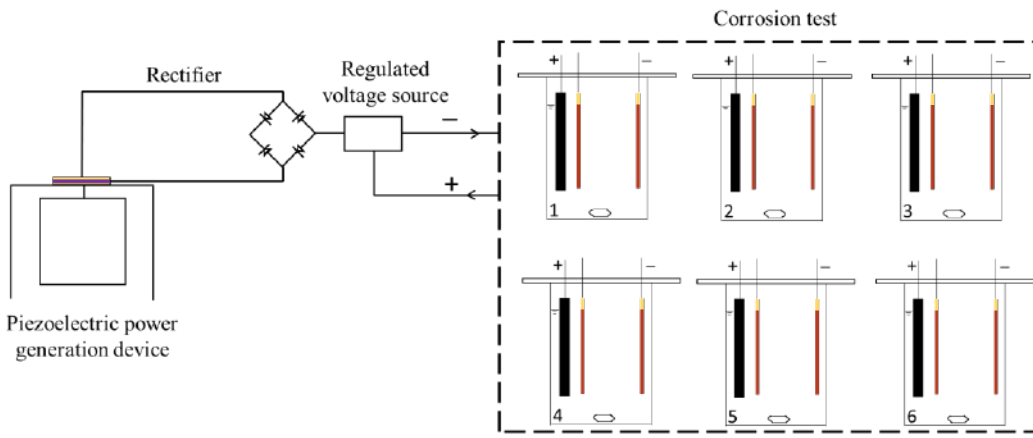

Fig. 3: Piezoelectric anticorrosion device schematic.

time, the current generated by the piezoelectric sheet was an alternating current, so the alternating current was changed to direct current through a rectifier to meet the basic conditions of cathodic protection. Then the regulated voltage source was passed to keep the current stable. Finally, the protection current generated by the piezoelectric sheet was externally connected to the cast iron sheet to be protected, and the cast iron corrosion test was conducted. As shown in Fig. 3, in the 6 beakers of the corrosion test apparatus, different solutions were placed according to the experiment, and two cast-iron sheets with silicone rubber were placed in a beaker containing a specific solution, and the rotor speed was adjusted to simulate the water flow rate. The anti-corrosion effect of the piezoelectric anticorrosive sheet was analyzed by comparing the corrosion changes of the cast iron with or without the piezoelectric protection device. The black bars in the beaker are anodes which are carbon rods.

Through reference to various literature studies, and based on the characteristics of environmental conditions in closed water pipes, experiments were carried out using four corrosion factors: pH, ammonium nitrate, sodium chloride, and sodium sulfate. Hydrogen ions participate in the cathodic reaction of iron corrosion. The pH is related to the solubility and form of the iron compound in the scale. And the change in pH also affects the formation of various oxides and hydroxides of iron. This in turn affects the corrosion rate of iron and the release of iron. In an acidic solution, nitrate reacts with zero-valent iron to form an ammonium-contaminated water body (Zhang & Edwards 2007), and ammonium causes rapid consumption of dissolved oxygen; for most bacteria, ammonium is a better source of nitrogen relative to nitrate, which can cause microbial growth and iron corrosion. Chloride and sulfate ions interfere with the formation of calcium and iron protective layers and can replace the hydrogen bonds in the passivation layer metal ions, thereby destroying the passivation film and chemically reacting with the scale to form dissolved ferrous ions. The passivation layer attached to the pipe scale layer is replaced by rust, which accelerates the corrosion rate of the pipe and increases the release of iron from the pipe network (Hu et al. 2018). Sulfate ions also participate in microbial reactions in the pipe network (Yang et al. 2014). Moreover, pH value, nitrate concentration, chloride ion concentration, and sulfate concentration are the typical influencing factors in the current corrosion process of cast iron. Therefore, the four influencing factors were selected as the optimization conditions for this study.

Deionized water was added to a 250 mL beaker to adjust the pH or to add different concentrations of the solution (see Table 1 for details) to obtain a 200 mL sample solution for the single factor impact test. In the experiment, other influencing factors were strictly controlled. In the experiment of pH influencing factors, NH_4NO_3, NaCl, and Na_2SO_4 were not added to the solution. When the NH_4NO_3, NaCl, or Na_2SO_4 concentration analysis experiment was carried out, the pH was controlled at around 7. For each of the NH_4NO_3, NaCl, and Na_2SO_4 solutions that were prepared, none of the other two compounds were added to the solution. For instance, the NH_4NO_3 solutions did not contain any NaCl or Na_2SO_4. The iron sheets were weighed daily to ensure accurate measurement of changes on each day. Three parallel experiments were performed.

Table 1: Details of the solution under different conditions (Room temperature 20°C~25°C).

Influence condition	Details
pH	3, 5, 7, 8, 9, 11
NH_4NO_3 concentration ($mg.L^{-1}$)	0, 100, 200, 250, 500, 1000
NaCl concentration ($mg.L^{-1}$)	0, 100, 200, 250, 500, 1000
Na_2SO_4 concentration ($mg.L^{-1}$)	0, 100, 200, 250, 500, 1000

Analytical Methods

The pH of the solution was measured using a pH meter (Mettler-Toledo 320). The weight-loss method was adopted. That is, the mass change of the cast iron sheet before and after the experiment is weighed to judge the corrosion rate of the cast iron and the protective effect of the piezoelectric anticorrosive sheet. The corrosion products on the cast-iron sheets were cleaned with deionized water, then the cast iron sheets were placed in an oven, dried at 50°C for 5 hours, then weighed and recorded (Yang et al. 2018). The voltage and current values in the environmental system during the whole experimental period were recorded by the voltage and current collector. The power consumption is obtained by voltage value and current value and is used to analyze the protection of cast iron in a corrosive environment under different power consumption conditions. The corrosion morphology of the cast iron was obtained by operating an electron scanning microscope (SEM (LEO-1450 Carl Zeiss) at 20.00 kV. The surface area of the SEM image was analyzed using Image-Pro Plus software.

RESULTS AND DISCUSSION

Effect of Initial pH

The initial pH of the solution has an important impact on the corrosion protection of the pipeline. This experiment explored the corrosion of cast iron with and without current protection at different pH.

Fig. 4 shows that the average rate of corrosion of cast iron decreases with increasing pH. The corrosion rate is relatively small and the difference is minimal when the pH

is neutral and alkaline and is lower than the daily average rate. In the acidic environment with pH=3, the corrosion rate is the highest on the first day, reaching 278 g.(m^{-2}.d^{-1}), and finally stabilized at around 146 g.(m^{-2}.d^{-1}). On the seventh day, the corrosion rate of the pH=3 solution is 122.9 g.(m^{-2}.d^{-1}) higher than that of the pH=7 solution (22.9 g.(m^{-2}.d^{-1}), which is mainly due to the hydrogen evolution corrosion of cast iron in an acidic environment. This is consistent with the study of Yang et al. (2017). The average corrosion rate of the cast iron sheet is sharply reduced with the protection device when compared with the corrosion rate without the protection device. In comparison, the corrosion rate drops to zero in neutral and alkaline solutions. In the acidic environment with pH=3 and pH=5, the corrosion rate is zero in the first four days, and slight corrosion occurs in the last two days. The highest corrosion rate is 7.08 g.(m^{-2}.d^{-1}). The protection current makes the cast iron in a state of excessive electrons so that the electron migration of metal corrosion is suppressed, and the occurrence of corrosion is avoided or reduced (Meng & Wang 2016).

As shown in Fig. 5, with the presence of the protection device's current, the protection degree in all solution systems is above 90%. Among them, in a neutral and alkaline environment, the protection degree can reach 100% for all seven days; however, it can reach 100% only in the first 4 days at pH=3 and pH=5. The cast iron without a protective device has obvious corrosion: the surface has rust and corrosion pit, and in contrast, the surface of the cast iron with protection device has no rust, is smooth, and less corroded, which indicates that the external protection device plays a good anti-corrosion role. Regarding power consumption, in different pH set-ups, the average daily electricity consumption gradually eases with time. The lowest power consumption (709.73 mW•h)

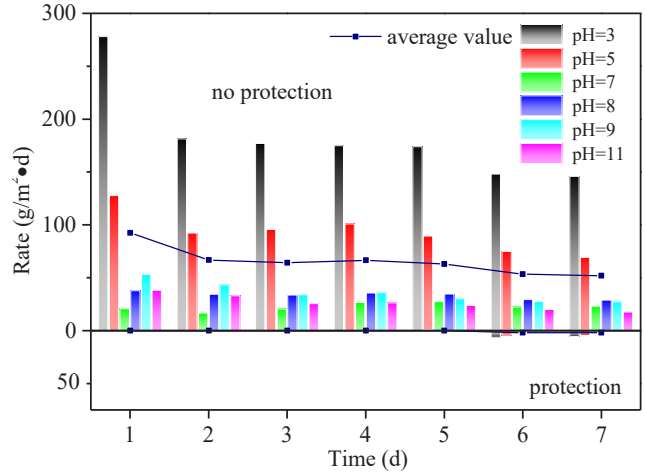

Fig. 4: Average rate change of cast iron under different pH conditions.

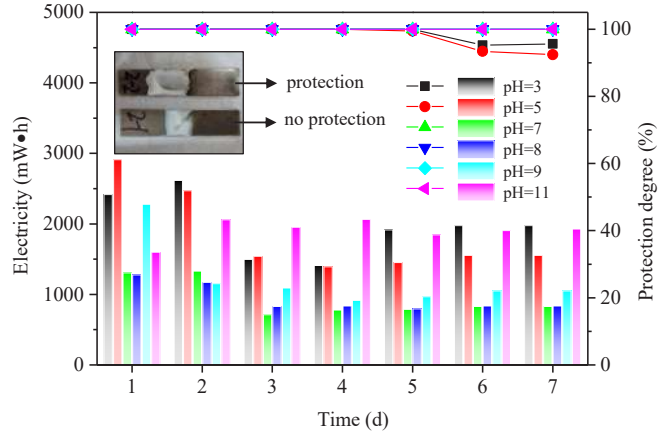

Fig. 5: Under the protection device, the changes in protection degree and power consumption of cast iron under different pH conditions.

at pH 7 is compared with the acidic conditions of the same time period, and the power consumption is shown to be reduced by about 50%.

Effect of Ammonium Nitrate Concentration

Nitrate ions have a great influence on the corrosion of cast iron. This experiment explored the corrosion of cast iron with and without current protection at different ammonium nitrate concentrations.

As shown in Fig. 6, in the ammonium nitrate solution environment system, the average corrosion rate increases with the increase of experiment time in the 5-day corrosion cycle. However, the corrosion rate of cast iron does not change regularly with the increase of nitrate ion concentration. Except for the 0 $mg.L^{-1}$ solution, the corrosion rate was the lowest for the 500 $mg.L^{-1}$ solution, which was 47.7 $g.(m^{-2}.d^{-1})$. The corrosion rate was the highest for the 1000 $mg.L^{-1}$ and 100 $mg.L^{-1}$ solutions, which exceeded the average, and reached their maximum levels on the fifth day: 59.3 $g.(m^{-2}.d^{-1})$ and 54.8 $g.(m^{-2}.d^{-1})$ respectively. When the protective current is applied, the average corrosion rate of the cast iron is greatly controlled in the ammonium nitrate solution system, and the corrosion rate is reduced to zero. In the deionized water environment, where there is poor electrical conductivity, the protection current is small and the corrosion is not effectively controlled.

From Fig. 7, the corrosion of cast iron is well controlled with the addition of the protective device, and the protection of cast iron is 100% except for the solution without ammonium nitrate. In the ammonium nitrate solution systems, the amount of electricity consumption is proportional to the concentration of the solution (except 0 $mg.L^{-1}$). Therefore, without protection, the solution has a minimum corrosion rate comparable to that of about 500 $mg.L^{-1}$. In the case of protection, combined with the corrosion rate and power consumption, the concentration of the solution is controlled at about 200 $mg.L^{-1}$. Its power consumption is reduced by 55% to 85% when compared to 500 $mg.L^{-1}$ and 1000 $mg.L^{-1}$, respectively. The minimum power consumption is 924.41 mW•h, although the power consumption is about 50% higher than that of 100 $mg.L^{-1}$. However, since the corrosion rate on the fourth day is about 18% lower than that of the 100 $mg.L^{-1}$ solution, controlling the solution concentration to 200 $mg.L^{-1}$ can completely protect the cast iron and save electricity.

Effect of Sodium Chloride Concentration

The chloride ion concentration has a large effect on the corrosion of cast iron. This experiment explored the corrosion of cast iron with or without current protection at different chloride ion concentrations.

From Fig. 8, in the chloride ion environment system, the average corrosion rate decreases gradually with the experiment time, and the higher the concentration, the faster the corrosion rate, indicating that the increase of Cl^- concentration will accelerate the release of iron and promote the corrosion of cast iron (Hu et al. 2018). This can be observed at chloride concentrations of 0 $mg.L^{-1}$ and 100 $mg.L^{-1}$, where the average rate of corrosion of cast iron is always below

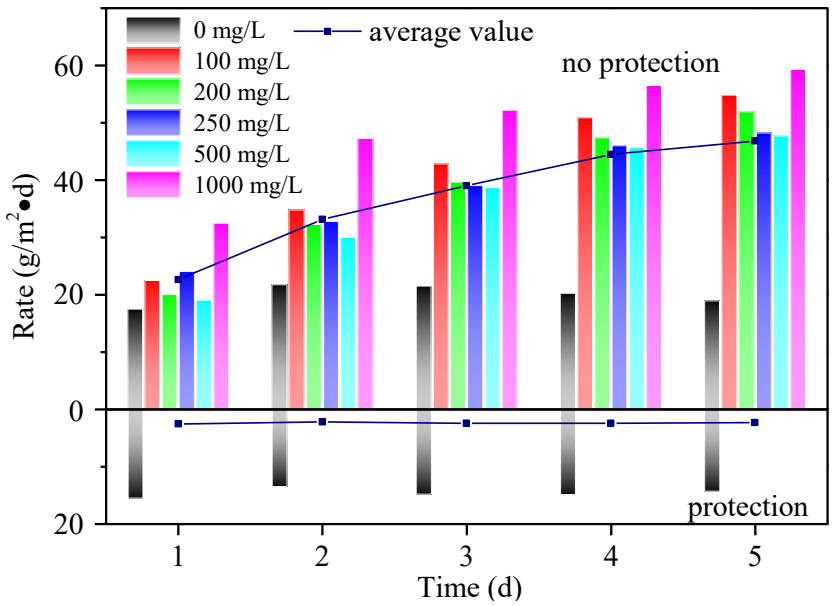

Fig. 6: Average rate change of cast iron under different ammonium nitrate concentrations.

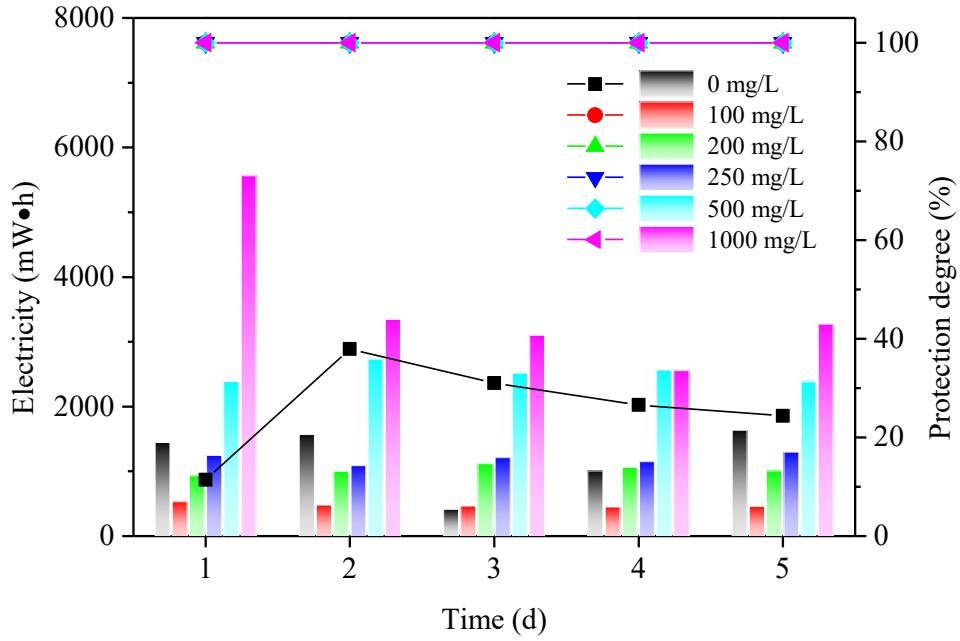

Fig. 7: Under the protection device, the changes in protection degree and power consumption of cast iron under different ammonium nitrate concentrations.

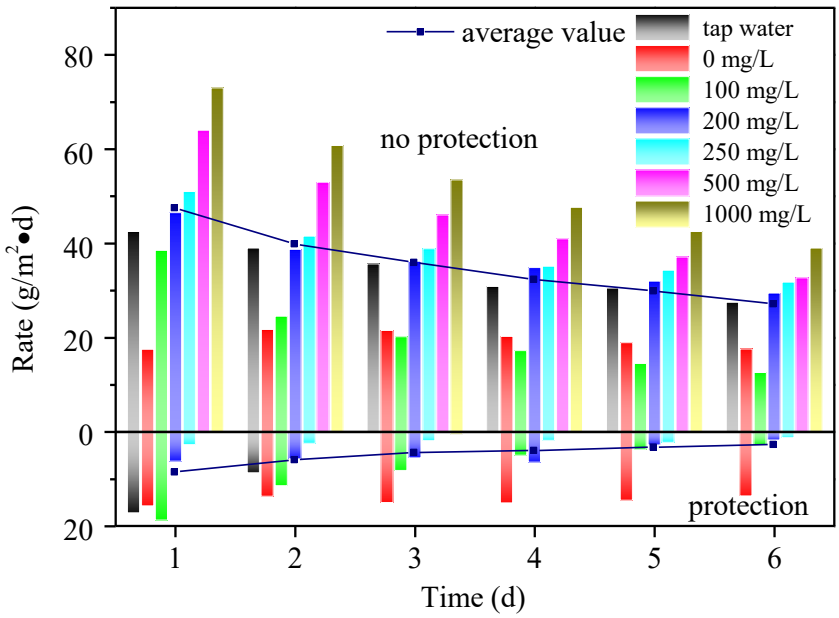

Fig. 8: Average rate change of cast iron under different chloride ion concentrations.

the overall average. Due to the presence of ionic substances in tap water, the corrosion rate of tap water is between the corrosion rates observed for the 100 mg.L^{-1} and 200 mg.L^{-1} solutions of sodium chloride. There is no ionic substance in the deionized water, and the corrosion rate is relatively low. We observe it first increasing, then falling, and then gradual. When the current is applied, the average corrosion rate of cast iron in the sodium chloride solution system is greatly reduced, especially for the solutions of 1000 mg.L^{-1} and 500 mg.L^{-1}, where the corrosion rate is almost zero. This is because the solution concentration is high and the protection current is large, so the average corrosion rate is very low, and the overall corrosion rate tends to decrease. When the current is applied, the average corrosion rate of cast iron in

tap water was higher than the corrosion rate of cast iron in high-concentration solutions. The maximum value of the average corrosion rate of cast iron in tap water reached 17 g.(m^{-2}.d^{-1}), while the maximum value in high-concentration solutions was 0.33 g.(m^{-2}.d^{-1}). However, due to the poor conductivity of deionized water, the corrosion rate in deionized water (0 mg.L^{-1}) is not significantly reduced, and the cathodic protection is not obvious.

As shown in Fig. 9, under tap water conditions, the degree of protection of the protected cast iron in the first two days was not ideal, the degree of protection was 60% and 78.2% respectively. While in a sodium chloride solution system with a protective current applied, the cast iron is well protected, especially at high concentrations (1000 mg.L^{-1}, 500 mg.L^{-1}). When the conductivity of the solution increases, the protection current also increases, and the degree of protection is over 99.3%. Therefore, from the perspective of the corrosion rate and degree of protection of cast iron, piezoelectric materials are more suitable for corrosion protection of cast iron in high-concentration solutions. Meanwhile, the daily electricity consumption is relatively stable. The power consumption is roughly positively correlated with the concentration of the solution. The corrosion rate of cast iron is also positively correlated with the solution concentration. Given that the protection degree can reach 100% at high concentrations, the cathodic protection effect is obvious. Therefore, from the perspective of anti-corrosion, it is advisable to try to control the lower concentration of sodium chloride without using a protection device. In the case of protection, the sodium chloride concentration is controlled at about 500 mg.L^{-1}, and the power consumption is 25% to 50% lower than that of the 1000 mg.L^{-1} solution, while the minimum power consumption is 2301.41 mW•h. This means that the system can save electricity and achieve a good anti-corrosion effect.

By visually comparing Fig. 10 (a~d) and (e~h) and using Image-Pro Plus software to analyze the SEM images, the proportion of the corrosion area can be obtained, defined as the degree of corrosion (Table 2). It can be seen from Fig. 10 that at 500 mg.L^{-1} without protection, the corrosion morphology is very detailed. So the scale was positioned to 10 μm. According to the actual situation at that time, the magnification was appropriately increased to better show the appearance of cast iron corrosion. Whether in the tap water solution or the sodium chloride solution, the corrosion of the cast iron without the protective device is serious, and the surface has obvious dense corrosion pits, and the products of corrosion can be clearly seen after the magnification. The corrosion degree of cast iron in tap water is 37.04%, the diameter of the corrosion pit is about 140 μm, and the corrosion degree of cast iron in sodium chloride solution is 50.72%. After the protection device is added, although certain corrosion occurs, the corrosion degree of cast iron in the tap water is 19.70%, and the corrosion degree of the cast iron in the sodium chloride solution is 22.86%. The corrosion condition is greatly improved compared to the results obtained

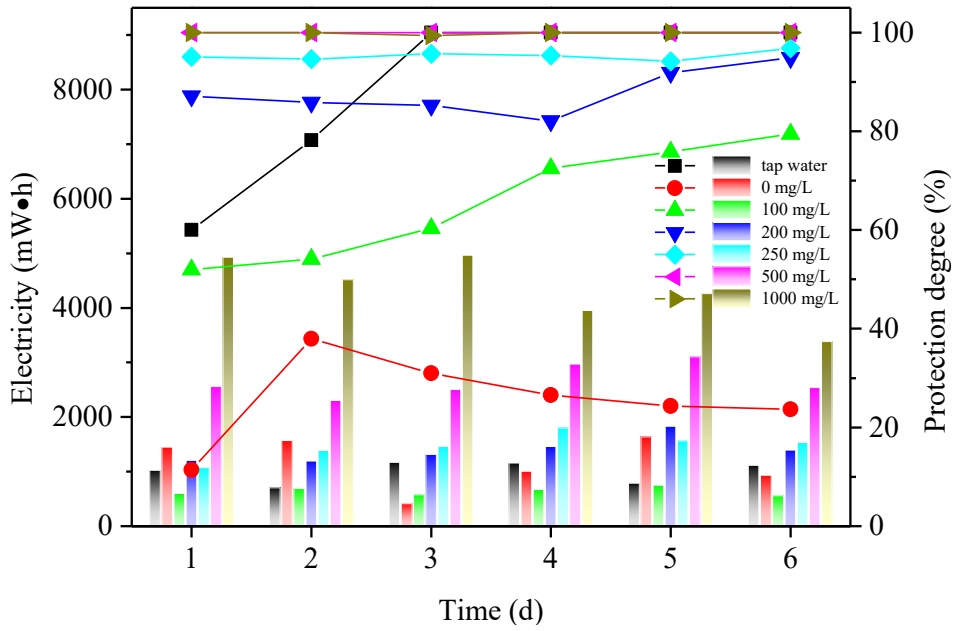

Fig. 9: Under the protection device, the changes in protection degree and power consumption of cast iron under different sodium chloride concentrations.

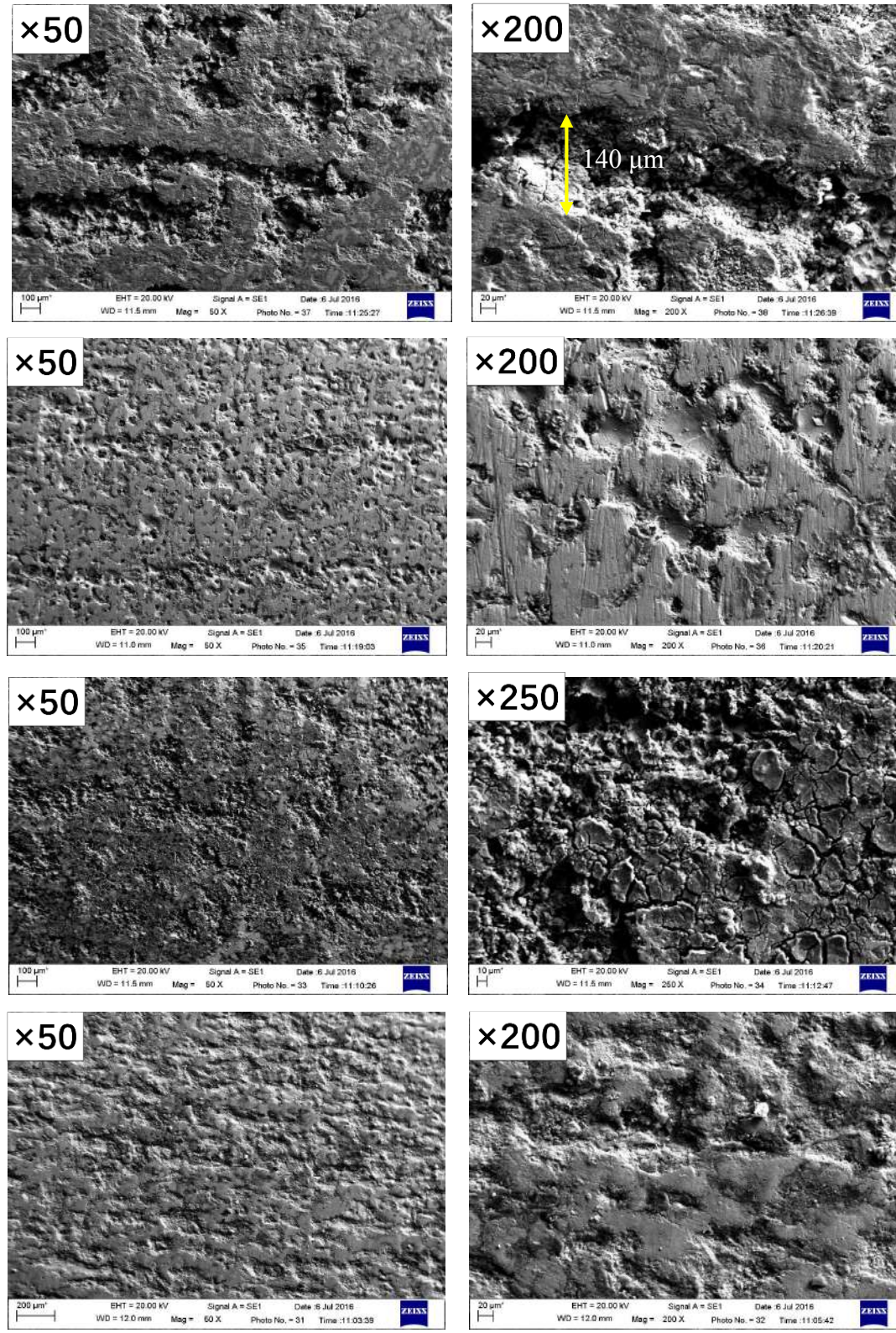

Fig. 10: SEM image of cast iron in different concentrations of sodium chloride solution, at 50, 200, or 250 times magnification.

Table 2: Cast iron corrosion degree table (data from images at 50 times magnification).

Solution condition	Tap water no protection	Tap water protection	500 mg.L^{-1} no protection	500 mg.L^{-1} protection
Corrosion degree (%)	37.04	19.70	50.72	22.86

without the use of the protection device. This shows that the protection device greatly improves the corrosion protection of cast iron. Without the protection device, the corrosion of cast iron in 500 mg.L^{-1}, sodium chloride solution is very high, the corrosion pit is dense, and the surface is very rough. Its corrosion degree to cast iron (50.72%) is stronger than that of tap water (37.04%), which corresponds to the conclusion of Fig. 8.

Effect of Sodium Sulfate Concentration

This experiment also explored the effect of sulfate ions on the corrosion of cast iron.

From Fig. 11, in the experimental sodium sulfate environment systems, the average corrosion rate is below 80 g.(m^2•d). The corrosion rate drops first and then increases in the solution of 200 mg.L^{-1} concentration of sodium sulfate. At other concentrations, the corrosion rate increases first, then decreases and then increases again. When the concentration of sodium sulfate is 0 mg.L^{-1}, the average rate of corrosion of cast iron is lower than the average value. At a concentration of 100 mg.L^{-1}, the average rate on the third day and after is below the average. Among all tested concentrations, cast iron has the fastest corrosion rate in a 500 mg.L^{-1} solution. This indicates that the increase of SO2- 4 concentration will accelerate the release of iron and promote the corrosion of cast iron (Hu et al. 2018, Yang et al. 2014). Comparingly, after the current is applied, the average corrosion rate of cast iron is greatly controlled in the sodium sulfate environment systems. Deionized water poses an exception, since the electrical conductivity is poor and the protection current is small, the corrosion rate is still large after the current is applied. The cast iron in other concentrations did not corrode in the first four days, while it was slightly corroded at 100 mg.L^{-1} and 500 mg.L^{-1} after four days, and the maximum rate on the sixth day was 1 g.(m^{-2}.d^{-1}) and 7.9 g.(m^{-2}.d^{-1}), respectively.

From Fig. 12, cast iron is well protected in a sodium sulfate solution with a protective current. For the concentrations of 200 mg.L^{-1}, 250 mg.L^{-1}, and 1000 mg.L^{-1} solution, the protection can reach 100%. In the solutions with concentrations of 500 mg.L^{-1} and 100 mg.L^{-1}, some corrosion began to appear after the 4th and 5th days, however, the degree of protection was still above 88.4%. In the deionized water system, the degree of protection is poor. The power consumption decreases first and then increase with the experiment time. The 200 mg.L^{-1} and 250 mg.L^{-1} solutions consume a large amount of electricity, while the 1000 mg.L^{-1} solution

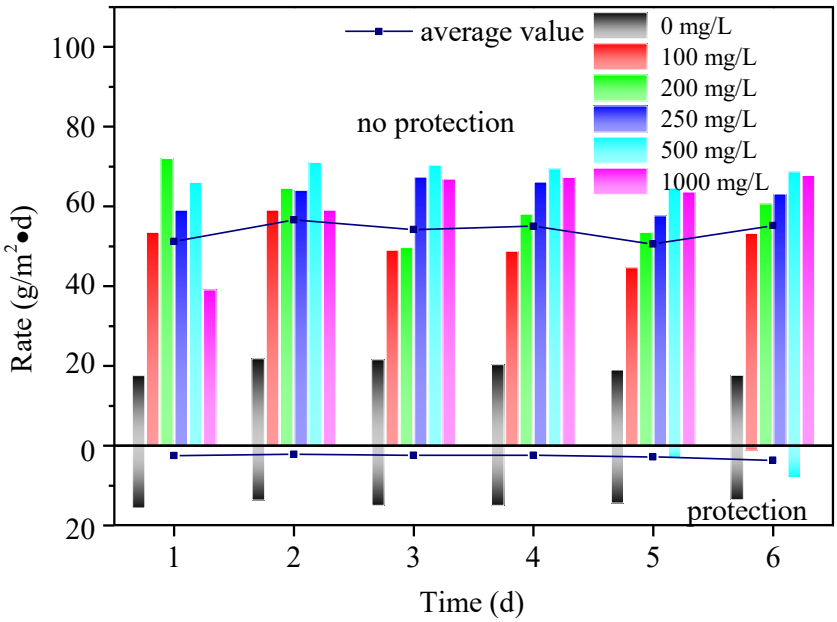

Fig. 11: Average rate change of cast iron under different sulfate ion concentrations.

consumes less power (390.70 mW•h), which is 5% to 90% lower than the other two solutions. The cast-iron protection of these three solution systems can reach 100%. Therefore, it is advisable to control the solution at a low concentration of about 100 mg.L^{-1} without protection. In the case of protection, the solution concentration should be controlled at about 1000 mg.L^{-1}.

By visually comparing Fig. 13 (a-d), and using Image-Pro Plus software to analyze the SEM image, the proportion of corrosion area is obtained, which is the corrosion degree (Table 3). Being under the protection of the device and being unprotected by the device have little effect on the corrosion of cast iron in deionized water, where the corrosion degree is between 60% and 70%. This is mainly due to the conductivity of deionized water being poor and not meeting the needs of cathodic protection. Comparing Fig. 13 (e~h), it can be observed that the corrosion without protective current is very evident: the surface has obvious corrosion products, and the corrosion degree is 73.71%. While under the protection current, the cast iron is slightly corroded, its surface is smooth, and the corrosion degree is 22.10%. This demonstrates that the protection device can greatly improve the corrosion protection of cast iron.

CONCLUSIONS

In this study, the corrosion behavior of cast iron in different environmental systems was studied with and without protective current, and the influencing factors were analyzed. The results show that during the protection of cast iron, when the cast iron is protected by electricity, in a neutral (pH=7) environment, the ammonium nitrate concentration is 200 mg.L^{-1}, the sodium chloride concentration is 500 mg.L^{-1}, or the sodium sulfate concentration is 1000 mg.L^{-1} and the protection can reach 100%, with the double effect of complete protection and power saving. In this study, a cathodic protection method similar to an applied current is used. That is, a protected metal is used as a cathode, and a piezoelectric anticorrosive sheet acting as an external power source is continuously vibrated to supply electrons to the cast iron sheet so that the cathode is always in an electron excess state. Only the reduction reaction occurs on the surface so that the corrosion of cast iron is suppressed. This pipeline anticorrosion method does not require external chemicals, it has better environmental protection characteristics, and has a demonstrable protective effect on the environment. The PVDF piezoelectric film has a low production cost and is easy to process. When put into use, it plays a protective role

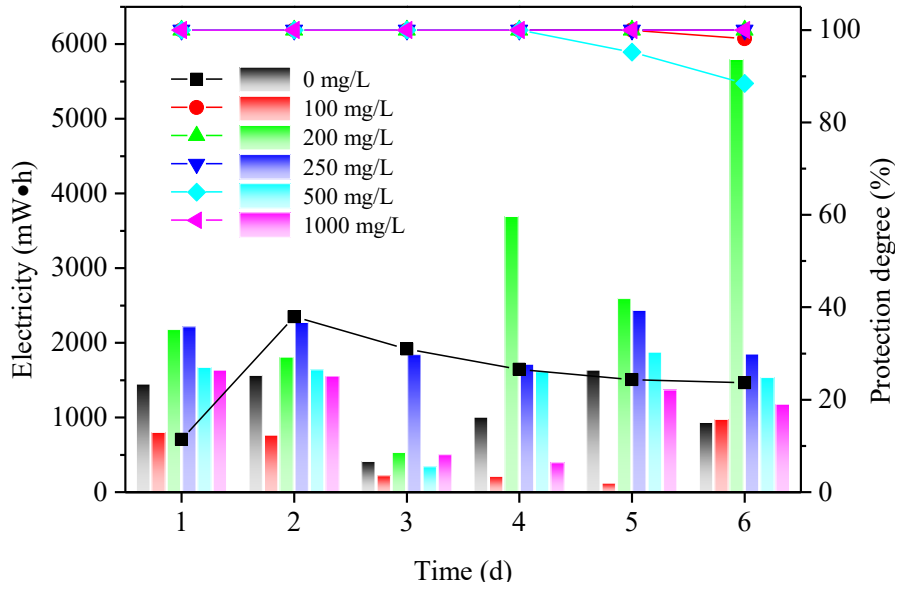

Fig. 12: Under the protection device, the changes in protection degree and power consumption of cast iron under different sodium sulfate concentrations.

Table 3: Cast iron corrosion degree table (data from images at 50 times magnification).

Solution condition	Deionized water no protection	Deionized water no protection	500 mg.L^{-1} no protection	500 mg.L^{-1} Protection
Corrosion degree (%)	63.41	66.37	73.71	22.10

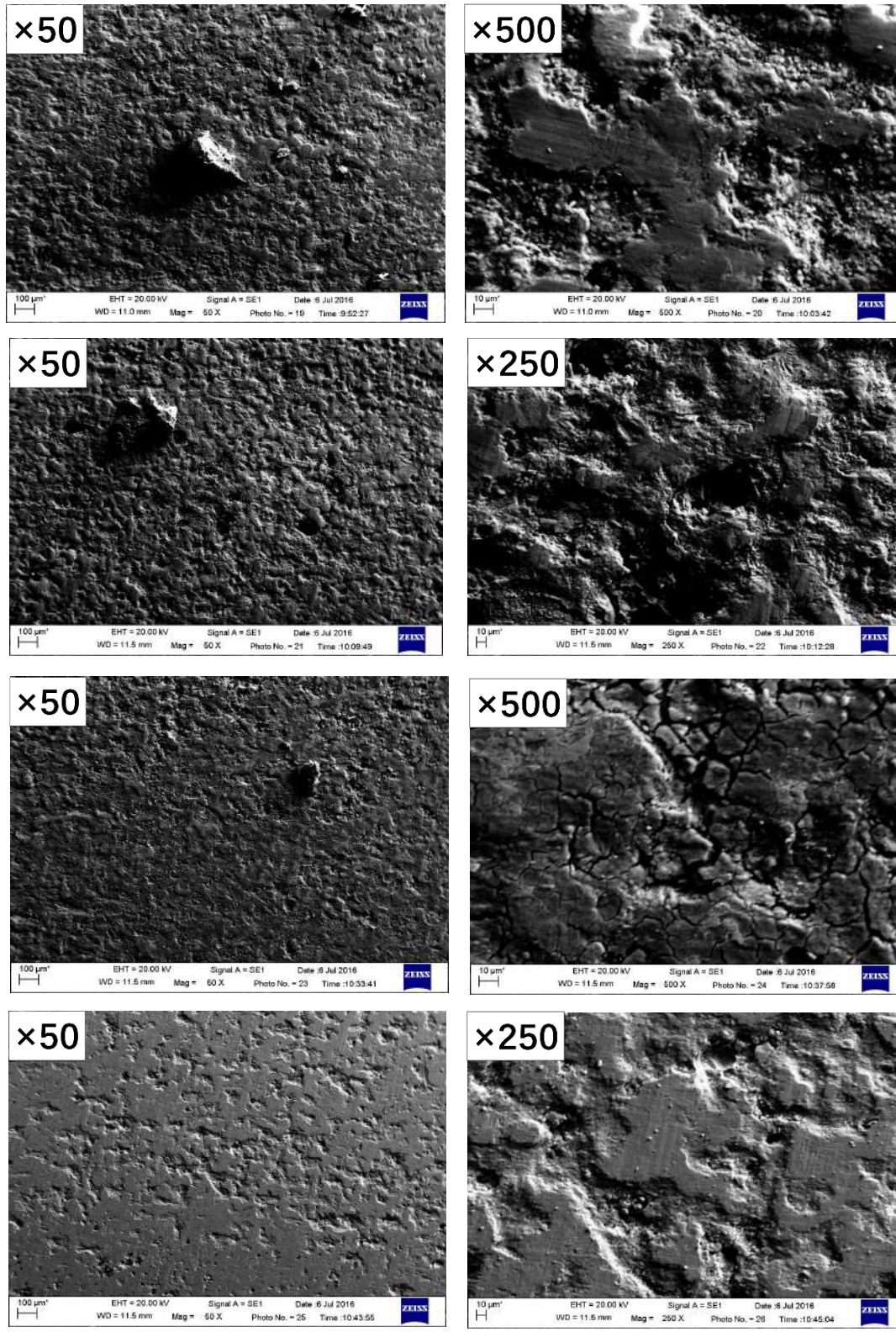

Fig. 13: SEM image of corrosion of cast iron in different concentrations of sodium sulfate solution, at 50, 250, or 500 times magnification.

on the pipeline, saves the cost of pipeline replacement, and has good economic benefits. The combination of this new material and traditional technology has advantages such as it is environment-friendly, conserves energy, has economic efficiency, and will certainly contribute to China's pipeline anti-corrosion process in the future.

ACKNOWLEDGEMENTS

This work was financially supported by the Research and Application of Piezoelectric Materials In Soil Remediation (04140007). The author would like to appreciate the support from the Brook Byers Institute for Sustainable Systems, the Hightower Chair, and the Georgia Research Alliance at Georgia Institute of Technology.

REFERENCES

Butt, Z., Pasha, R.A., Qayyum, F., Anjum, Z., Ahmad, N. and Elahi, H. 2016. Generation of electrical energy using lead zirconate titanate (PZT-5A) piezoelectric material: Analytical, numerical, and experimental verifications. J. Mech. Sci. Technol., 30: 3553-3558.

Chen, B., Li, H., Tian, W. and Zhou, C. 2019. PZT based piezoelectric sensor for structural monitoring. J. Electron. Mater., 1-8.

Dineva, P., Gross, D., Müller, R. and Rangelov, T. (eds) 2014. Dynamic Fracture of Piezoelectric Materials: Solution of Time-Harmonic Problems via BIEM. Springer International Publishing, USA, pp 7-32.

Duan, L. and Xing, J. 2015. Talking about the research status and development trend of piezoelectric materials. Shandong Ind. Technol., 271.

Hu, J., Dong, H., Xu, Q., Ling, W., Qu, J. and Qiang, Z. 2018. Impacts of water quality on the corrosion of cast iron pipes for water distribution and proposed source water switch strategy. Water Res., 129: 428-435.

Joseph, J., Singh, S.G. and Vanjari, S.R.K. 2018. Piezoelectric micromachined ultrasonic transducer using silk piezoelectric thin film. IEEE Electr. Device L.,5: 1-1.

Kim, H.S., Kim, J.H. and Kim, J. 2011. A review of piezoelectric energy harvesting based on vibration. Int. J. Precis. Eng. Man., 12: 1129-1141.

Li, M., Liu, Z., Chen, Y. and Hai, Y. 2016. Characteristics of iron corrosion scales and water-quality variations in drinking water distribution systems of different pipe materials. Water Res., 106: 593-603.

Li, Q. Research progress in piezoelectric materials used to design filters. In: 2009 Symposium on Piezoelectricity, Acoustic Waves, and Device Applications (SPAWDA 2009), 2009. IEEE, pp 11-11.

Loto, C.A., Loto, R.T. and Popoola, A.P. 2019. Performance evaluation of zinc anodes for cathodic protection of mild steel corrosion in HCL. Chem. Data Collect., 24: 100280.

McNeill, L.S. and Edwards, M. 2002. The importance of temperature in assessing iron pipe corrosion in water distribution systems. Environ. Monit. Assess., 77: 229-242.

Meng, C. and Wang, Y. 2016. The research of the cathodic protection corrosion for transmission station pipeline. Shandong Chem. Ind., 45: 75-77.

Ramatlo, D.A., Wilke, D.N. and Loveday, P.W. 2018. Development of an optimal piezoelectric transducer to excite guided waves in a rail web. NDT. E. Int., 95: 72-81.

Ribeiro, C., Sencadas, V., Ribelles, J.L.G. and Lanceros-Méndez, S. 2010. Influence of processing conditions on polymorphism and nanofiber morphology of electroactive poly(vinylidene fluoride) electrospun membranes. Soft Mater., 8: 274-287.

Sarin, P., Snoeyink, V., Bebee, J., Jim, K., Beckett, M., Kriven, W. and Clement, J. 2004. Iron release from corroded iron pipes in drinking water distribution systems: Effect of dissolved oxygen. Water Res., 38: 1259-1269.

Slaimana, Q.J. and Hasan, B. O. 2010. Study on the corrosion rate of carbon steel pipe under turbulent flow conditions. Can. J. Chem. Eng., 88: 1114-1120.

Sun, H., Shi, B., Lytle, D.A., Bai, Y. and Wang, D. 2014. Formation and release behavior of iron corrosion products under the influence of bacterial communities in a simulated water distribution system. Environ. Sci.: Processes Impacts, 16: 576-585.

Tang, E., Wang, L. and Han, Y. 2019. Space debris positioning based on two-dimensional PVDF piezoelectric film sensor. Adv. Space Res., 63(8): 2410-2421.

Wang, D. and Chen, J. 2016. Progress on the applications of piezoelectric materials in sensors. Mater. Sci. Forum, 848: 749-756.

Wang, R. and Ma, F. 2009. Discussion on corrosion and prevention of urban water supply pipeline. Sci. Technol. Inform., 51: 66-91.

Xu, X., Cao, D., Yang, H. and He, M. 2018. Application of piezoelectric transducer in energy harvesting in the pavement. Int. J. Pavement Res. Technol., 11: 388-395.

Yang, F., Shi, B., Bai, Y., Sun, H., Lytle, D.A. and Wang, D. 2014. Effect of sulfate on the transformation of corrosion scale composition and bacterial community in cast iron water distribution pipes. Water Res., 59: 46-57.

Yang, X., Jiang, H., Song, W., Wang, R., Sun, S. and Jia, R. 2017. Study on the influence of water quality change on iron release in a water supply network of a city and its control effect. J. China Urban Water Assoc., 38-43.

Yang, Y., Tang, H., Gu, L., Wang, H., Zhang, T. and Li, C. 2018. Influence factors of initial internal corrosion of grey cast iron pipes in the water distribution system. China Water & Wastewater, 34: 49-54.

Zhang, G., Li, B., Liu, J., Luan, M., Yue, L., Jiang, X., Yu, K. and Guan, Y. 2018. The bacterial community significantly promotes cast iron corrosion in reclaimed wastewater distribution systems. Microbiome, 6: 222.

Zhang, L., Yan, C., Rtimi, S. and Bandara, J. 2019. Piezoelectric materials for catalytic/photocatalytic removal of pollutants: Recent advances and outlook. Appl. Catal. B: Environ., 241: 256-269.

Zhang, Y. and Edwards, M. 2007. Anticipating effects of water quality changes on iron corrosion and red water. J. Water Supply Res. Technol.-AQUA, 56: 55-68.

Zhao, Z., Li, J.Q., Yuan, X., Li, X., Zhang, Y. and Sheng, J. 2005. Preparation and properties of electrospun poly (vinylidene fluoride) membranes. J. Appl. Polym. Sci., 97: 466-474.

Zhu, Y., Sun, F., Qian, H., Wang, H., Mu, L. and Zhu, J. 2018. A biomimetic spherical cactus superhydrophobic coating with durable and multiple anti-corrosion effects. Chem. Eng. J., 338: 670-679.

Nature Environment and Pollution Technology
An International Quarterly Scientific Journal

p-ISSN: 0972-6268
(Print copies up to 2016)
e-ISSN: 2395-3454

Vol. 20 | No.3 | pp. 955-972 | 2021

Original Research Paper

https://doi.org/10.46488/NEPT.2021.v20i03.004

Open Access Journal

The Increasing Trend of Black Carbon and Organic Carbon in Jordan During the Period of 2007 to 2018

K. M. Hamasha*†
*Department of Physics, Yarmouk University, Jordan
†Corresponding author: K.M. Hamasha; khamasha@yu.edu.jo

Nat. Env. & Poll. Tech.
Website: www.neptjournal.com

Received: 22-09-2020
Revised: 01-12-2020
Accepted: 08-12-2020

Key Words:
Black carbon
Organic carbon
Extinction
Scattering

ABSTRACT

During the last decades, carbonaceous aerosol extinctions such as black carbon and organic carbon extinctions exhibit an increasing trend across the globe. Measurements of carbonaceous aerosol in Jordan were done using satellite data during the period 2007 to 2018. These measurements were done in four locations of Jordan - Irbid in the north, Amman and Az-Zarqa in the middle, and Ma'an in the south. Black carbon extinction in Jordan increased slightly (slope = 0.0001) during this period, while organic carbon extinction increased slightly (slope = (0.7 – 10) $x10^{-5}$) in three locations and decreased slightly in one location (Irbid location (slope = $-2x10^{-5}$)). Organic carbon extinction measurements were greater than black carbon extinction measurements in all locations with varying ratios depending on the location of the measurements. Black carbon and organic carbon scattering measurements have the same behavior as extinction, with larger values in the north and smaller values in the south. Scattering values of organic carbon are larger than black carbon scattering values. Scattering values of organic carbon increased slightly in all locations (slope = 0.0001) while scattering values of black carbon decreased in three locations (Irbid, Amman, and Ma'an) and increased in one location (Az-Zarqa). Column mass density and surface mass concentration measurements show that organic carbon had larger values than black carbon in all locations besides that both organic carbon and black carbon had values decreasing when we go from north to south.

INTRODUCTION

Atmospheric aerosols have a significant impact on regional air pollution as well as on the radiation budget. Atmospheric aerosols directly affect the earth's radiative balance and climate by absorbing and scattering solar and thermal radiation (Myhre et al. 2013). Thus, in contrast to the greenhouse gases which only cause warming, atmospheric aerosols, depending on their properties, can cause either cooling or warming of the atmosphere (IPCC 2018). Aerosols also can indirectly affect the Earth's radiation balance and climate by changing the microphysical properties of clouds and their lifetimes, thereby modifying the precipitation regime (Zhanqing et al. 2017). Aerosols play a major role in atmospheric chemistry and hence affect the concentrations of the other minor atmospheric constituents like ozone (MacKenzie et al. 2011). Furthermore, aerosols have adverse effects on human health, and a strong relationship between aerosol concentration and human mortality and morbidity has been observed (Hime et al. 2018). Aerosols also have adverse effects on environmental quality including visibility (Lung et al. 2016).

Both the aerosol geographical and temporal distributions are very variable due to the short lifetime of particles in conjunction with various, not uniformly distributed sources and different extinction strengths. Additionally, particle transformations during transport as well as removal processes contribute to the observed variability. Hence, it is important to monitor the physical, chemical, and radiative properties of aerosol at a wide range of sites around the globe to build up a comprehensive picture of aerosols and their environmental impacts.

Carbonaceous aerosols are black carbon and organic carbon (McDonald et al. 2015). Black carbon (BC), often called soot, is composed of pure carbon clusters. BC is one of the most important absorbing aerosol species in the atmosphere. Organic carbon (OC) is clustered or aggregated organic molecules.

In Jordan few studies have been conducted to monitor the optical (Hamasha 2010, Hamasha and Arnott 2010, Hamasha et al. 2015) and physical properties of aerosol particles in Jordan (Huessien et al. 2011); still, there is a lack of information about this topic which has persuaded us to initiate this study.

In this study measurements of black carbon mass density, black carbon extinction at 550nm, black carbon scattering at 550 nm, black carbon surface mass concentration, organic carbon mass density, organic carbon extinction at 550 nm,

organic carbon scattering at 550 nm, and organic carbon surface mass concentration were recorded using satellite maps at four different sites in Jordan; Irbid in the North, Amman and Az-Zarqa in the middle, and Ma'an in the south for the period 2007 – 2018. Satellite maps were produced with the Giovanni online data system, developed and maintained by the NASA GES DISC.

MATERIALS AND METHODS

Black Carbon (BC) is one of the primary constituent components of atmospheric aerosols. Black carbon aerosols are highly absorbing, and an important factor in radiative forcing, radiative transfer, and pollution.

Organic carbon (OC) may refer to carbon in the atmosphere or ocean and refers to airborne chemical species with a biological origin (Mok et al. 2016) other than methane (CH_4), carbon monoxide (CO), or carbon dioxide (CO_2). Atmospheric OC is primarily an aerosol and has applications in pollution and radiative transfer.

This study on BC and OC is conducted in Jordan through measurements of extinction aerosol optical thickness (AOT) at 550 nm, scattering AOT at 550 nm, column mass density, and surface mass concentrations. BC and OC data was recorded from satellite using Giovanni online data system, developed and maintained by the NASA GES DISC during the period from 2007 to 2018 at four locations in Jordan.

Satellite remote sensing and model data play an important role in research and applications of tropical meteorology and climatology. Since the first weather satellite was launched by NASA in 1960, a large collection of NASA's Earth science data is freely available to the research and application communities around the world, significantly improving our overall understanding of the Earth system and environment. Established in the mid-1980s, the NASA Goddard Earth Sciences Data and Information Services Center (GES DISC) is a data archive center for multidisciplinary, satellite, and model assimilation data products (Liu et al. 2020). GES DISC hosts several important NASA satellite missions for tropical meteorology and climatology. Over the years, GES DISC has developed data services to facilitate data discovery, access, distribution, analysis, and visualization, including Giovanni. Giovanni is an online analysis and visualization tool without the need to download data and software (Acker & Leptoukh 2007). Using the Giovanni user interface, it is possible to easily find and display selected data on various types of plots. At the top of the interface are menus for the various kinds of visualizations available in Giovanni. The default visualization is a time-averaged map. The time-averaged map shows data values for each grid cell within the user-specified area, averaged over the user-specified time range as a map layer. Fill values do not contribute to the time average value. The generated map can be zoomed in and panned. Plot options include setting minimum and maximum values for the color scale and in some cases selecting other palettes.

The social and economic development in Jordan has been accompanied by an increase in the consumption of oil for different needs, including residential, commercial, industrial, transportation, and power generation. Combustion of oil and other fossil fuel is recognized as a major source of air pollution in urban areas. Several airborne substances can remain in the atmosphere for weeks, and travel over hundreds of kilometers, making air pollution a global problem. Measurements of black carbon light absorption coefficients (B_{abs}) using the photoacoustic instrument at the wavelength of 870 nm in different locations of Jordan show that B_{abs} is higher for the locations in the city centers than the locations in the industrial centers during summer 2007 (Hamasha et al. 2010). Low black carbon concentrations in the vicinity of industrial zones are attributed to the efficiency of tall stacks in reducing ground-level concentrations of emitted substances.

The study locations in Jordan (maps) are Irbid, Amman, Az-Zarqa, and Ma'an (Fig. 1). Irbid city (32^o 33' N, 35^o 51' E) is situated in the north of Jordan, in a fertile plateau, with an average elevation of 620 m. The city has a population of about 2 Million. Irbid is located about 70 km north of the capital city Amman and approximately 20 km south of the Syrian border. It has a hot-summer Mediterranean climate. Summers are hot on days with warm nights while winters are cool and wet with two snowy days on average. Rain averages about 500 mm a year.

Amman (31^{o}57' N, 35^{o}56' E) is the capital and most populous city of Jordan, situated in north-central Jordan. The city has a population of about 4.3 Million, and elevation ranged between 700 m – 1100 m. Originally, the city had been built on seven hills. Amman's position on the mountains near the Mediterranean climate zone places it under the semi-arid climate classification. Rain averages about 300 mm a year and periodic droughts are common, where most rain falls between October and April.

Az-Zarqa (32^{o}5' N, 36^{o}6' E) is located on the Az-Zarqa River basin in northeast Jordan. The city is situated 24 km northeast of Amman. Az-Zarqa has a cold semi-arid climate. The average annual temperature is 17.4°C, and around 182 mm of precipitation falls annually, mostly in the winter months.

Ma'an (30^{o}11' N, 35^{o}44' E) is a city in southern Jordan, 218 km southwest of the capital Amman. Ma'an has a cold desert climate, with hot summers and mild to cold winters due to its high altitude (above 1000 meters). Rainfall is extremely rare with an average of 44 mm a year only.

Fig. 1: Map of Jordan.

RESULTS AND DISCUSSION

Black Carbon Extinction AOT at 550 nm

Black carbon extinction AOT at 550 nm data was collected from Giovanni online data system satellite maps at four locations from Jordan - Irbid in the north, Amman and Az-Zarqa in the middle, and Ma'an in the south.

Fig. 2 shows yearly averaged BC extinction AOT at 550 nm. BC extinction values for all data, from greatest, were in Irbid, Amman, Az-Zarqa, and then Ma'an. Irbid and Amman had very close data, while Ma'an had faraway data from them. Ma'an has a very large area most of it desert with a low population compared with the other cities. Irbid has the largest BC extinction because of the many sources of BC in

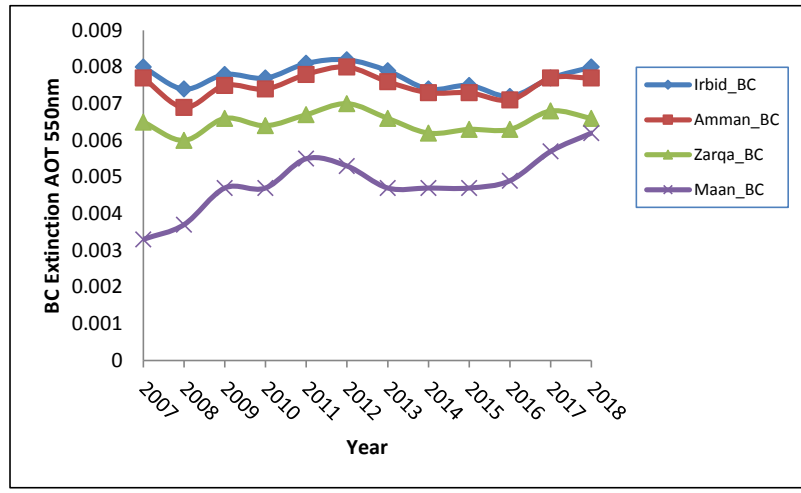

Fig. 2: Average black carbon extinction AOT at 550 nm for the period from 2007 to 2018 in Irbid, Amman, Az-Zarqa, and Ma'an locations.

the city and its location close to the border of Syria and Israel. Irbid, Amman, and Az-Zarqa had the largest average value of BC extinction in 2012, while Ma'an had the largest average value of BC extinction in 2018. Data for Irbid, Amman, and Az-Zarqa have the same behavior up and down. For Ma'an, BC extinction goes up from 2007 to 2011 then went down in 2013 and became stable in 2015 then kept going up till 2018. The reason for the increase in black carbon levels in 2012 is due to the Syrian civil war, as Syria is adjacent to the northern Jordanian border and close to central Jordan.

Organic Carbon Extinction AOT at 550 nm

Organic carbon extinction AOT at 550 nm data was collected from Giovanni online data system satellite maps at four locations from Jordan - Irbid in the north, Amman in the and Az-Zarqa in the middle, and Ma'an in the south.

Fig. 3 shows yearly averaged OC extinction AOT at 550 nm. For all data, Irbid had the largest OC extinction values and Ma'an had the lowest values. Ma'an has a very large area most of it desert with a low population compared with the other cities. Irbid has the largest OC extinction because of the many sources of OC in the city. Agricultural pollutants and livestock are the most important sources of organic carbon, which are abundant in an agricultural region such as Irbid.

All of the cities had the largest average value of OC extinction in 2017, and the lowest values of OC extinction in 2008. Data for Irbid, Amman, Az-Zarqa, and Ma'an have the same behavior fluctuations up and down.

Black Carbon and Organic Carbon Extinction AOT at 550 nm

Figs. 4-7 show the comparison of extinction AOT at 550

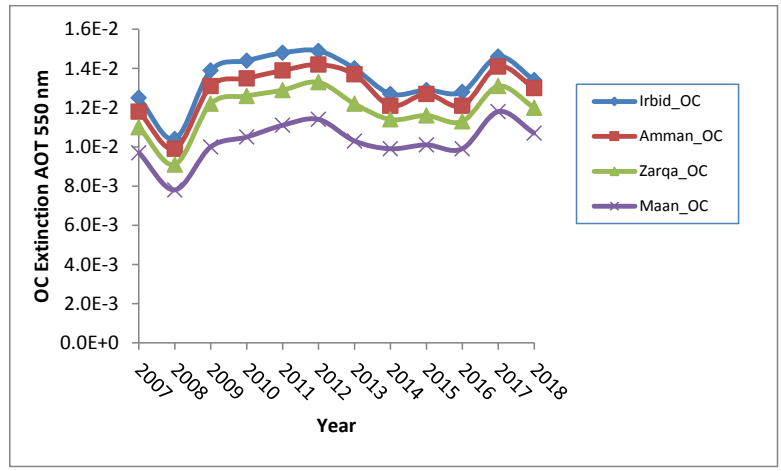

Fig. 3: Average organic carbon extinction AOT at 550 nm for the period from 2007 to 2018 in Irbid, Amman, Az-Zarqa, and Ma'an locations.

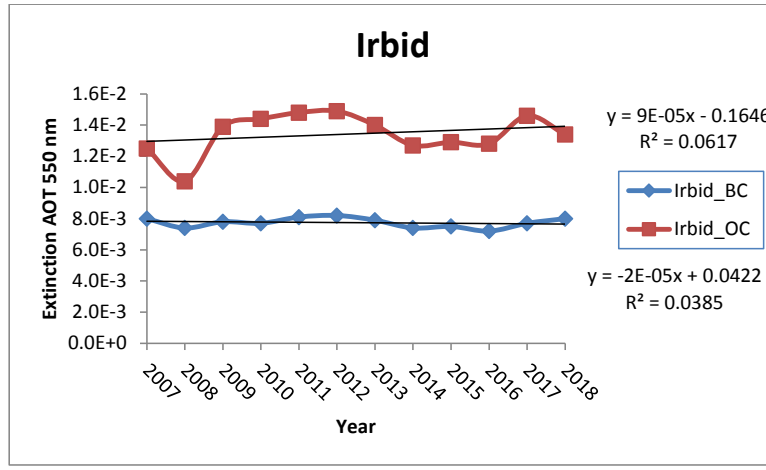

Fig. 4: Average extinction AOT at 550 nm for black carbon and organic carbon during the period from 2007 to 2018 in Irbid city.

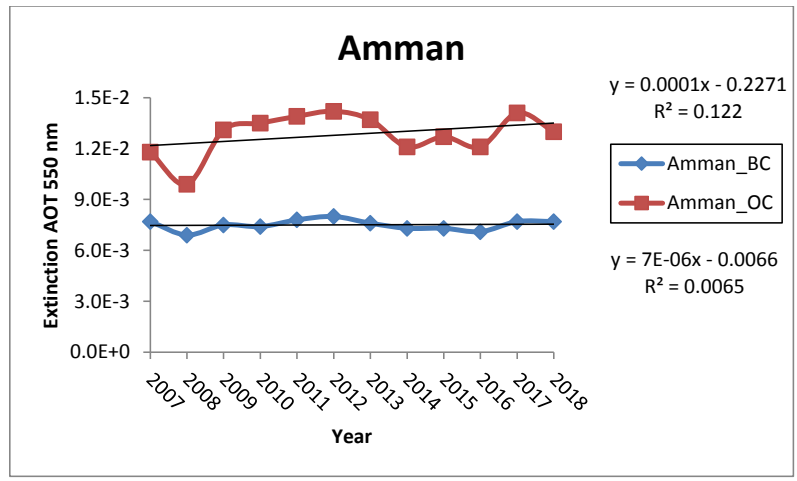

Fig. 5: Average extinction AOT at 550 nm for black carbon and organic carbon during the period from 2007 to 2018 in Amman city.

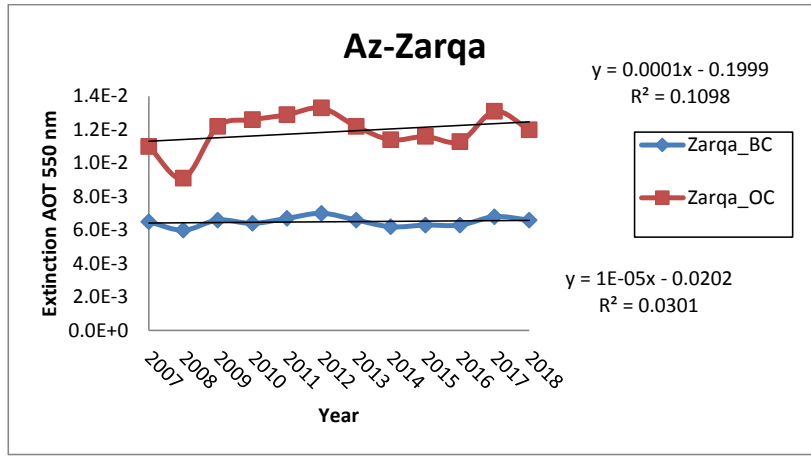

Fig. 6: Average extinction AOT at 550 nm for black carbon and organic carbon during the period from 2007 to 2018 in Az-Zarqa city.

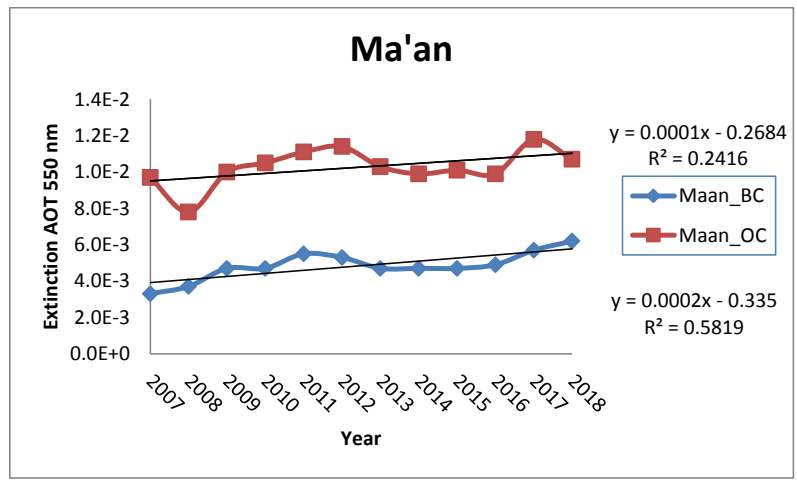

Fig. 7: Average extinction AOT at 550 nm for black carbon and organic carbon during the period from 2007 to 2018 in Ma'an city.

nm between BC and OC for the four locations during the period from 2007 to 2018. From Fig 4-7, for the yearly average extinction, OC is greater than BC in all four cities. OC extinction in Jordan increased slightly (slope = 0.0001) during this period, while BC extinction increased slightly (slope = (0.7 – 10) $x10^{-5}$) in three locations and decreased slightly in one location (Irbid location (slope = $-2x10^{-5}$)).

Figs. 8-11 show the correlations between the yearly average extinction values of BC and OC in four cities. For Irbid city, the yearly average extinction value of OC is about 2.5 times that of BC. For Amman city, the yearly average extinction value of OC is about 3 times that of BC, and for Az-Zarqa city, the yearly average extinction value of OC is about 3.5 times that of BC. While that for Ma'an city is almost the same.

Black Carbon Scattering AOT at 550 nm

Black carbon scattering AOT at 550 nm data was collected from Giovanni's online data system satellite maps at four locations from Jordan - Irbid in the north, Amman and Az-

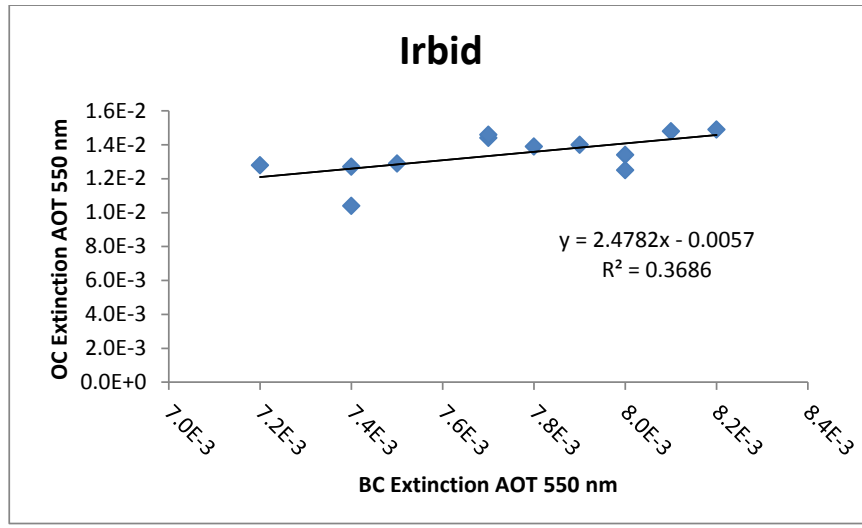

Fig. 8: Correlation between yearly average extinction value of black carbon and organic carbon in Irbid city.

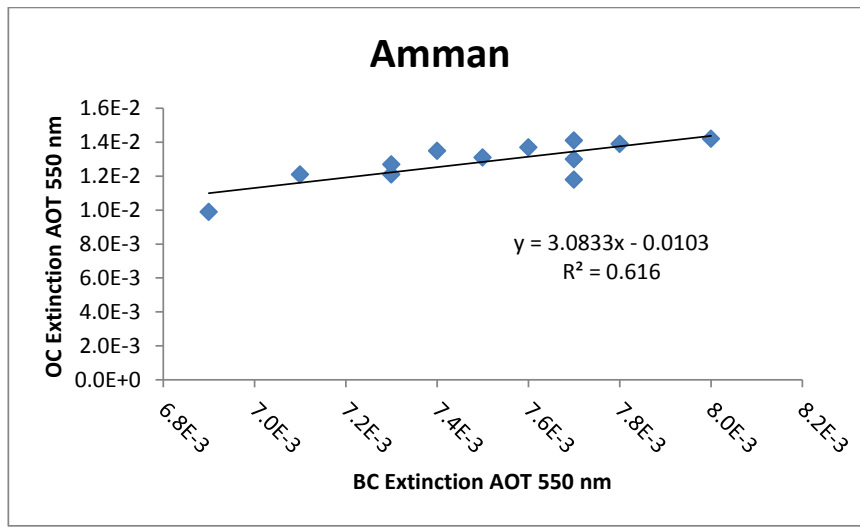

Fig. 9: Correlation between yearly average extinction value of black carbon and organic carbon in Amman city.

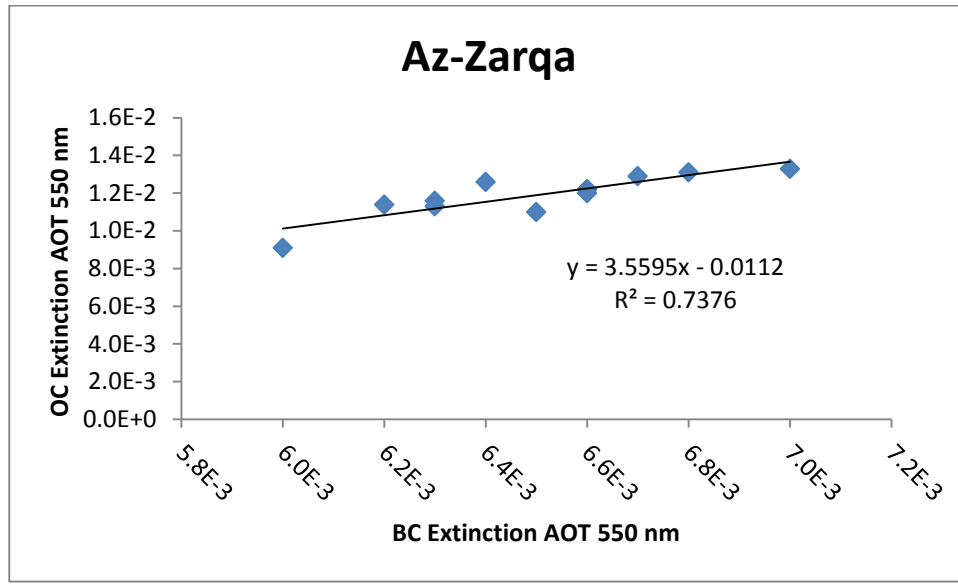

Fig. 10: Correlation between yearly average extinction value of black carbon and organic carbon in Az-Zarqa city.

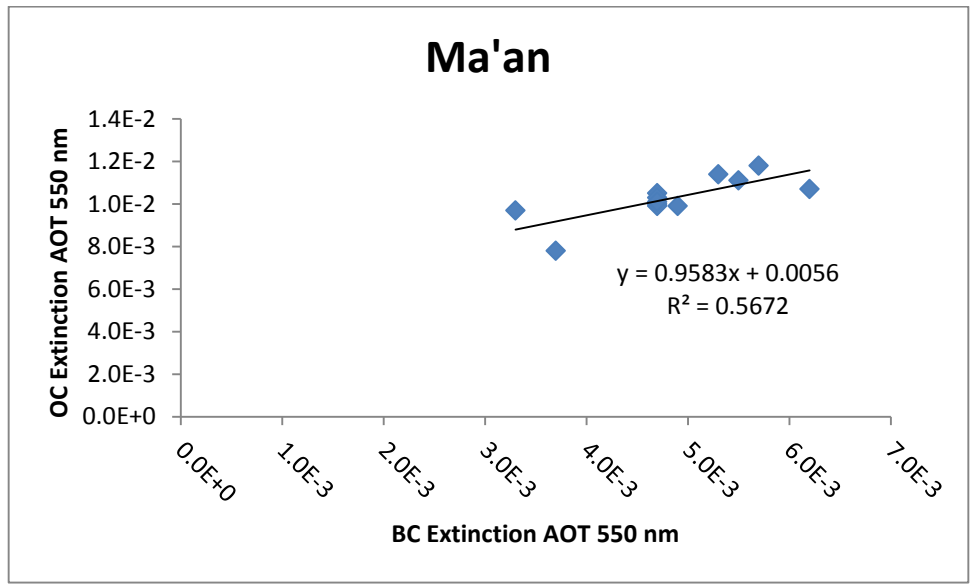

Fig. 11: Correlation between yearly average extinction value of black carbon and organic carbon in Ma'an city.

Zarqa in the middle, and Ma'an in the south. Fig. 12 shows the yearly average BC scattering AOT at 550 nm. For all data, Irbid had the greatest BC scattering values than Amman and Az-Zarqa, while Ma'an had the lowest value. Data were very close in Irbid and Amman. Ma'an has a very large area most of it desert with a low population compared with the other cities. Irbid has the largest BC scattering because of the many sources of BC in the city and its location close to the border of Syria and Israel.

Irbid's, Amman's, and Az-Zarqa's BC scattering values were almost constant, while Ma'an had a more fluctuating BC scattering, and had a maximum value in 2017.

Organic Carbon Scattering AOT at 550 nm

Fig. 13 shows the yearly averaged OC scattering AOT at 550 nm. For all data, Irbid had the greatest OC scattering values than Amman and Az-Zarqa, while Ma'an had the lowest

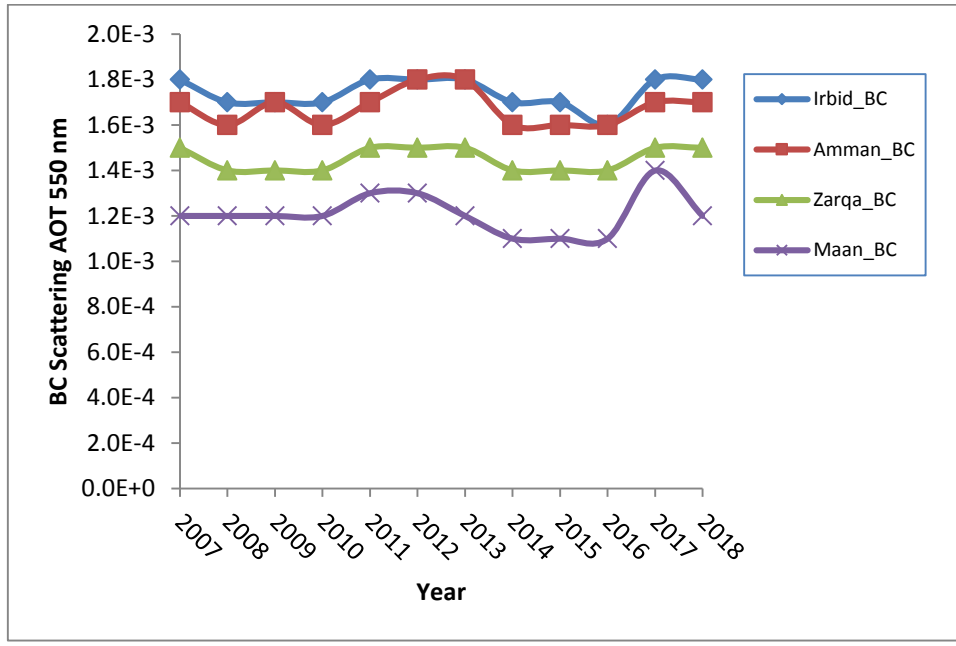

Fig. 12: Average black carbon scattering AOT at 550 nm for the period from 2007 to 2018 in Irbid, Amman, Az-Zarqa, and Ma'an locations.

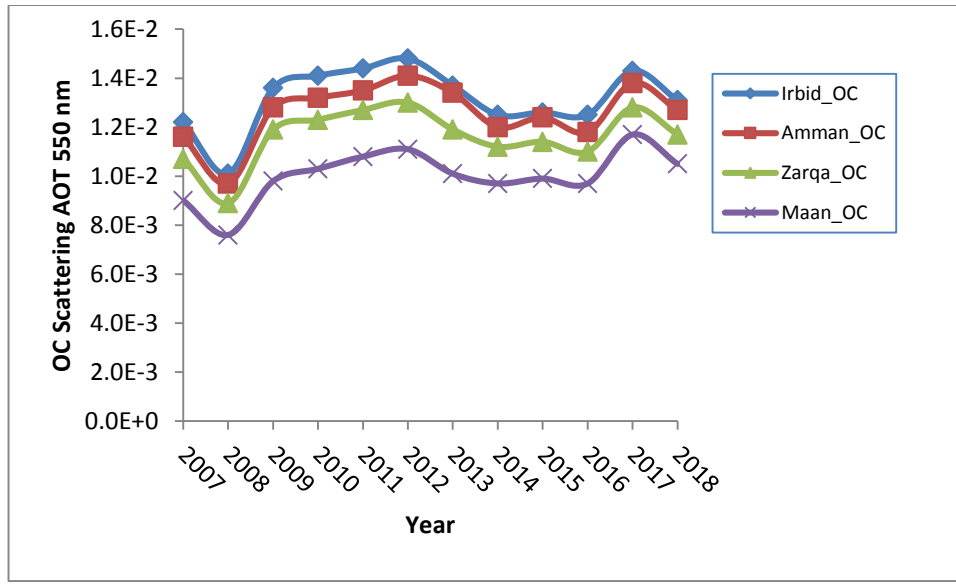

Fig. 13: Average organic carbon scattering AOT at 550 nm for the period from 2007 to 2018 in four locations from Jordan.

value. Ma'an has a very large area most of it desert with a low population compared with the other cities. Irbid has the largest OC scattering because of the many sources of OC in the city and its location close to the border of Syria and Israel.

All of the cities had the largest average value of OC scattering in 2017, and the lowest values of OC scattering in 2008. Data for Irbid, Amman, Az-Zarqa, and Ma'an show the same behavior fluctuations up and down.

BC and OC scattering measurements have the same behavior as extinction with larger values in the north and smaller values in the south. Scattering values of OC are larger than that of BC

Black Carbon and Organic Carbon Scattering AOT at 550 nm

Scattering values of OC increased slightly in all locations (slope = 0.0001) while scattering for BC decreased in three locations (Irbid, Amman, and Ma'an) and increased in the Az-Zarqa location (Figs. 14-17).

Comparison of scattering AOT at 550 nm between BC and OC for the four locations during the period from 2007 to 2018 shows that values of the yearly average scattering of OC are greater than that of BC in all four cities. Figs. 18-21 show the correlations between the yearly average scattering values of BC and OC in four cities. For Irbid city, the yearly average scattering value of OC is about 8.6 times that of BC. For Amman city, the yearly average scattering value of OC is about 9.8 times that of BC, and for Az-Zarqa city, the yearly average scattering value of OC is about 10.1 times that of BC. While in Ma'an city, the yearly average scattering value for OC is about 6.7 times that for BC.

Black Carbon Column Mass Density

Black carbon column mass density has values between 3×10^{-7} kg.m^{-2} and 8.5×10^{-7} kg.m^{-2} (Fig. 22). Irbid city has an average value of BC mass concentration of 7.8×10^{-7} kg.m^{-2}, while Amman, Az-Zarqa, and Ma'an have values of 6.7×10^{-7}

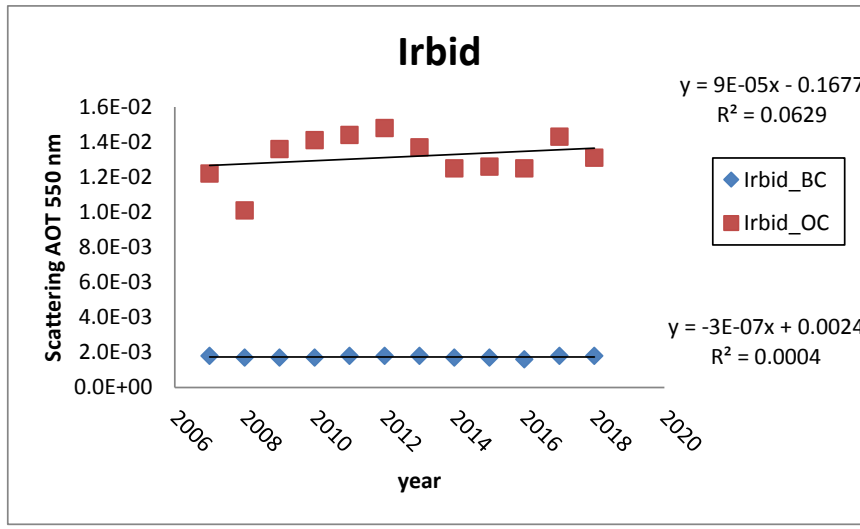

Fig. 14: Average scattering AOT at 550 nm for black carbon and organic carbon during the period from 2007 to 2018 in Irbid city.

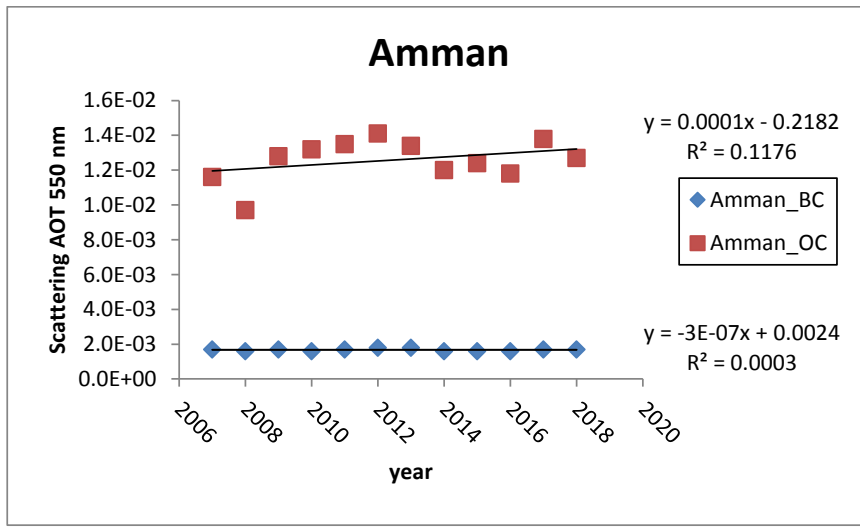

Fig. 15: Average scattering AOT at 550 nm for black carbon and organic carbon during the period from 2007 to 2018 in Amman city.

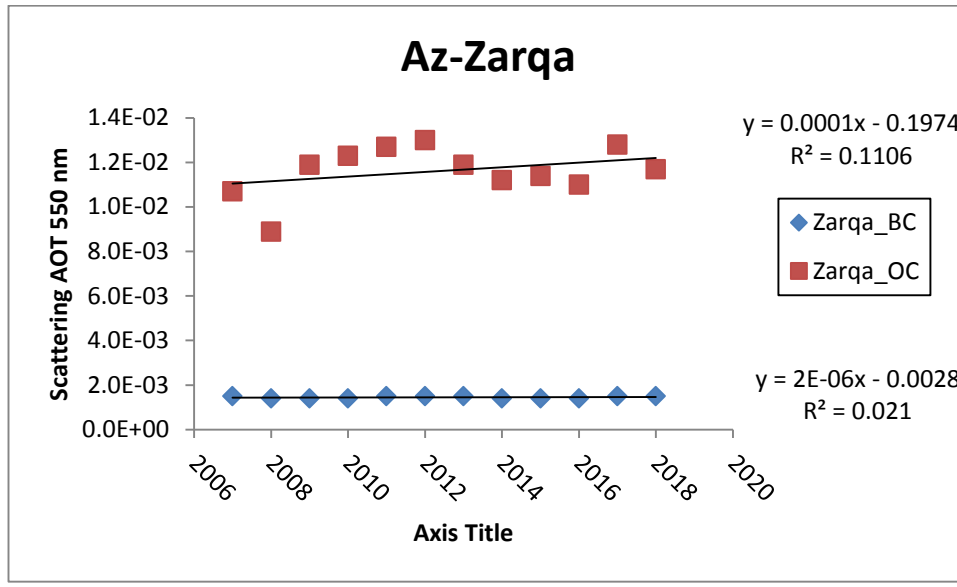

Fig. 16: Average scattering AOT at 550 nm for black carbon and organic carbon during the period from 2007 to 2018 in Az-Zarqa city.

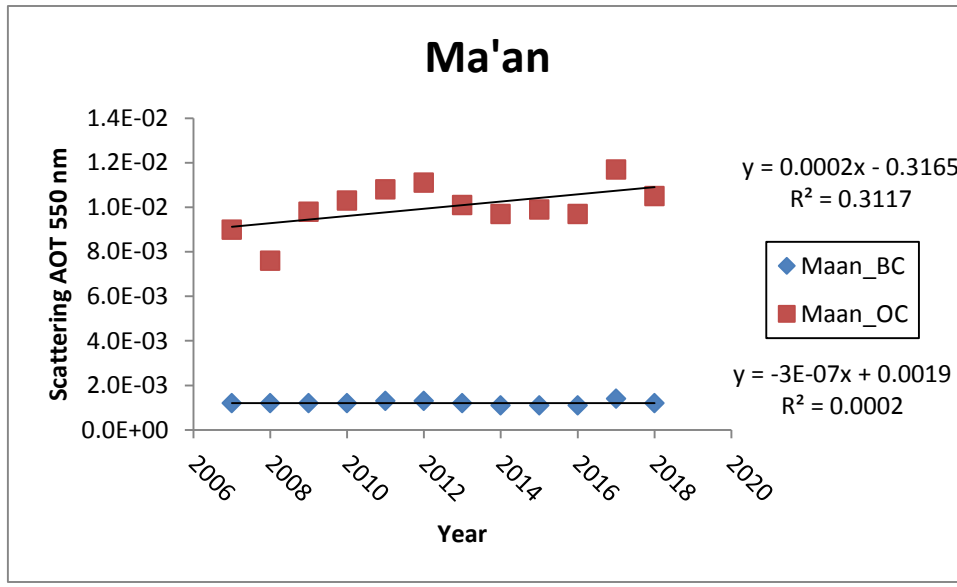

Fig. 17: Average scattering AOT at 550 nm for black carbon and organic carbon during the period from 2007 to 2018 in Ma'an city.

$kg.m^{-2}$, 5.1×10^{-7} $kg.m^{-2}$, and 5.1×10^{-7} $kg.m^{-2}$ respectively.

OC column mass density has values between 18.5×10^{-7} $kg.m^{-2}$ and 32.4×10^{-7} $kg.m^{-2}$ (Fig. 23). Irbid city has an average value of BC mass concentration of 28.8×10^{-7} $kg.m^{-2}$, while Amman, Az-Zarqa, and Ma'an have values of 28.1×10^{-7} $kg.m^{-2}$, 25.3×10^{-7} $kg.m^{-2}$, 23.2×10^{-7} $kg.m^{-2}$ respectively.

Figs. 24-27 show the correlation between BC column mass density and OC column mass density. OC column mass density in all sites has a greater value than BC column mass density. In Irbid and Amman, OC mass density is about 6 times BC mass density, while in Az-Zarqa, OC mass density is about 7 times that of BC mass density. Finally, in Ma'an, OC mass density is about 1.5 times that of BC mass density

Black Carbon and Organic Carbon Surface Mass Concentration

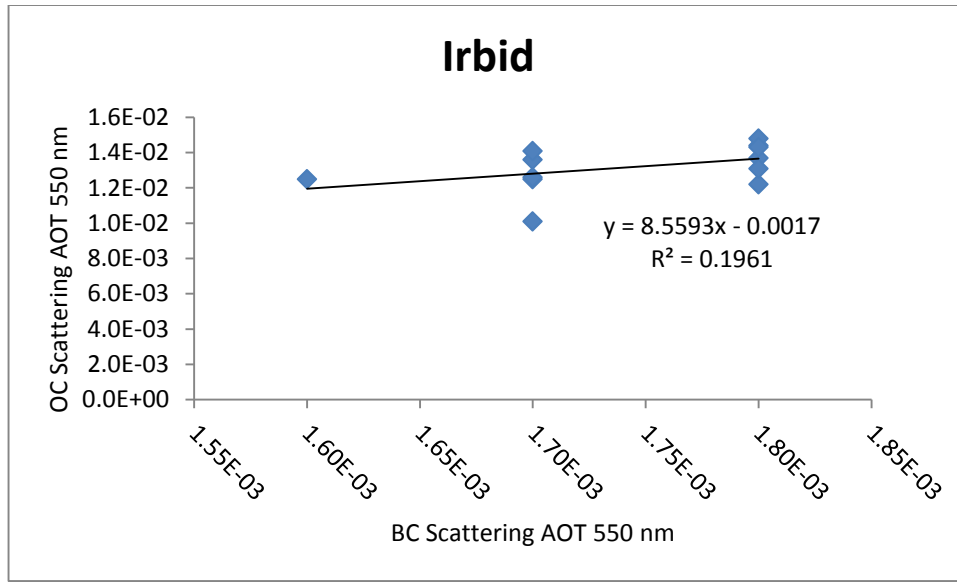

Fig. 18: Correlation between yearly average scattering value of black carbon and organic carbon in Irbid city.

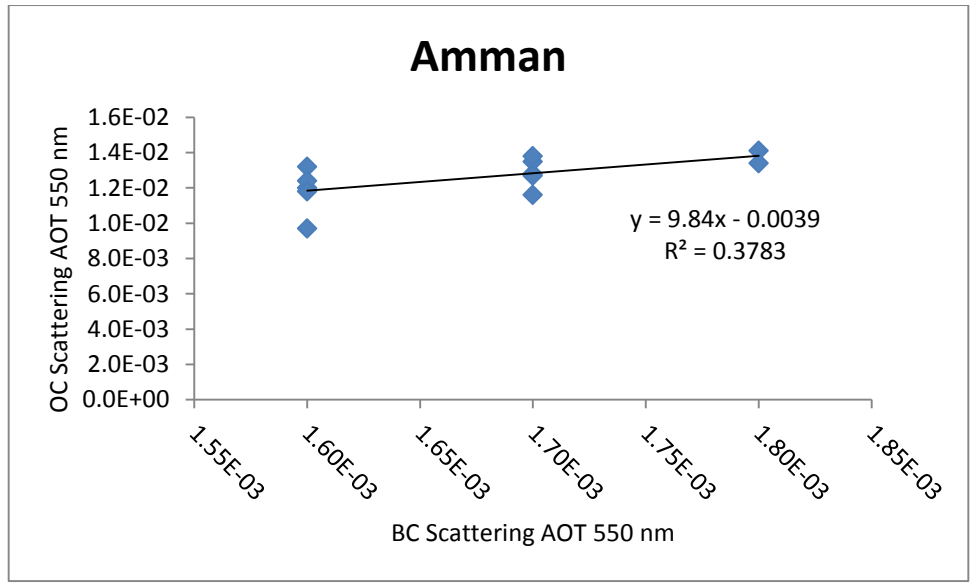

Fig. 19: Correlation between yearly average scattering value of black carbon and organic carbon in Amman city.

BC mass concentration has values between 1.5×10^{-4} mg.m^{-3} and 6×10^{-4} mg.m^{-3} (Fig. 28). Irbid city has an average value of BC mass concentration of 5.6×10^{-4} mg.m^{-3}, while Amman, Az-Zarqa, and Ma'an have values of 5.1×10^{-4} mg.m^{-3}, 3.6×10^{-4} mg.m^{-3}, 1.6×10^{-4} mg.m^{-3} respectively.

OC mass concentration has values between 4.6×10^{-4} mg.m^{-3} and 12.3×10^{-4} mg.m^{-3} (Fig. 29). Irbid city has an average value of BC mass concentration of 11.5×10^{-4} mg.m^{-3}, while Amman, Az-Zarqa, and Ma'an have values of 10.4×10^{-4} mg.m^{-3}, 10.0×10^{-4} mg.m^{-3}, 5.2×10^{-4} mg.m^{-3} respectively.

Figs. 30-33 show the correlation between BC mass concentration and OC mass concentration. OC mass concentration in all sites has a greater value than BC mass concentration. In Irbid city, OC mass concentration is about 3 times BC mass concentration, while in Amman, Az-Zarqa, and Ma'an it is about 2 times BC mass concentration.

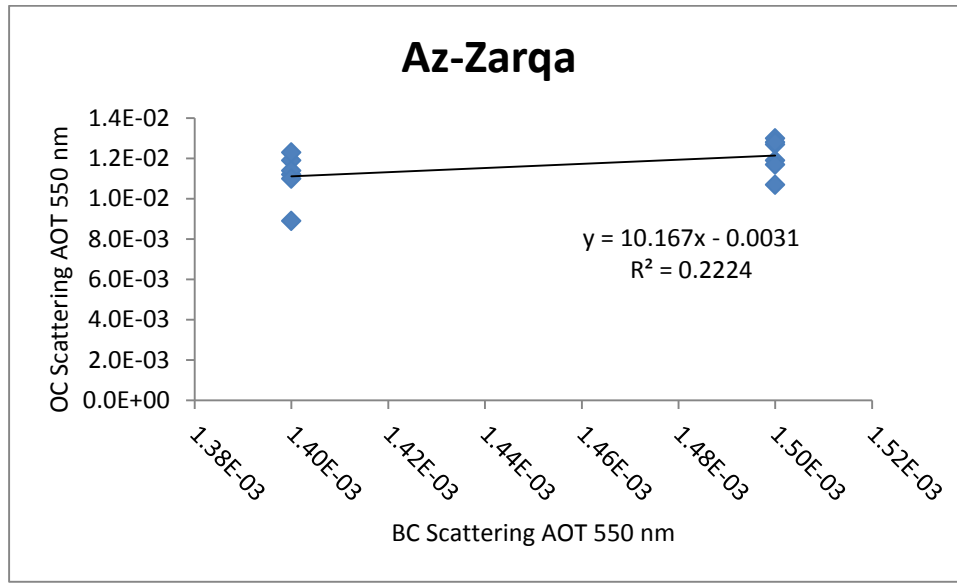

Fig. 20: Correlation between yearly average scattering value of black carbon and organic carbon in Az-Zarqa city.

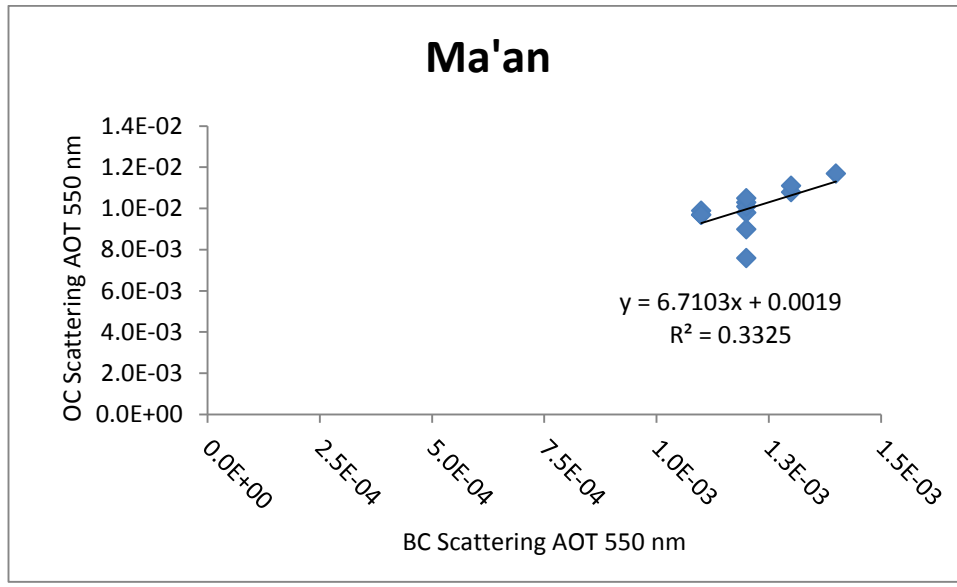

Fig. 21: Correlation between yearly average scattering value of black carbon and organic carbon in Amman city.

CONCLUSION

The amount of organic carbon at all sites is larger than black carbon and this leads to the belief that the sources of organic carbon in Jordan are more than the sources of black carbon. On the top of these sources is organic combustion.

Black carbon and organic carbon data keeps increasing as we go from south to north in Jordan. This increasing trend is because the south of Jordan is a desert with a low population density. While north of Jordan is a fertile plateau close to Syria from the north and Israel from the west. And since the prevailing direction of the winds in Jordan varies between the northwest and the southwest, the north of Jordan can be affected by more black and organic carbons from neighboring countries.

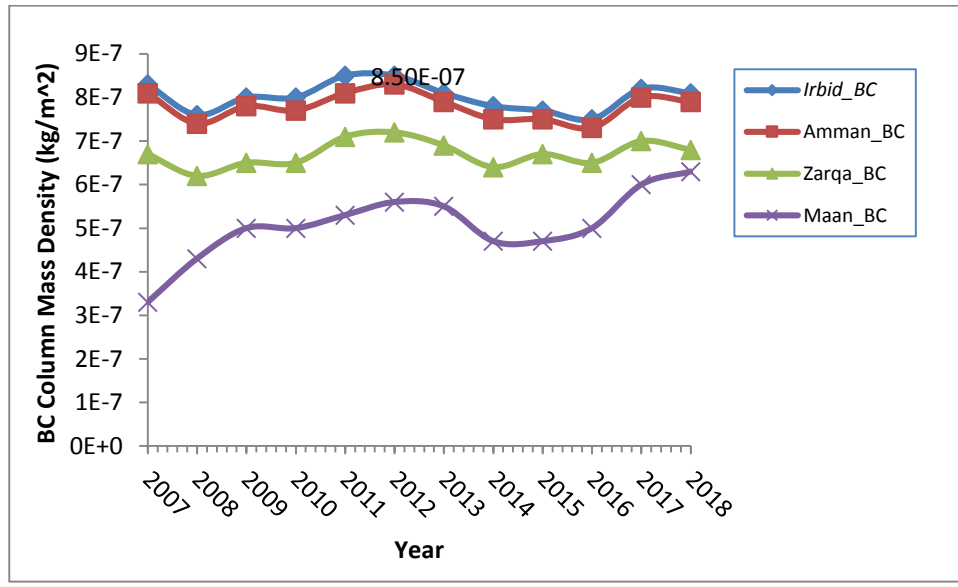

Fig. 22: Yearly average black carbon mass density during the period of 2007 to 2018 at Irbid, Amman, Az-Zarqa and Ma'an.

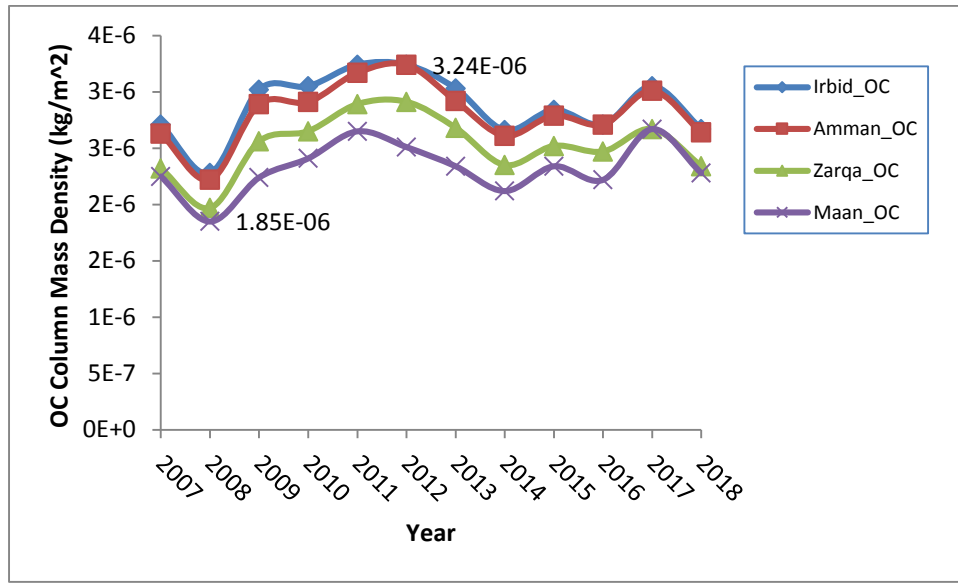

Fig. 23: Yearly average organic carbon mass density during the period of 2007 to 2018 at Irbid, Amman, Az-Zarqa and Ma'an.

Black carbon and organic carbon have maximum values in 2012 due to the Syrian civil war as Syria is adjacent to the northern Jordanian border. Air was polluted during the Syrian war as they used toxic weapons such as mortar bombs, artillery shells, barrel bombs, aircraft bombs, and missiles which have taken a toll on the environment and the population's health (Zwijnenburg & Kristine 2015). Besides that more than 1.5 M Syrian refugees entered Jordan and they are not in camps but are instead living in urban or rural areas, predominantly in the northern and eastern parts of the country. The rapid population growth and the development of the industrial and service sectors combined with increased vehicle traffic increased ambient air pollution levels. Sulfur dioxide is problematic due to the high sulfur content of Jordanian oil, carbon monoxide, nitrogen oxides, and particulate matter, with extinctions increasing proportionately in relation to population size, which pose risks to public health.

Black carbon and organic carbon kept increasing for the period of study (2007 to 2018), which leads to global warming and increasing temperature. This leads to the expectation that Middle East countries will be affected by increasing climate variability and extreme events such as droughts, loss of soil fertility and erosion, leaching of mineral fertilizers, and heat stress on animals. The energy demand also rises especially in summer due to an unexpected increase in temperature in countries that are used to living in mild weather conditions and do not need air-conditioning, such as Jordan. In addition, it is expected that climate change impacts hit water resources, which is the main issue in Middle East countries.

From extinction and scattering, we can calculate absorption which is the most important for global warming and increasing temperature.

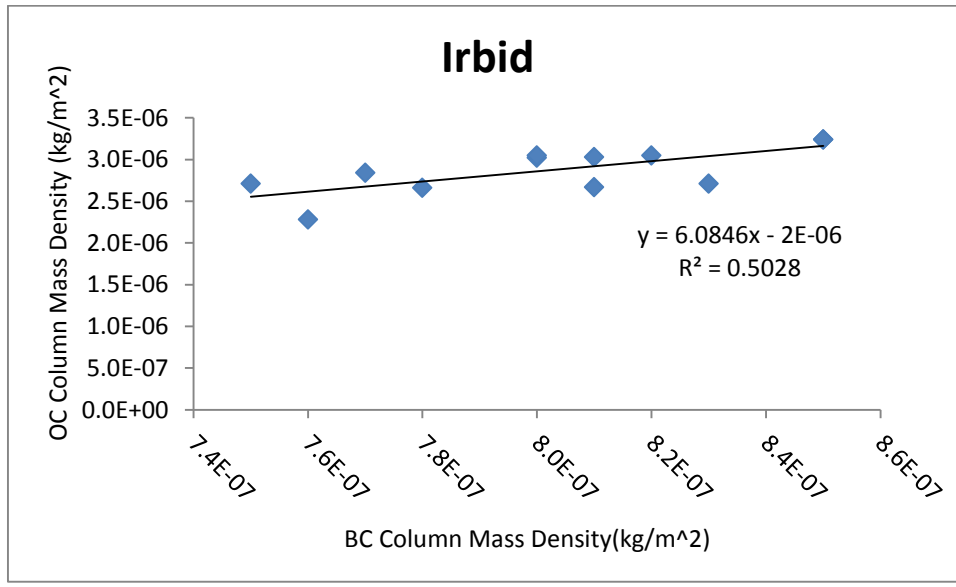

Fig. 24: Correlation between yearly average column mass density of black carbon and organic carbon in Irbid city.

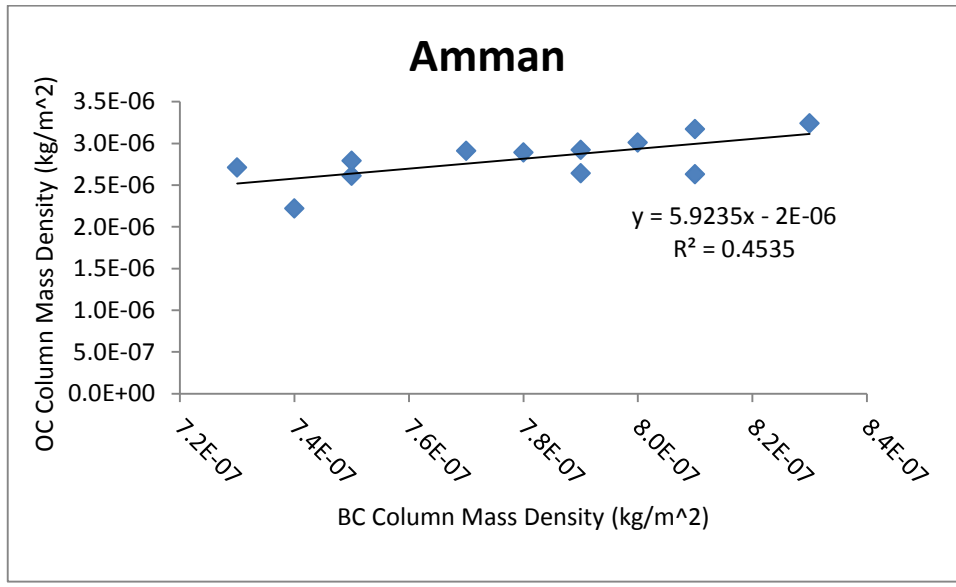

Fig. 25: Correlation between yearly average column mass density of black carbon and organic carbon in Amman city.

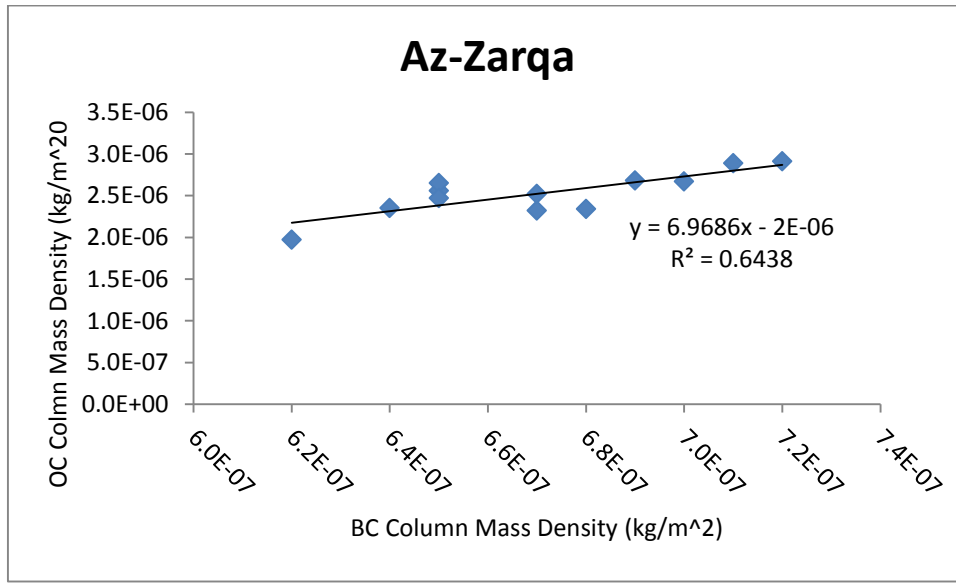

Fig. 26: Correlation between yearly average column mass density of black carbon and organic carbon in Az-Zarqa city.

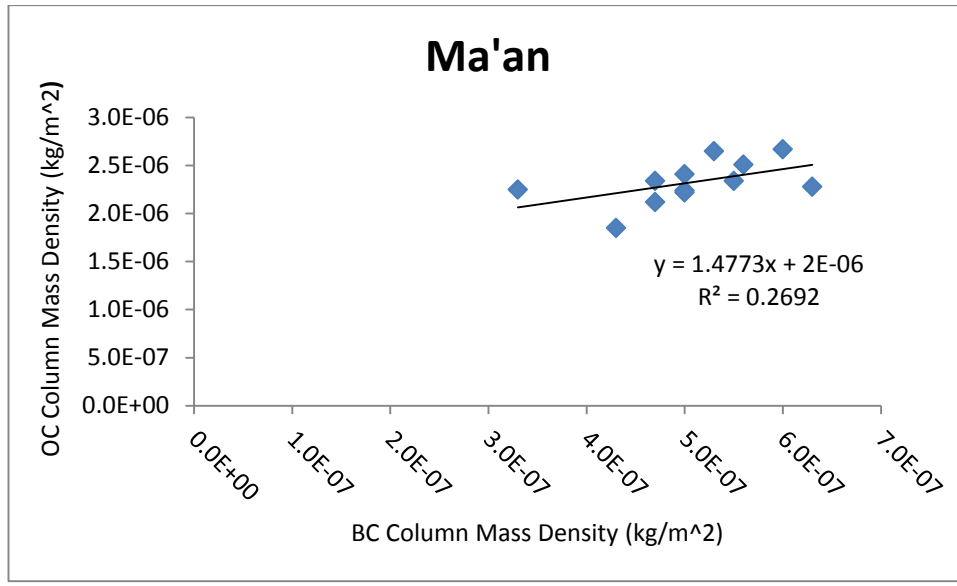

Fig. 27: Correlation between yearly average column mass density of black carbon and organic carbon in Irbid city.

ACKNOWLEDGMENT

Analyses and visualizations used in this paper were produced with the Giovanni online data system, developed and maintained by the NASA GES DISC.

REFERENCES

Acker, J.G. and Leptoukh, G. 2007. Online analysis enhances the use of NASA Earth science data. Eos. Trans. AGU, 88(2): 14 - 17.

Hamasha, K., Ababneh Z., Hamadneh H. and Hamasha K.H. 2015. Analysis of aerosol optical depth at Jordan during 2003-2012 using MODIS data. J. Nature Environ. Pollut. Technol., 14(1): 195-202

Hamasha, K. M., M. S., Almomani, M., Abu-Allaban, K.M. and Arnott, W.P .2010. Study of black carbon levels in city centers and industrial centers in Jordan. Jordan J. Phys., 3(1): 1-8.

Hamasha, K. 2010. Visibility degradation and light scattering/absorption due to aerosol particles in urban/suburban atmosphere of Irbid, Jordan. Jordan J. Phys., 3(2): 83 – 93.

Hamasha, K. and Arnott, W.P. 2010. Photoacoustic measurements of black carbon light absorption coefficients in Irbid city, Jordan. Environ. Monit. Assess. 166: 485-494.

Hime, N.J., Marks, G.B. and Cowie, C.T. 2018. A comparison of the health

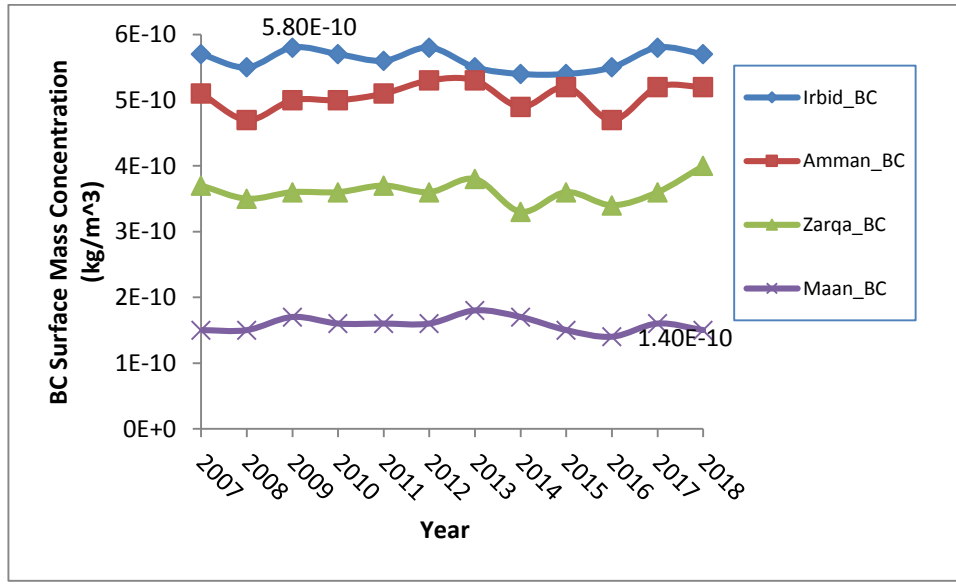

Fig. 28: Yearly average black carbon surface mass concentration during the period of 2007 to 2018 at Irbid, Amman, Az-Zarqa and Ma'an.

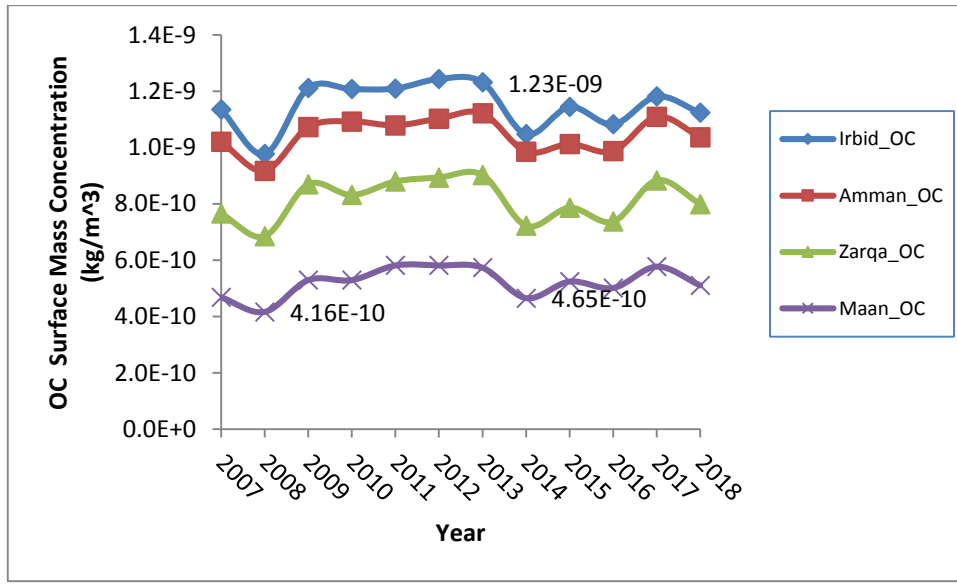

Fig. 29: Yearly average organic carbon surface mass concentration during the period of 2007 to 2018 at Irbid, Amman, Az-Zarqa and Ma'an.

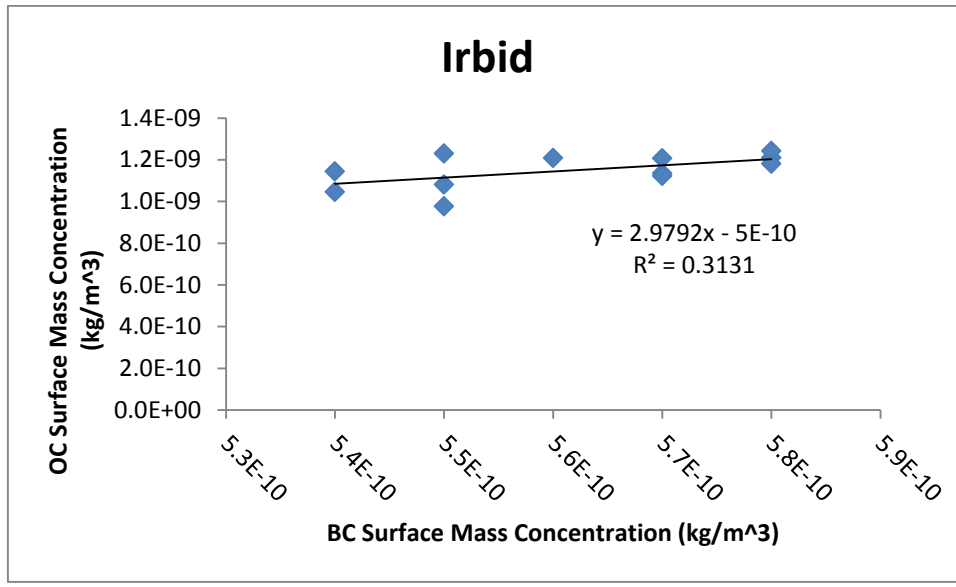

Fig. 30: Correlation between yearly average surface mass concentration of black carbon and organic carbon in Irbid city.

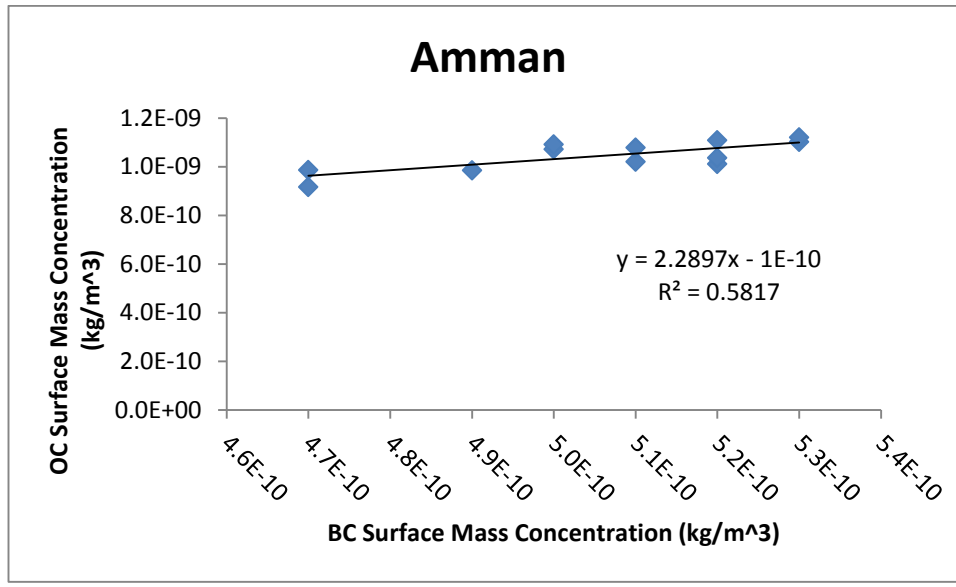

Fig. 31: Correlation between yearly average surface mass concentration of black carbon and organic carbon in Amman city.

effects of ambient particulate matter air pollution from five emission sources. Int. J. Environ. Res. Public Health., 15(6): 1206.

Hussein T., Abu Al-Ruz1 R., Petäjä T., Junninen H., Arafah D., Hämeri K. and Kulmala M. 2011. Local air pollution versus short-range transported dust episodes: a comparative study for submicron particle number concentration Aerosol Air Qual. Res., 11: 109–119.

Intergovernmental Panel on Climate Change (IPCC) 2018. Global warming of 1.5° C: an IPCC special report on the impacts of global warming of 1.5° C above pre-industrial levels and related global greenhouse gas emission pathways, in the context of strengthening the global response to the threat of climate change, sustainable development, and efforts to eradicate poverty. Intergovernmental Panel on Climate Change.

Liu Z., Lin Shi, C., Li, A. and Meyer, D. 2020. NASA Global satellite and model data products and services for tropical meteorology and climatology, Remote Sens., 12(17): 2821

Lung, C., Chen, S., Yang, C., Chen, Y., Chang, S., Tseng, W. and Liu S. 2016. Using atmospheric visibility to assess the effects of air pollution on hospital admissions for respiratory diseases. Aerosol Air Qual. Res., 16: 2237–2244.

McDonald, B.C., Goldstein, A.H. and Harley, R.A. 2015. Long-term trends in California mobile source emissions and ambient concentrations of black carbon and organic aerosol. Environ. Sci. Technol., 49(8): 5178-5188.

MacKenzie, A.R., Langford, B., Pugh, T.A.M. and Robinson, N.H. 2011.

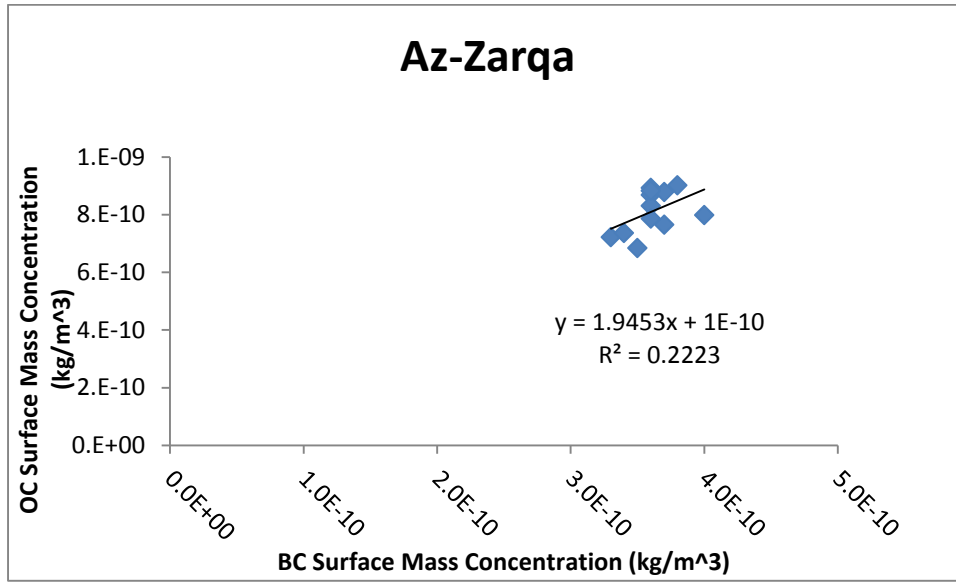

Fig. 32: Correlation between yearly average surface mass concentration of black carbon and organic carbon in Az-Zarqa city.

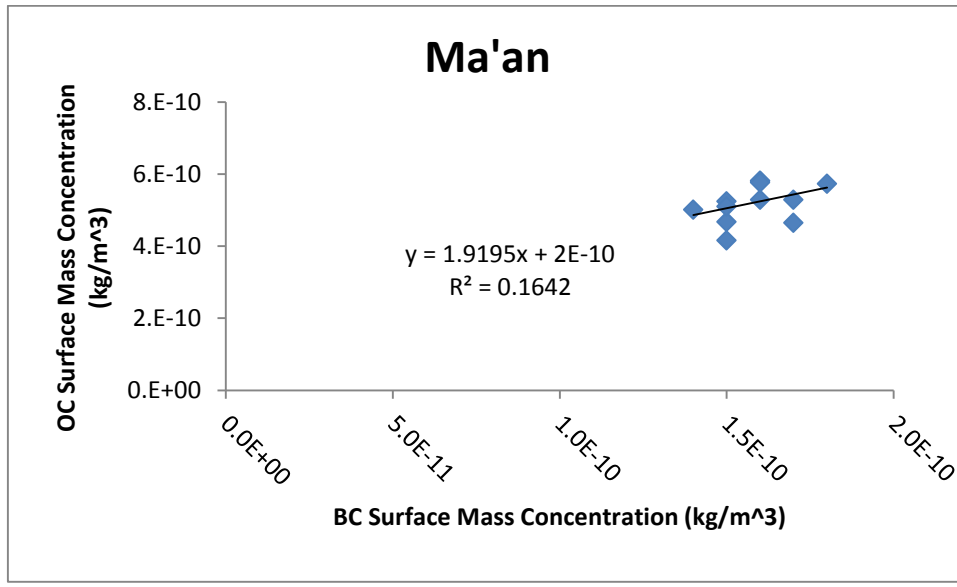

Fig. 33: Correlation between yearly average surface mass concentration of black carbon and organic carbon in Ma'an city.

The atmospheric chemistry of trace gases and particulate matter emitted by different land uses in Borneo. Philos. Trans. R. Soc. Biol Sci., 366(1582): 3177–3195.

Mok, J., Krotkov, N.A., and Arola, A. 2016. Impacts of brown carbon from biomass burning on surface UV and ozone photochemistry in the amazon basin. Sci. Rep. 6: 36940.

Myhre, G., Myhre, C.E.L., Samset, B.H. and Storelvmo, T. 2013. Aerosols and their relation to global climate and climate sensitivity. Nature Edu. Knowl., 4(5):7

Zhanqing, L., Rosenfeld, D. and Fan, J. 2017. Aerosols and their Impact on Radiation, Clouds, Precipitation & Severe Weather Events. Oxford Research Encyclopedia of Environmental Science, United States.

Zwijnenburg, W. and Kristine, P.T. 2015. Amidst the Debris. In: Weir, D. and Zeijden, V.D.W. (eds.). A desktop study on the environmental and public health impact of Syria's conflict. PAX, Syria, pp. 1-84.

Nature Environment and Pollution Technology
An International Quarterly Scientific Journal

p-ISSN: 0972-6268
(Print copies up to 2016)
e-ISSN: 2395-3454

Vol. 20 | No.3 | pp. 973-983 | 2021

Original Research Paper

https://doi.org/10.46488/NEPT.2021.v20i03.005

Open Access Journal

Procuring Plant Services for Ecological and Human Well Being

K. Saraswathi*† and K. Selvam**

*Department of Botany and National Centre of Excellence (MHRD), Thiagarajar College, Madurai -625 009, Tamil Nadu, India

**PG & Research Department of Botany, Thiagarajar College, Madurai- 625 009, Tamil Nadu, India

†Corresponding author: K. Saraswathi; krish.saras31@gmail.com

Nat. Env. & Poll. Tech.
Website: www.neptjournal.com

Received: 16-08-2020
Revised: 30-09-2020
Accepted: 16-10-2020

Key Words:
Ecosystem services
Native
Exotic
Carbon sequestration

ABSTRACT

Ecosystem services offered by two native tree species *viz. Azadirachta indica, Morinda tinctoria,* and four exotic species *viz. Tamarindus indica, Prosopis juliflora, Leucaena leucocephala,* and *Ipomoea carnea* in the Mathippanur village of Madurai district, Tamil Nadu, India were assessed to augment their valuable ecosystem services and to get the management strategy for sustainable use. The selected plant species provide economic benefit through their products, regulating soil health, sequestering carbon, and supporting nests of animals. However, they cause discomfort to the associated vegetation and human beings. Both native and exotic species play a crucial role in the ecosystem and the removal of exotic species will lead to disturbance in the ecosystem resilience. For sustainable management, mixed plantations of tree species can be raised in barren and fallow lands. The plantations will aid in monetary support to the local inhabitants, people's participation in resource management and conservation, and effective use of land and tree services.

INTRODUCTION

Human subsistence on Earth is impossible without the services of natural ecosystems (Daily 1997). Ecosystems play an important role in climate regulation, water circulation, plant reproduction, and soil nutrient dynamics (Costanza et al. 1997). These valuable functions of ecosystems are often termed ecosystem services. The ecosystem services include the delivery, provision, production, protection, or maintenance of a set of goods and services (Chee 2004). Ecosystem services include both goods and services which have a direct and indirect influence on human well-being (Daily 1997). Millennium Ecosystem Assessment (MEA 2003) also recognized the role of ecosystem services in human society.

Beyond whole ecosystem valuation, services of selected trees and shrubs on human well-being are evaluated as this biomass becomes the major source of many goods for human consumption, energy production, and genetic resources. They regulate microclimate and pollution. They also provide refuge sites and habitats for the reproduction of many other organisms. They play an inevitable role in biogeochemical cycles that interconnect air, soil, and water (Roeland et al. 2019). They also maintain the physical and mental health of human beings through their aesthetic value, spiritual enrichment, and recreation (de Groot et al. 2002).

The composition of the plant community has an influence on regular services in an ecosystem (Bennett et al. 2009). The complex ecosystem has both native species and new arrivals and each of the species play a critical role in ecosystem function. Some of the introduced species serve as a major food source (Pimentel et al. 2001). The management of exotic species and intensification of services rendered by the plant species require a methodical understanding of their functions in the ecosystem. Hence, a study was performed to assess the provisional, regulating, supporting services, and disservices offered by selected native and exotic plant species *viz., Azadirachta indica, Morinda tinctoria, Tamarindus indica, Prosopis juliflora, Leucaena leucocephala, and Ipomoea carnea,* and to augment their commercial and ecological benefits.

MATERIALS AND METHODS

Study Area and Climate

The study was performed during June 2015 - May 2016 in a village called Mathippanur in Thirumangalam Taluk of Madurai district, Tamil Nadu, India (Fig.1). It is located at 9.79878° N latitude and 77.851879°E longitude. It lies above 35 to 52 m above mean sea level. The climate is dry and hot with rains between October to December. The temperature during summer reaches a maximum of 40.0°C and a minimum of 26.3°C. Winter temperature ranges between 29.6°C and 18.0°C. The average annual rainfall is about 85 cm. According to the Census of India, in 2011, the village

Source: Google Satellite map at https://www.google.com/maps/place/Mathipanur,+Tamil+Nadu+638454/@11.4058688,77.2415686,768m/data-=!3m1!1e3!4m5!3m4!1s0x3ba91f74ff262283:0x2978d785c9fd1a7a!8m2!3d11.4057563!4d77.2437483

Fig. 1: Satellite map showing the study area Mathippanur village in Thirumangalam Taluk, Madurai District, Tamil Nadu, India

had a total adult population of 2008 with 984 males and 1024 females.

Socio-Economic Status of the Study Area

People in the study area are farmers and only a few who belong to the 20-30 years' age group are educated. Agriculture is their major occupation. Each family has 10-15 acres of own land for cultivation. They cultivate cotton, millets, and Sorghum in their fields. They move to nearby towns for their earnings during periods without sufficient rainfall.

Study Site Selection

The study sites with selected native and exotic plant species *viz., A. indica, T. indica, M. tinctoria, P. juliflora, L. leucocephala,* and *I. carnea* are found distributed in fallow lands and riparian zone of Mathippanur village. They can grow in loamy to sandy loamy soil. The selected plant species are distributed in a scattered manner. The age of the selected plants is 5-10 years.

A. indica and *M. tinctoria* are indigenous tree species. The native of *T. indica* is Tropical Africa, *P. juliflora* is North America, *L. leucocephala* is Southern Mexico and Northern Central America, and *I. carnea* is between Florida and Argentina.

Estimation of Plant Growth Parameters

Different plant growth parameters namely tree heights, girths, and densities were estimated. The biomass of tree species was calculated using the regression technique described as 'dimension analysis of woody plot' by Whittaker (1961) and 'allometry' by Chave et al. (2005). The carbon content of plant samples was estimated by using the wet acid digestion method (Jackson 1973).

Cost-Benefit Analysis

The productive services of selected native and exotic species were estimated based on the economic valuation of goods obtained from them. To collect this economic valuation, a

semi-structured interview was conducted with residents at Mathippanur village. The economic benefits derived from various products of selected plant species were estimated through the adjusted market price method (Godoy et al. 1993).

Herbaceous Density Analysis

The herbaceous community structure was analyzed by using the quadrat method.

Estimation of Soil Parameters

Soil bulk density was analyzed using a soil core method (Anderson & Ingram 1993). Soil moisture was determined by the gravimetric method (Jackson 1973). Soil respiration was measured by using the method described by Anderson (1982). Soil microbial biomass was determined in fresh soil by the Chloroform fumigation extraction technique (Vance et al. 1987).

Nest Analysis

The supporting service of the trees was analyzed by counting the number of nests made by different animals.

Statistical Analysis

One-way ANOVA was performed to find the significant mean value differences of selected parameters among the selected plant species using SPSS16.0. Post-hoc analysis was performed using Tukey's HSD at p = 0.05. Regression equations were also obtained using SPSS16.0.

RESULTS AND DISCUSSION

Density and Growth Parameters of Selected Plant Species

In the study area, *P. juliflora* was the most predominant species (Fig. 2) in terms of density. There were totally around 25 trees of *P. juliflora* found in an acre. This is because of the aggressive and invasive potential of *P. juliflora* when compared to other species. It tends to replace the native vegetation through encroachment (Bokrezion 2008). The other exotic plant *L. leucocephala* becomes an aggressive invader in Mexico and the Philippines (Orwa et al. 2009). However, in the present study areas, it is not as invasive as *P. juliflora*.

An exotic species *L. leucocephala* was significantly tall

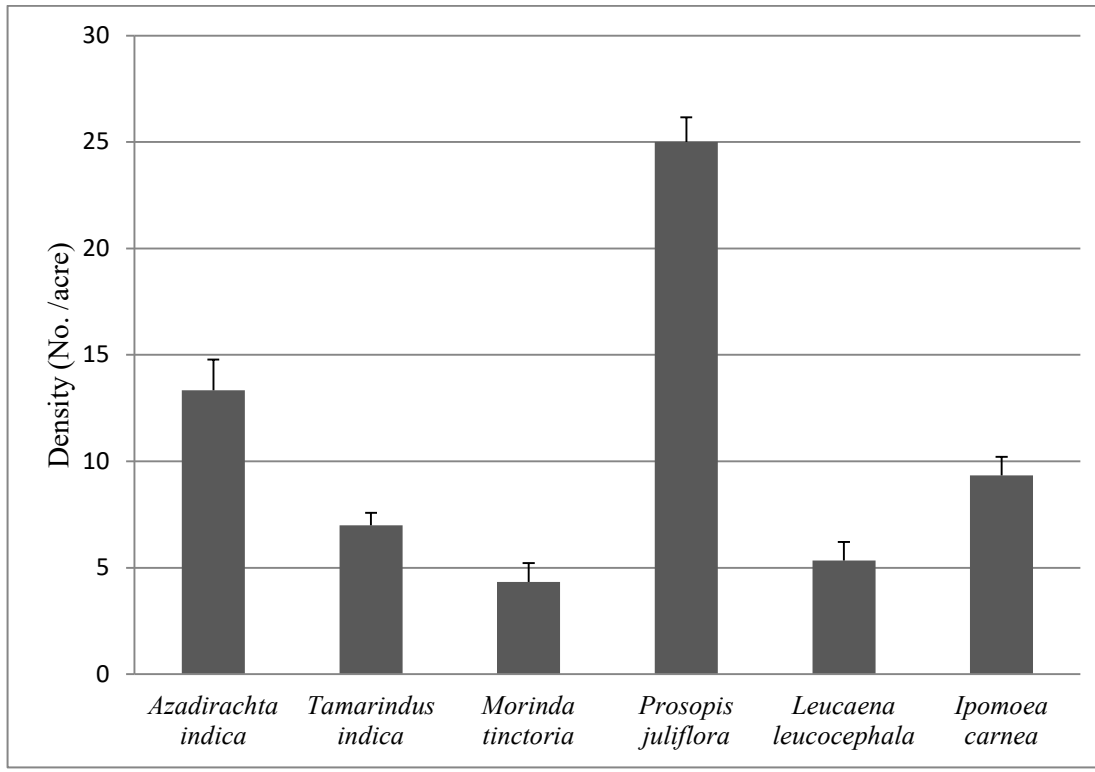

Fig. 2: Density of selected native and exotic plant species in Mathippanur Village, Thirumangalam Taluk, Madurai District, Tamil Nadu, India
Values – Mean ± SE

(2.17 ± 0.17 m) and has a large diameter (58.05 ± 2.35 cm) when compared to other species (Table 1). Earlier reports agreed that it can reach an average of 5 m height and a bole diameter of 10-50 cm (Orwa et al. 2009).

The average biomass of *T. indica* (968.86 ± 88.49kg) was incomparable with other species and it yielded significantly larger biomass than other native and exotic plant species. Next to it, *A. indica* produced a large amount of biomass (412.43 ± 46.76 kg). Biomass accumulation in a tree depends on the nature of the species and its density. In the present study, the density of *T. indica* was comparatively lesser than *A. indica*. This could be one of the reasons for its higher biomass yield per acre.

Provisioning Services

Domestic use of products: Certain products obtained from the selected plants are used for domestic purposes. They indirectly reduced the expenditure of food, medicine, and cooking fuel at the household-level (Table 2). *A. indica* has an alkaloid Azadiractin. Branch sticks of *A. indica* are used as toothbrushes. Dentists find twigs of *A. indica* effective in preventing periodontal disease. The leaves have high medicinal value and are used as germicidal agents. The leaves are also used to repel 300 different insect species (Ogah et al. 2011). The seed cake is used to control insects as well as fertilizers.

T. indica offers commercial as well as household-level benefits. Due to its variety of productive services, it is considered as one of the important agroforestry plant species. It is rich in vitamin B (thiamine and niacin) as well as has a small amount of carotene and vitamin C. Thus its flowers, leaves, and seeds are eaten and used to prepare a variety

Table 1: Growth parameters of selected native and exotic plant species in Mathippanur Village, Thirumangalam Taluk, Madurai District, Tamil Nadu, India

S. No.	Name of the plant species	Height (m)	Diameter (cm)	Biomass (kg)
1	*Azadiarachta indica* A. Juss.	1.78 ± 0.04 ^{bc}	20.43 ± 3.31 ^{ab}	412.43 ± 46.76 ^{b}
2	*Tamarindus indica* L.	1.95 ± 0.07 ^{cd}	20.56 ± 1.72 ^{ab}	968.86 ± 88.49 ^{c}
3	*Morinda tinctoria* Roxb.	1.16 ± 0.03 ^{a}	7.97 ± 0.55 ^{a}	92.42 ± 6.81 ^{a}
4	*Prosopis juliflora* (SW.) DC.	1.53 ± 0.08 ^{ab}	6.47 ± 0.63 ^{a}	118.86 ± 9.46^{a}
5	*Leucaena leucocephala* (Lam.) de Wit	2.17 ± 0.17 ^{d}	58.05 ± 2.35 ^{b}	76.14 ± 9.95 ^{a}
6	*Ipomoea carnea* Jacq.	1.34 ± 0.06 ^{a}	1.58 ± 0. 70 ^{a}	28.71± 3.57 ^{a}

Values – Mean ± SE. Different letters indicate significant differences among the mean values within a column at $p < 0.05$ level

Table 2: Provisioning services offered by selected native and exotic plant species at the house-hold level in Mathippanur Village, Thirumangalam Taluk, Madurai District, Tamil Nadu, India

S. No.	Name of the Plant species	Parts used	Uses
1	*Azadiarachta indica* A. Juss.	Leaves	Medicine, Mosquito repellent, Soap
		Wood and branches	Firewood
		Branch Sticks	Toothbrush
2	*Tamarindus indica* L.	Wood and branches	Firewood
		Flowers	Food (Soup)
		Seeds	Food, Medicine
3	*Morinda tinctoria* Roxb.	Wood and branches	Firewood
		Leaves	Medicine
		Bark	Rope for roof making
4	*Prosopis juliflora* (SW.) DC.	Thorny branches	Fence
		Fruit	Fodder
5	*Leucaena leucocephala* (Lam.) de Wit	Wood and branches	Firewood
		Branches	Fence
		Leaves	Fodder
6	*Ipomoea carnea* Jacq.	Leaves	Roof making
		Branches	Fence

of dishes marketed worldwide such as sauces, syrups, and processed foods. In the present study area, people reported that it is used to nourish malnourished children.

The leaves of *M. tinctoria* are used as medicine for scabies, hip pain, and joint pain. Rope prepared from the bark of *M. tinctoria* is used to tie roof thatches.

P. juliflora and *L. leucocephala* fruit pods are the major sources of fodder for the cattle. Their branches are used as a fence for houses and cattle sheds. *I. carnea* branches are also used as fencing material. Their leaves are laid under thatched roofs to get a cooling effect. Wood and branches of *A. indica, T. indica, M. tinctoria,* and *L. leucocephala* are used as fuelwood. *A. indica*, *T. indica*, and *L. leucocephala* offer tremendous services to ecosystem health, human health, and human sustenance (Orwa et al. 2009).

Commercial benefits from the products: The major occupation of people in the study area is agriculture. Due to erratic rainfall, farmers do not get money from agriculture throughout the year. So they avail the productive services of the plants for their livelihood. Although the commercial benefits offered by these plants are seasonal, they became one of the alternate sources of their economy. The products of these plants are used as such or processed into different forms.

T. indica produced significantly larger biomass in an acre (6782.00 ± 559.37 kg/acre) than other species (Fig. 3). It was followed by *A. indica* (5499.00 ± 599.24 kg/acre). These plant species support the livelihoods of several groups of people namely landowners, tenants, laborers, and people who help in transportation (Table 3 and 4). People who owned fallow land with exotic, invasive *P. juliflora* trees derived a substantial amount of money (INR 10,000) (US$ 132.65) without any investment. The charcoal production from *P. juliflora* provides a considerable monetary benefit to local people (Ilukor et al. 2016).

Regulating Services

Carbon sequestration capacity: Woody plant proliferation has been proposed as a significant terrestrial sink for atmospheric CO_2 (Scholes & Noble 2001) and to mitigate climate changes. Almost all the selected species had carbon content in 3/4th of their biomass. Carbon storage capacity in

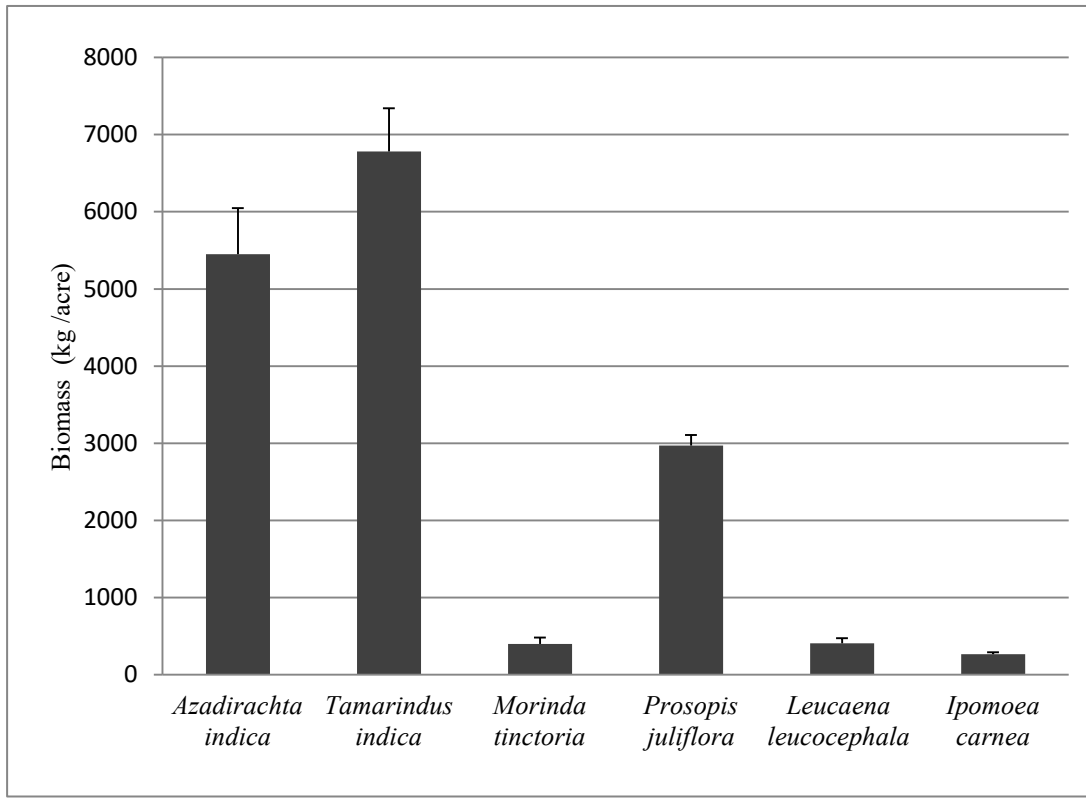

Fig. 3: Biomass (kg / acre) of selected native and exotic plant species in Mathippanur Village, Thirumangalam Taluk, Madurai District, Tamil Nadu, India
Values – Mean ± SE

Table 3: Economic valuations of provisioning services offered by selected native tree species in Mathippanur Village, Thirumangalam Taluk, Madurai District, Tamil Nadu, India

Name of the Tree	Type of Product	Yield per acre (kg)	Gross Benefit (acre)		Harvesting		Processing		Transport		Lease Amount to Land Owner		Net Benefit (acre)	
			INR	US$	INR	US$	INR	US$	INR	US$	INR	US$	INR	US$
Azadirachta indica A. Juss.	Wood	5000	110000	1450.00	Male 5days= 2000 (400/day) Female 5dyas=1000 (200/day)	26.53 (5.31) 13.27 (2.65)	-	-	2250	29.85	45,000	596.93	59750	792.59
	Seeds	100	2000	26.53	Female 750/day	9.95	-	-	-	-	-	-	1250	16.58
	Seed Cake (Fertilizer)	80	4000	53.06	Female 5days=750 (150/day)	9.95 (1.99)	200	2.65	50	0.66	-	-	3000	39.8
	Oil from seeds	25	3750	49.74	Female 5days =750 (150/day)	9.95 (1.99)	500	6.63	-	-	-	-	2500	33.16
Morinda tinctoria Roxb.	Wood	400	24000	31836	Male 3days= 1200 (400/day) Female 3days=600 (200/day)	15.92 (5.31) 7.96 (2.65)			750	9.95	500	6.63	20950	277.90
	Fruits (Dried)	80	1200	15.92	2days=700 (350/day)	9.29 (4.64)							500	6.63

INR Indian Rupees US$ United States Dollar

Table 4: Economic valuations of provisioning services offered by selected exotic trees and shrub in Mathippanur Village, Madurai District, Thirumangalam Taluk, Tamil Nadu, India

Type of Product	Yield per acre (kg)	Gross Benefit (acre)		Harvesting		Processing		Transport	Lease Amount to Land Owner			Net Benefit (acre)		Name of the Tree
		INR	US$	INR	US$	INR	US$	INR	US$	INR	US$	INR	US$	
Wood	6000	1,20,000	1591.82	Male 7days=2800 (400/day) Female 7days=1400 (200/day)	37.14 (5.31) 18.57 (2.65)	-	-	2,250	29.85	45,000	596.93	68,550	909.33	*Tamarindus indica* L.
Whole Pods	350	10,500	139.28	Female 5days=1750 (350/day)	23.21 (4.64)	250	3.32	550	7.30	-	-	7950	105.46	
Fleshy Fruits	300	18,000	238.77	Female 5days=1750 (350/day)	23.21 (4.64)	8days=2000 (250/day)	26.53 3.32	550	7.30	-	-	13,700	181.73	
Seeds	50	900	11.94	-	-	-	-	-	-	-	-	900	11.94	
Wood	3000	30,000	3967.95	1600	21.22	-	-	750	9.95	10,000	132.65	17,560	234.13	*Prosopis juliflora* (SW.) DC.
Charcoal	500	11,000	145.92	Male 8days=3200 (42.45)	42.45 (5.31)	Kerosene Oil 3000	39.80	-	-	-	-	4800	63.67	
Wood	500	5000	66.33	Male 3days=1350 (450/day)	17.91 5.97	-	-	750	9.95	-	-	2900	38.47	*Leucaena leucocephala* (Lam.) de Wit
Leaves	40	400	5.31	-	-	-	-	-	-	-	-	400	5.31	*Ipomoea carnea* Jacq.

INR Indian Rupees US$ United States Dollar

an acre was significantly high in *A. indica* (3919.7 ± 363.39 kg carbon/acre) followed by *T. indica* and the exotic species *P. juliflora* (Fig. 4). The woody plant *Prosopis* proliferation in grasslands of Texas resulted in the enhancement of carbon stock from 15 to 24 times greater than grasslands (Hibbard *et al.* 2003).

Air purification: The people in the study area realized the air purification property and feeling of freshness under *A. indica*. *M. tinctoria* was also reported for its high air pollution tolerance index. The study report of Krishnaveni *et al.* (2014) revealed the air pollution tolerance index of these two plants in Yercaud, Tamil Nadu.

Supporting Services

Understory herbaceous species density: There were eight different herbaceous plant species recorded under the canopy of selected plant species. Among the eight different herbs, the density of grasses *Cynodon dactylon, Cyperus rotundus,* and *Cynodon* spp. were higher than other species (Table 5). The mean density of herbaceous species was less under the canopy of the exotic species *I. carnea* (2.79 ± 0.78/m^2) and *P. juliflora* (3.5 ± 1.37/m^2) when compared to other species. Trees have shading effects due to their broad spreading crown and some of the trees have allelopathic effects. The growth and biomass production of herbaceous plant species were mainly affected by the shading effect (Frost & Edinger 1991).

Soil quality parameters and microbial biomass carbon: The soil quality parameters of selected plants are given in Table 6. Soil bulk density above 1 g.cm^{-3} has an influence on soil microbial community and their functions (Li et al. 2002). But the maximum soil bulk density of 0.08 g.cm^{-3} was recorded under *A. indica tree canopy. It shows the little inhibitory effect* of *A. indica. It had low* microbial biomass carbon and soil organic carbon when compared to other species (Diaz-Ravina *et al.* 1988). But the soil under *T. indica* had high organic carbon (22.60 ± 0.26%) and organic matter (87.12 ± 1.01%) and had a high soil respiration rate. A similar kind of observation was made by Faust *et al.* (2015). There were no significant differences in moisture content (%) in the soil with selected plant species.

Nests of birds and animals: The number of nests laid by birds and animals on *A. indica* (4.6 ± 0.88) was comparatively higher than other species (Fig. 5). Crow and Crane species build their nests on these trees. Squirrels prefer to construct their nests only on *M. tinctoria* and *P. juliflora*. There were

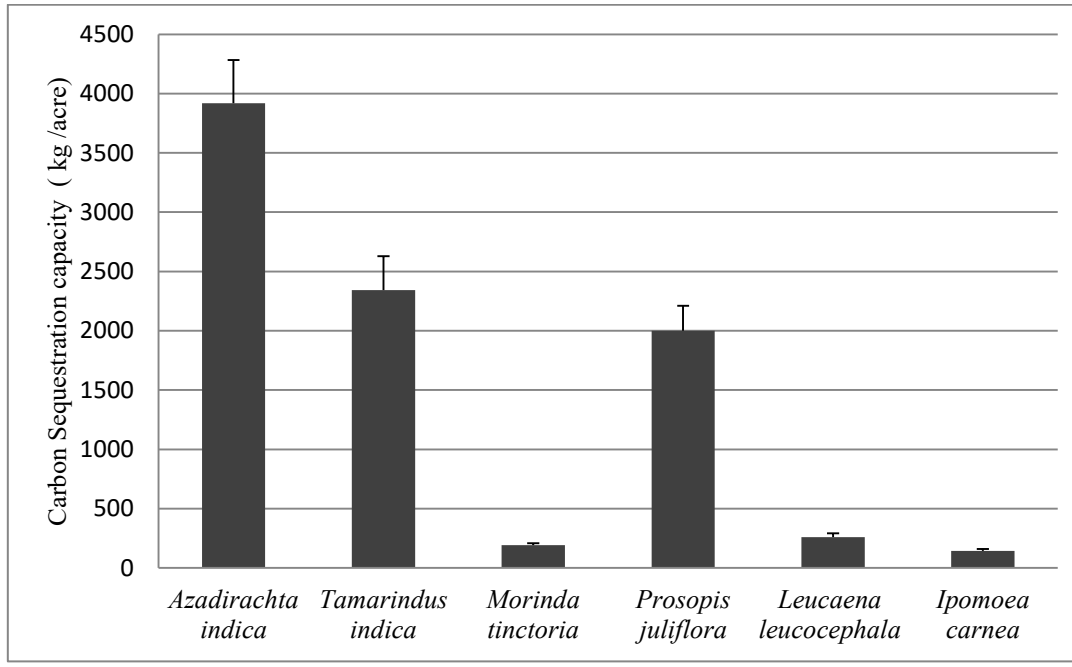

Fig.4: Carbon sequestered (kg / acre) in the biomass of selected native and exotic plant species in an acre at Mathippanur Village, Thirumangalam Taluk, Madurai District, Tamil Nadu, India
Values – Mean ± SE

Table 5: Density of herbaceous species under the canopy of selected native and exotic plant species in Mathippanur Village, Thirumangalam Taluk, Madurai District, Tamil Nadu, India

S. No.	Name of the Species	*Azadiarachta indica* A. Juss.	*Tamarindus indica* L.	*Morinda tinctoria* Roxb.	*Prosopis juliflora* (SW.) DC.	*Leucaena leucocephala* (Lam.) de Wit	*Ipomoea carnea* Jacq.
1	*Pedalium murex* L.	5.33	5.67	8	4.33	7	1.33
2	Cynodan spp.	7	7.67	6.67	8.33	7	4.67
3	*Cyperus rotundus* L.	6	10.3	5.33	10	5.33	6
4	*Cleome gynandra* L.	4.33	----	6	----	----	3.67
5	*Cynodan dactylon* (L.) Pers.	7	9.67	5.67	2.67	5.67	4
6	*Acalypha indica* L.	4.67	----	9.33	2.67	9.33	----
7	*Tephrosia purpurea* (L.)	6	7.33	8	---	6	2.67
8	*Eranthemum spp.* (L.)	6.67	4.33	----	---	6.67	----

Values – Mean ± SE. Different letters indicate significant differences among the mean values within a column at $p < 0.05$ level

Table 6: Soil quality parameters of selected native and exotic plant species in Mathippanur Village, Thirumangalam Taluk, Madurai District, Tamil Nadu, India

S. No.	Name of the Species	Bulk Density (g/cm^3)	Soil Moisture (%)	Organic Carbon (%)	Organic Matter (%)	Soil Respiration ($mg/hr/m^2$)	Microbial Biomass Carbon (%)
1	*Azadirachta indica* A. Juss.	0.08 ± 0.002 ^{c}	7.45 ± 0.57 ^{a}	12.20 ± 1.12 ^{a}	47.03 ± 4.34 ^{a}	21. 23 ± 2.86 ^{b}	3.16 ± 0.49 ^{a}
2	*Tamarindus indica* L.	0.079 ± 0.005 ^{c}	5.96 ± 0.77 ^{a}	22.60 ± 0.26 ^{d}	87.12 ± 1.01 ^{d}	105.57 ± 4.71 ^{d}	7.23 ± 0.38 ^{b}
3	*Morinda tinctoria* Roxb.	0.06 ± 0.0007 ^{b}	6.34 ± 1.28 ^{a}	17.30 ± 0.52 ^{c}	66.69 ± 2.03 ^{bc}	89.33 ± 2.87 ^{d}	6.7 ± 0.55 ^{b}
4	*Prosopis juliflora* (SW.) DC.	0.071 ± 0.0005^{bc}	7.08 ± 0.25^{a}	15.60 ± 0.45 ^{b}	60.14 ± 1.76 ^{b}	15.18 ± 4.32 ^{ab}	8.5 ± 1.37 ^{b}
5	*Leucaena leucocephala* (Lam.) de Wit	0.05 ± 0.0005 ^{a}	8.30 ± 2.66 ^{a}	18.70 ± 0.26 ^{c}	72.09 ± 1.01 ^{c}	47.15 ± 2.06 ^{c}	7.56 ± 0.53 ^{b}
6	*Ipomoea carnea* Jacq.	0.073 ± 0.0006 ^{b}	7.33 ± 1.05 ^{a}	17 .00 ± 0.10 ^{b}	65.53 ± 0.38 ^{bc}	2.99 ± 1.16 ^{a}	9.4 ± 0.53 ^{b}

Values – Mean ± SE. Different letters indicate significant differences among the mean values within a column at $p < 0.05$ level

no nests observed on *L. leucocephala* and *I. carnea*. The study reports of Chandrasekaran *et al.* (2014) implied that the tree species influence the reproductive success of the birds in wetland namely Vettangudi birds sanctuary, south India. The birds prefer to build their nests on the native tree *Acacia indica.*

Cultural services: The *T. indica* and *A. indica* have a large and extended crown. They offer shade and are used as shadow trees. They are also considered as a site for recreation and conducting meetings in villages. The people also recorded the warmness effect of *T. indica* and feeling of freshness by *A. indica*.

Disservices: People pointed out the release of heat by *T. indica* and the mechanical disturbances by *P. juliflora* (Mwangi & Swallow 2008). Above all, the trees provide space for snakes and harmful insects and it was registered as a negative service by the people of the study area, Mathippanur.

Services of Native and Exotic Species

In general, there are reports pointed out that invasive weeds threaten biodiversity by displacing native species and disrupting community structure (Sala et al., 2000). Exotic species tend to alter the natural cycles and they decrease water quality in degraded wetlands in Spain (Angeler et al. 2002). However, there were not many significant differences recorded on soil moisture percentage under both native and exotic invasive species in the study area. The tremendous productivity and other services by exotic species were recorded.

The results exemplify that both native and exotic plant species have financial and ecological significance. People who belong to different economic groups such as landowners, tenants, and laborers get revenue from the plants. The removal of exotic species is not advisable and its removal may induce a disturbance in the resilience of an ecosystem. People should be educated to be aware of unused valuable tree services (Davies et al. 2017). Monetary benefits provided by these plants can be enhanced through an effective management strategy.

Management Strategies suggested for Ecosystem Welfare and Socio-Economic Upliftment

The establishment of Plantation by the Government is the possible method to make use of uncultivable fallow land (around 300 acres) and barren land (around 250 acres) in the study area. The plantation should be mixed tree plantations with *A. indica, T. indica M. tinctoria,* and *L. leucocephala*. The plantations should contain combinations of these species with a minimum number of 40 to 100 per acre. I. *carnea* may not be included in the plantation because it prefers to grow in water-logged soil.

P. juliflroa is suitable for barren land and it is able to improve the soil pH and nutrient properties. It has already been proved that the plantations of *P. juliflroa* improved productivity of highly degraded sodic soil (Bhojvoid et al. 1996) and soil organic carbon and nitrogen were increased due to the growth of *P. juliflroa* in alkali soil (Singh 1996). Once the physico-chemical property of soil in barren land is enhanced, other trees can be planted.

Plantations should be managed by the Government. Specially trained personnel appointed by the Government can guide the people in pruning, weeding, adding nutrient supplements, and irrigation of plantation fields.

CONCLUSION

The tree species offer tremendous services to the ecosystem and human beings. The sustainable management of tree services and land will be achieved by means of establishing mixed plantations of the selected tree species. The plantations will assist in land utilization, conservation of soil health, nutrient cycling, air purification, and carbon sequestration along with offering employment opportunities and income to the local inhabitants. This will also provide an opportunity for people's participation in resource management and conservation.

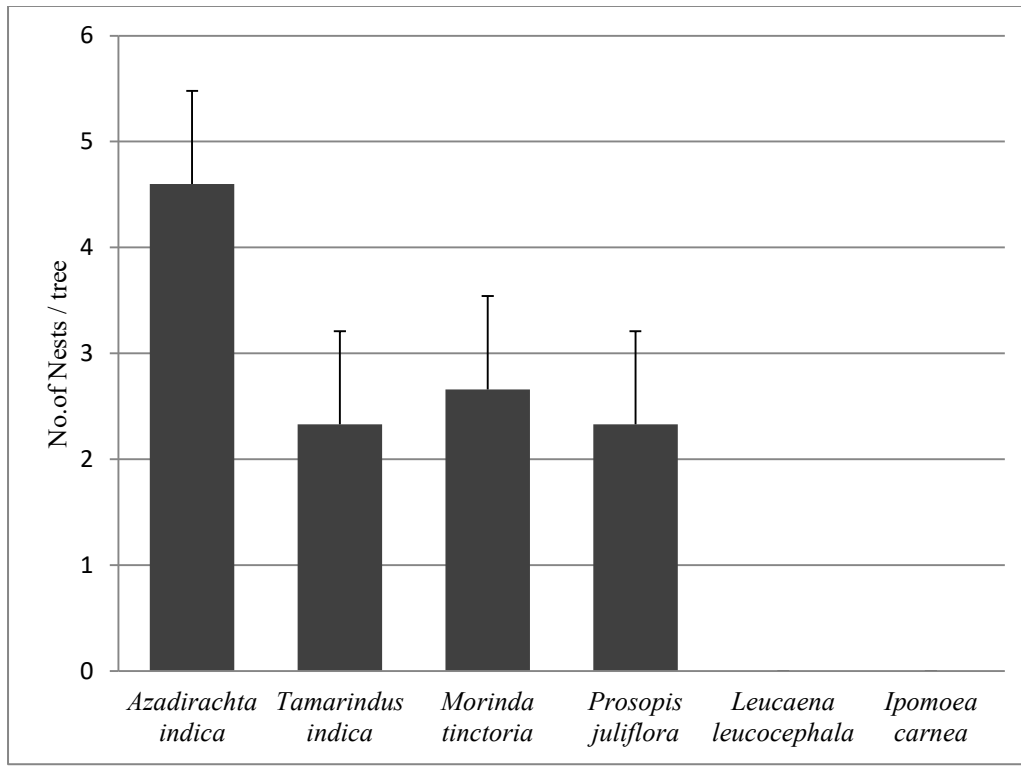

Fig. 5: Nests of birds and animals supported by selected native and exotic plant species in Mathippanur Village, Thirumangalam Taluk, Madurai District, Tamil Nadu, India
Values – Mean ± SE

ACKNOWLEDGEMENT

We would like to thank Mr. Joyson Joe Jeevamani, National Centre for Sustainable Coastal Management, Chennai for his timely help and valuable suggestions for the completion of work.

REFERENCES

Anderson, J.M. and Ingram, J.S.I. 1993. Soil Organic Matter and Organic Carbon. In*:* Anderson, J.M. and Ingram, J.S.I. (eds.) Tropical Soil Biology and Fertility: A Handbook of Methods. Second edition, CAB International, Wallingford, U.K., pp. 62-66.

Anderson, J.P.E. 1982. Soil Respiration. In: Page, A.L., Miller, R.H. and Keeney, D.R. (eds.) Methods of Soil Analysis, Part 2. American Society of Agronomy, Inc., Soil Science Society of America, Inc., Madison Wisconsin, pp. 831-871.

Angeler, D.G., Alvarez-Cobelas, M., Sanchez-Carrillo, S. and Rodrigo, M.A. 2002. Assessment of exotic fish impacts on water quality and zooplankton in a degraded semi-arid floodplain wetland. Aquat. Sci., 64: 76-86.

Bennett, E.M., Peterson, G.D. and Gordon, L.J. 2009. Understanding relationships among multiple ecosystem services. Ecol Lett., 12(12): 1394-404.

Bhojvoid, P.P., Timmer, V. R. and Singh, G. 1996. Reclaiming sodic soil for wheat production by *Prosopis juliflora* (Swartz) DC afforestation in India. Agrofor.Syst., 34: 139-150.

Bokrezion, H. 2008. The Ecological and Socio-economic Role of *Prosopis juliflora*in Eritrea: An analytical assessment within the context of rural development in the Horn of Africa, Ph.D Thesis, Mainz.

Chandrasekaran, S., Saraswathy K., Saravanan, S., Kamaladhasan, N. and Arun Nagendran, N. 2014. Impacts of *Prosopis juliflora* on nesting success of breeding wetland birds at Vettanguudi bird sanctuary. South India. Curr. Sci., 106(5): 676-678.

Chave, J., Andalo, C., Brown, S. and Cairns, M.A. 2005. Tree allometry and improved estimation of carbon stocks and balance in tropical forests. Oecologia, 145: 87-99.

Chee, Y.E. 2004. An ecological perspective on the valuation of ecosystem services. Biol. Conserv., 120: 549-565.

Costanza, R., d'Arge, R., de Groot, R., Farber, S., Grasso, M., Hannon, B., Limburg, K., Naeem, S., O'Neill, R., Paruelo, J., Raskin, R., Sutton, P. and van den Belt, M. 1997. The value of the world's ecosystem services and natural capital. Nature, 387: 253-260.

Daily, G.C. 1997. Introduction: What are ecosystem services? In: Daily, G.C. (ed.) Nature's Services: Societal Dependence on Natural Ecosystems. Island Press, Washington DC, pp. 1-10.

Davies, H.J., Doick, K.J., Hudson, M.D. and Schreckenberg, K. 2017. Challenges for tree officers to enhance the provision of regulating ecosystem services from urban forests. Environ. Res. 156, 97-107.

de Groot, R.S., Wilson, M.A. and Boumans, R.M.J. 2002. A typology for the classification, description, and valuation of ecosystem functions, goods, and services. Ecol Econ., 41: 393-408.

Diaz-Ravina, M., Caraballas, T. and Acea, M.J. 1988. Microbial biomass activity in four acid soils. Soil Biol. Biochem., 20: 817-823.

Faust, S., Hanisch, S., Buerkert, A. and Joergensen, R. G. 2015. Soil properties under manured *Tamarindus indica* in the littoral plain of south-western Madagascar. Arid Land Res Manag., 29(2): 167-179.

Frost W.E. and Edinger S.B. 1991. Effects of tree canopies on soil characteristics of annual rangeland. J. Range Manag., 44: 286-288.

Godoy, R., Lubowski, R. and Markandya, A. 1993. A method for the economic valuation of non-timber forest products. Econ. Bot., 47: 220-233.

Hibbard, K.A., Schimel, D., Archer, S., Ojima, D. S. and Parton, W. 2003. Grassland to woodland transitions: Integrating changes in landscape structure and biogeochemistry. Ecol Appl., 13: 911-926**.**

Ilukor, J., Rettberg, S., Treydte, A. and Birner, R. 2016. To eradicate or not to eradicate? Recommendations on *Prosopis juliflora* management in Afar, Ethiopia, from an interdisciplinary perspective. Pastoralism: Res. Pol. & Pract. 6(14): 1-8.

Jackson, M.L. 1973. Soil Chemical Analysis. Prentice of Hall of India Ltd., New Delhi.

Krishnaveni, M., Kalimuthu, R., Ponraj, K., Lavanya, K., Magesh, P. and JasbinShyni, G. 2014. Air pollution tolerance index assessment of Yercaud roadside plants. Int. J. Pharm. Sci. Rev. Res., 6(5): 362-4.

Li, C., Ma, B. and Zhang, T.Q. 2002. Soil bulk density effects on soil microbial populations and enzyme activities during the growth of maize (*Zea mays* L.) planted in large pots under field exposure. Can. J. Plant Sci., 82(2): 147-154.

Millennium Ecosystem Assessment (MEA). 2003. Ecosystems and Human Wellbeing: A Framework for Assessment. Island Press, Washington DC.

Mwangi, E. and Swallow, B. 2008. *Prosopis juliflora* invasion and rural livelihoods in the Lake Baringo area of Kenya. Conserv. Soc., 6: 130-140.

Ogah, E.O., Omoloye, A.A., Nwilene, F.E. and Nwogbaga, A.C. 2011. Effect of neem seed kernel extracts in the management of rice stem borers in the field in Nigeria. Nig J. Biotech., 23: 13-21.

Orwa, C., Mutua, A., Kindt, R., Jamnadass, R. and Anthony, S. 2009. Agroforestree Database: A tree reference and selection guide version 4.0. World Agroforestry Centre, Kenya

Pimentel, D., McNair, S., Janecka, J., Wightman, J., Simmonds, C., O'Connell., C., Wong, E., Russel, L., Zern, J., Aquino, T., and Tsomondo, T. 2001. Economic and environmental threats of alien plant, animal, and microbe invasions. Agric Ecosyst Environ., 84(1): 1-20.

Roeland, S., Moretti, M., Amorim, J.H., Branquinho,C., Fares, S., Morelli, F., Niinemets, U., Paoletti, E., Pinho,P., Sgrigna, G., Stojanovski, V., Tiwary, A., Sicard, P. and Calfapietra, C. 2019. Towards an integrative approach to evaluate the environmental ecosystem services provided by urban forest. J. For. Res., 30: 1981-1996.

Sala, O.E., Chapin, F.S., Armesto, J.J., Berlow, E. and Bloomfield, J. 2000. Global biodiversity scenarios for the year 2100. Science, 287: 1770-1774.

Scholes, R.J. and Noble, I.R. 2001. Storing carbon on land. Science, 294: 1012-1013.

Singh, G. 1996. Effect of site preparation techniques on *Prosopis juliflora* in an alkali soil. Forest Ecol Manag., 80: 267-278.

Vance, E.D., Brookes, P.C. and Jenkinson, D.S. 1987. An extraction method for measuring soil microbial biomass carbon. Soil Biol. Biochem., 19: 703-707.

Whittaker, R.H. 1961. Estimation of net primary production of forest and shrub communities. Ecol, 42: 177-180.

Nature Environment and Pollution Technology
An International Quarterly Scientific Journal

p-ISSN: 0972-6268
(Print copies up to 2016)
e-ISSN: 2395-3454

Vol. 20 | No.3 | pp. 985-996 | 2021

Original Research Paper

https://doi.org/10.46488/NEPT.2021.v20i03.006

Open Access Journal

The Current Use and Management of Single-Use Items (SUIs) in the Fast Food Industry in Ho Chi Minh City, Vietnam

Thi-Kim Chi Do*, Sunil Herat*, Le Van Khoa and Prasad Kaparaju†**

*School of Engineering and Built Environment, Griffith University, 170 Kessels Road, Nathan Campus, Brisbane 4111, Queensland, Australia

**Faculty of Environment and Natural Resources, Ho Chi Minh City University of Technology, Ly Thuong Kiet Street, District 10, Ho Chi Minh City, Vietnam

†Corresponding author: P. Kaparaju; p.kaparaju@griffith.edu.au

Nat. Env. & Poll. Tech.
Website: www.neptjournal.com

Received: 20-08-2020
Revised: 14-09-2020
Accepted: 09-10-2020

Key Words:
Fast food
Single-use items
Plastic items
Waste management

ABSTRACT

This study aims to determine the composition and the weight of individual single-use items (SUIs) generated in the selected fast-food restaurants (FFRs) in Ho Chi Minh City (HCMC), Vietnam. A semi-structured questionnaire was used to collect data of SUIs consumed per day from 126 FFRs covering six popular fast food companies (FFCs). At the same time, waste from 30 FFRs was collected, and its composition and weight were determined. Consequently, the amount and composition of the waste varied among the studied FFCs and is dependent on the food menu, the number of franchises for each FFC, customer number, size, and the type of SUIs used at these restaurants. Total waste collected across the six FFCs was 6 $t.d^{-1}$ and was equivalent to 1560 $t.yr^{-1}$ in HCMC. Of which, single-use plastic items (SUPIs) waste and single-use paper items (SUPaIs) waste accounted for 39% and 28%, respectively. The total weight of unnecessary SUPIs (condiment containers, straws, and forks) generated was about 44 $t.yr^{-1}$. The results suggest that the necessity of standardizing the type and size of the SUIs used at the FFRs, phasing out the use of unnecessary SUPIs, improving the local waste management practices through material recovery and recycling.

INTRODUCTION

The fast-food industry (FFI) has rapidly developed for decades due to the economic development and an increase in the "on the go" consumption culture. The global fast-food market is growing at a compound annual growth rate of 4.2% and is estimated to be worth more than $690 billion in 2022 (Zion Market 2017). Single-use plastic items (SUPIs) are commonly used in fast-food restaurants (FFRs), small packaging industries, and retail shop owners and grocery stores for product delivery, and they treat plastics as waste rather than a valuable resource. Thus, the FFI generates a considerable amount of packaging waste or single-use items (SUIs) that include cups, containers, cutlery, straws, lids, and bags. Most packaging waste comes from dining areas (39%), followed by kitchen areas (36%) and outside restaurants (25%) (Aarnio & Hämäläinen 2008). Plastic packaging accounted for 47% of the globally generated plastic waste, with more than 50% originating from Asia (UNEP 2018b). It is estimated that food delivery packaging waste account for 1% of the annual municipal solid waste generated in China (Song et al. 2018). Most packaging waste in the FFI is landfilled, although its theoretical recovery potential was 93%, and only 29% of the packaging waste is recovered (Aarnio & Hämäläinen 2008). The disposal of packaging waste, especially plastic waste, is considered as wasting resources, polluting the environment, especially, the marine environment where there is prolong biophysical breakdown of plastics (Leal Filho et al. 2019, Moharir & Kumar 2019). Therefore, addressing SUPIs and plastic packaging in the FFI should be considered as one of the priorities to deal with ocean pollution.

The consumption of SUIs, including single-use plastic items (SUPIs) and single-use paper items (SUPaIs), has been increasing due to the development of the FFI in urban areas (Gautam & Caetano 2017). With the introduction of online food ordering and home delivery, especially through the use of mobile devices, a sharp increase in SUIs consumption in the FFI has been reported (Gautam & Caetano 2017). It is estimated that more than 69% of customers have ordered food by using mobile devices (Gupta 2019). Notably, plastic packaging waste accounts for one-third of total plastic production, much of which is used for the production of SUPIs (UNEP 2016). Globally, 360 million tons of plastic were produced in 2018 with 51% of total plastic production originating from Asia (Plastics 2019) and nearly 40% of plastic was discarded after a single use (Ocean Conservancy 2019). It has been estimated that 12,000 Mt of plastic waste

will be disposed to landfills or in the natural environment by 2050 (Geyer et al. 2017). For example, in 2015, 146 Mt of primary non-fiber plastics was used in the packaging industry, which is mainly composed of polypropylene (PP), polystyrene (PE), and polyethylene terephthalate (PET), that contributed significantly to plastic packaging waste (Geyer et al. 2017). In particular, in the FFI, it is estimated that plastic packaging waste accounted for 11% of the waste generated in McDonald's restaurants in Finland (Aarnio & Hämäläinen 2008). Additionally, plastic containers made of PP and polystyrene (PS) accounted for approximately 75% of the total packing waste in high-populated megacities in China (Song et al. 2018), one of the major countries contributing to global marine plastic pollution (Ocean Conservancy 2019).

With a growing concern of ocean pollution caused by SUPIs, many countries have introduced policies to phase out SUPIs (Ocean Conservancy 2019). To date, 27 countries have introduced a ban on the manufacture, distribution, use, sale, and/or import of SUPIs (UNEP 2018a). However, only 22 countries have banned specific products, such as plastic plates, cups, and utensils while, 16 countries have prohibited materials of polymers, most commonly polystyrene and expanded polystyrene (UNEP 2018a). In ASEAN countries, 18 cities in Indonesia have planned to ban bags, straws, and foam containers for food by 2025 (Akenji et al. 2019). Similarly, Malaysia will also ban drinking straws by 2030, whilst Thailand is planning to phase out SUPIs in 2022 (Akenji et al. 2019).

Vietnam is one of the five major countries that is importing plastic waste through the transboundary agreement (UNEP 2018a). With the increased awareness about ocean plastic pollution, Vietnam has enacted limited policies on SUPIs, except a levy on plastic bags (UNEP 2018b). Vietnam is ranked as the eighth-most valuable market for global food chains (Vietnam: Vietnam ranks eighth for global franchise expansion - ProQuest, n.d.). In particular, the food and beverage sector accounts for the major share of consumers' monthly expenditure, which grew by 18% in 2018 (Vietnam: Vietnam's food processing, packaging sector thriving - ProQuest, n.d.). In Vietnam, Kentucky Fried Chicken (KFC), Lotteria, Jollibee, Pizza Hut, and The Pizza Company recorded revenues of VND5 trillion ($213.5 million) in 2018, an increase of 13% from 2017 (Vietnam: Fast food chains in the slow lane amid focus on health - ProQuest, n.d.). Interestingly, the waste generated by the FFI in Vietnam is considered commercial waste and is collected and landfilled along with the waste generated from hotels and restaurants (Verma et al. 2016). Ho Chi Min City (HCMC) is the largest city in Vietnam. In 2018, the amount of municipal solid waste generated in HCMC was about 8,900 $t.yr^{-1}$, of which, food waste accounted for 60%, followed by plastic waste (14%). A survey of 752,000 Vietnamese people, with 50% of respondents in HCMC, indicated that they would prefer either to eat out in quick services (36%) or to choose a restaurant (50%) because of its convenience (DecisionLab 2016). Data collected from websites of the above-mentioned six popular FFCs indicated that there are approximately 520 FFCs in Vietnam. Of which, Lotteria owns 210 franchise restaurants, followed by 140 KFC restaurants, 100 Jollibee restaurants, 26 Popeyes Stores, 20 Texas Chicken, and 23 McDonald's restaurants across the country. Nevertheless, research in solid waste management of the FFI is still limited (Aarnio & Hämäläinen 2008), especially of the FFI in Vietnam. To our knowledge, the composition and management of SUIs in the FFI in HCMC has not been investigated. The study aims to determine the weight and the composition of SUIs consumed and disposed of per day as well as to examine the waste generation and management in FFCs in HCMC.

MATERIALS AND METHODS

Research Design

The study aims to determine the type, composition, and total weight of individual SUIs consumed and disposed of per day as well as to examine waste generation and management in the selected FFCs in HCMC. Accordingly, this research was carried out by collecting both qualitative and quantitative data (see Fig. 1).

The qualitative data were collected by using a semi-structured questionnaire to quantify the daily and annual waste generation, and management practices at the selected FFRs in HCMC. The qualitative research collected data of SUIs from 126 respondents of 163 surveyed restaurants belonging to six popular FFCs (Lotteria, KFC, Jollibee's, Popeyes Stores, Texas Chicken, and McDonald's) in HCMC. The data was then calculated for 183 FFRs of six FFCs in total in HCMC during the period of the survey in 2017 (see Table 1).

The survey included four sections with 40 questions (from Q.1 to Q.40), and qualitative data were collected. The semi-structured questionnaire focused on the following main sections. Section 1: General information about fast food restaurant profile with seven questions (from Q.1 to Q.7) focused on the restaurant's location, and the number of customers visiting restaurants every day. Section 2: SUIs use and management with 18 questions (from Q.8 to Q.25). These questions were about the composition and the number of SUIs consumed per day. The data collected from the survey were also used in quantitative research. Section 3: Waste generation and management with 13 questions (from Q.26 to Q.38). These questions concentrated on current

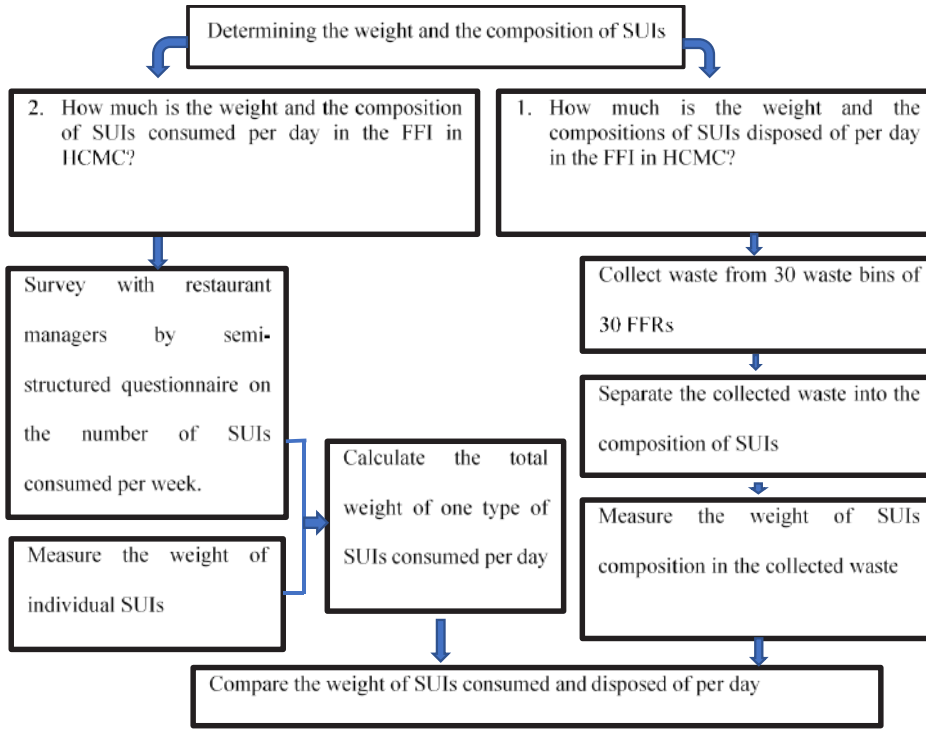

Fig. 1: The process of determining the weight and the composition of SUIs in FFRs in HCMC.

waste management in the surveyed restaurant. Section 4: Manager's experience in restaurant management with two questions (from Q.39 to Q.40). Most of the questions were multiple-choice questions. In this questionnaire, section 2 was used for quantitative research. Section 2 of the questionnaire focused on asking restaurant managers about the number of SUIs consumed per week. The respondents were restaurant managers who are responsible for waste management and general supervision. From the websites of FFCs, the information about restaurants' addresses was used for the survey process.

Primary data was collected from 30 waste bins randomly selected from the 30 restaurants (see Table 1). The collected waste was then separated and weighed into the following components: (1) SUPIs (condiment containers and lids; cutlery; bottles; cups; straws; condiment bags; other plastics); (2) food waste; (3) SUPaIs (cups, bags, other papers); (4) other waste. The weight of the individual components was also measured, and their percentage in the total sample was determined.

Fast Food Industry Survey

Fast food restaurant profile: Six popular FFCs in HCMC were selected for the study as presented in Table 1. In 2017,

Table 1: The total number of FFRs used for survey and waste collection through dedicated waste collection bins in HCMC in 2017.

FFC	Total restaurants		Number of FFRs surveyed (n_1)	Number of FFR used for waste collection from waste bins (n_2)
	r[1]	%		
Lotteria	90	49.18	62	11
KFC	49	26.78	34	6
Jollibee's	14	7.65	10	4
Popeyes Stores	11	6.01	8	3
Texas Chicken	10	5.46	7	3
McDonald's	9	4.92	5	3
Total	183	100	126	30

[1] Source: Websites of fast food companies in Vietnam in 2017

there were 183 FFRs for the six selected companies in HCMC. Data collected from websites of FFCs in Vietnam during the period of the survey shows that the biggest chain of FFCs in HCMC is Lotteria with 90 restaurants, followed by KFC, Jollibee, and Popeyes Stores with 49, 14, and 11 restaurants, respectively. Later, two more FFCs came into existence, Texas Chicken and McDonald's, with 10 and 9 restaurants, respectively. One hundred sixty-three restaurants belonging to the six selected FFCs were surveyed. Of which, 37 FFRs declined to respond. Thus, 126 FFRs participated in the survey and were randomized as per Solvin's formula (Perdana 2018). For each FFC, 50% of the sample size was surveyed in suburban districts, and the remaining rest were surveyed in central districts of HCMC.

Profile of the respondents: Of the total 163 FFRs, managers from only 126 FFRs agreed to participate in the survey. Some managers did not agree to participate or were too busy at the time of the survey. Sometimes, only one of the two shift managers agreed to participate in the survey. Most of the managers who participated in the survey had worked previously as a crew at the same restaurant before becoming a manager.

Sampling: Managers' participation in the research was voluntary and they signed a consent form with confidentiality of responses. The survey was carried out for four months (January 2017 through April 2017). The population size (N) was the total number of FFRs belonging to the selected six FFCs in HCMC (N =183 retrieved from websites of FFCs) during the period of the survey (2017). With confidence level e = 0.05%, using Solvin's formula (Perdana 2018), the total number of restaurants that participated in the survey (n= 126) was estimated as shown in the equation (1):

$$n = \sum_1^6 n_1 = \frac{N}{1+N(e)^2} = \frac{183}{1+183*(0.05)^2} = 126 \quad \ldots(1)$$

The number of FFR surveyed for each FFC (n_1) was calculated based on the percentage of the number of restaurants that each FFC owned in HCMC, which was multiplied by the sample size (n = 126). Value n_1 of one FFC was calculated by using the equation (2):

$$n_1 = r/N*100\%*n \quad \ldots(2)$$

Collection and Compositional Analysis of Fast Food Restaurant Waste

Grab samples of waste were collected from 30 FFRs belonging to the six selected FFCs (value n_2, column 5, Table 1). The collected waste was separated into five main compositions: (1) SUPIs (cutlery, cups or containers, condiment bags, condiment containers and lids, straws, other plastic); (2) food waste; (3) SUPaIs (cups, bags, other paper); and (4) other waste. The separated components were then weighed by using a weighing balance (Kingship, Model: KD-TBED). In each waste bin, a large plastic bag was placed to collect the waste. Upon filling up, the bag was brought and placed in the dedicated area of the restaurant yard. Thus, the bags in the study were collected from dedicated areas.

Calculations

The number and the weight of SUIs consumed per day: The total weight of individual SUI is denoted as w_1 (gram). Data on the number of SUIs consumed per week (Monday through Friday) is denoted as m (items/week) and this data was provided by the restaurant managers. The total number of SUIs consumed per day by an FFR is denoted by m_1 (items).

$$m_1 \sum_1^{n_1} m \quad \ldots(3)$$

The total average weight of SUIs consumed per day by all surveyed restaurants is denoted as q_1 (kg/day) in the equation [4].

$$q_1 = m_1 * w_1 \quad \ldots(4)$$

The average number of SUIs consumed per day by an FFR belonging to any FFC is denoted by m_2 (items/day).

$$m_2 = m_1/n_1 = (\sum_1^{n_1} m)\,/n1 \quad \ldots(5)$$

The total weight of SUIs consumed per day by one FFC is denoted by q_2 (kg/day). The value r (the number of FFRs of one FFC in HCMC during the period of the survey) is presented in Table 1.

$$q_2 = m_2*r*w_1 \quad \ldots(6)$$

The total weight of SUIs consumed per day by six selected FFCs is denoted by q_3 ($kg.week^{-1}$). The total number of SUIs consumed per day by an FFC is m_3 (items/day).

$$m_3 = m_2*r \quad \ldots(7)$$

$$q_3 = \sum_1^6 q_2 \quad \ldots(8)$$

The study also compares the q_2 value among the studied FFCs. The difference in q_2 value will provide the total weight of each SUIs consumed per day at each FFC. This q_2 value is variable and is dependent on the number of FFRs established in HCMC. Similarly, the q_3 value indicates the difference in the total weight of each type of SUIs consumed per day by six FFCs in HCMC. The q_3 and m_3 values vary depending on the weight, and the number of individual SUIs consumed per day.

Amount of SUIs waste collected from the waste bins and estimating the total amount of waste generated by six fast food companies**:** The total amount and the composition of waste generated per day by FFC were calculated by weighing each separated SUI collected from the waste bin

and expressed as a_1 (kg/day/bin). The number of waste bins generated per day at one FFR is denoted by u (bins/day/restaurant). The average weight of each SUI generated per bin at any FFR is denoted by a_2 (kg/day/bin/restaurant) in the equation (9).

$$a_2 = \frac{\sum_1^u a_1}{u} \quad \ldots(9)$$

The average number of waste bins generated per day by one FFR is u_1 (bins/restaurant) (10), while n_2 is the number of restaurants whose waste was collected (column 5, Table 1).

$$u_1 = \frac{\sum_1^{n_2} u}{n_2} \quad \ldots(10)$$

The estimated total weight of each SUI generated per day by FFC is denoted as a_3 (kg/day) and the number of FFRs for each FFC in HCMC is denoted as k (restaurants/company). From the above three values a_2, u_1, and k, the weight of SUIs generated per day by each FFC (a_3) was calculated by using the equation (11) shown below:

$$a_3 = a_2 * u_1 * k \quad \ldots(11)$$

The weight of SUIs generated per day by each FFC (a_3) is compared with the q_3 value.

RESULTS AND DISCUSSION

Waste Management in FFRs

Waste management at each FFR is started by collecting waste in the dining area and the kitchen area of the FFR. Therefore, each FFR has two types of waste bins, one in the dining area and the other in the kitchen area. A black plastic bag of 200 L capacity is generally placed in the waste bins. When the bag is full, it will be transferred to a dedicated area of the restaurant. Thereafter, a restaurant crew collects these bins and move them outside of the restaurant to be picked up by the waste collection truck and transported to landfills. The District Public Services Company Limited (DPSC) or HCMC Urban Environment Company Limited (CITENCO) of each district is responsible for transporting them to landfills. During the time before these bins are collected by DPSC or CITENCO, there are sometimes waste pickers coming to look for salable SUPIs such as plastic bottles in these bins. However, all cutlery, straws, and cups with lids as well as bags made of plastic are not picked up by these informal pickers due to their low values.

With respect to SUI management, each FFR places an order with the headquarter for the delivery of a certain number of SUIs. These SUIs are delivered directly to the concerned FFRs on a regular basis. SUIs used at each studied FFR are qualified and met the standard of QCVN 12-4:2015/BYT on national technical regulation on the safety and hygiene of glass, ceramic, porcelain, and enameled implements, containers, and packaging in direct contact with food. In turn, each FFCs orders their supply chain to manufacture SUIs meeting their requirements. Regarding the use of SUPIs at the FFRs, there are no policies to limit the use of SUIs per customer. These findings suggest that restaurant managers can improve the use of SUPIs by encouraging their staff to ask customers if they want to use SUPIs or limit the number of SUPIs delivered to their customers based on the order, which leads to a reduction in the number of SUPIs released into the environment.

Waste Generation and Waste Composition

Waste generation: The estimated daily waste (Monday through Friday) generated at the studied FFCs is presented in Fig. 2B and Fig.3. Results showed that approximately 6 t/d of waste was generated at the studied FFCs and is dependent on the location of the FFR and the number of customers visited. Of the total waste, SUPIs accounted for 39.4%, followed by food waste (32.7%) and SUPaIs waste (27.5%) (see Fig. 2B).

The survey result also indicated that the studied FFCs had only one day off due to the Tet holiday in HCMC. Thus, the total waste generated for one year (260 days) was estimated to be 1,560 $t.yr^{-1}$, excluding the weekends. Of which, plastic waste originating from SUPIs (SUPIs waste) would account for 590 $t.yr^{-1}$. These findings were in accordance with previous research, which reported that the percentage of food waste and inorganic waste accounted for 30% and 70%, respectively, of the waste generated in KFC outlets in Semarang, Indonesia in 2015 (Alfagi et al. 2015). These findings were also in line with previous research in Italy, which reported that food waste accounted for approximately 28% of the waste generated in Fano seafood restaurants in 2019 (Tatàno et al. 2017).

Among the six FFCs, Lotteria produced more than 2 t/d, followed by KFC with 1.4 t/d (Fig.3). The highest daily waste generation noticed for Lotteria than other FFCs in the study was because Lotteria had the highest number of restaurants (90) operating in HCMC. McDonald's with the lowest number of restaurants (9), produced 1 $t.d^{-1}$ of waste more than the other three FFCs (Fig.3).

Notably, the survey indicated that on average, more than 500 customers were registered at McDonald's every day - the highest average number of customers visited in comparison with other FFRs. Evidence shows that the food menu, material consumption, and waste management policies of FFC played a critical role in the amount of waste generated. The waste management policies of FFCs also influenced the composition and recovery of SUPIs (Hilario 2014). In particular, McDonald's generated a large amount

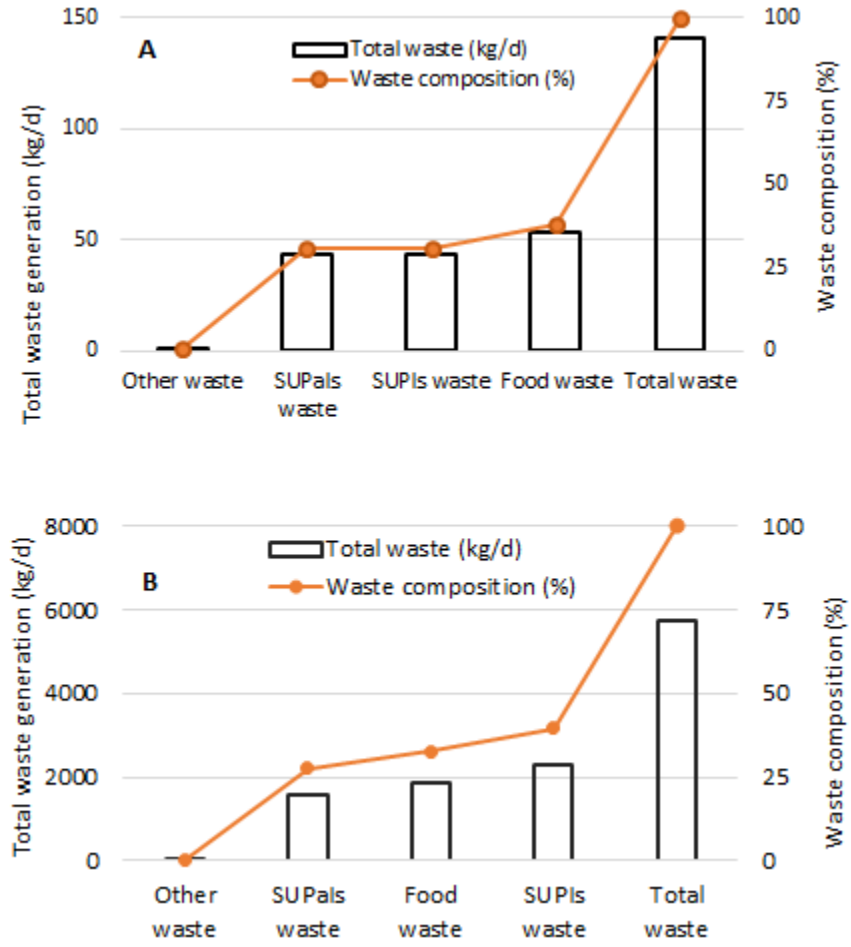

Fig. 2: Total waste amount (kg/d) and its composition (%) from the waste (A) collected from 30 waste bins across the selected six FFCs (B) Estimated for 183 FFRs in HCMC.

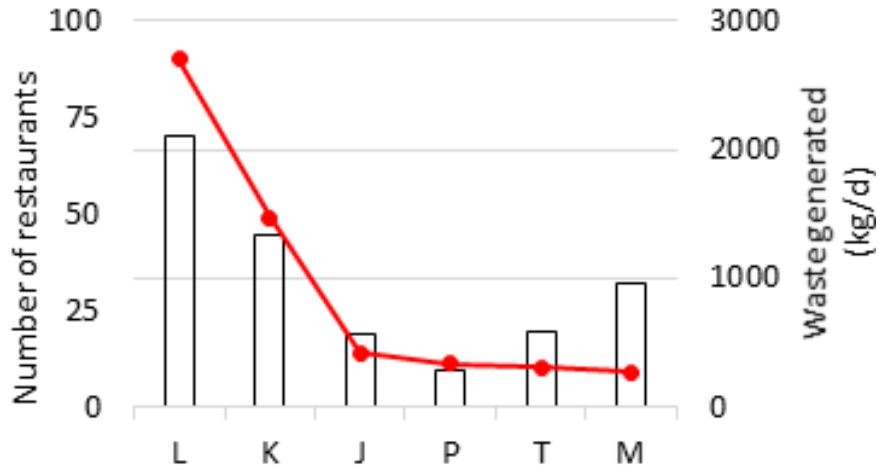

Fig. 3: Total number of FFRs and the amount of waste generated across the studied six FFCs in HCMC. Note: L: Lotteria; K: KFC; J: Jollibee's; P: Popeye Stores; T: Texas Chicken and M: McDonald's.

of paper waste and was planning to use packaging material that was 100% derived from renewable resources, recycled or certified by 2025 (Packaging and Recycling - McDonald's, n.d.). Accordingly, McDonald's policy currently indicatedthat 50% of the company's guest packaging originates from renewable or certified sources. These policies affected considerably the composition of waste the company-owned restaurants generate.

Organic waste and non-organic waste: The composition of waste generated in FFRs and the consumption of SUIs are presented in Fig 4. Overall, a significant variation in the composition of waste generated across the studied FFCs, especially with SUIs, was noticed for both 30 waste bin data and the calculated waste data for the 183 restaurants. Of the total waste, organic waste, i.e., food waste generated by the customers (post-consumption), accounted for 37.8% of the total waste in the 30 waste bins (Fig. 4A). This finding was in line with the previous research, which reported that organic waste accounted for 30% of waste reported in KFC outlets in Semarang, Indonesia (Alfagi et al. 2015).

The corresponding value for the 183 restaurant waste was 33% (Fig. 4B). The total SUIs waste, i.e. SUPIs and SUPaIs together accounted for 61.7% of the total waste in 30 waste bins (Fig. 4A) and 67% of total waste calculated for 183 FFRs (Fig. 4B). This difference in the composition of food waste and SUIs was obviously due to the difference in the number of restaurants, food menu, packaging material consumed, and policies adopted by each FFC on the use of SUIs. For instance, FFCs Lotteria and KFC consumed a large amount of diversified SUPIs in comparison with the other FFCs. Further, the number of restaurants for both Lotteria (90) and KFC (49) was higher than the other four FFCs in HCMC, thereby resulting in generating vast amounts of SUPIs wastes. Nevertheless, the proportion of SUIs waste (67%) noticed in the present study was 1.5 lower than the value of 93% reported for packaging waste at McDonald's in Finland in 2006 (Aarnio & Hämäläinen 2008) due to the improvement in material consumption and waste management policies of these FFCs over last ten years. In particular, for McDonald's, 50% of the company's guest packaging originated from renewable or certified sources (Packaging and Recycling - McDonald's, n.d.). This company has eliminated packaging through innovating material and design (Packaging and Recycling - McDonald's, n.d.). Similarly, KFC has applied and performed corporate social responsibility (CSR) successfully since 2012, which considered the environment as one of four factors in their CSR reports (Bediako 2018). On the other hand, the menu of both companies' restaurants in HCMC focused on Vietnamese traditional dishes (more rice) that were significantly different from the normal fast foods. All these solutions led to a reduction in the amount of packaging waste generated in comparison with the research in Finland in 2006. However, this result was also in accordance with 70% of inorganic waste reported at KFC outlets in Semarang, Indonesia in 2015 (Alfagi et al. 2015). It can be explained that the same component of waste was generated in both regions, which consist of plastic and beverages packaging and drinks leftover (Alfagi et al. 2015). In addition, in both countries, it was not obligatory for FFRs to separate the waste into different components for recycling. This led to the similarity in the component of the inorganic waste of KFC outlets in Semarang and HCMC.

Within SUIs, SUPIs and SUPaIs accounted for 30.8% and 30.9% respectively for the total SUIs generated in 30 waste bin data (Fig. 4A). The corresponding values for 183 FFR were 39.4% and 27.5%, respectively. Interestingly, SUPIs waste noticed in the present study was 2.3-3.5 times higher than the value reported in the literature. In particular,

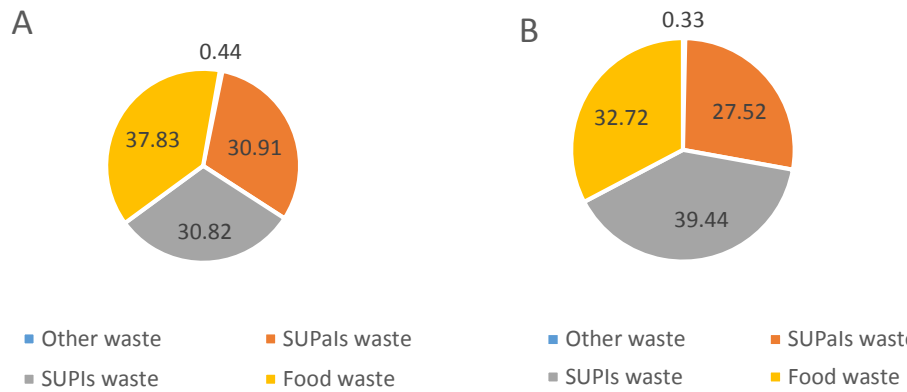

Fig. 4: The percentage of waste composition and SUIs disposed at the studied restaurants in HCMC: (A) Data of waste composition collected from 30 waste bins, (B) Data of waste composition estimated for 183 FFRs.

plastic waste accounted for 11% of total waste generated at McDonald's restaurants in Finland in 2006 (Aarnio & Hämäläinen 2008), which was 2.8 to 3.5 times lower than this study's findings. This can be explained as the consequence of the difference in McDonald's policies in several developed countries and Vietnam. In particular, although McDonald's has set its policy on the type of packaging materials to be used for its operations since the 2000s, the packaging material consumed was 22% of the global plastic packaging for function and safety of food worldwide (Packaging and Recycling - McDonald's, n.d.). However, the survey process in HCMC indicated that the McDonald's-owned restaurants still used a variety of SUPIs, such as spoons, forks, knives, straws, condiment containers, and cups as presented in Table 2. Thus, the percentage of plastic packaging waste at McDonald's in Finland in 2006 was lower than these findings. Similarly, SUPIs accounted for only 17% of the waste generated in seafood restaurants in Fano, Italy (Tatàno et al. 2017), which was 1.8 to 2.3 times lower than the percentage of SUPIs in the waste generated by the studied FFRs. It can be explained that restaurants in Fano, Italy served seafood that was preferred in the dining area instead of taking them away as fast food. Additionally, Finland and Italy were two of the European countries that issued policies on the limitation in the use of SUPIs (UNEP, 2018a). In contrast, the large percentage of SUPIs (30,8% of the waste in 30 bins and 39.4% of the waste calculated for 183 restaurants) in the waste generated the studied FFRs was 2.8 times higher than the value of 14% of plastic waste reported in the municipal solid waste in HCMC. The difference could be explained

Table 2: The type and the weight of individual SUPIs used by six FFCs (g).

Type of SUPIs	Lotteria	KFC	Jollibee's	Popeyes Stores	Texas Chicken	McDonald's
Plastic spoon 1	-	1.38	-	-	-	2.67
Plastic spoon 2	3.80	2.88	3.37	3.50	2.84	3.65
Plastic fork	2.83	3.08	3.02	2.85	2.99	3.57
Plastic knife	-	-	-	-	2.8	3.81
Plastic straw	0.64	0.47	0.44	0.52	0.56	0.52
Plastic condiment container	0.58	0.86	0.47	0.81	1.02	0.58
Small plastic lid	1.55	1.39	1.68	1.98	-	1.80
Big plastic lid	2.7	4.62	-	-	2.30	-
Plastic cup	14.4	13.6	-	-	13.21	20.39
Plastic ice cream cup	5.47	9.01	-	-	-	-
Plastic container	37.85	5.61	-	-	-	-
Plastic bag	4.22	6.07	6.36	-	-	3.13
Styrofoam container	-	-	4.03	-	-	-
Big paper cup	12.06	10.66	9.26	9.02	10.71	9.03
Small paper cup	7.08	9.00	7.16			
Paper ice cream cup	6.68	-	7.93	-	-	9.78
Paper tea cup 1	-	-	10.14	-	-	-
Paper tea cup 2	-	-	13.98	-	-	-
Medium paper bag	8.00	6.96	5.68	6.21	5.84	5.92
Large paper bag			6.19			9.18
Small paper bag	3.05	7.05	5.77	4.42	1.2	9.41
Wrapping paper	2.85	1.64	3.24	2.85	2.68	2.24
Paper container 1	-	8.32	-	-	-	7.57
Paper container 2	-	17.48	-	-	5.87	11.2
Paper container 3	-	27.09	25.29	28.40	34.98	13.09

Note: (-) Not used.

by the significant contribution of domestic waste (60-70%) to the municipal solid waste generated in HCMC (Thang et al. 2018).

Composition of SUPIs and SUPaIs

Data on the number and weight of SUIs consumed per day collected from the FFRs is presented in Table 2 and Fig. 5.

In particular, the estimated amount of SUIs consumed per day across the 183 FFR was 2.49 t (Fig. 5A and Fig. 5C). Of which, the amount of SUPaIs (57% - 1.41 t - Fig. 5C) was 1.3 times higher than the SUPIs (43% - 1.08 t - Fig. 5A). In contrast, the amount of SUIs waste generated was 3.87 t (Fig. 5B) with SUPIs share (2.27 t) was 1.42 times more than that of SUPaIs waste (1.6 t). The reason for this difference was that many customers brought takeaway drinks or food from other food services when they visited the studied FFRs. This increased the number of SUPIs disposed of in the studied FFRs.

Fig. 5B shows that the number, type, and weight of individual SUPIs consumed varied across the six FFCs in HCMC. Plastic cups accounted for the highest weight (400 kg), followed by plastic lids (193 kg). This result was in accordance with the previous results, which indicated that 75% of food delivery packaging waste in Chinese megacities

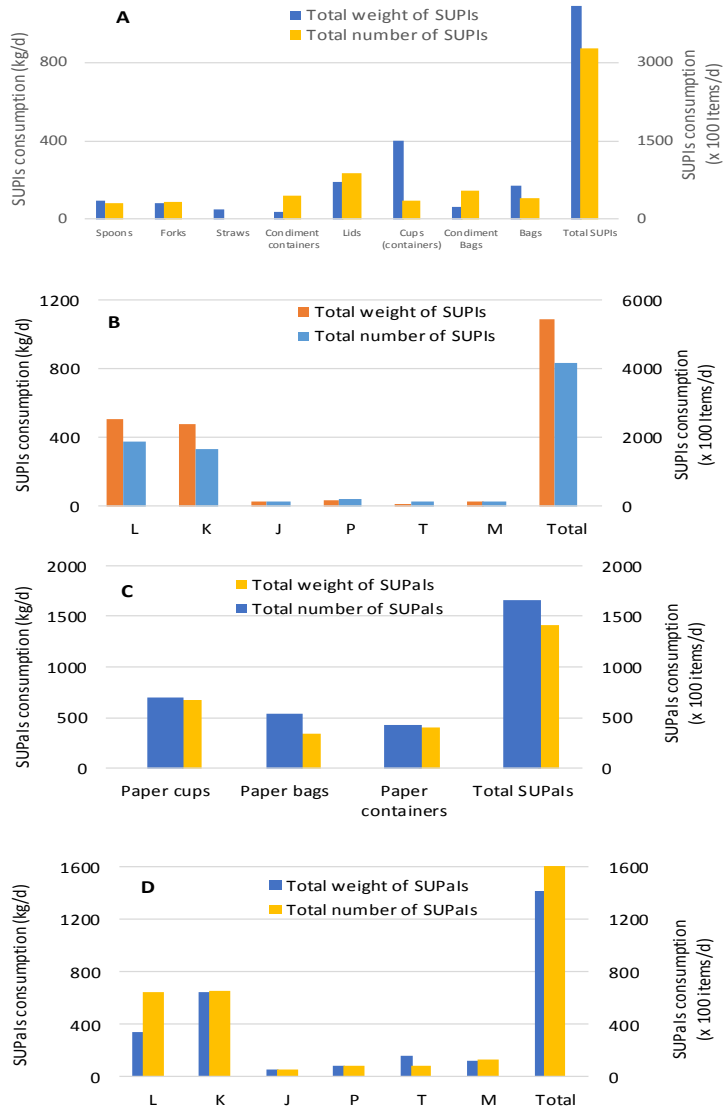

Fig. 5: The total weight and the number of SUIs consumed per day by six FFCs: (A) by each type of SUPIs, (B) by SUPIs across FFCs, (C) by each type of SUPaIs, and (D) by SUPaIs across FFCs. Note: L: Lotteria; K: KFC; J: Jollibee's; P: Popeye Stores; T: Texas Chicken and M: McDonald's.

was plastic containers (Song et al. 2018) and 32 million of SUPIs annually consumed were plastic bottles, cups, bags, and disposal plastics by food delivery (Jang et al. 2020).

In addition, the considerable number of SUPIs, including condiment containers, straws, and forks, appears to around 168 kg/day and was estimated to be about 43.7 t/yr (260 weekdays/yr). Most of these SUPIs have been identified as unnecessary SUPIs and have been enacted to be banned in many countries (UNEP 2018a).

In terms of the number of SUIs, the total number of individual SUPIs and SUPaIs consumed across the studied FFCs is presented in Fig. 5A and Fig. 5C. Results showed that the total number of SUPIs consumed across the studied FFCs was 415633 items and was 2.5 times higher than that of SUPaIs (166357 items). However, the total weight of SUPIs consumed was 1.3 times lower than that of SUPaIs. This variation in the weight distribution between SUPI and SUPaIs was obviously due to the difference in the weight of individual SUIs.

Regarding the weight of SUIs, the total weight of SUPaIs consumed per day was approximately 1.41 tons and 1.3 times higher than the weight of SUPIs (1.08 t). Results showed that the number, type, and weight of individual SUPIs consumed varied across the six FFCs in HCMC (Fig. 5B) and depended on the number of company-owned restaurants. The relatively high amount of SUPIs consumed by Lotteria (508 kg) and KFC (474 kg) was due to the fact that these two FFCs had the highest number of franchises in HCMC, 90 and 49 respectively. Accordingly, the weight of paper cups consumed was 670 kg/day and was the highest among the SUPaIs. This amount of consumption of SUPaIs in HCMC was half the consumption rate by the under 65 Portuguese population (Gautam & Caetano 2017). Among SUPaIs, paper bags were the least consumed item (338 kg) (see Fig. 5C). Among the FFCs, the highest SUPaIs consumption (646 kg/d) was noticed for KFC followed by Lotteria, Texas Chicken, and McDonald's (Fig. 5D). Conversely, Jollibee's and Popeyes Stores had the lowest consumption rate of SUPaIs.

In respect of the material for SUPIs, the SUPIs used in the studied restaurants were made of polypropylene (PP- the resin identification codification-6), such as forks, spoons, and knives or condiment containers or Polystyrene (PS – the resin identification codification-5). Among these SUPIs, only PP and PS have a high potential for recycling (Van der Harst & Potting 2014). SUPIs made of PS are expected to have a less environmental impact than those made of PP. Previous studies indicated that the effects of these SUPIs on the environment would be reduced by 20% through effective recycling (Gallego-Schmid et al. 2019). Therefore, PS instead of PP should be used for the manufacturing of SUPIs. Furthermore, Lotteria, Jollibee's, and KFC in HCMC used plastic utensils without resin identification codifications. The resin identification codifications enable consumers to identify the post-consumer plastic products that can be recycled (UNEP 2018a). Therefore, it is essential to regulate all plastic manufacturers to mark the resin identification codifications on their plastic products.

Regarding the diversity of SUIs, Table 2 presents the type and the weight of individual SUIs across six FFCs. Among FFCs, Lotteria, KFC, Jollibee's, and Popeyes Stores did not provide plastic knives to their customers. As a standout, Jollibee's provided Styrofoam containers as packaging material for a particular rice dish. The lighter weights of SUPIs used in these restaurants were plastic straws and condiment containers and their weight ranged from 0.44 g (company Jollibee's straw) to 0.86 g (KFC's condiment container). Interestingly, Jollibee consumed the lowest amount of these two items. In contrast, the plastic cup from McDonald's (20.39 g) and a single plastic container of Lotteria (37.85 g) were the heaviest SUPIs used in these FFCs. However, the weight of other individual SUPIs ranged between 2 and 6 g across the six studied FFCs. Interestingly, Lotteria and KFC were the only FFCs with more diversified usage of SUPIs. From Table 2, it can be seen that SUPIs such as spoon, fork, straw, and condiment container have the same function for all fast-food restaurants. If we regulate that, the same amount of plastic for one individual spoon, one individual fork, one individual straw, and condiment container is 2.84 g (Texas Chicken), 2.83 g (Lotteria), 0.44 g (Jollibee's), and 0.47 g (Jollibee's), respectively (Table 2); therefore, the amount of plastic that would be prevented from being released into the environment by six FFCs in HCMC will be 42.3 kg/day, equal to 11 tons/year. These results suggested that the standardization of the size and the weight of each SUPI would prevent a considerable amount of plastic waste coming from SUPIs releasing into the environment.

The evidence from this study shows that there are several recommendations to improve the use and management of SUIs in FFRs, which aim to reduce the amount of plastic waste released into the ocean. First, the role of restaurant managers in encouraging their staff to provide the accurate number of required SUPIs to their customers. Second, the government should regulate separating waste at the source to collect and recycle plastic waste and other waste. Third, the FFCs need to identify unnecessary SUPIs to be phased out in a short time, which has been done in several developed countries (Accorsi et al. 2014). In addition, the Vietnamese government should issue the Packaging and Plastic Act as a intervention policy to standardize the size and the weight of each type of SUPIs, which would prevent a considerable

amount of plastic waste from SUPIs released into the environment. Finally, it is necessary to use reusable items in dining areas of FFRs, which leads to a significant reduction of plastic cups and cutlery used once. Further research should focus on the role of managers in sustainable alternatives to SUPIs.

CONCLUSION

The study showed that amount and type of SUIs consumed and disposed of varied among the studied FFCs and was dependent on the local waste management technologies and the national policies in HCMC. Results showed that the total waste collected across the six FFCs was 6 $t.d^{-1}$ and was equivalent to 1560 $t.yr^{-1}$ in HCMC. Of the total waste generated, SUPIs and SUPaIs accounted for 39% and 28%, respectively. Among the six FFCs, Lotteria consumed and generated the highest amount of waste while Popeyes Stores generated the least amount of waste. The total weight of unnecessary SUPIs (condiment containers, straws, and forks) was about 44 $t.yr^{-1}$. For sustainable waste management and to reduce the amount of plastic waste generated by the FFI, policies on separating waste at source, standardization in the size, weight, and material used for SUPI are highly recommended. Further, the vital role of FFCs in the improvement of SUPI management is to identify unnecessary SUPIs to be phased out at all FFCs in the near future and improve the local waste management practices through material recovery and recycling.

ACKNOWLEDGEMENT

The author's acknowledgment is to the research team who assisted in collecting data of waste, especially Bon The Nguyen, a team leader of HCMC Open University. This research was sponsored by the Vietnamese Ministry of Education and Training, program 911-PH.

REFERENCES

Aarnio, T. and Hämäläinen, A. 2008. Challenges in packaging waste management in the fast-food industry. Resour. Conserv. Recy., 52(4): 612-621.

Accorsi, R., Cascini, A., Cholette, S., Manzini, R. and Mora, C. 2014. Economic and environmental assessment of reusable plastic containers: A food catering supply chain case study. Int. J. Prod. Econ., 152: 88-101.

Akenji, L., Bengtsson, M., Kato, M., Hengesbaugh, M., Hotta, Y., Aoki-Suzuki, C., Gamaralalage, D. J. P. and Liu, C. 2019. Circular Economy and Plastics: A Gap-Analysis in ASEAN Member States. Mission of the European Union to ASEAN, Association of Southeast Asian Nations, South-East Asia

Alfagi, A., Purnaweni, H. and Setiani, O. 2015. Waste Management in KFC and Pizza Hut: Case Study in Semarang , Indonesia. 2015.

Bediako, K. A. 2018. KFC's s sustainable competitive advantage in the international franchising. Univ. Incarnate Word, 23: 1-13.

DecisionLab. 2016. Out-of-Home Food and Drink Consumption Trends Vietnam. https://www.decisionlab.co/download-ooh-trends-vietnam

Gallego-Schmid, A., Mendoza, J. M. F. and Azapagic, A. 2019. Environmental impacts of takeaway food containers. J. Clean. Prod., 211 (2019): 417-427.

Gautam, A.M. and Caetano, N. 2017. Study, design, and analysis of sustainable alternatives to plastic takeaway cutlery and crockery. Energy Procedia, 136: 507-512.

Geyer, R., Jambeck, J.R. and Law, K.L. 2017. Production, use, and the fate of all plastics ever made. Sci. Adv., 3(7): 25-29.

Gupta, M. 2019. A study on the impact of online food delivery app on restaurant business special reference to Zomato and Swiggy. Int. J. Res. Anal.Rev., 6(1): 889-893.

Hilario, J. S. 2014. Responsiveness of fast-food chain managers along Far Eastern University (FEU-Manila) towards the implementation of green practices in restaurants. International Res. J. Pub. Environ. Health, 1(9): 183-191.

Jang, Y. C., Lee, G., Kwon, Y., Lim, J. H. and Jeong, J. H. 2020. Recycling and management practices of plastic packaging waste towards a circular economy in South Korea. Resour. Conserv. Recycl., 158(December 2019): 104798.

Leal Filho, W., Saari, U., Fedoruk, M., Iital, A., Moora, H., Klöga, M. and Voronova, V. 2019. An overview of the problems posed by plastic products and the role of extended producer responsibility in Europe. J. Clean. Prod., 214: 550-558.

Moharir, R.V. and Kumar, S. 2019. Challenges associated with plastic waste disposal and allied microbial routes for its effective degradation: A comprehensive review. J. Clean. Prod.., 208: 65-76.

Ocean Conservancy. 2019. Plastics Policy Playbook: Strategies for a Plastic-Free Ocean. Ace p. 164.

Packaging and Recycling | McDonald's. (n.d.). Retrieved March 10, 2020, from https://corporate.mcdonalds.com/corpmcd/scale-for-good/packaging-and-recycling.html approximately 22% percent of our packaging globally remains in plastic

Perdana. 2018. Book search methodologies. J. Chem. Inf. Model., 53(9).

Plastics 2019. Plastics: The Facts 2019. An Analysis of European Plastics Production, Demand, and Waste Data. https://www.plasticseurope.org/application/files/9715/7129/9584/FINAL_web_version_Plastics_the_facts2019_14102019.pdf

Song, G., Zhang, H., Duan, H. and Xu, M. 2018. Packaging waste from food delivery in China's megacities. Resour. Conserv. Recycl., 130 (November 2017): 226-227.

Tatàno, F., Caramiello, C., Paolini, T. and Tripolone, L. 2017. Generation and collection of restaurant waste: Characterization and evaluation at a case study in Italy. Waste Manag., 61: 423-442.

Thang, N. T., Liu, C., Hotta, Y., Fushimi, E. and Inoue, M. 2018. Vietnam, Country Chapter, State of the 3Rs in Asia and the Pacific. United Nations Centre for Regional Development.

UNEP. 2016. Marine plastic debris & Microplastic - Global lessons and research to inspire action and guide policy change. United Nations Environment Programme, Nairobi.

UNEP. 2018a. Legal Limits on Single-Use Plastics and Microplastics: A Global Review of National Laws and Regulations. https://www.unep.org/resources/publication/legal-limits-single-use-plastics-and-microplastics-global-review-national

UNEP. 2018b. Single-Use Plastics: A Roadmap for Sustainability Ministry of Environment, Forest and Climate Change. https://www.unep.org/resources/report/single-use-plastics-roadmap-sustainability.

Van der Harst, E. and Potting, J. 2014. Variation in LCA results for disposable polystyrene beverage cups due to multiple data sets and modeling choices. Environ. Model. Software, 51: 123-135.

Verma, R. L., Borongan, G. and Memon, M. 2016. Municipal solid waste management in Ho Chi Minh City, Vietnam: Current practices and future recommendation. Procedia Environ. Sci., 35: 127-139.

Vietnam: Fast food chains in the slow lane amid focus on health - ProQuest. (n.d.). Retrieved April 3, 2020, from https://search-proquest-com.libraryproxy.griffith.edu.au/docview/2242455477?pq-origsite=summon

Vietnam: Vietnam's food processing, packaging sector thriving - ProQuest. (n.d.). Retrieved April 3, 2020, from https://search-proquest com.libraryproxy.griffith.edu.au/docview/2295565133/fulltext/C77C6F-07009D4C64PQ/1?accountid=14543

Vietnam: Vietnam ranks eighth for global franchise expansion - ProQuest. (n.d.). Retrieved April 3, 2020, from https://search-proquest-com.libraryproxy.griffith.edu.au/docview/2275585814?pq-origsite=summon.

Zion Market. 2017. Global Industry Trends in Fast Food Market Size & Share Will Surpass USD 690.80 Billion by 2022. Zion Market Research. https://www.globenewswire.com/news-release/2019/07/12/1882007/0/en/Global-Industry-Trends-in-Fast-Food-Market-Size-Share-Will-Surpass-USD-690-80-Billion-by-2022.html

Nature Environment and Pollution Technology
An International Quarterly Scientific Journal

p-ISSN: 0972-6268
(Print copies up to 2016)
e-ISSN: 2395-3454

Vol. 20 | No.3 | pp. 997-1006 | 2021

Original Research Paper

https://doi.org/10.46488/NEPT.2021.v20i03.007

Open Access Journal

Soil Organic Carbon Stocks and Its Driving Factors Under Different Land-Use Patterns in Semiarid Grasslands of the Loess Plateau, China

Hao Zhang*, Jianping Li*(**)†, Yi Zhang*, Yutao Wang*, Juan Zhang*, Xu Luo* and Ru Zhang*
*School of Agriculture, Ningxia University, Yinchuan, Ningxia, 750021, China
**Breeding Base of State Key Laboratory for Preventing Land Degradation and Ecological Restoration, Ningxia University, Yinchuan, Ningxia, 750021, China
†Corresponding author: J. Li; lijianpingsas@nxu.edu.cn

Nat. Env. & Poll. Tech.
Website: www.neptjournal.com

Received: 30-09-2020
Revised: 28-10-2020
Accepted: 08-12-2020

Key Words:
Soil carbon stocks
Soil respiration
Fenced and grazed grassland
Soil properties
Semi-arid region

ABSTRACT

Fencing for grazing exclusion and grazing are common land-use methods in the semi-arid areas of the Loess Plateau in China, which have been widely found to change grassland soil organic carbon (SOC); however empirical studies that evaluated driving factors of soil carbon (C) stocks under the different land use are still weak. In this study, we investigated soil physicochemical and soil respiration (Rs) in the fenced and grazed grassland, to study the soil C stock variations and the main driving mechanism of soil C accumulation. The results showed that bulk density (BD), soil moisture content (SMC), and soil porosity (SP) had no significant difference between fenced and grazed grassland. Fencing increased the SOC, total nitrogen (TN), and C/N ratio, and significantly increased the aboveground biomass (AGB), belowground biomass (BGB), and the amount of soil large macro-aggregates in the topsoil layer (0-10 cm), and the soil stability was improved. Meanwhile, grazing increased soil temperature (ST) and Rs. The soil C stock in the topsoil layer (0-10 cm) of fenced grassland was significantly higher than that of grazed grassland. The soil C/N ratio, BD, and MWD explained large proportions of the variations in soil C stocks. Our results indicate that fencing can improve the stability of soil structure, and reduce Rs, then increase soil C stocks, which is an effective way to improve soil C stocks of grassland ecological in semi-arid areas of northwest China.

INTRODUCTION

The Intergovernmental Panel on climate change (IPCC) recently issued its special report on the impact of global climate change on global sustainable development. The report points out that without increased and urgent mitigation ambition in the coming years, leading to a sharp decline in greenhouse gas emissions by 2030, global warming will surpass 1.5°C in the following decades, leading to the frequent occurrence of extreme weather and gradual deterioration of global ecological environment (Lin et al. 2019). But it seems at present that global warming has continued unabated (Makarim et al. 2019). Global warming is related to the rising levels of atmospheric CO_2 over the past 23 million years (Cui et al. 2020). These data suggest present-day CO_2 (412 ppm) exceeds the highest levels that Earth experienced at least the past 800000 years (Keeling et al. 2001).

Soil C is the largest terrestrial C reservoir, containing about twice as much C as the atmospheric CO_2 pool globally, and the soil let 98 Pg C to the atmosphere with the soil respiration (Rs) annually, which is ten times of the burning of fossil energy (Shi et al. 2018). Therefore, we can reduce the atmospheric CO_2 concentration through strategies that both avoid loss of existing soil organic carbon (SOC) stocks and restore stocks in carbon (C) depleted soils, leading to mitigate the worsening global climate change (Smith et al. 2008, Thakur & Verma 2019). The role of soil organic matter as a regulator of climate has been recognized by scientists for decades (Bossio et al. 2020). Land-use change is identified as a cause of soil C losses and has been a significant source of atmospheric CO_2 over the last few centuries (Pradhan et al. 2019).

Grasslands cover 30-40% of the terrestrial surface area of the earth approximately and with 10% of the global soil C pool (Li et al. 2019, Zhang et al. 2020), which are the most widely distributed terrestrial ecosystems, play an important role in regional climate change and the global C cycle. In China, approximately 40% of the total land area is covered by grasslands; the grassland areas account for approximately 6-8% of the total global grassland area (Li et al. 2019). Compared to forest ecosystems, grasslands are marked by larger vegetation coverage and shorter vegetative growth cycles, which holds great potential as a C sink. And research has suggested that 47% of the total potential mitigation arises from SOC protection and sequestration in grasslands and agriculture, which is well above 9% of soil C mitigation

potential in the forest (Bossio et al. 2020). Fencing for grazing exclusion and free grazing are two common land-use patterns in the grassland ecosystem. Grazing exclusion is an effective practice for restoring overgrazed grasslands and an efficient grassland restoration management strategy that has been widely applied (Li et al. 2019). Generally, fencing increased SOC stocks and enhanced the capacity of soil functioning as a C sink. These studies show that overgrazing and conversion of freely grazed grassland to cropland lead to an annual average decline of 2.3-2.8% in SOC, but fencing increased the capacity of soil C stocks in china (Wang et al. 2011). Research on degraded grasslands in the arid desert regions of Northwest China suggests that although short-term grazing exclusion (three years) was not beneficial for C sequestration in the desert grassland, it is an effective strategy for improving the productivity of plants (Dong et al. 2020). Previous research by Yuan et al. (2020) had demonstrated that grazing exclusion for 14 years did not significantly affect soil SOC of the alpine meadow on the Tibetan Plateau, and differences in soil SOC were mainly controlled by the heterogeneity of the sites, rather than grazing exclusion (Yuan et al. 2020). Hafner et al. (2012) showed that sustainable moderate grazing is a suitable tool to preserve the high ability of the montane pasture land to store carbon, but fencing has a negative effect on soil surface C pool. In addition, Wang et al. (2009) showed that the Rs of grazed grassland is lower than that of grazing exclusion. Still, the study of soil respiration emission flux in alpine meadow suggested that compared with grazed grassland, grazing exclusion reduces CO_2 emission (Luo et al. 2020), and Rs increases with the increase of stocking rate (Cao et al. 2004).

The area of the grassland ecosystem accounts for about 1/3 of the land area of the Loess Plateau and 7.4% of the grassland area of China. With the large-scale implementation of the policy of converting slope farmland into forest and grassland, vegetation cover on the Loess Plateau has increased from 31.6% in 1999 to 59.6% in 2013, then up to 65.2% in 2017. Fencing for grazing exclusion and free grazing are two common land-use patterns in the grassland ecosystem on the Loess plateau (Li et al. 2019, Zhang et al. 2020). Different land-use patterns directly change the physical properties and structural stability of the soil, which is crucial for assessing the impact of enclosure and grazing on soil C stocks and surface flux and also helps us to understand the C sequestration potential of soil under different land-use patterns.

In this study, grazing exclusion grassland for eight years and free grazed grassland in the Yunwu Mountain grassland of the Loess Plateau were selected to measure soil C stocks and soil respiration along with physicochemical and water-stable aggregate. The objectives of this study were as follows: (1) to compare differences in soil C stocks between grazing exclusion and free grazing grasslands, and (2) to explore the effects of Rs, soil physicochemical and distribution characteristics of soil water-stable aggregates on soil C stocks between grazing exclusion and free grazed grasslands.

MATERIALS AND METHODS

Study Sites

The studied site was located in the Yunwu Mountain National Nature Reserve (36°10′-36°17′N, 106°21′-106°27′E), 45 km northeast of Guyuan City, Ningxia Autonomous Region, China in the southwest of the Loess Plateau at an altitude of 1,700-2,148 m. The soil type is dark loessial soil and mountain grey cinnamon soil, the average depth of the soil is 50 m. The underground water exists approximately 100 m below the land surface, and atmospheric precipitation mainly replenishes water resources. The experiment site has a temperate continental monsoon semi-arid climate with a mean annual temperature of 6.8°C and means annual precipitation of 410mm (1960-2010). Approximately 65%-85% of the total precipitation falls from July to September. The region's dominant plants are *Stipa bungeana*, *Stipa grandis*, *Thymus mongolicus*, *Artemisia stechmanniana*, and *Potentilla acaulis*. Since 1984, the regional government has implemented several mountain closure and grazing prohibition measures gradually from the center of Yunwu Mountain to the periphery, closing plots to livestock grazing and making them available for study. In this study, the fenced and grazed grasslands located in the periphery of Yunwu Mountain National Nature Reserve were selected with an interval of 1 km. Fenced grassland was built in 2011, and before the fencing was placed for grazing exclusion, the grasslands were used as grazed land, and the site's original condition (plant diversity and soil properties) was almost the same in both the grazed and fenced grasslands.

Experimental Design and Soil Sampling

The study was performed in October 2019. A single-factor (two levels, fenced grassland (FG) and grazed grassland (GG)) experiment was designed to investigate the differences between FG and GG. Three plots of 1 × 1 m were set up in each level, with an interval of 20 m. The livestock in GG included goats, and the average stocking rate was 2.5 goats.ha^{-1}.

Before sampling, grass, litter, or any other material on the soil surface were removed. Vertical soil profiles were dug in the sampling plots, and soil samples were collected from three soil layers (0-10, 10-20, 20-30 cm) using a ring knife (volume of 100 cm^3) and a spade for digging undisturbed soil weighing about a kilo. Soil samples were collected from the bottom to

the top of the soil profiles to avoid pollution and packed into Ziploc bags on-site for processing in the laboratory.

Measurements and Analysis Methods

We used a Li-8100 soil CO_2 flux system (LI-COR Inc., Lincoln, NE, USA) to measure Rs. A portable temperature probe connected to the Li-8100 was used to measure soil temperature (ST) at 5 cm depth, close to the PVC collar. The experimental measurement time is from 10:00 to 14:00 (local time). In the laboratory, the soil samples collected with the ring knife were used to measure the soil bulk density (BD, $g.cm^{-3}$), Soil moisture content (SMC, %) and soil porosity (SP, %) by the drying method in the laboratory. The sample remainders were air-dried, and each sample was split into two parts: one part passed through a two mm sieve to remove mixed litter and roots, then used for analyzing of soil organic carbon (SOC, $g.kg^{-1)}$, total phosphorus (TP, $g.kg^{-1}$) and total nitrogen (TN, $g.kg^{-1}$), and the other portion of the air-dried soil samples were used to determine the soil aggregate composition. Aggregates of six size classes were separated by wet sieving using Elliott's method (Elliott 1986). The aggregates were then split into three fractions: >2 mm (large macroaggregates), 0.25-2 mm (small macroaggregates), and <0.25 mm (microaggregates). The weight of aggregates for each class is used to calculate the mean weight diameter (MWD, mm). MWD was calculated as:

$$MWD = \sum W_i \times X_i$$

Where i is each aggregate fraction collected, Wi is the average diameter of fraction i and Xi is the dry mass of fraction i relative to the total soil mass.

The SOC stock was calculated using the following equation (Li et al. 2019):

$$C_s = \frac{BD \times SOC \times D}{10}$$

Where Cs, BD, SOC, and D are soil C stocks ($Mg.hm^{-2}$), soil bulk density ($g.cm^{-3}$), soil organic carbon ($g.kg^{-1}$), and soil depth (cm), respectively.

Statistical Analyses

All data were expressed as the mean ± standard deviation (SD). One-way ANOVA with Duncan test was performed to determine the differences in soil C stock and other soil properties were examined across the different soil depths, and a *t*-test was applied to determine the differences in the means of soil properties between GG and FG. Significant differences were assessed at the level of $P < 0.05$. We used redundancy analysis (RDA), a constrained ordination method, to determine the proportions of variability in soil C stock and Rs explained by environmental factors, using Canoco 5.0 software. The eigenvalues were proportional to the total variance explained for each axis, and were extracted from every variable as linear combinations of environmental attributes. In addition, the relationships of environmental factors with soil C stock were determined using Pearson's correlation analysis.

RESULTS

Variations in Soil Properties under Fenced Grassland and Grazed Grassland

Soil physicochemical properties: The soil bulk density (BD), moisture content (SMC), and porosity (SP) in the 0-30 cm soil layer were not significantly different between FG and GG, except the fencing significantly improved the SP in the soil layer of 20 to 30 cm of FG and led to significant differences between FG and GG ($P < 0.05$) (Table 1). As shown in Table 1, BD increased gradually with an increase in soil depth, whereas SMC decreased stepwise. FG and GG 20-30 cm soil layer BD was significantly higher than the 0-20 cm soil layer, and 0-10 cm SMC is significantly higher than 10-

Table 1: Soil physicochemical in fenced grassland (FG) and grazed grassland (GG).

Variables	FG			GG		
Soil layer(cm)	0-10	10-20	20-30	0-10	10-20	20-30
Bulk density ($g.cm^{-3}$)	1.04±0.05Ab	1.09±0.02Aab	1.15±0.02Aa	1.08±0.01Ab	1.08±0.01Ab	1.18±0.07Aa
Soil moisture (%)	21.03±0.10Aa	20.53±1.41Aab	18.22±1.25Ab	22.22±0.87Aa	19.92±0.41Ab	19.96±0.67Ab
Soil porosity (%)	54.23±2.86Aa	55.55±2.68Aa	54.39±0.13Aa	54.46±2.29Aa	56.39±1.39Aa	49.64±1.46Bb
Soil organic carbon($g.kg^{-1}$)	17.71±1.79Aa	14.98±1.31Aab	14.10±0.82Ab	14.22±0.61Aa	14.77±0.70Aa	15.5±1.4Aa
Total nitrogen ($g.kg^{-1}$)	2.02±0.04Aa	1.93±0.08Aab	1.81±0.11Ab	1.83±0.06Ba	1.89±0.08Aa	1.9±0.04Aa
Total phosphorus($g.kg^{-1}$)	0.66±0.02Aa	0.64±0.03Aa	0.67±0.01Aa	0.65±0.05Aa	0.67±0.01Aa	0.68±0.01Aa
Soil pH	8.24±0.47Aa	8.49±0.05Aa	8.56±0.06Aa	8.09±0.69Aa	8.47±0.04Aa	8.44±0.03Ba
C/N ratio	8.77±0.65Aa	7.76±0.41Aa	7.92±0.08Aa	7.78±0.57Aa	7.83±0.25Aa	8.15±0.75Aa

Note: Data represent the average of three replicates ± standard deviations. Different capital letters indicate significant differences ($P < 0.05$) among the grassland utilization ways. Different lower case letters indicate significant differences ($P < 0.05$) among the different soil layers, the same below.

30 cm. The SP of soil layers in FG changed little with depth, but the SP of 0-10 cm, 10-20 cm in GG was significantly higher than 20-30 cm. FG had greater SOC content, TN content, and C/N than GG in the 0-10 cm soil layer. The SOC content, TN content, and C/N in FG decreased gradually as soil depth deeper, and the SOC content and TN content of 0-10 cm were significantly higher than 20-30 cm. However, SOC content, TN content, and C/N in GG increased gradually as soil deeper. There was no significant difference in the TP content between FG and GG, and the distribution of TP content was relatively uniform between the vertical layers of the soil. The mean pH value in the topsoil layer (0-10 cm) of FG and GG was lower than 10-20 cm; their values are 8.24 and 8.09, respectively. The pH value of 20-30 cm in FG was significantly higher than that in GG.

Soil respiration and soil temperature: The Rs and ST of GG were higher than that of FG, the difference was not significant. The Rs of GG increased by 5.58%, and the average soil temperature increased by 1.2°C, compared with FG (Fig. 1).

Water-stable aggregate distribution and MWD: In the 0-10 cm soil layer, the amount of large macroaggregates (>2 mm) was significantly higher in FG (50.67%) than GG (36.69%), but the amount of small macroaggregates (0.25-2 mm) was significantly higher in GG (29.27%) than FG (13.13%)(Table 2). The amount of microaggregates (<0.25 mm) in each soil layer was higher in FG than GG, but not significantly.

The dominant fractions in the distribution of soil aggregates were the large macroaggregates (>2 mm) and microaggregates fractions (<0.25 mm) in each soil layer of FG and GG, and the large macroaggregates (>2 mm) fractions significantly decreased as soil depth increased. However, there was an inverse trend in the microaggregates (<0.25mm) fractions (Table 2).

The aggregate MWD in the 0-10 cm soil layer was significantly higher in FG than GG, and higher than the other soil layers. Among which, compared with 10-20 cm and 20-30

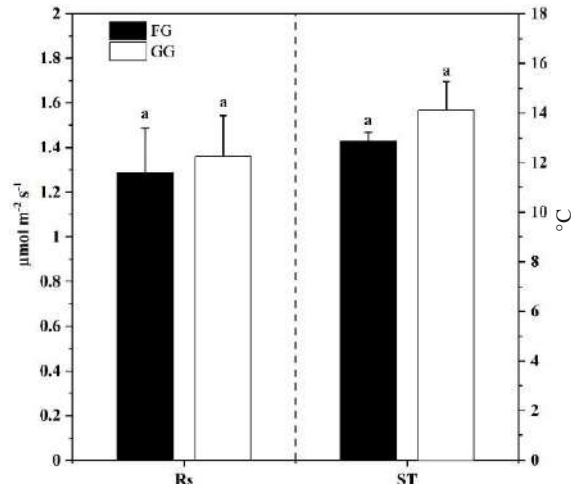

Fig. 1: Soil respiration (Rs) and soil temperature (ST) in fenced grassland (FG) and grazed grassland (GG)

Note: Different lower case letters indicate significant differences (P < 0.05) among the grassland utilization ways, the same below.

Table 2: Distribution of aggregate size and mean weight diameter (MWD) in fenced grassland (FG) and grazed grassland (GG)

Variables	Soil layer (cm)	Aggregate proportion in size class (%)			MWD
		>2mm	0.25-2mm	<0.25mm	
FG	0-10 cm	50.67±2.08Aa	13.13±2.93Ba	36.2±1.21Ab	3.78±0.14Aa
	10-20 cm	24.45±8.61Ab	16.89±10.57Aa	58.66±13.33Aa	1.90±0.61Ab
	20-30 cm	22.77±15.05Ab	13.13±5.21Aa	64.1±10.32Aa	2.35±0.26Ab
GG	0-10 cm	36.69±1.02Ba	29.27±7.93Aa	34.03±7.91Ab	2.83±0.25Ba
	10-20 cm	33.89±9.17Aa	15.27±1.65Ab	50.84±7.53Aa	2.57±0.67Aa
	20-30 cm	29.45±5.21Aa	13.12±0.35Ab	57.43±4.97Aa	2.25±0.36Aa

cm, aggregate MWD of 0-10 cm increased 98.9% and 60.6% in FG, respectively, and reach a significant level (Table 2).

Changes in Plant Biomass and Soil C Stocks Under Fenced Grassland and Grazed Grassland

FG had greater aboveground biomass (AGB) ($P<0.05$) than GG. The belowground biomass (BGB) ($P= 0.0669$) in the underlying soils was not significantly different between FG and GG (Fig. 2). AGB and BGB of FG increased by 193.62% and 154.32% respectively compared with GG. And the biomass of FG and GG are both BGB higher than AGB.

The soil C stock in the 0-30 cm soil layer did not significantly differ between FG and GG. And FG improved by only 8.92%, compared with GG in the 0-20 cm soil layer. However, the C stock in the 0-10 cm soil layer of FG was significantly higher than that of GG, which was 17.57 $Mg.hm^{-2}$ and 15.25 $Mg.hm^{-2}$, respectively. In addition, the changing trend of C stock in the 0-30 cm soil layer of FG and GG was different with the soil depth increased. Soil C stocks of FG decreased gradually with the increase of soil depth. But the changing trend of C stocks in GG is the opposite of that of FG. Moreover, the C stock in the 20-30 cm soil layer of GG was significantly higher than the other soil layers (Fig. 3).

Factors Affecting Soil C Stocks and Soil Respiration

The RDA showed that soil physicochemical and distribution characteristics of soil aggregates explained 92.70% of the total variation in surface soil C stock and Rs (Table 3). The Monte Carlo permutation test showed that surface soil C stock and Rs variations of FG and GG were explained by the first two axes (Table 3), with the first axis explaining 72.70% ($F=10.7$, $p=0.004$) and the second axis explaining 20.00% ($F=4.6$, $p=0.016$, Table 3). The C/N ratio and BD were the factors most strongly related to the first axis; the second axis was closely related to BGB and AGB (Table 3). The forward selection was conducted on the environmental variables, in turn until there was no obvious explanatory variable in the RDA ordinations, it indicated that surface soil C stock and Rs were mainly affected by the C/N ratio, TN, BD, and BGB (Table 3 and Fig. 4). The surface soil C stock was primarily affected by C/N, BD, and MWD while the Rs was primarily affected by the BGB and ST (Table 4). In addition, there is a positive correlation between Rs and soil C stocks under different land uses. The bivariate correlation analyses were used to evaluate the impact factors on soil C stocks (Fig. 5), the results show that there were large differences in the correlations on environmental factors and soil C stocks between different land uses. Surface soil C stock of FG and GG was positively correlated with SOC content and C/N ratio. And soil C stocks of GG had a significant positive relationship with BD alone, in addition to the SOC content and C/N ratio. However, surface soil C stock of FG was positively correlated with Rs, large macroaggregates, microaggregates, AGB, SMC, ST, and MWD (Fig. 5).

DISCUSSION

Soil is the most important component of the grassland ecosystem and the core of the ecosystem structure and function. The change of soil condition greatly affects the grassland ecosystem and closely related to human survival. Therefore, soil change caused by land-use change has always been a research hotspot in the field of the ecosystem. Normally, in the ways of traditional grazing, the soil compaction caused by animal weight is distributed vertically through the hoof

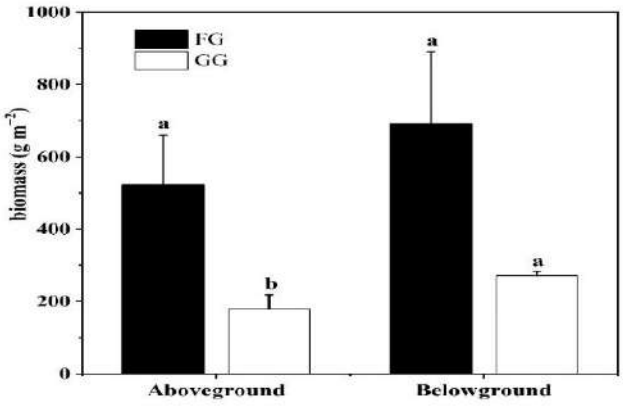

Fig. 2: Aboveground and belowground biomass in fenced grassland (FG) and grazed grassland (GG)

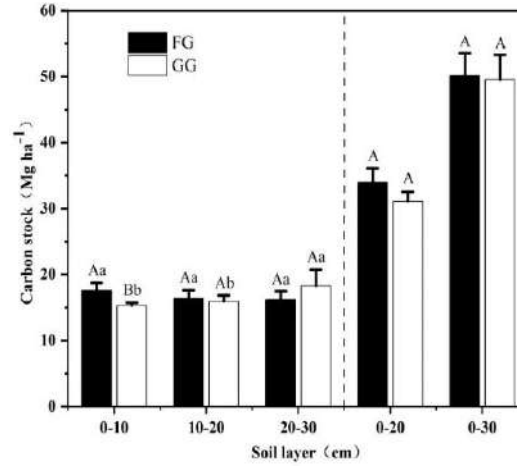

Fig. 3: Soil C stocks in fenced grassland (FG) and grazed grassland (GG).

Note: Different capital letters indicate significant differences ($P<0.05$) among the grassland utilization ways. Different lower case letters indicate significant differences ($P<0.05$) among the different soil layers.

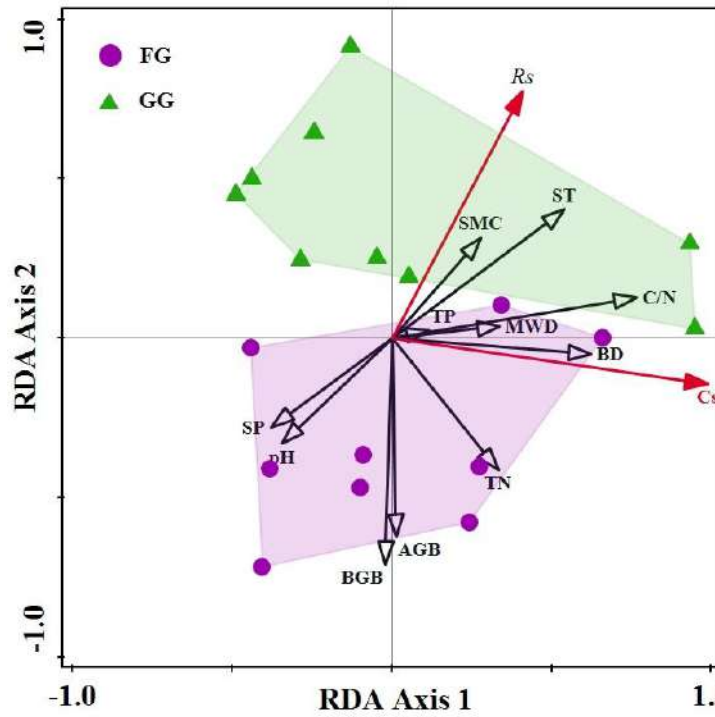

Fig. 4: Redundancy analysis (RDA) ordination diagram for soil carbon stock (Cs) and soil respiration (Rs) with environmental variables in fenced grassland (FG) and grazed grassland (GG).

Table 3: Statistic summary and canonical coefficients of Soil physicochemical and bio-mass characteristics for the first two axes of the RDA in fenced grassland (FG) and grazed grassland (GG).

Variables	Axis 1	Axis 2	λ-1	λ-A	*P*-value	F ratio
C/N	0.7652	0.1288	42.9	42.9	0.002	10.5
TN	0.3321	-0.4132	11.4	16	0.006	5.1
BD	0.6234	-0.0494	28.3	16.4	0.002	7.9
BGB	-0.0214	-0.7066	10	8.5	0.04	5.7
SMC	0.2787	0.316	7.6	5	0.054	4.5
TP	0.1147	0.0255	1	1.1	0.35	1
MWD	0.3375	0.0385	8.3	1.8	0.248	1.7
AGB	0.0126	-0.6217	7.7	0.6	0.484	0.6
ST	0.5397	0.4049	24.5	0.3	0.696	0.2
pH	-0.3445	-0.3304	10.8	0.1	0.782	<0.1
SP	-0.3772	-0.2778	11.9	<0.1	0.89	<0.1
Eigenvalues	72.70	20.00				
P value	0.004	0.016				
F ratio	10.7	4.6				

Note: C/N, C/N ratio; TN, total nitrogen; BD, bulk density; BGB, belowground biomass; SMC, soil moisture content; TP, total phosphorus; MWD, mean weight diameter; AGB, aboveground biomass; ST, soil temperature; pH, pH value; SP, soil porosity. λ-1: the variance when the variable is used as the only factor. λ-A: the additional variance of each variable explain when it is included in the model. *P*-value indicates the significance of λ-A.

area. This determines an increased BD and thus a reduction in SP and vertical water permeability. However, fencing for grazing exclusion is known to increase plant biomass and litter input to the soil, and consequently the quantity and quality of SOC. SOC plays a potential beneficial effect role in forming and stabilizing soil structure, enhancing soil physical properties. This may, in turn, increases the accumulation of organic matter on the soil surface that may reduce the volume, velocity, and erosive capacity of surface run-off (Yimer et al. 2015). Our results show that FG had greater AGB($P<0.05$) and BGB($P= 0.0669$) than GG, but grazing exclusion had weak effects on BGB in comparison to that in GG. This was similar to previous studies showing that AGB and BGB in long-term fenced and overgrazed temperate grasslands in northwest China, in that, fencing can enhance plant cover and biomass because it protects the soil seed bank and increases species composition recovery (Li et al. 2019). There was little difference in the soil physical properties under two soil-use patterns, in both FG and GG, such as BD, SMC, and SP. This was similar to previous studies showing that both BD and SMC did not vary with land-use types at the Central Rift Valley area of Ethiopia (Yimer et al. 2015). However, in contrast to the results from other studies, the SMC of the 0-10 cm layer of FG was lower than that of GG in our study. This is because vegetation restoration provided a favorable environment with rich moisture and moderate temperature, which facilitated the development of biocrusts at the early stage of grazing exclusion. The surface soil moisture was increased after eight years on fencing for grazing exclusion because biocrusts decreased the amount and depth of rain-

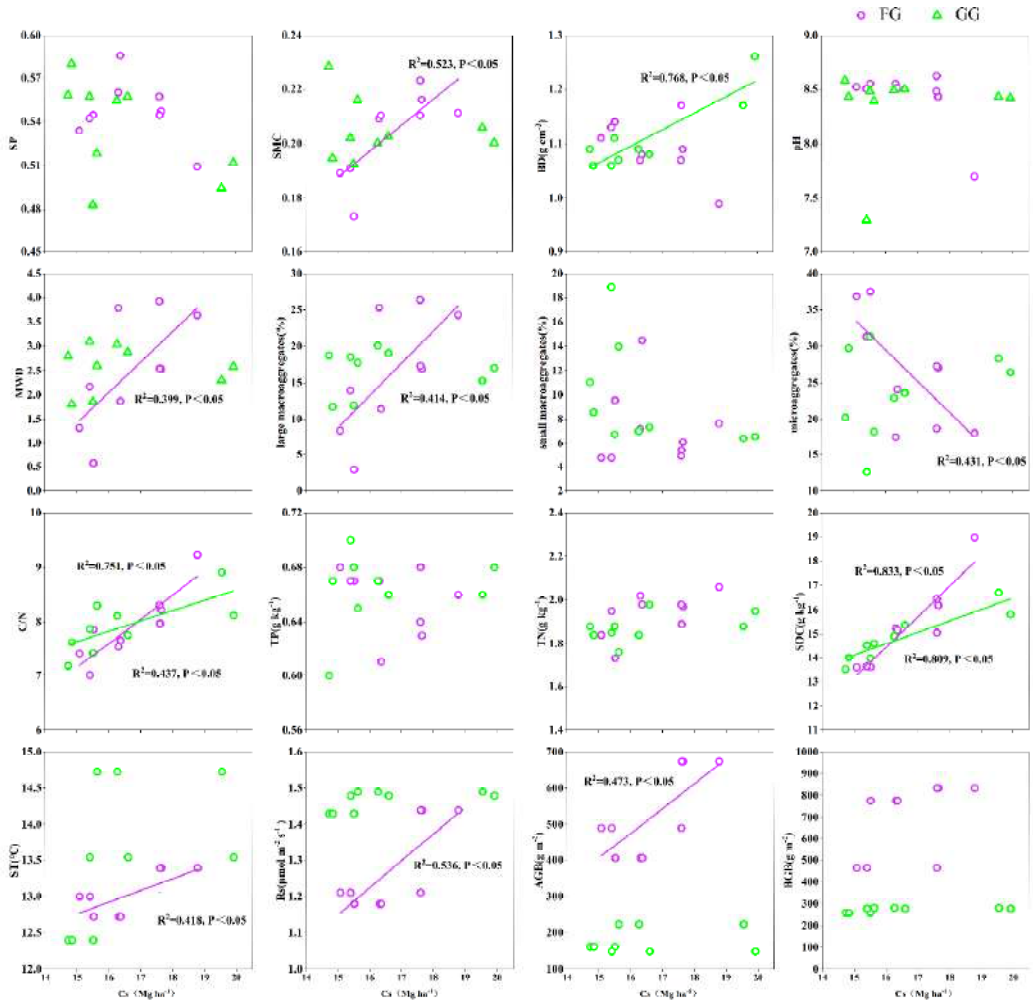

Fig. 5 Relationship of surface (0-30 cm) soil carbon stock with soil physicochemical and Soil aggregate stability of fenced grassland (FG) and grazed grassland (GG).

fall infiltration due to their lower infiltrability and higher water-holding capacity (Xiao et al. 2016).

Our findings indicate that the soil nutrient content showed strong variation under different land-use patterns. The difference was mainly observed topsoil layer (0-10 cm) between GG and FG, and distributions between the vertical layers of the soil. SOC content, TN content, and C/N in the 0-10 cm soil layer of FG are significantly higher than those of GG, and the TN content reaches a significant level ($p<0.05$). This is in line with previous studies in northern China's grasslands showing that the changes of the nutrient in the 0-10 cm soil layer between the different grasslands management and land use were the most evident (Wang et al. 2011). Our studies on the vertical direction of soil nutrients in grassland suggested that the SOC content, TN content, and C/N in FG decreased gradually as soil depth increased, which revealed the vertical transport of soil nutrients. On the contrary, the vertical direction of soil nutrients in GG increased as soil depth increased. This might be because frequent trampling by animals causes litter on the ground which mixed well with the soil (Carter et al. 2014) and then due to the higher SMC of GG compared with FG which facilitated decomposition and the release of labile-C inputs, it prompted a greater growth and activity of microbial biomass, resulting in the decomposition of both residue-C and native C (the C priming effect) (Shahbaz et al. 2017).

Well-developed soil structures are often seen as reliable indicators of grassland restoration. Soil aggregates are regarded as the basic unit of soil structure (Liu et al. 2020). Their formation and stabilization significantly affect SOC stocks and turnover. Our studies suggested that FG significantly improves the stability of soil aggregates in the 0-10 cm soil layer, compared with GG, and the MWD significantly increases by 33.6% (Table 2). At the same time, the amount of large macroaggregates in FG also increased significantly (Table 2). This might be because relatively abundant plant roots of FG enhance the formation of large macroaggregates and soil aggregate stability through physical entanglement, and provide root exudates and soil organic compounds as soil particle binders. However, frequent and severe grazing pressure will disturb the large macroaggregates and modify them into more microaggregates, and reduce the stability of soil aggregates. A study in Ghamishloo National Park, Isfahan, central Iran also showed that more proportions of large macroaggregates were observed in the protected area compared to the grazing-free area (Molaeinasab et al. 2018). However, we found that the amount of small macroaggregates in the 0-10 cm soil of FG was significantly lower than that of GG (Table 2), indicating that the soil large macroaggregates after the fencing for grazing exclusion were mainly composed of small macroaggregates. This is different from the view put forward by some scholars in perceptions that microaggregates formed from organic molecules are combined with clay and cations, which in turn are coupled to other microaggregates to form large macroaggregates following the hierarchy arrangements (Kurmi et al. 2020). This is perhaps a result of fencing for grazing exclusion.

Land-use change is identified as a cause of soil C losses and has been a significant source of atmospheric CO_2 over the past few centuries (Wang et al. 2011). Rs is the main way for CO_2 fixed by plants to return to the atmosphere, and it is the main factor affecting the carbon balance of the ecosystem (Hogberg & Read 2006). Changes in land use and management can cause changes in the structure or species composition of plant communities, soil physical and chemical properties, soil microclimate, and ground climate, thereby affecting the rate of Rs. Our study shows indicate that BGB is the primary factor affecting Rs under different land use patterns. Some studies have shown that 50%-93%

Table 4: Total variance of surface soil carbon stock and soil respiration explained by environmental variables based on redundancy analysis.

Ranking	Cs				Rs			
	Variables	Explains (%)	P	F	Variables	Explains (%)	P	F
1	C/N	54.5	0.004	16.8	BGB	30.9	0.024	6.3
2	BD	21.9	0.008	12.1	ST	16.4	0.062	4.0
3	MWD	10.7	0.008	10	SMC	10.6	0.108	3.0
4	ST	2.6	0.114	2.8	MWD	5.5	0.224	1.6
5	BGB	1	0.376	1	TP	7.5	0.122	2.6
6	pH	1.6	0.21	1.8	AGB	2.9	0.340	1.0
7	TP	0.3	0.612	0.3	pH	2.1	0.424	0.7
8	SMC	0.3	0.628	0.3	C/N	0.8	0.620	0.2
9	SP	<0.1	0.942	<0.1	TN	0.2	0.846	<0.1
10					SP	0.2	0.86	<0.1

of Rs is produced by plant root respiration in alpine regions (Kuzyakov & Blagodatskaya 2015), and some studies also show that CO_2 emission in the soil increases with the increase of BGB of plants (Liu et al. 2016). Past studies have shown that a better correlation between Rs and ST as well (Wang et al. 2020). As the soil temperature changes, the number and activity of microorganisms in the soil are enhanced or inhibited, which speeds up or slows down the decomposition rate of organic matter, resulting in a change in the Rs (Shao et al. 2017). Some studies have shown that the global temperature rise of 0.5°C will reduce the soil C stock in steady-state by about 6% (Trumbore et al. 1996). We found that the measurement of total CO_2 efflux from soil showed no significant differences between the land use types. This is consistent with the results of previous studies on grassland management in the Tibetan Plateau (Hafner et al. 2012). In addition, the Rs and ST of FG are lower than those of GG in our study. In general, the vegetation coverage and aboveground biomass of GG were significantly lower than that of FG due to the impact of trampling and feeding by livestock, which led to ST being strongly affected by light conditions, so ST was significantly higher than that of FG. And higher soil temperature accelerated the metabolic rate of the soil microbial community, both microbial metabolic quotients and microbial respiration of organic C in soil were also higher in the soils to warmer temperatures (Maranon-Jimenez et al. 2018). Our studies also indicate that soil temperature was an important factor affecting the Rs. We also identified a significant correlation between Rs and ST (Fig. 5).

Understanding the soil variables that affect the C stocks is a key goal for understanding the process of grassland vegetation restoration under different land use. The level of soil C/N ratio will facilitate or limit soil microbial activity to a certain extent, and the change of microbial activity will affect its respiration and ultimately affect soil C stocks. Microbial decomposition is faster in soils with lower C/N ratios (Zhao et al. 2019). In the study, the soil C/N ratio was an important factor affecting the soil C stocks. Our research also found that in FG there is a relatively low rate of Rs compared to GG (Fig. 1), which may cause the C stock in the 0-10 cm soil of FG to be significantly higher than that of GG (Fig. 3). In addition, the Rs showed a significant positive correlation with the C stock of FG (Fig. 5), which indicated that fencing for grazing exclusion promoted vegetation restoration, soil structure was stable, and higher C stock would increase its respiration rate. The C/N of 0-10 cm soil layer in GG was significantly lower than that of FG (Table1). This explains the results found in our study in which 0-10 cm C stock of GG is significantly lower than that of FG. Soil physical properties and aggregates also significantly affected the C stock (Table 4, Fig. 4). The soil C stocks of FG were positively correlated with SWC, large macroaggregates, and MWD, but the soil C stocks of GG were positively correlated with BD, consistent with previous findings (Yimer et al. 2015, Molaeinasab et al. 2018, Kurmi et al. 2020). This may be because fencing increased litter (fresh dead organic material) in the grassland ecosystem, and soil microorganism controls the content of soil organic matter and the stability of soil aggregates by directly transforming or physically intertwining secretion of extracellular polymeric substances or by changing the soil hydrophobic property (Tisdall & Oades 2006). SOC can promote the formation of stable soil aggregates, creating a large volume of mesopores and micropores, which hold capillary and hygroscopic water, respectively (Farley et al. 2004). This also explains the positive correlation between SMC and SOC of FG in this study. The soil aggregate contains about 90% of SOC, and the stable composition of soil aggregate can effectively reduce the decomposition of SOC (Jastrow 1996). Therefore, the soil surface C stock of FG is higher than that of GG, which is similar to the results of this study. Frequent and severe grazing pressures in GG disturb macroaggregates and modify them to more microaggregates, which weaken the stability of the surface soil structure and expose SOC to the ground surface (Molaeinasab et al. 2018), thus accelerating the decomposition of SOC. And trampling by livestock can significantly increase the BD of deep soil (Deng et al. 2014), so this study obtained a positive correlation between C stocks and BD.

CONCLUSION

We conclude that fencing for grazing exclusion can effectively increase AGB, BGB, and surface soil C stocks in semi-arid areas of the Loess Plateau. This is mainly due to the vegetation restoration of grassland after fencing for grazing exclusion enhances the formation of large macro-aggregates and soil aggregate stability. Rs may also be an important factor in affecting soil C stocks because the lower vegetation coverage of GG shows that ST was strongly affected by light conditions, and higher soil temperature accelerates the rate of Rs. This may result in lower C stocks on topsoil in GG than FG. In addition, grazing and trampling by livestock in GG may also affect surface soil C stocks. Therefore, further studies on mechanisms of Rs and grazing intensity on soil C stocks in grassland utilization are needed to fully explain how soil properties affect the vertical patterns of C stocks.

ACKNOWLEDGEMENT

The study was funded by the Key Research and Development Program of Ningxia (2020BEG03046), and the Top Discipline Construction Project of Pratacultural Science (NXYLXK2017A01)

REFERENCES

Bossio, D.A., Cook-Patton, S.C., Ellis, P.W., Fargione, J., Sanderman, J., Smith, P., Wood, S., Zomer, R.J., Von Unger, M., Emmer, I.M. and Griscom, B.W. 2020. The role of soil carbon in natural climate solutions. Nat. Sust., 3(5): 391-398.

Cao, G.M., Tang, Y.H., Mo, W.H., Wang, Y.A., Li, Y.N. and Zhao, X.Q. 2004. Grazing intensity alters soil respiration in an alpine meadow on the Tibetan plateau. Soil Biol. Biochem., 36(2): 237-243.

Carter, J., Jones, A., O'Brien, M., Ratner, J. and Wuerthner, G. 2014. Holistic management: misinformation on the science of grazed ecosystems. Int. J. Biodivers., 163431.

Cui, Y., Schubert, B.A. and Jahren, A.H. 2020. A 23 my record of low atmospheric CO_2. Geology, 48(9): 888-892.

Deng, L., Liu, G.B. and Shangguan, Z.P. 2014. Land-use conversion and changing soil carbon stocks in China's 'Grain-for-Green' Program: a synthesis. Glob. Change Biol., 20(11): 3544-3556.

Dong, Y.Q., Sun, Z.J., An, S.Z., Jiang, S.S. and Wei, P. 2020. Community structure and carbon and nitrogen storage of sagebrush desert under grazing exclusion in Northwest China. J. Arid Land, 12(2): 239-251.

Elliott, E.T. 1986. Aggregate structure and carbon, nitrogen, and phosphorus in native and cultivated soils. Soil. Sci. Soc. Am. J., 50(3): 627-633.

Farley, K.A., Kelly, E.F. and Hofstede, R.G.M. 2004. Soil organic carbon and water retention following conversion of grasslands to pine plantations in the Ecuadoran Andes. Ecosystems, 7(7): 729-739.

Hafner, S., Unteregelsbacher, S., Seeber, E., Lena, B., Xu, X.L., Li, X.G., Guggenberger, G., Miehe, G. and Kuzyakov, Y. 2012. Effect of grazing on carbon stocks and assimilate partitioning in a Tibetan montane pasture revealed by $^{13}CO_2$ pulse labeling. Glob. Change Biol., 18(2): 528-538.

Hogberg, P. and Read, D.J. 2006. Towards a more plant physiological perspective on soil ecology. Trends Ecol. Evol., 21(10): 548-554.

Jastrow, J.D. 1996. Soil aggregate formation and the accrual of particulate and mineral-associated organic matter. Soil Biol. Biochem., 28(4): 665-676.

Keeling, C.D., Piper, S.C., Bacastow, R.B., Wahlen, M., Whorf, T.P., Heimann, M. and Meijer, H.A. 2001. Exchanges of Atmospheric CO_2 and $^{13}CO_2$ with the Terrestrial Biosphere and Oceans from 1978 to 2000. I. Global Aspects. UC San Diego, Library - Scripps Digital Collection.

Kurmi, B., Nath, A.J., Lal, R. and Das, A.K. 2020. Water stable aggregates and the associated active and recalcitrant carbon in soil under rubber plantation. Sci. Tot. Environ., 703: 135498.

Kuzyakov, Y. and Blagodatskaya, E. 2015. Microbial hotspots and hot moments in soil: Concept & review. Soil Biol. Biochem., 83: 184-199.

Li, J.P., Ma, H.B., Xie, Y.Z., Wang, K.B. and Qiu, K.Y. 2019. Deep soil C and N pools in long-term fenced and overgrazed temperate grasslands in northwest China. Sci. Rep., 9: 16088.

Lin, J., Khanna, N., Liu, X., Teng, F. and Wang, X. 2019. China's Non-CO_2 greenhouse gas emissions: Future trajectories and mitigation options and potential. Sci. Rep., 9: 16095.

Liu, L.L., Wang, X., Lajeunesse, M.J., Miao, G.F., Piao, S.L., Wan, S.Q., Wu, Y.X., Wang, Z.H., Yang, S., Li, P. and Deng, M.F. 2016. A cross-biome synthesis of soil respiration and its determinants under simulated precipitation changes. Glob. Change Biol., 22(4): 1394-1405.

Liu, M., Han, G.L. and Zhang, Q. 2020. Effects of agricultural abandonment on soil aggregation, soil organic carbon storage and stabilization: Results from observation in a small karst catchment, Southwest China. Agric. Ecosyst. Environ., 288: 106719.

Luo, C.Y., Wang, S.P., Zhang, L.R., Wilkes, A., Zhao, L., Zhao, X.Q., Xu, S.X. and Xu, B. 2020. CO_2, CH_4 and N_2O fluxes in an alpine meadow on the Tibetan Plateau as affected by N-addition and grazing exclusion. Nutr. Cycl. Agroecosyst., 117(1): 29-42.

Makarim, S., Sprintall, J., Liu, Z.Y., Yu, W.D., Santoso, A., Yan, X.H. and Susanto, R.D. 2019. Previously unidentified Indonesian Throughflow pathways and freshening in the Indian Ocean during recent decades. Sci. Rep., 9: 7364.

Maranon-Jimenez, S., Soong, J.L., Leblans, N.I.W., Sigurdsson, B.D., Penuelas, J., Richter, A., Asensio, D., Fransen, E. and Janssens, I.A. 2018. Geothermally warmed soils reveal persistent increases in the respiratory costs of soil microbes contributing to substantial C losses. Biogeochemistry, 138(3): 245-260.

Molaeinasab, A., Bashari, H., Esfahani, M.T. and Mosaddeghi, M.R. 2018. Soil surface quality assessment in rangeland ecosystems with different protection levels, central Iran. CATENA, 171: 72-82.

Pradhan, B.B., Chaichaloempreecha, A. and Limmeechokchai, B. 2019. GHG mitigation in Agriculture, Forestry and Other Land Use (AFOLU) sector in Thailand. Carbon Bal. Manage., 14: 3.

Shahbaz, M., Kuzyakov, Y. and Heitkamp, F. 2017. Decrease of soil organic matter stabilization with increasing inputs: Mechanisms and controls. Geoderma, 304: 76-82.

Shao, S., Zhao, Y., Zhang, W., Hu, G.Q., Xie, H.T., Yan, J.H., Han, S.J., He, H.B. and Zhang, X.D. 2017. Linkage of microbial residue dynamics with soil organic carbon accumulation during subtropical forest succession. Soil Biol. Biochem., 114: 114-120.

Shi, Z., Crowell, S., Luo, Y.Q. and Moore, B. 2018. Model structures amplify uncertainty in predicted soil carbon responses to climate change. Nat. Commun., 9: 2171.

Smith, P., Martino, D., Cai, Z., Gwary, D., Janzen, H., Kumar, P., McCarl, B., Ogle, S., O'Mara, F., Rice, C., Scholes, B., Sirotenko, O., Howden, S., McAllister, T., Pan, G., Romanenkov, V., Schneider, U., Towprayoon, S., Wattenbach, M. and Smith, J. 2008. Greenhouse gas mitigation in agriculture. Phil. Trans. Royal Soc. London-B. Biol. Sci., 363(1492): 789-813.

Tisdall, J. and Oades, J. 2006. Organic matter and water-stable aggregates in soils. J. Soil Sci., 33: 141-163.

Thakur, M. and Verma, R.K. 2019. Biomass and soil organic carbon stocks under cedrus deodara forests in Mandi District of Himachal Pradesh. Nat. Environ. Pollut. Technol., 18(3): 879-887.

Trumbore, S., Chadwick, O. and Amundson, R. 1996. Rapid exchange between soil carbon and atmospheric carbon dioxide driven by temperature change. Science, 272: 393-396.

Wang, S.P., Wilkes, A., Zhang, Z.C., Chang, X.F., Lang, R., Wang, Y.F. and Niu, H.S. 2011. Management and land use change effects on soil carbon in northern China's grasslands: a synthesis. Agric. Ecosyst. Environ., 142(3-4): 329-340.

Wang, Y.Y., Hu, Z.H., Shang, D.Y., Xue, Y., Islam, A.R.M.T. and Chen, S.T. 2020. Effects of warming and elevated O_3 concentrations on N_2O emission and soil nitrification and denitrification rates in a wheat-soybean rotation cropland. Environ. Pollut., 257: 113556.

Wang, Z.W., Jiao, S.Y., Han, G.D., Zhao, M.l. and Walter, D.W. 2009. Soil respiration response to different stocking rates on Stipa breviflora Griseb. desert steppe. Acta Sci. Natur. Univ. Norm. Hunan., 40(2): 186-193.

Xiao, B., Hu, K.L., Ren, T.S. and Li, B.G. 2016. Moss-dominated biological soil crusts significantly influence soil moisture and temperature regimes in semiarid ecosystems. Geoderma, 263: 35-46.

Yimer, F., Alemu, G. and Abdelkadir, A. 2015. Soil property variations in relation to exclosure and open grazing land use types in the Central Rift Valley area of Ethiopia. Environ. Syst. Res., 4(1): 17.

Yuan, Z.Q., Epstein, H. and Li, G.Y. 2020. Grazing exclusion did not affect soil properties in alpine meadows in the Tibetan permafrost region. Ecol. Eng., 147: 105657.

Zhang, Y., Xie, Y.Z., Ma, H.B., Jing, L., Matthew, C. and Li, J.P. 2020. Rebuilding soil organic C stocks in degraded grassland by grazing exclusion: A linked decline in soil inorganic C. PeerJ, 8: e8986.

Zhao, Y.F., Wang, X., Ou, Y.S., Jia, H.X., Li, J., Shi, C.M. and Liu, Y. 2019. Variations in soil $\delta^{13}C$ with alpine meadow degradation on the eastern Qinghai-Tibet Plateau. Geoderma, 338: 178-186.

Nature Environment and Pollution Technology
An International Quarterly Scientific Journal

p-ISSN: 0972-6268
(Print copies up to 2016)
e-ISSN: 2395-3454

Vol. 20 | No.3 | pp. 1007-1019 | 2021

Original Research Paper

https://doi.org/10.46488/NEPT.2021.v20i03.008

Open Access Journal

Species Diversity, Soil Nutrients Dynamics and Regeneration Status of Sal (*Shorea robusta*) Forests in Western Himalayan Region of India

Akash†*, M. Zakir, Navneet* and B. S. Bhandari*****

*Department of Botany and Microbiology, Gurukul Kangri University, Haridwar, Uttarakhand, India

**Department of Biotechnology, Himalayan University, Itanagar, Arunachal Pradesh, India

***Ecology Laboratory, Department of Botany and Microbiology, H.N.B. Garhwal University, Shrinagar-246174, Uttarakhand, India

†Corresponding author: Akash; saklanibotany@gmail.com

Nat. Env. & Poll. Tech.
Website: www.neptjournal.com

Received: 03-09-2020
Revised: 03-11-2020
Accepted: 12-11-2020

Key Words:
Sal stand
Rajaji tiger reserve
Chilla forest
Species diversity
Soil nutrients

ABSTRACT

Sal (*Shorea robusta*) forest is found in an extensive array of conditions in Western Himalaya. It has been heavily used for commercial purposes. Thus, we did a study to gather the information on sal forests occupying a broad range of the Rajaji Tiger Reserve which spans across an extensive range in the Western Himalaya. We tested the species diversity, soil nutrients status, and regeneration potential of the Sal forest. Vegetation was sampled in 10 transects zone of 20×20 m^2 plots covering an area of 10.0 ha area. Trees, saplings, seedlings, shrubs, and herbs were sampled along the transects in the Chilla forest division of the tiger reserve. Samplings were done every 200 m along the transect with the help of the Nested quadrat method. Altogether 64 species were recorded: 24 trees, 12 shrubs, and 28 herbs. Environmental variables like pH, organic carbon, total nitrogen, available potassium, available phosphorous, and soil texture were also recorded to observe the effects of these environmental variables into diversity attributes. The Shannon Weiner index for trees was 1.350, for saplings 1.774, for seedlings 1.679. For shrub species, it was1.96. The Shannon Weiner index for herbaceous species in the rainy season was 2.8, in winter it was 2.36 whereas in summer it was 2.46. We concluded that the management of sal has enhanced the diversity and soil nutrients dynamics in the study area. Sal diversity also has enhanced the growth of co-dominant species like *Mallotus philippensis, Aegle marmelos, Listea chinensis, Naringi crenulata, Ehretia laevis, Cassia fistula,* etc. in the study area. Although we did not find any seedlings of the sal during the present study, the regeneration potential of sal forest increasing with a greater number of associated species provide a favorable environment for sal species.

INTRODUCTION

Sal (*Shorea robusta*) is one of the most important commercial timber trees in India. *Shorea robusta* forests of Western Himalaya are monocultures due to various silvicultural tasks at the time of British rule. Under these tasks, the natural associates of *S. robusta* were removed as 'Kokat' (Chauhan 2001, Negi et al. 2002). It is one of the most dominant forest communities in the lower region of Uttarakhand Himalaya. Acknowledging the ecological and economic distribution of *S.robusta* forest, different management regimes have been proposed under different land use classes and ownership. These forest types in India also come under Protected Area Network (PAN), Government managed forested areas which include National Parks and Wildlife Sanctuaries. The forest of Sal is mainly distributed in tropical regions of India and covers about 13.30 % of the total forest in the country (Satya & Nayaka 2005). In Uttarakhand Himalaya, *S. robusta* forest covers the major parts of Rajaji tiger reserve and Corbett tiger reserve. Sal in these reserves mainly occurs as a dominant tree under tropical moist and dry deciduous forests (Champion & Seth, 1968). In Western Himalaya, it occurs from the foothills of the Kangra region of Himachal Pradesh to the North-Eastern regions like Assam, Meghalaya, and Tripura through Uttar Pradesh, Uttarakhand, and Bihar at an altitude of 1,000 m (Satya & Nayaka 2005). It is generally found as a gregarious formation and tends to form pure to mixed forest stands in the foothills of Himalaya and the central part of India (Troup 1921). The whole Himalaya has a great diversity of plants that are still being utilized by the existing communities for their healthcare and traditional practice (Saklani et al. 2020).

To meet the increasing demand for timber trees due to the increasing human population, the tropical forests of Sal were converted into the urban landscape, various agricultural, and industries land which led to biodiversity and habitat loss (Jacquemyn et al. 2003). On the other hand, the quantitative

inventories play important role in the invention of economically important species (Keel et al. 1993) and further have enormous implications in the management and conservation of these tropical moist and deciduous forests (Campbell & Siepen 1994).

In western Himalaya, most of the forest of Sal is largely constituted by its plantation about many years ago. In Rajaji and Corbett tiger reserve, the forest of Sal is now a mature forest community. The associated plant species fairly mimics the structure and composition of natural-dominated sal (Champion & Seth 1968). In Himalaya, as the forest cover of sal is receding fast, the management of its natural forests would be an important strategy for conservation. The composition of forest plant species is strongly co-related to environmental gradients (Currie 1991) but the knowledge on the species composition and forest structure of the moist and dry tropical forests are still inadequate. Thus, the quantitative analysis based on species composition and structure is an important approach (Braun-Blanquet 1965). Further, it is evident that for effective conservation and management, the knowledge of forest structure and species composition is crucial (Kushwaha & Nandy 2012).

The leaves of Sal are used as fodder and also used in making various items like disposal plates (Jackson 1994). The phenology of this tree is debated in back years due to its deciduous versus evergreen paradox or nature (Troup 1921). In various parts of the world, especially the developing country, this tree fulfills the subsistence needs of humans (World Resources Institute 1996). Sal forests are also a source of timber, poles, and various medicinal wealth, mushrooms as

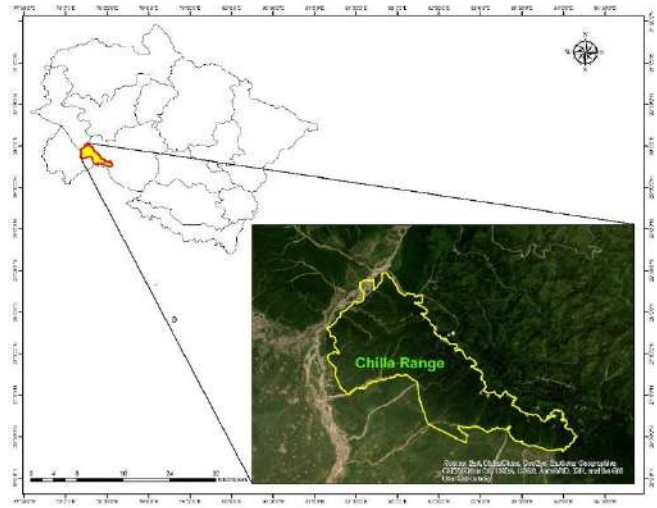

Fig. 1: Map of the study area.

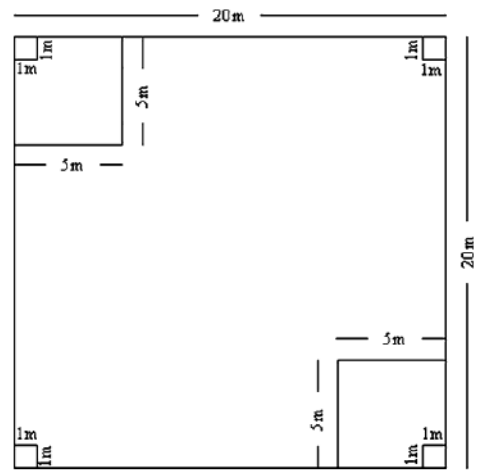

Fig. 2: Nested sampling design.

well as the ferns. Further, it also provides landscape-level conservation under wildlife sanctuary and national parks as it covers a large area of the forest (HMGN 2004).

STUDY AREA

Rajaji Tiger Reserve is located in Northern India at 29°51′ N to 30°15′ N, 077°52′ E to 078°22′ E at elevations from 250–1,100 above mean sea level. It falls within the Gangetic plains biogeographic zone and upper Gangetic plains province (Saklani et al. 2019). Rajaji tiger reserve (Earlier named as Rajaji National park) was established in 1983 with the aim of maintaining a viable population of Asian elephants and is designated as a protected area for 'Project Elephant' by the Ministry of Environment, Forest and Climate Change, Government of India. It spread in an area of 820.42 sq km. The tiger reserve is an essential part of the Terai landscape between the Sharda and Yamuna river in the Shivalik landscape (Saklani et al. 2018d). The study area comes under the Chilla forest division of the Rajaji tiger reserve which is an essential part of the tropical forest under Shivalik hill. The Chilla range of the reserve is one of the great centers of attraction for tourists (Saklani et al. 2018b). The Chilla forest division of Rajaji tiger reserve comes under the protected area network but undergoing rapid changes in fauna and vegetation pattern due to the large-scale anthropogenic forcing at some places in form of lopping, grazing, and hydropower project, scraping, trampling, and extraction of timber and non-timber forest products (Saklani et al. 2019). The anthropogenic gradients have rendered the system inhospitable for the growth of various associated plant species and regeneration resulting in a severe loss in plant diversity (Saklani et al. 2019, Pandey & Shukla 2001).

MATERIAL AND METHODS

The stratified random Nested sampling approach was followed for quantitative enumeration of the species survey in the present study. The sampling was carried out from 2016-2019 in all the strata viz. trees, shrubs and herbs. Quadrat size for enumeration of species was determined by the species-area-curve method (Misra 1968). For tree species, twelve 20 m × 20 m quadrat, sixty, 5 m ×5 m quadrats for shrubs, seventy-two 1 m ×1 m quadrats for herbs were laid randomly at each sample site. Further in each quadrat, circumference at breast height (CBH) of all the tree species with girthing tape was measured. A total of 60 and 50 plots were randomly laid in the forest of sal respectively and after that, the plant species were collected from the sal forest and identified by using regional flora, and all the species were confirmed from the Botanical Survey of India. Further, the herbarium was maintained in the Gurukul Kangri University, Haridwar, India. Plants were further confirmed from the Botanical Survey of India, Dehradun, Uttarakhand, India. Quantitative analysis of field data was done for density, abundance, frequency, and relative parameters (Curtis & McIntosh 1950). The Importance Value Index (IVI) for each tree, herb, and shrubs species was calculated (Curtis 1959). Further, all of the diversity indices were calculated in PAST Software Version 3.2. The species diversity index of both sites was determined using Shannon–Weiner Index (1949), Concentration of dominance by Simpson Index, Species richness index by Margaef, and Evenness by Jaccard Index. Analysis of variance (ANOVA) was done for statistical analysis by using the SPSS Version 20 (Statistical Package for Social Science). Species diversity profile and individual rarefaction curve of species were constructed in Paleontological Statistics (PAST) Software Program Version 3.14 based on presence and absence of plant species and the number of individual plant species in sal stand.

RESULTS AND DISCUSSION

Forest Structure and Composition

64 plant species were recorded from the stand of *S. robusta* in which 24 tree species (including saplings and seedlings), 12 shrubs, and 28 herbs of Chilla forest division of Rajaji tiger reserve representing 58 genera and 36 families were recorded within 10.0 ha of the Sal stands. The forest canopy was dominated by *S.robusta* as it was the most frequent species. After *S.robusta*, the next most frequent species were *Mallotus phillippensis, Cassia fistula, Naringi crenulata, Ehertia laevis, Legerstroemia indica, Crateva religiosa* and *Listea chinensis.* The understory of the Sal stand was quite sparse and dominated by shrubs such as *Lantana camara, Murrayya koenighii, Helicteres isora,* etc., and herbs like *Ageratum conyziodes, Achyranthus aspera, Aerva sanguinolenta, Adiantum* spp., *Cleome viscosa,* etc. The total density of trees was 318.29 ha^{-1} for saplings 12707.8 ha^{-1}, for seedlings 547.67 ha^{-1} whereas the total basal cover was of trees was 46.61 $m^2.ha^{-1}$, for saplings 39.23 $m^2.ha^{-1}$ and seedling 543.11 $cm^2.ha^{-1}$ in the study area. The highest density of tree in Sal stand was recorded for *S. robusta* (208.25 ha^{-1}), *E. laevis* (5000 ha^{-1}) for saplings, *M. philippensis* (287.5 ha^{-1}) whereas the rest of the species has shown moderate density in the study area. The total basal cover of trees was maximum recorded for *S. robusta* (43.25 $m^2.ha^{-1}$), *E. laevis* (12.25 $m^2.ha^{-1}$) for saplings, and *M. philippensis* (251.76 $m^2.ha^{-1}$) for seedlings. For shrub species, the highest density was recorded for *L.camara* and *C. viscosum* (1766.66 ha^{-1}) and the lowest was recorded for *Cassia occidentalis* (33.33 ha^{-1}), whereas the highest basal cover was recorded for *L.camara* (0.32 $m^2.ha^{-1}$) and the lowest basal cover was recorded for *C. occidentalis* (0.001

$m^2.ha^{-1}$). In herb species, the highest individuals density was observed for *A.conyzoides* (84.72 m^2) and lowest for *Oxallis latifolia* (1.39 m^2) in the rainy season whereas in winter *Ageratum conyzoides* and *Adiantum* spp. (56.94 m^2each) has been recorded with the highest density and lowest for *Boerhavia diffusa* (2.77 m^2). On the other hand, in summer, again highest density was observed for *A.conyzoides* (90.28 m^2) and lowest for *Oxallis latifolia* (1.38 m^2). The total basal cover was highest for *Achyranthus aspera* (3.16 cm^2/m^2) in the rainy season, *A.conyzoides* (2.12 $cm^2.m^{-2}$) in winter and summer, for *A.conyzoides* (3.03 $cm^2.m^{-2}$) has been recorded with the highest basal cover whereas other species showed moderate basal cover in all the season.

Diversity Indices

The maximum Shannon-Weiner was observed for tree saplings *viz.,* 1.679, Simpson Index was maximum observed for tree species (0.446), Margalef Index was a maximum recorded gain for Tree species (2.584) and Jaccard Index was for saplings (0.770). For herbaceous vegetation maximum value Shannon-Weiner in summer (2.46), Simpson Index in summer (0.07), Margalef Richness index in the rainy season (3.98), and Jaccard index was maximum in rainy and summer (0.87). Moderate diversity indices value was recorded for shrubs in the forest stand of Sal.

Regeneration Pattern

A comparison was made for the relative distribution of the total number of individuals in different girth classes. It was observed from the site that, trees girth class-wise density was highest was recorded for <10 cm diameter in comparison to other diameter classes. The density of the seedlings was highest (6600 $ind.ha^{-1}$) followed by the trees (3825 $ind.ha^{-1}$) and saplings (1525 $ind.ha^{-1}$). Maximum species showed new regeneration (39.13 %) followed by 17.39 % each by good and fair regeneration and 13.04% for each poor and no regeneration.

Soil Nutrients Dynamics

The pH value varied from 5.35±0.02 - 5.53±0.04 which was the maximum observed in a deep layer in the study site. The value of organic carbon varied from 1.27±0.01% - 1.33±005% which was highest recorded in the top layer of the soil whereas nitrogen varied from 0.23±0.008% - 0.27±0.005 % in which maximum content of nitrogen was also recorded in the top layer of soil. The value of Phosphorus varied from 10.33±0.88 $kg.ha^{-1}$ - 19.33±0.88 $kg.ha^{-1}$ which was highest recorded in the deep layer of the soil. Potassium varied from 165.55±0.70 - 245.63±0.86 which was maximum recorded in the uppermost layer of soil. The status of micronutrients for Boron was maximum observed in the upper and middle layer while the level of manganese and molybdenum didn't vary significantly in all the studied three layers. On the other hand, copper was altogether absent in the upper, middle, and lower layers. The whole strata of sal have been observed with sandy loamy texture in which sand covered the maximum content (64.86 %) of the texture in the top layer of the soil. ANOVA showed that pH, nitrogen, organic carbon, phosphorus, and potassium of soil vary significantly ($P<0.05$) among all the study sites.

The longest individual rarefaction curve of plant species reveals the maximum number of individuals in that strata. The longest individual rarefaction of seedlings species in Sal stand revealed that the highest number of individuals followed by trees and saplings (Fig. 3). Whereas for shrubs and herbs, the longest individual rarefaction curve has been observed for herbs in the rainy season followed by winter and summer seasons, and then for shrubs (Fig. 4). On the other hand, the diversity profile of plant species based on

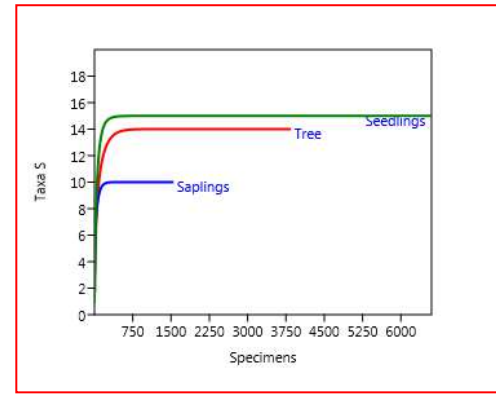

Fig. 3: Individual rarefaction curve of tree, seedlings and saplings in the Sal forest stand.

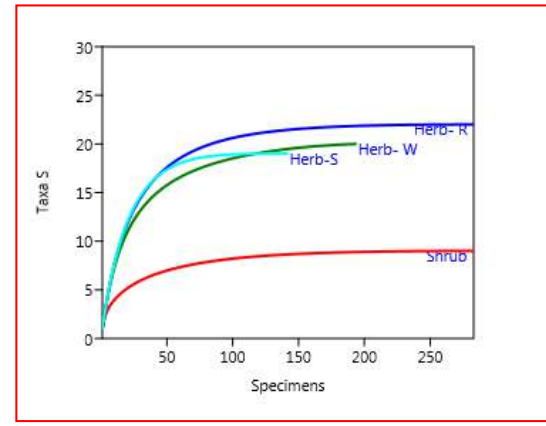

Fig. 4: Individual rarefaction curve of shrubs, herbs in rainy, winter, and summer in the Sal forest stand.

Table 1: Tree species composition of Sal forest along with ecological parameter.

Species	Family	D.ha^{-1}	TBC	IVI
Shorea robusta	Dipterocarpaceae	208.25	43.65	179.35
Mallotus philippensis	Euphorbiaceae	41.65	0.60	35.08
Aegle marmelos	Rutaceae	6.25	0.10	14.25
Listea chinensis	Lauraceae	10.25	0.12	13.82
Naringi crenulata	Rutaceae	10.25	0.18	12.23
Ehretia laevis	Ehertiaceae	16.66	0.48	11.45
Cassia fistula	Fabaceae	6.25	0.27	7.70
Ficus religiosa	Moraceae	6.25	0.90	7.33
Erythrina indica	Fabaceae	2.08	0. 19	4.49
Miliusa velutina	Annonaceae	2.08	0.07	4.28
Holoptelea integrifolea	Ulmaceae	2.08	0.13	2.66
Schleichera oleosa	Sapindaceae	2.08	0.06	2.50
Crateva religiosa	Capparaceae	2.08	0.04	2.46
Legestroemia parviflora	Lythraceae	2.08	0.01	2.41

D/ha = Density/hectare, TBC= Total basal cover, IVI= Importance value index

the number of species revealed seedlings with the highest number of species followed by trees, saplings in the sal stand (Fig. 5), whereas, for herbs, the highest diversity profile was observed in the rainy season followed by summer and then winter in the study area (Fig. 6).

DISCUSSION

The richness of species in sal forest was quite high (208 species in 24 ha) as compared to those of central India (Jha & Singh 1990) but less than 208 plant species (Pandey & Shukla 2003). In the present study, the total number of tree species was 64, which is much higher in number than that of the sal forest of eastern Himalayas (Uma Shankar 2001). In all of the above-mentioned studies of sal forest, the sampled area was a small variable which ranged from 0.2 to 2.9 ha**.** The present study of Sal forest is because of much greater diversity and the number of species of herbs and shrubs. The number of herbs and shrubs was quite high in the core of the tiger reserve as compared to the periphery of the reserve. This might be because lesser numbers of activities were observed in the core area of the Rajaji tiger reserve. Further, the canopy gaps of the sal forest in the Rajaji tiger reserve decrease as the periphery of the forest increases. A similar

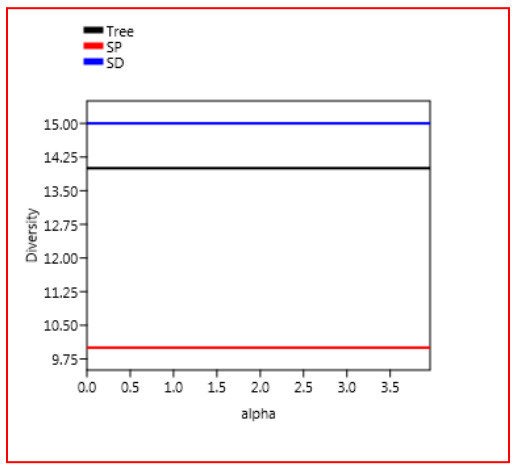

Fig. 5: Diversity Profile of tree, saplings, and seedlings.

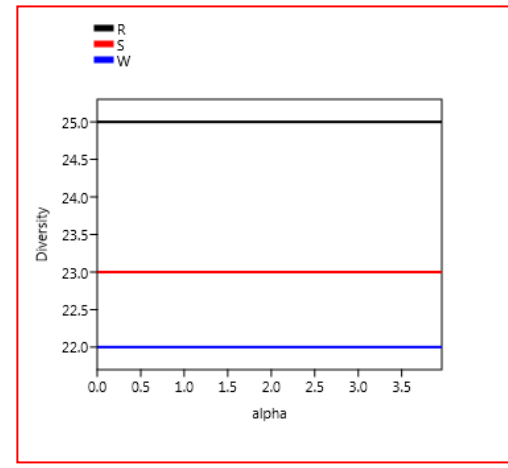

Fig. 6: Diversity Profile of herbs in rainy, winter, and summer.

Table 2: Sapling species composition of Sal forest along with ecological parameter.

Species	Family	D.ha^{-1}	TBC	IVI
Ehretia laevis	Ehretiaceae	5000.0	12.25	102.71
Listea chinensis	Lauraceae	2083.2	7.73	46.79
Mallotus philippensis	Euphorbiaceae	2083.2	6.18	46.44
Shorea robusta	Dipterocarpaceae	1041.6	4.78	31.09
Naringi crenulata	Rutaceae	1250	3.85	30.36
Aegle marmelos	Rutaceae	416.5	1.68	14.70
Salix alba	Saliaceae	208.32	1.20	8.32
Phyllanthus embilica	Phyllanthaceae	208.32	1.04	7.85
Crateva religiosa	Capparaceae	208.32	0.32	6.04
Trewia nudiflora	Euphorbiaceae	208.32	0.20	5.71

Table 3: Seedling species composition of Sal forest along with ecological parameter.

Species	Family	D.ha^{-1}	TBC	IVI
Mallotus philippensis	Euphorbiaceae	287.5	251.76	119.20
Ehretia laevis	Ehertiaceae	108.32	158.61	67.64
Naringi crenulata	Rutaceae	16.65	28.36	20.13
Randia longspina	Rubiaceae	14.57	64.01	19.54
Aegle marmelos	Rutaceae	33.33	6.48	8.91
Legerstroemia indica	Lythraceae	14.58	6.84	9.01
Syzygium cumini	Myrtaceae	12.5	3.98	8.10
Schleichera oleosa	Sapindaceae	8.33	7.0	7.90
Phyllanthus embilica	Phyllanthaceae	10.25	2.08	7.35
Cedrela toona	Meliaceae	8.33	2.65	7.10
Legerstroemia parviflora	Lythraceae	8.33	1.03	6.80
Ficus benghalensis	Moraceae	8.33	5.01	5.83
Cassia fistula	Fabaceae	6.25	0.49	4.62
Holoptelea integrifolia	Ulmaceae	4.15	0.33	4.21
Morus alba	Moraceae	6.25	4.48	3.65

interpretation was revealed by the study of Chandrashekara and Ramakrishnan (1994) while studying the forest structure of the Indian Western Ghat. The understory vegetation of the area was dominated by many shrubs like *L.camara, H.isora, C.viscosum, Zizyphus zujupa,* etc. Lianas like *Bauhinia vahlii* were most commonly observed towards the periphery whereas the herbs were less in comparison to the core area of the tiger reserve. The present interpretation is in sharp contrast with the study of Singh and Singh (1987) in the Central Himalayan region of India where the undergrowth of Sal is herbaceous. Further, the total number of species was higher than that of the sal forest of Doon Valley (Pandey & Shukla 2001). The richness of species observed in sal forest was 2.58 for trees, 2.19 for saplings, and 2.51 for seedlings which was almost similar to the earlier studies (Saklani et al. 2018a, b,c,d; 2019) from the forest stand of *Holoptelia integrifolea, Dalbergia sissoo, C.fistula* and *Trewia nudiflora* in Chilla forest range of the tiger reserve but much lower than that the study of (Pandey & Shukla 2001). This might be due to the anthropogenic pressures by Gujjars and their cattle which destroyed, trampled and scraped the vegetation in the study area. Although the overall regeneration for other

Table 4: Shrub species composition of Sal forest along with ecological parameter.

Species	Family	D.ha^{-1}	IVI
Lantana camara	Verbenaceae	1766.66	57.62
Murraya koenighii	Rutaceae	1033.33	52.79
Clerodendrum viscosum	Laminaceae	1766.66	49.18
Ziziphus jujupa	Rhamnaceae	816.67	37.48
Colebrookea oppositifolia	Laminaceae	483.33	34.66
Adatoda vesica	Acanthaceae	300.0	21.91
Asclepias curassavica	Apocynaceae	450.0	17.91
Calotropis gigentea	Apocynaceae	100.0	7.71
Helictres isora	Malvaceae	150.0	7.39
Desmodium ganeticum	Fabaceae	66.67	5.04
Calotropis procera	Apocynaceae	83.33	4.16
Cassia occidentalis	Fabaceae	33.33	4.16

Table 5: Herbs species composition of Sal forest along with ecological parameter.

Species	Family	Rainy		Winter		Summer	
		D.m^{-2}	IVI	D.m^{-2}	IVI	D.m^{-2}	IVI
Kyllinga monocephala	Cyperaceae	40.27	17.0	33.3	17.54	38.88	24.53
Ageratum conyziodes	Asteraceae	84.72	52.59	56.94	48.87	90.27	70.14
Adiantum spp	Pteridaceae	55.55	20.01	56.94	27.47	6.25	25.72
Cyprus rotundus	Cyperaceae	30.55	13.39	22.22	12.23	27.77	18.82
Achyranthus aspera	Amaranthaceae	51.38	48.45	27.77	34.36	-	-
Bidens pilosa	Asteraceae	26.38	11.12	9.72	3.66	27.77	17.43
Amarantus spinosus	Amaranthaceae	6.94	4.43	9.72	4.99	-	-
Aerva sanguinolenta	Amaranthaceae	48.61	22.08	33.33	14.32	-	-
Oxallis corniculata	Oxallidaceae	29.16	11.89	19.44	9.33	34.72	19.3
Tephrosia purpurea	Fabaceae	1.38	1.01	-	-	-	-
Abutilon indicum	Malvaceae	0.15	6.19	25	11.99	-	-
Oxallis debilis	Oxallidaceae	1.3	1.01	12.5	6.06	1.38	1.38
Cleome viscosa	Capparaceae	13.88	13.58	13.88	18.94	20.83	28.01
Euphorbia hirta	Euphorbiaceae	9.72	6.09	13.88	9.96	9.72	8.31
Ichnocarpus frutescens	Apocynaceae	9.7	4.78	19.44	11.06	-	-
Cassia tora	Fabaceae	20.83	9.84	20.83	13.02	-	-
Stellaria media	Caryophyllaceae	5.55	2.69	-	-	-	-
Cissampelos pareira	Memispermaceae	45.83	15.03	-	-	-	-
Christella dentata	Thelpteridaceae	20.83	9.52	22.22	12.22		
Blumea mollis	Asteraceae	16.66	8.64	16.66	8.99	16.66	12.73
Portulaca grandiflora	Portulacaceae	8.33	4.84	8.33	5.67	8.33	6.25
Urena lobata	Malvaceae	8.33	5.2	-	-	-	-
Polygonum spp.	Polgonaceae	11.11	4.87	20.83	10.96	20.83	13.04
Lygodium flexuosum	Lygodiaceae	6.94	3.70	-	-	6.94	5.91
Commelina benghalensis	Commelinaceae	2.77	1.95	-	-	2.77	2.67
Mimosa pudica	Fabaceae	-	-	6.94	2.76	6.94	3.85
Oxallis latiflolia	Oxallidaceae	-	-	27.77	13.10	34.722	39.10
Boerhavia diffusa	Nyctaginaceae	-	-	2.77	2.51	2.77	2.76
Total		572.22	299.99	480.46	300.0	413.87	300.0

Table 6: Summary of the species inventory in Sal forest.

	Trees	Saplings	Seedlings	Herbs			Shrubs
				R	W	S	
Number of genera	14	10	15	24	25	16	11
Number of families	13	08	12	15	15	14	8
Basal area ($m^2.ha^{-1}$)	46.61	39.23	543.11	11.05	7.50	8.38	1.69
Stand density (stems ha^{-1})	318.29	12707.8	547.67	572.21	480.46	413.82	7049.98
Shannon-Weiner index	1.350	1.774	1.679	2.8	2.36	2.46	1.96
Simpson index	0.446	0.214	0.321	0.06	0.06	0.07	0.17
Margalef Richness index	2.584	2.19	2.51	3.98	3.59	3.38	1.81
Jaccard Evenness index	0.511	0.770	0.620	0.87	0.76	0.87	0.79

Seedlings basal cover*= $cm^2.ha^{-1}$, Herb density* = $D.m^{-2}$, Herb basal cover* = $cm^2.m^{-2}$

Table 7: Chemical parameters of soil under Sal forest.

Depth (cm)	OC (%)	N (%)	P kg/ha)	K (kg/ha)	pH
0-10	1.33±005	0.27±0.005	10.33±0.88	245.63±0.86	5.36±0.01
15-25	1.32±0.01	0.24±0.005	14.41±0.50	165.55±0.70	5.35±0.02
30-40	1.27±0.01	0.23±0.008	19.33±0.88	195.35±0.65	5.53±0.04

OC = organic carbon, N = nitrogen, P = phosphorus, K = potassium

Table 8: Textural parameter of soil under Sal forest in different depth.

Depth (cm)	Texture	Sand (%)	Silt (%)	Clay (%)
0-10	Sandy loam	64.86	27.02	8.10
15-25	Sandy loam	52.63	42.10	5.26
30-40	Sandy loam	50	45	5

Table 9: Micronutrients analysis of soil under Sal forest.

	Micronutrients (ppm)				
Depth (cm)	Cu	Mo	Mn	Fe	B
0-10	-	0.0-0.05	0.2-1.0	-	>2.0
15-25	-	0.0-0.05	0.2-1.0	-	>2.0
30-40	-	0.0-0.05	0.2-1.0	-	2.0

Cu = copper, Mo = molybdenum, Fe = iron, B = boron

species in the study area is fairly good, the main species *S.robusta* has shown no regeneration. It was observed that the plant species which showed poor and no regeneration in a forest stand, might show good and fair regeneration in the other sites of the study area. Similar result was observed in our earlier study (Saklani et al. 2018c, 2019) in six different sites of the Chilla forest division of the tiger reserve. Nil and poor regeneration could be due to the various anthropogenic activity such as grazing, lopping, scraping, and trampling. Overgrazing harms the ground flora and inversely affects the regeneration pattern of the species. Many researchers like Ballabha et al. (2013) pointed out the factor like lopping, grazing, fires adversely affecting the regeneration pattern of species in Western Himalaya.

The physico-chemical property of soil always determines the status of nutrients in the soil which may change according to the type of vegetation, the climatic condition of the area (Rundel 1989). Disturbances like trampling, grazing,

scraping, and looping are the main pressures that affect the dynamism and upsetting cycling of nutrients in a forest as these pressures influence the physico-chemical property of soil in a forest [Knight 1975]. It was observed from the study area that organic carbon (1.27±0.01%-1.33±005%), nitrogen (0.23±0.008%-0.27±0.005 %), and potassium (0.23±0.008%-0.27±0.005 %) and all the studied micronutrients like copper, molybdenum, iron, boron were maximum recorded in the top layer (0-10 cm) of the soil except for pH (5.35±0.02-5.53±0.04), and phosphorus (10.33±0.88 $kg.ha^{-1}$-19.33±0.88 $kg.ha^{-1}$) which was maximum found in the deep layer (30-40cm). Optimum organic carbon and nitrogen support the diversity status and regeneration potential of *S. robusta, M. philippensis, C. fistula,* etc. The nutrients status from the present study can be comparable with Bharti and Kamboj (2018) from the Haridwar forest division of Uttarakhand whose values of the physico-chemical parameter was were more or less similar to the present study. The maximum amount of soil nutrients in the top layer could be due to the accumulation of the huge amount of organic matter which makes humus in the top layer. So good and fair regeneration potential of the species was observed in the sal forest. High nutrients in the lower layer are sometimes fascinated by the downwards movement of the particles of soil transfer of various nutrients of soil to the lower layer (Sukumar 1992).

The assessment of soil nutrients dynamics, diversity, and the regeneration pattern of the tree species are important for conservation, management as well as for their sustainable utilization. The present study area is rich in trees along with their saplings and seedlings except for the seedlings of Sal. Overall regeneration potential is fairly good but in some areas, there is a poor regeneration pattern of species due to anthropogenic activities. So, it is necessary to give sufficient time to the forest to reduce pressure. Therefore, the seedlings of Sal have much time established and reach the mature stage. Further, closing each compartment of the sal forest that is close to the residing locals would be the best strategies to provide vegetational regeneration. Enrichment planting in the closed compartment of Sal forest with useful species will also favor the best regeneration of species in the area.

Enhancement of Sal Forest Through Management and Species Regeneration

The management of the sal forest has played a significant contribution in the conservation of forest wildlife in the Rajaji tiger reserve. Effective and sustainable forest management of sal requires the various functions of forests which can be considered across various stands The main objective for sal forest management is to fulfill the goals associated with forest and requirements of the current generation and to meet their various needs. The different participatory approaches for degraded sal management are woodlot management, agroforestry, and coppice management (Alam 2006, Safa 2004). Another significant approach for the management of sal forests is the establishment of ecotourism areas. In the Rajaji tiger reserve, many ecotourism spots have already proved to be an effective tool for the management of forest communities in the area. The three aspects of ecotourism are conservation of nature along with the natural resources, participation of local inhabitants, and sustainable management of resources so that profits can be gained. The main objectives of the conservation and participatory sal coppice cannot be achieved until these strategies are aimed at reducing the rate of the vulnerability of sal stands from denudation and encroachment. For the management of forests, there are ample opportunities for the official Rajaji tiger reserve and the government in terms of woodlots and agroforestry. Local villagers and Gujjars of the tiger reserve are still using implemented small-scale agroforestry and land management which has contributed to a green economy through sustainable and renewable management of the forest inside the tiger reserve.

In the present study, it was observed that the sal forest in Chilla is fully mature as there was a lack of seedlings and saplings in the stand. Direct use of sal by local people or tribal people associated with this forest or indirect effects of their activities in past, e.g. grazing, fire, or litter collection are responsible for lack of sal saplings and seedlings. The forest of the sal stand was planted along with the natural stand about many years ago. The earlier emphasis of policies and management plans of sal forest was on increasing productivity by creating high value of timber stock through clear-felling the existing natural stands followed by artificial regeneration with exotics or fast-growing species. The financial strategies were overcome by strict implementation of the Wildlife Act, 1972, but there is, at times, less concern for the livelihoods of ethnic and local communities. Further, where possible, replanting and filling with *S. robusta* and its associated species like *M. philippensis, Terminalia chebula, Terminalia bellerica*, *Acacia catechu, Bombex ceiba, Albizzia lebbeck, Lagerstroemia parviflora* and *Cassia fistula* must be examined every year. The sal forest harbors a wide variety of medicinal plants, so protection and identification of species, and detailed study of medicinal plants of the forest are also required.

The forest of sal is a natural home for *S.robusta*, so greater attention should be on its increasing productivity rather than the replacement of other plant species. Sal coppice could be much productive than the block plantation per hectare (Rahman et al. 2005). First, in the Rajaji tiger reserve, agro-

Table 10: Stumps density (stump.ha^{-1}) regeneration status of woody species in a Sal Stand.

Species	Density (Ind./h)			
	TR	SP	SD	RS
Shorea robusta	2500	125		Poor
Holoptelea integrifolia	25	-	50	Fair
Cedrela toona	-	-	100	New
Alstonia scholaris	-	-	-	-
Naringi crenulata	125	150	200	Good
Cassia fistula	75	-	75	Fair
Mallotus philippensis	500	250	3475	Good
Ehretia laevis	200	600	1300	Good
Oroxylum indicum	-	-	-	-
Listea chinensis	125	250	-	Poor
Terminalia bellirica	-	-	-	-
Ziziphus oenoplia	-	-	-	-
Aegle marmelos	75	50	400	Good
Crateva religiosa	25	25	-	Poor
Syzygium cumini		-	150	New
Ficus religiosa	75	-	-	No
Adina cordifolia	-	-	-	-
Morus alba	-	-	75	New
Celtis australis	-	-	-	-
Ficus palmata	-	-	-	-
Dalbergia sissoo	-	-	-	-
Trewia nudiflora	-	25	-	New
Cordia dichotoma	-	-	-	-
Phyllanthus emblica	-	25	125	New
Butea monosperma	-	-	-	-
Psidium guajava	-	-	-	-
F. Glomerata	-	-	-	-
Legerstroemia indica	-	-	100	New
Acacia spp.	-	-	-	-
Melia azadirachta	-	-	-	-
Acacia catechu	-	-	-	-
Pterospermum acirifolium	-	-	-	-
Caliandra haematocephala	-	-	-	-
Bombex ceiba	-	-	-	-
Bauhinia variegata	-	-	-	-
Holarrhena pubescens	-	-	-	-
Salix alba	-	-		New

Table Cont....

Species	Density (Ind./h)			
	TR	SP	SD	RS
Azadirachta indica	-	25	-	-
Schleichera oleosa	25	-	100	Fair
Eugenia oogenesis	-	-	-	-
Delonix regia	-	-	-	-
Putranjiva roxburghii	-	-	-	-
Legerstroemia parviflora	25	-	175	Fair
Erythrina indica	25	-		No
Millusa velutina	25	-		No
Randia longspina	-	-	175	New
Ficus benghalensis	-	-	100	New

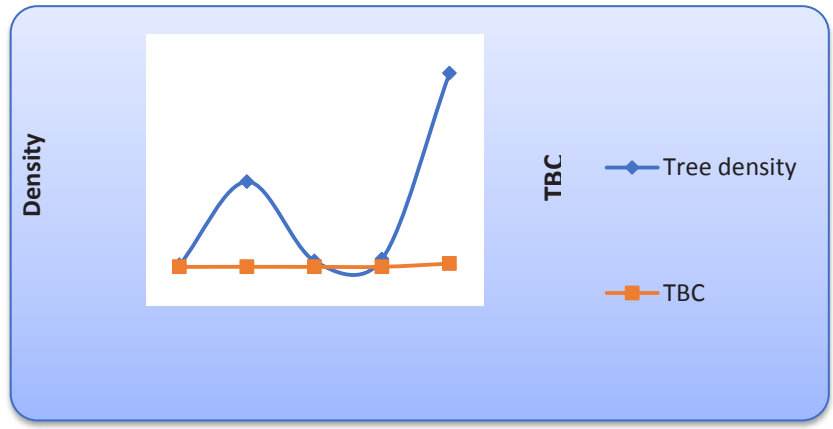

Fig.7: Trees stand density (Ind.ha) and total basal cover ($m^2.ha^{-1}$) on different girth classes (in cm) in Sal stand.

forestry should be given priority as far as the management of sal is concerned. Second, woodlots could be another better approach for conservation initiatives. Agroforestry is more viable and reliable than woodlot management in terms of budget (Safa et al. 2004). Regeneration of sal has been a serious issue in its management in different parts of India. The management of sal forest was initiated in the past few centuries which did not get the successful output. A different study suggested high soil water and poor aeration of soil are responsible for the poor regeneration pattern in sal (Hole 1921). High water in the soil is related to precipitation or drought whereas poor aeration of soil is caused by high rainfall and the dried leaves of sal as well as the grazing of animals (Troup 1986). Although dried leaf provides humus to the soil which provides essentials nutrients like N, P, and K, bad aeration to such soil is injurious. The study of Sukumar (1992) also had argued that deficient or poor aeration during monsoon seasons and compaction of soil in the dry season, and unfavorable topographic localities are responsible for failure in sal regeneration. The important character of sal is it tends to grow and regenerate as a mass of seedlings in favorable conditions of soil, light, and good drainage of moisture (Rautiainen & Suoheimo 1997). Troup (1986) also had explored the mechanical effects of leaf litter on the seedling formation of sal by experiment and recorded that seed germinated on a layer of dead leaves under good light and moisture content with good drainage of the area. Sometimes vigorous growth of seedlings could be achieved by the complete removal of the overhead canopy (Troup 1986).

It was further observed that only a little portion of seedlings (about 4 %) of the sal-dominated forest has been recorded with seed origin and the rest were originated from coppice seedlings (Suoheimo et al. 1999), which reveals the strength of coppice origin in sal regeneration. Moreover,

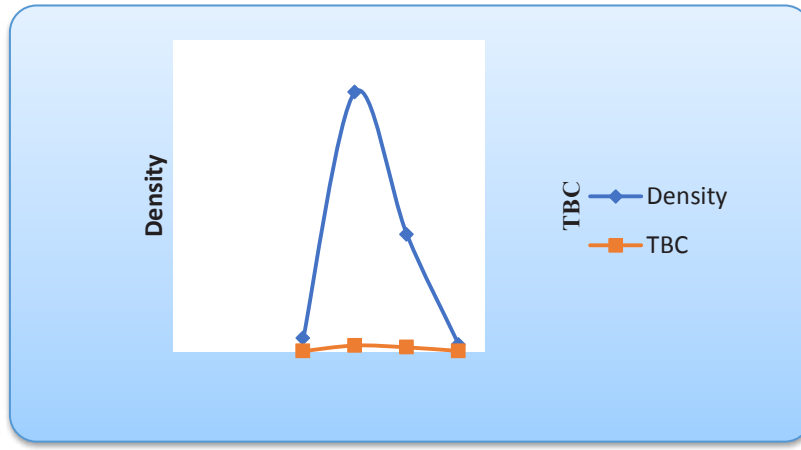

Fig. 8: Saplings density (Ind.ha^{-1}) and total basal cover (m^2.ha^{-1}) on different girth classes (in cm) in Sal stand.

the perennating character of sal enables it to coppice the unnecessary shoots and felling back which repeats year by year and allows the forest to regenerate. Various young sal shoots of uniform height developed from roots which had survived in the ground due to the protection against grazing of animal (Jackson 1994). In the Rajaji tiger reserve, similar conditions were observed but the poor regeneration of sal is the main problem.

CONCLUSION

Western Himalaya covers the huge stand of sal forest providing essential ecosystem services for livelihood and has a significant role in the performance of different ecological functions. Rajaji tiger reserve which is an important part of Western Himalaya is dominated by *H. integrifolea, D. sissoo, S. robusta, C. fistula,* and *T. nudiflora* and co-dominated with *M. philippensis, T. nudiflora, H. pubescens, A. cordifolia, P. emblica,* etc. The result of the present study revealed that the sal stand has a great diversity of 64 species. A huge canopy of trees in sal stands also provides ample nutrients in the soil which further support the growth of ground flora. It was also observed that soil parameters like pH, organic carbon, total nitrogen, available potassium, available phosphorous favor the growth of various species in sal forest. It was also concluded that the sal forest in Chilla is fully mature as there was a lack of seedlings and saplings in the stand. So, the management of sal stands through regeneration could be an important point for improving the overall diversity status of *S.robusta* in the present study area. Further, the involvement of the community in the conservation of sal should be implemented in the tiger reserve so that in the natural stand of sal, many non-wood forest products can be sustainably used by the locals.

ACKNOWLEDGEMENTS

The authors are grateful to the Director and Forest guards of the Rajaji tiger reserve for their help during the fieldwork.

REFERENCES

Alam, M., Furukawa, Y., Sarker, S.K. and Ahmed, R. 2008. Sustainability of Sal (Shorea robusta) forest in Bangladesh: Past, present and future actions. Int. For. Rev., 10(1): 29-37.

Ballabha, R., Tiwari, J.K. and Tiwari,P. 2013. Regeneration of tree species in the sub-tropical forest of Alaknanda Valley, Garhwal Himalaya, India. For. Sci. Prac., 15: 89-97.

Bharti, M. and Kamboj, N. 2018. Impact of different land uses on soil characteristics in Ranipur Rao Watershed in Haridwar district, Uttarakhand. Int. J. Creat. Res. Thoughts, 6(1): 1147-1154.

Braun-Blanquet, J. (eds.) 1965. Plant Sociology (translated by Fuller, GD and Conard, HS). IBS Press, USA, pp. 1-228.

Campbell, A. and Siepen, G. 1994. Landcare: Communities Shaping the Land and the Future. ICON Group International, San Deigo, CA, pp. 21-85

Champion, S.H. and Seth, S.K. (eds.) 1968. A Revised Survey of the Forest Types of India.World Cat, pp. 21-85.

Chandrashekara, U. M. and Ramakrishnan, P. S. 1994. Vegetation and gap dynamics of a tropical wet evergreen forest in the Western Ghats of Kerala, India. J. of Tro. Eco., 10(3), 337-354.

Chauhan, P.S., Manhas, R.K. and Negi, J.D.S. 2001. Demographic and diversity analysis of tree species in sal (*Shorea robusta* Gaertn. f.) forests of Doon Valley. Ann. For., 9(2): 188-198.,

Currie, D.J. 1991. Energy and large-scale patterns of animal-and plant-species richness. Amer. Nat., 137(1): 27-49.

Curtis, J.T. 1959. The Vegetation of Wisconsin: An Ordination of Plant Communities. University of Wisconsin Press, Madison, Wisconsin, pp. 1-450.

Curtis, J.T. and Mcintosh, R.P. 1950. The interrelations of certain analytic and synthetic phytosociological characters. Eco., 31(3): 434-455.

Gentry, A.H., Bullock, S.H., Mooney, H.A. and Medina E. (eds), 1995. Seasonally dry tropical forests. Div. Flor. Comp. Neotrop. Dry For.. 146-194.

His Majesty's Government of Nepal (HMGN), 2004. Terai Arc Landscape: Nepal: Strategic Plan 2004-2014. Ministry of Forests and Soil Conservation, Kathmandu, Nepal.

Hole, R.S. 1921. The regeneration of sal forests. Ind. For., 47(4): 152-159.

Jackson, J.K. 1994. Manual of afforestation in Nepal: Forest Research and Survey Center. Kath. Nep., 21-50

Jacquemyn, H., Butaye, J. and Hermy, M. 2003. Influence of environmental and spatial variables on the regional distribution of forest plant species in a fragmented and changing landscape. Ecography, 26: 768–776.

Jha, C.S. and Singh, J.S. 1990. Composition and dynamics of dry tropical forest in relation to soil texture. J. of Veg. Sci., 609-614.

Keel, S., Gentry, A.H. and Spinzi, L. 1993. Using vegetation analysis to facilitate the selection of conservation sites in eastern Paraguay. Cons. Bio., 7(1): 66-75.

Knight, D.H. 1975. A phytosociological analysis of species-rich tropical forest on Barro Colorado Island, Panama. Eco. Mono., 45(3): 59-284.

Kushwaha, S.P.S. and Nandy, S. 2012. Species diversity and community structure in sal (*Shorea robusta*) forests of two different rainfall regimes in West Bengal, India. Biod. Cons., 21(5): 1215-1228.

Misra, R. (eds.) 1968. Ecology Workbook. Oxford & IBH Publisher, England.

Negi., J.D.S. and Chauhan, P.S. 2002. Greenhouse gases mitigation potential by sal (*Shorea robusta* Gaertn. F.) forest in Doon Valley. Int. For., 128(7): 771-778.

Pandey, S.K. and Shukla, R.P. 2003. Plant diversity in managed sal (*Shorea robusta* Gaertn.) forests of Gorakhpur, India: Species composition, regeneration, and conservation. Biod. Cons., 12(11): 2295-2319.

Pandey. S.K. and Shukla, R.P. 2001. Regeneration strategy and plant diversity status in degraded sal forests. Curr. Sci., 81: 95-102.

Rahman, M., Nishat, A. and Vacik, H. 2009. Anthropogenic disturbances and plant diversity of the Madhupur Sal forests (*Shorea robusta* C. Gaertn) of Bangladesh. I. J. of Bio. Sci. & Manag., 5(3): 162-173.

Rautiainen, O. and Suoheimo, J. 1997. Natural regeneration potential and early development of *Shorea robusta* Gaertn. f. forest after regeneration felling in the Bhabar-Terai zone in Nepal. For. Eco. and Man., 92(1-3): 243-251.

Rundel, P.W. 1989. Ecological success in relation to plant form and function in woody legumes. Adv. in Leg. Biol., 377-398.

Safa, M.S., Siddiqui, M.R., Asanoy, A. and Abdu, A. 2004. Financial viability of small farm forestry based on no-cost sharing arrangement in sal (*Shorea robusta*) forest of Bangladesh. MRPA, 6: 1-5.

Saklani, A., Navneet and Bhandari, B.S. 2019. Community analysis of woody species in a tropical forest of Rajaji Tiger Reserve. Env. and Eco., 37 (1): 48-55.

Saklani, A., Navneet and Bhandari, B.S. 2018a. Phytosociological studies, biodiversity conservation in a subtropical moist deciduous forest of Rajaji Tiger Reserve, Uttarakhand. India. J. Res. Ana. Rev., 5(3): 39-51.

Saklani, A., Navneet and Bhandari, B.S. 2018b. The phyto-sociological investigation, biodiversity conservation and life form pattern in a *Holeptela integrifolia* community under Rajaji Tiger Reserve, Uttarakhand, India. I. Res. J. of Bio. Sci, 7(7): 1-8.

Saklani, A., Navneet and Bhandari, B.S. 2018c. Tree diversity, stand structure, and community composition in the tropical forest of Rajaji tiger reserve. Northern India. J. App. Sci. Nat. Sci., 10(3): 945-953.

Saklani, A., Navneet, Bhandari, B.S. and Bijlwan, K. 2018d. Phytodiverd sity, stand structure, and biodiversity conservation in a tropical forest community under Rajaji tiger reserve, Uttarakhand, India. ENVIS Bull. Him. Eco., 26: 7-16.

Saklani, A., Navneet and Bhandari, B.S. (eds.). 2020. Ethnomedicinal Plant Use and Practice in Traditional Medicine. IGI Global, USA, pp. 1-300.

Satya, U.D. and Nayaka, S. 2005. *Shorea robusta*: An excellent host tree for lichen growth in India. Cur. Sci., 89(4): 21-25.

Shankar, U. 2001. A case of high tree diversity in a sal (*Shorea robusta*)-dominated lowland forest of Eastern Himalaya: Floristic composition, regeneration, and conservation. Cur. Sci., 776-786.

Singh, J.S. and Singh, S.P. 1987. Forest vegetation of the Himalayas. The Bot. Rev., 53(1): 80-192.

Sukumar, R. 1992. The Asian elephant: Ecology and Management. Cambridge University Press, Cambridge, UK, pp. 1-190.

Suoheimo, J., Li, C. and Luukkanen, O. 1999. Isozyme variation of natural populations of sal (*Shorea robusta*) in the Terai region, Nepal. Sil. Gen., 7: 32-37.

Troup, R.S. (eds.) 1921. The Silviculture of Indian trees. Clarendon Press, Oxford, pp. 1-225.

Troup, R.S. 1986. The Silviculture of Indian Trees. International Book Distributors, Dehradun, India, pp. 1-300.

World Resources Institute. 1996. World Resources 1996-1997. Oxford University Press, New York.

Nature Environment and Pollution Technology
An International Quarterly Scientific Journal

p-ISSN: 0972-6268
(Print copies up to 2016)
e-ISSN: 2395-3454

Vol. 20 | No.3 | pp. 1021-1031 | 2021

Original Research Paper

https://doi.org/10.46488/NEPT.2021.v20i03.009

Open Access Journal

Climate Responsive Strategy Matrix for Designing Buildings in India

N. Thakur*, D. Parashar*, C. Chidambaram* and M. Dharwal†**
*School of Architecture and Planning, Sharda University, Greater Noida, India
**School of Business Studies, Sharda University, Greater Noida, India
†Corresponding author: M. Dharwal; mriduldharwal22@gmail.com

Nat. Env. & Poll. Tech.
Website: www.neptjournal.com

Received: 05-09-2020
Revised: 09-11-2020
Accepted: 12-11-2020

Key Words:
Climate responsive strategies
Thermal comfort
Green buildings
Climatic zones

ABSTRACT

The starting point for a good design of any building project is the analysis of the macroclimate and microclimate of the building site that encompasses an understanding of temperature, radiation, wind, precipitation, topography, vegetation, ground cover, etc., which together describe the site climate. Although urban context somewhat unifies, climate and topography prevalent in India are varied and diverse. Most part of the country is hot, while some regions are dry throughout the year, some are humid and some others are composite. The building design features, therefore, need to vary with the diversity to provide comfortable environments naturally. The context and the requirements for thermal comfort provide the basis for building siting, selection of building form and envelope, fenestration design, choice of materials, and other aspects. The paper proposes and discusses the various climate-responsive design strategies that are best adapted for the different climatic zones of India and presents such design interventions and features as a comparative matrix. Such a comparative presentation is novel, convenient, easy to comprehend, and provides a useful toolkit for building designers. The climate-responsive interventions in building design proposed in this study have the potential to enhance built environments naturally, thereby mitigating the adverse environmental impact. The proposed strategies are also validated through a sample field survey responded by building professionals from various climatic zones of the country.

INTRODUCTION

The built environment has evolved continuously over a period of time and ages along with the rapid developments as well as technological advancements. Traditionally, local contextual features dominated Architecture by considering aspects of climate, availability of local materials, and local techniques. In recent times, architecture has evolved leaving its local and vernacular forms and adopted global unifying characters, which depend largely on using active means of making buildings thermally comfortable that has resulted in large consumption of energy by the buildings. With increasing energy consumptions and concerns of severe environmental impacts like climate change, depleting ozone layer, and issues of global warming have been on the rise (Jung et al. 2013). The energy efficiency of buildings is the norm prescribed in most environmental policies at the International as well as the National levels (Perez-Lombard et al. 2008).

The building design is the major aspect that provides energy efficiency and enables thermally comfortable living environments. It is imperative that the design processes become appropriate and aid in achieving thermal comfort thereby reducing energy demand. Sustainable development requires reducing energy consumption and minimizing the impact of the environment on built structures (Choi et al. 2016). The overall energy consumption by buildings is 40% which is responsible for high carbon emissions. Efforts in recent years have been to reduce CO_2 emissions through the conservation of energy (Harish & Kumar 2016). The building energy consumption is also a response to the climatic zone. Any two climatic zones cannot be considered and addressed as one (Yilmaz 2007). Designing energy-efficient buildings in different climatic conditions would need the study and analysis of the various climatic zones and their impacts. This also includes the study of the use of materials and components that are suitable to the climate and also crucial for sustainable development.

Each climatic zone requires different design techniques which need to be addressed appropriately by understanding climate variables including temperature, radiation, rainfall, wind speed and direction, and humidity, to design sustainable buildings. Designing for the climate is crucial for design sustainability, which if addressed correctly can save massive amounts of heating and cooling energy whilst sustaining occupants' thermal comfort (Albatayneh et al. 2018). Several methods and software on energy simulations of buildings have been developed but still lack a high interaction capability between the real energy data and theoretical data (Venkataraman & Kannan 2013). There is a need to co-relate

the outputs of the models based on the study of the indicators with the strategies adopted and practiced in the various climatic zones. In this perspective, it is imperative that the design processes become appropriate and aid in addressing the issues. It has been noted that the initial phases of design are crucial in setting out the building performance in terms of choice of resources, the energy consumption, and life cycle costs of the buildings (Kovacic & Zoller 2015).

This study attempts to identify and develop strategies that are responsive to the different climatic zones within India. It identifies the strategies based on the design parameters/ groups that form a part of the preliminary design of any building. The aim is to develop a strategy matrix that could be a ready reckoner for practitioners in the fields of architecture, design, and allied disciplines. The study has been conducted during 2019-2020 in India.

MATERIALS AND METHODS

The study firstly adopts the methodology cited by Krishnan et al. (2014) in the "Climate Responsive Architecture, A Design Handbook for Energy Efficient Buildings" for identifying the parameters to be addressed to design a climate-responsive building. Further, the conventional approaches of architects and designers while designing buildings are evaluated objectively. These are co-related with the parameters cited above to give "groups" that are synonymous with the building design process. Relevant sources in the area of sustainability and green buildings in India like TERI (Tata Energy and Research Institute) GRIHA (Green Rating for Integrated Habitat Assessment) have been analyzed for inputs against the parameters. The Climate consultant software that helps in climate analysis has been used for assessing thermal comfort through the study of Psychrometric charts, and the indicators of climate that are to be addressed in terms of the design process related to the parameter groups. A climate strategy matrix is then developed addressing the parameters and the five climatic zones within India. The matrix has been then validated through a survey from professionals in the area for further contextual inputs. The final matrix is collated and presented as a ready reference appropriate to all climatic zones in India.

The scope of the study is to develop a matrix on a given set of parameters. As the building design is a complex process and driven largely by the understanding of local contexts and inputs therein, it does not directly measure the indicators and relies on the existing database available as inputs for making the inferences.

Climatic Zones in India

The diversity of India is also reflected in its climate due to the various geographical features around and within its boundaries. India lies in the tropical climatic zone and is primarily dominated by high temperatures. Within its boundaries, the entire country from the North to the South and from East to West is divided into 5 climatic zones as indicated in Fig. 1. The climatic zones in India are as below:

1. Cold Climate
2. Composite Climate
3. Hot and Dry
4. Warm and Humid
5. Temperate Climate

The high altitudes in the Northern part of the country are demarcated as the cold zone. The great Himalayan mountain range further divides it into two zones, the lower part of the Himalayas being cold and cloudy whereas the upper part is cold and dry. The western part which lies within the purview of the great Indian Thar desert, flanked by the Aravalli range is the hot and dry zone that receives minimal rainfall. The coastal strip along the west, south and east due to its vicinity to the Arabian sea, Indian Ocean, and the Bay of Bengal respectively are classified as the warm and humid zone. The central part of the country which is prominently land-locked within these three zones experiences composite climatic conditions. The country also has moderate climatic conditions known as the temperate zone which is experienced by only two cities of India -Pune, and Bengaluru.

Climate Responsive Building Design

The building design is complex and involves the building to be built around complex parameters of the natural environment. Prior to the advent of air conditioning and mechanical ventilation systems, sun and wind were the only determinant forces for the design of the building. Therefore, the building typologies varied from place to place which gave a distinct vernacular character to the built form which responded well to the climatic conditions without relying on any active mechanical means to keep the occupants thermally comfortable. Similarly, as the buildings were designed keeping in mind the impact of the climate on them, so was the use of local materials or native technologies, that did not have an adverse impact on the local micro climate of the place at large. The buildings relied on providing thermally comfortable living conditions to the occupants through climate-responsive building design. Although the primary objective of the built spaces is still the same in current times i.e. to provide healthy and comfortable living conditions to the occupants, since the advent of the new technologies and gradual developments in the building industry, the building designers have drifted their ways to provide habitats with more reliance on the mechanical means rather than passive means.

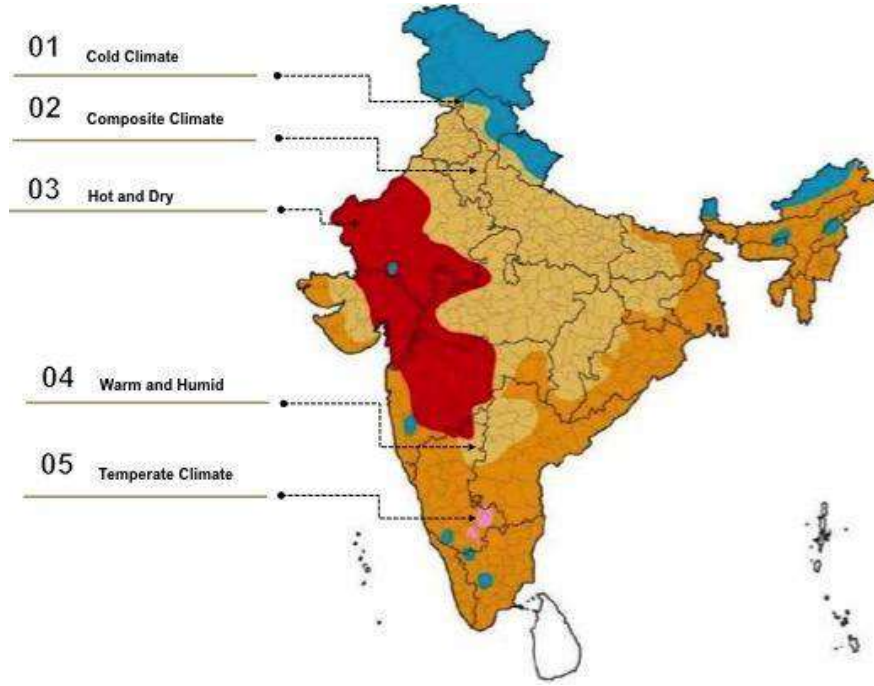

Fig. 1: Map of India indicating the 5 climatic zones.
Source: ECBC (2007)

Design Process

The urban areas encompass a network of buildings serving for living and performing activities. Vitruvius states that the primary function of architecture is that it should provide shelter from the dynamic conditions of the environment. An architect designs buildings and cities considering a complex of laws, rules, sciences including servicing and services, the environment, and the context of the people and society.

An architect/ designer plans a building keeping in mind certain aspects as indicated in Fig. 2. Considerations include, first, the design program including the local bylaws, local context, and surroundings followed by the provisions of urban planning of the respective city. Second, designing an appropriate building form that is often creative in approach while considering certain local conditions. Third, the building facade design is to be functional in terms of addressing the climatic conditions of temperature, humidity,

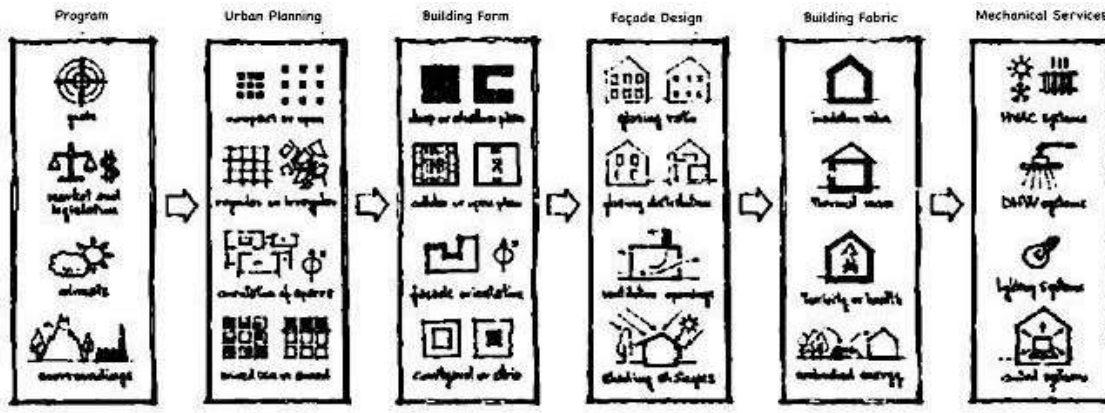

Fig. 2: Phases of design process influencing buildings energy performance and comfort.
Source: Aste et al. (2014)

wind movement, etc. as well as the aesthetic appearance of the building. The building fabric is evolved based on the desired effect of temperature as well as the availability of natural resources. This is then followed by working out of the various services crucial for achieving thermal comfort as well as essential servicing of the building system for effective functioning of the building. Much of the building details are finalized even before the building is built on the site.

Once the building is designed, the only option to ensure thermal comfort would then by using active forms and at the expense of energy consumption. The design process is a major factor in influencing the building's energy performance and comfort as well as energy consumption that directly influence the life costs of the buildings as well as the running costs.

Thermal Comfort

The fundamental aspect of the environmental quality of the indoor spaces of buildings that are directly related to the satisfaction of occupants and energy use is thermal comfort (Schiavon et al. 2014). Many books used by architects and designers use the 'bioclimatic chart'. Victor Olgyay was the pioneer of thermal comfort who considered Effective Temperature (ET) as the basis for the comfort diagram known as the 'Bioclimatic Chart'. He identified the space within the perimeter of the comfort zone outlined as comfortable to the occupants (Olgyay 1963). The chart also depicted the various ways of extending the comfort zone through increasing radiation, wind speed, and humidity. Givoni (1992, 1998) further depicted the comfort zone in the psychrometric chart with strategies for heating and cooling as depicted in Fig. 3.

The strategies that the thermal comfort area reports through the Bioclimatic Chart have been inconsistent with ASHRAE 55 thermal comfort areas (Schiavon et al. 2014). There are also inconsistencies that have been identified between the initial climate-based files and the later simulations due to the influence of construction, building program, and also the preferences of occupants (Arsano & Reinhart 2017). Extended boundaries of comfort zones can be formed when wind speeds are taken into account as they have the potential to offset temperatures and are dependent on climate-specific adaptations and comfort expectations (Kumar et al. 2016). Thus, the microclimate of the area where the building is designed also influences thermal comfort. Furthermore, the current comfort standards do not take into account that the thermal comfort requirements also vary in the different climatic zones. The range of solutions to provide thermally comfortable indoors varies from place to place and the right techniques need to be carefully chosen so that there is less reliance on energy consumption.

Parameters for Climate Responsive Building Design

Architect and environmentalist Arvind Krishan defines that the idea of climatically responsive design is to moderate the conditions around and inside such that they are always within or as close as possible to the comfort zone. The prevalent climatic conditions are generally harsh for most parts of the year and hence the importance of the building design in moderating the indoor conditions to suit the occupants. The difference in the natural climatic conditions to a thermally comfortable built space can be mitigated through a climate-responsive building design (Fig. 4) by incorporating appropriate site planning, building form, envelope materials, opening, daylighting, etc., and without the reliance on active measures.

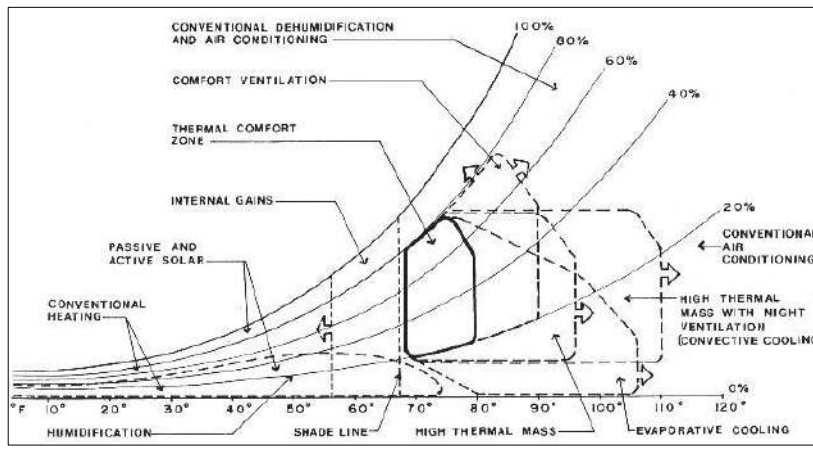

Fig. 3: Summary of design strategies as a function of ambient conditions of climate.
Source: Psychrometric-Bioclimatic Chart by Baruch Givoni & Murray Milne

Design is initiated by considering the context as the most important parameter and in which the geographical location, as well as the local climate, is of utmost importance. The identification, understanding, and control of the climatic effects at the location of the building are crucial. Arvind Krishan has stratified the design process into 20 aspects (Table 1) of the building and the built environment in a sequence from macro-level details to micro-level aspects in the process of climate-responsive building design wherein climate as a parameter is considered at each level at each aspect. Though all of these aspects are addressed, at some point in any typical design process, the design approach is never a step by step, material by material, or aspect-wise approach. The approach to design is comprehensive and holistic with several aspects addressed together. The recommendations provided are also generic and not specific to the climatic zones in India.

Climate Responsive Strategies by GRIHA and TERI

Green Rating for Integrated Habitat Assessment (GRIHA) is an Indian rating system, based on accepted energy and environmental principles, that has been instrumental in raising awareness about green design. It assesses the performance of building against nationally acceptable benchmarks. It evaluates the environmental performance of a building holistically over its entire life cycle. It also promotes climate-responsive building design measures, including progressive use of renewable energy. The GRIHA initiative is being followed by various development agencies throughout the country now and is picking up amongst Architects, Engineers, and Construction companies and is now mandated for public buildings. However, the use of the same is also limited and more as guidelines and in terms of suggestions for the climate-based design of buildings.

GRIHA was developed by the Energy and Resources Institute (TERI), a policy research organization working in the fields of energy, environment, and sustainable development. GRIHA addresses the common design elements that directly or indirectly affect the thermal comfort conditions and thereby the energy consumption in a building. It provides recommendations more like generalized suggestions rather than specific inputs for different climatic zones. The inputs from these have also been incorporated into the final climate-based strategy matrix.

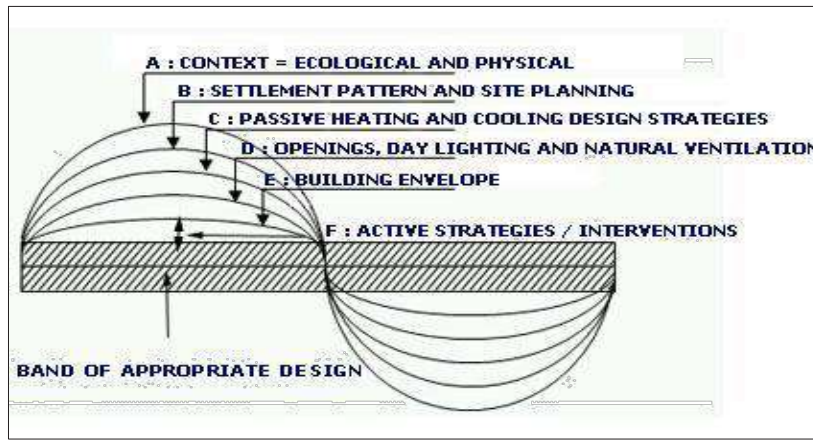

Fig. 4: Addressing conditions to achieve thermally comfortable buildings.
Source: Krishnan et al. (2014)

Table 1: The 20 Aspects of the design process for climate-responsive building design.

1. Landform: topography and slope orientation	7. Plan Form	12. Fenestration pattern and Configuration	18. Internal layout and partitions
2.Vegetation type and pattern	8. Plan Elements	13.Fenestration orientation	19. Internal materials
3. Water bodies	9. Building orientation	14. Fenestration Controls	20. Internal finishes
4. Street widths and orientation	10. Surface area to volume ratio	15. External Colours and textures	
5. Open spaces and built spaces	11. Roof Forms	16. Roof materials	
6. Ground Character		17. Walls	

Source: Krishan et al. (2014)

DEVELOPING THE CLIMATE RESPONSIVE STRATEGY MATRIX

Today's buildings in developed countries including India consume a significant portion of the total primary energy. In many of these buildings, adopting energy efficiency strategies, which can be readily adopted by architects and designers, can significantly reduce energy consumption.

Strategies for Climatic Zones by Climate Consultant

The data available on Psychrometric charts for specific cities that can be viewed on the climate consultant software used for analyzing the prevailing climatic conditions have been extracted as indicated in Table 2 for each of the climatic zones in India.

Grouping of Climate Based Building Design Parameters

From Arvind Krishan's climate-based building design aspects, 18 aspects have been logically listed down into four groups (Fig. 5) of pre-requisites in line with the normal design process as indicated in Fig. 1 for the purpose of designing a climate-responsive building through a comprehensive, grouped approach. The aspects range from the microenvironment surrounding the site to the finishes of the structure.

These individual groups are further discussed below with strategies for all 5 Indian climatic conditions considering inputs of the climate consultant software, and recommendations of TERI & GRIHA through a descriptive analysis to present the matrix with strategies. The matrix has further been validated by sample architectural experts from cities cited in Table 3.

CLIMATE RESPONSIVE STRATEGY MATRIX

The groups described above have been listed below with the suggestions for the corresponding climatic zones. The process follows a four-fold methodology as indicated in Fig. 6.

Table 2: Indicative strategies extracted from Climate Consultant 6.0 for the 5 climatic regions of India.

Climatic Zone	Representative City	Conditions & Indicative Design Strategy
Cold Climate	Shillong	11% is the comfort conditions without reliance on any mechanical means , while through incorporation of passive means it can be made 70% comfortable through out the year.
Composite Climate	Delhi	Through passive techniques, indoor temperature can be made 52% for human comfort condition while the prevalent climatic conditions indicate only 14% comfort
Hot and Dry Climate	Ahmedabad	17% in the human comfort zone, building design required to moderate natural conditions to make indoors comfortable without mechanical support. High heat, strong solar radiations and low water content in the air to be dealt in design
Warm and Humid Climate	Chennai	2.2 % of prevalent conditions lie in human comfort zone and majority of the time the design needs to create an comfortable ambient atmosphere to reduce moderate high humidity, high temperature.
Temperate Climate	Bengaluru	26% the natural environment is in the human comfort level and through passive means 94% can be made brought to comfort level through out the year.

Source: Compiled by the authors by accessing Climate Consultant 6.0 on April 25, 2020

Table 3: Cities representative of the 5 climatic zones in India.

Climatic Zone	Representative City
Cold Climate	Nainital, Shillong
Composite Climate	Delhi, Bhopal
Hot and Dry Climate	Ahmedabad, Jaipur
Warm and Humid Climate	Chennai, Panjim (Goa)
Temperate Climate	Bengaluru, Pune

Source: Cities identified by authors for validation of climate responsive strategy matrix

Site Micro Climate

Siting a building is a critical exercise as microclimate at times may vary even within the site boundaries at a short distance. Table 4 details the strategy matrix based on aspects related to the site micro and suggests strategies for all 5 zones of Indian climate conditions. For the hot and dry region, where the topography is generally flat, buildings should be located in the valleys and depressions, if such a situation is encountered on site, as these would have a slight dip in the temperature due to the higher density of cool air. Vegetation varies across all climatic zones and hence it is important to utilize its existence to benefit the built environment at large. For instance, in a hot and humid climate, vegetation can be utilized to channelize the naturally occurring high wind velocity to enhance the wind flow towards desired parts of the buildings or they can be utilized as barriers to harsh regional winds in a hot and dry or a harsh cold climate. Similarly, the existence of moisture in the air can produce varying results depending upon the external temperature conditions as moist air can hold more heat than dry air. In hot and dry weather with moderate wind velocity, the introduction of more moisture

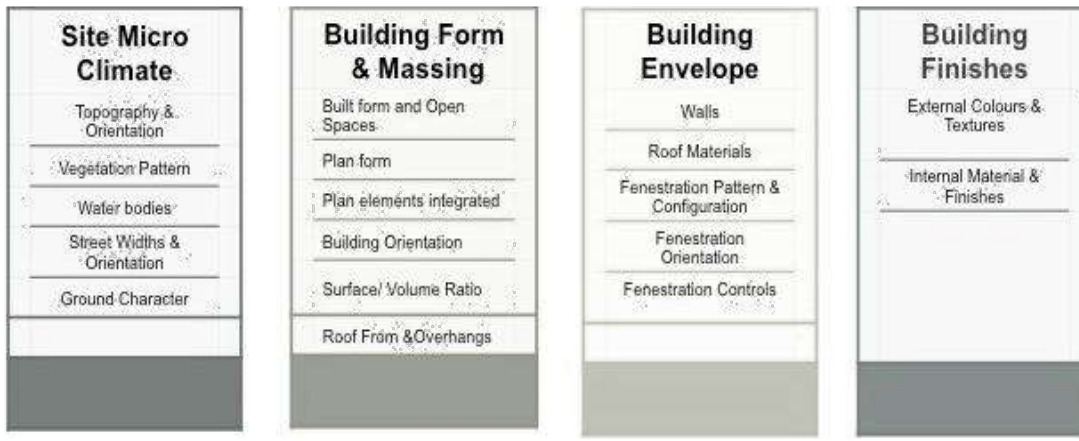

Fig. 5: Groups of parameters for climate-responsive building design.
Source: Adapted by authors from Arvind Krishnan's 20 design aspects

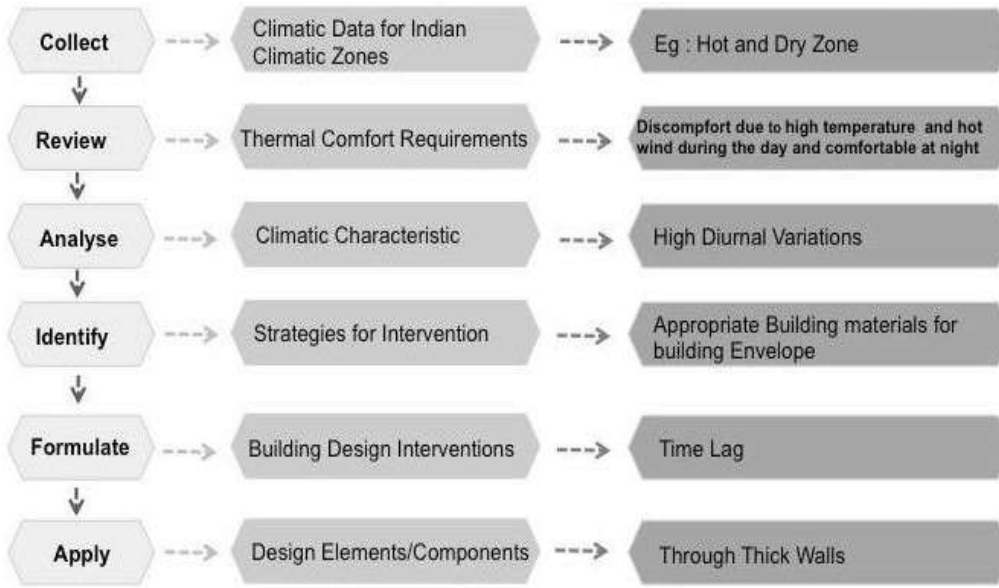

Fig. 6: Methodology followed for developing recommendations.
Source: Authors

Table 4: Strategies to address site microclimate in all the 5 climatic zones.

	Cold	Composite	Hot and Dry	Warm & Humid	Temperate
Landform : Topography Orientation	Generally high altitudes / hills. South-facing slopes preferred.	Plains & Plateaus. Higher levels are preferred	Generally Flat. Depressions and valleys preferred	Generally sloping towards the coast. North slopes in shade and slopes facing wind direction are preferred.	High Plateaus
Vegetation Pattern	a) Dense Forest. Evergreen trees cut cold winds but shade may block sun. b) Cold Desert. Scanty vegetation.	Seasonal. Deciduous vegetation to control sun.	Usually Scanty & dry surrounding. Trees planted to cut off east-west sun.	Dense vegetation, Tree should channel the wind and maximize airflow.	Well Vegetated. Trees planted to shade.
Water Bodies	When enclosed can store heat and control heat loss. For Cold Dry add humidity to air	Preferred during summers but should be drained during monsoons and winters	Enables evaporative cooling and directs cool breeze indoors.	Not recommended as it adds to humidity levels.	Enable cooling and direct cool breeze indoors.
Street Widths & Orientation	Narrow to prevent cold drafts (E-W Oriented)	Should be narrow (N-S Oriented) and oriented to receive monsoon winds.	Should be narrow and shaded (N-S Oriented)	Preferably wide to promote air movement	Shaded streets
Ground Character	Paved, dark and smooth to increase absorptivity and avoiding Glare	Green Non-reflective ground cover	Not reflective, rough surface for diffusing radiation, more softscape, light coloured paving	Not absorptive, rough, some hardscape and dry ground around buildings	Balanced softscape and hardscape

Source: Compiled by authors and validated by a survey

can induce a feeling of more comfort, whereas in an already humid condition, more discomfort can be experienced and in a cold climate, water can be used to trap the heat and release it to the interior environment.

Along with moderating the natural conditions to benefit the manmade environment, careful planning of the built environment too can create a positive impact on the thermal comfort conditions inside the built envelope. The orientation and spacing between buildings can be varied to either promote or to cut off the impact of one or more elements of climate. It is favorable in some conditions of the cold climatic zones of the country to increase the absorptivity of solar radiations to release the absorbed heat at lower temperatures at night, but in the case where the atmospheric temperature is already soaring, having reflective or absorptive surfaces can further add on the heat in the environment.

The surrounding environment, as well as the building, can positively or negatively impact each other and therefore careful considerations must be given to locating the building or planned elements on the site as well as surface treatments of the ground around it.

Building Form and Massing

The next step in the building design process after the contextual analysis is to moderate and orient the built mass with an underlying understanding of the solar geometry, wind directions, precipitation, and other determinants of climate to maximize or minimize the impact of solar radiation, wind movements, and moisture content within the building depending on the climatic data available for that zone. In a hot and dry region, a more compact built form is preferred with contained inward-looking open spaces so that there is a minimum interface with outside temperature hence also having a minimum perimeter to area ratio. It bears similarity to the structure in a cold zone where a similar compact form is desired to contain the heat within the space, but orienting windows towards the south side to trap the south sun. And similarly, the other climate suggestions are provided that may suit the respective climatic zone.

Apart from working out an appropriate form of the structure, planning of some elements like courtyards, atriums, Trombe walls, etc. can help in creating a thermally suitable atmosphere for the inhabitants. In the cold climatic zones like Leh and Ladakh, utilization of the solar radiation is the only source of natural heating of the indoor environment and hence providing sunspaces that are oriented towards the south or providing the traditional technique of Trombe wall that can trap the heat and later release the trapped heat at

night can be beneficial in a responsive design by relying less on heating through active means. Table 5 below discusses strategies for built form and mass.

Building Envelope

The building envelope as discussed in Table 6 is the thermal barrier between the external and the internal environment. Each element of the building envelope i.e. floor, walls, roof, fenestration, etc. contributes to heat exchange between the two sides and if appropriately designed by selecting the right materials and construction details, it could minimize the thermal impact (Akeel et al. 2017). Fenestration itself can constitute a large part of undesired heat ingress or egress not appropriately planned for the climatic situation where it has to be located. In designing fenestration, the following factors may be considered for a climate-responsive building design which are the size of the openings, its material selection, and assembly, the orientation, the pattern whether openable or closed, and the shading requirements. Due to the potential heat intake it can have a hot and dry climate, windows should be planned smaller in size and well shaded, located at two levels preferably their orientation towards East and West should be avoided. In warm and humid conditions, where the wind is required in all parts of the buildings, windows are placed keeping in mind cross ventilation, openable yet an assembly that can keep the heat out as much as possible. In the colder zone, windows that allow the south sun during the windows are provided.

Walls and roofs take in a large amount of heat in the typical heat-dominated tropical climate. Selection of material for the roofs and wall is done with an underlying understanding of how a material would behave when subjected to heat on one of the sides and accordingly appropriate construction techniques and wall assemblies are then constituted to create the envelope that would keep the interiors comfortable. Mud or brick walls have a very different thermal property from concrete and glass. Shading devices protecting the external openings and fenestration from the harsh climates enhance the performance of the envelope, particularly in a hot country like ours. The material and construction technique used in the envelope modifies the thermal characteristics of the envelope. While dark heat-insulating material like timber is preferred in cold climates, massive heat-storing materials or cavity walls are preferred in hot dry and lighter masonry structures transparent to wind performs best in humid zones.

Building Finishes

Surface finishes (see strategies for building Finishes in Table 7) in terms of color and texture also modify the thermal characteristics of a built environment. External and internal surface finishes, colors, and textures impact the heat transfer into the structure due to their various properties such as density, specific heat capacity, emissivity, color, albedo, absorptivity, transmittance, and roughness (Hwaish, 2018). One or a combination of the above factors can increase or decrease the amount of thermal transfer through conduction, convection,

Table 5: Strategies to address building form and massing in all the 5 climatic zones.

	Hot & Dry	Warm & Humid	Composite	Cold	Temperate
Built Form & Open Spaces	Compact for mutual shading with small open spaces	Open Planning to promote air circulation	Compact planning, low rise development	Open spaces to be small but allow south sun.	Open Planning for thermal comfort
Plan Form	Minimum Perimeter to Area ratio, Shaded and semi covered areas as buffers	Minimum Perimeter to Area ratio but shaped and supporting maximum air movement.	Minimum Perimeter to Area ratio. Mutual shading. Open to monsoon winds.	Minimum Perimeter to Area ratio for reduce heat loss.	Minimum Perimeter to Area ratio for minimum heat gain.
Plan Elements Integrated	Shaded Courtyards, Fountains, water channels, wind towers/catchers, earth air tunnel, Terrace/Roof gardens, window planters	Open courtyards/atrium, balconies, patios, verandahs. Wind Tunnels, Windcatchers to catch breeze.	Shaded Courtyards, Fountains, hybrid structures (separate summer/monsoon areas), earth air tunnel, pergola with creepers	Sun spaces, Greenhouse, trombe wall, light wells, light shelves, thermal chimney, water walls	Shaded courtyards, Shading devices for fenestration, balconies, Roof gardens
Building Orientation	Longer facades facing North South, primarily to minimize heat gain	Longer facades North South or more preferably oriented as per the wind direction	Longer facades facing North South, primarily to minimize heat gain and to catch monsoon winds	Oriented for maximum sun, preferably South	Longer facades facing North South, primarily to minimize heat gain
S/V Ratio	minimum S/V ratio	S/V ratio to create shaded airy spaces	minimum S/V ratio	minimum S/V ratio	minimum S/V ratio
Roof Form & Overhangs	Flat or Shaded roofs to minimize heat gain	Pitched roofs with large overhangs	Large eaves to shade walls and openings	Flat roofs to minimize heat loss	Light roofs with deep overhangs

Table 6: Strategies to address building envelope in all the 5 climatic zones.

	Hot & Dry	Warm & Humid	Composite	Cold	Temperate
Fenestration Pattern & Configuration	Small Openings to prevent wind carrying sand, shaded to cool hot breeze. High level heat vents	Large and body level well-shaded fenestration. Cross ventilation arrangement	Two level small openings. Operable and shaded. Maximum on monsoon windward side.	Large glazed areas, unshaded but well sealed.	Large well shaded and sealed fenestration
Fenestration orientation	North facing primarily, also sunny spaces for winter sun	Staggered and in the direction of airflow	Towards south for cold season and towards monsoon winds	South facing	North facing
Fenestration Controls	Shaded Fenestration, Low E Value Glass, Louvers, sun breaks	Solar radiation is diffuse. So shading not important. Flywire net to ward off insects	Shaded openable Fenestration, Low E Value Glass, Louvers, sun breaks	Optimum glazing, well-sealed, unshaded	openable windows
Walls	Adobe construction, masonry with high thermal mass, low U, reflective insulation, green walls, AAC blocks, hollow blocks, composite masonry, stone/ tile cladding	Low U walls. Low thermal mass. Insulation are effective	Masssive walls at lower levels. Light structures at upper levels.	Wall to have low U value. Thermal mass for heat storage. Trombe walls, Trombe wall with vents, Solar wall, Water wall	Walls with low U factor for minimum heat loss. Trombe walls, Trombe wall with vents, Solar wall, Water wall
Roof Materials	Adobe construction, roof with high thermal mass, reflective insulation, green roofs, earthen pots, roofing tiles	Roof to have low U value and have low heat capacities (light roofs).	Light roofs, well insulated, low U values	Low U value roofs, adobe, stone roof with high thermal mass	Roofs with low U value and roofing tiles

Table 7: Strategies to address building finishes in all 5 climatic zones.

	Hot & Dry	Warm & Humid	Composite	Cold	Temperate
External Colors & Textures	Light Colours , textured walls for shading	Light Colours , rough textured walls	Light Coloured exteriors (white wash in summer)	Dark Colours & flat surfaces	Light / Dark, Smooth/ Rough textures
Internal Materials & Finishes	Light furniture and interiors to reduce heat absorption, matt finishes	Light furniture and interiors to reduce heat absorption and improve lighting levels	Light Colours and textures to reduce heat absorption	Dark Colours and heavy furniture to promote heat absorption	Light /Dark

or radiation. Smooth light-colored plasters radiate much of the incoming radiation while textured coatings absorb and add heat into the building. Within the buildings, the color of walls, ceilings, and furniture also reflects or absorbs incoming radiations and modifies the thermal properties of the inside space. It is a known fact that darker colors absorb more heat than lighter shades. Hence warmer the climate, lighter shades are preferred and colder the climate the dark colors help to absorb or retain the heat within the interior atmosphere.

CONCLUSIONS

The building industry is a large contributor to the rising environmental degradation and every year the energy consumption in buildings is increasing alarmingly. The major reason being the utilization of active energy-consuming appliances for the creation of desired comfort conditions within the building. The architects and designers, who have a major role in the building design process, need to acknowledge the need for designing naturally for thermal comfort thereby reducing the pressure on artificial conditioning of indoor environs.

The paper provides a very simplified way of the entire design process that should be carried out to create a thermally responsible structure, which not only provides comfortable indoor spaces to the inhabitants but also reduces the need for energy-consuming cooling/heating appliances/systems and its negative impacts on the environment at large. The paper provides an easy to comprehend concise matrix that should be considered to create suitable massing and choosing the

building component and materials for each climate condition that also is essential for sustainable development. Not every building has the same weather exposure. Regional climate conditions, macro environment, and site microclimate all affect the built-up indoor environment and must be taken into account in the design process of a climate-responsive building.

REFERENCES

Akeel, H., Al-Mulla, N. and Almulla, H. 2017. Impacts of heat exchange on building envelope in hot climates. J. Int. J. Emerg. Technol. Adv. Eng., 5 (2): 47-57.

Albatayneh, A., Alterman, D., Page, A. and Moghtaderi, B. 2018. The significance of building design for the climate. J. Environ. Clim. Technol., 22: 165-178.

Arsano, Y A. and Reinhart, C. 2017. A comparison of methods for evaluating ventilation cooling potential building program-based climate analysis for early design decisions. In: 15th International Conference. Proceedings of International Building Performance Simulation Association (IBPSA), San Francisco, USA.

Aste, N., Butera, F. and Adhikari, R. 2014. Sustainable Building Design for Tropical Climates: Principles and Applications for Eastern Africa. UN-Habitat, Nairobi, Kenya

Choi, J., Shin, J., Kim, M. and Kim, I. 2016. Development of open BIM-based energy analysis software to improve the interoperability of energy performance assessment. J. Auto. Const., 72: 52-64.

Givoni, B. 1998. Climate Considerations in Buildings and Urban Design. Wiley & Sons, New Jersey, USA, pp.185.

Givoni, B. 1992. Comfort, climate analysis, and building design guidelines. Energy and Buildings, 18:11-23.

Hwaish, A. N. A. 2018. Sustainable design for building envelope in hot climate; a case study for the role of the dome as a component of the roof in heat exchange. International Journal of Advanced Engineering, Management and Science, 4(2): 126-134.

Harish, V.S. and Kumar, A. 2016. A review on modeling and simulation of building energy systems. J. Renew. Sust. Energy Rev., 56: 72-92.

Jung, D.K., Lee, D.H., Shin, J.H., Song, B.H. and Park, S.H. 2013. Optimization of energy consumption using BIM-based building energy performance analysis. J. Appl. Mech. Materials, 281: 649-652.

Kovacic, I. and Zoller, V. 2015. Building life cycle optimization tools for early design phases. Energy, 92: 409-419.

Krishnan, A., Baker, N., Yannas, S. and Szokolay, S. 2014. Climate Responsive Architecture: A Design Handbook for Energy Efficient Buildings. Tata McGraw-Hill Education, New York.

Kumar, S., Mathur, J., Mathur, S., Singh, M. K. and Loftness, V. 2016. An adaptive approach to define thermal comfort zones on psychrometric chart for naturally ventilated buildings in the composite climate of India. J. Build. Environ., 109: 135-153.

Olgyay, V. 1963. Design with Climate: A Bioclimatic Approach to Architectural Regionalism. Princeton University Press, New Jersey, USA.

Perez-Lombard, L., Ortiz, J. and Pout, C. 2008. A review on buildings energy consumption information. Energy Build., 40(3): 394-398.

Schiavon, S., Hoyt, T. and Piccioli, A. 2014. Web application for thermal comfort visualization and calculation according to ASHRAE standard 55. J. Build. Simul., 7(4): 321-334.

Venkataraman, A. and Kannan, R. 2013. Whole Building Energy Analysis using BIM. In: 4th International Conference Proceedings of International Conference on Advances in Civil Engineering AETACE, NCR, India, pp. 935-943.

Yilmaz, Z. 2007. Evaluation of energy-efficient design strategies for different climatic zones: Comparison of thermal performance of buildings in temperate-humid and hot-dry climate. J. Energ. Build., 39: 306-316.

Nature Environment and Pollution Technology
An International Quarterly Scientific Journal

p-ISSN: 0972-6268
(Print copies up to 2016)
e-ISSN: 2395-3454

Vol. 20 | No.3 | pp. 1033-1039 | 2021

Original Research Paper

https://doi.org/10.46488/NEPT.2021.v20i03.010

Open Access Journal

Effect of Wheat Straw Biochar on Thermophysical Properties of Loessial Soil

B. W. Zhao†, Y. Zhao, H. Liu, Y. Q. Li, K. X. Duan and X. Zhang

School of Environmental and Municipal Engineering, Lanzhou Jiaotong University, No. 88, West Anning Rd., Lanzhou 730070, P. R. China

†Corresponding author: B. W Zhao; zhbw2001@sina.com

Nat. Env. & Poll. Tech.
Website: www.neptjournal.com

Received: 22-08-2020
Revised: 23-10-2020
Accepted: 01-11-2020

Key Words:
Biochar
Bulk density
Thermophysical properties
Loessial soil

ABSTRACT

Soil thermophysical properties are the key factors affecting the internal heat balance of soil. In this paper, biochars (BC300, BC500 and BC700) were produced with wheat straw at the temperatures of 300, 500 and 700°, respectively. The effects of biochar amendment at the rates of 0%, 1%, 3%, and 5% on the thermophysical properties (thermal conductivity, heat capacity, and thermal diffusivity) of a loessial soil were investigated with and without water content respectively. Although the bulk density of soil significantly decreased with biochar amendment, due to enhancing soil porosity and organic matter content, the thermophysical properties of soil did not change largely with biochar amendment rate and pyrolysis temperature. Water content exhibited significant effects on the thermophysical properties of soils added with biochars, where the thermal conductivity and heat capacity of soil were linearly proportional to water content, the thermal diffusivity initially increased and then decreased with the increase of water content. In the meanwhile, there was no significant correlation between the biochar amendment rate or pyrolysis temperature and thermophysical properties. The results show that water content should be mainly concerned as a factor when the internal heat balance of loess soil is evaluated, even though the soil is amended with biochar.

INTRODUCTION

Biochar is a solid carbon material obtained by the pyrolysis of biomass (such as straw, sawdust, sludge, etc.) under high temperature and a limitative oxygen condition (Ding et al. 2016, Tripathi et al. 2016, Li et al. 2017). Related studies had shown that biochar played an important role in reducing greenhouse gas emission, slowing global warming, improving soil quality, promoting crop yields, and remedying contaminated soil (Chan et al. 2007, Liu et al. 2012, Herath et al. 2013, Lu et al. 2014, Lehmann & Joseph 2015, Elzobair et al. 2016, Lin et al. 2019). As a large agricultural country, China has abundant straw resources, and the current disposal of straw in China has always been an environmental problem. According to statistics, the annual amount of straw by incineration in China is about 1.4×10^8 t (Mohan et al. 2014), which causes severe pollution to the atmospheric environment. To realize the proper disposal and utilization of straw, it is an economical and feasible way to convert straw into biochar. In addition, loess soil is widespread and accounts for one-tenth of the global land area. Loess soil has the characteristics of loose structure, large porosity and water permeability, low agglomerating force, and organic matter content, which result in nutrient leaching from the loess soil, causing the soil to have poor quality (Tuo et al. 2017). Therefore, biochar could be a modifier to improve the fertility of loess soil and enhance crop yields.

Biochar amendment into the soil will change the composition and properties of soil, such as soil organic matter and bulk density, and thus indirectly affect the soil thermophysical properties and temperature (Wang et al. 2009). Zhang et al. (2013) found that the application of biochar could reduce daily or seasonal temperature fluctuations of soil. Genesio et al. (2012) found that the soil treated by biochar had an albedo being lower than that of the control by 80%. During the crop growing season, the albedo of soil treated by biochar decreased by 20-26%. Usowicz et al. (2016) noted that there was no significant change in soil thermal conductivity and thermal diffusivity after application of biochar in grassland, while in fallow land, both of them decreased with the increase of biochar amendment. Yadav & Saxena (1973) found that the heat capacities of sand and clay were a linear function of the water content, and the compaction treatment had no significant effect on the heat capacity of the soil. However, there have been few studies on the effect of biochar amendment on the thermophysical properties of loess soil.

Thus, the loessial soil was sampled, wheat straw was used as the biomass to prepare biochar, and the biochar was added into the loessial soil. The changing laws and mechanisms of wheat straw biochar influencing the thermophysical properties of loessial soil were explored. The results could provide a reference for the subsequent evaluation of the physical environmental effects of biochar on loess soil.

MATERIALS AND METHODS

Biochars and Soil

Wheat straw was obtained in Wushan County, Tianshui City, Gansu Province, China. The straw was washed 3 times with tap water, air-dried for 2 days, and dried in an oven at 70-80°C overnight. Then the straw was crushed and passed through a 40 mesh sieve. The straw crumbs were put into a crucible with compaction and pyrolyzed in a muffle furnace (HWL-12XC, Shandong Huawei Luye company, China) at 300, 500 and 700°C for 6 h, and then taken out after the sample was cooled (Ren et al. 2018). The biochars were denoted as BC300, BC500 and BC700. The basic properties of biochars are listed in Table 1, where the yield of the biochar was obtained by the ratio of the sample mass difference before and after pyrolysis to the mass of biomass; the pH value was measured by the potentiometric method (Zhou et al. 2015); the content of C, H, and N in biochar was determined by an element analyzer (Vario EL, Elementar, Germany), and the content of O was calculated by a subtraction method (Peterson et al. 2012); the average pore size and the specific surface area were measured by BET physical adsorption instrument (Autosorb-1, Quantachrome, USA).

The loessial soil was sampled from the 0-20 cm surface soil at Elephant Mountain Town, Gangu County, Tianshui City, Gansu Province, China, which is the cultivated soil for growing wheat all year round. The impurities such as small stones, rhizomes, and leaves were removed. The soil sample was air-dried and passed through a 40 mesh sieve for use. The basic properties of soil are also listed in Table 1, where the total carbon was determined by soil carbon and nitrogen analyzer (DK-3, Shenzhen Deka Precision Instrument Company, China); the moisture content was determined by calculating the ratio of the difference between the quantity of the sample before and after drying to the initial quantity of the sample; the organic matter content was obtained by potassium dichromate oxidation method (Shuang et al. 2016); the porosity was measured by the standard method (GB/T 24203-2009); for determining bulk density, a sample of 100 mL was taken, its mass weighted, and the ratio of mass to volume calculated.

Experimental Design

The biochars were thoroughly mixed with loessial soil in the amount of 0%, 1%, 3%, and 5% (mass ratio) and placed in a 100 mL plastic container with a sealed lid. The containers were put into an incubator at 25°C for one week to ensure the equilibrium and then the bulk density, organic matter content, and thermophysical properties of soils were determined. Three parallel samples were set for each run. The sample with no biochar addition was the control (CK). The treatments with BC300, BC500 and BC700 at the amendment rates of 1%, 3% and 5% were denoted as BC300-1, BC300-3, BC300-5; BC500-1, BC500-3, BC500-5; BC700-1, BC700-3 and BC700-5, respectively. As far as the effects of water content on the thermophysical properties were concerned, distilled water was added at the rates of 0%, 20%, 30%, and 40% respectively into the soil sample under different treatments.

Determination Methods

The determinations of organic matter content and bulk density of loessial soil were the same as mentioned in the earlier section. The thermophysical properties of loessial soil were analyzed by KD2 Pro thermal characteristic analyzer (METER Group, Inc., USA).

Data Analysis

Origin Pro 8.5 software was used for data fitting; SPSS 19.0 statistical analysis software was used for Pearson correlation analysis and the least significant difference method was used for multiple comparisons (Uppercase letters represented differences between groups, lowercase letters represented differences within groups).

RESULTS AND DISCUSSION

Effect of Biochar on Soil Property without Water Content

The effects of biochars on the bulk density of loessial soil are shown in Fig. 1. Biochar amendment had significant effects on the bulk density of loessial soil. The bulk density of CK was 1.002 g.cm^{-3}, and the decreasing percentages of bulk

Table 1: Basic properties of biochars and soil.

Biochar	Yield (%)	pH	Average pore size (nm)	Specific surface area ($m^2.g^{-1}$)	Element (%)			
					C	H	O	N
BC300	45.63	7.11	/	0.43	63.10	3.91	27.07	0.46
BC500	27.22	9.66	2.33	23.12	71.41	2.83	19.72	0.58
BC700	23.94	10.43	2.00	311.51	86.60	1.86	5.47	0.61

Soil	Total carbon（%）	pH	Organic matter（%）	Porosity（%）	Bulk density（g/cm^3）
Loessial soil	2.2	8.22	0.79	60.9	1.002

density in soils with BC300-1, BC500-1, and BC700-1 were 12.9%, 6.4% and 4.4%; BC300-3, BC500-3, and BC700-3 were 23.8%, 16.3% and 13.6%; BC300-5, BC500-5, and BC700-5 were 36.4%, 24.9% and 21.7%, respectively.

The reduction in bulk density of soil could be attributed to the increment in the organic matter content and porosity of soil due to biochar amendment. The effects of BC300, BC500, and BC700 on the organic matter content of loessial soil are shown in Fig. 2. It can be observed that the organic matter content of loessal soil significantly increased by BC300, BC500, and BC700 amendment The organic matter content of CK was 0.79%, and the increasing percentages of organic matter in soils with BC300-1, BC500-1, and BC700-1 were 55.7%, 67.1%, and 75.9%; BC300-3, BC500-3, and BC700-3 were 164.6%, 169.6%, and 219.0%; BC300-5, BC500-5, and BC700-5 were 226.6%, 225.3%, and 229.1%, respectively. Hua et al. (2014) also found that the effect of biochar on soil with low organic matter content was significantly higher than that with high organic content. In addition, biochar has a low density and rich pore structure (Lehmann & Joseph 2015). According to the relevant research, the soil bulk density was related to the soil porosity and compaction (Neves et al. 2003, Hong et al. 2011, Wu et al. 2015, Das et al. 2017, Zhao et al. 2018). Biochar amendment would result in increasing of soil porosity and decreasing soil bulk density. The conclusion was consistent with previous research results (Oguntunde et al. 2008).

The effects of biochar amendment on the thermophysical properties of loessial soil without water content are shown in Fig. 3. The thermal conductivity of soils with BC300-1, BC500-1 and BC700-1 were 0.193, 0.195 and 0.201 w.m·K^{-1}; BC300-3, BC500-3 and BC700-3 were 0.173, 0.180 and 0.188 w.m·K^{-1}; while BC300-5, BC500-5 and BC700-5 were 0.167, 0.173 and 0.181 w.m·K^{-1}, respectively (Fig. 3a). The thermal conductivity of loessial soil increased by the biochar addition at the rate of 1%. The thermal conductivity was inversely proportional to the biochar addition amount. The reason was that the thermal conductivity of biochar itself was low and the addition of biochar was conducive to the formation of large pores in loessial soil. In addition, the increase of organic matter content of loessial soil was also an important reason for the decrease of thermal conductivity with the increase of biochar addition amount (Abu-Hamdeh et al. 2000).

As seen from Fig. 3b, when compared with CK, the heat capacity of soils with BC700-1 and BC700-3 increased by 6.7% and 1.6%, respectively. The heat capacity decreased by the addition of biochar at the rate of 5%. Since the organic matter content of loessial soil increased by the high addition of biochar, the organic matter content was an important factor for the decline of the heat capacity (Abu-Hamdeh et al. 2000, Zhao et al. 2016). The heat capacity of loessial soils added with BC500 and BC700 reduced with the increase of biochar amendment, where those with BC500-1, BC500-3, and BC500-5 were 1.104, 1.046, and 1.035 MJ.m^3·K^{-1}, respectively. However, the changing laws between the heat capacity and the addition amount with BC300 were not significant.

Thermal diffusivity is the ratio of thermal conductivity to thermal capacity. The effects of biochars on the thermal diffusivity of loessial soil are shown in Fig. 3c. When compared with the CK, the thermal diffusivity of soils with BC300-1, BC500-1, BC700-1, and BC700-5 increased by 0.99%, 3.0%, 1.2%, and 3.0%, respectively. The thermal diffusivity of loessial soils with BC300-3, BC500-3, BC500-5, and BC700-3 decreased by 4.9%, 8.5%, 1.2%, and 0.79%, respectively. The addition of BC300 and BC500 was inversely proportional to

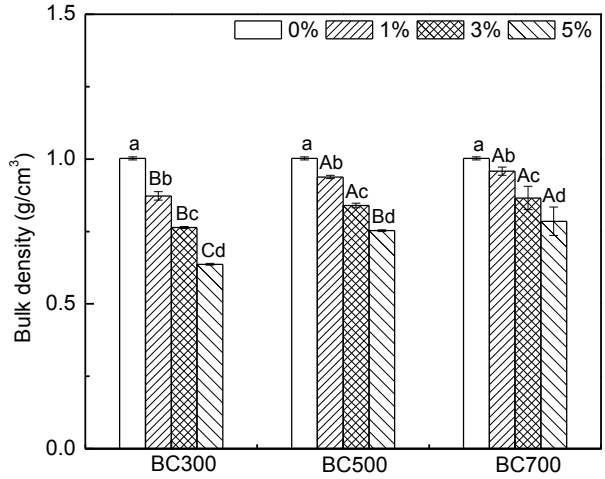

Fig. 1: Effects of biochars on bulk density of loessial soil

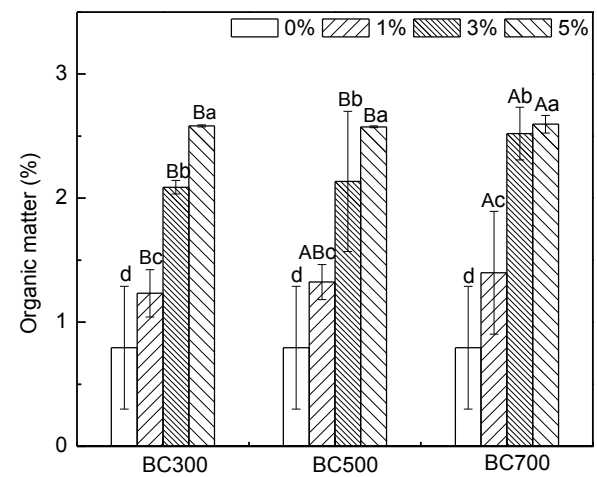

Fig. 2: Effects of biochars on organic matter contents of the soil.

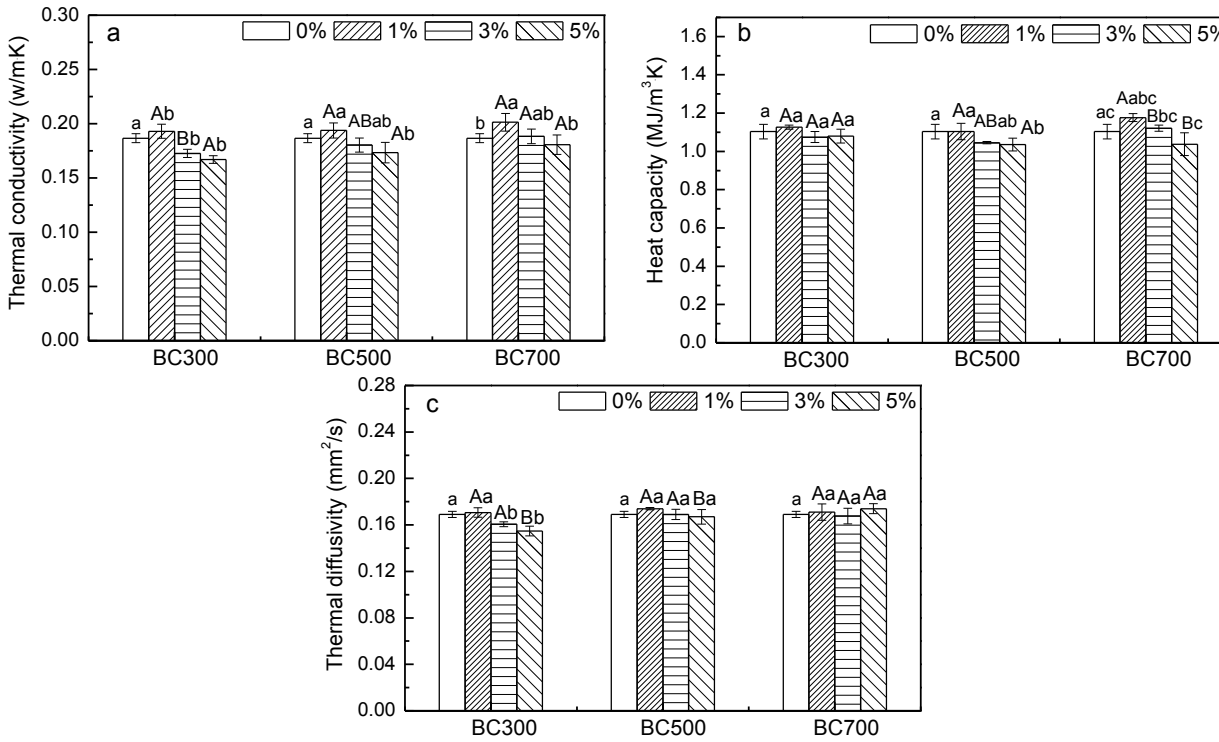

Fig. 3: Effects of biochars on thermal conductivity (a), heat capacity (b) and thermal diffusivity (c) of loessial soil.

the thermal diffusivity. It was mainly due to the low thermal diffusivity of the biochar itself (Bachmann et al. 2001, Zhao et al. 2016). The effect of pyrolysis temperature on the heat capacity and the thermal diffusivity of loessial soil was not significant (Usowicz et al. 2014).

Effect of Biochar on Soil Property with Water Content

The effects of water content on the thermophysical properties of loessial soil are illustrated using BC300 systems and shown in Fig. 4 (no data shown for BC500 and BC700 systems). There was a close linear positive correlation between the thermal conductivity and water content with biochar amendment, indicating that the thermal conductivity could be heavily affected by a slight change in water content. The reason is that the thermal conductivity of water is almost 30 times that of air and the thermal conductivity was increased by the formed water film (Zhao et al. 2016). When the water content was 0% and 40%, the thermal conductivity of soils with BC300-5 was 0.2 and 1.19 w.m·K^{-1}, respectively, with an increase of 495%, which shows that the thermal conductivity would be greatly improved by water content.

The effects of water content on the heat capacity of loessial soil are shown in Fig. 4b. There was a close linear positive correlation between heat capacity and water content. When the water content was 0% and 40%, the heat capacity of soils with BC300-5 was 0.87 and 2.50 MJ.m^{-3}·K^{-1}, respectively, with an increase of 187%. The reason is that the specific heat capacity of water is much larger than that of air and the positive effect of the heat capacity caused by increasing the water content was significantly higher than the negative effect caused by increasing porosity.

The effects of water content on the thermal diffusivity of loessial soil are shown in Fig. 4c. The fitted curves between the thermal diffusivity and water content are logarithmic. The thermal diffusivity of loessial soils with biochar amendment initially increased and then decreased with the increase of water content. The peak thermal diffusivity of soils with CK, BC300-1, BC300-3, and BC300-5 were 0.415, 0.433, 0.389 and 0.349 mm^2.s^{-1}, respectively. At low water content, the thermal conductivity of loessial soil increased with the water content more obviously than the heat capacity, and after the peak value, the heat capacity increased with the moisture content more obviously than the thermal conductivity, which caused the thermal diffusivity to increase and then decrease (Bachmann et al. 2001).

Correlation Analysis

The correlation between the thermophysical properties of

loessial soil added with biochars and influencing factors is shown in Table 2. In the absence of water content, there was a significant correlation between the thermal properties and the biochar amendment rate and the bulk density of soil. There was a significant negative correlation between the biochar amendment rate and thermal conductivity, heat capacity, and thermal diffusivity with correlation coefficients of -0.532**, -0.549**, and -0.411*, respectively. A significant positive correlation was found between the bulk density of soil and the thermophysical properties, with high correlation coefficients of 0.908**, 0.852** and 0.869**. However, with water content, the thermal properties were only significantly correlated with the water content. The correlation coefficients of thermal conductivity, heat capacity, and thermal diffusivity were 0.936**, 0.957** and 0.841**, respectively, which showed that water content was the main factor to evaluate the internal heat balance of loess soil, even though the loessial soil was treated with biochars.

CONCLUSIONS

Wheat straw biochar amendment could enhance the porosity

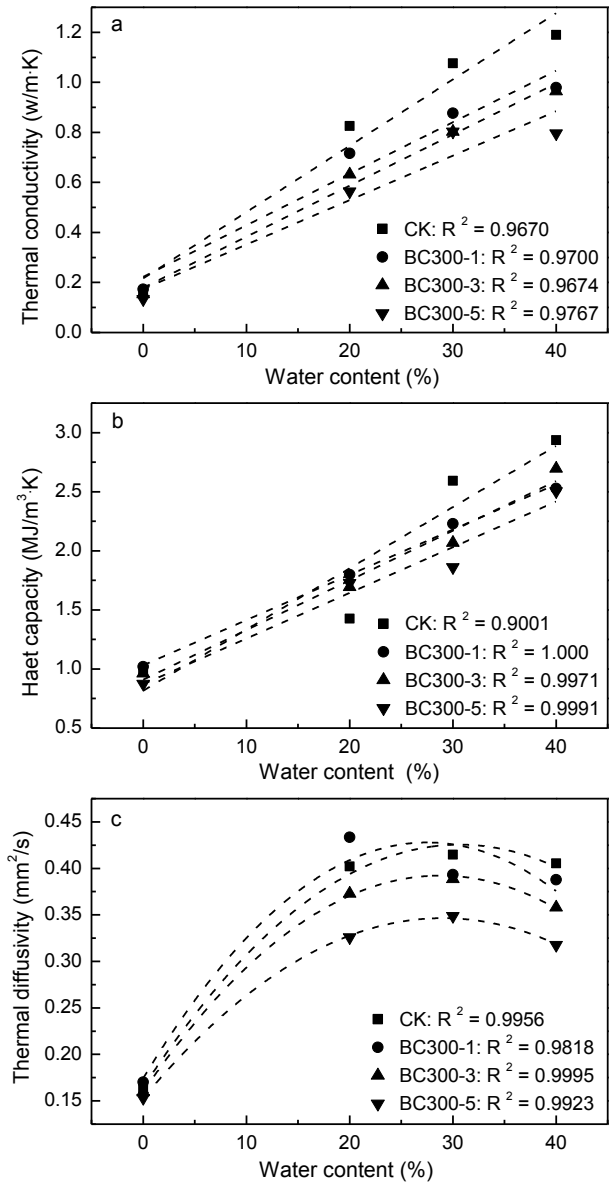

Fig. 4: Effects of water content on thermal conductivity (a), heat capacity (b) and thermal diffusivity (c) of loessial soil.

Table 2: Correlation between thermophysical properties and influencing factors.

	Thermal property	Factor			
		Pyrolysis temperature	Biochar amendment rate		Bulk density
Without water content	Thermal conductivity	0.169	-0.532**		0.908**
	Heat capacity	0.132	-0.549**		0.852**
	Thermal diffusivity	0.221	-0.411*		0.869**
	Thermal property	Factor			
		Water content	Biochar amendment rate	Pyrolysis temperature	Bulk density
With water content	Thermal conductivity	0.936**	-0.257	-0.012	0.18
	Heat capacity	0.957**	-0.12	0.01	0.091
	Thermal diffusivity	0.841**	-0.213	-0.012	0.176

* Significant correlation at 0.05 level; ** Significant correlation at 0.01 level

and organic matter content of loessial soil. Thus, the bulk density of loessial soil decreased significantly with the biochar amendment rate. Without water content, although the thermal conductivity, heat capacity, and thermal diffusivity of soil did not change largely with biochar amendment rate and pyrolysis temperature, there was a significant negative correlation between the biochar amendment rate and thermal properties, while there was a significant positive correlation between the bulk density of soil and the thermophysical properties. In the presence of water content, there was no significant correlation between the biochar amendment rate and pyrolysis temperature and thermophysical properties. The thermophysical properties changed significantly with water content increasing. It is shown that water content was a more important factor to evaluate the internal heat balance of loess soil.

ACKNOWLEDGMENT

This work was financially supported by the National Natural Science Foundation of China (51766008, 21467013, 21167007).

REFERENCES

Abu-Hamdeh, N. H. and Reeder, R. C. 2000. Soil thermal conductivity effects of density, moisture, salt concentration, and organic matter. Soil Sci. Soc. Am. J., 64: 1285-1290.

Bachmann, J., Horton, R., Ren, T. and Van der Ploeg, R. R. 2001. Comparison of the thermal properties of four wettable and four water-repellent soils. Soil Sci. Soc. Am. J., 65: 1675-1679.

Chan, K. Y., Van Zwieten, L., Meszaros, I., Downie, A. and Joseph, S. 2007. Agronomic values of greenwaste biochar as a soil amendment. Aust. J. Soil Res., 45: 629-634.

Das, O., Kim, N., Kalamkarov, A. L., Sarmah, A. K. and Bhattacharyya, D. 2017. Biochar to the rescue: Balancing the fire performance and mechanical properties of polypropylene composites. Polym. Degrad. Stabil., 144: 485-496.

Ding, Z., Wan, Y., Hu, X., Wang, S. and Zimmerman, A. R. 2016. Sorption of lead and methylene blue onto hickory biochars from different pyrolysis temperatures: importance of physicochemical properties. J. Ind. Eng. Chem., 37: 261-267.

Elzobair, K. A., Stromberger, M. E. and Ippolito, J. A. 2016. Stabilizing effect of biochar on soil extracellular enzymes after a denaturing stress. Chemosphere, 142: 114-119.

Genesio, L., Miglietta, F., Lugato, E., Baronti, S., Pieri, M. and Vaccari, F. P. 2012. Surface albedo following biochar application in durum wheat. Environ. Res. Lett., 7: 014025.

Herath, H. M. S. K., Camps-Arbestain, M. and Hedley, M. 2013. Effect of biochar on soil physical properties in two contrasting soils: An Alfisol and an Andisol. Geoderma, 209-210: 188-197.

Hong, X., Zhang, L., Wei, G. and Qing, Z. 2011. Effects of biochar amendment on cropland soil bulk density, cation exchange capacity, and particulate organic matter content in the North China Plain. J. Appl. Ecol., 22: 2930-2934.

Hua, L., Lu, Z., Ma, H. and Jin, S. 2014. Effect of biochar on carbon dioxide release, organic carbon accumulation, and aggregation of soil. Environ. Prog. Sustain. Energy, 33: 941-946.

Lehmann, J. and Joseph, S. 2015. Biochar for Environmental Management: Science, Technology and Implication. Routledge, New York. pp 33-46.

Li, B., Yang, L., Wang, C., Zhang, Q., Liu, Q. and Li, Y. 2017. Adsorption of Cd(II) from aqueous solutions by rape straw biochar derived from different modification processes. Chemosphere, 175: 332-340.

Lin, Y., Yi, S., Zhang, Z., Wang, M. and Nie, T. 2019. Study on the effect of water, fertilizer, and biochar interaction on N_2O emission reduction in paddy fields of northeast China. Nat. Environ. Pollut. Technol., 18(3): 955-961.

Liu, X. H., Han, F. P. and Zhang, X. C. 2012. Effect of biochar on soil aggregates in the Loess Plateau: Results from incubation experiments. Int. J. Agr. Biol., 14: 975-979.

Lu, N., Liu, X. R., Du, Z. L., Wang, Y. D. and Zhang, Q. Z. 2014. Effect of biochar on soil respiration in the maize growing season after 5 years of consecutive application. Soil Res., 52: 505-512.

Mohan, D., Sarswat, A., Ok, Y. S. and Pittman, C. U. 2014. Organic and inorganic contaminants removal from water with biochar, a renewable, low cost and sustainable adsorbent: A critical review. Bioresource Technol., 160: 191-202.

Neves, C. S. V. J., Feller, C., Guimarães, M. F., Median, C. C. and Fortier, M. 2003. Soil bulk density and porosity of homogeneous morphological units identified by the cropping profile method in clayey Oxisols in Brazil. Soil Till. Res., 71: 109-119.

Oguntunde, P. G., Abiodun, B. J., Ajayi, A. E. and Nick, V. D. G. 2008. Effects of charcoal production on soil physical properties in Ghana. J. Plant Nutr. Soil Sci., 171: 591-596.

Peterson, S. C., Appell, M. and Jackson, M. A. 2012. Comparing corn stover and switch grass biochar: Characterization and sorption properties. J. Agr. Sci., 5: 1-8.

Ren, X., Wang, F., Zhang, P., Guo, J. and Sun, H. 2018. Aging effect of minerals on biochar properties and sorption capacities for atrazine and phenanthrene. Chemosphere, 206: 51-58.

Shuang, L., Ni, S. N., Du, J., Ying, C. Y. and Shi, C. G. 2016. Determination of organic carbon content in geochemical exploration soil samples by potassium dichromate oxidation-external heating method. Anhui Chem. Ind., 42: 110-112.

Tripathi, M., Sahu, J. N. and Ganesan, P. 2016. Effect of process parameters on production of biochar from biomass waste through pyrolysis: A review. Renew. Sus. Energy. Rev., 55: 467-481.

Tuo, D., Xu, M., Li, Q. and Liu, S. 2017. Soil aggregate stability and associated structure affected by long-term fertilization for a loessial soil on the loess plateau of China. Polish J. Environ. Stud., 230: 849-861.

Usowicz, B., Lipiec, J., Łukowski, M., Marczewski, W. and Usowicz, J. 2016. The effect of biochar application on thermal properties and albedo of loess soil under grassland and fallow. Soil Till. Res., 164: 45-51.

Usowicz, B., Lukowski, M. and Lipiec J. 2014. Thermal properties of soils: Effect of biochar application. EGU General Assembly, 16: 9533.

Wang, Y., Chen, S., Sun, H. and Zhang, X. 2009. Effects of different cultivation practices on soil temperature and wheat spike differentiation. Cereal Res. Commun., 37: 575-584.

Wu, W., Sun, X., Dong, D. and Wang, H. N. 2015. Environmental Effects of Biochar in Soil. Science Press, Beijing.

Yadav, M. R. and Saxena, G. S. 1973. Effect of compaction and moisture content on specific heat and thermal capacity of soils. J. Ind. Soc. Soil Sci., 21: 129-132.

Zhang, Q., Wang, Y., Wu, Y., Wang, X., Du, Z. and Liu, X. 2013. Effects of biochar amendment on soil thermal conductivity, reflectance, and temperature. Soil Sci. Soc. Am. J., 77: 1478-1487.

Zhao, J., Ren, T., Zhang, Q., Zhang, Q. and Du, Z. 2016. Effects of biochar amendment on soil thermal properties in the North China Plain. Soil Sci. Soc. Am. J., 80: 1157-1166.

Zhao, S., Ta, N., Li, Z., Yang, Y., Zhang, X. and Liu, D. 2018. Varying pyrolysis temperature impacts application effects of biochar on soil labile organic carbon and humic fractions. Appl. Soil Ecol., 123: 484-493.

Nature Environment and Pollution Technology
An International Quarterly Scientific Journal

p-ISSN: 0972-6268
(Print copies up to 2016)
e-ISSN: 2395-3454

Vol. 20 | No.3 | pp. 1041-1046 | 2021

Original Research Paper

https://doi.org/10.46488/NEPT.2021.v20i03.011

Open Access Journal

Water Quality Evaluation of Wenyu River Based on Single Factor Evaluation and Comprehensive Pollution Index Method

Li Linjun, Men Baohui† and Peng Rui

School of Water Resources and Hydropower Engineering, North China Electric Power University, Beijing 102206, China

†Corresponding author: Men Baohui; menbh@ncepu.edu.cn

Nat. Env. & Poll. Tech.
Website: www.neptjournal.com

Received: 03-08-2020
Revised: 18-09-2020
Accepted: 09-10-2020

Key Words:
Wenyu River
Single-factor index method
Comprehensive Pollution Index Method
Water quality evaluation

ABSTRACT

Wenyu River is the "mother river" in Beijing. In recent years, the research on the water quality of the Wenyu River has increased gradually. In this paper, the monitoring data at Shahe Reservoir, Lu Tuan Gate, Xin Bao Gate, and Ma Fang sections for each month in 2019 were adopted. The single-factor evaluation method and the comprehensive pollution index method were selected to analyze the current situation of the water quality of Wenyu River in the Chang Ping section and its temporal and spatial variation trend. The single factor evaluation method showed that the dissolved oxygen exceeded the standard seriously in all other months of the year except that the situation was better in May, June, and July. The ammonia nitrogen content reached the highest level in January, followed by a month-by-month decreasing trend. After June, each section basically met the requirements of Class v water quality. The comprehensive pollution index method shows that the water quality of Shahe reservoir varies greatly throughout the year, and it is in grade v for 6 months. The evaluation results of both methods show that the water quality of all sections of Wenyu River in 2019 was mostly in category v.

INTRODUCTION

Wenyu Originating in the southern foothills of the Yan Mountains River, the Wenyu River is the only one of the five major river systems in the city that originates in Beijing and has water all year round. Shahe Reservoir is called Wenyu River. In the lower reaches of Shahe Reservoir, there are mainly Lin Gou River, Qing He River, Dam River, small and medium-sized river confluence through Chaoyang and, Shun Yi District from North Tong Zhou District Gate into North Canal. Wenyu River has more water than the rest of Beijing. In recent years, with the rapid development of Chang Ping District's economy and the acceleration of urban industrialization, the Wenyu River has gradually become a river with industrial and domestic sewage as its main supply of water. From 2005 to 2006, the sewage treatment rate of Wenyu River was less than 61%. In the survey in 2013, it was found that there were still many direct discharge of sewage. Yang et al. (2015) team found that the non-point source pollution in Changping section of Wenyu River mainly comes from commercial land and transportation land, as well as fertilization of farmland, Yu et al. (2012) systematically analyzed the evolution process of water environmental quality of Wenyu River from 1980 to 2010, and found that the sewage discharged from the centralized treatment facilities became the primary supply source of Wenyu River (70.1%). Additionally, the discharge of factory wastewater and domestic sewage will increase the content of heavy metals in sediments. The leachate produced by garbage stacking contains a large amount of heavy metals such as Cu, Zn, Pb and Cr, which enter rivers through surface runoff or soil runoff, resulting in the increase of heavy metal content in river sediments. Though the heavy metal pollution and potential ecological risk in surface sediments of Changping section of Wenyu River are slight, the water quality of Wenyu River still needs to be paid enough attention to prevent further deterioration.

In recent years, with the development of society and the improvement of people's living standards, water environment management is extremely urgent. And reasonable water environment management measures need to be formulated according to accurate water quality assessment. However, water environment pollution is affected by many factors at the same time, has a certain complexity. Therefore, the selection of the evaluation method has always been a major problem in the process of water environment management.

In the early days, people evaluated water quality by its sensory properties (i.e. color, smell, turbidity, etc.). Later, with the progress of science and technology, chemical and biological indexes were added as the basis for water quality evaluation, which greatly improved the accuracy of water

quality evaluation. At present, the approach for water quality evaluation mainly includes single factor water quality index method, fuzzy mathematics method, comprehensive water quality identification index method, principal component analysis method, etc., but these methods have some shortcomings. The single factor water quality index method is simple to calculate and easy to use, but it is greatly affected by the worst of the selected factors, and there is a certain gap between the evaluation results and the real water quality. The comprehensive water quality identification index method can express abundant water quality information, but it ignores the difference in the importance of different water quality indicators in the evaluation (Wu et al. 2019). The fuzzy mathematics method is subjective in the determination of index weight. TOPSIS is a sorting method approaching ideal points, which is a common and efficient multi-objective decision analysis. In the process of normalization of the multi-objective decision matrix, there are many different methods for data processing, and different data normalization methods will have different impacts on the result (Milani et al. 2005). From the perspective of weights, traditional TOPSIS has a strong subjectivity of index weights, so it is more objective to allocate weights by using the entropy weight method (Liu & Hua 2007). From the perspective of the correlation among the indexes, TOPSIS does not link water quality indicators and their officially defined criteria with each indicator, however, the TOPSIS-based informative weighting and ranking (TIWR) approach can combine the water quality indicators with the relevant standards, and consider the correlation among the indicators by using the importance of the standards through the inter-standard correlation method (Li et al. 2018). The comprehensive pollution index method can compare the water pollution degree of different river sections in space, which is convenient for classification. Index of biotic integrity (BIB) is usually carried out with river bottom fish and benthic animals, and rarely with plankton. In fact, plankton can reproduce rapidly and have a short life cycle and can respond to changes in water quality (Zhu et al. 2018), therefore, based on the IBI, the P-BIB factor analysis method was improved and summarized. Due to slow action and long growth cycle of large invertebrates, they can be indicators of changes in the river water environment, therefore, based on the biological evaluation of IBI, the B-IBI index analysis method was summarized (Yang et al. 2012). Microbial health risk assessment based on indicator bacteria is based on the fact that pathogenic microorganisms pose a threat to human health to a certain extent (Chen et al. 2017). The water quality evaluation based on matter-element analysis is convenient and intuitive, and can comprehensively reflect the water quality (Liu et al. 2019, Bowen et al. 2018). Water quality assessment based on attribute recognition theory of attribute recognition theoretical model can effectively overcome the two common problems of fuzzy classification or unreasonable evaluation, but the subjective confidence is set too high, and through the concept of grey correlation degree analysis in grey system theory, the numerical relationship between subsystems (or factors) in the system can be found (Cai et al. 2019). Principal component analysis (PCA) can cover up some important factors due to the excessive number of related factors. The water pollution index method can collect and summarize the pollutants in the water and comprehensively reflect the water pollution situation in the form of numerical values, and the results are intuitive and accurate. The multivariate analysis technique helps us to determine the water quality status through the physical, chemical, and biological indicators of water. When the multivariate statistical HJ-Biplot method is used for water quality evaluation, the joint representation of physical, chemical, and biological variables of different months in two research fields can be observed simply and clearly on a plane (Carrasco et al. 2019). WQI_{min} model was established by using stepwise multiple linear regression analysis for the water quality index method. The study showed that the WOI_{min} model could effectively evaluate and manage water quality, but the potential risks of algae proliferation were not taken into account in this model.

Difficulties in water quality evaluation:

1. Allocation of multiple index weights. There are often multiple indicators in water quality evaluation, and the problems in the weight allocation of these indicators are that the evaluation results are greatly influenced by the worst or the best factors, the important differences of different water quality indicators are ignored, and the subjectivity is affected.
2. The classification is unreasonable or fuzzy.
3. Some important factors are covered up because of the excessive number of factors. Therefore, water quality evaluation needs us to think from multiple aspects, or through the comparison of a variety of water quality evaluation methods, to get a more reasonable evaluation method.

The interannual variation of water quality in the Wenyu River is influenced by seasonal climate. The runoff from 1982 to 2014 at the hydrological station of the Shahe Gate was simulated based on the Swat model to simulate the hydrological cycle process in the Upper Wenyu River Basin. It is found that in the upper reaches of Wenyu River, the contribution rate of meteorological factors to runoff is 21. According to the analysis of the natural economic situation around Wenyu River, there are a lot of farmland along the river, and the largest source of organic matter in the sediment may be the crop residues such as crop stalks that enter the riv-

er with rainfall and runoff. Therefore, the terrigenous organic matter in the sediment will account for a larger proportion. Rivers are seriously affected by non-point source pollution.

MATERIALS AND METHODS

In 2019, data on pH, nh3-n2, COD, and DO was collected in four sections of Wenyu River Shahe Reservoir, Ma Fang, Lu Tuan Gate, and Xin Bao Gate for each month. In this paper, the water quality of Wenyu River is evaluated by a single factor evaluation method and a comprehensive index evaluation method.

Water quality of rivers is affected by rainfall and runoff, and climate change and land use change will affect runoff. Yang et al. (2018) showed that in Changping section of Wenyu River, the contribution of climate change to runoff change was much greater than that of land use change. Therefore, when we study the change of water quality of Wenyu River in one year, we focus on observing the change of water quality from the seasonal change. In recent years, the water quality of Wenyu River has improved because the water quality of Wenyu River has been inferior for a long time. To better understand the water quality of Wenyu River, in this paper, the water quality of the Wenyu River is investigated in four sections: reservoir, Ma Fang, Lu Tuan Gate, and Xin Bao Gate. To avoid accidental factors, the above four sections are sampled every month. The data are shown in Fig. 1.

Methodology: The idea of the single-factor index method is to select the worst index in the series of water quality indexes and use the index calculated by the index as the standard to evaluate the water quality grade. The single factor evaluation method only focuses on one index, which can reflect the water quality index, but only one water quality factor is considered, which cannot reflect the water quality of the river comprehensively.

Water quality indicators can be divided into general water quality assessment factors and special water quality assessment factors (for example: DO, pH).

1. General water quality evaluation factor:

$$S_{i,j} = C_{i,j}/C_{s,j} \quad \ldots(1)$$

$S_{i,j}$: Standard Index； $C_{i,j}$: The measured value of evaluation factor i in j section， ml/L：$C_{i,j}$: Standard limit of i。

2. Special water quality evaluation factor:
How to work out pH:

$$PH_j \leq 7.0$$

Fig. 1: Measured results of water quality objectives.

$$SPH_j = \frac{7.0 - PH_j}{7.0 - PH_{sd}} \quad \ldots(2)$$

$$PH_j \leq 7.0$$

$$SPH_j = (PH_j - 7.0)/(PH_{sn} - 7.0) \quad \ldots(3)$$

PH_j: Measured value of PH; SPH_j: Standard Index; PH_{sn}: Upper limit of Ph in evaluation criteria; PH_{sd}: Lower limit of Ph in evaluation criteria.

How to work out DO:

When $DO_j \geq DO_s$

$$S_{DO,j} = /DO_f - DO_j/ /(DO_f - DO_s) \quad \ldots(4)$$

When $DOj < DOs$

$$S_{DO,j} = 10 - 9DO_j/DOs_s \quad \ldots(5)$$

$S_{DO,j}$ is the standard exponent of DO; DO_f is Saturation dissolved oxygen concentration under water temperature and air pressure, $mg.L^{-1}$ Rentenformel (Germany): $DO_f = 468/(31.6 + t)$, t means temperature, °C; DO_j is the measured value of dissolved oxygen at Point j, $mg.L^{-1}$; DO_s Standard limit for evaluation of dissolved oxygen, $mg.L^{-1}$.

The comprehensive pollution index method is to obtain the comprehensive pollution index of the water body and to grade the water quality according to the standard of water quality classification. The formula is:

$$P = \frac{1}{n}\sum_{i=1}^{n} P_i \quad \ldots(6)$$

Table 1: Water quality assessment indicators and standard classification

Indicators	I	II	III	IV	V
pH	6.5	7.5	7.5	8.5	9
COD/(mg/L)	15	15	20	30	40
DO/(mg/L)	7.5	6	5	3	2
NH_4^+N/(mg/L)	0.15	0.5	1	1.5	2

P is the comprehensive pollution index, P_i single factor evaluation method for calculating the value of I index.

Case Study

Because the water quality of Wenyu River is in the category of v for a long time, the water quality of Wenyu River was sampled in 2019 in accordance with the water quality standard of surface water (gb3838-12002) as shown in Table 1. The single factor evaluation method and the comprehensive pollution index method were used.

RESULTS AND DISCUSSION

Results of Single Factor Analysis

According to the division of the functional zone objects of surface water environment in the "surface water environment standard" (GB 3838-2002), the single factor index analysis of the above-mentioned four sections of Wenyu River was

Fig. 2: Single-factor index.

carried out with the standard of type v water. Insert the data from Fig.1 into equations (1), (2), (3), (4), and (5) to get Fig. 2.

Since the single-factor evaluation method only selects the results of one evaluation factor as the evaluation index, therefore, in the single-factor evaluation, it cannot reflect the comprehensive water quality of the river, but for the evaluation factor, you can see how far it's gone. According to the calculation, the DO of the 4 sections reached the V Type Water Standard most of the time, but the DO of Lu Tuan Gate exceeded the standard in July, and the water quality was poor V type water. In the whole year, the CODCR indexes of each section generally exceeded the standard, which indicated that the Wenyu River was seriously polluted. In the treatment of the Wenyu River, we should strengthen the treatment of sewage, strictly in accordance with the national comprehensive sewage discharge standards. In the first half of 2019, the phenomenon of ammonia nitrogen exceeding the standard was common in all sections. After June, except for a small amount of ammonia nitrogen exceeding the standard in Shahe Reservoir, the other sections basically met the standard of V type water. The single factor index of ammonia nitrogen showed an obvious difference between the first half-year and the second half-year. While the Wenyu River pH showed a long-term stability in the V Water Standard, and not too large fluctuations.

Results of Composite Pollution Index Analysis

The single factor analysis method lays too much emphasis on the influence of single factor, and the evaluation of river water quality is not comprehensive enough. In order to reflect the water quality of the river in a more comprehensive way, on the basis of single factor analysis, this paper adopts the comprehensive pollution method to distinguish the water quality of Wenyu River. The results are shown in Fig. 3.

In summer (June, July and August), the water quality of each sampling section experienced a process of gradual deterioration and gradual improvement. Beijing has entered flood season in summer, and the water quality of rivers has gradually deteriorated, reaching the worst of the year. And after the end of the flood season, the water quality gradually improved. Compared with the other three sections, the water quality of Shahe Reservoir is usually worse. But in the flood season, Lutuan gate water quality deterioration is the most obvious. The water quality of each section basically belongs to class V water, and the fluctuation range is small with time.

CONCLUSIONS

1. Combining single factor and comprehensive pollution index method, it is found that the water quality of Shahe Reservoir is poor and belongs to the Inferior v water body.
2. Beijing has a temperate monsoon,-it is hot and rainy in summer while cold and dry in winter .Rainy summers increase the runoff of rivers. However, because Wenyu River has been polluted for a long time, part of nitrogen, phosphorus and inorganic gel metal may eventually settle in the bottom mud. In the flood season, due to heavy rainfall, not on the basis of non-point source pollution, but also accompanied by the release of endogenous pollution, this makes the water quality of the river in the summer flood season when coming an obvious deterioration. After the flood season, the river water quality improved under the river's self-regulation ability.
3. In the single-factor evaluation, it was found that the single-factor index of ammonia nitrogen in Wenyu river exceeded the standard in the first half of the year and the second half of the year, especially in January, February and March. It may be that the low temperature

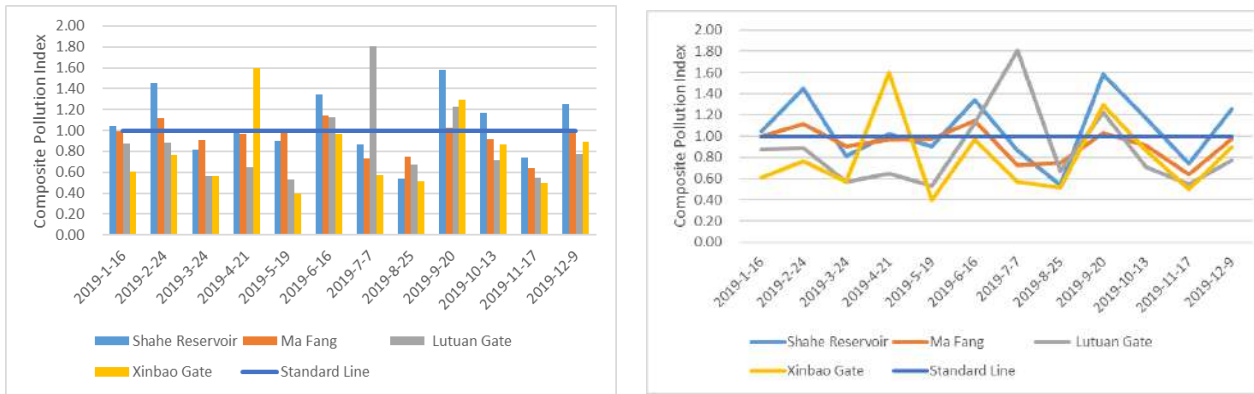

Fig. 3: Composite Index.

in Beijing at this time caused high ammonia nitrogen. The low temperature not only affected the growth rate and activity of nitrifying bacteria but also affected the speed and efficiency of denitrification. The nitrification reaction will decrease when the temperature is lower than 15°C, which caused the ammonia nitrogen levels to go off the charts.

4. The water quality of the Wenyu River varies with seasons, and the water quality monitoring indexes are affected by temperature and rainfall. In the treatment of the Wenyu River, we must first understand the causes of water quality changes to take proper measures.

ACKNOWLEDGMENTS

This paper is supported by the funds for the undergraduate innovative experiment plan of North China Electric Power University, the National Key R& D Program of China (Grant No. 2016YFC0401406), and the Famous Teachers Cultivation planning for Teaching of North China Electric Power University (the Fourth Period).

REFERENCES

Bowen, L., Baohui, M., Min, G., Zhengda, D., Dongfei, W. and Chengyu, H. 2018. Water environmental quality evaluation of the karst water in Beijing. Nat. Environ. Pollut. Technol., 17(2).

Cai, C.X., Men, B.H. and Liu, C.J. 2019. Water quality assessment of Wenyu River based on attribute recognition theory. Beijing Water, 3: 26-30.

Carrasco, G., Jose-Luis, M. and María-Carmen, P. 2019.Water quality evaluation through a multivariate statistical HJ-Biplot approach. J. Hydrol., 577: 1-9.

Chen, C., Wang, M.N. and Wang, J.Q. 2017. Microbial health risk assessment of Wenyu River based on indicator bacteria. J. Environ. Sci., 378: 3177-3184.

Liu, C.J., Men, B.H. and Cai, C.X. 2019. Preliminary study on water quality assessment of Wenyu River based on Matter Element Analysis. Water Resources Development and management, 10: 11-15.

Liu, M.Y. and Hua, L. 2008. Analysis of water environmental capacity of Wenyu River, Proceedings of the Capital Normal University, 293: 80-82.

Milani, A.S., Shanian, A. and Madoliat, R. 2005. The effect of normalization norms in multiple attribute decision-making models: Select methods. Eu.J. Oper. Res.,107(3): 312-318.

Wu, R., Hou L.L. and Lang F.X. 2019. Application comparison of different water quality evaluation methods in Sui Chuan River J. Jiangxi Water Sci. Technol., 45(6): 435-443.

Yang, M.X., Ma, W.L. and Zhang, Z.M. 2018. Impacts of land-use change and climate change on runoff variation in the upper reaches of Wenyu River. J. South-to-North Water Transfer and Water Science and Technology., 16(3): 72-78.

Yang, L., Li, Y.H. and Wang, J.C. 2012 Ecological health assessment of Wenyu River based on B-IBI Index. J. Ecol., 32(11): 3314-3322.

Yang, L., Wu, Z., Han, Y.,Wu, Q.Y., Wang,Z.M. and Yang, Y.G. 2015. Analysis of non-point source pollution load in Wenyu River basin based on L-THIA Model., Journal of Safety and Environment.,15(1): 208-212.

Yu, D.W., Yu, M., Wei, Y.S., Wang, Y.W., Deng, X., Yang,Y. and Xiao, Q.C. 2012. Spatio-temporal evolution of water quality in Wenyu River from 1980 to 2010. J. Environ. Sci., 32(11): 2803-2813.

Zhu, L.Y., Chen, Y.Y. and Liu, J. 2018. Temporal and spatial variation of water quality and phytoplankton community structure in Wenyu River. Environ. Sci., 7: 1-21.

Nature Environment and Pollution Technology
An International Quarterly Scientific Journal

p-ISSN: 0972-6268
(Print copies up to 2016)
e-ISSN: 2395-3454

Vol. 20 | No.3 | pp. 1047-1057 | 2021

Original Research Paper

https://doi.org/10.46488/NEPT.2021.v20i03.012

Open Access Journal

Real-Time Fine-Scale Measurement of Water Quality Parameters Along the Bagmati River in the Kathmandu Valley

M. P. Adhikari*†, N. B. Rawal* and N. B. Adhikari**

*Central Department of Chemistry, Tribhuvan University, Kirtipur 44613, Kathmandu, Nepal

**Department of Electronics and Computer Engineering, Pulchowk Campus, Institute of Engineering, Tribhuvan University, Kathmandu 44700, Nepal

†Corresponding authors: M. P. Adhikari; mandira43@hotmail.com

Nat. Env. & Poll. Tech.
Website: www.neptjournal.com

Received: 28-07-2020
Revised: 30-09-2020
Accepted: 09-10-2020

Key Words:
Mobile sensor system
Water quality
Bagmati river
Water pollution

ABSTRACT

Real-time fine-scale data was collected along the Bagmati River, in Kathmandu Valley, using mobile and fixed sensor system during the winter season. The water quality parameters; pH, conductivity, total dissolved salt (TDS), salinity, oxygen reduction potential (ORP), dissolved oxygen (DO), and turbidity were measured in the space domain using a fixed sensor and mobile sensor (small rafting boat loaded with sensor) systems. The water quality parameters from the fixed sensor system revealed that the Bagmati River was comparatively less polluted upstream from Gokarna to Tilganga sites and molecular oxygen present in the water was enough to decompose organic pollutants. However, the water quality downstream from Tinkune to Balkhu sites was degraded drastically making it unfit for living organisms. Temporal variation of water quality attributes that human activity significantly enhanced pollutants which severely degraded the water quality in the daytime. The fine-scale space domain heat map data of the mobile sensor system also suggested that the water quality continuously deteriorated from Shankhamul to Sundarighat sites. The ORP value was always negative and decreased with downflow and becomes -263 mV near the Sundarighat Bridge. The mixing of tributaries and increment of solid waste and untreated sewer along the river enhanced pollutants excessively and decreased oxygen level to zero. The results attributed that decomposition of the sewer by microorganism consumed almost all oxygen which produced volatile compounds and generated malodorous odor downstream of Bagmati River.

INTRODUCTION

Bagmati River originates from the Shivapuri Hill and passes through different culturally important places of the Kathmandu Valley. It enters the valley at Sundarijal and ends at Chovar. It stretches about 51 km inside the Kathmandu Valley and it has a catchment area of about 678 square km (Shrestha & Tamrakar 2012). It is immensely important culturally, historically, biologically, and geologically among the river system of the Kathmandu Valley. It is one of the holy rivers of Hindu, hence, culturally and historically, there are no alternatives of river water for the Hindu people. People use this river for taking bath and also for paying homage to their ancestors and gods and take small quantities of water to their home for use in rituals. In addition, some people living near the bank are still using Bagmati River water for bathing, washing vegetables, utensils, and clothes; for agriculture, industry, and irrigation purposes (Wolfe 2000, Milner et al. 2015). Although the Bagmati River is immensely important, most of the portion in Kathmandu Valley was found to be critically polluted (Paudyal et al. 2016, Mehta & Rana 2017, Adhikari et al. 2019, Sharma et al. 2020).

There are five major tributaries, namely, Manohara, Dhobi, Tukucha, Bishnumati, and Balkhu Khola in the Kathmandu Valley. Hence, tributaries significantly affect the water chemistry of the Bagmati River inside the Kathmandu Valley (Adhikari & Sah 2017). In addition, the uncontrolled and mismanaged growth of the population in the Kathmandu Valley is destroying the palatability of river water. People are directly discharging untreated sewage and personal garbage into the river. The river is converting into one of the easily accessible dumping sites for solid wastes and untreated domestic, industrial, and agricultural effluents (Kannel et al. 2007, Mishra et al. 2017, Pratum et al. 2019). It was reported that Bagmati River water is in pristine condition upstream, however, downstream it is critically polluted (Regmi 2013, Mishra et al. 2017, Sharma et al. 2020). Shrestha et al. (2015) observed DO concentration of more than 10 $mg.L^{-1}$ upstream and less than 1 $mg.L^{-1}$ downstream of Bagmati River in Kathmandu Valley. The river water was grey color upstream while it was black color downstream (Adhikari et al. 2019, Mehta & Rana 2017). Although numerous campaigns were conducted to clean the Bagmati River, the stinking smell and blackish

color of the water are still existing. These characteristics of river water and the ecology of the Bagmati River threaten not only humans but also living organisms that rely on the river because pollutants including toxic elements present in the river water potentially affect the aquatic ecosystem (Tripathee et al. 2016, Mahmud et al. 2019). Hence, the determination of the level of pollutants and identification of the source of pollutants is important to rectify the problem and implement the action effectively. In traditional water quality monitoring systems, the water samples used to be collected and analyzed manually in a limited number in the laboratory. Therefore, there was a lack of freedom for the collection of enough data, hence real-time information in fine scales could not be delivered.

To resolve these queries, real-time and spatial profiling and characterizations of the pollutants using sophisticated mobile tracers and analyzers are of the highest need. Due to the exponential development of information technology, these days it becomes possible to track the pollutants in fine temporal and spatial scales. Besides collecting data from fixed monitoring stations, mobile tracers provide fine-scale analysis which would be the first experience in the case of the Nepalese River.

MATERIALS AND METHODS

The spatial variation of water quality parameters along the Bagmati River inside the Kathmandu Valley was conducted in December 2019 and January 2020 using a fixed sensor system. The portable Multi-Parameter Analyzer (Hanna, HI-9829) was used to collect data from different locations. It measures and logs real-time data of different physical parameters such as pH, conductivity, salinity, total dissolved solids (TDS), dissolved oxygen (DO), temperature, and turbidity. Data were continuously measured and logged in every 5 secs from 14 fixed stations (Fig. 1, Table 1) and at least 120 data sets were collected from each site. The observation was started from the farthest upstream site of Bagmati River, Gokarna site (B-1), which is located about 8 km from the entrance point (Sundarijal) of Bagmati River inside the Kathmandu Valley. This is a rural area and there are few local residents but lack of visible source of pollutants (Green 2003). The second and third sites were the B-2 and B-3 just upstream and downstream of Guheshwori Wastewater Treatment Plant, respectively. The B-2 and B-3 sites include the influence of residential as well as industrial areas such as wool dying companies, medical colleges, hotels, etc. The wastewater treatment plant collects wastewater from sewage lines and is treated before discharging into the Bagmati River. The next sampling site was the Guheshwori temple (B-4). The source of pollutants in this site is the activities of people along the banks of the river such as bathing, washing, conducting picnic, etc. The Gaurighat sampling site (B-5) represents the effects of the local residential area before entering the Pashupatinath temple site. Pashupatinath temple is the most holistically important Hindu temple of Nepal as well as the world. People take bath and use water for praying to gods and in cultural rituals. This place is also popular for the cremation of the human body. The ash remaining after the cremation is discharged directly into the river. The B-6 data was collected from Pashupatinath temple (Aryaghat

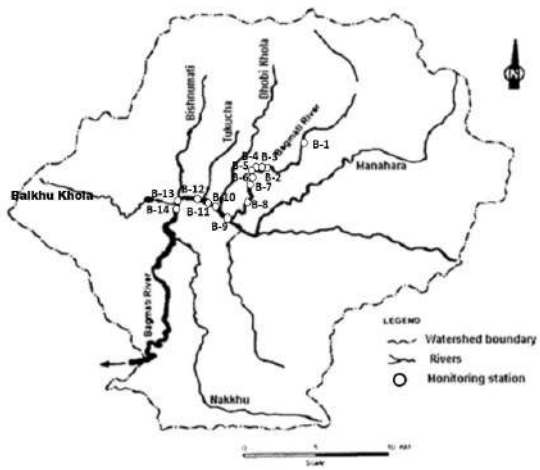

Fig. 1: Water quality monitoring station along the Bagmati river inside Kathmandu Valley.

Table 1: Water quality data monitoring stations along the Bagmati River.

Sample name	Observation site
B-1	Gokarna Temple: 8 km distance from the entrance of Bagmati River in Kathmandu Valley
B-2	Upstream of Guheshwori Wastewater Treatment Plant
B-3	Downstream of Guheshwori Wastewater Treatment Plant
B-4	Guheshwori Temple
B-5	Gaurighat: Upstream of Pashupatinath Temple
B-6	Pashupatinath Temple (Aryaghat)
B-7	Tilganga: Downstream of Pashupatinath Temple
B-8	Tinkune (Min Bhawan)
B-9	Shankhamul: Just downstream of Manohara confluence
B-10	Dhobikhola: Just downstream of Dhobikhola confluence
B-11	Thapathali: Just before the Bagmati Bridge
B-12	Tukuchakhola: Just downstream of the Tukuchakhola confluence
B-13	Bishnumatikhola: Just downstream of Bishnumatikhola)
B-14	Balkhukhola: Just downstream of Balkhukhola confluence

site). Pashupatinath area is bypass through a tunnel for the discharge of untreated wastewater and effluent from the treatment plant and are discharged at the Tilganga area into the Bagmati river (Green 2003). Next data was collected at Tilganga (B-7). The data was collected just downstream of discharge of the Guheshwori Wastewater Treatment Plant. The sampling site B-7 was the Tinkune. It was observed that solid waste and sewer lines connected directly to the river and noticeably dark and turbid water was observed from this site. The remaining observation sites were selected for the determination of the effect of tributaries on the Bagmati River. The observation sites B-9, B-10, B-12, B-13, and B-14 represent the confluence of Manahara, Dhobi, Tukuchha, Bishnumati, and Balkhu, respectively. Observation at Thapathali site R-11 represents the upstream of the most polluted tributary (Tukucha) of the Bagmati River (Bajracharya 2014). The daily and diurnal variations of the water quality parameter of the Bagmati River were observed at the Shankhamul site before mixing with the tributaries. The observation was conducted at effective working hours i.e., from 9:00 to 16:00 hour so that influence of domestic and industrial effluent on the Bagmati River could be clearly observed.

The next observation comprised the compilation of extremely minute and fine-scale real-time data using a mobile sensor system along the Bagmati River from Shankhamul to Sundarighat Bridge. The observation of spatio-temporal variation of water quality parameters was conducted on November 13, 2019, from 11:00 to 16:30. The portable Multi-Parameter Analyzer (Hanna, HI-9829) and Global positioning system (GPS) device were onboard in the small rafting boat. The data was measured and logged continuously every 5 sec (a few meters). The boat was sailed slowly and possibly at the center of the water stream and center of the river (Fig. 2).

RESULTS AND DISCUSSION

At first, spatial and temporal variations of water quality parameters along the Bagmati River were determined using a fixed sensor system to find out the sources of pollutants. Then, the Bagmati River was characterized in the space domain using fine-scale real-time data from a mobile sensor system.

Spatial Variation of Physiochemical Parameters along the Bagmati River

The physicochemical characterization of water indicates the quality of river water. The data from 14 different sites (Fig. 1) was collected randomly at different times and dates in the winter season. The average and standard deviation of collected data were tabulated in Table 2 and some key parameters were plotted in Fig. 3 and 4. The observed temperature of river water was varied between 9 and 15 degrees Centigrade. The variation of observed temperature was consistent with the air temperature reported for different days by Weather Nepal (2020). Therefore, it was considered that there was a lack of thermal pollutants. The observed turbidity was as low as 51.22 ±10.63 FNU at the B-1 site but higher than 300 FNU at other sites (Table 2, Fig 3a). The enhancement of turbidity at downflow may be either due to leaching of soil or mixing of domestic and industrial effluent in the river water during flowing (Costa et al. 2015). Fig. 3b shows that the pH of the river was almost neutral upstream up to the B-6 site and becomes more and more alkaline downstream from B-7. The slightly alkaline pH at downstream sites indicated that river water consists of a weak base such as carbonate and bicarbonates from soil or sand and/or ammonical compound from domestic sewage and agricultural run-off (Aggarwal & Arora 2012) and/or microbial decomposition of organic matter (Sundararajan et al. 2018).

The spatial variation of conductivity, Oxidation Reduction Potential (ORP), and Dissolved Oxygen (DO) were plotted in Fig. 4. The observed conductivity was less than 228.28 ±10.76 µS/cm till B-6 and that was more than two times at B-7 (485.53 ±2.86 µS/cm) then increased almost continuously from B-8 to B-14 sites (Fig. 4a). The observed conductivity indicated that effluents of domestic and industrial pollutants were low upstream till B-6 but loading of municipal wastes from the residential area and tributaries enhanced conductive substances and increased conductivity downstream (Okeke & Adinna 2013). Further, Table 2 showed that total dissolved solids (TDS) were low about 67.02±0.70 ppm at B-1, and increased linearly till B-6 site then enhanced drastically after B-7, and it was almost

Fig. 2: Water quality data collection along Bagmati River using mobile tracing system (rafting boat loaded with measuring instrument).

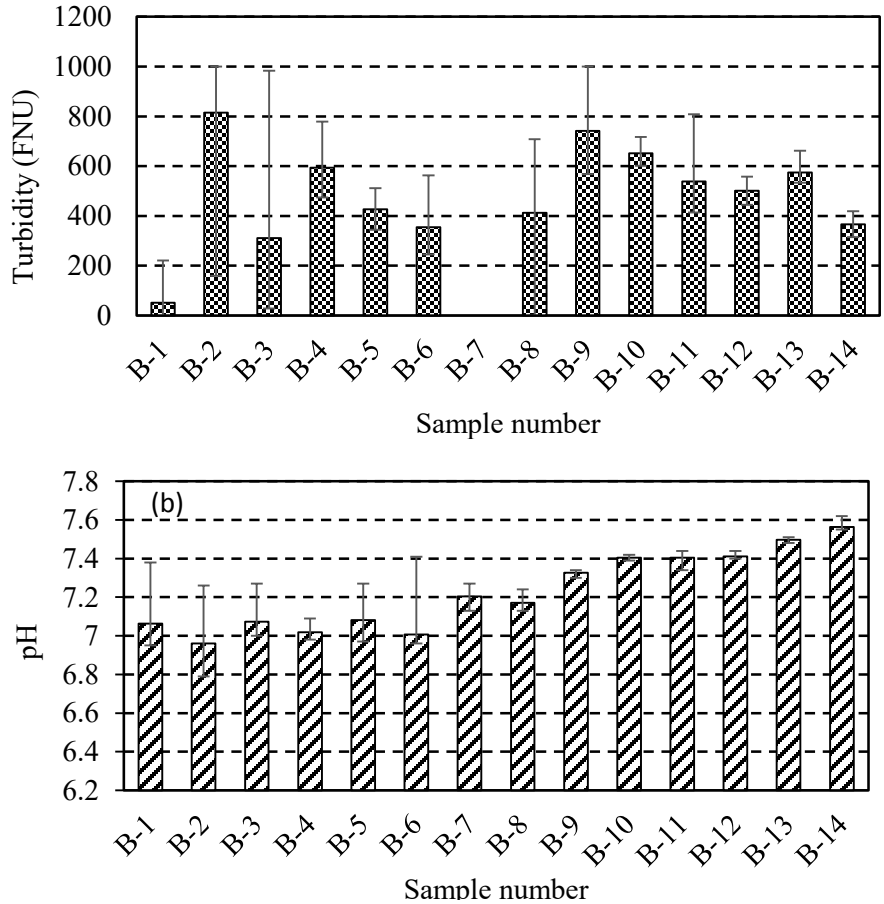

Fig. 3: Spatial variation of (a) Turbidity and (b) pH along the Bagmati River from Gokarna (B-1) to Balkhu (B-14) site.

seven-folds high at the end of the observation site (B-14). Similarly, salinity was less than 0.1 psu till the B-6 site but it enhanced continuously downstream and becomes 0.46 psu at the B-14 site. McCarthey et al. (2008) and Malla et al. (2015) reported that domestic and industrial wastewater is typically enriched in salts therefore inflow of municipal and industrial discharge enhanced the conductivity, salinity, and TDS of water. The oxidation-reduction potential (ORP) is a critical water quality parameter that measures the water disinfection potential. This parameter is most prominently used in wastewater treatment plants (Suslow 2004, Goncharuk et al. 2010). The presence of oxidizing agent (oxygen) increases the ORP value and a reducing agent (substrate or carbon and hydrogen-containing compound) decreases the ORP value. The observed ORP of river water varied differently between upstream and downstream (Fig. 4b). In the case of upstream, the ORP was positive and the potential was mostly more than 50 mV. However, the ORP value was negative and it ranged from -30 to -114 downstream. Suslow (2004) and Goncharuk et al. (2010) reported that the ORP value between +50 to +250 mV is useful for the degradation of an organic compound with free molecular oxygen and nitrification process. The ORP value between +50 and -50 mV is suitable for denitrification and between -50 and -250 mV is suitable for sulfide formation and biological phosphorus release. The negative ORP value suggested that the river water downstream consists of reducing agents from wastewater which may produce sulfide and biological phosphorus. Another most important parameter to determine the water quality is the Dissolved Oxygen (DO). At upstream, the DO concentration was within the acceptable limit (4-10 ppm), however, it was less than 3 ppm downstream except at B-12 and B-14 (Fig. 4c). The microbial decomposition of organic material utilized molecular oxygen which drastically decreases the DO in water (Okeke & Adinna 2013). The DO concentration attributed that organic substance in the river water was low upstream which consumed a lesser amount of molecular oxygen. However, the enhanced organic substance downstream consumed a higher amount of molecular oxygen and reduced the DO concentration. All the results attributed

Table 2: Water quality parameters measured along the Bagmati River at 14 observation sites.

Sample number	Temperature [°C]	Turbidity [FNU]	pH	ORP [mV]	Conductivity [µS/cm]	TDS [ppm]	Salinity [PSU]	DO [ppm]	No of sample
B-1	12.75 ± 0.24	51.22 ±10.63	7.06 ±0.05	68.42±8.16	133.83 ±1.29	67.02 ±0.70	0.06 ±0.00	7.23 ±0.58	1621
B-2	10.74 ± 0.64	814.45 ±201.21	6.96 ±0.07	40.57 ±18.91	193.91 ±14.92	96.95 ±7.46	0.09 ±0.01	7.032 ±0.59	1953
B-3	9.21 ± 0.02	310.73 ±252.37	7.07 ±0.05	55.43 ± 15.62	167.01 ±9.51	83.49 ±4.81	0.08 ±0.0	4.81 ±0.27	711
B-4	9.34 ± 0.00	594.29 ±56.11	7.02 ±0.02	73.66 ±6.30	163.30 ±1.13	81.61 ±0.54	0.08 ±0.0	6.90 ±0.23	196
B-5	13.06 ± 0.03	426.79 ±27.64	7.08 ±0.07	77.51 ±1.22	204.69 ±0.80	102.41 ±0.49	0.1 ±0.0	6.79 ±0.11	212
B-6	13.06 ± 0.15	354.56 ±44.24	7.00 ±0.05	76.38 ±8.82	228.28 ±10.76	114.13 ±5.41	0.11 ±0.01	6.85 ±0.64	1005
B-7	11.85 ± 0.02	-	7.20 ±0.03	26.08 ±6.38	485.53 ±2.86	242.73 ±1.41	0.24 ±0.0	7.94 ±0.38	172
B-8	12.31 ± 0.05	412.32 ±236.02	7.17 ±0.02	-30.96 ±8.61	470.09 ±44.96	235.09 ±22.47	0.23 ±0.02	1.07 ±0.53	206
B-9	15.2 ±0.12	741.06 ±117.62	7.33 ±0.01	-24.40 ±2.19	708.44 ±23.62	354.24 ±11.84	0.35 ±0.01	3.12 ±0.77	216
B-10	14.39 ±0.04	652.11 ±22.01	7.41 ±0.01	-76.24 ±4.97	859.56 ±19.34	429.74 ±9.65	0.43 ±0.01	0.75 ±0.27	135
B-11	14.95 ±0.08	538.87 ±64.67	7.40 ±0.01	-114.84 ±21.55	728.06 ±24.14	364.04 ±12.08	0.36 ±0.01	0.49 ±0.25	1275
B-12	14.78 ±0.06	501.00 ±18.99	7.41 ±0.01	-64.27 ±5.30	862.4 ±7.14	431.12 ±3.56	0.43 ±0.0	5.52 ±0.33	123
B-13	14.57 ±0.04	574.19 ±21.60	7.50 ±0.01	-45.70 ±6.81	917.39 ±14.09	458.75 ±7.06	0.46 ±0.01	0.39 ±0.13	122
B-14	13.78 ± 0.12	366.07 ±18.89	7.56 ±0.01	-71.93 ±16.23	927.72 ±3.71	463.84 ±1.89	0.46 ±0.0	6.38 ±0.43	122

that the water quality at the upstream site was less polluted due to treatment of water before discharging into the river. However, lack of enough wastewater treatment plants and direct connection of sewer lines and discharge of solid waste along the Bagmati River at the downstream site (from B-7 downward) enhanced organic waste and soluble conductive substances which consumed almost all DO, hence, ORP value of river water becomes negative.

Temporal Variation of Water Quality Parameter of the Bagmati River

Daily variation of water quality parameters at Shankhamul (before the confluence of tributaries) and Balkhu (after confluences of tributaries) sites was plotted in Fig. 5. Fig. 5 (a) shows that the pH of river water varied between 7.3 and 7.5 at Shankhamul and between 7.4 and 7.7 at the Balkhu site. The daily variation of conductivity (Fig. 5b) in both Shankhamul and Balkhu sites was non-steady and it varied between 814 and 886 µS/cm. The turbidity was very high (>600 FTU) at the Shankhamul site but that was comparatively low in the Balkhu site especially on first Day-1 (Fig. 5c). The dissolved oxygen at the Shankhamul site was almost zero on most of the days except Day-2 but it was more than 3 ppm at the Balkhu site on all days (Fig. 5d). ORP varied from day to day but the values were always negative in both sites (Fig. 5e). The ORP value was close to -50 mV at the Shakhamul site whereas it was mostly less than -50 mV at the Balkhu site. Results attributed that river water of both Shankhamul and Balkhu sites were extensively polluted permanently. The comparatively low DO and turbidity value at the Balkhu site may be because of the check dam erected below Balkhu Bridge. This is because aeration of water during flowing across the dam increased the concentration of DO and removed the suspended particles (Regmi 2013).

The diurnal variation of water quality parameters at the Shankhamul site showed that there were great variations of water quality parameters with time (Fig. 6). As expected, the temperature was 19^{o}C at 9 am and increased linearly with time and peaked in the afternoon then decreased slowly in the evening (Fig. 6a). Similarly, pH and conductivity were 7.4 and about 600 µS/cm at 9 am and increased linearly to 7.6 and 850 µS/cm, respectively at 10 pm and remained almost constant till 2 pm and decreased slowly again (Fig. 6b). Interestingly, the DO and ORP value changed differently than as expected in normal condition (Fig. 6c). Both concentrations were high in the morning indicating cleanness of water, however, it decreased continuously with time in the day. The observation was conducted before the confluence of tributaries. Hence, the enhancement of pollutants in the daytime was considered to be due to the effect of human activity i.e., the discharge of domestic and industrial effluent into the river water rather than mixing of tributaries. The DO was as high as 8 ppm at 9:00 am and decreased to almost zero after 11:30 am. Generally, the dissolved oxygen increases in the daytime

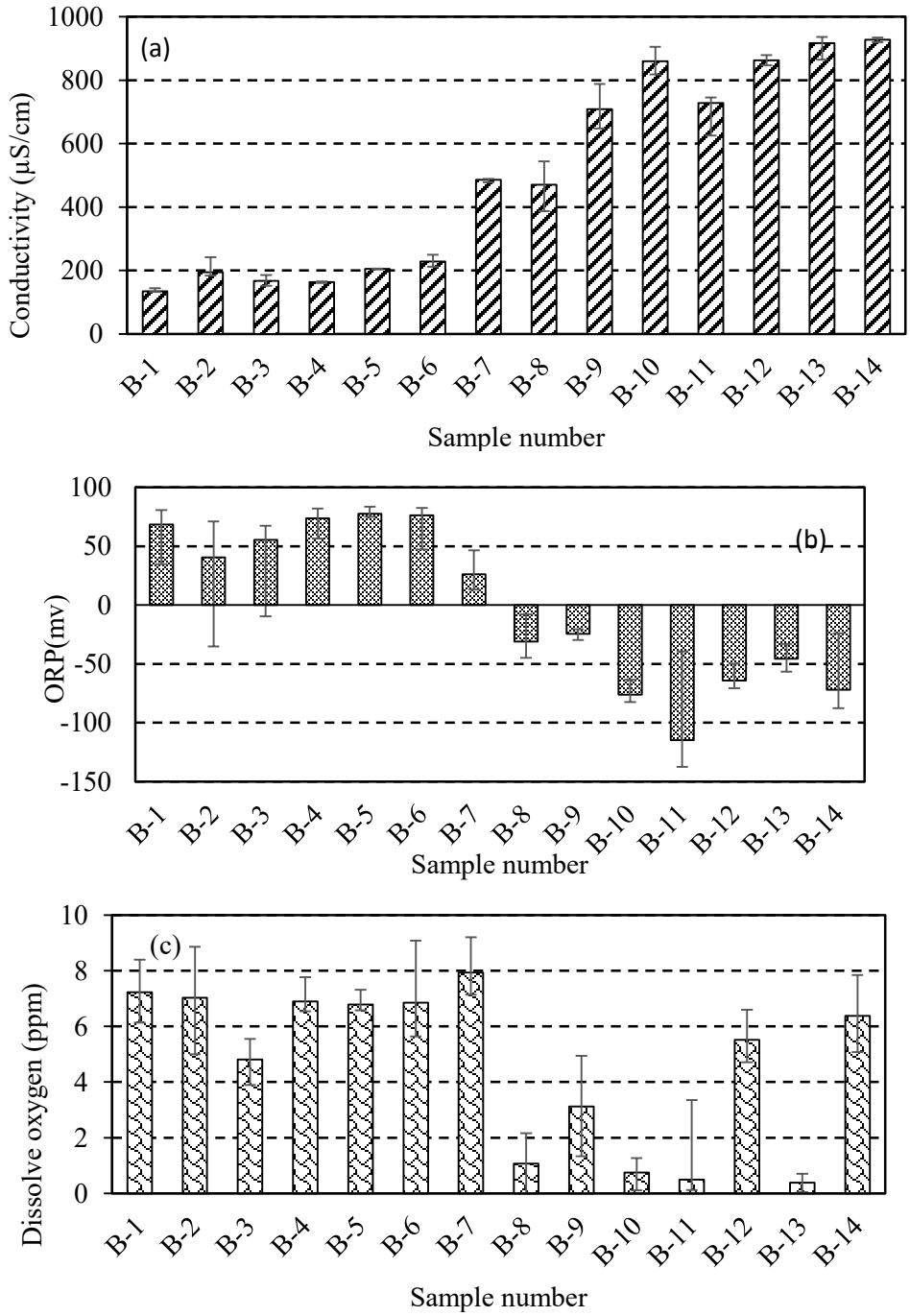

Fig. 4: Spatial variation of (a) Conductivity, (b) Oxidation Reduction Potential (ORP), and (c) Dissolve Oxygen (DO) along the Bagmati River.

due to the photosynthetic activity of plants and algae present in the river water (Martinez-Tavera et al. 2017). The tendency of DO concentration attributed that instead of enhancement of DO by photosynthesis it was used by microorganisms originated from wastewater to decompose the organic matter present in the river water. ORP was positive and about 50 mV initially and decreased linearly to -80 mV at 14:00. The high ORP value in the morning indicated that there was the presence of an oxidizing agent but enhancement of a reducing agent such as ammonia, nitrites, organic substances reduced ORP value in the daytime (Goncharuk et al. 2010). From the result, it is considered that human activities enhanced

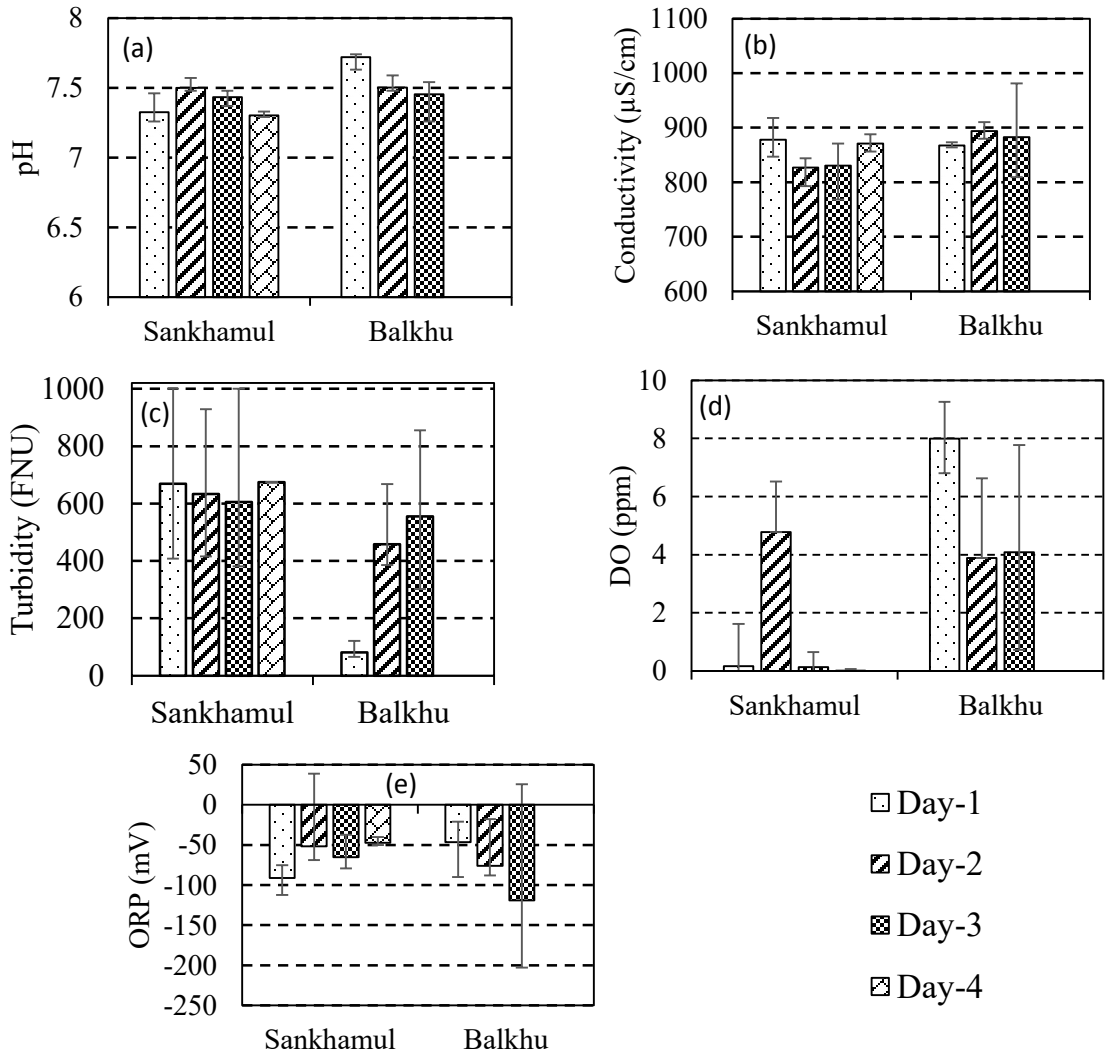

Fig. 5: Daily variation of water quality parameters (a) pH, (b) conductivity, (c) turbidity, (d) DO and (e) ORP at Shankhamul and Balkhu sites.

pollutants extremely at the daytime which consume almost all DO producing an anoxic condition in the river water at the downstream site (AliAl-Samawi & Al-Hussaini 2016).

Real-Time Fine-Scale Variation of Water Quality Parameters Along the Bagmati River

Real-time fine-scale spatial variations of water quality parameters along the Bagmati River from a mobile tracer system were plotted in Fig. 7. The heat map (Fig. 7) insights interesting results of water quality parameters in space domains. The temperature during the observation period was recorded between 20.64 and 22.34^{o}C. The temperature range suggested that the effect of temperature on water quality parameters was insignificant. The pH was slightly alkaline (7.28±0.041) and varied between pH 7.18 to 7.39, therefore variation of pH was less pronounced in the heat map (Fig. 7a). Fig. 7b shows that the conductivity enhanced slowly towards the downflow till the Bishnumati tributary and sharply enhanced after mixing it and continuously enhanced till the end of the observation site. Initially, the conductivity was about 700 µS/cm but it enhanced to more than 800 µS/cm downstream. The effect of tributaries on conductivity was clearly observed. The enhancement of conductivity after mixing with the Manohara, Dhobikhola, and Tukuchakhola tributaries was insignificant but that was significant after mixing with the Bishnumati and Balkhukhola tributaries (Fig. 7b). The variation of turbidity along the river was just opposite to that of pH and conductivity (Fig. 7c). The turbidity was high initially from Shankhamul to Thapathali and decreased slowly along the downstream. Visibly decreased

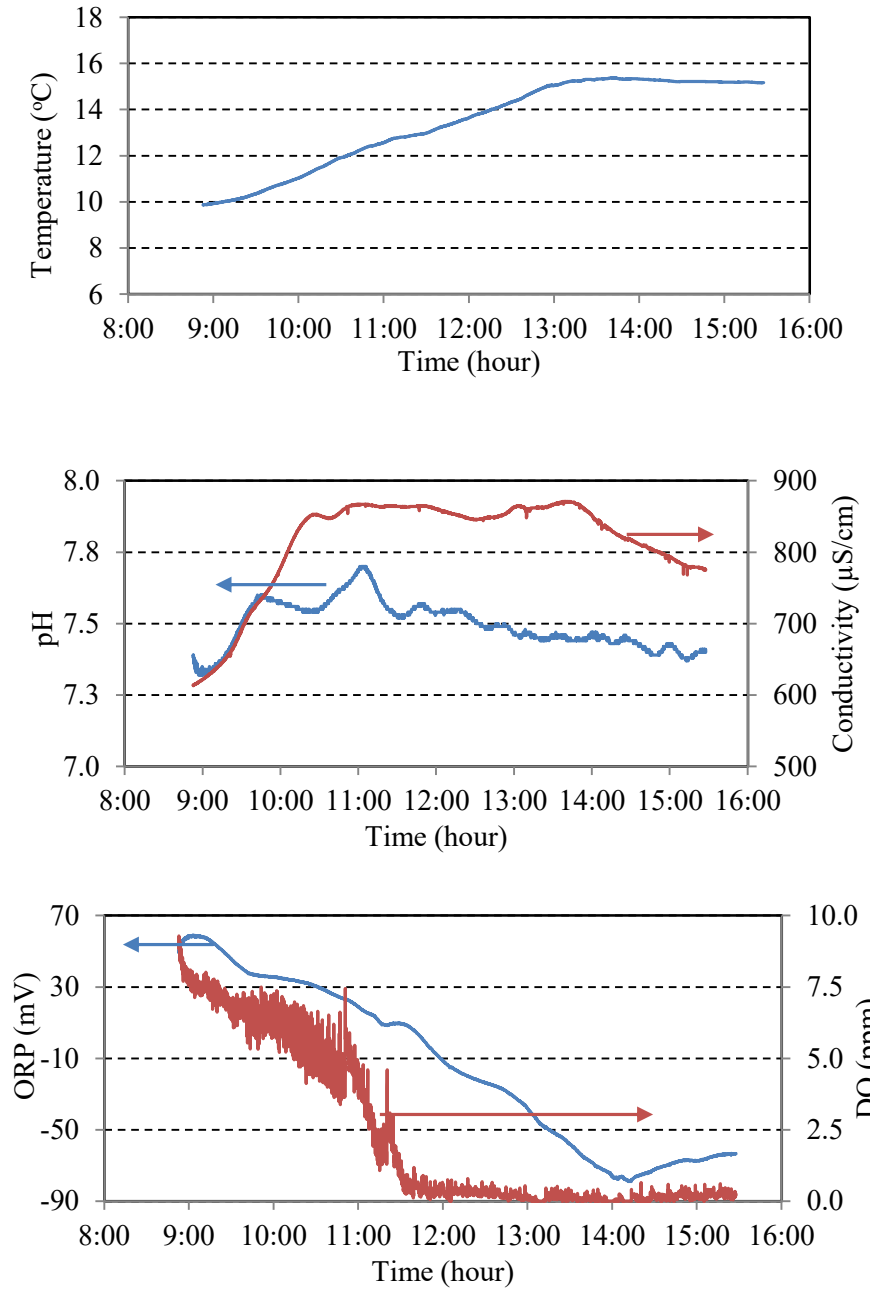

Fig. 6: Diurnal variation of water quality parameters (a) Temperature (b) pH and conductivity (c) ORP and DO at Shankhamul site.

turbidity near the end of the observation site illustrates the possibility of either decomposition or settlement of macromolecules during flowing. The photograph of river water taken at a different point (Fig. 7d) also indicated that the color of river water was unlike from point to point. The color was comparably dark downstream than that at the Shankhamul site and was extremely black at the Sundarighat site. Previous studies also reported that the turbidity was low but the color of the water was darkest downstream near the Sundarighat (at Jalbinayak) (Adhikari et al. 2019).

There was a consistency of spatial variations of DO concentration (Fig. 7e) and ORP (Fig. 7f). The DO concentration was low in between Shankhamul and Thapathali site and suddenly enhanced after Thapathali site and again decreased continuously to zero till the end, slight increment at Balkhu Bridge was observed but it was less pronounced. The fixed

station data (Fig. 4c) also indicated that the dissolved oxygen was high at B-12 (nearby Thapathali) and B-14 (Balkhu) sites. Similarly, the ORP value was negative along the river except just after Thapathali (50 mV) where DO content was around 7 ppm (Fig. 7e). The enhancement of DO and ORP values at the Thapathali site was may due to the presence of a check dam under the Bagmati bridge at Thapathali. As discussed previously, the dam retains a large amount of river water and spread throughout the riverbank, further, falling water from the dam hits the surface. Both these processes help to dissolve atmospheric oxygen causing aerobic conditions (Regmi 2013). The ORP value varied between -100 and -263 mV and the lowest ORP value was observed near the Suhdarighat Bridge. Suslow (2004) and Ali Al-Samawi (2016) reported that negative ORP (<250 mV) is a critical event in an anaerobic digester, where the sulfide serves as a

Fig. 7: Micro-scale spatial variation of water quality parameters (a) pH, (b) conductivity (c) turbidity (d) photograph of water (e) DO and (f) ORP along the Bagmati River.

sulfur nutrient for anaerobic and anaerobic bacteria, which produces a large variety of volatile compounds, where many of these volatile compounds are malodorous. The results suggested that the collection of pollutants along the river during downflow and connection of pipeline of untreated wastewater and dumping of solid waste near the Sundarighat area might be responsible for the production of a huge amount of sulfate-containing pollutants in the river water (Regmi 2013). These sulfate-containing compounds turned into acid and methane at the anaerobic condition which forms dark black sediment and generates malodorous volatile compounds (Castro & Huber 2005). This is the reason for black-colored water with stinky odor observed along the Bagmati River downstream. During the observation time, the research team observed a stinky smell at the Sundarighat bridge which made it difficult to stand over the bridge even for a few minutes. From the results of fine-scale real-time data, it was confirmed that human activities such as solid waste disposal along the bank of the river and direct discharge of sewer and mixing of polluted tributaries tremendously enhanced the pollutants (Kannel et al. 2007, Adhikari & Sah 2017) that turned out Bagmati River into a biologically dead river.

CONCLUSIONS

The water quality parameter of the Bagmati River in Kathmandu Valley was characterized using real-time data. The dissolved oxygen (DO) content was more than 5 ppm at upstream from Gokarna to Tilganga sites which was enough to oxidize organic compound. However, the dissolved oxygen content decreased to almost zero downstream from Tinkune to Balkhu sites indicating less chances of survival for the living organisms. Immense change of water quality parameters before mixing with the tributaries was the indication of mixing of untreated domestic and industrial wastewater into the Bagmati River from urban industrialized areas. The diurnal variation of water quality parameters at the Shankhamul site showed an amazing trend. The increase in pH and conductivity but the decrease in ORP and DO in the daytime suggested that the activity of people in the daytime was responsible to convert pristine water to perilous river water.

The real-time fine-scale space domain data indicated that pollutants increased continuously along the downflow of the river. Likely polluted tributaries enhanced the conductivity of Bagmati River instead of dilution. DO concentration was almost zero and ORP decreased from -100 to -263 mV at the end of the observation site. The results attributed that the solid waste, domestic sewer as well as tributaries loaded sulfur-containing organic pollutants reduced molecular oxygen to such an extent that living organisms could not survive in it. In absence of oxygen, the decomposition of pollutants by microorganisms generated volatile substances, which was responsible for the hazardous fouling smell along the bank of the river.

ACKNOWLEDGEMENTS

The authors are grateful to the University Grant Commission (UGC), Nepal for supporting us with faculty research grants. We are very much thankful to Mr. Ram Prasad Rimal and Mr. Laxman Prasad Rimal, RamLaxman Innovations, Lazimpat for providing us with an expertized technical support. Thanks are due to Mausam Khanal, Nepal River Conservation Trust for providing support with the river rafting arrangements. We kindly acknowledge Mr. Biplab Bhudhathoki, Mr. Sushant Gautam, and Mr. Janak Bhatta, Tribhuvan University for lending their supports in the observations.

REFERENCES

Adhikari, M.P. and Sah, M.K. 2017. Chlorine Demand and water pollutants of pond and river water. J. Nepal. Chem. Soc., 36: 39-48.

Adhikari, M.P., Neupane, M.R. and Kafle, M. 2019. Physio-chemical parameterization and determination of the effect of tributaries on the enhancement of pollutants in Bagmati River. J. Nepal Chem. Soc., 40: 36-43.

Aggarwal, R. and Arora, S. 2012. A study of water quality Kaushalya River in the submountaneous Shivalik region. Int. J. Sci. Technol. Res., 1(8): 52-68.

AliAl-Samawi, A.A. and Al-Hussaini, S. N. H. 2016. The oxidation-reduction potential distribution along Diyala river within Baghdad city. Mesop. Environ. J. 2(4): 54-66.

Bajracharya, S.B. 2014. Bagmati Action Plan (2009-2014), 2009 Government of Nepal & National Trust for Nature Conservation Khumaltar, Lalitpur, Nepal ISBN No. 978-993933933-702:8-4.

Castro, P. and Huber, M.E. 2005. Marine Biology (5th ed.) McGraw Hill, New York.

Costa, J.S., Braga, F.S., Almeida, R.S., Ramos, D.C., Brito, A.C., Cunha, C. and Santos, B. R. 2015. Physicochemical characterization of water quality-Lagoa dos Indios in Bacapa, Brazil. J. of Amer. Chem. Sci., 5(2): 122-134.

Goncharuk, V.V., Bagrii, V.A., Mel'nik, L.A., Chebotareva, R.D. and Bashtan, S.Y. 2010. The use of redox potential in water treatment processes. J. of Water Chem. Technol. 32(1): 1-9

Green, H.M. 2003. The effects of carpet dye on the Bagmati River. Masters of Engineering Thesis. Massachusetts Institute of Technology, Cambridge, Massachusetts, USA.

Kannel, P.R., Lee, S., Kanel, S.R., Khan S.P. and Lee, Y.S. 2007. Spatial-temporal variation and comparative assessment of water quality of urban river system: A case study of the river Bagmati (Nepal). Environ. Monit. Assess., 129: 433-459.

Mahmud, N.S., Abdullah, S.Z., Jalal, K.C.A., Rimatulhana, R. and Amal, M.N. 2019. Assessment of bacteria and water quality parameters in cage cultured Pangasius hypophthalmus in Temerloh, Pahang River, Malaysia. Nat. Env. & Poll. Tech., 18(5).

Malla, R., Shrestha S., Chapagain S.K., Shakya, M. and Nakamura, T. 2015. Physio-chemical and oxygen-hydrogen isotopic assessment of Bagmati and Bishunumati rivers and the shallow groundwater along the river corridors in Kathmandu Valley, Nepal. J. of Water Res. Prot., 7: 1435-1448.

Martinez-Tavera, E., Rodriguez-Espinosa, P.F., Shruti, V.C., Sujitha, S.B.,

Morales-Garcia, S.S. and Munoz-Sevilla, N.P. 2017. Monitoring the seasonal dynamics of physicochemical parameters from Atoyac River Basin (Puebla), Central Mexico: Multivariate approach. Environ. Earth Sci., 76: 95.

McCarthy, M., Scott, C., Ensink, J., Jiang, B. and Biggs, T. 2008. Salinity implications of wastewater irrigation in the Musi River catchment in India. Cey. J. Sci. (Bio. Sci.)., 37(1): 49-59.

Mehta, K.R. and Rana, S.V.S. 2017. Study of physico-chemical parameters of Bagmati River, Kathmandu, Nepal. Int. J. of Chem. Stud., 5(6): 2042-2048.

Milner, C., Basnet, H., Gurung, S., Maharjan, R., Neupane, T., Shah, D.N., Shakya, B.N., Tachamo, R., Shah, R.D and Vaidya, S. 2015. Bagmati river expedition 2015: A baseline study along the length of the Bagmati River in Nepal to gather data on physical, chemical, and biological indicators of water quality and pollution, and document human-river interaction. Nepal River Conservation Trust and Biosphere Association. Kathmandu, Nepal.

Mishra, B.K., Regmi, R.K., Masago, Y., Fukushi, K., Kumar, P. and Sarawat, C. 2017. Assessment of Bagmati River pollution in Kathmandu Valley: Scenario-based modeling and analysis for sustainable urban development. Sust. Water Qual. Ecol., 9: 67-77.

Okeke, P.N. and Adinna, E.N. 2013. Water quality study of Ontamiri River in Owerri, Nigeria. Uni. J. of Environ. Res. Technol. 3(6): 641-649.

Paudyal, R., Kang, S., Sharma, C.M., Tirpathee, L. and Sillanpaa, M. 2016. Variations of the physicochemical parameters and metal levels and their risk assessment in urbanized Bagmati river, Kathmandu, Nepal. J. of Chem., 1-13.

Pratum, C., Arunrat, N., Sereenonchai, S., Huang, J.C. and Xu, T. 2019. Water quality situation of the Tha Chin river and the riverbank community's understanding. Nat. Env. and Poll. Tech., 18(3): 1045-1051.

Regmi, S. 2013. Wastewater treatment in Khatmandu: management, treatment, and alternative. Bachelor's Thesis. Mikkeli University of Applied Science, Finland.

Sharma, C.M., Kang, S., Tripathee, L., Paudyal, R. and Sillanpää, M. 2020. Major ions and irrigation water quality assessment of the Nepalese Himalayan rivers. Environ. Develop. and Sust., 23: 2668-2680.

Shrestha, N., Regmi, R.K. and Mishra, B.K. 2015. Current status of water environment in Kathmandu Valley, Nepal. Water and Urban Initiative Working Paper Series-3: 1-5.

Shrestha, P. and Tamrakar, N.K. 2012. Morphology and classification of the main stem Bagmati River, Central Nepal. Bull. Depart. Geol.., 15: 23-34.

Sundararajan, S., Kamalakannan, B., Karthikeyan, R., Khadangaand, M.K. and Jena, B.K. 2018. Diurnal variation and water quality parameters of three different ecosystems in the Gulf of Mannar, Southeast Coast of India. 2018. J. Marine Sci. Res. Dev., 8(3): 1-6.

Suslow, T. V. 2004. Oxidation-deduction potential for water disinfection monitoring, control, and documentation. UC Agric. Nat. Resour. ANR Pub., 8: 1-5.

Tripathee, L., Kang, S., Sharma, C.M., Rupakheti, D., Paudyal, R., Huang, J. and Sillanapää. 2016. Preliminary health risk assessment of potentially toxic metals in surface water of the Himalayan Rivers, Nepal. Bull. Environ. Contam. Toxicol., 97: 855-862.

Weather Nepal. 2020. The temperature of Kathmandu on Dec 2019 and Jan 2020 (Retrieved on Mar 28, 2020. https://www.timeanddate.com/weather/nepal/kathmandu/historic?month=1&year=2020

Wolfe, A.N.C. 2000. Microbial contamination in the Kathmandu valley drinking water supply and Bagmati river. Master of Eng. Thesis. Civil and Environ Eng. Dep. Massachusetts Ins. of Techno. Cambridge, Massachusetts, USA.

Nature Environment and Pollution Technology
An International Quarterly Scientific Journal

p-ISSN: 0972-6268
(Print copies up to 2016)
e-ISSN: 2395-3454

Vol. 20 | No.3 | pp. 1059-1068 | 2021

Original Research Paper

https://doi.org/10.46488/NEPT.2021.v20i03.013

Open Access Journal

Reagent Activated Cotton Fiber for Rapid Determination of Aldehydes in Diverse Matrices

S. Tantry*, K. Tharpa*, Ajay Kumar*, Arun Kumar* and B.H.S. Thimmappa†**

*SABIC Research & Technology Pvt. Ltd., Plot No. 81 to 85, Chikkadunnasandra, Sarjapura-Attibele State Highway, Bengaluru-562125, Karnataka, India

**Department of Chemistry, Manipal Institute of Technology, Manipal Academy of Higher Education, Manipal-576104, India

†Corresponding author: B.H.S. Thimmappa; bhs.thims@manipal.edu

Nat. Env. & Poll. Tech.
Website: www.neptjournal.com

Received: 02-09-2020
Revised: 01-10-2020
Accepted: 06-11-2020

Key Words:
Reagent activated cotton fiber
O-benzyl hydroxylamine (OBA)
Formaldehyde
Acetaldehyde
Diverse matrices

ABSTRACT

A method to capture and analyze aldehydes in either solution or gas samples on cotton fiber, activated with *O*-benzyl hydroxylamine (OBA), is developed. The stability of the reagent activated cotton fiber (RACF) with and without capturing aldehydes was 17 days and 24 Hrs, respectively, qualifying the technique for field applications. Thus the aldehyde capturing can be done outside the lab using RACF in any closed environment and bring back to the lab for the quantitative analysis.. The analytical method is based on the gas chromatographic analysis of aldoxime formed between aldehydes and OBA on RACF. Optimized experimental conditions required 50 mg of RACF to capture aldehydes with a reaction time of 15 minutes. The technique detects aldehydes much below the permissible exposure limits of 25 ppm for acetaldehyde (CH_3CHO) and 0.75 ppm for formaldehyde (HCHO). The method's detection limits are 4 ppb of HCHO, 8 ppb of CH_3CHO in the gas sample, and 1.5 ppb of HCHO, and 19 ppb of CH_3CHO in the solution or aqueous sample. The analytical method was validated within the established quantitation ranges as per the required International Council for Harmonization Guidelines (CPMP/ICH/381/95). The RACF is a quick tool to measure aldehydes in a polymer sample, laboratory cupboards or refrigerators, and chemical products. The method described here complies with green analytical chemistry principles such as reduction in a solvent, chemical sample size and waste generation, cost-effectiveness, and usage of a biodegradable substrate.

INTRODUCTION

Simple aldehydes such as formaldehyde and acetaldehyde are building blocks of many essential chemicals of daily use. They are universal air pollutants sourcing from the air, water, and products such as paint, cosmetics, and plastics. Both monitoring and limiting the concentration of aldehydes in the air, workplace, and consumer products, are essential because they are known or suspected carcinogens as per the Evaluation of Carcinogenic Risks to Humans (WHO-IARC 2002) More recently, there are many publications on the development of an aldehyde monitoring system using different sampling techniques and analytical methods suitable for measuring aldehyde in the air, water, or products (Szulejko & Kim 2015). Using ortho-benzylhydroxylamine (OBA) as a derivatizing agent, the ppm level analysis of aldehydes in triethanolamine was developed, but it requires a long derivatization time (Jain & Thielen 1995). Methods were developed using o-2,3,4,5,6-(pentaflurobenzyl) hydroxylamine hydrochloride agent (Nawrocki et al. 1996, Koziel et al. 2001), which involves a solid-phase extraction for the analysis of low-ppb amounts of aldehydes-ozonation by-products. The well-known reagent 2,4-dinitrophenyl hydrazine derivatization for determination of aldehydes in fish (Veloso et al. 2001) and simultaneous determination of ketoconazole and formaldehyde in shampoo (Vander et al. 2002) by high-performance liquid chromatography (HPLC) was studied. Formaldehyde is highly toxic, and the levels are regulated in many products, including cosmetics, textiles, household products, indoor work, and the environment. A simple and sensitive flow injection method with fluorimetry and 5,5-dimethylcyclohexane-1,3-dione (dimedone) was developed for the determination of formaldehyde (Sakaia et al. 2002). However, this needs a heating system for a longer time. The solid-phase microextraction technique combined with GCMS (Tsai et al. 2003 , Qing et al. 2011) involves multiple steps and applicable to only water samples. Atmospheric pressure photoionization-mass spectrometry (APPI-MS) is used for the analysis of aldehydes and ketones after derivatization with 2,4-dinitrophenylhydrazine (DNPH) and liquid chromatographic separation (Suze et al. 2004), but

this is not much linear to quantify in automobile and cigarette exhaust samples. Using pentafluorophenyl hydrazine reagent, determination of formaldehyde in cosmetics using combined headspace-solid-phase microextraction-gas chromatography (Rivero 2004) involves a tedious cleanup process. Japan has a water quality standard in place for formaldehyde levels in drinking water (0.08 $mg.L^{-1}$).

Determination of aldehydes using 2,4-dinitrophenylhydrazine derivatization is well known, and the same is applied for the quantification of linear aliphatic aldehydes in water in the presence of heavy metals by HPLC (Lin et al. 2009). Derivatization using fluorescein 5-thiosemicarbazide through capillary electrophoresis is very sensitive to temperature and time. This technique is applied for the analysis of low-molecular-mass aldehydes in drinking waters using laser-induced fluorescence detection (Eugenia et al. 2010). Simultaneous determination of thirteen polycyclic aromatic hydrocarbons and twelve aldehydes in cooked food by an automated on-line solid-phase extraction ultra-high-performance liquid chromatography-tandem mass spectrometry (Gosetti et al. 2011, Guan & Rubin 2012) was very promising. However, the observed matrix effect and the need for lots of solvent for washing of SPE sorbent makes it a technique of low practical value. Many methods have been developed using GCMS and LCMS. The new concept of a microfluidic lab-on-chip using o-2,3,4,5,6-(pentafluorobenzyl) hydroxylamine hydrochloride derivatizing agent for gaseous carbonyls analysis (Pang et al. 2013) was very promising and executed for a specific application. Reviews on formaldehyde gas sensors and analytical methods to assess carbonyl compounds in foods and beverages provided more insight into this area (Chung et al. 2013, Vanessa & Zenilda 2013, Jeong et al. 2015). Formaldehyde quantification in hair straightening products was established using the proton nuclear magnetic resonance technique (NMR) (Kuballa et al. 2013). However, it is not sensitive for low-level detection, and the standard deviation was found to be very high. Solid-phase microextraction with fiber derivatization for the sampling of formaldehyde indoor involves the use of a combination of two reagents, and the stability of fibers is not found to be that effective. For determining aldehydes in the gas phase of mainstream smoke by headspace gas chromatography-mass spectrometry, PET bottled mineral waters and beverages, and derivatization techniques for determining carbonyls in the air/food/monomer samples was very useful but limited to specific matrices (Valentina et al. 2014). Determination of low-level aldehydes in detergents, cosmetic products, and airborne aldehydes in-cabin air of aircraft (Rosenberger et al. 2016) involves photoluminescence and HPLC detection, respectively (Gholami et al. 2016). Aerosol samples generated from e-cigarettes and tobacco smoke were collected manually using 2,4-dinitrophenylhydrazine (DNPH) cartridges at a constant sampling (puffing) velocity of 1 $Lmin^{-1}$ or another, and the result was directly linked to the number of puffs and consistency in reproducing the same (Sang et al. 2016, Mumiye et al. 2017, Zhao et al. 2017, Zhang et al. 2018). In a few cases, the analysis was not handy and involved expertise, and the techniques used also need modification for a particular application. Other challenges include interference from other pollutants, not user-friendly, not cost-effective, less sensitive mass analysis reproducibility, metric effect, and stability issues. No single technique is both economical yet sensitive and universal in its application to measuring aldehydes in all three types of samples. Further, so far, the use of reagent activated cotton has not been reported for such an analytical application.

We used pure dried cotton fiber activated with *O*-benzylhydroxyl for both sampling and analysis of aldehydes in the air, the solution, or the solid product. Besides low-cost cotton offers many advantages as an ideal sampling tool such as i) fast, uniform distribution and transportation of the reagents or the sample, ii) absorbs and hold reagents, iii) a large, lightweight network structure with large surface area to hold excess reagents, iv) withstands against external forces and v) natural, highly biodegradable, and disposable (Dochia et al. 2012). Upon optimizing all experimental conditions, we use just 50 mg of reagent activated cotton to capture aldehydes from the air or solution sample and 15 minutes reaction time to form quantifiable aldimine products. The long hours of stability of the reagent activated cotton, as well as the captured aldehyde in the form of aldimine, enabled this technique to measure aldehyde in both laboratory environments and products. The captured aldehydes are analyzed by gas chromatography with flame ionization detection (GC-FID) as formaldehyde *O*-benzyl oxime and acetaldehyde *O*-benzyl oxime within the quantifiable range.

MATERIALS AND METHODS

Reagents and Materials

Aqueous solution of 0.1 % (w/w) *o*-Benzylhydroxylamine hydrochloride (Sigma Aldrich, India) and 0.01 % (w/w) benzyl alcohol (Sigma Aldrich, India) were prepared. Reagents such as 0.1 M solution of potassium dihydrogen orthophosphate (SDFCL, India), 0.1 M solution of dipotassium hydrogen phosphate (K_2HPO_4-Sigma Aldrich), 0.1 M hydrochloric acid (Merck, India) were prepared in deionized Millipore water. About 36 % (w/v) aqueous formaldehyde (SDFCL, India) was diluted as required, and n-hexane (Merck, India) was used as received. Acetaldehyde (Fluka, USA) was distilled at 40°C until its purity was 99.9 % achieved on the GC-FID. Commercially available absorbent

cotton (Indian or British Pharmacopeia grade) was used for all the experiments.

Instrumentation

A Shimadzu 2010 gas chromatography (GC) system was used for the study. The system is equipped with a flame ionization detector (FID), and an auto-injector which can be used for all types of analysis. A fused silica capillary column (DB-210, Agilent) having a dimension of 30 m in length, 0.25 mm internal diameter, 0.5 µm film thickness was used for the GC analysis. Helium was the carrier gas (1.0 $mL.min^{-1}$). The column temperature gradient program was, first starts with 50°C isothermal for 1 min, ramped up to 200°C at 6° $C.min^{-1}$ withholding time of 1 min, ramped again at 25°C. min^{-1} to 220°C, and held for 2 minutes. The injection port temperature was 225°C, and the detector temperature was 250°C, respectively. The split ratio was at 10:1, with an injection volume of 1.0 microliter.

Methods and Procedures

Distillation of acetaldehyde: The commercially supplied acetaldehyde, although stored under 8°C, contains many impurities. Paraldehyde was found to be one of the major impurities. Therefore, the acetaldehyde was distilled at 30°C and collected in ice-cold water through a de-activated silica column. The set-up for acetaldehyde distillation is shown in Fig. 1.

Cotton pre-treatment: Cotton was repeatedly washed in water, followed by hexane and allowed to dry in the air for several hours. The dried cotton is referred to as pre-treated cotton and use for activation with the reagents.

Cotton activation: About 3 g of pre-treated cotton was dipped overnight in a 500 mL beaker containing 100 mL of 1:1 (v/v) of pH 4 buffer solution and 0.1% *O*-benzylhydroxylamine (OBA) hydrochloride solution. The reagent activated cotton was dried in the air for several hours and used for the analysis of aldehydes in the air or aqueous sample. Since cotton has a high resistance to solvents and alkali, it will not react with any chemicals; however, due to its multilayered structure and better adsorption property (Textile Fashion Study 2012), it will hold the reagent for a longer time. The reagent *O*-benzylhydroxylamine (OBA) hydrochloride will be absorbed entirely and detected in the gas chromatography technique.

Physical and chemical properties of cotton before and after activation: Cotton, the seed hair of plants of the genus Gossypium, is the purest natural form of cellulose, containing more than 90% of the polysaccharide. It is a dominant natural fiber and recognized as a chemically and biologically inert material. Hence, in the chemical field, it showed positive results for inertness and is an eco-friendly material. After hexane washing and reagent activation, the color of the cotton was remaining the same as shown in Fig. 2.

Cotton has excellent resistance to degradation by heat, damage after 240°C due to oxidation. The blank runs using

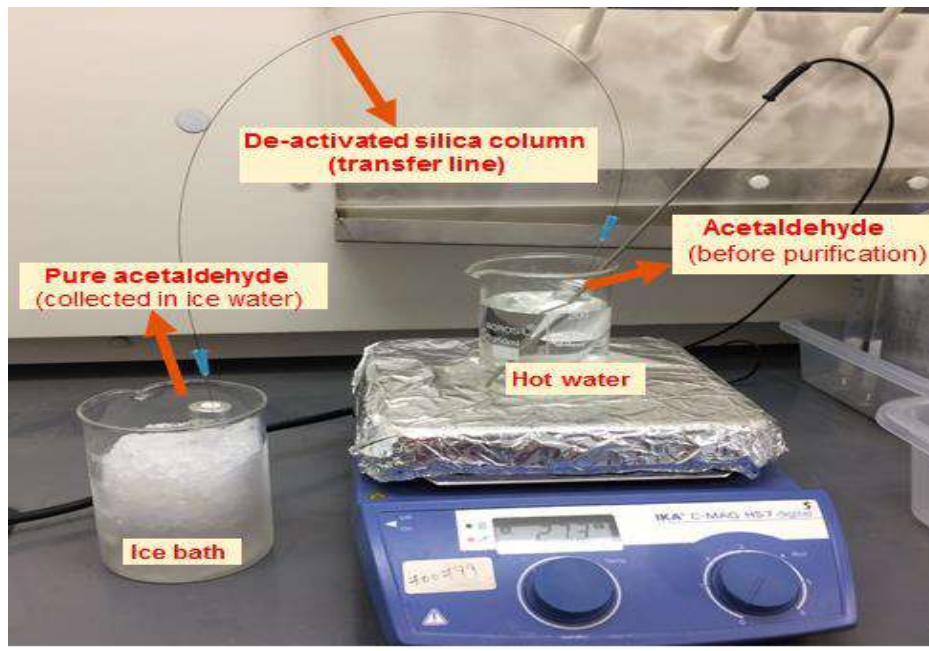

Fig.1: Acetaldehyde distillation.

reagent activated cotton fiber did not show any new peaks during GC-FID analysis, as shown in Fig. 3.

Calibration of Aldehydes in Vapor and Solution States

Calibration of aldehydes in vapor state: About 50 mg of reagent activated cotton taken in different headspace vials were crimped and connected using deactivated fused silica capillary transfer line to another set of crimped headspace vials containing varying concentrations of aldehydes. Deactivated fused silica capillary columns will play a very vital role in gas chromatography for trace analysis of polar/low boiler components since they will not interfere with any chemical components in the sample matrix. For aldehydes calibration, formaldehyde and acetaldehydes in the range of 0.1 to 1 ppm are prepared in water. The headspace vial containing aldehydes was heated in an oil bath at 90°C, and the resulting vapor was collected in a vial containing activated cotton for one hour. Later, the reagent activated cotton was transferred into a series of polypropylene (PP) tubes, and each PP tube had an added 1 mL of 0.01% benzyl alcohol as the internal standard, 1 mL of 0.15 M H_2SO_4 and 1mL of n-hexane solution and vigorously shaken for 1 min. The 1 mL of the hexane layer was analyzed using the method described in section 2.2.

Calibration of aldehydes in the solution state: The same procedure was followed as in vapor state calibration, except that the different concentration of aldehydes was directly added to the reagent activated cotton.

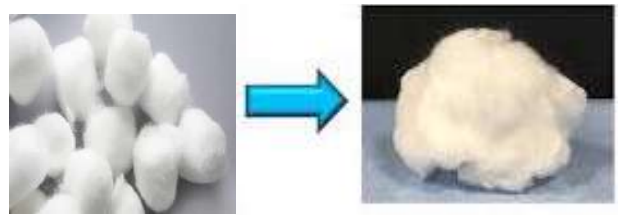

Raw/IP/BP cotton Reagent activated cotton

Fig. 2**:** Cotton before and after activation process.

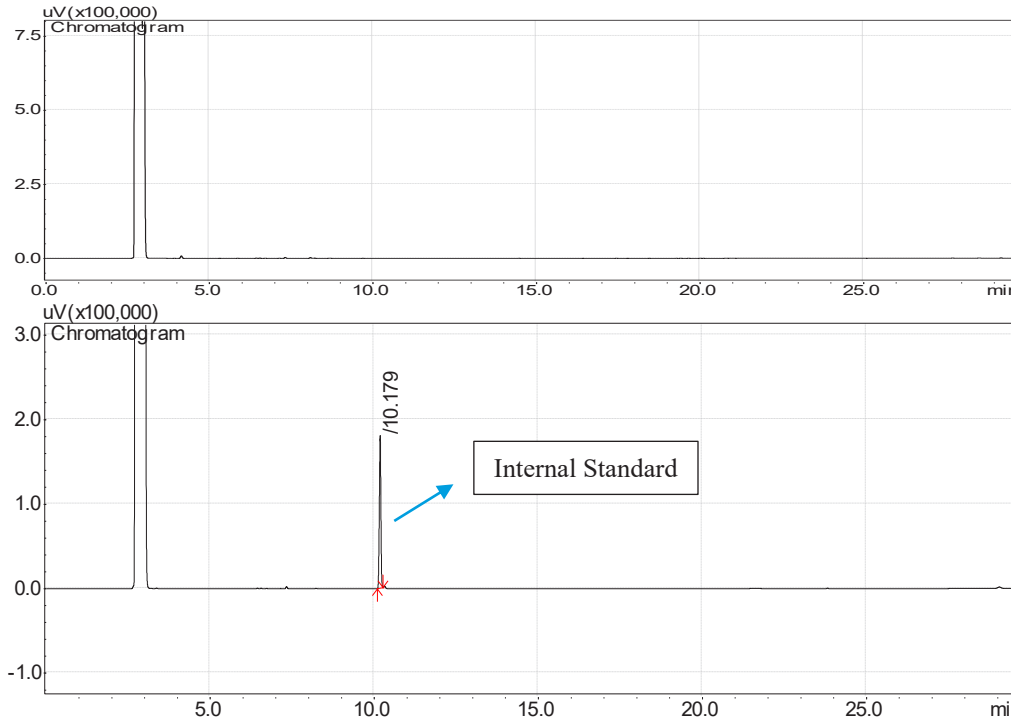

Fig. 3: Blank cotton analysis before and after activation.

Sampling of Aldehydes in Air or Solution State

For an analysis of the gas sample, about 50 mg of reagent activated cotton in an open glass vial or beaker was placed in the aldehyde sampling area for a minimum of 1 hour. The sampling area could be any closed or open environment such as a chemical storage area or cupboards, laboratory, and chamber. The sampling of the aqueous solution was done by adding 1 mL of the filtered liquid sample into 50 mg of reagent activated cotton placed in a PP tube.

Aldehydes content in solids such as polymer was sampled using the setup described under section 2.3.5 for calibration of aldehydes in the vapor state. A known amount of solid sample was weighed, depending upon the content of aldehyde, in a headspace vial, crimped, and heated in an oil bath for one hour at 90°C. The resulting vapor was collected through a transfer line in another crimped vial containing 50 mg of reagent activated cotton.

RESULTS AND DISCUSSION

Most of the derivatizing agents for the measurement of aldehyde require strong acidic conditions, limiting its application to samples that are compatible with acid media. Jain et al. (1995) proposed OBA as a derivatizing agent for the ppm level analysis of aldehydes in a neutral medium. However, the application is limited to triethanolamine and requires a long derivatization time. Since the pH can increase the rate of nucleophilic addition reaction (Fig. 4) between aldehyde and OBA, first, the effect of different pH was studied.

After that, to improve on the application of this method, experimental conditions were optimized to coat reagent on cotton fiber and for analysis of aldehydes in different matrices such as air, water, and polymer.

Effect of pH

The effect of pH on oxime formation was studied using different pH buffer solutions ranging from pH 2.0 to 8.0. The pH of the reaction media is essential because a highly acidic pH may protonate primary amine, whereas neutral/basic pH may not facilitate the reaction. Based on the effect of different pH studied (Fig. 5) for both formaldehyde and acetaldehyde derivatization, the maximum conversion to the OBA-FA (*O*-benzyl hydroxylamine-formaldehyde) derivative was observed between pH 4 to 7 and for the OBA-AA

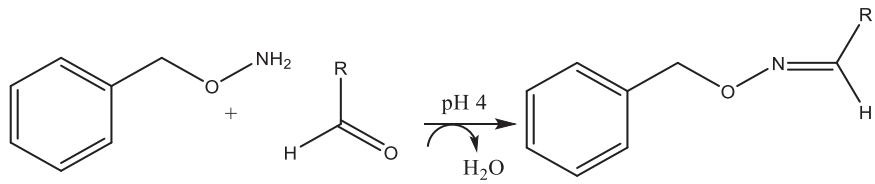

Fig. 4: Reaction of *O*-benzyl hydroxylamine hydrochloride with an aldehyde at the buffer of pH 4.0.

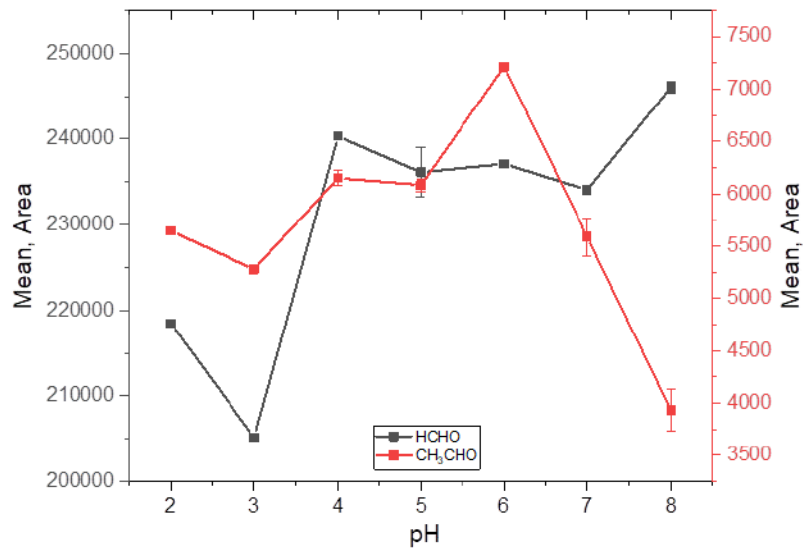

Fig. 5: pH optimization for formaldehyde and acetaldehyde.

(*O*-benzyl hydroxylamine -acetaldehyde) derivative was found between pH 4 to 6.

It is apparent that below pH 2 the protonation of amine or above pH 7 non-ionization of the carbonyl group of aldehyde are two rate-determining steps. The buffer of pH 4.0 was finalized as the reaction medium.

Optimization of Reaction Time

At pH 4, the time required for derivatization was studied by measuring the product at different intervals (Fig.6). It was found that the reaction is instantaneous and completes anywhere between 5 to 15 minutes.

However, when the same solution was kept for longer than 15 minutes, the product tends to degrade. This tendency is because FA/AA-OBA derivative, which is Schiff's base, is reversible in the presence of water. Therefore, within 10-15 minutes of reaction time, 1 mL of hexane was added to extract the Schiff's base, thereby increasing the product stability.

Cotton Weight Optimization

Since cotton is lightweight and bulky, the weight of cotton is crucial for a reproducible result. The different values of the known weight of reagent activated cotton fiber (20 mg to 200 mg) were taken in a PP tube and added to a fixed concentration of standard FA-AA mixture. The effect of different weights of reagent activated cotton on the aldehyde response (Fig. 7) shows the optimum weight of cotton required.

Above 50 mg of the activated cotton, the duration of the Schiff base desorption becomes impractical. Due to a large surface area, it bulges after absorption, and the more amount

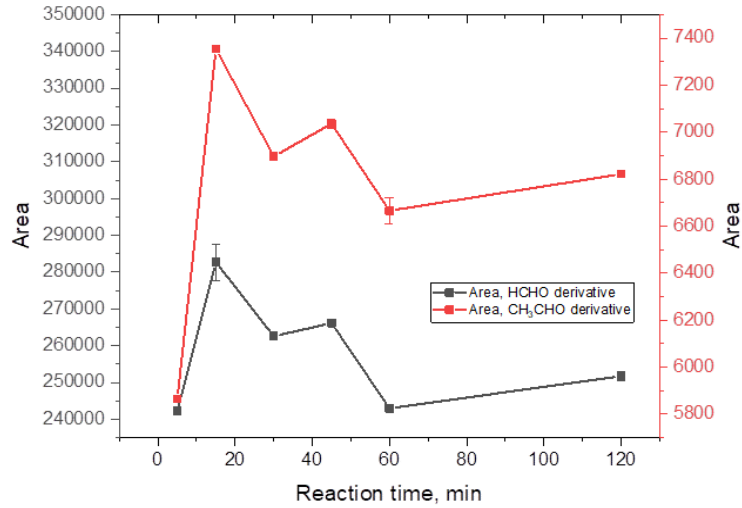

Fig. 6: Reaction time optimization for formaldehyde and acetaldehyde.

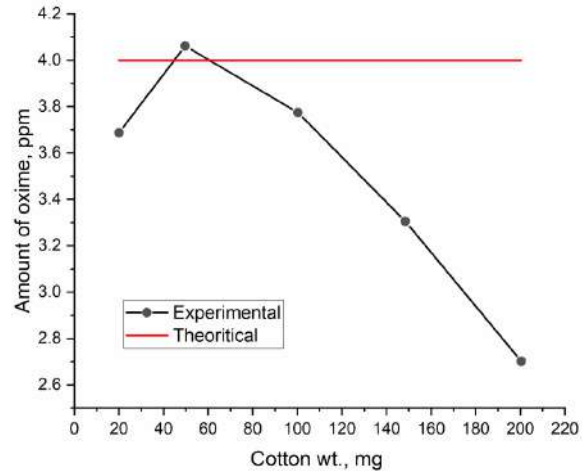

Fig. 7: Cotton weight optimization for formaldehyde and acetaldehyde.

of cotton will create challenges for effective extraction or desorption.

Stability of Activated Cotton and the Derivatized Product

The study of the stability of the reagent absorbed cotton fiber and the derivatized product (oxime), carried out at different intervals of time and days, is shown in Fig. 8.

It shows that the cotton activated with OBA was stable for many days; however, the derivative is stable for at least 24 Hrs. The representative chromatogram (Fig. 9) shows two peaks for the AA-OBA product, which are geometrical isomers, and the area of both the peaks was added for calculating.

The blank reagent activated cotton fiber analysis rules out any adsorption of aldehydes from the atmospheric air, which contains some ppb level of aldehydes. We have not observed any peaks related to aldehydes during experiments in the blank injections, which were subjected to the same procedures during quantification. The coefficient of determination, $R^2 > 0.99$ (Fig. 10), was achieved for aldehydes in both liquid and vapor in a concentration range of 0.1-1.1 ppm.

The linearity curve indicated that the solubility of aldehyde O-benzyl oxime derivative in water, particularly 1 mL of 0.15 M H_2SO_4, is consistent, reproducible, and no other interferences were observed. The analytical method was validated for the below-mentioned parameters, as per the

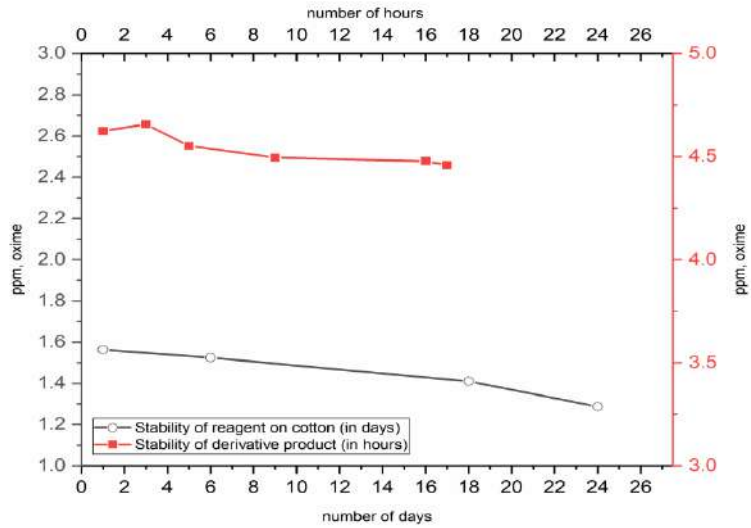

Fig. 8: Pre-reagent absorbed cotton and derivatized product oxime stability study.

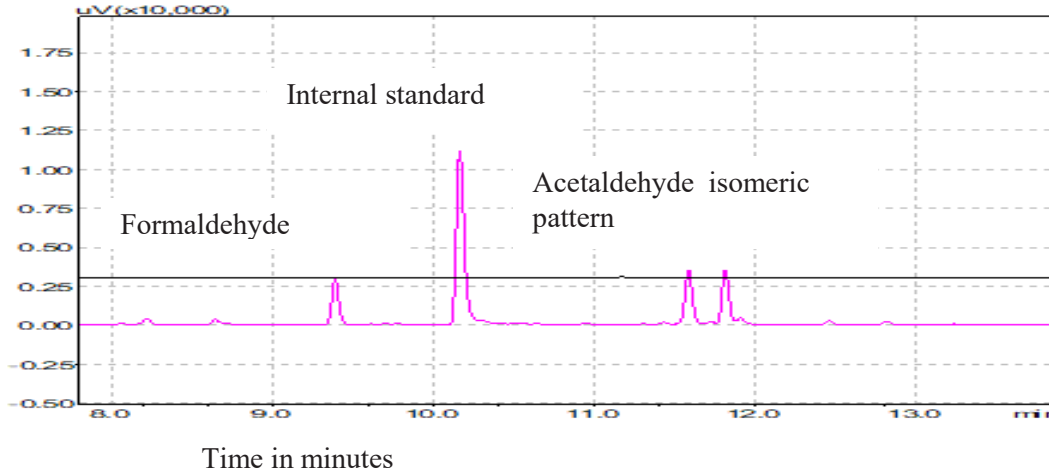

Fig. 9: GC trace for formaldehyde and acetaldehyde in presence of internal standard.

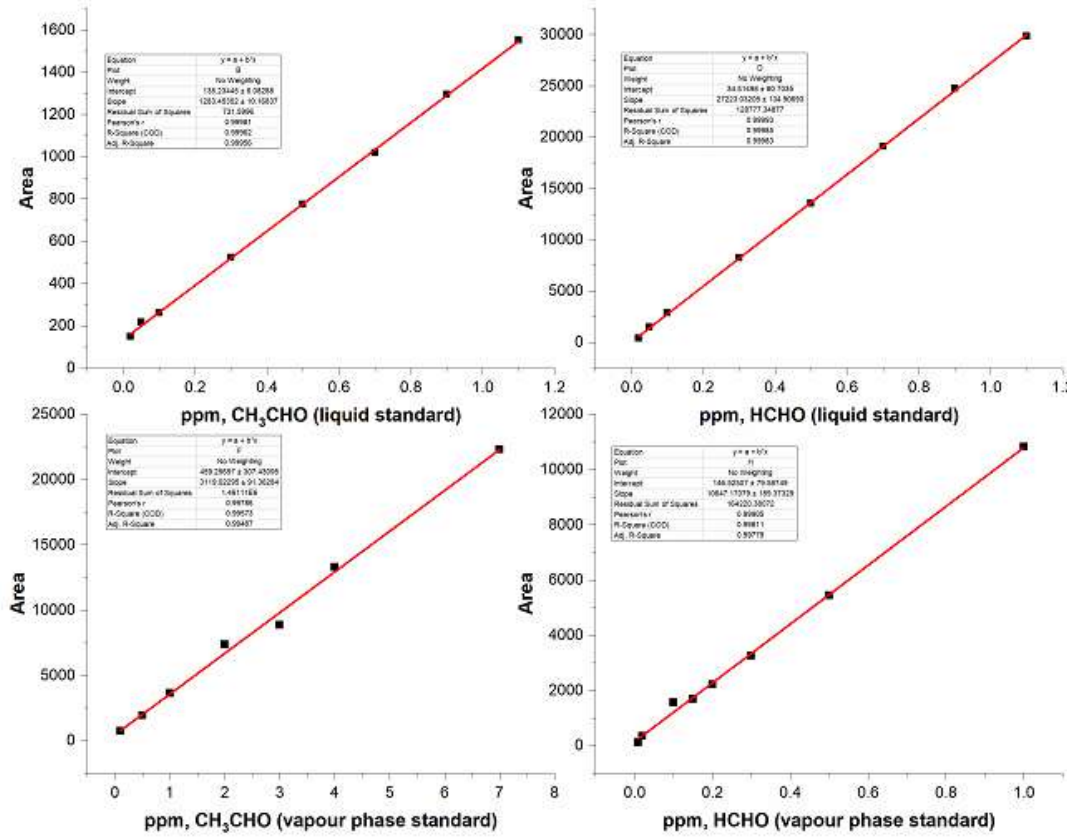

Fig. 10: Linearity graphs in solution phase and vapor phase for formaldehyde and acetaldehyde.

ICH guidelines [35]. The range, regression coefficient, limit of detection (LOD), and limit of quantification (LOQ), accuracy, and precision of the methods are included in Table 1.

Applications: Aldehydes were measured in an effluent treatment plant, laboratory environment, inside a chemical storage refrigerator, and in a polymer sample, following the sampling procedure described in section 2.3.5. The results are shown in Table 2.

The methods for the quantification of carbonyl compounds in the chemical field, specifically aldehydes, have been established by researchers and industries. Many methods using chromatographic techniques are useful in quantifying aldehydes at a meager ppm/ppb limit of detection and quantification levels within reasonable ranges. However, in practice, industries or researchers are facing challenges to meet the other critical criteria like cost, time, and waste generation. Aldehyde quantification in indoor air or food matrix using solid-phase, microextraction followed by on-fiber derivatization or 2,4-dinitrophenylhydrazine technique enables to detect in ppb level (Bourdin & Desauziers 2014). However, it will generate a large amount of waste since it needs lots of solvents for washing of sorbents and very laborious. The derivatization techniques using acetoacetanalide

Table 1: Analytical method validation parameters for formaldehyde and acetaldehyde in solution and vapor phase.

Method	Coefficient of determination (R2) and range		Detection limit		% RSD (Precision)		Accuracy (recovery)
	FA, (ppm)	AA, (ppm)	FA, (ppb)	AA, (ppb)	FA	AA (isomeric)	
Solution	0.9999 (0.01 -1.1)	0.9978 (0.01 -1.1)	1.5	19	0.59	1.95	93.2-102%
Vapour	0.9990 (0.01 -1.1	0.9998 (0.01 -7)	4	8	0.22	1.45	96.2-101.98%

Table 2: Summary of representative sample analysis in various matrices.

Sample	Solution analysis		Vapor analysis	
	Mode of study	FA, (RSD) n = 3	AA, (RSD) n = 3	FA, (RSD) n = 3	AA, (RSD) n = 3
ETP	Liquid	0.59 ppm (1.45%)	16.4 ppm (2.3%)	Not Applicable	Not Applicable
CSR	Vapour	Not Applicable	Not Applicable	0.53 ppm (0.71%)	0.36 ppm (0.65%)
Lab / cabinet	Vapour	Not Applicable	Not Applicable	Less than 4 ppb	Less than 8 ppb
Polymer (PET)	Vapour	Not Applicable	Not Applicable	Not Applicable	0.21 ppm (0.51%)

or O-(2,3,4,5,6-pentafluorobenzyl) hydroxylamine are used to monitor aldehydes in detergents, cosmetic products, raw water during ozonation, and gaseous carbonyl compounds in the air are describing only for specific customized applications. They are not cost-effective and involve cumbersome processes. The metric effects, challenges with the stability of SPME fibers, mass source modification for the specific application are also observed in some of these techniques, and few are very limited to only the lab/research field. The reagent O-benzylhydroxylamine hydrochloride used for the determination of aldehydes in Triethanolamine work reported the very loner derivatization time of 2hrs. The pre-column derivatization followed by fluorescence detection is very sensitive to pH, temperature, and time. The methods developed to determine aldehydes in cosmetics, detergents, indoor air using spectroscopy and proton NMR techniques are not sensitive for low-level detection and observed high standard deviation.

CONCLUSIONS

Based on the challenges observed in the literature methods including the green analytical chemistry challenges, the new methodology using cotton fiber is established for the quantification of formaldehyde and acetaldehyde. The method can be applied to any other aldehydes and used in many applications. The new method has been reported for the pre-concentration and determination of acetaldehyde and formaldehyde using *O*-benzylhydroxyl amine treated cotton, which is subsequently extracted and analyzed using simple gas chromatography with a flame ionization detector from various matrices. The stability of the RACF with and without captured aldehydes was 17 days and 24 Hrs, respectively, qualifying the technique for field applications. The advantages of the reported method are the avoidance of separate reagent preparation, ease of sampling, and low monetary requirements. The process complies with green analytical chemistry principles, such as using biodegradable material, reducing a large amount of waste generation for sample preparation/analysis, using water-soluble reagents in a minimal amount, and less expensive. By using the innate high adsorption capacity of the cotton, the reagent activated cotton is conveniently used to measure aldehydes in various sample matrices such as air, aqueous, and polymer sample. The integration regarding sampling and in-situ detection would make advanced techniques further attractive for a large domain of applications. This blending may be achieved by having cotton activated with a 'marker' within the derivatizing agent that can be measured under IR (Infrared), UV, or fluorescence detector. The RACF technology could be explored to other analytes determination using respective derivatizing agents or chemicals.

REFERENCES

Bourdin, D. and Desauziers, V. 2014. Development of SPME on-fiber derivatization for the sampling of formaldehyde and other carbonyl compounds in indoor air. Anal. and BioAnal. Chem., 406: 317-328.

Chung, P.R., Tzeng, C.T., Ke, M.T. and Lee, C.Y. 2013. Formaldehyde gas sensors: A review. Sensors, 13: 4468-4484.

CPMP/ICH/381/95 Validation of analytical methds and terminology, ICH topic Q2A 1995. http://www.pharma.gally.ch/ich/q2a038195en.pdf

Dochia, C. M., Sirghie, R.M. and Kozłowski, R. 2012. Handbook of natural fibers. Wood-Head Pub. Ser. in Textiles, 1: 11-23.

Eugenia, C. and Silva, B.M. 2010. Analysis of low-molecular mass aldehydes in drinking waters through capillary electrophoresis with laser-induced fluorescence detection. Electrophoresis, 31: 2028-2036.

Gholami, A., Mohsenikia, A. and Masoum, S. 2016. Determination of very low level of free formaldehyde in liquid detergents and cosmetic products using photoluminescence method. J. Anal Methods Chem, 50(3): 1014-1022.

Gosetti, F., Chiuminatto, U., Mazzucco, E., Robotti, E., Calabrese, G., Gennaro, M.C. and Marengo, E. 2011. Simultaneous determination of thirteen polycyclic aromatic hydrocarbons and twelve aldehydes in cooked food by an automated online solid-phase extraction ultra-high-performance liquid chromatography-tandem mass spectrometry. J. Chromatogr. A, 1218: 6308-6318.

Guan, X. and Rubin, E. 2012. An optimized method for the measurement of acetaldehyde by high-performance liquid chromatography. Alcohol Clin. Exp. Res., 36: 398-405.

ICH guidelines-http//www.fda.gov/cder/guida, (2016), US, Q7 Good Manufacturing Practice Guidance for Active Pharmaceutical Ingredients, Guidance for Industry

Jain, V. and Thielen, D. 1995. Determination of aldehydes in the basic medium by gas chromatography using O-benzylhydroxylamine derivatization. J. Chromatogr. A, 709(2): 387-392.

Jeong, H.S., Chung, H., Hoon Song, S., Kim, C. Joon-Goo, L. and Young-

Suk, K. 2015. Validation and determination of the contents of acetaldehyde and formaldehyde in foods. Toxicol. Res., 31: 273-278.

Koziel, J. A., Noah, J. and Pawliszyn, J. 2001. Field sampling and determination of formaldehyde in indoor air with solid-phase microextraction and on-fiber derivatization. Environ. Sci. Technol., 35: 1481-1486.

Kuballa, T., Mildau, G., Kratz, E., Keck-Wilhelm, A., Tschiersch, C. and Lachenmeier, D.W. 2013. Formaldehyde in hair straightening products: Rapid ^{1}H NMR determination and risk assessment. Intl. J. of Cos. Sci., 35: 201-206.

Lin, Y.L., Wang, P.Y., Hsieh, L.L., Ku, K.H., Yeh, Y.T. and Wu, C.H. 2009. Determination of linear aliphatic aldehydes in heavy metal containing waters by high-performance liquid chromatography using 2,4-dinitrophenylhydrazine derivatization. J. Chromatogr. A, 1216: 6377-6381.

Mumiye, A., Ogunwale, Mingxiao Li., Mandapati, V., Ramakrishnan, R., Yizheng, C., Michael, H., Nantz, Daniel, J., Conklin, R. and Xiao-An, F. 2017. Aldehyde detection in electronic cigarette aerosols. ACS Omega, 2: 1207-1214.

Nawrocki, J., Kalkowska, I. and Dabrowska, A. 1996. Optimization of solid-phase extraction method for analysis of low-ppb amounts of aldehydes-ozonation by-products. J. Chromatogr. Sci., 749: 157-163.

Pang, X., Lewis, A.C. and Ródenas-García, M. 2013. Microfluidic lab-on-a-chip derivatization for gaseous carbonyl analysis. J. Chromatogr. A, 1296: 93-103.

Qing, Y., Zheng, D., Liu, L. M. and Hong., L. 2011. Rapid analysis of aldehydes by simultaneous microextraction and derivatization followed by GC-MS. J. of Sepr. Sci., 34: 1607-1612.

Rivero, R.T. and Topiwala, V.J. 2004. Quantitative determination of formaldehyde in cosmetics using combined headspace-solid-phase micro extraction-gas chromatography. Cosmet Sci., 55: 343-350.

Rosenberger, W., Beckmann, B. and Wrbitzky, R. 2016. Airborne aldehydes in cabin-air of commercial aircraft: Measurement by HPLC with UV absorbance detection of 2,4-dinitrophenylhydrazones, J. Chromatogr. Sci. B, 1019: 117-127.

Sakaia, T., Tanaka, S.I., Teshima, N., Yasuda, S. and Ura, N. 2002. Fluorimetric flow injection analysis of trace amount of formaldehyde in the environmental atmosphere with 5,5- dimethylcyclohexane-1,3-dione, Talanta, 58: 1271-1278.

Sampson, M.M., Chambers, D.M., Pazo, D.Y., Moliere, F., Blount, B.C. and Watson, C.H. 2014. Simultaneous determination of four aldehydes in the gas phase of mainstream smoke by headspace gas chromatography-mass spectrometry, Anal. Chem., 86: 7088-7095.

Sang, H. J. and Kim, K.H. 2016. Development of a sampling method for carbonyl compounds released due to the use of electronic cigarettes and quantitation of their conversion from liquid to aerosol, J. Chromatogr. A, 1429: 369-373.

Suze, M., Leeuwen, V., Hendriksen, L. and Uwe, K. 2004. Determination of aldehydes and ketones using derivatization with 2,4-dinitrophenylhydrazine (DNPH) and liquid chromatography/atmospheric pressure photoionization-mass spectrometry (LC/APPI-MS), J. Chromatogr. A, 1058: 107-112.

Szulejko, J. E. and Kim, K. H. 2015. Derivatization techniques for determination of carbonyls in air. Trends Anal. Chem., 64: 29-41.

Textile Fashion Study. 2012. Cotton-fiber-manufacturing physical and chemical properties. http://textilefashionstudy.com/cotton-fiber-physical-and-chemical-properties-of-cotton/

Tsai, S.W. and Chang, C.M. 2003. Analysis of aldehydes in water by solid-phase microextraction with on-fiber derivatization, J. Chromatogr. A, 1015: 143-150.

Valentina, L., Christova, B., Julieta, A. and Tishkova, V.G. 2014. Health risks associated with PET bottled mineral waters and beverages: Overview, analysis, and evaluation. J. Environ. Sci., Comp. Sci. Eng.Technol, 3(4): 1856-1876.

Vander, H., Nguyet, A.N., Detaevenier, M.R., Massart, D.L. and Plaizier, V. 2002. Simultaneous determination of ketoconazole and formaldehyde in a shampoo: Liquid chromatography method development and validation. J. Chromatogr A., 958: 191-201.

Vanessa, M.O. and Zenilda, L.C. 2013. Analytical methods to assess carbonyl compounds in foods and beverages. Chem. Soc., 24: 1711-1718.

Veloso, M.C.C., Silva,V.M., Santos, G. V. and Andrade, J. B. 2001. Determination of aldehydes in fish by high-performance liquid chromatography, J. Chromatogr. Sci. 39: 173-176.

World Health Organization- International Agency for Research on Cancer (WHO_IARC). 2002. IARC Monographs on the Evaluation of Carcinogenic Risks to Humans. https://monographs.iarc.who.int/wp-content/uploads/2018/06/mono81.pdf

Zhang, X., Wang, R., Zhang, Li., Wei, Jianke., Ruan, Y., Wang, W., Houwei, Ji. and Jian, Liu. 2018. Simultaneous determination of four aldehydes in the gas phase of mainstream smoke by headspace gas chromatography-mass spectrometry, Int. J. Anal. Chem., 2019(2): 1-6

Zhao, W., Zhang, Q.B., Lu, S., Sun, Zhang, S. and Zhang, J. 2017. Rapid determination of six low molecular carbonyl compounds in tobacco smoke by the APCI-MS/MS coupled to data mining. J. Anal. Metds. Chem., 1-7.

Nature Environment and Pollution Technology
An International Quarterly Scientific Journal

p-ISSN: 0972-6268
(Print copies up to 2016)
e-ISSN: 2395-3454

Vol. 20 | No.3 | pp. 1069-1076 | 2021

Original Research Paper

https://doi.org/10.46488/NEPT.2021.v20i03.014

Open Access Journal

Photoelectrocatalytic Oxidation of Textile Industry Wastewater by $RuO_2/IrO_2/TaO_2$ Coated Titanium Electrodes

R. Rathinam*† and M. Govindaraj**

*Department of Chemistry, Sri Eshwar College of Engineering, Coimbatore-641 202, Tamil Nadu, India

**Department of Chemistry, K.Ramakrishnan College of Technology, Samayapuram, Trichy-621112, Tamil Nadu, India

†Corresponding author: R. Rathinam; rathinam.r@sece.ac.in

Nat. Env. & Poll. Tech.
Website: www.neptjournal.com

Received: 14-10-2020
Revised: 13-12-2020
Accepted: 08-12-2020

Key Words:
Photoelectrocatalytic oxidation
Textile wastewater
Titanium electrodes
Colour removal

ABSTRACT

Photoelectrocatalytic Oxidation (PECO) system prominently increases the migration of photoexcited charges, hinders the fast recombination of electron-hole, and increases the period of photogenerated holes. In this article, we constructed a novel PECO system to degrade textile industry wastewater by $RuO_2/IrO_2/TaO_2$ coated titanium electrodes. The result shows that PECO treatment can effectively reduce the color and true color of the secondary pollutants present in the wastewater. It is confirmed that a synergistic effect exists between photocatalysis (PC) and electrocatalysis (EC). Moreover, we discussed the influence of pH, current density, electrolyte concentration, and stirring speed. The maximum decolorization efficiency of textile industry wastewater with a pH of 8.2 was found to be 96% under the optimum condition stirrer speed of 200 rpm, an electrolyte concentration of 0.05M, a current density of 15 $mA.cm^{-2,}$ and at a treatment time of 30 mins. The UV-Visible spectra confirm the degradation of textile industry wastewater.

INTRODUCTION

The widespread disposal of industrial wastewater containing organic dyes onto the land and water bodies led to serious contamination in many countries worldwide because of their toxicity and threat to human life and the environment (Thangamani et al. 2007, Han et al. 2009). Every day, industries, agriculture, and the general population are using water and discharging many mixtures in wastewaters. Indeed, agriculture practices, industrial discharges, and human beings play an important role in polluting water. All these practices have generated various pollutants and altered the water cycle causing a global concern linked to their eventual impact on wildlife and human health (Deblonde et al. 2011). For 20 years, many articles have reported the presence of new compounds, called "emerging pollutants", in wastewater and aquatic environments (Vogelsang et al. 2006, Rosal et al. 2010, Thattil & Rose 2019). Traditional treatment technologies in practice for the removal of dye wastewater, fail to meet strict discharge standards. Therefore, an efficient method to treat wastewater containing dye is an urgent need to comply with the discharge standards (Dai et al. 2013). Wastewater generated by textile dyeing and finishing activities is known to contain a considerable amount of pollutants, which are biologically difficult to degrade. So far, several biochemical, chemical and physical treatment methods were applied to treat textile industry wastewater, however with limited success (Arslan-Alaton et al. 2008).

Recently, Advanced Oxidation Processes (AOPs) and electrochemical methods have been established to treat the impurities of drinking water and industrial effluents (Rathinam et al. 2015). As the guidelines worldwide have become stringent, the effluents of textile and related industries have to be treated carefully before discharge. This has resulted in a demand for environmentally friendly technologies to remove dyes from effluents (Rajabi et al. 2016).

The textile industry is one of the most water-consuming industries with a huge volume of high-quality water demand. Textile industrial wastewater is contaminated with a wide range of potential organic and inorganic pollutants that adversely affect the aquatic environment. Most annually produced dyes that are estimated at hundreds of thousands of tons are used in the textile industry. The textile industry is considered as one of the most-dye consuming industries. There are various types of dyes involved in the dying process; reactive dyes are one among them. (Nasr et al. 2019). High quantities of wastewaters containing unconsumed dyes are released into the environment by textile dyeing and printing industries which have high biological oxygen demands (BOD), high chemical oxygen demands (COD), high concentrations of suspended solids, high salt content, and high levels of color caused by residual dyes. The presence of color and its causative compounds have always been undesirable

in water used for either industrial or domestic needs (Singh et al. 2010).

Photoelectrocatalytic oxidation method nowadays has received increasing attention in the field of environment because of its ability to destroy undesirable organic compounds in the aqueous phase and to remove traces of organic species that are stable and difficult to oxidize by means of conventional water treatment methods (Daghrir et al. 2012). In the photoelectrocatalytic process, the rate of conversion does not depend directly on the applied potential but depends on several factors: (i) the specific feature of the semiconductors, (ii) diffusion light, (iii) adsorption and desorption of the reactant and products, and (iv) the intensity of the electric field in the space charge region (Daghrir et al. 2012). The combined treatment process of the photoelectrocatalytic oxidation process was observed to be effective for the removal of organic pollutants from wastewater (Zhao et al. 2010). This work was aimed at treating the textile industry wastewater using the photoelectrocatalytic oxidation technique for color removal.

MATERIALS AND METHODS

The photoelectrocatalytic oxidation experiments were performed in a 750 mL photoelectrochemical reactor (Fig. 1) equipped with a UV lamp with quartz jacketed 15W immersion low-pressure mercury arc lamp (Philips, model TUV) as irradiation with the wavelength of 254 nm and the electrodes are assembled within a single compartment cylindrical glass cell. The reactor is connected to a cooling water circulation bath for controlling the temperature at 27±2°C. The top of the reactor is provided with a holder for holding the UV lamp, electrodes, gas outlet, and thermometer. An internal light source is surrounded by a quartz jacket and the light source is a UV lamp. The gaps between the plates were maintained at 7 mm to minimize the ohmic losses. Electric power was supplied by a regulated DC power supply, which was obtained from M/s. Mighty Electronics Equipments Corporation Pvt. Ltd., Coimbatore, India. The four electrodes, two anodes, and two cathodes are alternatively looped internally. The UV lamp and electrodes are connected to the respective terminals of the power source. The textile industry wastewater samples containing dyes were found to contain a pH of 8.2 and electrolyte is added to the solution taken in the photoelectrocatalytic reactor. Using the magnetic stirrer we stir the sample wastewater solution in the reactor. The treated wastewater sample was centrifuged at 5000 rpm for 15 mins and the supernatant liquid was taken for analysis. The color removal is measured using a spectrophotometer.

Fig. 1: Schematic diagram of the experimental setup for photoelectrocatalytic reactor.

The analysis of textile industry wastewater and its removal during photoelectrocatalytic oxidation were recorded using a UV-Visible spectrophotometer (UV-1700 Pharma Spec, Shimadzu, Japan). Decolorization efficiency calculated as follows:

$$\text{Colour removal efficiency (\%)} = \left(\frac{\text{Ao} - \text{A}}{\text{Ao}}\right) \text{X } 100$$

Where;

A_o: Initial concentration of dye before electrochemical oxidation ($mg.L^{-1}$)

A: Present concentration of dye after electrochemical oxidation ($mg.L^{-1}$)

RESULTS AND DISCUSSION

Effect of Initial pH on Colour Removal

The pH value is an important parameter in the photoelectrocatalytic process because the species of the reaction compounds and their adsorption equilibrium depend on the pH values of the solution. The pH values of solutions can influence the process through the following three routes: (i) the semiconductor flat-band potential variation (ii) adsorption isotherm of electroactive species (the adsorption of electroactive species is governed by the Langmuir adsorption equilibrium equation) (iii) photoelectrochemical oxidation of water and OH^- ions competing with other reactants to form powerful oxidants on irradiation (Shaogui et al. 2006). It affects the capacity of adsorption and dissociation of the target compounds, the charge distribution to photocatalyst surface, and the oxidation potential of the valence band. The experiment demonstrates that the dye solution concentration decreases much faster in acidic solution than that in alkaline solution.

To study the influence of pH, experiments were conducted with pH 3, 5, and 10 in addition to sample wastewater orig-

inal pH. The solution pH was adjusted using sulfuric acid (0.1N H_2SO_4) or sodium hydroxide (0.1N NaOH). During the treatment process, the current density was maintained at 15 $mA.cm^{-2}$, electrolysis time of 30 mins, stirrer speed of 200 rpm, under UV illumination, and 0.05 M of NaCl as the supporting electrolyte. Fig. 2 shows that the influence of initial pH on the percentage of color removal by photoelectrocatalytic oxidation within 30 mins of the reaction.

It is clear that varying the pH strongly affected color removal efficiency and reached 98% with sample wastewater's original pH of 8.2 within 30 mins of the treatment process, while lower color removal was observed at higher pH. This is due to the oxidation and hydrolysis of chlorine yields hypochlorous acid (HOCl) or the hypochlorite ion (OCl^-) depending on the solution pH 10. On the other hand, a low pH solution will corrode the electrode and inhibit the activity of the electrode, even hinder the proceeding of degradation reaction (Ju et al. 2012).

When the pH value was less than 4, the molecule in the dye was in cationic form and its adsorption on the catalyst surface became difficult because of an electrostatic repulsive force. As a result, the efficiency of the photoelectrocatalytic degradation of textile wastewater was relatively low with pH less than 4 while the efficiency was increased with pH greater than 4. Thus, the oxidizing ability of photo-generated holes was raised, i.e. the hydroxyl radicals production was facilitated in the oxidation of water (or hydroxide ions) by photo-generated holes. At neutral pH, more readily water (or hydroxide ions) underwent oxidation to generate hydroxyl radicals on the catalyst surface (Daghrir et al. 2013). The degradation capacity of the system in this extremely dark-colored media is mainly due to the electrochemical generation of oxidant species, which can be photochemically transformed in the bulk of the solution in an even more reactive radical (Tauchert et al. 2006). Therefore, the photoelectrocatalytic degradation of textile industry dye wastewater was more efficient at the original pH of 8.2.

In the photoelectrocatalytic method, the degradation rate of certain contaminants such as pentachlorophenol, humic acid, and benzotriazole is found to be maximum and much faster in an acidic solution than in an alkaline solution. It is proven that the degradation rate of 4-chlorophenol was enhanced in both alkaline and acid solutions (Wang et al. 2009), However, the effect of pH in photocatalytic reactions cannot be generalized (Daghrir et al. 2012). Studies have reported that photoelectrocatalytic oxidation without initial pH adjustment was more effective in removing phenol, compared to pH 3.0 and pH 11. Photoelectrocatalytic oxidation degradation of BPA is favored at strongly acidic conditions with the extent of enhancement reaching as much as about 90%. Working at slightly acidic, neutral, or alkaline conditions reduces degradation rates by as much as 3 to 4 times (Yavuz & Kaporal 2006). Therefore, pH is an important operational parameter determining the efficiency of photocatalytic removal of different pollutants in wastewaters (Hadjiltaief et al. 2016).

Effect of Electrolyte Concentration on Colour Removal

An electrolyte plays a vital role in the photoelectrocatalytic process. In the photoelectrocatalytic process, the efficiency of current intensity, voltage, and consumption of electrical energy is affected by the conductivity of the solution. The conductivity must be high to ensure good ion transfer in the effluent. When the conductivity is too low, the resistance is

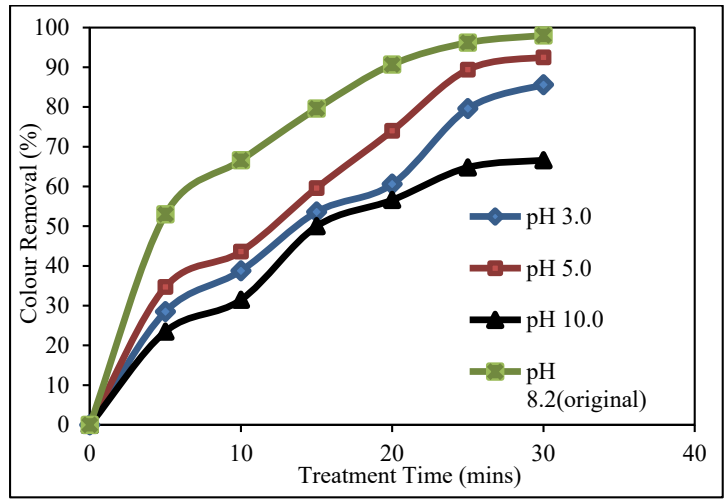

Fig. 2: Effect of initial pH on color removal.

too high and consequently, an increase of the applied voltage is observed. High ionic strength leads to faster electron transport and better degradation rate (Ju et al. 2012) so that the effect of electrolyte on the degradation of textile wastewater was investigated. Solutions with various ionic strengths were obtained by preparing various concentrations of NaCl aqueous solution in this study. As anions of the supporting electrolyte participate in the decomposition reaction of dye molecules, careful selection of electrolytes is essential in maximizing the decolorization efficiency of a given compound.

In this study, the supporting electrolyte used is NaCl. The NaCl concentrations (0.025, 0.05, 0.1M) were tested. Each test was performed with sample wastewater with a pH of 8.2 and under a constant current density of 15 $mA.cm^{-2}$, electrolysis time of 30 mins, stirrer speed of 200 rpm under UV illumination. The result shown in Fig. 3 indicates that the textile industry wastewater degradation efficiency increases with the concentration of electrolyte. This can be attributed to the surplus free Cl^- since the electrolyte can enhance charge transfer to the reactor, leading to an increase in the efficiency of direct electrochemical oxidation and the capture of a photogenerated electron by the external electric field (Wenbing et al. 2005). In chloride solutions, the Cl^- ions adsorbed on the working electrode may be oxidized to produce Cl2 as oxidants which may decolorize dye wastewater (Ali Baddouh et al. 2018). In addition, the photogenerated hole or OH• can oxidize free chloride ion into active chlorine as one of the products in dye wastewater degradation, and then the active chlorine (Cl•, ClO^-) promotes oxidation of dye wastewater. These results indicate that the adsorption of chloride ions is preponderant at lower pH. As a consequence, the contribution of chloride oxidation is diminished under conditions where the pH of the solution is neutral or alkaline, and the formation of hydroxyl radicals under these conditions could be the preponderant process.

An increase in the concentration of NaCl has been found to increase the generation of active chlorine (Murugananthan et al. 2011). Decolourization of paper mill effluents was found to increase with the increase in NaCl concentration (El–Ashtoukhy et al. 2009). Additionally, it must be assumed that due to the high complexity of chemical, photochemical and electrochemical reactions involving chlorine generation one could possibly form other oxidants during this photoelectrochemical process (Fraga et al. 2009). NaCl releases chloride ions in the liquid phase, which can electrochemically and/or photochemically generate highly reactive chlorohydroxyl radicals ($ClOH^•$), as well as chloride radicals (Kiwi et al. 2000); Furthermore, anodic reactions may generate free chlorine, chlorine dioxide, and hypochlorite (Daskalaki et al. 2013). To minimize the chlorides' negative influence, an optimum concentration of 0.05 M was adopted in other experiments.

Effect of Current Density on Color Removal

As most applications of photoelectrochemical systems involve the transfer of electrons across the solid/electrolyte interface, current density applied potential recording techniques are commonly used for their characterization. It is reported that the rate of degradation increases significantly when the applied current density increased (Mohan et al. 2007). To investigate the influence of current density on treatment efficiency of the electrochemical system, different current densities from 5 to 25 $mA.cm^{-2}$ were experimentally analyzed under the conditions:

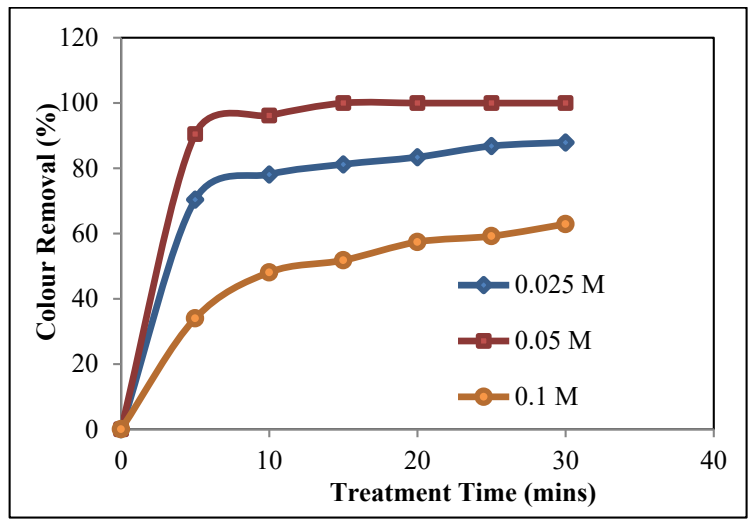

Fig. 3: Effect of supporting electrolyte concentration on color removal.

30 mins treatment time and 200 rpm stirrer speed. Fig. 4 shows that color removal percentage increased with electrolysis time and increased with applied current density.

In all cases, the color removal rate was much faster during the first 20 mins of electrolysis. With the current density of 15 mA.cm^{-2} and at 5 mins electrolysis time, color removal efficiency reached 96.2%. The complete color removal was achieved at 15 mA.cm^{-2} after 30 mins of electrolysis.

After 30 mins, the total removal efficiency of color was 92.4% for the current density of 5 mA.cm^{-2}, while almost complete degradation was obtained at the current densities 10, 15, 20, and 25 mA.cm^{-2}. It is clear that percentage color removal increases with increasing current density; this is attributed to an increase of Cl_2, HOCl, and OCl^- concentrations in the solution, which eventually increases the dye degradation (Raghu & Ahmed Basha 2008). Beyond 15 mA.cm^{-2}, there is no significant increase in the percentage of color removal; this may be attributed to the fact that the discharge potential of Cl_2 increases with current density and becomes close to the discharge potential of O_2. It is explained by the fact that an external electric field could not only decrease the rate of recombination of electron-hole pairs but could also improve direct and/or indirect electrooxidation reactions of anodes under higher applied cell voltages.

It is well known that the amount of applied current density determines production rate, and adjusts the rate and size of the bubble production, hence affects the growth of flocs (Daneshwar et al. 2003). Current density can be formulated as CD = I/S, where CD is the current density (mA^{-2}), I is the current (A), and S is the total area of the anode (m^2) (Parsa et al. 2011)

From these results, it is clear that applied current improves the photoelectrochemical process due to minimization of charge e–/h+ recombination up to 15 mA.cm^{-2}, when maximum optimization is obtained. In addition, at higher current density the process could be limited by mass transporting conditions and/or chlorate production as a parallel reaction occurring at the photoanode following the electrochemical reaction expressed in Eq. 1 or aqueous solution by a chemical reaction in Eq. 2 as demonstrated below:

$$6OCl^- + 3H_2O \rightarrow 2ClO_3^- + 6H^+ + 4Cl^- + 1.5O_2 + 6e^- \quad \ldots(1)$$

$$2HOCl + OCl^- \rightarrow ClO_3^- + 2H^+ + 2Cl^- \quad \ldots(2)$$

Effect of Treatment Time and Stirring Speed on Colour Removal

The influence of electrolysis time was explored at a constant current density of 15 mA.cm^{-2}, stirrer speed 200 rpm, and supporting electrolyte concentration of 0.05 M. Fig. 5 shows the effect of treatment time on the color removal. It was noted that the color removal increased from 0 to 60 mins, indicating that dye wastewater color removal was directly proportional with treatment time. The rate of degradation is high at the beginning of the process and reduces gradually to a monotonical value at the end of the process. This phenomenon was consistent with that of the electrochemical degradation of 4–chlorophenol reported by Wang et al. (2009). In view of reducing power consumption and further optimizing the electrochemical oxidation, all other experiments were conducted within 30 mins of treatment time.

To verify the important role of mass transfer on the photoelectrocatalytic oxidation of textile industry wastewater, the influence of stirrer speed during anodic oxidation of waste-

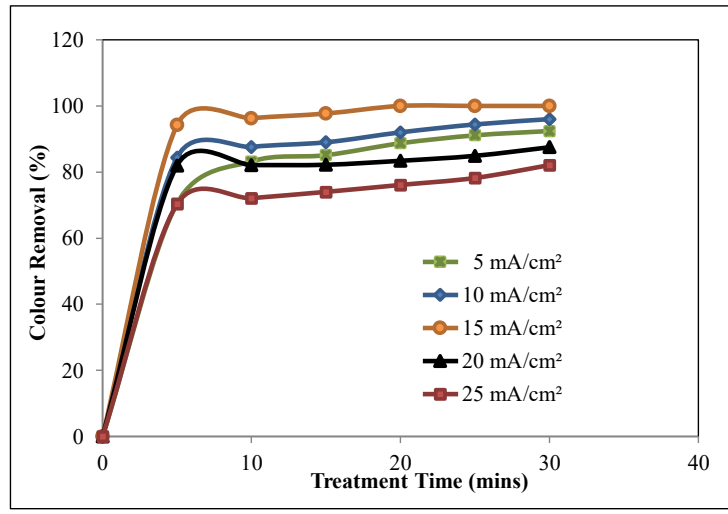

Fig. 4: Effect of current density on color removal.

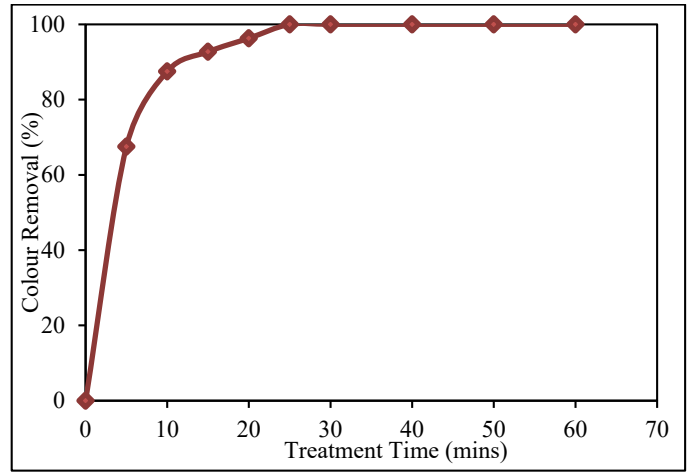

Fig. 5: Effect of treatment time on color removal.

water was studied by varying the stirrer speed. The stirring speed of the solution causes an increase of contact between flocs and agglomeration during the process. Experiments were performed at different stirrer speeds, in the range of 150 to 300 rpm under the following experimental conditions; 15 mA.cm^{-2} of applied current density and treatment time of 30 mins. Fig. 6 shows that the percentage color removal decreases from 90.98% to 85.72% as the stirrer speed increases from 150 to 300 rpm.

It can be seen from the results that increasing color removal was obtained under different stirrer speeds and the color removal is higher with the presence of a stirrer. The result shows that enhancing effect of stirrer speed on the rate of color removal becomes less pronounced at high stirrer speeds (e.g. >200 rpm) probably because of the diffusion-controlled cathodic reduction of hypochlorite and its anodic oxidation reaction are favored at higher stirrer speed. Also by increasing stirrer speed, color removal is increased up to 200 rpm, beyond that there is a significant decrease in colour removal. An increase in stirrer speed leads to a more rapid and more actual electrochemical process. This confirms that the color removal reaction is diffusion-controlled when there is an increase in rotational speed. There will be an increase in the intensity of turbulence and a reduction in the diffusion layer thickness at the surface of the electrode that improves the mixing conditions in the electrolyte in bulk. This enhances the rate of transfer of reactants and products to anode surface (El-Ashtoukhy et al. 2009).

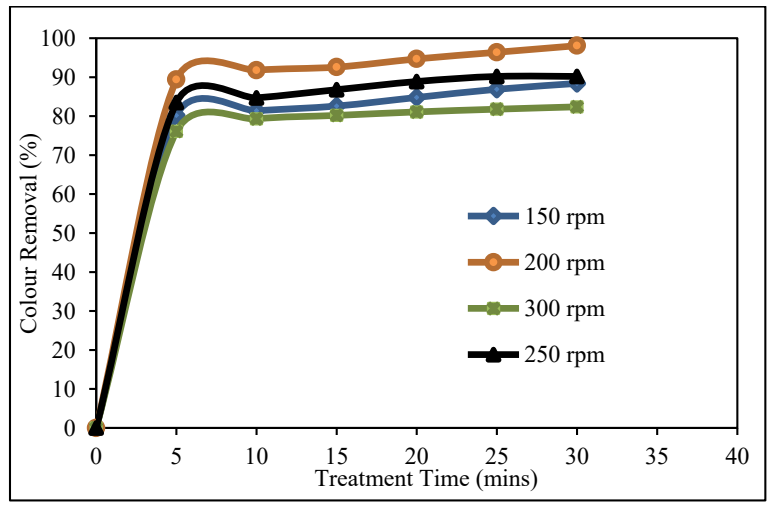

Fig. 6: Effect of stirrer speed on color removal.

Effect of Applied Current Density on Energy Consumption

It is critical to evaluate the electrical energy consumption in textile wastewater treatment to determine whether photoelectrocatalytic oxidation is financially viable for the removal of color from textile industry wastewater. Once the required currents and corresponding voltages were obtained from the photoelectrocatalytic oxidation tests, the amount of energy used was estimated.

In Fig. 7, the minimum energy consumption was 5.64 $kWh.m^{-3}$ at 5 $mA.cm^{-2}$ current density for 30 mins treatment time under the optimum conditions. The energy consumption in the high current density was increased because of polarization. The energy consumption was increased from 5.64 $kWh.m^{-3}$ to 18.52 $kWh.m^{-3}$ while increasing applied current density from 5 $mA.cm^{-2}$ to 25 $mA.cm^{-2}$ under the optimum conditions. The present experiment was conducted at an applied current density of 15$mA.cm^{-2}$.

UV-Visible Absorbance Spectra Analysis

Fig. 8 shows the time-dependent UV–visible spectrum of textile industry wastewater during the photoelectrocatalytic oxidation process. As it is clear from this figure, the absorption peaks diminished and finally disappeared under reaction, which indicates that the wastewater had been degraded and color was removed. However, it is remarkable to note that the overall absorbance of the curve decreases when the photoelectrocatalytic treatments are applied, likely due to colloidal and suspended particles. It is found that there is no new absorption bands appeared in either the visible or ultraviolet regions.

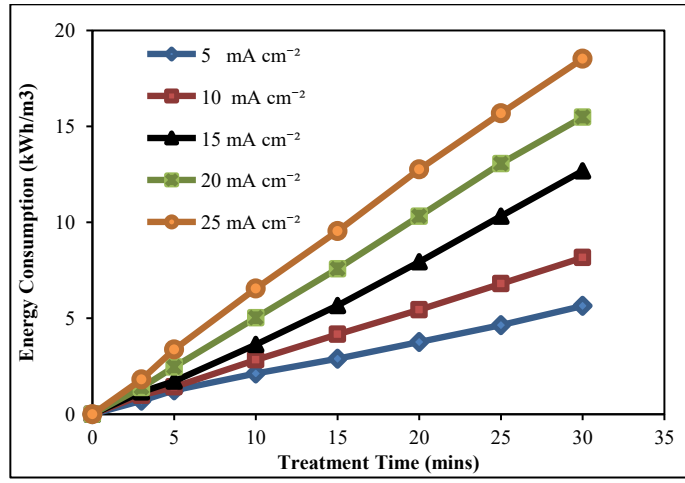

Fig. 7: Effect of applied current density on energy consumption.

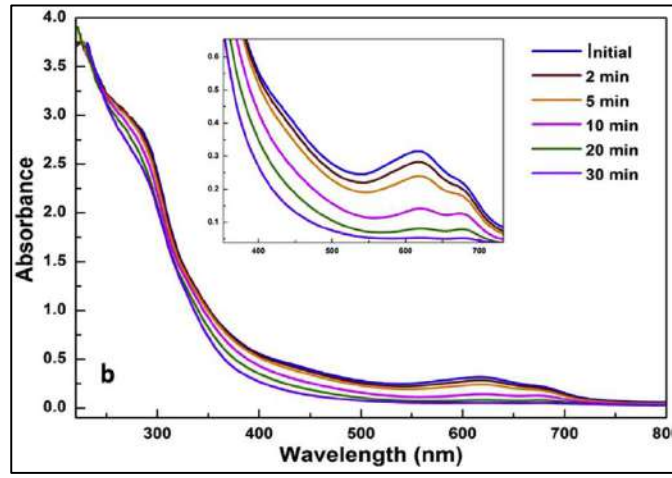

Fig. 8: UV-visible spectrum of textile industry wastewater.

CONCLUSION

From the results, it can be concluded that the color removal efficiency of textile industry wastewater reached 98% within 30 mins, while lower color removal was observed at higher pH. The maximum color removal was achieved at a current density of 15 $mA.cm^{-2}$, electrolysis time of 30 mins, stirrer speed of 200 rpm under UV illumination. The color removal was directly proportional to treatment time and photo-electrocatalytic oxidation was found to be effective for color removal. The color removal efficiency of textile industry wastewater after treatment was confirmed using UV-visible spectroscopy. This study suggests that the photoelectrocatalytic oxidation technique is effective and reliable for a wide variety of future applications.

REFERENCES

Ali, B., Guilherme, G.B., Mohamed, M. R., Brahim, E.I., LahcenBazzi, M.H. and Maria, V.B.Z. 2018. Electrochemical decolorization of Rhodamine B dye: Influence of anode material, chloride concentration, and current density. J. Environ. Chem. Eng., 6: 2041-2047.

Arslan-Alaton, I., Kabdash, I. and Sahin, Y. 2008. Effect of operating parameters on the electrocoagulation of simulated acid dye bath effluent. The open environment & Biol. Monit. J., 1(1): 7-12.

Daghrir, R., Drogui, P. and El Khakani, M.A. 2013. Photoelectrocatalytic oxidation of chlortetracycline using Ti/TiO2 photo-anode with simultaneous H_2O_2 production. Electrochem. Acta, 87: 18-31.

Daghrir, R., Drogui, P. and Robert, D. 2012. Photoelectrocatalytic technologies for environmental applications. J. Photochem. Photobiol. A-Chem., 238: 41-52.

Dai, Q., Shen, H., Xia, Y., Chen, F., Wang, J. and Chen, J. 2013. The application of a novel Ti/SnO2–Sb2O3/PTFE-La-Ce-β-PbO2 anode on the degradation of cationic gold yellow X-GL in sono-electrochemical oxidation system. Sep. Purif. Technol., 104: 9-16.

Daneshwar, N., Ashassi-SorKhahi, N. and Tizpar, A. 2003. Decolourization of Orange II by electrocoagulation method. Sep. Purif. Technol., 31: 153-162.

Daskalaki, V.M., Fulgione, I., Frontistis, Z., Rizzo, L. and Mantzavinos, D. 2013. Solar light-induced photoelectrocatalytic degradation of bisphenol-A on TiO_2/ITO film anode and BDD cathode. Catal. Today, 209: 74-78.

Deblonde, T., Cossu-Leguille, C. and Hartemann, P. 2011. Emerging pollutants in wastewater: A review of the literature. Int. J. Hyg. Environ. Health, 214: 442-448.

El-Ashtoukhy, E.S.Z., Amin, N.K. and Abdel-Wahab, O. 2009. Treatment of paper mill effluents in a batch stirred electro chemical tank reactor. Chem. Eng. J., 146: 205-210.

Fraga, L.E., Anderson, M.A., Beatriz, M.L.P.M.A., Paschoal, F.M.M., Romãoluciane, P. and Zanoni, M.V.B. 2009. Evaluation of the Photoelectrocatalytic method for oxidizing chloride and simultaneous removal of microcystin toxins in surface waters. Electrochem. Acta, 54: 2069-2076.

Hadjltaief, H.B., Zina, M.B., Galvezb, M.E. and Costab, P.D. 2016. Photocatalytic degradation of methyl green dye in aqueous solution over natural clay-supported ZnO–TiO_2 catalysts. J. Photochem. Photobiol. A-Chem., 315: 25-33.

Han, F., Kambala, V.S.R., Srinivasan, M., Rajarathnam, D. and Naidu, R. 2009. Tailored titanium dioxide photocatalysts for the degradation of organic dyes in wastewater treatment: A review. Appl. Catal. A-Gen., 359: 25-40.

Ju, P., Fan, H., Guo, D., Meng, X. and Xu, M. and Ai, S. 2012. Electrocatalytic degradation of bisphenol A in water on a Ti-based PbO2–ionic liquids (ILs) electrode. Chem. Eng. J., 179: 99-106.

Kiwi, J., Lopez, A. and Nadtochenko, V. 2000. Mechanism and kinetics of the OH-radical intervention during Fenton oxidation in the presence of a significant amount of radical scavenger (Cl-*).* Environ. Sci. Technol., 34: 2162-2168.

Mohan, N., Balasubramanian, N. and Basha, C.A. 2007. Electrochemical oxidation of textile wastewater and its reuse. J. Hazard. Mater, 147: 644-651.

Murugananthan, M., Latha, S.S., Bhaskarraju, G. and Yoshihara, S. 2011. Role of electrolyte on anodic mineralization of atenolol at boron-doped diamond and Pt electrodes. Sep. Purif. Technol., 79: 56-62.

Nasr, F.A., Sadik, M.A. and El-Shafai, S.A. 2019. Innovative electrochemical treatment of textile dye wastewater. Egypt. J. Chem., 62(11): 2019-2032.

Parsa, J.B., Vahidian, H.R., Soleymani, A.R. and Abbasi, M. 2011. Removal of acid brown 14 in aqueous media by electrocoagulation: Optimization parameters and minimizing of energy consumption. Desalination, 278: 295-302.

Raghu, S. and Ahmed Basha, C. 2008. Dye destruction and simultaneous generation of sodium hydroxide using a divided electrochemical reactor. Ind. Eng. Chem. Res., 47: 5277-5283.

Rajabi, A.A., Yamini, Y., Faraji, M. and Nourmohammadian, F. 2016. Modified magnetite nanoparticles with acetyltrimethylammonium bromide as superior adsorbent for rapid removal of the disperse dyes from wastewater of textile companies. Nanochem. Res., 1(1): 49-56.

Rathinam, R., Govindaraj, M., Vijayakumar, K. and Pattabhi, S. 2015. Decolourization of Rhodamine B from aqueous by electrochemical oxidation using graphite electrodes. Desalin. Water Technol., 57: 16995-17001.

Rosal, R., Rodriguez, A., Perdigon-Melon, J.A., Petre, A., Garcia-Calvo, E., Gomez, M.J., Aguera, A. and Fernandez-Alba, A.R. 2010. Occurrence of emerging pollutants in urban wastewater and their removal through biological treatment followed by Ozonation. Water Resour., 44: 578-588.

Shaogui, Y., Yazi, L. and Cheng, S. 2006. Preparation of anatase TiO_2/Ti nanotube-like electrodes and their high Photoelectrocatalytic activity for the degradation of PCP in aqueous solution. Appl. Catal. A-Gen., 301: 284-291.

Singh, K.P., Gupta, S., Singh, A.K. and Sinha, S. 2010. Experimental design and response surface modeling for optimization of Rhodamine B removal from water by magnetic nanocomposite. Chem. Eng. J., 165: 151-160.

Tauchert, E., Silvana, S., Josmaria, L.M. and Patricio, P.Z. 2006. Photochemically-assisted electrochemical degradation of landfill leachate. Chemosphere, 64: 1458-1463.

Thangamani, K.S., Sathishkumar, M., Sameena, Y., Vennilamani, N., Kadirvelu, K., Pattabhi, S. and Yun S.E. 2007. Utilization of modified silk cotton hull waste as an adsorbent for the removal of textile dye (reactive blue MR) from aqueous solution. Bioresour. Technol., 98: 1265-1269.

Thattil, P.P. and Rose, A.L. 2019. Photodegradation of congo red dye via simple and effective air oxidation using copper (II) chloride and sunlight. Nat. Env. Pol. Tech., 18(4): 1243-1248.

Vogelsang, C., Grung, M., Jantsch, T.G., Tollefsen, K.E. and Liltved, H. 2006. Occurrence and removal of selected organic micropollutants at mechanical, chemical, and advanced wastewater treatment plants in Norway. Water Resour., 40: 3559-3570.

Wang, N., Li, X., Wang, Y., Quan, X. and Chen, G. 2009. Evaluation of bias potential enhanced photocatalytic degradation of 4-chlorophenol with TiO_2 nanotube fabricated by anodic oxidation method.Chem. Eng. J., 146(1): 30- 35.

Wenbing, Z., Taicheng, A., Mingchao, C., Guoying, S. and Jiamo, F. 2005. Effects of anions on the photocatalytic and photoelectrocatalytic degradation of reactive dye in a packed-bed reactor. J. Chem. Technol. Biotechnol., 80: 223-229.

Yavuz, Y. and Kaporal, A.S. 2006. Electrochemical oxidation of phenol in a parallel plate reactor using ruthenium metal oxide electrode. J. Hazard. Mater, B136: 296-302.

Zhao, X., Qu, J., Liu, H., Wang, C., Xiao, S., Liu, R., Liu, P., Lan, H. and Hu, C. 2010. Photo-electro chemical treatment of landfill leachate in a continuous flow reactor. Bioresour. Technol., 101: 865-869.

Nature Environment and Pollution Technology
An International Quarterly Scientific Journal

p-ISSN: 0972-6268
(Print copies up to 2016)
e-ISSN: 2395-3454

Vol. 20 | No.3 | pp. 1077-1085 | 2021

Original Research Paper

https://doi.org/10.46488/NEPT.2021.v20i03.015

Open Access Journal

Reliable and Sophisticated Techniques to Evaluate LDPE Degraded Compounds by *Streptomyces werraensis* SDJM

N. Deepika and R. Jaya Madhuri†
Department of Applied Microbiology, Sri Padmavati Mahila Visvavidyalayam, Tirupati-517502 India
†Corresponding author: R. Jaya Madhuri

Nat. Env. & Poll. Tech.
Website: www.neptjournal.com

Received: 17-07-2020
Revised: 17-11-2020
Accepted: 09-01-2021

Key Words:
LDPE
LCMS technique
GCMS-SPME technique
Streptomyces werraensis
SDJM strain

ABSTRACT

The modern world in the present era made life miserable due to extensive usage of plastic. Low-density polyethylene (LDPE) is widely consumed in every part of the world starting from baby products to garbage bags. Humans and animals are affected due to the usage and disposal of LDPE in the environment. To safeguard the environment from deleterious effects, biodegradation of LDPE was studied by isolating a potent *Streptomyces werraensis* SDJM strain from garbage soil. The degradation assessment was performed to identify the LDPE degraded compounds such as octane, decane, tetracosane, hexacosane, dotriacontene, tetratiacontene, tridecone, tetracontane, and pentacosane, using a sophisticated technique - liquid chromatography-mass spectroscopy (LCMS). The end product of LDPE biodegradation, carbon dioxide was measured by the GCMS-SPME technique. Field trials in garbage soil for a period of three months reveal 71.26% weight loss compared to laboratory test results where the weight loss was 60.05%. The morphological changes and structural changes of the polymer in fields were assessed by SEM analysis and FTIR analysis after one month of incubation. The test results in field trials were promising and convincing to overcome the LDPE pollution in presence of *S.werraensis* SDJM strain.

INTRODUCTION

Low-density polyethylene is a synthetic polymer that plays a vital role in every facet of human life, primarily for packaging food (milk, cereals, pulses, and vegetables), computer components, dispensing bottles, laboratory equipment, garbage bags, etc. Amongst synthetic plastics, one of the most problematic plastics in this regard is polyethylene (PE). Polyethylene or PE is the most common plastic and about 80 million tons of polyethylene is produced worldwide (Piringer & Baner 2008). LDPE, a polyolefin is produced from olefin (alkene) monomers because olefins contain a reactive double bond. LDPE was first introduced through radical polymerization under high pressure by Imperial Chemical Industries (ICI) in 1933 (Dennis 2010).

Disposal of LDPE through landfills and incineration creates huge environmental pollution (Einas & Hago 2014, Ingavale & Raut 2018). Polyethylene waste disposed into oceans disperse all over the water due to buoyancy and is considered as hazardous waste killing aquatic habitat. Incineration of polyethylene waste such as trash bags, grain storage bags, and shopping bags under an open atmosphere at low to high temperatures release toxic fumes such as methane and carbon monoxides that pollute the environment and cause significant health hazards. Some of the significant VOCs released at the time of incineration are polycyclic aromatic hydrocarbons (PAHs), polychlorinated dibenzofurans (PCDFs,) and dioxins which are major carcinogenic hazards to humans (Environment Pollution Board 433 2012).

Physical and chemical methods of degradation techniques are employed to safeguard our ecosystem from toxic carcinogens but none of the methods are really effective to overcome pollution. Low-density polyethylene degradation is enhanced by exposing the polymer to abiotic conditions using UV, chemicals, and high temperature before subjecting to biotic degradation (Gajendiran et al. 2016). Among all the methods of degradation, biodegradation is one of the projecting ways in recent research to reduce environmental pollution and health hazards. The biodegradation of low-density polyethylene can be carried out under aerobic environment and anaerobic environment. Aerobic microbes in the presence of oxygen form thick biomass around the polymer and degrade slowly by releasing carbon dioxide and water as end products whereas, under anoxic conditions, anaerobes release carbon dioxide, methane, hydrogen sulfide, and water (Muthukumar & Veerappapillai 2015).

There are various analytical techniques to determine the biodegradation of low-density polyethylene. These techniques were used to identify structural changes of the polymer which include physical or morphological changes, chemical changes, and further confirmation through analysis of degraded products. The physical and morphological changes of the low-density polyethylene can be determined visually

through biofilm formation but further confirmation can be done based on a scanning electron microscope (SEM). SEM technique undoubtedly identifies the changes on the surface of any material as it reveals the details of abrasions and incisions created by the microorganism (Shalini & Sasikumar 2015).

The chemical changes of the polymer or chemical properties are determined based on the formation or disappearance of functional groups. Functional groups of the polymers were analyzed by Fourier transform infrared spectroscopy (FTIR). The polymer was oxidized through the β-oxidation process forming carbon dioxide and water as end products (Nupur et al. 2017). The degradation products of low-density polyethylene can be determined either by using gas chromatography-mass spectroscopy (GCMS) or liquid chromatography-mass spectroscopy (LCMS) techniques. Polyethylene samples treated with microorganisms were tested by performing GCMS analysis and the spectra reveal that the linear polymer chain was broken into different compounds confirming that microbes play a key role in the degradation of polyethylene.

Soil burial methods or field trails were employed by using a potent microbial strain to reduce pollution. Weight loss, SEM analysis, and thermogravimetric analysis were performed to identify the changes of the PE, true graft of PE-g starch, and the composite of PE-g starch samples through soil burial method using garden soil (Neena & Inderjeet 2013). The field trials were compared with laboratory conditions using synthetic media through weight loss analysis and it was observed that the soil burial method with compost is more efficient in degrading polyethylene. This confirms that microorganisms in soil play a predominant role to degrade low-density polyethylene (Okoh & Atuanya 2014).

This study aims to investigate the role of microorganisms from garbage soil to degrade low-density polyethylene under both laboratory and field conditions.

MATERIALS AND METHODS

1. Low-density polyethylene powder (LDPE) from Sigma Aldrich Chemical Co (Product of USA) was used for degradation studies. LDPE size is 53-75µm and its density was 0.94g.ml^{-1} at 25°C.
2. Low-density polyethylene film from Pack Worth Polymers (Hyderabad, India) was used for degradation studies
3. Mineral salts medium (MSM g.L^{-1}): KH_2PO_4, 0.2; K_2HPO_4,1.6; $(NH_4)_2SO_4$, 1.0; $MgSO_4.7H_2O$, 0.2; $CaCl_2.2H_2O$, 0.02; $FeSO_4.7H_2O$, 0.01; NaCl, 0.1; pH, 7.2 ± 0.2

LCMS (Liquid Chromatography-Mass Spectroscopy) Analysis to Identify the LDPE Degrading Compounds

Mineral salt broth with LDPE at a concentration of 1%w/v was prepared and inoculated with *Streptomyces werraensis* SDJM. Control was maintained without organism to check the parent polymer peak. Liquid phase mass spectroscopy was performed to identify the degraded products of low-density polyethylene after one month of incubation along with a control sample. Sample and control were injected into triple quadrupole LCMS sample port.

LCMS was performed using a thermo scientific instrument with LC-ultimate 3000 which was coupled with TSQ-Endure MS with a trace finder data system. The fragmented ions were detected with an electron multiplier detector to develop a chromatogram. The chromatogram obtained was compared with the NIST library to identify the degraded products of low-density polyethylene (Samuel et al. 2009).

GCMS Analysis (Gas Chromatography-Mass Spectroscopy) by SPME Method (Solid Phase Micro Extraction) for Identification of LDPE Degraded Products

Gas chromatography-mass spectroscopy-solid phase microextraction technique was used to extract the degraded products of low-density polyethylene after one month of incubation with *S. werraensis* SDJM. The fiber was exposed to the medium for 15 min and retracted slowly into the protective sheet. Then it was inserted into the injector to desorb and GCMS was started simultaneously.

Gas chromatography Mass spectroscopy (GCMS) was performed using Agilent instruments. In this instrument, GC-7890A was coupled with 5975C-MS with a chemstation data system. The chromatogram of the degraded products was compared with NIST 2014 spectra library.

Field Tests

Field tests were performed to determine the capability of isolated strain *S.werraensis* SDJM to degrade low-density polyethylene in garbage soil. LDPE bags' initial weight was noted and buried in garbage soil at a depth of 5-30cm and 10% *S.werraensis* SDJM inoculum was incorporated along with 1000 mL of mineral salt broth for a period of three months. A control sample was buried without organisms at a different location for comparative studies. After one month of incubation, both control and inoculated LDPE samples were washed with distilled water and air-dried, and weight was recorded. SEM analysis was performed for both control and sample to observe the morphological changes, and structural changes of the polymer were determined

by FTIR analysis. The weight loss data is recorded for three months and correlated with laboratory experiments (Kathiresan 2003).

RESULTS AND DISCUSSION

The end products of degradation of low-density polyethylene by *S.werraensis* SDJM were assessed by liquid chromatography mass spectroscopy. The degraded products were determined by LCMS analysis through the fragmentation pattern and m/z values. These unknown compounds formed were evaluated comparing with known compounds through the national institute standard and technology (NIST).

Low-density polyethylene is a linear polymer made up of monomers. The LCMS data reveals that the polymer parent peak was formed at 17.69 RT with 1064 molecular weight. In the treated sample, parent polymer was degraded into small linear aliphatic compounds such as octane, decane, tetracosane, hexacosane, dotriacontene, tetratiacontene, tridecone, tetracontane, and pentacosane. The LCMS spectra and molecular weight of the unknown compounds are represented in Table 1. This data reveals that the *S.werraensis* SDJM breaks the polymer and forms aliphatic straight chains of alkenes and alkanes (Figs. 1 & 2).

GCMS Analysis of LDPE

GCMS analysis was performed through solid-phase mi-

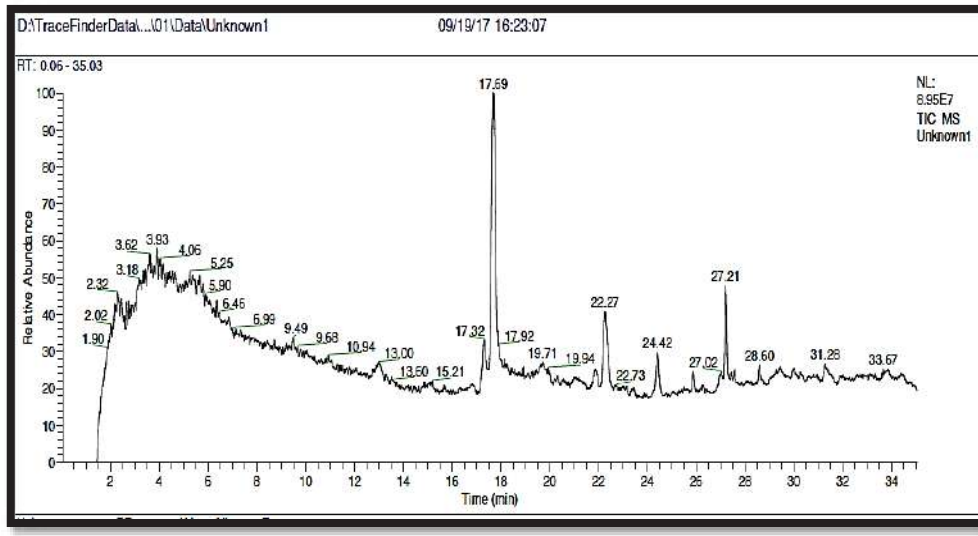

Fig. 1: Mass spectrum of LDPE control.

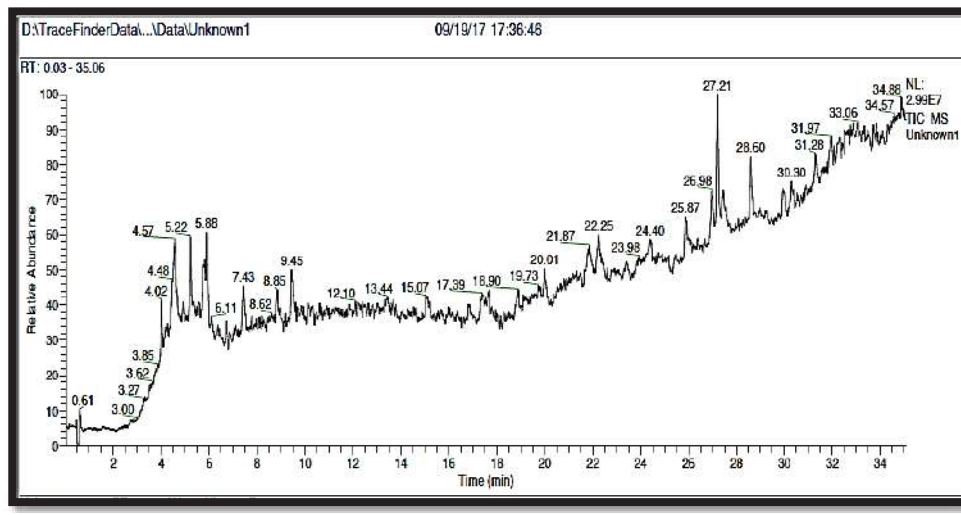

Fig. 2: Mass spectrum of LDPE sample with *S.werraensis* SDJM.

croextraction method using GC-7890A and 5975C-MS to identify the volatile compounds of the degraded low-density polyethylene after a period of one month along with control. The SPME fiber was inserted into the sample and kept for 15 min to adsorb the degraded compounds. Then the fiber was removed and inserted into the sample inlet of GCMS to desorb and analyzed the compounds.

The compound detected was identified as carbon dioxide through the NIST library as the peak formation was identified at 3.365 min. In control, peaks were absent indicating the absence of organism and degradation (Figs. 3 & 4).

Field Tests for Assessment of LDPE Degradation in Garbage Soil Using *Streptomyces werraensis* SDJM

Table 1: Degradation products of LDPE.

S.NO	Retention time(min)	Molecular weight	IUPAC name of the compound	Structure
1	4.02	114.232	Octane(C_8H_{18})	
2	4.02	142.29	Decane($C_{10}H_{22}$)-	
3	4.48	338.65	Tetracosane($C_{24}H_{50}$)	
4	4.57	366.718	Hexacosane($C_{26}H_{54}$)-	
5	5.22	448.864	Dotriacontene($C_{33}H_{64}$)	
6	5.22	478.934	Tetratiacontene($C_{34}H_{70}$)	
7	5.88	184.4	Tridecone($C_{13}H_{28}$)	
8	5.88	563.096	Tetracontane($C_{40}H_{82}$)--	
9	7.43	338.65	Tetracosane($C_{24}H_{50}$)	
10	7.43	352.69	Pentacosane($C_{25}H_{52}$)	

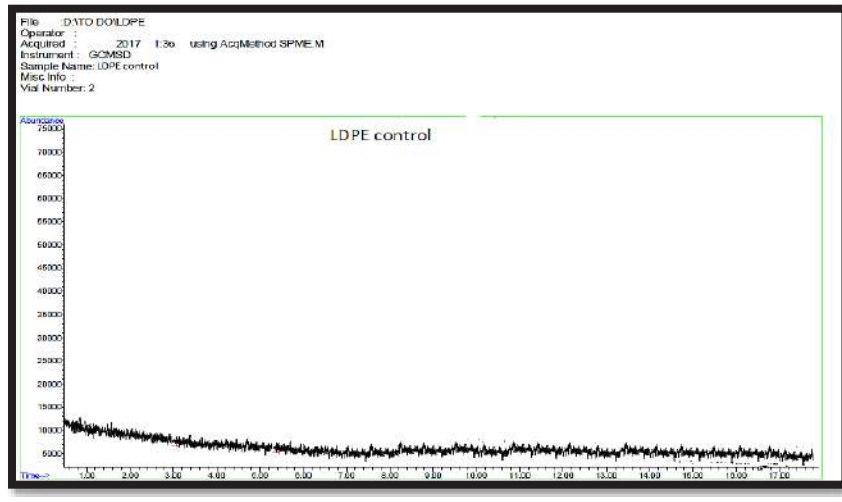

Fig. 3: Mass spectra of control.

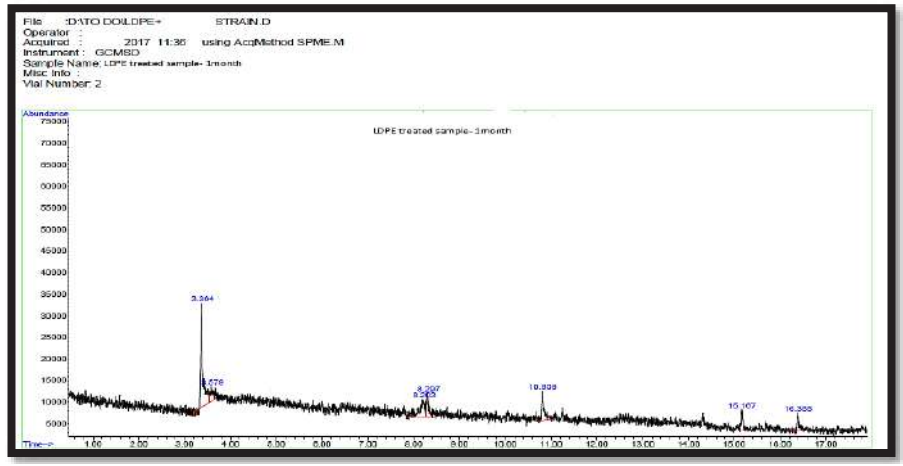

Fig. 4: Mass spectra of the sample.

Field tests were performed to check the efficiency of LDPE degradation using *S.werraensis* SDJM in garbage soil. The results were correlated with control by burying LDPE at a different location without organism for a period of one month. The changes in the polymer were determined by weight loss, morphological changes by SEM analysis, and structural changes by performing FTIR analysis.

Weight Loss of LDPE

The initial weight of the LDPE film was measured and buried in garbage soil. After one month, biofilm formation with crack and pits was observed on the surface of LDPE in both control and sample. Yellowing of the film was more in the sample compared to the control sample (Fig. 5). It has been observed the weight loss of the sample buried with *S.werraensis* SDJM is 60.01% and the weight loss of the control is 13.97% in one month (Fig. 6). The weight loss results of field trials were compared with laboratory weight loss results for a period of three months and it was observed that *S.werraensis* SDJM reduces more weight of the polymer in garbage soil up to 71.26% by associating with other microbes under natural conditions compared to laboratory conditions i.e 60.05% (Fig. 7).

Scanning Electron Microscopy (Sem) Analysis for Buried LDPE

Morphological changes on the surface of both control and sample were analyzed using SEM analysis. Biofilm formation, cracks, pits, and abrasions were observed in both control and sample but more cracks were identified in the sample compared to control (Fig. 8).

FTIR Analysis of Buried LDPE Samples

FTIR analysis was performed for both LDPE control and sample buried in garbage soil for a period of one month and it was observed that both exhibit structural change due to shift in absorbance and formation of new functional groups.

FTIR spectrum of control LDPE was buried without organism degradation due to soil inhabitants and form peaks at

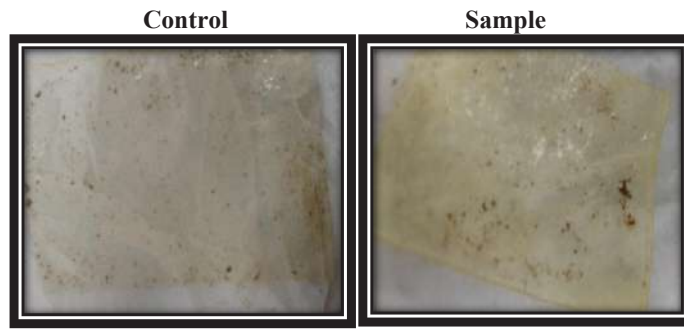

Fig. 5: Biofilm formation on LDPE in field trials.

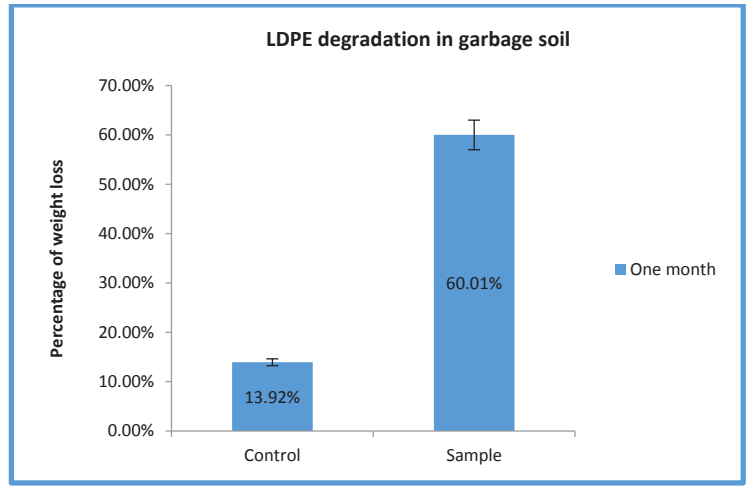

Fig. 6: Weight loss of LDPE in garbage soil.

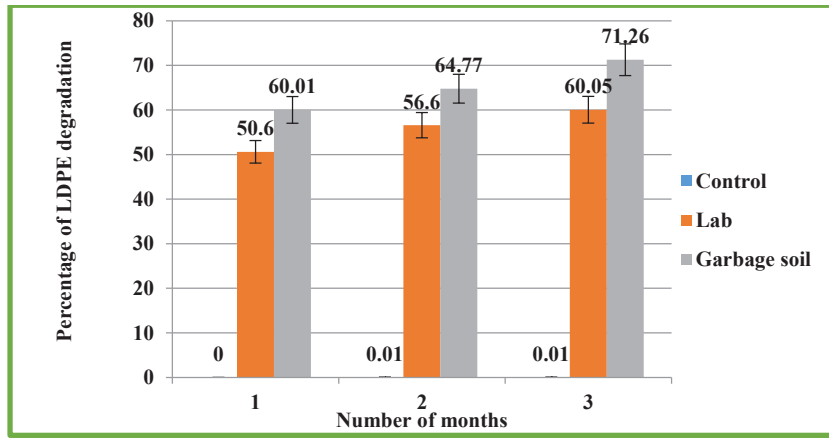

Fig. 7: Comparative studies between laboratory and field conditions through weight loss.

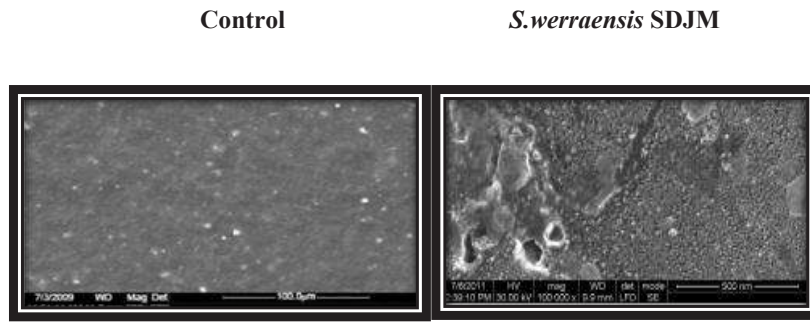

Fig. 8: SEM analysis of buried LDPE film.

2663.63 cm^{-1},1721.81 cm^{-1},1031.23 cm^{-1} and 912.92 cm^{-1}. In the treated sample, new peaks were formed at 2663.63 cm^{-1},1722.63 cm^{-1}, 1081.28 cm^{-1}, and 966.12 cm^{-1}. These peaks represent the formation of carbonyls and carboxylic acid in both control and sample by oxidizing the alkane and alkene bonds (Fig. 9 & 10). The changes in the control are due to microbes present in the garbage soil.

DISCUSSION

There are wide ranges of plastics that can be molded into desired shapes. For three decades' plastics have been extensively used as they are light in weight, strong and persistent for a long time without any damage (Kathiresan 2003). Low-density polyethylene was the first polyethylene derived through the polymerization of ethylene monomers. The hydrocarbon chain of low-density polyethylene is straight, crystalline, and tough to degrade after throwing away under normal environmental conditions. Disposal of low-density polyethylene is unmanageable in society and creates numerous deleterious effects polluting the environment and causing various health hazards. In the present research, the potent *S.werraensis* SDJM strain was isolated from LDPE dumped garbage sites, screened, and the effectiveness of biodegradation was assessed in both laboratory conditions and at garbage sites to control various anomalies created by LDPE pollution.

In the present research, LDPE degraded compounds were analyzed after 30 days of incubation by *S.werraensis* SDJM.

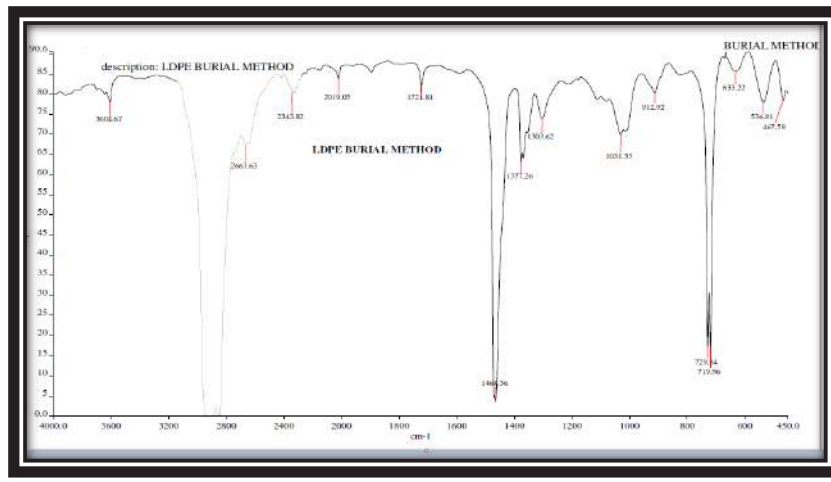

Fig. 9: FTIR spectrum of control without culture in garbage soil.

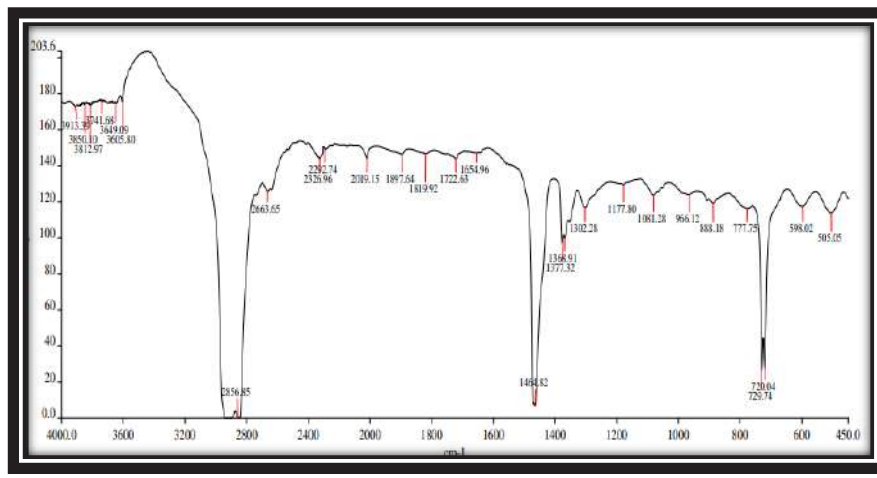

Fig. 10: FTIR spectrum with *Streptomyces werraensis* SDJMin garbage soil.

Compounds like octane, decane, tetracosane, hexacosane, dotriacontene, tetratiacontene, tridecone, tetracontane, and pentacosane were detected in the treated sample through LCMS analysis whereas they were absent in control. Carbon dioxide released due to β-oxidation and TCA cycle was confirmed by GCMS using solid phase microextraction technique. These two sophisticated techniques prove that *S.werraensis* SDJM has the capacity to degrade LDPE in a short period of time.

The analysis data obtained was correlated with other researchers and found that GCMS analysis of LDPE treated with *Acinetobacter baumannii* revealed the formation of new peaks such as 2-butene, 2-methyl at 7.646 RT, acetone at 8.250 RT, and ethene at 17.288 RT. Acetone presence confirms *A.baumannii degrade* polymer and form carbonyl compound (Pramila & Vijaya 2015). LDPE treated with *Pseudomonas aeruginosa* PAO1 for 120 days were analyzed through GCMS and identified alkanes, fatty acids (hexadecanoic acid, octanoic acid), hydrocarbons, oxygenated chemical compounds (aldehydes, ketones, esters, ether groups), and aromatic compounds formation (Bhone et al. 2012). The degraded products of LDPE were analyzed using HPLC and it was observed that the peak at 14.13 disappeared in treated samples of 40% and 50% of starch blend compared to the control sample. This confirms LDPE can be degraded by microorganisms (Veethahavyaa et al. 2016).

Microorganisms isolated from compost soil were tested for polyethylene degradation. Degraded products in the culture supernatant were collected, extracted using distilled ether, and analyzed by GCMS. The polyethylene degraded products were identified as octadecadienoic acid, octadecatrienoic acid, benzene dicarboxylic acid, and cyclopropanebutanoic acid (Mahalakshmi et al. 2012). Streptomyces species was isolated from East Azerbaijan, Iran soil, and the efficiency of HDPE degradation was tested through GCMS analysis. The degradation compounds were identified as tetradecanoic acid, eicosane, heneicosane, docosane, tricosane, tetracosane, hexacosane and benzoic acid (Ali et al. 2017). Aldehydes, ketones, and carboxylic acids were identified during the LDPE extrusion coating process. Biodegradation of polyethylene releases Ergosta-5, 22-dien-3-ol, acetate (3, 22 E), 1-monanalinoeoglycerol trimethylsilyl ether, betamethasone acetate, azafrin, 9, 12, 15-octadecatrienoic acid, 2, 3-bis [(trimetylsilyl) oxy] propyl ester, and (Z, Z, Z)-C27H52O4Si2) (Pranita 2010). The degraded products of low-density polyethylene by *Achromobacter denitrificans* was analyzed through GCMS and it was observed that octadecadienoic acid, octadecatrienoic acid, benzene dicarboxylic acid, and cyclopropanebutanoic acid were produced in 60 days of incubation (Ambikadevi et al. 2015).

Field trials were performed under natural garbage soil conditions and the obtained data was compared with laboratory trials. Garbage soil is a rich source of polyethylene degrading microorganisms as the soil is enriched with various waste materials along with plastic bags and the available nutrients in garbage endures them to grow for a long life by harboring the natural habitats. In the present study, LDPE was dumped in garbage soil with *S.werraensis* SDJM, and control without organism was kept in another location for comparative studies.

In one month, the weight loss of the sample is 60.01% and control is 13.92%. SEM analysis and FTIR analysis were performed to identify the morphological and structural changes before and after degradation. It has been observed that degradation was more prominent in the sample compared to control. Finally, the results of weight loss in three months conducted in fields were compared with laboratory test results and found that *S.werraensis* SDJM could degrade LDPE by more than 10% by associating with soil microbes compared to laboratory conditions.

The above experimental data was compared with a field trial conducted to degrade the polymer and it was found that the soil burial method for degradation of polyethylene was determined by weight loss and SEM analysis. It has been noticed that the weight loss of composite sample (PE-g-starch) and true graft (PE) was about 88% and 84% respectively. Degradation of PE and PE-g starch was further confirmed by scanning electron microscopy (SEM analysis). This helps to identify the topographical changes of the polymer created by soil microorganisms due to degradation (Neena & Inderjeet 2013).

Fourier transform infrared spectroscopy (FTIR) and SEM analysis were performed to identify the structural and surface changes of the degraded low-density polyethylene using bacterial consortium in enriched soil. The results obtained in the presence and absence of the consortium were compared with the untreated LDPE control sample. LDPE buried in soil exhibits CH/CH2 stretching, bending, deformation and results in the formation of C-O at 1,218.6 cm^{-1} and 1,031.6 cm^{-1}. FTIR spectrum of LDPE treated with consortium reveals that there is the disappearance of CH3 bending and complete change was noticed between 1,300 cm^{-1} and 950 cm^{-1}. A peak at 1628.4–1628.7 cm^{-1} was observed in both treated and untreated samples. SEM analysis was performed to LDPE control, untreated sample, and sample treated with consortia. In both the treated and untreated samples there is a noticeable change when compared with control. The reason behind the changes in the untreated sample is mainly due to natural habitants present in the soil (Shahbaz et al. 2013).

Low-density polyethylene was subjected to environmental degradation by burying the sample in soil under natural conditions. To test the efficiency of degradation by soil microbes the samples were removed periodically from soil and tested using FTIR analysis. This helps us to identify structural changes of the polymer due to biodegradation and major absorption at 1400-1800 cm^{-1} indicating the presence of carbonyl peaks was found (Tabassum et al. 2010).

REFERENCES

Ali, F., Alireza, D., Najibeh, S. and Faezeh, N. 2017. Biodegradation of high density polyethylene using *Streptomyces species*. J. Coast. Life Med., 5(11): 474-479.

Ambikadevi, K., Lakshmi, B.K.M. and Hemalatha, K.P.J. 2015. Degradation of low-density polythene by *Achromobacterdenitrificans* strain S: A novel marine isolate. Int. J. Rec. Sci. Res., 6(7): 5454-5464.

Bhone, M.K., Ravi, C., Meena, K., Chu, S.L. and Kishore, S. 2012. Biodegradation of low-density polythene (LDPE) by pseudomonas species. Indian J. Microbiol., 52(3): 411-419.

Dennis, B.M. 2010. Book: Introduction to Industrial Polyethylene, Properties, Catalysts, and Processes. Wiley, New York, pp. ***1–150.***

Einas, I.A.M. and Hago, E.F.H. 2014. Effect of the low-density polyethylene carry bags waste on the asphalt mixture. Int. J. Eng. Res. Sci. Technol. 3(2): 86-93.

Environment Pollution Board 433. 2012. Health and Environmental Effects of Burning Waste Plastics. pp. 1-3.

Gajendiran, A., Krishnamoorthy, S. and Abraham, S. 2016. Microbial degradation of low-density polyethylene (LDPE) by *Aspergillus clavatus* strain JASK1 isolated from landfill soil. Biotech, 6(1): 52.

Ingavale, R.R. and Raut, P.D. 2018. Comparative biodegradation studies of LDPE and HDPE using Bacillus weihenstephanensis isolated from garbage soil. Nature Environment and Pollution Technology, 17(2): 649-655.

Kathiresan, K. 2003. Polyethylene and plastic degrading microbes from the mangrove soil. Revista de Biol. Trop., 51: 629-633.

Mahalakshmi, V., Abubakker, S. and Niren, A.S. 2012. Analysis of polyethylene degrading potentials of microorganisms isolated from compost soil. Int. J. Pharm. Biol. Arch., 3(5): 1190-1196.

Muthukumar, A. and Veerappapillai, S. 2015. Biodegradation of plastics: A brief review. Int. J. Pharm. Sci. Rev. Res., 31(2): 204-209.

Neena, G. and Inderjeet, K. 2013. Soil burial biodegradation studies of starch grafted polyethylene and identification of *Rhizobium meliloti*. J. Environ. Chem. Ecotoxicol., 5(6): 147-158.

Nupur, O., Neha, P., Surjit, S., Anil, B., Anamikashrivastava, P., Vivek, R. and Sutapa, B. 2017. Evaluation of hdpe and ldpe degradation by fungus, implemented by statistical optimization. Sci. Rep., 7: 1-10.

Okoh, E.B. and Atuanya, E.I. 2014. Impacts of soil composting and poultry manure on biodegradation of polyethylene. Int. J. Appl. Microbiol. Biotechnol. Res., 2: 18-29.

Piringer, O.G. and Baner, A.L. 2008. Plastic Packaging: Interactions with Food and Pharmaceuticals (2nd ed.). Wiley-VCH, Weinheim, Germany.

Pramila, R. and Vijaya Ramesh, K. 2015. Potential biodegradation of low-density polyethylene (LDPE) by Acinetobacterbaumanni. Afr. J. Biotechnol. Res., 7(3): 24-28.

Pranita, N.A. 2010. Studies on Biodegradation of Polythene, Thesis, Dr.Babasaheb Ambedkar Marathwada University, Aurangabad, pp.1-135.

Samuel, O. A., Sajid, S., Anicia, M. **and** Wayne, S. 2009. Chromatographic and spectral analysis of two main extractable compounds present in aqueous extracts of laminated aluminum foil used for protecting LDPE-filled drug vials. Int. J. Anal. Chem., 2009: 1-9.

Shahbaz, A., Mohd, N., Harshita, G., Haider, Z. and Sanjay, G. 2013. Biodeterioration studies of thermoplastics in nature using indigenous bacterial consortium. Environ. Sci., 56(3): 475-484.

Shalini, M. and Sasikumar, C. 2015. Effect of microbes on low-density polyethylene material degradation with reference to sem analysis. Int. J. Pharma Biosci., 6(4): 447-452.

Tabassum, M., Khan, M.R. and Mohd, A.H. 2010. Study of environmental biodegradation of LDPE films in soil using optical and scanning electron microscopy. Micron, 41(5): 430-438.

Veethahavyaa, K.S., Rajath, B.S., Sabike, N. and Manoj Kumar B. 2016. Biodegradation of low-density polyethylene in aqueous media. Procedia Environ. Sci., 35: 709-713.

Nature Environment and Pollution Technology
An International Quarterly Scientific Journal

p-ISSN: 0972-6268
(Print copies up to 2016)
e-ISSN: 2395-3454

Vol. 20 | No.3 | pp. 1087-1096 | 2021

Original Research Paper

https://doi.org/10.46488/NEPT.2021.v20i03.016

Open Access Journal

Spatial and Temporal Characteristics of $PM_{2.5}$ Sources and Pollution Events in a Low Industrialized City

R. Xu*, Q. Tian*, H. Wan†, J. Wen***, Q. Zhang* and Y. Zhang***

*College of Computer and Information Security, Guilin University of Electronic Technology, Guilin 541004, China
**Key Laboratory for City Cluster Environmental Safety and Green Development of the Ministry of Education, Institute of Environmental and Ecological Engineering, Guangdong University of Technology, Guangzhou, 510006, China
***Guilin Environmental Monitoring Center Station, Guilin 541002, China
†Corresponding author: H. Wan; wanhang@gdut.edu.cn

Nat. Env. & Poll. Tech.
Website: www.neptjournal.com

Received: 28-08-2020
Revised: 04-11-2020
Accepted: 08-12-2020

Key Words:
$PM_{2.5}$
Air pollution
Pollution events
Spatial characteristics

ABSTRACT

In recent years, cities in southern China have experienced severe air pollution, despite having few sources of pollutants. To study the pollution characteristics of $PM_{2.5}$ in these "low industrialized" cities, a numerical method based on the HYSPLIT4 Model and Kriging Spatial Interpolation Technology was established. Simulation results showed that the $PM_{2.5}$ pollution in Guilin was affected by both internal and external sources. The backward air mass trajectory from July 2017 to June 2018 was simulated using the HYSPLIT model. The cluster analysis results indicated that the direction of trajectory ② accounted for 63.09% of the air pollution in the city. The average concentration of $PM_{2.5}$ pollution was 45.94 $\mu g.m^{-3}$. The pollutant originated from the "Xiang-Gui Corridor." The location of the sources was collocated with high industry regions. The spatial characteristics of the four pollution processes in the winter of 2017 were analyzed using a spatial interpolation method. The results showed that the transport of air masses in the direction of trajectory ② was obstructed by a mountain system in the northeast. Therefore, two air pollution accumulation centers and a topographic weakening zone dominated by internal and external sources were formed. It can be inferred that the air pollution in Guilin is affected by both internal and external factors. These results provide important theoretical and technical support for regional air pollution control and environmental protection.

INTRODUCTION

The Chinese government implemented a series of air pollution prevention and control measures to improve the country's air quality. Under this situation, air quality in most regions has improved, but pollution remains serious in some areas (Luan et al. 2018, Jiang et al. 2018, Cui et al. 2019, Sun et al. 2019). It is worth noting that tourist areas in southern China, such as Guilin, have also suffered serious air pollution, despite having fewer sources of pollutants. However, there is no clear conclusion about the cause of air pollution in tourist areas, which are quite different from those in industrial cities because of their characteristics. In recent years, with the development of tourism, the eco-environmental problems in Guilin have been a cause of concern for environmental workers. Bai et al. (2017) studied the impact of climate re(sources on the tourism development of Guilin International Resort and found that air pollution would affect tourism development. As a tourism city, ensuring the air quality of Guilin is necessary and important.

Scholars adopted several tools to analyze the sources of air pollutants and characterize pollution characteristics. For example, Zhang et al. (2019) employed the Comprehensive Air Quality Model Extensions (CAMx) based on the Particulate Source Apportionment Technology (PSAT) to simulate and analyze the sources of $PM_{2.5}$ in Beijing. They found that 47.6% of the $PM_{2.5}$ originated from local sources. Zhang et al. (2018) used the Community Multiscale Air Quality Modeling System (CMAQ) to simulate the changes of surface $PM_{2.5}$ in Qingdao during winter. They found that $PM_{2.5}$ accounted for 72.7%–93.2% of the daily emissions. This percentage would decrease by about 21% when considering the pollution process, and the proportion of aerosol accumulation would increase by about 6%. Another study by Yang et al. (2019) used the WRF-SMOKE-CMAQ model to analyze the life cycle of $PM_{2.5}$ in Xi'an from 2014 to 2017. The study concluded that the $PM_{2.5}$ concentrations increased from 82.4 $\mu g.m^{-3}$ to 95.4 $\mu g.m^{-3}$ as a result of dust emissions into the atmosphere. Wang et al. (2015) analyzed the air pollution in the Yangtze River Delta in December 2013 using a Principal Component Analysis (PCA). They found that the concentration of fine particulate matter increased due to the anthropogenic emission of dust from Northwest China. This method of research uses a meteorological grid, which

needs to be analyzed with an internal source list data. This research model is suitable for the pollution source analysis of large-scale regions but is ineffective when extrapolating the source of a pollutant from pollution monitoring points.

The Hybrid Single-Particle Lagrangian Integrated Trajectory (HYSPLIT) model can be used to trace the transport and diffusion trajectory of pollutants from the monitoring points. Arif et al. (2018) used the HYSPLIT4 model to study the source of atmospheric pollutants in Patna in 2015. The Concentration Weighted Trajectory (CWT) method was also used to analyze pollution levels in source regions. Mukherjee and Agrawal (2018) studied the sources of $PM_{2.5}$ pollution in Varanasi, India, from 2014 to 2017. They quantified the contribution from traffic, road dust, and internal combustion activities, and found that Northwest India was the main source area. Liu et al. (2013) used the CWT method to track the origin and transport of atmospheric pollutants in Lanzhou. Results showed that the HYSPLIT model and CWT analysis methods are effective tools when analyzing external sources and their corresponding contributions (Sun et al. 2015, Perrone et al. 2018). However, it is difficult to clarify the temporal and spatial characteristics of air pollution processes under the combined action of internal and external sources in small-scale regions.

The internal sources of air pollution are studied using set pair analysis and the spatial interpolation method used by some scholars. Zhou et al. (2016) constructed the set pair analysis method for internal and external sources of $PM_{2.5}$ and then studied the proportion of internal to external sources in Dongguan. However, this study did not consider the spatial and temporal characteristics of the pollutants. Yang et al. (2018) employed a Spatiotemporal Ordinary Kriging (STOK) technique and analyzed the daily concentrations of $PM_{2.5}$ in southern Jiangsu province in 2014. Their results showed that 29.3% of the area was polluted by $PM_{2.5}$ in 2014. Additionally, the number of polluted days varied from 59 to 164 in different parts of the study region. The spatial interpolation method can be used to study the spatial and temporal distribution of pollutants, but previous studies typically focused on the correlation between a pollutant and various meteorological parameters. The correlation analyses speculated the causes of regional pollution but failed to consider that transport, emissions, and accumulation are affected by topography.

Previous studies failed to capture the complete life cycle of a pollutant (Zdun et al. 2016, Zhao et al. 2015, Liu et al. 2017). To fully understand the emission and transport of pollution, this study needs to track the trajectory of a pollutant, locate and quantify its sources, and consider the effects of topography. In this paper, the HYSPLIT method is adopted to determine the trajectory of an air mass and estimate air pollution sources. Then, the PSCF and CWT methods are used to quantify and analyze the internal pollution sources. Furthermore, spatial interpolation and topographic element methods are adopted to determine the temporal and spatial distribution characteristics of pollutants.

MATERIALS AND METHODS

Study Object and Data

Guilin was selected as the research area. Guilin covers an area of 27,809 km^2 and has a population of over 5 million. The research area borders Yongzhou and Shaoyang of Hunan Province in the northeast and Liuzhou in the south. All three are heavy industrial cities.

The topographical distribution of the study area is presented in Fig. 1. The west, north, and southeast regions are mountainous and have higher terrain. The central regions have relatively low terrain. There is a long narrow channel in the northeast between the Yuechengling and Dupangling-Haiyangshan Mountain chains. The depth of this channel, also known as the "Xiang-Gui Corridor," ranges from 600 to 1600 m between the mountain peak and the basin.

Guilin has lower pollution emissions than surrounding cities, but its air quality is significantly worse. The overall amount of $PM_{2.5}$ remains high, especially in Quanzhou County, Pingle County, Yongfu County, and downtown Guilin.

The research area contains 19 fixed atmospheric environmental quality automatic monitoring stations ("fixed stations" in short) and 51 mini ones ("mini stations" in short). Guilin University of Electronic Technology Yaoshan Station (Yaoshan Station) was selected as the background value reference station because it was considered to be free from the influence of internal sources. Yaoshan Station is 13 km from downtown Guilin. Vegetation covers more than 78% of this station, and consequently, this station is only weakly influenced by the air pollution from downtown.

The following basic data was used to analyze the sources and spatial distribution of air pollution in the research area: hourly average data of the 19 fixed stations in Guilin, including wind direction, wind speed, temperature, rainfall, barometric pressure, humidity, and $PM_{2.5}$ concentration; Landsat8 satellite 30 m resolution full-band image, administrative division data, and elevation DEM image data provided by Geographic Cloud; and the GDAS data (spatial resolution 1°×1°) provided by US National Centers for Environmental Prediction (Table 1).

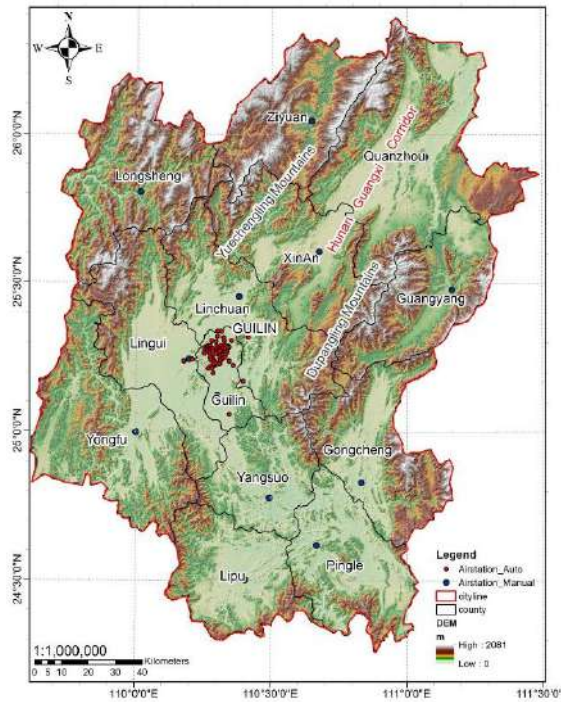

Fig. 1: Topography of the study area and distribution of monitoring stations.

Table 1: Datasheet.

Data category	Data contents	Data source	Time range	Resolution
Meteorological data	$PM_{2.5}$	Guilin Environmental Monitoring Station	2014.3–2019.6	Day
Meteorological analysis data	Wind speed, wind direction, temperature, rainfall, barometric pressure, moisture content	Guilin Environmental Monitoring Station	2017.7–2018.6	Day
Air mass trajectory data	GDAS data	NCEP	2017.7–2018.6	1°×1°
Geographic data	DEM data, Administrative division data	China Geographic cloud space website	2017.7–2018.6	30m×30m

Study Methods

The internal and external sources and the transport pattern of the air pollutants in the research area were analyzed using the data described above. First, the trajectory of the air mass was simulated for 365 consecutive days using the HYSPLIT4 model. Using a spatial clustering method, it was found that air pollution was transported from several directions. Second, the PSCF method was used to grid the potential source areas. Third, the CWT method was employed to quantify the grid value of the pollutants in the potential source areas. Fourth, four periods with severe pollution were selected. The changes of $PM_{2.5}$ were calculated using the spatial interpolation method, which analyzed the spatial and temporal distributions of pollutants. Finally, the temporal and spatial characteristics of air pollution in the study area under the influence of meteorological and topographic changes were discussed.

External Source Transmission

The HYSPLIT4 model was used to simulate the trajectory of an air mass for continuous periods to determine the direction of air pollutant transmission from external sources. The HYSPLIT4 model is a hybrid single-particle orbit model developed by the Air Resources Laboratory (ARL) under the US National Oceanic and Atmospheric Administration (NOAA). This model is used to calculate and analyze the trajectories of atmospheric pollutants and diffusion. Trajectories were categorized according to their spatial variation

(SPVAR) to obtain the relationship between the total spatial variation (TSV) (the sum of SPVAR) and n (the number of trajectories). Based on the clustering results, the locations of source regions were determined using the PSCF method. Then CWT method was used to quantify the pollution weight and thus estimate the total pollutants carried out.

(1) Potential Source Contribution Function - PSCF

The PSCF method determines the location of a pollution source by setting the atmospheric backward trajectory and the meteorological values. The PSCF function is defined as the conditional probability that the value of an element corresponding to the monitoring grid, namely $PM_{2.5}$ concentration, exceeds the set threshold when an air mass passing through an area reaches the monitoring grid. The PSCF value of the *i-th* grid within the research area is shown in Equation (1):

$$PSCF_i = \frac{m_i}{n_i} \quad \ldots(1)$$

where n_i and m_i separately represent the relative standing time of backward air quality and pollutant concentration in the retention area. The PSCF method calculates the contribution of the grid to pollutant concentrations in the research area.

(2) Concentration-Weighted Trajectory (CWT)

The PSCF method can determine the correlation between the corresponding element value and the threshold value of the trajectory in the grid. Therefore, the CWT method is used to quantify and analyze the weighted concentration of pollutants. The weighted concentration of grid *i* refers to the time-averaged concentration of monitoring points passing through grid *i*, as shown in Equation (2):

$$CWT_i = \frac{1}{\sum_{l=1}^{t} n_{il}} \sum_{i=1}^{t} C_{il}, \quad \ldots(2)$$

Where CWT_i denotes the weighted concentration of grid *i*, *l* denotes the serial number of the trajectories, *t* denotes the total number of trajectories, n_{il} denotes the time spent by *l-th* trajectory passing through grid *i*, and C_{il} is the $PM_{2.5}$ concentration of trajectory *l* while passing through grid *i*.

Internal Source Diffusion

A spatial interpolation method was used for the internal source diffusion analysis. The regional changes in concentration were estimated, and the influence of internal sources was analyzed, as were the topographic characteristics.

If it is assumed that there are *n* points of actual measurements within the area of point x_0, namely $x_1, \ldots, x_n$. Then, the Kriging interpolation method is expressed as Equation (3):

$$Z^*(x_0) = \sum_{i=1}^{n} P_i Z(x_i), , \quad \ldots(3)$$

where $Z^*(x_0)$ denotes the concentration grid values of $PM_{2.5}$; *n* stands for the number of stations used for $PM_{2.5}$ interpolation; $Z(x_i)$ is the average $PM_{2.5}$ concentration of *i-th* station, and P_i is the undetermined weighting coefficient. After the unbiased minimum variance estimation is executed, Equation (4) is derived by introducing the Lagrange coefficient *Q*:

$$\sum_{i=1}^{n} P_i C(x_i, x_j) + Q = C(x_0, x_j), \; j = 1, 2, \ldots n \quad \ldots(4)$$

$$\sum_{i=1}^{n} P_i = 1, \quad \ldots(5)$$

where $C(x_i, x_j)$ is the co-variance function of $Z(x_i)$ and $Z(x_j)$ in Equation (4). Equations (4) and (5) are combined to get the weighting coefficient $P_i (i = 1, 2, \ldots, n)$ and Lagrange coefficient *Q*. Then, the interpolation estimation of any point within the research area can be obtained by Equation (3).

The Kriging interpolation method is employed to reflect the accumulation of $PM_{2.5}$ and the changes in its concentration in different areas. The landscape's influence on $PM_{2.5}$ transport is also determined. Therefore, the air pollution emission is influenced by both the transport of air pollution from external sources, and the diffusion of air pollution from internal sources.

RESULTS AND DISCUSSION

Pollution Characteristics

Data was collected from Yaoshan Station, Longyin Station, Guilin Environmental Monitoring Station, and No. 8 Middle School Station from 2014 to 2019, and then the data was analyzed to determine changes in $PM_{2.5}$ in different regions. As shown in Fig. 2, the Yaoshan Station presented lower concentrations. The $PM_{2.5}$ concentrations at this station were highest from December to January of the following year and lowest from June to July.

The pollution and meteorological conditions differed significantly from March to August (Period 1) and September to February of the following year (Period 2). Table 2 summarizes the results from Fig. 2. The atmospheric pressure is less correlated with the meteorological parameter ($PM_{2.5}$, PM_{10}), and the humidity is directly related to rainfall. The corresponding statistical results were not listed in Table 2.

(1) $PM_{2.5}$ concentration: During Period 1, $PM_{2.5}$ concentrations were greater than 70 $\mu g.m^{-3}$ and less than 20

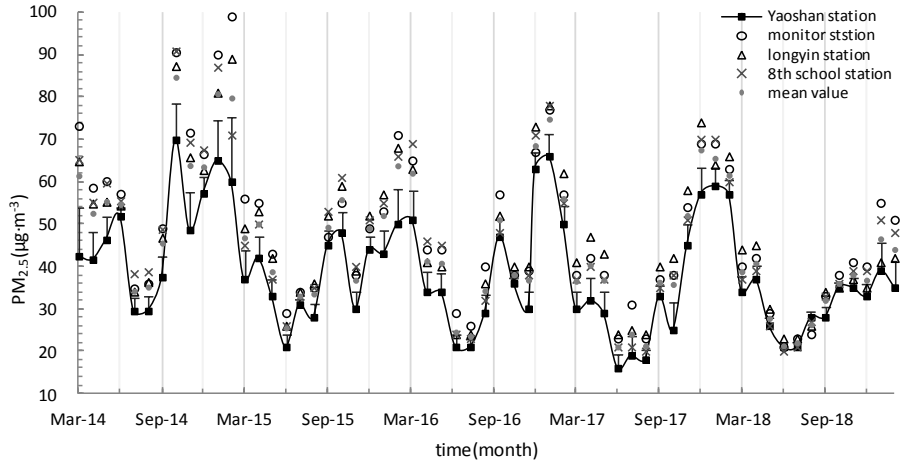

Fig. 2: Comparison of atmospheric environmental quality data of fixed stations in 2014-2019.

μg.m^{-3}, and between these two values accounted for 2%, 44%, and 54% of the observed $PM_{2.5}$ concentrations, respectively. During Period 2, $PM_{2.5}$ concentrations were greater than 70 μg.m^{-3} and less than 20 μg/m^3, and between these two values accounted for 21%, 20%, and 59%, of the observed $PM_{2.5}$ concentrations, respectively.

(2) Wind direction: During Period 1, eight wind directions had relatively uniform values, with westerly winds and northwesterly winds occurring 4% and 5% of the time, respectively. During Period 2, northerly and northwesterly winds were most frequent and accounted for 43% and 25% of all the winds, respectively.

(3) Wind speed: During Period 1, weak winds occurred the most frequently. As shown in Table 2, 95% of the observed wind was less than 3.5 m.s^{-1}. During Period 2, strong winds occurred with greater frequency, and only 83% of the observed winds were less than 3.5 m.s^{-1}.

(4) Temperature: During Period 1, the temperatures between 15°C and 30°C accounted for 72% of the observed temperature. Temperatures below 15°C and above 30°C accounted for 16% and 12%, respectively. During Period 2, the temperatures between 10°C and 25°C accounted for 62% of the observed temperature, while temperatures below 10°C and above 25°C accounted for 25% and 13%, respectively.

(5) Rainfall: During Period 1, there was no rainfall 41% of the time. Rainfall between 0.1 and 20 mm occurred on 56% of the days, and more than 20 mm of rainfall occurred on 3% of the days. During Period 2, there was no rainfall 79% of the time, rainfall between 0.1 and 20 mm occurred 21% of the time, and more than 20 mm rainfall occurred 0% of the time.

To summarize, Period 1 typically had temperatures ranging from 15°C to 30°C. This period also had weak, uniform wind directions, larger amounts of precipitation, bad meteorological conditions for pollutant diffusion, and low $PM_{2.5}$ concentrations. Period 2 primarily had temperatures between 10°C and 25°C, strong northeasterly and northerly winds, little rainfall, good meteorological conditions for pollutant diffusion, and high $PM_{2.5}$ concentrations.

Table 2: Proportion of pollution characteristics in Guilin from July 2014 to June 2019.

$PM_{2.5}$ (μg/m^3)	Period one (%)	Period two (%)	wind direction	Period one (%)	Period two (%)	wind speed (m/s)	Period one (%)	Period two (%)	temperture (℃)	Period one (%)	Period two (%)	rainfall (mm)	Period one (%)	Period two (%)
0~20	44%	20%	N	12	25	0~0.5	27	12	0~5	0	2	0	41	79
21~30	23%	15%	NE	20	43	0.6~1.0	26	20	6~10	3	23	0.1~1	21	9
31~40	16%	16%	E	9	5	1.0~1.5	13	14	11~15	13	24	1~2	8	3
41~50	8%	1%	SE	10	4	1.6~2.0	11	11	16~20	12	17	2~3	4	3
51~60	5%	15%	S	17	3	2.1~2.5	8	12	21~25	29	21	3~5	6	2
61~70	2%	12%	SW	23	6	2.6~3.0	6	9	26~30	31	10	5~10	7	3
71~90	2%	11%	W	4	5	3.1~3.5	4	8	31~35	11	3	10~20	10	1
⩾90	0%	10%	NW	5	9	⩾3.6	5	14	⩾35	1	0	>20	3	0

Note: Period 1 is from March to August, and Period 2 is from September to February of the following year.

The research area is located in a subtropical zone, with little demand for heat in the winter and little seasonal difference in atmospheric pollution emissions. Period 1 had more unfavorable meteorological conditions for pollutant diffusion than Period 2, but the air quality was better. This indicates that the transport of pollutants from external sources needs to be focused on.

Table 3 showed the variation of $PM_{2.5}$ concentration from December 8 to 19 in 2019. As a background station, the variation of $PM_{2.5}$ concentration at Yaoshan station was quite different from the other three stations. In the monitoring period, $PM_{2.5}$ concentration at Yaoshan station increased rapidly compared to other stations. After that, $PM_{2.5}$ concentration at the other three stations just began to increase, which reflected the spatial differences of stations.

Analysis of External Source Transmission

The HYSPLIT4 model was used to calculate the backward air mass trajectory in the research area, while the PSCF and CWT methods were used to locate and quantify the trajectory sources.

Analysis of trajectory simulation results: The first simulation used the Guilin Environmental Monitoring Station as the target. The simulated altitude was 1000 m, which corresponds to 700 m in Guilin. The simulation ran from July 1, 2017, to June 30, 2018, and 48 hours was used as the backward trajectory parameter. The TSV changed over 30%, indicating an acceptable allocated clustering number. The 365-day air mass trajectory lines were organized into three categories: Trajectories ①, ② and ③ (Fig. 3).

Trajectory fractal number and spatial distribution are shown in Table 4.

The majority of the air masses were transported along Trajectory ②. This trajectory also had the highest $PM_{2.5}$ concentrations. The two parameters during Period 2 were higher than those in Period 1, which demonstrates better atmospheric quality during Period 1 (Table 2).

Trajectory ① originated from the south of the research area, and 25.62% of the air masses were transported along this path. The average concentration of $PM_{2.5}$ for this trajectory was 39.47 $\mu g.m^{-3}$, the lowest among the three trajectories. Its daily frequency of pollution was 12.63%. The trajectory ②was the largest and originated from the northeast. Its average concentration of $PM_{2.5}$ was 45.94 $\mu g.m^{-3}$, however, the daily frequency of pollution was 14.41%, which was significantly higher than trajectories ① and ③. The trajectory ③ had a length of 662.9 km and originated from the southwest, and had the least quantity of air masses (11.29%). Its average concentration of $PM_{2.5}$ was 55.27 $\mu g.m^{-3}$, however, its daily frequency of pollution was only 9.7%.

Yaoshan station was regarded as the background value station of external pollution. The clustering results of the air masses and $PM_{2.5}$ concentrations were used to divide pollution sources into internal and external sources and calculate their proportion. The results are shown in Table 5.

External sources were responsible for more than 76% of the pollution, on average. Referring back to Table 4, the air quality was good, and the pollution in period 1 was generally lower.

Table 3: $PM_{2.5}$ concentration at four stations from December 8 to 19 in 2019.

$PM_{2.5}(\mu g.m^{-3})$	8th School station	Longyin station	Monitor station	Yaoshan station
Dec-8	31	34	32	66
Dec-9	38	41	39	72
Dec-10	75	75	68	90
Dec-11	92	93	89	123
Dec-12	94	101	98	128
Dec-13	98	103	93	93
Dec-14	129	136	121	85
Dec-15	128	134	122	68
Dec-16	95	98	96	45
Dec-17	82	88	85	36
Dec-18	75	78	76	30
Dec-19	49	65	59	42

In the second period, pollution was more severe. External sources contributed 84.7% of the total pollution, and Trajectory ① accounted for the highest proportion (95.1%). External sources accounted for 83% of the annual pollution, of which Trajectory ③ accounted for the highest proportion (94.2%). The contribution of external pollution from the "Xiang Gui corridor" (Trajectory②) was 83.2%. Trajectory ② mainly represented pollution from external sources. In Trajectory ③, the contribution of pollution from external sources was high, but few air masses were transported along this trajectory. Therefore, this trajectory could not represent the primary cause of pollution in the study region.

The majority of the air masses traveled along Trajectory ②. It is not surprising that this trajectory carried more pollutants and had higher $PM_{2.5}$ concentrations. Trajectory ③also had high concentrations of $PM_{2.5}$, but fewer air masses were transported along this trajectory. The trajectory 1 concentration of $PM_{2.5}$ was close to the value of the target area.

Trajectories ① and ③ had longer transmission distances and low $PM_{2.5}$ concentrations. These trajectories do not transport enough pollution from external sources and should be taken as the main direction for the diffusion of internal source pollution in the research area. Additionally, by comparison in Table 4, Fig. 3, and Fig. 1, it was found that Trajectory ② was coincident with the "Xiang-Gui Corridor." It showed that this area should be taken as the key point for impact analysis of topographical changes.

PSCF result analysis: The daily mean concentration of $PM_{2.5}$ (75 $\mu g.m^{-3}$) was used as the threshold. The total residence time of the trajectory in the grid and the daily average value was 48 h. The simulation was run for 365 days, and 10 days was used as the average residence time in the grid. To

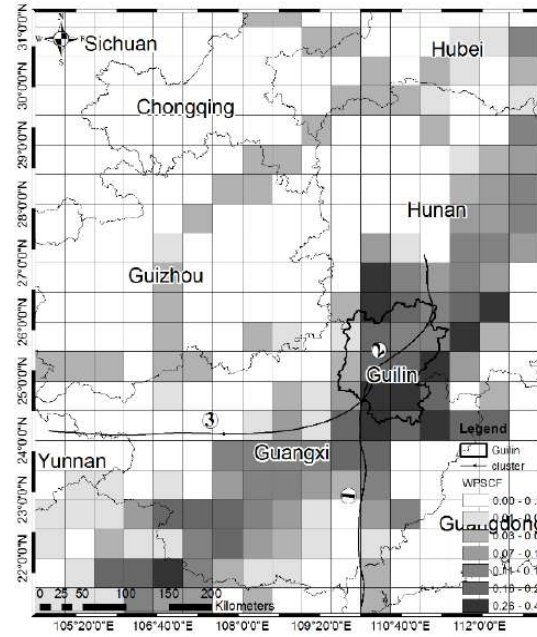

Fig. 3: The WPSCF distribution and clustering analysis results of backward trajectory

Table 4: Result analysis of trajectory clustering.

cluster	period one trajectory (number)	period one $PM_{2.5}$ ($\mu g/m^3$)	period two trajectory (number)	period two $PM_{2.5}$ ($\mu g/m^3$)	year trajectory (number)	path length（km）	year trajectory number ratio（%）	year $PM_{2.5}$ ($\mu g/m^3$)	PM2.5>75（number）	day pollution frequency（%）
1	34	47.9	61	33.21	95	448.5	25.62	39.47	12	12.63
2	125	54.64	104	35.48	229	276.2	63.09	45.94	33	14.41
3	23	75.33	18	29.63	41	662.9	11.29	55.27	4	9.7
all	182	57.37	183	34.15	365	1387.6	100	45.05	50	13.71

Note: Period 1 is from March to August, and Period 2 is from September to February of the following year

Table 5: Proportion of internal and external pollution sources in different periods.

cluster	Period 1 $PM_{2.5}$ proportion of external pollution sources	Period 1 $PM_{2.5}$ proportion of internal pollution sources	Period 2 $PM_{2.5}$ proportion of external pollution sources	Period 2 $PM_{2.5}$ proportion of internal pollution sources	Annual $PM_{2.5}$ proportion of external pollution sources	Annual $PM_{2.5}$ proportion of internal pollution sources
1	76%	23%	95.10%	4.90%	73.80%	26.20%
2	76.40%	23.60%	84%	16%	83.20%	16.80%
3	80.10%	19.90%	88%	12%	94.20%	5.80%
ALL	76.70%	23.30%	84.70%	15.30%	83%	17%

avoid distortion caused by too high PSCF values in grids n_i, empirical weight function, W_i, was introduced:

$$W_i = \begin{cases} 1.0 & n_i > 10 \\ 0.7 & 5 < n_i \leq 10 \\ 0.42 & 2 < n_i \leq 5 \\ 0.17 & n_i \leq 2 \end{cases} \quad . \qquad \ldots (6)$$

This formula indicates values of W_i when n_i trajectories pass through grids *i* at the above time points. The PSCF value is then given by $WPSCF_i = PSCF_i \times W_i$.

The WPSCF values were distributed as the grid values of Fig. 3. The northeast grid had large gray values, which indicated that the air pollution was transported along Trajectory ②. Therefore, the source was located in the grid in the northeast of Trajectory ②. Trajectories ① and ③ had smaller grid values outside the research area and larger values within the research area, which suggests that the internal pollution source was consistent with the results obtained from the trajectory data.

CWT results analysis: The PSCF method was used to analyze the influence of pollution in the research area from a semi-quantitative perspective. The CWT method was also used to determine the source of the pollutants. The backward trajectories are shown in Fig. 4. The trajectories from the northeast and south are presented as dark grids in a consistent direction of the cluster trajectory line. By comparison, areas with dark grids could coincide in Fig. 3 and Fig. 4, indicating that the sources were located in the northeast and south of the research area.

Characteristics of external source transmission: According to the WCWT distribution and clustering results of backward trajectories, it is known that (1) Trajectory ② accounted for 63.09%, with an average $PM_{2.5}$ concentration of 45.94 μg.m^{-3}. (2) The dark grids were in the northeast, implying that the "Xiang-Gui Corridor" is the source of the pollutants. (3) Dark grids were also located in the north and northeast of the research area, where there is a lot of industries. In other areas of the research region, the darker grids coincided with trajectories ① and ③.

Based on the above analysis, it can be inferred that the air pollution in the research area was emitted from a combination of external sources (i.e., from the "Xiang-Gui Corridor") and internal sources.

Analysis of Internal Source Pollution

The previous section analyzed external sources of air pollution and air mass trajectories. It is natural to next consider how external and internal sources jointly impact pollution using a spatial interpolation method.

As shown in Table 4, $PM_{2.5}$ concentrations peaked between September 2017 and February 2018. Four pollution events were selected to interpolate the mean $PM_{2.5}$ concentrations from 19 stations using the Kriging interpolation method. The four events chosen were from October 31 to November 9, December 13 to December 22, December 28 to January 6, and January 23 to February 1. The results are shown in Fig. 5.

$PM_{2.5}$ concentrations were high in Quanzhou County and urban areas. However, the $PM_{2.5}$ concentration in Longsheng County and Gongcheng County was relatively low. This is consistent with Fig. 3 and Fig. 4, which showed that the external source of pollution came from the northeast. During the four pollution events, Ziyuan County, the northeast of Xing'an County, and Guanyang in the "Xiang-Gui Corridor" showed relatively low $PM_{2.5}$ concentrations.

The distribution of the blue belt varied with the pollution events. Its core area was northeast of Xing'an County, with the Yuechengling Mountains to the northwest and the Ocean Mountains in the Dupangling Mountains to the southeast. The peaks affect the direct transport of the air masses and form obvious weakening zones. The Yaoshan Mountains to the northeast of the urban areas act as barriers and prevent

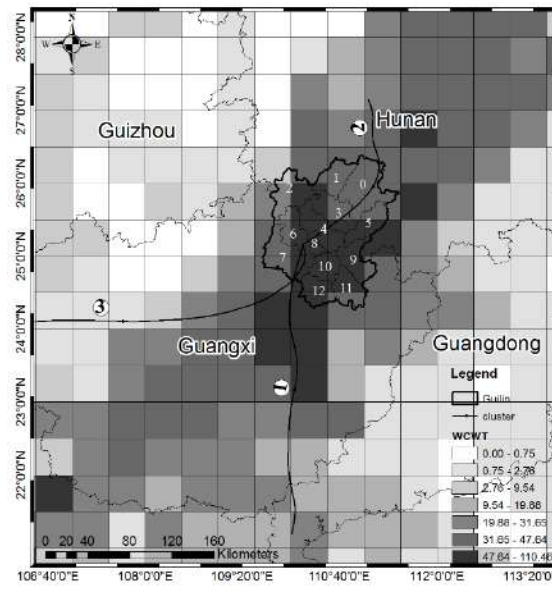

Note: 0 Quanzhou County, 1 Ziyuan County, 2 Longsheng County, 3 Xing'an County, 4 Lingchuan County, 5 Guanyang County, 6 Lingui County, 7 Yongfu County, 8 the urban area, 9 Gongcheng County, 10 Yangshuo County, 11 Pingle County, and 12 Lipu County

Fig. 4: The WCWT distribution and clustering analysis results of backward trajectory

the air masses from directly entering the urban areas, causing the four pollution events.

The four periods in Fig. 5 all showed that Quanzhou County in the northeast and the urban areas in the center contain high concentrations of pollution. This shows the effect of the internal and external sources and suggests that while Quanzhou County is affected by the northeastern air mass, the internal sources also contribute toward the accumulation of pollution in the urban areas.

CONCLUSIONS

This study focused on the sources and transport of $PM_{2.5}$ in the city of Guilin. A combination of $PM_{2.5}$ daily average and meteorological parameters data, and simulations using the HYSPLIT model were used to analyze pollutant sources, internal source diffusion, and the effect of topography on pollutants in the research area. Conclusions could be drawn as follows.

1. From 2014 to 2019, heavy pollution periods in the research area occurred from September to February.

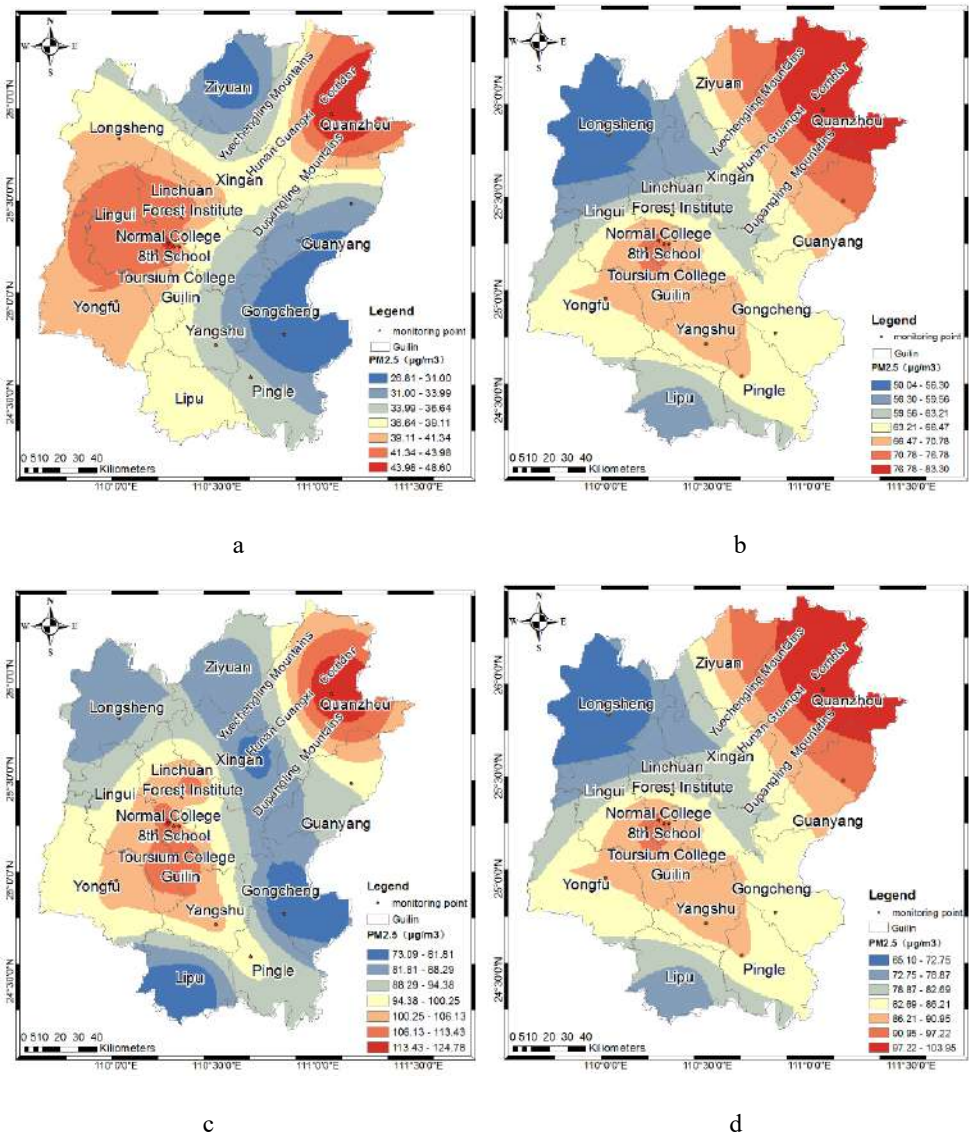

Note: A: October 31 to November 9, B: December 13 to December 22, C: December 28 to January 6, D: January 23 to February 1

Fig. 5: The interpolation results of four pollution processes in Winter in Guilin.

2. External sources were predominantly from the northeast direction, and the trajectory of the pollutants coincided with the "Xiang-Gui Corridor." Potential source areas were concentrated in industrial regions in the Hunan Province, which lies to the northeast of the research area. The internal sources were located to the south and southeast. In particular, pollution originated in Yongfu County, Lipu County, and Pingle County.
3. Multiple pollution events showed that the temporal and spatial characteristics of pollutant transport were affected by special terrain. The "Xiang-Gui Corridor" was affected by external sources in the northeast and formed a regional center of atmospheric pollution. The urban areas, which were under the influence of internal, southern, and southeastern sources, formed a second regional center.

ACKNOWLEDGMENTS

This work was supported by the National Natural Science Foundation of China [grant number 41967042]; the State-supported Special Fund Project for Local Science and Technology Development [grant number ZY1949005]; the Guangxi Key Research and Development Program [grant number AB18221108]; the Guilin Key Scientific Research and Technological Development Program (grant number 20190213-1).

REFERENCES

Arif, M., Kumar, R., Kumar, R., Eric, Z. and Gourav, P. 2018. Ambient black carbon, $PM_{2.5,}$ and PM_{10} at Patna: Influence of anthropogenic emissions and brick kilns. Sci. Total Environ., 624: 1387-1400.

Bai, X., Zhang, Y., Wang, C. and Tan, Y. 2016. Analysis of climate resources impact on Guilin international resort tourism development. Int. J. Environ. Protect. Policy, 4(6): 196-200.

Cui, J., Lang, J., Chen, T., Cheng, S. and Chen, S. 2019. Emergency monitoring layout method for sudden air pollution accidents based on a dispersion model, fuzzy evaluation, and post-optimality analysis. Atmos. Environ., 222: 117124.

Jiang, N., Yin, S., Guo Y., Li, J., Kang, P., Zhang, R. and Tang, X. 2018. Characteristics of mass concentration, chemical composition, source apportionment of PM25 and PM10, and health risk assessment in the emerging megacity in China. Atmos. Pollut. Res., 9(2): 309-321.

Liu, B., Wu, J., Zhang, J., Wang, L., Yang, J., Liang, D., Dai, Q., Bi, X., Feng, Y., Zhang, Y. and Zhang, Q. 2017. Characterization and source apportionment of PM2.5 based on error estimation from EPA PMF 5.0 model at a medium city in China. Environ. Pollut., 222: 10-22.

Liu, N., Yu, Y., He, J. and Zhao, S. 2013. Integrated modeling of urban-scale pollutant transport: application in a semi-arid urban valley, Northwestern China. Atmos. Pollut. Res., 4(3): 306-314.

Luan, T., Guo, X., Guo, L. and Zhang, T. 2018. Quantifying the relationship between PM2.5 concentration, visibility, and planetary boundary layer height for long-lasting haze and fog-haze mixed events in Beijing. Atmos. Chem. Phys., 18(1): 203-225.

Mukherjee, A. and Agrawal, M. 2018. Assessment of local and distant sources of urban $PM_{2.5}$ in the middle Indo-Gangetic plain of India using statistical modeling. Atmos. Res., 213: 275-287.

Perrone, M.G, Vratolis, S,. Georgieva, E., Török, S., Šega, K. Veleva, B.. Osán, J., Bešlić, I., Kertész, Z., Pernigotti, D., Eleftheriadis, K. and Belis, C. A. 2018. Sources and geographic origin of particulate matter in urban areas of the Danube macro-region: The cases of Zagreb (Croatia), Budapest (Hungary), and Sofia (Bulgaria). Sci. Tot. Environ., 619-620: 1515-1529.

Sun, K., Liu, X., Gu, J., Li, Y., Qu, Y., An, J. Wang, J. 2015. Chemical characterization of size-resolved aerosols in four seasons and hazy days in the megacity Beijing of China. J. Environ. Sci., 32: 5-167.

Sun, R., Fan, L. and Chen, Z., 2019. Temporal and spatial distribution characteristics of atmospheric PM 2.5 concentrations in Guiyang, China. Nat. Environ. Pollut. Technol., 18(2).

Wang, M., Cao, C., Li, G. and Singh, R. P. 2015. Analysis of a severe prolonged regional haze episode in the Yangtze River Delta, China. Atmos. Environ., 102: 112-121.

Yang, X., Wu, Q., Zhao, R., Cheng, H., He, H., Ma, Q., Wang, L. and Luo, H. 2019. A new method for evaluating winter air quality: PM2.5 assessment using Community Multi-Scale Air Quality Modeling (CMAQ) in Xi'an. Atmos. Environ., 4: 18-28.

Yang, Y., Christakos, G., Yang, X. and He, J. 2018. Spatiotemporal characterization and mapping of PM2.5 concentration in southern Jiangsu province, China. Environ. Pollut., 234: 794-803.

Zdun, A., Rozwadowska, A. and Kratzer, S. 2016. The impact of air mass advection on aerosol optical properties over Gotland (Baltic Sea). Atmos. Res., 182: 142-155.

Zhang, Q., Xue, D., Liu, X., Gong, X. and Gao, H. 2019. Process analysis of PM2.5 pollution events in a coastal city of China using CMAQ. J. Environ. Sci., 5(79): 225-238.

Zhang, Y., Li, X., Nie, T., Qi, J., Chen, J. and Wu, Q. 2018. Source apportionment of PM2.5 pollution in the central six districts of Beijing, China. J. Clean. Prod., 174: 661-669.

Zhao, Y. Z., Man, S. W. and Kwon, H. L. 2015. Estimation of potential source regions of PM2.5 in Beijing using backward trajectories. Atmos. Pollut. Res., 6(5): 173-177.

Zhou, Y., Zhou, J. and Xiao, R. 2016. Research for regional contribution rate of internal source and external source of PM2.5 based on a set pair analysis method. Meteorol. Environ. Res., 2: 36-40+44.

Nature Environment and Pollution Technology
An International Quarterly Scientific Journal

p-ISSN: 0972-6268
(Print copies up to 2016)
e-ISSN: 2395-3454

Vol. 20 | No.3 | pp. 1097-1106 | 2021

Original Research Paper

https://doi.org/10.46488/NEPT.2021.v20i03.017

Open Access Journal

Water Erosion, its Relationship to Total Suspended Solids and Water Quality in the Lower Basin of the Usumacinta River, Tabasco, Mexico

G. Rodríguez-Martínez*†, I. Galaviz-Villa*, S. Partida-Sedas, C.A. Sosa-Villalobos*, R. de G. Bernal-Ramírez*, V. Alcántara-Méndez* and A. García-Saldaña****

*Tecnológico Nacional de México/Instituto Tecnológico de Boca del Río, carretera Veracruz- Córdoba km 12 C.P. 94290. Boca del Río, Veracruz, México.

**Tecnológico Nacional de México/ Instituto Tecnológico Superior de Huatusco, Av. 25 Poniente No.100, col. Reserva Territorial Huatusco, Veracruz, México, C.P. 94100.

†Corresponding author: G. Rodríguez-Martínez; guadaluperguezmtz@gmail.com

Nat. Env. & Poll. Tech.
Website: www.neptjournal.com

Received: 10-09-2020
Revised: 23-11-2020
Accepted: 12-12-2020

Key Words:
Agricultural waste
Erosion risk
Loss of fertile soil
Water quality

ABSTRACT

Total suspended solids are an indicator of material constituted by sedimentable solids, suspended solids, and colloidal, whose origin is erosion, wastewater discharges, and agricultural waste. The objective of this research was to determine territorial water erosion, its relation with total suspended solids, and the water quality in the lower basin of the Usumacinta River in Tabasco. Three sampling points were established, located in the municipalities of Tenosique, Emiliano Zapata, and Jonuta, in the state of Tabasco. Water samples were collected during 12 monthly sampling campaigns in an annual cycle, and the total suspended solids were determined according to the provisions of the NMX-AA-034-SCFI-2015 standard. Water erosion was calculated based on the Universal Soil Loss Equation (USLE) and with the use of geographic information systems (GIS). The results obtained were statistically analyzed, finding that the measured maximum TSS concentrations are 130.92 $mg.L^{-1}$ in Boca del Cerro, 165.28 $mg.L^{-1}$ in Chablé, and 113.91 $mg.L^{-1}$ in Jonuta which are within the permissible concentrations for protection of freshwater aquatic life and agricultural irrigation according to ecological criteria of water quality (CE-CCA-001/89), in Mexico. The lower basin of the Usumacinta River has areas with extreme erosion (990 $tons.ha^{-1}yr^{-1}$), with conditions that accelerate the erosion process, such as annual rainfall between 1805 mm and 2250 mm, clay soils located on slopes greater than 16%, and agricultural soils. These events cause loss of the soil fertile layer where agriculture is developed, also giving rise to the accelerated transport of suspended solids; which negatively alter the quality of the water of the Usumacinta River.

INTRODUCTION

Of the total border basins in Mexico, the Usumacinta River is the one with the largest extension and hydrological development. It covers an area of more than seven million hectares distributed in three countries; 58% correspond to Guatemala, 41.91% to Mexico, and 0.001% to Belize (Soares & García 2017). According to its physical characteristics of relief, hydrology, and altitude, the Usumacinta River basin can be divided into three sectors: low basin (21.5%), medium (48.5%), and high (30%) (March & Castro 2010). Tabasco's economy is based on the development of agriculture, livestock, forestry, fishing, industry, commerce, and tourism; agriculture and livestock being the main activities in the municipalities of Tenosique, Emiliano Zapata, and Jonuta (INEGI 2016). These activities cause soil degradation from the physical, chemical, and biological point of view, manifesting as erosion (Alvarado-Cardona et al. 2007).

At present, there is a combination of factors that accelerate the erosion phenomenon of the Grijalva-Usumacinta basin, causing 83% to present a medium to a high level of erosion risk, and only 17% present a low-risk level (Sánchez-Hernández et al. 2013). Eroded soil is transported by runoff to surface water bodies, turning into sediments. In this regard, Paz González (2004) indicated that when the drag force decreases, the thicker particles begin to settle in areas of less slope, while the finer materials are often held in suspension in the perennial stream.

Total suspended solids in surface water are an indicator of material constituted by sedimentable solids, suspended solids, and colloidal, whose origin is wastewater discharges, soil erosion, and agricultural waste (CONAGUA 2018). Suspended solids modify the penetration of light in water in addition to affecting photosynthesis, temperature, and turbidity processes (Vargas & Linero 2017). Therefore, the objective of this work was to determine territorial water

Table 1: Geographical location of sampling sites.

Municipality	Sampling site	UTM Coordinates 15 N Zone	
		(X)	(Y)
Tenosique	Puente Boca del Cerro (R1)	660265.3	1927441.6
Emiliano Zapata	Puente Chablé (R2)	628676.6	1974718.7
Jonuta	Puente Jonuta (R3)	587847.4	2001480.2

erosion, its relation with total suspended solids, and the water quality of the lower basin of the Usumacinta River.

MATERIALS AND METHODS

Study Area

Sampling sites are located in the municipalities of Tenosique, Emiliano Zapata, and Jonuta in the state of Tabasco (Table 1, Fig. 1).

Sampling

Ten sampling campaigns were carried out from May to December 2018, and from May to June 2019. Water samples were collected monthly based on the CAQAF4-01 procedure, which establishes methodology and criteria for collecting, handling, packaging, preserving, and transferring samples, during prevailing seasons in Tabasco - rainy (June-November) and dry season (December-May). In addition, 20 composite soil samples were collected (each one made up of 16 subsamples or simple samples), in accordance with the procedure established by NOM-021-RECNAT-2000, which establishes specifications for fertility, salinity and soil classification, study, sampling, and analysis.

Laboratory Analysis

Total suspended solids (TSS) were characterized in surface waters of the lower basin of the Usumacinta River, Tabasco, according to the method established in the NMX-AA-034-SCFI-2015 standard. The granulometric analysis and the determination of soil texture were carried out in accordance with the AS-28 and AS-09 methods established in NOM-021-RECNAT-2000.

Statistical Analysis

Descriptive statistics was used to compare the results of physicochemical analyzes with the Ecological Criteria for Water Quality (CE-CCA-001/89) in Mexico, and interna-

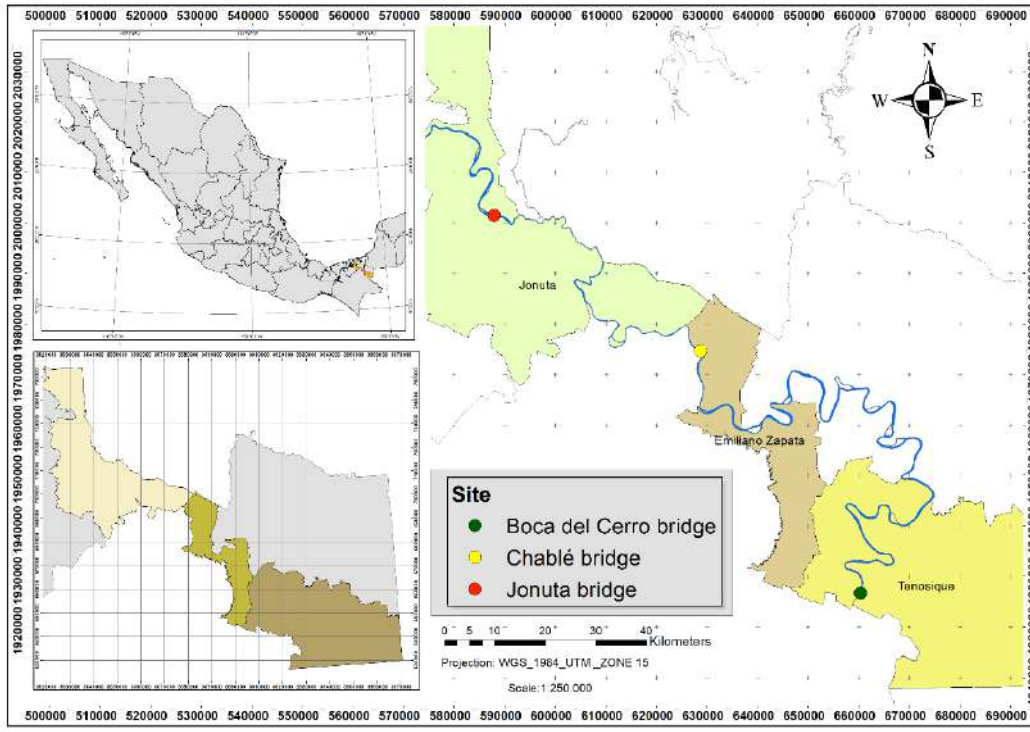

Fig. 1: Location of sampling sites in the lower basin of the Usumacinta River, Tabasco.

Table 2: Concentration of total suspended solids (TSS) recorded at sampling sites and mentioned in Normativity of Mexico and the USA (mg.L^{-1}).

Statistical	TSS Concentration			Normativity	
	R1 Boca del Cerro	R2 Chablé	R3 Jonuta	CE-CCA-001/89	US-EPA-2001/2003
Media	95.70	91.10	69.94		
Standard Dev.	35.22	74.18	43.97	50[a]	50[a]
Maximum	130.92	165.28	113.91	500[b]	150[c]
Minimum	60.48	16.92	25.96		

(a): For agricultural irrigation; (b): For drinking water supply source; (c): For protection of freshwater aquatic life.

tionally, with the Water Quality Criteria of the United States Environmental Protection Agency (US-EPA 2001/2003).

Water Erosion

Water erosion was determined based on the Universal Soil Loss Equation (USLE) (Wischmeier & Smith 1978), and the ArcGIS information system (version 10.3) with which the georeferenced information is represented. The equation consists of six factors that influence the erosion process:

$$A = R*K*LS*CP$$

In which *A* is the estimation of average annual soil loss (tons.ha^{-1}.yr^{-1}); *R* is the rainfall erosivity factor, accounts for the energy and intensity of rainstorms (MJ.mm.ha^{-1}h^{-1}); *K* is the soil erodibility factor and measures the susceptibility of a soil to erode under a standard condition (tons.h.MJ^{-1} mm^{-1}); *LS* is the slope length and steepness factor, accounts for the effect of length and steepness of slope on erosion; *C* is the cover and management and crop factor and estimates the soil loss ratio for 4 or 5 crop stage periods throughout the year, accounting for the combined effect of all the interrelated cover and management variables; *P* is the support practice factor, accounts for the effect of conservation support practices, such as contouring, contour strip cropping, and terraces on soil erosion.

For the determination of each of the factor, the annual precipitation obtained from the database of the Ensenada Scientific Research Center and Higher Education databases (CLICOM 2017) and the digital elevation model of the basin in scale 1: 50,000 (INEGI 2015) were used, in addition to the granulometry and soil texture data generated in this study. Also, the types of land use and vegetation of the study area were considered (INEGI 2016).

RESULTS

Total Suspended Solids

The results of maximum TSS concentrations obtained at site R1 (130.92 mg.L^{-1}), R2 (165.28 mg.L^{-1}), and R3 (113.91 mg L^{-1}) comply with the ecological criteria for water quality (CE-CCA -001/89) established for water supply sources, however, exceeding the criteria for agricultural irrigation use. According to the Environmental Protection Agency (US-EPA 2001/2003), the quality criteria for drinking water supply sources are not met, noting that site R2 exceeds the limits that guarantee the protection of aquatic life in freshwater (Table 2). In general, the water quality of the river is worse in the upper part of the lower basin, although the maximum TTS concentration was observed in the middle part of it. The water quality is good for irrigation and river ecology but it is bad for drinking purposes and needed treatment considering this parameter among many others. It should be noted that the Usumacinta River is the principal source of drinking water supply for the municipalities of Tenosique (Boca del Cerro) and Jonuta.

The concentration of TSS registered in Boca del Cerro (R1) was 163 mg.L^{-1}. In the rainy season, June is when the highest TSS concentration was recorded, while in the dry season, for April and May, concentrations of TSS were not detected (Fig. 2).

Regarding the concentration of total suspended solids registered in Chablé, during the rainy season (in June 2018), it was 300 mg.L^{-1}. On the other hand, in the dry season (in May 2018 and 2019), the detected concentration was 13 mg L^{-1} (Fig. 3). Furthermore, the concentration of TSS recorded in Jonuta was 133 mg.L^{-1} at the end of June. In May (2018 and 2019), the concentration of TSS detected was 14 mg.L^{-1}, while at the end of the dry season, in the first week of June, it was 18 mg.L^{-1} (Fig. 4).

Rainfall Erosivity factor (R)

Results obtained in this study show that the municipality of Jonuta has the lowest erosivity value (24,225.14 MJ.mm. ha^{-1}h^{-1}), while its average annual rainfall is 1,805 mm. On the other hand, Tenosique (where the sampling site Boca del Cerro is located) presents a maximum value of 36,258.55 MJ.mm.ha^{-1}h^{-1} while its average annual rainfall is 2,250

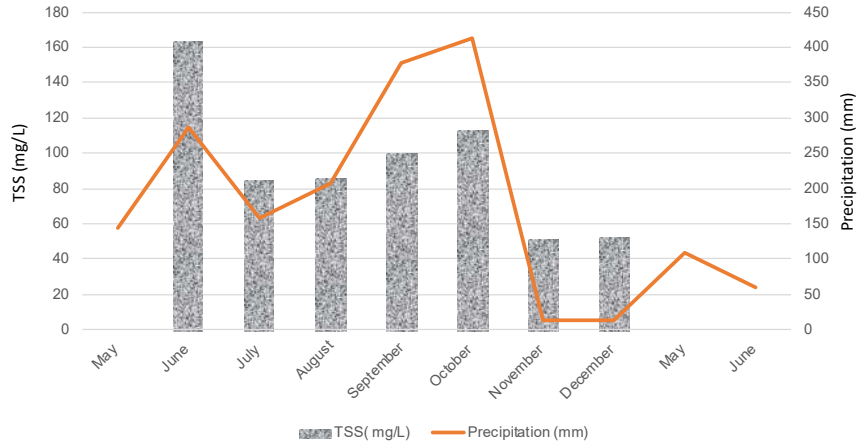

Fig. 2: TSS concentration registered in Boca del Cerro (R1) in the rainy season (June-November, 2018) and dry season (December-May, 2019).

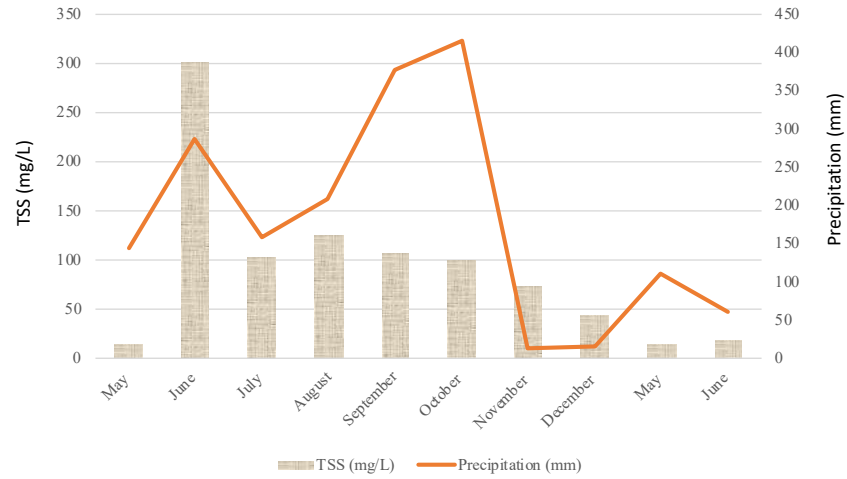

Fig. 3: TSS concentration recorded in Chable (R2) in the rainy season (June-November, 2018) and dry season (December-May, 2019).

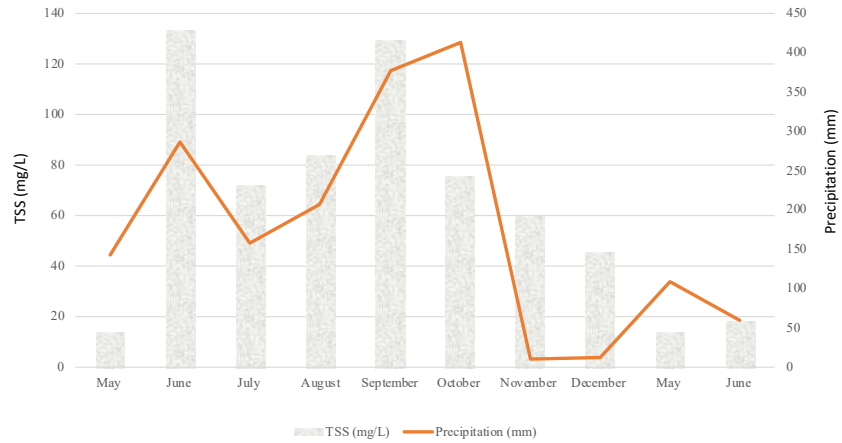

Fig. 4: TSS concentration recorded in Jonuta (R3) in the rainy season (June-November, 2018) and dry season (December-May, 2019).

mm (Fig. 5). It was observed that the area with the highest potential energy (in raindrops) corresponds to the municipality of Tenosique.

Soil Erodibility Factor (K)

A range of values between 0.23-0.89 tons.h.MJ^{-1}mm^{-1} was obtained within the study area. The municipality of Emiliano Zapata was the area with the greatest susceptibility to erosion (Fig. 6).

Slope-Length factor (LS)

Results obtained in this study show that the municipality of Tenosique, where the town of Boca del Cerro is located, presents a slope value of 16% being a territory prone to erosion. On the contrary, Jonuta presents a value of 0.03%, which makes it stable against erosion (Fig. 7). It is observed that the highest factor (LS = 27,423) is associated with the steepest slopes located in the municipality of Tenosique, and the lowest value (LS = 0.03) was registered in the municipality of Jonuta (Fig. 8).

Cover Management and Crop Factor (C)

In the municipality of Jonuta, there are areas with little natural vegetation and water bodies. On the contrary, in the municipalities of Emiliano Zapata (where the sampling site

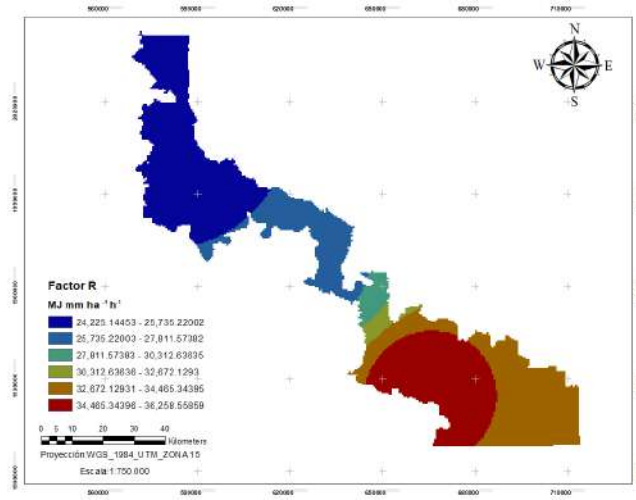

Fig. 5: Distribution of erosivity (Factor R) in the lower basin of the Usumacinta River, Tabasco.

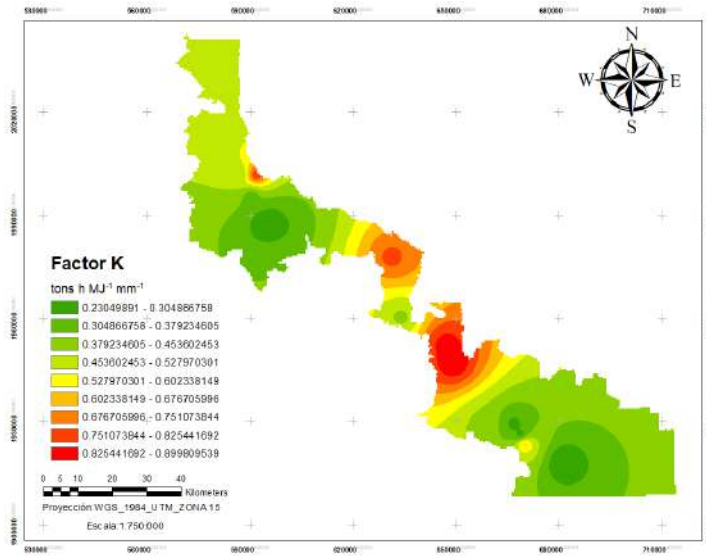

Fig. 6: Distribution of soil erodibility (K Factor) in the lower basin of the Usumacinta River, Tabasco.

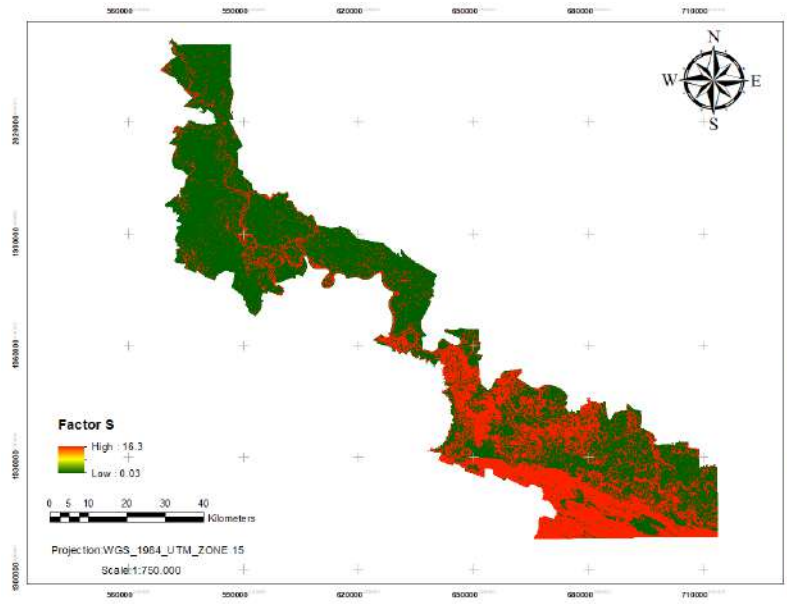

Fig. 7: Degree of steepness (Factor S) in the lower basin of the Usumacinta River, Tabasco.

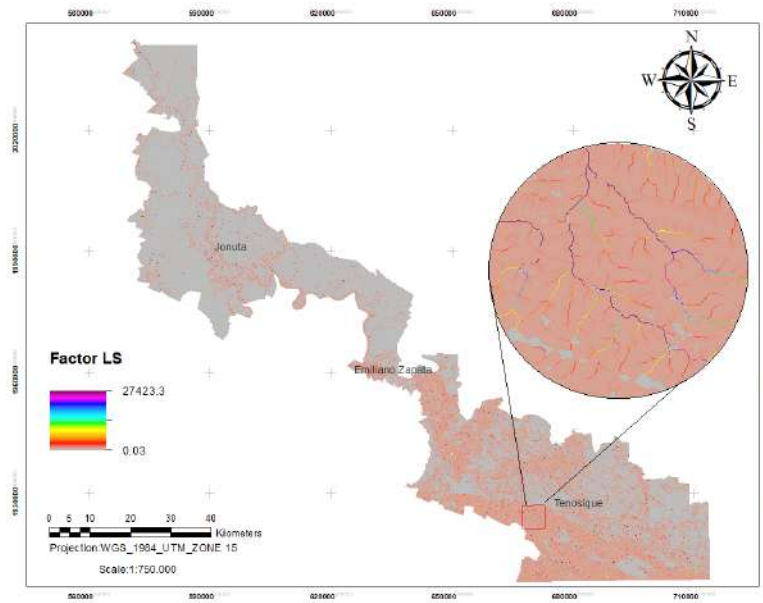

Fig. 8: Slope-length factor (LS) in the lower basin of the Usumacinta River, Tabasco.

of Chablé is located) and Tenosique, there are jungles along with agricultural lands and pastures (Fig. 9).

Water Erosion

The results obtained from average annual erosion in Tenosique (Boca del Cerro), Emiliano Zapata (Chablé), and Jonuta are 990 tons.ha^{-1}year^{-1}, 174 tons.ha^{-1}year^{-1}, and 65.tons. ha^{-1}yr^{-1}, respectively (Fig. 10).

DISCUSSION

Total Suspended Solids

In the lower basin of the Usumacinta River, concentrations of total suspended solids between 13 and 18 mg.L^{-1} were

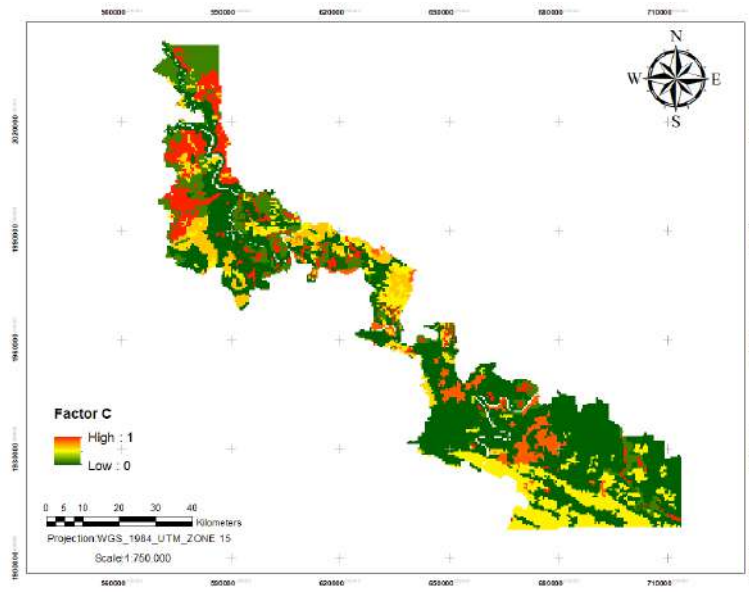

Fig. 9: Cover management and crop factor (C) in the lower basin of the Usumacinta River, Tabasco.

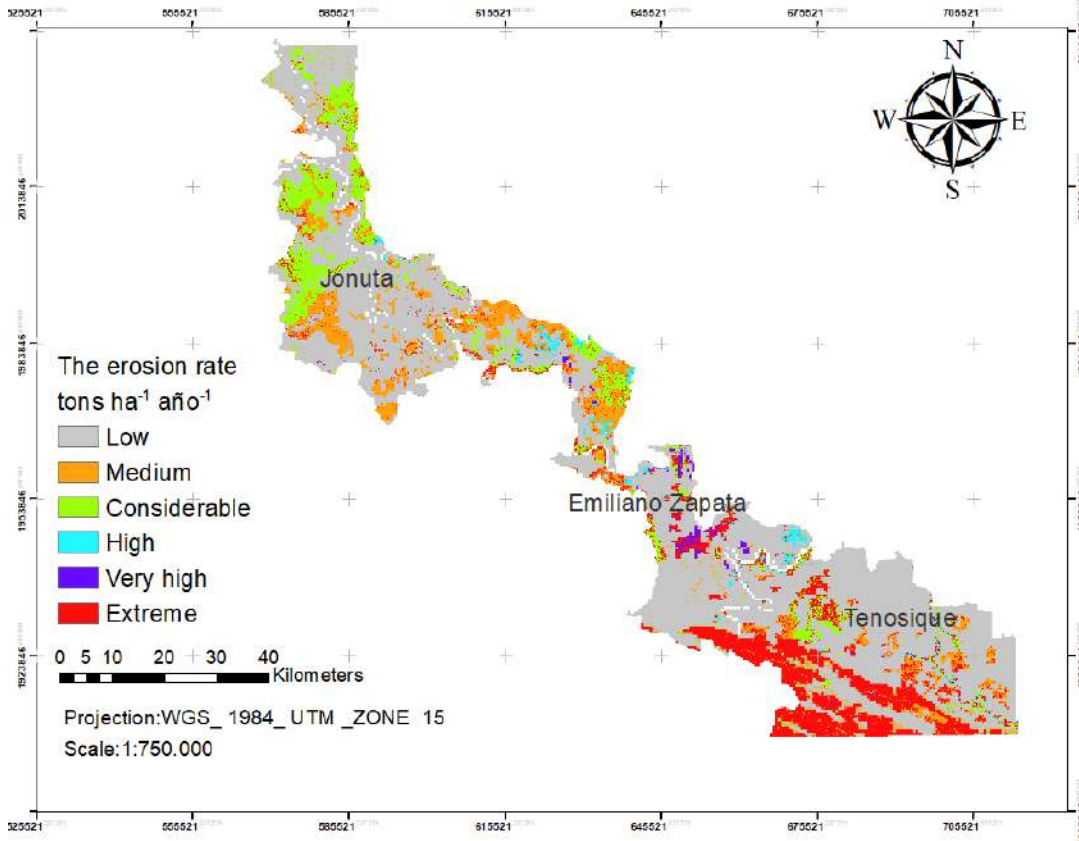

Fig. 10: Erosion rate in the lower basin of the Usumacinta River, Tabasco, Mexico.

registered in the dry season; and from 72 to 300 mg.L^{-1} in the rainy season. According to Laino-Guanes et al. (2016), rivers in the state of Tabasco reported TSS concentrations between 1.8 mg.L^{-1} and 4.3 mg.L^{-1} in the dry season, and 31.1 mg.L^{-1} and up to 548.8 mg.L^{-1} in the rainy season. This increase in TSS concentrations may be due to the dragging of material accumulated or deposited on the banks of the effluents in the dry season, or by landslides and loss of soil due to erosion in the rainy season (Almazán-Juárez et al. 2016). The TSS concentrations are associated with turbidity. Kulkarni (2011), indicated that TSS values greater than 1000 mg.L^{-1} affect the entry of light, limiting the development of aquatic life, as well as making possible the transport of toxic substances when there are small particles (less than 63 μm).

Rainfall Erosivity factor (R)

Erosivity factor (R) in territories is correlated with the rainfall present, Cerdà (2001) mentioned that the greater the intensity of the precipitation, the greater the raindrops, and thus the loss of soil increases. Tenosique presents a maximum value of 36,258.55 MJ.mm.$ha^{-1}h^{-1}$ associated with a mean annual rainfall of 2,250 mm (Fig. 5), considered the municipality with the highest potential energy (in raindrops). In this regard, López and Romero (1993), point out that rainfall of 100 mm to 300 mm registered in a few hours, releases enormous amounts of energy reflected in high soil losses, sinkholes, embankments, thick layers of sediments, and floods, as observed in the study area and sampling sites. Losses of soil due to water erosion can affect agricultural activity in this regard, López et al. (2003), mention that as a consequence of the impoverishment of the soil and loss of its productivity, the effects on crop yields arise, and fertilization requirements also increase, in addition to the difficulty in tillage.

Soil Erodibility Factor (K)

Soil erodibility is related to the stability of the aggregates and the cohesion forces that hold them together with the texture. The types of soil that predominate in this area are vertisols and gleysols, which are soils with a slow permeability characteristic (Palma-López 2007). A range of values between 0.23-0.89 tons.h.$MJ^{-1}mm^{-1}$ was obtained within the study area. The municipality of Emiliano Zapata was the area with the greatest susceptibility to erosion. This municipality has an area of 31,492 ha for livestock (INEGI 2016). This implies the use of heavy machinery and trampling by the cattle that generates superficial compaction, altering the structure of the soil, thus, decreasing permeability. Furthermore, the nature of the soil increases erosion, lowers its permeability and the cohesion of its elements (structure) (Alfonso-Linares & Monedero-García 2004). According to Duarte (2006), phenomena such as erosion, compaction, reduction in depth, acidification and decrease in biological activity, loss of nutrients, pesticides, and sediments from agricultural plots to surface and groundwater increases (Fig. 6).

Slope-Length Factor (LS)

The slope-length factor (LS) represents the effect of slope length on erosion. Results obtained in this study show that the municipality of Tenosique, where the town of Boca del Cerro is located, presents a slope value of 16% being a territory prone to erosion. On the contrary, Jonuta presents a value of 0.03%, which makes it stable against erosion. It is also observed that the highest LS factor is associated with steeper slopes and low values occur in plains areas (Figs. 7, 8). According to Alvarado-Cardona et al. (2007), the parts of a basin that present the greatest risk of erosion are those slopes greater than 25%.

Cover Management and Crop Factor (C)

According to the coverage of the basin, the cover management and crop factor varies from 0.1 to 0.85, considering the value of 1 for water bodies (Fig. 9). In the municipality of Jonuta, there are areas with little vegetation and water. This makes it an area susceptible to erosion. This municipality has an area of 3,151 ha for agriculture and 129, 202 ha for livestock (INEGI 2016). On the contrary, in the municipalities of Emiliano Zapata (Chablé sampling site) and Tenosique (Boca del Cerro sampling site), there are jungle areas. In this regard, García-Fayos (2004) mentioned that vegetation influences erosion by increasing the stability of the soil aggregates, protecting it from the impact of drops of water, increasing the infiltration capacity, and stopping runoff, as could be seen in this study. Despite this and generated by the change in land use to activities such as agriculture and livestock, there is a loss of 427 ha.yr^{-1} of vegetation (CONANP 2010).

Water Erosion

According to Montes-León et al. (2011), water erosion was classified into six ranges, which are: low (<50 tons.ha^{-1}.yr^{-1}), medium (50-100 tons.$ha^{-1}yr^{-1}$), considerable (100-150 tons.ha^{-1} yr^{-1}), high (150-200 tons.$ha^{-1}yr^{-1}$), very high (200-250 tons.ha^{-1} $year^{-1}$), and extreme (> 250 tons.$ha^{-1}yr^{-1}$). Thus, the results of erosion in the lower basin of the Usumacinta River ranges from low to extreme, Jonuta is classified as low (<50 tons.$ha^{-1}yr^{-1}$), Emiliano Zapata as medium (50-100 tons.$ha^{-1}yr^{-1}$), and Tenosique as extreme (> 250 tons.$ha^{-1}year^{-1}$). There is a combination of factors that accelerates the erosion phenomenon in the upper part of the lower basin of the Usumacinta River, causing areas with extreme erosion to appear (Fig. 10), just as it was observed in the municipality

of Tenosique - unlike those reported by Sánchez-Hernández et al. (2013), where 83% of the Grijalva-Usumacinta basin presented a medium to a high level of erosion, and only 17% presented a low level of risk.

CONCLUSION

According to the current situation of water erosion in the lower basin of the Usumacinta River in the state of Tabasco, there are areas with extreme erosion, a product of a steep slope, high rainfall, and clay soils that are dedicated to agriculture and livestock. A certain pattern has been established in the distribution of territorial water erosion (TWE), total suspended solids (TSS), and the water quality (WQ) of the Usumacinta River in its lower basin. WQ is good for aquatic life and agricultural irrigation in its lower basin. The mean annual TSS value is greater in the upper part of the lower basin (municipality of Tenosique) than in other parts of the basin and is equal to 95.7 $mg.L^{-1}$. This is due to the intense water erosion of the soil (TWE= 990 $t.ha^{-1}.year^{-1}$), a product of a steep slope (greater than 16%), high rainfall (greater than 1805 $mm.yr^{-1}$), and clay soils used for agriculture and pastures. Therefore, it is necessary to provide measures to reduce soil erosion by considering soil conservation technologies and surface water runoff control. In the downstream parts of the basin with significantly lower surface slopes, the TSS and TWE values are 91.10 $mg.L^{-1}$ and 174 $t.ha^{-1}$ yr^{-1} in the municipality of Emiliano Zapata, and 69.94 $mg.L^{-1}$ and 65 $t.ha^{-1}$yr in the municipality of Jonuta. Such distribution of TSS values indicates the influence of local factors and less corresponds to the upstream parts of the river. The influence of municipal wastewaters on the TSS value can be neglected because its volume is insignificant compared to the river flow in the rainy season. However, this influence cannot be ruled out because the treatment plants of each municipality in the study area do not operate, or do not operate properly, which causes environmental and health problems in the dry season.

ACKNOWLEDGEMENT

To the National Water Commission (CONAGUA) and to the National Council of Science and Technology (CONACYT) 2014-248265 Project "Evaluation of the effect of diffuse sources of pollution on the quality of the water of the Usumacinta River, in the state of Tabasco. To the Postgraduate College, Veracruz Campus; and the Boca del Río Technological Institute.

REFERENCES

Alfonso-Linares, C. A. and Monedero-García, M. 2004. Uso, manejo y conservación de suelos. Asociación Cubana de Técnicos Agrícolas y Forestales. La Habana, Cuba., pp. 68.

Almazán-Juárez, M. T., Almazán-Juárez, Á., Carreto-Pérez, B. E., Hernández, E., Castro, A. D. N. and Almazán-Núñez, R. C. 2016. Calidad y clasificación de usos del agua en la cuenca baja del río Papagayo, Guerrero México. Ecosistemas y Recursos Agropecuarios, 3(9): 293-305.

Alvarado-Cardona, M., Colmenero, R.J.A. and Valderrábano, A.M.L. 2007. La erosión hídrica del suelo, en un contexto ambiental, en el estado de Tlaxcala. Ciencia ergo sum 14(3): 317-326.

Cerdà, A. 2001. La erosión del suelo y sus tasas en España. Revista ecosistemas, Madrid, España, 10(3). Available in: https://www.revistaecosistemas.net/index.php/ecosistemas/article/download/268/264

CE-CCA-001/89. 1989. Criterios Ecológicos de Calidad del Agua. Diario Oficial de la Federación, México. Available in: http://www.dof.gob.mx/nota_detalle.php?codigo=4837548&fecha=13/12/1989

CONAGUA. 2018. Estadísticas del agua en México. CONAGUA, México. 294 pp. Available in: http://sina.conagua.gob.mx/publicaciones/EAM_2018.pdf

CONANP. 2010. Comisión Nacional de Áreas Naturales Protegidas 2010. Identificación de cambios en el uso del suelo y vegetación, y cálculo de la tasa de transformación del hábitat en el periodo 2000-20210. Área de protección de flora y fauna "Cañon del Usumacinta". 55 pp.

Duarte, A.F.C. 2006. Contaminación difusa originada por la actividad agrícola de riego, a la escala de la cuenca hidrográfica. Tesis doctoral, Universidad de Córdoba. Escuela técnica superior de ingenieros agrónomos y montes.

García-Fayos, P. 2004. Interacciones entre la vegetación y la erosión hídrica. Pp:309-334. En: Valladares, F.2004. Ecología del bosque mediterráneo en un mundo cambiante. 2 [a] edición. Ministerio de Medio Ambiente, EGRAF, S.A., Madrid. ISBN: 84-8014-552-8.

INEGI. 2016. Anuario estadístico y geográfico de Tabasco, México. 461p Available in: http://internet.contenidos.inegi.org.mx/contenidos/Productos/prod_serv/contenidos/espanol/bvinegi/productos/nueva_estruc/anuarios_2016/702825084363.pdf

Kulkarni, A. 2011. Water quality retrieval from landsat TM imagery. Procedia Comp. Science, 6: 475-480. https://doi.org/10.1016/j.procs.2011.08.088

Laino-Guanes, R., González-Espinosa, M., Ramírez-Marcial, N., Bello-Mendoza, R., Jiménez, F., Casanoves, F. and Musálem-Castillejos, K. 2016. Human pressure on water quality and water yield in the upper Grijalva river basin in the Mexico-Guatemala border. Ecohydrology & Hydrobiology, 16(3): 149-159.

López, H.E.F., Menes, M.M., Mota, J.L.O., Saens, E.M. and González, R.C. 2003. Integración de la EUPS a un SIG para estimar la erosión hídrica del suelo en una cuenca hidrográfica de Tepatitlán, Jalisco, México. Terra Latinoamericana, 21(2): 233-244.

López, B.F. and Romero D.M.A. 1993. Génesis y consecuencias erosivas de las lluvias de alta intensidad en la región mediterránea. Cuadernos I: Geográfica Vol. 18,19: Ediciones Logroño, España., pp. 7-28.

March, M.I. and Castro, N. 2010. La Cuenca del Río Usumacinta: Perfil y perspectivas para su conservación y desarrollo sustentable. Las cuencas hidrográficas de México. Diagnóstico y priorización. México DF: SEMARNAT-INE-Gonzálo Río Arronte, IAP., pp. 193-197.

Montes-León, M.A.L., Uribe-Alcántara, E.M. and García-Celis, E. 2011. Mapa nacional de erosión potencial. Tecnología y ciencias del agua, 2(1): 05-17.

NMX-AA-034-SCFI-2015. Norma Mexicana. Análisis de agua- Medición de sólidos y sales disueltas en aguas naturales, residuales y residuales tratadas- Método de prueba.

Palma-López, D.J., Cisneros, D.J., Moreno, C.E. and Rincón-Ramírez, J.A. 2007. Suelos de Tabasco: su uso y manejo sustentable. Colegio de Postgraduados-ISPROTAB-FUPROTAB. Villahermosa, Tabasco, México., pp. 195.

Paz González, A. and Vidal Vázquez, E. 2004. Erosión y Escorrentía. Universidad de La Coruña. Facultad de Ciencias. España., pp. 11.

Sánchez-Hernández, R., Mendoza-Palacios, J., De la Cruz Reyes, J., Mendoza-Martínez, J. and Ramos-Reyes, R. 2013. Mapa de erosión potencial en la cuenca hidrológica Grijalva-Usumacinta México mediante el uso de sig. Universidad y Ciencia, 29 (2): 153-161.

Soares, D. and García, A.G. 2017. La cuenca del río Usumacinta desde la perspectiva del cambio climático. Instituto Mexicano de Tecnología del Agua, México., pp. 425.

US EPA 2001. Parameters of water quality: Interpretation and standards. Environmental Protection Agency. Johnstown Castle, Ireland., pp. 132.

US EPA 2003. Developing water quality criteria for suspended and bedded sediments (SABS). US EPA Office of Water.

Vargas, V.B. and Linero, C. J. 2017. Caracterización de sólidos suspendidos y sedimentos superficiales en humedales del departamento del Magdalena (Zapayán, Pijiño y Chilloa). 212-216 pp. In: Memorias III *Seminario Internacional de Ciencias Ambientales,* SUE- Caribe, 2017.

Wischmeier, W.H. and Smith, D.D. 1978. Predicting rainfall erosion losses: A guide to conservation planning. Washington, D.C., U.S. Dep. Agric., Agric. Handb. No. 537, 1978.

Nature Environment and Pollution Technology
An International Quarterly Scientific Journal

p-ISSN: 0972-6268
(Print copies up to 2016)
e-ISSN: 2395-3454

Vol. 20 | No.3 | pp. 1107-1113 | 2021

Original Research Paper

https://doi.org/10.46488/NEPT.2021.v20i03.018

Open Access Journal

Optimization of the Water and Fertilizer of Rice in the Cold Field and the Biochar Application Amount Based on RAGA Model

Y. Li *(***)(****), S. Yi *(***)(****)†, Y. Lin(***)(****) and S. Liu**(***)(****)**

*College of Engineering, Heilongjiang Bayi Agricultural University, Daqing 163319, China

**College of Civil Engineering and Water Conservancy, Heilongjiang Bayi Agricultural University, Daqing 163319, China

***Engineering Research Center of Processing and Utilization of Grain By-products, Ministry of Education, Daqing, 163319, China

****Heilongjiang Engineering Technology Research Center for Rice Ecological Seedlings Device and Whole Process Mechanization,Daqing, 163319, China

†Corresponding author: Shujuan Yi; yishujuan_2005@yeah.net

Nat. Env. & Poll. Tech.
Website: www.neptjournal.com

Received: 10-08-2020
Revised: 09-09-2020
Accepted: 09-10-2020

Key Words:
RAGA model
Cold rice
Water use efficiency
Comprehensive warming potential

ABSTRACT

This paper proposes an optimization method based on the RAGA model. Taking rice from a cold area as the research object, this article selects irrigation volume, nitrogen application volume, and biochar application volume as experimental factors, and rice yield, water use efficiency, greenhouse gas emission comprehensive warming potential as influencing indicators. The research design is D311 Field trials by 3 factors of 5 levels of saturation. Hence, we can obtain the data on rice yield, water use efficiency, greenhouse gas emissions and comprehensive warming potential under different levels of water and fertilizer, and biochar application, and regression equations were established respectively. The RAGA model was used to simulate the regression equations. The optimal combination of water and fertilizer, and biochar was obtained as follows: irrigation amount is 7230 $m^3.hm^{-2}$, nitrogen fertilizer application amount is 92.13 $kg.hm^{-2}$, and biochar application amount is 30 $t.hm^{-2}$. The optimal rice yield obtained under this combination is 9452.20 $kg.hm^{-2}$. The water use efficiency is 1.94 $kg.m^{-3}$, and the comprehensive warming potential of greenhouse gas emissions is 4546.73 $kg.hm^{-2}$. The combined application of water and fertilizer, and biochar optimized by this model can provide a theoretical basis for achieving high yield, water-saving, and emission reduction of rice in cold areas, and it can also provide a reliable calculation method and idea for solving similar optimization problems in the field of agricultural production.

INTRODUCTION

Due to the good taste of rice in black soil in cold areas, the area of rice fields in Northeastern China has increased rapidly in the past ten years (Wang & Come 2010). The rational combination of irrigation, fertilizer, and biochar is the key to increasing crop yield and water use efficiency and reducing greenhouse gas emissions (Sun et al. 2009, Frolking et al. 2002, Wang et al. 2008). However, in the process of rice growth, there are problems such as extensive irrigation and uneven rainfall, resulting in rice water consumption accounting for more than 90% of agricultural water. At present, the average irrigation quota in my country is 9000 $m^3.hm^{-2}$, and the water use efficiency is less than 1 $kg.m^{-3}$, which is less than half of that in developed countries (Li et al. 2013).

According to statistics, the current application rate of chemical fertilizers on arable land in my country is close to 400 $kg.hm^{-2}$, which is seriously exceeding the safety limit of 225 $kg.hm^{-2}$ set internationally for the prevention and control of air and water pollution (Rao et al. 2011, Mao 2009). A long-term unreasonable application of fertilizers will cause crop lodging, white seedlings, weak nitrogen fixation capacity, and a sudden increase in greenhouse gas emissions. Biochar has the characteristics of high carbon content, hard to decompose, high specific surface area, and is loose and porous. The use of biochar can improve the soil's physical and chemical properties and microbiological properties of rice fields, which reduce greenhouse gas emissions (Chen et al. 2014, Liu et al. 2013, Zhou et al. 2017). Therefore, the establishment and perfection of a theoretical system explain the relationship between crop yields, water use efficiency, greenhouse gas emissions and water and fertilizer, and biochar, and the construction of a multi-objective mathematical model finds the best combination to ensure national food security. The major issues facing the implementation of the sustainable agricultural development strategy are using the best combination of irrigation, fertilization, and biochar for agricultural production activities to ensure crop yields,

save agricultural production resources, reduce agricultural non-point source pollution, improve the ecological environment, and enhance crops quality, which is very significant (Muoneke et al. 2007).

At present, domestic and foreign research reports on the relationship between high yield, water-saving, emission reduction, water and fertilizer, and biochar, mostly adopt orthogonal or orthogonal rotating experimental design methods to design experimental plans, obtain data relationships corresponding to different combinations, use least two multiplying parameter estimation, and establishing nonlinear equations between targets and factors. Then regression analysis method, variance analysis method, single factor effect method, main effect and interaction effect method used to analyze the test results, and find out the best water fertilizer and biochar combined application program (Li et al. 2004, Ai & Li 2005, Shapiro &Wortmann 2006, Widdicomde &Thelen 2002, Cox & Cherney 2001, Cox et al. 2006). However, this method has shortcomings such as large errors, high difficulty in multivariate replacement, and poor processing capability of sample data with noise. In the process of agricultural production, crop growth is interactively affected by a variety of factors. The factors and indicators have strong nonlinear and black box characteristics. It is difficult to quantitatively describe the causal relationship between them with traditional analysis methods (Zhang et al. 2003). The current research based on the RAGA model can successfully deal with complex problems such as high-dimensionality, multi-peak, nonlinearity, discontinuity, non-convexity, noise, and so on. Then the optimal combination is obtained, which is gradually becoming one of the best tools for solving complex problems. It has been widely used in hydrology, meteorology, geology, economy, medicine, machinery, humanities, etc. (Howell 2009, Zhang et al. 2017, Zhu et al. 2015).

This paper takes rice from a cold area as the research object, and conducts field experiments according to the saturated D311 (Xu 1997) test plan to obtain data on yield, water use efficiency, and greenhouse gas comprehensive warming potential under different water and fertilizer, and biochar combinations, and establish a multi-objective regression equation. An optimization algorithm based on RAGA is proposed for multi-objective optimization, to find the optimal water and fertilizer, and biochar application plan, to provide a reference field management technology for high yield, water-saving, and emission reduction of rice in the northeast cold region.

MATERIALS AND METHODS

Overview of the Test Area

The experiment was conducted at the National Rice Irrigation Test Center Station (125°44'E, 45°63'N) in Heping Town, Qing'an County, Suihua City, Heilongjiang Province from May to October 2019, which has typical black soil in a cold area. The annual mean temperature is 2.5°C, the annual mean precipitation reached 550 mm, and the annual mean water surface evaporation was 750 mm. The crop has a hydrothermal growth period of 156 to 171 days and a frost-free period of 128 days throughout the year. The climate is characterized by a cold temperate continental monsoon climate. The soil type is albic soil rice field, with a bulk density of 1.01 $g.cm^{-3}$ and a porosity of 61.8%. Basic physical and chemical properties of soil include organic matter mass ratio 41.4 $g.kg^{-1}$, pH value 6.40, total nitrogen mass ratio 15.06 $g.kg^{-1}$, total phosphorus mass ratio 15.23 $g.kg^{-1}$, total potassium mass ratio 20.11 $g.kg^{-1}$, alkaline hydrolysis nitrogen mass ratio 154.36$mg.kg^{-1}$, effective phosphorus mass ratio 25.33$mg.kg^{-1}$ and available potassium mass ratio 157.25 $mg.kg^{-1}$.

Experimental Design and Process

The test adopts the optimal design of saturated D311. The test factors are irrigation amount, nitrogen fertilizer, and biochar. The specific application amount is as follows: the irrigation amount is 5000~10000$kg.hm^{-2}$, nitrogen fertilizer (pure nitrogen) is 50~150$kg.hm^{-2}$, and biochar is 0~40$t.hm^{-2}$. The experimental design scheme is shown in Table 1.

The experiment set up 11 treatments, repeated 3 times and arranged in random blocks. Each block has an area of 10 m×10 m=100m^2. Rice is planted around the block to add protection rows. The technical measures such as rice seedling raising, transplanting, plant protection, and medication, as well as field management conditions are the same. To reduce the influence of lateral penetration on the test, the isolation treatment is adopted among the plots, that is, plastic boards and cement ridges are used as the barriers around the plots. Materials are buried in the field 40cm deep below the ground surface. The irrigation method adopts a pipeline water supply, and each pipeline is equipped with a water meter to control the amount of irrigation. Nitrogen fertilizer is applied according to the ratio of base fertilizer, tiller fertilizer, and ear fertilizer at 5:3:2. P-fertilizer is used as base fertilizer at one time, and the amount of application is 45$kg.hm^{-2}$. K-fertilizer is divided into basal fertilizer and 8.5 leaf age (young ear differentiation period), the front and the back ratio is 1:1, the application rate is 80$kg.hm^{-2}$. Biochar is applied to the surface of the soil, and the biochar is used with the rotary tiller. Layers of soil are evenly mixed. The tested fertilizers were urea (N content is 46%), diammonium phosphate (N content is 18%, P_2O_5 content is a46%), potash fertilizer (K_2O content is 40%), and the tested biochar was a straw biochar product of Liaoning Jinhefu Agricultural Development Co. Ltd.

Table 1: Saturated D-311 optimal design processing table.

Treatment number	Coded value			Actual value			GWP ($kg.hm^{-2}$)
	X_1	X_2	X_3	$W(m^3.hm^{-2})$	$N(kg.hm^{-2})$	$BC(t.hm^{-2})$	
1	0	0	2	5000	100	40	3450.11
2	0	0	-2	5000	100	0	5955.66
3	-1.414	-1.414	1	3200	65	30	5119.64
4	1.414	-1.414	1	6800	65	30	5098.78
5	-1.414	1.414	1	3200	135	30	4593.49
6	1.414	1.414	1	6800	135	30	4377.51
7	2	0	-1	7500	100	10	4731.18
8	-2	0	-1	2500	100	10	4269.39
9	0	2	-1	5000	150	10	4782.40
10	0	-2	-1	5000	50	10	5087.59
11	0	0	0	5000	100	20	4133.44

The tested rice variety was Longqingdao No. 3, the local main cultivars, with a planting density of 4 plants per hole. Base fertilizer was applied on May 6, transplanted on May 17, and tillering fertilizer was applied on May 31 and Panicle fertilizer was applied on July 19. Ear fertilizer harvested on September 20. The growth period of rice is 127 days, which is divided into the returning green stage (May 17 to May 30), the tillering period (May 31 to July 7), the jointing-booting stage (July 8 to July 25), heading date (July 26 to August 4), milky maturity (August 5 to August 24), and yellow ripening stage (August 25 to September 20).

Test Index Determination

Yield: This test observes the number of productive ears, the number of rows per ear, the thousand-grain weight, and the seed-setting rate of each treatment to calculate the theoretical yield. Theoretical yield = effective panicle number × grain number per panicle × thousand-grain weight × seed setting rate.

Water consumption: Accurately record the irrigation time and amount of each treatment through the water meter, and observe the changes of the water surface scale every day. At the same time, observe the reference crop water demand.

Greenhouse Gas: The sampling of flue gases was carried out on sunny days, which adopts the static chamber/gas chromatogram. When sampling, a syringe was used to extract about 100 mL of gas from the box, collect samples at 0, 5, 10, and 15 minutes respectively, then the gas in the syringe was immediately transferred to the aluminum foil sampling bag, and the sampling bag was brought back to the laboratory for measurement in time. The gas concentration is detected by Shimadzu GC-14B gas chromatograph, and the standard gas is provided by the National Standard Material Center.

Calculation Method and Data Analysis

Water use efficiency: Water use efficiency calculation formula:

$$WUE=Y/ETc \quad \ldots(1)$$

Where WUE is water use efficiency, Y is yield, ETc is water consumption

Greenhouse gas emissions: The formula for calculating greenhouse gas emission flux from rice fields (Zheng et al. 1998): $F = \rho \cdot h \cdot dc/dt \cdot 273/(273 + T)$.

Among them, F is the gas emission flux ($mg \cdot m^{-2} \cdot h^{-1}$), ρ is the gas density under standard conditions ($kg \cdot m^{-3}$), h is the box height (m), and dc/dt is the inside of the sampling box. The concentration change rate of the gas is ($mL \cdot m^{-3} \cdot h^{-1}$), 273 is the gas equation constant, and T is the average temperature (°C) in the sampling box during the sampling process. Calculate the gas emission flux according to the relationship curve of the gas sample concentration and time. The emission during the growth season is the product of the average flux value of each growth period and the total length of the growth period and then accumulated.

In this study, the global warming potential GWP (the GWP of CO_2 is 1) is used to express the relative radiation effect of different greenhouse gases of the same quality on the greenhouse effect enhancement. Taking 100a as the time scale, the GWP of CH_4 and N_2O per unit mass are 21 and 310 times that of CO_2 respectively (Nie et al. 2019). The calculation formula of GWP is as follows:

$$GWP = fCH_4 \times 21 + fN_2O \times 310 \quad \ldots(2)$$

In the formula, f is the emission of different greenhouse gases in the rice field ecosystem during the whole growth period of rice.

Data Analysis: The test data are analyzed and calculated using Excel2003, SPSS17.0 and MATLAB7.0.

Introduction and Construction of RAGA Model

Introduction to the RAGA Model

The RAGA model is an accelerated genetic algorithm model based on real number coding (Jin et al. 2001), overcomes the shortcomings of traditional genetic algorithms (GA). This paper adopts real number coding. It can search a larger space and can be mixed with other classic optimization algorithms to facilitate the processing of complex decisions. Variable constraint conditions by order-based evaluation function model are used to evaluate the individual fitness value, so that is not affected by the actual target value. In the evolutionary iteration, the parallel calculation of the genetic algorithm is realized, and all the offsprings are evaluated uniformly, to ensure the superiority of understanding as much as possible, further accelerate the evolution time, and gradually adjust the search space of optimized variables, and the algorithm optimization speed is greatly improved, which speeds up the convergence speed. The principle is as follows.

$$\min f = \sum_{i=1}^{n} \left\| F(C, X_i - Y_i \right\|^q \quad \ldots(3)$$

Where: C=[*Ci*] is the model p variables (parameters) to be optimized. [a_j, b_j] is the initial change interval (search interval) of c_i. X is the N-dimensional input variable of the model. Y is the M-dimensional yield vector of the model. F is the nonlinear model, namely F: $R^N \rightarrow R^M$. $\{(X_i, Y_i) | i = 1,2,\cdots m\}$ is the input and yield by m sets of data for the model. $\| \ \|$ is the norm. q is a real number. When q=1, it is a linear function criterion, and when q=2, it is a quadratic function criterion, which may be determined by specific modeling requirements. f is the optimization function criterion.

RAGA Model Construction

This study takes minimization as an example.

$$\min f(x)$$
$$\text{s.t } a(j) \le x(j) \le b(j) \quad \ldots(4)$$

Step 1: Real-number the variables. The following linear transformation is used as follows.

$$X(j) = a(j) + y(j)[b(j) - a(j)], (j = 1,2,...p) \quad \ldots(5)$$

In the formula, a(j) and b(j) are the initial variables. y(j) is the jth variable x(j) to be optimized on a(j), b(j) corresponds to a real number in the interval [0, 1], that is, the genetic gene in RAGA. At this time, the genes corresponding to all variables are connected together to form the coding form of the problem solution, which is called a chromosome, [y(1), y(2)...y(p)].

Step 2: Initialize the parent population. Suppose the parent population is n, randomly generate random numbers between n groups [0, 1], each group has p, that is $\{u(j,i)\}(j = 1,2...p; i = 1,2...n)$, $u(i, j)$will be the parent individual value of the initial population $y(j, i)$. The optimized variable $x(j, i)$ can be obtained by formula (7-17), and the corresponding objective function value can be obtained by formula (7- 15). The corresponding individual $f(i)$ will be sorted from small to large. The value $\{f(i)(i = 1,2...n)\}$ of the objective function is smaller, the individual's adaptability is stronger. After sorting, the first k individuals are selected as excellent individuals and directly enter the next generation.

Step 3: Evaluation of the fitness of the parent population. A certain probability is set for each chromosome $y(j, i)$ in the population so that it will be selected in a certain proportion. The adaptability of the chromosomes is stronger, the possibility of being selected greater. In this paper, we choose an evaluation function based on order (represented by eval [y(j,i)]). The idea is to use the order of chromosomes to make random combinations instead of based on the target value, and its evaluation function is as follows:

$$eval[y(j,i)] = \alpha(1-\alpha)^{i-1} \quad \ldots(6)$$

Where α is a random number between (0, 1). When i=1, it means the chromosome is the best, and when i=n, the chromosome is the worst.

Step 4: Choose. The selection process is based on the principle of rotating the gambling wheel, defining n times as the basis, and one rotation will generate a new chromosome. The gambling wheel selects chromosomes based on the fitness of each individual. The process is as follows:

$$\begin{aligned} & q_0 = 0 \\ & q_i = \sum_{j=1}^{i} eval[y(j,i)](j = 1,2...p; i = 1,2...n) \\ & q_{i-1} \le r \le q_i \\ & r \in [0, q_i] \end{aligned} \quad \ldots(7)$$

Repeat step 2 and step 3 for n times, so that n duplicate chromosomes can be obtained to form a new generation of individuals.

Step 5: Hybridization operation. First, select the cross probability p_c, then there are a total of chromosomes $p_m.n$

in the population for crossover operation. If r≤pc, choose y(j,i) as a parent and pair them randomly: [y1'(j,i), y2'(j,i)], [y3'(j,i) , y4'(j,i)], [y5'(j,i), y6'(j,i)]. To ensure their pairwise pairing, when the parent individual has an odd number, one chromosome can be increased or decreased. The crossover adopts the arithmetic crossover method, and the specific algorithm is as follows:

$$x = cy_1'(j,i) + (1-c)y_2'(j,i); y = (1-c)y_1'(j,i) + cy_2'(j,i) \quad \ldots(8)$$

Where: c is a random number between (0, 1).

If the calculated solution set is convex, it is guaranteed that the two offspring are feasible. If it is not a convex set, the feasibility of the offspring must be verified at this time. If the two offspring are feasible, they can be used instead of the parent to produce a new one. With a random number 'c', repeat the crossover operation until a new viable offspring is obtained. This process only replaces the parent with a viable offspring. If a new generation of individuals is not feasible, some correction methods must be adopted to make it a viable chromosome.

From i=1 to n, repeat step 5 to obtain a new generation of population {y2(j,i)} (j=1,2...p; i=1,2...n) through the hybridization operation.

Step 6: Mutation operation. The mutation process is similar to the hybridization process. The mutation probability p_m is selected, that is $p_m \cdot n$ so that there will be chromosomes in the population for mutation operation. If r≤pm, select y(j, i) as the parent of the mutation, and use y3'(j,i) for each selected parent. The expression is as follows.

$$y_3(j,i) = y_3'(j,i) + Md(i = 1,2,...p) \quad \ldots(9)$$

In the formula, M is a random number between (0, M), and d is the randomly selected variation direction in R^n. If no feasible solution is found in the predetermined number of cycles, set M=0 and restart the calculation.

From i=1 to n, step 6 is repeated to get a new generation of population after mutation

$$\{y_3(j,i)\} = \{j = 1,2...p; i = 1,2...n\}$$

Step 7: Iterative evolution. The 3n offspring individuals obtained through step 4 to step 6 are sorted according to their fitness function values from large to small, and the previous (n- k) offspring individuals are selected as the new parent population. Then proceed to the next round of optimization process, repeat step 3, re-evaluate, select, cross, and mutate the parent individuals.

Step 8: Speed up processing. Because too many evolution times may lead to the weakening of the algorithm's optimization ability, the new outstanding individuals produced by the first and second evolutions are taken as the new change space for the next optimization, and the above step 1 to step 7 are repeated to speed up. The range of excellent individuals will gradually shrink and get closer to the optimal value until the program reaches a certain preset number of times or the objective function value is less than the preset value. At this time, the algorithm ends. The result comes from the above steps by the optimized current optimal individual.

RESULTS AND DISCUSSION

The Establishment of Multi-Objective Regression Equation

According to the test plan, the test data of production, water use efficiency, and greenhouse gas comprehensive warming potential indicators are shown in Table 2.

Taking $X_1(W)$, $X_2(N)$, $X_3(C)$ coding values as independent variables, and the yield, water use efficiency, and greenhouse gas comprehensive warming potential are shown in Table 2 as dependent variables A quadratic polynomial regression analysis is carried out to obtain the regression equation of the target:

$$\begin{cases} \max Y = 14535.96 + 1306.28x_1 + 456.02x_2 + 137.63x_3 + 299.97x_1x_2 - 177.75x_1x_3 - \\ 93.63x_2x_3 + 905.01x_1^2 + 354.33x_2^2 - 328.57x_3^2 \\ \max WUE = 2.04 + 1.019x_1 + 0.768x_2 + 0.980x_3 + 0.142x_1x_2 - 0.134x_1x_3 + \\ 0.763x_2x_3 - 1.226x_1^2 - 1.347x_2^2 - 1.191x_3^2 \\ \min GWP = 4583.31 + 36.79x_1 - 148.42x_2 - 291.81x_3 - 24.39x_1x_2 - 84.38x_1x_3 - \\ 72.08x_2x_3 - 141.04x_1^2 - 28.40x_2^2 - 16.74x_3^2 \\ -2 \le x_1, x_2, x_3 \le 2 \end{cases} \quad \ldots(10)$$

Perform F test on each regression equation: (F_Y = 5.37, F_{WUE} = 4.75, F_{GWP} = 144.48)> ($F_{0.01}$ (10, 20) = 3.37), indicating that the relationship between the regression equation is extremely significant, that is, the regression equation can reflect the relationship between each target and the relationship between irrigation volume, nitrogen fertilizer and biochar. The *t*-test was performed on the regression coefficients in each target regression equation, $t_i > t_{0.05}(11)$=1.796, indicating that the influence of each factor on the index was significant.

Optimal Combination of Yield, Water Use Efficiency, and Greenhouse Gas Comprehensive Warming Potential Based on RAGA Model

This article uses the RAGA model steps 1 to 8 to optimize the formula (10) and calculates the optimal solution of the above-mentioned multi-objective optimization problem. In this article, the initial number of individuals is set to 1200,

Table 2: Experimental treatment data of different water and fertilizers, and biochar.

Treatment number	Coded value			Actual value			Y	WUE	GWP
	X1	X2	X_3	W(m^3/hm^2)	N(kg/hm^2)	BC(t/hm^2)	(kg/hm^2)	(kg/m^3)	(kg/hm^2)
1	0	0	2	5000	100	40	7187.72	1.88	3450.11
2	0	0	-2	5000	100	0	9086.00	1.68	5955.66
3	-1.414	-1.414	1	3200	65	30	8462.00	1.57	5119.64
4	1.414	-1.414	1	6800	65	30	9213.00	1.92	5098.78
5	-1.414	1.414	1	3200	135	30	8202.65	1.54	4593.49
6	1.414	1.414	1	6800	135	30	8259.44	2.04	4377.51
7	2	0	-1	7500	100	10	6065.62	1.96	4731.18
8	-2	0	-1	2500	100	10	8025.00	1.73	4269.39
9	0	2	-1	5000	150	10	9500.00	1.80	4782.4
10	0	-2	-1	5000	50	10	14535.96	1.66	5087.59
11	0	0	0	5000	100	20	9020.00	1.95	4133.44

the maximum genetic algebra is 60, and the binary number of variables is 20. The crossover probability is taken as 0.7. The yield (Y), water use efficiency (WUE), greenhouse gas comprehensive warming potential (GWP), and the curve of the overall model with the number of iterations are shown in Fig. 1.

It can be seen from Fig. 1 that each curve has a larger amplitude when the number of iterations is small. The comprehensive temperature increase trend and the overall model curve decline rapidly at the beginning of the iteration, which stabilizes after the iteration number reaches a certain value. The yield and water use efficiency curve presents an up and down trend, and the yield curve is more stable than the water use efficiency curve. The final optimal yield is 9452.20 kg. hm^{-2}, the optimal water use efficiency is 1.94 $kg.m^{-3}$, and the optimal warming potential is 4546.73 $kg.hm^{-2}$. The coded value of water is 1.784 when the optimal solution is obtained, the coded value of nitrogen fertilizer is 1.685, and the coded value of biochar is 1.0, and the actual value is converted into irrigation amount is 7230m^3.hm^{-2}, nitrogen

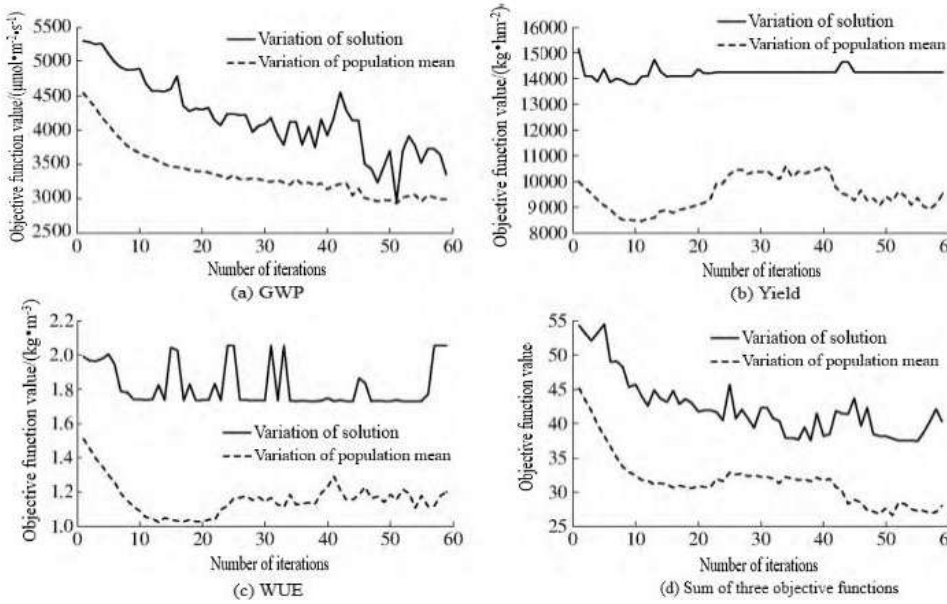

Fig.1: GWP, Yield, Water use efficiency, and the optimal solution of the whole model and performance tracking.

fertilizer application amount is 92.13kg.hm^{-2}, and biochar application amount is 30t.hm^{-2}.

CONCLUSION

Based on the traditional regression equation fitting, this paper proposes an optimization method based on the RAGA model and applies it to the practical problem of irrigation, fertilization, and biochar optimization in rice planting and production in cold areas, which expands the RAGA model Application scope.

RAGA algorithm proposed in this paper is used to optimize the experimental data of rice water and fertilizer, and biochar in cold areas. The rice yield under the experimental conditions is 9452.20 kg.hm^{-2}, the water use efficiency is 1.94 kg.m^{-3}, the greenhouse gas emission comprehensive warming potential is 4456.73 kg.hm^{-2}, the corresponding irrigation amount is 7230m^3.hm^{-2}, the amount of nitrogen fertilizer application is 92.13kg.hm^{-2}, and the amount of biochar application is 30t.hm^{-2}. This method can provide a theoretical basis for increasing production, saving water, and reducing emissions in the process of rice production in cold areas.

The application of the optimization method based on the RAGA model in the optimization of rice irrigation, fertilization, and biochar application amount has important theoretical and practical significance for guiding the production of rice in cold areas, increasing rice yield, reducing production water consumption, and reducing agricultural non-point source pollution. At the same time, it provides a reliable calculation method and idea for solving similar multi-objective complexity optimization problems in the field of agricultural production.

ACKNOWLEDGMENTS

This work was supported by Heilongjiang Bayi Agricultural University Support Program for San Heng San Zong (TDJH201803), Engineering Research Center of Processing and Utilization of Grain By-products, Ministry of Education, Heilongjiang Engineering Technology Research Center for Rice Ecological Seedlings Device and Whole Process Mechanization.

REFERENCES

Ai, F.Q. and Li, G.Z. 2005. Rotating regression analysis of the relationship between nitrogen application rate, density, and rape yield. Chinese Agric. Sci. Bull., 21(4): 142-144.

Chen, W.F., Zhang, W.M. and Meng, J. 2014. Review and prospects of research on biochar and agricultural environment. J. Agric. Environ. Sci., 33(5): 821-828.

Cox, W.J. and Cherney, D.J.R. 2001. Row spacing, plant density, and nitrogen effects on corn silage. Agro. J., 93(3): 597-602.

Cox, W.J., Hanchar, J.J. and Knoblauch, W.A. 2006. Growth, yield, quality, and economics of corn silage under different row spacing. Agro. J., 98(1): 163-167.

Frolking, S., Qiu J. and Boles S. 2002. Combing remote sensing and ground census data to develop new maps of the distribution of rice agriculture in China. Global Biogeochem Cyc., 16: 1091-1101.

Howell, T.A. 2009. Relationship between crop production and transpiration, evapotranspiration, and irrigation. Irrig. Agric. Crop Agro. Monog., 30: 292-427.

Jin, J.L., Yang, X.H. and Ding, J. 2001. Improved scheme of standard genetic algorithm-accelerated genetic algorithm. Sys. Eng. Theory Pract., (4): 8-13.

Li, G.Z., Ai, F.Q. and Zhao, Y.H. 2004. The effect of different densities and nitrogen fertilizers on rape yield. J. Mount. Agric. Biol., 23(3): 198-201.

Liu, Y.X., Wang, Y.F. and Lu, H.H. 2013. Effects of biomass carbonization on rice field greenhouse gas emissions and soil physical and chemical properties. J. Appl. Ecol., 24(8): 2166-2172.

Mao, Z. 2009. Construct water-saving and anti-pollution ecological irrigation area. China Water Resour., (19): 28.

Muoneke, C.O., Ogwuche, M.A.O. and Kalu, B.A. 2007. Effect of maize planting density on the performance of maize/soybean intercropping system in a guinea savannah agroecosystem. Afr. J. Agric. Res., 2(12): 667-677.

Nie, T.Z., Chen, P., and Zhang, Z.X. 2019. Effects of different types of water and nitrogen fertilizer management on greenhouse gas emissions, yield, and water consumption of paddy fields in a cold region of China. Int. J. Environ. Res. Pub. Health, 16: 1639.

Rao, J., Xu, X.Y. and Ji, X.T. 2011. Research on the status, mechanism, and countermeasures of agricultural non-point source pollution in my country. Issues Agric. Eco., (8): 81-82.

Shapiro, C.A. and Wortmann, C.S. 2006. Corn response to nitrogen rate, row spacing, and plant density in Eastern Nebraska. Agro. J., 98(3): 529-535.

Sun, A.H., Zhang, Z.X. and Zhu, S.J. 2009. Experimental study on water consumption law and water use efficiency of rice with different irrigation modes in Sanjiang Plain. Water-Saving Irrig., (11): 12-14.

Wang, Q.J. and Come, Y.C. 2010. On the countermeasures and suggestions for rice production and sustainable utilization of water resources in Heilongjiang Province. China Rice, 16(4): 25-28.

Wang, Y.Y., Chen, W.W. and Zhao Z.C. 2008. CH_4 and N_2O emission characteristics and emission estimation of rice in a cold area in Sanjiang Plain. Trans. Chinese Soc. Agric. Eng., 24(10): 170-176.

Widdicomde, W.D. and Thelen, K.D. 2002. Row width and plant density effects on corn grain production in the Northern corn belt. Agro. J., 94(5): 1020-1023.

Xu, Z.R. 1997. Regression analysis and experimental design. Beijing: China Agric. Press, 1997: 102-143.

Zhang, S.J., He, Y. and Fang, H. 2003. The application of artificial neural networks in the analysis of the relationship between crop yield and soil spatial distribution information. Sys. Eng. Theory Pract., (12): 121-127.

Zhang, Z.X., Zhang, S.W. and Guo, D.D. 2017. Coupling effect analysis of different water and fertilizer conditions on maize and optimal water and fertilizer application scheme. J. Agric. Mach., 48(9): 206-214.

Zheng, X.H., Wang, M.X. and Wang, Y.S. 1998. Comparison of manual and automatic methods for measurement of methane emission from rice paddy fields. Adv. Atmos. Sci., 15(4): 569-579.

Zhou, F., Xu, C.Y. and Wang, Y.L. 2017. The impact of biochar on soil CH_4 and N_2O emissions. Environ.Sci., 38(9): 3831-3839.

Zhu, D.L., Zhan, T. and Zhang, Y. 2015. Multi-neighborhood structure and multi-objective genetic algorithm. Trans. Chinese Soc. Agric. Mach., 46(4): 309-315.

Nature Environment and Pollution Technology
An International Quarterly Scientific Journal

p-ISSN: 0972-6268
(Print copies up to 2016)
e-ISSN: 2395-3454

Vol. 20 | No.3 | pp. 1115-1126 | 2021

Original Research Paper

https://doi.org/10.46488/NEPT.2021.v20i03.019

Open Access Journal

The Construction of Regional Ecological Security Pattern Based on a Multi-Factor Comprehensive Model and Circuit Theory

H.R. Yu*, Y.Z. Wang*(**) †, Z. Liang*and C.K. Min***

*School of architecture and planning, Anhui Jianzhu University, Hefei 230022, China
**Anhui Urbanization Development Research Center, Hefei 230022, China
***School of English, Welsh School of Architecture, Cardiff University, Cardiff CF10 3BA, UK
†Corresponding author: Y.Z. Wang; rockyhust@126.com

Nat. Env. & Poll. Tech.
Website: www.neptjournal.com

Received: 19-11-2020
Revised: 09-12-2020
Accepted: 22-02-2021

Key Words:
Regional Security pattern
Circuit theory
Residents' needs
Development strategy

ABSTRACT

Various ecological problems have become increasingly prominent due to the accelerated growth of urbanization. Ecological security and ecological conservation have become an important topics in the current scenario. This study took southern Anhui as an example, constructing comprehensive assessment models to conduct source identification from three perspectives, i.e. ecosystem services, ecological sensitivity and residents' ecological needs. Landscape resistance surface was built based on the reciprocal of habitat quality and night-time light data. According to the circuit theory, the ecological process in the heterogeneous landscape was simulated to identify ecological corridors, extract pinch points and divide barriers that need improvement, thereby to construct the southern Anhui ecological security pattern (ESP). The pattern comprised 20 ecological sources, 37 ecological corridors, 9 pinch points and 2 levels of improvement areas. Specifically, ecological sources were mainly distributed within the area of Huangshan city and Xuancheng city, mostly covered with trees; ecological corridors were mostly located in the northern part of the research area; pinch points were mainly farmland or beside construction land; the primary improvement area was mainly in Chaohu city and Maanshan city, while the secondary improvement area was distributed around the primary area. The study discussed the diversified improvement strategies of different barriers and introduced the optimization scheme "one centre, two wings, one belt", providing planning advice for decision-makers. The study expanded the construction of regional ESP, and partly guided the steady development of ESP of southern Anhui.

INTRODUCTION

The rapid development of urbanization has caused an increasingly intense contradiction between economic development and ecological conservation. Ecological systems like forests, waters, and wetlands have been destroyed, causing deterioration in the habitat quality and a decline in the biodiversity. On the other hand, people have higher needs for life thanks to the economic development, as well as new demands for ecosystem services. Ecological security pattern, the bridge between ecosystem services and societal development, is regarded as a crucial strategic tool to guarantee regional ecological security and increased well-being. The planning of ecological security pattern (ESP) has become a key for the Chinese governments at all levels to ensure the sustainable development of the regional economy, and coordinate the relationship between ecosystem and economic society. Also, it is regarded as a fundamental and a crucial method to realize regional ecological security, and one of the strategic modes for national land development and protection (Nathwani et al. 2019, Huang et al. 2020).

Currently, scholars in various fields at home and abroad have discussed the structure (He et al. 2020) and function (Song et al. 2020) of ESP, as well as its construction (Xun et al. 2018) and assessment (Yin et al. 2011, Schröter et al. 2020). In addition, scholars have conducted massive research concerning biodiversity conservation (Chen et al. 2017), nature reserve planning (Jia et al. 2005), remedy for ecosystem (Meng et al. 2012), etc. The research on ESP construction in China has formed a mainstream paradigm of "source identification—resistance surface construction—corridor construction". Generally speaking, the identification of sources should provide important ecological services and own nice landscape connectivity, greatly needed in regions. Traditional ecological source identification mostly comprises two methods: the first is to directly determine natural reserves, national parks, scenic spots, etc. as an ecological source. Though convenient to operate, it may lack the accuracy of patch assessment. Some scholars chose patches with a relatively stable type of eco-utilization in the long term as ecological sources, for example, woodland, grassland, farmland, etc. However, this method does not take land-use heterogeneity

into account, as a land of the same type in different regions still differs to a certain degree. Another more scientific method is to construct a comprehensive indicator system to assess regional parcels, and then to determine ecological sources. The chosen indicators are determined by the functional importance of ecosystem services, ecological sensitivity, etc. (Peng et al. 2018). The weight and constitution of indicators in different areas are determined according to the local situation. Specifically speaking, indicators comprises important ecosystem services indicators like water conservation, biodiversity, carbon fixation ability, soil conservation, etc. (Gao et al. 2020), and ecological sensitivity indicators like elevation, slope, etc. However, scholars at home and abroad have not thoroughly considered the relationship between ecosystem services, ecological sensitivity and residents' needs for ecosystem services. The natural ecosystem cannot survive without "people", which means that a sustainable society needs a balanced development between ecological basic services and residents' ecological needs (Li et al. 2020). The construction of ESP is a multi-goal optimization process based on the coordinated "society-economy-ecology" development. In this regard, this study considered residents' needs for ecosystem services when selecting ecological sources.

The key to the ecological corridor selection is to simulate species migration and construct a resistance surface. Currently, scholars mainly apply circuit theory (Guo et al. 2020), minimum cumulative resistance (MCR) model (Li et al. 2007), and cellular automaton (Zhou et al. 2020) to simulate the movement of species migration. MCR model and ant colony optimization algorithms can only determine the position of the ecological source, as well as the position and direction of ecological corridor, unable to further identify patches and corridors that are more crucial. While circuit theory can be applied to study the movement pattern of ecological flow in a heterogeneous landscape, identify important patches and corridors by calculating isolation degree between patches, and then determine the range of corridor. For resistance surface construction, researchers often determine the resistance value of each patch based on their experience, leading to relatively large differences in the resistance value of different regions. The relatively more scientific method at present is to construct a resistance surface based on the reciprocal of habitat quality coupling with night-time light data (Wang et al. 2019).

This study chose southern Anhui as a research area and attempted to: (1) comprehensively consider the coordination between ecosystem services and residents' needs in the construction of ESP, determine ecological sources and verify their rationality; (2) based on the reciprocal of habitat quality, utilize the modification of night-time light data to construct regional landscape resistance surface; (3) based on circuit theory, select ecological corridor and its range, determine the pinch points that could influence the connectivity of ecological corridor and barrier, and study diversified strategies of ecological conservation, to provide advice for the planning of regional ecological conservation.

MATERIALS AND METHODS

Study Area and Data Sources

Southern Anhui, located in southern Anhui Province (29°31'-31°N, 116°31'-119°45'E) (Fig. 1), has an area of 31.2 thousand km^2. It has abundant forest resources and soils, with 20.5 thousand km^2 forest area, accounting for 45.7% of the total forest area in Anhui province. Southern Anhui is an important ecological source of the Yangtze River Delta, and also one of the most famous tourist spots in China. Long-term land development has caused severe

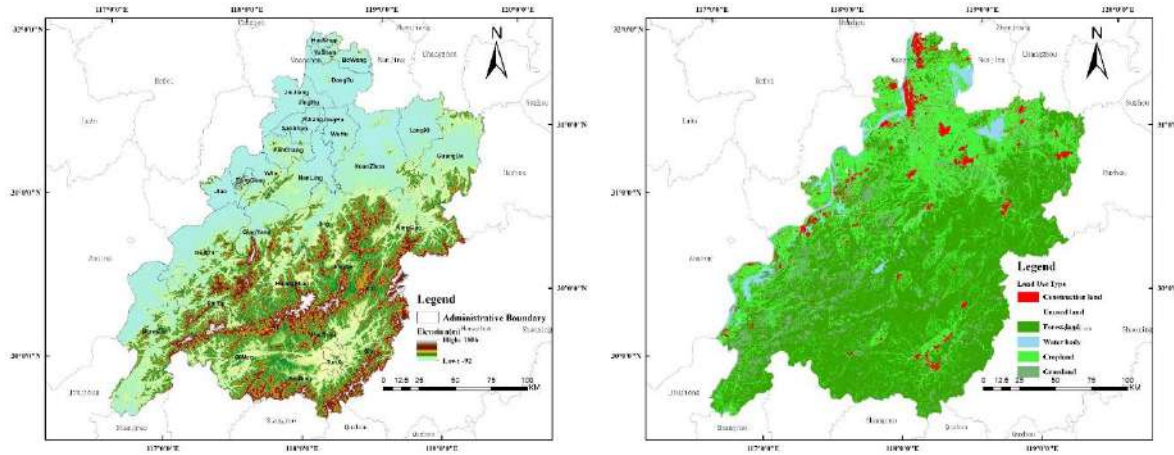

Fig. 1: Land-use type and elevation in southern Anhui.

influences on the ecosystem in southern Anhui, causing problems like habitat deterioration, biodiversity loss, deforestation, soil erosion, etc. Relatively large differences in environment exist within the region. Also, southern Anhui has not formed an interconnected ecological network.

The data sources used in this study were as follows: (1) the 2018 land use and NDVI database was provided by the Resource and Environment Data Cloud Platform; (2) digital elevation model (DEM) data was obtained from the Geospatial Data Cloud website at a spatial resolution of 90m; (3) meteorological data from National Tibetan Plateau Data; (4) soil data from Food and Agriculture Organization of the United Nations (FAO). (5) the 2018 NPP-Virrss was provided by the National Oceanic and Atmospheric Administration. We reclassified all data using the nearest-neighbour to ensure that the spatial resolution was 30m × 30m.

Research Framework and Methods

Identification of the ecological source: The ecological source refers to the area that, from the perspective of human services, plays a decisive role in maintaining regional ecological stability. It normally consists of ecological patches that have relatively important ecosystem services, high ecological sensitivity, and can satisfy residents' ecological needs (Dondina et al. 2016). The methodological framework is shown in Fig. 2, and each process has been described in detail thereafter.

This study applied relevant assessment models (InVEST model (Tallis et al. 2011), CASA model and water and soil conservation model (Zhang et al. 2019)) to quantitatively assess the ecosystem services in southern Anhui. According to the previous research and the local situation of the research area, the study gave four types of ecosystem services the weights of 0.2, 0.3, 0.2, and 0.3 respectively, and divided them into five levels based on natural breakpoint method. The assessment of ecosystem services in southern Anhui was then generated after overlaying the weights.

Ecological sensitivity reflects the complexity and probability of regional ecological problems. Its degree reflects the probability of ecological problems in the disturbance of unreasonable activities (Peng et al. 2018). To maintain regional ecological stability, it is supposed to protect areas with relatively high sensitivity. Southern Anhui is a hilly and mountainous region. According to relevant research (Zhang et al. 2011, Peng et al. 2018, Peng et al. 2017) and the actual situation of the research area, five types of indices, i.e. soil erosion intensity, vegetation coverage, land use type, elevation and slope were selected as assessment factors. The analytic hierarchy process was adopted to determine the weight of each indicator, and then the sensitivity of five

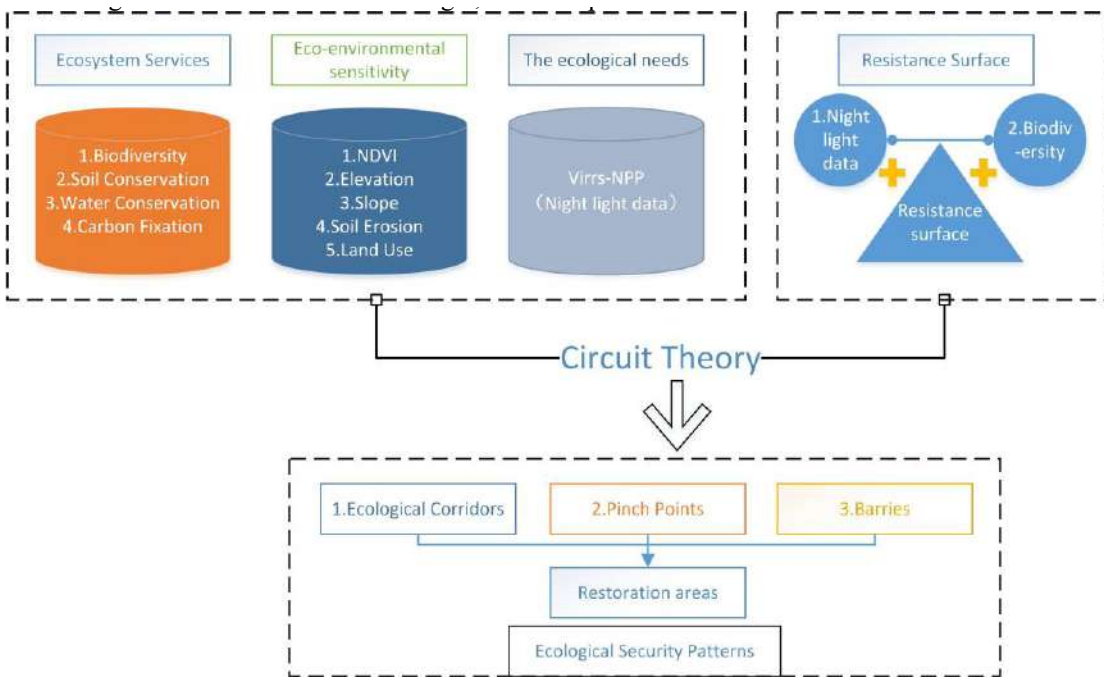

Fig. 2: Construction framework of ecological security pattern in southern Anhui.

Table 1: Classification and weighting of ecological sensitivity evaluation factors.

Evaluation factor/unit	Sensitivity assignment					Weights
	9	7	5	3	1	
NDVI		(0.65, 0.75]	(0.65, 0.75]	(0.35, 0.50]		0.20
Elevation (m)		(500, 800]	(800, 1100]	(1100, 1400]	1400	0.15
Slope		(5, 10]	(10, 15]	(15, 25]		0.15
Land-use type	Forest land or Waterbody	Grassland	Cropland	Construction land	Unuse land	0.20
Soil erosion intensity	Extremely strong erosion	Strong erosion	Moderate erosion	Mild erosion	Slight erosion	0.30

factors was valued and calculated according to their weight. According to the natural breakpoint method, five levels including no sensitivity, light sensitivity, medium sensitivity, high sensitivity and extreme sensitivity were divided to assess the ecological sensitivity. The specific valuation and weights are shown in Table 1.

Generally, land of ecological services with a closer distance towards human activities are applied by residents more often, accordingly with higher ecological importance. Therefore, further analysis based on population density distribution data is required to acquire the spatial distribution of ecological needs. As night-time light data based on VIIRS-NPP has proven to be accurate in reflecting the intensity and range of human activities, the nuclear density analysis was applied to calculate the aggregated intensity of ecological needs in different expanded radii. The radium of needs was set to be 10 km to calculate night-time aggregated intensity. The specific equations and explanations have been mentioned in some research (Peng et al. 2018, Peng et al. 2017).

At last, three assessment results, i.e. ecosystem services, ecological sensitivity and residents' ecological needs were valued respectively, based on the reference to associated statistics, at the weights of 0.5, 0.3 and 0.2, thereby generating the final result of the importance to protect the ecological sources. According to the natural breakpoint method, five levels were divided, and patches that were greater than level three were selected as an ecological source candidate. Considering that ecological source needs certain habitat area and is capable of providing important ecological services, some relatively small patches were eliminated according to the actual situation. In the meantime, patches that are relatively aggregated were combined with other patches, thereby generating the southern Anhui ecological source.

The construction of ecological resistance surface: The difficulty of species migrating to patches of different habitats can be reflected by the resistance surface. Resistance surface depicts the influence of landscape heterogeneity towards ecological process flow. The resistance value is related not only to the distance to the ecological source but also to the land use and human disturbance. For example, human activities will prevent material circulation and energy exchange between different landscape patches. Therefore, traditional resistance surfaces were mainly applied to simulate ecological resistance according to the land use of patches, and could not accurately simulate the distribution of resistance surface. Generally speaking, the higher of the habitat quality in the region, the more complex will be the biodiversity in the region, and easier will be the migration of species. Regarding relevant research (Zhou et al. 2020, Peng et al. 2017), the study considered the actual situation in southern Anhui and adopted the reciprocal of habitat quality to construct a resistance surface. In the meantime, night-time light data were applied as a calibration factor. Considering that the value can be zero, the study assigned the data at no-zero value, and it exerted no influence to the construction of the actual resistance surface.

$$R_Z = R_0 \times OLS$$

In the equation, R_Z represents the resistance value after the calibration of each grid, R_0 represents the original resistance value constructed based on land use type, OLS represents night-time light index.

Ecological corridor and security pattern: Circuit theory is generally required to identify sticking points and pinch points, and thereby to construct the complete regional ecological security pattern, as shown in Fig. 3 (Dondina et al. 2016). In the construction of an ecological corridor, the tool Linkage Mapper developed based on circuit theory can explicitly depict the exact positions of barriers and pinch points. Sticking points are the barriers to effective species migration and ecological process. Under the circumstances of high urbanization, it is of great significance to determine and ameliorate sticking points. Pinch points are the area of too frequent ecological processes, and also the key node of ESP construction, unable to eliminate or hamper. Circuit theory can identify the ecological corridors that suit real species migration routes, combined with the improvement of sticking points and the protection of nodes, and it helps scholars to have a clear understanding towards ESP construction and propose targeted advice for protection (Liu et al. 2018).

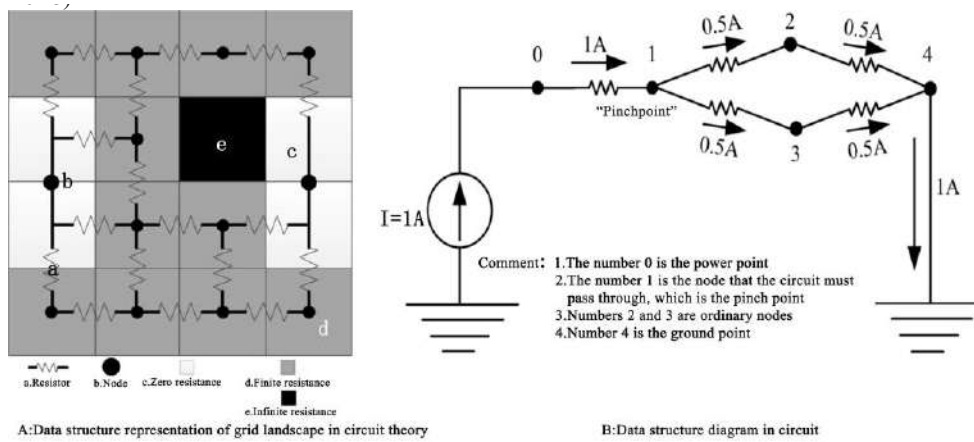

Fig. 3: Circuit theory grid circuit expression and resistance distribution diagram.

RESULTS AND DISCUSSION

Spatial Distribution Pattern of Factors

Every ecosystem service was divided into five levels according to the natural breakpoint method, and the significance from low to high was ranked from level one to five (Fig. 4). Results showed that ecosystem services presented a relatively significant spatial variation on overall quality which may result from the fact that the southern Anhui is higher than the northern. To analyze it in the context of the whole region, the biodiversity and water conservation of southern Anhui ranked the best, with the area greater than level three

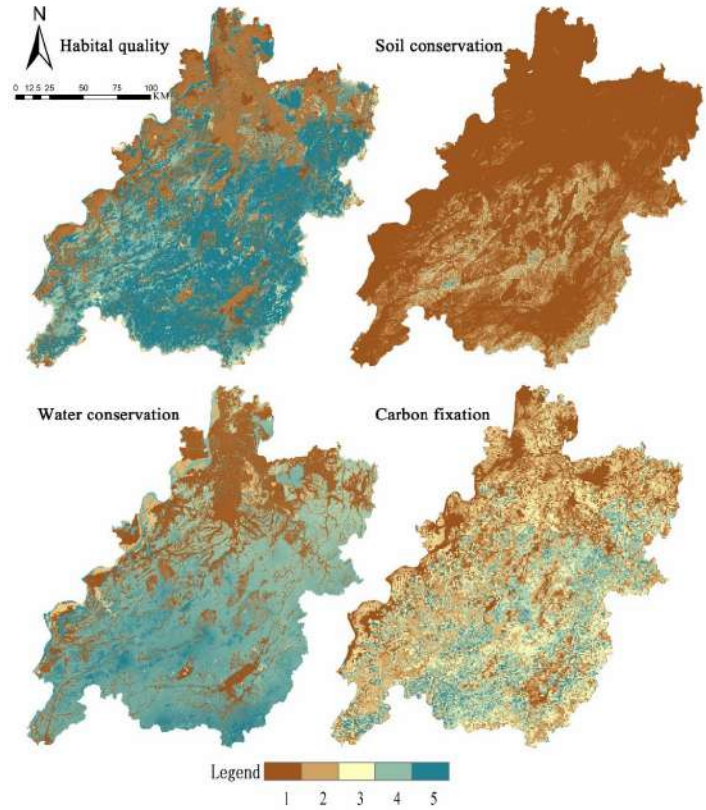

Fig. 4: Spatial distribution map of ecosystem service grades in southern Anhui.

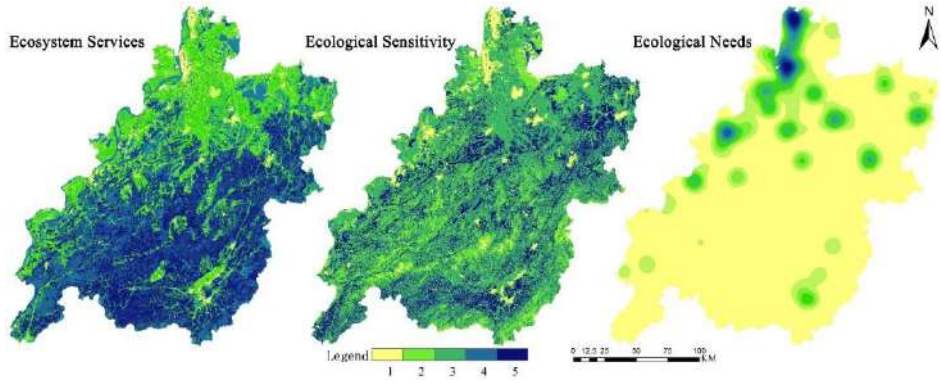

Fig. 5: The spatial distribution of factors for ecological source identification.

accounting for 62.7% and 48.5% of the total respectively, while the area of soil conservation and NPP that ranks greater than level three accounted for 1.17% and 34.6% of the total respectively. The soil conservation of southern Anhui is at serious risk, urging for certain protection strategies to renovate this function. Chaohu city and Maanshan city have high population density with rapid economic development, and face severely degenerated functions of biodiversity and water conservation and serious ecological problems, compared to Huangshan city and Xuancheng city.

Value water conservation, soil conservation, NPP and biodiversity at the weights of 0.2, 0.3, 0.2 and 0.3, and divide them respectively into five levels according to the natural breakpoint method. The assessment of ecosystem services in southern Anhui was then generated after overlaying the weights (Fig. 5). To understand the variations of ecosystem functions within the southern Anhui, the zonal statistics function in ArcGIS was applied to calculate the score of normalized ecosystem functions, as shown in Fig. 6. Qimen county ranked the highest in the assessment of ecosystem functions, while Jinghu district within Chaohu city ranked the lowest. The ecosystem functions presented an overall tendency of high in the south but low in the north. The overall ecosystem functions were related to elevation and population density.

The areas that rank greater than level three were mainly distributed in the south and the east, mostly consisting of woodland and grassland, accounting for 28.1% of the total area. The areas that have low sensitivity were mostly construction land, as well as the bare land at high elevation, located in the south of southern Anhui.

Residents' ecological needs were mainly distributed in the north and part of the east of southern Anhui, contrary to the distribution of ecosystem services and ecological

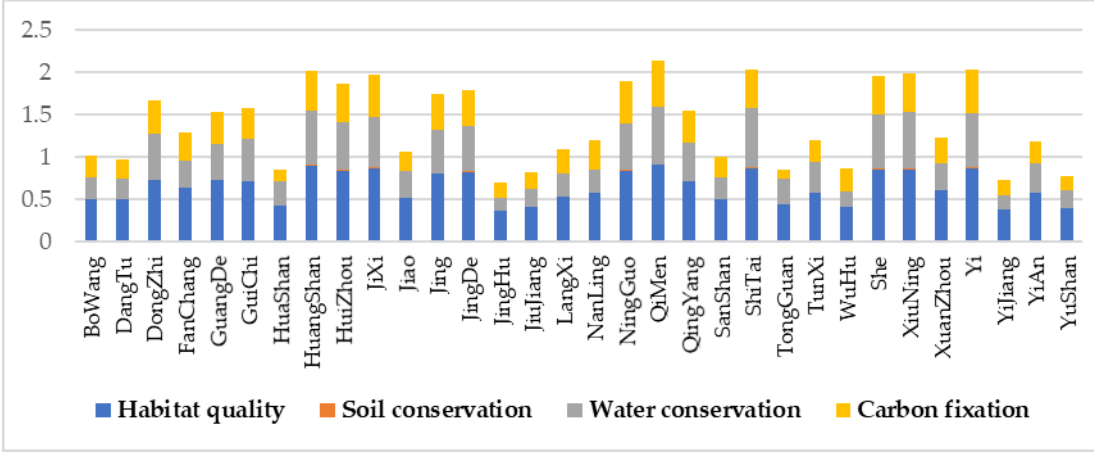

Fig. 6: The importance score of ecosystem services of counties.

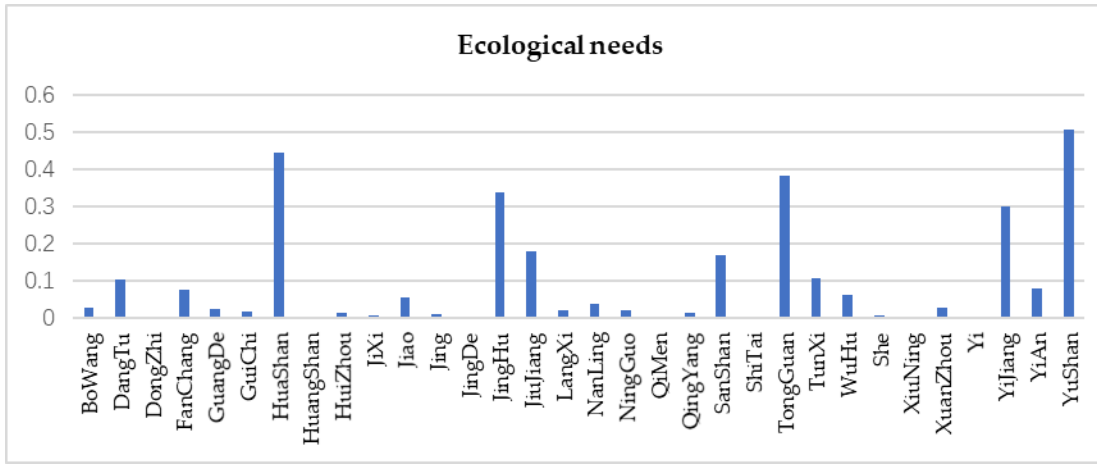

Fig. 7: The rank of residents' ecological needs in the counties and districts of southern Anhui.

sensitivity as shown in Fig. 7. For example, Jinghu district and Yunshan district are the economic centres of the region, and the ecological conditions within the region cannot satisfy the living needs of the majority; while the south and east of southern Anhui have sparse population, thereby they have relatively small residents' needs compared to the north. It means that apart from satisfying residents' needs, it is required to strengthen the connection between internal ecological lands within the region and construct a regional ecological network. It can help maintain regional ecological security and satisfy the coordinated development of "nature-society-ecology".

Ecological Source Extraction

Based on the assessment of ecosystem services, ecological sensitivity and residents' ecological needs in southern Anhui, patches that ranked greater than level three were extracted to identify the distribution of ecological sources, as shown in Fig. 8. The total area of ecological source in southern Anhui is 19269.54km^2, accounting for 51.3% of the total area. The areas are mainly distributed in the regions of Huangshan city, Xuancheng city and Chizhou city. These are the prime areas which can guarantee the ecological security of southern Anhui, as well as the ecological bottom line of urbanization

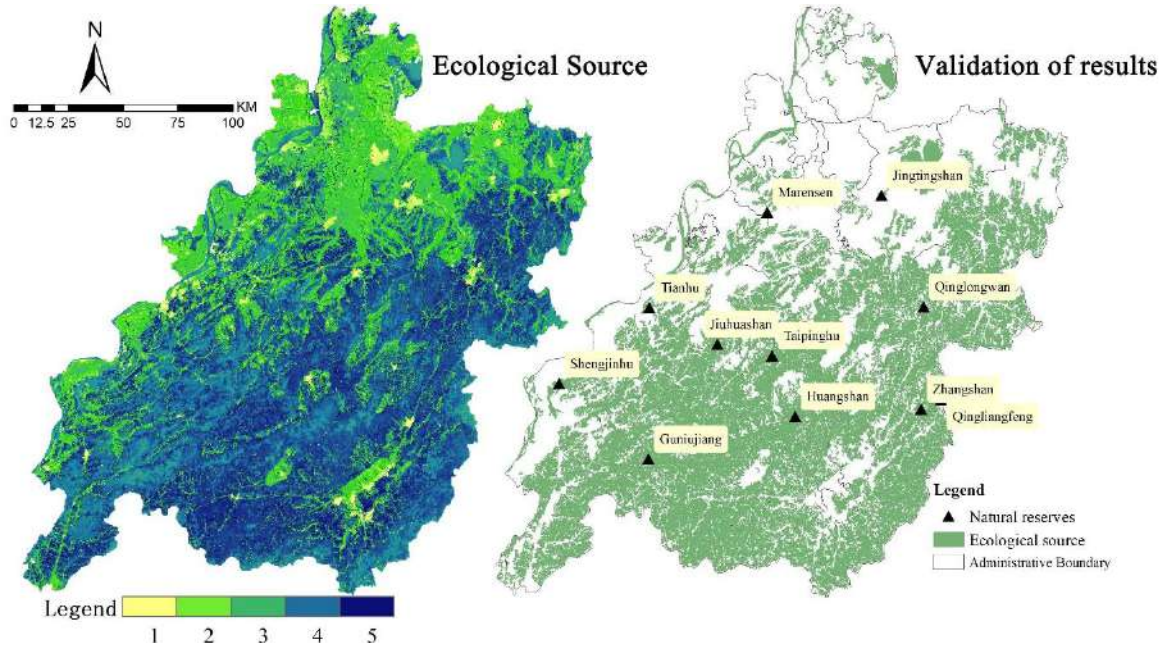

Fig. 8: Validation of results of ecological source extraction in southern Anhui.

Table 2:The area and the percentage of land-use in the ecological source region.

Land-use type	Area (km^2)	Proportion (%)
Cropland	432.34	2.2
Frost land	15369.49	79.7
Grassland	2557.99	13.3
Waterbody	896.53	4.7
Construction land	13.38	0.0995
Other land	0.1	0.0005

and environmental resource development. Exploitation and construction should be strictly prohibited in these areas. Among them, woodland was the most primary land use type, accounting for 79.7% of the total; grassland and waters accounted for 13.3% and 4.7% receptively; farmland accounted for 2.2%. It can be seen that certain ecological sources were exploited or constructed unreasonably. Besides, construction area and bare land accounted for less than 1% (Table 2).

To verify the effectiveness of the ecological source extraction based on a multi-factor comprehensive model, the study overlay the geographic position of ten national and provincial natural reserves and patches extracted from ecological sources. It can be found that natural reserves were basically within the extraction range of the ecological source, proving the validation of source extraction results.

The Construction of Minimum Accumulated Resistance Surface

The minimum accumulated resistance surface in an ecological source is shown in Fig. 9. Among them, the area along the Yangtze River, located in the north of research area, ranked the highest of the minimum accumulated resistance value, especially in the areas of Wuhu city and Maanshan city (Dangtu county, Jinghu District, Wuhu county and Fanchang county). The middle and south of the research area had complex surrounding landscape. As woodland and grassland limit human activities, thereby exerting a relatively small influence on the ecological environment, the minimum accumulated resistance surface is relatively small.

The ESP Construction of Southern Anhui

The spatial distribution of ecological corridors: The identification of the ecological corridor plays an important role in maintaining the ecological process. The ecological function of corridor closely relates to its spatial range such as the edge effect of corridor. The width of the ecological corridor based on circuit theory is determined according to the accumulated resistance and certain specific threshold. As shown in Fig.10, the range of ecological corridor was determined as the threshold of accumulated resistance increased from 1000 to 6000, and the ratio of the ESP area increased accordingly. The figure shows that as threshold increases, the area of ecological corridor increases accordingly, while there is slight or no change in the ecological corridor's spatial distribution.

Considering the urgent need for economic development, the limitation of financial investment in ecological conservation in southern Anhui, as well as the discussion of relevant research on ecological corridor, this study assumed that the investment in ecological conservation supported 10% of the whole research area, and applied threshold 3000 to determine the spatial range of ecological corridor. There were 37 ecological corridors determined, with a total length of 440.42

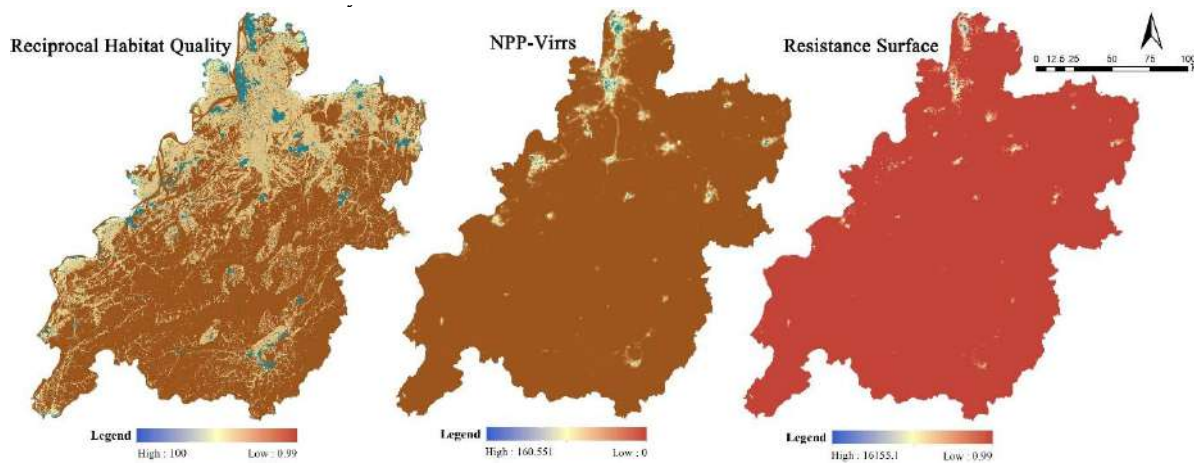

Fig. 9: Ecological resistance surface in southern Anhui.

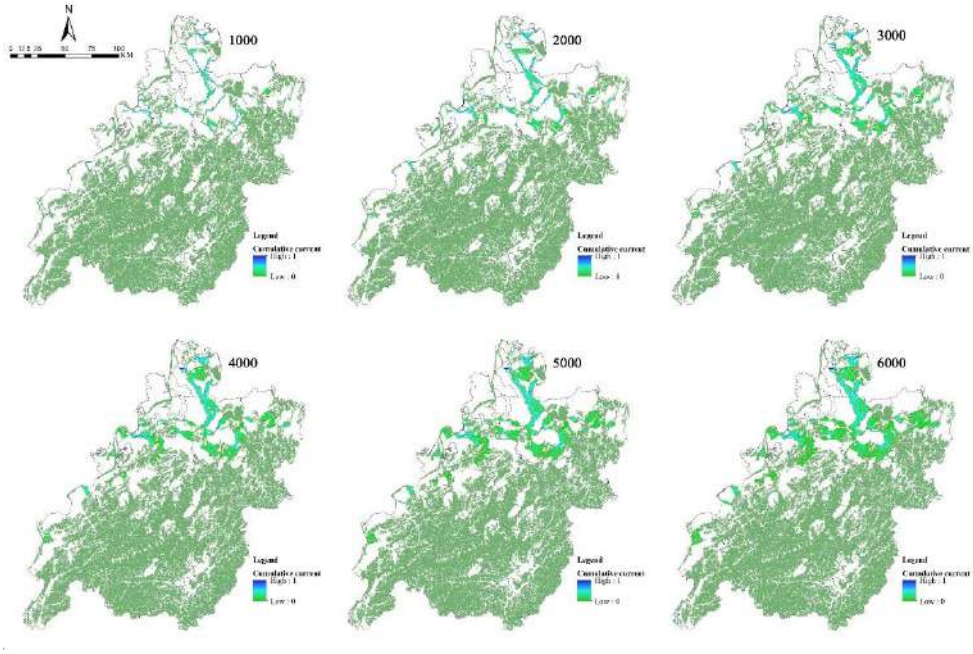

Fig. 10: Spatial distributions of ecological corridors for thresholds from 1000 to 6000.

km, mostly consisting of farmland. The ecological corridors in the south had high current density and presented a shape of cobweb, while the southwest and east had relatively small current density and presented a clustered distribution. The longest ecological corridor in the region was 59 km; the shortest 1.2 km.

The spatial distribution of barriers and pinch points: Linkage Mapper tool developed based on circuit theory was applied to determine the barriers that could influence the connection quality of ecological corridors, divide improvement areas in ecological corridors, and identify pinch points based on current corridors. The method is applied to give priority to the areas that are important to the connectivity of the research area, as shown in Fig. 11.

The ecological corridor barriers in southern Anhui were divided into primary and secondary improvement areas. The

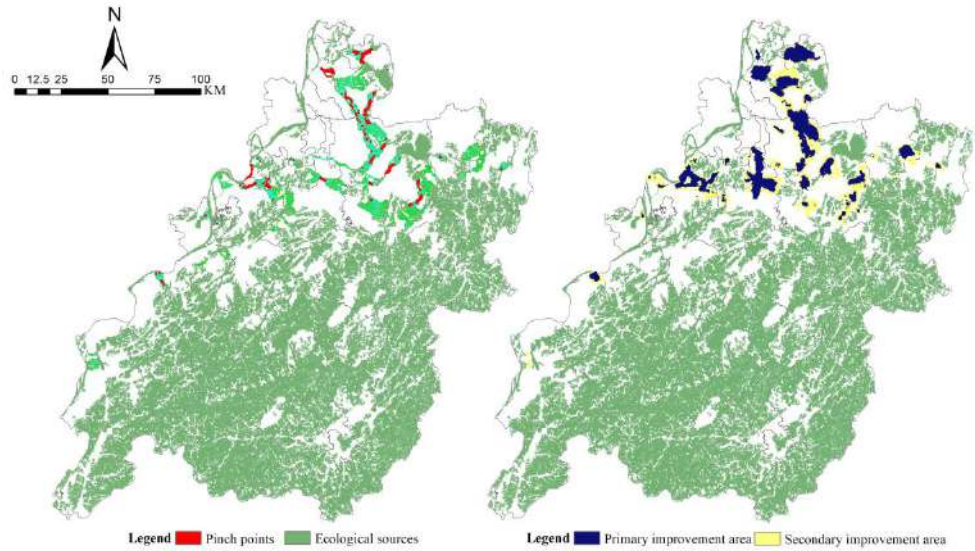

Fig. 11: Spatial distribution of pinch points and improvement areas.

area of the primary area was 1144.42 km^2, mostly distributed between sources or in the fringe area of sources; the area of the secondary area was 969.18km^2, mainly distributed around the primary improvement area. The range of secondary area depended on the number of connective sources and the distance between sources, influenced by both construction land and farmland.

According to the natural breakpoint method, the area with the highest ecological corridor density of the three levels was regarded as a pinch point area, with a total area of 119.24 km^2. The pinch points were mainly distributed close to the fringe area of the northern research area, with many cornerstones–small ecological sources within. The pinch points of the southwest were mainly distributed between the Yangtze River and ancient forests in southern Anhui, with a complete ecological conservation system and good landscape connectivity. According to the distribution of pinch points, 9 important pinch points were extracted for ecological conservation and improvement.

The Construction and Planning Strategies for ESP in Southern Anhui

The construction of ESP in southern Anhui is based on the comprehensive consideration of the ecological corridor, improvement area and the pinch point. There were 20 ecological sources, 37 ecological corridors, 9 important pinch points and 2 levels of improvement areas. The ecological corridors, pinch points and improvement areas were mainly distributed in the north, relating to the actual situation of southern Anhui. Southern Anhui, the important area with ecological functions of the Yangtze River Delta, has a major district of woodland and grassland, mostly distributed within Huangshan city, Chizhou city and Xuancheng city. Maanshan city and Wuhu city in the region are the bridge between southern Anhui and the external area. The rapid economic development causes significant ecological degradation in the area. To maintain the ecological connection of southern Anhui to the outside world and perform its important ecological function of serving residents, the ESP of southern Anhui is designed accordingly (Fig. 12).

Currently, scholars believe that barrier improvement, ecological pinch point protection and buffering zone construction are effective methods to optimize regional ESP under the circumstances of urbanization. In this study, the improvement area in southern Anhui mainly consisted of farmland and construction land. The improvement area was

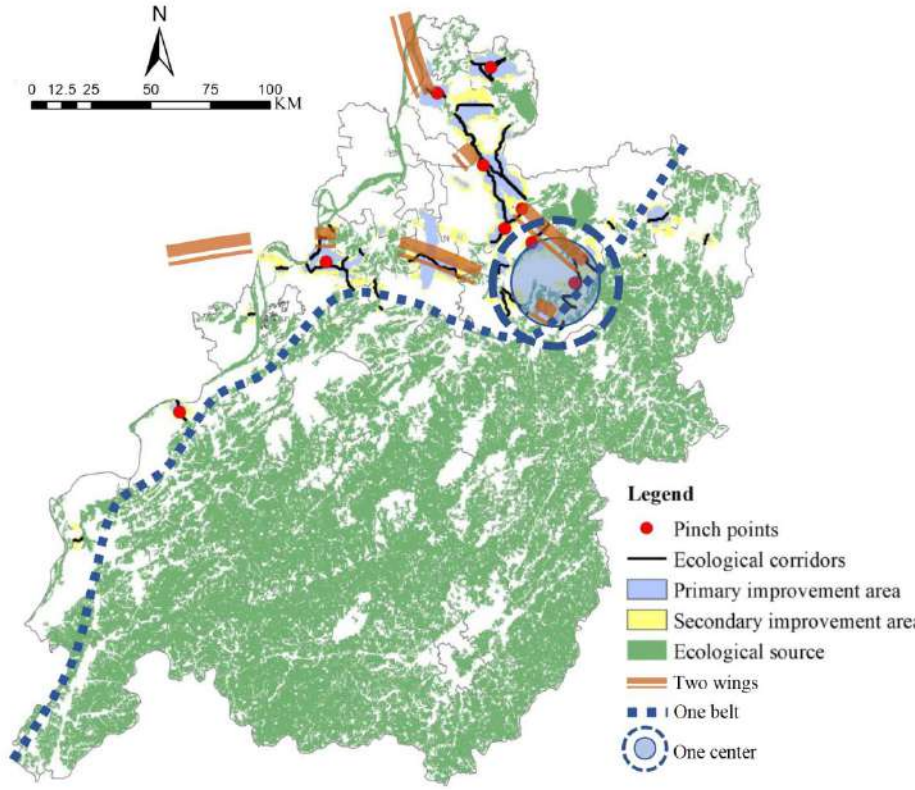

Fig. 12: Spatial distribution map of ecological security patterns.

located in the construction area, mainly around the urban area of Maanshan city of Wuhu city. The urban areas are the center for economic and population growth. Therefore, it is inappropriate to eliminate barriers in practical improvement strategies. Generally speaking, setting urban green belts in an economically developed area is a proper method to deal with the problem. Barriers besides farmland or sources should be eliminated in place, to enhance corridor connectivity. For pinch points that are important to the connection to the ecological source, the development-prohibited area should be set. In the meantime, unified planning at the provincial, city and county level should be conducted to ensure the connectivity of the ecological corridor. In this regard, a comprehensive spatial pattern of "one centre, two wings, one belt" should be generated at the regional level. "One centre" refers to the intersection of Chaohu city, Maanshan city and the southern mountainous area, regarded as an important node allowing species to accept ones from other sources; "two wings" refers to the ecological corridors from the southern mountainous area to Chaohu city and Maanshan city. Due to the overlength of the corridor, policymakers should adopt effective methods to ensure the connectivity of corridor and safeguard species to successfully migrate to the intersection of the southern mountainous area; "one belt" refers to the biological buffering zone that should be set between the southern mountainous area and northern plain area, to prevent the land expansion or population increase in the plain area and thereby avoiding the ecological degradation in the southern mountainous area.

Currently, there is no unified agreement about the method and indices of source extraction at home and abroad. Therefore, it is necessary to conduct validation after indices construction. The study overlaid the geographic positions of national and provincial natural reserves on source identification results, partly verifying the reasonability of the indices extracted from ecological sources. However, limited by manpower and material resources, the study did not construct a quantitative assessment standard of long-term dynamic monitoring. It is required to conduct more in-depth research to verify the reasonability of extracted indices.

Besides, southern Anhui is a region that has a close connection to its surrounding cities, and it surely could be influenced by the outside material and energy flow. Therefore, further research should consider breaking the boundaries of administrative divisions, as well as the influence of surrounding ecological factors on the ecological pattern of the research area.

CONCLUSION

The study constructed identification indices of "people-oriented" ecological source based on ecosystem services, ecological sensitivity and residents' needs and applied the reciprocal of habitat quality and night-time light data to construct landscape resistance surface. At last, based on circuit theory, ESP of southern Anhui was constructed, and then the optimization scheme was generated accordingly.

The main conclusion comprises: (1) the multi-factor comprehensive assessment model based on ecosystem services, ecological sensitivity and residents' needs was applied to identify 20 ecological sources in southern Anhui that suited "nature-ecology-society". Compared with the geographic positions of national and provincial nature reserves, the feasibility and rationality of the model were verified. The area of ecological source accounted for 51.3% of the total, mainly consisting of woodland and grassland; (2) the regional landscape resistance surface in the study was built according to the reciprocal of habitat quality and night-time light data. Compared with the valuation that only considers the land-use type, this valuation considered the important influence of human activities on the ecological process. Therefore, this construction of resistance surface is more reasonable; (3) the range and direction of 37 ecological corridors in southern Anhui were identified according to circuit theory, and then two levels of improvement areas and 9 important pinch points were divided accordingly. The area of the primary improvement area was 1144.42km^2, mainly distributed in the north of southern Anhui; the area of the secondary area was 969.18km^2, mostly consisting of farmland and construction land.

REFERENCES

Chen, X., Peng, J., and Liu, Y. 2017. Construction of Ecological Security Pattern of Yunfushan City Based on the Framework of "Importance-Sensitivity-Connectivity". Geogr. Res., 36(3):471-484.

Dondina, O., Kataoka, L., Orioli, V., and Bani, L. 2016. How to manage hedgerows as effective ecological corridors formammals: A two-species approach. Agric. Ecosyst. Environ., 231, 283–290.

Gao, J., Zou, C., Zhang, K., Xu, M., and Wang, Y. 2020.The establishment of Chinese ecological conservation redline and insights into improving international protected areas. J. Environ. Manag., 264:110505.

Guo, X., Zhang, X., and Du, S. 2020. The impact of onshore wind power projects on ecological corridors and landscape connectivity in Shanxi., Chin. J. Clean. Prod., 254.

He, J., Pan, Y., Liu, D. 2020. Analysis of the wetland ecological pattern in Wuhan from the perspective of an ecological network. Acta Ecologica Sinica, 40(11):3590-3601.

Huang, J., Hu, Y., and Zheng, F. 2020. Research on recognition and protection of ecological security patterns based on circuit theory: a case study of Jinan City. Environ. Sci. Pollut. Res. Int, 27(11):12414-12427.

Jia, L., OuYang, Z., Zhao, T. 2005. The ecological function regionalization of Anhui Province., Acta Ecologica Sinica, 25(2):254-260.

Li, Z., and Li, M. 2020. Spatio-temporal dynamics of ecological security pattern of the Pearl River Delta urban agglomeration based on LUCC simulation. Ecol. Indic., 114.

Li, Z., Yang, G., and Dong, Y. 2007. Establishing the ecological security pattern in rapidly developing regions: A case in the AYRAP. J. Nat. Res. 22(1): 106-113.

Liu J, Yin H W., Kong F H., and Li M H. 2018. Structure optimization of circuit theory-based green infrastructure in Nanjing, China. Acta Ecologica Sinica, 38(12):4363-4372.

Meng, J., Zhu, L., and Yang, Q. 2012. Construction of the ecological security pattern of land use in Ordos City. Acta Ecological Sinica, 32(21):6755-6766.

Nathwani, J., Lu X., Wu, C., Fu, G., and Qin, X. 2019. Quantifying security and resilience of Chinese coastal urban ecosystems. Sci. Total Environ., 672:51-60.

Peng, J., Yang, Y., and Liu, Y. 2018. Linking ecosystem services and circuit theory to identify ecological security patterns. Sci Total Environ, 644(10):781-790.

Peng, J., Yang, Y., Liu, Y., Hu, Y., Du, Y., Meersmans, J., and Qiu S. 2018. Linking ecosystem services and circuit theory to identify ecological security patterns. Sci. Total Environ., Dec 10,644:781-790.

Peng, J., Zhao, H., and Liu, Y. 2017. Urban ecological corridors construction: a review. Acta Ecologica Sinica, (37):23-30.

Schröter, M., Kraemer, R., Remme, and R.P. 2020. Distant regions underpin interregional flows of cultural ecosystem services provided by birds and mammals. Ambio, 49(5).

Song, T., Li, D., Zhang, L. 2020.Evaluation of the importance of regional ecosystem services in the Qinba Mountains and construction of ecological security patterns. Eng. Sci. 22(01): 64-72.

Wang, Y., Jin, X., and Shen, C. 2019. The construction of ecological security pattern in the developed areas in the east—A Case Study in southern Jiangsu. Acta Ecologica Sinica, 39(07):2298-2310.

Xiaona L., Chunlan L., and Long C. 2020. Gradient effects and ecological zoning of ecosystem services in transition zone of Beijing Bay. Transactions of the Chinese Society of Agricultural Engineering, 36(12):276-285.

Xun, F., Luo, K., and Li, Y. 2018. Evaluation of urban water system corridor ecosystem service value based on high-score remote sensing data- Taking the water system corridor in central Beijing as an example. Chin. Gard., 34(10):50-54.

Yin, H.W., Kong F.H., Qi, Y., Wang, H.Y., Zhou, Y.N., and Qing, Z.M. 2011. Developing and optimizing ecological networks in urban agglomeration of Hunan province; China.Acta Ecologica Sinica, 31(10): 2863-2874.

Zhang, D., Qu, L., and Zhang, J. 2019. Construction and optimization of ecological security pattern based on the perspective of ecological supply and demand- Taking the Yangtze River Delta as an example. Acta Ecologica Sinica, 39(20):7525-7537.

Zhou, R., Lin, M., and Wu, Z. 2020. Construction of Ecological Security in Guangdong-Hong Kong-Macao Greater Bay Area from the Perspective of Importance of Ecosystem Services. Ecol. Econ., 36(07):189-196.

Nature Environment and Pollution Technology
An International Quarterly Scientific Journal

p-ISSN: 0972-6268
(Print copies up to 2016)
e-ISSN: 2395-3454

Vol. 20 | No.3 | pp. 1127-1135 | 2021

Original Research Paper

https://doi.org/10.46488/NEPT.2021.v20i03.020

Open Access Journal

Amylase Production by *Aspergillus niger* and *Penicillium* Species by Solid-State and Submerged Cultivation Using Two Food Industrial Wastes

J. Mary Sheela†, K. Divya and S. Premina
Department of Microbiology, Ethiraj College for Women, Chennai, Tamilnadu, India
†Corresponding author: J. Mary Sheela; marysheela_j@ethirajcollege.edu.in

Nat. Env. & Poll. Tech.
Website: www.neptjournal.com

Received: 01-10-2020
Revised: 31-10-2020
Accepted: 12-11-2020

Key Words:
Amylase enzyme
Coconut oil cake (CW)
Brewery wastewater (BW)
Penicillium species
Aspergillus niger

ABSTRACT

Amylase enzymes are starch degrading enzymes and have received a great deal of attention due to their perceived technology importance and economic benefit. Amylase enzymes are considered important enzymes used in starch processing industries for the hydrolysis of polysaccharides like starch into simple sugar constituents. This enzyme is also involved in the commercial production of glucose. Solid-state cultivation and submerged cultivation have tremendous potentials for enzyme amylase production by using different solid substrates like rice bran, wheat bran, coconut oil cake, and groundnut oil cake which are rich in starch. These agro-industrial wastes are considered cheap raw materials for the production of amylase. Wastewater from the industry like brewery can also be used as a liquid substrate for submerged cultivation. It may have the possibility of depurination of wastewater. In the present study, *Aspergillus niger* and *Penicillium* species were isolated and their amylase activity was determined by the starch hydrolysis method. Enzyme production was done by using coconut oil cake as a substrate for solid-state fermentation and brewery wastewater as a substrate for submerged fermentation. The enzyme produced by the organisms was extracted and enzyme assay was done by the Dinitrisalicilic method (DNS method). The protein estimation was done by Lowry Folin's method. The qualitative assay was carried out by performing Gas Chromatography-Mass Spectroscopy (GC-MS).

INTRODUCTION

Enzymes are proteins and consist of long chains of amino acids that fold to produce a three-dimensional structure. Each amino acid sequence produces a specific structure, which has different properties. Enzymes are also responsible for many important biochemical reactions in microorganisms, plants, animals, and human beings. Enzymes differ in their function so that they have the unique ability to facilitate biochemical reactions without undergoing any change themselves. This catalytic ability makes enzymes unique.

Enzymes are biological catalysts with high selectivities. They have been used in the food industry for hundreds of years and play a vital role in many other industries (Detergents, textile manufacturing, pharmaceuticals, pulp, and paper). Recently, enzymes are becoming increasingly important in sustainable technology and green chemistry. They are also produced by various microorganisms including bacterial and fungal species (Esfahanibolandbalaie *et al.* 2008). Generally, enzymes are active at mild temperatures. Above specific temperature, the enzyme is denaturated. It has characteristic pH at which their activity is maximum. Extreme pH values result in electrostatic interactions within the enzyme, leading to the inactivation of enzymes (Prasanna 2005). Other important factors that affect the enzymatic effect are the enzyme concentration, treatment time, additives such as surfactants and chelators, and mechanical stress. The enzyme can break down a particular compound. The molecule that an enzyme acts upon is known as its substrate, which is then converted into a product or products. Some of the most common include amylase which converts starch into simple sugars, proteases that break down proteins, cellulases that break down cellulose, and lipases that split fats into glycerol and fatty acids (Alva et al. 2007). For each type of reaction in a cell, different enzymes are involved and they are broadly classified into six categories such as hydrolytic, oxidizing and reducing, synthesizing, lytic, transferring, and isomerizing. The important characteristic of enzymes is their catalytic function.

Microorganisms particularly have been considered as a treasure of useful enzymes. In recent years, using microorganisms as biotechnological sources of enzymes that are industrially important has stimulated great interest in the exploration of extracellular enzymatic activity in many microorganisms (Pandey et al. 2000). The first industrially produced enzyme was amylase from a fungal source in 1894, which was used for the digestive disorder treatment. Amylases are a class of enzymes that acts as a catalyst in the hydrolysis of starch into simple sugars such as glucose and maltose (Farzana et al. 2016). Amylase is commonly present in human saliva,

where it begins the chemical process of digestion. Starch degrading enzymes such as amylase have been receiving a great deal of attention and interest due to their perceived technological significance and economic benefits. This enzyme is also used for the industrial production of glucose (Saranraj & Stella 2013).

Historically, around 1857 the application of enzymes in textile industrial processes began when malt extract was used to remove size from fabrics before the printing process. Starch is widely used as a sizing agent, because it is readily available, relatively cheap, and based on natural, also sustainable raw materials (Adinarayana et al. 2005). About 75% of the sizing agents used worldwide are starch and its derivatives. In medicinal and clinical areas, there are several processes that involve the application of amylases (Kundu A.K et al. 1970). Because of the increasing demand for these enzymes in various industries, there is more interest in developing enzymes with better and desirable properties such as raw starch degrading amylases that is suitable for industrial applications and their cost-effective production methods (Rodriguez, S.C. and Sanroman, A.M. 2006). They can be obtained from several sources, such as plants, animals, and microorganisms (Saleem et al. 2014).

Amylases are commercially important enzymes and it represents about 25-33% of the worldwide enzyme market (Mouna Sahnoun et al. 2012). Amylases are of various types, namely α, β, and glucoamylase. α-amylases (endo-1,4-α-D-glucan glucohydrolase) are extracellular enzymes that randomly cleaves the 1,4-α-D-glycosidic bonds between adjacent glucose units in the linear amylase chain(Sundarram et al. 2014). β-amylases (β-1,4-glucan maltohydrolase) are mostly of plant origin, but some microbial strains are also known to produce them. It is an exoacting enzyme that cleaves amylose at non-reducing ends, amylopectin, and glycogen molecule (Mojsov et al. 2012). Glucoamylase also called amyloglucosidase, gluconeogenic enzymes, starch glucogenase, and exo-1,4-α-D-glucan glucanohydrolase. It hydrolyses single glucose units from the non-reducing ends of amylose and also amylopectin in a stepwise manner (Singh et al. 2014).

Although many microorganisms are able to produce this enzyme, some of the most widely used for their industrial applications are *Bacillus licheniformis, Bacillus amyloliquefaciens, Aspergillus niger*, *Penicillium chrysogenum* (Saranraj & Stella 2013). When compared to other microbial sources, the fungal amylases are preferred because of their more acceptable GRAS (Generally Recognized As Safe) status, the conditions such as hyphal mode of growth and good tolerance to low water activity (aw) and high osmotic pressure makes fungal species most efficient for bioconversion of solid substrates and thus attracting more interest as source of amylolytic enzymes suitable for industrial applications as given below (Singh et al. 2014).

Industrial Applications	Microbial Source	Role
Conversion of starch	*Bacillus* amyloliquefaciens	Liquefaction, saccharification of starch.
Bakery	*Bacillus* stearothermophilus	Converting starch into smaller sugars.
Detergent industries	*Bacillus* species *Aspergillus* species	Degrade the starchy foods residues such as potatoes, custard, etc.

Solid-state cultivation is more simple, also requires lower capital, has superior productivity, reduce energy needs, requires simple fermentation media and absence of vigorous control of fermentation parameters, uses less water and produces lower wastewater, has easier control of bacterial contamination, and require a lower cost of downstream processing (Sivaramakrishnan et al. 2007).

Submerged fermentation is advanced and industrially important enzymes are commonly produced by using this method. Brewery industries produce large quantities of wastewater. The utilization of this wastewater as a substrate for submerged fermentation may reduce environmental pollution. Usage of solid substrates like coconut oil cake acts as a low-cost substrate for solid-state fermentation (Mabel et al. 2006).

MATERIALS AND METHODS

Isolation of *Aspergillus niger* and *Penicillium* Species

Sabouraud Dextrose Agar (SDA) plates were prepared and a settle plate technique was performed. The SDA plates were kept open for 10 mins and incubated at room temperature for 4 days. After incubation, fungal species were observed on SDA medium.

Two different fungal cultures were selected based on their colony morphology and subcultured on SDA slants. These two fungal cultures were subjected to lactophenol cotton blue staining for observing the morphology.

Slide Culture Technique

A rectangular slab of SDA was prepared and was placed on a clean glass slide. The culture isolate was then inoculated and another glass slide was placed over the top of it to form

a sandwich. This slide was kept inside a petri dish along with moist cotton and incubated for about 3 days at room temperature. After incubation, the coverslip was placed on a drop of lactophenol cotton blue stain and viewed under the microscope (45x). The morphology of *A.niger* and *P.species* were observed and photographed.

Determination of Amylase Activity

A.niger and P.species isolates were tested for amylase production by starch hydrolysis. Starch agar medium was prepared and inoculated with the isolated organisms and then incubated at room temperature for about 2-3 days. After incubation, the plates were flooded with the iodine solution, and the zone of clearance was observed around the microbial growth, which indicates the production of amylase. Based on the zone of clearance, the fungal isolates were used for further studies on the production of the enzyme amylase.

Enzyme Production

Enzyme production was done by two methods namely,

- Submerged fermentation (SmF)
- Solid-state fermentation (SSF)

Submerged Fermentation (SmF)

The inocula were prepared by transferring 2ml of 60-hours old culture slant in 50ml of a medium composed (g/L) as follows, Glucose-20; (NH_4) SO_4-6.6; KH_2PO_4- 3.5; $FeSO_4.7H_2O$-0.15; $MgSO_4.7H_2O$-0.10;

$MnCl_2.2H_2O$-0.45; Mycological peptone-3.0. The media pH was adjusted at 6.8 and then autoclaved at 121°C for 15 mins. The media was allowed to cool and inoculated. After inoculation, the culture was incubated at 30°C for 48h.

Brewery wastewater, which was used as the culture media base, was collected from the local brewery plant. The brewery wastewater was subjected to centrifugation at 12,000 rpm for 15 mins to remove the solids suspensions. The supernatant was collected for further use. The production media was obtained by supplementing this supernatant with the following nutrients (g/l): Mycological peptone-3.0; $(NH_4)SO_4$-6.6; $CacO_3$-8.0; NaCl-5; KH_2PO_4-3.5; $FeSO_4.7H_2O$-0.15; $MgSO_4.7H_2O$-0.10; Soluble potato starch-40. The media pH was adjusted at 6.0 and sterilized (121°C for 15 mins), inoculated with 2% inoculum level, and incubated at 30°C.88 h^{-1} (Mabel et al. 2006).

Solid-State Fermentation (SSF)

Substrates like coconut oil cake were used as a solid substrate for solid-state fermentation. Ten g of coconut oil cake was weighed and hydrated with 10 mL of basal salt solution and adjusted with moisture content from 43-81% (Ramachandran et al. 2004). The substrate was sterilized by autoclaving at 12°C for 15 mins. 1% of inoculum was inoculated after sterilization and then incubated at room temperature for 6 days (Suganthi et al. 2011).

Enzyme Extraction for Submerged Culture

After incubation, the culture sample was filtered by using Whatman filter paper No.1. The paper-filtered media was used to perform analytical determinations (Mabel et al. 2006).

For Solid-state Culture

After incubation, 0.1 M phosphate buffer saline was prepared and pH was adjusted to pH 7.0. 22 mL of freshly prepared phosphate buffer saline was added to the substrate beds and shaken vigorously in a rotary shaker for 15-20 mins at 120 rpm.

The mixture was then filtered through a cheese cloth and the filtrate was subjected to centrifugation at 8000 rpm at 4 for 15 mins. The supernatant was collected in a clean fresh tube and it was filtered through a cheese cloth, the filtrate was used as the crude enzyme preparation (Suganthi et al. 2011).

Assay of Amylase Activity

Dinitro Salicylic Acid Method (DNS)

For standard preparation, different concentration of maltose (1 mm, 2 mm, 3 mm, 4 mm, 5 mm, 10 mm) was prepared and DNS assay was performed. 6 tubes were arranged in a row of test tube rack and labeled as S1, S2, S3, S4, S5, S6, T1 (*A.niger* BW), T2 (*Penicillium* sps BW), T3 (*A. niger* CW), T4 (*Penicillium* sps CW). 1 mL of the respective stocks and samples were transferred to the labeled tubes. 1mL of DNS reagent was added to all the tubes, then all the tubes were heated at 100° for 5 mins. After heating, the tubes were allowed to cool. All the tubes were made into 10 mL with distilled water. Then it was transferred to cuvettes and the absorbance value was noted at 540 nm using a calorimeter. The graph was plotted with a concentration of maltose at the x-axis and absorbance value (OD value) at the y-axis.

Estimation of Protein Lowry-Folin's Method

A series of tubes were taken and labeled as Blank, S1, S2, S3, S4, S5, S6, T1, T2, T3, T4 respectively. 0.5 mL, 1mL, 1.5 mL, 2 mL, 2.5 mL, and 3 mL of Bovine serum albumin (standard) was added to the S1, S2, S3, S4, S5, S6 respectively. 1 mL of samples were added to T1, T2, T3, T4. All the tubes were made up to 3mL with distilled water. Then 4.5 mL of Alkaline copper reagent was added to all the test tubes. 0.5 mL of Folin's reagent was added to all the test

tubes and incubated at room temperature for 10 mins. After incubation absorbance value was noted at 560 nm using a calorimeter. The graph was plotted with a concentration of protein at the x-axis and absorbance value (OD value) at the y-axis.

Gas Chromatography-Mass Spectroscopy (GC- MS)

The enzyme samples were qualitatively assayed by performing Gas Chromatography-Mass Spectroscopy (GC-MS). GCMS was performed by using equipment 7000 Series Triple Quad GC/MS for the enzyme samples to identify the amount and type of chemicals present in the sample by measuring the mass-to-charge ratio and abundance of gas-phase ions. This equipment is a standalone capillary GC detector for use with the Agilent 7890A Series gas chromatograph. Mass spectroscopy works by the principle of ionizing chemical compounds to generate charged molecules and measuring their mass-to-charge ratio.

In GCMS, the sample is ionized. Molecules of the samples break into a charged fragment during the ionization process. Ions are separated based on their mass-to-charge ratio (m/z). Ions are detected by using a mechanism that has the ability to detect charged particles (e.g. electron multiplier). Results are finally displayed as spectra of the relative abundance as a function of the m/z ratio. Identification is carried out by correlating known masses to the identified masses or by a characteristic fragmentation pattern.

RESULTS AND DISCUSSION

Isolation of Organisms

Fungal cultures like *P.species* and *A.niger* were isolated by the settle plate technique. The colony morphology on the SDA plate was observed as follows,

- The colonies cottony in texture, initially white and later became gray-green or olive-gray (Fig. 1a).

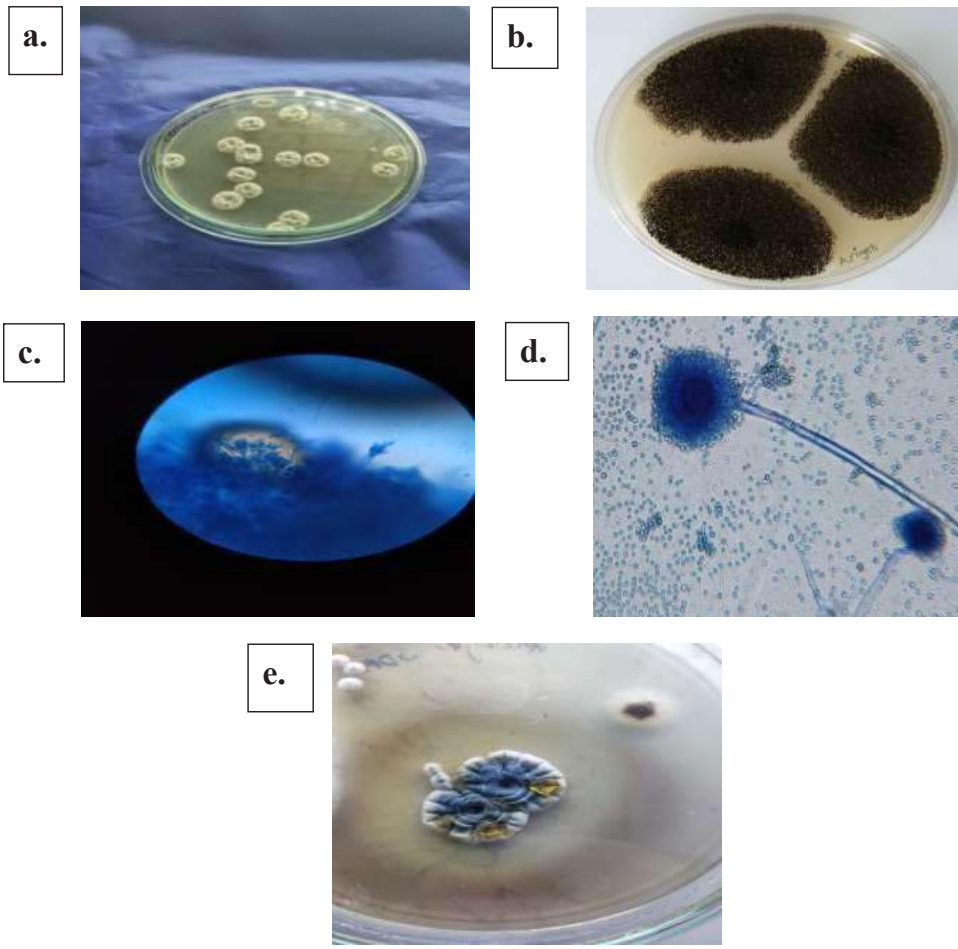

Fig. 1: a. SDA plates showing *Penicillium species* b. SDA plates showing *Aspergillus niger* c. Lacto phenol cotton blue staining showing *Penicillium species* d. Lacto phenol cotton blue staining showing *Aspergillus niger* e. Plate showing zone of clearance around *Penicillium species* colonies.

- Salt and pepper appearance and reverse turning pale yellow (Fig. 1b).

Slide Culture Technique

The morphology was microscopically observed by performing slide culture technique and the structure was identified by staining with lactophenol cotton blue stain as follows,

- Dense, brush-like, spore-bearing structures. Simple or branched conidiophores and terminated by flask-shaped phialides. It confirms *P.species* (Fig. 1c).
- Dark brown in color, globose vesicle with primary and secondary sterigmata, and conidiospores cover the entire surface of the conidial head. It confirms *A.niger* (Fig. 1d).

Determination of Amylase Activity

A starch hydrolysis test was performed. Zone of clearance was observed around the colonies on each plate containing *A.niger* and *P.species* (Fig.1e). It indicates the ability of the isolated organisms to produce the enzyme amylase.

Submerged Fermentation

The brewery wastewater supplemented with nutrients was used as a liquid medium. *A.niger* and *P.species* were inoculated in two different conical flasks containing liquid medium and incubated (Fig. 2a, 2b).

After incubation, the culture medium was paper filtered (Fig. 2c, 2d). The filtrate was used as a crude enzyme (Fig. 2e, 2f).

Solid-State Fermentation

Coconut oil cake was used as a solid substrate. The substrate was inoculated with *A.niger and P.*species in two different conical flasks and incubated.

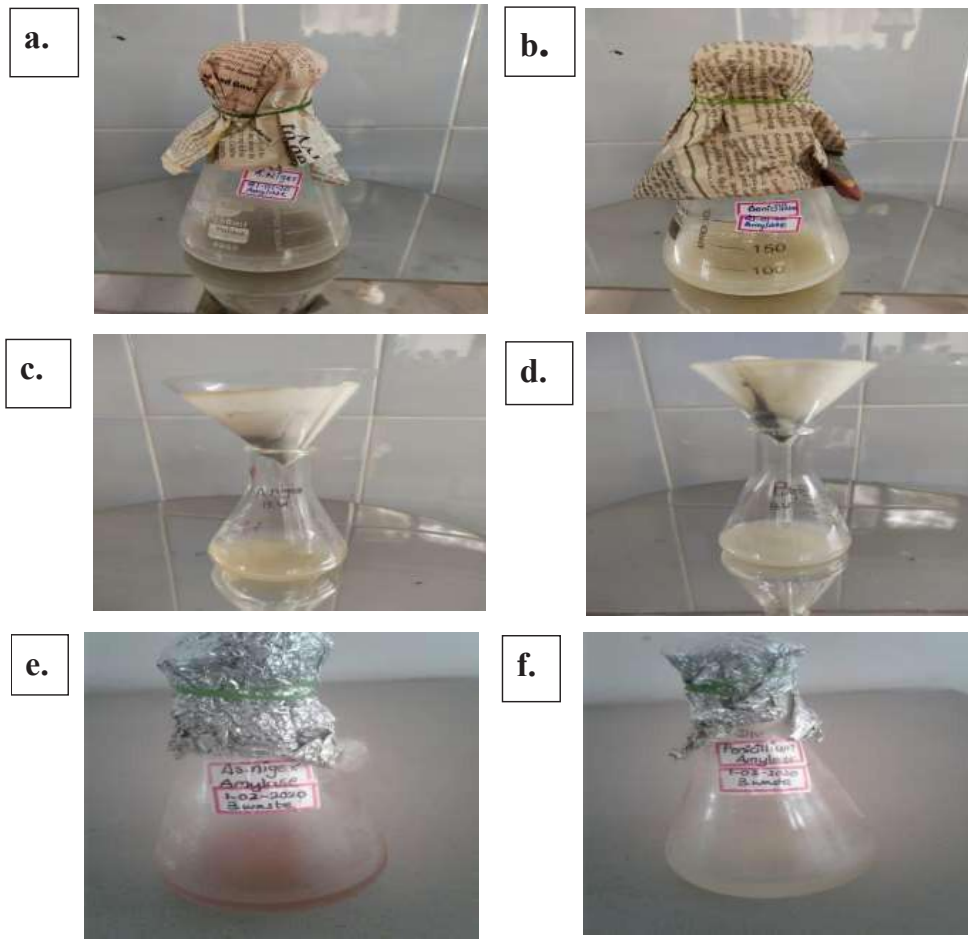

Fig. 2: a. Submerged fermentation of *Aspergillus niger* b. Submerged fermentation of *Penicillium species* c. Filteration of culture medium (BW) for *Aspergillus niger* d. Filtration of culture medium (BW) for *Penicillium species* e. Crude enzyme obtained from submerged fermentation of *Aspergillus niger* f. Crude enzyme obtained from 0submerged fermentation of *Penicillium species.*

After incubation, the mat growth was observed (Fig. 3a, 3b). It was then centrifuged and the supernatant (Fig. 3c, 3d) was filtered using a cheese cloth and used as a crude enzyme (Fig. 3e, 3f).

Assay of Amylase Activity Dinitrosalicyclic Acid Method

Dinitrosalicylic method was performed. The absorbance value was noted at 540 nm using a calorimeter for enzyme samples and standards (Fig. 4b). The graph was plotted with a concentration of maltose against absorbance (OD value) (Fig. 4a). From the graph, the concentration of amylase in the enzyme samples was determined (Fig. 4c).

Estimation of Protein by Lowry Folin's Method

The protein content of the samples was estimated using Lowry Folin's method. The absorbance value for the standards and test were noted at 560 nm using a calorimeter (Fig. 5b). The graph was plotted with concentration along the x-axis against absorbance value along the y-axis (Fig. 5a). The concentration of protein of crude enzyme extracts was estimated (Fig. 5c).

Gas Chromatography-Mass Spectroscopy

GC-MS was performed for the enzyme samples for qualitative analysis. Various chemi-

Fig. 3: a. Solid-State fermentation(SSF) of *Aspergillus niger* b. Solid-State fermentation of *Penicillium species* c. Supernatant obtained from centrifugation of filtrate from SSF of *Aspergillus niger* d. Supernatant obtained from centrifugation of filtrate from SSF of *Penicillium species* e. Crude enzyme obtained from SSF of *Aspergillus niger* f**.** Crude enzyme obtained from SSF of *Penicillium species*

a.

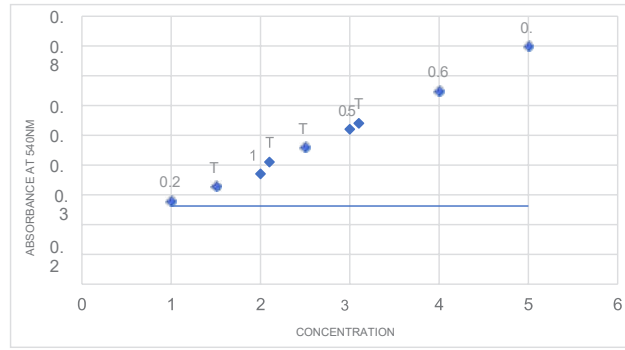

b.

	CONCENTRATION	ABSORBANCE (nm)
S1	1mm	0.31
S2	2mm	0.35
S3	3mm	0.40
S4	4mm	0.65
S5	5mm	0.80
T1	-	0.33
T2	-	0.26
T3	-	0.50
T4	-	0.41

c.

TEST SAMPLES	CONCENTRATION ($mg.mL^{-1}$)
T1	2
T2	1.5
T3	3.1
T4	2.5

Fig. 4: a. Graph plotted with concentration against absorbance b. Absorbance value of standards and samples in DNS method c. Concentration of amylase in test samples.

a.

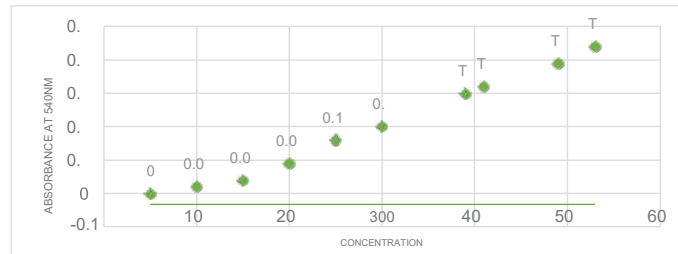

b.

	CONCENTRATION (mL)	ABSORBANCE (nm)
S1	50	0
S2	100	0.02
S3	150	0.04
S4	200	0.09
S5	250	0.16
S6	300	0.2
T1	-	0.32
T2	-	0.30
T3	-	0.44
T4	-	0.39

c.

TEST SAMPLES	CONCENTRATION (µg.mL)
T2	410
T2	390
T3	530
T4	490

Fig. 5: a. Graph plotted with concentration against absorbance b. Absorbance values obtained from Lowry Folin's method **c.** Concentration of protein in crude enzymes by Lowry Folin's method.

cal compounds for each test sample were observed (Tables 1, 2, 3 and 4).

DISCUSSION

Amylase is a vital enzyme involved not only in modern biotechnology but also employed in various industries like starch processing industries for the hydrolysis of polysaccharide and paper industries. Enzyme amylase obtained from fungal species has large applications in the food and pharmaceutical industries and also widely used for the preparation of oriental foods.

The present study states that the enzyme amylase can be produced by using food wastes like brewery wastewater and coconut oil cake that are cost-effective and easily available when compared to the conventional substrates. Using brewery wastewater as a substrate may also reduce environmental pollution. *A.niger* and *P.species* were isolated by using the settle-plate technique. The slide culture technique was carried out to observe the morphology of the organisms.

Starch hydrolysis test was performed, zone of clearance around the colonies indicates their ability to produce the enzyme amylase. Enzyme production was done by submerged cultivation using brewery wastewater as a liquid substrate, and solid-state fermentation using coconut oil cake as a solid substrate. Crude enzymes were obtained by using the

Table 1: GC-MS analysis of the crude extract from SSF of *Penicillium* species.

S. No.	Compound Name	Structural Formula	Molecular Weight ($g.mol^{-1}$)	Retention Time
1	Naphtho[1,2-b]furan2- one,2,3,3a,4,5,5a,6,7,9a,9 b-decahydro-3,5a,9- trimethyl-7,9a-peroxy	$C_{15}H_{20}O_4$	262.17	12.864
2	7,9-Di-tert-butyl-1- oxaspiro(4,5)deca6,9- di-ene-2,8-dione	$C_{17}H_{24}O_3$	276.36	18.899
3	2-Oxepanone,5-(1,1- dimethylethyl)	$C_{10}H_{18}O_2$	170.24	29.022

Table 2: Qualitative analysis of the crude extract from SSF of *Aspergillus niger.*

S. No.	Compound Name	Structural Formula	Molecular Weight ($g.mol^{-1}$)	Retention Time
1	Dodecanal	$C_{12}H_{24}O$	184.3	8.724
2	Phthalic acid, butyl cyclobutyl ester	$C_{16}H_{20}O_4$	276.32	18.891
3	Bis(2-ethylhexyl) phthalate	$C_{24}H_{38}O_4$	390.55	29.010

Table 3: Qualitative analysis of the crude extract from SmF of *Penicillium* species.

S. No.	Compound Name	Structural Formula	Molecular Weight ($g.mol^{-1}$)	Retention Time
1	Benzothiazole,2-(2- hydroxyethylthio)-	$C_9H_9NOS_2$	211.30	19.862
2	1,4-Benzenediamine, N-(1,3- dimethylbutyl)-N'- phenyl	$C_{18}H_{24}N_2$	268.39	29.002
3	1,3Benzenedicarboxylic acid,bis(2-ethylhexyl) ester	$C_{24}H_{38}O_4$	390.55	37.291

Table 4: Qualitative analysis of the crude extract from SmF of *Aspergillus niger.*

S. No.	Compound Name	Structural Formula	Molecular Weight ($g.mol^{-1}$)	Retention Time
1	Z-8-Methyl-9- tetradecenoic acid	$C_{15}H_{28}O_2$	240.38	9.691
2	7,9-Di-tert-butyl-1- oxaspiro(4,5)deca-6,9- diene2,8dione	$C_{17}H_{24}O_3$	276.36	18.891
3	cis-13-Octadecenoic acid	$C_{18}H_{34}O_2$	282.46	29.023

performed. Qualitative analysis of enzyme extract was done by performing Gas Chromatography-Mass Spectroscopy (GC-MS).

CONCLUSION

Amylase enzyme was produced by using food industrial wastes such as coconut oil cake as a solid substrate for solid-state fermentation and brewery wastewater as a liquid substrate for submerged fermentation. It indicates that the utilization of these wastes as a substrate may decrease environmental pollution and also reduces the production cost of the enzyme amylase.

REFERENCES

Adinarayana, K., Kugan, P. and Suren, S. 2005. Amylase production in solid-state fermentation by the *Thermophilic lanuginosus*. J. Biosci. Bioeng., 100(2): 168-171.

Alva, S., Anupama, J., Savla, J., Chiu, Y.Y., Vyshali, P., Sruthi, M., Yogeetha, B.S., Bhavya, D., Purvi, J., Ruchi, K., Kumudini, B. S. and Varalakshmi, K.N. 2007. Production and characterization of fungal amylase enzyme isolated from *Aspergillus species*. JGI 12 in solid-state culture. Afr. J. Biotechnol., 6(5): 576-581.

Esfahanibolandbalaie, Z., Rostami, K. and Mirdamadi, S.S. 2008. Some studies of α-Amylase production using *Aspergillus oryzae.* Pak. J. Biol. Sci., 11(22): 2553-2559.

Farzana,Y., Minhal, A., Amna, A., Hafsa, S., Azra, N., Asma, A., Shakeel, A.K. and Shah, A.U.Q. Solid state fermentation: A cost-effective approach for the production of starch liquefying fungal amylase using agro-industrial wastes. Sci. Int., 28(3): 2703-2706.

Kundu, A.K. and Das, S. 1970. Production of amylase in liquid culture by strains of *Aspergillus oryzae.* Amer. Soc. Microbiol., 19(4): 598-603.

Mabel. S.H., Marilu, R., Ne, l.P.G. and Renato, P.R..2006. Amylase production by *Aspergillus niger* in submerged cultivation on two wastes from food industries. J. Food Eng., 73: 93-100.

Mojsov, K. 2012. Microbial α-amylases and their industrial applications: A review. Int. J. Manag., 2(10): 583-609.

Naidu, M.A. and Saranraj, P. 2013. Bacterialamylase: A review. Int. J. Pharm. Biol. Arch., 4(2): 274-287.

Prasanna, V.A.. 2005. Amylase and their applications. Afr. J. Biotechnol., 4(13): 1525-1529.

Ramachandran, S., Patel, A.K., Nampoothiri, M., Francis, F., Nagy, V., Szakacs, G. and Pandey, A. 2004. Coconut oil cake: A potential raw material for the production of α- amylase. Biosource Technol., 93: 169-174.

Rodriguez, S.C. and Sanroman, A.M. 2006. Application of solid-state fermentation to the food industry. J. Food Microbiol., 76: 291-302.

Saranraj, P. and Stella, D. 2013. Fungal amylase: A review. Int. J. Microbiol. Res., 4(2): 203-211.

Saleem, A., Mohsen, K.H. and Ebrahim, E. 2014. Production of amylase by fungi isolated from legume seeds collected in Almadinah Almunawwarah, Saudi Arabia. J. Taibah Univ. Sci., 8: 90-97.

Singh, S., Singh, S., Bali, V., Sharma, L. and Mangla, J. 2014. Production of fungal amylases using cheap, readily available agriresidues, for potential application in textile industry. Biomed Res. Int.., 2014(8): 1-9.

Sivaramakrishnan, S., Gangadharan, D., Nampoothiri, K.M., Soccol, C.R. and Pandey, A. 2007. Alpha-amylase production by *Aspergillus oryzae* employing solid-state fermentation. J. Sci. Ind. Res., 66(8): 621-626. Sundarram, A. and Thirupathihali, P.K.M. 2014. Alpha-amylase production and application: A review. J. Appl. Environ. Microbiol., 2(4): 166-175.

Suganthi, R., Benazir, J.F., Santhi, R., Ramesh Kumar, V., Anjana, H., Nitya, M., Nidhiya, K.A., Kavitha, G. and Lakshmi, R. 2011. Amylase production by *Aspergillus niger* under solid-state fermentation using agroindustrial wastes. Int. J. Eng. Sci. Technol., 3(2): 1756-1763.

Nature Environment and Pollution Technology
An International Quarterly Scientific Journal

p-ISSN: 0972-6268
(Print copies up to 2016)
e-ISSN: 2395-3454

Vol. 20 | No.3 | pp. 1137-1145 | 2021

Original Research Paper

https://doi.org/10.46488/NEPT.2021.v20i03.021

Open Access Journal

The Physicochemical Characteristic of Activated Carbon Based on Sludge and Preparation Method

H. Lu†, F. Luo, Q. Zhang, J. Li and L. Cai

School of Civil Engineering and Architecture, Wuhan Polytechnic University, Wuhan 430023, P.R. China

†Corresponding author: H. Lu; lhj_whpu@163.com

Nat. Env. & Poll. Tech.
Website: www.neptjournal.com

Received: 28-08-2020
Revised: 19-10-2020
Accepted: 08-12-2020

Key Words:
Sludge
Activated carbon
Adsorption

ABSTRACT

To understand the features and best preparation of sludge activated carbon (SAC), and the pore structure, component, adsorption characteristics, and the yield rate of SAC, many tests have been carried out. The study illustrated that the pore structure was mostly mesopore and amorphous pore such as the ink bottle hole. In terms of different preparations to obtain SAC, the yield of SAC in sample No.1 achieved 88.09%. Using the preparation of $ZnCl_2$ as an activator, the iodine adsorption value was significantly higher than other preparations. However, the content of quartz in sample No.1 achieved a maximum of 52.51%. Charcoal was detected in all samples except sample nos 9-12. The adsorption capacity of Cu(II) and Cd(II) reached a maximum of 600.02 $mg.kg^{-1}$ and 383.2 $mg.kg^{-1}$. The results showed an optimum preparation condition, which was by using the $ZnCl_2$ as an activator, 2:1 as the impregnated ratio, 40% concentration in activator and at 400ºC reaction temperature could create rich pore structure and charcoal inside.

INTRODUCTION

A number of problems in sewage treatment plants directly appear in real life such as continual increasing cost, sewage, sludge, and the low rate of resource utilization. According to government statistics, the amount of dry sludge produced when it is handled by municipal sewage bureaus in China is 15 million t which accounts for 32% of total solid waste in China, and the annual growth rate is higher than 10% (Yang 2010). The contamination of water by heavy metal ions has become a big problem in China. To effectively prevent and improve this situation, many scientists are trying to find innovative methods like creating a strong and brand-new adsorption material to adsorb heavy metal ions instead of using traditional methods such as the chemical precipitation method and ion exchange. As we all know, activated carbon has the ability to remove heavy metal ions in water, which is a huge advantage. However, scientists indicate that the preparation of activated carbon is not easy, and the raw material cost is expensive especially if activated carbon is prepared using coal or wood as raw material. Hence, finding an alternate material is critical to resolving the cost problem (Lai et al. 2012). The inner composition of sludge contains high organic matters which can be used to generate activated carbon by using a rational method. Then the wasted sludge can be converted into a new material with adsorption properties. Wang et al. (2012) claimed that when the temperature in the pyrolysis test was set at 400-700°C, with the thermal decomposition temperature enhancement, the decomposition fluid's production rate increased gradually. Li et al. (2012) found it was highly effective to prepare sludge activated carbon using $ZnCl_2$ as an activator with rational concentration (45%), and with the reaction temperature set at (600°C), the immersed temperature set at (45°C), and the reaction time being(50 mins). Moreover, he discovered that sludge activated carbon (SAC) had the adsorption ability to remove heavy metal ions as well. Li et al. (2013) found that when SAC is prepared from sewage sludge from a municipal sewage treatment plant combined with corn stalks, the results showed that when activated carbon was produced under the condition of 25% corn straw content and 500°C pyrolysis temperature, the BET surface area achieved 756 $m^2.g^{-1}$. The yield presented a trend of gradually dropping with increasing temperature. When activated carbon was prepared under the temperature of 450°C and corn straw content of 25%, yield attained the maximum value of 43.1%.Liu and Liu (2013) stated that when the optimal combination was set at 3 $mol.L^{-1}$ of $ZnCl_2$, pyrolysis temperature was set at 550°C, chemical activation was set for 2 hours and a liquid-solid ratio of 1.5:1, it showed that the adsorption of methylene blue in SAC was 41.9 $mg.g^{-1}$ with a yield of 48.9%. Bao et al. (2012) revealed that the SAC surface with rich acidic functional groups played a crucial role in the adsorption of heavy metals, especially in terms of the adsorption of

Cd(II). Neither the Langmuir nor Freundlich model described the isotherms satisfactorily, suggesting that the number of binding sites for Cd(II) on the surface of SAC was small. The adsorption of SAC was in ion exchange, and SAC could easily remove COD and TP from landfill leachate (Wu et al. 2017). SAC prepared by using ZnCl2 as an activator achieved good quality, the concentration of SAC was at 180 $g.L^{-1}$, and pollutants in wastewater decreased (Duan et al. 2016, Zheng et al. 2016). The product rate of SAC might be affected by temperature, time, and others, but the key influence is pyrolysis temperature (Agrafioti et al. 2013). The study illustrated that it was potential to use dewatering sludge as a modified agent for landfill liners, and the changes in the plastic index, hydraulic conductivity, and compressive strength were the main factors (Li et al. 2014).

In this paper, the rational preparation method, the inner pore structure, and the adsorption ability of SAC were performed. Several laboratory tests were conducted such as low-temperature nitrogen adsorption measurement, batch adsorption test, SEM, X-ray diffraction test, and the iodine adsorption value test. The low-temperature N_2 adsorption test and the iodine adsorption value test were used to analyze pore structure, and the X-ray diffraction and SEM were used to examine the composition analysis. A batch adsorption test was used to understand the adsorption ability of Cd(II) and Cu(II) to the SAC.

MATERIALS AND METHODS

Test Materials

The sludge was fresh from the Hanxi sewage treatment plant in Wuhan, Hubei Province, and the sludge used in the test was after the removal of water. The X-ray diffraction test was performed to obtain the elemental composition of sludge and the results are shown in Table 1. The determination method exhibited the physical characteristics of the sludge taken from the municipal sludge the wastewater treatment plant, which is shown in Table 2.

Test Methods

The recovered fresh sludge was dried in a drying oven at 105°C. After the removal of all water, dried sludge was ground into powder in a ball grinding mill. The treated sludge was sieved through a 1 mm sieve, and then, the reaction condition was set for different impregnation ratios, different temperatures, and different activation concentrations. Finally, different activators were mixed with treated sludge till all the chemical reactions were completed. After 24 hours, a series of complex chemical reactions were performed. In the end, the SAC was sealed, after washing and drying it

Table 1: The elemental composition of sludge.

Element name	C	O	Mg	Al	Si	P	S	K	Ca	Fe	Other
m(%)	7.87	54.1	1.28	5.80	14.83	2.34	1.87	1.54	3.77	5.19	1.41

Table 2: The basic physical characteristics of sludge.

pH	Specific gravity (g/mL)	Organic (%)	W (%)	e	K (cm/s)
6.96	1.24	43.2	80.3	3.36	1.20×10^{-8}

Table 3: The orthogonality experiment.

Affect / Number	A	B	C	D
	Activators	Temperature (°C)	Impregnation Ratio	Concentration of Activator (%)
1	$ZnCl_2$	400	2:1	40
2	$ZnCl_2$	500	1:1	45
3	$ZnCl_2$	600	1:2	50
4	$ZnCl_2$	700	1:3	55
5	H_3PO_4	400	1:1	55
6	H_3PO_4	500	2:1	50
7	H_3PO_4	600	1:3	45
8	H_3PO_4	700	1:2	40
9	Na_2CO_3	400	1:3	50
10	Na_2CO_3	500	1:2	55
11	Na_2CO_3	600	1:1	40
12	Na_2CO_3	700	2:1	45

again. According to the preparation conduction, as shown in Table 3, a series of tests was conducted.

To check the yield of SAC obtained from different preparations, the formula is as below:

$$P=\frac{m_a}{m_c}\times 100\% \quad \ldots(1)$$

Where P is the yield of activated charcoal, m_a is the weight of the sample after carbonizing, m_c is the weight of the sample before carbonizing.

Iodine adsorption value test: According to the test method of wooden activated carbon-determination of iodine number (GB/T12496.8-1999), 10 mL of hydrochloric acid solution with 0.50 g SAC was added into a conical bottle, and the bottle was shaken to fully moist the solution in the bottle. Then, it was heated, boiling for 30 seconds. After the temperature cooled down, 50.0 mL of iodine standard solution was added into the conical bottle, after that the bottle was sealed. The bottle vibrated in an oscillator for 15 mins and was filtered quickly. The 10 mL solution extracted from the conical bottle was mixed with 100 mL distilled water, and finally, it was titrated with the standard solution of sodium thiosulfate. The iodine adsorption value was calculated by the following formula:

$$A=\frac{5(10C_1\text{-}1.2C_2V_2)\times 126.93}{m} \quad \ldots(2)$$

Where A is the iodine adsorption value, C_1 is the concentration of the standard solution of iodine, C_2 is the concentration of the standard solution of sodium thiosulfate, V is the volume of sodium thiosulfate, c is the concentration of the rest of the filtrate solution and m is the weight of the SAC.

Low-temperature nitrogen adsorption measurement: Using the JW-BK static nitrogen adsorption instrument, the pore structure characteristics of SAC were examined. 0.50 g of SAC was dipped in 99.99% liquid nitrogen, then the reaction was observed and the results were obtained. The JW-BK static nitrogen adsorption instrument uses different values of P/P_0 to predict the pore distribution. In the end, the specific surface area, pore size, and pore volume distribution of SAC were calculated according to the standard BET method.

X-ray diffraction test and SEM test: The samples used in the XRD test were samples after different chemical activation preparation methods. The XRD test was repeated about four times with SAC which was obtained from different chemical activation preparation methods. The composition of the samples was determined by using X-ray diffraction (Holland PA Nalytical Co.Ltd) with a Cu-Kα operating at 45 kV and 40 mA. The divergence slit was 0.19 mm. The scanning speed was $6°.min^{-1}(2\theta)$. Data were recorded between 5° and 85° with a step size of 0.04°.

The microstructure of the SAC was observed by using an S-3000 N scanning electron microscope. To obtain detailed data of SAC, the samples of SAC were selected carefully, and the SEM test was carried out in three groups of parallel tests with the same sample. The samples were air-dried and stored at 5°C. However, the surface of SAC was gilt with a thickness of approximately 20 nm according to the "General rules for analytical scanning electron microscopy" (JY/T 010-1996). Surface micromorphology was tested by using an S-3000N scanning electron microscope (Hitachi, Japan). SEM images with magnifications of 1000 × were obtained.

Batch adsorption test: The 3 g sample in the test, which was obtained from three different preparation methods, was numbered 1, 5, and 9, respectively, and then immersed in 25 mL Cd(II) or Cu(II) chemical solutions. The initial concentration of Cd(II) or Cu(II) was 50-350 $mg.L^{-1}$. After mixing evenly, the mixture was placed in a water bath instrument at 25°C. Then, the mixed solution was quiesced for 24 hours, and the concentration of Cd(II) or Cu(II) in the suspension solution after centrifugation was measured by spectrophotometry (Shanghai Third Analytical Instruments Factory) according to GB 7467-87 DPC. The concentration of heavy metal ions adsorbed on the SAC was calculated from the mass balance:

$$q_e=\frac{(C_0-C_e)\cdot V}{M}\times 100\% \quad \ldots(3)$$

Where q_e is the adsorbed amount of Cd(II) or Cu(II) onto SAC, C_0 is the initial concentration of Cd(II) or Cu(II), C_e is the equilibrium concentration of Cd(II) or Cu(II), V is the volume of the aqueous phase and M is the weight of the SAC.

RESULTS AND DISCUSSION

Iodine Adsorption Value Test

As depicted in Fig. 1, it was revealed that different preparation methods affected the overall yield of SAC, and the range of yield was between 62.01% to 88.09 %. When the activator was $ZnCl_2$, H_3PO_4, Na_2CO_3, the highest yield of SAC was 88.09%, 83.98%, and 79.63%, respectively. It was obvious that the yield of SAC was more than 80% when $ZnCl_2$ was chosen as the activator, and the least yield of SAC, which was less than 80%, was when Na_2CO_3 was chosen as the activator. Thus, the best order of acquisition rate of SAC was $ZnCl_2 > H_3PO_4 > Na_2CO_3$. The results claimed that by selecting $ZnCl_2$ as an activator, the maximum yield of SAC could be achieved. Even if the rest of the conditions were different, except activators, the SAC prepared by $ZnCl_2$ achieved a high yield compared to the others.

Fig. 2 shows SAC produced by different preparation methods presented by the difference in the degree of pores, directly causing the value of iodine adsorption capacity.

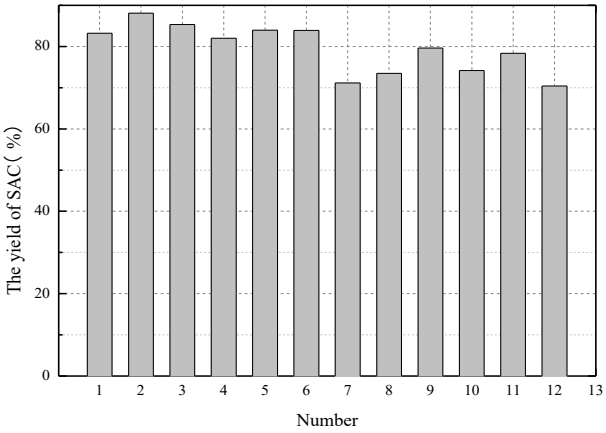

Fig. 1: The yield of SAC.

As shown in Fig. 2(a), with the increase of activation temperature, by selecting $ZnCl_2$ and H_3PO_4 as the activators to prepare SAC, the curves showed a downward trend as a whole. When the activation temperature was at 400ºC, taking $ZnCl_2$, H_3PO_4, and Na_2CO_3 as the activators, the maximum value of iodine adsorption capacity was achieved, and the iodine adsorption value was 452.16, 363.69, 257.80 $mg.g^{-1}$, respectively. Fig. 2(b) showed the value of iodine adsorption in the sample was variable with the change of impregnated ratio under different preparation methods. By choosing H_3PO_4 as an activator to produce SAC, the impregnated ratio was 1: 1, the iodine adsorption value in the sample reached a maximum of 363.69 $mg.g^{-1}$, and the iodine adsorption value corresponding to the impregnated ratio was in the range of 240.37 to 273.88 $mg.g^{-1}$. However, when using Na_2CO_3, as an activator, the curve is stable and the iodine adsorption value in the sample was in the range of 221.61 to 263.16 $mg.g^{-1}$. According to Fig. 2(c), with the increase of the concentration in the activator, it was evident that there was a change in the curves once the activator chosen was either $ZnCl_2$ or H_3PO_4. Moreover, when using $ZnCl_2$ as an activator to prepare SAC, and the concentration is at 40%, the value of iodine adsorption was the maximum at 452.16 $mg.g^{-1}$. However, the concentration of H_3PO_4 at 50% to prepare SAC resulted in a maximum iodine adsorption value of 363.69 mg/g^{-1}. Hence, as shown in Fig. 2, the curves of $ZnCl_2$ as an activator were all distributed at the top of other curves which depicted other activators, and the iodine adsorption value in the sample was obviously higher than that of the others. Moreover, the development of micropores (> 1.0 nm) was better than the others as well. By contrast experiments, for the preparation of SAC, the best option was $ZnCl_2$ as an activator, the impregnated ratio at 2: 1, the concentration in activator at 40 %, and the reaction temperature at 400°C.

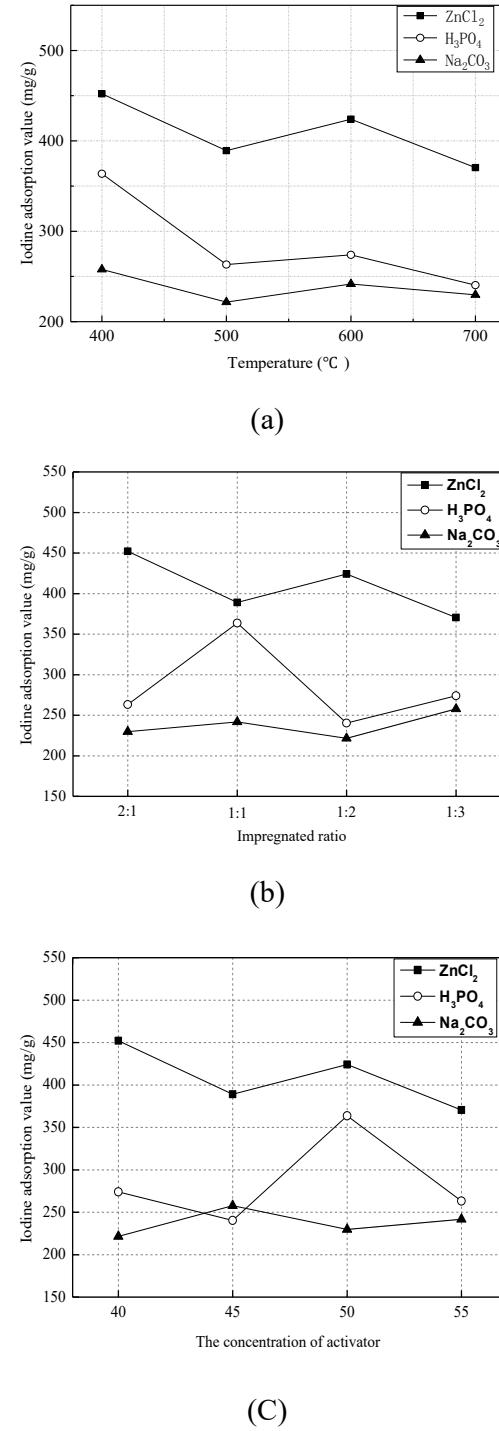

Fig. 2: The value of the iodine adsorption curve.

Low-Temperature Nitrogen Adsorption Measurement

According to Fig. 3, it was revealed that the adsorption-desorption isotherm curves and the tendency were similar

even if the SAC was prepared under different conditions. Selecting $ZnCl_2$ as an activator, the temperature at 400ºC, the impregnated ratio at 2:,1 and the concentration of activator at 40% to analyze, N_2 absorbed to SAC varied with variation in relative pressure ($P/P_{0)}$. When the relative pressure was low, the main adsorption method was single-molecule adsorption and the speed of adsorption was slow, however, the trend of the curve was more stable. When the relative pressure (P/P_0) was close to 0.4, N_2 was forced to enter the pores. Due to the action of capillary condensation, the gas state of N_2 was converted into liquid nitrogen, thus the surface of SAC was accumulated with nitrogen, and the isotherm curve continued moving upward. The liquid nitrogen was adsorbed to the pores of SAC until the relative pressure approximately reached 1. In terms of IUPAC classification, the isotherm was the IV category. There was an H2 hysteresis loop in the process of adsorption and desorption. Moreover, the hyster-

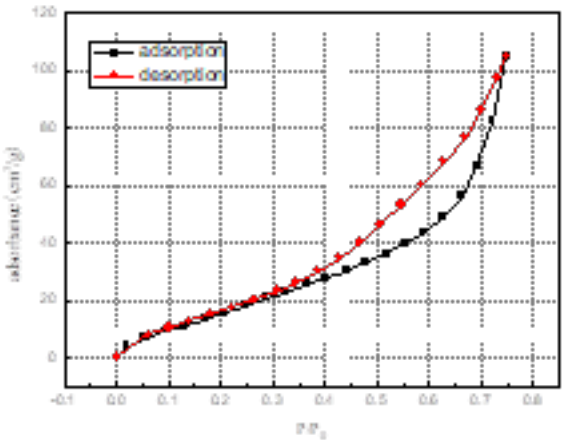

Fig. 3: Sorption isotherm of SAC.

Table 4: The microstructure parameters of SAC.

Number	Total pore volume (cm^3.g-1)	D (nm)	Specific surface area ($m^2.g^{-1}$)
1	0.1017	5.67	537.22
2	0.1028	8.05	457.84
3	0.0910	7.96	493.99
4	0.1232	7.63	427.37
5	0.0879	5.33	415.65
6	0.0925	5.71	297.92
7	0.0752	5.39	307.16
8	0.0797	5.48	267.08
9	0.1304	8.24	294.63
10	0.1318	7.63	250.88
11	0.0926	7.94	271.09
12	0.0220	7.31	255.17

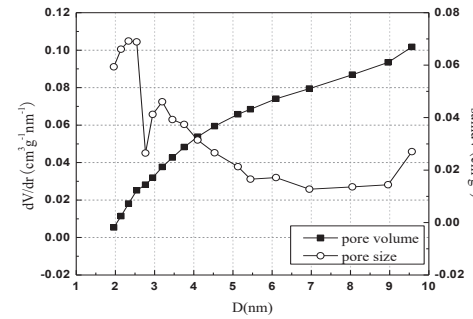

(a)

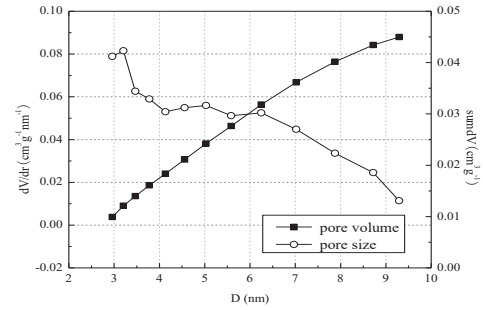

(b)

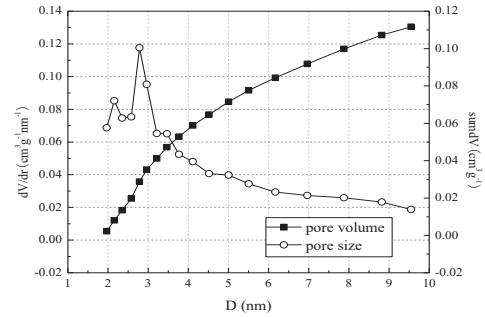

(c)

Fig. 4: The pore volume and pore size distributions of SAC (a) $ZnCl_2$ (b) H_3PO_4 (c) Na_2CO_3.

etic curve reflected the pore kind was amorphous pores such as the ink bottle hole. The reasons were as follows: With abundant pores in SAC, there was enough room for nitrogen to enter. The nitrogen inside was not allowed to come out because of the changing pressure or the pores in SAC which easily blocked nitrogen into the orifice.

Fig. 4 showed the analysis of the pore size and pore volume under the different preparation methods. Due to the high similarity of samples from the same activator, three SAC samples with the largest specific surface area, prepared

by using $ZnCl_2$, H_3PO_4, and Na_2CO_3, were selected for the analysis, which were numbered No. 1, No. 5, and No. 9, respectively. Fig. 4(a) shows that sample No. 1 had a peak value of 2.34 nm and 3.19 nm; the peak value of sample No. 5 was 3.21 nm as shown in Fig. 4(b). Moreover, the peak value of sample No.9 was 2.8nm and 2.78 nm as shown in Fig. 4(c). The microstructure parameters such as total pore volume, average pore size, and specific surface area of SAC are shown in Table 4. The total pore volume of the sample was between 0.0220 to 0.1318 $cm^3.g^{-1}$, and the average pore size was between 5.33 to 11.60 nm, however, the specific surface area was distributed in the range of 250.88 to 537.22 $m^2.g^{-1}$. According to the IUPAC classification, the pore size distribution of 2-50 nm is called mesoporous. Since the pore size distribution was in the range of 2-10 nm, as shown in the results, the pore in SAC was mainly mesoporous. The above results could be explained as follows: It was obvious that the preparation method using $ZnCl_2$ as an activator was beneficial for the development of pore structure and specific surface area. Moreover, the skeleton in the process of carbonation forced newly formed charcoal to attach to it. During the conditions of pyrolysis, catalysis, and dehydration, at high temperatures, it produced a rich pore structure inside the sludge (Yuan & Liu 2015). It was indirectly observed that the adsorption capacity was the highest because SAC provided lots of contact areas in its abundant specific surface area.

X-ray Diffraction Test

Fig. 5 showed the X-ray diffraction pattern in SAC with different preparation methods. The main mineral composition of SAC is seen in Table 5. Thus, the data proved that the compositions of SAC were different under different pyrolysis with different activators. The quartz composition in the samples was stable and more than 50%, however, the quartz contents of samples 9-12, which was in the range of 53.45% to 54.01%, was high compared to others. Charcoal in samples 1-8 shows that it was feasible to prepare carbon-containing material by compatible processing. Among those samples, the content of charcoal was pretty high, and when the preparation method was by using $ZnCl_2$, the maximum percentage of charcoal was 52.51%. At the same time, charcoal was not detected in samples 9-12. Moreover, quartz was the main peak in all samples. Furthermore, the main components of SAC prepared by $ZnCl_2$ or H_3PO_4 were similar, including quartz (26.70°, 50.2°), charcoal (22.00°, 42.00°), muscovite (19.90°, 35.00°), and berlinite (21.00°, 26.60°). However, SAC had an obvious diffraction peak at 22.00° and 42.00°. The diffraction peak (2θ = 22°) was the crystal plane of microcrystal (002) in graphite-like structure, and the diffraction peak (2θ = 42°) was the crystal plane of microcrystal (100) with graphite-like structure. The reasons

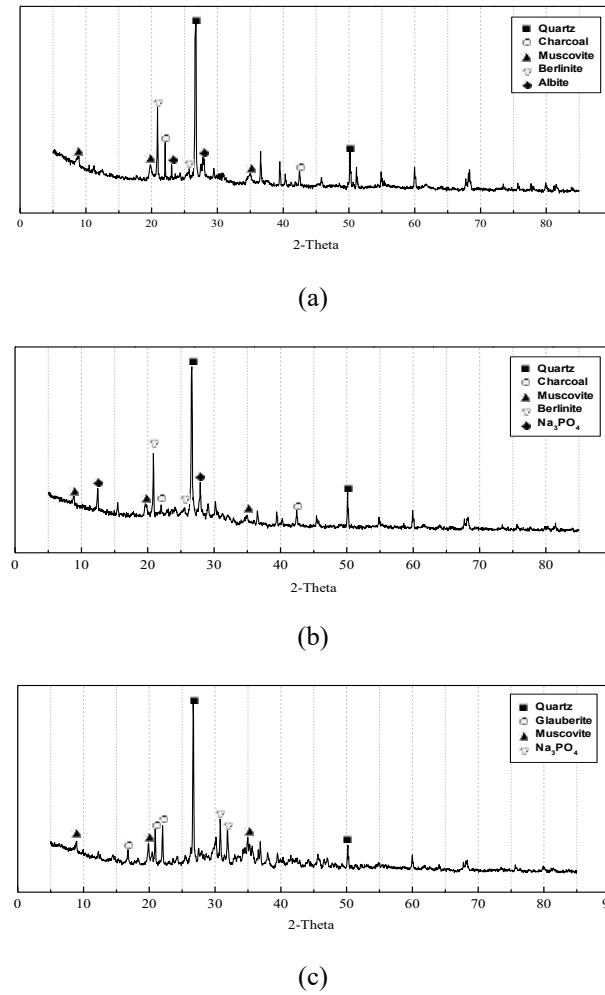

Fig. 5: The X-ray diffraction pattern (a) $ZnCl_2$ (b) H_3PO_4 (c) Na_2CO_3.

were as follows: Because $ZnCl_2$ had little effect on the cellulose in SAC, more and more celluloses were crystallized into graphite. Moreover, the diffraction peak of microcrystalline graphite was enhanced. Furthermore, the higher the degree of crystallization, the more stable carbon compounds were formed. It was proved that this preparation method was the best option to prepare SAC because of the evidence of abundant pore structure, the high content of charcoal and stable substances.

As shown in Fig. 6(a), the magnification of samples was 1000 times. It could be seen that the structure of sample No. 1 was a honeycomb structure, and the surface of the sample was rough with a porous carbon skeleton structure inside. Moreover, the particle unit body was mainly composed of flake, and the structure of sample No. 1 was characterized by simple stacking, mostly edge-surface contact and edge-edge contact with a large number of pores and rich pore structure.

Table 5: The mineral composition of SAC.

Activator	Number	Quartz	Charcoal	Muscovite	Berlinite	Albite	Others
$ZnCl_2$	1	52.45%	3.84%	31.71%	3.82%	6.57%	1.61%
	2	52.43%	4.12%	32.47%	4.15%	5.03%	1.80%
	3	52.51%	4.06%	32.92%	4.28%	4.94%	1.29%
	4	52.35%	3.97%	31.28%	3.35%	7.57%	1.48%
Activator	Number	Quartz	Charcoal	Muscovite	Berlinite	Na_3PO_4	Others
H_3PO_4	5	52.93%	2.94%	31.79%	6.14%	4.71%	1.49%
	6	53.11%	2.52%	33.64%	5.46%	3.91%	1.36%
	7	52.91%	2.89%	34.07%	6.03%	2.85%	1.25%
	8	52.89%	2.31%	33.27%	5.90%	3.67%	1.96%
Activator	Number	Quartz	Charcoal	Muscovite	Na_3PO_4	Glauberite	Others
Na_2CO_3	9	53.56%	-	32.82%	5.66%	6.59%	1.37%
	10	54.01%	-	33.37%	7.34%	3.50%	1.78%
	11	53.62%	-	32.67%	5.25%	6.92%	1.54%
	12	53.45%	-	34.23%	6.73%	4.34%	1.25%

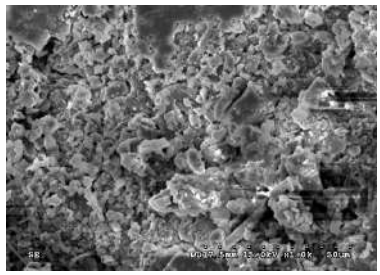

(a)

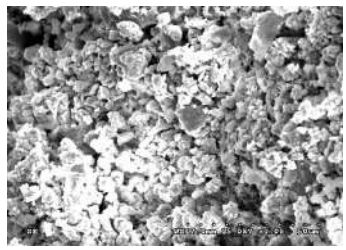

(b)

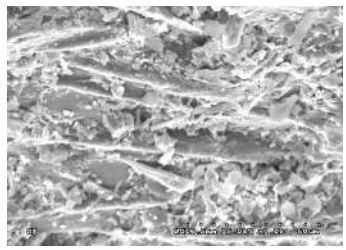

(c)

Fig. 6: SEM Images (magnified 1000 times) of SAC (a) $ZnCl_2$ (b) H_3PO_4 (c) Na_2CO_3.

As shown in Fig. 6(b), sample No. 5 was mainly composed of aggregated granular structure, and the pore structure was not more obvious than sample No.1. As shown in Fig. 6(c), the structure of sample No. 9 was a flake structure that was mainly surface-to-surface contact. Moreover, the surface of the sample had folds with rich irregular strip debris on the surface. The results of the iodine adsorption value test and low-temperature nitrogen adsorption test show that sample No. 1 had a large number of pores, rich pore structures, and specific surface areas compared to other samples, therefore, the activation of $ZnCl_2$ had a positive effect on the pore structure of SAC.

Batch Adsorption Test

The adsorption isotherm for Cu(II) and Cd(II) under different preparation methods are shown in Fig 7. With the different preparation methods, the adsorption capacity of Cu(II) increased dramatically. Moreover, the adsorption capacity reached the highest value at 600.02 $mg.kg^{-1}$ when SAC was prepared using $ZnCl_2$ as an activator, and the least value was 412.17 $mg.kg^{-1}$ when Na_2CO_3 was used as an activator. In the preparation method using H_3PO_4 as an activator, the adsorption capacity had a mid-value (between the highest and least) and the value of adsorption was 512.97 $mg.kg^{-1}$. When the curves of adsorption capacity of Cd(II) was highly similar to Cu(II), the highest adsorption value was 383.2 $mg.kg^{-1}$, and the minimum value for the adsorption capacity was 227.75 $mg.kg^{-1}$, and the highest adsorption capacity was 315.25 $mg.kg^{-1}$ when H_3PO_4 was the activator. In the last phase, the adsorption did not take place because of the phenomenon of Coulomb repulsion. The values of the isotherm

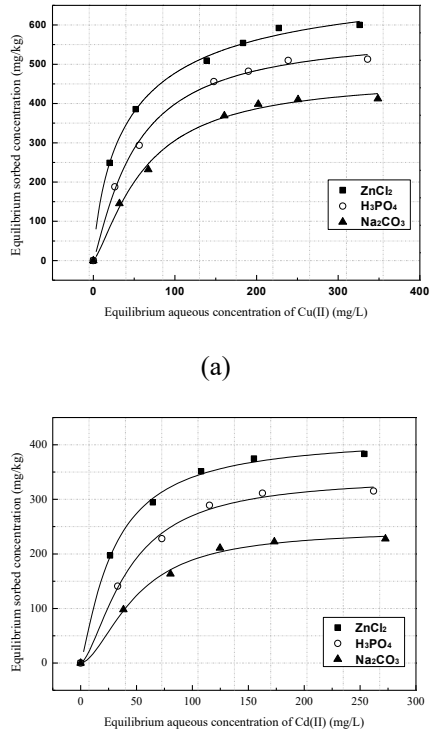

Fig. 7: The adsorption isotherm with different preparation methods (a) Cu(II) (b) Cd(II).

parameters are given in Table 6. All adsorptions belonged to the Langmuir isotherm model, especially the adsorption of Cu(II). Moreover, the high accuracy of the model and the R^2 which almost reached 1 was the best evidence to prove that SAC had loose structure, large porosity, and specific surface area, however, SAC has the potential and feasibility to adsorb all polluted matters regardless of the method used to prepared SAC. In terms of the various preparation methods, to get SAC, sample No.1, which was the preparation method using $ZnCl_2$, provided more pores for the heavy metals. However, using others preparation were also rational choices expect the number of pores was not enough when compared to sample No. 1.

CONCLUSION

To explore the physicochemical characteristics and the optimum preparation condition of SAC, a series of tests were conducted, such as low-temperature nitrogen adsorption measurement, XRD, SEM, batch adsorption test, and the iodine adsorption value test. To analyze the yield of SAC the iodine adsorption value test was performed. The adsorption capacity of Cu(II) and Cd(II) to SAC was observed by performing the batch adsorption test. The pore structure, pore volume, and components of the SAC were observed by performing the low-temperature N_2 adsorption test, XRD, and SEM. The following conclusions can be drawn:

1. The order of yield rate of SAC prepared by different activators is $ZnCl_2 > H_3PO_4 > Na_2CO_3$. When $ZnCl_2$ is selected as the activator for the preparation of SAC, the iodine adsorption value is significantly higher than that of other activators, and the micropores (> 1.0 nm) in the obtained SAC are highly developed.
2. In accordance with the IUPAC classification method, the SAC isotherms belong to the IV category, and the hysteretic curve is H2 kind, moreover, the pore of SAC is mostly mesopore.
3. The quartz composition in all samples is more than 50%, and charcoal was observed in sample Nos 1-8 but not in sample Nos 9-12. The content of charcoal was maximum at 52.51% when the preparation method of SAC is with $ZnCl_2$ as an activator.
4. The results showed an optimum preparation condition - which was by using the $ZnCl_2$ as an activator, 2:1 as the impregnated ratio, 40% concentration in activator and at 400ºC reaction temperature - could create rich pore structure and charcoal inside. .

ACKNOWLEDGEMENTS

The authors would like to express their great appreciation for funding provided by the "National Natural Science Foundation of China (U20A20320)".

REFERENCES

Agrafioti, E., Bouras, G., Kalderis, D. and Diamadopoulos, E. 2013. Biochar production by sewage sludge pyrolysis. J. Anal. Appl. Pyrol., 101(5): 72-78.

Bao, H. F., Yang, W. W., Zhang, L. Q. and Feng, L. 2012. Efficiency and

Table 6: The isotherm parameter for Cd(II) and Cu(II).

Number	Cu(II)			Cd(II)		
	q_m (mg.kg^{-1})	b (L.mg^{-1})	R^2	q_m (mg.kg^{-1})	b (L.mg^{-1})	R^2
1	740.046	0.04694	0.992	416.635	0.01625	0.987
5	582.691	0.00949	0.992	341.408	0.00292	0.975
9	467.713	0.00401	0.983	244.191	0.00116	0.975

kinetics of heavy metal removal from water by sludge-based activated carbon. J. China environmental science, 32(02): 254-259.

Duan, J.Q., Liu, Y.J. and Zhou, L. 2016. Preparation of activated carbon from sludge and its application in the treatment of blue carbon wastewater. J. Environ. Eng., 10(12) 6337-6342.

Lai, B., Zhou, Y.X. and Yang,P. 2012. Bioactive carbon treatment of ABS resin production wastewater. J. China Environ. Sci., 32(02): 254-259.

Li, G., Li, W.G. and Wang, G.Z. 2012. Preparation characterization and application of sludge-based activated carbon. J. Anhui Agric. Sci., 30(02): 489-493.

Li, Y.L., Li-Ping, L.L., Weng-Jun, l. and Li, J. 2013. Optimization and preparation of sludge-based activated carbon by two-step pyrolysis and performance. J. Beijing Univ. Technol., 39(12): 1887-1897.

Liu, H.P. and Liu, X.Z. 2013. The preparation of sludge-substrate activated charcoal and its property analysis. J. Fujian Univ. Technol., 33(01): 69-74.

Li, Y.L., Liu, J.W., Chen, J.Y. and Shi, Y.F. 2014. Reuse of dewatered sewage sludge conditioned with skeleton builders as landfill cover material. J. Int J Environ Sci Technol, 11(1): 233-240.

Wang, R.F., Li, T. and Fan, L.Q. 2012. Bioactive carbon treatment of ABS resin production wastewater. J. Anhui Agric. Sci., 40(08): 4848-4849.

Wu, C.S., Huang, F.W., Liu, W.W., Liu, C.Q., Guo, Y.Y. and Zheng, Y.Y. 2017. Study on adsorption performance of sludge-based biochar to landfill leachate. J. Environ. Eng., 35(02): 1-4.

Yuan, L. and Liu, Y.Q. 2015. Catalytic effect of $MgSO_4$ and $ZnCl_2$ on the rapid pyrolysis of pine wood. J. Acta Energ. Sol. Sini., 36(07): 1775-1761.

Yang, H.Y. 2010. The present situation of municipal sewage and sludge treatment in China. J. North Environ. Mag., 22(01): 79-80.

Zheng, K.Q., Wang, J. C., Liu, S.T., Xue, H.B., Wu, J.Y., Liu, T.Y., Yi, W.Q. and Wang, X.Z. 2016. Adsorption characteristics of sludge Biochar for Pb^{2+} and Cd^{2+} at different pyrolysis temperatures. Chinese J. Environ. Eng., 10(12): 7277-7282.

Nature Environment and Pollution Technology
An International Quarterly Scientific Journal

p-ISSN: 0972-6268
(Print copies up to 2016)
e-ISSN: 2395-3454

Vol. 20 | No.3 | pp. 1147-1156 | 2021

Original Research Paper

https://doi.org/10.46488/NEPT.2021.v20i03.022

Open Access Journal

Contributions of Land Utilization Differences and Changes in Zhongyuan Urban Agglomeration to Regional Thermal Environment

Qingkong Cai*, Erjun Li†, Yafei Zhang***, Guo Wang* and Chao Chen***

*College of Civil Engineering, Henan University of Engineering, Zhengzhou, Henan 451191, China
**College of Human and Social Sciences, Henan University of Engineering, Zhengzhou, Henan 451191, China
***College of Geological Engineering and Geomatics, Chang'an University, Xi'an, Shanxi 710054, China
†Corresponding author: Erjun Li; hnwxlej@163.com

Nat. Env. & Poll. Tech.
Website: www.neptjournal.com

Received: 12-04-2021
Revised: 20-08-2021
Accepted: 28-08-2021

Key Words:
Contribution index
Land utilization
Urban agglomeration
Urban thermal environment

ABSTRACT

Accelerated urbanization has given rise to sharp environmental changes in urban underlying surfaces, thus changing the regional thermal environment and endangering the ecosystem balance. The thermal environment is complex, and the influence laws of land utilization differences and changes in the thermal environment in different seasons and under different daytime and nighttime conditions are unclear. In this regard, effective measures should be implemented to reduce the regional thermal environmental effect and determine the influence laws of land utilization differences and changes in the regional thermal environment. Zhongyuan urban agglomeration was applied as the study area. Two-year MODIS eight-day synthesized surface temperature product and land utilization monitoring data were obtained by remote sensing and used to analyze the influencing characteristics of different cities and land utilization types on the thermal environment of urban agglomeration from the angles of interannual differences and seasonal differences. During 2010-2018, the area changes in different land utilization types in the study area are significant with decreasing farmland area and increasing forest land and construction land. The farmland and forest land have the most significant influences on the regional thermal environment, where the farmland exerts a warming effect on the regional thermal environment and the forest land exerts a cooling effect. In different seasons and under different daytime and nighttime conditions, the construction land shows a strong warming effect on the regional thermal environment. The contribution indices of Changzhi city and Jincheng city to the thermal environment of the urban agglomeration are negative, so they exert the cooling effect. The warming or cooling role played by Handan city, Liaocheng city, and Xingtai city in the thermal environment is transited under different daytime and nighttime conditions, namely, they exert the warming effect in the daytime and the cooling effect in the nighttime. The seasonal differences in the contributions of different cities to the regional thermal environment are the most apparent in summer and winter. The contribution indices are generally high in summer and winter and low in spring and autumn. Conclusions have theoretical significance for scientifically regulating the regional thermal environment.

INTRODUCTION

Rapid urbanization has resulted in drastic environmental changes in the urban underlying surface, and one of the most obvious negative effects is the rise of urban surface temperature. Land utilization/coverage change (LUCC), which is the most direct pattern of manifestation of the interaction between human activity and the natural environment, plays a significant role in the regional thermal environment (Liu et al. 2014). Urban heat island (UHI) is a concentrated reflection of urban thermal environmental characteristics (Memon et al. 2008). Since the concept of "heat island" was proposed by Howard at the beginning of the 19th century, scholars have carried out a large quantity of research work regarding the monitoring and recognition (Dai et al. 2009, Zhou et al. 2008), evaluation and diagnosis (Oke et al. 1987, Zhang et al. 2012), simulation and regulation (Meng et al. 2010, Yue et al. 2010), etc. of UHI. With the rapid outward urban expansion and continuous population aggregation toward the cities, the thermal environment of urban agglomeration is faced with unprecedented challenges under the impact of global warming (Chi et al. 2015).

Scholars have explored eco-environmental problems triggered by changes in the urban thermal environment during urbanization in recent years. When studying the relationship between surface temperature and landscape patterns, Zhou et al. pointed out the importance of seasonal aspect changes (Zhou et al. 2014). Carlson et al. put forward a method for extracting impervious surface by using the vegetation coverage; however, the vegetation coverage was affected by seasonal changes, which generated a certain influence on studies with respect to impervious surface and surface temperature (Carlson

et al. 2000). Taking Houston in America for example, Streuker discussed the relationships of the spatial distribution of urban heat island with the urban heat island intensity and suburb temperature (Streutker 2002). Rigo et al. analyzed differences in urban surface temperatures measured by different satellites from those obtained through field measurement; the difference value between the surface temperature provided by MODIS and the measured surface temperature was smaller than 5% (Rigo et al. 2006). The urban thermal environment has been frequently investigated also in China. Tang et al. used three-period Landsat ETM+ image data to discuss the relationships of the surface temperature in Changchun city in summer with the coverage of impervious surface and vegetation coverage (Tang et al. 2017). Taking the mountainous city Chongqing for example and considering altitude, slope, aspect, surrounding landform, etc., Jia found that the surface temperature with an altitude of above 1,000 m presented an obvious linear relation to the altitude (Jia 2014). Han et al. used the MODIS surface temperature product to discuss the influences of spatial-temporal changes in the thermal environmental safety pattern in Yangtze River Delta urban agglomeration and the changes in the land utilization; the results showed that the excessively high proportion of construction land and excessively low proportion of forest land were the primary causes for the declining safety level of the thermal environment (Han et al. 2017). Xie et al. analyzed the spatial-temporal change laws of the urban thermal environment in the Nanchang City area during 1996-2016 and displayed the relationships of the urban thermal environment with land utilization and manmade heat discharge (Xie et al. 2019). Qiao et al. analyzed the spatial-temporal pattern of urban thermal environmental risks and their characteristics in Beijing city; the results indicated that the urban thermal environmental risks presented a rising trend in Beijing, where the proportion of extremely high-risk areas was elevated from 9.66% to 12.08% (Qiao et al. 2019). Wang et al. analyzed the relationships of urban land utilization type and pattern features with the surface thermal environment and stated that the surface temperature varied considerably with land utilization types; among which, the surface temperatures of industrial land, land for roads and squares, and residential land were higher than those of river, garden, and forest land (Wang et al. 2013).

To sum up, eco-environmental problems induced by changes in the thermal environment during the urbanization progress have been analyzed in detail; however, considering the complexity of the urban thermal environment, few studies have involved interannual and seasonal differences in the influences of land utilization types on the urban thermal environment. In addition, most studies used a single city as the study object, few works were conducted at the scale of urban agglomeration. The thermal environmental problem triggered by the rapid urbanization stands out in Zhongyuan urban agglomeration, which is one of 19 national-level urban agglomerations in China. Based on the above analysis, Zhongyuan urban agglomeration was taken as the study area, and the influence mechanism and action laws of different cities and different land utilization types on the thermal environment in this urban agglomeration were analyzed from the respective angles of interannual differences and seasonal differences to reasonably utilize land resources, optimize urban construction planning, relieve and control urban high temperature, and provide a theoretical and practical basis for constructing a beautiful Zhongyuan region.

MATERIALS AND METHODS

Profile of the Study Area

Zhongyuan urban agglomeration is Central Plains (centering on Henan Province) located in Central and East China and the junction between the coastal open region and central and western regions in China. It is one of the core regions with enormous vigor and potential in the future economic development pattern of China and has an important node for forging a new growth pole of China's economic development. The geographical location is between east longitude of 110°15'-118°10'E and northern latitude of 30°23'-37°47'N. According to the Development Plan of Zhongyuan urban agglomeration approved by the State Council on December 28, 2016, Zhongyuan urban agglomeration has jurisdiction over 30 cities in five provinces: Henan, Shanxi, Hebei, Shandong, and Anhui (Fig. 1). The land area of the administrative region is 287,000 km^2, accounting for 3.0% of the total land area of the nationwide administrative region. The main regional landform is plain, along with low hills and mountains. It belongs to temperate monsoon climate and subtropical monsoon climate, with four distinctive seasons (high temperature and rainy summer and cold and dry winter). By the end of 2017, the urban built-up area in Zhongyuan urban agglomeration is 7,400 km^2, accounting for 12.0% of the total national urban built-up area; the total population was 188,881,400 at the end of the year, accounting for 13.6% of the total national population. The city size in Zhongyuan urban agglomeration has been continuously expanded, the population absorption ability continuously strengthened, and the cohesion and overall competitiveness continuously enhanced. Promoting the development of Zhongyuan urban agglomeration will be of great strategic importance for accelerating and facilitating the rising of Central China, thereby boosting the new-type urbanization and expanding the new space for China's economic development.

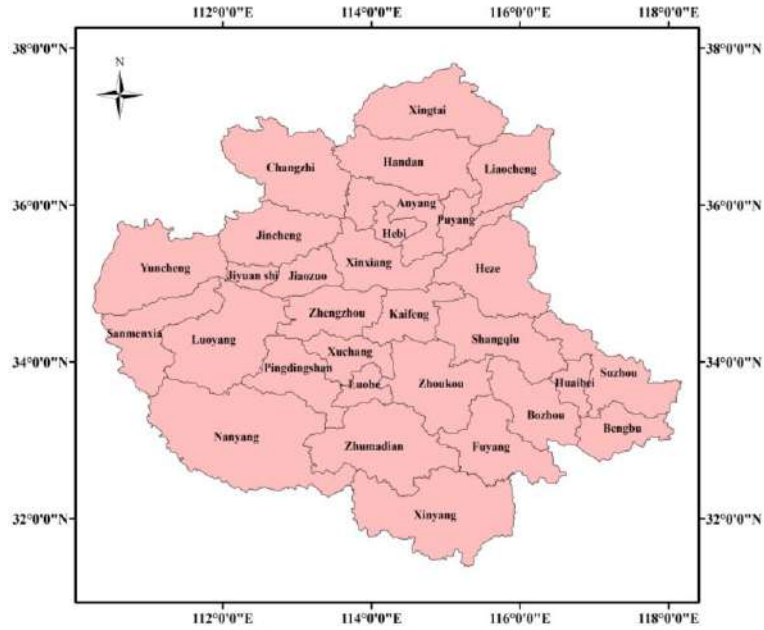

Fig. 1: Geographical location of the study area.

Data Collection and Preprocessing

The data sources used in this study mainly included MODIS surface temperature data and land utilization data, where the surface temperature data derived from the MODIS eight-day synthesized surface temperature product (MOD11A2) provided by the National Aeronautics and Space Administration (NASA) of the United States of America, the spatial resolution of images was 1000 m and the column numbers were h26v05 and h27v05. The year-round data in two periods, namely, 2010 and 2018, were downloaded. The original data were acquired by Aqua Satellite when passing the territory at 13:30 and 01:30 to characterize the surface reflection conditions in the surface warming and cooling time periods (Qiao et al. 2014, Sun et al. 2018, Peng et al. 2014). The surface temperature data product was acquired through the inversion using the split-window algorithm, with the precision reaching as high as 1 K (Wan et al. 2004). The preprocessing work mainly included image reprojection, image synthesis, image splicing, and image clipping. The images were re-projected using the MODIS reprojection tool (MRT), the temperature product was then synthesized into the monthly average surface temperature data through the maximum value composite method, and the monthly average surface temperature data were finally obtained through image splicing and image clipping. The synthesized surface temperature data of the study area in June are presented in Fig. 2.

The land utilization data originated from 1:100000 China land utilization remote sensing monitoring datasets in 2010 and 2018 provided by the Resource and Environment Science and Data Center, Chinese Academy of Sciences. The land utilization types included six level I types (Farmland, forest land, grassland, water area, residential land and unused land) and 25 level II types, all of which have been widely applied to various fields, such as spatial-temporal pattern analysis of the urban thermal environment and comprehensive eco-environmental evaluation (Liu et al. 2004). In this study, the urban and rural land, industrial and mining land, and residential land were called by a joint name, that is, construction land and the two-period land use classification maps (Fig. 3) were obtained through image splicing and image clipping.

Methodology

Acquisition of surface temperature data: The MODIS eight-day synthesized surface temperature product only recorded the surface thermal radiation values under cloudless conditions; as such, the surface thermal radiation value should be transformed into surface temperatures. Based on the data header files, the radiation scaling ratio of the MODIS temperature product was obtained as 0.02, and radiation scaling intercept was set as 0, so the conversion formula for surface temperature is:

$$T = 0.02 \cdot DN - 273.15 \quad \ldots(1)$$

where T is the surface temperature (unit, °C), and DN is the brightness value of the image element.

The seasonal differences in the contributions of different land utilization types to the thermal environment in urban

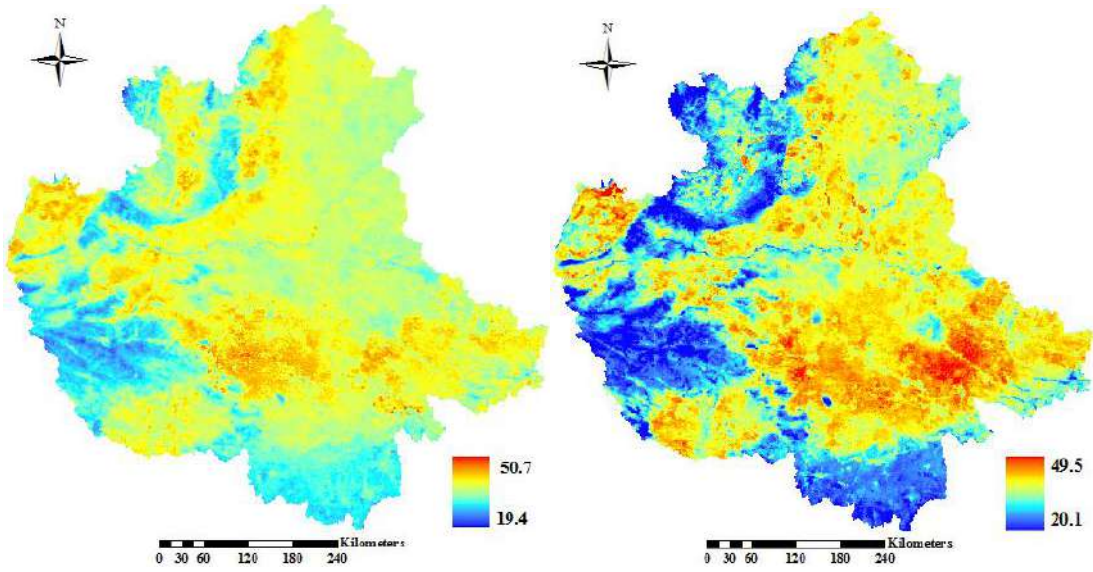

(a) June 2010 (b) June 2018

Fig. 2: Surface temperature graphs in Zhongyuan urban agglomeration in June 2010 and 2018.

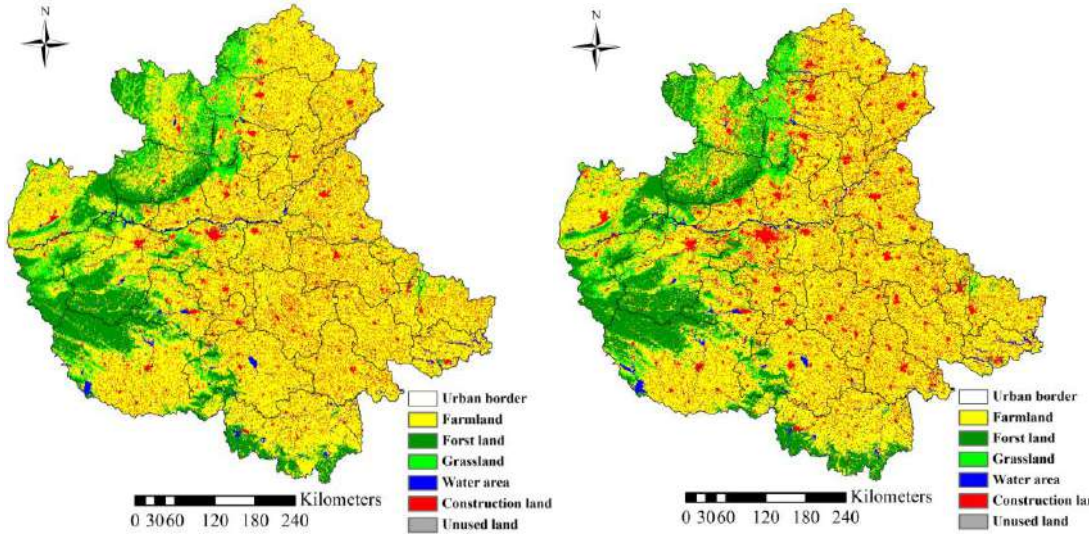

(a) 2010 (b) 2018

Fig. 3: Land utilization classification maps of Zhongyuan urban agglomeration in 2010 and 2018.

agglomeration were compared. The synthesized MODIS monthly average temperature data were used to calculate the seasonal average and daily (daytime and nighttime) average surface temperatures in spring (March-May), summer (June-August), autumn (September–November), and winter (December-February in the next year).

Calculation of contribution index: The influence mechanism of different cities on the regional thermal environment differed to some extent due to the spatial heterogeneity of land utilization types. The contribution index (CI) was used to quantitatively characterize the contributions of land utilization types to the urban thermal environment. CI is the

product of the difference value between the average surface temperature of one land utilization type and regional average surface temperature with the proportion of the area of this land utilization type in the total regional area (Xu 2009, Qiao et al. 2013). CI is calculated by the following formula:

$$CI = D_t \times S \quad \ldots(2)$$

Where CI is the CI of one land utilization type to the thermal environment; D_t is the difference value between the average surface temperature of one land utilization type and regional average surface temperature, and S is the proportion occupied by one land utilization type in the total regional area. The positive or negative CI represents the warming or cooling effect of land utilization type on the urban thermal environment, and its value denotes the contribution of this land utilization type to the urban thermal environment. In a similar way, the CI of each city to the regional thermal environment is the product of the difference value between average surface temperature and regional average surface temperature with the proportion occupied by the city area in the total regional area (Sun et al. 2018).

RESULTS AND DISCUSSION

Differences in the Contributions of Different Land Utilization Types to the Thermal Environment of the Urban Agglomeration

Interannual differences: The area proportion of each land utilization type in the two periods was calculated based on the land utilization data in 2010 and 2018. By using the vector data and surface temperature data of land utilization types, the daytime average surface temperatures in 2010 and 2018 were respectively extracted to obtain the CI value of each land utilization type to the thermal environment (Table 1).

As given in Table 1, among different land utilization types, the proportion of farmland was the largest in the total study area, followed by forest land, construction land, grassland, water area, and unused land. From 2010 to 2018, the area proportion of farmland in the study area was reduced from 66.43% to 63.70%, while the areas of forest land, water area, and construction land were increased. The surface temperatures of farmland and construction land were higher than the regional average surface temperature, and their CI values were increased from 0.31 and 0.06 in 2010 to 0.43 and 0.12 in 2018, respectively; the warming effect on the regional thermal environment was obviously enhanced. The surface temperatures of forest land, grassland, water area, and unused land were all lower than the regional average surface temperature, indicating that they exerted a cooling effect on the regional thermal environment, where the CI value of forest land was transformed from -0.31 in 2010 to -0.41 in 2018, and the cooling effect was enhanced somehow. The temperature anomaly value of grassland was transformed from -0.29 in 2010 to -0.89 in 2018, and the CI values of water area and unused land were negative, manifesting their cooling effect on the regional thermal environment.

Seasonal differences: Based on the vector data of each land utilization type and MODIS temperature product data, the average temperatures of each land utilization type in the daytime and nighttime in 2010 and 2018 were extracted by four seasons, respectively. The seasonal CI value of each land utilization type to the thermal environment was obtained (Table 2). The broken line graphs of seasonal CI of each land utilization type to the thermal environment of Zhongyuan urban agglomeration in 2010 and 2018 were drawn (Fig. 4).

As given in Table 2 and Fig. 4, the CI value of farmland presented significant daytime and nighttime differences. The daytime warming effect was more obvious than the nighttime warming effect, which was mainly ascribed to the solar radiation and seasonal characteristics of crops. Except that the CI values of farmland in the daytime of spring and nighttime of winter were smaller than 0, the CI values in other seasons were all greater than 0, with a significant warming effect. The cooling effect of forest land was the most remarkable in sum-

Table 1: CI values of land utilization types to thermal environment of Zhongyuan urban agglomeration in 2010 and 2018.

Land-use type	2010			2018		
	Area ratio	Temperature anomaly	CI	Area ratio	Temperature anomaly	CI
Farmland	66.43%	0.46	0.31	63.70%	0.68	0.43
Forest land	13.85%	-2.27	-0.31	14.04%	-2.92	-0.41
Grassland	6.47%	-0.29	-0.02	6.11%	-0.89	-0.05
Water area	2.05%	-0.78	-0.02	2.20%	-0.74	-0.02
Construction land	11.13%	0.54	0.06	13.91%	0.87	0.12
Unused land	0.07%	-0.69	-0.00	0.04%	-0.10	-0.00

Table 2: CI values of land utilization types to the thermal environment of Zhongyuan urban agglomeration in 2010 and 2018.

Land-use type		Contribution index in 2010				Contribution index in 2018			
		Spring	Summer	Autumn	Winter	Spring	Summer	Autumn	Winter
Day	Farmland	-0.06	0.50	0.61	0.16	0.21	0.56	0.74	0.21
	Forest land	-0.02	-0.56	-0.56	-0.12	-0.31	-0.65	-0.68	-0.00
	Grassland	0.16	-0.04	-0.18	-0.02	0.03	-0.10	-0.18	0.03
	Water area	-0.02	-0.02	-0.02	-0.00	-0.03	-0.03	-0.02	-0.00
	Construction land	-0.06	0.14	0.15	0.00	0.11	0.22	0.15	0.01
	Unused land	-0.00	-0.00	0.00	-0.00	-0.00	0.00	-0.00	-0.00
Night	Farmland	0.06	0.28	0.05	-0.15	0.03	0.27	0.05	0.46
	Forest land	-0.04	-0.32	-0.06	0.14	-0.09	-0.33	-0.08	0.21
	Grassland	-0.04	-0.07	0.23	-0.04	-0.04	-0.08	-0.03	0.05
	Water area	0.03	0.02	0.03	0.02	0.02	0.02	-0.04	0.07
	Construction land	0.04	0.09	0.04	0.01	0.07	0.13	0.06	0.28
	Unused land	0.00	0.00	-0.00	-0.00	0.00	0.00	0.00	0.00

mer and autumn, and the CI values were increased from -0.56 and -0.56 in 2010 to -0.65 and -0.68 in 2018, respectively; the cooling effect on the regional thermal environment was enhanced. The CI values of grassland in the daytime of spring and nighttime of autumn were greatly different, exerting a certain cooling effect on the regional surface temperature. In different seasons and under different daytime and nighttime conditions, the construction land showed a strong warming effect on the regional thermal environment. The daytime and nighttime differences in the CI value of water area to the thermal environment were significant; the CI value was negative in the daytime (cooling effect) and it was positive in the nighttime (warming effect). The CI value of unused land to the thermal environment of this urban agglomeration was approximately 0 mainly because the unused land accounted for a small proportion in the regional area. Therefore, the unused land contributed little to the thermal environment.

Differences in CI Values of Different Cities to the Thermal Environment of Zhongyuan Urban Agglomeration

Interannual differences: The 30 cities in the study area were taken as the statistical units, and their vector data and MODIS temperature data were used to calculate the CI values of each city to the urban thermal environment under different daytime and nighttime conditions in 2010 and 2018. The statistical results were plotted into a histogram (Fig. 5).

As shown in Fig. 5, the CI values of Changzhi city and Jincheng city to the study area in different years and different daytime and nighttime conditions were all negative, so they exerted a cooling effect on the thermal environment of this urban agglomeration in the daytime and nighttime, where the cooling effect of Changzhi city was the most significant. The CI value in the daytime was transformed from -0.04 in 2010 to -0.08 in 2018, and that in the nighttime from -0.21 in 2010 to -0.18 in 2018. The CI values of Xingtai city, Handan city,

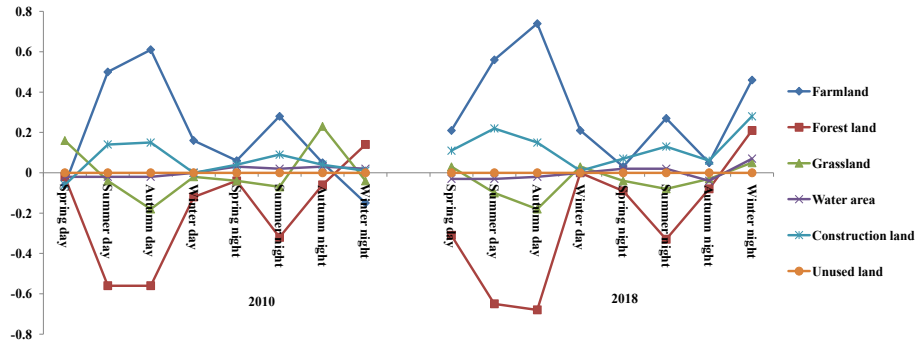

Fig. 4: Seasonal CI values of land utilization types to the thermal environment of Zhongyuan urban agglomeration in 2010 and 2018.

and Liaocheng city were greater than 0 in the daytime and smaller than 0 in the nighttime, so they exerted a warming effect in the daytime and cooling effect in the nighttime. In the diurnal changes, the warming and cooling roles of the urban thermal environment were transited, namely, the warming effect was exerted in the daytime and the cooling effect in the nighttime. The CI values of other cities were positive, indicating that the average temperatures in these cities were always higher than the average temperature in the urban agglomeration, they generated a warming effect in daytime and nighttime, among which Nanyang city was the most typical; this city generated a warming effect on the regional thermal environment.

Seasonal differences: The CI values of each city to the thermal environment of Zhongyuan urban agglomeration under different daytime and nighttime conditions were statistically analyzed based on the MODIS temperature data and vector data of each city in 2018 (Table 3 and Fig. 6).

Table 3 and Fig. 6 show that different cities presented seasonal differences in the CI value to the thermal environment of this urban agglomeration. To be more specific, the CI value was greater than 0 in spring and summer, and it might be positive or negative in autumn and winter. The seasonal differences in the CI value to the thermal environment were the most obvious in summer and winter, and the CI values in spring and autumn fluctuated around 0, where Pingdingshan

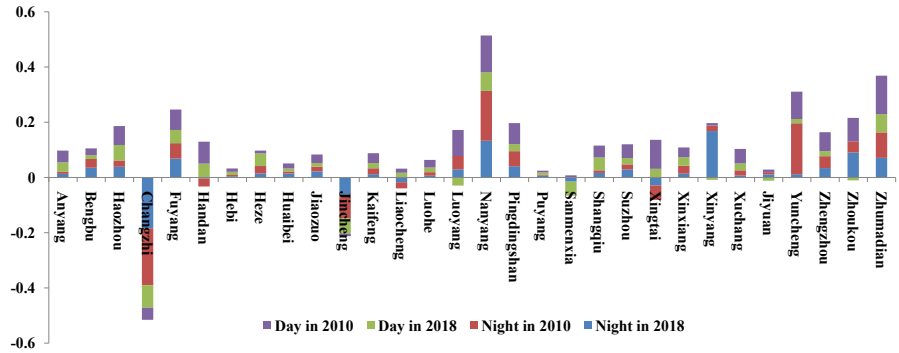

Fig. 5: CI values of different cities to the thermal environment of Zhongyuan urban agglomeration in 2010 and 2018.

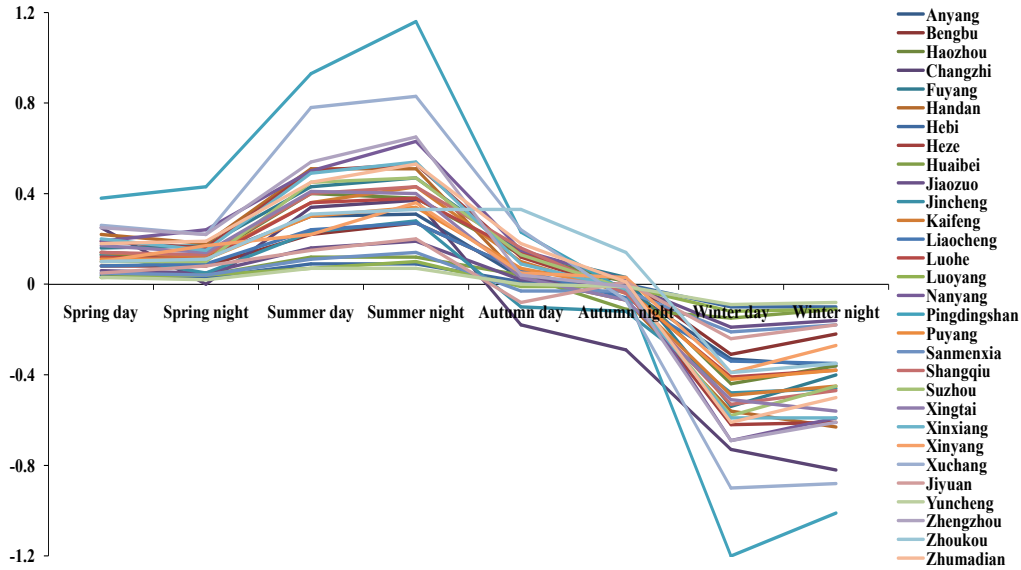

Fig. 6: Seasonal CI values of each city to the thermal environment of Zhongyuan urban agglomeration in 2018.

Table 3: Seasonal CI values of each city to the thermal environment of Zhongyuan urban agglomeration in 2018.

City	Spring		Summer		Autumn		Winter	
	Day	Night	Day	Night	Day	Night	Day	Night
Anyang	0.14	0.12	0.30	0.31	0.03	-0.02	-0.33	-0.36
Bengbu	0.08	0.08	0.22	0.27	0.06	0.02	-0.31	-0.22
Haozhou	0.13	0.12	0.40	0.38	0.13	0.01	-0.44	-0.36
Changzhi	0.25	0.00	0.34	0.37	-0.18	-0.29	-0.73	-0.82
Fuyang	0.16	0.17	0.43	0.47	0.14	0.03	-0.54	-0.40
Handan	0.22	0.18	0.51	0.51	0.03	-0.07	-0.56	-0.63
Hebi	0.04	0.03	0.09	0.09	0.01	0.00	-0.10	-0.10
Heze	0.19	0.16	0.50	0.53	0.12	-0.03	-0.62	-0.61
Huaibei	0.03	0.04	0.12	0.12	0.04	-0.11	-0.15	-0.11
Jiaozuo	0.06	0.05	0.16	0.19	0.02	0.00	-0.19	-0.16
Jincheng	0.13	0.05	0.23	0.28	-0.10	-0.12	-0.48	-0.46
Kaifeng	0.14	0.12	0.36	0.43	0.10	-0.04	-0.49	-0.45
Liaocheng	0.08	0.09	0.24	0.27	0.06	-0.06	-0.34	-0.35
Luohe	0.12	0.11	0.36	0.38	0.14	-0.03	-0.41	-0.38
Luoyang	0.03	0.04	0.07	0.10	-0.01	-0.01	-0.12	-0.11
Nanyang	0.19	0.24	0.50	0.63	0.15	0.02	-0.69	-0.59
Pingdingshan	0.38	0.43	0.93	1.16	0.23	-0.03	-1.20	-1.01
Puyang	0.11	0.11	0.30	0.34	0.07	-0.02	-0.42	-0.38
Sanmenxia	0.05	0.04	0.11	0.14	-0.03	-0.03	-0.21	-0.18
Shangqiu	0.14	0.13	0.40	0.43	0.16	-0.04	-0.53	-0.47
Suzhou	0.10	0.10	0.45	0.47	0.13	-0.02	-0.58	-0.45
Xingtai	0.17	0.14	0.41	0.40	0.03	-0.07	-0.51	-0.56
Xinxiang	0.20	0.15	0.49	0.54	0.09	-0.02	-0.59	-0.59
Xinyang	0.10	0.17	0.22	0.36	0.05	0.03	-0.39	-0.27
Xuchang	0.26	0.22	0.78	0.83	0.24	-0.07	-0.90	-0.88
Jiyuan	0.05	0.08	0.15	0.20	-0.08	0.01	-0.24	-0.18
Yuncheng	0.03	0.02	0.07	0.07	0.00	-0.01	-0.09	-0.08
Zhengzhou	0.25	0.22	0.54	0.65	0.04	-0.01	-0.69	-0.61
Zhoukou	0.10	0.11	0.31	0.33	0.33	0.14	-0.39	-0.35
Zhumadian	0.18	0.19	0.45	0.53	0.18	0.01	-0.61	-0.50

city was the most typical. The diurnal CI value to the thermal environment was 1.05 in summer and -1.10 in winter, which was smaller than those in spring (0.41) and autumn (0.10). The absolute CI values of Yuncheng city, Luoyang city, Huaibei city, and Hebi city were generally low, and the seasonal differences in the CI value were minor; among which, the diurnal average CI values of Yuncheng city in the four seasons all fluctuated around 0, being 0.02, 0.07, 0.00 and -0.08 in spring, summer, autumn, and winter, respectively. The difference between daytime CI and nighttime CI to the thermal environment was not large. In general, the abovementioned cities exerted a warming effect on the thermal environment

in the study area in spring and summer and a cooling effect in autumn and winter.

CONCLUSIONS

This study aimed to clarify the influence laws of land utilization type differences and changes in the regional thermal environment in different seasons and under different daytime and nighttime conditions. Zhongyuan urban agglomeration was taken as the study area, and the MODIS temperature product and land utilization data were utilized to analyze the influence laws of different cities and different land utilization types on the regional thermal environment by using the contribution index from the angles of interannual differences and seasonal differences. The following conclusions could be drawn:

(1) The farmland and forest land appeared to influence the thermal environment of Zhongyuan urban agglomeration most significantly, which was mainly manifested by two aspects: influenced area and influence intensity. The farmland accounted for the largest proportion in the total study area, with the CI value increasing from 0.31 in 2010 to 0.43 in 2018, and the warming effect on the regional thermal environment was apparently strengthened. The CI value of forest land was transformed from -0.31 in 2010 to -0.41 in 2018, and its cooling effect on the regional thermal environment was also enhanced.

(2) The contribution of farmland to the regional thermal environment showed significant daytime and nighttime differences, where the warming effect in the daytime was more obvious than that in the nighttime. The seasonal CI values of forest land were basically negative, and the cooling effect was the most remarkable in summer and autumn. In different seasons and under different daytime and nighttime conditions, the construction land showed a strong warming effect on the thermal environment of the urban agglomeration.

(3) In different years and different daytime and nighttime conditions, the CI values of Changzhi city and Jincheng city to the thermal environment were negative, exerting a certain cooling effect on Zhongyuan urban agglomeration. The CI values of Handan city, Liaocheng city, and Xingtai city were positive in the daytime and negative in the nighttime. The cooling and warming roles of the urban thermal environment were transited under different daytime and nighttime conditions from the warming role into the cooling role.

(4) The contributions of different cities to the thermal environment in Zhongyuan urban agglomeration presented seasonal differences. The CI value was greater than 0 in spring and summer, and it could be either positive or negative in autumn and winter. Meanwhile, the seasonal differences in the contribution to the thermal environment were the most apparent in summer and winter.

Besides being affected by human factors and natural factors, the CI index to the thermal environment is also related to the landform, anthropogenic emissions, etc. Hence, some uncertain factors still exist in research on the thermal environment of urban agglomeration by using the CI index. Furthermore, the MODIS temperature product with the precision of 1 K used in this study can meet the research needs to some extent. However, the thermal environment of urban agglomeration with higher precision data remains to be further investigated.

ACKNOWLEDGEMENTS

This study was supported by Key Scientific Research Projects of Colleges and Universities in Henan Province (21A420003), Doctoral Fund of Henan Institute of Engineering (D2016005) and The Ninth Batch of Provincial Key Discipline (Geodesy and Surveying Engineering) Project in Henan Province (JiaoGao [2018] No.119). The authors are grateful to the student of Henan Institute of Engineering for their support during data processing.

REFERENCES

Carlson, T.N. and Arthur, S.T. 2000. The impact of land use-land cover changes due to urbanization on surface microclimate and hydrology: a satellite perspective. Global and Planetary Change, 25(1-2):49-65.

Chi, W.F., Shi, W.J. and Kuang, W.H. 2015. Spatio-temporal characteristics of intra-urban land cover in the cities of China and USA from 1978 to 2010. Journal of Geographical Sciences, 25(1): 3-18.

Dai, X.Y., Zhang, L.Q. and Guo, Z.Y. et al. 2009. Mechanism of formation of urban heat island effect and its spatial pattern in Shanghai. Acta Ecologica Sinica, 29(7): 3995-4004.

Han, D.R., Xu, X.L. and Li, J. et al. 2017. Study on the security pattern of the heat environment and the influence of land use change in the Yangtze River Delta urban agglomeration. Journal of Geo-information Science, 19(1): 39-49.

Jia, J.T. 2014. Estimation of evapotranspiration in mountainous city- A case study in Chongqing. Chongqing: Master Degree Thesis of Chongqing Normal University, China.

Liu, J.Y., Liu, M.L., Zhuang, D.F. et al. 2003. Study on spatial pattern of land-use change in China during 1995-2000. Science in China (Series D:Earth Sciences), 46(4): 373-384+420-422.

Liu, J.Y., Kuang, W.H., Zhang, Z.X. et al. 2014. Spatiotemporal characteristics, patterns and causes of land use changes in China since the late 1980s. Journal of Geographical Sciences, 24(2): 195-210.

Memon, R.A., Leung, D.Y.C. and Liu, C. 2008. A review on the generation, determination and mitigation of Urban Heat Island. Journal of Environmental Sciences, 20(1): 120-128.

Meng, W.G., Zhang, Y.X., Li, J.N. et al. 2010. Application of WRF/UCM in the simulation of a heat wave event and urban heat island around Guangzhou city. Journal of Tropical Meteorology, 26(3): 273-282.

Oke, T.R. and Cleugh, H.A. 1987. Urban heat-storage derived as energy-balance residuals. Boundary-Layer Meteorology, 39(3): 233-245.

Peng, S.S., Piao, S.L., Zeng, Z.Z. et al. 2014. Afforestation in China cools local land surface temperature. Proceedings of the National Academy of Sciences of the United States of America, 111(8): 2915-2919.

Qiao, Z., Sun, Z.Y., Sun, X.H. et al. 2019. Prediction and analysis of urban thermal environment risk and its spatio-temporal pattern. Acta Ecologica Sinica, 39(2): 649-659.

Qiao, Z. and Tian, G.J. 2014. Spatiotemporal diversity and regionalization of the urban thermal environment in Beijing. Journal of Remote Sensing, 18(3): 715-734.

Qiao, Z., Tian, G.J. and Xiao, L. 2013. Diurnal and seasonal impacts of urbanization on the urban thermal environment: A case study of Beijing using MODIS data. ISPRS Journal of Photogrammetry & Remote Sensing, 85: 93-101.

Rigo, G., Parlow, E. and Oesch, D. 2006. Validation of satellite observed thermal emission with in-situ measurements over an urban surface. Remote Sensing of Environment, 104(2): 201-210.

Streutker, D.R. 2002. A remote sensing study of the urban heat island of Houston, Texas. International Journal of Remote Sensing, 23(13): 2595-2608.

Sun, Z.Y., Sun, X.H., Xu, X.L. et al. 2018. Study on the contribution of land use heterogeneity and change to regional thermal environment: a case study of Beijing-Tianjin-Hebei urban agglomeration. Ecology and Environmental Sciences, 27(7): 1313-1322.

Tang, Z., Zheng, H.F., Ren, Z.B. et al. 2017. Spatial and temporal changes to urban surface thermal landscape patterns: a case study of Changchun city. Acta Ecologica Sinica, 37(10): 3264-3273.

Wang, M., Meng, H., Bai, Y. et al. 2013. Relationships between landscapes spatial pattern and land surface temperature in Shanghai. Ecology and Environmental Sciences, 22(2): 343-350.

Wan, Z., Zhang, Y., Zhang, Q. et al. 2004. Quality assessment and validation of the MODIS global land surface temperature. International Journal of Remote Sensing, 25(1): 261-274.

Xie, Z.Y., Huang, T., Li, Y.J. et al. 2019. Study on the relationship between spatial-temporal evolution of land use and of urban heat environment in Nanchang. Environmental Science & Technology, 42(S1): 241-248.

Xu, S.L. 2009. An approach to analyzing the intensity of the daytime surface urban heat island effect at a local scale. Environmental Monitoring and Assessment, 151(1): 289-300.

Yue, W.Z., Xu, L.H. and Xu, J.H. 2010. Thermal environment change and its socioeconomic drivers in Shanghai City during the 1990s. Acta Ecologica Sinica, 30(1): 155-164.

Zhang, Y., Bao, W.J., Qi, Y. et al. 2012. Study on seasonal variations of the urban heat island and its interannual changes in a typical Chinese megacity. Chinese Journal of Geophysics, 55(4): 1121-1128.

Zhou, R.W., Jiang, W.M. and He, X.F. 2008. Numerical simulation of the impacts of the thermal effects of urban canopy structure on the formation and the intensity of the urban heat island. Chinese Journal of Geophysics, 51(3): 715-726.

Zhou, W.Q., Qian, Y.G., Li, X.M. et al. 2014. Relationships between land cover and the surface urban heat island: seasonal variability and effects of spatial and thematic resolution of land cover data on predicting land surface temperatures. Landscape Ecology, 29(1): 153-167.

Nature Environment and Pollution Technology
An International Quarterly Scientific Journal

p-ISSN: 0972-6268
(Print copies up to 2016)
e-ISSN: 2395-3454

Vol. 20 | No.3 | pp. 1157-1164 | 2021

Original Research Paper

https://doi.org/10.46488/NEPT.2021.v20i03.023

Open Access Journal

Chemical Composition and Nutritional Value of Paddy Straw Milky Mushroom (*Calocybe indica*)

G. Chelladurai*, T.K. Yadav and R.K. Pathak†*****

*PG & Research Department of Zoology, Bishop Heber College (Autonomous), Trichy-620017, Tamil Nadu, India

**Centre for Environmental Studies, Institute of Interdisciplinary Studies, University of Allahabad, Allahabad-211002, India

***Centre for Biotechnology, Institute of Interdisciplinary Studies, University of Allahabad, Allahabad-211002, India

†Corresponding author: Ravi Kant Pathak; pathakravi68@gmail.com

Nat. Env. & Poll. Tech.
Website: www.neptjournal.com

Received: 12-10-2020
Revised: 24-11-2020
Accepted: 18-12-2020

Key Words:
Milky mushroom
Biochemical composition
Cultivation techniques
Paddy straw
Nutritional value

ABSTRACT

The edible milky mushroom is the most widely cultivated mushroom in tropical and sub-tropical regions. Studies were conducted on the cultivation and nutritional analysis of this mushroom. The pure culture of *Calocybe indica* was carried out in the laboratory. The culture was maintained on potato dextrose agar slant and sub-cultured at a regular monthly interval to sustain their fruiting vigor. The above stock culture was used in studies. Wheat grain spawn of *C. indica* was prepared in glass bottles. The filled paddy grain spawn of *C. indica* was used at 6% level to the wet weight of the substrate and the beds were spawned. After harvest, the mushrooms were dried at 40°C under the hot air oven to make it powered for further analysis. The collected fresh mushrooms were dried in shade and coarse powder was analyzed for nutrients namely moisture, crude protein, lipid, ash, crude fiber, and minerals. It shows the dominant compounds of protein, fiber, and carbohydrate and the contents are 14.11%, 8.30% and 5.62% respectively. Lipid, ash, ether extract and p^H contents are 4.06%, 7.04%, 3.15% and 5.4% respectively. The carbon and nitrogen contents are 33.60% and 3.56% respectively. In the estimation of saturated fatty acids and unsaturated fatty acids present in *C. indica,* totally, 17 fatty acids were recorded. In the estimation of essential and non-essential amino acids present in *C. indica*, totally, 15 amino acids were recorded. In the estimation of minerals composition present in *C. indica,* it was recorded that the species had a good resource of mineral composition. Totally, 6 macro minerals and 8 micro minerals were recorded. This investigation may provide that the paddy straw substrates can be recommended for the commercial cultivation of *C. indica* to obtain highly nutritious mushrooms.

INTRODUCTION

Mushrooms can be used as food to solve malnutrition problems. Mushrooms have good nutritional value particularly as a source of protein that can enrich human diets, especially in some developing countries where animal protein may not be available and are expensive (Gopinath et al. 2012). Many genera of mushrooms are edible and rich in essential nutrients such as carbohydrates, proteins, vitamins, minerals, fat, fibers, and various amino acids (Okwulehie & Odunz 2000). The *Calocybe indica* is an easily cultivable edible mushroom in India. They are distributed in the tropical regions of the world. In India, it is widely distributed in the genetic plains of West Bengal. They are considered to be more popular because of their robust size, attractive color, sustainable yield, delicious taste along with its unique texture. It has become the third commercially grown mushroom in India, after the button and oyster's mushroom (Purakayasatha & Nayak 1979). The bioactive potential of some commercially important mushrooms like milky and button mushroom is a source of essential amino acids and fatty acids for infants and the elderly (Nakalem & Kabasa, 2013).

The annual production of the milky mushroom in seasonal farms concentrated in the southern states of Tamil Nadu, Kerala and Karnataka have now been estimated to be nearly 10,000 tons. It is purely of Indian origin and highly suitable for the tropical climatic conditions of central India, northern India, and southern India. Its cultivation is now spreading very fast in many states of the country like Tamil Nadu, Kerala, Odisha, Haryana, and West Bengal due to its longer shelf life and adaptability to warm and humid conditions. In Tamil Nadu, this mushroom is commonly grown in sunken beds where humidity and temperatures are ideal for vegetative growth and fruit body development. Mushroom species have been shown to possess antioxidant capacity in in-vitro systems. Like other matrices containing antioxidant compounds, e.g. phenolics, organic acids, and alkaloids from mushrooms can be used both as a food supplement and in the pharmaceutical industry. The public is becoming

increasingly aware of problems with the over-prescription and misuse of traditional antibiotics (Mary & Sahana 2014). *C. indica* is more popular due to its robust size, attractive color, sustainable yield, delicious taste, and unique texture. It is rich in carbohydrates, protein, lipids, fats, fiber, ash, and essential amino acids (Mary & Sahana 2014). They have become an attractive functional food mainly because of their biochemical composition and antioxidant properties which have been reported to prevent oxidative damage by free radical and reactive oxygen species (ROS) and may prevent the occurrence of diseases like carcinogenesis, aging, physical injury, infection, and cardiovascular disease. Therefore, the milky mushroom is considered a better proxy for oyster mushroom. The aim of this investigation was to analyze the biochemical composition and nutritional values of this mushroom cultivated on a paddy straw bed, to increase awareness of the beneficial effects of edible mushrooms among the consumers.

MATERIALS AND METHODS

Culture and Maintenance

The pure culture of *C. indica* was cultivated from the Zoology research laboratory, Kamaraj College, Tuticorin. The pure culture was maintained on the potato dextrose agar slant and sub-cultured at a regular monthly interval to sustain their fruiting vigor. They were stored at 4°C for further usage.

Spawn Preparation

The wheat grain spawn of *C. indica* was prepared in glass bottles as described (Pani 2011a). The wheat grain (1kg) was semi-boiled, then 2% calcium carbonate and 0.2% gypsum were added. The mother culture was prepared in glass bottles filling them ½ full and the working spawn was prepared in plastic bags capped with cotton plugs by rubber bands. The mother culture was then subcultured on potato dextrose agar and after its full growth, it was transferred to the working spawn bags of *C. indica.*

Cultivation and Harvesting

The paddy straws were collected from local farmers of the Tuticorin district, Tamil Nadu, India. The straw was used as a substrate for cultivation. The substrate was soaked in cold water for 4 h. After draining excess water, the materials were treated in hot water (80°C) for 60 mins and dried in shade. For the bed preparation, polythene bags of 60 × 30 cm size and 100 gauge thickness was used and cylindrical beds were prepared using 0.5 kg of substrate (dry weight) per bed. The filled wheat grain spawn of *C. indica* was used at 6% level to the wet weight of the substrate (Pani 2011b). After 10 to 15 days, when the beds were fully colonized by the mycelium of *C. indica* (mushroom), they were cut into two halves and applied with casing soil to a height of about 2 cm over the spawn run. The beds were uniformly and regularly sprayed with water until it was the last harvest. In total, three crops were harvested at intervals of 3 to 5 days.

Nutritional Status of *C. indica*

The collected fresh mushrooms were shade dried and its coarse powder was analyzed for the presence of nutrients namely, protein, fat, ash, fiber, moisture, and minerals.

Estimation of Protein

Five grams of grounded mushroom was mixed with 50 mL of 0.1 N NaOH and then boiled for 30 mins. After cooling the solution to room temperature, it was subjected to centrifugation at 1000 rpm. The supernatant was analyzed for total protein contents (Lowry et al. 1951).

Estimation of Lipid

The total lipid was determined by a slightly modified method (Floch et al. 1956). Primarily, five grams of finely ground mushroom was suspended in 50 mL of chloroform: methanol (2:1 v/v) mixture. After mixing thoroughly, it was allowed to stand for 3 days. Then the solution was filtered and centrifuged at 1000 rpm for 15 mins.

Estimation of Fiber

The total fiber contents were determined by the following method (Raghuramulu et al. 2003). Ten grams of moisture and fat-free sample was taken in a beaker. To which 200 mL of con 0.255 N H_2SO_4 was added and boiled for 30 mins. While boiling, constant volume was maintained by adding water at frequent intervals. Then, it was filtered through a muslin cloth and the residues were washed with hot distilled water for the complete removal of acid from it. After which, it was transferred to the same beaker and 200 mL of 0.313 N NaOH was added to it. After boiling it for 30 mins, the mixture was filtered through a muslin cloth then, and the residues were washed thoroughly in hot water until it was freed from alkali. It was then washed with ethyl alcohol and followed by ether. Finally, it was transferred to a crucible, dried overnight at 80°C to 100°C and its weight was recorded in an electric balance. The crucible was heated in a muffle furnace at 600°C for 5 to 6 h and its weight was recorded after it cooled.

Estimation of Ash

The ash contents were determined by innerving or burning the pre-weighed test sample (1 g dry weight) in a muffle furnace at 560°C for a period of 5 h. Then, the residues were

weighed and the percentage was calculated according to AOAC (1990). It was subjected to further analysis.

Estimation of Nitrogen and Carbon Contents

The total nitrogen and carbon contents were determined using the wet digestion extraction methods (Nivozamsky et al. 1983).

Determination of pH

The 5% (w/v) (5g in 100 mL of water) finely powdered mushroom was kept on a shaker for 5h at 140 rpm and then subjected to filtration. The filtrates were analyzed for the pH using a pH meter (Elico, India) (Iqbal et al. 2010).

Estimation of Amino Acids

The collected tissues were dried at 60°C for 24 h in an oven and they were packed in airtight polyethylene covers and kept in desiccators. The oven-dried samples were finely ground before estimating the amino acid profile. Amino acids were estimated in HPLC-Lachrome Merck in SPD-10A VP Detector (Baker et al. 1994).

Estimation of Fatty Acids

The samples were oven-dried at 70°C for 24 h until no more weight reduction was observed. After that, it was ground finely with pestle and mortar. To the 100 mg to 200 mg of finely ground tissue samples, 2 mL of chloroform and methanol (1:1 ratio) was added and kept aside for 30 sec. Then the residual matter was removed through filtration with the Whatman no:1 filter paper (125 mm). After that, it was subjected to washing with 1mL of chloroform and methanol (2:1 ratio) for removing the inorganic substance. Next, the extracts were infected with chloroform: methanol: water (8:4:3) where the residual phase was evaporated to dryness. Then the dried matter was sealed in a test tube with 3% methanolic HCl and stored at 80°C for 18 h. To this, 2 mL of hexane was added for extraction of the fatty acid ethyl esters from the methanol by hexane. 1 mL of the supernatant containing hexane phase was collected in a microvel. After which, the residual fraction was dissolved in the ratio of 10:1 with ethyl acetate and 1:1 aliquot of which was injected into gas chromatography equipped with flame identification detector and column HP ULTRA -2 (25 m, 0.2 mm 1D) (Babu et al. 2012).

Estimation of Minerals

The concentration of the metals like calcium, sodium, magnesium, potassium, phosphorous, barium, iron, zinc, cobalt, chromium, copper, manganese, gallium, lithium, nickel, selenium, aluminum, and boron, were estimated from 1g of mechanically ground and oven-dried samples at 175°C. Then it was digested with sulphuric acid and 40% nitric acid and was allowed to stand overnight at room temperature, before being analyzed for specific metals, using Atomic Absorption Spectrophotometer (AAS) Shimadzu –AA-65015 (Guzman & Jimenez 1992).

RESULTS AND DISCUSSION

Cultivation of *C. indica*

On casing the spawn bed into the soil, a small mushroom is developed which is shown in Fig. 1. After 4 days the mushroom growth is increased to 5-6 cm in length. It's ready to harvest. After harvest, the mushroom was dried at 40°C under the hot air oven to make it powered for further analysis (Fig.1).

Proximate Composition of *C. indica*

The results of the proximate and nutritional composition

Fig. 1: Harvesting stage of *C. indica.*

of dried *C. indica* are shown in Fig. 2. It shows that the dominant compounds are protein (14.11%), fiber (8.30%), carbohydrate (5.62%), lipid (4.06%), ash (7.04%), ether extract (3.15%), and pH (5.4%). The carbon and nitrogen content of *C. indica* are (33.60%) and (3.56%) respectively (Fig. 2).

Fatty acids profile of *C. indica*

In the estimation of saturated fatty acids and unsaturated fatty acids present in *C. indica*, a total of 17 fatty acids were recorded. Among the available saturated fatty acids (SFA) include stearic acid (20.36%), lignoceric acid (1.57%), myristic acid (1.49%), lauric acid (1.42 %), palmitic acid (1.30 %), heneicosylic acid (0.41%), pentadecyclic acid (0.65%), margaric acid (0.27%), and arachidic acid (0.28%) (Fig. 3a). The unsaturated fatty acids include linoleic acid (42.88%), elaidic acid (22.47%), myristoleic acid (1.56%), eicosapentaenoic acid (1.86%), erucic acid (0.34%), palmitoleic acid (0.21%), gondoic acid (1.24%), and dichomo-linolenic acid (0.657%) (Fig. 3b). In the analysis of fatty acids, it was observed that

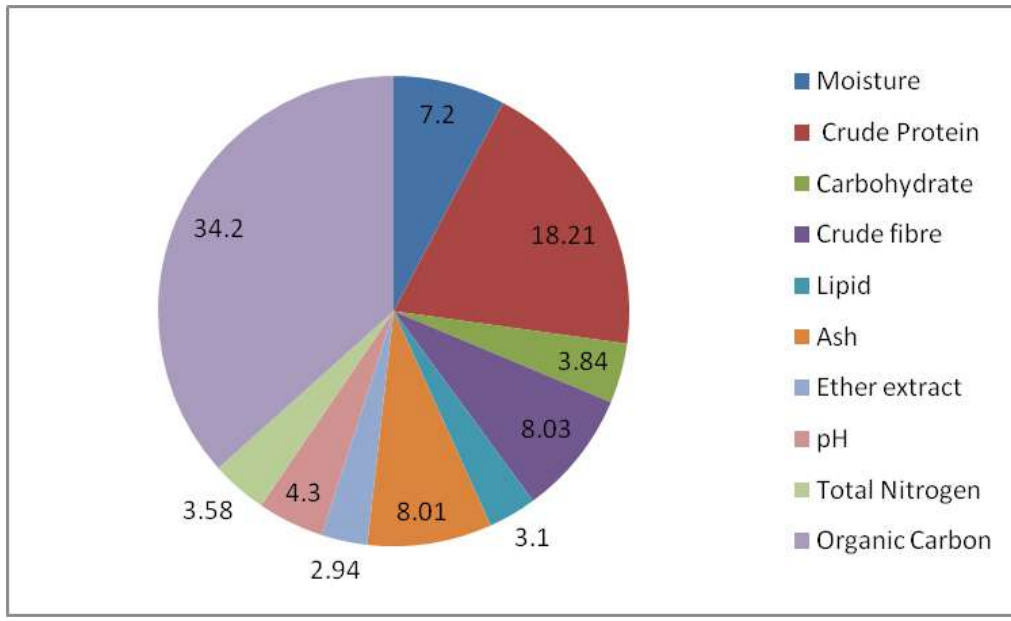

Fig. 2: Proximate composition of *C. indica.*

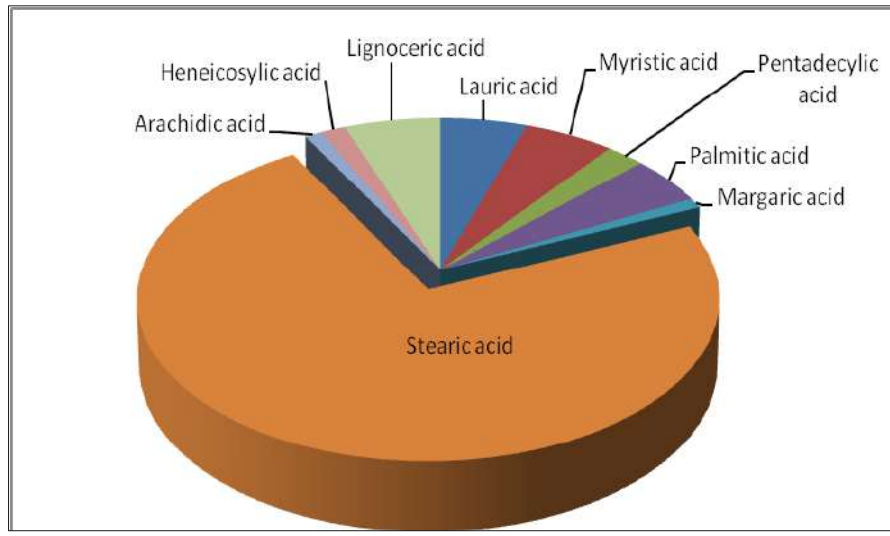

Fig. 3a: Composition of saturated fatty acids of *C. indica.*

the most abundant fatty acids present in the *C. indica* were linoleic acid and elaidic acid.

Amino acids content of dried *C. indica*

In the estimation of essential and non-essential amino acids present in dried powder of *C. indica,* totally 15 amino acids were recorded. Among the non-essential amino acids, analine was found to be the most abundant amino acids followed by glutamic acid and Isoleucine. Among the essential amino acids, isoleucine (12.37%), histidine (8.07%), leucine (5.17%), valine (4.33%), threonine (3.70%), lysine (2.26%), phenylalanine (2.29%) and methionine (0.27%) were recorded (Fig. 4a). The non-essential amino acids like analine (16.05 %), glutamic acid (14.75%), aspartic acid (11.85%), glycine (7.41%) Serine (6.78%), tyrasine (3.42%) and arginine (2.37%) were recorded (Fig. 4b).

Minerals Composition

In the analysis of the minerals in dried mushrooms, results show that there is a good source of minerals. Among the minerals totally, 6 macro minerals and 8 micro minerals were recorded. The maximum macro mineral was potassium (28209ppm), followed by magnesium (1012ppm), phosphorus (381ppm), and barium (9.3ppm) were recorded (Fig. 5a). Micro minerals

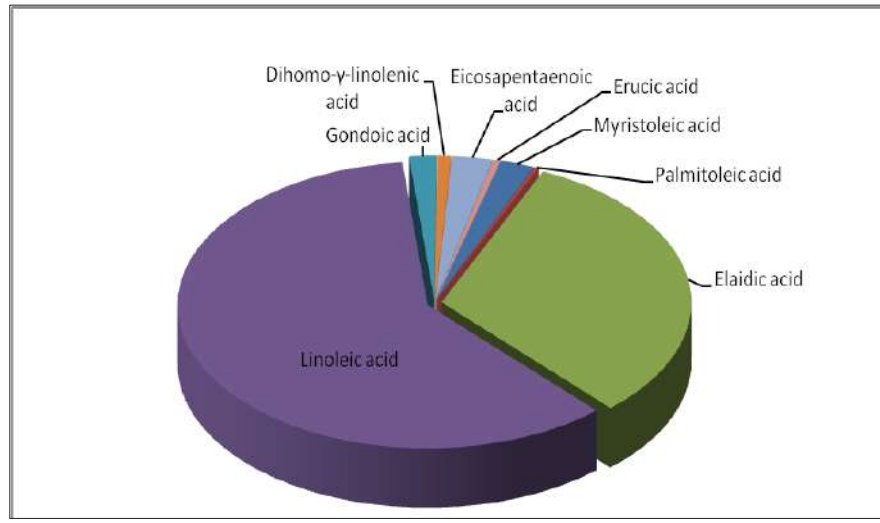

Fig. 3b: Composition of unsaturated fatty acids of *C. indica.*

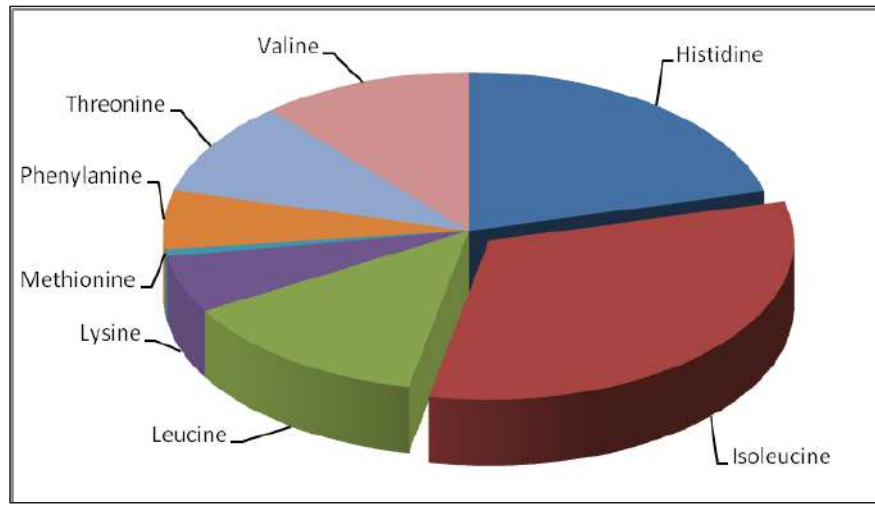

Fig. 4a: Composition of essential amino acids of *C. indica.*

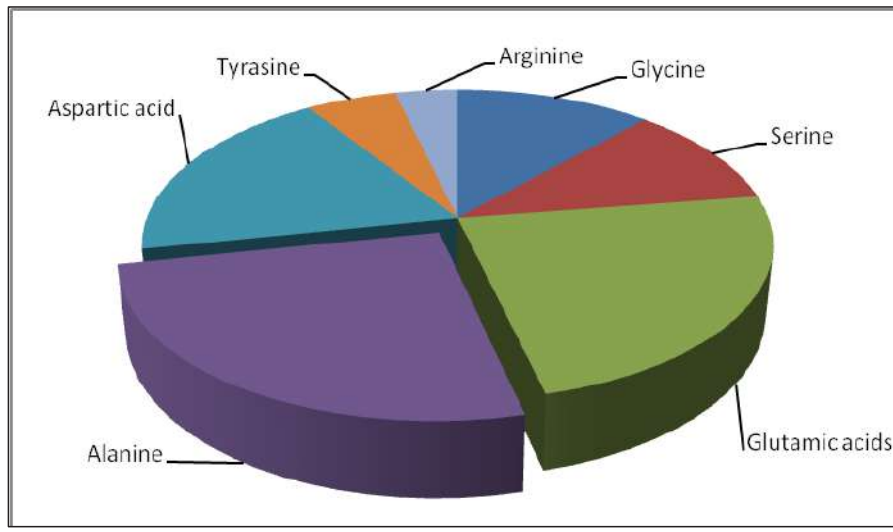

Fig. 4b: Composition of non-essential amino acids of *C. indica.*

such as iron (77.55ppm), aluminum (38.92ppm), manganese (20.56ppm), copper (28.20ppm), zinc (35.12ppm), boron (18.87ppm), nickel (0.85ppm), chromium (0.89ppm) were recorded (Fig. 5b).

DISCUSSION

The *C. indica* (Milky Mushroom) could be easily grown on a wide range of substrate including the straw of paddy, wheat, ragi, maize, bajra, cotton stalks, and leaves, sugarcane biogases, cotton and jute wastes, dehulled maize cobs, tea/coffee waste, etc. Saranya et al. (2011) investigated the cultivation of milky mushrooms, *C. indica*, which was conducted to find out the growth and yield performance on different substrates. The yield of fresh mushroom obtained from paddy straw, teak leaves, and sugarcane trash substrates were 1140, 745, and 570 $g.kg^{-1}$ respectively. The nutritional significance of *C. indica* cultivated on different substrates was assessed in terms of protein, carbohydrate, amino acids, and lipids. The cellulolytic activity and coir pith compost were also tested using *C. indica*. The present result suggested the lignocellulosic substrate like paddy straw, teak leaves, and sugarcane trash show great potential for use as a raw material since this substrate provides an economically acceptable production for *C.*

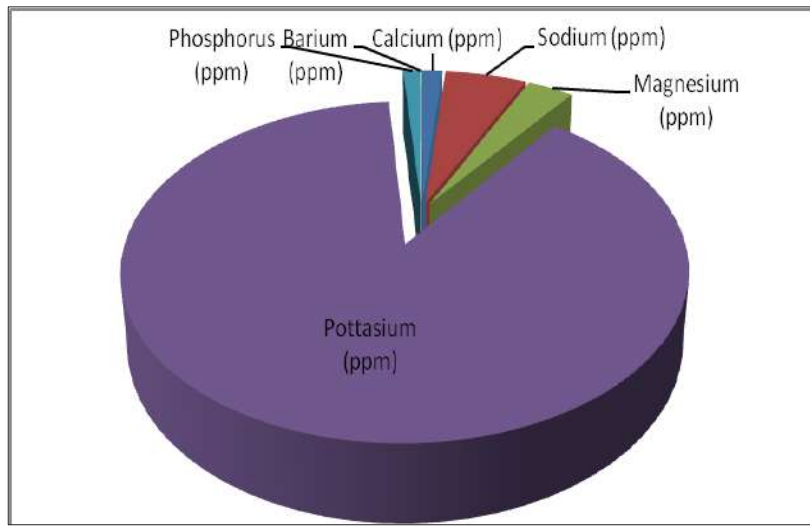

Fig. 5a: Composition of macro minerals of *C. indica.*

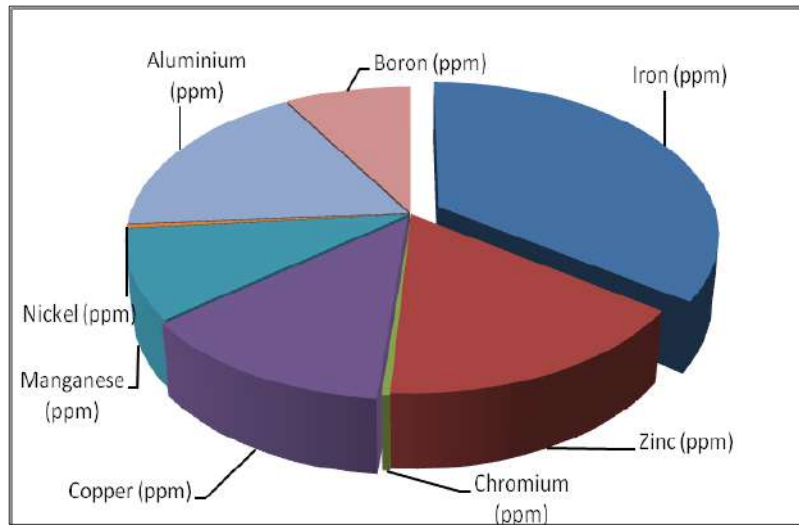

Fig. 5b: Composition of micro minerals of *C. indica.*

indica. Mushrooms are neutraceuticals which contain edible fruit body. The nutritive value of mushrooms is equal to that of milk and it has low calories, sodium, fats, and cholesterol. In addition to this, they are rich in protein, unsaturated fatty acids, vitamin B, D, C as well as minerals such as potassium, phosphorus, calcium, and magnesium. (Krishnaveni et al. 2014). The high yield strain of *C. indica* grows well at room temperature between 24°C to 27°C and can be cultivated even on unfermented materials. The advantages of this mushroom over other mushrooms are easy method of cultivation, less investment, very attractive fruiting body, pleasing milk-white color, long shelf life, more nutritious and less time to grow (Kathiravan & Krishnakumari 2015). In the present study, the cultivation of *C. indica* was carried out on paddy straw waste and has been observed to produce an excellent yield after 15 days.

Mushrooms are a good source of digestible proteins and less fat in nature. The present study also reveals that the nutritional composition of *C. indica* was protein (14.11%), fiber (8.30%), carbohydrate (5.62%), fat (4.06%), ash (7.04 %), ether extract (3.15%), p^H (5.4), carbon (33.60%) and nitrogen (3.56%). Mushrooms contain higher nutritional values of protein (4.22g), carbohydrate (1.11g), fat (1.05g), ash (2.30g), and moisture (85.95) (Krishnamoorthy et al. 1998). Mushrooms consist mostly of unsaturated fatty acids, which are less hazardous to the health than the saturated fatty acids of animal fats (Zahid et al. 2010). The moisture percentage depends on the mushroom species and the parameters related to harvest, culinary, and storage conditions. Mushrooms also contain a rich amount of amino acids (Kalac 2013). Leucine, valine, glutamic, and aspartic acid are the most abundant amino acids in mushrooms (Guillamónet et al. 2010). The present study with *C. indica* showed 8 essential and 7 non-essential amino acids. The amino acid aniline (16.05%) was served to be the most significant and it's followed by glutamic acid (14.75%) and isoleucine (12.37%). Mushrooms can be used as food to solve malnutrition problems. Mushrooms have good nutritional value particularly as a source of protein that can enrich human diets, especially in some developing countries where animal protein may not be available and are expensive (Proksch et al. 2002). The presence of linoleic acid and oleic acid were observed to be the major unsaturated fatty acid present in *C. indica*. Usually, in mushrooms, the fat contents seem to be very low when compared with proteins and carbohydrates. Moreover, the fats present in the mushroom fruiting bodies are dominated by unsaturated fatty acids. In the present study, 17 fatty acids were recorded. From the analysis of fatty acids, it was observed, the most abundant fatty acids present in the *C. indica* were linoleic acid (42.88%) followed by elaidic acid (22.47%). Mushrooms are considered to be a dietary supplement for aquaculture because of their higher protein contents when compared with that of fats.

Sodium, magnesium, potassium, and calcium are the essential macronutrient absorption in the intestine and are used for their normal metabolism (Satish et al. 2013). Their imbalance would result in the diseased or infected conditions exhibiting their significant impact on the immune system of *Babylonia spirata.* The present study on the minerals composition of *C. indica* revealed the presence of 6 macro minerals and 8 micro minerals, among them, potassium (28209 ppm) as maximum in macro minerals and iron (77.55ppm)

as maximum in micro minerals. Similarly, the nutraceutical properties of *C. indica* have reported the presence of vitamins, proteins, minerals, amino acids, polyphenols such as flavonoids and alkaloids (Mirunalini et al. 2012).

Mushroom seems to be an important source of bioactive compounds for the development of new therapeutic agents (Sumathy et al. 2015). Since mushrooms are abundant in nature, cost-effective, and easily can be cultivated, there is a promising solution for a variety of health issues in the upcoming years. These data suggest that dietary mushrooms cultivated on paddy straw are a good source of nutrients especially minerals and fatty acids. So, this result also indicates that the studied mushrooms have good nutritive value for humans. In addition, mushrooms are a promising food that may overcome the protein-energy malnutrition problem in the nation.

ACKNOWLEDGEMENTS

The authorities of Kamaraj College, Manonmaniam Sundaranar University for providing the necessary facilities, and the author, in addition, thank the Centre for Marine Living Resources and Ecology (CMLRE), Project (Grant No. MoES/10-MLR/01/12), Government of India for their financial support.

REFERENCES

AOAC 1990. Official Method of Analysis (15th Edition). Association of Official Analytical Chemists, Washington DC, U.S.A.

Babu, A.V., Venkatesan, M. and Rajagopal, S. 2012. Biochemical composition of different body parts of *Gafrarium tumidum* (Roding 1798) from Mandapam, South East Coast of India. Afr. J. Biotechnol., 11(7): 1700-1704.

Baker, D.H. and Han, Y. 1994. Ideal amino acid profile for broiler chicks during first three weeks post-hatching. Poult. Sci.,73: 1441-1447.

Floch, J., Lees, M. and Sloane-Stanley, G.H. 1956. A simple method for the isolation and purification of total lipids from animal tissues. J. Biol. Chem., 226: 497-509.

Gopinath, L., Arunkumar, J., Meera, A. and Shantha, P.R. 2012. Optimization of growth parameters for increased yield of the edible mushroom *Calocybe indica.* Afr. J. Biotechnol., 11(11): 7701-7710.

Guillamón, E., García-Lafuente, A., Lozano, M., D´Arrigo, M., Rostagno, M.A., Villares, A. and Martínez, J.A. 2010. Edible mushrooms: Role in the prevention of cardiovascular diseases. Fitoterapia, 81: 715-723.

Guzman, H.M. and Jimenez. 1992. Concentration of coral reefs by heavy metals along the Caribbean coast of central Africa (Costarica and Panama). Mar. Pollut. Bull., 24: 554-561.

Iqbal, Z., Lateef, M., Jabbar, A. and Gilani, A. H. 2010. In vivo anthelmintic activity of *Azadirachta indica* A. Juss seeds against gastrointestinal nematodes of sheep. Vet. Parasitol., 168: 342-345.

Kalac, P. 2013. A review of the chemical composition and nutritional value of wild-growing and cultivated mushrooms. J. Sci. Food Agric., 93(2): 209-218.

Kathiravan, S. and Krishnakumari, S. 2015. Optimization of casing process for enhanced bioefficiency of *Calocybe indica*, an indigenous tropical edible mushroom. Int. J. Rec. Sci. Res., 6(2): 2594-2598.

Krishnamoorthy, A.S., Muthusamy, M., Marimuthu, T., Narasimhan, V. and Muthusankaranaraynman, A. 1998. Milky mushroom, APK 2. Bulletin on new mushroom variety release. Regional Research Station, TANU, Aruppukottai, India. 16.

Krishnaveni, M. and Saranya, R. 2014. Cultivation of *Pleurotus florida* and *Calocybe indica* using various agrowaste. Res. J. Pharm.Technol., 7(3): 307- 309.

Lowry, O.H., Rosebrough, N.J., Farr, A.L. and Randall, R.J. 1951. Protein measurement with the tolin phenol reagent. J. Biol. Chem.,193: 265-273.

Mary, J. and Sahana, B. 2014. Cultivation of milky mushroom using paddy straw waste. Int. J. Curr. Microbiol. Appl. Sci., 3(12): 404-408.

Mirunalini, S., Dhamodharan, G. and Deepalakshmi. K. 2012. Antioxidant potential and current cultivation aspects of an edible milky mushroom-*Calocybe indica.* Int. J. Pharm. Sci., 4(1): 137-143.

Nakalem, B. and Kabasa, J.D. 2013. Fatty and amino acids composition of selected wild edible mushrooms of Bunyoro sub-region, Uganda. AJFAND, 13(1): 7225-7240.

Nivozamsky, I., Houba, V.J.G., Van Eck, R. and Van Vark, W. 1983. A novel digestion technique for multi-element plant analysis. Commun. Soil Sci. Plant Anal., 14: 239-248.

Okwulehie, I.C. and Odunze, E.I. 2000. Evaluation of the nutritional value of some tropical edible mushrooms. J. Sustain. Agric. Environ., 6(2): 157-162.

Pani, B.K. 2011a. Response of summer white mushroom (*Calocybe indica*) to supplementation of cultivation substrate. Asian J. Exp. Biol. Sci., 2(4): 766-768.

Pani, B.K. 2011b. Evaluation of straw of some paddy varieties as substrates for cultivation of milky mushroom (*Calocybe indica*) in Orissa. Biosci. Discov., 2(3): 341-342.

Proksch, P., Edrada R.A. and Ebel, R. 2002. Drug form the seas-current status and microbiological implication. Appl. Microbiol. Biotechnol., 59: 125-134.

Purakayasatha, R.P. and Nayak, D. 1979. A new method of cultivation of *Calocybe indica:* An edible mushroom. Taiwan Mushroom, 3: 14-18.

Raghuramulu, N., Madhavan, N.K. and Kalyanasundaram, S.A. 2003. Manual of Laboratory Techniques. Hyderabad, India: National Institute of Nutrition. Indian Council of Medical Research, pp. 59-58

Saranya, V., Madhanraj, P. and Panneerselvam, A. 2011. Cultivation, composting, biochemical and molecular characterization of *Calocybe indica* (C and A). Asian J. Pharm. Res., 11(1): 55-57.

Satish, K., Sharma, M., Alok, R. and Abalisha, A. 2013. Effect of various organic supplements on non-enzymatic antioxidant and minerals expression in *Calocybe indica*. The Biosean, 8(2): 421-424.

Sumathy, R., Kumuthakalavalli, R. and Krishnamoorthy, A.S. 2015. Proximate, vitamin, amino acid, and mineral composition of milky mushroom, *Calocybe Indica* (P&C). Var. Apk2 commonly cultivated in Tamil Nadu. J. Nat. Prod. Plant Resour., 5 (1): 38-43.

Zahid, M.K, Barua, S. and Haque, S.M. 2010. Proximate composition and mineral content of selected edible mushroom varieties of Bangladesh. Bangladesh J. Nutr., 22-23: 61-68.

Nature Environment and Pollution Technology
An International Quarterly Scientific Journal

p-ISSN: 0972-6268
(Print copies up to 2016)
e-ISSN: 2395-3454

Vol. 20 | No.3 | pp. 1165-1171 | 2021

Original Research Paper

https://doi.org/10.46488/NEPT.2021.v20i03.024

Open Access Journal

Study on Catalytic Oxidation, Flocculation and Sedimentation of Acidizing and Fracturing Wastewater

T. Yu*(**)*, F. Wang*(**), H. Hu*(**), C. Qu*(**)† and Le Zhang*(**)**

*College of Chemistry and Chemical Engineering, Xi'an Shiyou University, Xi'an 710065, P. R. China

**Shaanxi Key Laboratory of Environmental Pollution Control Technology and Reservoir Protection of Oil Field, Xi'an Shiyou University, Xi'an 710065, China

***State Key Laboratory of Petrochemical Pollution Control and Treatment, Beijing 102206, P. R. China

†Corresponding author: Chengtun Qu; xianquct@163.com

Nat. Env. & Poll. Tech.
Website: www.neptjournal.com

Received: 21-08-2020
Revised: 00-00-2020
Accepted: 01-11-2020

Key Words:
Waste aciding fluid
Catalytic oxidation
Flocculating settling
Treatment process

ABSTRACT

The acidizing and fracturing waste fluid in a wellsite in northern Shaanxi was treated by catalytic oxidation and flocculation precipitation. It investigated the effect of different coagulants and their dosage and the wastewater pH on coagulation precipitation. As for chemical oxidation experiment, it investigated the effect of oxidant dosage and reaction time on its treatment effect. The results showed that when 30% hydrogen peroxide (volume percentage) was added at the dosage of 0.3% and oxidized for 50 min, the pH was adjusted to 7.5 and 350 mg/L polyaluminum chloride (PAC) and 4 mg/L polyacrylamide were added (PAM); after processing the waste liquid, total iron, chemical oxygen demand (COD), chromaticity, and average corrosion rate were reduced from 252.75 mg/L, 3427.50 mg/L, 624.15°, and 0.1226 mm/a to 0.12 mg/L, 275.18 mg/L, 125° and 0.0217 mm/a, respectively; effective removal of iron and color, reduced COD, and controlled corrosion was achieved.

INTRODUCTION

In the process of shale gas exploitation, hydraulic fracturing technology is needed to increase the recovery rate (Barati & Liang 2014, Mauter & Alvarez 2014, Lester et al. 2013). Hydraulic fracturing is accomplished by injecting a large amount of fracturing fluid into the formation to improve reservoir permeability (Glaze & Kang 1989). Combining acidizing and fracturing operations for oil and gas well transformation is an important method used for oil and gas field stimulation (Olsson et al. 2013, Davarpanah 2018). After the fracturing operation is completed, most of the fracturing fluid will be returned to the ground after breaking the rubber to form shale gas fracturing flowback fluid. A variety of additives are often added to the fracturing fluid to meet the requirements of sand carrying and drag reduction (Adham et al. 2018, Puspita 2015). At the same time, it will contact with oil and gas, water and rocks in the stratum during the fracturing process, resulting in many types of pollutants in the fracturing fluid. The viscosity is high and the treatment is difficult (Poyatos et al. 2010, Amr et al. 2013, Boczkaj et al. 2010, Bello et al. 2017) . If it is not treated, it will cause environmental pollution. The development of shale gas fracturing flowback fluid treatment and reuse technology is of great significance for shale gas development and environmental protection (Reilly et al. 2015, You et al. 2019). Recently, advanced oxidation process (AOP) has been successfully used to treat industrial wastewaters that are non-biodegradable and toxic to microorganisms (Kim et al. 2004, Boczkaj & Fernandes 2017, Li et al. 2018) Especially, Fenton oxidation has been applied for the decolorization of effluents from textile dyeing process and dye manufacturing process. Compared to other oxidation processes, such as UV/H_2O_2 process, costs of Fenton oxidation are quite low (Dutta et al. 2001). Fenton oxidation has been lately used for different treatment processes because of its ease of operation, the simple system and the possibility to work in a wide range of temperatures (Solozhenko et al. 1995). At present, the main treatment method for fracturing waste liquid is oxidation viscosity reduction with coagulation and precipitation. The main treatment technology for acidification waste liquid is alkali neutralization with coagulation and precipitation (Makhathini et al. 2020, Mao 2018 et al). In recent years, research has focused on identifying highly efficient, widely applicable, and economical treatment technologies for acidizing and fracturing waste fluid.

Water quality characteristics of the acidizing and fracturing waste liquid from a wellsite in northern Shaanxi, was analyzed. According to the characteristics of fracturing wastewater, the suspended solids and colloidal in waste liquid

were removed by coagulation sedimentation. Removal of iron and color, reduction of COD removal, and corrosion control were investigated using catalytic oxidation and flocculation precipitation (Zhang et al. 2020). Then the COD of wastewater was reduced by chemical oxidation treatment in order to achieve recycling standard of enterprise. The hydroxy radicals (·OH) produced in the process could oxidate the organic compounds in the wastewater so that the wastewater can meet the discharge standard (Szpyrkowicz et al. 2001, Arslan & Balciolu 1999). This study aims to provide technical guidance for effective waste processing of acidizing and fracturing waste liquid through discussing experimental conditions. It investigated the effect of different coagulants and their dosage and the wastewater pH on coagulation precipitation. As for the chemical oxidation experiment, it investigated the effect of oxidant dosage and reaction time on its treatment effect.

MATERIALS AND METHODS

Instrumentation and Reagents

Instrumentation used in the study was the following: UV-Vis spectrophotometer (UV-2350, Shanghai Right Instrument Co., LTD.), electronic balance (CP214, Mr. Hauser Instrument Co., LTD.) and circulating water vacuum pump (SHZ-D (III), Gongyi City Instrument Co., LTD in China). Reagents used in the experiment were the following**:** hydrogen peroxide (30%), concentrated sulfuric acid, congo red test paper, hydroxylamine hydrochloride, sodium hydroxide, polyaluminum chloride (PAC), polyacrylamide (PAM).

Water Quality Characteristics Analysis Method

The determination of Fe^{2+}, Fe^{3+} plasma, and COD in waste liquid was performed in accordance with water and wastewater detection methods and an oil and gas field water analysis method (Ferrer & Thurman 2015). Oil and suspended matter content were determined using a recommended index and an analysis method of water injection quality of a clastic reservoir (Oetjen & Thomas 2016). Corrosion rates were determined using a water corrosion test method (Pier et al. 2018).

Determination of Viscosity, Chromaticity and Light Transmittance

(1) Viscosity: The passage time of distilled water and the passage time of water sample were determined using a Uhler viscometer, and water sample viscosity was calculated according to equation (1).

$$\mu = (t_2 \times r)/t_1 \quad \ldots(1)$$

t_1 = time required for distilled water, s

t_2 = passage time required for water sample, s

r = density of water sample g/cm^3

m = viscosity of water sample, mPa·s

(2) Chromaticity: The water sample absorbance was measured at 350 nm. According to the chromaticity standard curve and due to the high chromaticity of the water sample, the measured value was calculated after making a 1:10 dilution.

(3) Light transmittance: The light transmittance of the water sample was measured at 680 nm. Due to the low light transmittance of the water sample, the measured value was calculated after making a 1:10 dilution.

Optimization Method for Catalytic Oxidation Agent System

The pH was adjusted to 7.5 after a certain volume of hydrogen peroxide was added and oxidized for a certain time. PAC, an inorganic flocculant, and PAM, a coagulant, were added and allowed to stand for 30 min. The light permeability of the clear liquid was based on optimal dosage of H_2O_2, the oxidant, oxidation time, flocculant dosage, and interval time.

RESULTS AND DISCUSSION

Analysis of Water Quality Characteristics

The water sample was taken from the acidizing and fracturing waste fluid of a well site in northern Shaanxi. Following the standards and methods mentioned in Section 1.2, the water quality characteristics of the waste liquid were analyzed. The results are shown in Table 1. The content of divalent iron was 218.25 mg/L. The viscosity was relatively low at 1.11 mPa·s. Oil content and suspended substance content were low, at 9.69 mg/L and 37.00 mg/L, respectively. Chromaticity

Table 1: The characteristics of wastewater.

Serial number	Test items	Content
1	pH	3.5
2	Fe^{2+} (mg·L^{-1})	218.25
3	Fe^{3+} (mg·L^{-1})	34.50
4	Oil (mg·L^{-1})	9.69
5	Suspended solids (mg·L^{-1})	37
6	Chromaticity (°)	624.15
7	Viscosity (mPa·s)	1.11
8	Light transmittance (%)	25.82
9	COD (mg·L^{-1})	3427.50
10	Mean corrosion rate (mm/a)	0.1226

was high and reached 624.15° in the case of 1:10 dilution. Light transmittance was low at only 25.82% in a 1:10 dilution, and COD was high at 3427.50 mg/L. The average corrosion rate was high at 0.1226 mm/a, suggesting strong corrosion.

Analysis of Catalytic Oxidation Process

The concentration of Fe^{2+} in the acidizing and fracturing liquid concentration was high, up to 218.25 mg/L, and the pH was 3.5. According to the principle of Fenton's reagent, a solution of H_2O_2 in an acidic environment (pH is generally 3 to 4) (Tang et al. 2018) , with Fe^{2+} as a catalyst can produce hydroxyl free radicals (·OH) and organic macromolecules, which reduces ion in the waste liquid. Bacteria and other pollutants have strong oxidation capabilities and can degrade macromolecular structures, and Fe^{3+} and Fe^{2+} can be converted to waste liquid. Stable gel breaking off can be achieved, which strengthens flocculation and bactericidal activities (Yoon et al. 2001, Watts et al. 2005). Therefore, the acidic environment and water quality characteristics of the waste liquid, such as high content of iron divalent, were utilized to conduct catalytic oxidation treatment of the acidified and fracturing waste liquid according to the method described in the section 1.4. As for chemical oxidation experiment, it investigated the effect of the oxidant dosage and reaction time on its treatment effect.

Effect of H_2O_2 Addition on the Reaction

The oxidant dosage (H_2O_2) were optimized. The effects of oxidant dosage on COD removal rate and transmittance rate were investigated. The experimental results of H_2O_2 optimization amount are shown in Fig. 1 and Table 2 .

As shown in Fig. 1, when the dosage of H_2O_2 increases from 0.1% to 0.3%, the COD removal rate of wastewater gradually increases in the proportion of the increase of the amount of H_2O_2. However, when the dosage of H_2O_2 increases from 0.3% to 0.5%, the removal rate of COD in wastewater gradually decreases. When the dosage of H_2O_2 is 0.3%, the COD removal rate reaches the maximum. When the concentration of H_2O_2 is low, the COD removal rate of wastewater increases with the increase of H_2O_2 concentration ($Fe^{2+}+H_2O_2 \rightarrow Fe^{3+}+\cdot OH+OH^-$). When the amount of H_2O_2 exceeds 0.3%, the removal effect of H_2O_2 on ·OH increases with the increase of H_2O_2 added ($H_2O_2+\cdot OH \rightarrow H_2O+\cdot OH_2$). Moreover, the high concentration of ·OH produced by the decomposition of high concentration of H_2O_2 will also oxidize Fe^{2+} to Fe^{3+}, thereby reducing the utilization of ·OH and reducing the COD removal rate. It can be seen from Figure 1 that the transmittance of wastewater increases with the increase of H_2O_2 dosage. The flocculation and settlement phenomena are shown in Table 2.

Effect of Oxidation Time on the Reaction

The oxidation time was optimized. The effects of oxidation time on COD removal rate and transmittance rate was

Table 2: H_2O_2 optimization amount.

H_2O_2 addition/%	Flocculation and sedimentation
0.1	The floc was loose and less in quantity, and the supernatant was turbid.
0.2	The floc was loose and less in quantity, and the supernatant was turbid.
0.3	The floc volume is large and dense, and the supernatant is clear
0.4	The floc volume was large and dense, and the supernatant was clear and had air floatation.
0.5	The floc volume was large and dense, and the supernatant was clear and had air floatation.

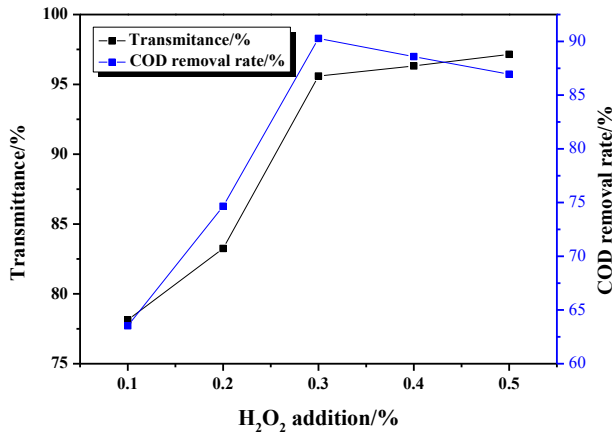

Fig. 1: H_2O_2 optimization amount.

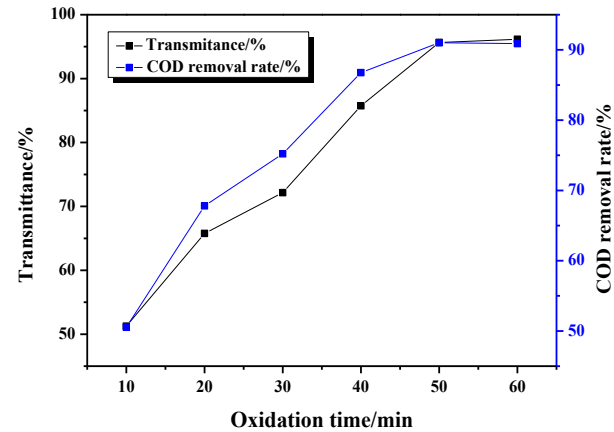

Fig. 2: Optimization of oxidation time.

investigated. the experimental results of optimization of oxidation time are shown in Tables 3 and Fig. 2.

It can be seen from Fig. 2 that with the extension of time, the COD removal rate of wastewater increases gradually. The COD removal rate reached the highest in 50 min. With the extension of time, the COD removal rate tends to be stable, and the transmittance of wastewater increases with the increase of H_2O_2 dosage. H_2O_2 produced an increase in ·OH in the Fe^{2+} catalyzed waste liquid (Oetjen & Thomas 2016). In the waste liquid, organic macromolecular chain structures play an important role in oxidative damage, which destroys the stability of the waste liquor colloid system (Gordalla et al. 2013), and in turn, flocculation settlement is reinforced. Therefore, from the oxidation-flocculation effect, it can be concluded that the addition of H_2O_2 in the catalytic oxidation-flocculation experiment of the waste aciding fluid is optimal at 0.3% and when the oxidation time is 50 min. The flocculation and settlement phenomena are shown in Table 3.

Analysis of Flocculation and Precipitation Process

Waste aciding fluid will produce a strong corroding and alkaline environment required by the flocculant. At the same time, the Fe^{2+} remaining in the waste liquid after catalytic oxidation treatment will be converted into Fe^{3+}. In an alkaline environment, a Fe $(.OH)_3$ precipitate will be formed, which has strong adsorption, coagulation, and flocculation characteristics (Costa et al. 2017, Kreipl & Kreipl 2017, Wisen et al. 2019). Therefore, neutralization of the alkaline environment first occurs during flocculation precipitation, followed by flocculation precipitation treatment. According to the method described in section 1.4, after catalytic oxidation the waste liquid was flocculated and precipitated. It investigated the effect of different coagulants and their dosage and the wastewater pH on coagulation precipitation.

The Effects of the Wastewater pH on Coagulation

The effects of pH on COD removal rate and transmittance rate were investigated. The experimental results of pH optimization in flocculation and precipitation are shown in Fig. 3.

Table 3: Optimization of oxidation time.

Oxidation time/min	Flocculation and sedimentation
10	Loose flocs, less amount, slow settlement
20	Loose flocs, less amount, slow settlement
30	Loose flocs, less amount, slow settlement
40	Loose flocs, less amount, slow settlement
50	The floc is compact, large in quantity and quick in settling
60	The floc is compact, large in quantity and quick in settling

It can be seen from Fig. 3 that the COD removal rate of wastewater increases with the increase of pH. With the increase of pH, COD removal rate tends to be stable. At the same time, with the increase of pH, the transmittance of wastewater increases gradually, and tends to be stable with the increase of pH. However, considering the reagent cost and reason of sludge discharge, and alkalinity neutralization at the optimal pH of 7.5, the transmittance can reach more than 95% after processing wastewater.

The Effects of Different Flocculants and Their Dosage on Coagulation

The effects of different flocculants and their dosage on COD removal rate and transmittance rate were investigated.

The experimental results of optimization of flocculant types are shown in Table 4.

It can be seen from Table 4 that the light transmittance can reach 90% when PAC flocculant is used, but it is lower when PFC flocculant is used. Therefore, PAC was used as the best flocculant.

The experimental results of optimization of flocculant PAC addition are shown in Fig. 4.

From Fig. 4 it can be infrerred that the COD removal rate increases with the increase of PAC dosage, when PAC dosage is 350 mg/L, the COD removal efficiency reaches at its best,

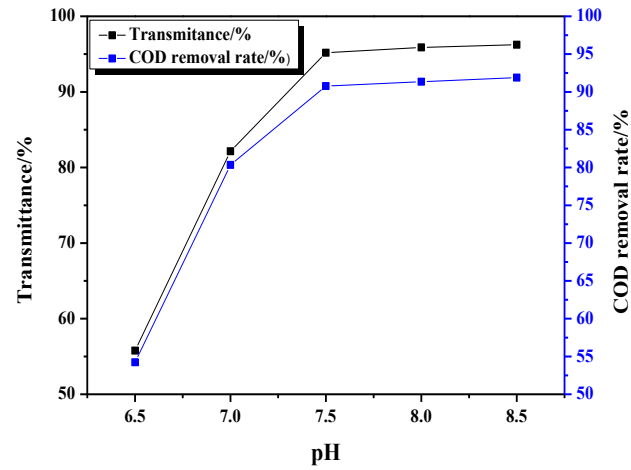

Fig. 3: pH optimization in flocculation and precipitation.

Table 4: Optimization of flocculant types.

Types of flocculants	PAC	PFS
Transmittance (%)	97.3	45.6

and the COD removal rate is 91.95%. When PAC dosage continued to increase, the COD removal rate decreased slightly. From Fig. 4 it can be inferred that the transmittance of wastewater increases with the increase of PAC dosage.

The Effects of Different Coagulants and Their Dosage on Coagulation

The experimental results of preferred coagulant types are given in Table 5, which show that when a coagulant has an ion degree of 12% and a molecular weight of 8×10^6 and the Types of PAM is $7^{\#}$, the water transmittance after treatment can reach more than 98.8%.

The experimental results of Optimization of coagulant $7^{\#}$ addition are shown in Fig. 5. The COD removal rate increases with the increase of the PAC dosage. When the dosage of PAC is 3mg/L, the COD removal effect reaches at its best, and the COD removal rate is 91.84%; when the dosage of PAC continues to increase, the COD removal rate decreases slightly. Fig. 5 shows that the transmittance of wastewater increases with the increase of coagulant $7^{\#}$ dosage,and the coagulant $7^{\#}$ is dosed at 4 mg/L, the water transmittance after treatment can reach more than 99%.

As shown by Fig. 3, as the pH increased, and flocculation improved. With an increase in alkalinity, ferric iron ion and hydroxyl ions form iron hydroxide precipitation, resulting in a flocculation precipitation strengthening effect (Ge et al. 2015). However, considering the reagent cost and reason of sludge discharge, and alkalinity neutralization at the optimal pH of 7.5, the light transmittance can reach more than 95% after processing wastewater. The flocculation and precipitation conditions were optimized successively. As can be seen from Table 4 and Fig. 4, PAC was selected as the inorganic flocculant, and the effect was improved when the PAC dosage was 350 mg/L. It is shown in Table 5 and Fig. 5 that when a coagulant has an ion degree of 12%, and a molecular weight of 8×10^6, and the PAM is dosed at 4 mg/L, the water transmittance after treatment can reach more than 99%.

The most effective catalytic oxidation and flocculation precipitation process for treating shale gas fracturing and acidizing liquid wastewater is indicated by the water quality indicators shown in Table 6. Results are as follows: pH increased to 7.5, Fe^{2+} was reduced to 0.10 mg/L, COD was reduced to 275.18 mg/L, chromaticity was reduced to 125°, and the average corrosion rate decreased to 0.0217 mm/a.

CATALYTIC OXIDATION WITH FLOCCULATION AND PRECIPITATION TREATMENT PROCESS

Based on the experiment results, the process of catalytic oxidation with flocculation and precipitation was proposed to treat waste liquid. The process flow is shown in Fig. 6.

Table 5: Preferred coagulant types.

Types of PAM	1	2	3	4	5	6	7	8
Ion/%	20	30	40	50	60	Non-ionic	12	Anion
Molecular weight/ (ten thousand)	800	800	1200	800	800		800	
Transmittance/%	96.0	95.6	95.0	97.0	98.8	98.3	98.8	97.6

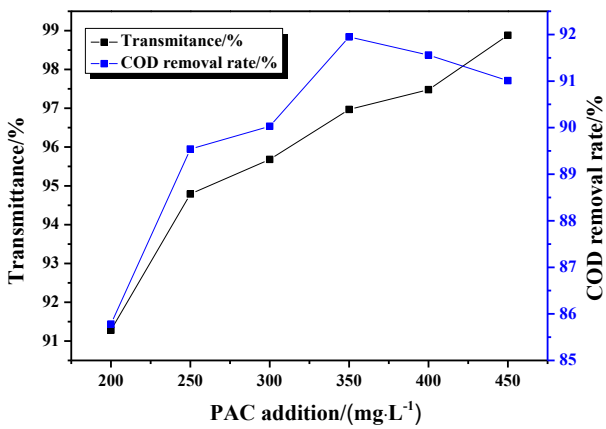

Fig. 4: Optimization of flocculant PAC addition.

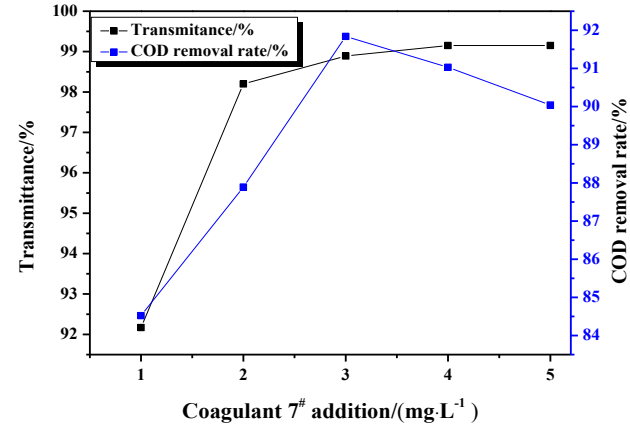

Fig. 5: Optimization of coagulant $7^{\#}$ addition.

Table 6: Water quality analysis after treatment.

S. No.	Test items	Content
1	pH	3.5
2	Fe^{2+} ($mg \cdot L^{-1}$)	0.10
3	Fe^{3+} ($mg \cdot L^{-1}$)	0.02
4	Oil ($mg \cdot L^{-1}$)	2.98
5	Suspended solids ($mg \cdot L^{-1}$)	8
6	Chromaticity (°)	125
7	Viscosity (mPa·s)	0.97
8	Light transmittance (%)	99.15
9	COD ($mg \cdot L^{-1}$)	275.18
10	Mean corrosion rate (mm/a)	0.0217

The treatment process can be divided into three stages. The first stage is catalytic oxidation, which mainly includes Fenton's reagent condition optimization (pH, catalyst, oxidant) and oxidation time optimization. The second stage is flocculation precipitation, including alkali neutralization, flocculant optimization and, coagulant optimization. The third stage is feasibility analysis and treatment of water reuse mixture, including a feasibility analysis of a water reuse mixture after treatment and removal of related heavy metal ions.

CONCLUSION

(1) Acidified fracturing waste liquid is characterized by low pH, high chromaticity, high iron content, high COD, and low light transmittance. Catalytic oxidation with flocculation and precipitation is the process selected for treatment.

(2) The water transmission rate increased from 25.82% to 99.15% and the average corrosion rate decreased from 0.1226 mm/a to 0.0217 mm/a after catalytic oxidation with flocculation and precipitation treatment. The dosage of H_2O_2 was 0.3% in the catalytic oxidation process, and pH was 7.5 during flocculation and precipitation. The PAC concentration dosage was 350 mg/L, and the dosage of PAM with ion degree of 12% and molecular weight of 8×10^6 was 4 mg/L.

ACKNOWLEDGMENTS

This work was supported by the Open Project Program of State Key Laboratory of Petroleum Pollution Control, and Shaanxi Youth Science and technology new star project (2017KJXX-49); and Scientific Research Program Funded by Shaanxi Provincial Education Department (Program No.18JS088), and Natural Science Basic Research Plan in Shaanxi Province of China (Program 2019JM-506).

REFERENCES

Adham, S., Hussain, A., Minier-Matar, J., Janson, A. and Sharma, R. 2018. Membrane applications and opportunities for water management in the oil & gas industry. Desalination, 2-17.

Amr, S. S. A., Aziz, H. A. and Adlan, M. N. 2013. Optimization of stabilized leachate treatment using ozone/persulfate in the advanced oxidation process. Waste Management, 33(6): 1434-1441.

Arslan, I. and Balciolu, I. A. 1999. Degradation of commercial reactive dyestuffs by heterogenous and homogenous advanced oxidation processes: a comparative study. Dyes & Pigments, 43(2): 95-108.

Barati, R. and Liang, J. T. 2014. A review of fracturing fluid systems used for hydraulic fracturing of oil and gas wells. J. Appl.Polym. Sci., 131(16): 318-323.

Boczkaj, G., Kamiński, Marian and Przyjazny, A. 2010. Process control and investigation of oxidation kinetics of postoxidative effluents using gas chromatography with pulsed flame photometric detection (gc-pfpd). Ind. Eng. Chem. Res., 49(24): 12654-12662.

Bello, M. M. and Raman, A. A. A. 2017. Trend and current practices of palm oil mill effluent polishing: application of advanced oxidation processes and their future perspectives. J. Environ. Manag., 198(pt.1): 170-182.

Boczkaj, G. and Fernandes, André. 2017. Wastewater treatment by means of

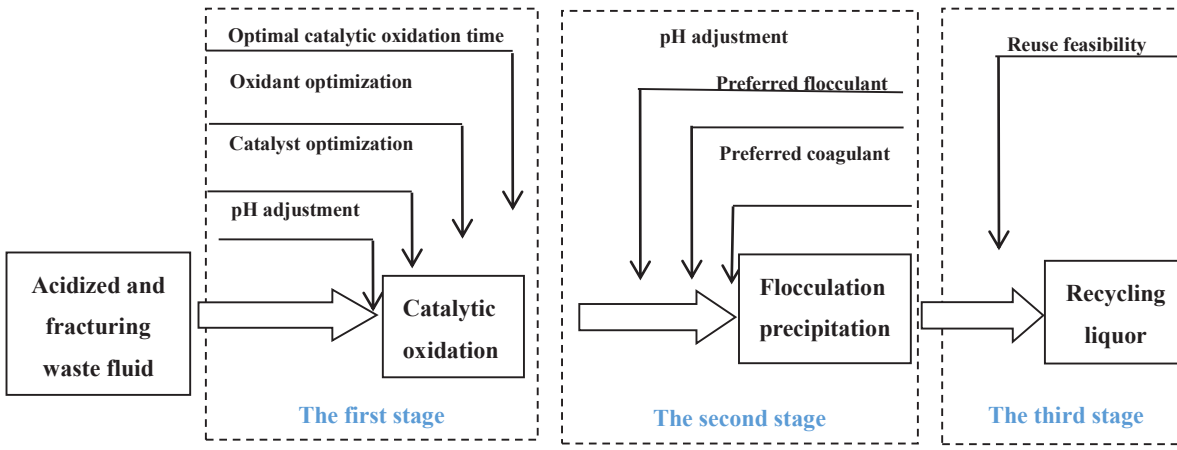

Fig. 6: Catalytic oxidation with flocculation precipitation treatment process.

advanced oxidation processes at basic ph conditions: a review. Chem. Eng. J., 320: 608-633.

Costa, D., Jesus, J., Branco, D., Danko, A. and Fiúza, António. 2017. Extensive review of shale gas environmental impacts from scientific literature (2010-2015). Environ. Sci. & Pollut. Res., 24(17): 1-16.

Davarpanah A. 2018. Feasible analysis of reusing flowback produced water in the operational performances of oil reservoirs. Environ.Sci.Pollut. Res. Int., 25(35):35387-35395.

Dutta, K., Mukhopadhyay, S., Bhattacharjee, S. and Chaudhuri, B. 2001. Chemical oxidation of methylene blue using a fenton-like reaction. J. Hazard. Mater., 84(1): 57-71.

Ferrer, I. and Thurman, E.M. 2015. Analysis of hydraulic fracturing additives by lc/q-tof-ms. Anal. Bioanal. Chem., 407(21): 6417-6428.

Glaze, W. H. and Kang, J. W. 1989. Advanced oxidation processes. description of a kinetic model for the oxidation of hazardous materials in aqueous media with ozone and hydrogen peroxide in a semibatch reactor. Ind. Eng. Chem. Res., 28(11):1573–80

Gordalla, B. C., Ewers, U. and Frimmel, F. H. 2013. Hydraulic fracturing: a toxicological threat for groundwater and drinking-water? Environ. earth Sci., 70(8): 3875-3893.

Ge, H., Yang, L., Shen, Y., Ren, K., Meng, F., Ji, W. and Wu, S. 2015. Experimental investigation of shale imbibition capacity and the factors influencing loss of hydraulic fracturing fluids. Pet. Sci., 12(4): 636-650.

Kim, T. H., Park, C., Yang, J. and Kim, S. 2004. Comparison of disperse and reactive dye removals by chemical coagulation and fenton oxidation. J. Hazard. Mater., 112(1-2): 95-103.

Kreipl, M. P. and Kreipl, A. T. 2017. Hydraulic fracturing fluids and their environmental impact: then, today, and tomorrow. Environ. Earth Sci., 76(4): 160.

Lester, Y., Yacob, T., Morrissey, I. and Linden, K. G. 2013. Can we treat hydraulic fracturing flowback with a conventional biological process? the case of guar gum. Environ. technol. lett., 1(1): 133-136.

Li, L., Yang, Z., Yu, Z., Hong, T. and Tian, Y. 2018. Study on the Oxidation Process of As (III) in Acidic Wastewater Containing Arsenic by Electrolysis and Ultrasonic Coupling. Nature Environ. Pollut. Technol., 17(4): 1419-1424.

Mauter, M. S., Alvarez, P. J. J., Burton, A., Cafaro, D. C., Chen, W. and Gregory, K. B. et al. 2014. Regional variation in water-related impacts of shale gas development and implications for emerging international plays. Environ. Sci. Technol., 48(15): 8298-306.

Makhathini, T. P., Mulopo, J. and Bakare, B. F. 2020. Possibilities for acid mine drainage co-treatment with other waste streams: a review. Mine Water Environ., 39(1): 1-14.

Mao J, Zhang C, Yang X, Zhang Z. 2018. Investigation on problems of wastewater from hydraulic fracturing and their solutions. Water, Air, & Soil Pollut.

Olsson, O., Weichgrebe, D. and Rosenwinkel, K. H. 2013. Hydraulic fracturing wastewater in germany: composition, treatment, concerns. Environ. Earth Sci., 70(8): 3895-3906.

Oetjen, K. and Thomas, L. 2016. Volatile and semi-volatile organic compound patterns in flowback waters from fracturing sites within the marcellus shale. Environ. Earth Sci., 75(12): 1043.

Oetjen, K. and Thomas, L. 2016. Volatile and semi-volatile organic compound patterns in flowback waters from fracturing sites within the marcellus shale. Environ. Earth Sci., 75(12): 1043.

Puspita, P., Roddick, F. and Porter, N. 2015. Efficiency of sequential ozone and uv-based treatments for the treatment of secondary effluent. Chem. Eng. J., 268: 337-347.

Poyatos, J. M., Munio, M. M., Almecija, M. C., Torres, J. C., Hontoria, E. and Osorio, F. 2010. Advanced oxidation processes for wastewater treatment: state of the art. Water Air Soil Pollut, 205(1-4), 187-204.

Pier, R., Gaspar-Vargas, B., Romero, A. and Nilsson, M. 2018. Comparative study using ion exchange resins to separate and reduce norm from oil and gas flowback wastewater. J. Radioanal. Nucl. Chem., 318(1): 497-503.

Reilly, D., Singer, D., Jefferson, A. and Eckstein, Y. 2015. Identification of local groundwater pollution in northeastern pennsylvania: marcellus flowback or not?. Environ. Earth Sci., 73(12): 8097-8109.

Solozhenko, E. G., Soboleva, N. M. and Goncharuk, V. V. 1995. Decolourization of azodye solutions by fenton's oxidation. Water Res., 29(9): 2206-2210.

Szpyrkowicz, L., Juzzolino, C. and Kaul, S. N. 2001. A comparative study on oxidation of disperse dyes by electrochemical process, ozone, hypochlorite and fenton reagent. Water Res., 35(9): 2129-2136.

Tang, Y., Ren, H., Yang, P., Li, H., Zhang, J. and Qu, C. et al. 2018. Treatment of fracturing fluid waste by fenton reaction using transition metal complexes catalyzes oxidation of hydroxypropyl guar gum at high ph. Environ. Chem. Lett., 17(1):559–64.

Watts, R. J., Sarasa, J., Loge, F. J. and Teel, A. L. 2005. Oxidative and reductive pathways in manganese-catalyzed fenton's reactions. J. Environ. Eng., 131(1): 158-164.

Wisen, J., Chesnaux, R., Wendling, G. and Werring, J. 2019. Water footprint of hydraulic fracturing in Northeastern British Columbia, Canada. Environ. Earth Sci., 78(24): 1-13.

You, L., Zhou, Y., Kang, Y., Yang, B., Cui, Z. and Cheng, Q. 2019. Fracturing fluid retention in shale gas reservoirs:mechanisms and functions. Arab. J. Geosci., 12(24): 1-17.

Yoon, J., Lee, Y. and Kim, S. 2001. Investigation of the reaction pathway of oh radicals produced by fenton oxidation in the conditions of wastewater treatment. Water Sci.Technol., 44(5), 15-21.

Zhang, B., Li, B., Zhang, D. and Li, J. 2020. Experimental research on permeability variation from the process of hydraulic fracturing of high-rank coal. Environ. Earth Sci., 79(1).

Nature Environment and Pollution Technology
An International Quarterly Scientific Journal

p-ISSN: 0972-6268
(Print copies up to 2016)
e-ISSN: 2395-3454

Vol. 20 | No.3 | pp. 1173-1183 | 2021

Original Research Paper

https://doi.org/10.46488/NEPT.2021.v20i03.025

Open Access Journal

Removal of Various Contaminants by Highly Porous Activated Carbon Sorbent Derived from Agricultural Waste Produced in Malaysia - A Review

N.Z. Zabi, W.N. Wan Ibrahim†, N.S. Mohammad Hanapi and N. Mat Hadzir
Faculty of Applied Sciences, Universiti Teknologi MARA, 40450 Shah Alam, Selangor, Malaysia
Corresponding author: W.N. Wan Ibrahim; wannazihah@uitm.edu.my

Nat. Env. & Poll. Tech.
Website: www.neptjournal.com

Received: 28-05-2020
Revised: 29-07-2020
Accepted: 16-09-2020

Key Words:
Activated carbon
Adsorption
Agricultural waste
Environmental pollutants

ABSTRACT

This paper aims to review recent studies in preparing activated carbons from different types of agricultural wastes in Malaysia and how it can help Malaysia manage agricultural waste. It can be seen that most biomasses can be used as precursors to produce activated carbon for a wide range of pollutants and this adsorbent can be modified to optimally function depending on the types of pollutants. Under optimum dosages, modification through chemical activation using acidic, basic, or drying agents has significant effects on the selectivity of the analyte adsorption. The acidic activating agent causes the activated carbon to have negatively charged acid groups which enable it to adsorb cationic adsorbate while the basic activating agent causes the adsorbent to have a positive surface charge and enable it to adsorb anionic adsorbate.

INTRODUCTION

In Malaysia, the agricultural sector contributes 7.3% to the Gross Domestic Product (GDP). In 2018, oil palm (37.9%) was the major contributor to the GDP of the agricultural sector followed by other agricultural products (25.1%) such as paddy, cocoa beans, pepper, kenaf (dried stem), and rubber which contributed 2.8% per year (Department of Statistics Malaysia 2019). Since oil palm is the major contributor, 77% of total residues are from the oil palm industry, 9.1% of rice residues, 8.2% of forestry residues and 5.7% of other residues like rubber, cocoa, and coconut (Griffin et al. 2014).

The waste management expenditure increased from RM 755.5 million to RM 789.0 million from the year 2015 to 2017 and constantly has become a challenge to manage the wastes (Department of Statistics Malaysia 2019). In the agricultural sector, the simplest way to dispose of the wastes is through burning but it causes serious air pollution (Teimouri et al. 2019). However, agricultural wastes are renewable sources that can be converted into energy, bio-based products, and value-added products (Marsin et al. 2018). Thus, there are many studies and reviews on how these biomasses can be useful resources instead of disposing them (Sulaiman et al. 2011, Saba et al. 2015, Aditiya et al. 2016). Some studies used agricultural wastes as potential biosorbent such as activated carbon (Teimouri et al. 2019).

Originally, coal was the best source of activated carbon but it is limited and non-renewable. Therefore, agricultural waste was used as an alternative source to produce activated carbon since it is renewable and low-cost (Danish & Ahmad 2018). Activated carbons produced from biomasses are cheaper compared to commercialized activated carbon and can improve the economy by re-using these biomasses. Other than that, activated carbon obtained from biomasses may have a higher surface area compared to commercialized activated carbon. (Maneerung et al. 2016). Most agricultural wastes are lignocellulosic material and these types of materials are suitable to produce activated carbon (Nabais et al. 2013). Lignocellulosic material is a plant-based material, which is made of cellulose, hemicellulose, and lignin (Jiang et al. 2020). There are three major categories of this type of material which are wood-based like oak, energy crop like bamboo, and agricultural waste like palm and rubber trees (Ufodike et al. 2020). This paper reviews activated carbon produced from agricultural wastes that can be found in Malaysia and potentially act as an adsorbent to remove environmental pollutants from aqueous solutions.

Activated Carbon from Agricultural Wastes

Activated carbon can be produced through two types of activation process namely physical and chemical activation. The chemical properties (ash content and surface properties) and physical properties (surface area and pore size) depend on the types of the activation process. Chemical activation use dehydrating agents to impregnate the precursor material. The agent can either be acidic or basic depending on the analytes.

Li et al. (2008) stated that physical activation involves two steps which are carbonization step (400°C - 850°C) and activation step (600°C - 900°C).

Cheah et al. (2013) stated that chemical activation has more advantages as it produces activated carbon with a higher BET surface area compared to physical activation. Comparison of two different studies that used the same precursor (oil palm shell), showed that activated carbon from physical activation obtained a lower BET surface area approximately 151 $m^2.g^{-1}$ (Abioye & Ani 2015) whereas a study that employed chemical activation obtained surface area of 1254 $m^2.g^{-1}$ surface (Hoseinzadeh Hesas et al. 2013). Besides, chemical activation produces a higher yield of activated carbon, has less activation time, and provides suitable functional groups (Danish & Ahmad 2018).

Chemical activating agents such as phosphoric acid and zinc chloride are always used to activate lignocellulosic material because these agents would immediately react with lignocellulose when mixed together (Yakout & Sharaf El-Deen 2012). Zinc chloride can produce activated carbon in small and uniform-sized micropores (Hoseinzadeh Hesas et al. 2013) but phosphoric acid is more preferred because it produces both mesopores and micropores and safer compared to zinc chloride (Yacob et al. 2013). Gueye et al. (2014) reported that phosphoric acid depolymerized cellulose, hemicellulose, and lignin, which causes the formation of cross-linking through dehydration, cyclization, and condensation reaction. In addition, phosphoric acid also stimulates the formation of phosphate and polyphosphate bridges, which connects and cross-links the fragments obtained from macromolecules. Hui and Zaini (2015) stated that potassium hydroxide is also used to activate lignocellulosic material since it can produce well-developed pores and high specific surface areas. Unfortunately the activated carbon yield is frequently low. This is supported by the study of Foo and Hameed (2011) who managed to produce activated carbon with total surface area, total pore volume, and average pore size of 807.54 $m^2.g^{-1}$, 0.45 $cm^3.g^{-1}$, and 2.193 nm respectively.

Besides that, activated carbon can have different types of pores based on their pore sizes. Xue et al. (2019) stated that pore size can be characterized as ultramicropore (< 0.7 nm), supermicropore (0.7 nm-2.0 nm), small mesopore (2.0 nm-2.5 nm) and large mesopore (2.5 nm -50 nm). The types of pores depend on activating agents used and also activation temperature. Heidari et al. (2014) showed that a high percentage of micropore can be obtained using potassium hydroxide and zinc chloride. For phosphoric acid, mesopores can be formed due to the presence of phosphate linkage that expands the biomass structure.

Chen et al. (2017) used phosphoric acid activation to produce activated carbon with high BET surface area and large pore volume. The hydrochar described here can be obtained from hydrothermal carbonization of corn cob residue (CCR). The porous structure of activated carbons was characterized by nitrogen adsorption and scanning electron microscopy (SEM). Results showed that the specific surface area and total pore volume of activated carbon were increased to 2192 $m^2.g^{-1}$ and 1.269 $cm^3.g^{-1}$, respectively, under conditions of 400°C, 1 h, and an impregnation ratio of 3, from 5.69 $m^2.g^{-1}$ and 0.136 $cm^3.g^{-1}$ of the starting material. The chemical properties of hydrochar and activated carbons were further characterized by Fourier transform infrared spectroscopy (FT-IR), which confirmed the chemical transformation. Furthermore, the localized graphitic nature of the porous carbon was shown by the X-ray diffraction pattern. Thus, the adsorption capacity was enhanced for activated carbon in comparison with commercial carbon. The process of activated carbon preparation provided a high value-added application of hydrochar.

In recent years, many researchers developed activated carbon from different types of biomass for various application such as adsorption (Kaveeshwar et al. 2018), catalyst supports (Mateo et al. 2020), medicine (Lakshmi et al. 2018), electrode materials (Tripathi et al. 2020), air filters (Gallego et al. 2013) and gas storage (Biloé et al. 2002). This is because activated carbon can be produced in large quantities (Mateo et al. 2020). Synthesis of activated carbon from biomass can reduce environmental pollution and the cost of disposal (Muniandy et al. 2014). Although activated carbons from biomasses are used in many industrial applications, the biggest challenge in producing activated carbon is the cost of production, uncertain methods, and also regeneration process (Danish & Ahmad 2018). Table 1 and Table 2 shows properties of activated carbon from agricultural wastes produced through chemical activation and physical activation respectively.

Activated Carbon as Adsorbent

In the adsorption process, adsorbent primarily depends on the surface chemistry and pore structure of the material. Method of activation and nature of precursor tremendously affect the surface functional groups and pore structure. The surface functional groups provide vital information involving removal of cationic and anionic adsorbate (Marsin et al. 2018). For example, when activated carbon is treated with acid, the activated carbon will have negatively charged acid groups and able to adsorb cationic adsorbate and vice versa (Bhatnagar et al. 2013).

Removal of Dyes using Activated Carbon

Dye is a molecule that contains chromophore and auxochrome. The chromophore group causes the dye to have

Table 1: Properties of activated carbons produced through chemical activation.

Material	Agent	S_{BET} ($m^2.g^{-1}$)	Reference
Coconut spathe	KOH	1705	Prashanthakumar et al. (2018)
Rice husk	NaOH	2786	Zhang et al. (2020)
Coconut shell	KOH	265	Purnomo et al. (2018)
Oil palm kernel shell	H_3PO_4	630	Yacob et al. (2013)
Cocoa shell	H_3PO_4	1077	Pereira et al. (2014)
Oil palm empty fruit bunch	KOH	807.54	Foo and Hameed (2011)
Rubber seed shell	KOH	620	Pagketanang et al. (2015)
Oil palm shell	$ZnCl_2$	1254	Hoseinzadeh Hesas et al. (2013)
Kenaf stem	H_3PO_4	1154	Meryemoglu et al. (2016)

Table 2: Properties of activated carbons produced through physical activation.

Materials	Agent	S_{BET} ($m^2.g^{-1}$)	Reference
Oil palm empty fruit bunch	Steam	718	Kadir et al. (2014)
Rice straw	Steam	243	Yang et al. (2020)
Cocoa shell	CO_2	558.25	Ahmad et al. (2013)
Oil palm shell	CO_2	151	Abioye and Ani. (2015)
Coconut shell	CO_2/Steam	610	Chandana et al. (2019)
Rubberwood sawdust	CO_2	465	Mazlan et al. (2016)
Coconut husk	Steam/O_2	415.85	Fu et al. (2020)
Oil palm shell	CO_2	905	Herawan et al. (2013)
Waste tea	Steam	995	Zhou et al. (2018)

its own color since it has a double bond that oscillates to adsorb light (Liang et al. 2014). Dyes are commonly used in foods, clothes, and also medicines which has increased the production rate of dyes. Many different types of dyes have been produced such as acidic, basic, disperse, azo, anthraquinone based and metal complex dyes (Ratna & Padhi 2012).

Dyes can have health effects due to their toxicity and non-biodegradable characteristics (Kalkan et al. 2013). Examples of health problems are cancer, allergic respiratory problem, and skin and mucous membrane irritation (Kausar et al. 2018). Besides health effects, dyes also cause environmental pollution as it affects the symbiotic process in water as it prevents light penetration and causes the photosynthetic activity to decrease (Nidheesh et al. 2018).

It is difficult to remove dyes using ordinary water treatments due to its complex chemical structure and poor biodegradability (Khorasani & Shojaosadati 2019). Therefore, a lot of studies have been conducted to find the best methods to remove dyes such as flocculation or coagulation (Sharma et al. 2011), electrochemical destruction (Narayana & Kariyajjanavar 2019), ozonation (Sekar 2008), and ion exchange (Yang et al. 2019). However, adsorption is preferable since it is more efficient and easier to conduct (Rai et al. 2015). There are various adsorbents that have been introduced such as disposable paper cups (Shukla et al. 2020), chitosan/polyamide nanofibers (Dotto et al. 2017), and amino grafted MCM-41 (Rizzi et al. 2019) but activated carbon is still the most used adsorbent because of its remarkable characteristics (Maneerung et al. 2016). Table 3 summarizes activated carbon from different agricultural wastes for the removal of dyes.

Macedo et al. (2006) prepared mesoporous activated carbon from coconut coir dust to remove methylene blue (cationic) and remazol yellow (anionic) dyes. Zinc chloride was used as an activating agent with a ratio of 3 $ZnCl_2$:1 coir dust. This adsorbent contained both acidic and basic sites which enabled it to adsorb both basic and acidic dyes simultaneously. The study revealed that the interaction forces between the adsorbent and dyes are related to the pH solution which affects the charge distribution on the adsorbent surface. The optimum pH to adsorb methylene blue was pH 8 while remazol yellow was pH 4. In addition, the activated carbon had a short equilibrium time (approximately 120 min) to adsorb both dyes.

Sellaoui et al. (2017) used cocoa shells as a source of activated carbon to adsorb reactive violet 5 dye. The adsorption process is described as multilayer adsorption and it is thermally activated where the number of dye molecules per site increases when the temperature increases. From this study, the number of dye molecules per site on cocoa shell activated carbon is higher compared to commercialized activated carbon due to the interaction between functional groups in cocoa shell activated carbon and dye.

Guo et al. (2020) modified the activated carbon produced from peanut shell with $FeCl_3$ and $MgCl_2$ as a bimetallic activating agent to remove malachite green. Prepared adsorbent obtained a total surface area of 633.35 $m^2.g^{-1}$ with a high maximum adsorption capacity of 4031.96 $mg.g^{-1}$. The high adsorption rate is due to the increment of the area of the adsorbent rather than the change of contact areas between the adsorbent and the dye. The adsorption rate was narrowed to the intra-particle diffusion rate of dye molecules compared to the availability of active sites. Interactions between MG dye and Fe-Mg15 including the H-bonding, π-π stacking, and the electrostatic attraction triggered considerable adsorption performance. The dominant interaction was the H-bonding between Mg-OH and N-containing groups in MG. The chemical regeneration method could not have achieved an effective removal of adsorbed malachite green, whereas the adsorptive properties of Fe-Mg BACs could be well regenerated via the thermal regeneration method. The adsorption for this study fits the Freundlich isotherm model.

Mahamad et al. (2015) used activated carbon produced from pineapple biomass to remove methylene blue from an aqueous solution. The total surface area of the adsorbent was 914.67 $m^2.g^{-1}$ with a maximum adsorption capacity of 288.34 $mg.g^{-1}$. In this study, the mechanism involved in the removal of the dye was the migration of dye from the bulk of solution and diffusion of the dye through boundary layer to surface of the adsorbent and intra-particle diffusion of dye into interior pores of adsorbent. The boundary layer resistance was affected by the rate of adsorption.

Islam et al. (2017) produced mesoporous activated carbon using hydrochar prepared from coconut shell. The maximum adsorption capacity was 200.01 $mg.g^{-1}$ and the total surface area of the adsorbent was 876.14 $m^2.g^{-1}$. The adsorption in this study fitted the Langmuir isotherm and pseudo-second-order model. Results showed higher adsorption of dye when pH increased from 7 to 9, due to the high number of ^-OH groups which contributed a slightly negative charge on the surface and enhanced the adsorption of the dye.

Removal of Pesticides Using Activated Carbon

Pesticides are chemically prepared from different types of substances such as such as fungicides, rodenticides, weed killers, insecticides, and antimicrobials (Elhag et al. 2017). This organic material is used to kill targeted pests (Chawla et al. 2018). Pesticides can be divided into classes which are organophosphates, organochlorine, carbamates, chlorophenol, and synthetic pyrethroids pesticides (Hamza et al. 2016). Organophosphorus pesticides (OPs) are the most used pesticides in agriculture because it is more biodegradable and has shorter persistence compared to organochlorine pesticides (Chen et al. 2010). It protects the crops by inhibiting acetylcholinesterase enzyme activity in insects (Sapahin et al. 2014).

Nonetheless, continuous and excessive usage of pesticides inadequately can lead to many environmental and health problems (Blankson et al. 2016). As a matter of fact, improper use of any kind of pesticides can cause agricultural products to have residues of it (Chen et al. 2010). There are few major groups of pesticides that are carcinogenic to living organisms which are organophosphates, organochlorines, carbamates, and pyrethroids (George & Shukla 2011).

Table 3: Literature studies on different agricultural wastes for removal of dyes.

Materials	Activation method	Activation agent	Dyes	Removal uptake ($mg.g^{-1}$)	Reference
Oil palm empty fruit bunch	Chemical	KOH	Methylene blue (Cationic)	344.83	Foo and Hameed (2011)
Coconut coir dust	Chemical	$ZnCl_2$	Methylene blue	14.36	Macedo et al. (2006)
			Remazol yellow (Anionic)	n.a.	
Cocoa shell	Chemical	$ZnCl_2/FeCl_3$	Reactive violet 5	n.a.	Sellaoui et al. (2017)
Peanut shell	Chemical	$FeCl_3$ /$MgCl_2$	Malachite green (Cationic)	4031.96	Guo et al. (2020)
Pineapple waste	Chemical	$ZnCl_2$	Methylene blue	288.34	Mahamad et al. (2015)
Oil palm shell	Chemical	KOH	Methylene blue	243.90	Tan et al. (2008)
Coconut shell	Chemical	KOH	Methylene blue	200.01	Islam et al. (2017)

*n.a. – not available

Besides health problems, pesticides affect the ecosystems as well due to their persistent nature. (Marican & Durán-Lara 2017). Thus, monitoring residues of pesticides in soil, water, plants, and food is important.

There are three types of methods to remove pesticides which are biological, chemical, and physical processes (Mojiri et al. 2020) For biological processes, Nie et al. (2020) used microalgae to bioremediate water containing pesticides. Fiorenza et al. (2020) used a chemical process to remove pesticides from water by molecular imprinting on titanium dioxide photocatalyst. For physical processes, the most common technique is adsorption. Table 4 summarizes activated carbon from different agricultural wastes for the removal of pesticides.

Chang et al. (2014) used rice straw as a precursor to remove carbofuran from an aqueous solution. Based on this study, the adsorption of the pesticides was optimum at a lower pH and temperature. At a high temperature, the target molecules eluded from solid phase to bulk phase due to an increase in energy while at high pH value. Carbofuran tends to deprotonate due to the presence of OH^- ions and this causes weaker interaction between the neutral molecular form of carbofuran with the adsorbent. The adsorption process best fits the Langmuir model. The maximum carbofuran adsorption capacity was 296.52 $mg.g^{-1}$.

Salman et al. (2011) removed 2,4-dichlorophenoxyacetic acid from an aqueous solution. The activated carbon was produced from the oil palm frond. Based on the result, the adsorption of the pesticides depended on the availability of sites on the adsorbent compared to the concentration of the pesticides. The adsorption process best fits the Langmuir model. Ioannidou et al. (2010) used four agricultural residues as sources of activated carbon (olive kernel, corn cob, rapeseed stalks. and soya stalks). However, corn cob activated carbon had the highest adsorption capacity which is 18.9×10^{-2} $mg.g^{-1}$ since it contains more micropores and also spongy like cross-interconnected pores.

Abdelhameed et al. (2020) used orange peel and apricot kernel to produce activated carbon for the removal of prothiofos and its degradation compounds from an aqueous solution. Based on the result, the maximum adsorption capacities of the pesticide were 185.9 ± 1.8 $mg.g^{-1}$ and 145.8 ± 2.4 $mg.g^{-1}$ for orange peel and apricot kernel, respectively. The adsorption process best fits the Langmuir model. The adsorption of the pesticides occurs when prothiofos that contain P-O functional groups bind with free hydroxyl and carboxyl groups of the adsorbent through hydrogen bonds.

Removal of Polycyclic Aromatic Hydrocarbon using Activated Carbon

Polycyclic aromatic hydrocarbons (PAHs) are a group of compounds, which are composed of two or more fused aromatic rings (Cao et al. 2017). PAHs have different functional groups in the benzene rings or lateral chains which causes it to have different chemical properties (Tsibart & Gennadiev 2013). PAHs are usually emitted as a mixture and the relative molecular concentration ratios are usually treated as the characteristics of the emission source (Tobiszewski & Namieśnik 2012).

Every year, there are production and processing of plasticizers, dyes, and pigments that cause the release of PAHs. Besides that, PAHs can also enter the environment through incomplete combustion processes such as the processing of coal and crude oil during refining, coal gasification, and coking (Pérez-Gregorio et al. 2010). The prevalence of this compound is released into various water bodies which will cause serious health and environmental problems (Mojiri et al. 2019). PAHs are known for their genotoxic, mutagenic, and carcinogenic effects on humans (Idowu et al. 2019). Other than that, due to its persistent nature, toxicity and bioaccumulation this compound also affects the environment especially soil.

Thus, it is necessary to remove this compound from the environment. Chemical such as chemical precipitation and solvent liquid-liquid extraction (Ates & Argun 2018, Naik et al. 2017) and biological methods such as phytoremediation technology (Włóka et al. 2019) are used to remove PAHs,

Table 4: Literature studies on different agricultural wastes for removal of pesticides.

Materials	Activation method	Activation agent	Pesticides	Removal uptake/ percentage	Reference
Rice straw	Chemical	KOH	Carbofuran	296.52 $mg.g^{-1}$	Chang et al. (2014)
Oil palm frond	Chemical	KOH	2,4-dichlorophenoxyacetic acid	352.89 $mg.g^{-1}$	Salman et al. (2011)
Corn cobs	Physical	Steam	Bromopropylate	18.9×10^{-2} $mg.g^{-1}$	Ioannidou et al. (2010)
Orange peel	Physical	Hot air	Prothiofos	185.9 ± 1.8 $mg.g^{-1}$	Abdelhameed et al. (2020)
Coconut frond	Chemical	H_3PO_4	Carbofuran	80%	Njoku et al. (2014)
Oil palm shell	Chemical	NaOH	4-chloroguaiacol	454.45 $mg.g^{-1}$	Hamad et al. (2010)

however some of the techniques produce toxic by-products. Due to this occurrence, physical methods such as filtration (Ndiaye et al. 2005) and adsorption (Kumar et al. 2019) are commonly used. Compared to other physical methods, adsorption is the best method because of its safety, affordability, universal nature, and simple operation process (Akinpelu et al. 2019). Table 5 summarize activated carbon from agricultural waste for the removal of PAHs compounds.

Kumar et al. (2019) used palm shells as a source of activated carbon. The activated carbon was modified through pyrolysis to increase the adsorption of PAH compounds. The activated carbons have been induced with potassium hydroxide. Based on the result, the maximum adsorption capacity of acenaphthalene for pyrolysis-assisted activated carbon (131.7 $mg.g^{-1}$) was higher than normal activated carbon (96.54 $mg.g^{-1}$) because it had a higher surface area (430 $m^2.g^{-1}$) compared to normal activated carbon (286 $m^2.g^{-1}$). Both adsorption process fits the Freundlich model which shows heterogeneous adsorption.

Gupta and Gupta (2015) produced activated carbon from banana peel to remove naphthalene, fluorene, and phenanthrene from aqueous system. The adsorbent had good adsorption capacity and a large BET surface area (>900 $m^2.g^{-1}$). Since the adsorption process was endothermic (positive enthalpy change, $\Delta H°$), the adsorption of PAH compounds was better at a higher temperature. Besides that, a positive value of entropy change, $\Delta S°$ showed that the adsorption process was spontaneous and good affinity between PAHs and adsorbent because there was an increase in randomness at the interface (solid/liquid). Gupta (2015) used orange rind as a source of activated carbon. In this study, the adsorption of PAH compounds was preferable at lower pH because the adsorbent surface had a more positive charge due to the presence of H^+ ions and which has led to high interaction between the adsorbent surface and π-electron cloud of phenanthrene molecules.

Yakout et al. (2013) used rice husk to produce activated carbon. The activated carbon was used to adsorb naphthalene, phenanthrene, and pyrene. Based on the result, the adsorption of PAH compounds onto the adsorbent depended on the weight and solubility of the adsorbate. There was a higher removal rate of pyrene followed by phenanthrene and naphthalene.

Removal of Heavy Metal using Activated Carbon

Heavy metals are metals that have densities greater than 5 $g.cm^{-3}$ such as arsenic, cadmium, chromium, mercury, lead, copper, zinc, and nickel (Chen et al. 2015). Heavy metal pollution is one of the most serious environmental problems. Industries such as metal plating, mining operations, surface finishing industry, radiator manufacturing, alloy, and batteries industries usually release heavy metals in wastewater (Tounsadi et al. 2016). Other than that, nickel and zinc are persistent in nature and tend to accumulate in soils and plants which can be transferred to living organisms through the food chain (Alam et al. 2020). When humans or animals consume any of these heavy metals it can cause negative health effects like cancer, nausea, vomiting, mental retardation, liver, and kidney failure (Masjedi et al. 2020).

Therefore, the removal of heavy metals from the environment is important. There are three types of methods to remove heavy metal ions which are biological methods such as synergistic actions of microorganisms and waste molasses (Sun et al. 2020), a chemical method such as joint EDTA-acid treatment (Kou et al. 2020), and physical method such as adsorption using nanoparticles (Das & Rebecca 2018). Although nowadays, the removal of pollutants using activated carbon is considered an effective purification process since it can reduce trace amounts of heavy metal to reach environmental standards and regulations (Treviño-Cordero et al. 2013). Table 6 summarizes activated carbon from agricultural waste for the removal of heavy metals.

Table 5: Literature studies on different agricultural wastes for removal of PAHs compounds.

Materials	Activation method	Activation agent	PAHs	Removal uptake (mg.g-1)	Reference
Palm shell	Chemical	KOH	Acenaphthalene	131.7	Kumar et al. (2019)
Banana peel	Physical	n.a.	Naphthalene	333.33	Gupta and Gupta. (2015)
			Fluorene	285.71	
			Phenanthrene	217.39	
Orange rind	Chemical	H_3PO_4	Phenanthrene	70.92	Gupta (2015)
Rice husk	Chemical	H_3PO_4	Naphthalene	n.a.	Yakout et al. (2013)
			Phenanthrene	n.a.	
			Pyrene	n.a.	

*n.a. – not available

Chandana et al. (2019) produced activated carbon using coconut shells to remove Cr (VI) from industrial overflows. The activated carbon was produced through physical activation with three different types of activating agents. From the study, the best activating agent was a mixture of carbon dioxide and steam with a surface area of 610 $m^2.g^{-1}$. The adsorption of Cr (VI) depended on the pH of the solution and showed maximum adsorption capacity (~26 $mg.g^{-1}$) at pH 2.

Borhan et al. (2016) prepared activated carbon from rubber seed shells to remove copper (II) and zinc ions from an aqueous solution. Based on the result, the highest percentage removal of copper (II) ions and zinc ions were 99.6% and 94%, respectively at the optimum condition of 200 ppm of initial concentration, 400 rpm stirring rate, and 45 minutes of contact time. This study stated that increasing the stirring rate causes a higher rate of diffusion of metal ions. This is because there was an enhancement of turbulence and reduction in thickness of the liquid boundary layer.

Rahman et al.(2014) produced activated carbon from oil palm shells and coconut shells to remove nickel (II), lead (II), and chromium (IV) ions from aqueous solution. The activated carbon from the oil palm shells was activated in two different impregnation conditions where the oil palm shell powder was either wet or semi-dried with phosphoric acid before placing it in the furnace. A comparison between prepared and commercial activated carbon was also made in this study. Based on the result, prepared activated carbons had higher adsorption capacity for Ni (II) and Pb (II) ions while commercial activated carbon was able to adsorb more Cr (IV) ions although it had lower adsorption capacity in a low concentration range. The adsorption process for Ni (II) and Pb (II) ions best fits the Langmuir model. For the adsorption process of Cr (IV) ions, only two adsorbents were used which are activated carbon from oil palm shells (semi-dried) and commercial activated carbon and the process best fits both Langmuir and Freundlich model. This study stated that the prepared activated carbon is more suitable to be used in drinking water purification compared to commercial activated carbon since it has a stronger affinity towards all heavy metals even at low concentrations. The removal uptake of heavy metal ions for every adsorbent is shown in Table 6.

Chowdhury et al. (2012) used kenaf fiber as a starting material to produce activated carbon for the removal of copper (II) ions from wastewater. Based on the data, the adsorption process best fits the Langmuir model compared to Freundlich and this shows that it is a monolayer adsorption process. In addition, for kinetic study, the adsorption fits pseudo-second-order model where the rate-limiting step

Table 6: Literature studies on different agricultural wastes for removal of heavy metals.

Materials	Activating method	Activating agent	Heavy metals	Removal uptake/percentage	Reference
Coconut shell	Physical	CO_2 /steam	Cr^{6+}	~26 $mg.g^{-1}$	Chandana et al. (2019)
		CO_2		n.a.	
		O_3		n.a.	
Rubber seed shell	Chemical	KOH	Zn^{2+}	99.6%	Borhan et al. (2016)
			Cu^{2+}	94%	
Kenaf fibre	Chemical	KOH	Cu^{2+}	n.a.	Chowdhury et al. (2012)
Oil palm shell (wet)	Chemical	H_3PO_4	Ni^{2+}	10.83	Rahman et al. (2014)
			Pb^{2+}	74.63	
			Cr^{4+}	n.a.	
Oil palm shell (semi-dried)	Chemical	H_3PO_4	Ni^{2+}	19.61	Rahman et al. (2014)
			Pb^{2+}	63.69	
			Cr^{4+}	46.30	
Coconut shell	Chemical	H_3PO_4	Ni^{2+}	12.18	Rahman et al. (2014)
			Pb^{2+}	73.53	
			Cr^{4+}	n.a.	
Oil palm empty fruit bunch	Chemical	NaOH	Pb^{2+}	100%	Wahi et al. (2009)
			Hg^{2+}	100%	
			Cu^{2+}	25%	

*n.a. – not available

may be chemisorption which involves valency forces through sharing and exchange of electrons.

Wahi et al. (2009) prepared activated carbon from oil palm empty fruit bunch for removal of mercury, lead, and copper from aqueous solution. The EFB activated carbon showed excellent efficiency in removing Pb(II) and Hg(II) with a percentage of removal up to 100 % even at low adsorbent dosage. In contrast, only 25 % removal of Cu(II) by the EFB activated carbon was observed. The study also showed that the adsorption of Hg(II), Pb(II), and Cu(II) by EFB activated carbon is dependent on the dosage of adsorbent and initial metals concentration. The use of EFB as activated carbon is not only effective for Hg(II) and Pb(II) removal from wastewater but also helps in solving the problem of the over-abundance of EFB as an agricultural waste product. Based on the result, the adsorption of lead (II) and mercury (II) ions best fits the Freundlich model while the adsorption of copper (II) best fits the Langmuir model.

Future Prospect of Activated Carbon from Agricultural Waste

For the past years, most of the activated carbon produced from agricultural wastes is in powdered form. Recently, many studies have shifted their focus in producing activated carbon in fiber form and it is known as activated carbon fiber (ACF). This material is a combination of activated carbon and carbon fiber. Based on a review done by Hassan et al. (2020), there was an increasing number of publications (>300) about ACF from the year 2017 to 2019. The advantages of this material are higher adsorption rates, high accessible porosity, high surface area, improved contact efficiencies, adequate design flexibility, and easy regeneration. The four major precursors for the production of this material are polyacrylonitrile, phenolic resins, pitch resins, and bio-based materials mainly lignocellulosic. Therefore, for future studies, agricultural waste can be used as precursors to determine the best method to produce ACF as a highly potential adsorbent.

CONCLUSION

It is proven that agricultural biomasses can be used to produce activated carbon for the removal of different types of pollutants. This adsorbent is cheaper and sometimes even better than commercial activated carbon. By utilizing these wastes, it can reduce the expenditure for waste management and also improve the economy of this country. The biomass-based activated carbon can be a better adsorbent once surface modification through physiochemical methods is done. Different types of biomass require different activation treatments for optimum removal of targeted pollutants. For removal of dyes, chemical activation is preferable and adsorption efficiency can be increased by controlling the pH of the solution. For the removal of pesticides, the removal uptake using chemical activation is higher than physical activation since there are more pores formed and the presence of suitable active sites to adsorb the pesticides. For removal of PAHs compound, chemical activation using acid is preferable since the adsorption of PAHs is based on positive charge surface area and π-electron cloud. For the removal of heavy metals, using phosphoric acid as an activating agent has a high removal uptake of certain heavy metals. Besides that, choosing the right precursor is also important for the adsorption process because the precursor materials control the carbon pore structure.

ACKNOWLEDGEMENTS

The authors gratefully acknowledge Universiti Teknologi MARA for the facilitation and Ministry of Education Malaysia for their financial supports through vote number 600-IRMI/FRGS 5/3 (416/2019).

REFERENCES

Abdelhameed, R.M., Abdel-Gawad, H. and Hegazi, B. 2020. Effective adsorption of prothiofos (O-2,4-dichlorophenyl O-ethyl S-propyl phosphorodithioate) from water using activated agricultural waste microstructure. J. Environ. Chem. Eng., 8(3): 103768.

Abioye, A.M. and Ani, F.N. 2015. The characteristics of oil palm shell biochar and activated carbon produced via microwave heating. Retrieved April 13, 2020, from Applied Mechanics and Materials, website: http://www.scientific.net/AMM.695.12

Aditiya, H.B., Chong, W.T., Mahlia, T.M.I., Sebayang, A.H., Berawi, M.A. and Nur, H. 2016. Second-generation bioethanol potential from selected Malaysia's biodiversity biomasses: A review. Waste Manag., 47: 46-61.

Ahmad, F., Daud, W.M.A.W., Ahmad, M.A., Radzi, R. and Azmi, A.A. 2013. The effects of CO2 activation, on porosity and surface functional groups of cocoa (Theobroma cacao)-Shell-based activated carbon. J. Environ. Chem. Eng., 1(3): 378-388.

Akinpelu, A.A., Ali, M.E., Johan, M.R., Saidur, R., Qurban, M.A. and Saleh, T.A. 2019. Polycyclic aromatic hydrocarbons extraction and removal from wastewater by carbon nanotubes: A review of the current technologies, challenges, and prospects. Process Saf. Environ. Prot., 122: 68-82.

Alam, M., Hussain, Z., Khan, A., Khan, M. A., Rab, A., Asif, M., Shah, M. A. and Muhammad, A. 2020. The effects of organic amendments on heavy metals bioavailability in mine impacted soil and associated human health risk. Sci. Hort., 262: 109067.

Ates, H. and Argun, M.E. 2018. Removal of PAHs from leachate using a combination of chemical precipitation and Fenton and ozone oxidation. Water Sci. Technol., 78(5): 1064-1070.

Bhatnagar, A., Hogland, W., Marques, M. and Sillanpää, M. 2013. An overview of the modification methods of activated carbon for its water treatment applications. Chem. Eng. J., 219: 499-511.

Biloé, S., Goetz, V. and Guillot, A. 2002. Optimal design of activated carbon for an adsorbed natural gas storage system. Carbon, 40(8): 1295-1308.

Blankson, G.K., Osei-Fosu, P., Adeendze, E.A. and Ashie, D. 2016. Contamination levels of organophosphorus and synthetic pyrethroid

pesticides in vegetables marketed in Accra, Ghana. Food Cont., 68: 174-180.

Borhan, A., Abdullah, N.A., Rashidi, N.A. and Taha, M.F. 2016. Removal of Cu2+ and Zn2+ from single metal aqueous solution using rubber-seed shell-based activated carbon. Procedi. Engi., 148: 694-701.

Cao, H., Chao, S., Qiao, L., Jiang, Y., Zeng, X. and Fan, X. 2017. Urbanization-related changes in soil PAHs and potential health risks of emission sources in a township in Southern Jiangsu, China. Science of The Total Environment., 575: 692-700.

Chandana, L., Krushnamurty, K., Suryakala, D. and Subrahmanyam, C. 2019. Low-cost adsorbent derived from the coconut shell for the removal of hexavalent chromium from an aqueous medium. Mater. Today: Proceed., 26: 1-8

Chang, K.L., Chen, C.C., Lin, J.H., Hsien, J.F., Wang, Y., Zhao, F., Shih, Y.H., Xing, Z.J. and Chen, S.T. 2014. Rice straw-derived activated carbons for the removal of carbofuran from an aqueous solution. New Carb. Mater., 29(1): 47-54.

Chawla, P., Kaushik, R., Shiva Swaraj, V.J. and Kumar, N. 2018. Organophosphorus pesticides residues in food and their colorimetric detection. Environ. Nanotechnol. Monit. Manag., 10: 292-307.

Cheah, W.K., Othman, R. and Yeoh, F.Y. 2013. Organic and inorganic acid activation of activated carbon fiber from palm oil empty fruit bunch. Adv. Mater. Res., 858: 122-130.

Chen, J., Duan, C. and Guan, Y. 2010. Sorptive extraction techniques in sample preparation for organophosphorus pesticides in complex matrices. J. Chrom. B., 878(17-18): 1216-1225.

Chen, H., Teng, Y., Lu, S., Wang, Y. and Wang, J. 2015. Contamination features and health risk of soil heavy metals in China. Sci. Tot. Environ., 512-513: 143-153.

Chen, J., Zhang, L., Yang, G., Wang, Q., Li, R. and Lucia, L. A. 2017. Preparation and characterization of activated carbon from hydrochar by phosphoric acid activation and its adsorption performance in prehydrolysis liquor. Bioresour., 12(3).

Chowdhury, Z.Z., Zain, S.M., Khan, R.A. and Islam, M.S. 2012. Preparation and characterizations of activated carbon from kenaf fiber for equilibrium adsorption studies of copper from wastewater. Kor. J. Chem. Eng., 29(9): 1187-1195.

Danish, M. and Ahmad, T. 2018. A review on the utilization of wood biomass as a sustainable precursor for activated carbon production and application. Renew. Sustain. Energy Rev., 87: 1-21.

Das, M.P. and Rebecca, L.J. 2018. Removal of lead (II) by phyto-inspired iron oxide nanoparticles. Nat. Environ. Pollut. Technol., 17(2): 569-574.

Department of Statistics Malaysia. 2019, May 31. Review of Survey of Environmental Protection Expenditure 2018. Retrieved May 11, 2020, from Department of Statistics Malaysia, Official Portal website: https://www.dosm.gov.my/v1/index.php?r=column/cthemeByCat&cat=154&bul_id=L1BTVXhaaEFPeERDc2Y1K3JLWVdMQT09&menu_id=NWVEZGhEVlNMeitaMHNzK2htRU05dz09

Department of Statistics Malaysia. 2019, November 29. Review of Selected Agricultural Indicators, Malaysia, 2019. Retrieved May 11, 2020, from Department of Statistics Malaysia, Official Portal website: https://www.dosm.gov.my/v1/index.php?r=column/cthemeByCat&cat=72&bul_id=SEUxMEE3VFdBcDJhdUhPZVUxa2pKdz09&menu_id=Z0VTZGU1UHBUT1VJMFlpaXRRR0xpdz09

Dotto, G.L., Santos, J.M.N., Tanabe, E.H., Bertuol, D.A., Foletto, E.L., Lima, E.C. and Pavan, F.A. 2017. Chitosan/polyamide nanofibers prepared by force spinning technology: A new adsorbent to remove anionic dyes from aqueous solutions. J. Cleaner Prod., 144: 120-129.

Elhag, D.E., Abdalla, B.S., Suliman, S.A. and Ali, I. 2017. Multi-residue analysis of organophosphorus pesticides in vegetables using GC-MS. J. Agric. Chem. Environ., 6(4): 232-241.

Fiorenza, R., Di Mauro, A., Cantarella, M., Iaria, C., Scalisi, E.M., Brundo, M.V., Gulino, A., Spitaleri, L., Nicotra, G., Dattilo, S., Carroccio, S.C., Privitera, V. and Impellizzeri, G. 2020. Preferential removal of pesticides from water by molecular imprinting on TiO2 photocatalysts. Chem. Eng. J., 379: 122309.

Foo, K.Y. and Hameed, B.H. 2011. Preparation of oil palm (Elaeis) empty fruit bunch activated carbon by microwave-assisted KOH activation for the adsorption of methylene blue. Desalination, 275(1-3): 302-305.

Fu, J., Zhang, J., Jin, C., Wang, Z., Wang, T., Cheng, X. and Ma, C. 2020. Effects of temperature, oxygen, and steam on pore structure characteristics of coconut husk activated carbon powders prepared by the one-step rapid pyrolysis activation process. Bioresour. Technol., 310: 123413.

Gallego, E., Roca, F.J., Perales, J.F. and Guardino, X. 2013. Experimental evaluation of VOC removal efficiency of a coconut shell activated carbon filter for indoor air quality enhancement. Build. Environ., 67: 14-25.

George, J. and Shukla, Y. 2011. Pesticides and cancer: Insights into toxicoproteomic-based findings. J. Proteomics., 74(12): 2713-2722.

Griffin, W., Michalek, J., Matthews, H. and Hassan, M. 2014. Availability of biomass residues for co-firing in Peninsular Malaysia: Implications for cost and GHG emissions in the electricity sector. Energies, 7(2): 804-823.

Gueye, M., Richardson, Y., Kafack, F.T. and Blin, J. 2014. High efficiency activated carbons from African biomass residues for the removal of chromium (VI) from wastewater. J. Environ. Chem. Eng., 2(1): 273-281.

Guo, F., Jiang, X., Li, X., Jia, X., Liang, S. and Qian, L. 2020. Synthesis of MgO/Fe3O4 nanoparticles embedded activated carbon from biomass for high-efficient adsorption of malachite green. Mater. Chem. Phy., 240: 122240.

Gupta, H. 2015. Removal of phenanthrene from water using activated carbon developed from orange rind. Int. J, Sci.. Res. Environ. Sci., 3(7): 248-255.

Gupta, H. and Gupta, B. 2015. Adsorption of polycyclic aromatic hydrocarbons on banana peel activated carbon. Desal. Water Treat., 57(20): 9498-9509.

Hamad, B.K., Noor, A.M., Afida, A.R. and Mohd Asri, M.N. 2010. High removal of 4-chloroguaiacol by the high surface area of oil palm shell-activated carbon activated with NaOH from aqueous solution. Desalination, 257(1-3): 1-7.

Hamza, R.A., Iorhemen, O.T. and Tay, J.H. 2016. Occurrence, impacts, and removal of emerging substances of concern from wastewater. Environ. Technol. Innov., 5: 161-175.

Hassan, M.F., Sabri, M.A., Fazal, H., Hafeez, A., Shezad, N. and Hussain, M. 2020. Recent trends in activated carbon fiber production from various precursors and applications-A comparative review. J. Anal. Appl. Pyrolysis., 145: 104715.

Heidari, A., Younesi, H., Rashidi, A. and Ghoreyshi, A. 2014. Adsorptive removal of CO_2 on highly microporous activated carbons prepared from Eucalyptus camaldulensis wood: Effect of chemical activation. J. Taiwan Inst. of Chem. Eng., 45(2): 579-588.

Herawan, S.G., Hadi, M.S., Ayob, M.R. and Putra, A. 2013. Characterization of activated carbons from the oil-palm shell by CO_2 activation with no holding carbonization temperature. The Sci. World J., 2013: 1-6.

Hoseinzadeh Hesas, R., Wan Daud, W.M.A., Sahu, J. N. and Arami-Niya, A. 2013. The effects of a microwave heating method on the production of activated carbon from agricultural waste: A review. J. Anal. Appl. Pyrol., 100: 1-11.

Hui, T.S. and Zaini, M.A.A. 2015. Potassium hydroxide activation of activated carbon: A commentary. Carbon Lett., 16(4): 275-280.

Idowu, O., Semple, K.T., Ramadass, K., O'Connor, W., Hansbro, P. and Thavamani, P. 2019. Beyond the obvious: Environmental health implications of polar polycyclic aromatic hydrocarbons. Environ. Int., 123: 543-557.

Ioannidou, O.A., Zabaniotou, A.A., Stavropoulos, G.G., Islam, M.A. and Albanis, T.A. 2010. Preparation of activated carbons from agricultural residues for pesticide adsorption. Chemosphere, 80(11): 1328-1336.

Islam, M.A., Ahmed, M.J., Khanday, W.A., Asif, M. and Hameed, B.H.

2017. Mesoporous activated coconut shell-derived hydrochar prepared via hydrothermal carbonization-NaOH activation for methylene blue adsorption. J. Environ. Manag., 203: 237-244.

Jiang, C., Yakaboylu, G.A., Yumak, T., Zondlo, J.W., Sabolsky, E.M. and Wang, J. 2020. Activated carbons prepared by indirect and direct CO2 activation of lignocellulosic biomass for supercapacitor electrodes. Renew. Energy., 155: 38-52.

Kadir, S.A.S.A., Matali, S., Mohamad, N.F. and Abdul Rani, N.H. 2014. Preparation of activated carbon from oil palm empty fruit bunch (EFB) by steam activation using response surface methodology. Int. J. Mater. Sci. Appl., 3(5): 159.

Kalkan, E., Nadaroğlu, H., Celebi, N. and Tozsin, G. 2013. Removal of textile dye reactive black 5 from aqueous solution by adsorption on laccase-modified silica fume. Desal. Water Treat., 52(31-33): 6122-6134.

Kausar, A., Iqbal, M., Javed, A., Aftab, K., Nazli, Z.-i.-H., Bhatti, H.N and Nouren, S. 2018. Dyes adsorption using clay and modified clay: A review. J. Mol. Liq., 256: 395-407.

Kaveeshwar, A.R., Ponnusamy, S.K., Revellame, E.D., Gang, D.D., Zappi, M.E. and Subramaniam, R. 2018. Pecan shell-based activated carbon for removal of iron (II) from fracking wastewater: Adsorption kinetics, isotherm, and thermodynamic studies. Process Saf. Environ. Prot., 114: 107-122.

Khorasani, A.C. and Shojaosadati, S.A. 2019. Magnetic pectin-chlorella vulgaris biosorbent for the adsorption of dyes. J. Environ. Chem. Eng., 7(3): 103062.

Kou, Y., Zhao, Q., Cheng, Y., Wu, Y., Dou, W. and Ren, X. 2020. Removal of heavy metals in sludge via joint EDTA-acid treatment: Effects on seed germination. Sci. Tot. Environ., 707: 135866.

Kumar, J.A., Amarnath, D.J., Sathish, S., Jabasingh, S.A., Saravanan, A., Hemavathy, R.V., Anand, K.V. and Yaashikaa, P.R. 2019. Enhanced PAHs removal using pyrolysis-assisted potassium hydroxide induced palm shell activated carbon: batch and column investigation. J. Mol. Liq., 279: 77-87.

Lakshmi, S.D., Avti, P.K. and Hegde, G. 2018. Activated carbon nanoparticles from biowaste as new generation antimicrobial agents: A review. Nano-Struct. Nano-Objects., 16: 306-321.

Li, W., Zhang, L., Peng, J., Li, N. and Zhu, X. 2008. Preparation of high surface area activated carbons from tobacco stems with K_2CO_3 activation using microwave radiation. Ind. Crops and Prod., 27(3): 341-347.

Liang, C.Z., Sun, S.P., Li, F.Y., Ong, Y.K. and Chung, T.S. 2014. Treatment of highly concentrated wastewater containing multiple synthetic dyes by a combined process of coagulation/flocculation and nanofiltration. J. Memb. Sci., 469: 306-315.

Macedo, J. de S., da Costa Júnior, N. B., Almeida, L. E., Vieira, E. F. da S., Cestari, A. R., Gimenez, I. de F., Carreño, N. L. V. and Barreto, L. S. 2006. Kinetic and calorimetric study of the adsorption of dyes on mesoporous activated carbon prepared from coconut coir dust. J. Colloid Interface Sci., 298(2): 515-522.

Mahamad, M.N., Zaini, M.A.A. and Zakaria, Z.A. 2015. Preparation and characterization of activated carbon from pineapple waste biomass for dye removal. Int. Biodeter. Biodegrad., 102: 274-280.

Maneerung, T., Liew, J., Dai, Y., Kawi, S., Chong, C. and Wang, C.H. 2016. Activated carbon derived from the carbon residue from biomass gasification and its application for dye adsorption: Kinetics, isotherms, and thermodynamic studies. Bioresour. Technol., 200: 350-359.

Marican, A. and Durán-Lara, E.F. 2017. A review on pesticide removal through different processes. Environ. Sci. Pollut. Res., 25(3): 2051-2064.

Marsin, F.M., Wan Ibrahim, W.A., Nodeh, H.R., Sutirman, Z.A., Ting, N.N. and Sanagi, M.M. 2018. Recent advances in the preparation of oil palm waste-based adsorbents for removal of environmental pollutants: A review. Malaysian J. Anal. Sci., 22(2): 175-184.

Masjedi, A., Askarizadeh, E. and Baniyaghoob, S. 2020. Magnetic nanoparticles are surface-modified with tridentate ligands for the removal of heavy metal ions from water. Mater. Chemi. Phy., 249: 122917.

Mateo, W., Lei, H., Villota, E., Qian, M., Zhao, Y., Huo, E., Zhang, Q., Lin, X., Wang, C. and Huang, Z. 2020. Synthesis and characterization of sulfonated activated carbon as a catalyst for bio-jet fuel production from biomass and waste plastics. Bioresour. Technol., 297: 122411.

Mazlan, M.A.F., Uemura, Y., Yusup, S., Elhassan, F., Uddin, A., Hiwada, A. and Demiya, M. 2016. Activated carbon from rubberwood sawdust by carbon dioxide activation. Process Eng., 148: 530-537.

Meryemoglu, B., Irmak, S. and Hasanoglu, A. 2016. Production of activated carbon materials from kenaf biomass to be used as catalyst support in the aqueous-phase reforming process. Fuel Process. Technol., 151: 59-63.

Mojiri, A., Zhou, J. L., Ohashi, A., Ozaki, N. and Kindaichi, T. 2019. A comprehensive review of polycyclic aromatic hydrocarbons in water sources, their effects, and treatments. Sci. Tot. Environ., 696: 133971.

Mojiri, A., Zhou, J. L., Robinson, B., Ohashi, A., Ozaki, N., Kindaichi, T., Farraji, H. and Vakili, M. 2020. Pesticides in aquatic environments and their removal by adsorption methods. Chemosphere, 253: 126646.

Muniandy, L., Adam, F., Mohamed, A.R. and Ng, E.P. 2014. The synthesis and characterization of high purity mixed microporous/mesoporous activated carbon from rice husk using chemical activation with NaOH and KOH. Micropor. Mesopor. Mate., 197: 316-323.

Nabais, J.M.V., Laginhas, C., Carrott, M.M.L.R., Carrott, P.J.M., Amorós, J.E.C. and Gisbert, A.V.N. 2013. Surface and porous characterization of activated carbons made from a novel biomass precursor, the esparto grass. Appl. Surf. Sci., 265: 919-924.

Naik, P.K., Paul, S. and Banerjee, T. 2017. Liquid equilibria measurements for the extraction of polyaromatic nitrogen hydrocarbons with a low-cost deep eutectic solvent: Experimental and theoretical insights. J. Mol. Liq., 243: 542-552.

Narayana, S.J. and Kariyajjanavar, P. 2019. Studies on degradation of pulp and paper mill industrial dye fast red by indirect electrochemical method. Nat. Env. Pollut. Technol., 18(2): 657-662.

Ndiaye, P.I., Moulin, P., Dominguez, L., Millet, J.C. and Charbit, F. 2005. Removal of fluoride from electronic industrial effluent by RO membrane separation. Desalination., 173(1): 25-32.

Nidheesh, P.V., Zhou, M. and Oturan, M.A. 2018. An overview on the removal of synthetic dyes from water by electrochemical advanced oxidation processes. Chemosphere, 197: 210-227.

Nie, J., Sun, Y., Zhou, Y., Kumar, M., Usman, M., Li, J., Shao, J., Wang, L. and Tsang, D.C. W. 2020. Bioremediation of water containing pesticides by microalgae: Mechanisms, methods, and prospects for future research. Sci. Tot. Environ., 707: 136080.

Njoku, V.O., Islam, M.A., Asif, M. and Hameed, B.H. 2014. Preparation of mesoporous activated carbon from coconut frond for the adsorption of carbofuran insecticide. J. Anal. Appl. Pyrolysis, 110: 172-180.

Pagketanang, T., Artnaseaw, A., Wongwicha, P. and Thabuot, M. 2015. Microporous activated carbon from KOH-activation of rubber seed-shells for application in Capacitor Electrode. Energy Procedia, 79: 651-656.

Pereira, R.G., Veloso, C.M., da Silva, N.M., de Sousa, L.F., Bonomo, R.C.F., de Souza, A.O., da Guarda Souza., M.O. and da Costa, I.F.R. 2014. Preparation of activated carbons from cocoa shells and siriguela seeds using H_3PO_4 and $ZnCl_2$ as activating agents for BSA and α-lactalbumin adsorption. Fuel Process. Technol., 126: 476-486.

Pérez-Gregorio, M.R., García-Falcón, M.S., Martínez-Carballo, E. and Simal-Gándara, J. 2010. Removal of polycyclic aromatic hydrocarbons from organic solvents by ashes wastes. J. Hazard. Mater., 178(1-3): 273-281.

Prashanthakumar, T.K.M., Ashok Kumar, S.K. and Sahoo, S.K. 2018. A quick removal of toxic phenolic compounds using porous carbon prepared from renewable biomass coconut spathe and exploration of a new source for porous carbon materials. J. Env. Chem. Eng., 6(1), 1434-1442.

Purnomo, C.W., Kesuma, E.P., Perdana, I. and Aziz, M. 2018. Lithium recovery from spent Li-ion batteries using coconut shell activated carbon. Waste Manag., 79: 454-461.

Rahman, M., Adil, M., Yusof, A., Kamaruzzaman, Y. and Ansary, R. 2014. Removal of heavy metal ions with acid-activated carbons derived from oil palm and coconut shells. Materials, 7(5): 3634-3650.

Rai, P., Gautam, R.K., Banerjee, S., Rawat, V. and Chattopadhyaya, M.C. 2015. Synthesis and characterization of a novel $SnFe_2O_4$ @ activated carbon magnetic nanocomposite and its effectiveness in the removal of crystal violet from an aqueous solution. J. Environ. Chem. Eng., 3(4): 2281-2291.

Ratna, K. and Padhi, B.S. 2012. Pollution due to synthetic dye toxicity and carcinogenicity studies and remediation. Int. J. Environ. Sci., 3(3): 940-947.

Rizzi, V., Prasetyanto, E.A., Chen, P., Gubitosa, J., Fini, P., Agostiano, A., De Cola, L. and Cosma, P. 2019. Amino grafted MCM-41 as a highly efficient and reversible eco-friendly adsorbent material for the Direct Blue removal from wastewater. J. Mol. Liq., 273: 435-446.

Saba, N., Jawaid, M., Hakeem, K.R., Paridah, M.T., Khalina, A. and Alothman, O.Y. 2015. Potential of bioenergy production from industrial kenaf (Hibiscus cannabinus L.) based on Malaysian perspective. Renew. Sustain. Energy Rev., 42: 446-459.

Salman, J.M., Njoku, V.O. and Hameed, B.H. 2011. Batch and fixed-bed adsorption of 2,4-dichlorophenoxyacetic acid onto oil palm frond activated carbon. Chem. Eng. J., 174(1): 33-40.

Sapahin, H.A., Makahleh, A. and Saad, B. 2014. Determination of organophosphorus pesticide residues in vegetables using solid-phase micro-extraction coupled with gas chromatography–flame photometric detector. Arabian J. Chem., 2015: 1-11.

Sekar, A.S.S. 2008. Removal of color from tannery dye wastewater using ozone. Nat. Env. Pollut. Technol., 7(3): 505-508.

Sellaoui, L., Lima, É. C., Dotto, G. L., Dias, S. L. P. and Ben Lamine, A. 2017. Physicochemical modeling of reactive violet 5 dye adsorption on the homemade cocoa shell and commercial activated carbons using the statistical physics theory. Results in Physics., 7: 233-237.

Sharma, S., Mathur, S. and Sharma, R. 2011. Efficacy of electrocoagulation in the treatment of textile wastewater containing basic red dye using iron electrodes. Nat. Environ. Pollut. Technol., 10(2): 225-228.

Shukla, K., Verma, A., Verma, L., Rawat, S. and Singh, J. 2020. A novel approach to utilize used disposable paper cups for the development of adsorbent and its application for the malachite green and rhodamine-B dyes removal from aqueous solutions. Nat. Environ Pollut. Technol., 19(1): 57-70.

Sulaiman, F., Abdullah, N., Gerhauser, H. and Shariff, A. 2011. An outlook of Malaysian energy, oil palm industry and its utilization of wastes as useful resources. Biomass Bioenerg., 35(9): 3775-3786.

Sun, Y., Lan, J., Du, Y., Li, Z., Liao, X., Du, D., Ye, H., Zhang, T. C. and Chen, S. 2020. Efficient removal of heavy metals by synergistic actions of microorganisms and waste molasses. Bioresour. Technol., 302: 122797.

Tan, I.A.W., Ahmad, A.L. and Hameed, B.H. 2008. Adsorption of basic dye using activated carbon prepared from oil palm shell: batch and fixed bed studies. Desalination, 225(1-3): 13-28.

Teimouri, Z., Salem, A. and Salem, S. 2019. Clean and new strategy for catalytic conversion of agriculture waste shells to activated carbon via microwave-assisted impregnation: Applied and eco-friendly aspect for decoloration of industrial corn syrup and process identifications. J. Environ. Chem. Eng., 7(3): 103161.

Tobiszewski, M. and Namieśnik, J. 2012. PAH diagnostic ratios for the identification of pollution emission sources. Environ. Pollut., 162: 110-119.

Tounsadi, H., Khalidi, A., Abdennouri, M. and Barka, N. 2016. Activated carbon from Diplotaxis Harra biomass: Optimization of preparation conditions and heavy metal removal. J. Taiwan Inst. Chem. Eng., 59: 348-358.

Treviño-Cordero, H., Juárez-Aguilar, L.G., Mendoza-Castillo, D.I., Hernández-Montoya, V., Bonilla-Petriciolet, A. and Montes-Morán, M.A. 2013. Synthesis and adsorption properties of activated carbons from biomass of Prunus domestica and Jacaranda mimosifolia for the removal of heavy metals and dyes from water. Ind. Crops Prod., 42: 315-323.

Tripathi, M., Dixit, A. and Bobade, S.M. 2020. Fabrication of supercapacitor using banyan leaves-based activated carbon electrode and formic acid-based polymer electrolyte. Mater. Today: Proceed., 28: 320-324.

Tsibart, A.S. and Gennadiev, A.N. 2013. Polycyclic aromatic hydrocarbons in soils: Sources, behavior, and indication significance (a review). Eurasian Soil Sci., 46(7): 728-741.

Ufodike, C.O., Eze, V.O., Ahmed, M.F., Oluwalowo, A., Park, J.G., Liang, Z. and Wang, H. 2020. Investigation of molecular and supramolecular assemblies of cellulose and lignin of lignocellulosic materials by spectroscopy and thermal analysis. Int. J. Biol. Macromol., 146: 916-921.

Wahi, R., Ngaini, Z. and Uson Jusok, V. 2009. Review of removal of mercury, lead, and copper from aqueous solution by activated carbon of palm oil empty fruit bunch. World Appl. Sci. J., 5: 84-91.

Włóka, D., Placek, A., Smol, M., Rorat, A., Hutchison, D. and Kacprzak, M. 2019. The efficiency and economic aspects of phytoremediation technology using Phalaris arundinacea L. and Brassica napus L. combined with compost and nano SiO_2 fertilization for the removal of PAH's from the soil. J. Environ. Manag., 234: 31-319.

Xue, C., Hao, W., Cheng, W., Ma, J. and Li, R. 2019. Effects of the pore size distribution of activated carbon (AC) on CuCl dispersion and CO adsorption for CuCl/AC adsorbent. Chem. Eng. J., 375: 122049.

Yacob, A. R., Wahab, N., Suhaimi, N. H. and Mustajab, M. K. A. A. 2013. Microwave-induced carbon from waste palm kernel shell activated by phosphoric acid. Int. J. Eng. Technol., 5(2): 214-217.

Yakout, S.M. and Sharaf El-Deen, G. 2012. Characterization of activated carbon prepared by phosphoric acid activation of olive stones. Arab. J. Chem., 9: S1155-S1162.

Yakout, S. M., Daifullah, A. A. M. and El-Reefy, S. A. 2013. Adsorption of naphthalene, phenanthrene, and pyrene from aqueous solution using low-cost activated carbon derived from agricultural wastes. Adsorp. Sci. Technol., 31(4): 293-302.

Yang, Z., Asoh, T. A. and Uyama, H. 2019. Removal of cationic or anionic dyes from water using ion-exchange cellulose monoliths as adsorbents. Bull. Chem. Soc. Japan., 92(9): 1453-1461.

Yang, W., Chen, H., Han, X., Ding, S., Shan, Y. and Liu, Y. 2020. Preparation of magnetic Co-Fe modified porous carbon from agricultural wastes by microwave and steam activation for mercury removal. J. Hazard. Mater., 381: 120981.

Zhang, Y., Song, X., Zhang, P., Gao, H., Ou, C. and Kong, X. 2020. Production of activated carbons from four wastes via one-step activation and their applications in Pb2+ adsorption: Insight of ash content. Chemosphere, 245: 125587.

Zhou, J., Luo, A. and Zhao, Y. 2018. Preparation and characterization of activated carbon from waste tea by physical activation using steam. J. Air Waste Manag. Assoc., 68(12): 1269-1277.

Nature Environment and Pollution Technology
An International Quarterly Scientific Journal

p-ISSN: 0972-6268
(Print copies up to 2016)
e-ISSN: 2395-3454

Vol. 20 | No.3 | pp. 1185-1191 | 2021

Original Research Paper

https://doi.org/10.46488/NEPT.2021.v20i03.026

Open Access Journal

Experimental Investigation on Concrete with E-waste - A Way to Minimize Solid Waste Deposition

P. Muthupriya† and B. Vignesh Kumar
Department of Civil Engineering, N.G.P. Institute of Technology, Coimbatore-641 048, T.N., India
†Corresponding author: P. Muthupriya; drmuthupriya@gmail.com

Nat. Env. & Poll. Tech.
Website: www.neptjournal.com

Received: 07-09-2020
Revised: 05-11-2020
Accepted: 08-12-2020

Key Words:
E-waste
Coarse aggregate
Solid waste
Strength properties

ABSTRACT

In recent years, the generation of Electronic waste (E-waste) has increased to a greater extent worldwide. The use of electronic devices has proliferated in recent decades and proportionality, and the quantity of electronic devices that are disposed of is growing rapidly throughout the world. Electronic waste (E-waste) typically includes general household electronics, discarded electronic gadgets, and circuit boards. With the growing use of consumer electronics, there is a huge generation of E-waste every day. Reuse of E-waste plastics as aggregates or filler in some or other forms of in construction industry may be considered as economical and technically viable for solving the disposal of a large amount of waste and this can be used as aggregates and fine filler in concrete or the construction of flexible pavement. The idea was to determine whether E-waste plastic components can be used as an alternative to conventional material like bitumen, filler in the bituminous mix in a flexible pavement structure. This is an effective alternative solution to reduce the growing quantity of E-waste.

INTRODUCTION

Electronic and electrical waste, commonly known as E-waste items, do not disintegrate or degenerate. The blasting use of electronic and electrical equipment has made another yet extremely hazardous stream of waste, called "electronic-waste", or basically known as e-waste. Used electronics which are sorted for reuse, resale, salvage, recycling, or disposal are also considered e-waste.

On one hand, the development of electronics products has made life easy for all but on the other hand, it has encouraged the "use and throw" mentality. Nowadays people prefer to buy a new appliance rather than taking the pains to get the old appliance repaired. Such a trend not only leads to an increase in the volume of electrical and electronic waste but also poses a serious threat to public health and the environment. E-waste is growing exponentially in recent years because the markets for these products are also growing rapidly. E-waste is presently one of the quickest developing waste streams.

Consistently, countless old PCs, cellular telephones, TV sets, and radio gear are tossed, a large portion of which is either disposed of in landfills or unapproved reusing yards. Informal processing of electronic waste in developing countries may cause serious health and pollution problems, as these countries have limited regulatory oversight of e-waste processing.

The problem of disposing and managing solid waste materials in all countries has become one of the major environmental, economical, and social issues. A complete waste management system including source reduction, reuse, recycling, land-filling, and incineration needs to be implemented to control the increasing waste disposal problems. Typically e-plastics are not recycled into the same type of plastic products made from recycled plastics that are often not recyclable. The use of biodegradable plastics is increasing. If some of these get mixed in the other plastics for recycling, the reclaimed plastic is not recyclable because of the variance in properties and melt temperatures.

PAST STUDIES

Kaniskha et al. (2019) studied the concrete mixes of various percentages of e-waste. disposal of a large amount of E-waste material, reuse of E-waste in the concrete industry is considered as the most feasible application. The work was conducted on M30 concrete. The replacement of coarse aggregate with E-waste in the range of 0%, 5%, 10%, 15%, 20% and 25%. Finally, the mechanical properties of the concrete mix specimens obtained from the addition of these materials are compared with the control concrete mix. The test results showed that a significant improvement in compressive strength was achieved in the e-waste concrete compared to conventional concrete and can be used effectively in concrete. Balasubramaniam et al. (2018) carried experimental investigation on e-waste. They have confirmed that no major changes are found in the compressive strength of concrete with the presence of e-plastic. However, when

1% of e-plastic for 5cm is added, the compressive strength gets reduced by 2.59% when compared to the control mix. With the addition of the e-plastic-4cm and e-Plastic-3cm, the compressive strength increases to a maximum of 5.9% and 10.6% respectively when compared to the control mix. In addition, they have confirmed that an increase in strength is found in the tensile strength of concrete with the presence of e-plastic. When 1% of the e-plastic for 5cm is added, the tensile strength gets increased by 2.3%; when 1% of the e-plastic for 4cm is added, the strength increase observed is 4.6%, and when 1% of e-plastic for 3cm is added, the tensile strength initially increases by 4.6% when compared to control mix at 28 days of curing and then decreases with the percentage increase. Thus, they have concluded that strength was achieved in the e-plastic concrete compared to conventional concrete.

Raut et al. (2018) observed that the coarse aggregate can be replaced by e-waste and the research strongly showed the possibility of e-waste being used as a substitute for fine and coarse aggregate. More use of this waste material tends to reduce the demand for natural resources used in concrete and it is of prime importance that a substitute of coarse aggregate can be explored. Manjunath (2017) conducted an experimental investigation on concrete with e-waste and reported that by adding various ratios of e-waste in M20 grade concrete, its compressive strength, tensile strength, and flexural strength are tested. The use of e-waste products in concrete not only makes it economical but also helps in reducing disposal problems. Total replacement of concrete is not possible because no material plays the role of concrete in terms of strength, durability, and workability.

Akram (2017) observed that the strength was decreased on the addition of e-waste and hence 10% fly ash was added. It is reported that the addition of e-waste in concrete will reduce the value of landfill cost and saving energy. It will protect the environment from solid waste pollutions and its effects indirectly. The generation of waste materials creates the most ecological problems for the environment. Especially e-waste materials are harmful and toxic waste materials compared to other solid waste. Selvam et al. (2015), studied the strength characteristics by conducting the tests on e-waste concrete with e-waste and the results revealed that up to 20% replacement e-waste for coarse aggregate in concrete shows improvement in compressive & tensile strength. By comparing the results with conventional concrete at 28 days strength it is observed that the strength of concrete is reduced by 30.7% when coarse aggregate is replaced beyond 20 % of e-waste. It is identified that e-waste can be disposed by using them as construction materials and the e-waste is not suitable to replace fine aggregate but it is used to replace the coarse aggregate. Also the compressive strength and split tensile strength of concrete containing e plastic aggregate is retained more or less in comparison with controlled concrete specimens. However, strength is noted to be decreased when the e plastic content was more than 20%. And they have also concluded that, 20% of e-waste aggregate can be replaced as coarse aggregate replacement in concrete without any long term detrimental effects and with acceptable strength development properties.

Kumar (2018) studied the partially replacement of coarse aggregate with e-waste. He casted concrete cubes with 5%, 7.5%, and 12.5% e-waste and compared the compressive strength of M25 grade concrete with conventional concrete cubes of M25 grade. His study concludes that the electronic waste can replace coarse aggregate up to 12%. It provides an effective way to disposal the e-waste. Makes the concrete light weight and thus the self-weight is reduced. Makes the concrete more flexible hence can easily bear the seismic loads. It reduces the stress on the natural resources. It increases the workability of concrete. Sustainable development is possible. It reduces the risk of harmness to land.

Prasanna & Rao (2014) conducted the research on replacing the coarse aggregate with e-waste by 5%, 10%, 15% and 20% in one batch and they also made another batch with using same percentage of e-waste and also adding 10% of fly ash. The concrete strength is found out to be optimum when 15% of coarse aggregate is replaced with e-waste.

E-WASTE CONCRETE

Components of e-waste are Cathode ray tubes (used in TVs, computer monitors, ATM, video cameras, and more), a Printed circuit board (image behind the table - a thin plate on which chips and other electronic components are placed), Chips and other goldplated components, Plastics from printers, keyboards, monitors, etc., and Computer wires.

E-waste is defined as the type of concrete in which e-waste is used as the materials for concrete by partial replacement.

For solving the disposal of a large amount of recycled plastic material, the reuse of plastic in the concrete industry is considered the most feasible application. Recycled plastic can be used as coarse aggregate in concrete.

Objectives of this Experimental Investigation are (a) To identify e-waste that can be disposed of by using them as construction material. (b) Replacement of e-waste as coarse aggregate. (c)To limit the amount of toxic substances in certain electronic products. (d) To develop and improve the technology for e-waste management. (e) To reduce the pollution due to recycling of e-waste in the unorganized sec-

tion. (f)To determine the compressive and flexural strength of concrete containing e-plastic aggregate.

MATERIALS AND METHODS

- Cement: Prozolona Portland cement, 53 grade conforming to IS: 455-1987 and other properties like finess,specific gravity etc., are pointed in Table 1.
- Fine aggregate: Locally available manufacturing sand conforming to grading zone II of IS: 383-1970
- Coarse aggregate: Locally available crushed blue granite stones conforming to a graded aggregate of nominal size 12.5 mm as per IS: 383-1970.
- Tables 2 and 3 explain the properties of fine and coarse aggregate respectively.
- Water: Potable water
- E-waste used: Chipboard (plastic e-waste)

E-waste

In this experimental investigation, e-waste has been used as a partial substitute for coarse aggregate in concrete, that is high impact polystyrene (HIPS) plastic from all the electronic gadgets and its accessories are used in the concrete as a partial substitute for coarse aggregate in various percentages. In this present experimental investigation, a chipboard is used for e-waste.

MIX DESIGN AND METHODOLOGY

Design Mix prepared based on Indian Standard Code of Practice and the below mix proportions were derived, are Shown in Table 4.

Table 1: Properties of cement.

S.No.	Property of Cement	Values
1	Fineness of cement	7.5%
2	Grade of cement	43
3	Specific gravity	3.15
4	Initial setting time	28 min
5	Final setting time	600 min

Table 2: Properties of fine aggregates.

S.No.	Characteristics	Value
1	Type	M-sand
2	Specific gravity	2.68
3	Total water absorption	1.02%
4	Grading zone	II

Mix Proportion

Cement=438.1 kg/m^3, Fine aggregate=641.07 Kg.m^{-3},Coarse aggregate =1120.82 7 Kg.m^{-3}, Water content=197.16 L.m^{-3}, Mix Ratio = 1 : 1.46 : 2.55 : 0.45

Mix Ratio = Cement: Fine aggregate: Coarse aggregate: Water

EXPERIMENTAL INVESTIGATION

Slump Cone Test

The slump test is a means of assessing the consistency of fresh concrete. It is used indirectly, as a means of checking if the correct amount of water has been added to the mix. The steel slump cone is placed on a solid, impermeable, level base and filled with fresh concrete in three equal layers. Table 5 shows the testes carried out on harded concrete after a curing period.

Compression Strength

The compressive strength of concrete is determined at the age of 7days and 28 days. The specimens are cast and tested as per IS: 516-1959. The compressive strength of cubes is tested with a replacement of 10%, 15%, and 20% of the mass of coarse aggregates with e-waste with selected quality of water. The tests are carried out on a 150x150x150 mm size cube, as per IS: 516-1959. The test specimens are removed from the molds and unless required for the test within 24 hours, immediately submerge in clean fresh water and keep there until taken out just prior to the test. A 3000 kN capacity standard compression testing machine is used to conduct the test. The specimen is placed between the steel plates of the compression-testing machine. The load is applied at the rate

Table 3: Properties of coarse aggregate.

S.No	Characteristics	value
1	Type	Crushed
2	Maximum size	20mm
3	Specific gravity(20mm)	2.825
4	Total water absorption(20mm)	3.645%

Fig. 1: Slump cone test.

Table 4: Mix Proportion for a different mix.

Mix	E-waste %	Cement ($Kg.m^{-3}$)	F.A ($Kg.m^{-3}$)	C.A ($Kg.m^{-3}$)	E-waste ($Kg.m^{-3}$)	Mix proportion (C: F.A: C.A: E-waste)
M0	0	438.1	641.07	1120.82	0	1: 1.46 : 2.55 : 0
M1	10	438.1	641.07	1008.73	112.08	1: 1.46 : 2.30 : 0.25
M2	15	438.1	641.07	952.69	168.12	1: 1.46 : 2.17 : 0.38
M3	20	438.1	641.07	896.65	224.16	1: 1.46 : 2.04 : 0.51

Table 5: Test on hardened concrete.

S.No.	Type of Test	Properties studied	Size of the Specimen
1.	Compression Test	Compression Strength	150X150X150 mm
2.	Flexural Strength Test	Flexural Strength	500X100X100 mm prism
3.	Split Tensile Strength Test	Tensile Strength	150 mm diameter cylinder

of 140 $kg.cm^{-2}$.min, and the failure load in kN is observed from the dial gauge of the compression testing machine.

Flexure Strength Test

The flexure strength of concrete was determined at the age of 28 days. The specimens were cast and tested as per IS: 516-1959. The compressive strength of cubes is tested with a replacement of 20% of the mass of cement with selected quality of e-waste, and 0.5% of the load shall be applied at a rate of loading of 400 $Kg.min^{-1}$ for the 15.0 cm specimens and at a rate of 180 $Kg.min^{-1}$ for the 10.0 cm specimens.

Split Tensile Test

The tensile strength of concrete is determined at the age of 28 days. The specimens are cast and tested as per IS: 516-1959. The compressive strength of cubes is tested with a replacement of 20% of the mass of cement with selected quality of E-waste, and 0.7% of CONPLASTSP-36 with selected quality of water. The load was applied continuously without shock at a rate within the range of 0.7 to 1.4 MPa. min^{-1} (1.2 to 2.4 $MPa.min^{-1}$ based on IS 5816 1999). The breaking load is noted.

RESULTS AND DISCUSSION

The compressive strength result of the M25 grade of E-waste concrete trial mixes at the age of 7 and 28 days is tabulated in Table 6. The development of compressive strengths of M25 grade of e-waste concrete trial mixes containing 10%, 15%, and 20% coarse aggregate replacement level by fly ash and superplasticizer is added to the mixes.

All the mixes were tested at a period of 7 and 28 days. It is observed that the compressive strengths at the age of 28 days for M25 grade of e-waste concrete trial mixes containing 15% and 20% were 25 and 24MPa respectively; and at the age of 7 days were 18 and 17 MPa respectively.

Table 6 presents the compressive strength of concrete mixes with and without e-plastic aggregates, where M0 is a conventional mix with 0% of e-plastic, M1 with 10% of e-plastic, M2 with 15% of e-plastic, and M3 with 20% of e-plastic. Graph 1& 2 shows the graphical representations of compressive strength of all mixes M0, M1, M2, and M3 for 7 and 28 days. Hence, the maximum compressive strength was found to be 15 percent replacement of coarse aggregates by e-waste for M25 grades of concrete

Table 6: Compressive strength at 7 days and 28 days.

Mix	E-Waste (%)	Compressive Strength (MPa)	
		7 days	28 days
M0	0	19	27
M1	10	15	23
M2	15	18	25
M3	20	17	24

Fig. 2: Compressive strength test.

Fig. 3: Flexural strength test.

The results of the flexural test of e-waste concrete are given in Table 7. The influence of e-waste in concrete at different ratios is tabulated below.

All the mixes were tested at a period of 7 and 28 days. It is observed that the flexural strengths at the age of 7 days for M25 grade of E-waste concrete trial mixes for M0, M1, M2, M3, M4 were 2.65, 2.25, 2.59, and 2.43 Mpa respectively; and at the age of 28 days were 4.15, 3.54, 3.81 and 3.63 MPa respectively.

The experimental result for flexural strength is given in Table 7. All the mixes were tested at a period of 7 and 28 days. It is observed that the flexural strengths at the age of 7 days for M25 grade of E-waste concrete trial mixes for M0, M1, M2, M3, M4 were 2.4, 2.05, 2.31, and 2.26 MPa respectively; and at the age of 28 days were 3.45, 3.13, 3.34, and 3.28 MPa respectively. From Table 8, the flexural strength is maximum when replacing 15% of coarse aggregate with e-waste in concrete. The development of tensile strengths

Table 7: Flexural strength at 7 days and 28 days.

Mix	E-WASTE (%)	Flexural Strength (MPa)	
		7 days	28 days
M0	0	2.65	4.15
M1	10	2.25	3.54
M2	15	2.59	3.81
M3	20	2.43	3.63

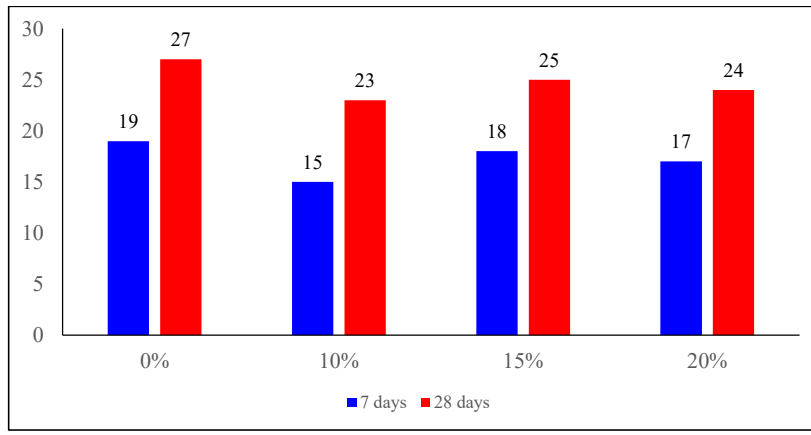

Fig. 4: Compressive strength of E-waste concrete at 7days and 28 days.

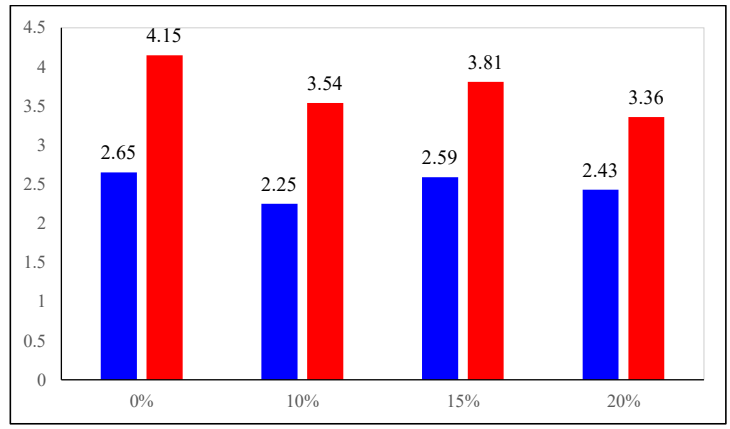

Fig. 5: Flexural strength of E-waste concrete at 7days and 28 days.

of M25 grade of concrete trial mixes containing 10%, 15%, and 20% replacement of coarse aggregates by e-waste and are relatively compared.

All the mixes were tested at a period of 7 and 28 days. It is observed that the tensile strengths at the age of 7 days for M25 grade of e-waste concrete trial mixes for M0, M1, M2, M3, M4 containing 10%,15%, and 20% of e-waste were 2.4, 2.05, 2.31, and 2.26 MPa respectively; and at the age of 28 days were 3.45,3.13, 3.34 and 3.28 MPa respectively

The experimental result for tensile strength is given in Table 8. From Table 8, the tensile strength is high when replacing 15% of coarse aggregate with e-waste in concrete.

Table 8: Tensile strength at 7 days and 28 days.

Mix	E-Waste (%)	Split Tensile Strength (MPa)	
		7 days	28 days
M0	0	2.4	3.45
M1	10	2.05	3.13
M2	15	2.31	3.34
M3	20	2.26	3.28

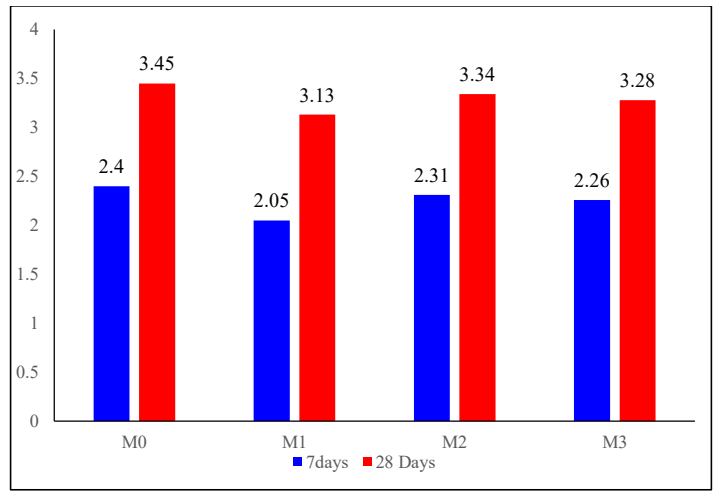

Fig. 6: Tensile strength of E-waste concrete at 7days and 28 days.

From all the strength tests carried out on e-waste concrete, it is observed that the replacement of coarse aggregate by e-waste results in an increase in compressive strength, flexural strength and split tensile strength.

CONCLUSION

- Following are the conclusions that can be made based upon the studies made by various experimental investigations. E-waste plastics can be used to replace some of the aggregates in a concrete mixture. This contributes to reducing the unit weight of the concrete. This is useful in applications requiring non-bearing lightweight concrete.
- The effect of the water-cement ratio of strength development is not prominent in the case of plastic concrete. It is because the plastic aggregates reduce the bond strength of concrete. Therefore, the failure of concrete occurs due to the failure of the bond between the cement paste and plastic aggregates.
- For a given w/c, the use of e-waste plastics in the mix lowers the density, compressive strength, and tensile strength of concrete.
- The inclusion of recycled aggregates in the concrete of the buildings under investigation is shown to be advantageous from an energy point of view.
- As a result of the experimental investigation, it is well understood that e-waste can be used as an alternative for concrete making materials and it leads to less disposal of e-waste in the environment. Thus resulting in reduced pollution.

So, it can be concluded that e-waste can partially replace the coarse aggregates in concrete and it gives a sustainable solution to the natural resources like aggregates and reduction in the accumulation of e-waste. It also reduces the excess landfill due to the e-waste deposition. As a result, we can reduce pollution of the environment as the use of e-waste in concrete reduced its deposition in an open environment and thus reduce solid waste and its impacts.

SCOPE FOR FUTURE WORK

- E-waste material can be used instead of fine aggregates and strength can be verified.
- Along with e-waste some other chemical and mineral admixtures can be added and tested.

REFERENCES

Akram, A. 2017. E-waste management by utilization of e-plastics in concrete mixture as coarse aggregate replacement, Int. J. Innov. Res. Sci. Eng. Technol., 4(7), 24-39.

Balasubramaniam, B., Gopala Krishna, G.V.T. and Saraswathy, V. 2018. Review of literature on electronic waste materials used in concrete. Int. J. Eng. Manag. Res., 3(2): 31-35.

Kaniskha, N.B., Pavithran, P., Sanjai, J., Sheela, F. and Balaji, V. 2019. Study on concrete with e-waste as partial replacement of coarse aggregate and m-sand as fine aggregate. Int Rese. J. Eng. Technol., 6(5): 2255-2265.

Kumar, Ankit 2018. Utilisation of e-waste in concrete by partial replacement of coarse aggregate. IEEE International Conference on Recent Advances in Engineering, Technology and Computational Sciences (RAETCS-2018) At: Sam Higginbottom University of Agriculture, Technology & Sciences, Allahabad 05 Sep 2018.

Manjunath, A. 2017. Partial replacement of e-waste as coarse aggregate in concrete, Int. Conf. Solid Waste Manag., 35: 731-739.

Prasanna, P.K. and Rao, M.K. 2014. Strength variations in concrete by using E-waste as coarse aggregate. International Journal of Education and applied research, 4(2).

Raut, S.R., Dhapudkar, R.S. and Mandoakar, M.G. 2018. Experimental study on utilization of e-waste in cement concrete. Int. J. Eng. Sci., 23(19): 82-86

Selvam, N.P. and GVT, G.K. 2016. Recycle of E-waste in concrete. International Journal of Science and Research (IJSR), 5(4): 1590-1593.

Nature Environment and Pollution Technology
An International Quarterly Scientific Journal

p-ISSN: 0972-6268
(Print copies up to 2016)
e-ISSN: 2395-3454

Vol. 20 | No.3 | pp. 1193-1199 | 2021

Original Research Paper

https://doi.org/10.46488/NEPT.2021.v20i03.027

Open Access Journal

Fabrication of Ag/TiO_2 Cotton Fabric to Enhance Photocatalytic Degradation of Anionic Dye

S. Fu*, Y. Dong*, L. Liang* and X. Meng*(**)(***)†

*College of Textile and Garment, College of Life Science, Shaoxing University, Shaoxing, China

**Key Laboratory of Clean Dyeing and Finishing Technology of Zhejiang Province, Shaoxing University, Shaoxing, China

***Zhejiang Sub-center of National Carbon Fiber Engineering Technology Research Center, Shaoxing, China

†Corresponding author: Xu Meng; mengqiaoshen@163.com

Nat. Env. & Poll. Tech.
Website: www.neptjournal.com

Received: 09-08-2020
Revised: 10-10-2020
Accepted: 01-11-2020

Key Words:
Ag/TiO_2
Photocatalysis
Anionic dye
Degradation

ABSTRACT

Ag/TiO_2 composite fabric was prepared by coprecipitation with $TiCl_4$ as a titanium source and $AgNO_3$ as a silver source. The samples were characterized by scanning electron microscope (SEM), thermogravimetric analyzer (TG) and Fourier transform infrared spectrometer (FTIR). The photocatalytic activity of synthetic fabrics was measured by the degradation of anion dyes under ultraviolet light. The effects of silver loading concentration, fabric area, initial concentration, and photocatalytic time on photocatalytic activity were investigated. The experimental results showed that the degradation rate of Ag/TiO_2 composite fabric on anion dyes could reach 70.76% in 50 minutes, indicating that the prepared Ag/TiO_2 composite fabrics had high photocatalytic activity.

INTRODUCTION

The rapid development of the printing and dyeing industry has brought us a wealth of printing and dyeing products as well as pollution problems (Holkar et al. 2016, Anastasi et al. 2011). The research of efficient and economical sewage treatment technology has become a research hotspot. Traditional water treatment methods mainly include physicochemical methods and biological methods (Banks et al. 2020). However, these methods have several disadvantages such as low degradation efficiency and unsatisfactory effect, and cannot meet the increasingly strict wastewater discharge standards, which pose a serious threat to the water environment.

Photocatalytic technology, as a new green environmental protection technology, can oxidize and decompose organic molecules into carbon dioxide, water, and some inorganic small molecules under light irradiation (Lu & Zhao 2018). Because of its excellent photoactivity, chemical and thermal stability, and the ability to degrade toxic organic pollutants in water, TiO_2 has become one of the most promising environmental remediation materials (Riegel & Bolton 1995, Farbod & Khademalrasool 2011, Kaneco et al. 2006). It was widely used in wastewater treatment, organic degradation, air treatment, and other fields. However, the practical application of TiO_2 has been extremely limited. The wide bandgap (e.g. = 3.2 eV) reduces the utilization rate of sunlight (Zhao et al. 2020, Habibi-Yang & Feizpoor 2019). Meanwhile, the recombination of electrons and holes that generate on the TiO_2 is unfavorable to the efficiency of the TiO_2 photocatalysts (Ma et al. 2020).

To overcome these shortcomings, a large number of studies have concentrated on the improvement of the photocatalytic efficiency and visible light utilization of TiO_2. At present, various strategies including noble metal deposition (Benz et al. 2020), semiconductor composite (Lv et al. 2014), metal or non-metal doping (Khan et al. 2017, Li et al. 2018), and load modification (Zhao et al. 2012) have been explored. Among them, noble metal (Pt, Ag, Au) deposition of TiO_2 significantly improves the electron capture efficiency, which is one of the most effective ways to improve its photocatalytic activities. Due to the large Fer between nano TiO_2 and noble metal, it is thermodynamically possible to transfer electrons brought by TiO_2 conduction to metallic particles, resulting in the formation of electron accumulation center on the surface of noble metal. This is a kind of photoelectron trap, which achieves a good separation of electrons and holes and greatly improves the photocatalytic activity of TiO_2 (Kulkarni et al. 2015). In this work, Ag was selected as the deposited noble metal. Considering the properties of easy doping, high electrical conductivity, and good light absorption ability, it is

one of the most suitable materials for industrial applications. What's more, there is a synergy between Ag and TiO_2 at room temperature. Working as an electron receiver, Ag helps to reduce the recombination rate of electron-hole pairs. Ag/TiO_2 materials can receive light energy in both ultraviolet and visible light, optimizing the utilization of solar energy. A large number of studies have shown that silver deposition can effectively improve the photocatalytic of TiO_2 (Zheng et al. 2019, Rana et al. 2016).

MATERIALS AND METHODS

Materials and Reagents

The titanium tetrachloride ($TiCl_4$, 99.5%), nitric acid (HNO_3, 65-68%), and absolute ethanol were purchased from Aladdin Industrial Corporation. The silver nitrate ($AgNO_3$) was obtained from Shanghai Fine Chemical Research Institute.

Preparation of Ag/TiO_2 Cotton Fabric

Add 2 g of $TiCl_4$ into 10 mL absolute ethanol, and mark it as solution A. Add $AgNO_3$ (0%, 2%, 5%, 8%, 10%, 15%) into 40 mL absolute ethanol and altering the pH level to 2, marking it as solution B. Soak the washed cotton cloth into B solution. Lastly, add solution A to B at a slow rate of about 2 sec per drop while constantly stirring the solution. After stirring for about 2 hours, wash the fabric with distilled water and dry it in the oven (60°C, 15 mins).

Characterization of Ag/TiO_2 Cotton Fabric

FTIR was used to detect the chemical groups of unmodified and Ag/TiO_2 cotton fabric in the wavelength range of 500-4000 cm^{-1}. We use TG to analyze the thermal performance and decomposition kinetics. The microstructure and morphology of the prepared fabric were analyzed by SEM.

Photocatalytic Activity of Ag/TiO_2 Cotton Fabric

The photocatalytic activity of Ag/TiO_2 fabric was evaluated by testing the degradation of anionic dye solution as a model pollutant by using UV light. The photocatalytic activity of the Ag/TiO_2 fabric area varies from 15 cm^2 to 35 cm^2. The effect of initial concentration on the photocatalytic activity of the dye solution varies from 5 $mg.L^{-1}$ to 25 $mg.L^{-1}$. The distance of the UV lamp was kept 15 cm above the dye solution. We use the ultraviolet-visible spectrophotometer to measure the absorbance of the solution every 5 minutes.

RESULTS AND DISCUSSION

Morphology of the Fabric

The morphology of the non-modified, pure TiO_2 and 15% Ag/TiO_2 fabric is shown in Fig. 1. The surface of the pure TiO_2 and 15% Ag/TiO_2 composite fabric looked uneven with particles attached, indicating that TiO_2 and Ag were successfully supported on the fabric. The surface agglomeration of

Fig. 1: The morphology of the non-modified (a), pure TiO_2 (b), 15% Ag/TiO_2 (c) fabric.

pure TiO_2 fabric is obvious, which may be because TiO_2 is attracted and then agglomerated by polar groups of cotton fabric. The surface of the Ag/TiO_2 composite fabric also has some pellets. However, compared with pure TiO_2, doping Ag reduced the particle agglomeration and the dispersion degree is higher.

Chemical Structure

In Fig. 2, no new absorption peak appeared in the infrared spectra of a, indicating that Ag-doped would not affect Ti-O bond, O-O bond and Ti-Ti bond in the TiO_2 structure. 3338 cm^{-1} is the stretching vibration peak of O-H on the fabric surface, which confirmed the strong interaction of water molecules on the surface of TiO_2. The peak at 1644 cm^{-1} is caused by the bending vibration of O-H and is due to the absorption of water molecules. The peaks in the range of 526-664 cm^{-1} are caused by the stretching vibration and variable angle vibration of Ti-O. It indicated that Ag/TiO_2 indeed existed on the surface of the fabric. The peak near 2901 cm^{-1} is C-H stretching vibration, and the peak at 1167, 1108, and 1050 cm^{-1} is -C-O-C stretching vibration, which is in line with the characteristic peak of the infrared spectrum of cotton fiber.

Thermo Gravimetric Analysis

Fig. 3 shows the thermogravimetric characterizations of non-modified cotton and 15% Ag/TiO_2 fabric. The results show that the decomposition of 15% Ag/TiO_2 fabric is earlier than unmodified fabric. At room temperature of 275°C, there is dehydration of physically adsorbed water and evaporation of waxes and other small molecules. Between 275°C and 355°C, both of them had a large mass loss, which is caused by the decomposition of fibrous macromolecules of organic matter. It is obvious that the residual value of the weight of unmodified cotton is lower than that of 15% Ag/TiO_2 fabric, which proved that the thermal stability of the modified fabric is improved.

Factors Influencing the Photocatalytic Activity

Effect of Doped Silver Content on Photocatalytic Degradation

Fig. 4 shows that under the same irradiation time, the photocatalytic efficiency of Ag/TiO_2 composite fabric with different silver loads ss improved to different degrees compared with pure TiO_2 fabric. At the same time, Ag increases the content of hydroxyl and O_2, promoting the redox reaction. However, the composite of Ag and TiO_2 has a saturation value. The photocatalytic activity of the fabric peaked when the silver load was 5%. This may be because too much silver forms excessive contact sites. Ag itself constantly accepted electrons, however, it could not transmit electrons to O_2, and its ability to accept holes was constantly enhanced, leading to the combination of electrons and holes captured by Ag (Parastar et al. 2013). Other studies have shown that excessive Ag will cover the surface of TiO_2, resulting in the decrease

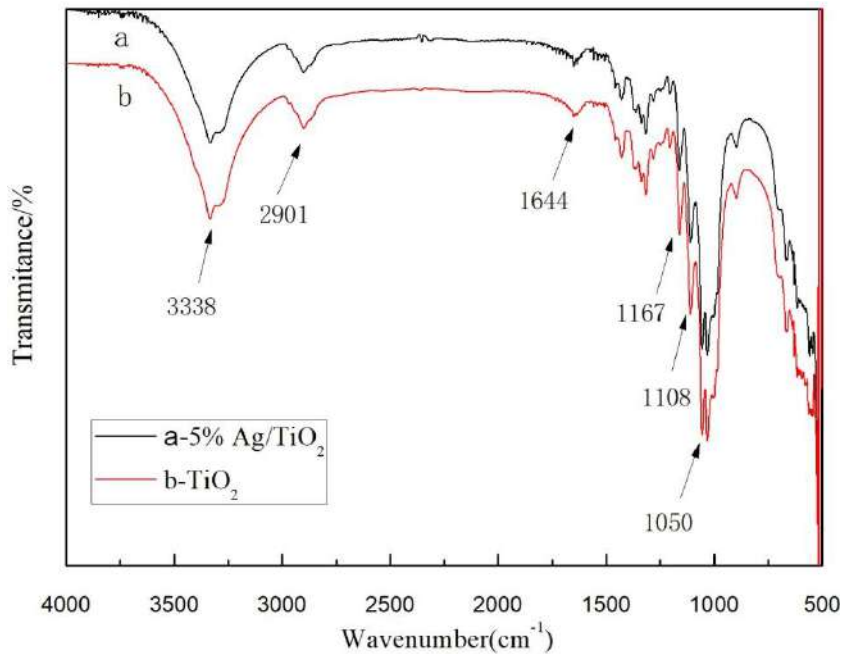

Fig. 2: FTIR spectra of pure TiO_2 and 5% Ag/TiO_2 fabric.

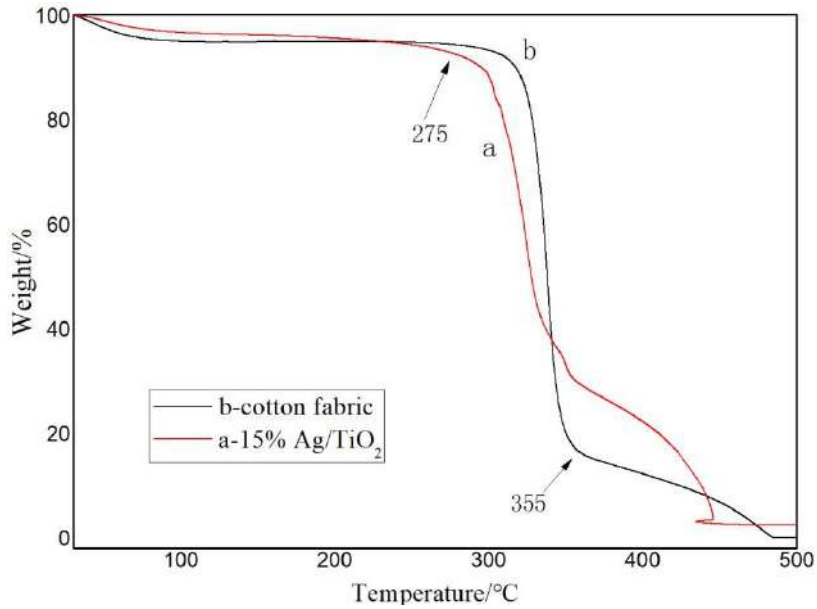

Fig. 3: Thermogravimetric characterizations of 15% Ag/TiO_2 cotton fabric (a) and cotton fabric (b).

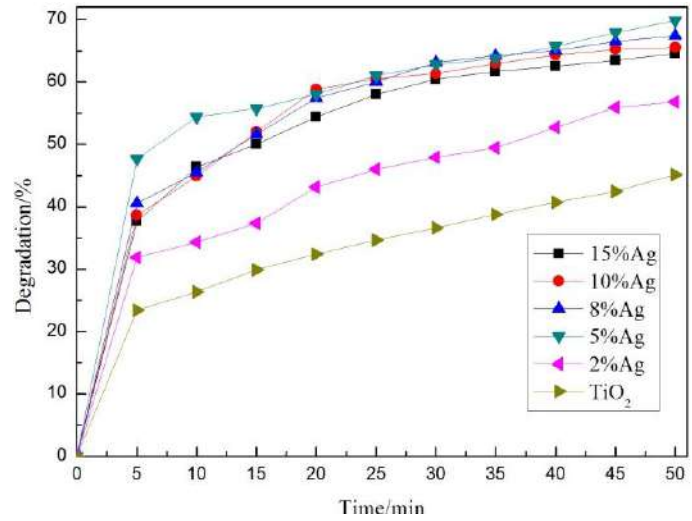

Fig. 4: Effect of doped silver content on photocatalytic degradation.

of hole concentration (Suwarnkar et al. 2014).

Effect of Initial Concentration of Dye on Photocatalytic Degradation

In Fig. 5, the influence of initial dye concentration on photocatalytic degradation is shown. As shown in this figure, when the dye concentration is lower than 15 $mg.L^{-1}$, the degradation rate increase with an increase in the initial concentration. This may be because the degradation process conformed to the first-order reaction kinetics in a certain range of dye concentration. Dye molecules competitively adsorbed on the catalyst surface which accounted for the increase of reaction rate and degradation rate. When the concentration is higher than 15 $mg.L^{-1}$, the initial degradation rate slows down, and the final degradation rate decreases. Excessive dye molecules adsorbed on TiO_2, preventing the reaction of dye molecules with free radicals and electron holes.

Effect of Fabric Area on Photocatalytic Degradation

The effect of fabric area on anionic dye degradation under

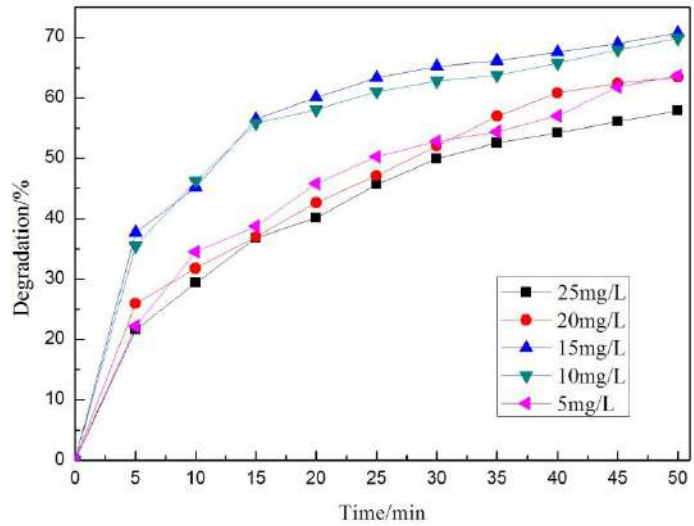

Fig. 5: Effect of initial concentration on photocatalytic degradation.

UV irradiation is shown in Fig. 6. When the fabric area is below 25 cm^2, the initial degradation rate increased rapidly with the increase of fabric area, and the degradation rate was also improved. The increase of fabric area was equivalent to the increase in the amount of catalyst and catalytic active centers. The result is the opposite when the fabric area is larger than 25 cm^2. This may be because when the fabric area is too large, the light transmittance is affected, the light absorption and the O_2 contact of the lower layer are reduced, resulting in the decrease of photocatalytic activity.

Effect of Irradiation Time on Photocatalytic Degradation

Fig. 7 shows the degradation of dye at different irradiation times. With the increase of illumination time, the degradation degree of anionic dyes increased. And the degradation rate of 5% Ag/TiO_2 composite fabric was higher than that of pure TiO_2 fabric, indicating that Ag was an effective catalyst. When the UV light lasted for more than 50 minutes, the degradation rate of the two fabrics no longer significantly increased, indicating the photocatalytic reaction basically approached equilibrium.

Catalytic Mechanism Analysis

The possible catalytic mechanism is shown in Fig. 8. When Ag/TiO_2 is exposed to ultraviolet light (hv > 3.2 eV), electrons are stimulated and transfer from the valence band (VB) to the conduction band (CB), leaving holes in the valence

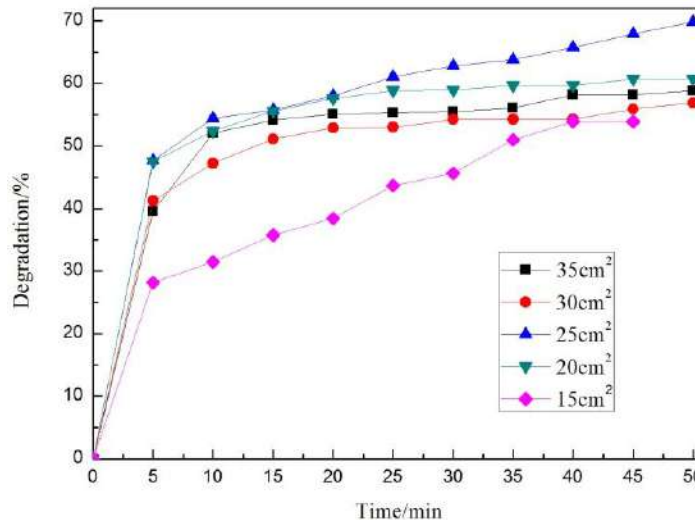

Fig. 6: Effect of fabric area on photocatalytic degradation.

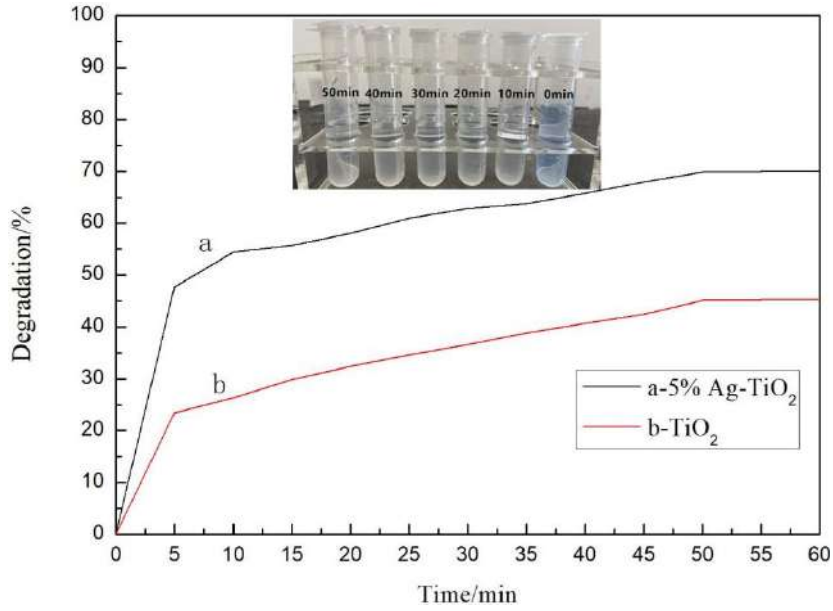

Fig. 7: Effect of irradiation time on photocatalytic degradation.

band. The silver then acts as an electron receiver, capturing electrons from TiO_2 and storing them on its surface. Ag can effectively attract and conduct electrons, and effectively prevent electrons from recombining with holes. The adsorbed oxygen molecules on the silver are quickly captured by electrons, reduced to form superoxide radical (O_2^-), and further react with H^+ to form hydroxyl radical (•OH). On the other hand, the holes of Ag^+ can react with H_2O to form •OH. The e^- and h^+ get more chances to react with O_2 and H_2O. •OH and O_2^- have high oxidation capacity, which can oxidize and degrade organic molecules to H_2O and CO_2. The degradation reactions are shown in the following equations.

CONCLUSIONS

These experiments studied the photocatalytic degradation of anionic dye with Ag-doped TiO_2 cotton fabric (produced by coprecipitation method) under UV irradiation. The effects of Ag-doped, initial concentration, fabric area, and irradiation time were investigated. The experiments confirmed that Ag/TiO_2 was successfully doped on cotton fabric and the photocatalytic property of the modified fabric was improved. In this study, results showed that the optimal silver content doped on TiO_2 was 5%, the fabric area was 25 cm^2, the initial concentration was 15 $mg.L^{-1}$, and the optimal irradiation time

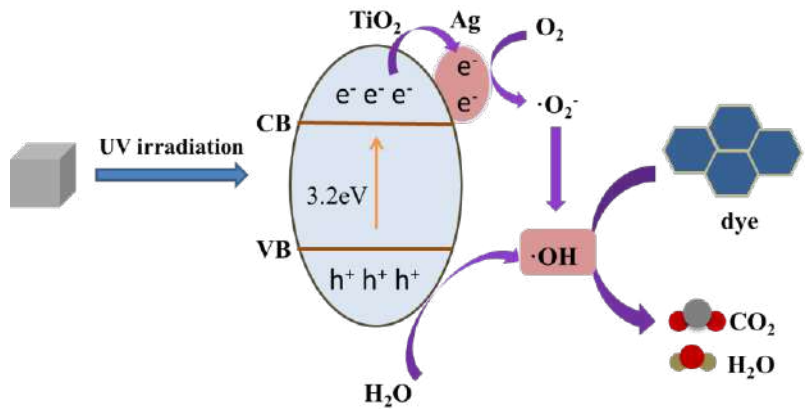

Fig. 8: Catalytic mechanism of Ag/TiO_2.

was 50 mins. Under the best conditions, the degradation rate could reach 70.76%.

ACKNOWLEDGMENTS

The authors gratefully acknowledge the financial support of the National Natural Science Foundation of China (Grant No. 51703130), and the International Science and Technology Cooperation Project of Shaoxing University (Grant No. 2019LGGH1004).

REFERENCES

Anastasi, A., Parato, B., Spina, F., Tigini, V., Prigione, V. and Varse, G.C. 2011. Decolourisation and detoxification in the fungal treatment of textile wastewaters from dyeing processes. N. Biotechnol., 29(1): 38-45.

Banks, D., Jun, B.M., Heo, J., Her, N., Park, C.M. and Yoon, Y. 2020. Selected advanced water treatment technologies for perfluoroalkyl and polyfluoroalkyl substances: A review. Sep. Purif. Technol., 231: 115929

Benz, D., Felter, K.M., Köser, J., Thöming, J., Mul, G. and Grozema, F.C. 2020. Assessing the role of Pt clusters on TiO_2 (P25) on the photocatalytic degradation of Acid Blue 9 and Rhodamine B. J. Phys. Chem., 124(15): 8269-8278.

Farbod, M. and Khademalrasool, M. 2011. Synthesis of TiO_2 nanoparticles by a combined sol-gel ball milling method and investigation of nanoparticle size effect on their photocatalytic activities. Powder Technol., 214(3): 344-348.

Habibi-Yangjeh, A. and Feizpoor, S. 2019. Combination of $NiWO_4$ and polyaniline with TiO_2: Fabrication of ternary photocatalysts with highly visible-light-induced photocatalytic performances. J. Iran. Chem. Soc., 17(2): 351-365.

Holkar, C.R., Jadhav, A.J., Pinjari, D.V., Mahamuni, N.M. and Pandit A.B. 2016. A critical review on textile wastewater treatments: possible approaches. J Environ. Manag., 182: 351-366.

Kaneco, S., Katsumata, H., Suzuki, T. and Ohta, K. 2006. Titanium dioxide mediated photocatalytic degradation of dibutyl phthalate in aqueous solution-kinetics, mineralization, and reaction mechanism. Chem. Eng. J., 125(1): 59-66.

Khan, M.I., Bhatti, K.A., Qindeel, R., Fazale, A., Naeemur, R. and Alonizan, N. 2017. Sol-gel deposition and characterization of multilayer 2% Cu doped TiO_2 nanostructured thin films. J. Mater. Sci. - Mater. Elect., 28(13): 9471-9477.

Kulkarni, R.M., Malladi, R.S., Hanagadakar, M.S., Doddamani, M.R. and Bhat, U.K. 2015. Ag-TiO_2 nanoparticles for photocatalytic degradation of lomefloxacin. Desal. Water Treat., 57(34): 16111-16118.

Li, X., Wu, Y., Shen, Y., Sun, Y., Yang, Y. and Xie, A. 2018. A novel bifunctional Ni-doped TiO_2 inverse opal with enhanced SERS performance and excellent photocatalytic activity. Appl. Surf. Sci., 427: 739-744.

Lu, Y. and Zhao, P., 2018. Preparation of ZnO Nano-photocatalysts and their performance on photocatalytic degradation of coking wastewater. Nat. Environ. Pollut. Technol., 17(3): 953-956.

Lv, J., Su, L., Wang, H., Liu, L., Xu, G. and Wang, D. 2014. Enhanced visible-light photocatalytic activity of TiO_2 nanotube arrays modified with CdSe nanoparticles by electrodeposition method. Surf. Coat. Technol., 242: 20-28.

Ma, H., Zheng, W., Yan, X., Li, S., Zhang, K. and Liu, G. 2020. Polydopamine-induced fabrication of Ag-TiO_2 hollow nanospheres and their application in visible-light photocatalysis. Coll. Surf. A- Physicochem. Eng. Asp., 586.

Parastar, S., Nasseri, S., Borji, S.H., Fazlzadeh, M., Mahvi, A.H. and Javadi, A.H. 2013. Application of Ag-doped TiO_2 nanoparticle prepared by photodeposition method for nitrate photocatalytic removal from aqueous solutions. Desal. Water Treat., 51(37-39): 7137-7144.

Rana, M., Hao, B., Mu, L., Chen, L. and Ma, P.C. 2016. Development of multi-functional cotton fabrics with Ag/AgBr–TiO_2 nanocomposite coating. Comp. Sci. Technol., 122: 104-112.

Riegel, G. and Bolton, J.R. 1995. Photocatalytic efficiency variability in TiO_2 particles. J. Phys. Chem., 99(12): 4215-4224.

Suwarnkar, M.B., Dhabbe, R.S., Kadam, A.N. and Garadkar, K.M. 2014. Enhanced photocatalytic activity of Ag-doped TiO_2 nanoparticles synthesized by a microwave-assisted method. Ceramics International, 40(4): 5489-5496.

Zhao, H., Su, F., Fan, X., Yu, H., Wu, D. and Quan, X. 2012. Graphene-TiO_2 composite photocatalyst with enhanced photocatalytic performance. Chinese J. Catal., 33(4-6): 777-782.

Zhao, L.N., Jia, Y.H., You, H., Wang, S.T. and Fu, L. 2020. Photocatalytic performance and application outlook of 3D TiO_2/titanium mesh modified by GO-Ag joined-deposition. Catal. Today, 340: 106-114.

Zheng, X., Zhang, D., Gao, Y., Wu, Y., Liu, Q. and Zhu, X. 2019. Syntheses and characterization of cubic Ag/TiO_2 nanocomposites for the photocatalytic degradation of methyl orange in aqueous solutions. Inorg. Chem. Comm., 110.

Nature Environment and Pollution Technology
An International Quarterly Scientific Journal

p-ISSN: 0972-6268
(Print copies up to 2016)
e-ISSN: 2395-3454

Vol. 20 | No.3 | pp. 1201-1208 | 2021

Original Research Paper

https://doi.org/10.46488/NEPT.2021.v20i03.028

Open Access Journal

Time Series Analysis of Decadal Precipitation Pattern at Selected Cities of Southern India

T. S. Subbiah*, P. Parthiban*, R. Mahesh* and A. Das*†
*Centre for Environmental Engineering, PRIST Deemed University, Thanjavur, Tamil Nadu, India
†Corresponding author: A. Das; scientists.crd@gmail.com

Nat. Env. & Poll. Tech.
Website: www.neptjournal.com

Received: 24-09-2020
Revised: 26-10-2020
Accepted: 12-11-2020

Key Words:
Time series modeling
Forecasting
ARIMA
Precipitation pattern

ABSTRACT

To characterize and explore the short-term climatic patterns over the last decade (Jan. 2009 to Dec. 2018), the present research has been carried out, involving time series analysis of precipitation pattern in three cities of Tamil Nadu, namely, Thanjavur, Nagapattinam, and Chennai, referring to deltaic, coastal and highly urbanized cities of Tamil Nadu, respectively. The study involves time series empirical analysis, decomposition, exponential smoothing, and various stochastic modeling. Herein, the location-specific suitable models are obtained and specific predictions are being carried out, as well.

INTRODUCTION

Rainfall trends in response to climate change and probability analysis have been studied by various researchers (Jayawardene et al. 2005, Parta & Kahya 2006, Kumar & Singh 2011, Obot et al. 2010, Kumar & Jain 2010, Manikandan & Tamilmani 2012, Manivannan et al. 2016, Mohanty et al. 2000) and they have emphasized that the knowledge of location-specific rainfall variations is essential for proper water harvesting and water management practices.

In India, nearly 65% of the cultivable area is under rainfed agriculture. Rainfall is one of the important factors deciding the success of rainfed agriculture of a particular agro-ecological region where the major part of the precipitation is rainfall, which shows definite changes over time (Banze et al. 2018, Sharma et al. 2018). Kumar and Jain (2010) reported that higher or lower rainfall or changes in rainfall distribution would influence the spatial and temporal distribution of runoff, soil moisture, groundwater storage and would alter the frequency of droughts and floods. While the observed monsoon rainfall at the national level does not show any significant trend, regional monsoon variations have been recorded. An increasing trend of monsoon season rainfall has been found along the west coast, northern Andhra Pradesh, and northwestern India (+10% to +12% of the normal over the last 100 years) while a decreasing trend of monsoon seasonal rainfall has been observed over eastern Madhya Pradesh, North-eastern India and some parts of Gujarat and Kerala (6 to 8% of the normal over the last 100 years) (Kumar & Singh 2011, Singh & Kumar 2016).

In fact, comprehensive knowledge of the trend and persistence in rainfall of the area is of great importance because of the economic implications of rain-sensitive operations (Sharma et al. 2015, Sharma & Dubey 2013, Jakhar et al. 2011). Keeping the above in view, the present study has been conducted to analyze the precipitation pattern of selected study areas and evaluation of various modeling options and predictability.

STUDY AREA

The locations selected for the study are Thanjavur, Nagapattinam and Chennai to have a synoptic coverage of major hydro-lithographic domains namely deltaic and agricultural region, coastal and metropolitical region respectively. The study area lies in the following geocoordinates: $10^{o}45'00''$ N to $10^{o}49'30''$ N, $79^{o}6'00''$ E to $79^{o}10'30''$E; $10^{o}41'32.787''$ N to $10^{o}49'50.541''$ N, $79^{o}49'33.907''$E to 79^{o} $51'13.19''$E and $12^{o}.58'38.203''$ N to $13^{o}8'31.381$ N, $80^{o}14'7.673''$E to $80^{o}18'42.037''$E for Thanjavur, Nagapattinam and Chennai respectively. The base map of the study area is shown in Fig. 1.

The average temperature in Thanjavur is 28.7°C and the precipitation averages 938 mm. The average maximum temperature of Nagapattinam during the summers remains around 35°C. The relative humidity hovers around 60 to 65%.

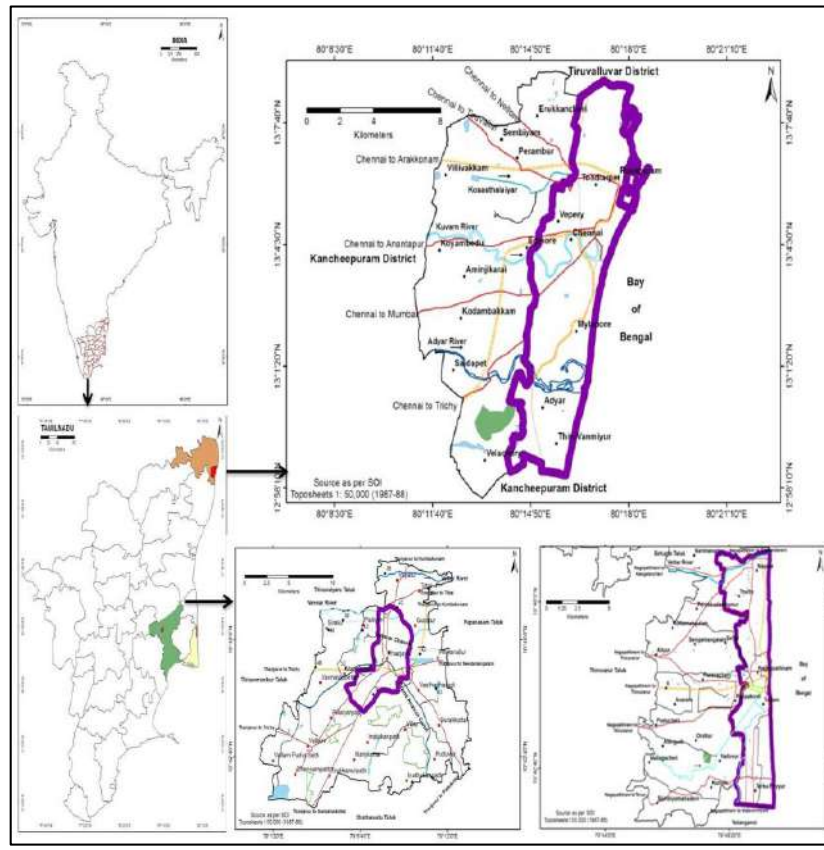

Fig. 1: Location map of the study area.

In Chennai, the average annual temperature is 28.6°C. In a year, precipitation is around 5.43 mm and humidity at 70%.

MATERIALS AND METHODS

General Analyses of Decadal Rainfall Pattern

Monthly rainfall data of 10 years for the period 2009 to 2018 was collected from the meteorological observatory center (IMD) and annual rainfall data was computed from monthly rainfall data. The statistical analysis of rainfall dissimilarity of the study regions (Thanjavur, Nagapattinam, and Chennai) displays a quite good range from 0 to 449.6, 0 to 522.45, and 0 to 780.2 mm respectively with an annual average rainfall value of 60.38, 83.47, and 66.8 mm respectively.

The Descriptive Statistics and Box Whisker Plots of Rainfall Data

Statistical parameters such as mean, median, standard deviation, range, coefficient of variation, skewness, and kurtosis of these rainfalls were also calculated. The trend of annual, seasonal, and monthly rainfall data was calculated using box-whisker plots.

Decomposition of Time Series Data of Study Area

R (Version 1.1.463) was used to carry out the multiplicative decomposition of the time series data in terms of trend, cyclicity, and seasonality. Decompose and forecast functions of the R tool are used to split the time series into seasonality, trend, and error components.

Time Series Modelling

Four standard time series modeling approaches were adopted to explore the frequency domain of the precipitation data, namely:

1. Holt-Winters: The Holt-Winters forecasting algorithm allows users to smooth a time series and use that data to forecast areas of interest.
2. Linear Regression: It is used to predict the value of an outcome variable Y based on one or more input predictor variable (X-variables). The aim is to establish a linear relationship (a mathematical formula) between the predictor variable(s) and the response variable, so that, we can use this formula to estimate the value of the response Y when only the predictors (Xs) values are known.

3. ETS (Error, Trend, and Seasonal): ETS method is an approach method for forecasting time series univariate.
4. ARIMA (Autoregressive Integrated Moving Average): ARIMA is a statistical analysis model that uses time series data to either better understand the data set or to predict future trends.

The Auto-ARIMA algorithm was used to obtain the optimal parameters (p, d & q), rather than using ACF and PACF (plots), manually.

In addition to the standard metrics (namely, mean, standard deviation, and R^2), three other important metrics (viz. AIC (Akaike's Information Criteria), AICc (corrected AIC), and BIC (Bayesian information criteria)) are being employed for model evaluation and selection for ETS and ARIMA, being an unbiased estimate of the model prediction error.

The basic idea of AIC is to penalize the inclusion of additional variables in a model. It adds a penalty that increases the error when including additional terms, thereby discouraging overfitting. The lower the AIC, the better the model (Akaike 1974).

Let k be the number of estimated parameters in the model. Let L be the maximum value of the likelihood function for the model. Then the AIC value of the model is the following.

$$AIC = 2k - \ln(L)$$

AICc is a version of AIC corrected for small sample sizes (Burnham & Anderson 2002), which is defined in terms of the correction term below, where K is the number of parameters and n is the sample size.

$$AICc = AIC + \frac{2k^2 + 2k}{n - k - 1}$$

BIC is a variant of AIC with a stronger penalty for including additional variables in the model.

RESULTS AND DISCUSSION

Time Series Variation of Precipitation Pattern

All three-study area shows a more or less similar pattern of temporal periodicity. The rainfall pattern from 2009-2012 and 2015 shows higher precipitation compared to that during 2013, 2014, 2016, and 2017. The time series of annual rainfall has been presented in Fig. 2.

However, the precipitation in 2018 has been the highest compared to the previous 9 years. Interestingly maximal contribution has been recorded during November 2018 (possibly due to the striking of the Gaja cyclone in November 2018). Among the three study areas, the maximum monthly rainfall had been obtained in Thanjavur during 2009-2014.

As indicated in the summary statistics, Thanjavur experiences the highest mean and median rainfall, compared to the other two study areas (namely, Chennai and Nagapattinam), whereas standard deviation, standard error, and range are the least for Chennai. All the locations show negatively skewed and leptokurtic and positively skewed, the highest being at Nagapattinam. (Table 1).

Monthly Variability of Rainfall Pattern Since Last Decade

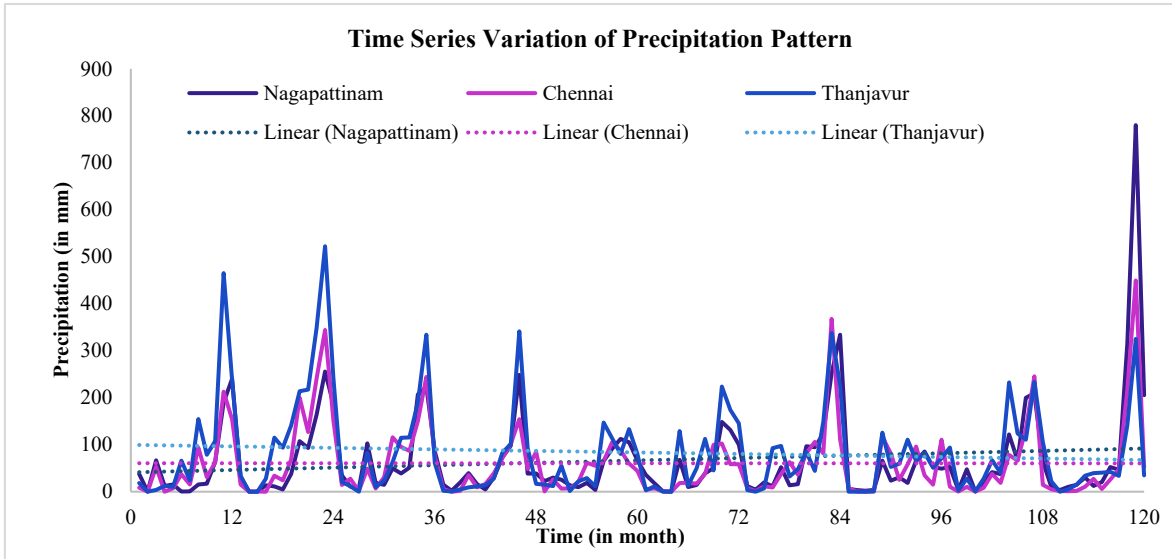

Fig. 2: Time Series Variation of Precipitation Pattern in the Study Area.

This was estimated using box plots (Figs. 3, 4 and 5) and during November-December (NE monsoon), all the places experience the highest rainfall, with another secondary peak during May-June (South-West Monsoon) indicating two distinct monsoon showers contributing the majority of the rainfall.

As evident from box plots, in all three locations, there are two distinct periods of heavy shower primarily during October to December corresponding to Northeast monsoon and secondarily during May to August corresponding to Southwest monsoon. The onset of the southwest monsoon is early in Thanjavur and Nagapattinam (i.e. May) compared to Chennai (i.e. June) and correspondingly its duration is longer in Chennai followed by Nagapattinam and Thanjavur .

The sporadic showers as indicated by the outliers in the box plot is limited from January to June in Thanjavur and Nagapattinam whereas it extended up to August in the case of Chennai. Interestingly in all three locations, the minimum average rainfall as indicated by the first quartile is higher than 20 mm from August to December, the highest minimum being during October to November. Similarly, the highest monthly mean rainfall as indicated by the third quartile is observed during May to December in all the locations with more than 100 mm rainfall.

Table 1: Descriptive statistics.

S. No	Parameters	Chennai	Thanjavur	Nagapattinam
1	Mean	60.387	83.471	66.864
2	Standard Error	7.131	9.102338941	8.905
3	Median	35.055	48.585	36.765
4	Mode	0	0	0
5	Standard Deviation	78.123	99.711	97.559
6	Sample Variance	6103.351	9942.308	9517.834
7	Kurtosis	7.394	4.499	23.807
8	Skewness	2.439	1.979	3.974
9	Range	449.6	522.45	780.16
10	Minimum	0	0	0.04
11	Maximum	449.6	522.45	780.2
12	Sum	7246.45	10016.55	8023.77
13	Confidence Level (95.0%)	14.121	18.023	17.634

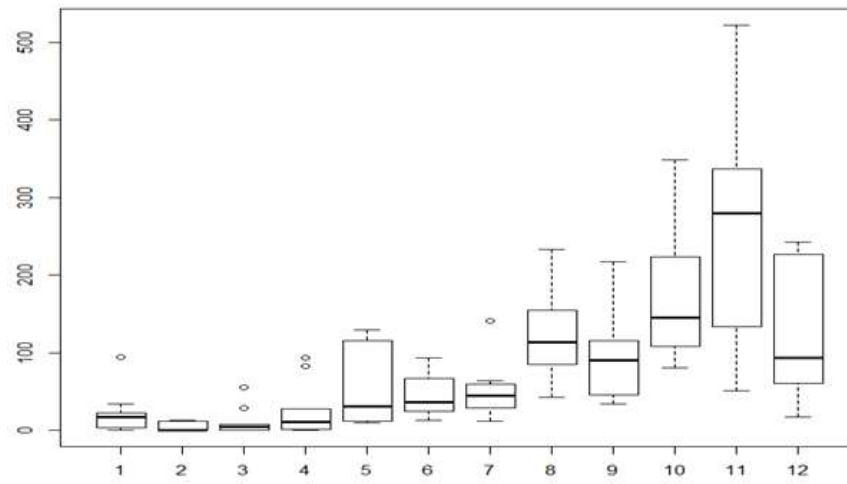

Fig. 3: Box Plots for Monthly Rainfall at Thanjavur from 2009 to 2018.

Decomposition of Multiplicative Series

On the multiplicative decomposition of the time series data of precipitation of study area, although the trend appears to be similar (i.e. primary peak during March) there is a distinct decrease in rainfall over the years compared to 2003 except 2008. In the case of Chennai, however, the magnitude of rainfall during 2008 is much lesser than the other two study areas (Fig. 5)

The seasonality of the rainfall pattern over the years is similar in all three locations in relation to the highest rainfall during November whereas, in the case of Chennai, there are two more peaks which are the secondary and tertiary peaks corresponding to May and August through the decade and only less significant peak in Thanjavur during May. Nagapattinam, shows no distinct secondary and tertiary peaks, indicating uni-model periodicity throughout the years studied.

Time Series Modeling and Forecasting of the Rainfall Data

Various models (namely, Holt-Winters, ETS, Linear Regression, and ARIMA) were attempted to model and forecast rainfall pattern, and ARIMA (0,0,1) was found to be the best model for all three locations for non-seasonal components, as reflected by the least value of error as represented by AIC, although seasonality components do vary.

This means all the time series data of the study area is stationary, as indicated by the integrated parameter zero. Besides, the autoregression of the data series is also zero, thereby establishing the requirement of only first-order moving average-term to model the rainfall data for the whole decade. Thus, the required model (non-seasonal) for forecasting the rainfall data is given by,

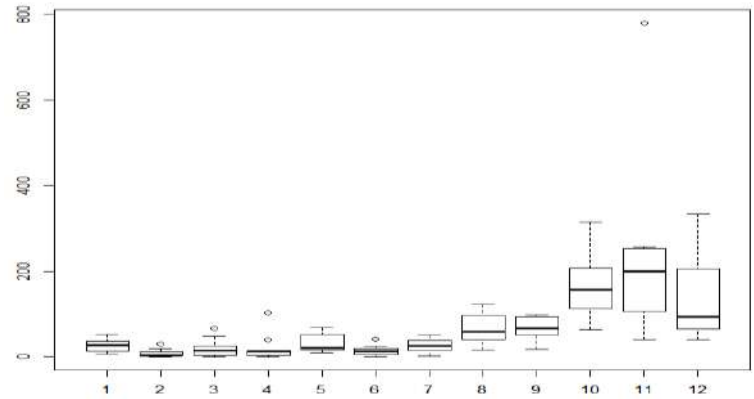

Fig. 4: Box Plots for Monthly Rainfall at Nagapattinam from 2009 to 2018.

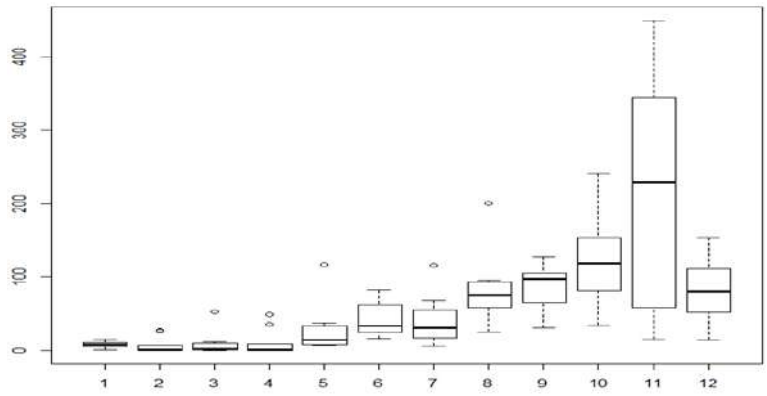

Fig. 5: Box Plots for Monthly Rainfall at Chennai from 2009 to 2018.

$$X_t = \mu + \varepsilon_t + \theta_1 \varepsilon_{t-1}$$

Where μ is the mean of the series, the θ_1 is the coefficient of the model and the εt is white noise error terms. However to be specific, even among the first-order moving average model that satisfies all the three time series data of the precipitation, the complete model, involving the seasonal component as well, for the locations are given by ARIMA (0,0,1) (2,0,0) [12], ARIMA (0,0,1) (0,1,1) [12], and ARIMA (0,0,1) (1,0,0) [12] for Thanjavur, Nagapattinam, and Chennai, respectively. This means, the seasonal component of the locations does show distinct variation in the model, as represented by autoregression of 2nd order for Thanjavur, first-order differentiated and first-order moving average for Nagapattinam, and first-order autoregression for Chennai.

The diagnostics of various models attempted are presented in Table 2, which shows that considering standard error, the most suitable models for Thanjavur is ARIMA followed by ETS, whereas for Chennai, the most suitable models are ETS and Holt-Winters, and for Nagapattinam, Linear Regression and ETS are the most suitable models. Hence ETS and ARIMA are by far the best models for all the three places considered.

CONCLUSIONS

Based on the studies carried out, it is clear that the same seasonality and cyclicity pattern of rainfall of the three distinct study areas has been maintained over time, i.e., heavy shower primarily during October to December corresponding to Northeast monsoon and secondarily during May to August corresponding to Southwest monsoon. However, the onset and duration of the monsoon as well as the magnitude and variability do show distinct variability in these locations, with increasing sporadic variation between January to June, as reflected by the outliers. The time series analysis of precipitation pattern is stationary in all three locations, with the non-seasonal component of the precipitation pattern obeying first-order moving average, whereas the non-seasonal component does show very distinct variation, as observable in the additional secondarily peak in Chennai and tertiary peak in Thanjavur and varying seasonal terms in ARIMA Thanjavur (2,0,0), Nagapattinam (0,0,1) and Chennai (1,0,0). As far as the suitability of the modeling method is concerned, ETS and ARIMA are found to be the best forecasting models for all three locations, as inferred from the diagnostic matrices.

The rainfall pattern over the years is similar in all three locations in relation to the highest rainfall during November whereas in the case of Chennai during May and August through the decade and only less significant in Thanjavur during May. In the case of Nagapattinam, there are no distinct variations indicating uni-model periodicity throughout the years studied. The time series study of the three locations also reveals that the most suitable models for Thanjavur are ARIMA followed by ETS, whereas for Chennai, the most suitable models are ETS and Holt-Winters and for Nagapattinam, Linear Regression and ETS are the most suitable models. Hence ETS and ARIMA are by far the best models for all the three places considered.

Table 2: Diagnostics for Models Used

Model	Locations	Mean	SE	Additional Diagnostics
Holt-Winter	Thanjavur	42.95	3.2145	-
	Nagapattinam	63.45	18.4235	-
	Chennai	58.51	14.2541	-
Linear	Thanjavur	44.62	29.5967	-
	Nagapattinam	72.84	15.6951	-
	Chennai	59.5	19.2205	-
ETS	Thanjavur	61.30	4.3652	σ^2 = 6721, AIC=1599.51, AICC= 1604.13, BIC=1641.32
	Nagapattinam	60.1178	16.3915	σ^2 = 3621,AIC=1431.087, AICC=1435.70,BIC=1472.90
	Chennai	43.2	11.2395	σ^2 = 3256,AIC=1236.02, AICC=1568.65, BIC=1352.91
ARIMA	Thanjavur	46.83	0.2507	σ^2 = 4594,AIC=1235.08 AICC=1235.4, BIC=1245.8
	Nagapattinam	70.54	20.2281	σ^2 = 5671,AIC=1387.63 AICC=1387.28,BIC=1398.43
	Chennai	61.7962	16.9503	σ^2 = 3810,AIC=1341.2, AICC=1341.73, BIC=1355.14

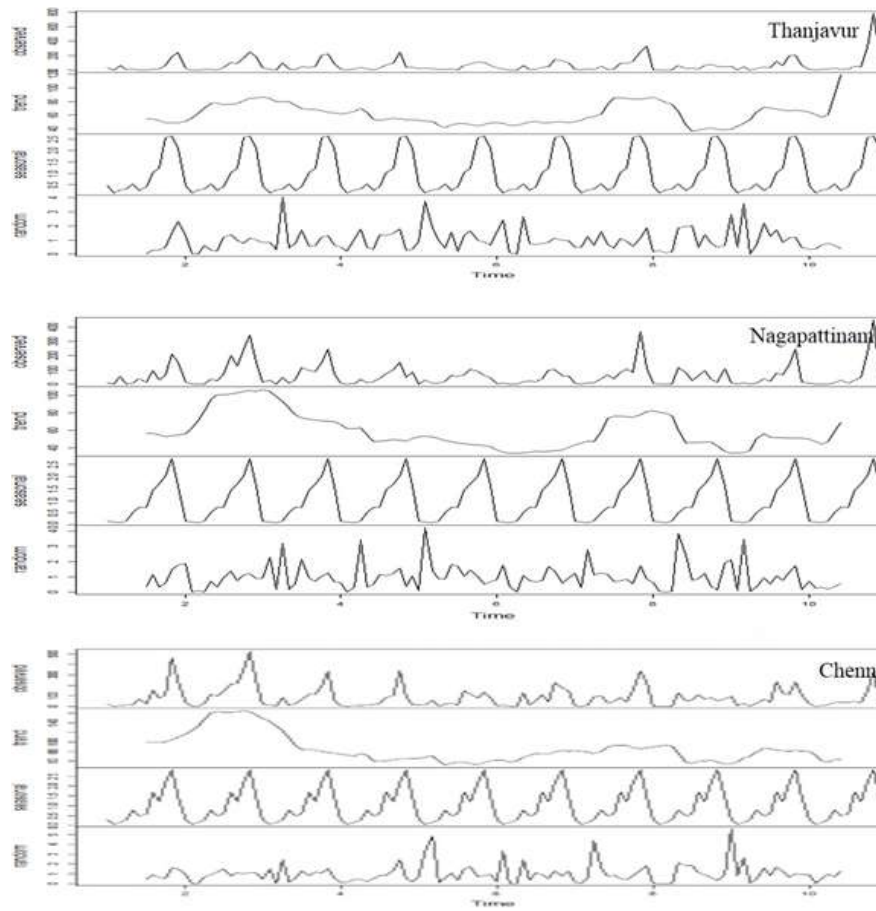

Fig. 6: Decomposition of Multiplicative Series for the Study Area during 2009 to 2018.

ACKNOWLEDGEMENTS

The authors acknowledge Dept. of Science and Technology (DST): SUTRAM FOR EASY WATER (DST/TM/WTI/WIC/2K17/82(G)) and Indian Space Research Organization (ISRO): (ISRO/RES/4/684/19-20) for financial support for carrying out this research.

REFERENCES

Akaike, H. 1974. A new look at the statistical model identification. IEEE Trans. Automat. Contr., 19(6): 716-723. doi:10.1109/TAC.1974.1100705, MR 0423716.

Banze, F., Guo, J. and Xiaotao, S. 2018. Impact of climate change on precipitation in Zambeze river basin in Southern Africa. Nat. Env. and Pol. Tech., 17(4): 1093-1103.

Burnham, K.P. and Anderson, D.R. 2002. Model Selection and Multimodel Inference: A Practical Information-Theoretic Approach (2nd ed.). Springer-Verlag, Berlin/Heidelberg, Germany.

Jakhar, P., Gowda, H.C.H., Naik, B.S. and Barman, D. 2011. Probability analysis of rainfall characteristics of Semiliguda in Koraput, Orissa. Indian. J. Soil Cons., 39(1): 9-13.

Jayawardene, H.K.W.I., Sonnadar, D.U.J. and Jayawardene, D.R., 2005. Trends of rainfall in Sri Lanka over the last century. Sri Lanka J. Phy., 6: 7-17.

Kumar, C.P. and Singh, S. 2011. Impact of climatic on water resources and national water mission of India. In: National seminar on global warming and its impact on water resources held on 14th January, 2011 at Kolkata (West Bengal).

Kumar, V. and Jain, S.K. 2010. Rainfall trends in Ganga-Brahmputra-Meghna river basins of India. J. Hydrol., 33: 59-66.

Manikandan, M. and Tamilmani, D. 2012. Statistical analysis of special pattern of rainfall trends in Parambikualam Aliyar subbasin, Tamilnadu. Indian. Water Resour. Soc., 32(1-2): 40-49.

Manivannan, S., Khola, O.P.S. and Dinesh, D. 2016. Probability analysis of weekly rainfall for crop planning in Nilgiris hills of Tamil Nadu. J. Agromet., 18(1): 163-164.

Mohanty, S., Marathe, R.A. and Singh, S. 2000. Probability models for prediction of annual maximum daily rainfall for Nagpur. J. Soil Water Cons., 44(1-2): 38-40.

Obot, N.I., Chendo, M.A.C., Udo, S.O. and Ewona, I.O. 2010. Evaluation of rainfall trends in Nigeria for 30 years. Int. J. Phys. Sci., 5(14): 2217-2222.

Parta, T. and Kahya, E. 2006. Trend analysis in Turkish precipitation data. Hydrol. Process, 20: 2011-2026.

Sharma, K.K. and Dubey, S.K. 2013. Probability analysis of rainfall for planning water harvesting and irrigation in semi-arid region of Uttar Pradesh. Indian. J. of Soil Cons., 41(1): 14-19.

Sharma, K.K., Singh, A.K. and Dubey, S.K. 2015. Analysis of one-day probable maximum precipitation for designing soil and water conservation structures in Agra, U. P. J. Agromet., 17(2): 268-270.

Sharma, K.K., Singh, A.K., and Dubey, S.K. 2018. Rainfall trend analysis for crop planning under rainfed conditions in district Agra of Uttar Pradesh. Mausam, 69(4): 599-606.

Singh, S. and Kumar, S. 2016. Trend analysis of rainfall of Sagar district, Madhya Pradesh. Indian. J. of Soil Cons., 44(1): 44-49.

Nature Environment and Pollution Technology
An International Quarterly Scientific Journal

p-ISSN: 0972-6268
(Print copies up to 2016)
e-ISSN: 2395-3454

Vol. 20 | No.3 | pp. 1209-1216 | 2021

Original Research Paper

https://doi.org/10.46488/NEPT.2021.v20i03.029

Open Access Journal

Analysis on Pollution Hazards and Recycling Strategies of Logistics Packaging Wastes of E-Commerce Enterprises

Zhongchao Hao
Department of Information Engineering, Changzhou Institute of Industry Technology, Changzhou 213164, China
†Corresponding author: Zhongchao Hao; haozc@ciit.edu.cn

Nat. Env. & Poll. Tech.
Website: www.neptjournal.com

Received: 16-04-2021
Revised: 19-06-2021
Accepted: 28-06-2021

Key Words:
E-commerce enterprise
Logistics wastes
Package pollution
Recycling strategies
SEM

ABSTRACT

The emergence of China's e-commerce industry leads to the rapid expansion of the express delivery industry, and the environmental pollution problem triggered by the express packaging wastes has become increasingly critical, severely impacting human health and sustainable social development. The literature regarding the pollution and recycling strategies of e-commerce logistics packaging wastes was first complied with and summarized in this work. Then, the research hypothesis of multi-subject (e-commerce enterprise, government, and third-party enterprises) in the recycling of e-commerce logistics packaging wastes was established. Finally, the effect of multi-subject participation in the recycling of e-logistics packaging wastes was surveyed via questionnaires using structural equation modeling. Results demonstrate that under the background of high-speed e-commerce development, the package pollution problem has become an important problem influencing environmental pollution in various countries across the world. The overall Cronbach's alpha value of the questionnaires was 0.903, indicating good reliability. The observable variable- standard factor loading coefficient, was always greater than 0.5, indicating that the construct validity was accurate. Third-party and e-commerce enterprises played a significant positive role in the recycling effect of e-commerce logistics packaging wastes, with regression coefficients of 1.981 and 0.575, respectively. The government did not show any obvious influence on the recycling effect of e-commerce logistics packaging wastes. The pollution hazards of logistics packaging wastes of e-commerce enterprises can be effectively mitigated if e-commerce enterprises lead the green consumption needs, the government accelerates the perfection of laws and regulations related to the e-commerce logistics packaging, and a third-party professional recycling system is established, among others things. The study results will be of great reference significance for deeply analyzing the problems existing in the current express package pollution control and their causes, exploring the factors influencing the recycling effect of e-commerce logistics packaging wastes and enriching the multi-subject recycling strategies for express package pollution.

INTRODUCTION

With the popularization and rapid development of the internet, the emerging consumption model-online shopping has been increasingly favored and gradually become an important constituent part of people's daily life. Fig. 1 shows that China's express business volume in 2010 reached 2,340,000,000, and the expression business income was RMB 57,460,000,000. The express business volume is increasing in consecutive years owing to the growing popularity of online shopping. Up to 2019, the express business volume was 63,520,000,000, and the expression business income was RMB 749,780,000,000, which increased by 27.15 and 13.05 times, respectively. However, behind the prosperous development of the express delivery industry is the great demand for express packaging materials, which, in China, mainly include plastic bags, woven bags, express waybills, packaging boxes, packaging tapes, envelopes, and internal fillers. These packaging materials will result in certain environmental problems in the manufacturing and terminal treatment links. Most express packages are disposable, meaning that they will no longer serve as packaging ones after the express transportation is completed and will become packaging wastes without use-value.

In certain big cities in China, the increment in express packaging wastes already accounts for the vast majority of the increase in household wastes. The recycling rate of express packaging wastes is lower than the massive express packaging wastes. The overall recycling rate of express packaging wastes is low in China. Given that the proportion of green packaging materials currently used in the express delivery industry is low, most plastic bags and scotch tapes are non-degradable materials made of polyvinyl chloride (PVC), which, if arbitrarily discarded, will pollute the environment.

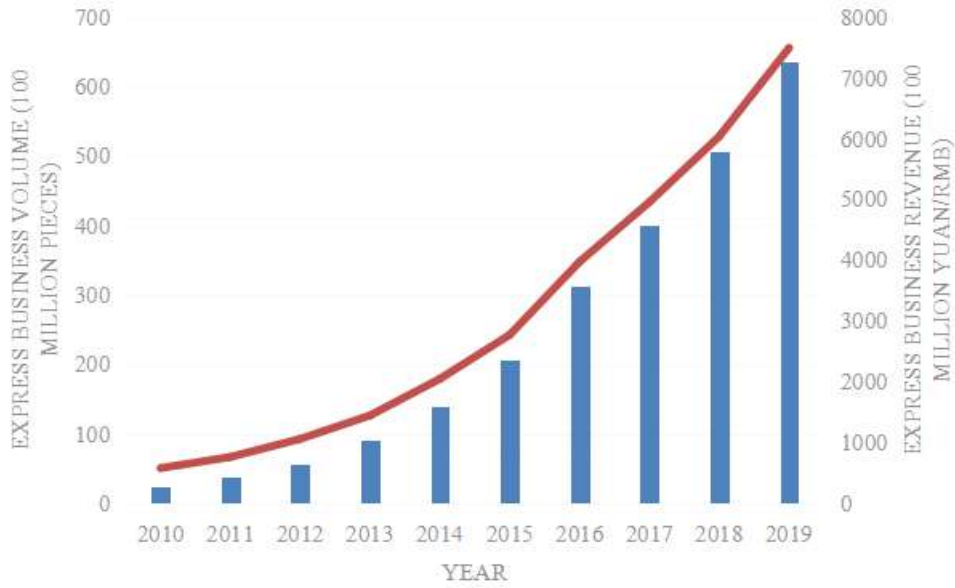

Fig. 1: China's express business volumes and incomes during 2010–2019.
(Data derived from Report on China Express Development Index [2020])

The express packages are faced with recycling difficulty, and a considerable number of packages are directly burnt or landfilled without the recycling link, leading to serious environmental pollution. In the era featured by the rapid development of online shopping and express delivery industry, the pollution hazards of express packages must be analyzed, and the multi-subject recycling strategies for the e-commerce express packaging wastes must be systematically explored.

OVERVIEW OF THE STUDY AREA

The environmental destruction and waste of resources, which are induced by express packages, have become more serious with the rapid increase in the express business volume in China. The multi-subject recycling strategy for express packages has become a resource, environmental protection and social problem to be solved urgently. The recycling strategy, logistics pattern, and package design have been mainly analyzed with respect to the recycling of e-commerce logistics wastes. Bamberg (2003) analyzed the decisions of students with high and weak environmental awareness in applying for the information manual of green electronic products. The author stated that the recycling willingness was affected by the richness level of environmental knowledge. Robinson et al. (2005) surveyed two large families, namely, Royal Kensington and Chelsea in Great London, and pointed out that the large-scale propaganda of environmental protection could effectively improve the recycling effect; more residents were required to trust in the necessity of garbage recycling. Kelly et al. (2006) surveyed 1400 students and staff in Massey University, New Zealand and stated that the recycling behavior was significantly correlated with two factors: attitude toward recycling and occupational identity. Feng et al. (2006) studied two problems: design and coordination of reverse supply chain, traditional channel, and online recycling channel. The results showed that from the perspective of the recyclable distributor and system, the performance of the double-loop channel was always superior to that of the single-loop channel. Knussen et al. (2008) conducted a questionnaire survey on 252 participants from Scotland, Britain and thought that both past behaviors and lack of habit significantly contributed to the diversity in recycling willingness. Lin et al. (2009) used the analytical hierarchy process to analyze the consumer willingness to recycle discarded home appliances and proposed measures that could strengthen consumer willingness to take a part in e-waste recycling. Veiga (2013) analyzed the effect of compulsory waste control and recycling policy in Brazil; The results manifested that the reverse logistics project achieved an overall success, but its efficiency was not high for small-sized rural communities. Wang et al. (2016) explored the factors deciding the residential e-waste recycling behavioral intention in China; the author stated that the cognition of informal recycling influenced residential behavioral intention, and

the standardization and propaganda had positive influences on the cognition of informal recycling. Yamaguchi et al. (2016) used the contingent value method to assess consumer preferences for low-quality packaging. The results showed that economic means could influence consumers to purchase products with simplified packages because high disposal costs reduced the attraction of product sources. Klaiman et al. (2016) assessed the consumer willingness to pay (WTP) for packaging materials and recoverability of beverages via a discrete choice experiment. The results showed that the packaging materials enjoying the maximum consumer WTP were the plastic package, followed by glass, carton, and aluminum. Bai et al. (2018) explored the pattern and trend of recycling attitudes and behaviors of Chinese consumers and pointed out that economic incentive, recycling convenience, and information security were the primary requirements of consumers for recycling smartphones. From the perspective of university green education, Yu et al. (2019) corrected and verified the citizens' pro-environmental behavioral model and stated that green education could improve citizens' environmental awareness and generate the intentions of environmental sustainability and cyclic utilization. Taking Hangzhou City, for example, Pei (2019) discovered that the neighborhood relationship and community attachment generated direct positive influences on residents' willingness to recycle wastes. Arain et al.(2020) deemed that America lacked a set of unified e-waste recycling methods, which led to a low e-waste recycling rate among consumers and evaluated the influences of consumer behaviors on e-waste recycling. The results showed that the primary factors influencing consumer decisions are consumers' poor understanding of products and disposal sites and uneasy acquisition of recycling facilities within a reasonable distance. Aboelmaged (2020) believed that young consumers played an important role in the generation of e-waste problems and used the partial least squares SEM to perform a multivariate statistical analysis of survey data. The survey results showed that the recycling habit and consciousness generated significant effects on young people's willingness to recycle e-waste. Existing research literature has shown that the express package pollution problem under the rapid development of e-commerce has raised wide concern in domestic and foreign academic circles. However, the recycling strategies for express packaging wastes have been less involved, and the few studies regarding this have not been systematic and deep enough. The SEM was used in this study to empirically study the effect of multi-subject participation in express package recycling by analyzing the pollution hazards of e-commerce express packages. The corresponding countermeasures were proposed from the angle of e-commerce logistics wastes to provide a certain reference for the practice of express package pollution control under the high-speed e-commerce development in China.

POLLUTION HAZARDS OF E-COMMERCE PACKAGING WASTES

Water Pollution Caused by Package Production

Express package pollution mainly refers to the pollution generated in the manufacturing and terminal treatment process of express packaging materials. In daily life, express packaging bags are mostly processed from domestic and chemical wastes, which may contain a large quantity of residues of toxic and harmful substances. During the recycling, the raw wastes should be first washed, while most reprocessed plastic enterprises are family workshop-style small enterprises with incomplete pollution discharge equipment and arbitrary sewage discharge, thus leading to water resource pollution.

Waste Pollution Caused by the Package Treatment Link

In China's express delivery industry, the overall recycling rate of package wastes is low, and plastic bags and scotch tapes are mostly non-degradable packaging materials made of PVC, which is mainly disposed of through landfills or burning. However, the waste PVC, if buried in soil, can be completely degraded only after 100 years, which will result in soil hardening and reduce the nutrient substances in soil, thus impeding the plant growth. The degraded plastic packages will also enter the groundwater system by forming tiny plastic particles, intrude into the food chain of human beings, and harm human health. When these degraded packages are inappropriately burnt, solid-state pollution will be transformed into gaseous-state pollution or pollution in other forms and continue to pollute the environment.

MODEL PROFILE AND HYPOTHESIS SETTING

Structural Equation Modeling (SEM)

The structural equation reflecting the causal relationship between the measurable variable and latent variable was established according to SEM. This equation consists of two parts: measurement and structural equations. The specific model can be expressed as follows:

Measurement equation: $X=\Lambda_x\xi+\delta, Y=\Lambda_y\eta+\varepsilon$ …(1)

Structural equation: $\eta=\gamma\xi+\beta\eta+\zeta$ …(2)

where X is the vector consisting of exogenous indexes; Y denotes the vector composed of endogenous indexes; δ and ε represent the measurement errors of X and Y, respectively; Λ_x expresses the relationship between the index X and latent variable ξ; Λ_y is the relationship between the

index Y and latent variable η; ξ and η stand for exogenous and endogenous latent variables, respectively; γ and β are the structural coefficient matrixes that reflect the interaction between exogenous ξ and endogenous η latent variables; and ζ is the residual error term.

Hypothesis Setting

According to the research results of several scholars worldwide, the multiple subjects that participate in the recycling of express packages were defined as e-commerce and third-party recycling enterprises. The recycling effect was taken as a dependent variable, and the hypotheses were made, as illustrated in Table 1.

EMPIRICAL STUDY

Reliability and Validity Analysis of Samples

The questionnaire respondents were managers of micro, small, and medium-sized e-commerce enterprises, government officials from the e-commerce and environmental protection department, and managers from third-party professional garbage recycling institutions. The investigation was conducted by combining interviews and questionnaires. The questionnaires were distributed online and offline. A total of 394 questionnaires were recovered, where 362 were valid questionnaires, and the effective recycling rate was 91.9%. The reliability analysis was performed for the 11 observable variables of four latent variables-recycling by e-commerce enterprises, government recycling, third-party recycling, and recycling effect-via statistical software SPSS22.0 to further confirm the reliability and validity of questionnaires (Table 2). The overall Cronbach's *a* value of the questionnaires was 0.903, and those of the four latent variables were 0.702, 0.614, 0.677, and 0.500, respectively, indicating favorable consistency of measurement indexes and strong questionnaire homogeneity. Meanwhile, the standard factor loading coefficients of all observable variables were greater than 0.5, manifesting a good construct validity of each latent variable (Table 3).

Exploratory Factor Analysis

First, the correlation coefficient matrix of the observable variables in the structural equation was calculated. The results showed that most correlation coefficient values exceeded the critical value (0.396). Second, the KMO sample measurement and Bartlett spherical test analysis were conducted for the survey data via SPSS22.0. According to the results, the

Table 1: Hypothesis setting for the effect of multi-subject participation in the recycling of express packages

Code number	Content
H1	Recycling of express package wastes by e-commerce enterprises has a significant positive influence on the recycling effect.
H2	The government recycling of express package wastes generates a remarkable positive influence on the recycling effect.
H3	The recycling effect is positively influenced at a significant level by the participation of third-party enterprises in the recycling of express package wastes.

Table 2: Sample reliability and validity and factor analytical results.

Latent variable	Latent variable number	Observable variable	Observable variable number	Standard factor load	Cronbach's *a*	
E-commerce enterprise recycling	Factor1	Sense of responsibility	A1	0.700	0.702	0.903
		Corporate culture	A2	0.744		
		Regional policy	A3	0.675		
Government recycling	Factor2	Tax relief	B1	0.734	0.614	
		Low-interest loan	B2	0.448		
		Financial assistance	B3	0.771		
Third party recycling	Factor3	Online store layout	C1	0.739	0.677	
		Supply system	C2	0.761		
		Working capital	C3	0.598		
Recycling effect	Factor4	Recovery quantity	D1	0.848	0.500	
		Secondary utilization rate	D2	0.843		

Table 3: Estimated value of the residual error term.

Item	Nonstandard estimation coefficient	Standard error	z	p
Factor1	0.473	0.063	7.466	0.000
Factor2	0.732	0.085	8.640	0.000
Factor3	0.653	0.075	8.667	0.000
a1	0.433	0.039	11.000	0.000
a2	0.418	0.041	10.078	0.000
a3	0.571	0.054	10.539	0.000
b1	0.418	0.042	9.855	0.000
b2	0.777	0.061	12.751	0.000
b3	0.500	0.052	9.694	0.000
c1	0.391	0.037	10.642	0.000
c2	0.744	0.062	12.039	0.000
c3	0.549	0.047	11.718	0.000
d1	0.470	0.047	9.994	0.000
d2	0.229	0.039	5.867	0.000

KMO value was 0.90, which is greater than the critical value (0.7). Meanwhile, the *X* value of the Bartlett spherical test was 2300.781 (P<0.001). Therefore, the survey data were of high correlation, indicating that they are suitable for the factor analysis.

Result Analysis

The path coefficient of SEM was calculated through Stata16.0, and the relationship between latent variables and that between latent and observable variables are illustrated in Table 4. When the e-commerce enterprises participated in the recycling, the standardized path coefficient value was 0.575. This path presented a significance level of 0.05 (z=2.041, p=0.041<0.05), indicating that the participation of e-commerce enterprises generated a significant positive influence on the recycling of e-commerce logistics package wastes. Government and third-party recycling generated remarkable negative and positive influences on the recycling effect, respectively.

Fig. 2 shows that the proposed H1 and H3 held true, while H2 did not.

(1) Hypothesis H1 was true. This study verified that the participation of e-commerce enterprises could exert an apparent positive influence on the recycling of e-commerce logistics package wastes, which was largely consistent with most previous research conclusions. E-commerce enterprises are the direct participators in the recycling of express packages. Consumers and e-commerce enterprises should be informed about logistics package recycling through a variety of channels to elicit a high level of interest and ensure express packages recycling is carried out in a timely and orderly manner. The recycling concept of express packages should be actively promoted through various channels, such as networks and news media, to raise environmental awareness among e-commerce enterprises and establish the foundation for express package recycling. E-commerce enterprises should take full utilization of online channels to recycle express packages, develop an online appointment platform, and collaborate with logistics companies in the offline collection of goods to improve the ease of recycling channels and encourage recycling behaviors.

(2) Hypothesis H2 was not true. This study verified that the government participation in the recycling of e-commerce logistics package wastes did not generate any practical effect, indicating that no actual recycling effect was achieved when the government served as a market subject in the recycling of logistics package wastes. To figure out the reason behind

Table 4: Model regression coefficient.

X	->	Y	Standardization coefficient	SE	z	p
Factor1	->	Factor4	0.575	0.282	2.041	0.041
Factor2	->	Factor4	−1.46	0.654	−2.233	0.026
Factor3	->	Factor4	1.981	0.657	3.016	0.003

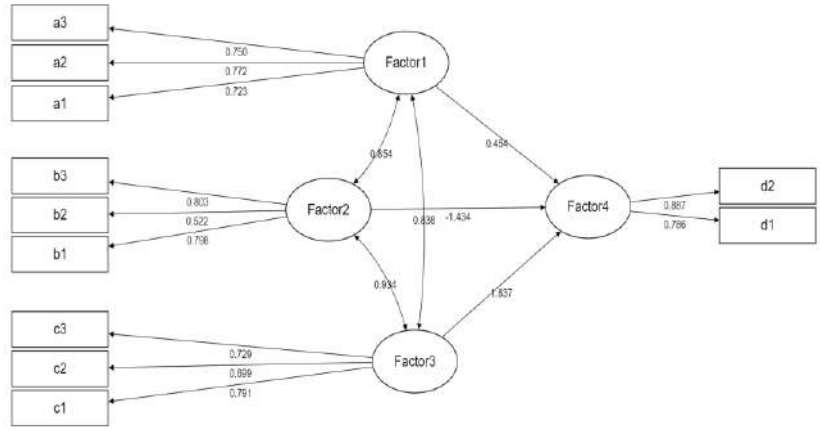

Fig. 2: Graphical SEM result.

this situation, given that the existing e-commerce enterprises are primarily concerned with the development of e-commerce platforms, basic government economic policies and self-recycling fail to completely draw the e-commerce enterprises' attention. Although the government establishes up e-commerce waste recycling platforms and provides subsidies for the recycling of e-commerce logistics packages and to enterprises for their door-to-door recycling, these measures are insufficient to encourage e-commerce enterprises to participate more actively in the recycling of logistics package wastes. At present, only a few recycling sites of e-commerce logistics package wastes can be found in many Chinese cities, all of which have poor accessibility, and residents cannot conveniently participate in the recycling process. Accordingly, it is not realistic for the government to actively undertake the subject responsibility for e-commerce waste recycling.

(3) H3: Third-party enterprises play a significant positive role in the recycling of e-commerce logistics package wastes, and the recycling effect is stronger than that achieved by e-commerce enterprises. If consumers can initiatively send the package wastes to third-party recycling sites on their own initiative, or if third-party recycling sites assign personnel to provide paid door-to-door service for the waste collection, then the recycled express package wastes will be classified by the recycling sites and differently disposed of according to the classification result. The packages that can be repeatedly used will be returned to the express companies. Those packages that can be reused after processing and treatment will be sent to the package production enterprises. The unrecyclable packages will be sent to third-party waste disposal companies for landfilling or burning. Therefore, the express package recycling systems established by third-party professional waste recycling enterprises may fully utilize their professional expertise and enable garbage disposal to reach a professional level.

POLICY SUGGESTIONS

E-Commerce Enterprises Should Guide the Green Consumption Needs and Realize the Environmental Protection of Source Package

E-commerce platforms can guide merchants to use environmentally friendly express packages through the rule negotiation or reward and punishment measures and further promote environmentally friendly e-commerce packaging. Furthermore, these platforms can provide suitable preferential treatment in settlement expense or transaction commission and impose certain punishments on merchants that do not use green packages. Besides guiding the green consumption needs of merchants, consumers' green consumption needs can also be led through some marketing means. E-commerce enterprises encourage consumers to initiatively select green packages by increasing the credit points and endowing coupons, and they can also enhance the propaganda of such marketing activities. Meanwhile, the R&D of package production enterprises should be strengthened to increase the green supply of express packages. The package production enterprises, which are important subjects in the express package pollution control, should strengthen the sense of responsibility and concept of green development among the subjects and actively implement national rules and standards regarding the green package. Moreover, these enterprises should comprehensively assess the environmental protection property of express packaging supplies in the whole cycle, such as the source of raw materials, package production, and waste recycling. Finally, such enterprises should give full play to their guiding role in advocating rational consumption and promoting green packages.

The Government Should Perfect the Related Laws and Regulations to Standardize Enterprises' Recycling Behaviors. The package recycling problem faced by express enterprises is a significant problem of structural optimization and transformation of the express delivery express. The Chinese government should attach importance to the overall regulation of the express delivery industry, perfect the corresponding laws and regulations with respect to the package problem, improve the utilization efficiency of express resources, and facilitate the progress and development of the express delivery industry. Related departments should promulgate express package recycling laws and form a complete normative system to ensure that the express packaging and delivery industries have laws to abide by during the operation period. When guiding and standardizing the existing express business, the government should provide supplementary explanations about the package production, use, and recycling and urge the express delivery industry to perform according to related stipulations. The government sectors should give preferential tax policies to enterprises specialized in waste recycling, develop green loan channels, enact related documents, and provide subsidies. The related government sectors should provide financial and policy support to some express package recycling enterprises to encourage their development.

Establish A Third-Party Professional Recycling System and Increase the Technology Content of Recycling Work

To improve the recycling efficiency of express packages, e-commerce enterprises should establish a professional recycling system to cover core links, such as production, recycling, and use, and realize the whole process real-time monitoring of express packaging and recycling work. Related administrative departments should unite core enterprises in the industrial chain, such as express and package production enterprises, to establish a complete recycling system and fulfil enterprise obligations. Manufacturers, users, consumers, and government administrative departments are required to undertake joint responsibilities. The professional express package recycling system should cover all persons of interest during the use period of packaging materials. After the express package system is perfected, the express enterprises can systematically carry out the express package recycling work. The recycling organizations should conduct the recycling work reasonably according to the recycling labels specified on the packaged articles. Taking package recycling into account, enterprises producing cartons should reduce the product breakage rate in the follow-up use, properly improve the carton design, and enhance the compressive strength. Packaging tapes should not be excessively used to intertwine the expressages because they make the unboxing process extremely inconvenient and result in environmental pollution.

CONCLUSIONS

China's online shopping has entered an omni-channel period, and the express delivery industry is also developed at full speed. With the high-speed growth of express business volume, the environmental destruction and waste of resources triggered by express packages have become increasingly serious, and the recycling of express packages has become a resource, environmental and social problem that remains to be urgently solved. The research hypotheses were established for the multi-subject (e-commerce enterprise, government, and third-party enterprise) participation in the recycling of e-commerce logistics package wastes. The SEM was used to empirically study the recycling effect of e-logistics package wastes with multi-subject participation. The results showed that the overall Cronbach's alpha value of the questionnaire was 0.903, indicating good reliability. The standard factor loading coefficients of all observable variables were greater than 0.5, manifesting satisfactory construct validity. Third-party and e-commerce enterprises generated significant positive influences on the recycling effect of e-commerce logistics package wastes, with the regression coefficients of 1.981 and 0.575, respectively. However, the recycling effect was not affected by the government participation. The policy suggestions for the multi-subject governance and control of e-commerce logistics package wastes include the following: The e-commerce enterprises should guide the green consumption needs, and the government should perfect the related laws and regulations of e-commerce logistics packages and establish a third-party professional recycling system. This study suggests that the multi-subject governance pattern of express package pollution, public participation mechanism in the field of express package pollution control, and double-track system construction for professional express package recycling should be deeply explored.

ACKNOWLEDGMENTS

This study was sponsored by Changzhou Science and Technology Project(No. CR20202010).

REFERENCES

Aboelmaged, M. 2021. E-waste recycling behaviour: An integration of recycling habits into the theory of planned behaviour. Journal of Cleaner Production, 278: 124182.

Arain, A. L., Pummill, R., Adu-Brimpong, J., Becker, S., Green, M., Ilardi, M. and Neitzel, R. L. 2020. Analysis of e-waste recycling behavior based on survey at a Midwestern US University. Waste Management, 105: 119-127.

Bai, H., Wang, J. and Zeng, A. Z. 2018. Exploring Chinese consumers' attitude and behavior toward smartphone recycling. Journal of Cleaner Production, 188, 227-236.

Bamberg, S. 2003. How does environmental concern influence specific environmentally related behaviors? A new answer to an old question. Journal of Environmental Psychology, 23(1): 21-32.

Feng, L., Govindan, K. and Li, C. 2017. Strategic planning: Design and coordination for dual-recycling channel reverse supply chain considering consumer behavior. European Journal of Operational Research, 260(2): 601-612.

Kelly, T. C., Mason, I. G., Leiss, M. W. and Ganesh, S. 2006. University community responses to on-campus resource recycling. Resources, Conservation and Recycling, 47(1): 42-55.

Klaiman, K., Ortega, D. L. and Garnache, C. 2016. Consumer preferences and demand for packaging material and recyclability. Resources, Conservation and Recycling, 115: 1-8.

Knussen, C. and Yule, F. 2008. I'm not in the habit of recycling, the role of habitual behavior in the disposal of household waste. Environment and Behavior, 40(5): 683-702.

Lin, C. H., Wen, L. and Tsai, Y. M. 2010. Applying decision-making tools to national e-waste recycling policy: an example of analytic hierarchy process. Waste Management, 30(5): 863-869.

Pei, Z. 2019. Roles of neighborhood ties, community attachment and local identity in residents' household waste recycling intention. Journal of Cleaner Production, 241: 118217.

Robinson, G. M. and Read, A. D. 2005. Recycling behaviour in a London Borough: Results from large-scale household surveys. Resources, Conservation and Recycling, 45(1): 70-83.

Veiga, M. M. 2013. Analysis of efficiency of waste reverse logistics for recycling. Waste Management & Research, 31(10): 26-34.

Wang, Z., Guo, D. and Wang, X. 2016. Determinants of residents' e-waste recycling behaviour intentions: evidence from China. Journal of Cleaner Production, 137: 850-860.

Yu, T. K., Lin, F. Y., Kao, K. Y., Chao, C. M. and Yu, T. Y. 2019. An innovative environmental citizen behavior model: Recycling intention as climate change mitigation strategies. Journal of Environmental Management, 247: 499-508.

Yamaguchi, K. and Takeuchi, K. 2016. Consumer preferences for reduced packaging under economic instruments and recycling policy. Waste Management, 48: 540-547.

Nature Environment and Pollution Technology
An International Quarterly Scientific Journal

p-ISSN: 0972-6268
(Print copies up to 2016)
e-ISSN: 2395-3454

Vol. 20 | No.3 | pp. 1217-1223 | 2021

Original Research Paper

https://doi.org/10.46488/NEPT.2021.v20i03.030

Open Access Journal

Biosorption of Malachite Green by Dry Cells of Isolated Free Living Nitrogen Fixing Bacteria

A.M.M. Mawad*(***)†, H. Albasri* and H. A. Temerk**

*Biology Department, College of Science, Taibah University, Al-Madinah Al-Munawarah, Saudi Arabia
**Botany and Microbiology Department, Faculty of Science, South Valley University, Qena, Egypt
***Botany and Microbiology Department, Faculty of Science, Assiut University, Assiut 71516, Egypt
†Corresponding author: A.M.M. Mawad; ammawad@taibahu.edu.sa

Nat. Env. & Poll. Tech.
Website: www.neptjournal.com

Received: 19-10-2020
Revised: 17-11-2020
Accepted: 11-12-2020

Key Words:
Azotobacter
Biosorption
Malachite green
Nitrogen fixing bacteria

ABSTRACT

Contamination of water with Malachite green (MG) may threaten aquatic and human life. Nitrogen-fixing *Azotobacter* sp. is an efficient adsorbent for the removal of MG from dye solutions. The optimum pH for the biosorption process was determined. The maximum adsorption capacity and the effect of different adsorbate concentrations were detected. The kinetics and isotherm models for biosorption were constructed. Optimum adsorption of MG by *Azotobacter* sp. was obtained at pH 6.0, biomass concentration was 0.05%, initial dye concentration was 50 $mg.L^{-1}$, and contact time was 600 mins. Dye adsorption exhibited an increase with contact time and initial malachite green concentration. The kinetics of the adsorption process was best followed by the pseudo-second-order kinetic model which confirms the chemisorption process. The adsorption equilibrium data fit well to the Langmuir model indicating a monolayer adsorption behavior onto a surface of *Azotobacter* sp. with a finite number of active sites. Maximum biosorption capacity was found to be 142.8 $mg.g^{-1}$ of bacterial biomass. The dry biomass *of Azotobacter* sp. has proved to be an efficient biosorbent for the removal of synthetic dyes from actual industrial effluent that is contaminated with up to 400 $mg.L^{-1}$ dye concentration.

INTRODUCTION

Malachite green (MG) is a cationic triphenylmethane dye that is extensively used in many industries such as textile, pharmaceutical, and the aquaculture industry (Nath & Ray 2015; Wu et al. 2020). It is used as a food coloring agent, food additive, disinfectant, and anthelminthic (Srivastava et al. 2004, Gao et al. 2017). It is also used to stain silk, wool, jute, leather, cotton, paper, and acrylic industries (Culp & Beland 1996). Malachite green represents a major part of the total production of dye-containing wastewater in the textile industry (Nemerow 1963). The major sector of the economy worldwide mainly depends upon the textile industry; this has led to an increase in the release of large amounts of organic chemicals including dyes and many inorganic chemicals in industrial effluents and wastewater (Kumar et al. 2006).

The discharge of these pollutants in the aquatic environment may alter the chemical, physical and biological characteristics of the aquatic system (Erdem et al. 2005; Dos Santos et al. 2007). Malachite green particularly has a negative impact on the immune and reproductive systems (Gouranchat 2000; Inyinbor et al. 2020). Moreover, the US Food and Drug Administration (FAD) has nominated MG as a priority chemical for carcinogenicity investigations (Culp & Beland 1996). Although the use of MG has been forbidden in many countries and not FAD approved (Cha et al. 2001), it is still being consumed in other countries due to its low cost and availability (Schnick 1988).

The removal of color from dye wastewater is a complicated method due to its high solubility and low biodegradability (Gupta & Saleh 2013). Chemical precipitation, oxidation, and degradation are commonly used for that purpose however, they are only effective at a high solute concentration (Mawad et al. 2020). The adsorption process is an effective alternate strategy for the removal of dye wastewater (Mawad et al. 2014; Mawad et al. 2016). Microorganisms play an efficient role as biosorbent for the removal of pollutants from aqueous solutions (Mawad et al. 2016). The cell surface of microorganisms has a high affinity towards charged molecules such as cationic dyes. Adsorption of dyes by dry, non-viable microorganisms is characterized by no nutrient needed for cell growth, the high removal efficiency of colored effluents, and lack of toxicity limitations (Adhikari et al. 2010, Mawad et al. 2015, Liu et al. 2018).

Therefore, the main objective of this study is to determine the efficiency of isolated nitrogen-fixing *Azotobacter* sp. for adsorption of MG from an aqueous solution.

MATERIALS AND METHODS

Isolation of *Azotobacter* sp.

Free-living nitrogen-fixing bacteria *Azotobacter* sp. was isolated from cultivated soil. The isolate was cultivated on the nitrogen-free (NF) medium consisting of per liter, 10 g mannitol, 10 g $CaSO_4$, 2 g $MgSO_4.5H_2O$, 2 g NaCl, 2 g $FeSO_4$ and 5 g K_2HPO_4 and 15 g agar and pH adjusted at 7.0. The medium was autoclaved, poured into Petri dishes and supplemented with 0.5 g of fine soil particles after solidification, and incubated at 30°C for 24 h. The growing colonies were purified using the streaking plate method and preserved at 4°C for further use.

Preparation of Biosorbent

The bacterial isolate Azot-6 was selected for adsorption of dye based upon heavy growth on the NF medium. The bacterial cells were cultivated on 1L of broth NF medium for 24-48 h, centrifuged at 5000 rpm for 10 mins. The pellets were collected and washed three times by deionized water. The bacterial cells were completely dried in a vacuum hood cabinet for 7 days. The dried cells were then directly used as an adsorbent surface.

Biosorption Experiments of Malachite Green

Malachite green (MG), a synthetic basic (cationic) dye was used as a sorbent in this study. The batch dye removal was investigated in an Erlenmeyer flask (50 ml) containing 20 mL of 100 $mg.L^{-1}$ of MG and 0.05 g of bacteria. The experiment was performed at 30°C agitated on a rotary shaker at 150 rpm for 12 h to reach adsorptive equilibrium.

The biosorbent (dried bacteria) along with adsorbed dye then was separated from the solution by centrifugation at 8000 rpm for 5 mins and the remaining concentration in the supernatant was analyzed using a UV spectrophotometer at maximum absorption wavelengths, λmax = 618 nm.

The calibration curve was constructed by dissolving 10-600 $mg.L^{-1}$ of MG in deionized water and the absorbance was plotted against a certain concentration using a UV spectrophotometer (Deep Vision 301 E) at λmax = 618 nm. The linear plot equation was used to determine the remaining concentration of the solution during the biosorption process.

Effect of pH Values on Biosorption Process

The impact of initial pH was determined by the addition of 0.05 g of *Azotobacter* sp. to 20 mL of dye solution (50 $mg.L^{-1}$) at different pH solutions ranging from 3 to 7. The remaining MG concentrations were determined at adsorptive equilibrium time.

Biosorption equilibrium studies were performed by the addition of 0.05 g of *Azotobacter* sp. in a series of Erlenmeyer flasks containing 20 mL of MG solution of different concentrations (50, 100, 200, 300, 400 $mg.L^{-1}$) at 30°C. A shaking was provided for 12 h, to reach equilibrium. After equilibrium, the concentrations in the samples were determined as mentioned before.

Malachite green uptake: The amount of adsorbed dye onto the unit weight of adsorbent (*Azotobacter* sp.), qe ($mg.g^{-1}$) was estimated using the mass balance equation given by:

$$qe(mg/g)= (C0-Ce)V/M \quad ...(1)$$

where C0 and Ce represent the concentrations of MG ($mg.L^{-1}$) in the solution at time, t=0 and at any time t (h), respectively.

RESULTS AND DISCUSSION

Effect of pH on Biosorption of Malachite Green

The initial pH results in Fig. 1 show that the maximum adsorption capacity (34.88 $mg.g^{-1}$) was recorded at pH 6.0 while the minimum biosorption capacity (1.5 $mg.g^{-1}$) was determined at pH 2.0.

Functional groups that are found in the cell wall of *Azotobacter* sp. are carboxyl, sulfate, and amine. At low pH solutions, the protonation of functional groups enhances a net positive charge on *Azotobacter* sp. This allows the electrostatic repulsion of malachite green dye molecules that are positively charged (cationic groups) which consequently, led to a decrease in the malachite green removal (Sekhar et al. 2009; Nath & Ray 2015). On the other hand, at higher pH, the cell wall of bacteria was negatively charged which enhance the electrostatic attraction force between the cell wall and cationic dyes. So, the adsorption capacity increased from 7.5 $mg.g^{-1}$ to 34.88 $mg.g^{-1}$ at pH from 3-6.

A similar result was reported for biosorption of malachite green on *Pithophora* sp. at pH 6.0 (studied in the range 2.0–7.0), biomass load 0.03 g/30 mL, and initial dye concentration up to 100 $mg.L^{-1}$ within 5 h (Kumar et al. 2006). Nath and Ray (2015) and Jasińska et al. (2013) reported maximum biosorption of malachite green on 0.5 $g.L^{-1}$ of *Bacillus cereus* M116 (MTCC 5521) at pH 5.0.

Effect of the Contact Time and the Initial Malachite Green Concentration

In the present study, initial dye concentration varied from 50,100, and 300 $mg.L^{-1}$ up to contact time of 600 mins using 0.05% biomass concentration at 30°C and 120 rpm. The adsorption rate increased gradually from 30 mins to 360 mins.

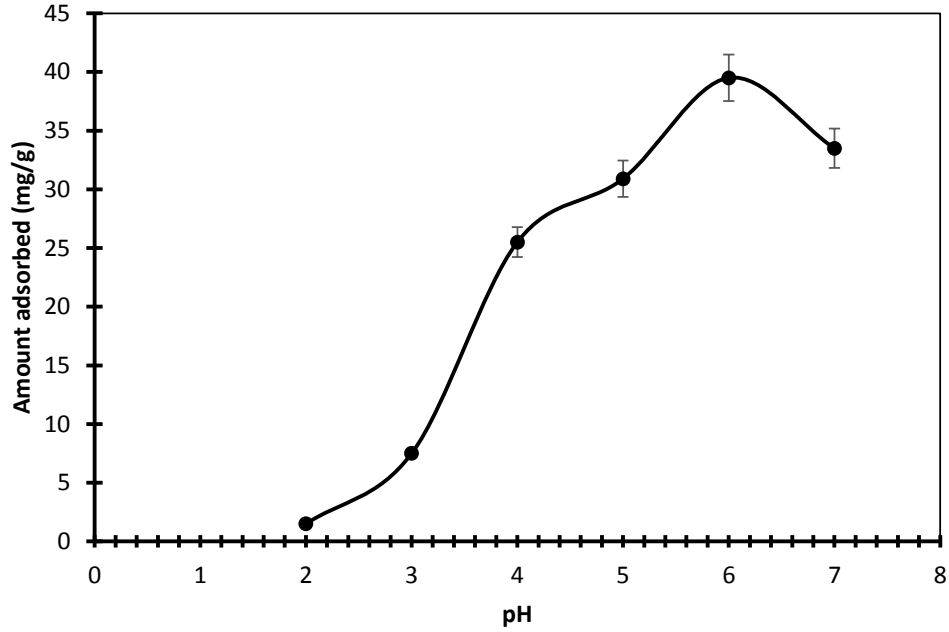

Fig. 1: Effect of pH on surface charge of *Azotobacter* sp. and on amount adsorbed (mg.g^{-1}) of malachite green by *Azotobacter* sp. (volume of dye solution: 50 mL; biomass concentration: 0.05%; initial dye concentration: 50 mg.L^{-1}; temperature: 30°C; incubation time: 10 h; shaking speed: 150 rpm)

The biosorption rate reached saturation after 360 mins as illustrated in Fig. 2. The results exhibited that the equilibrium capacity of dye was 38.6 mg.g^{-1}, 81.3 mg.g^{-1}, and 112.6 mg.g^{-1} that were determined when the initial concentration of dye was 50, 100, and 300 mg.L^{-1}, respectively.

The cell surface of *Azotobacter* sp. consists of a large number of negatively charged functional groups which serve as active sites for adsorption of positively charged cationic dyes. This explains the reason for the rapid biosorption rate at the initial period. After a lapse of time, all active sites were occupied with dye molecules and became saturated. So, any additional particles of dyes would encourage a repulsion force between the external adsorbed layer of dye on the adsorbent's active sites and the added one (Mawad et al. 2014).

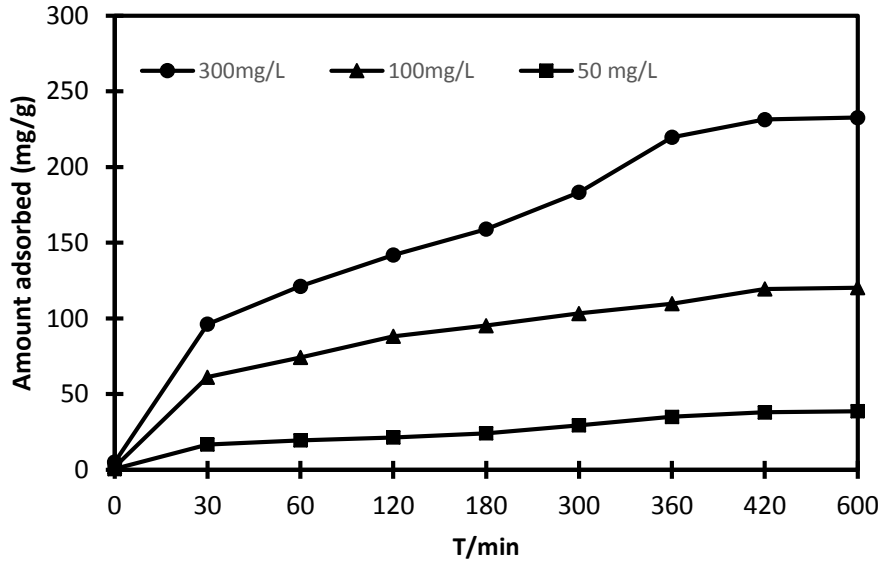

Fig. 2.: Impact of contact time and initial dye concentration on adsorption of malachite green (50 mL) by *Azotobacter* sp. (0.05%) at 30°C; shaking speed: 150 rpm.

Biosorption Kinetics

The investigation of batch biosorption kinetics provides information for designing batch sorption systems. Adsorption kinetics clarify the speed of the adsorption process. The kinetics of solute uptake gives information about the optimum operating conditions for a full-scale batch process (Kim & Choi 2017). Many kinetic models have been established to describe the reaction order of the adsorption process that represents the experimental data. In this study, the kinetics experiments were achieved at the optimum pH value (6.0) and initial dye concentrations of 50,100, 200, 300, and 400 mg. L^{-1}; the kinetics parameters of adsorption were determined by pseudo-first-order which is expressed as (Töwe et al. 2007)

$$\text{Log}(qe\text{-}qt)=\text{log}qe\text{-}K1t/2.303 \quad ...(2)$$

where k1 is the pseudo-first-order rate constant and qe and qt are the adsorption capacity of the dye molecules on adsorbent at equilibrium and at time t, respectively. The values of k1 and qe were estimated by plotting log(qe - qt) versus the time (Fig.3a). The calculated qe is demonstrated in Table 1 when the initial concentrations were 50, 100, and 300 mg.L^{-1}, the theoretical values of qe of MG were 2.5, 1.5, and 1.6 mg.g^{-1}, the R^2 values of the plots were 0.98, 0.87, and 0.97, and the values of k1 were 0.0045, 0.0034 and 0.0035, respectively. The results showed that the calculated qe values seemed to be much lower than the experimental values of 38.4, 81.2, and 112.8, when the initial concentrations were 50, 100, and 300 mg.L^{-1}. respectively (Fig.3a).

The linear form of the pseudo-second-order kinetics model (Ho & McKay 1999) was represented by the equation

$$t/q_t = 1/k_2qe^2 + t/q_e \quad ...(3)$$

Where k_2 is the pseudo-second-order adsorption rate constant. The values of k_2 and q_e were estimated from the slope and intercept of the plots of t/qe versus t at different concentrations of 50, 100, and 300 mg.L^{-1} of MG (Fig. 3b).

It was observed that the values of R^2 were 0.96, 0.99, and 0.95 while the values of K_2 were $8.6x10^{-5}$, $1.1x10^{-4}$, and $2.7x10^{-5}$ for biosorption of 50, 100, and 300 mg.L^{-1} of MG, respectively. Moreover, the theoretical amount adsorbed (qe) were 40.3, 83.2, and 120.2 mg.g^{-1} (Table 1).

In most studied adsorption systems, the pseudo-first-order model does not fit well over the entire adsorption stage and is generally applicable for the very early stage of the adsorption process. The pseudo-second-order model can expect the sorption attitude along with the whole-time adsorption (Ho 2006). The pseudo-second-order kinetics model is based on the adsorption capacity of the solid phase and confirms the chemisorption process.

Table 1: Kinetic parameters for adsorption of malachite green on *Azotobacter* sp.

	Pseudo-first-order			Pseudo-second-order		
Adsorbate (mg.L^{-1})	q_e (mg.g^{-1})	K_1(min^{-1})	R^2	q_e (mg.g^{-1})	K_2 (gmg.min^{-1})	R^2
50	2.5	0.004	0.98	40.1	$8.6x10^{-5}$	0.96
100	1.2	0.004	0.87	38.2	$1.1x10^{-4}$	0.99
400	6.7	0.036	0.95	120.2	$2.7x10^{-5}$	0.96

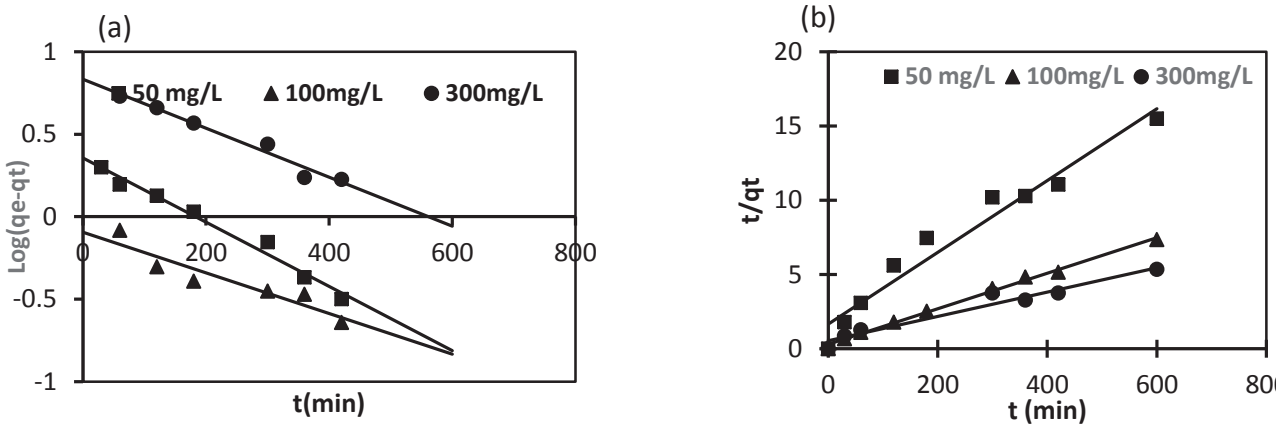

Fig. 3: (a) Pseudo first order (b) pseudo-second-order kinetic plot for adsorption of malachite green by *Azotobacter* sp..

The results of pseudo-second-order depicted that the R^2 values were close to 1.0 and the theoretical qe ($mg.g^{-1}$) was close enough to the experimental values. So, the most suitable model to describe the biosorption of malachite green by *Azotobacter* sp. is the pseudo-second-order kinetic model. Moreover, the obtained results suggested the chemisorption behavior of malachite green on the surface of *Azotobacter* sp. as it followed the pseudo-second-order model. These results came in the context of much literature that discussed the absorption kinetics of malachite green by microorganisms (Jasińska et al. 2013; Nath & Ray 2015).

Equilibrium Adsorption Isotherms

Adsorption isotherm is requested in the study of biosorption because it provides the description of the stoichiometric solute–solid interaction (Das & Guha 2007). Biosorption equilibrium gives the essential physiochemical information for evaluating the applicability of the sorption process as a unit operation (Nath & Ray 2015) as shown in Fig. 4. To investigate the adsorbate–adsorbent interaction, the adsorption equilibrium data was analyzed by Langmuir (Langmuir 1918) and Freundlich (Freundlich 1906) isotherm models as shown in equations (4) and (5), respectively.

$$Ceq/qe = 1/qmaxb+ceq/qmax \quad ...(4)$$

$$Lnqeq = (1/n)lnceq+lnkf \quad ...(5)$$

Where b is the Langmuir constant ($dm^3.mg^{-1}$) related to the affinity between adsorbate and adsorbent and qmax is the maximum monolayer adsorption capacity ($mg.g^{-1}$). K_f ($dm^3.g^{-1}$) and n are the adsorption capacity and the intensity of adsorption, respectively.

The Langmuir isotherm is valid for monolayer adsorption onto a surface with a finite number of identical sites. Langmuir's equation proposed that the surface is homogenous. If the experimental data fitted to the Langmuir isotherm model, it indicates the monolayer coverage of solute onto the adsorbent surface and the homogenous distribution of solute on active sites. On the other hand, Freundlich isotherm proposed that the adsorption process performs on heterogeneous surfaces and considers the multilayer adsorption phenomenon (Nath & Ray 2015).

Results in Fig. 4 show the adsorption equilibrium plot of malachite green. Isotherm model parameters were estimated from the slope and intercept of their respective equilibrium plots (Fig. 5a & 5b). The values of isotherm parameters and linear regression correlation coefficient (R^2) for the two isotherm models have been summarized in Table 2. Based on linear regression correlation coefficient (R^2) values of the two isotherm models, results were found to be described best by Langmuir (Fig. 5a). These observations indicate that the adsorption mechanism is a hybrid one and does not follow the ideal monolayer adsorption behavior. These results were in accordance with the results of biosorption of malachite green by *Bacillus cereus* (Kumar et al. 2005; Pan et al. 2006; Dahri et al. 2014).

CONCLUSION

Malachite green is a toxic triphenylmethane dye that is still being used in many countries. *Azotobacter* sp. is known to play a viable role in atmospheric nitrogen fixation and fertility of the soil. This study is considered the first that

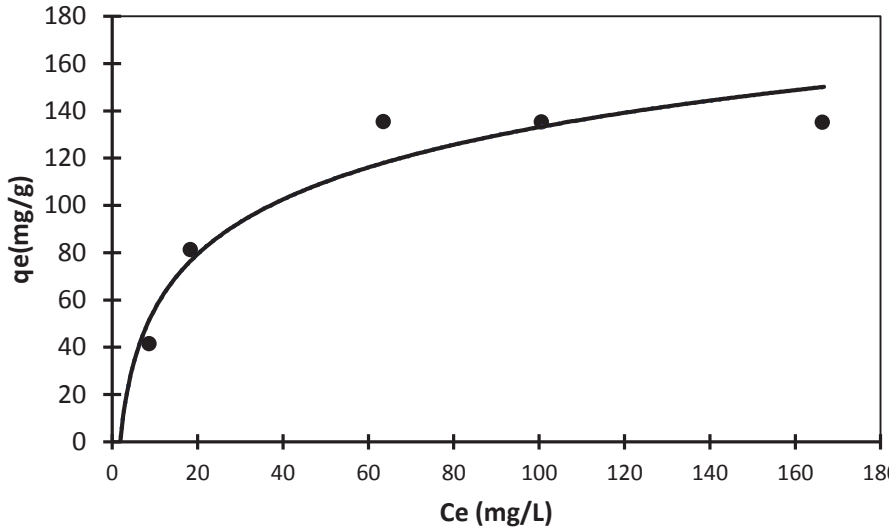

Fig. 4: Equilibrium adsorption isotherm for adsorption of malachite green by *Azotobacter* sp..

Table 2: Equilibrium adsorption isotherm constants for the fitted isotherm models

Langmuir			Freundlich		
Q_{max}	b(L.mg^{-1})	R^2	K_F(mg.g^{-1})	n	R^2
141.2	0.45	0.99	13803.1	0.5	0.92

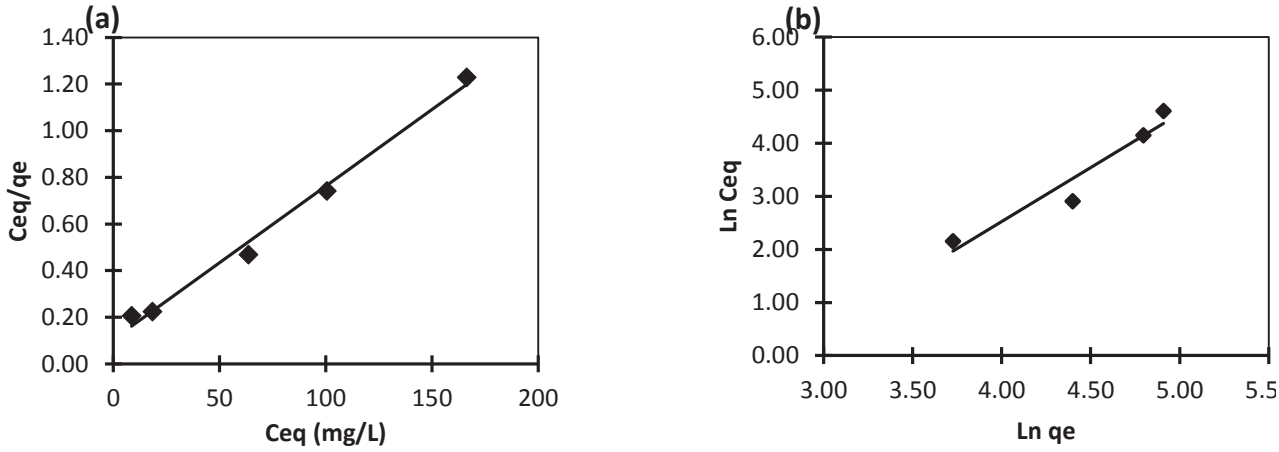

Fig. 5: Langmuir (a) and Freundlich (b) isotherm plots at 30°C (volume of dye solution: 50 mL; biomass concentration: 0.05%; temperature: 30°C; incubation time: 10 h; shaking speed: 150 rpm).

discussed the role of *Azotobacter* biomass in the biosorption of toxic dyes from the aquatic environment. The biomass of *Azotobacter* sp. is characterized by low cost and easy to be provided without any toxic constraints. In this study, *Azotobacter* exhibited an efficient adsorption capacity of malachite green within 360 mins.

REFERENCES

Adhikari, S., Chattopadhyay, P. and Ray, L. 2010. Biosorption of malathion by dry cells of an isolated *Bacillus* sp. S14. Chem. Speciat. Bioavailab., 22: 207-213.

Cha, C.J., Doerge, D.R. and Cerniglia, C.E. 2001. Biotransformation of malachite green by the fungus *Cunninghamella elegans*. App. Env. Microbiol., 67: 4358-4360.

Culp, S.J. and Beland, F.A. 1996. Malachite green: A toxicological review. J. Am. Coll. Toxicol., 15: 219-238.

Dahri, M.K., Kooh, M.R.R. and Lim, L.B. 2014. Water remediation using a low-cost adsorbent walnut shell for removal of malachite green: Equilibrium, kinetics, thermodynamic and regeneration studies. J. Environ. Chem. Eng., 2: 1434-1444.

Das, S.K. and Guha, A.K. 2007. Biosorption of chromium by Termitomyces clypeatus. Colloids Surf. B-Biointerfaces, 60: 46-54.

Dos Santos, A.B., Cervantes, F.J. and van Lier, J.B. 2007. Review paper on current technologies for decolorization of textile wastewaters: Perspectives for anaerobic biotechnology. Bioresour. Technol., 98: 2369-2385.

Erdem, E., Çölgeçen, G. and Donat, R. 2005. The removal of textile dyes by diatomite earth. J. Colloid Interface Sci., 282: 314-319.

Freundlich, U. 1906. On adsorption in solutions. J. Phys. Chem., 57: 385-470.

Gao, R., Geng, Y., Li, G., Gu, Y. and Qian, S. 2017. Influence of tourmaline on DPC pore structure and removal effect on the malachite green. Nat. Environ. Pollut. Technol., 16(2): 667.

Gouranchat, C. 2000. Malachite green in fish culture (state of the art and perspectives): Bibliographic study. Ecole Natl. Veterinaire, 142: 2000.

Gupta, V.K. and Saleh, T.A. 2013. Sorption of pollutants by porous carbon, carbon nanotubes and fullerene: An overview. Environ. Sci. Pollut. Res. Int., 20: 2828-2843.

Ho, Y.S. 2006. Review of second-order models for adsorption systems. J. Hazard. Mater., 13: 681-689.

Ho, Y.S. and McKay, G.1999. Pseudo-second order model for sorption processes. Process Biochem., 34: 451-465.

Inyinbor, A., Dada, O.A., Bello, O.S., Oluyori, A.P., Fanawopo, O.F., Oreofe, T.A. and Ajayi, O. 2020. Surface modified low-cost adsorbent in malachite green scavenging, malachite green/rhodamine B, and malachite green/rhodamine b/Cu2+ composite treatment. Orbital: E-J. Chem., 12: 87-94.

Jasińska, A., Bernat, P. and Paraszkiewicz, K. 2013. Malachite green removal from aqueous solution using the system rapeseed press cake and fungus *Myrothecium roridum*. Desal. Water. Treat., 51: 7663-7671.

Kim, S.H. and Choi, P.P. 2017. Enhanced Congo red dye removal from aqueous solutions using iron nanoparticles: adsorption, kinetics, and equilibrium studies. Dalton Trans., 46: 15470-15479.

Kumar, K.V., Ramamurthi, V. and Sivanesan, S. 2006. Biosorption of malachite green, a cationic dye onto *Pithophora* sp., freshwater algae. Dyes Pigm., 69: 102-107.

Kumar, K.V., Sivanesan, S. and Ramamurthi, V. 2005 Adsorption of malachite green onto *Pithophora* sp., freshwater algae: Equilibrium and kinetic modeling. Process. Biochem., 40: 2865-2872.

Langmuir, I. 1918 The adsorption of gases on plane surfaces of glass, mica and platinum. J. Am. Chem. Soc., 40: 1361-1403.

Liu, J., Zhang, L., Zha, D., Chen, L., Chen, X. and Qi, Z. (2018) Biosorption of malachite green onto *Haematococcus pluvialis* observed through synchrotron Fourier-transform infrared microspectroscopy. Lett. Appl. Microbiol., 67: 348-353.

Mawad, A., Yousef, N. and Shoreit, A. 2014. Bioremediation of acid blue 25 dye by anthracene degrading Pseudomonas pseudoalcaligenes ASU-016. Int. J. Environ. Sci. (CAT), 10: 27-34.

Mawad, A.M., Abd Hesham, E.L., Yousef, N.M., Shoreit, A.A., Gathergood, N. and Gupta, V.K. 2020. Role of bacterial-fungal consortium for enhancement in the degradation of industrial dyes. Curr. Genomics, 21: 283-294.

Mawad, A.M., Yousef, N.M. and Shoreit, A.A. 2016. Robust Aspergillus terreus biofilm supported on graphene oxide/hematite-nanocomposites for adsorption of anthraquinone dye. Desalin. Water Treat., 57: 24341-24351.

Nath, J. and Ray, L. 2015. Biosorption of malachite green from aqueous solution by dry cells of *Bacillus cereus* m116 (MTCC 5521). J. Environ. Chem. Eng., 3: 386-394.

Nemerow, N.L. 1963. Theories and practices of industrial waste treatment. J. Amer. Water Resour., 4(4): 66-67

Pan, J., Ge, X., Liu, R. and Tang, H. 2006. Characteristic features of *Bacillus cereus* cell surfaces with biosorption of Pb (II) ions by AFM and FT-IR. Colloids Surf. B Biointerfaces, 52: 89-95.

Schnick, R.A. 1988. The impetus to register new therapeutants for aquaculture. Prog. Fish-Cult., 50: 190-196.

Sekhar, C.P., Kalidhasan, S., Rajesh, V. and Rajesh, N. 2009. Bio-polymer adsorbent for the removal of malachite green from an aqueous solution. Chemosphere, 77: 842-847.

Srivastava, S., Sinha, R. and Roy, D. 2004. Toxicological effects of malachite green. Aquat. Toxicol., 66: 319-329.

Töwe, S., Leelakriangsak, M., Kobayashi, K., Van Duy, N., Hecker, M., Zuber, P. and Antelmann, H. 2007. The MarR-type repressor MhqR (YkvE) regulates multiple dioxygenases/glyoxalases and an azoreductase which confer resistance to 2-methylhydroquinone and catechol in Bacillus subtilis. Mol. Microbiol., 66: 40-54.

Wu, L., Xu, Z., Meng, Q., Xiao, Y., Cao, Q., Rathi, B., Liu, H., Han, G., Zhang, J. and Yan, J. 2020. A new aptamer/black phosphorus interdigital electrode for malachite green detection. Anal. Chim. Acta., 1099: 39-45.

Nature Environment and Pollution Technology
An International Quarterly Scientific Journal

p-ISSN: 0972-6268
(Print copies up to 2016)
e-ISSN: 2395-3454

Vol. 20 | No.3 | pp. 1225-1229 | 2021

Original Research Paper

https://doi.org/10.46488/NEPT.2021.v20i03.031

Open Access Journal

Urban and Rural Airborne Particulate Matter: Seasonal Variation of Alpha Activity in Kanyakumari District

C. Jesu Raj† and J. Prema Kumari
Department of Chemistry, Scott Christian College (Autonomous), Nagercoil, Manonmaniam Sundaranar University, Tirunelveli, India
†Corresponding author: C. Jesu Raj; jesuraj.jpp@gmail.com

Nat. Env. & Poll. Tech.
Website: www.neptjournal.com

Received: 24-08-2020
Revised: 01-10-2020
Accepted: 16-10-2020

Key Words:
Airborne particulate matter
Alpha counter
Alpha activity
Kanyakumari district

ABSTRACT

All forms of life on earth including man have evolved in the presence of radiation and have always been exposed to them from the natural environment. The health effect from exposure to alpha particles depends greatly on how a person is exposed. If alpha-emitters are inhaled, swallowed, or get into the body through a cut, the alpha particles can damage sensitive living tissue. In this paper, investigations have been made to determine the presence of alpha activity in the air. Hence, the alpha activity was measured by collecting Airborne Particulate Matter (APM) non-simultaneously on Whatman filters from ten sampling sites in Kanyakumari District during the summer and winter seasons using a high volume sampling method. The sampling sites are characterized by different contributions from ore refining factories like Indian Rare Earths (IRE) Limited, mountain areas, some industrial, non-nuclear activities like tiles and brick factories in and around the Kanyakumari district. The alpha activity in airborne particulate matter collected was determined by Alpha Counter and their results were tabulated.

INTRODUCTION

Alpha particles come from the decay of the heaviest radioactive elements, such as uranium, radium, and polonium. Even though alpha particles are very energetic, they are so heavy that they use up their energy over short distances and are unable to travel very far from the atom. Alpha particles lack the energy to penetrate even the outer layer of skin, so exposure to the outside of the body is not a major concern (Songul et al. 2012). Radioactivity in the atmosphere originates from naturally radioactive material, cosmogenic production, nuclear weapons testing, and nuclear accidents (Arkian et al. 2007, Nakpil et al. 2019).

Alpha radiation is an average of about 20 times more dangerous, and in experiments with inhaled alpha emitters, up to 1000 times more dangerous than an equivalent activity of beta-emitting or gamma-emitting radioisotopes. An increase in the background ionization radiation from numerous sources has various health side effects on the populace (Avwiri & Go 2006).

Sources and levels of air pollution can vary from place to place. In urban areas, different kinds of motor vehicles, industries, and other commercial activities may cause air pollution. In rural areas, air pollution is caused by the use of wood, crop residues, and dung cakes as fuel for domestic purposes and the dust generated from unpaved roads (Roy & Adhikari 2009).

The activity of natural ionization sources such as soil, rocks, outer space nuclides, and radiation is a determinant factor for air ion concentration in a particular place (Samotaev & Nikolay 2015).

The interaction between humans and the environment has resulted in variation in the quantity and quality of the background radiation to which human beings are exposed. It is virtually impossible for people to avoid radiation from their living environment. Therefore, it is necessary to keep a constant vigil on the changes caused by the various sources of ionizing radiation exposures. For these reasons, the examination of alpha activity and trace elements concentration size distribution is a useful tool for the characterization and apportionment of the sources of rural and urban airborne particulate matter.

The Kanyakumari district is recognized as the area with the highest level of air pollution. This is because in a relatively small area of 1684 km^2 the district has a dense population (over 1.8 crores inhabitants). Indian Rare Earths (IRE) Limited, Cashew nut factories, Tiles and brick factories are the industrial sources in Kanyakumari District. The present research focused on the presence of alpha activity in ambient

particulate matter. The comparison of the results obtained for ten sites in the district in diverse periods of the year allows appraisal of the input of different pollution sources in the district. The aim of this study is the identification and assessment of gross alpha radioactivity levels in air-suspended particulate matter in and around the Kanyakumari District.

MATERIALS AND METHODS

A high-volume air sampler running on electrical energy has been purchased to collect air samples contaminated with automobile exhaust at the above-mentioned sampling sites. The extent of absorption of heavy metals in each sample is calculated and correlated with the results obtained earlier. The suspended particles of air are retained in the filter. With the help of a blower, the duration of sampling is measured in an elapsed time meter which is placed in series. The sampler was placed 2m above the ground level. Each sampling lasted to minimize the influence of short-term weather condition changes.

For measuring the presence of alpha activity in the air, the radiation counting system (Nucleonix RC 605A) is used with an alpha counter of ZnS (Ag) solid scintillation detector. A punched filter paper of size 2.5cm diameter was inserted into the alpha counter. The alpha activity calculation was corrected for the mass thickness of the aerosol deposit collected in the filters. The background of the detector was determined with measurements that routine samples were counted and was measured using clean filters. The average detection limit for this apparatus was approximately 0.3 ± 0.1 $mBq.m^{-3}$ background activities for alpha. A background subtraction procedure was applied to each of the gross alpha analyses. For each measurement of alpha emitters in the filters, counting times of 5h were used.

Gross measurements are used as a method to screen samples for relative levels of radioactivity in the air. It is simply a measurement of all alpha activity present, regardless of specific radionuclide source. The samples were counted for gross alpha radioactivity using a low background multiple detector gas flow proportional counter. Alpha emitter radionuclides are listed below:

- Americium-241
- Plutonium-239
- Uranium-238
- Thorium-232
- Radium-226
- Radon-222
- Polonium-210

Equation (1) used to calculate the alpha radioactivity is given below:

$$\alpha \text{ Activity} = \frac{N}{T} * \frac{100}{E} * P * \frac{1}{V * 8 * 60} \quad \ldots 1$$

Where N is the net alpha count rate (gross alpha count rate minus the background count rate) at the alpha voltage plateau; E is the efficiency of the alpha counter; P is a paper factor; V is the volume of air in the sample.

SAMPLING LOCATION

The samples were taken in diverse periods in the years 2014-2016 non-simultaneously at ten measuring points to analyze the influence of traffic intensity and other sources on ambient air pollution. Fig.1 shows the six sampling points from the urban areas and four sampling points from the rural areas of the Kanyakumari district. The sampling locations of the Kanyakumari district were characterized by dense buildings, narrow streets and heavy traffic, local combustion, high wind, and seashore with dense buildings, factories like cashew nut factory, ore refining factory, tiles, and brick factories, and agriculture specialization. All these factors contribute to gross alpha radioactivity levels, especially in the winter period.

The samples were taken by placing the high volume air sampler at 1m above the ground at the following urban locations:

- Kaliyakkavilai - Dense buildings, narrow streets, and heavy traffic and are available in between the border of Tamilnadu and Kerala.
- Marthandam – Intensive traffic and dense population.
- Thuckalay - 14km near Marthandam, immense with dense population and vehicular traffic area.

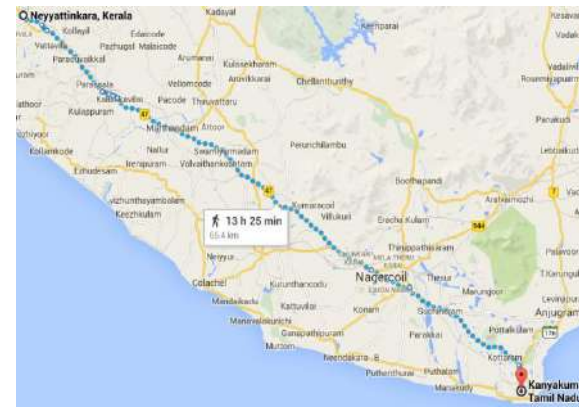

Fig.1: Roadmap of Kanyakumari District.

- Villukuri - A mountain area exposed to vehicular traffic and located with many Cashew Nut Factories.
- District Nagercoil junction, Nagercoil – Specialized for Latex industry, exposed to vehicular traffic, but with elevated smoke and dust affected area during all seasons.
- Kanyakumari- A tourist area characterized by high wind and seashore exposed to vehicular traffic.

The samples were taken by placing the high volume air sampler at 1m above the ground at the following rural locations:

- Colachel Municipality - Known to be densely populated area, coastal and inland areas, Marine and inland fisheries, harvesting, processing, marketing, and distribution, and is characterized by high wind and seashore with dense buildings, narrow streets, and heavy traffic.
- Manavalakurichi - Characterized by ore refining factory (IRE) and seashore exposed to vehicular traffic.
- Monday Market - Known for tiles, brick factories, and cashew nut factories.
- Kurunthencode - Specialized for agriculture located at a distance of 7kms from Monday Market.

RESULTS AND DISCUSSION

In general, alpha activity value increases during the winter season. Likewise, in the area of Kanyakumari district, the highest alpha activity value was found during the winter season based on the observations made on two consecutive years between December 2014 and May 2016.

Table 1 summarizes the results obtained from airborne particulate samples. It was observed that the highest and the lowest gross alpha activity values were found in the urban areas of Kanyakumari District based on seasonal variation.

From the overall results obtained in Kanyakumari District, during the winter season, the place Kanyakumari indicates the highest value due to the reason of being a coastal area, which contains a mixture of rare minerals such as garnet, ilmenite, rutile, leucoxene, zircon, sillimanite and monazite. The lowest activity values were found in Thuckalay and Nagercoil during the years 2014 and 2015 due to the absence of the characteristics that relate to alpha activity since those places were meant for high vehicular traffic intensity.

During the summer season of 2014-2016, it is found that the maximum alpha activity value was found in Kanyakumari due to the reason mentioned above. But the minimum activity value was found in the place Thuckalay during the first consecutive year and in the areas such as Kaliyakkavilai, Marthandam, and Nagercoil during the second consecutive year because those areas are not open to the mining process.

Fig. 2 shows the graphical representation of season-based analysis of Alpha Activity in Urban areas of Kanyakumari District. The dark grey line in the figure shows the recorded alpha radioactivity during the winter season and the light grey line represents the recorded alpha radioactivity during the summer season.

The results obtained from airborne particulate samples in the rural areas of Kanyakumari District based on seasonal variation are listed in Table 2. During the winter season, it has been found that the maximum alpha activity value was found in Manavalakurichi for the reason being a coastal area and having refining factories (IRE).

The minimum alpha activity value was found in the Kurunthencode area since the area is known for the cultivation of paddy fields and trees like plantain and coconut. Also, the maximum alpha activity value was found in Manava-

Table 1: Alpha activity values in the urban areas of Kanyakumari District.

Alpha Activity Values -Urban Area [in $Bq.m^{-3}$]				
Area / Season	Winter Season (Dec, Jan, Feb)		Summer Season (Mar, Apr, May)	
	2014-2015	2015-2016	2014-2015	2015-2016
Kaliyakkavilai	0.000771	0.000926	0.000617	0.000463
Marthandam	0.000617	0.000771	0.000463	0.000463
Thuckalay	0.000463	0.00108	0.000309	0.000617
Villukuri	0.000309	0.000771	0.000463	0.000617
Nagercoil	0.000617	0.000617	0.000463	0.000463
Kanyakumari	0.000926	0.001234	0.000771	0.000926
Minimum	0.000309	0.000617	0.000309	0.000463
Maximum	0.000926	0.001234	0.000771	0.000926
SD Value	0.0002334	0.000227	0.000159	0.00018

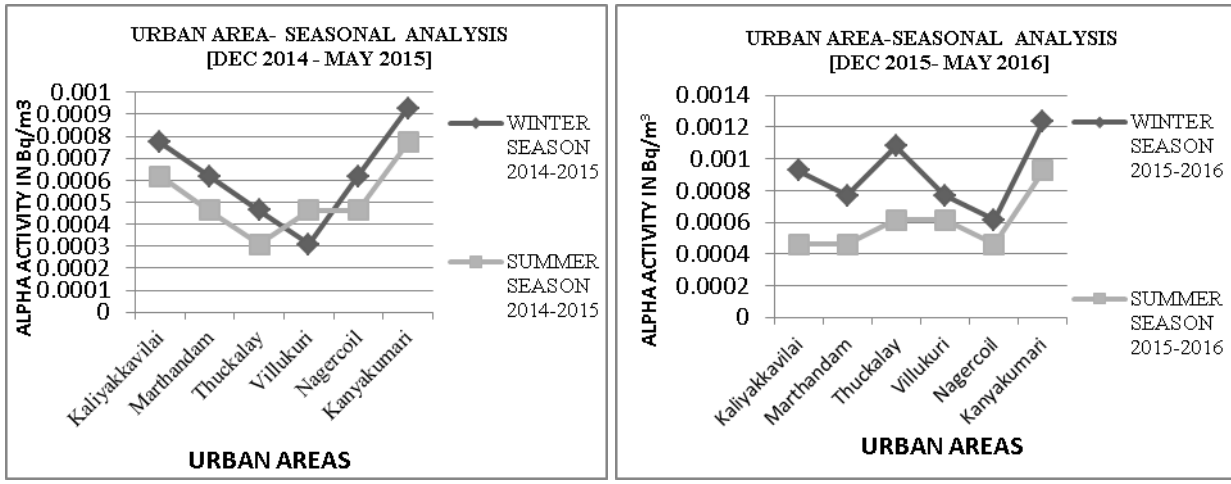

Fig. 2: Season-based analysis of the alpha activity in the urban area.

Table 2: Alpha activity values in the rural area of Kanyakumari District.

Area / Season	Alpha Activity Values -Rural Area [in Bq.m^{-3}]			
	Winter Season (Dec, Jan, Feb)		Summer Season (Mar, Apr, May)	
	2014-2015	2015-2016	2014-2015	2015-2016
Colachel	0.00108	0.001234	0.000771	0.000926
Manavalakurichi	0.001234	0.001388	0.000926	0.00108
Monday Market	0.000926	0.00108	0.000463	0.000771
Kurunthencode	0.000771	0.000926	0.000309	0.000617
MIN	0.000771	0.000926	0.000309	0.000617
MAX	0.001234	0.001388	0.000926	0.00108
SD	0.0001992	0.000199	0.0002815	0.0001993

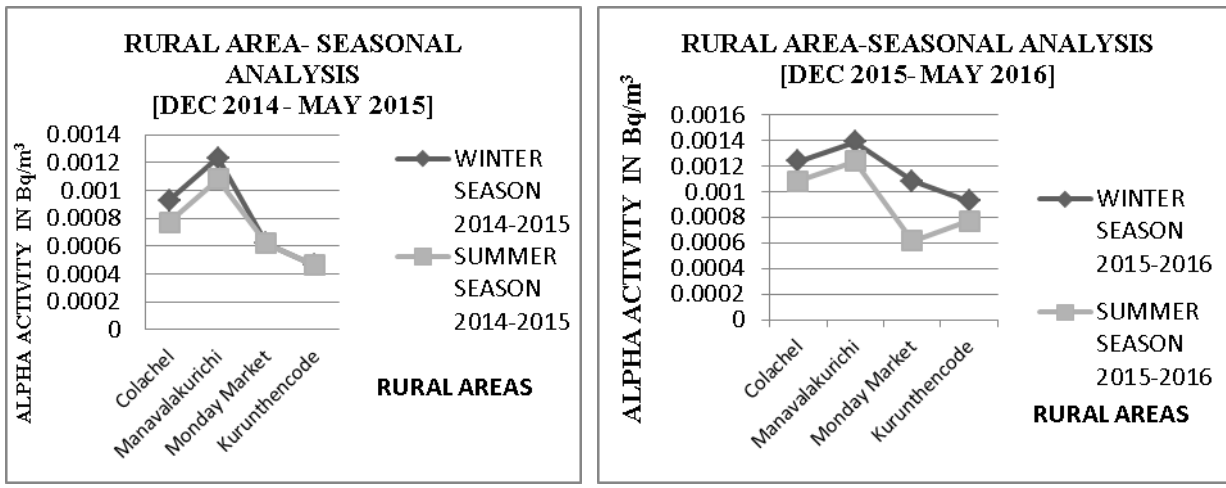

Fig. 3: Season-based analysis of the alpha activity in the rural area.

lakurichi and the minimum activity value was found in the Kurunthencode due to the reason as mentioned previously.

The graphical representation of season-based analysis of Alpha Activity in rural areas of Kanyakumari District is depicted in Fig. 3. The dark grey line in the figure shows the recorded alpha radioactivity during the winter season and the light grey line represents the recorded alpha radioactivity during the summer season.

So far the findings of both the tables and figures state that the winter season shows the maximum alpha activity value in the air when compared with the summer season, due to the higher rate of sedimentation of Suspended Particulate Matter (SPM) collected from ambient air.

CONCLUSION

The radioactivity levels of aerosols were studied based season-wise in the urban and rural areas of Kanyakumari district in Tamil Nadu. The gross alpha activities were detected in the collected aerosol samples. The primary conclusion is that sampling locations and particle fractions showed a difference for alpha activity dispersion due to the sources of radioactivity and characteristics of sampling locations. Apart from the above, meteorology plays an important role in the dispersion and transport of radioactivity. To the best of knowledge, the study will be important in the future to use atmospheric activity studies to investigate the influence of the origin of the air masses on concentrations of the gross alpha levels or different radionuclides in the urban and rural areas of the Kanyakumari district. Thus, the analysis made concludes that the alpha activity was found in maximum during the winter season due to the low rate of wind flow in both urban and rural areas.

ACKNOWLEDGEMENT

We are indebted to the Head, Department of Chemistry, Scott Christian College (Autonomous), Nagercoil for providing the instruments for the collection of the samples and the generous help and permission for using High Volume Air sampler and Nucleonix 605A for analyses of the samples.

REFERENCES

Arkian, F., Salahinejad, M., Bidokhti, A.A. and Meshkatee, A. 2007. Analysis of gross alpha, gross beta activities and beryllium-7 concentrations in surface air: Their variations and statistical prediction model. Environmental Monitoring and Assessment, 140(1-3): 325-330.

Avwiri, O.G. 2006. Determination of radionuclide levels in soil and water around cement companies in port Harcourt. Journal of Applied Sciences and Environmental Management, 9(3): 26-29.

Roy, S. and Adhikari, G.R. 2009. Seasonal variation in suspended particulate matter vis-a-vis meteorological parameters at Kolar gold fields, India. International Journal of Environmental Engineering, 1(4): 432.

Nakpil, A.S., Baja, E.S. and Medina, P.M.B. 2019. Mutagenicity of bulk, aqueous and organic partitions of air particulate matter in differentially ventilated wards in a public urban hospital. Nat. Env. Poll. Tech., 18(4): 1463-1469.

Samotaev, N., Gurkovskivy, B., Miroshnichenko, V., Onischenko and Simakov, A. 2015. Alpha-radioactive isotopes monitoring of human body contamination by a trace of air ions presence. Procedia Engineering, 120: 874-877.

Songul A., Barbara, K., Anna, W., Ugur, C., Halim, T., Rene, V. G., Lucyna, S. and Ewa, Wi. 2012. Gross alpha and beta activities of airborne particulate samples from Wawel Royal Castle museum in Cracow, Poland. Journal of Radioanalytical and Nuclear Chemistry, 295(2): 1567-1573.

Nature Environment and Pollution Technology
An International Quarterly Scientific Journal

p-ISSN: 0972-6268
(Print copies up to 2016)
e-ISSN: 2395-3454

Vol. 20 | No.3 | pp. 1231-1236 | 2021

Original Research Paper

https://doi.org/10.46488/NEPT.2021.v20i03.032

Open Access Journal

Influence of Evaporation on the Hydrogen and Oxygen Stable Isotopes in an Enclosed Water Body: A Case Study

X. Zhao*(**), L. H. Sun*(**)† and X. Y. Qiu*(**)
*School of Resources and Civil Engineering, Suzhou University, Suzhou 234000, China
**School of Earth and Environment, Anhui University of Science and Technology, Huainan 232001, China
†Corresponding author: L. H. Sun; sunlinh@126.com

Nat. Env. & Poll. Tech.
Website: www.neptjournal.com

Received: 17-08-2020
Revised: 09-09-2020
Accepted: 09-10-2020

Key Words:
Isotopes
D-excess
Influence of evaporation
Water resource protection

ABSTRACT

It is of great significance to study the influence of evaporation on the protection and management of regional water resources. In this study, water samples have been collected from a typical enclosed water body, Liuxi, a small brook in the campus of Suzhou University in May and June, and then analyzed for their hydrogen and oxygen stable isotopes. The results indicate that the samples collected in June have higher $\delta^{18}O$ and δD values relative to the samples collected in May, and both of them have $\delta^{18}O$ and δD values plotted at the right of the meteoric line, in combination with their lower deuterium excess (d-excess) values relative to the meteoric line, implying that the water has been influenced by evaporation. Moreover, the d-excess values showed decreasing and increasing in different sampling sites, which was demonstrated to be influenced by different extents of evaporation. Based on the calculation, the residual water quantities were 70–75% and 51–70% for May and June relative to the initial water, which indicates that about 10% of the water had evaporated during May and June.

INTRODUCTION

Surface water is not only the main component of natural water resources, but also an important source for sustaining human life. Compared to the groundwater, surface water is not only the most basic water resource for agriculture, industry and human lives, but also an important resource for natural landscape and entertainment. Surface water is extremely vulnerable to the impact and pollution of the external environment, (Xu et al. 2016). Therefore, a large number of studies related to the surface water environment, quantity, quality and other related issues have been carried out in recent years (Zhang et al. 1997, Xu 2005, Joshi & Seth 2011, Fan et al. 2017, Gao et al. 2018, Wu et al. 2018).

At present, scholars have conducted a great deal of research on the hydraulic connection between surface water and groundwater, the evolution of surface water in the process of precipitation, evaporation and runoff, and the treatment and restoration of surface water environment by using hydrogeochemistry and isotope technology (Buttle 1994, Wang et al. 2018, Xia et al. 2019). In these studies, hydrogen and oxygen stable isotopes, play an important role in the hydrological cycle and water balance calculation, as good tracers (Jiang et al. 2000, Zhang et al. 2006, Zhang et al. 2020).

Suzhou city is located on the Huaibei plain. It is an important industrial and agricultural city in China. Although there are only small lakes and rivers in Suzhou, they are still very important for urban development and have played an important role in the beautifying of the environment. However, because of their special characteristics, e.g. strong sealing, poor water mobility, small water environment capacity and low self-purification capacity (Zhao 2019), these small lakes and rivers can be easily influenced by human activities.

There were some studies that were carried out for the water bodies in Suzhou city. Most of these focused on the assessment and source approximation of pollutants (Li et al. 2015, Zhang et al. 2018), but there is no report related to their stable isotopes, which is considered to be important for the study of regional water cycle. Therefore, in this study, water samples have been collected from a typical enclosed water body, Liuxi, a small brook in the campus of Suzhou University in May and June, and then analyzed for hydrogen and oxygen stable isotopes. The goals of the study include: (1) obtaining information regarding the compositions of hydrogen and oxygen stable isotopes of the water; (2) finding out the main influencing factors; (3) calculating the degree of influence of evaporation. This brook was chosen because of its relatively closed characteristics and the fact that no rainfall occurred during the two sampling periods, hence, the influence of evaporation can be better obtained. The study can provide the basis for water resources protection and management of regional closed water bodies.

MATERIALS AND METHODS

Study Area

Suzhou city is located in the north of Anhui province, China. It is at the northern gate of Anhui province between longitude 116°09'-118°10' E and latitude 33°18'-34°38' N, with a total area of 9787 square kilometers. The rainfall is concentrated between the middle of July to the beginning of August every year, and may cause floods. The average annual rainfall is 840 mm, and the rainfall is mainly concentrated in summer, fulfilling 50%-60% of the total annual rainfall.

The Liuxi brook is located in the middle of the East Campus of Suzhou University, with a total length of about 500m, a depth of one to one and a half meters, and a width of about ten meters. Because of the dams built on either side of the brook, it is an enclosed water body in the absence of atmospheric precipitation and artificial water supplement, and the loss of water in it is mainly influenced by evaporation.

Sampling and Analyses

According to the hydrogeological conditions of the Liuxi brook, a total of 20 samples were collected on May 5 and June 5, 2019 (10 samples each time, the specific location and number are shown in Fig. 1). There was no rainfall or artificial water supplement during the period. The samples were collected in was recorded during sampling.

After collection, all of the samples were filtered by a 0.45 μm microporous filter membrane, and the stable hydrogen and oxygen isotopes were measured by liquid isotope analyzer (LGR iwa-45ep). The accuracy shown is $\delta D<0.5‰$, $\delta^{18}O<0.1‰$, respectively. The results were then calculated with Vienna Standard Mean Ocean Water (VSMOW) standard. The analyzing quality is controlled by the standard sample, and the relative standard deviation is within five percent. All of the measurements were processed in the Key Laboratory of Mine Water Resource Utilization of Anhui Higher Education Institute.

Calculation Methods

The global meteoric water line (GMWL) has been established by (Craig 1961) based on the global atmospheric precipitation isotopic data. Because of the differences of geographical factors and meteorological conditions in different regions, the meteoric water line is different in different regions. At

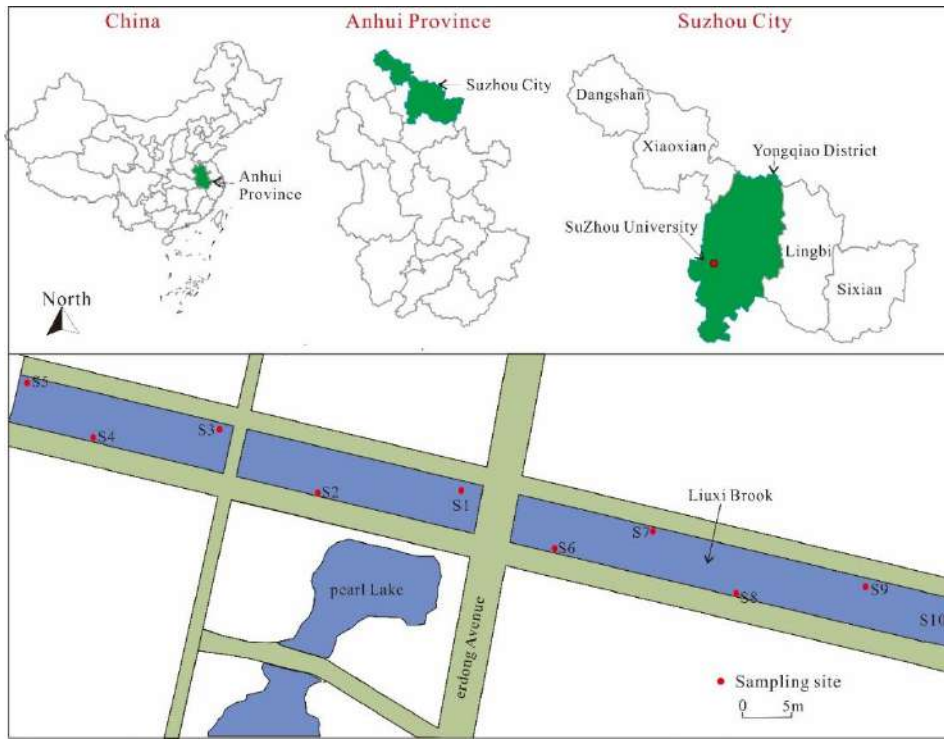

Fig. 1: Location of the study area and sampling sites.

present, due to the lack of precipitation data in Suzhou, the national meteoric water line of China (CMWL) was adopted in this study, and the equation is as follow:

$$\delta D=7.89\delta^{18}O+8.16 \quad \ldots(1)$$

The evaporation line is a linear regression line between δD and $\delta^{18}O$ of the surface water in a region, and the deviation of the line relative to the meteoric line is a reflection of the degree of evaporation of the region, which varies in different areas. In this study, the evaporation line (MEL) (Chen et al. 2008) in the Huaihe River region have been chosen for comparison, and the equation is as follow:

$$\delta D=5.89\delta^{18}O-7.68 \quad \ldots(2)$$

Isotopic fractionation refers to the fractionation of light and heavy isotopes in the evaporation process. Because the bonds of the relatively light isotopes are easier to destroy and remove from the water, while the heavy ones remain to enrich the residual water. The isotopic fractionation of water with Rayleigh equilibrium is mainly affected by temperature under evaporation, and its isotopic composition increases exponentially with the decrease of volume ratio of residual water (Shi et al. 2003, Philip 2019). The stable isotope value δ_0 in the initial water body has the following relationship with the stable isotope value δ in the remaining water body:

$$\delta=(\delta_0+1)f^{(a-1)}-1 \quad \ldots(3)$$

In the equation, a is the fractionation coefficient, *f* is the ratio of the residual water. Because the absolute value of δ is small, then the equation (3) can be simplified to be:

$$\delta-\delta_0=-10^3(a-1)\ln f \quad \ldots(4)$$

The fractionation coefficient a is a function of temperature and their relationships are as follows:

Table 1: Results of stable isotope analysis of hydrogen and oxygen in Liuxi water

Sample ID	May			June		
	$\delta^{18}O$/‰	δD/‰	d-excess	$\delta^{18}O$/‰	δD/‰	d-excess
S1	-4.90	-38.88	0.35	-4.67	-30.25	7.11
S2	-4.68	-38.66	-1.25	-4.24	-30.97	2.92
S3	-4.60	-39.10	-2.33	-2.26	-38.18	-20.10
S4	-4.67	-38.80	-1.48	-2.60	-36.25	-15.48
S5	-4.66	-38.55	-1.23	-3.33	-32.74	-6.14
S6	-4.58	-38.71	-2.06	-3.61	-30.97	-2.06
S7	-4.72	-37.72	0.03	-3.02	-30.87	-6.68
S8	-4.68	-37.83	-0.39	-3.45	-30.49	-2.87
S9	-4.63	-38.26	-1.23	-4.56	-25.72	10.74
S10	-5.26	-36.62	5.43	-1.74	-39.66	-25.72

$$10^3\ln a^{18}O=1.137(10^6/T^2)-0.4156(10^3/T)-2.0667 \quad \ldots(5)$$

$$10^3\ln aD=24.844(10^6/T^2)-76.248(10^3/T)+51.612 \quad \ldots(6)$$

RESULTS AND DISCUSSION

Compositions of Hydrogen and Oxygen Isotopes

The hydrogen and oxygen stable isotopes of water samples collected from the Liuxi brook are shown in Table 1. As can be seen from the table, the May samples have δD values range from -39.10‰ to -36.62‰, with an average of -38.31‰, and the $\delta^{18}O$ values range from -5.26‰ to -4.58‰, with an average of -4.74‰. Comparatively, the June samples show higher values of δD and $\delta^{18}O$, the δD are from -38.18‰ to -25.72‰ (mean is -32.61‰), and the $\delta^{18}O$ are from -4.67‰ to -2.26‰ (mean is -3.35‰). Except for the sample S10 in June, the $\delta^{18}O$ and δD values of other samples increased with different extents from May to June, which indicates the influence of evaporation (Tian et al. 2000, Kim et al. 2011). Moreover, in combination with the meteoric line and evaporation line in Fig. 2, except for the sample S9, all the samples are plotted below the meteoric line but near the evaporation line, which further demonstrates that the water in the Liuxi brook has been influenced by evaporation.

Analysis of d-excess

The relationship between δD and $\delta^{18}O$ in different regions tends to deviate from the global meteoric line. This difference was quantified as deuterium excess (d-excess) (Dansgaard 1964), and the equation for it is d-excess = $\delta D - 8\times\delta^{18}O$. For the water samples from the Liuxi brook, the d-excess values of samples in May range from -2.33‰ to 5.43‰, with an average of 0.42‰ (Table 1), whereas the d-excess values of samples in June are from -20.10‰ to 10.74‰, with an average value of -5.82‰. All of the samples except for S9 have lower d-excess values relative to the GMWL (Fig. 3), implying the influence of evaporation,

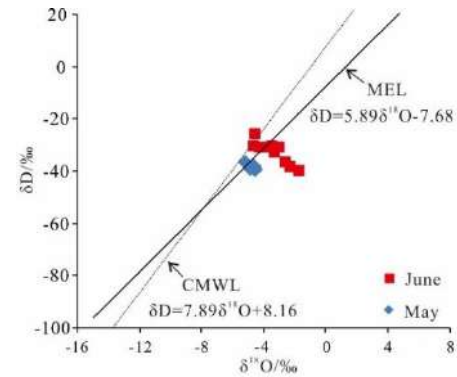

Fig. 2: Relationships between $\delta^{18}O$ and δD.

similar to the results obtained by the comparison of δD and $\delta^{18}O$ in the Fig. 2.

As can be seen from the relationship between d-excess, δD and $\delta^{18}O$ (Fig. 4), the correlation of coefficients between d-excess and δD is 0.865, and is 0.956 between d-excess and $\delta^{18}O$. Both of them are higher than the critical value (r = 0.765, a = 0.01, n = 10), implying that the d-excess values of water samples have been obviously affected by the stable isotope compositions of hydrogen and oxygen. However, it can be obtained from Fig. 3 that the d-excess values of 7 samples decreased while 3 samples increased. During water rock interaction, the $\delta^{18}O$ values in silicate and carbonate rocks are higher than that in water, and the oxygen isotope of the water can be influenced (increasing) during water rock interaction with temperature > 60°C. Comparatively, the δD values in these rocks is low and cannot influence the hydrogen isotope in water. Under this situation, the d-excess value of the water will decrease (Yao & Lu 2017). However, the water in this study is only 27°C(<60°C), and therefore, the influence from the water rock interaction can be ruled out.

There are two types of isotopes (^1H and ^2H) related to the δD, and other two types (^{16}O and ^{18}O) related to the $\delta^{18}O$. Comparatively, the isotopes of hydrogen can be more easily influenced by evaporation relative to the oxygen isotopes because of their different weights. Under the condition of low degree evaporation, the hydrogen isotopes can be more easily fractionated relative to the oxygen isotopes. With the increasing of the degree of evaporation, the differences of fractionation between hydrogen and oxygen isotopes will decrease. Therefore, if the change of δD higher than the change of $8\times\delta^{18}O$, which means the low degree evaporation, and leading to the increasing of d-excess, alternatively, means the high degree evaporation and leading to the decreasing of d-excess.

From this point of view, although all of the water samples except for the S10 have δD and $\delta^{18}O$ increased, their changing rate are different, which therefore leading to the increasing (S1, 2 and 9) and decreasing (S3, 4, 5, 7, 8 and 10) of the d-excess. From the perspective of change rate, the average change rate of δD between the two month samples is 14.8%, while the average change rate of $\delta^{18}O$ is 29.0%. Therefore, the d-excess values of most samples in June are lower than those in May.

Quantity of Residual Water Relative to Initial Water

The stable isotopic compositions of hydrogen and oxygen in the initial water body is determined by the intersection of local meteoric line and evaporation line, which was calculated to be $\delta^{18}O$ = -7.92‰ and δD = -54.32‰ (based on equation (1) and (2)). According to the meteorological data of the Suzhou, the mean temperature in May and June is 27°C(300.15 K). The results of the calculations of the proportion of the residual water, relative to initial water based on $\delta^{18}O$ and δD are shown in Table 2 and Fig. 5.

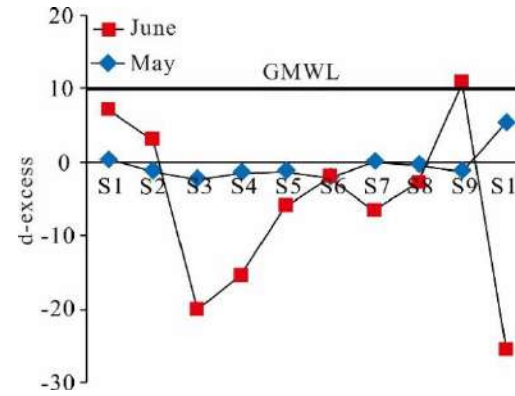

Fig. 3: Variation of the d-excess values.

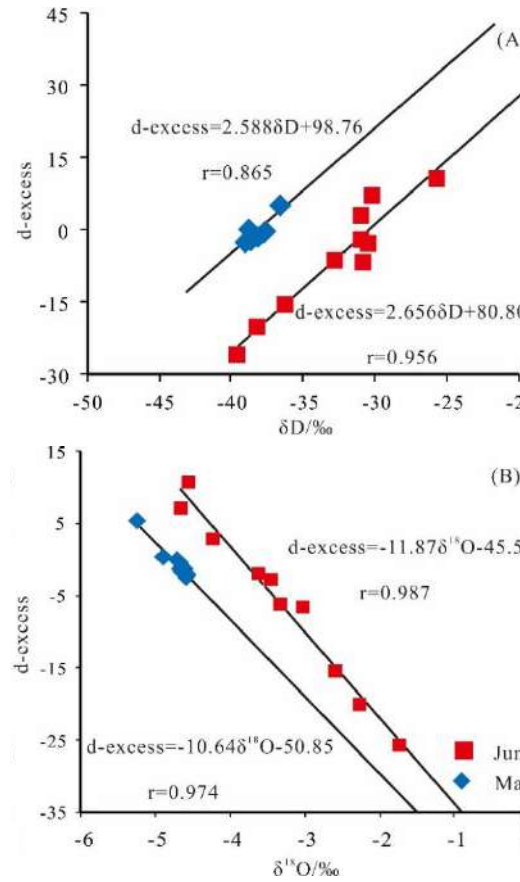

Fig. 4: Relationships between d-excess, δD and $\delta^{18}O$.

As can be seen from the table and figure, based on the values of $\delta^{18}O$, the proportion of the residual water in May is 70% to 75%. Comparatively, the results are 79%–82% based on the values of δD. As to the June samples, the residual water proportions are 51%–70% for May and 69–82% for June based on the values of δD, respectively. Previous studies revealed that the calculation of the water loss caused by evaporation by using $\delta^{18}O$ is more accurate, because in the actual situation, water evaporation is also affected by some meteorological conditions such as wind speed and air humidity (Qian et al. 2007). Therefore, the results obtained from the $\delta^{18}O$ have been accepted in this study. By calculating the proportionate difference of residual water in June and May of each sampling point, the average value of residual water proportion difference calculated by $\delta^{18}O$ is 10%, which indicates that the water loss of the Liuxi brook is about 10% and influenced by evaporation from May to June.

CONCLUSIONS

Based on the hydrogen and oxygen isotopes of water samples collected in the Liuxi brook during May and June, the following conclusions have been obtained:

(1) Most of the samples have higher $\delta^{18}O$ and δD values in June relative to May, implying that the hydrogen and oxygen isotopes of the water have been influenced by evaporation.

(2) The influence of evaporation was further confirmed by the lower d-excess values of the water samples relative to the meteoric line. However, the change of d-excess

Table 2: Calculation results of evaporation ratio of each sampling point.

Sample ID	May				June			
	$\delta^{18}O$/‰	*f*	δD/‰	*f*	$\delta^{18}O$/‰	*f*	δD/‰	*f*
S1	-4.90	0.72	-38.88	0.82	-4.67	0.70	-30.25	0.73
S2	-4.68	0.70	-38.66	0.81	-4.24	0.67	-30.97	0.74
S3	-4.60	0.70	-39.10	0.82	-2.26	0.54	-38.18	0.81
S4	-4.67	0.70	-38.80	0.82	-2.60	0.56	-36.25	0.79
S5	-4.66	0.70	-38.55	0.81	-3.33	0.61	-32.74	0.75
S6	-4.58	0.70	-38.71	0.81	-3.61	0.63	-30.97	0.74
S7	-4.72	0.71	-37.72	0.80	-3.02	0.59	-30.87	0.73
S8	-4.68	0.70	-37.83	0.81	-3.45	0.62	-30.49	0.73
S9	-4.63	0.70	-38.26	0.81	-4.56	0.69	-25.72	0.69
S10	-5.26	0.75	-36.62	0.79	-1.74	0.51	-39.66	0.82

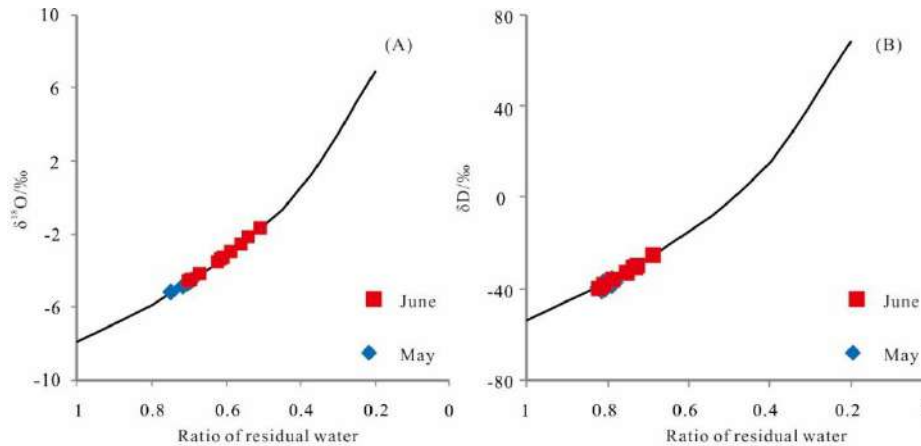

Fig. 5: The relationships between $\delta^{18}O$, δD and the proportion of residual water.

value has been demonstrated to be influenced by the changing of $\delta^{18}O$ and δD, which was related to the evaporation.

(3) According to the calculation based on Rayleigh equilibrium evaporation, the residual water quantities were 70–75% and 51–70% for May and June relative to the initial water, which indicates that about 10% of the water has been evaporated during the period between May and June.

ACKNOWLEDGEMENTS

This work was financially supported by Natural Science Research Project of Universities in Anhui Province (KJ2020ZD64).

REFERENCES

Buttle, J.M. 1994. Isotope hydrograph separations and rapid delivery of pre-event water from drainage basins. Progress in Physical Geography, 18(1): 16-41.

Chen, L.W., Gui, H.L. and Yin, X.X. 2008. Composing characteristic of hydrogen and oxygen stable isotopes and tracing of hydrological cycle. Int. J. Coal Sci. Technol., 30(10): 1107-1111.

Craig, H. 1961. Isotopic variations in meteoric waters. Sci. 133(3465): 1702-1703.

Dansgaard, W. 1964. Stable isotopes in precipitation. Tellus, 16(4): 436-468.

Fan, B.L., Zang, D., Tao, Z.H. and Zhao, Z.Q. 2017. Compositions of hydrogen and oxygen isotope values of Yellow River water and the response to climate change. China Environ. Sci., 37(5): 1906-1914.

Gao, H.B., Li C.Y., Sun, B., Shi, X.H., Zhao, S.N. and Fan, C.R. 2018. Characteristics of hydrogen and oxygen stable isotopes in Lake Hulun Basin and its indicative function in evaporation. Lake Sci, 30(1): 211-219.

Jiang, H.H., Liang, D.H. and Wu, Z.L. 2000. Compasion of comprehensive assessment method of river water quality. Arid Environmental Monitoring, 14(2): 139-142.

Joshi, A. and Seth, G. 2011. Hydrochemical profile for assessing the groundwater quality of Sambhar lake city and its adjoining area. Environ. Monit. Assess., 174(1-4): 547-554.

Kim, K. and Lee, X.H. 2011. Isotopic enrichment of liquid water during evaporation from water surfaces. J Hydrol, 399(3-4): 364-375.

Li, Z.C., Gui H.L. and Chen, S. 2015. Source and degree of heavy metal pollution in the sediment of the moat of Suzhou city, Anhui province. J. Ecology Rural Environ., 31(4): 559-565.

Philip, B. 2019. Hydrogeology: Groundwater science and engineering. Groundwater, 57(3): 356-357.

Qian, H., Dou, Y., Li, X.J., Yang, B.C. and Zhao, Z.H. 2007. Changes of $\delta^{18}O$ and δD along Dousitu River and its indication of river water evaporation. Hydrogeology & Engineering Geology, 1(24): 107-112.

Shi, H., Liu, S.R. and Zhao, X.G. 2003. Application of stable hydrogen and oxygen isotope in water circulation. J Soil Water Conserv, 17(2): 163-166.

Tian, L.D., Yao, T.D. and Sun, W.Z. 2000. Numagui Atusi. Study on stable isotope fractionation during water evaporation in the middle of the Tibetan Plateau. J. Glaciol. Geocryol, 22(6): 159-164.

Wu, H.B., Zhao, Q., Qin, X.B., Gao, Q.Z. and Lv, C.W. 2018. Temporal and spatial variations of hydrogen and oxygen isotopes in Tuoji Raive and its influencing factors. Chinese Journal of Applied Ecology, 29(5): 1461-1469.

Wang, X.Y., Xu, H.L., Yan, J.J., Ling, H.B. and Zhao, X.F. 2018. Conversion of river water to groundwater based on oxygen isotope ($\delta^{18}O$) in the lower reaches of Tarim River. J. Hydrol. Eng., 29(2): 81-89.

Xia, C., Mei, J., Liu, W., Zhou, J. and Liu, G. 2019. Variations of environmental isotopes in precipitation and surface water in plain area influenced by summer monsoon: a case study in Jinjiang river basin, Chengdu, China. Nat. Env. and Poll. Tech., 18(3): 825-833.

Xu, H.S., Zheng, H., Chen, X.S., Ren, Y.F. and Ouyang, Z.Y. 2016. Relationships between river water quality and landscape factors in Haihe River Basin, China: Implications for environmental management. Chin. Geogr. Sci., 26(2): 197-207.

Xu, Z.X. 2005. Comprehensive water quality identification index for environmental quality assessment of surface water. Journal of TongJi University(Natural Science), 33(4): 482-488.

Yao, P. and Lu, G.P. 2017. Hydrochemical and isotopic characteristics of the Juma River and their implications. Environmental Chemistry, 36(7): 1525-1536.

Zhang, L.X., Zhao, B., Xu, G. and Guan, Y.T. 2018. Characterizing fluvial heavy metal pollutions under different rainfall conditions: Implication for aquatic environment protection. Sci. Total Environ., 635(4): 1495-1506.

Zhang, Q.Q., Wang, H.W. and Lu, C. 2020. Tracing sulfate origin and transformation in an area with multiple sources of pollution in northern China by using environmental isotopes and Bayesian isotope mixing model.Environ Pollut, 265: 115105.

Zhang, X.P. and Yao, T.D. 1997. Estimation of lake evaporation by stable isotopic ratio. J. Glaciol. Geocryol., 19(2): 161-166.

Zhang, Y.H., She, Y.Q., Wang, X.H. and Shu, J.P. 2006. Application of environmental isotopes in water cycle. Advances in Water Science, 17(5): 738-747.

Zhao, H.L. 2019. Study on distribution characteristics of heavy metal pollution in semi-closed rivers in cities. Sichuan Environment, 38(6): 120-124.

Nature Environment and Pollution Technology
An International Quarterly Scientific Journal

p-ISSN: 0972-6268
(Print copies up to 2016)
e-ISSN: 2395-3454

Vol. 20 | No.3 | pp. 1237-1242 | 2021

Original Research Paper

https://doi.org/10.46488/NEPT.2021.v20i03.033

Open Access Journal

Insilico Molecular Docking Studies of Volatile Compounds Identified by GC-MS from *Tagetes* Species Against *Mamestra brassicae* (Linnaeus, 1758)

S.R. Krishna Motukuri †, D. Vijaya Nagini, J. Nallamothu and S. Karthikeyan
Department of Biotechnology, K. L. University, Vaddesweram-522502, Guntur, Andhra Pradesh, India
† Corresponding author: S.R. Krishna Motukuri; msrkrishna81@gmail.com

Nat. Env. & Poll. Tech.
Website: www.neptjournal.com

Received: 26-08-2020
Revised: 29-09-2020
Accepted: 15-10-2020

Key Words:
Insect Repellents
Tagetes species
GC-MS
Molecular docking
Mamestra brassicae

ABSTRACT

Plants evolved to be a potential source of pharmacologically active compounds that are being widely accepted as insect repellent compounds for generations. Products of natural origin are mostly preferred over synthetic compounds because of fewer side effects on human health and the environment, have the potential to be produced locally, cost-effective, and are proved to be more efficient. They are best suited in organic food production and can play a much greater role in developing countries as a new class of eco-friendly products for controlling pests. In turn, the development of repellents is desirable alternatives to synthetic chemical insecticides for controlling pests. In the process of continual search for insect-based repellents of natural origin, a wide number of *Tagetes* species have been archived and all parts of this plant from root to seed possess a range of phytochemicals that are responsible for the repellent activity. The present study concentrates on the identification of active volatile compounds from *Tageteserecta* leaves by Gas chromatography-mass spectrometry (GC-MS) analysis and further evaluation through molecular docking studies of identified compounds against *Mamestra brassicae*.

INTRODUCTION

Over the decades, the tradition of utilizing plant derivatives as a potential defense barrier against a wide variety of insects has been globally accepted (Luthria et al.1993). In numerous cases, the botanicals have a long history of usage as traditional remedies to kill or repel insects and are in continual use to date (Broussalis et al.1999). It was estimated that around 2000 species of botanicals are known to inherit some insecticidal activity (Klocke 1989). It is a well-known fact that solvent extracts and other secondary metabolites especially essential oils of many plants show differential levels of insect or bug-repellent properties (Chogo & Crank 1981, Curtis et al. 1991, Trigg & Hill 1996, Thorsell et al. 1998).

Tagetes that originates from the Asteraceae family is an annual, herbaceous ornamental plant that is reported native to Mexico (Tosco1970). It is a genus probably recognized as a source of natural colors (Timberlake & Henry 1986). The genus is also known to have very attractive biologically active compounds such as essential oils (Marotti et al. 1996) and thiophenes (Hulst et al. 1989) that are known for repelling insects (López et al. 2011). In the process of evolution, the interplay between plants and pests or insects is an important determinant of plant yield. These plant-pest interactions that include volatile chemical passages have been widely utilized in the regulation of agricultural pests. In response to the attack, plants have developed a scope of resistance mechanisms to lessen the risk of damage and loss of yield or productivity (Mitchell et al. 2016).

The present work involves the isolation of the volatile compounds of *Tagetes* species by using activated charcoal and analyzing those compounds by GC-MS and also describes the further evaluation of identified compounds against *Mamestra brassicae* through molecular docking studies.

MATERIALS AND METHODS

Viton-lined glass lid, glass jars, aluminum foil, pot, activated charcoal, steel cartridge, pump, N-hexane, methanol, and acetyl chloride

Collection of Plant Material

Tagetes errecta plants were collected from the fields which were maintained in the good physical condition and were grown to a height of 20 centimeters suitable for the extraction experiment.

Extraction and Purification of Volatile Compounds

Extraction of volatile compounds is carried out in a closed-loop stripping system as described by Boland et al. (1984) in which the entire plant is placed in a pot and covered with an aluminum foil and kept inside the closed glass jar which consists of a Viton-lined glass lid with an inlet and outlet.

Air is continuously circulated and the emitted volatile compounds were collected from empty glass jars and also from aluminum-wrapped pots filled with autoclaved soil to collect non-plant-related volatiles. Prior to the collection of volatiles, one end is allowed to supply air through the aquarium motor air pump and on the other side, approximately 100 mg of activated charcoal in the cotton plug is fixed. Plant volatiles were collected in a stainless steel cartridge by drawing air from the glass jars by using an external pump. The whole jar is enclosed without any air leakage either inside or outside (Kroes et al. 2017). The extracted volatile compounds from charcoal were further purified by soxhlet extraction. A sample of organic volatile compounds was extracted by n-hexane in soxhlet extraction. This sample was mixed with equal volumes of methanol and acetyl chloride to attain a final concentration of up to 10 mL.

GC-MS Analysis

The identification and quantification of plant volatiles were performed according to the method described by Pangesti et al. (2015). The plant volatiles were separated and detected using a thermo trace ultra gas chromatograph (GC) which was coupled to a thermo trace DSQ quadrupole mass spectrometer (MS) (Thermo Fisher Scientific, Waltham, USA). The volatiles were thermally discharged from the Tenax TA cartridges at 250 °C for 10 min with a helium stream of 20 mL min^{-1} on an Ultra 50:50 warm desorption unit (Markes, Llantrisant, UK). A cool sorbent trap at 0°C (Unity, Markes) was focused, and after the end of the desorption procedure, volatiles were discharged from the cold trap by ballistic warming at 40°C s^{-1} to 280°C, which was kept up for 10 min and was then moved in a splitless mode to an analytical column [(ZB-5MSi; 30 m × 0.25 mm i.d. × 0.25 µm film thickness with 5 m implicit guard column (Phenomenex, Torrance, CA, USA)] arranged inside the GC oven. The temperature of the GC oven was at first held at 40°C for 2 min, which was then maintained at 10°C min^{-1} and finally raised to a final temperature of 280°C and held for 4 min under a helium stream of 1 mL min^{-1}. The DSQ MS was worked in a scan mode with 35–350 amu mass range at 5.38 scans s^{-1} and spectra were recorded in electron impact ionization (EI) mode at 70 eV. MS transfer line and particle or ion source were set to 275°C and 250°C, separately. Volatiles were probably distinguished by correlation of mass spectra with those in the NIST 2005 and the Wageningen Mass Spectral Database of Natural Products MS libraries, as well as utilizing experimentally acquired Linear Retention Indices (LRI) (Kroes et al.2017).

Molecular Docking

Currently, multiple docking tools have been in use that run based on structure-based drug design strategies. The auto dock is one of the componential software tools that work on such a strategy. In the present work, the molecular docking studies were performed using auto dock – docking tool module to study the intermolecular interactions of chemosensory protein2 (CSP2) identified from the moth *M. brassicae* with standard lead inhibitor DEET (N,N-Diethyl-meta-toluamide) at the active site 3D space of protein of interest and also used to study the binding energy of lead inhibitor DEET.

Protein Structure Preparation

A typical protein structure was obtained from a protein data bank (PDB) with a PDB ID as 1k19 (www.pdb.org/pdb/) (Runthala A et al. 2010) for the molecular docking study; *i.e.* CSP2 structure PDB ID was 1k19. To obtain the protein structure, all hydrogen atoms were added, removed water molecules from the cavity, lower occupancy residue structures were deleted, filled the missing residues, generated the side chains and any incomplete side chains were replaced using the ADT version 4.2. The suitable ligand structures for docking were then saved in PDBQT file format.

Preparation of Ligands

ChemDraw Ultra 7.0 was utilized in the designing of the structure of the 2D light and these structures were changed over to 3D structures utilizing Chem3D ultra 7.0. MM2 was used for the minimization of energy levels. These energy-minimized ligands were utilized for docking assessment. All ligand structures were saved in .pdb file format to provide as an input to 2 (Version AutoDock 4.2). After evaluation, the ligand structures were saved in the PDBQT record design.

Validation of Molecular Docking

Protein-Ligand interactions happen through the sub-atomic mechanics resulting in the conformational changes in which the ligand-binding changes the protein state and its function. To know the reliability of such interactions, the technique of molecular docking should be validated preliminarily for the analysis of ligands. The co-crystallized ligand was extracted from the CSP2 and re-docked onto its active dynamic site. The reference standard ligand (DEET) was extracted from the PDB and re-docked again onto the active site to compute the docking energy level.

Auto Docking

AutoDock vina version (4.0) was used for molecular docking studies which utilize gradient-based conformational search. Volatile chemical compounds namely docosane, docosanoic acid, eicosane, heneicosane, heptacosane, heptadecanedipentyl, hexacosane, hexadecanoic acid methylester, hexatriacontane, octacosane, octadecanoic acid methylester,

pentacosane, pentacosane-13 undecyl, tetracosane and a standard active ingredient in most of the insect repellents i.e. DEET were docked against 1k19 and results were analyzed based on their binding energies. Based on binding free energies almost for all ligands, 100 stimulations were performed for every docking experiment. The relatedness of the docked structure was estimated by calculating the root mean square deviation (RMSD) (Runthala et al. 2010) between the coordinates of the atoms. The least binding energy conformations were considered as the best docking posture.

RESULTS AND DISCUSSION

In the context of farming, insect or pests management plays a vital role in deciding the yield of the crop. Presently, a wide range of synthetic insect repellents or insecticidal compounds is in trade. The most common of all the synthetic repellents with an excellent insect repellency property used worldwide is DEET (Fig.1) (N,N- diethyl-3-methylbenzamide) (Yap 1986, Coleman et al. 1993, Walker et al. 1996). Although it is widely accepted its usage is limited because of its noticeable effects like unpleasant odor, it has the ability to penetrate the skin, damages the plastic, painted surfaces and synthetic fabrics thus resulting in a search for new alternative approaches (Miller 1982, Roland et al. 1985, Briassoulis 2001, Clem et al. 1993). A substitute for synthetic repellents is to use natural products with good efficacy and which are eco-friendly. Botanical insecticides have been recommended as an alternative to synthetic insecticides for reducing the loss of crop yield that is being invaded by various pests or insects and pose only a negligible threat to the environment and human health. However, only a few of the botanicals are in current use in the farming community and there is an urgent need for the development and trading of new botanical insecticides (Isman 2006). The tradition of using plant-derived compounds, particularly essential oils, has been recently launched into the market which is found to be active against hematophagous arthropods (Curtis et al. 1991).

A wide variety of *Tagetes* species have gained researchers interest as it possesses essential volatiles with a remarkable insecticidal property. The essential volatile compounds of the *T. errecta* plant were extracted by using charcoal and further purified. The volatile compounds present in *T. errecta* were identified by the GC-MS technique. Molecular

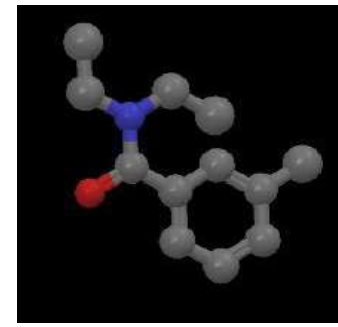

Fig. 1: Structure of DEET.

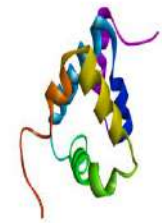

Fig. 2: Structure of 1k19.

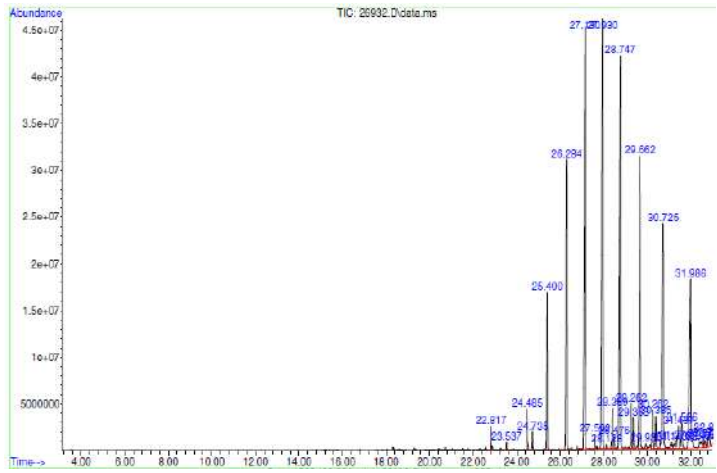

Fig. 3: GC-MS chromatogram of volatile compounds of *Tagetes errecta.*

Table 1: Volatile Compounds of *Tagetes errecta* obtained by GC MS reports.

Peak	R. T. Min	Compound name	Structure	Peak height	Corr. Area	Quality	Structure
1	22.817	Hexadecanoicacid,methyl ester	$C_{17}H_{34}O_2$	2397957	42882341	98	
2	23.537	Eicosane	$C_{20}H_{42}$	779053	14533637	98	
3	24.485	Heneicosane	$C_{21}H_{44}$	4207688	90714880	99	
4	24.735	Octadecanoic acid, methyl ester	$C_{19}H_{38}O_2$	1915660	33984466	99	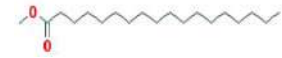
5	25.400	Docosane	$C_{22}H_{46}$	14962963	304217950	96	
6	27.130	Tetracosane	$C_{24}H_{50}$	42719981	1280463770	99	
7	27.592	Heptadecane, 8,8- dipentyl-	$C_{27}H_{56}$	1474031	2741475	91	
8	27.930	Pentacosane	$C_{25}H_{52}$	42116615	1311990887	94	
9	28.128	Docosanoic acid, methyl ester	$C_{23}H_{46}O_2$	467389	11435367	99	
10	28.389	Hexatriacontane	$C_{36}H_{74}$	4144778	93809392	97	
11	28.476	Pentacosane,13-undecyl-	$C_{36}H_{74}$	1260881	27132915	72	
12	28.747	Hexacosane	$C_{26}H_{54}$	39741656	1255452851	98	
13	29.262	Tetracosane	$C_{24}H_{50}$	4529030	117897533	98	
14	29.363	Pentacosane	$C_{25}H_{52}$	2991924	67853632	89	
15	29.662	Heptacosane	$C_{27}H_{56}$	30665082	1053795210	98	
16	29.936	Octacosane	$C_{28}H_{58}$	481534	17865430	98	
17	31.986	Octacosane	$C_{28}H_{58}$		803393205	99	

docking studies reveal the presence of novel compounds by comparing their highest binding affinity with Chemosensory Protein CSP2 (1k19) (Fig. 2) identified from the moth *M. brassicae.* The GC-MS analysis shown in Fig.3 reveals that 14 volatile compounds were present in extracts of *T. errecta* including docosane, docosanoic acid, eicosane, heneicosane, heptacosane, heptadecanedipentyl, hexacosane, hexadecanoicacidmethylester, hexatriacontane, octacosane, pentacosane, tetracosane octadecanoic acid methylester, pentacosane13undecyl (Table 1). From the GC-MS analysis tetracosane, pentacosane, hexacosane, heptacosane are the compounds present more in the volatile organic compounds of *T. erecta.* Based on the correlation area of the peaks of GC-MS results, pentacosane is the highest amount present in the sample with a correlation area of 1311990887, the second-highest compound is tetracosane with a correlation area of 1280463770, and the least amount of compound is Heptadecane, 8,8- dipentyl- with a correlation area of 2741475.

To explore the accurate intermolecular interactions between the ligand and the protein target, molecular docking studies were performed. AutoDock vina version 4.0 was used which executes grid-based ligand docking between tiny ligand molecules and complex receptor molecules which

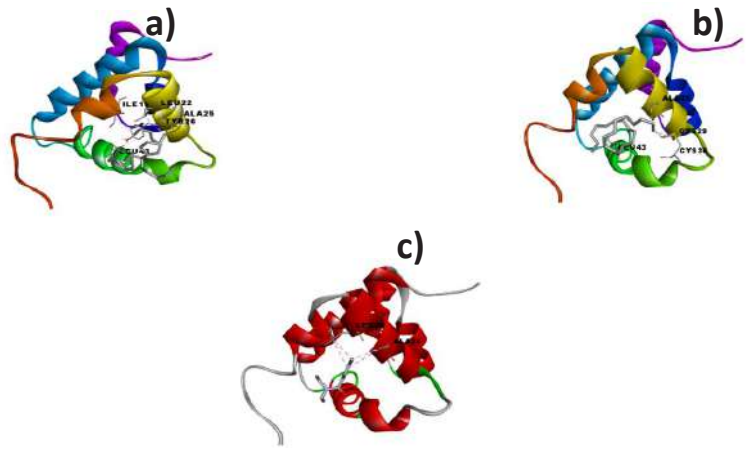

Fig. 4: Docking of a) Heptadecanediphenyl ,b) Docosane, c) DEET with 1k19.

usually is a protein of interest. The 3-dimensional structural information of the protein of interest i.e Chemosensory Protein CSP2 identified from the moth *M. brassicae* was taken from the Protein Data Bank (PDB) with PDB ID as 1k19. Initially, the protein preparation was performed by deleting the water molecules, adding the hydrogen bonds, and by generating the side chains. The volatile compounds extracted from the *T. erecta* species obtained from GC-MS analysis were docked into the active site of 1k19. Molecular docking methodologies are basically used in the current generation drug design process to figure out the protein-ligand interactions **(**Gaddaguti et al.2012**)**. Thus, understanding the detailed 3D structure of a protein-ligand composite at the very basic atomic level could be served as a significant subject in biological sciences (Gaddaguti et al. 2012, Ahmed et al. 2018). The most accurate method of determining the exactness of a docking protocol is to determine how closely the lowest energy pose i.e the binding conformation is predicted between the ligand and the target protein.

All the volatile compounds obtained from the GC-MS analysis of *T. erecta* were docked with the CSP2 protein 1k19. Among the volatile compounds (ligands) identified through GC-MS analysis docked in this study (Fig. 4), two compounds, namely, heptadecanediphenyl and docosane showed lower binding energy as -4.8 than the standard inhibitor DEET which showed the binding energy as -6.2 (Table 2). The least binding energy conformation pose was identified and this energy was regarded as a favorable docking pose (Ghosh et al. 2017). These volatile botanical compounds of *T. erecta* have potential insect repellency property activity against 1k19 Chemosensory Protein CSP2 of the moth *Mamestra brassicae*.

Table 2: Binding free energies for the insilco binding of ligands with 1k19.

S.No.	Ligand Name	Binding Free Energy (kCal.mol^{-1})
1	Heptadecanediphenyl	-4.8
2	Docosane	-4.8
3	DEET	-6.2

CONCLUSION

Plant-derived products (PDPs) are very useful on grounds with low mammalian toxicity, reduced environmental persistence, and complex chemistries that limit the development of pest resistance against them. In turn, for controlling pests, the development of repellents from PDPs is the best alternatives to chemical insecticides. In the present study, among 14 volatile botanical compounds screened with autodocking, two compounds namely heptadecanediphenyl and docosane showed lower binding energy than the standard compound DEET. These two bioactive volatile compounds of *T. erecta* have potential insect repellency property activity against 1k19 Chemosensory Protein CSP2 of the moth *M. brassicae*. The results of this study could be used for further characterization and in vivo inhibitor activity studies against moth *M. brassicae.*

LIST OF ABBREVIATIONS

GC-MS-Gas chromatography-Mass spectrometry, mg-milligram, DSQ-Dual Stage Quadrupole, °C-degree centigrade, min-minute, mL-millilitre, min−1-per minute, s−1-per second, amu-atomic mass unit, eV-Electron volt, NIST-National Institute of Standards and Technology, PDBQT- Protein Data

Bank, Partial Charge (Q) & Atom Type (T), MM2-Molecular Mechanics

REFERENCES

Ahmed, H.A., Alkali, I.Y. and Mahmud, A.F. 2018. In silico molecular docking studies of some phytochemicals against dipeptidyl peptidase 4. Int. Res. J. Pharm. Med. Sci., 1(6): 65-68.

Boland, W., Ney, P., Jaenicke, L. and Gassmann, G. 1984. A 'closed-loop-stripping' technique as a versatile tool for metabolic studies of volatiles. In: Chreier, P. (Ed.), Analysis of Volatiles, Walter de Gruyter, Berlin, pp. 371-373.

Briassoulis, G. 2001. Toxic encephalopathy associated with the use of DEET insect repellents: A case analysis of its toxicity in children. Hum. Exp. Toxicol., 20: 8-14.

Broussalis, A.M., Ferraro, G.E., Martino, V.S., Pinzón, R., Coussio, J.D. and Alvarez, J.C. 1999. Argentine plants as potential source of insecticidal compounds. J. Ethnopharmacol., 67(2): 219-223.

Chogo, J.B.A. and Crank, G. 1981. Chemical composition and biological activity of the Tanzanian plant Ocimum suave. J. Nat. Prod., 44(3): 308-309.

Clem, J.R., Havemann, D.F. and Raebel, M.A. 1993. Insect repellent (N,Ndiethyl-m-toluamide) cardiovascular toxicity in an adult. Ann. Pharmacother., 27: 289-293.

Coleman, R.E., Robert, L.L., Roberts, L.W., Glass, J.A., Seeley, D.C., Laughinghouse, A., Perkins, P.V. and Wirtz, R.A. 1993. Laboratory evaluation of repellents against four anopheline mosquitoes (Diptera: Culicidae) and two phlebotomine sand flies (Diptera: Psychodiae). J. Med. Entomol., 30: 499-502.

Curtis, C.F., Lines, J.D., Lu, B. and Renz, A. 1991. Natural and synthetic repellents. In: Curtis, C.F. (Ed.), Control of Disease Vectors in the Community. Wolfe Publishers Ltd, London, pp. 75-92.

Gaddaguti, V., Mounika, S.J., Sowjanya, K., Rao, T., Chakravarthy, M.S.R.K. and Allu, R., 2012. GCMS analysis and in silico molecular docking studies of mosquito repellent compounds from Hyptissuaveolens. Int. J. Bioassays, 1: 36-41.

Ghosh, A.K., Palit, S. and Samajdar, S. 2017. Insilco molecular docking study of dihydroisoquinolinium derivatives as DPP IV inhibitors in type II diabetes mellitus. Pharma. Tutor, 5(6): 22-28.

Hulst, A.C., Meyer, M.M.T., Breteler, H. and Tramper, J. 1989. Effect of aggregate size in cell cultures of *Tagetes patula*on thiophene production and cell growth. Appl. Microbiol. Biotechnol., 30: 18-25.

Isman, M.B. 2006. Botanical insecticides, deterrents, and repellents in modern agriculture and an increasingly regulated world. Annu. Rev. Entomol., 51: 45-66.

Klocke, J.A. 1989. Plant compounds as source and models of insect-control agents. Econ. Med. Plant Res., 3: 103-144.

Kroes, A., Weldegergis, B.T., Cappai, F., Dicke, M. and van Loon, J.J. 2017. Terpenoid biosynthesis in Arabidopsis attacked by caterpillars and aphids: effects of aphid density on the attraction of a caterpillar parasitoid. Oecologia, 185(4): 699-712.

López, S.B., López, M.L., Aragón, L.M., Tereschuk, M.L., Slanis, A.C., Feresin, G.E. and Tapia, A.A. 2011. Composition and anti-insect activity of essential oils from *Tagetes* L. species (Asteraceae, Helenieae) on *Ceratitis capitata* (Wiedemann) and *Triatoma infestans* (Klug). J. Agric. Food Chem., 59(10): 5286-5292

Luthria, D.L., Ramakrishnan, V. and Banerji, A. 1993. Insect antifeedant activity of furochromones: Structure-activity relationships. J. Nat Prod., 56(5): 671-675.

Marotti, M., Piccaglia, R., Brunelli, A. and Flori, P. 1996. Preliminary studies on the control of fungal phytopathogens with *Tagetes* extracts. Proceeding of the Third European Symposium on Industrial Crops and Products, Reims, France.

Miller, J.D. 1982. Anaphylaxis associated with insect repellent. N Engl. J. Med., 307(21): 1341-1342.

Mitchell, C., Brennan, R.M., Graham, J. and Karley, A.J. 2016. Plant defense against herbivorous pests: Exploiting resistance and tolerance traits for sustainable crop protection. Front. Plant Sci., 7: 1132.

Pangesti, N., Weldegergis, B.T., Langendorf, B., Van Loon, J.J.A., Dicke, M. and Pineda, A. 2015. Rhizobacterial colonization of roots modulates plant volatile emission and enhances the attraction of a parasitoid wasp to host-infested plants. Oecologia, 178: 1169-1180.

Roland, E.H., Jan, J.E. and Rigg, J.M. 1985. Toxic encephalopathy in a child after brief exposure to insect repellents. Can. Med. Assoc. J., 132: 155-156.

Runthala, A. and Singh, A.K. 2010. Tegument based in-silico Drug targeting of herpes simplex virus-1. Saratov J. Med. Sci. Res., 2(6): 353-357.

Thorsell, W., Mikiver, A., Malander, I. and Tunon, H. 1998. Efficacy of plant extracts and oils as mosquito repellents. Phytomedicine, 5: 311-323.

Timberlake, C.F. and Henry, B.S. 1986. Plant pigments as natural food colors. Endeavour, 10: 31-36.

Tosco, U. 1970. Diccionario de Bota´nica; Instituto Geogra´fico de Agostini: Teide, Barcelona.

Trigg, J.K., and Hill, N. 1996. Laboratory evaluation of eucalyptus-based repellent against four biting arthropods. Phytother. Res., 10: 43-46.

Walker, T.W., Robert, L.L., Copeland, R.A., Githeko, A.K., Wirtz, R.A., Githure, J.I. and Klein, T.A. 1996. Field evaluation of arthropod repellents, deet, and a piperidine compound, AI3-37220, against *Anopheles funestus* and *Anopheles arabiensis* in West Kenya. J. Am. Mosq. Control Assoc., 12: 172-176.

Yap, H.H. 1986. Effectiveness of soap formulations containing deet and permethrin as personal protection against outdoor mosquitoes in Malaysia. J. Am. Mosq. Control Association, 2: 63-67.

Nature Environment and Pollution Technology
An International Quarterly Scientific Journal

p-ISSN: 0972-6268
(Print copies up to 2016)
e-ISSN: 2395-3454

Vol. 20 | No.3 | pp. 1243-1250 | 2021

Original Research Paper

https://doi.org/10.46488/NEPT.2021.v20i03.034

Open Access Journal

Study on Spatiotemporal Evolution Characteristics of Regional Annual Precipitation

Xianqi Zhang*(**)(***), Zhiwen Zheng*† and Rulin Ouyang****

*School of Water Conservancy, North China University of Water Resources and Electric Power, Zhengzhou 450046, China

**Collaborative Innovation Center of Water Resources Efficient Utilization and Protection Engineering, Zhengzhou 450046, China

***Technology Research Center of Water Conservancy and Marine Traffic Engineering, Henan Province, Zhengzhou 450046, China

****Water Resources Management Center, Ministry of Water Resources, Beijing 100038, China

†Corresponding author: Zhiwen Zheng; 604267813@qq.com

Nat. Env. & Poll. Tech.
Website: www.neptjournal.com

Received: 23-12-2020
Revised: 21-07-2020
Accepted: 04-03-2021

Key Words:
Innovation trend analysis (ITA)
Precipitation
Wavelet analysis

ABSTRACT

The study of the temporal and spatial evolution of precipitation is of great importance for the efficient use of water resources. This paper examines the long series of precipitation in Henan province from 1959-2018. Innovative Trend Analysis (ITA) method and Mann-Kendall (MK) test were used to analyze the characteristics of precipitation trend changes. Mann-Kendall (MK) mutation test and the sliding T method were used to study the jump features of precipitation. Wavelet analysis of the cyclical characteristics of precipitation. The results show that the spatial distribution of precipitation in Henan Province is uneven, with a gradual increase from north to south. The precipitation of northern, central and southern regions showed a downward trend, while that of western regions showed an upward trend. Both the northern and southern regions experienced jump features in precipitation around 1975 and 2008, while the western region experienced jump features around 1962 and 1980, and the central region experienced jump features around 1980; There are 3.5 different scales of "abundance and depletion" in the northern, western and southern regions, with a first principal cycle of 28a, and 5.5 different scales of "abundance and depletion" in the central region, with a first principal cycle of 17a.

INTRODUCTION

With global warming, the hydrological cycle processes such as regional precipitation, evaporation and runoff have changed. The frequency of extreme weather and climate events raises widespread concerns about climate change. Rainfall is a major component of the water cycle and its variability is closely linked to droughts and floods, which can threaten water supply, agricultural irrigation and socio-economic development. The study of precipitation characteristics is therefore essential for flood control and drought prevention, rational use, optimal allocation and scientific management of water resources. (Zhou et al. 2020) analyzed precipitation trends and mutation characteristics in the North Canal basin from 1960-2016 using linear regression, Mann-Kendall mutation test, wavelet analysis and other methods. (Animashaun et al. 2020) Investigation of the temporal and spatial variability of rainfall in 33 micro-watersheds in the Central Hydrological Zone of Niger, Nigeria, from 1911-2015. (Wang et al. 2020) studied precipitation trends in the Yangtze River Delta from 1961 to 2016 using the Innovative Trend Analysis (ITA), Theil-Sen and Mann-Kendall methods, and verified the validity of the ITA method. (Chen et al. 2016) analyzed the trend and cyclical evolution of annual and seasonal precipitation from 1960-2006 at 49 meteorological stations in Liaoning province. At present, the evolution of precipitation is mostly studied in terms of trends and cycles in a single time series for an area or river basin, which does not sufficiently reflect the representativeness and spatial variability of regional precipitation evolution.

Henan Province is located in central China and covers a total area of 167000km^2, spanning four river basins: the Yangtze River, the Yellow River, the Huai River and the Hai River. The climate is characterized by a transition from subtropical to warm-temperate from south to north and from plain to hilly mountainous from east to west, and the precipitation is unevenly distributed over time and space.

As shown in Fig. 1, the daily measured precipitation data for the period 1959-2018 was selected from four weather

stations in Anyang, Lushi, Zhengzhou and Xinyang. An analysis of 60-year precipitation trends in Henan Province using the Innovative Trends Analysis (ITA) and Mann-Kendall methods. The Mann-Kendall mutation test and the sliding T method for analyzing precipitation mutation characteristics. Analysis of its period using Morlet wavelets. The temporal and spatial characteristics and patterns of precipitation sequences are fully studied to provide reference for flood control and drought prevention, scientific management of water resources and agricultural production in Henan Province.

DATA SOURCES

In this paper, daily precipitation data for 60 years from 1959 to 2018 from four meteorological stations in Anyang (north), Lushi (west), Zhengzhou (central) and Xinyang (south), provided by the China Meteorological Data Network, are used. Daily precipitation data is collated into adult precipitation data for study.

METHODS

Innovative Trends Analysis (ITA) Method

There are a number of methods for studying trends in precipitation, such as the Mann-Kendall (MK) test and the Spearman's rho (SR) test. These methods provide a better picture of precipitation trends, however, they require restrictive assumptions such as data length, normality, series independence, etc. (Alashan 2018). These features may sometimes be absent in the structure of the hydrological time series. ITA method is a trend analysis method that does not rely on restrictive assumptions and is highly effective (Alifujiang et al. 2020, Gedefaw et al. 2018, Huang et al. 2018, Li et al. 2019).

ITA is a graphical method for displaying hydrometeorological trends based on time series on a Cartesian coordinate system. The raw data is divided equally into two parts according to the time series, each part being arranged in ascending order. The top half of the data is defined as the first subsequence on the x-axis and the bottom half as the second subsequence on the y-axis, as shown in Fig. 2. A 1:1 (45°) line represents a non-trend line and a scatter falling above (below) a 1:1 line represents an upward (downward) trend in the time series. A scatter falling within 5% of the 1:1 (45°) straight line means that there is no significant trend in the time series. In this paper, rainfall is divided into three sub-areas: 'low', 'medium' and 'high' to detect trends in rainfall within the different sub-areas (Şen 2012, Şen 2017).

The slope s of the innovative trend analysis method can be calculated according to the following equation.

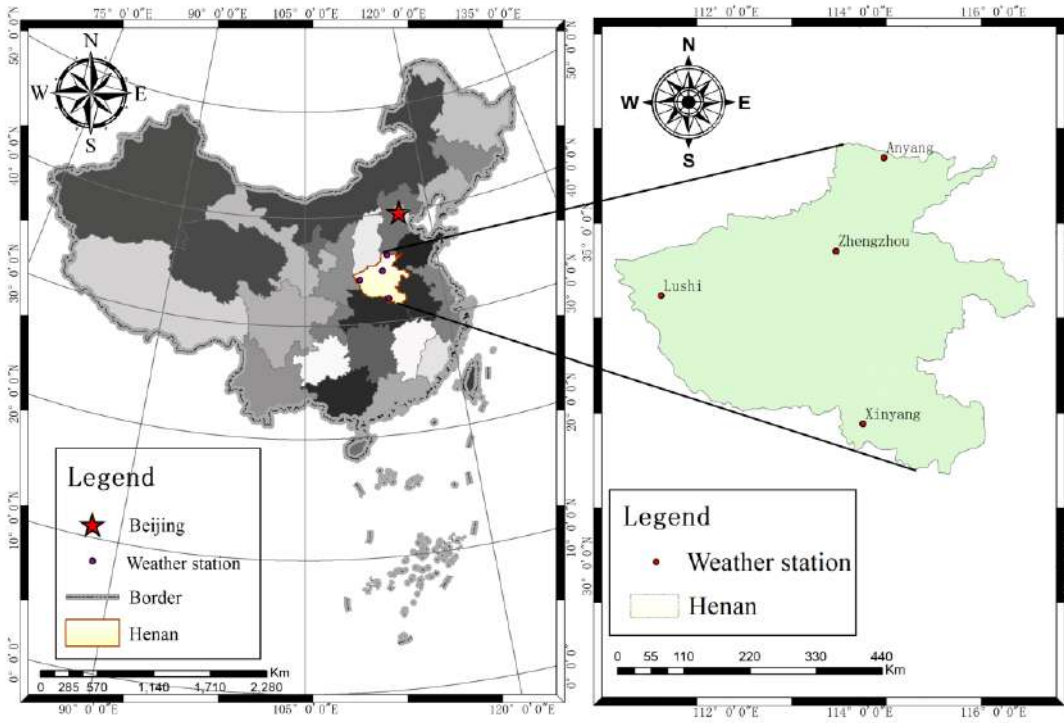

Fig. 1: Diagram of the study area.

$$s = \frac{2(\bar{y}_2 - \bar{y}_1)}{n} \quad ...(1)$$

Where: n is the length of the sequence, $\bar{y}_2$ is the arithmetic mean of the vertical coordinates and $\bar{y}_1$ is the arithmetic mean of the horizontal coordinates.

Mann-Kendall (MK) Test

The MK test is a non-parametric trend detection method. The advantage is that the data is not required to be normally distributed and is rarely disturbed by outliers. (Liu et al. 2012b). The basic formula is as follows:

$$S = \sum_{i-1}^{n-1} \sum_{j=i+1}^{n} \operatorname{sgn}\left(x_j - x_i\right) \quad ...(2)$$

$$\operatorname{sgn}(x_j - x_i) = \begin{cases} +1, if(x_j - x_i) > 0 \\ 0, if(x_j - x_i) = 0 \\ -1, if(x_j - x_i) < 0 \end{cases} \quad ...(3)$$

Where: x_j, x_i denotes the sample data values and $j > i$; n denotes the length of the data series. When n>10, the S distribution tends to be normal. The variance is calculated is as follows:

$$\operatorname{var}(S) = [n(n-1)(2n+5) - \sum_t t(t-1)(2t+5)]/18 \quad (4)$$

$$Z = \begin{cases} \frac{S-1}{\sqrt{\operatorname{var}(S)}}, & S > 0 \\ 0 \quad , & S = 0 \\ \frac{S+1}{\sqrt{\operatorname{var}(S)}}, & S < 0 \end{cases} \quad (5)$$

In bilateral trend tests, for a given level of significance, the original hypothesis is considered unacceptable if $|Z| \geq Z_{1-\alpha/2}$ That is, at a confidence level of α, there is a clear upward or downward trend in the time series data. For a given level of significance, a is considered an unacceptable hypothesis. When |z| is greater than or equal to the threshold value $Z_{1-\alpha/2}$ =1.96, 2.58 it means that both an upward and downward trend is evident, passing the 95% and 99% level of significance test respectively (Guo et al. 2015, Liu et al. 2012a, Yu & Chen 2013).

Morlet Wavelets

Wavelet analysis is a high-resolution analytical method that enables the decomposition of time series into the time and frequency domains in order to obtain the inherent evolution of the sequence. Its wavelet function is oscillatory and can quickly decay to zero (Heng 2003, Li et al. 2011).

For any function $f(t) \subset L^2(R)$, where $L^2(R)$ denotes the squared productive space and R denotes the set of real numbers, the continuous wavelet transformation is:

$$W_f(a,b) = \frac{1}{\sqrt{|a|}} \int_{-\infty}^{+\infty} f(t) \overline{\psi}\left(\frac{t-b}{a}\right) dt \quad (6)$$

Where: $W_f(a, b)$ is the wavelet coefficient; a is the periodic scale factor; b is the time shift factor; $\overline{\psi}\left(\frac{t-b}{a}\right)$ is the complex conjugate function for $\psi\left(\frac{t-b}{a}\right)$.

Wavelet variance is a parameter reflecting the main time scale of the sequence, the value of which can be obtained by integrating the continuous wavelet transform coefficients, calculated by the following formula:

$$Var(a) = \int_{-\infty}^{+\infty} \left|W_f(a,b)\right|^2 db \quad (7)$$

$$\psi(t) = e^{w_0 ti} e^{-t^2/t} \quad (8)$$

RESULTS AND DISCUSSION

Trend Analysis

The trends in precipitation at the four stations in Anyang, Lushi, Zhengzhou and Xinyang are quantitatively analyzed using the MK test method and the Innovative Trend Analysis (ITA) method. The results of the calculations are shown in Table 1.

According to the calculations in Table 1, the annual precipitation MK values for Anyang, Zhengzhou and Xinyang are -0.53, -1.73 and -0.11 respectively, which are all less than zero and $|Z_c| < 1.96$, indicating a non-significant downward trend. Whereas the annual precipitation MK for the Lushi is 1.05 greater than 0 but $|Z_c| < 1.96$ with a non-significant upward trend. The Innovative Trend Analysis (ITA) method agrees with the results of the MK trend analysis. Precipitation in Anyang shows an upward trend in the 'low' zone and a downward trend in the 'medium' and 'high' zones. In combination with Fig. 2(a), there is a clear upward trend in precipitation for less than 300mm and a downward trend for more than 650mm, but not significant. The precipitation trends in the 'low' and 'medium' divisions of Lushi are consistent

Table 1: Trend test calculation results

Sites	Z_c	S			
		Year	low	medium	High
Anyang	-0.53	-0.80	2.20	-0.15	-7.93
Lushi	1.05	0.17	0.65	1.43	-25.62
Zhengzhou	-1.73	-0.04	3.14	0.42	-25.21
Xinyang	-0.11	-1.06	0.29	-3.94	-9.60

with the annual precipitation trends, with a non-significant upward trend, but with a significant downward trend in the 'high' divisions. In combination with Fig. 2(b), most of the precipitation in Lushi is concentrated in the 400-700mm range and the trend is not significant, with a significant downward trend below the 5% trend line for precipitation greater than 900mm. The trend of precipitation in the 'low' and 'medium' subdivisions of Zhengzhou is increasing but not significantly, while the downward trend of precipitation in the 'high' subdivisions is significant. According to Fig. 2(c), precipitation greater than 900mm in Zhengzhou is below the 5% trend line and it shows a significant downward trend. According to Fig. 2(d), there is a significant downward trend in precipitation in Xinyang between 1300 and 1500 mm.

Rainfall in Henan Province increases from north to south. Precipitation in the north and west-central regions is mostly in the range of 300-1000 mm, while in the south it is mostly in the range of 800-1600 mm, with an uneven spatial distribution of precipitation. In the northern and south-central parts of Henan there is a downward trend in precipitation over the years and an upward trend in the west, but the change in trend is not significant.

Mutational Analysis

The Mann-Kendall mutation test and the sliding T-test were used to analyze the characteristics of the annual precipitation mutations in Henan Province.

The Mann-Kendall mutation test plot (Fig. 3) and the sliding T-test plot (Fig. 4) for the four stations in Henan were plotted using MATLAB.

As can be seen from the Mann-Kendall mutation test curve (Fig. 3a). The intersections of UF statistics and UB

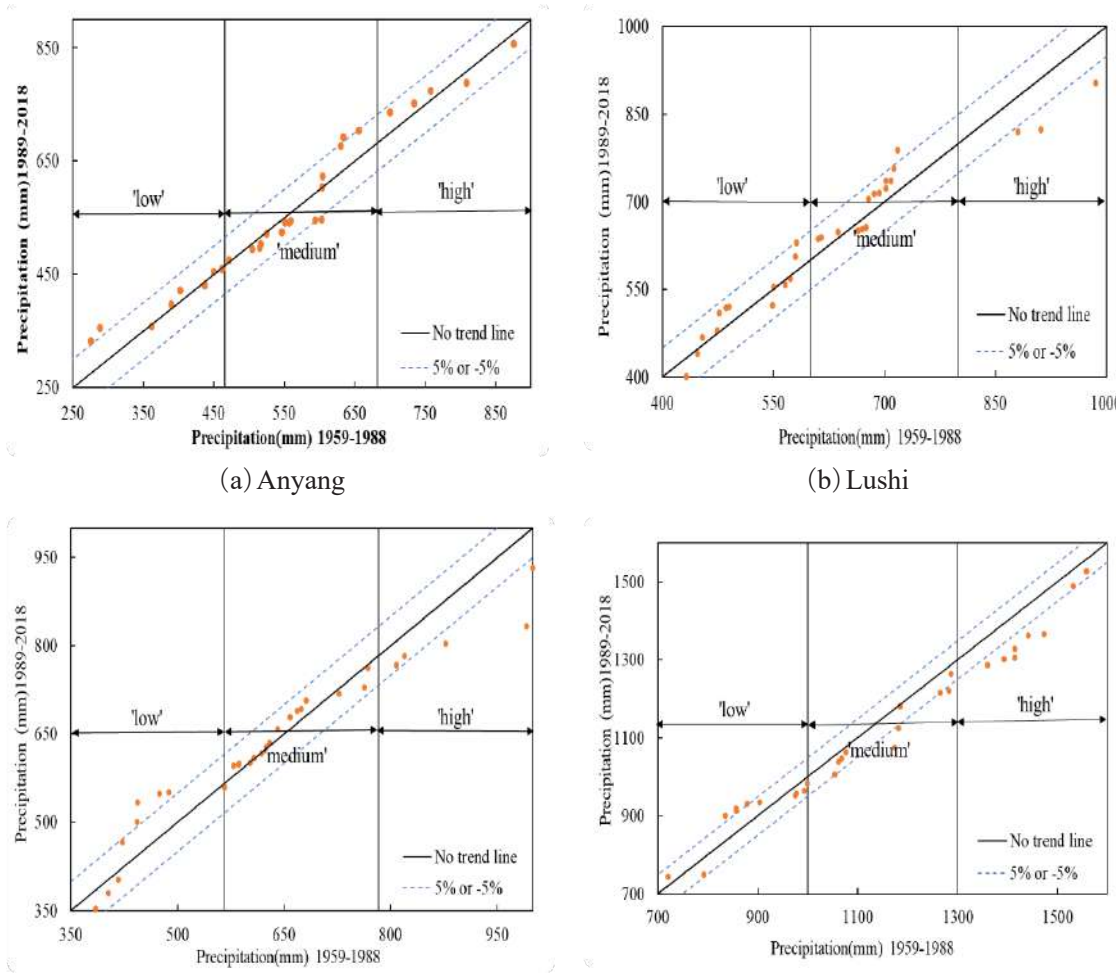

Fig. 2: ITA precipitation trends at four stations in Henan.

statistics are 1961, 1966, 1974, 2008 and 2017 respectively, indicating that the precipitation in Anyang was abruptly changed in 1961, 1966, 1974, 2008 and 2017.The UF statistics for the period 1965-2018 are all negative, indicating a decreasing trend in precipitation in Anyang. According to Fig. 3(b), the years in which the mutation occurred in Lushi were 1961, 1980, 1986, 2006 and 2013, and the UF statistic was negative in 1969-1981, indicating that there was a decreasing trend in precipitation in Lushi in 1969-1981 and an increasing trend in precipitation in Lushi in the remaining years. According to Fig. 3(c), Zhengzhou underwent mutations in 1961, 1980, 1985, 1995, 2011 and 2016, with UF statistics fluctuating up and down with no clear trend. According to Fig. 3(d), the years of the Xinyang mutation were 1963, 1973 and 1979.

The annual precipitation at each station is subjected to a sliding T-test and the sliding T-test is plotted at the level of significance A (Fig. 4). As shown in Fig. 4(a), the Anyang mutation years are 1975, 1981 and 2008. See Fig. 4(b) for the year of the Lushi mutation, 1980, 1985. See Fig. 4(c) for the Zhengzhou mutation years of 1964, 1981, 1985 and 2002. As shown in Fig. 4(d), the year of the Xinyang mutation is 2008.

Combining the results of the Mann-Kendall mutation test and the sliding T-test plots, which are shown in Table 2, it was determined that precipitation in Anyang and Xinyang was mutated around 1975 and 2008, in Lushi around 1962 and 1980, and in Zhengzhou around 1980.

Cyclical Analysis

The cumulative anomaly of 60 years of sequential annual

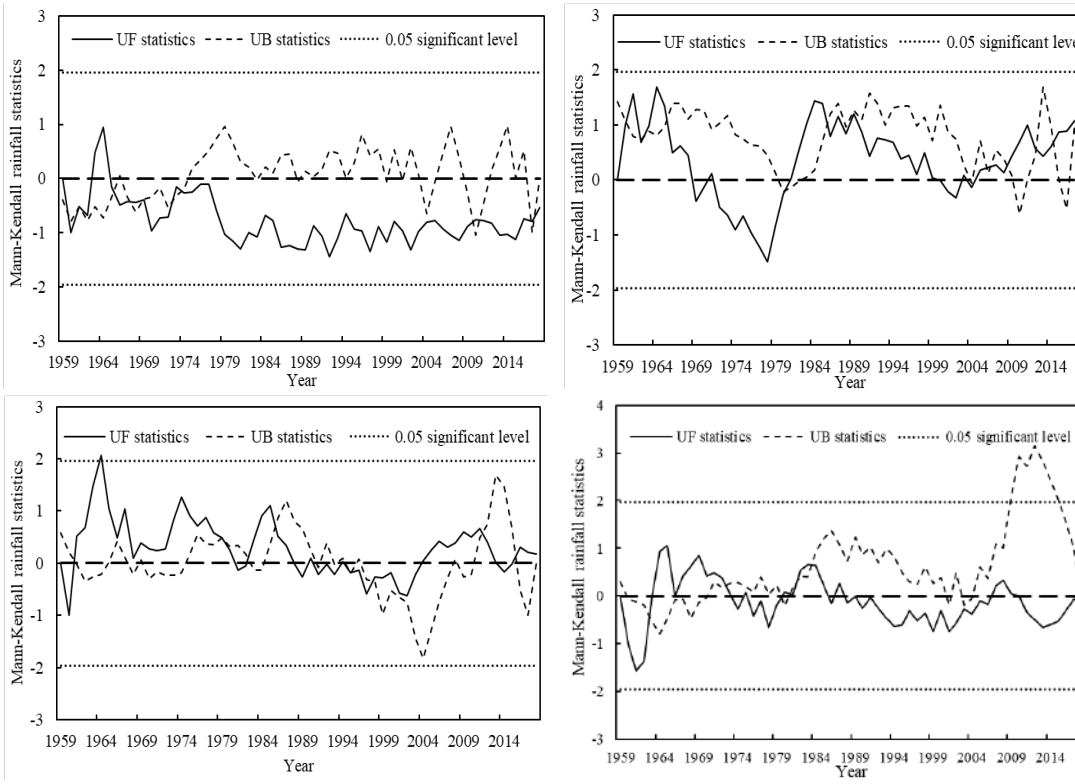

Fig. 3: Mann-Kendall mutation test curve.

Table 2: Rainfall mutation year

	Anyang	Lushi	Zhengzhou	Xinyang
Mann-Kendall mutation test results	1961 , 1966, 1974, 2008, 2017	1961, 1980, 1986, 2006, 2013	1961, 1980, 1985, 1995, 2011, 2016	1963, 1973, 1979
Sliding T mutation test results	1975, 1981, 2008	1980, 1985	1964, 1981, 1985, 2002	2008
Mutation year	1975, 2008	1980	1962, 1980	1975, 2008

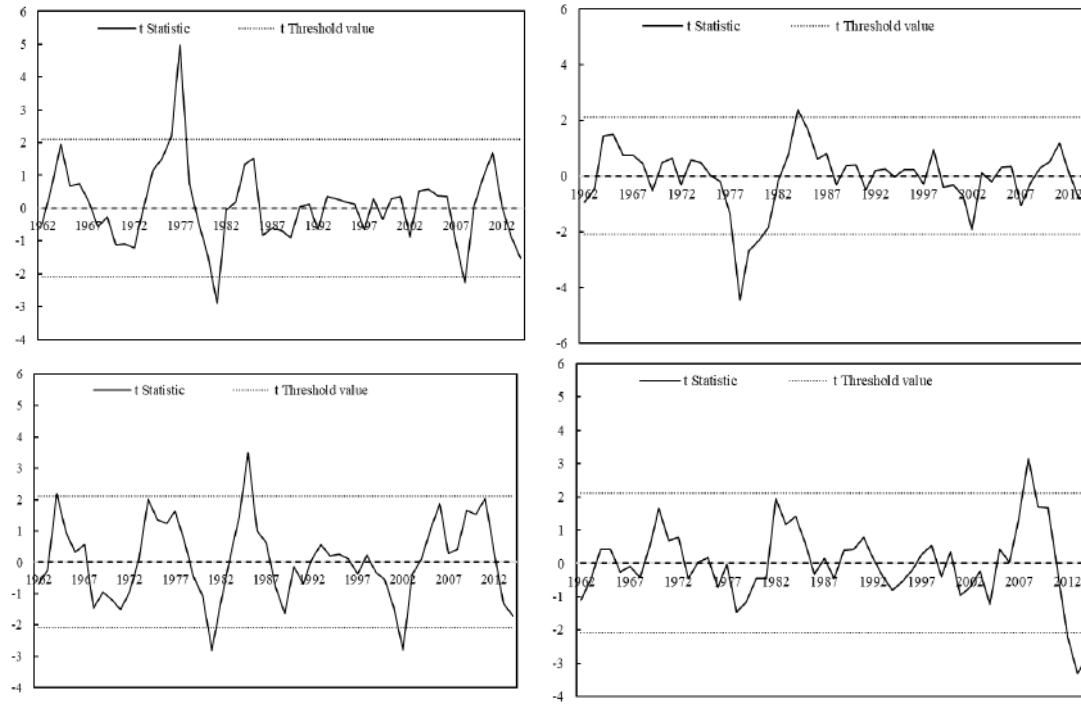

Fig. 4: Sliding T-test curve

precipitation data in Henan was processed, and Kolmogorov-Smirnov test was conducted on the annual precipitation data of four stations in Henan by SPSS software. The results showed that the annual precipitation data of the four stations in Henan presented an approximate normal distribution. Therefore, the MATLAB program is used to perform a wavelet transform on the series data, calculate the Modulus and real part of wavelet transform, and draw the wavelet variance plot of the annual precipitation of Henan 4 stations from 1959 to 2018 and the contour plot of the real part of wavelet, as shown in Fig. 5 and 6 respectively.

In the wavelet variance plot of annual precipitation at four stations in Henan from 1959-2018 (Fig. 5), the larger the variance value, the stronger the cyclical oscillation on the corresponding time scale. From Fig. 5(a), it can be seen that there are three peaks in the variance curve of annual precipitation in Anyang city, corresponding to time scales of 28a, 23a and 8a, respectively. This indicates that the oscillation cycles of the main flood precipitation in the northern region are 28a, 23a and 8a, with the largest peak on the 28a time scale and the strongest oscillation cycle being the first main cycle, and the second and third main cycles corresponding to the 23a and 8a time scales in turn. In combination with Fig. 6(a), the first main cycle 28a precipitation in Anyang experienced 3.5 alternations of abundance and depletion.

The fact that the 2018 precipitation wavelet contours are not closed and are roughly in the center of the solid part of the line suggests that the region will remain in an abundance state for the next 5 years.

The analysis in Fig. 5(b)-(d) is the same, with three peaks in Lushi, Zhengzhou and Xinyang, the first main period in Lushi being 28a and the second and third main periods corresponding to time scales 17a and 8a, the first main period in Zhengzhou being 18a and the second and third main periods corresponding to time scales 28a and 8a, and the first main period in Xinyang being 28a and the second and third main periods corresponding to time scales 18a and 8a. According to Fig. 6(b)-(d), the first principal cycle of 28a rainfall in Lushi experienced 3.5 alternations of abundance and depletion, the first principal cycle of 17a rainfall in Zhengzhou experienced 5.5 alternations of abundance and depletion, and the first principal cycle of 28a rainfall in Xinyang experienced 3.5 alternations of abundance and depletion. In summary, Anyang, Lushi and Xinyang all have a first principal cycle of 28a and experience 3.5 alternate periods of abundance and dryness in their rainfall.

CONCLUSIONS

(1) Precipitation in Henan Province is in the range of 300-800mm in the north and west-central regions, and

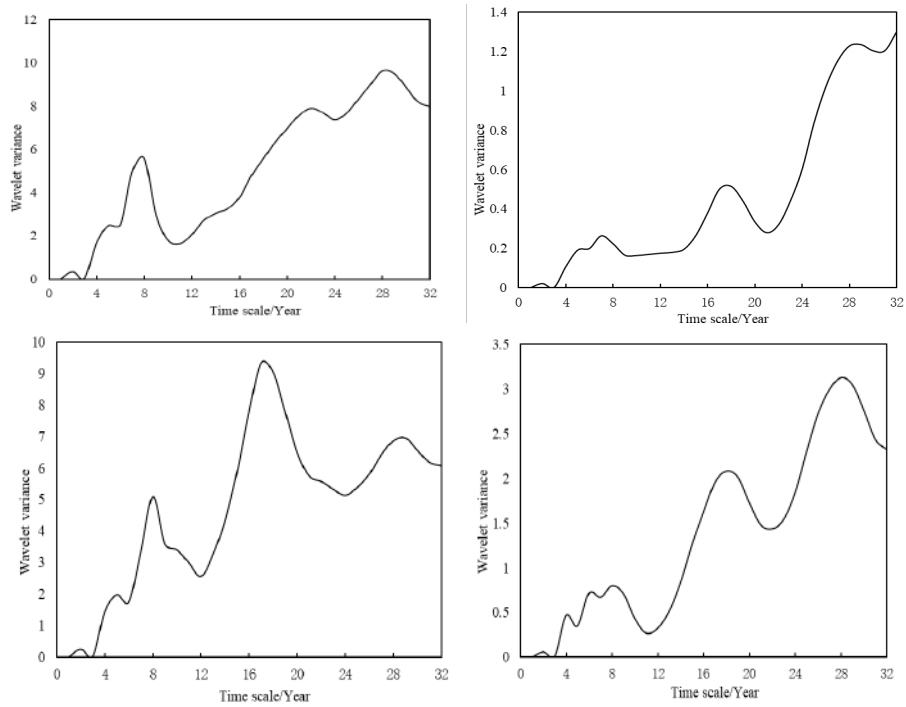

Fig. 5: Wavelet variance plot of annual precipitation at four stations in Henan, 1959-2018.

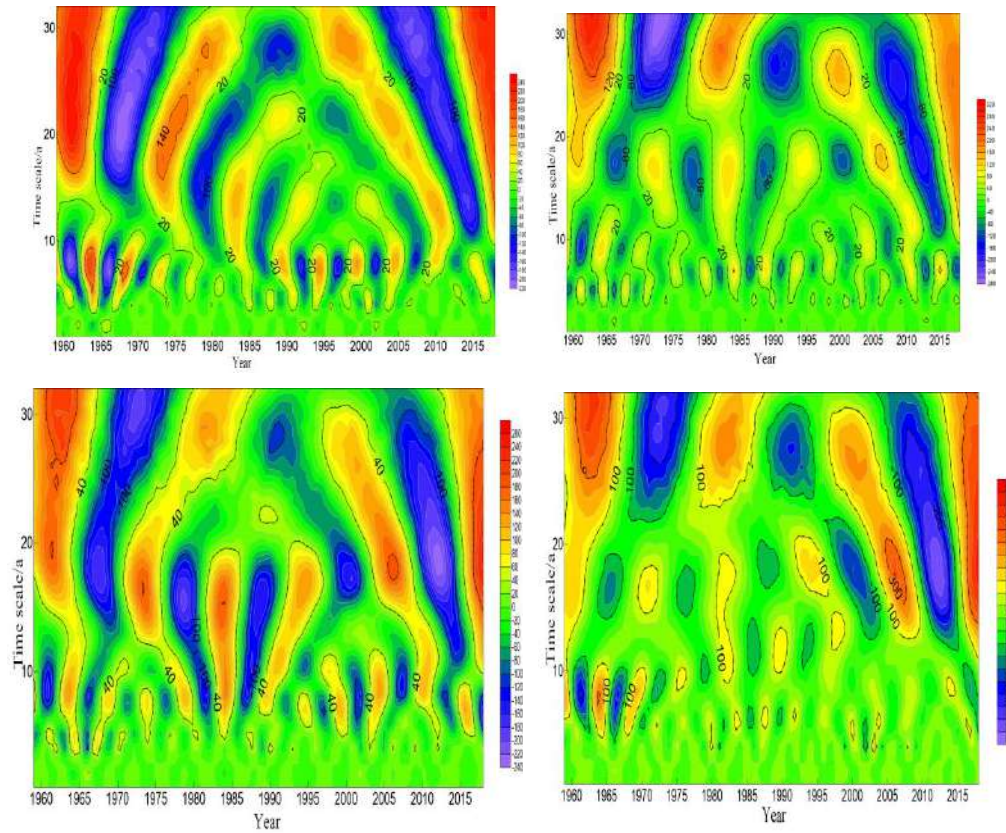

Fig. 6: Wavelet contours of annual precipitation at four stations in Henan, 1959-2018.

800-1500mm in the southern regions, with the overall manifestation being a gradual increase in annual precipitation from north to south and west to east, and a gradual increase in precipitation intensity. The northern, central and southern regions of Henan show a non-significant downward trend in precipitation over the last 60 years, while the western regions show an upward trend, but the trend is not obvious. High-intensity precipitation in all regions shows a significant decreasing trend.

(2) Precipitation in the north and south of Henan Province was mutated around 1975 and 2008, in the west around 1962 and 1980, and in the central areas around 1980.

(3) Multiscale analysis of annual precipitation time series in Henan Province using Morlet wavelet analysis. There are three main cycles of annual rainfall in the northern, central and southern regions of Henan Province, with the first main cycle of 28a experiencing 3.5 alternations of abundance and dryness, and the first main cycle of 17a in the central region experiencing 5.5 alternations of abundance and dryness, and the annual rainfall in each region will remain in an abundance state in the next 5a.

(4) The evolution of regional precipitation is influenced by a variety of factors, but in this paper we only use mathematical methods to mine information within the 60 years of statistics themselves to study their evolutionary characteristics.

REFERENCES

Alashan, Sadik 2018. An improved version of innovative trend analyses. Arab. J. Geosci., 11(3): 50.

Alifujiang, Y., Abuduwaili, J., Maihemuti, B., Emin, B. and Groll, M. 2020. Innovative trend analysis of precipitation in the Lake Issyk-Kul Basin, Kyrgyzstan. J. Atmos., 11(4).

Animashaun, I.M., Oguntunde, P.G., Akinwumiju, A.S. and Olubanjo, O.O. 2020. Rainfall analysis over the Niger central hydrological area, Nigeria: variability, trend, and change point detection. J. Sci. Afr., 8.

Chen, T., Xia, G., Wilson, L.T., Chen, W., Chi, D. and Dietrich, S. 2016. Trend and cycle analysis of annual and seasonal precipitation in Liaoning, China. J. Adv. Meteorol., 2016.

Gedefaw, M., Yan, D., Wang, H., Qin, T., Girma, A., Abiyu, A. and Batsuren, D. 2018. Innovative trend analysis of annual and seasonal rainfall variability in Amhara regional state, Ethiop. J. Atmos., 9(9).

Guo, S., Guo, B., Wang, G. and Xiao, Q. 2015. Mann-Kendall method based water-sediment trend analysis of the upper Han River. J. Water Resour. Power, 33(11): 140-142.

Heng, T. 2003. Research on wavelet analysis and its applications. PhD thesis, Sichuan University.

Huang, D., Liu, Z. and Jiang, Q. 2018. Applying non-parametric MK and ITA methods to characterise changes in groundwater quality parameters - an example of the New Three Mine Aquifer. J. Water Resour. Water Engineering, 29(03): 7-13.

Li, J., Wu, W., Ye, X., Jiang, H., Gan, R., Wu, H., He, J. and Jiang, Y. 2019. Innovative trend analysis of main agriculture natural hazards in China during 1989-2014. J. Nat. Hazards, 95(3).

Li, M., Xia, J., Chen, S. and Meng, D. 2011. Wavelet analysis of precipitation changes in Beijing over the last 300 years. J. N. Resour., 26(06): 1001-1011.

Liu, Y., Zhuo, X. and Qing, A. 2012. Mann-Kendall analysis of precipitation trends in the Guanzhong Basin. Yellow River, 34(02): 28-30+33.

Şen, Z. 2012. Innovative trend analysis methodology. J. Hydrol Eng., 17(9).

Şen, Z. 2017. Innovative trend significance test and applications. Theor. Appl. Climatol., 127(3-4).

Wang, Y., Xu, Y., Tabari, H., Wang, J., Wang, Q., Song, S. and Hu, Z. 2020. Innovative trend analysis of annual and seasonal rainfall in the Yangtze River Delta, eastern China. Atmos. Res., 231.

Yu, Y. and Chen, X. 2013. Mann-Kendall based process delineation of runoff abundance change. J. Water Res. Water Eng., 24(01): 60-63.

Zhou, J., Wang, S., Liu, C., Han, Z., Du, Y. and Jiang, Z. 2020. Analysis of precipitation trends and abrupt changes in the last 57a in the North Canal basin. Hydropower Technol., 51(S1): 21-29.

Nature Environment and Pollution Technology
An International Quarterly Scientific Journal

p-ISSN: 0972-6268
(Print copies up to 2016)
e-ISSN: 2395-3454

Vol. 20 | No.3 | pp. 1251-1256 | 2021

Original Research Paper

https://doi.org/10.46488/NEPT.2021.v20i03.035

Open Access Journal

Assessment of Heavy Metal and Pesticide Contamination in Banana Fields and Development of Phytoremediation System in Kozhikode District, Kerala, India

T. Arathi, K. P. Rahna, Delse P. Sebastian† and Satheesh George
Department of Botany, St. Joseph's College (Autonomous), Devagiri, Calicut, Kerala, India
†Corresponding author: Delse P. Sebastian; delsbotany@gmail.com

Nat. Env. & Poll. Tech.
Website: www.neptjournal.com

Received: 31-08-2020
Revised: 29-10-2020
Accepted: 01-11-2020

Key Words:
Heavy metals
Banana fields
Ornamental plants
Lead phytoremediation

ABSTRACT

Analysis of soil samples collected from various banana fields in Kozhikode district was carried out to identify the extent of heavy metal and pesticide contamination. Analysis by atomic absorption spectrometry revealed contamination of lead in some of the banana fields (Omasseri, Balussery, Vengeri & Nanmanda) in the district. The Gas Chromatogram analysis revealed that the banana fields in Kozhikode district were free of organo-chloride and organo-phosphate pesticide contamination. Among the several ornamental plants evaluated for assessing lead phytoremediation potential, *Dianthus chinensis* L. showed the highest phytoaccumulation potential. *Chrysanthemum indicum* L., *Ruellia simplex* C. Wright and *Lantana camara* L.also showed high lead accumulation. Therefore, these ornamental plants could be used in phytoremediation to remove lead from contaminated soils.

INTRODUCTION

Mining, processing, and smelting activities have contaminated soil and water resources with heavy metals at various places in the world. Act of geochemical weathering processes upon metallurgical wastes and by-products instigate the process of carrying heavy metals from contaminated places and redistributing them into soils, streams, and groundwater of surrounding areas (Fuge et al.1993, Paulson 1997). Thus, soil and water resources, the health of the ecosystems, and human populations are adversely affected by heavy metals. Many reports have shown that short-term or long-term exposure to toxic metals results in the reduction of microbial diversity and activities in soil (Kelly et al. 2003).

Heavy metals include arsenic (As), cadmium (Cd), chromium (Cr), copper (Cu), iron (Fe), lead (Pb), mercury (Hg), platinum (Pt), silver (Ag), and the zinc (Zn) group elements. Heavy metal concentrations beyond certain limits have adverse health effects because they interfere with the normal functioning of living systems. Lead poisoning causes inhibition of hemoglobin synthesis, problems in the functioning of kidneys, reproductive systems, cardiovascular system, and acute and chronic damage to the central nervous system (CNS) and peripheral nervous system (PNS). Mercury poisoning in its organic forms, like monomethyl and dimethylmercury, causes erethism (an abnormal irritation or sensitivity of an organ or body part to stimulation), acrodynia (also called Pink disease, which is characterized by rash and desquamation of the hands and feet), gingivitis, neurological disorders, stomatitis, total damage to the brain and CNS, and are also connected with a congenital malformation (Duruibe et al. 2007).

Contamination by xenobiotic chemicals has been reported in a large number of hazardous waste sites. Considering the increasing contamination of the environment, many remediation technologies have been developed to treat soil, water, and air contaminated by various pollutants, including in situ and ex situ methods (Aboulroos et al. 2006). Soil remediation is the return of soil to a condition of ecological stability together with the establishment of plant communities it supports or supported to conditions prior to disturbance. Conventional technologies for the removal of metals from polluted soils involve transportation of soil to laboratories, soil washing with chemicals to remove metals, and finally replacing the soil at its original location after disposing of its hazardous waste (Francis et al. 1999). This decontamination strategy is an ex situ approach and can be very expensive and damaging to the soil structure and ecology (Salt et al. 1998). Immobilization of heavy metals through the addition of lime (Krebs et al.1999), phosphate (Ebbs & Kochian 1998), and calcium carbonate (Chen et al. 2000) has been suggested as remediation techniques. These remediation methods have the advantage of instantaneously reducing the risk factors arising from metal contamination, but these are considered

temporary alternatives because the metals have not been fully removed from the soil environment. Conventional methods to remediate metal-contaminated soils like soil flushing, solidification/stabilization, vitrification, thermal desorption, encapsulation, etc. can be used at highly contaminated sites but these methods are not suitable for larger areas. Furthermore, these remediation techniques require high energy input and expensive machinery (Schnoor 1997). Conventional methods may destroy soil structure and decrease soil productivity (Leumann et al. 1995). Considering the problems associated with conventional methods, some organism-based remediation techniques, such as bioremediation was developed to degrade and detoxify certain contaminants. Compared to traditional methods, these biological systems are less amenable to environmental extremes but they are more cost-effective (Cunningham & Berti 1993). Over the past decade, there has been increasing interest in the development of plant-based remediation technologies which have the potential to be low-cost, low-impact, and environmentally sound, a concept called phytoremediation (Cunningham & Ow 1996).

Phytoremediation is applicable at sites containing organic, nutrient, or metal pollutants that can be absorbed by the roots of plants and sequestered, degraded, immobilized, or metabolized in place (Vijayan & Sushama 2018). Phytoremediation is accepted because of its cost-effectiveness, aesthetic advantages, and long-term applicability (Yadav et al. 2010). To obtain the optimum remediation for the prevailing conditions, a particular contaminated site may require a combination of procedures. Biological, physical, and chemical methods may be used in combination with one another to reduce contamination to a safe and acceptable level. Considering all these, the present study was conducted to identify the extent of heavy metal and pesticide contamination and the development of a phytoremediation system in banana fields of Kozhikode District.

MATERIALS AND METHODS

Study Area

Kozhikode or Calicut district of Kerala state, India was selected as the study area for the present study. Bananas in their raw and value-added forms become an inseparable part of daily life and celebrations of the district.

Soil Samples

Soil samples collected from different banana fields of Kozhikode district were used for the study. Ten typical locations Omassery, Balussery, Kanthapuram, Vengeri, Vazhayur, Kakkur, Kuttiadi, Vanimel, Thiruvambadi, and Nanmanda were selected. In each of the selected banana field, soils were collected from a depth of 0-50 cm.

Plant Materials

Ten common ornamental plants were chosen for the present study. *Galphimia gracilis* Bartl., *Lantana camara* L., *Dahlia pinnata* Cav., *Chrysanthemum indicum* L., *Tithonia rotundifolia* (Mill.) S.F.Blake, *Ruellia simplex* C.Wright, *Dianthus chinensis* L., *Otacanthus caeruleus* Lindl., *Tecomaria capensis* (Thunb.) Spach, and *Catharanthus roseus* (L.) G.Don .The plants were collected from Kozhikode district and acclimatized in the Botanical Garden of St. Joseph's college Devagiri.

Glassware and Chemicals

Beakers, distilled water, filter paper, funnels, grinder, heating mantle, measuring cylinders, oven, round bottom flasks, trays, weighing balance, Lead Acetate, Nitric acid (HNO_3), Perchloric acid ($HClO_4$), Hydrogen peroxide(H_2O_2), Hydrochloric acid(HCl), etc. were used for the present study. The chemicals used were obtained from HiMedia Laboratories Private Limited and Qualigen Chemicals, Mumbai, India.

Experimental Protocol and Procedure

Test for heavy metals: Soil samples collected from 10 different banana fields of Kozhikode district were used for the present study. One gram of each soil sample was digested with repeated addition of 10ml nitric acid (HNO_3) and Hydrogen peroxide (H_2O_2). The solutions were heated to boiling and filtered. 20ml of Hydrochloric acid (HCl) was added to the initial digestate and the sample was refluxed. After filtration, the digestate was diluted to a final volume of 100 mL. The heavy metal concentration in all the samples was analyzed by Flame Atomic Absorption Spectrophotometer at CWRDM (Centre for Water Resources Development and Management), Kozhikode, Kerala.

Test for pesticides: 5g of each soil sample collected from different places of Kozhikode district were taken. It was then shaken with 20ml of hexane for one hour. After filtration, the volume of the solutions thus obtained was made to 50ml each. The Pesticide concentration in all the samples was tested by a Varian-make CP-3800 gas chromatograph equipped with Ni63 ECD electron-capture detector at CWRDM (Centre for Water Resources Development and Management), Kozhikode, Kerala.

Phytoremediation: For the phytoremediation study, ten common species of ornamental plants were selected. Twenty plants of each species were collected and acclimatized in the college garden for two weeks. These plants were divided

into two sets. The first set of ten plants of each species was kept as the control plants. The second set of ten plants of each species was kept for Lead treatment. The heavy metal treatment was carried out for 10 days after the acclimatization period. Each plant of the control set was given 100 mL of water regularly for 10 days. Each plant of the second set was treated with 100 mL of lead solution regularly for 10 days. The lead solution was prepared by dissolving 10 g of lead in 10 L of water. After the treatment period, the plants were taken out of the soil, washed with distilled water to remove the soil particles, dried in an oven for 48 hours at 80°C, and were ground into powder. 0.5 g ground powder of plants of each set were weighed accurately and digested with a 40 mL mixture of nitric acid (HNO_3) and perchloric acid ($HClO_4$) taken in the ratio of 4:1. The resulting mixtures were evaporated to dryness and were extracted with distilled water. The solutions were heated to boiling and filtered. The volume of the solutions thus obtained was made to 50 mL each. The metal ion concentrations in all the samples were analyzed by Flame Atomic Absorption Spectrophotometer at CWRDM (Centre for Water Resources Development and Management), Kozhikode, Kerala.

RESULTS AND DISCUSSION

Soil Analysis

The soil in agricultural areas may be contaminated by toxic heavy metals, pesticides, etc. The presence of such toxic substances may cause various health and environmental issues. Results obtained in the present study by the analysis of soil samples collected from various banana fields in Kozhikode district were summarised in Tables 1 & 2.

Table 1: Amount of Pb present in soil collected from banana fields of different places in Kozhikode District.

Serial No.	Fields	Pb Present in Soil ($mg.kg^{-1}$)	Hg Present in Soil ($mg.kg^{-1}$)
1	Omassery	0.02	BDL
2	Balussery	0.07	BDL
3	Kanthapuram	BDL	BDL
4	Vengeri	0.19	BDL
5	Vazhayur	BDL	BDL
6	Kakkur	BDL	BDL
7	Kuttiadi	BDL	BDL
8	Vanimel	BDL	BDL
9	Thiruvambadi	BDL	BDL
10	Nanmanda	0.26	BDL

BDL: Below Detection Level

Table 2: Amount of pesticides (Organochlorine & Organophosphorus) present in soil collected from banana fields of different places in Kozhikode district.

Organo phosphorus pesticides		Organochlorine pesticides	
Name of the pesticide	Concentration in soil	Name of the pesticide	Concentration in soil
Mevinphos	BDL	Lindane	BDL
Phorate	BDL	Aldrin	BDL
Disulfoton	BDL	Daldrin	BDL
Methyl parathion	BDL	α -Endosulfan	BDL
Thionazin	BDL	β -Endosulfan	BDL
Parathion	BDL	DDE	BDL
Triazophos	BDL	DDT	BDL
Piperonyl butoxide	BDL		
Dimethoate	BDL		
Famphur	BDL		
O,O,O Triethyphosphorothioacetal	BDL		
Sulfotep	BDL		

BDL: Below Detection Level

The study revealed that in several places of Kozhikode district like Omassery, Balussery, Vengeri, and Nanmanda soil of banana fields was contaminated with lead. The amount of lead present was found to be 0.02 $mg.kg^{-1}$, 0.07 $mg.kg^{-1}$, 0.19 $mg.kg^{-1}$ and 0.26 $mg.kg^{-1}$ respectively. In places like Kanthapuram, Vazhayur, Kakkur, Kuttiadi, Vanimel, and Thiruvambadi, soil in banana fields was devoid of lead pollution. Mercury contamination was not at all observed in the soil of banana fields of Kozhikode district.

The present study also revealed that organochlorine and organophosphate pesticide contamination was absent in soils of banana fields of various places in Kozhikode district. This may be due to increased awareness among farmers about the harmful effects of synthetic pesticides and also may be due to legal restrictions enforced by the Government of Kerala.

Phytoremediation Studies

Results of soil analysis revealed the presence of lead contamination in some of the banana fields in Kozhikode district. Hence phytoremediation studies were conducted to identify suitable ornamental plants that can be used for phytoremediation of lead in soil. Results observed in comparative analysis of the accumulation of lead-in-control and experimental plants are summarized in Fig.1 and Table 3.

In control plants, the absorption level of lead was very low. This clearly showed that the concentration of lead in the soil used for the present study was very low. Among the various treated plants used for the study, the highest level of lead absorption was shown by *D. chinensis* L. (32.55 $mg.kg^{-1}$), *C. indicum* L. (30.65 $mg.kg^{-1}$), *R. simplex* C. Wright (23.11

Table 3: Phytoaccumulation levels of Lead-in-Control and Lead-treated Plants.

Serial No.	Plants	Lead accumulated in control plant(mg/kg)	Lead accumulated in treated plant(mg/kg)
1	*Galphimia gracilis* Bartl.	BDL	3.79
2	*Lantana camara* L.	0.18	22.83
3	*Dahlia pinnata* Cav.	0.07	4.43
4	*Chrysanthemum indicum* L.	0.19	30.65
5	*Tithonia rotundifolia* (Mill.) S.F.Blake	2.56	3.67
6	*Ruellia simplex* C.Wright	0.60	23.11
7	***Dianthus chinensis*** L.	0.07	32.55
8	*Otacanthus caeruleus* Lindl.	0.10	5.58
9	*Tecomaria capensis* (Thunb.) spach	0.04	7.24
10	*Catharanthus roseus* (L.) G.Don	2.25	3.01

BDL-Below Detection Level

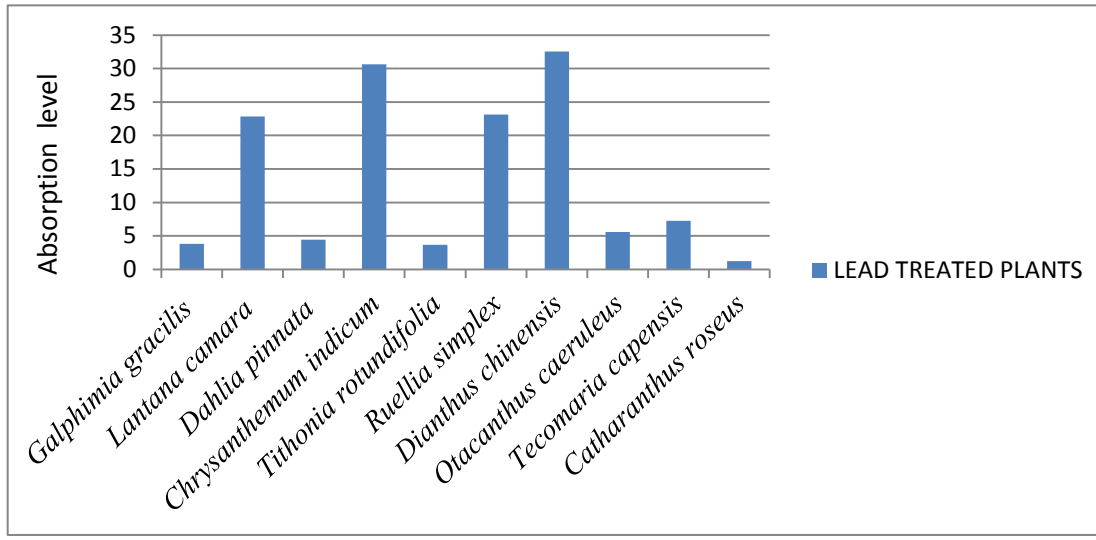

Fig. 1: Graph showing phytoaccumulation of lead by treated plants.

mg.kg^{-1}), and *L. camara* L. (22.83 mg.kg^{-1}). Lead absorption of *C. roseus* (L.) G.Don (3.01 mg.kg^{-1}) was found to be very low. Similar results showing a difference in lead absorption potential of different plant species were reported earlier by several workers (Ramana et al. 2008, Chirakkara & Reddy 2015, Adesodun et al. 2010).

Observations on Each Plant

***Galphimia gracilis* Bartl:** The concentration of lead-in-control and lead-treated *G. gracilis* plants were BDL (Below Detectable Level) and 3.79mg/kg respectively. Lead-treated *G. gracilis* plants showed yellowing of leaves within 10 days.

***Lantana camara* L.:** The concentration of lead-in-control and lead-treated *L. camara* plants were 0.18 mg/kg and 22.83 mg/kg respectively.

The treated *L. camara* plants accumulated a high amount of lead (22.83 mg/kg) in their plant body. Treated plants did not show any observable symptoms which indicated the high lead tolerance capacity of the *L. camara* plants.

***Dahlia pinnata* Cav.:** The concentration of lead-in-control and lead-treated *D. pinnata* Cav. plants were 0.07 mg/kg and 4.43 mg/kg respectively.

White spots appeared on the leaves of treated *D. pinnata* Cav. plants within 10 days. Moreover, the leaves of treated plants were getting dried during the treatment, which showed that *D. pinnata* Cav plants cannot tolerate high lead content in the soil. Therefore in the present study, *D. pinnata* Cav plants were found to be less effective in the phytoremediation of lead-contaminated soil.

***Chrysanthemum indicum* L.:** *C. indicum* L. plants showed accumulation of a high amount of lead. The concentration of lead-in-control and lead-treated plants of *C. indicum* L. plants were 0.19 mg/kg and 30.65mg/kg respectively.

Lead-treated plants showed yellowing and drying of leaves within 10 days. Hence it was found that *C. indicum* L. plants cannot tolerate high lead content in the soil. Therefore *C. indicum* L. plants could not be used for phytoremediation of lead-contaminated soil.

***Tithonia rotundifolia* (Mill.) S.F.Blake:** The concentration of lead-in-control and lead-treated *T. rotundifolia* (Mill.) S.F.Blake plants were 2.56 mg/kg and 3.67mg/kg respectively. Plant showed only slight wilting during the treatment period. *T. rotundifolia* (Mill.) S.F.Blake plants were found to be less effective in the phytoremediation of lead-contaminated soil.

***Ruellia simplex* C.Wright:** *R. simplex* C. Wright plants were found to be good accumulators of lead. The concentration of lead-in-control and lead-treated *R. simplex* C. Wright were 0.60 mg/kg and 23.11 mg/kg respectively. The *R. simplex* C. Wright plants showed only slight wilting during the treatment period.

***Dianthus chinensis* L.:** Among the plants used for the study, *D. chinensis* L. plants showed the highest phyto accumulation potential.

The concentration of lead-in-control and lead-treated *D. chinensis* L. plants were 0.07 mg/kg and 32.55 mg/kg respectively. Slight wilting of the leaves of lead-treated *D. chinensis* L. plants was observed during the study.

***Otacanthus caeruleus* Lindl.:** *O. caeruleus* Lindl. plants were found to be less effective in phytoremediation of lead in contaminated soil. The concentration of lead-in-control and lead-treated plants of *O. caeruleus* Lindl.were 0.10 mg/kg and 5.58 mg/kg respectively. *O. caeruleus* Lindl. plants did not show any noticeable symptoms during treatment.

***Tecomaria capensis* (Thunb.)Spach**: The concentration of lead-in-control and lead-treated plants of *T. capensis (*Thunb.) Spach were 0.04 mg/kg and 7.24 mg/kg respectively. *T. capensis (*Thunb.)Spach plants did not show any symptoms during treatment.

***Catharanthus roseus (*L.)G.Don:** The concentration of lead-in-control and lead-treated plants of *C. roseus (*L.) G.Don were 2.25 mg/kg and 3.01 mg/kg respectively. Hence, the plant was found to be the least effective in lead phytoremediation of soil. In the present study *C. roseus (*L.) G.Don plants did not show any symptoms of lead toxicity during the treatment.

CONCLUSIONS

In the present study, *D. chinensis* L. showed the highest lead accumulating capacity. *C. indicum* L., *R. simplex* C. Wright, and *L. camara* L.also showed high lead accumulation. Hence the present study revealed that these ornamental plants could be used in phytoremediation to remove Lead from contaminated soils. Further studies are required to identify the concentration at which plants having phytoremediation potential shows the highest absorption. As the ornamental plants used for the present study were not edible, the risk of contaminants entering the food chain was reduced. Ornamental plants have the additional benefit of enhancing the aesthetics of the environment in addition to cleaning up the environment and generating additional income, including additional employment opportunities.

ACKNOWLEDGEMENT

The authors greatly acknowledge the Rusa, MHRD, Department of Higher Education, Government of India for the

financial assistance for the purchasing of chemicals and other equipment needed for completing the work.

REFERENCES

Aboulroos, S.A., Helal, M.I.D. and Kamel, M.M. 2006. Remediation of Pb and Cd polluted soils using in situ immobilization and phytoextraction techniques. Int J. Soil Sediment Contam., 15(2): 199-215.

Adesodun, J.K., Atayese, M.O., Agbaje, T.A., Osadiaye, B.A., Mafe, O.F. and Soretire, A.A. 2010. Phytoremediation potentials of sunflowers (*Tithonia diversifolia* and *Helianthus annuus*) for metals in soils contaminated with zinc and lead nitrates. Water Air Soil Poll., 207 (1): 39-48.

Chen, H.M., Zeng, C.R., Tu, C. and Shen, Z.G. 2000. Chemical methods and phytoremediation of soil contaminated with heavy metals. Chemosphere, 41: 229-234.

Chirakkara, R.A. and Reddy, K.R. 2015. Plant Species Identification for phytoremediation of mixed contaminated soils. J. Hazard. Toxic Rad. Waste, 15: 128-129.

Cunningham, S.D. and Berti, W.R. 1993. Remediation of contaminated soils with green plants: An overview. In Vit ro Cell. Dev. Biol., 29P: 207-212.

Cunningham, S.D. and Ow, D.W.1996. Promises and prospects of phytoremediation. Plant Physiol., 110(3): 715.

Duruibe, J.O., Ogwuegbu, M. O. C. and Egwurugwu, J. N. 2007. Heavy metal pollution and human biotoxic effects. Int. J. Phy. Sci., 2(5): 112-118.

Ebbs, S.D. and Kochian, L.V. 1998. Phytoextraction of zinc by oat (*Avina sativa*), barley *(Hordeum vulgare*), and indian mustard (*Brassica juncea*). Environ. Sci. Technol., 32: 802-806.

Francis, C.W., Timpson, M.E. and Wilson, J.H. 1999. Bench- and pilot-scale studies relating to the removal of uranium from uranium-contaminated soils using carbonate and citrate lixiviants. J. Hazard. Mater., 66: 67-87.

Fuge, R., Pearce, F.M., Pearce, N.J.G. and Perkins, W.T. 1993. Geochemistry of Cd in the secondary environment near abandoned metalliferous mines. Wales. Appl. Geochem., Suppl. Iss., 2: 29-35.

Kelly, J. J., Häggblom, M. M. and Tate, R. L. 2003. Effects of heavy metal contamination and remediation on soil microbial communities in the vicinity of a zinc smelter as indicated by analysis of microbial community phospholipid fatty acid profiles. Bio. Fert. Soils, 38(2): 65-71.

Krebs, R., Gupta, S.K., Furrer, G. and Schulin, R. 1999. Gravel sludge as an immobilizing agent in soils contaminated by heavy metals: A field study. Water Air Soil Poll., 115: 465-479.

Leumann, C.D., Rammelt, R. and Gupta, S.K. 1995. Soil remediation by plants: Possibilities and limitations. (In German.) Agrarf Orschung (Switzerland), 2: 431-434.

Paulson, A.J. 1997. The transport and fate of Fe, Mn, Cu, Zn, Cd, Pb, and SO4 in a groundwater plume and in downstream surface water in the Coeur d'Alene mining district. Idaho, USA. Appl. Geochem., 12: 447-464.

Ramana, S., Biswas, A.K., Ajay and Rao, S. 2008. Phytoextraction of lead by marigold and chrysanthemum. Ind. J. Plant Physiol., 13(3): 297-299.

Salt, D.E., Smith, R.D. and Raskin, I. 1998. Phytoremediation. Plant Mol. Bio., 49: 643-668.

Schnoor, J. L. 1997. Phytoremediation: Technology Evaluation Report. Ground-Water Remediation Technologies Analysis Center, pp. 98-101.

Vijayan, V.D. and Sushama, P.K., 2018. Phytoremediation as an effective technology for the removal of heavy metals from dump yard soils. Nat. Env. Poll. Tech., 17(4): 1353-1358.

Yadav, R., Arora, P., Kumar, S. and Chaudhury, A. 2010. Perspectives for genetic engineering of poplars for enhanced phytoremediation abilities. Ecotoxicology, 19(8): 1574-1588.

Nature Environment and Pollution Technology
An International Quarterly Scientific Journal

p-ISSN: 0972-6268
(Print copies up to 2016)
e-ISSN: 2395-3454

Vol. 20 | No.3 | pp. 1257-1261 | 2021

Original Research Paper

https://doi.org/10.46488/NEPT.2021.v20i03.036

Open Access Journal

Contamination of Cadmium, Lead, Mercury and Manganese in Leachate from Open Dump, Controlled Dump and Sanitary Landfill Sites in Rural Thailand: A Case Study in Sakon Nakhon Province

K. Ruengruehan*, R. Junggoth, S. Suttibak***, C. Sirikoon**** and N. Sanphoti*†**

*Department of Community Health Faculty of Public Health, Kasetsart University, Chalermphrakiat Sakon Nakhon Province Campus, Thailand

**Department of Environmental Health Occupational Health and Safety, Faculty of Public Health, Khon Kaen University, Thailand

***Department of Civil Engineering, Faculty of Science and Engineering, Kasetsart University, Chalermphrakiat Sakon Nakhon Province Campus, Thailand

****Senior-Professional Environmental Officer, Sakon Nakhon Provincial Offices for Natural Resources and Environment, Thailand

†Corresponding author: N. Sanphoti; nirawan.s@ku.th

Nat. Env. & Poll. Tech.
Website: www.neptjournal.com

Received: 27-07-2020
Revised: 15-09-2020
Accepted: 01-11-2020

Key Words:
Heavy metals
Open dump
Controlled dump
Sanitary landfill

ABSTRACT

The contamination of heavy metal in leachate was investigated at various sites with different solid waste management, namely an open dump, controlled dump, and sanitary landfill. The results indicated that all four heavy metals investigated (cadmium, lead, mercury, and manganese) were present in the leachate at all solid waste management sites. The highest cadmium and lead concentrations were each observed in open dump leachate samples, while the highest manganese and mercury concentrations were each observed in controlled dump leachate samples.

INTRODUCTION

Currently, population growth in Thailand is causing a huge demand for basic living factors, and consequently, many problems stem from the utilization of many kinds of products, with many unused materials resulting in a huge amount of solid waste. In addition, waste products from daily consumption such as plastic foam boxes and food waste are increasing every day, and these are contributing further to increased waste management problems. There are various methods of waste management such as incineration of solid waste, landfill waste, or the use of 3R (reuse, recycling, reduce) practices (Chiemchaisri et al. 2007), with the method used depending on the municipality. Many government agencies in Thailand have different methods of waste management (sanitation landfill and improper landfill to deal with the waste problem) (Chinnathan et al. 2017, Muttamara et al. 2017). However, local government in many areas still lack the budget and knowledgeable staff to manage solid waste disposal. Local administrative organizations in Sakon Nakhon province have chosen to use three different methods of management: open dump, controlled-open dump, and sanitary landfill. Although the forms of waste disposal are different, all of them face the same problem of leachate contaminating the environment. Leachate is the water caused by waste degradation by microorganisms and it can permeate through the waste pile and dissolve various contaminants into the soil in the form of a solution mixed with suspended solids and sediment (Xaypanya et al. 2018). External water sources, such as rainwater, can enter the waste and these contribute to the leachate. Leachate often has a high concentration of pollutants such as COD, heavy metals, and various kinds of organic substances. Contamination in sampled water may vary due to the humidity, rainfall, waste composition, and season (Ogundiran & Afolabi 2008). Compared with water generally, leachate is very dirty and can pollute and deteriorate the soil through which it passes, making the soil unsuitable for plant growth which affects, directly and indirectly, human health and other organisms in the ecosystem (Kanmani & Gandhimathi 2013). Heavy metal contamination, especially in potable water supplies makes

the water unsuitable for human use (Fauziah et al. 2013). The leachate normally consists of pathogens, solutions, suspensions, and various contaminants, especially, toxic heavy metals (Chiemchaisri et al. 2015). A study of heavy metal contamination in the leachate at the On Nut Waste Disposal Facility, Bangkok, Thailand reported that the contamination levels of mercury, manganese, and cadmium were in the ranges 2.4-39.1 $mg.L^{-1}$, 0.01-2.88 $mg.L^{-1}$, and 0.008-0.013 $mg.L^{-1}$ respectively (Thapanandana 1993). However, there has been less research on heavy metal contamination in various types of solid waste management in rural areas. Thus, the current study investigated the contamination of cadmium, lead, mercury, and manganese in leachate under various types of solid waste management, namely open dump, controlled dump, and sanitary landfill in the rural area of Sakon Nakhon municipality, Thailand.

MATERIALS AND METHODS

Cross-sectional research was used to investigate the contamination of heavy metals in leachate under various types of solid waste management. Cadmium, lead, mercury, and manganese were chosen as representative heavy metals in the leachate. The methodology of this study was separated into two parts: 1) the collection and survey of municipal waste landfill sites and 2) sampling of heavy metals in leachate under various types of solid waste management. Groundwater samples were taken from an observed well using Bailer and Peristaltic pumps. To reduce sampling error, water sampling was carried out after pumping had drained some water until the acid-alkali value, electrical conductivity, and temperature of the water sampled in the well were constant. A polyethylene or polypropylene pipe was inserted into the well to the desired depth. Then water was pumped up to the ground and the sample was treated by adding HNO_3 solution to lower the pH level to less than or equal to pH 2 before analysis in the laboratory. The surface water sampling process was achieved by grab sampling to collect the sample at a specified time, and then the sample was treated by adding HNO_3 solution to reduce to pH 2. An atomic absorption spectrophotometer (Perkin Elmer; Model A, Analyst 100; USA) was used for the heavy metal analysis.

RESULTS AND DISCUSSION

Sanitary Landfill Disposal Site

Three sanitary landfill sites were identified in Sakon Nakorn, namely in Tha Rae, Sakon Nakhon subdistrict, and Phang Khon subdistrict. Tha Rae subdistrict municipality had a landfill area of 48,000.0 m^2, with 12.9 t/day of community waste entering the landfill system and the amount of community waste accumulated was 5.46 t. The landfill was surrounded by a fence; however, there was a problem due to people scavenging waste from the area. The Sakon Nakhon municipality had a landfill waste area of 260,000.0 m^2, with 66.89 t/day of community waste entering the landfill system and the amount of community waste accumulated was 42.5 t. The solid waste landfill site in Phang Khon subdistrict municipality had a landfill area of 78,400.0 m^2 based on sanitary landfill. The amount of solid waste entering the landfill system was 29.7 t/day and the amount of accumulated waste was 25.2 t. The details are provided in Table 1.

Controlled Dumpsite

The disposal site in Dong Mafai municipality was 35,200.0 m^2 in size and the amount of waste entering the disposal site was 19.0 t/day and the amount of accumulated waste in the system was 5.4 t. The site was completely fenced with gates for access. There was no incineration of waste. Behind the site, a wall had been built with some trees as a buffer and to prevent waste scavenging. The solid waste site in Nong Lat subdistrict municipality had an area of 6,400.0 m^2, with 10.2 t/day of solid waste entering the system and the amount of accumulated waste in the system was 3.5 t. Solid waste was open-dumped and then incinerated behind a wall. In addition, there was an area for dumping garbage and incineration outside the wall behind the incinerator. The solid waste site in Sawang Daen Din sub-district municipality had an area of 51,200.0 m^2. The amount of municipal solid waste was 19.0 t/day and the amount of accumulated waste was 312.0 t. There was open dumping, plowing of old solid waste, and modifying the area for new solid waste, but no burning of solid waste. There was no perimeter fence with gates nor a buffer, so there was a problem with scavenging by people.

Table 1: Information on sanitary landfill sites.

Type of solid waste management	Location Name	Location of site		Landfill size (m^2)	Solid waste (t/day)	Accumulated solid waste (t)
		Latitude	Longitude			
Sanitary landfill	Tha Rae	17.29288	104.22897	48,000	12.9	5.4
	Sakon Nakhon	17.06875	104.18266	260,000	66.8	42.5
	Phang Khon	17.39227	103.73387	78,400	29.7	25.2

The solid waste site in Wanon Niwat municipality had an area of 11,200.0 m^2. The amount of solid waste delivered to the site was 10.5 t/day and there was 120.0 t of accumulated waste. There was open dumping and burning around the entrance area. The details for these sites are provided in Table 2.

Uncontrolled Dumpsite

The disposal system in the Bong Tai sub-district municipality had an area of 43,200.0 m^2. The amount of solid waste delivered to the site system was 5.0 t/day and the amount of accumulated solid waste was 63.0 t. There was open dumping and burning of solid waste. There was no gate but there was a wire fence with some trees as a buffer and there was a moat around the area. There was no plowing of old solid waste. The waste disposal site in the Nong Luang sub-district municipality had an area of 8,000.0 m^2. The amount of solid waste delivered to the site was 0.5 t/day and the amount of accumulated waste was 22.5 t. Plowing, spreading, and landfilling occurred. The waste site in Song Dao municipality had a landfill area of 9,600.0 m^2. The amount of solid waste delivered to the site was 4.0 t/day and the amount of accumulated waste in the area was 30.0 t. No incineration was evident. The site had gates and a perimeter wire fence, so there was no evidence of scavenging. The disposal system in Ban Phon sub-district municipality had an area of 3,200.0 m^2. The amount of solid waste delivered to the site was 0.60 t/day and the amount of accumulated waste was 3.6 t. There was waste burning but there were no gates or a fence and no solid waste collection service (villagers dumped their waste themselves). The solid waste site in the Kut Bak sub-district municipality had an area of 6,720.0 m^2. The amount of waste delivered to the site was 0.92 t/day and the amount of accumulated waste was 68.0 t. There was no landfilling using the old waste. The site was gated and fenced and located near the community. A sewage fermentation tank was located in the same area. The details for these sites are provided in Table 3.

Contamination of Heavy Metal in Leachate

The analysis considered the contamination of cadmium, lead, mercury, and manganese in the leachate of municipalities with a sanitary landfill in three subdistrict municipalities, namely Tha Rae, Sakon Nakhon, and Phang Khon. The results indicated the leachate samples had pH values in the range 6.8-8.7 and electrical conductivity in the range 4.5-8.6 µs/cm. The conductivity of the leachate in Phang Khon subdistrict municipality was quite high at 4,499.0 µs/cm. The leachate temperature was in the range 27.5-33.0 ^oC and turbidity was in the range 14.5-185.0 NTU (Table 4). The concentrations of cadmium, lead, mercury, and manganese were in the ranges of 0.01-0.24, 0.01-0.12, 0.02-0.12, and 0.18-0.76 $mg.L^{-1}$ respectively (Table 5). For the controlled dumps (Dong Mafai, Nong Lat, Sawang Daen Din, and Wanon Niwat subdistrict municipalities), the leachate samples had pH values in the range 4.7-8.3, electrical conductivity in the range 8.30-4341.0 µs/cm, temperature in the range 28.2-33.0 ^oC, and turbidity in the range 8.2-340.0 NTU (Table 4). The concentrations of cadmium, lead, mercury, and manganese were in the ranges 0.20-0.48, 0.21-0.35, 0.12-1.22, and 0.26-1.89 $mg.L^{-1}$ respectively (Table 5). The cadmium, lead, mercury, and manganese concentrations were analyzed

Table 2: Information on controlled dumpsites.

Type of solid waste management	Location name	Location of site		Landfill size (m^2)	Solid waste (t/day)	Accumulated solid waste (t)
		Latitude	Longitude			
Controlled dump	Dong Mafai	17.29876	104.04488	35,200	19.0	5.4
	Nong Lat	17.31089	103.59319	6,400	10.2	3.2
	Sawang Daen Din	17.50000	103.46523	51,200	32.0	312.0
	Wanon Niwat	17.62784	103.75658	11,200	10.5	120.0

Table 3: Information on uncontrolled dumpsites.

Type of solid waste management	Location name	Location of site		Landfill size (m^2)	Solid waste (t/day)	Accumulated solid waste (t)
		Latitude	Longitude			
Open dump	Bong Tai	17.41993	103.30216	43,200	5.0	63.0
	Nong Luang	17.40499	103.38456	8,000	0.5	22.5
	Song Dao	17.35378	103.48229	9,600	4.0	30.0
	Ban Phon	17.24517	103.82255	3,200	0.6	3.6
	Kut Bak	17.08435	103.82255	6,720	9.2	68.0

in the leachate from five subdistrict municipalities with open dumpsites (Bong Tai, Nong Luang, Song Dao, Phon Na Kaeo, and Kut Bak). The leachate samples had pH values in the range 6.5-7.6, electrical conductivity in the range 4.5-2461.0 µs/cm, temperature in the range 22.8-33.0^{o}C, and turbidity in the range 21.2-1033.0 NTU (Table 4). The concentrations of cadmium, lead, mercury, and manganese were in the ranges 0.01-1.25, 0.02-1.25, 0.17-0.57, and 0.21-0.46 mg.L^{-1} respectively (Table 5).

CONCLUSION

The contamination of heavy metal in leachate was investigated at different dumpsites (sanitary landfill, controlled dump, and open dump) by sampling for cadmium, lead, mercury, and manganese in municipal waste leachate and comparing the concentrations. The results indicated that the heavy metals were present in the leachate from all types of solid waste management.

(a) The highest cadmium concentration was observed in the open dump leachate, followed by controlled dump leachate, and sanitary landfill leachate.

(b) The highest lead concentration was observed in the open dump leachate, followed by controlled dump leachate, and sanitary landfill leachate.

(c) The highest manganese concentration was observed in the controlled dump leachate, followed by open dump leachate, and sanitary landfill leachate.

Table 4: pH, conductivity, temperature, and turbidity of leachate from different sites.

Type of solid waste management	Location name	pH	Conductivity, mS.c^{-1}	Temperature	Turbidity, NTU
Sanitary landfill	Tha Rae	7.6	4.5	27.5	131.0
	Sakon Nakhon	8.7	8.6	29.5	185.0
	Phang Khon	6.8	4,499.0	33.0	14.5
Controlled dump	Dong Mafai	8.3	8.3	28.9	8.4
	Nong Lat	4.7	64.6	28.2	8.2
	Sawang Daen Din	7.1	2,413.0	30.0	184.0
	Wanon Niwat	7.0	4,341.0	33.0	340.0
Open dump	Bong Tai	7.2	962.0	33.0	438.0
	Nong Luang	6.5	2,461.0	33.0	1033.0
	Song Dao	6.9	1,005.0	31.0	347.0
	Ban Phon	6.8	320.0	22.8	21.2
	Kut Bak	7.6	4.5	27.5	131.0

Table 5: Concentration of heavy metals (Cd, Pb, Mn, Hg) in leachate.

Type of solid waste management	Location name	Cd (mg.L^{-1})	Pb(mg.L^{-1})	Mn(mg.L^{-1})	Hg(mg.L^{-1})
Sanitary landfill	Tha Rae	0.01	0.01	0.18	0.02
	Sakon Nakhon	0.24	0.12	0.25	0.04
	Phang Khon	0.02	0.02	0.76	0.12
Controlled dump	Dong Mafai	0.35	0.21	0.26	0.12
	Nong Lat	0.48	0.25	0.93	1.22
	Sawang Daen Din	0.20	0.35	1.89	0.25
	Wanon Niwat	0.21	0.32	1.53	0.14
Open dump	Bong Tai	0.02	0.15	0.43	0.18
	Nong Luang	0.01	0.02	0.47	0.21
	Song Dao	0.21	0.45	0.46	0.17
	Ban Phon	0.04	1.25	0.21	0.57
	Kut Bak	1.25	0.87	0.41	0.28

(d) The highest mercury concentration was observed in the controlled dump leachate, followed by open dump leachate, and sanitary landfill leachate.

REFERENCES

Chiemchaisri, C., Juanga J.P. and Visvanathan, C. 2007. Municipal solid waste management in Thailand, and disposal emission inventory. Environ. Monit. Assess., 135(1-3): 13-20.

Chiemchaisri, C., Chiemchaisri, W. and Witthayapirom, C. 2015. Remediation of MSW landfill leachate by a permeable reactive barrier with vegetation. Water Sci. Technol., 71(9): 1389-1397.

Chinnathan, A., Jarudej, A., Supachot, S., Jeerattikul, K., Bundit, I., Phatavee, P., Chanoknunt, K., Wichai, S. and Chiemchaisri, C. 2017. Municipal plastic waste composition study at transfer station of Bangkok and possibility of its energy recovery by pyrolysis. Energy Procedia, 107: 222-226.

Fauziah, S.H., Izzati, M.N. and Agamuthu, P. 2013. Toxicity on Anabas Testudineus: A case study of sanitary landfill leachate. Procedia Environ. Sci., 18: 14-19.

Kanmani, S. and Gandhimathi, R. 2013. Assessment of heavy metal contamination in soil due to leachate migration from an open dumping site. Appl. Water Sci., 3: 193-205.

Muttamara, S., Visvanathan, C. and Alwis, K.U. 1994. Solid waste recycling and reuse in Bangkok. Waste Manag. Res., 12(2): 151-163.

Ogundiran, O.O. and Afolabi, T.A. 2008. Assessment of the physicochemical parameters and heavy metals toxicity of leachates from the municipal solid waste open dumpsite. Int. J Environ. Sci. Technol., 5(2): 243-250.

Thapanandana, T. 1993. The contamination of mercury, cadmium, and manganese in leachate from solid waste disposal sites of Bangkok metropolitan administration. Thesis (M.Sc.), Chulalongkorn University, Bangkok, Thailand.

Xaypanya, P., Takemura, J., Chiemchaisri, C., Seingheng, H. and Tanchuling, M. 2018. Characterization of landfill leachates and sediments in major cities of Indochina peninsular countries: Heavy metal partitioning in municipal solid waste leachate. Environment, 5(6): 65.

Nature Environment and Pollution Technology
An International Quarterly Scientific Journal

p-ISSN: 0972-6268
(Print copies up to 2016)
e-ISSN: 2395-3454

Vol. 20 | No.3 | pp. 1263-1268 | 2021

Original Research Paper

https://doi.org/10.46488/NEPT.2021.v20i03.037

Open Access Journal

In-vitro Effects of Chlorpyrifos and Monocrotophos on the Activity of Acetylcholinesterase (AChE) in Different Tissues of Apple Snail *Pila globosa* (Swainson, 1822)

S. Pal*, S. Maity, S. Balachandran*† and S. Chaudhury***

*Department of Environmental Studies, Siksha-Bhavana, Visva-Bharati, Santiniketan-731235, West Bengal, India

**West Bengal Zoo Authority, Aranya Bhawan, Salt Lake City-700106, West Bengal, India

†Corresponding author: S. Balachandran; s.balachandran@visva-bharati.ac.in

Nat. Env. & Poll. Tech.
Website: www.neptjournal.com

Received: 07-09-2020
Revised: 09-11-2020
Accepted: 12-11-2020

Key Words:
Apple snail
Chlorpyrifos
Monocrotophos
AChE activity
Hepatopancreas

ABSTRACT

The impact of two organophosphorus insecticides [Chlorpyrifos (CPF) and Monocrotophos (MCP)] on non-target wild natural gastropod, *Pila globosa* (apple snail) from the paddy fields was studied. The activity of acetylcholinesterase (AChE) was monitored on foot-muscle and hepatopancreas tissues of control and exposed snails. In the foot- muscle AChE inhibition progressed and reached 54.19% and 63.13% of the control, whereas, the AChE inhibition in the hepatopancreas reached 46.96% and 53.67% over control after 48 hours of exposure to 1.5 $mL.L^{-1}$ and 2.5 $mL.L^{-1}$ CPF respectively. After 48 hours of MCP exposure at 1.5 $mL.L^{-1}$ and 2.5 $mL.L^{-1}$ separately, the AChE inhibition of foot muscle was 49.07% and 57.59% respectively while in hepatopancreas it was 44.65% and 48.84% respectively. Our results show more inhibition of AChE activities on the foot-muscle than hepatopancreas in a concentration and time-dependent manner with greater severity by CPF in comparison to MCP. AChE inhibition increased with the increasing exposure time.

INTRODUCTION

Today's agricultural work is unthinkable without the use of pesticides. These widely spread pesticides are used to control agricultural pests, but at the same time, they are highly toxic to non-target natural populations particularly in the aquatic environment. This necessitated the need to understand and evaluate the biological effects of xenobiotics on the aquatic ecosystem (Ullah et al. 2018). According to Sunanda et al. (2016), organophosphorus (OP) insecticides are increasingly used in agriculture as a substitute for organochlorine and carbamate insecticides because of their high efficiency and low persistence in the environment. Chlorpyrifos (CPF) and monocrotophos (MCP) are the commonly used OP insecticides that are often detected in the freshwater system (Narra et al. 2017). Unfortunately, organophosphorus pesticides due to their lack of target specificity can cause serious, long-lasting effects on aquatic non-prey species, especially invertebrates (Wang et al. 2018). Therefore, an appropriate monitoring strategy is needed to measure the environmental risks and to protect the non-target organism like invertebrate species from the effects of OP pesticides.

Although OP compounds can break down rapidly in the environment, non-target organisms may suffer from chronic effects, such as AChE inhibition (Nguyen et al. 2018) due to indiscriminate applications of these OPs in the paddy fields. OP compounds have several toxic properties but the most concern is AChE inhibition. OP interferes with the activity of the enzyme AChE, leading to prolonged muscle contraction (Bolton-Warberg et al. 2007). Moreover, the inhibition of AChE results in abnormal respiration, swimming, feeding due to loss of coordination, tremors, muscle spasms, convulsions, and even death (Tam et al. 2015, Ihsan et al. 2019). AChE activity is therefore widely used in biomonitoring studies as a biomarker of OP pesticide exposure (Khalil 2015). Freshwater molluscs display high sensitivity to aquatic pollutants, making them an ideal bio-indicator model in the field (Wang et al. 2018).

Molluscs are well-known for their capacities to accumulate different classes of chemicals in their tissues such as the head, kidney, foot muscle, and particularly the hepatopancreas (Regoli et al. 2006). But AChE activity has only been studied in a limited number of molluscan species exposed to xenobiotics and often using only one kind of tissue, which makes it difficult to compare the results obtained by different authors (Kopecka-Pilarczyk 2010).

Pesticide pollution in the agricultural fields is a matter of growing interest. Since the real toxicological impacts remain

largely unexplored in field conditions, the main objective of the present study was to develop an integrated ecotoxicological approach with the apple snail *P. globosa* (Swainson) for monitoring toxicological effects caused by two extensively used organophosphate pesticides, chlorpyrifos (CPF) and monocrotophos (MCP).

P. globosa is a very common economically important gastropod found in paddy fields and ponds of West Bengal, India. Apple snails being herbivore and detritivore play a major role in numerous ecosystems. It is a prey to several predators such as reptiles, birds, and mammals thus, it can be the base point at the origin of the food web, transfer xenobiotics (Laskowski & Hopkin 1996) to higher trophic levels leading to biomagnification.

Due to the paucity of information on the effects of CPF and MCP on AChE of *P. globosa* an attempt has been made to investigate the short-term effect of these two OP pesticides in the metabolically active tissues (hepatopancreas and foot muscle) of the said gastropod.

MATERIALS AND METHODS

Experimental Design

84 mature apple snail *P. globosa*, weighing 15 ± 2g were collected during monsoon from an untreated pond not having pollution history far away from the agricultural sites and subjected to experiments. 4 snails were considered as control and other 80 snails confined with nylon net was exposed in the separate paddy fields sprayed with the different concentrations of the two OP pesticides; chlorpyrifos (CPF) and monocrotophos (MCP) with the concentrations of 1.5 $mL.L^{-1}$ water and 2.5 $mL.L^{-1}$ water for a period of 48 hours (exposure periods of 3, 6, 12, 24 and 48 hours). Finally, the experimental groups were as follows.

Group I– Control, snails unexposed to the pesticide; *Group II*–20 snails exposed to 1.5 ml L^{-1} of CPF for different time periods; *Group III*–20 snails exposed to 2.5 $ml.L^{-1}$ of CPF for different time periods; *Group IV*–20 snails exposed to 1.5 $mL.L^{-1}$ of MCP for different time periods; *Group V*–20 snails exposed to 2.5 $mL.L^{-1}$ of MCP for different time periods.

For enzyme assay, four specimens from each exposed group were collected randomly per exposure duration (3, 6, 12, 24, and 48 hours) and quickly transported to the laboratory in an icebox to avoid tissue degradation.

Chemicals

All chemicals used were of analytical grade purchased from Sigma Chemical Company (USA).

AChE assay (EC 3.1.1.7)

AChE activity of *P. globosa* was determined spectrophotometrically under laboratory conditions according to the method of Ellman et al. (1961) by measuring the rate of hydrolysis of the substrate. To improve the standard of analytical accuracy and precision of the enzyme assay, the present investigation focuses on the conditions under which it is measured. Considered parameters for the present quality assurance and quality control procedure are temperature, pH, ionic strength, and concentrations of the reactants (substrate and enzyme) which influence the enzyme sensitivity in a reaction mixture. For each assay, four collected specimens from each concentration of CPF and MCP (one from each replicate) at an interval of 3, 6, 12, 24, 48 hours were sacrificed and pooled together before homogenization of the tissue sample. Foot muscle and hepatopancreas tissues were taken out immediately by breaking shells and 10% (w/v) tissue homogenate were prepared separately in ice-cold 0.1 M phosphate buffer of pH 8.0 standardized specifically for *P. globosa* AChE activity. Tissue homogenate was centrifuged at 10000 rpm for 30 min at 4^{o} C in a Remi CM-8 plus cooling centrifuge. A reaction cocktail of 3ml volume was prepared using 60 µl clear supernatant (enzyme source), 0.1 M of phosphate buffer (pH 8.0), 0.5 M of dithiobisnitrobenzoic acid (DTNB), and 1.84 mm acetylthiocholine iodide standardized for the AChE activity of this species. The change in optical density at 412 mm was recorded on a Beckman DU 640 UV/Vis spectrophotometer for a 3 min time scan under optimum temperature (30^{o} C) in a 10 mm path length cuvette. A freshly prepared thiocholine standard curve (Jash et al. 1982) was used to measure the specific activity of AChE and expressed as $n.mole^{-1}$ thiocholine produced min^{-1} mg^{-1} protein. The protein content of the tissue samples was estimated using the Bovine Serum Albumin standard curve following the method of Lowry et al. (1951). All assays were done in triplicate to avoid errors and pitfalls during enzyme assay.

Statistical Analysis

The AChE activities of *P. globosa* are tabulated as mean± standard error of three replicates (each comprising four snails). Test of significance was performed by one-way analysis of variance followed by Duncan's multiple range test ($P< 0.05$) using the statistical SigmaStat 3.0 program.

RESULTS AND DISCUSSION

AChE Activity

The AChE activity in the foot muscle and hepatopancreas of *P. globosa* following separate applications of low (1.5 $mL.L^{-1}$

of water) and high (2.5 mL.L^{-1} of water) concentrations of chlorpyrifos (CPF) and monocrotophos (MCP) is given in Tables 1 & 2 respectively. Statistically significant differences were observed in the inhibition of AChE activity between the control and CPF and MCP exposed foot muscle and hepatopancreas tissues after application of both low (1.5 mL.L^{-1}) and high (2.5 mL.L^{-1}) concentrations.

The studies have revealed that in the foot muscle of *P. globosa,* AChE inhibition progressed and reached 54.19% and 63.13% of the control after 48 hours of exposure to 1.5 mL and 2.5 mL.L^{-1} chlorpyrifos respectively. Whereas the AChE inhibition in hepatopancreas reached 46.96% and 53.67% over control after 48 hours exposed to lower and higher concentrations of CPF respectively. In the case of 1.5 mL and 2.5 mL.L^{-1} of MCP exposure, the AChE inhibition of foot muscle was 49.07 % and 57.59 % respectively, while in hepatopancreas it was 44.65 % and 48.84% respectively at the end of the exposure period. From the above results, it was clear that both organs exhibited more than a 30% decrease in the AChE activity when exposed to OP which reflects an indication of the risk of overexposure (Aprea et al. 2002). Therefore, the results indicated that the apple snails in the rice fields exposed to OP may be stressed for long hours even after the spraying has stopped.

When OP pesticides enter into the body of the snails, they move to all parts of the body and block AChE which hydrolyses the neurotransmitter acetylcholine. In this study, the reduction of AChE activity is assumed to result from the direct action of CPF and MCP exposure on the active site of this enzyme (Blodgett 2006). As with other OP, CPF and MCP inhibit nervous system function by binding with AChE, the enzyme responsible for the hydrolysis of the neurotransmitter acetylcholine at the cholinergic synapses. Binding AChE with OP pesticides allows the accumulation of acetylcholine at the nerve junction which leads to overstimulation of nicotinic and muscarinic receptors, thus disrupting neurotransmission (Yu et al. 2008).

The present study exhibited that the CPF and MCP inhibited the AChE activity in a similar pattern in both foot muscle and hepatopancreas tissues. A similar trend of AChE activities in all tissues exposed to the OP is in accordance with the previous study of Yaqin & Hansen (2010). Gangnaire et al. (2008) reported that the inhibition of AChE activities has been found in a similar pattern in different tissues of freshwater snails, *Potamopyrgus antipodarum,* and *Valvate piscinalis*.

Dose and Time-Dependent Response in AChE Activity

The results in Tables 1 & 2 clearly show that the AChE activities in the foot muscle and hepatopancreas of *P. globosa* were influenced by the concentrations and duration of the exposure to CPF and MCP. The maximum negative effect was seen among the snails exposed to the highest concentration and a maximum exposure period. A relevant decrease was observed in the AChE activity by 22.89 to 54.19 % and 29.17 to 63.13% in the foot muscle and 20.86% to 46.96 % and 23.37 to 53.67 % in the hepatopancreas following the exposure to lower and higher concentrations of CPF respectively at the interim from 3 to 48 hours. Similarly, the decreased AChE activity was seen 19.07 to 49.07 % and 24.35 to 57.59% in the foot muscle and 15.10 to 44.65% and 20.08 to 48.84% in the hepatopancreas following the lower and higher concentrations of MCP respectively throughout the exposure period.

From the above result, it was confirmed that *P. globosa* exposed to both CPF and MCP exhibited greater inhibition of AChE activity in both organs during the long exposure time and at medium concentrations of these OP pesticides. Such concentration-time response has also been found for a variety of OP insecticides in the tissues of gastropod, *Planorbarius corneus* (Cacciatore et al. 2013)

OP insecticides are highly toxic to aquatic animals, even at low concentrations (Humphrey et al. 2004, Narra et al. 2011). The time gap between the spraying of pesticides and the elevated AChE inhibition levels in the case of apple snails was indicative of the time required for the apple snail to absorb the pesticides. It also emphasized the stress responses of the apple snail and how the snail failed to endure the elevated stress. The OP needs time to be activated into its oxon- metabolite by cytochrome P450 enzyme to become toxic and inhibit AChE activity (Barata et al. 2004, Narra et al. 2011). The reaction of OP pesticides with AChE is progressive in that the longer the inhibitor is in contact with the enzyme the greater the inhibition (Sturn et al. 2007). In *P. globosa* AChE activity gradually decreased when the exposure time was increased. This was because the OP reduced the power of muscle contraction of the snail resulting in losing the ability to close its operculum making it more susceptible to the toxicity of the OP pesticides for the prolonged period of exposure. The most severe sign of neurotoxicity was the abnormal protrusion of the head-foot region from the shell in freshwater gastropod *Chilina gibbosa* (Cossi et al. 2015). A positive correlation with chlorpyrifos concentrations and time of exposure associated with the degree of AChE inhibition of *Lanistes carinatus* was recorded in the successive durations of exposure (Khalil 2015). These findings were in accordance with the results of the present investigation, which indicated that different pesticides will have different affinities to the active site of the AChE and therefore different concentrations and exposure times have a direct relationship

between the degree of inhibition of AChE and toxicity of the OP pesticides (Kristoff et al. 2006)

Tissue-Specific Analyses of AChE

The significant inhibition of AChE in the foot muscle of *P. globosa* was observed at 48 hours of exposure, which was a maximum of 54.19% and 63.13% over the control after respective low and high concentrations of CPF exposure compared to 49.07% and 57.59% over the control after exposure in low and high concentrations of MCP respectively (Tables 1 & 2). But no significant difference in AChE inhibition was recorded throughout the exposure period in the hepatopancreas tissue between low and high concentrations of CPF and MCP exposure though at 48 hrs of exposure a remarkable inhibition was observed which were 46.96% and 53.67% over the control for the respective low and high concentrations of CPF while 44.65% and 48.84% inhibition were noted after low and high concentrations of MCP exposure respectively (Tables 1 & 2).

The inhibitory AChE activity in both foot muscle and hepatopancreas AChE activities exhibited a similar pattern of inhibition but the degree of AChE inhibition was higher in foot muscle than hepatopancreas at all the time intervals in the CPF and MCP exposed snails. This is the reflection of the higher sensitivity of foot muscle than hepatopancreas as the foot muscle is the main direct interacting organ of the surrounding toxic medium (Mundhe & Pandit 2014). Foot muscle tissues of the apple snails evidenced an extremely decreased activity in the levels of AChE in both concentrations of CPF and MCP. The changes in the hepatopancreas suggest that it was relatively less affected than the foot muscle tissue. OP compounds were most likely, acting as neurotoxic agents with greater potency on the foot muscle of the apple snail because the foot muscle is innervated by nerves from several ganglia which represent the main target organ for high AChE activity.

The AChE inhibition is fairly related to the tissue innervation level. Hence, it can be concluded that the highest AChE concentration the highest inhibition susceptibility (Ram et al. 2011) which may be the cause behind the higher reduction in AChE activity in foot muscle than hepatopancreas in *P. globosa*. The depleted sequence in terms of decrement in AChE activity levels was: foot muscle > hepatopancreas. Such sequence of depletion was reported by Putkome et al. (2008) where higher AChE inhibition was exhibited in muscle than digestive gland (hepatopancreas) when the golden apple snail *Pomacea canaliculata* was exposed to organophosphates CPF and dichlorvos.

Pesticide Specific Inhibition of AChE

The CPF was found to be more effective against this snail followed by MCP. CPF produced a maximum of 63.13% and 53.67% AChE inhibition over control in the foot muscle and hepatopancreas respectively whereas MCP produced a maximum of 57.59% and 48.84% AChE inhibition over control in foot muscle and hepatopancreas respectively, after 48 hours of exposure to a higher dose (2.5 mL L^{-1}). From this result, it was obvious that the inhibition was however more pronounced in CPF exposed snails indicating that the toxic potential of CPF is greater than that of MCP because CPF has a relatively persistent nature compared to MCP (Palma et al. 2009). CPF is metabolically converted by oxidative desulfuration into chlorpyrifos – oxon (CPO). The insecticidal action of CPF stems from the inhibition of AChE by CPO, resulting in severe cholinergic toxicity (Crane et al. 2012). The effect was confirmed by the observation of Rao et al. (2005) where at all the time intervals the CPF treated termites (*Odontotermes obesus*) exhibited more AChE inhibition than those exposed to MCP. A study by Tripathi & Pandey (2016) found that the gill of *P. globosa* was affected by CPF with greater severity in comparison to MCP.

CONCLUSIONS

The present study indicated that CPF and MCP cause considerable inhibition of the AChE activity of a freshwater snail *P.*

Table 1: Biochemical responses of *Pila globosa* exposed to chlorpyrifos in paddy fields (n=4).

Biochemical measurements	Tissue	Concentrations of chlorpyrifos 20% EC	Duration of exposure (hour)					
			0(control)	3	6	12	24	48
AChE activity n.mol.mg^{-1} protein min^{-1}	Foot	1.5 mL.L^{-1} water	144.56 ± 2.49(100) ^{Aa}	111.42±2.61 (77.11) ^{Bb}	105.09±2.03 (72.73) ^{Bb}	89.18±3.42 (61.72) ^{Bc}	78.55±3.65 (54.36) ^{Bc}	66.19±2.98 (45.81) ^{Bd}
		2.5 mL.L^{-1} water	144.56 ± 2.49 (100) ^{Aa}	102.34±1.36 (70.83) ^{Bb}	95.58±1.82 (66.15) ^{Bb}	82.49±2.73 (57.09) ^{Bc}	74.89±2.08 (51.83) ^{Bc}	53.26±1.67 (36.87) ^{Cd}
AChE activity n.mol.mg^{-1} protein min^{-1}	Hepatopancreas	1.5 mL.L^{-1} water	118.20 ± 1.53(100) ^{Aa}	93.54±2.98 (79.14) ^{Bb}	87.71±3.11 (74.21) ^{Bb}	78.80±1.65 (66.67) ^{Bc}	73.44±2.82 (62.14) ^{Bc}	62.69±2.48 (53.04) ^{Bd}
		2.5 mL.L^{-1} water	118.20 ± 1.53(100) ^{Aa}	90.57±3.07 (76.63) ^{Bb}	85.43±2.19 (72.28) ^{Bb}	74.17±1.36 (62.75) ^{Bc}	65.17±3.01 (55.81) ^{Bc}	54.76±2.39 (46.33) ^{Bd}

Table 2: Biochemical responses of *Pila globosa* exposed to monocrotophos in paddy fields (n=4).

Biochemical measurements	Tissue	Concentrations of monocrotophos 36% SL	Duration of exposure (hour)					
			0(control)	3	6	12	24	48
AChE activity n.mol.mg^{-1} protein min^{-1}	Foot	1.5 mL.L^{-1} water	144.56 ± 2.49(100) ^{Aa}	116.94±1.41 (80.93) ^{Bb}	108.49±3.56 (75.05) ^{Bb}	99.31±3.05 (68.73) ^{Bc}	89.15±3.72 (61.69) ^{Bc}	73.59±3.94 (50.93) ^{Bd}
		2.5 mL.L^{-1} water	144.56 ± 2.49(100) ^{Aa}	109.31±2.04 (75.65) ^{Bb}	102.64±2.96 (71.28) ^{Bb}	90.94±4.76 (62.94) ^{Bc}	82.61±1.56 (57.17) ^{Bc}	61.28±2.10 (42.41) ^{Cd}
AChE activity n.mol.mg^{-1} protein min^{-1}	Hepatopancreas	1.5 mL.L^{-1}water	118.20 ± 1.53(100) ^{Aa}	100.35±2.39 (84.90) ^{Bb}	92.49±3.01 (78.21) ^{Bb}	84.93±2.92 (71.86) ^{Bc}	80.74±1.85 (68.31) ^{Bc}	65.42±2.57 (55.35) ^{Bd}
		2.5 mL.L^{-1} water	118.20 ± 1.53(100) ^{Aa}	94.46±3.90 (79.92) ^{Bb}	88.67±2.49 (75.02) ^{Bb}	81.16±3.05 (68.67) ^{Bc}	76.65±1.15 (64.85) ^{Bc}	60.45±3.11 (51.16)^{Bd}

Results are exposed as mean ± standard error. AChE, acetylcholinesterase. All values indicate mean ± SE of three replicates, each comprising four snails. Significance was tested statistically by one-way analysis of variance (ANOVA) and Duncan's multiple range tests ($P < 0.05$) within the same concentration among different exposure duration as well as within the same exposure duration between different concentrations of chlorpyrifos and monocrotophos. Values with the same superscript smaller case letters in a row are not significantly different from each other. Values with the same superscript capital letters in a column are not significantly different from each other. Values in parenthesis indicate percent enzyme activity with control taken as 100%.

globosa under field conditions. Our findings show that AChE activity in *P. globosa* was a very useful bioindicator species showing a strong sensitivity and increasing the possibility to indirectly detect the presence of OP compounds in the aquatic system. The fluctuating levels of AChE in *P. globosa* can be used for biomonitoring the non-target aquatic species exposed to xenobiotics.

REFERENCES

Aprea, C., Colosio, C., Mammone, T., Minoia, C. and Maroni, M. 2002. Biological monitoring of pesticide exposure. Review of analytical methods. J. Chromatogr B, 769: 191-219.

Barata, C., Solayan, A. and Porte, C. 2004. Role of cholinesterases in assessing the toxicity of OP (Chlorpyrifos, malathion) and carbamate (carbofuran) pesticides to *Daphnia magna*. Aquatic Toxicol., 66: 125-139.

Blodgett, D. J. 2006. Organophosphate and Carbamate Insecticide. In: Peterson, M.E. and Talcott, P. A. (eds.) Small Animal Toxicology. Elsevier.

Bolton-Warberg, M., Coen, L. D. and Weinstein, J.E. 2007. Acute toxicity and acetylcholinesterase inhibition in grass shrimp (*Palaemonetes pugio*) and oysters (*Crassostrea virginica*) exposed to the organophosphate Dichlorvos: Laboratory and field studies. Arch. Environ. Contam. Toxicol, 52: 207-216.

Cacciatore, L.C., Guerrero, N.V. and Cochon, A.C. 2013. Cholinesterase and carboxylesterase inhibition in *Planorbarius corneus* exposed to a binary mixture of azinphos-methyl and chlorpyrifos. Aquat. Toxicol., 128-129: 124-134.

Cossi, P.F., Beverly, B., Carlos, L. and Kristoff, G. 2015. Recovery study of cholinesterase and neurotoxic signs in the non -target freshwater invertebrate *Chilina gibbosa* after acute exposure to an environmental concentration of azinphos-methyl. Aquat. Toxicol., 167: 248-56.

Crane, A.L., Klein, K., Zanger, U.M. and Olson, J.R. 2012. Effect of CYP2B6*6 and CYP2C19*2 genotype on chlorpyrifos metabolism. Toxicology, 293: 115-122.

Ellman, G.L., Courtney, K.D., Andres, V. and Featherstone, R.M. 1961. A new and rapid colorimetric determination of acetylchololinesterase activity. Biochem. Pharm., 7: 88-95.

Gangnaire, B., Geffard, O., Benoit, X., Margoum, C. and Garrie, J. 2008. Cholinesterase activities as potential biomarkers: Characterization in two freshwater snails, *Potamopyrgu santipodarum* and *Valvata piscinalis*. Chemosphere, 71: 553-560.

Humphrey, C.A., Klump, D.W. and Raethke, N. 2004. *Pomancentrus amboinensis* as a bioindicator organism for the Great Barrier Reef: Responses to chlorpyrifos. Bull. Environ. Contam. Toxicol., 72: 888-895.

Ihsan, T., Edwin, T. and Yanti, R.D. 2019. The effect of sublethal exposure of chlorpyrifos to Nile Tilapia (Oreochromis niloticus): case study of Twin Lakes of West Sumatra, Indonesia. Nat. Env. Poll. Tech., 18(4): 1399-1403.

Jash, N.B., Chatterjee, S. and Bhattacharya, S. 1982. Role of acetylcholine in the recovery of brain acetylcholinesterase in *Channa punctatus* (Bloch) exposed to furadan. Comp. Physiol. Ecol., 7: 56-58.

Khalil, A.M. 2015. Toxicological effects and oxidative stress responses in freshwater snail, *Lanistescarinatus*, following exposure to chlorpyrifos. Ecotox. Environ. Safety, 116: 137-42.

Kopecka-Pilarczyk, J. 2010. In vitro effects of pesticides and metals on the activity of acetylcholinesterase (AChE) from different tissues of the blue mussel, *Mytilus trossulus* L. Journal of Environmental Science and Health, Part B, 45: 46-52.

Kristoff, G., Guerroro, N.Y., de D'Angelo, A.M.P. and Cochon, A.C. 2006. Inhibition of cholinesterase activity by azinphos-methyl in two freshwater invertebrates *Biomphalaria glabrata* and *Lumbriculus variegatics*. Toxicology, 222: 185-194.

Laskowski, R. and Hopkin, S.P. 1996. Accumulation of Zn, Cu, Pb, and Cd in the garden snail (*Helix aspersa*): Implications for predators. Environ. Pollut., 91: 289-297.

Lowry, O.H., Rosenbrough, N.J., Farr, A.L. and Randall, J. 1951. Protein measurement with the folin-phenol reagent. J. Biol. Chem., 193: 265-275.

Mundhe, A.Y. and Pandit, V.S. 2014. Assessment of toxicity of monocrotophos in freshwater bivalve *Lamellidens marginalis*, using different markers. Toxicol. Int., 21(1): 51-56.

Narra, M.D., Ghousia, B., Rajendar, K. and Rao, J.V. 2011. The toxic impact of two organophosphate insecticides on biochemical parameters of a food fish and assessment of recovery response. Toxicology and Industrial Health. DOI: 0748233711 412423: 1-10.

Narra, M.R., Rajender K, Reddy, R.R., Murty, U.S. and Begum, G. 2017. Insecticides induced stress response and recuperation in fish: Biomarkers in blood and tissues related to oxidative damage. Chemosphere, 168: 350-357.

Nguyen, T., Håkan, B. and Nguyen, V.C. 2018. Evaluation of the joint toxicity of chlorpyrifos ethyl and fenobucarb on climbing perch (*Anabas testudineus*) from rice fields in the Mekong Delta, Vietnam. Environ. Sci. Pollu. Res., 25(14): 13226-13234.

Palma, P., Palma, V.L., Fernandez, R.M., Bohn, A., Soares, A.M.V.M. and Barbosa, I.R. 2009. Embryo-toxic effects of environmental concen-

trations of chlorpyrifos in the crustacean *Daphnia manga*. Ecotoxicol. Environ. Saf ., 72: 1714-1718.

Putkome, S., Cheevarporn, V. and Helander, H.F. 2008. Inhibition of acetylcholiesterase activity in the golden apple snail (*P. canaliculata*) exposed to chlorpyrifos, dichlorvos, and carbaryl insecticides. Environ. Asia, 2: 15-20.

Ram, S.B.H., Devi, C.U., Susma, C., Jasti, V.R., Kumar, T.M.V. and Thirumurugan, G. 2011. Effect of polytrin C (combination pesticide) on the acetylcholiesterase inhibition in plasma and brain of Wistar rats. Am. J. Biochem. Mol. Biol., 1: 101-105.

Rao, V.J., Parvathi, K., Kavitha, P., Jakka, N. M., Pallela, R. 2005. Effect of chlorpyrifos and monocrotophos on locomotor behavior and acetylcholiesterase activity of subterranean termites. Pest Manag. Sci., 61: 417-421.

Regoli, F., Gorbi, S., Fattorini, D., Tedesco, S., Notti, A., Machella, N., Bocchetti, R., Benedetti, M. and Piva, F. 2006. Use of the land snail *Helix aspersa* as sentinel organism for monitoring ecotoxicological effects of urban pollution. Environ. Health Perspect., 114: 63-69.

Sturn, A., Radau, T.S., Hahn, T. and Schulz, R. 2007. Inhibition of rainbow trout acetylcholinesterase by aqueous and suspended particle-associated OP insecticides. Chemosphere, 68 (4): 605-612.

Sunanda, M., Rao, C. S. J., Neelima, K., Rao, G. and Simhachalam, G. 2016. Int. J. Pharm. Sci.: Rev. Res., 59: 299-305.

Tam, N. T., Berg, H., Tuyen, P. T. B. and Cong, N. V. 2015. Effect of chlorpyrifos ethyl on acetylcholinesterase activity in climbing perch (*Anabas testudineus*, Bloch, 1972). Arch. Environ. Contam. Toxicol., 69: 515-524.

Tripathi, N. and Pandey, R. 2016. Histochemical study of *Pila globosa* gill when exposed to a sublethal dose of monocrotophos and chlorpyrifos. Bioglobia, 3(2): 73-78.

Ullah, S., Li, Z., Hasan, Z., Khan, S. U. and Fahad, S. 2018. Malathion-induced oxidative stress leads to histopathological and biochemical toxicity in the liver of *Labeorohita* at acute concentration. Ecotoxicol. Environ. Saf., 161: 270-280.

Wang, Q., Hong, X., Chen, H., Yuan, L. and Zha, J. 2018. The neuropeptides of Asian freshwater clam (*Corbicula fluminea*) as new molecular biomarker basing on the responses of organophosphate chemicals exposure. Ecotoxicol. Environ. Saf., 160: 52-59.

Yaqin, K. and Hansen, P.D. 2010. The use of cholinergic biomarker, cholinesterase activity of blue mussel *Mytilus edulis* to detect the effect of organophosphorus pesticides. Afr, J. Biochem. Res., 4: 265-272.

Yu, F., Wang, Z., Ju, B., Wang, Y., Wang, J. and Bai, D. 2008. Apoptotic effects of organophosphorus insecticide chlorpyrifos on mouse retina in vivo via oxidative stress and protection of combination of vitamins C and E. Exp. Toxicol. Pathol., 59: 415-423.

Nature Environment and Pollution Technology
An International Quarterly Scientific Journal

p-ISSN: 0972-6268
(Print copies up to 2016)
e-ISSN: 2395-3454

Vol. 20 | No.3 | pp. 1269-1275 | 2021

Review Research Paper

https://doi.org/10.46488/NEPT.2021.v20i03.038

Open Access Journal

Portrayal of Textile Based Pollutants and its Impact on Soil, Plants and Fisheries

M. Riza*†, M. N. Ehsanand S. Hoque*****

*Department of Environmental Science, Bangladesh University of Professionals, Dhaka, Bangladesh
**Department of Textile Engineering, Southeast University, Dhaka, Bangladesh
***Department of Soil, Water & Environment, University of Dhaka, Dhaka, Bangladesh
†Corresponding author: M. Riza; mumtahina@seu.edu.bd

Nat. Env. & Poll. Tech.
Website: www.neptjournal.com

Received: 26-09-2020
Revised: 18-11-2020
Accepted: 08-12-2020

Key Words:
Agriculture
Effluents
Fisheries
Textile Pollutants
Soil
Plants

ABSTRACT

The textile industry occupies a significant hold on the global economy. This substantial industry often generates a large volume of effluents exceeding the permissible limit of discharge in the different regions of the world. Therefore, textile effluents act as pollutants altering the natural composition of various components of the environment. This paper discusses the impact of textile-based pollutants on agriculture including plants, soil, water and fisheries. The observed result is significant because textile effluents exert a widespread negative impact on the respective respondents, though plants show few positive effects. Prior treatment of textile wastewater is necessary before applying it to the soil, as there is a possibility of affecting the plant ecosystem via soil media. Plants are benefitted in terms of germination and growth, due to irrigation by textile effluents with proper dilution. The physical and biochemical properties of water streams along with aquatic organisms are impacted by these specific discharges, leading to even severe deterioration of particular living creatures. Pollutants released from various steps of textile processing have adverse effects on the environment, disturbing the food chain, ecosystem, and overall ecological balance.

INTRODUCTION

Industrialization reflects the economic improvement of countries (Sarayu & Sandhya 2012) especially the textile industry is a boon for fiscal sustainability. Clothing is the second most fundamental need of human beings, agriculture being the prime essentials (Elango et al. 2017)**.** Textile trade, especially exporting and importing, plays a prominent role in sustaining the economic growth of a country. According to the World Trade Statistical Review 2019, the share in the world export of textile (%) of China, the European Union (28), Bangladesh, Vietnam, India, Turkey, Indonesia, Cambodia, and the United States of America in 2018 was 31.3, 28.4%, 6.4%, 6.2%, 3.3%, 3.1%, 1.8%, 1.6%, and 1.2%, respectively (WTO 2019). There are skilled and unskilled labor forces who work in different segments of the textile industry like dyeing, finishing, knit-composite, garments, printing, and washing factories. While the textile industry is scattered, it creates around 1 trillion dollars business, contributing to 7% of the total world exports, and about 35 million workers are engaged globally (Desore & Narula 2018).

As 8,000 chemicals and a large volume of freshwater are used in the textile industry, this is one of the prime contributors to surface and groundwater pollution (Bhatia et al. 2017). The textile industry consumes a large volume of water in various processing stages, such as pretreatment, scouring, bleaching, dyeing, printing, washing, and finishing (Yin et al. 2017); however, the main pollution load originates from processes of dyeing and finishing (Lotito et al. 2014). Fig. 1 shows the influence of textile discharges on agricultural segments like soil, plants and fisheries.

Textile effluents discharged into surface water lead to contamination of water. The effluent acts as a pollutant because it disrupts the natural quality and composition of water and other environmental segments like soil and biodiversity. The wastewater generated in large volume by the textile industry is considered the most polluting effluents among all industrial effluents (Mani et al. 2019). Dyes and chemicals are prominent constituents in textile effluents that are not easily decomposable in the environment (Ghaly et al. 2014). Various types of chemicals such as wetting agents, sequestering agents, scouring, bleaching, dyeing, finishing, and printing chemicals are used in the pretreatment, dyeing, and finishing stages of textile processing. Approximately 280,000 tons of dyes are generated as effluents every year around the world (Maas & Chaudhari 2005). Effluent discharged from textile processing into water bodies has sweeping implications on the environment as it contains numerous contaminants like solids, oils, metal complexes, organics, complex synthetic dyes, and remainders from different stages of fabric pretreatment and coloration (Bhatia et al. 2018)**.** Textile effluent usually contains

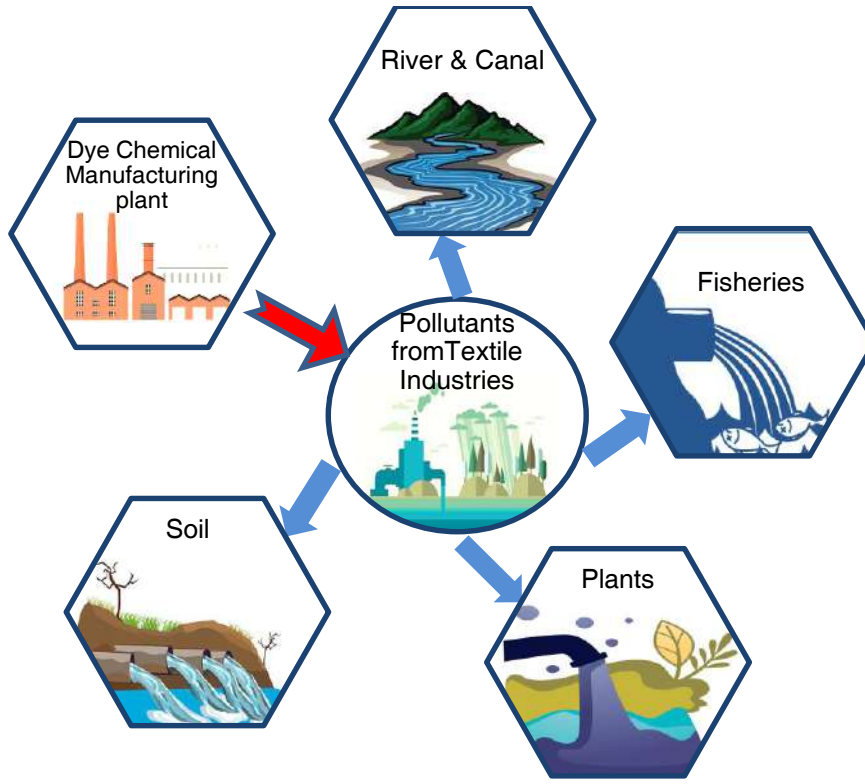

Fig. 1: Schematic diagram representing the impact of textile-based pollutants on soil, plant, water, and fisheries.

a higher concentration of total dissolved solids (TDS), total suspended solids (TSS), biochemical oxygen demand (BOD), and chemical oxygen demand (COD) when discharged into the environment (Mani et al. 2019).

Different categories of dyes like direct, acid, reactive, disperse, vat, basic, azoic, sulfur, etc. are used for the coloration and dyeing of different types of fabrics. Many of the dyes are usually metal salts. Heavy metals that occur in textile effluent are As, Ba, Cd, Cu, Fe, Hg, Os, Ni, and Sb (Nagajyoti et al. 2010). This paper summarizes the agricultural issues along with the characterization of the textile effluents.

RATIONALE OF THE STUDY

The effluents of different industries deteriorate the various components of the environment to a vast extent based on the composition of their respective discharges and the category of the industry. The deleterious impacts of these industries (mining, coal, oil, leather, tannery, distillery, chemicals, etc.) on surrounding nature have been reviewed in several studies. However, the attention given to the impact of textile effluents on agriculture such as plants, ecosystem, soil, fisheries and water remains limited. The human health-related issues, as well as the condition of air and water, have been discussed earlier in terms of textile releases. As agriculture plays a prime role in the economy, a review is done to analyze how textile-based pollutants disturb the different sectors of agriculture.

IMPACT OF TEXTILE-BASED POLLUTANTS ON AGRICULTURE

Effects on Soil

Soil acts as a basic source of agricultural growth and influences almost all parts of the life cycle (Emadodin et al. 2020). Around the world, wastewater irrigation is common in tropical and subtropical regions (Pandey et al. 2015). Irrigating the agricultural lands using different industrial wastewaters may alter the soil's physical, chemical, and biological properties (Mani et al. 2019). Several heavy metals such as chromium, copper, and zinc remain in high amounts in textile effluent, which may affect soil and the plant ecosystem. (Dey & Islam 2015). Agricultural lands irrigated by industrial effluents may affect the soil's physical and chemical properties as well as soil fertility by augmenting the activity and diversity of microorganisms (Mani et al. 2019).

The dye bath auxiliaries having nitrogen and phosphorus (such as urea, ammonium acetate, ammonium sulfate, and

phosphate) are the prime origin of nutrients in textile wastewater (Correia et al. 1994). Industrial effluent irrigation often increases the availability of nutrients for microbes (Jain et al. 2005, Li et al. 2015). The use of both treated and untreated wastewater has a temporal impact on the accumulation of heavy metals in soil (Khan et al. 2008, Ullah et al. 2012). Several researchers have stated that heavy metals accumulate in the soil because of the continuous watering of agricultural lands with industrial effluents (Hare et al. 2017, Chowdhary et al. 2018). Cai et al. (2012) observed that the concentrations of heavy metals such as Cu, Zn, Ni, Cr, Pb, Cd, As, and Hg in agricultural soils of Huizhou in China was found to be in the range of 1.65 to 99.8, 16.8 to 248.8, 2.61 to 112, 1.12 to 81.1, 4.92 to 108.1, 0.01 to 1.12, 1.1 to 137.8, 0.01 to 3.39 $mg.kg^{-1}$, respectively. However, the reference values recommended by the Chinese National Environmental Monitoring Centre (1990) for these heavy metals were 17, 47.3, 14.4, 50.5, 36, 0.056, 8.9, and 0.078 $mg.kg^{-1}$, respectively. Because of the higher content of heavy metals in effluent sludge, a pre-treatment process for reducing the amount of heavy metal is mandatory before the sludge can be used as a soil conditioner or fertilizer in the agricultural soil (Islam et al. 2009). An effective effluent treatment system should be an integral part of the textile industry and be kept functional as well to protect agricultural land, water, and the surrounding environment.

Effects on the Plants

It is reported that African and Asian cities fulfill their demand (50%) for vegetables from agricultural lands irrigated with wastewater (Bjuhr 2007). The amount of nitrogen in the textile effluent reported by Begum et al. (2018) in two regions of Narayanganj and Gazipur, Bangladesh was high - about 0.05% and 0.07% respectively. There were six treatments of different effluent levels including different proportions of fresh water and Recommended Dose of Fertilizer (RDF). It was observed that all the treatments showed a significant positive effect on the yield parameters of jute vegetables over the control on agricultural soils. However, in contaminated soils, effluent irrigation showed a negative effect over the control (Begum et al. 2018). Ganesan and Chellappan (2018) studied the growth of Sea Marigold planted in soil irrigated with partially diluted textile effluents. The result demonstrated a positive effect on plant shoot length and root length, plant biomass, chlorophyll content, and carotenoid of three different cultivars of wheat, when compared with raw effluent irrigated plants. Moreover, the responding plant exhibited maximum development and growth because of the absence of textile effluent. At low concentrations, textile effluent did not show an impeding effect on seed germination, whereas seeds germinated in undiluted effluents did not survive for a longer

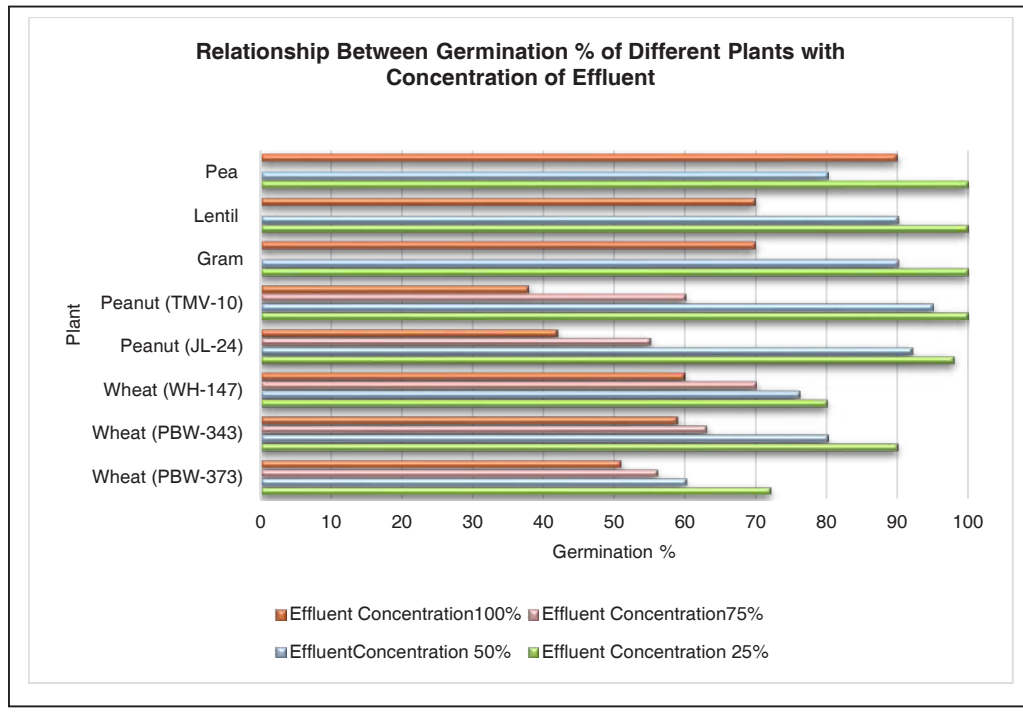

Fig. 2: Effect of various concentration of textile effluent on germination percentage (%) of different plants (Kaushik et al. 2005, Saravanamoorthy & Kumari 2007, Gufrankhan et al. 2011).

period (Kaushik et al. 2005). The relationship between the germination of different plants with various concentrations of textile effluent is depicted in Fig. 2, based on data collected from several related research works.

Several other studies reported similar outcomes on germination, biomass, chlorophyll pigments, and root growth of peas, lentil, and gram seedlings by textile effluents when irrigated in low concentrations, compared to adverse impact on plants when irrigated with highly concentrated textile effluents (Gufrankhan et al. 2011). The usage of textile wastewater on planting and irrigation of two varieties of peanut exhibited an increased chlorophyll content, growth yield, and germination positively contributing to root length and shoot length, etc. (Saravanamoorthy & Kumari 2007).

Metals play an essential role in the formation of dyes, and copper, zinc, chromium, lead, cobalt, nickel, and manganese are commonly used heavy metals in several dyes (Madhav et al. 2018). Heavy metals exert an impending threat to the food security of the contaminated area and show precarious influence on the ecosystem (Lu et al. 2012, Mombo et al. 2016). As noted by Gopalakrishnan and Jeyadoss (2011), textile effluent contains a very high concentration of zinc, copper, and cadmium at 4.56, 2.69, and 2.49 $mg.L^{-1}$, respectively, beyond their acceptable limits (Zn: 0.5 g $mg.L^{-1}$, Cu: 0.05 $mg.L^{-1}$, Cr: 0.05 $mg.L^{-1}$) and causing numerous environment-related problems. Though copper is a necessary micronutrient required in a small quantity for the growth of the plant, yet toxicity is imposed upon plants when assimilated in high amounts (Mahmood & Islam 2006). Likewise, cadmium displays toxicity by hindering the growth of plants (Hu et al. 2013).

In the case of soil-plant interaction, high concentrations of heavy metals in the soil showed adverse effects on different plants such as alfalfa, lettuce, radish, and alpine pennycress, but at low concentrations, their effects were moderate on those plants (Guala et al. 2010). As industrial effluent acts as a prime key source for accretion of heavy metals in crops, prior treatment is necessary for the effluent before release into the surrounding environment (Chowdhary et al. 2018). Toxic metal ions and nutrients from the soil reach the tissues of the plant (DalCorso et al. 2013) and an extreme accumulation of heavy metals in plant tissue impact seed germination, root elongation, plant biomass, and chlorophyll biosynthesis and consequently, affect crop productivity (Shahid et al. 2015).

Fresh and dry biomass of plants decreased with an increase in the concentration of textile effluents; a high concentration of the effluent inhibited the survival of plants (Rehman et al. 2009). Textile wastewater can be used safely for the irrigation of plants and crops after appropriate treatment of the effluent if there is a shortage of water for irrigation (Rehman et al. 2009). Most of the studies have shown that the growth and development of other morphological parameters of plants improved if the plants are irrigated by partially diluted effluents. In contrast, the highly concentrated textile effluent negatively impacted the plants.

Effects on Water and Fisheries

The release of textile effluents, whether solid, liquid, or gaseous, affected the aquatic ecosystem by decreasing the penetration of sunlight and hence diminishing the photosynthesis rates and raising the biological oxygen in water (Kant 2012, Singh et al. 2015). Ahmed et al. (2011) conducted studies on the Buriganga and Karnatoli rivers near Dhaka, Bangladesh at the proximity of the textile industries and reported that the values of physicochemical properties of textile effluent like BOD, salinity, TDS, TSS, sodium, potassium, calcium, iron, phosphate, chloride, nitrite and nitrate were 46.9 to 58.5, 0.75 to 1.03, 984 to 1148, 872.75 to 1282.4, 390 to 411.1, 12.4 to 31, 37.21 to 54.82, 0.12 to 0.18, 18.25 to 19.88, 72.21 to 135.87, 0.07 to 0.74 and 0.47 to 1.02 $mg.L^{-1}$, respectively. These values were beyond the acceptable limit for open water recommended by the Department of Environment, Bangladesh, and might threaten the living organisms in the surface water and ecosystem of Buriganga and Karnatoli river (Ahmed et al. 2011).

The constituents of natural water streams may have an increased possibility to be solubilized because of the high pH in effluents and aquatic life is hampered due to these high pH values (Younas et al. 2017). Highly alkaline condition is not suitable for the existence of living organisms in the water bodies. Besides heavy metals, organic pigments, and dyes, for example, C.I. Pigment Yellow-12, C.I. Disperse Yellow-7, C.I. Direct Yellow-1, etc., salt, acid, alkalis, bleaching, and finishing agent have an adverse impact on the health of living things to a large scale (Imtiazuddin et al. 2012). The pH value of textile effluent collected from the release point of seven different textile mills situated in Pakistan was in the range of 7.5 and 11.5, whereas the value recommended by National Environmental Quality Standards (NEQS), Pakistan was 6 to 9 (Imtiazuddin et al. 2012).

The physical and biochemical properties of water and aquatic life are interlinked and impact one another, directly or indirectly (Sanga & Sirsat 2016). High temperature reduces the solubility of gases in water that ultimately increases BOD or COD. Short-term temperature variation in waterbodies near textile and dyeing industries might create problems for fish egg hatching and even lead to death, thus affecting the fish population (Roy et al. 2010). The excessive levels of TSS in water systems can have a significant detrimental impact on the physical, chemical, and biological properties of the waterbodies (Bilotta & Brazier 2008). The changes

in the water system due to the discharge of effluent impair the osmoregulatory mechanism of aquatic lives and make water unsuitable for the intended use (Kaur & Soodan 2020).

Textile industries around the world consume more than 10,000 tons of dyes each year. 100 tons of toxic textile effluents are discharged into water resources/bodies every year that can damage the ecosystem (Iqbal & Ashiq 2007, Dizge et al. 2008). For instance, zinc displays harmful effects on the initial stages of aquatic life when it is present in large concentrations in water. Furthermore, exposure to nickel for a longer duration can reduce body weight, damage the heart and liver of aquatic species, and also cause skin irritation (Imtiazuddin et al. 2014). Thus, in consequence, contaminated natural water bodies have a deadly impact on fishes and inhibit the growth of microorganisms (Puvaneswari et al. 2006).

Soni et al. (2006) conducted a study to observe the toxicity of textile dye wastewater on a freshwater fish, *Gambusia affinis,* and found noticeable changes in the shape and variation of red blood cells. Also because of high BOD and COD values of dyes, aquatic organisms and fish confront toxicity (Al Prol 2019). When textile wastewater reaches the water stream, the amount of total dissolved solids and total suspended solids increases as unfixed dyes, remnants of starch, different finishing chemicals, agents, and salts are carried along with the effluents, and further, these fragments increase the salinity of the water. Because of high salinity in the freshwater system, contaminated water has a harmful impact on organisms of water bodies, especially exposing osmotic imbalance and hampering homeostasis in aquatic lives (Ahmed et al. 2011). It is reported that mortality of *Tilapia* was increased with the increase of concentration of textile effluent in Lake Hawassa, Southern Ethiopia. Berehanu et al. (2015) indicated the mortality of that fish was about 16.1, 65, 86.8, and 88.7% at 1%, 5%, 10%, and 20%, concentration levels of textile effluents, respectively. Other scientists (Table 1) also reported mortality rates of tilapia fish.

So, textile effluent discharge exerted a potential threat to the existence of aquatic life especially fish (Berehanu et al. 2015). Muley et al. (2007) carried out a study on *Labeo rohita* with exposure to effluent around Kolhapur, India. In the acute toxicity (96 hr) experiment, the fingerlings of freshwater fish Labeo rohita were exposed to tannery, electroplating, and textile mill effluents. It was found that electroplating effluent was more toxic than tannery and textile mill wastes. After acute toxicity experiments for different industrial effluents, various tissues viz. gill, liver, muscle and kidney were obtained separately. The glycogen content in all the tissues decreased considerably upon acute toxicity of three industrial effluents. The total protein content decreased in all tissues in three effluents. In general total lipid content decreased in all tissues after acute exposure when compared to control group. The results obtained in the present study showed that, the industrial effluents from tannery, electroplating and textile mills caused marked depletion in biochemical composition in various tissues of the fish Labeo rohita after acute exposure.

Using the acute toxicity (96 hr) and chronic (30 days) exposure experiment, Nikalje et al. (2011) investigated the *Labeo rohita* in the polluted Panchganga river near Kolhapur, India. There was a remarkable decrement in protein, total glycogen, and lipid content in all tissues of *Labeo rohita* because of the presence of heavy metals in high amounts (Nikalje et al. 2011). The decline was more significant at higher concentrations of effluent than lower concentrations. In summary, proper dilution of textile effluent before discharge is a prerequisite to lessen the negative impact on fisheries.

CONCLUSION

The textile industry releases diverse and high amounts of pollutants into the environment, which consequently affects different segments of the agricultural ecosystem including soil, plants, water, and fisheries. Thus, pollutants disrupt the food chain, ecosystem, and agricultural productivity over

Table 1: Effect of concentration of textile effluent on mortality rate of Tilapia (*Oreochromis niloticus*)

	Mortality % of Tilapia (*Oreochromis niloticus*)		
Concentration of Effluent %	1 day	4 days	7 days
1	-	-	16.1
5	-	-	65
10	23	10	86.8
20	64	20	88.7
30	-	50	-
40	-	70	-
100	-	100	-

time. To maintain the ecological balance, it is important to take necessary initiatives with utmost importance. Imparting cost-effective and eco-friendly chemicals, techniques and methods might be a better option to combat environmental degradation. An effective effluent treatment plant should be an integral part of each textile factory to minimize pollution. The law enforcing bodies and monitoring committees of different countries can play a significant role to ameliorate the damage to agriculture as well as other organisms due to textile effluent pollution by enacting stringent laws, rules, and regulations for protecting the environment from textile-based pollution.

REFERENCES

Ahmed, M.K., Das, M., Islam, M.M.,Akter M.S. and Islam,M. 2011. Physico-chemical properties of tannery and textile effluents and surface water of river Buriganga and Karnatoli, Bangladesh. World Appl. Sci. J., 12: 152-159

Al Prol, A.E. 2019. Study of environmental concerns of dyes and recent textile effluents treatment technology: a review. Asian J. Fish Aquat. Res., 3: 1-18.

Begum, M., Gani, M.N. and Alam, M.D. 2018. Effect of textile effluent on the yield of jute leaves (*Corchorus capsularis*) in winter season. J. Biodivers. Conserv. Bioresour. Manag., 4: 53-60.

Berehanu, B., Lemma, B. and Tekle-Giorgis Y. 2015. Chemical composition of industrial effluents and their effect on the survival of fish and eutrophication of Lake Hawassa, Southern Ethiopia. J. Environ. Prot. (Irvine, Calif), 06: 792-803.

Bhatia, D., Sharma, N.R., Singh, J. and Kanwar, R.S. 2017. Biological methods for textile dye removal from wastewater: A review. Crit. Rev. Environ. Sci. Technol., 47: 1836-1876.

Bilotta, G.S. and Brazier, R.E. 2008. Understanding the influence of suspended solids on water quality and aquatic biota. Water Res., 42: 2849-2861.

Bjuhr, J. 2007. Trace metals in soils irrigated with wastewater in a periurban area downstream Hanoi City, Vietnam. Dissertation, Swedish University of Agricultural Sciences.

Cai, L., Xu, Z., Ren, M., Guo, M., Hu, X., Hu, G., W. H. and Peng, P. 2012. Source identification of eight hazardous heavy metals in agricultural soils of Huizhou, Guangdong Province, China. Ecotoxicol. Environ. Saf.,78: 2-8.

Chavan, R.B. 2001. Indian textile industry: Environmental issues. Indian J. Fibre. Text. Res. 26: 11-21.

China National Environmental Monitoring Centre (CNEMC) 1990. Soil element background values in China. Beijing: China Environmental Science Press (in Chinese), pp. 330-483.

Chowdhary, P., Raj, A. and Bharagava, R.N. 2018. Environmental pollution and health hazards from distillery wastewater and treatment approaches to combat the environmental threats: A review. Chemosphere, 194: 229-246.

Correia, V.M., Stephenson, T. and Judd, S.J. 1994. Characterisation of textile wastewaters: A review. Environ. Technol., 15: 917-929.

DalCorso, G., Fasani, E. and Furini, A. 2013. Recent advances in the analysis of metal hyperaccumulation and hypertolerance in plants using proteomics. Front. Plant Sci., 4: 1-8.

Desore, A. and Narula, S.A. 2018. An overview on corporate response towards sustainability issues in textile industry. Environ. Dev. Sustain., 20: 1439-1459.

Dey, S. and Islam, A. 2015. A review on textile wastewater characterization in Bangladesh. Resour. Environ., 5: 15-44.

Dizge, N, Aydiner, C, Demirbas, E., Kobya, M. and Kara, S. 2008. Adsorption of reactive dyes from aqueous solutions by fly ash: Kinetic and equilibrium studies. J. Hazard Mater., 150: 737-746.

Elango, G., Rathika, G. and Elango, S. 2017. Physico-chemical parameters of textile dyeing effluent and its impacts with case study. Int. J. Res. Chem. Environ., 7: 17-24.

Emadodin, I., Reinsch, T., Rotter, A.,Orlando-Bonaca, M., Taube, F. and Javidpour, J. 2020. A perspective on the potential of using marine organic fertilizers for the sustainable management of coastal ecosystem services. Environ. Sustain., 3: 105-115.

Ganesan, S. and Chellappan, R.K. 2018. Morphological, biochemical, and antioxidant enzyme adaptation of *Suaeda maritima* growing in textile dye effluent irrigated soil. Indian J. Plant Physiol., 23: 128-139.

Ghaly, A., Ananthashankar, R., Alhattab, M. and Ramakrishnan, V. 2014. Production, characterization and treatment of textile effluents: a critical review. J. Chem. Eng. Process Technol., 05: 1-18.

Gopalakrishnan, K. and Jeyadoss, T. 2011. Comparative study on biosorption of Zn(II), Cu(II), and Cr(VI) from textile dye effluent using activated rice husk and activated coconut fiber. Indian J. Chem. Technol., 18: 61-66.

Guala, S.D., Vega, F.A. and Covelo, E,F. 2010. The dynamics of heavy metals in plant-soil interactions. Ecol. Modell., 221: 1148-1152.

Gufrankhan, M. Daniel, G. and Konjit, M. 2011. Impact of textile wastewater on seed germination and some physiological parameters in pea (*Pisum sativum* L.), lentil (*Lens esculentum* L.), and gram (*Cicer arietinum* L.). Asian J. Plant Sci., 10: 269-273.

Hare, V., Chowdhary, P. and Baghel, V.S. 2017. Influence of bacterial strains on *Oryza sativa* grown under arsenic tainted soil: Accumulation and detoxification response. Plant Physiol. Biochem., 119:93-102.

Hu, Y.F., Zhou, G. and Na, X.F. 2013. Cadmium interferes with maintenance of auxin homeostasis in *Arabidopsis* seedlings. J. Plant Physiol., 170: 965-975.

Imtiazuddin, S.M. and Mumtaz, M. and Mallick, K.A. 2012. Pollutants of wastewater characteristics in textile industries. J. Basic Appl. Sci., 8: 554-556.

Imtiazuddin, S.M., Mumtaz, M. and Ahmed, T. 2014. Physico-chemical analysis and heavy metals concentration in textile effluent in Karachi region of Pakistan. Glob. J. Environ. Sci. Technol., 2: 71-74.

Iqbal, M.J. and Ashiq, M.N. 2007. Adsorption of dyes from aqueous solutions on activated charcoal. J. Hazard Mater., 139: 57-66.

Islam, M., Halim, M.A., Safiullah, S., Hoque, S.M. and Islam, M.S. 2009. Heavy metal (Pb, Cd, Zn, Cu, Cr, Fe, and Mn) content in textile sludge in Gazipur, Bangladesh. Res. J. Environ. Sci., 3: 311-315.

Jain, R.K., Kapur, M., Labana, S., Lal, B., Sarma, P.M., Bhattacharaya, D. and Thakur, S. 2005. Microbial diversity: Application of microorganisms for the biodegradation of xenobiotics. Curr. Sci., 89: 101-112.

Kant, R. 2012. Textile dyeing industry an environmental hazard. Nat. Sci., 4: 22-26

Kaur, S., and Soodan, M. 2020. Literature review on the effect of textile and paper mill effluents on aquatic organisms. Sustain. Humanosph., 16: 1528-1541.

Kaushik, P., Garg, V.K. and Singh, B. 2005. Effect of textile effluents on growth performance of wheat cultivars. Bioresour. Technol., 96: 1189-1193.

Khan, S., Cao, Q., Zheng, Y.M. Huang, Y.Z. and Zhu, Y.G. 2008. Health risks of heavy metals in contaminated soils and food crops irrigated with wastewater in Beijing, China. Environ. Pollut., 152: 686-692.

Li, C., Zhang, Z., Li, Y. and Cao, J. 2015. Study on dyeing wastewater treatment at high temperature by MBBR and the thermotolerant mechanism based on its microbial analysis. Process Biochem., 50: 1934-1941.

Lotito, A.M., De Sanctis, M., Rossetti, S., Lopez, A. and Di Iaconi,C. 2014. On-site treatment of textile yarn dyeing effluents using an integrated biological-chemical oxidation process. Int. J. Environ. Sci. Technol., 11: 623-632.

Lu, A., Wang, J., Qin, X., Wang, K., Han, P. and Zhang, S. 2012. Multivariate and geostatistical analyses of the spatial distribution and origin of heavy metals in the agricultural soils in Shunyi, Beijing, China. Sci. Total Environ., 425: 66-74.

Maas, R. and Chaudhari, S. 2005. Adsorption and biological decolorization of azo dye Reactive Red 2 in semicontinuous anaerobic reactors. Process Biochem., 40: 699-705.

Madhav, S., Ahamad, A., Singh, P. and Mishra, P.K. 2018. A review of textile industry: wet processing, environmental impacts, and effluent treatment methods. Environ. Qual. Manag., 27: 31-41.

Mahmood, T. and Islam, K.R. 2006. Response of rice seedlings to copper toxicity and acidity. J. Plant. Nutr., 29: 943-957.

Mani, S., Chowdhary, P. and Hare, V. 2019. Industrial Effluents: Impact on Agricultural Soils and Microbial Diversity. In: Varma, A., Tripathi, S. and Prasad, R. (eds) Plant Biotic Interactions. Springer Nature, Switzerland AG, pp 43-60

Mombo, S., Foucault, Y., Deola, F. Gaillard, I., Goix, S., Shahid, M., Schreck, E., Pierart, A. and Dumat,C. 2016. Management of human health risk in the context of kitchen gardens polluted by lead and cadmium near a lead recycling company. J. Soils Sediments, 16: 1214-1224.

Muley, D.V., Karanjkar, D.M. and Maske, S.V. 2007. Impact of industrial effluents on the biochemical composition of fresh water fish Labeo rohita. J. Environ. Biol., 28: 245-249.

Nagajyoti, P., Lee, K. and Sreekanth, T. 2010. Heavy metals occurrence and toxicity for plants: A review. Environ. Chem. Lett., 8: 199-216.

Nikalje, S.B., Muley, D.V., Pailwan, S.M. and Angadi, I.F. 2011. Biochemical alterations in different tissues of a freshwater major carp *labeo rohita* after acute and chronic exposure to textile mill effluent (TME). In: International conference on climate change, forest resource, and environment. The Ecoscan, Thiruvananthapuram, pp 341-345.

Pandey R., Singh, J. and Ababa, A. 2015. Effect of textile factory effluent irrigation on productivity of the wheat crop. Int. J. Sci. Environ. Technol., 4: 727-736.

Puvaneswari, N., Muthukrishnan, J. and Gunasekaran, P. 2006. Toxicity assessment and microbial degradation of azo dyes. Indian J. Exp. Biol., 44: 618-626

Rehman, A., Bhatti, H.N. and Athar, H.U.R. 2009. Textile effluents affected seed germination and early growth of some winter vegetable crops: a case study. Water Air Soil Pollut., 198:155-163.

Roy, R., Fakhruddin, A., Khatun, R., Islam, M.S., Ahsan, M.A. and Negar, A.J.M.T. 2010. Characterization of textile industrial effluents and its effects on aquatic macrophytes and algae. Bangladesh J. Sci. Ind. Res., 45: 79-84.

Sanga, R.M. and Sirsat, P. 2016. Toxicity of industrial effluent on fry of exotic carp, *Cyprinus carpio*. J. Environ. Res. Dev., 10: 729-733.

Saravanamoorthy, M.D. and Kumari, B.D.R. 2007. Effect of textile wastewater on morphophysiology and yield on two varieties of peanut (*Arachis hypogaea* L .). J. Agric. Technol. Eff., 5: 1432-1435.

Sarayu, K. and Sandhya, S. 2012. Current technologies for biological treatment of textile wastewater: A review. Appl. Biochem. Biotechnol., 167: 645-661.

Shahid, M., Khalid, S. and Abbas, G. 2015. Heavy metal stress and crop productivity. In: Hakeem, K. R. (ed), Crop production and global environmental issues. Springer International Publishing Switzerland, pp 1-15.

Singh, A.L., Chaudhary, S., Kayastha, A.M. and Yadav, A. 2015. Decolorization and degradation of textile effluent with the help of *Enterobacter asburiae*. Indian J. Biotechnol., 14: 101-106.

Soni, P., Sharma, S. and Sharma, S. 2006. A comparative study on the toxic effects of textile dye wastewaters (untreated and treated) on mortality and RBC of a freshwater fish *Gambusia affinis* (Baird and Gerard). J Environ. Biol., 27: 623-628.

Ullah, H., Khan, I. and Ullah, I. 2012. Impact of sewage-contaminated water on soil, vegetables, and underground water of peri-urban Peshawar, Pakistan. Environ. Monit. Assess., 184:6411-6421.

WTO. 2019. World Trade Organization. World Trade Stat. Rev. https://www.wto.org/english/res_e/statis_e/wts2019_e/wts2019_e.pdf. Accessed 25 Jun 2020

Yin, H., Guo, H., Qiu, P., Yi, L. and Li, J. 2017. Case analysis on textile wastewater subjected to combined physicochemical-biological treatment and ozonation. Desalin. Water Treat., 66: 140-148.

Younas, U., Iqbal, S., Saleem, A. Iqbal, M., Nazir, A., Noureen, S., Mehmood, K. and Nisar, N. 2017. Fertilizer industrial effluents: Physicochemical characterization and water quality parameters evaluation. Acta. Ecol. Sin., 37: 236-239.

Nature Environment and Pollution Technology
An International Quarterly Scientific Journal

p-ISSN: 0972-6268
(Print copies up to 2016)
e-ISSN: 2395-3454

Vol. 20 | No.3 | pp. 1277-1284 | 2021

Original Research Paper

https://doi.org/10.46488/NEPT.2021.v20i03.039

Open Access Journal

Impact of Environmental Subsidies on Environmental Technology Innovation of Polluting Enterprises

Chunwei Han†
School of Accounting, Henan University of Engineering, Zhengzhou 451191, China
†Corresponding author: Chunwei Han; huehan@126.com

Nat. Env. & Poll. Tech.
Website: www.neptjournal.com

Received: 12-04-2021
Revised: 30-05-2021
Accepted: 12-06-2021

Key Words:
Environmental subsidies
Green innovation
Green patent
Strategic innovation

ABSTRACT

Environmental technology innovation plays an important role in solving pollution control problems. Under the background of the green development of the polluting industry, environmental subsidies have become an important financial instrument to make up for the lack of capital market. To explore the motivation of environmental technology innovation supported by environmental subsidies, using the data of listed polluting enterprises in China from 2013 to 2019, the impact of environmental subsidies on environmental technology patents of polluting enterprises was discussed from the perspective of selective industrial policies. Results show that environmental subsidies stimulate the total number of environmental technology patents and non-invention patents to increase significantly, showing the behavior characteristics of enterprises pursuing innovation quantity while ignoring quality. When enterprises expected to get more environmental subsidies, they make environmental technology patents to seek support. The above phenomenon is only significant in the state-owned enterprise group and senior executives group with a technical background in the group analysis results. The number of environmental technology invention patents of private enterprises increased significantly. The selective environmental subsidies policy stimulates the strategic innovation of enterprises, while the environmental technology invention patents representing substantive innovation and high-quality innovation are not improved significantly. The managerial implication of the conclusions is that the government should not only consider increasing environmental subsidies to polluting enterprises in the future but also should support better regulatory policies to improve the level of pollution prevention and control through environmental technology innovation.

INTRODUCTION

Environmental pollution has become a common problem all over the world. Polluting enterprises as the main emitters of pollutants in the process of economic and social development, should actively increase investment in environmental technology innovation, develop energy-saving and low-carbon advanced environmental protection technology and equipment, comprehensively improve the operation quality of pollution control facilities, and assume the important responsibility of environmental protection. It is generally believed that the externality, indivisibility, and uncertainty of innovation activities would inevitably lead to market failure, thus hindering enterprises from achieving the socially optimal level of spontaneous R&D activities. In this regard, selective innovation incentives are widely used in the world (Luo et al. 2020). However, it is difficult for the government to effectively supervise the R&D activities of all applicants, so there is a possibility of adverse selection and moral hazard. This means that in addition to substantial innovation aimed at technology upgrading and competitive advantage, enterprises may also participate in strategic innovation. They aim to cover up the actual innovation ability, to cater to the government and achieve other interests. However, in the initial R&D stage, enterprises face financing constraints from the capital market, which is also an objective reality. To this end, the Chinese government has arranged a large number of environmental subsidies to encourage environmental technology innovation (Wang et al. 2020).

The existing literature has classified the enterprise environmental technology innovation from the innovation content, innovation intensity, or innovation mode, but less literature analyzed innovation behavior from the perspective of motivation (Li et al. 2016). In fact, in addition to the substantial innovation motivation for core technology breakthrough, enterprises also have the intention of the one-sided pursuit of innovation quantity to meet the industrial policy and seek other interests, which is a kind of "strategic" behavior. Therefore, it is of great academic value and policy significance to study the motivation of different innovation activities for understanding the interaction between the government and enterprises in the implementation process of China's industrial subsidy policy, evaluating the effectiveness of policy implementation, and exploring the mechanism of action.

Given this, this study attempts to distinguish environmental technology innovation behaviors with different motives and to investigate the impact of environmental subsidies on environmental technology innovation of micro-enterprises and internal mechanisms. The conclusions are expected to provide empirical basis for formulating scientific and effective environmental subsidy policies and give full play to the positive role of environmental technology innovation in environmental protection.

PAST STUDIES

Theoretically, environmental technology innovation can improve the environmental performance of enterprises, and has a positive contribution to the financial performance of enterprises (Xie et al. 2019). At the same time, environmental subsidies also lead to stronger government regulation and supervision pressure on enterprises, forcing enterprises to enhance the legitimacy of environmental behavior through environmental technology innovation (Li et al. 2017).

However, in enterprise practice, the difference between the "outsider" role of local government and the professional and technical background of enterprise environmental technology innovation makes it difficult for the government to implement effective external governance and intervention mechanism. The impact of environmental subsidies on environmental technology innovation has been independent of government supervision and intervention. Innovation behavior measured by the patent application is typical strategic behavior.

From the perspective of policy implementation, the government has the inertia of directly intervening in the economy and implements the "selective" industrial policy led by the government. For example, the catalog of encouraging industries or the guidance catalog of industrial structure adjustment and other similar documents issued by the government every year had regulatory characteristics of the government choosing to replace market mechanism and restricting competition (Jiang et al. 2010). However, the information asymmetry between policymakers and enterprises, as well as the limitations of professional knowledge and practice, also made it difficult for the government to correctly predict the future of technology. Therefore, for the consideration of being responsible for financial funds, the government had its precondition to issuing subsidies, that was, to select the subsidy object according to innovation signals released by enterprises in advance. At this time, it was easy to induce enterprises to make adverse selection behavior of "seeking support" (Hall et al. 2012, Mao et al. 2015).

From the perspective of the technology cycle and policy timeliness, although the strategic value brought by environmental technology innovation would eventually show higher environmental performance, social performance and behavioral legitimacy, its economic benefits could not be realized in the short term. The goal of local government to implement industrial policies was to achieve short-term results (Jiang et al. 2010). This showed that there were great differences between the short-term goal orientation of China's industrial policy and the long-term sustainable investment needed for substantive innovation. From the perspective of incentive compatibility, enterprises could not achieve effective unification of "private interest" and "public interest" in the short term through environmental technology innovation (Wang et al. 2020).

In addition, the selection system of government officials also provided an institutional basis for enterprises to implement strategic innovation. If local officials wanted to occupy an advantage in the promotion competition, they must make greater achievements in the short period, which conflicted with the long-term nature of substantive innovation. To achieve the short-term achievements, officials chose enterprises with more and faster achievements to provide strong financial support, while enterprises carried out low-level innovation to meet the political needs of officials.

This study divides the environmental technology innovation behavior of enterprises into two types from the perspective of motivation. The one is the behavior of applying for high-level invention patents identified as substantive innovation, which aims to promote technological progress and to obtain a competitive advantage. The other is the act of applying for other patents recognized as strategic innovation, which caters to the supervision by pursuing the quantity of innovation, to seek other interests. Then, this study selects characteristics of industrial policy to investigate the effect and mechanism of environmental subsidies on environmental technology innovation.

METHODOLOGY

Samples and Data

This study selects polluting listed enterprises of China's A-share market in Shanghai and Shenzhen from 2013 to 2019 as research samples. The environmental technology patent data are from the State Content of Patent Database of China (SCPD) and the State Intellectual Property Office of China (SIPO). The subsidy comes from the annual report of listed enterprises. The financial data of enterprises come from the CSMAR database.

To reduce the impact of outliers, enterprises under special treatment and samples with missing data of important variables are excluded. Final samples include 1100 enterprises and 6180 effective observations. The observation results

of the samples in the chemical industry, medicine, metal smelting, electricity, heat, gas and water production and supply, transportation, storage and postal services industries are relatively concentrated, accounting for 14.63%, 11.42%, 10.61%, 9.9%, and 8.48%, respectively. To eliminate the influence of extreme values, all continuous variables are winsorized at 1% and 99% levels. Stata15.0 software was used for all data processing.

Variable Definition

This study uses environmental technology patent applications to measure the environmental technology innovation behavior of enterprises. The data of "environmental technology innovation" has not been classified and disclosed in the patent database. Therefore, it obtains enterprise environmental technology patent information through keyword screening (Cormier et al. 2015, Yu 2021).

Environmental subsidy refers to the government's special subsidies, special funds, and achievement awards for environmental protection projects such as enterprise environmental governance, environmental protection technology R&D, energy conservation, and emission reduction. Its content generally includes keywords such as energy conservation and emission reduction, environmental protection, energy, environment technology, waste gas, carbon emissions, carbon trading, recycling, sustainable development, and so on. This study sorts out details of government subsidies in the notes to the annual report of enterprises through keyword selection and calculates the number of environmental subsidies received every year.

It chooses enterprise size, business age, debt ratio, asset structure, profitability, equity balance, and growth ability as control variables. The variable definition is shown in Table 1.

Modeling

To explore the impact of environmental subsidies on environmental technology innovation, this study constructs the following model by referring to the methods of existing literature (Guo 2018):

$$Y_{i,t}\left(LnGp_{i,t},\ lnGpti_{i,t},\ LnNgpti_{i,t}\right)=\alpha_0+\alpha_1 Esub_{i,t+1}+\alpha_2 Size_{i,t-1}+\alpha_3 Age_{i,t-1}+\alpha_4 Lev_{i,t-1}+\alpha_5 Opr_{i,t-1}+\alpha_6 Assets_{i,t-1}+\alpha_7 Shareb_{i,t-1}+\lambda_i+\tau_t+\varepsilon_{i,t} \quad \ldots(1)$$

In the above formula (1), Y represents the enterprise's environmental technology innovation behavior, which is measured by the number of applications for two types of patents. I represents the enterprise. T represents the time. α is the coefficient. ε represents the error term. Definitions of other variables are shown in Table 1. The control variables lag for one period to reduce the influence of endogenous. The reason why environmental subsidy is postponed is that there is a time lag of about one year between the government's appropriation to enterprises and the patent output. At the same time, to control the time-invariant impact and macro-economic impact at the enterprise level, λ_i and τ_t are added. They represent the fixed effect and year fixed effect at the enterprise level. The study establishes a two-factor fixed effect regression model.

According to the requirements of panel data regression analysis, model selection is required. Therefore, the Haussmann test is carried out for each model. If the Haussmann test value is significant, the fixed-effect model is selected. If the Haussmann test value is not significant, the random effect model is selected. For cases that cannot be distinguished, the random effect model should also be selected.

Table 1: Variable definition.

Variable name	Code	Calculation instructions
Total amount of environmental technology innovation	Gp	Ln (1+ environmental technology patent total number)
Environmental technology invention innovation	Gpti	Ln (1+number of environmental technology invention patents)
Other environmental technology innovations	Ngpti	Ln (1+ the number of other environmental technology patents)
Environmental subsidy	Esub	(Environmental subsidy/Total assets at the end of the period)×100%
Enterprise size	Size	Ln (total assets)
Business age	Age	Number of years since the establishment of the company
Debt ratio	Lev	(Total Liabilities/Total Assets)×100%
Asset structure	Assets	(Net fixed assets/Total assets)×100%
Profitability	Opr	(Operating profit/Operating income)×100%
Equity checks and balances	Shareb	The largest shareholder's shareholding ratio
Growth ability	Growth	Operating income growth rate

RESULTS AND DISCUSSION

Model Selection

Test statistics of the three models are significant at the 1% significance level, which shows that the fixed effect of each model is better than the random effect, which proves that the model setting is appropriate (see Table 2).

The estimated value of *Esub* coefficient in column (1) is significant at the level of 10%, indicating that the number of environmental technology patent applications increases under the incentive of environmental subsidies. The estimated value of *Esub* coefficient in column (3) is less than the significant level of 10%, and the estimated value of *Esub* coefficient in column (5) is significant at the level of 5%, which indicates that the impact of environmental subsidies results in a significant increase in the number of non-invention patent applications. However, the number of invention patent applications is not significantly affected. This shows that under the incentive of selective environmental subsidies, enterprises show more patent applications to obtain subsidy resources to demonstrate innovation ability. Since enterprises can arrange innovation activities in advance to meet the preference of the government, to improve their chances of success, the increase of environmental technology innovation output is only a strategic behavior, reflecting the adverse selection motivation of enterprises to cater to policies and to seek support.

Table 2: Model selection.

Variable	(1)	(2)	(3)	(4)	(5)	(6)
	Model 1 FE	Model 1 RE	Model 2 FE	Model 2 RE	Model 3 FE	Model 4 RE
	Gp	Gp	Gpti	Gpti	Ngpti	Ngpti
Esub	0.0482*	0.104***	0.0391	0.0773***	0.0539**	0.123***
	(0.0290)	(0.0280)	(0.0280)	(0.0269)	(0.0257)	(0.0246)
Size	0.123***	0.257***	0.158***	0.246***	0.0928***	0.259***
	(0.0361)	(0.0254)	(0.0348)	(0.0245)	(0.0320)	(0.0214)
Age	-0.348***	-0.0494***	-0.355***	-0.0417***	-0.223***	-0.0255***
	(0.0343)	(0.00748)	(0.0331)	(0.00722)	(0.0304)	(0.00594)
Lev	-0.224*	-0.266**	-0.185	-0.206*	-0.0903	-0.103
	(0.121)	(0.110)	(0.117)	(0.106)	(0.107)	(0.0958)
Assets	0.311*	-0.0748	0.204	-0.187	0.181	-0.103
	(0.161)	(0.144)	(0.155)	(0.138)	(0.142)	(0.124)
Opr	0.261	-0.00192	0.362*	0.187	-0.148	-0.274*
	(0.209)	(0.165)	(0.202)	(0.159)	(0.185)	(0.140)
Shareb	-0.00518**	-0.00130	-0.00197	0.00108	-0.00500**	-0.00206
	(0.00229)	(0.00174)	(0.00221)	(0.00168)	(0.00203)	(0.00147)
Growth	-0.0161	-0.0160	-0.0163	-0.0175	-0.00202	-0.00573
	(0.0421)	(0.0415)	(0.0407)	(0.0399)	(0.0373)	(0.0366)
_cons	5.993***	-2.765***	4.702***	-3.364***	3.866***	-3.703***
	(0.976)	(0.567)	(0.943)	(0.547)	(0.865)	(0.473)
N	6180	6180	6180	6180	6180	6180
R2	0.051		0.043		0.050	
F Value	20.40***		17.21***		19.87***	
Wald chi2		386.77***		333.09***		419.76***
Hausman Test						
Chi-square	158.82		181.53		102.24	
P-Value	0.0000		0.0000		0.0000	

Note: Standard errors are in parentheses. *, **, *** represent the significance level of 10%, 5%, and 1%, respectively.

Heterogeneity Analysis

Nature of ownership: The estimated value of *Esub* coefficient in columns (1) and (4) is significant; it means that the total environmental technology patent applications of both state-owned enterprises and private enterprises are not significantly affected by environmental subsidies (see Table 3). The estimated value of *Esub* coefficient in column (3) is significant at the level of 5%, which indicates that the number of non-patent applications of state-owned enterprises has increased significantly under the incentive of environmental subsidies. The estimated value of *Esub* coefficient in column (2) is less than 10%, indicating that the number of invention patent applications of state-owned enterprises has not been significantly affected. In contrast, the number of invention patent applications of private enterprises has increased significantly, and the estimated value of *Esub* coefficient in column (5) is significant at the level of 5%. The estimated coefficient in column (6) is less than 10%, indicating that the number of non-invention patent applications of private enterprises is not significantly affected.

The phenomenon means that compared with private enterprises, state-owned enterprises have less willingness to survive in the market by high-tech environmental technology invention patents. Selective industrial policy guides the increase of "quantity" rather than "quality" of environmental technology innovation of state-owned enterprises. Private enterprises are facing fierce market competition and they need high-quality technology innovation to win. Therefore, private enterprises need substantial environmental technology innovation, pay attention to the improvement of innovation quality. They will not blindly innovate to meet the policy and to strive for the subsidy resources that may or may not be available, resulting in the strategic behavior of only pursuing innovation "quantity".

Technical background of senior executives: When the government chooses innovation subsidy objects, it will rely

Table 3: Results Grouped by Ownership Nature.

Variable	State-owned enterprise			*Private enterprise*		
	(1)	(2)	(3)	(4)	(5)	(6)
	Gp	Gpti	Ngpti	*Gp*	*Gpti*	*Ngpti*
Esub	0.0679	0.0146	0.0943**	0.0346	0.0735**	0.00445
	(0.0453)	(0.0421)	(0.0430)	(0.0381)	(0.0330)	(0.0371)
Size	0.287***	0.216***	0.302***	0.109**	0.0635	0.162***
	(0.0631)	(0.0586)	(0.0599)	(0.0509)	(0.0440)	(0.0495)
Age	-0.327***	-0.229***	-0.350***	-0.359***	-0.222***	-0.359***
	(0.0582)	(0.0541)	(0.0553)	(0.0430)	(0.0373)	(0.0419)
Lev	-0.0324	-0.0466	-0.0458	-0.316*	-0.120	-0.273*
	(0.201)	(0.187)	(0.191)	(0.162)	(0.141)	(0.158)
Assets	0.766***	0.691***	0.594**	0.211	0.00654	0.137
	(0.266)	(0.247)	(0.253)	(0.214)	(0.185)	(0.208)
Opr	-0.433	-0.656*	-0.145	0.451*	-0.0261	0.481*
	(0.371)	(0.344)	(0.352)	(0.264)	(0.229)	(0.257)
Shareb	-0.000778	-0.00135	0.00121	-0.00667**	-0.00710***	-0.00230
	(0.00401)	(0.00373)	(0.00381)	(0.00294)	(0.00255)	(0.00286)
Growth	-0.107	-0.00711	-0.138*	0.0213	0.00692	0.0301
	(0.0744)	(0.0691)	(0.0706)	(0.0528)	(0.0457)	(0.0513)
_cons	2.817	2.014	2.182	6.048***	4.174***	4.274***
	(1.860)	(1.728)	(1.766)	(1.240)	(1.074)	(1.207)
N	2164	2164	2164	4016	4016	4016
R^2	0.079	0.075	0.072	0.045	0.041	0.038
F value	11.55***	10.89***	10.42***	11.38***	10.31***	9.43***

Note: Standard errors are in parentheses. *, **, *** represent the significance level of 10%, 5%, and 1%, respectively.

on some dominant signals to make decisions, to avoid the interference of information asymmetry. The technical R&D background of the enterprise's top management team is the government's key consideration (Peng et al. 2017).

The estimated value of *Esub* coefficients in column (4), column (5), and column (6) of Table 4 do not reach the significance level of 10%, indicating that the total number of environmental technology patents, invention patents and other patent applications of enterprises with no technical background of senior executives are not significantly affected by environmental subsidies. In contrast, the total number of environmental technology patent applications and the number of non-invention patent applications of enterprises with technical backgrounds have increased significantly. For example, the estimated value of *Esub* coefficient in column (1) is significant at the level of 10%, and the estimated value of *Esub* coefficient in column (3) is significant at the level of 5%. However, the estimated coefficient in column (2) does not reach the significance level of 10%, indicating that the number of environmental technology invention patent applications of enterprises with technical backgrounds is not significantly affected by environmental subsidies.

This phenomenon shows that executives with technical R&D backgrounds are more likely to consciously invest more capital in R&D and technology innovation when allocating resources. Under the incentive of selective environmental subsidy, the top management team with professional background and experience chooses the non-invention patent declaration with lower difficulty, shorter R&D cycle, and lower risk. The aim is to make the formulation and implementation of future environmental subsidy schemes more reliable, rather than blindly carrying out the high-quality innovation with high difficulty, long cycle, and high risk.

Managerial Implications

Polluting enterprises should increase investment in environmental technology innovation. In the practical application

Table 4: Results grouped by executive background.

Variable	Executives with technical background			Executives without technical background		
	(1)	(2)	(3)	(4)	(5)	(6)
	Gp	*Gpti*	*Ngpti*	*Gp*	*Gpti*	*Ngpti*
Esub	0.0506*	0.0394	0.0578**	0.00614	0.0705	0.0115
	(0.0304)	(0.0293)	(0.0273)	(0.111)	(0.107)	(0.0901)
Size	0.126***	0.156***	0.0968***	0.0430	0.0380	0.0512
	(0.0383)	(0.0369)	(0.0344)	(0.135)	(0.130)	(0.110)
Age	-0.362***	-0.371***	-0.233***	-0.243	-0.159	-0.191
	(0.0355)	(0.0342)	(0.0318)	(0.149)	(0.144)	(0.121)
Lev	-0.0526	-0.0467	0.0165	-0.597	-0.581	-0.128
	(0.132)	(0.127)	(0.118)	(0.404)	(0.389)	(0.329)
Assets	0.221	0.0880	0.198	-0.00442	0.581	-0.780
	(0.170)	(0.164)	(0.153)	(0.599)	(0.576)	(0.487)
Opr	0.193	0.362*	-0.256	1.018	0.281	0.930
	(0.220)	(0.212)	(0.197)	(0.799)	(0.769)	(0.651)
Shareb	-0.00588**	-0.00127	-0.00649***	-0.000793	-0.00792	0.00484
	(0.00249)	(0.00239)	(0.00223)	(0.00765)	(0.00737)	(0.00623)
Growth	-0.0173	-0.0150	-0.00246	-0.0656	-0.0229	-0.0110
	(0.0445)	(0.0428)	(0.0398)	(0.153)	(0.148)	(0.125)
_cons	6.223***	4.978***	4.058***	5.072	3.775	3.087
	(1.024)	(0.985)	(0.917)	(4.041)	(3.890)	(3.289)
N	5661	5661	5661	519	519	519
R^2	0.052	0.046	0.050	0.050	0.043	0.062
F value	18.91***	16.66***	18.11***	1.37	1.18	1.73*

Note: Standard errors are in parentheses. *, **, *** represent the significance level of 10%, 5%, and 1%, respectively.

of environmental protection, the continuous breakthrough of technologies including desulfurization and denitration, bag dust removal, and catalytic conversion can play a sustainable role in improving the environment. Therefore, polluting enterprises should pay attention to the continuous promotion of environmental technological innovation, improve the utilization efficiency of resources from the source and process, use efficient environmental protection equipment to save energy, and reduce environmental pollution, which will bring significant improvement in environmental performance.

In the process of implementing the environmental subsidies policy, the government should strictly control the pollution sources, and the relevant regulatory authorities should strengthen the implementation of energy conservation and emission reduction, formulate a more targeted regulatory system to control pollution emissions, and improve the regulatory efficiency in the innovation process. At the same time, the government should actively carry out public supervision of environmental pollution, encourage the public to participate in the complaints and suggestions of environmental pollution, open a network interactive platform and create a good atmosphere for environmental protection supervision.

The effectiveness of the environmental subsidy policy cannot be measured by only one performance index. We should build a more scientific performance evaluation system for enterprises of different nature and industries to comprehensively evaluate the effectiveness of the policy. Environmental subsidies should have a strict evaluation system, which involves not only the evaluation of economic performance but also the evaluation of social and environmental benefits. Design a reasonable and comprehensive analysis and evaluation system for different types of enterprises, and then build a reasonable and effective policy support model to maximize the use efficiency of government funds.

CONCLUSIONS

Environmental technology innovation is an important factor for polluting enterprises to achieve sustainable development and has an important impact on improving the quality of environmental protection. Based on the data of China's listed polluting enterprises from 2013 to 2019, the impact of environmental subsidies on environmental technology innovation of enterprises from the perspective of selective industrial policy was discussed and the heterogeneous impact of the nature of enterprise ownership and the technical background of executives was analyzed. Following conclusions are drawn.

(1) Environmental subsidies promote the overall growth of environmental technology patent applications of polluting enterprises. Among them, the number of invention patents representing the high-tech level is not significantly affected, while the number of non-invention patents increases significantly. It shows the phenomenon of pursuing quantity while ignoring the quality of environmental technology innovation.

(2) From the perspective of enterprise property rights, environmental subsidies significantly increase the number of non-invention patent applications of state-owned enterprises. They also significantly increase the number of invention patent applications of private enterprises but have no significant impact on other aspects.

(3) From the perspective of whether the senior executives with technical background, the total number of patent applications and the number of non-invention patent applications of enterprises with senior executives of technical background increase significantly. However, the number of invention patents and enterprises without senior executives of technical background is not significantly affected by environmental subsidies.

(4) From the perspective of selective industrial policy, there is a phenomenon that enterprises use environmental technology innovation strategy to cater to the government and to seek support. In terms of motivation, it is an innovation strategy rather than a substantial innovation.

ACKNOWLEDGMENT

This study was supported by the Henan Soft Science Project (182400410659), and the Doctoral Fund Project of Henan University of Engineering (D2017027).

REFERENCES

Cormier, D. and Magnan, M. 2015. The economic relevance of environmental disclosure and its impact on corporate legitimacy: An empirical investigation. Business Strategy & the Environment, 24(6): 431-450.

Guo, Y. 2018. Signal transmission mechanism of government innovation subsidy and enterprise innovation. China Industrial Economics, (9): 98-116.

Hall, B. H. and Harhoff, D. 2012. Recent research on the economics of patents. Annual Review of Economics, 4(1): 541-565.

Jiang, F.T. and Li, X.P. 2010. Direct market intervention and restrict competition: the orientation of China's industrial policy and its fundamental defects. China Industrial Economics, (9): 26-36.

Li, D., Zheng, M., Cao, C., Chen, X., Ren, S. and Huang, M. 2017. The impact of legitimacy pressure and corporate profitability on green innovation: evidence from China's top 100. Journal of Cleaner Production, (141): 41-49.

Li, W.J. and Zheng, M.N. 2016. Is it substantive innovation or strategic innovation: impact of macroeconomic policies on micro-enterprises' innovation. Economic Research Journal, (4): 60-73.

Luo, S. and Sun, Y. 2020. Do selective R & D incentives from the government promote substantive innovation? Evidence from Shanghai technological enterprises. Asian Journal of Technology Innovation, 28(3): 323-342.

Mao, Q.L. and Xu, J.Y. 2015. The effect of government subsidy on firms' new product innovation: an analysis based on the moderate interval of subsidy intensity. China Industrial Economics, (6): 94-107.

Peng, H.X. and Mao, X.S. 2017. Government subsidies for innovation, company executives background and R&D investment: evidence from the high-tech industry. Finance & Trade Economics, (3): 147-161.

Wang, X. and Wang, L. 2020. The major shareholders unavoidable: a new explanation for the failure of government subsidies on green innovation. R&D Management, (2): 24-36.

Xie, X., Huo, J. and Zou, H. 2019. Green process innovation, green product innovation, and corporate financial performance: a content analysis method. Journal of Business Research, 101(8): 697-706.

Yu, Z.M. 2021. Environmental protection interview, government environmental protection subsidies and enterprise green innovation. Foreign Economics & Management, (7): 22-37.

Nature Environment and Pollution Technology
An International Quarterly Scientific Journal

p-ISSN: 0972-6268
(Print copies up to 2016)
e-ISSN: 2395-3454

Vol. 20 | No.3 | pp. 1285-1293 | 2021

Original Research Paper

https://doi.org/10.46488/NEPT.2021.v20i03.040

Open Access Journal

Chemical and Pathogen Impacts on Human Health near Aquaculture Areas in West Godavari District of Andhra Pradesh, India

D. Nageswara Rao*, T. Bhaskara Rao*† and P.V.S. Machiraju**
*Department of Chemistry, Koneru Lakshmaiah Education Foundation, Guntur-522502, A.P., India
**Department of Chemistry, Pragati Engineering College (A), Surampalem-533437, A.P., India
†Corresponding author: T. Bhaskara Rao: tbhaskararao208@gmail.com

Nat. Env. & Poll. Tech.
Website: www.neptjournal.com

Received: 05-10-2020
Revised: 25-11-2020
Accepted: 08-12-2020

Key Words:
Groundwater
Aquaculture
Microbial characterization
Water quality
Toxicity

ABSTRACT

Water is essential for all living organisms in the universe. Chemicals can cause contamination in groundwater near aquacultural activity areas. Keeping in view the hectic aquacultural activity in surrounding locations of Akividu town in West Godavari District of AP, India, it is proposed to assess the chemical and microbial contamination of waters to suggest remedial measures to protect the quality of water for safeguarding the health of the public residing in the nearby habitations who consume these waters for drinking purposes. 16 Groundwater samples were collected and analyzed for assessing the physicochemical parameters viz., pH, Electrical conductivity (EC), Total Dissolved solids (TDS), Total hardness (TH), Total Alkalinity (TA), Na^+, K^+, Calcium, Magnesium, Chloride, Sulphate, Nitrate and Phosphate, Irrigation parameters like %Na, SAR, KR RSC, and microbial analysis. The study results revealed that the samples were contaminated chemically and also with pathogenic bacteria like *Pseudomonas, Citrobacter freundii* and *Escherichia coli* which can cause water-borne diseases. Further, a health survey was carried out to verify the adverse effects to be caused by the chemical and microbial contamination of water on people's health. The health survey results indicated the sufferings of the people who consume this water for drinking and domestic purposes. The waters are to be treated accordingly to control the chemical and bacterial contamination by using the available treatment methodologies before considering them for drinking purposes.

INTRODUCTION

Groundwater recharge is being done by various water bodies. Physico-chemical characteristics of an aquatic body not only reflect the type and diversity of aquatic biota but also the water quality and its contamination (Mir et al. 2004). Research studies (Raveen et al. 2008) revealed the necessity for the restoration of degrading freshwater bodies to ensure the sustainability of a healthy ecosystem. The environmental impact of aquaculture in the country came to the limelight for the first time with the reports of NEERI (1995). Intensive aquaculture requires huge quantities of freshwater from groundwater sources (Ramesh et al. 2008). Using significant volumes of groundwater to create the required salinity levels of brackish water for aquaculture activity can cause salinization of groundwater aquifers (Dahdouh-Guebas et al. 2006). The research studies (Alagarswamy 1995) revealed that shrimp farming and other farming systems can lead to pollution and result in adverse impacts on the environment. Higher quantities of nitrogen and phosphorus in feeds during aquaculture can also cause an increase in nutrient concentration in waters. The excess nutrient concentrations may deteriorate the water in the aquatic environment (Falconer et al. 2018). The research studies indicated that the values of SAR and RSC indicate 97% of the waters and their suitability for domestic, irrigation, and industrial purposes (Nagaraju & Papanna 2009).

The bacteria and pathogenic organisms present in drinking water can cause health hazards like dysentery, cholera, fevers, hepatitis, intestinal disorders, etc. Presence of *coli form* in water is an indicator of harmful bacteria but all the bacteria are not harmful (Massoud et al. 2010, Joao 2010). Microbial pathogenic bacteria in water can cause diarrhoeal diseases nearly up to 82% of diseases (WHO 2010). Several microbial communities that survive in waters start multiplying and depreciate the water quality (Ikonen et al. 2017). Pathogen contamination of waters is a significant health risk and also a threat to the water supplies essential for living and other recreational activities. Low levels of contact with contaminated water are significant and can cause an outbreak of gastroenteritis (Madoux-Humey et al. 2016, Boehm & Sassoubre 2014). Though *coli forms* do not cause serious illness, they act as an indicator for the presence of more (Ibrahim et al. 2014). Approximately 3.4 million people particularly children die from water-borne diseases (WHO

2014). Various studies (Arnone & Walling 2007) revealed that gastrointestinal problems can be caused by different microbes and germs present in water bodies which indicate the symptoms like diarrhea, nausea, vomiting, fever, and abdominal pains (Arnone & Walling 2007).

Keeping in view of hectic aquaculture activity and the release of backwaters due to its activity and the seepage of these waters into groundwater sources, it is proposed to carry out the characterization of groundwater near aquaculture activity areas to evaluate the chemical and pathogenic impacts through groundwater sources on the public health through their utility for drinking and domestic purposes and to suggest remedial measures to protect the health of the public.

MATERIALS AND METHODS

The sampling locations are identified near aquacultural activity areas around Akividu of West Godavari District of Andhra Pradesh, India. The samples were collected in polythene containers and preserved for analysis as per the standard procedures (Ramteke & Moghe 1988, APHA 1992). The details of sample code, sampling locations along with their coordinates are presented in Table 1 and the study area map is presented in Fig. 1.

Table 1: Sample code, location and coordinates.

Sample Code	Sample Location	GPS Co-ordinates	
		Latitude	Longitude
AE-1	Cherukuvada main road, near Hossanna mandir	16.58411	81.39045
AE-2	Cherukuvada main road, near Anjanayaswami temple	16.58390	81.39041
AE-3	Akivedu, near Vinayaka Industry	16.58473	81.40942
AE-4	Cherukuvad (undi road), near Church	16.58644	81.41901
AW-1	Manchineeti Cheruvugattu	16.57885	81.38296
AW-2	Kaikaluru road, near SV Godowns	16.57785	81.35683
AW-3	Near SV Godowns	16.57880	81.35907
AW-4	Near SV Godowns	16.57856	81.35921
AN-1	Near Alapadu main road	16.57494	81.32997
AN-2	Kolletikota, near Alapadu turning	16.58087	81.32201
AN-3	Kalletikota road, near Alapadu Panchayathi Cheruvu	16.58207	81.32103
AN-4	Kolletikota road, near Hanuman Temple	16.59303	81.31828
AS-1	Main road, near Telephone Exchange	16.58241	81.38025
AS-2	Near Telephone Exchange	16.58257	81.38027
AS-3	Argumuru Garuvu	16.58253	81.39849
AS-4	Main road, near Anjanaya temple	16.58435	81.40992

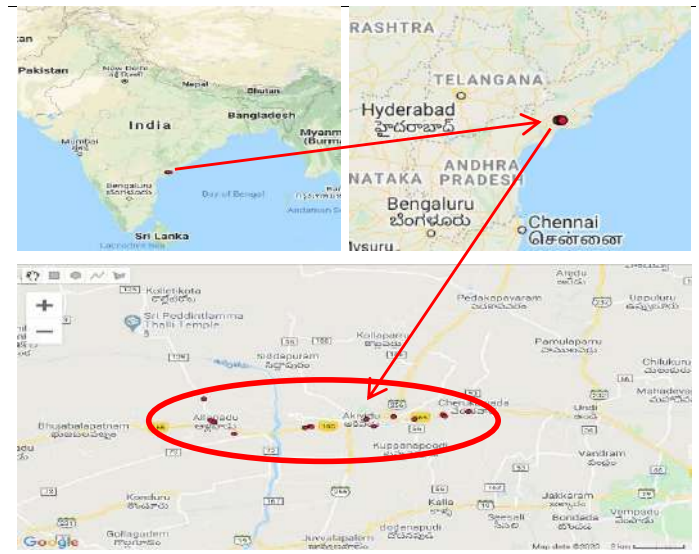

Fig. 1: Study area map (Google map).

Physicochemical Parameters

The waters were characterized for physicochemical parameters viz., pH, Electrical conductivity (EC), Total Dissolved solids (TDS), Total hardness (TH), Total Alkalinity (TA), Na+, K+, Calcium and Magnesium, Chloride, Sulphate, Nitrate, and Phosphate. pH is determined by pH Meter (Model-PCS Tester35, Eutech) and conductivity measured by portable EC sensor (Electrode based). TDS is determined by TDS Sensor (Electrode based). Total Hardness, Total Alkalinity, and Chloride are estimated by titrimetry. Sulfate and Phosphate are estimated by spectrophotometer (Model-106, Systronics), Na^+ and K^+ by Flame photometer (Model-128, Systronics), and Nitrate by using Ion-selective electrode (Model-HI 3222 pH/ORP/ISE Meter, HANNA). The irrigation parametric levels, Percent Sodium (%Na), Sodium Adsorption Ratio (SAR), Residual Sodium Carbonate (RSC), Kelly's Ratio (KR), Magnesium Hazard (MH) are determined by using equations.

$$\text{Percent Sodium (\%Na)} = \frac{Na^+ X100}{Ca^{2+} + Mg^{2+} + Na^+ + K^+} \text{ (meq/l)}$$

$$\text{Sodium Adsorption Ratio (SAR)} = \frac{Na^+}{\sqrt{\frac{Ca^{2+} + Mg^{2+}}{2}}} \text{(meq/I)}$$

Residual Sodium Carbonate (RSC) = $(CO_3^{2-} + HCO_3^-) - (Ca^{2+} + Mg^{2+})$ (meq/L)

$$\text{Kelly Ratio (KR)} = \frac{Na^+}{Ca^{2+} + Mg^{2+}}$$

$$\text{Magnesium Hazard (MH)} = \frac{Mg^{2+}}{Ca^{2+} + Mg^{2+}} X100$$

Microbial Characterization

MPN Count: MPN count in water samples was done by the standard MPN index method.

Identification of Bacteria: The identification of bacterial species was carried out by the cultural characteristics using staining reactions to identify the shape and the color of the microorganisms and biochemical characterization which include IMViC (Indole production test, Methyl red test, Voges Proskauer test, Citrate utilization) tests (Obiri-Danso & Jones 1999a, 1999b, Sohan & Iqbal 2012).

RESULTS AND DISCUSSION

The values of physicochemical characteristics of the groundwater near aquacultural areas are presented in Tables 2, 3 and 4 and values for irrigational param-

Table 2: Physicochemical characteristics of groundwater near aquacultural areas.

Sample Code	Temp (°C)		pH		EC (µmhos/cm)		TDS (mg/L)		Salinity (mg/L)		TH (mg/L)		TA (mg/L)	
	Monsoon		Monsoon		Monsoon		Monsoon		Monsoon		Monsoon		Monsoon	
	Pre	Post	Pre	Post	Pre	Post	Pre	Post	Pre	Post	Pre	Post	Pre	Post
AE-1	29.0	30.4	8.43	8.15	3920	1575	2770	1120	2150	826	350	500	70	1300
AE-2	28.9	30.5	8.10	6.93	8630	1230	6080	870	4960	640	1700	2150	130	1700
AE-3	29.0	30.4	7.60	7.57	3730	1270	2640	917	2040	977	780	1150	80	1070
AE-4	28.9	30.4	8.45	7.84	2630	1510	1850	1070	1400	795	430	450	100	1660
AW-1	29.1	30.5	8.08	8.14	3100	927	2190	663	1680	481	630	300	100	1420
AW-2	29.0	30.3	8.75	7.94	5720	670	4040	476	3210	3850	580	2800	90	1850
AW-3	29.0	30.5	8.83	8.18	3100	4320	2190	3080	1680	2410	240	700	80	2030
AW-4	29.1	30.5	7.84	8.11	15000	1745	10590	1250	9030	932	2300	700	100	1570
AN-1	29.1	30.3	7.77	8.19	14710	4320	10385	3080	8770	2420	2800	900	70	1700
AN-2	29.1	30.4	8.33	8.92	10100	5250	7140	3740	5910	2970	1060	600	100	1830
AN-3	29.1	30.4	8.03	8.67	7370	3680	5190	2630	4200	2020	820	1000	90	890
AN-4	29.1	30.4	7.73	8.12	6900	3680	4860	2660	3900	2080	860	1700	50	1650
AS-1	29.0	30.5	7.68	8.15	1659	1320	1180	937	873	690	240	300	50	1130
AS-2	29.1	30.5	8.21	7.25	2060	736	1460	524	1110	379	370	100	60	280
AS-3	29.0	30.4	8.14	7.20	2370	1400	1670	1010	1260	742	470	900	60	1250
AS-4	29.1	30.4	8.11	7.49	3070	1600	2170	1140	1660	852	1110	700	50	350
BIS value	-		6.5-8.5		-		500		-		200		200	

Table 3: Physicochemical characteristics of groundwater near aquacultural areas.

Sample Code	Cl^- (mg/L)		SO_4^{2-} (mg/L)		PO_4^{3-} (mg/L)		NO_3^- (mg/L)	
	Monsoon		Monsoon		Monsoon		Monsoon	
	Pre	Post	Pre	Post	Pre	Post	Pre	Post
AE-1	1155.67	744.45	73.57	133.57	0.61	1.13	29.5	17.4
AE-2	2431.87	2906.9	334.57	270.71	2.33	1.78	36.4	30.5
AE-3	765.72	744.45	244.29	1742.80	0.11	0.62	109.0	13.4
AE-4	446.67	744.45	178.00	128.71	0.13	0.53	54.2	43.7
AW-1	517.57	567.2	225.29	56.85	3.19	1.07	19.3	18.4
AW-2	1474.72	15030.8	307.14	3.54	0.00	1.29	95.3	69.7
AW-3	588.47	1807.95	235.71	308.71	0.64	4.73	112.0	70.1
AW-4	5835.07	921.7	348.43	170.00	3.86	0.7	153.0	19.2
AN-1	6083.22	2197.9	334.57	114.14	3.29	0.43	66.9	36.3
AN-2	3708.07	2552.4	184.86	307.57	0.14	1.93	60.3	337
AN-3	2502.77	2197.9	135.14	234.85	1.01	3.89	47.6	37.9
AN-4	2396.42	2906.9	257.00	230.85	1.63	1.4	50.2	71.7
AS-1	233.97	212.7	118.57	101.42	0.50	1.2	194.0	48.4
AS-2	304.87	567.2	170.57	60.00	0.47	3.87	191.0	9.65
AS-3	588.47	921.7	128.71	219.71	2.08	1.01	18.9	19.9
AS-4	907.52	1276.2	74.14	145.00	3.39	0.14	29.3	17.5
BIS value	250		200		-		45	

Table 4: Physicochemical characteristics of groundwater near aquacultural areas.

Sample Code	Ca^{2+} (mg/L)		Mg^{2+} (mg/L))		Na^+ (mg/L)		K^+ (mg/L)	
	Monsoon		Monsoon		Monsoon		Monsoon	
	Pre	Post	Pre	Post	Pre	Post	Pre	Post
AE-1	120	80	12.2	73.2	1936.2	293.8	59.4	10.6
AE-2	500	160	109.8	427	828.0	607.6	23.6	6.4
AE-3	200	120	68.32	207.4	1722.8	400.0	605.0	13.5
AE-4	120	80	31.72	61	497.6	228.0	186.4	93.7
AW-1	220	80	19.52	24.4	678.2	89.3	332.7	24.2
AW-2	180	160	31.72	585.6	2296.8	1962.2	18.4	29.2
AW-3	40	120	34.16	97.6	1137.3	872.7	16.5	25.5
AW-4	760	120	97.6	97.6	3738.0	384.6	114.8	8.5
AN-1	780	160	207.4	122	3576.8	925.1	109.6	14.5
AN-2	400	80	14.64	97.6	2378.2	916.5	70.8	293.9
AN-3	240	120	53.68	170.8	1669.0	807.8	25.4	66.1
AN-4	260	80	51.24	366	1662.4	901.1	111.2	26.3
AS-1	80	80	9.76	24.4	238.8	122.6	255.2	151
AS-2	120	40	17.08	BDL	276.0	77.9	401.8	17.1
AS-3	100	120	53.68	146.4	564.6	235.5	17.6	9.8
AS-4	220	80	136.64	122	540.2	326.9	26.0	8.5
BIS Value	75		30		-		-	

Table 5: Irrigation parametric values of groundwater near aquacultural areas.

Sample Code	% Na (me/L)		SAR (me/L)		RSC (me/L)		Kelly's Ratio		MH	
	Monsoon		Monsoon		Monsoon		Monsoon		Monsoon	
	Pre	Post	Pre	Post	Pre	Post	Pre	Post	Pre	Post
AE-1	90.8	55.8	45.1	5.8	BDL	16.1	12.1	1.3	14.0	59.4
AE-2	51.1	38.4	8.8	5.8	BDL	BDL	1.1	0.6	26.0	81.0
AE-3	70.8	43.1	26.9	5.2	BDL	BDL	4.8	0.8	35.3	73.4
AE-4	61.9	46.8	10.5	4.7	BDL	24.3	2.5	1.1	29.7	55.0
AW-1	58.3	37.1	11.8	2.3	BDL	22.4	2.3	0.7	12.4	32.8
AW-2	89.3	60.5	41.6	16.3	BDL	BDL	8.7	1.6	22.0	85.4
AW-3	90.6	72.4	32.1	14.4	BDL	26.8	10.4	2.7	57.7	56.5
AW-4	76.9	54.4	34.0	6.4	BDL	17.6	3.5	1.2	17.0	56.5
AN-1	72.7	68.9	29.5	13.5	BDL	16.2	2.8	2.3	29.8	55.0
AN-2	81.8	67.3	31.8	16.4	BDL	24.2	4.9	3.4	5.5	66.1
AN-3	81.1	62.2	25.4	11.2	BDL	BDL	4.5	1.8	26.4	69.5
AN-4	78.4	53.6	24.7	9.6	BDL	BDL	4.2	1.2	24.0	88.0
AS-1	47.9	35.2	6.7	3.1	BDL	16.6	2.2	0.9	16.3	32.8
AS-2	40.5	58.2	6.3	3.4	BDL	3.6	1.6	1.7	18.5	0.0
AS-3	71.6	36.3	11.4	3.4	BDL	7.3	2.6	0.6	46.2	66.1
AS-4	51.0	50.4	7.1	5.4	BDL	BDL	1.1	1.0	49.8	70.9
Standard Value	60		26		1.0		1.0		50	

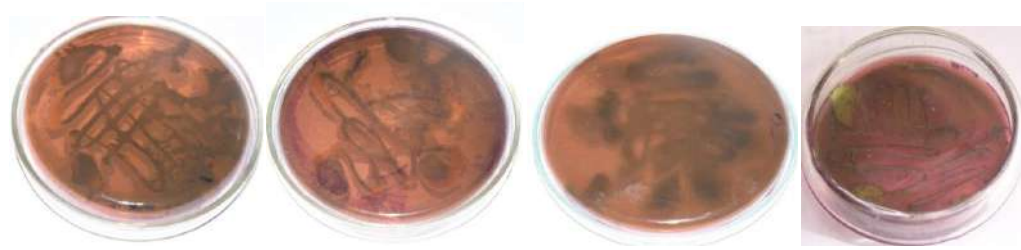

AE-1: *Pseudomonas* AE-2: *Citrobacter* AW-1: *Citrobacter* AW-2: *E.*coli

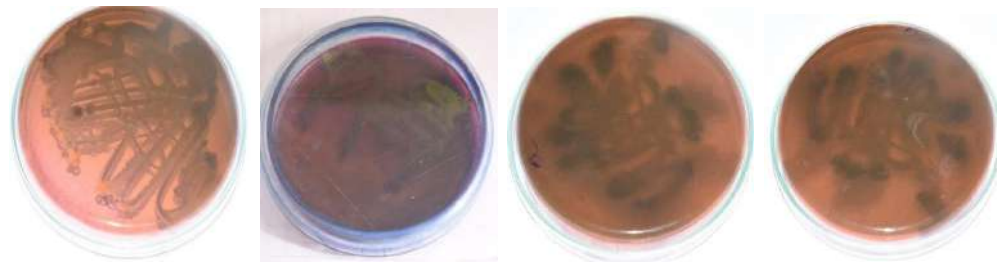

AN-1: *Pseudomonas* AN-2: *E. coli* AS-1: *Citrobacter* AS-2: *Citrobacter*

Fig. 2: Photographs of the identified microbial species.

Table 6: Correlation analysis.

Pre Monsoon															
	Temp	pH	EC	TDS	Salinity	TH	TA	Cl^-	SO_4^{2-}	NO_3^-	PO_4^{3-}	Na^+	K^+	Ca^{2+}	Mg^{2+}
Temp	1														
pH	-0.314	1													
EC	0.341	-0.273	1												
TDS	0.341	-0.273	1	1											
Salinity	0.344	-0.277	1	1	1										
TH	0.285	-0.421	0.905	0.905	0.908	1									
TA	-0.361	0.256	0.373	0.373	0.367	0.282	1								
Cl^-	0.402	-0.306	0.991	0.992	0.993	0.906	0.269	1							
SO_4^{2-}	-0.04	-0.115	0.665	0.665	0.663	0.639	0.517	0.597	1						
NO_3^-	0.083	-0.158	-0.022	-0.021	-0.009	-0.075	-0.218	-0.012	0.148	1					
PO_4^{3-}	0.391	-0.386	0.468	0.468	0.474	0.684	0.037	0.49	0.286	-0.271	1				
Na^+	0.362	-0.138	0.875	0.876	0.875	0.712	0.214	0.88	0.573	0.026	0.255	1			
K^+	0.05	-0.459	-0.293	-0.292	-0.286	-0.179	-0.104	-0.295	0.023	0.433	-0.216	-0.197	1		
Ca^{2+}	0.307	-0.401	0.952	0.952	0.954	0.978	0.368	0.944	0.675	-0.02	0.63	0.763	-0.159	1	
Mg^{2+}	0.171	-0.385	0.603	0.602	0.603	0.850	0.004	0.623	0.417	-0.199	0.682	0.437	-0.193	0.723	1
Post Monsoon															
	Temp	pH	EC	TDS	Salinity	TH	TA	Cl^-	SO_4^{2-}	NO_3^-	PO_4^{3-}	Na^+	K^+	Ca^{2+}	Mg^{2+}
Temp	1														
pH	-0.2	1													
EC	-0.23	0.675	1												
TDS	-0.231	0.674	1	1											
Salinity	-0.612	0.548	0.582	0.582	1										
TH	-0.431	-0.201	-0.07	-0.067	0.536	1									
TA	-0.16	0.349	0.405	0.404	0.544	0.4	1								
Cl^-	-0.536	0.057	-0.094	-0.094	0.737	0.803	0.357	1							
SO_4^{2-}	-0.05	-0.138	-0.015	-0.012	-0.086	0.085	-0.075	-0.18	1						
NO_3^-	-0.156	0.577	0.632	0.63	0.563	0.01	0.402	0.165	-0.034	1					
PO_4^{3-}	0.372	0.166	0.326	0.325	0.201	-0.094	-0.04	-0.003	-0.108	0.13	1				
Na^+	-0.606	0.314	0.36	0.36	0.939	0.775	0.53	0.883	-0.081	0.365	0.141	1			
K^+	-0.014	0.593	0.457	0.454	0.308	-0.237	0.208	-0.033	-0.061	0.874	0.073	0.084	1		
Ca^{2+}	-0.386	-0.097	0.106	0.105	0.443	0.701	0.513	0.506	0.14	-0.11	-0.11	0.603	-0.291	1	
Mg^{2+}	-0.418	-0.206	-0.09	-0.087	0.524	0.995	0.367	0.807	0.074	0.026	-0.088	0.763	-0.22	0.629	1

eters in Table 5. The details of MPN count and the identified bacterial species are presented in Table 7. The Photographs of the identified microbial species in waters are presented in Fig. 2.

The MPN count observed in waters is presented in Fig. 3. A health survey was carried out in the study area and the age details of the public and diseases experienced by them are summarized in Table 8.

The percentage of diseases experienced by the people in the study area is represented in Fig. 4.

Physicochemical characteristics: The analytical results of physicochemical parameters are presented in Tables 2, 3 and 4 along with the BIS standard values which reveal that the temperature during the collection of samples ranges from 28.9°C to 29.1°C and the pH of waters during pre-monsoon and post-monsoon seasons range from 7.60-8.83 and 6.93-8.92 respectively. The values indicate the slight alkaline nature of waters. Microorganisms depend on water for their growth depending on the water activity gradient. All microorganisms prefer pH 7 (neutral) for their optimum growth but they can grow more in acidic pH values. They

Table 7: Details of MPN count and identified *bacterial species* in waters.

Sample Code	MPN Index	No. of bacterial colonies on EMB	Bacterial colony Morphology on EMB	Gram's Nature	* (IMViC tests)				Bacteria Species
					I	MR	VP	C	
AE-1	02	02	Colourless	-ve	-	-	-	-	*Pseudomonas*
AE-2	31	02	Colourless	-ve	+	+	--	+	*Citrobacter freundii*
AW-1	22	01	Colourless	-ve	+	+	-	+	*Citrobacter freundii*
AW-2	02	01	Green Metallic Sheen	-ve	+	+	-	-	*E. coli*
AN-1	02	01	Colourless	-ve	-	-	-	-	*Pseudomonas*
AN-2	02	02	Green Metallicsheen	-ve	+	+	-	-	*E. coli*
AS-1	01	01	Colourless	-ve	+	+	-	+	*Citrobacter freundii*
AS-2	01	01	Colourless	-ve	+	+	-	+	*Citrobacter freundii*

*I = Indole, MR=Methyl red, VP=VogesProskauer, C=Citarte

Table 8: Details of people's age and disease experienced.

Age in Yrs	Diseases Experienced					Total
	Fever	Gastro Intestinal troubles	Joint pains	Typhoid	Skin Allergy	
1-10	12	0	1	0	5	18
11-20	0	0	0	0	1	1
21-30	2	3	3	0	1	9
31-40	3	5	1	1	5	15
41-50	2	6	1	0	1	10
51-60	0	1	0	0	2	3
Above 60	0	1	1	0	0	2
Total	19	16	7	1	15	58

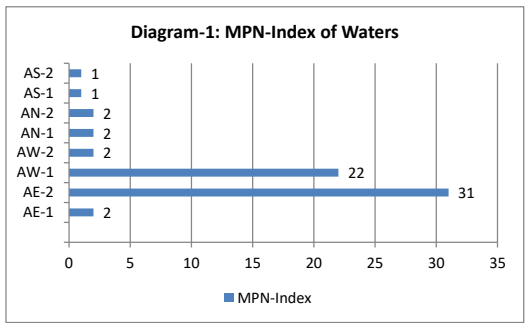

Fig. 3: MPN Index of waters.

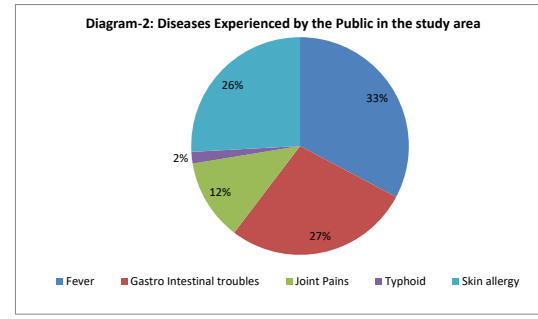

Fig. 4: Diseases experiences by the public in the study area.

stop their growth at pH 5.0 whereas some microorganisms can grow as low as 4.6-4.4 (pH 4.6 was considered to be the lower growth limit). The observed pH values of water samples are in the range of 6.93-8.92 in both seasons and are observed around pH 7 which is favorable for the growth of microorganisms in the waters of the study area (Meter Group n.d.). Higher EC values indicate the presence of salt content in the waters and it is revealed by the higher values of TDS and salinity. TDS values crossed the permissible limit in all parameters. Total hardness values in all samples in the study area exceeded the permissible limit. TA values during the pre-monsoon season are within the permissible limit while it crossed the permissible limit during post-monsoon in all samples. Chloride and sulfate ion concentration values during pre- and post-monsoon seasons crossed the permissible limit during pre- and post-monsoon seasons. Phosphate ion concentration values range from 0.11-3.86 $mg.L^{-1}$ and 0.14-4.73 $mg.L^{-1}$ during pre- and post-monsoon seasons respectively. Nitrate ion concentration values during pre- and post-monsoon seasons are within the permissible limit in the majority of samples collected near the aquaculture activity area. Calcium and magnesium values in the waters exceeded the permissible limit in the majority of the samples. Na levels during pre-monsoon range from 238-3738 $mg.L^{-1}$ and during post-monsoon range from 77.9-1962.2 $mg.L^{-1}$. K levels range from 16.5-605.0 $mg.L^{-1}$ during pre-monsoon season and it ranges from 6.4-293.9 $mg.L^{-1}$ during post-monsoon which reveals higher levels of salt content present in the waters collected near aquaculture activity areas.

Irrigation parameters: Irrigation parametric values are presented in the Table 5 along with the BIS standard values which reveal percent sodium values during pre-monsoon season exceeded in major locations while during the post-monsoon season these values are within the permissible limit in the majority of the sample which reveals the unsuitability of these waters in terms of %Na values for irrigation during the pre-monsoon season while these waters can be considered for irrigation in the majority of the sampling locations. SAR in most of the samples during pre- and post-monsoon seasons indicates the suitability for irrigation in terms of SAR values. RSC values during pre- and post-monsoon seasons in the study area are within the irrigation standards which confirm the suitability for irrigation. Kelly's ratio values during pre- and post-monsoon seasons exceeded the permissible limit for irrigation. Magnesium hazard values during pre-monsoon season in the majority of the samples are within the irrigation standards while in post-monsoon these values exceeded irrigation standard value.

Correlation analysis: During the pre-monsoon season, EC, TDS, salinity, chloride, TH, sodium, calcium, and magnesium values strongly correlated and influences the water quality in the study area (Table 6). While in the post-monsoon season, EC, salinity, TH, chloride, TH, sodium, magnesium, and nitrate correlated strongly and majorly affects the water quality (Table 6).

MPN count: The water sample AE-1 was found with an MPN count of 2 and water sample AE-2 with MPN count 31. Water sample AW-1 is observed with MPN count 22 while the water sample AW-2 is with MPN count 2. Water sample AN-1 is found to contain MPN count 2 and the water sample AN-2 with MPN count 2. Water samples AS-1 and AS-2 are observed with MPN count 1 each. Except for the water samples AS-1 and AS-2, the remaining samples are observed with MPN count 2 and more than 2 which indicates microbial contamination of these water samples in the study area.

Bacterial species: The bacteria *Pseudomonas* generally tend to live and breed in water, soil, and damp areas. People with a weakened immune system are prone to severe infections like fever, skin rashes, joint pains, and ear infections. *C. freundii* is a species of facultative anaerobic gram-negative bacteria. Bacteria are often found in the water, soil, food, and intestines of humans and animals. The bacteria can cause several types of infections in bones, intestines, respiratory and urinary tracks. *E. coli* is a type of bacteria and normally exists in the intestines. Most types of *E. coli* are harmless and even help the digestive tract healthy. But some strains can cause diarrhea if contaminated water is consumed or by eating contaminated food. *E. coli* stains can also cause abdominal cramps, fever, and acute kidney failure.

The water sample AE-1 was found to have *bacterial species Pseudomonas* and the *w*ater sample AE-2 was found to have *C. freundii.* Water sample AW-1 was found to have *C. freundii and the* water sample AW-2 was found to have *E. coli.* Water sample AN-1 was found to have *Pseudomonas* while the water sample AN-2 was found to have *E. coli.* Water sample AS-1 was found to contain *C. freundii* while the water sample AS-2 was found to have *C. Freundii.* Due to the presence of pathogenic bacteria like *Pseudomonas, C. freundii, and E. coli* in the waters of the study area, health problems like fever, bone-related problems like joint pains, gastrointestinal troubles, and skin diseases can be caused.

Health survey: The health survey information (Table 8) revealed the details of the sufferings of people residing in the nearby areas of the aquacultural activity. People of different ages (from 1yr to 60 yrs) and the health problems viz., fever, gastrointestinal troubles, typhoid, and skin diseases experienced by them are correlated with the presence of the pathogenic species present in waters.

CONCLUSION

The parametric values of temperature and the pH of water

samples are in favor of pathogenic *bacteria*l growth in waters of the study areas indicating the microbial contamination of waters. Physicochemical parametric values of the majority of the parameters confirm the chemical contamination of waters and indicate their unsuitability for drinking purposes. Irrigation parameters like %Na, SAR, Kelly's Ratio, and MH also reveals the unsuitability of these waters in the majority of the sampling locations. The study results revealed that health problems like fever, gastrointestinal troubles, bone-related health problems like joint pains, and skin diseases experienced by the people residing in the nearby areas of aquacultural areas are the actual contribution of *pathogenic bacteria* like *Pseudomonas, C. freundii, and E. coli* in waters. Disinfection and sterilization are to be done continuously every time to eliminate microbial contamination. Very sensitive and frequent monitoring of waters is suggested and a wide range of biosensor systems are to be developed for usage from time to time to assess the quality of waters to protect the health of the people if these waters are proposed for consumption or drinking.

ACKNOWLEDGEMENT

The authors express their sincere thanks and gratitude to the authorities of Pragati Engineering College (A), Surampalem, A. P India for their support in carrying out the analysis in R&D laboratories. The authors also convey their thanks to the faculty, Department of Microbiology, Y.N.College (A), Narasapuram for their cooperation in microbial analysis.

REFERENCES

Alagarswamy, K. 1995. Report on a regional study and workshop on the environmental assessment and management of aquaculture development, FAO Corporate Document Repository,pp. 1-26.

APHA1992. The Standard Method for the Examination of Water and Wastewater (19th ed.). American Public Health Association, Washington.

Arnone, R.D. and Walling, J.P. 2007. Waterborne pathogens in urban watersheds. Water Health, 5(1): 149-162.

Boehm, A. and Sassoubre, L.M. 2014. Enterococci as Indicators of Environmental Contamination. In: Gilmore MS, Clewell DB, Ike Y. (eds.) Enterococci: From Commensals to Leading to Causes of Drug-Resistant Infections. Massachusetts Eye and Ear Infirmary, Boston, PMID: 24649503.

Dahdouh-Guebas, F., Collin, S., Lo Seen, D., Ronnback, P., Depommier, D., Ravishankar, T. and Koedam, N. 2006. Analysing ethnobotanical and fishery-related importance of mangroves of the East-Godavari Delta (Andhra Pradesh, India) for conservation and management purposes. J. Ethnobiol. Ethnomed., 2(24): 1-22.

Falconer, L., Telfer, T.C. and Ross, L.G. 2018, Modelling seasonal nutrient inputs from non-point sources across large catchments of importance to aquaculture. Aquaculture, 495: 682-692.

Ibrahim, A.B., Mohd Khan, A. and Norrakiah, A.S. 2014. Microbiological risk assessment of freshwater aquaculture fish: From farm to table. Adv. Environ. Biol., 8(14): 105-111.

Ikonen, J.M., Hokajärvi, A.M., Heikkinen, J., Pitkänen, T., Kolehmainen, M. and Pursiainen, A. 2017. Drinking water quality in distribution systems of surface and ground water works in Finland. J. Water Secur., 3: 1-10.

Joao, C., P.S. 2010. Water microbiology: Bacterial pathogens and water. Int. J. Environ. Res. Pub. Health, 7(10): 3657-370.

Madoux-Humery, A.S., Dorner, S., Sauve, S., Aboulfadl, K., Galarneau, M., Servais, P. and Prevost, M. 2016. The effects of combined sewer overflow on riverine sources of drinking water. Water Res. 92: 218-227.

Massoud, A., Jurdi, M. and Nuwayhid, I. 2010. The challenges of sustainable access to safe drinking water in rural areas of developing countries: Case of Zawtan Elcharkieh, Southern Lebanon. J. Environ. Health, 72(10): 24-30.

Mir, A.B.Q., Pandey, G.C. and Sarwar, S.G. 2004. Impact of SKIMS effluent on the water quality of Anchar lake, Kashmir. Indian J. Environ. Ecoplan., 8(2): 389-394.

Nagaraju, D and Papanna, C. 2009. Hydrogeochemical Studies of Kabini River Basin, Karnataka, India. Nat. Environ. Pollut. Technol., 8(1): 111-118.

NEERI 1995. Investigation report on impacts of aquaculture farming and remedial measures in ecologically fragile coastal areas in the states of Andhra Pradesh and Tamilnadu. Submitted to Hon'ble Supreme Court, National Environmental Engineering Research Institute, Nagpur, India, p. 143.

Obiri-Danso, K. and Jones, K. 1999. Distribution and seasonality of microbial indicators and thermophilic campylobacters in two freshwater bathing sites on the River Lune in northwest England. J. Appl. Microbiol., 87: 822-832.

Obiri-Danso, K. and Jones K. 1999. The effect of a new sewage treatment plant on fecal indicator numbers, campylobacters, and bathing water compliance in Morecambe Bay. J. Appl. Microbiol., 86: 603-614.

Ramesh, R.P., Gkigbo, R.N., Madhusoodan, S.A. and Radha, L. 2008. Groundwater pollution due to aquaculture in the east coast region of Nellore district, Andhra Pradesh, India. Afr. J. Environ. Sci. Technol. 2(3): 40-50.

Ramteke, D.S. and Moghe, C. A. 1988. Manual on Water and Wastewater Analysis. National Environmental Engineering Research Institute, Nagpur, India.

Raveen, R., Chennakrishnan, C. and Stephen, A. 2008. Impact of pollution on the quality of water in three freshwater lakes of sub-urban Chennai. Nat. Environ. Pollut. Technol., 7(1): 61-64.

Sohan, S. and Iqbal, S. 2012. Microbiological analysis of surface water in Indore, India. Res. J. Recent Sci., 1(ISC-2011): 323-325.

World Health Organization (WHO). 2010. Unsafe water, sanitation, and hygiene, 2010. http://www.who.int/publications/cra/chapters/volume2/1321-1352.pdf

World Health Organization (WHO). 2014. Water Quality and health. Drinking water chlorination – A review of disinfection practices and issues. http://www.waterandhealth.org/drinkingwater/wp.html. Accessed 28 Apr 2014.

Meter Group n.d. How water activity and pH work together to control microbial growth. https://www.metergroup.com/food/articles/how-water-activity-and-ph-work-together-to-control-microbial-growth.

Nature Environment and Pollution Technology
An International Quarterly Scientific Journal

p-ISSN: 0972-6268
(Print copies up to 2016)
e-ISSN: 2395-3454

Vol. 20 | No.3 | pp. 1295-1300 | 2021

Original Research Paper

https://doi.org/10.46488/NEPT.2021.v20i03.041

Open Access Journal

Evaluation of LDPE Degradation Under Controlled Composting

S. Singh*, S. Shankar and Shikha*†**

*Department of Environmental Science, School for Earth & Environmental Science, Babasaheb Bhimrao Ambedkar University (A Central University) Vidya Vihar, Raebareli Road, Lucknow-226 025, Uttar Pradesh, India

**Department of Environmental Science, School of Vocational Studies and Applied Sciences, Gautam Buddha University, Yamuna Expressway, Greater Noida, Gautam Buddh Nagar-201 312, U.P., India

†Corresponding author: Shikha; envscibbau@ymail.com

Nat. Env. & Poll. Tech.
Website: www.neptjournal.com

Received: 07-10-2020
Revised: 09-11-2020
Accepted: 09-01-2021

Key Words:
LDPE degradation
Compost treatment
Plastic waste

ABSTRACT

The compost burial test was performed to determine the degradation of commercially available low-density polyethylene in natural compost for a period of six months. Biodegradability of polyethylene films in compost was monitored using scanning electron microscopy (SEM), Energy dispersive X-Ray, Fourier transform infrared spectroscopy (FTIR), X-Ray diffraction (XRD), thermal gravimetric analysis (TGA), differential scanning calorimetry (DSC), and weight reduction analysis. After six months of compost exposure, a major change over the surface of LDPE was observed. SEM images clearly showed the exfoliation and cracks on the film leading to degradation. The other analysis also showed a change in the thermal properties and crystallinity of the LDPE films. The composting method could prove to be the reliable and ecological method of degrading plastic waste without hindering the natural ecosystem.

INTRODUCTION

Composting is basically a natural process by which organic material gets decomposed into humus, which is a soil-like material. The major groups of microorganisms that are involved in composting are bacteria and fungi. These microorganisms decompose the organic substances as their source of food. This process of degradation requires carbon, nitrogen, oxygen, water, and heat. Organisms decompose the organic substance to use carbon and nitrogen as the source of energy and for building their cell structure (Mierzwa-Hersztek et al. 2019). Degradation of the polymers in the compost environment occurs primarily through mechanical, chemical, and thermal degradation (Calabia & Tokiwa 2004). Of all the mechanisms of degradation, chemical degradation is considered the most important for polymers. In the compost method, the specific weight of the plastic is buried under the mixture of a definite amount of mature compost and soil and then kept under natural weathering conditions with maintained moisture content. Biodegradation of polymer is measured based on the amount of carbon present in the polymer converted to gaseous carbon dioxide. The nature and type of compost affect the extent and degree of degradation of polymer (Das & Kumar 2015). This is the natural way of decomposing plastic in an eco-friendly manner. The increased accumulation of plastics in the environment has forced researchers across the world to develop several degradation methods to deal with plastic waste which does not create further stress on the natural environment (Vázquez-Morillas et al. 2016). The study presented here is one such attempt at dealing with plastic waste. To evaluate biodegradability in realistic disposal conditions, a compost burial test of LDPE films was performed for six months. In the experiment, different concentrations of compost were used and kept in pots to degrade the low-density polyethylene (LDPE) films. The investigations on the chemical and morphological changes in LDPE films revealed the extent of degradation.

MATERIALS AND METHODS

Compost Setup

For composting method, different concentration of compost 20%, 40%, 60%, 80% and 100% (w/w) was made. For this, approximately 1 kg of the compost and soil was maintained in different concentration in different pots. The experiment was done in triplets. The LDPE films of area 5cm^2 were buried under the compost in pots for a period of six months.

Characterization of Degraded LDPE Samples

After six months LDPE samples were taken out, washed, and characterized using weight reduction, SEM, EDX, FTIR, TGA, XRD, and DSC analysis.

Scanning Electron Microscopy and Energy Dispersive X-ray Analysis

The LDPE films were subjected to SEM and EDX analysis for determining the changes induced in their morphological structure and elemental composition. The analysis was done using the Scanning Electron Microscope of JEOL (JSM 6490 LV) present at University Scientific Instrument Center (USIC), Babasaheb Bhimrao Ambedkar University, Lucknow (Ambika et al. 2015).

Fourier Transform Infra-red Spectroscopy (FTIR)

The FTIR analysis serves the purpose of detecting the functional group in the substance, which is subjected to the analysis. FTIR scan was taken at a spectrum ranging from 400 cm^{-1} to 4000 cm^{-1} at room temperature. The relative absorbance intensities of the keto carbonyl bond (1740 cm^{-1}) and a double bond (908 cm^{-1}) to that of the methylene bond (1465 cm^{-1}) were calculated using the following equation (Albertsson et al. 1998): keto carbonyl bond index (KCBI) = I_{1715}/I_{1465}; and internal double bond index (IDBI) = I_{908}/I_{1465}. The crystallinity percentage of the polyethylene films was calculated by using following equation: % crystallinity = $100 - [\{1 - (Ia/1.233Ib) / 1 + (Ia/Ib)\} \times 100]$: where *Ia* is absorbance at 1473 and *Ib* is the absorbance at 1463 (Averous & Pollet 2012).

X-Ray Diffraction Analysis (XRD)

XRD analysis was done by the fifth generation Rigaku (Modal no Mini Flex 600) X-ray diffractometer. XRD analysis gives detail about the crystalline nature of the substance subjected to the analysis. In the case of LDPE, the analysis is very important as it shows whether the polymer material has undergone a change or not after its treatment with the compost. For this purpose, LDPE films were cut into pieces and inserted inside the diffractometer.

Thermal Gravimetric Analysis (TGA) and Differential Scanning Calorimetry (DSC)

For TGA analysis, Shimadzu's TGA50 series thermogravimetric analyzer was used while for DSC analysis, Shimadzu Modal no. DSC-60Plus was used. TGA and DSC analysis are performed for determining the thermal properties of the LDPE films. For the analysis, the LDPE films were cut into very small pieces and then kept in the crucible, which was then loaded in the instrument for analysis.

RESULTS AND DISCUSSION

The LDPE films were subjected to the compost treatment of varying concentrations from 20% to 100%. After a period of six months, LDPE films were recovered from the compost and various analysis such as SEM, EDX, FTIR, TGA, DSC, XRD and weight reduction analysis was performed for determining the extent of degradability. The physicochemical parameter of the compost sample was also estimated to observe the post-treatment changes in the compost parameters. The results obtained for various analyses are given as follows.

Scanning Electron Microscopy

In SEM analysis the untreated LDPE film appeared as a smooth, uniform, and homogeneous sheet, whereas, other LDPE films that were kept under the treatment with different concentrations of compost showed significant changes in the morphology (Fig 1). After six months of treatment, the most prominent change was observed in LDPE film that was treated with 80% compost followed by 100%, 60%, 40%, and 20% compost. In LDPE film treated with 100% compost, the deterioration was observed over the surface but it was less prominent than 80% compost treated LDPE. In 60% and 40% compost treated LDPE, some changes such as exfoliation of surface and peeling were observed. The least change was observed in 20% compost treated LDPE due to less amount of compost and more amount of dry soil sample. The LDPE film appeared as a continuous, uninterrupted sheet. SEM micrographs in this study revealed that upon exposure to compost, surface erosion took place and the matrix became perforated. This ultimately resulted in a thinning of the matrix with inconsistent properties which corresponds to the deterioration of the mechanical properties of the LDPE sheets (Kale et al. 2015). Exfoliation was clearly demonstrated in the LDPE. This peeling of a thin layer (exfoliation) can happen only if there is a major erosion of the more accessible amorphous regions in the polyethylene, leaving a crystalline region that degrades very slowly. The SEM analysis clearly reveals the change in the surface structure of the LDPE and moreover, the degradation was observed to be more prominent in 80% compost treated LDPE sample (Bhardwaj et al. 2012).

X-Ray Diffraction Analysis

The crystallinity of the polymer is directly proportional to the diffraction peak intensity. The peaks at 21° and 23.5° are the characteristic peaks of the semi-crystalline polyethylene molecule. The intensities of the different compost treated samples were compared for the intensities at these two significant peaks. The change in crystallinity of treated and untreated samples was compared according to the change in X-Ray intensities at different 2 theta angles. The two obvious diffractive peaks of about 21° and 23.5° correspond to a typical crystalline plane (110), and (200) of the orthorhombic

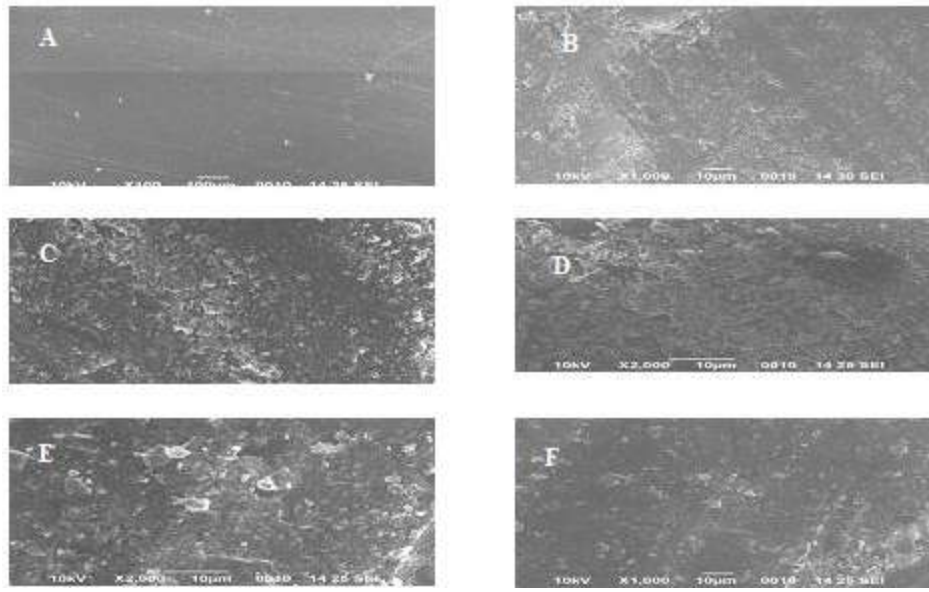

Fig. 1: SEM micrographs: (A) Untreated LDPE (B) 20% compost (C) 40% compost (D) 60% compost (E) 80% compost (F) 100% compost treated LDPE samples.

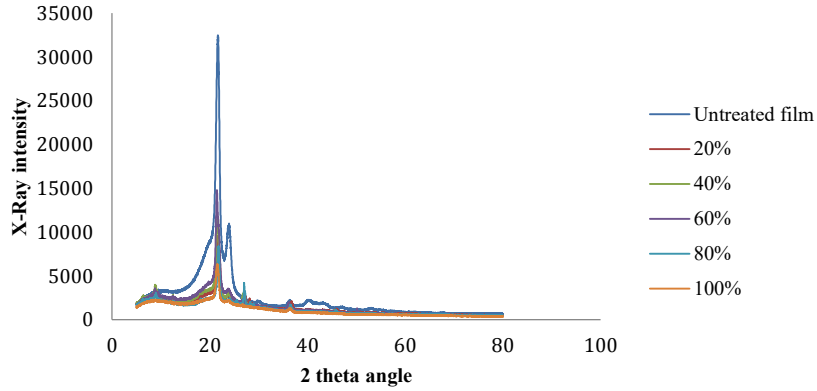

Fig. 2: XRD graph of different compost treated and untreated samples.

phase respectively (Caruso 2015). The graph shown in Fig. 2, clearly shows that the lowest intensity at 21° and 23.5° was observed on 80% compost treated LDPE sample. Maximum intensity was found in untreated LDPE sample followed by 20%, 40%, 60%, and 100% compost treated sample

Energy Dispersive X-Ray (EDX) Analysis

The weight percent of carbon and oxygen of LDPE treated with different concentrations of compost is given in Table 1 below. The EDX analysis revealed that the lowest carbon content was observed in 80% compost treated sample and higher oxygen content was also found in the LDPE treated with 80% compost treated sample. This signifies that the microbial attack began at the surface of the polymer resulting in higher oxygen content on the surface. This step can be described as a development of oxidation skin and as a result, the polymer's surface is damaged with fine cracks indicat-

Table 1: Weight percent of carbon and oxygen.

Sample	Carbon	Oxygen
Untreated LDPE	77.29%	22.71%
20% Compost treated	73.01%	26.42%
40% Compost treated	67.75%	32.25%
60% Compost treated	53.11%	44.20%
80% Compost treated	46.29%	50.26%
100% Compost treated	50.22%	46.32%

ing morphological transformations after which degradation proceeds towards the inner part of the polymer depending on the diffusion rate (Gu 2003).

Thermal Gravimetric Analysis

After six months of incubation in compost, a significant drop in thermal stability of LDPE films was recorded with respect to the untreated LDPE sample. The thermal gravimetric analysis graph shown in Fig. 3 reveals that the maximum reduction in thermal stability was observed in 80% compost treated LDPE. The onset temperature was found to be 403°C and the final decomposition temperature was 486°C with no residue left. Both the temperature for 80% compost treated LDPE obtained were found to be least among all the compost treated samples and untreated samples. TGA results showed the presence of endothermic effects in the compost treated sample. The endothermic effect was due to three processes, which are intermolecular dehydration, vaporization, and solid-state decomposition. The total burning and degradation of the residual polymer backbone took place at a temperature interval of 200°C to 500°C (Sen & Raut 2015).

Differential Scanning Calorimetric (DSC) Analysis

From the curve of DSC analysis shown in Fig. 4, some of the parameters such as glass transition temperature (T_g), onset melting temperature (T_o), melting point temperature (T_m) and end melting point temperature (T_f) were recorded.

The glass transition temperature, onset melting temperature, melting point temperature and end melting point temperature for 80% compost treated sample are 120°C, 395°C, 472°C, 507°C respectively. These values recorded for 80% compost treated sample are highest among all the compost treated and untreated samples. This signifies the increase in crystallinity of the sample. This might be due to the fact that biotic degradation by microbial communities on the LDPE sample attacked the amorphous region, due to which crystalline region remained intact which increased the crystallinity of the polymer. DSC results clearly reveal the increased crystallinity, increased chain scissoring, oxidation, and a minor decrease in tensile strength (Bhatia et al. 2014).

Fourier Transform Infra-red (FTIR) Spectroscopic Analysis

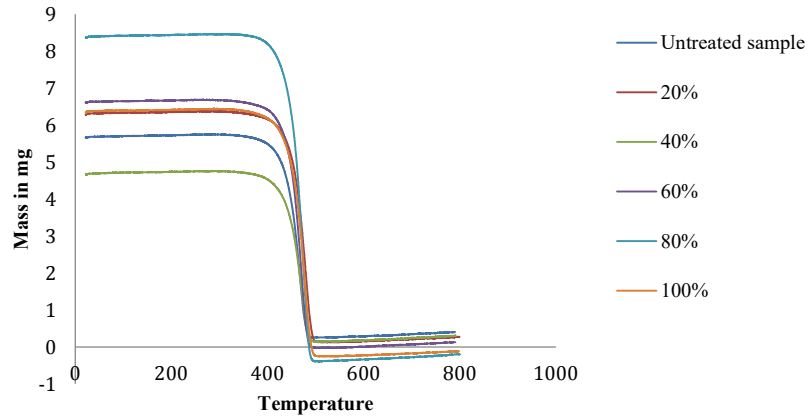

Fig. 3: Thermal gravimetric analysis graph of compost treated LDPE sample.

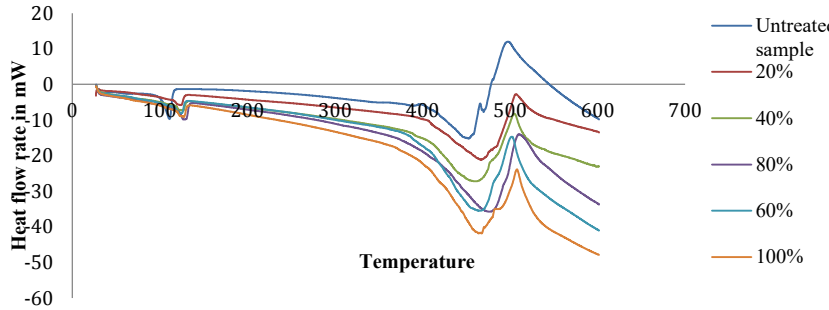

Fig. 4: Differential scanning calorimetry curve of LDPE samples.

FTIR study was conducted to determine the functional groups of the treated and untreated LDPE samples. The spectroscopic graphs are shown below in Fig. 5 & 6 and various functional groups observed in the treated LDPE samples are show in Table 2. The overall trend obtained after aging LDPE by burying it under the different concentrations of compost is that there are higher transmittance values at certain wavenumbers like 2840 cm^{-1}, 2916 cm^{-1}, 1480 $cm^{-1,}$ and 719 cm^{-1}), representing an increase in C-H bond intensity, which can be explained by chain scissoring or increase of CH_3 endings (Sathiskumar & Madras 2011). All the compost treated samples composted formed new spectra at a wavenumber of 1380 cm^{-1}, representing the hydroxyl group. Furthermore, new transmittance peaks were also observed at wavenumbers 997 cm^{-1} and 933 cm^{-1}, indicating the formation of C=C bonds (Giudicianni et al. 2013).

The keto carbonyl bond index and the internal double bond index were found to be maximum in the case of 80% compost treated LDPE. The formation of double bonds in the polymeric chain can be due to the Norrish type II reaction and an increase in the concentration of the carbonyl group could be responsible for a higher carbonyl bond index.

Low-density polyethylene is insoluble in nature due to its crystalline. In this study, there was an observed reduction in the crystallinity of the polyethylene after six months of incubation with the compost. The crystallinity percent for untreated LDPE and 20%, 40%, 60%, 80% and 100% compost treated samples were 86.32%, 81.67%, 79.51%, 74.91%, 65.48% and 71.13% respectively. The lowest crystallinity value was observed in 80% compost treated LDPE. The decrease in crystallinity supports the conversion of crystalline structures of the LDPE films into an amorphous structure as a consequence of degradation.

Weight Reduction Analysis

Polyethylene degradation was monitored by dry weight reduction of polyethylene films treated with the different composts. The present findings revealed that the compost treatment showed some deterioration effect on the LDPE samples. Among all the samples, a maximum weight reduction of approximately 17% was observed in 80% compost treated sample (Fig 7). For rest of the 20%, 40%, 60%, 100% compost treated samples, weight reduction obtained was 6.3%, 8.45%, 11.97% and 14.29%.

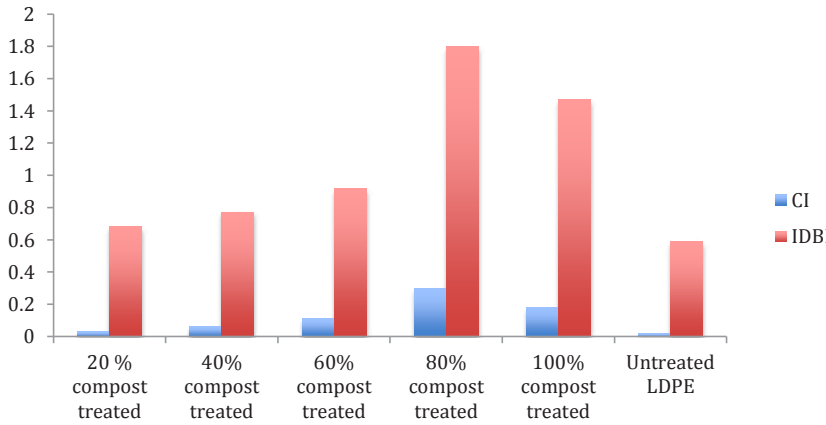

Fig. 5: Graph of carbonyl and internal double bond index of composted LDPE.

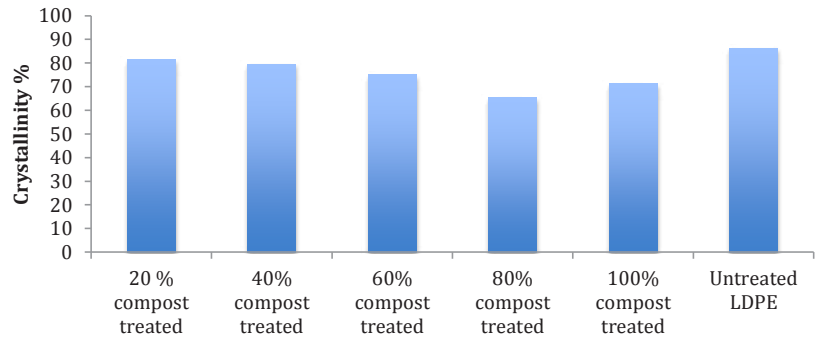

Fig. 6: Graph of crystallinity percent of composted LDPE.

Table 2: Functional groups detected in composted and control LDPE samples.

Origin	Peaks	Functional group	Detected sample
CH_2	2920 cm^{-1}	Alkyl asymmetric stretching	20%, 40%, 60%, 80%, 100% and control LDPE
CH_2	2850 cm^{-1}	Alkyl symmetric stretching	20%, 40%, 60%, 80%, 100% and control LDPE
C=C	1473, 1462, 1437 cm^{-1}	Bending deformation of carbon double bond	60%, 80%, 100% LDPE
C-H	727 and 723 cm^{-1}	Alkane bend mono	20%, 40%, 60%, 80%, 100% and control LDPE
O-H	3200-3450 cm^{-1}	Hydroxyl stretching (intermolecular)	20%, 40%, 60%, 80%, 100% and control LDPE
O-H	1380 cm^{-1}	Hydroxyl bending	80% LDPE
C-O	1160 cm^{-1}	Carbonyl group	20%, 40%, 60%, 80%, 100% LDPE

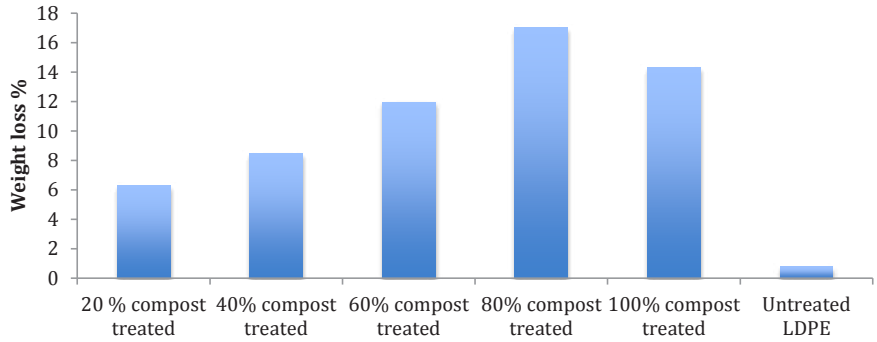

Fig. 7: Graph of weight loss percent of different composted LDPE samples.

CONCLUSION

All the composted LDPE samples showed the changes induced in the polymer. Major changes were observed in LDPE samples treated with 80% compost. A maximum weight reduction of 17% was noted in the 80% compost treated sample. Thermal gravimetric analysis revealed the lowest onset and decomposition temperature with no residue left in the LDPE sample treated with 80% compost treated sample. EDX analysis showed minimum carbon content and maximum oxygen content in 80% compost treated LDPE sample after six months of treatment. In FTIR analysis, a maximum value of carbonyl and double bond index supported the greater extent of degradation in 80% composted LDPE.

REFERENCES

Ambika, D.K., Lakshmi, B.K.M. and Hemalatha, K.P.J. 2015. Degradation of low-density polythene by *Achromobacter denitrificans* strain s1, a novel marine isolate. Int. J. Rec. Sci. Res., 6(7): 5454-5464.

Albertsson, A.c., Erlandsson, B., Hakkarainen, M., and Karlsson, S. 1998. Molecular weight changes and polymeric matrix changes correlated with the formation of degradation products in biodegraded polyethene. J. Polym. Environ., 6: 187-195.

Averous, L. and Pollet, E. (ed.) 2012. Biodegradable Polymers. In: Averous, L. and Pollet, E. (eds.) Environmental Silicate Nano-Biocomposites. Springer Nature, Switzerland, pp. 13-39.

Bhardwaj, H., Gupta, R. and Tiwari, A. 2012. Microbial population associated with plastic degradation. Sci. Rep., 1(2): 1-4.

Bhatia, M., Girdhar, A., Tiwari, A. and Nayarisseri, A. 2014. Implications of a novel *Pseudomonas* species on low-density polyethylene biodegradation: An in vitro to in silico approach. Springer Plus, 3(497): 1-10.

Calabia, B.P. and Tokiwa, Y. 2004. Microbial degradation of poly (D-3-hydroxybutyrate) by a new thermophilic *Streptomyces* isolate. Biotechnol. Lett., 26(1): 15-19.

Caruso, G. 2015. Plastic degrading microorganisms as a tool for bioremediation of plastic contamination in aquatic environments. J. Pollut. Eff. Cont., 3(3): 1-2

Das, M.P. and Kumar, S. 2015. An approach to low-density polyethylene biodegradation by *Bacillus amyloliquefaciens*. Biotech, 5(1): 81-86.

Giudicianni, P., Cardone, G. and Ragucci, R. 2013. Cellulose, hemicellulose, and lignin slow steam pyrolysis: thermal decomposition of biomass components mixtures. J. Anal. Appl. Pyrolysis, 100: 213-222.

Gu, J.D. 2003. Microbiological deterioration and degradation of synthetic polymeric materials: Recent research advances. Int. Biodeterior. Biodegrad., 52(2): 69-91.

Kale, S.K., Deshmukh, A.G., Dudhare, M.S. and Patil, V.B. 2015. Microbial degradation of plastic: A review. J. Biochem. Technol., 6(2): 952-961.

Mierzwa-Hersztek, M., Gondek, K. and Kopeć, M. 2019. Degradation of polyethylene and biocomponent-derived polymer materials: An overview. J. Polym. Environ., 27(3): 600-611.

Sathiskumar, P.S. and Madras, G. 2011. Synthesis, characterization, degradation of biodegradable castor oil-based polyesters. Polym. Degrad. Stab., 96(9): 1695-1704.

Sen, S.K. and Raut, S. 2015. Microbial degradation of low-density polyethylene (LDPE): A review. J. Environ. Chem. Eng., 3: 462-473.

Vázquez-Morillas, A., Beltrán-Villavicencio, M., Alvarez-Zeferino, J. C., Osada-Velázquez, M. H., Moreno, A., Martínez, L. and Yañez, J. M. 2016. Biodegradation and ecotoxicity of polyethylene films containing pro-oxidant additive. J. Polym. Environ., 24(3): 221-229.

Nature Environment and Pollution Technology
An International Quarterly Scientific Journal

p-ISSN: 0972-6268
(Print copies up to 2016)
e-ISSN: 2395-3454

Vol. 20 | No.3 | pp. 1301-1308 | 2021

Original Research Paper

https://doi.org/10.46488/NEPT.2021.v20i03.042

Open Access Journal

Successive Saccharification of Waste Paper as a Resource for Bio-product Development

K.M.P. Mokatse and J.P.H. van Wyk†
Department of Pharmacology and Therapeutics, Sefako Makgatho Health Sciences University, Ga-Rankuwa, South Africa
†Corresponding author: J.P.H. van Wyk; bioenergy.res@gmail.com

Nat. Env. & Poll. Tech.
Website: www.neptjournal.com

Received: 24-04-2020
Revised: 30-06-2020
Accepted: 16-07-2020

Key Words:
Saccharification
Waste paper
Trichoderma viride
Cellulase

ABSTRACT

Environmental pollution and the exploitation of fossil-based products are topical issues that should be a matter of concern to the global population. The production of bio-based substances from waste biomass is a way to reduce the consumption of fossil fuels and limit environmental pollution. Enzymatic catalysed saccharification of cellulose is an important step for the bio-conversion of biomass such as waste paper into glucose that could be utilized as a feedstock for the production of value added bioproducts and this process can also be considered as an alternative route of waste management. During this study, fresh cellulase enzyme from *Trichoderma viride* was incubated separately with seven different waste paper materials during twelve successive incubation periods of 2 h each. The amount of sugar released from each paper material during each incubation period was determined. The highest sugar concentration released from each paper materials was produced during the first incubation period except the filter paper for which the highest amount of sugar was produced during the 9th period of incubation. During these optimum sugar producing incubation periods the highest total sugar concentration was released from brown envelope paper (3.3 mg.mL^{-1} followed by foolscap paper (3.0 mg.mL^{-1}) and office paper (2.8 mg.mL^{-1}) while the lowest amount of sugar was released from Pick 'n Pay paper (0.6 mg.mL^{-1}). The relative saccharification percentage was also calculated which showed that filter paper produced the highest amounts of sugar followed by newspaper, and foolscap paper with advertising paper from a retailer. Pick 'n Pay offered the highest resistance towards cellulase catalysed bio-conversion into sugar.

INTRODUCTION

Globally the accumulation of municipal solid waste (MSW) amounts to 1300 tons per year with solid waste contributing approximately 3% of the total greenhouse gas emissions worldwide, which makes it as one of the biggest contributors to global warming and climate change (Ndlovu & Van Wyk 2019). High amounts of solid waste and its improper management worsens air quality in cities which affects the health of human beings negatively (Tahir et al. 2015).

Cellulosic waste biomass such as sawdust, agricultural residues, and municipal solid waste (waste paper) are quite cheap and abundant alternative substrates for bio-product development (Canilha et al. 2013). Paper materials can be categorized as useful commodities because paper is a way to present information, can act as a protective agent and also serves as a packaging material (Van Wyk et al. 1999). The large consumption of different types of papers such as newspaper, office paper and advertising paper on a daily basis indicate that paper is an important commodity that is used worldwide and affects human life (Wu & Cheng 2005). Waste paper is a heterogeneous mixture of plant material, especially which is rich in cellulose (50-60%) (Veluchamy 2017), a glucose biopolymer that constitutes thousands of glucose units and hemicellulose that is composed of two kinds of pentoses (xylose and arabinose) and three kinds of hexoses (glucose, mannose and galactose) (Saini et al. 2015). Lignin which is another biopolymer in paper materials is made up of aromatic compounds only which can't be easily hydrolysed as it works as a glue cementing cellulose and hemicellulose together (Seidl & Goulart 2016).

The hydrolysis of cellulose can be performed in different ways, either by strong acids and bases or by an enzymatic catalysed process using cellulase as the hydrolytic agent. The enzymatic process favours having a selection of the substrate and less production of by-products under mild conditions (Hamelinck et al. 2005). Cellulase is a hydrolytic, multi-component enzyme system responsible for the saccharification of cellulose. The complete hydrolysis of cellulose into glucose can be achieved synergistically by a combination of three types of cellulases namely, endoglucanases which cleave internal glucosidic bonds in the cellulose structure, exoglucanases which are responsible to cleave cellobiosyl units from the end of a cellulose chain and the third enzymatic

component is a β-glucosidase enzyme that is responsible for the removal of glucose units from cello-oligosaccharides and the hydrolysis of cellobiose into glucose (Jeoh et al. 2006, Kim et al. 1998).

The hydrolysis of waste cellulose into fermentable sugars for the production of bio-products such as bioethanol and bio-pharmaceuticals, is an important step in the use of alternative feedstocks and thus reduces pollution caused by solid waste accumulation. Industries and businesses are the biggest users of paper which amounts to 52% of the total papers produced and it is estimated that about 10% of recovered waste paper comes from offices (Rodriguez et al. 2017). During the current investigation *T. viride* cellulase was used to successively hydrolyse the cellulose content of seven different paper materials namely, office paper, foolscap paper, newspaper, filter paper, brown envelope paper and advertising paper from retailers, Pick 'n Pay and Woolworths into fermentable sugars such as glucose. During the successive cellulase treatment of the waste paper materials, the produced sugar was removed from the incubation mixture after each incubation period. The regular removal of sugars from the incubation mixture was aimed at limiting end-product inhibition and regularly adding fresh cellulase could assist in constructing a sugar production profile from different cellulose materials when treated regularly and successively with fresh *T. viride* cellulase enzymes.

MATERIALS AND METHODS

Waste Paper Materials and Cellulase Enzyme

Seven different types of paper materials were used as cellulose substrates during the *T. viride* cellulase catalysed degradation of these waste cellulose materials into fermentable sugars such as glucose. These paper materials included, office paper, foolscap paper, Pick 'n Pay advertising paper, Woolworths advertising paper, newspaper, brown envelope paper and filter paper that were prepared as circular discs of 6.0 mm in diameter.

Cellulase Catalysed Saccharification of Waste paper

Twenty pieces of each paper material were transferred into a test tube and then mixed with 800 µL of tris-buffer (0.5 $mL.dm^{-3}$, pH 5.0) and 200 µL of the *T. viride* cellulase enzyme solution (2 $mg.mL^{-1}$, prepared in the buffer solution). These paper-enzyme mixtures were incubated for 2 h at 50°C and thereafter centrifuged for 15 min at 4000 rpm with the supernatants transferred into clean test tubes and used to determine the amount of sugar released from each paper material during the cellulase catalysed action. The non-degraded paper materials (precipitate after centrifugation) were kept at 4°C for a re-incubation with fresh *T. viride* cellulase during a subsequent successive treatment of 2 h. Successive treatments were repeated for 12 consecutive incubation intervals and all incubations with the distinctive paper materials were performed in triplicate (Ndlovu & Van Wyk 2019).

Determination of Reducing Sugars

The amount of sugars released from various paper materials (present in the supernatant after centrifugation) during successive treatment with *the T. viride* cellulase was determined by adding 1500 µL of DNS solution to each supernatant according to the method described by Miller (Miller 1959). To accelerate the colour formation, each solution was placed in a boiling water bath for a period of 10 min and thereafter cooled in ice water. The cooled and coloured samples were read on a spectrophotometer (Shimadzu, Kyoto, Japan) at 520 nm in order to determine the amount of reducing sugars released from each paper material. The concentration of sugars released during each of the successive incubation periods was calculated by using a calibration curve constructed with glucose standards and expressed as $mg.mL^{-1}$.

Calculation of Percentage Saccharification

The percentage saccharification of each paper material caused by the cellulase enzyme was calculated as described by Alrumma (2016), where the percentage saccharification is equal to the concentration of reducing sugars ($mg.mL^{-1}$) divided by the initial substrate concentration ($mg.mL^{-1}$) × 0.9 × 100. The factor 0.90 was used to convert polysaccharide to monosaccharide accounting for water uptake during hydrolysis.

RESULTS AND DISCUSSION

Rising environmental problems such as the accumulation of solid waste and release of carbon dioxide and other toxic compounds into the air as a result of fossil fuel combustion will force the global community to identify and develop renewable resources that could be used as feedstocks for the synthesis of many chemical substances. A possible solution to these negative environmental issues could be the development of bio-products such as bio-ethanol, biodiesel and other biochemicals from the cellulose component of organic waste like the waste paper. To produce bio-products, the cellulosic component of biomass or waste cellulose has to be hydrolysed by cellulolytic enzymes producing glucose which is finally fermented into bio-products (Mazzoli 2012). The different types of biomass available show high recalcitrance to enzymatic rupture due to the barrier properties of lignin and other admixtures. Most of the different types of waste papers and boards such as newspaper, packaging paper,

cardboard, corrugated board, coated or impregnated paper and the board can contain not only lignin, but other barrier components such as waxes, fats, rubbers, synthetic polymers and resins, and hydrophobic substances that prevent the enzymatic cleavage of the paper materials (Loelovich 2014).

When office paper (Fig. 1) was exposed to successive treatment with *T. viride* cellulase, a sugar concentration of 2.8 $mg.mL^{-1}$ was produced during the first incubation period of 2 h. The amount of sugar released from office paper during the second incubation period was lower at a concentration of 1.0 $mg.mL^{-1}$. The tendency of decreasing sugar production during successive treatment continued until the 6^{th} incubation period (12 h of degradation) when a sugar concentration of 0.4 $mg.mL^{-1}$ was released from this paper material. During the rest of the incubation periods, the amount of sugar released stayed relatively constant as it varied between 0.4 $mg.mL^{-1}$ and 0.6 $mg.mL^{-1}$. The rate at which the amount of sugar production decreased during the first six successive treatments was calculated at -0.2 $mg.mL^{-1}.h^{-1}$.

All other six paper materials degraded with the *T. viride* cellulase enzymes exhibited almost the same tendency in sugar production with the highest sugar concentration releasing during the first incubation period. When foolscap paper (Fig. 2) was degraded, a sugar concentration of 3.0 $mg.mL^{-1}$ was released which decreased to a concentration of 0.4 $mg.mL^{-1}$ after 14 h (7^{th} incubation period) of cellulase treatment. During the rest of the incubation periods, a relatively constant amount of sugar ($mg.mL^{-1}$) was released during each incubation period from 14 h to 21 h. With brown envelope paper (Fig. 3) exposed to the enzymatic catalysed degradation the amount of sugar released during the first incubation period was 3.3 $mg.mL^{-1}$ which decreased at a rate of -0.21 $mg.mL^{-1}.h^{-1}$ until a concentration of 0.4 $mg.mL^{-1}$ was released after 14 h of treatment. During the rest of the incubation period, the sugar concentration varied between 0.7 $mg.mL^{-1}$ and 0.5 $mg.mL^{-1}$.

When newspaper (Fig. 4) was saccharified with *T. viride* cellulase a relative high amount of sugar was released during

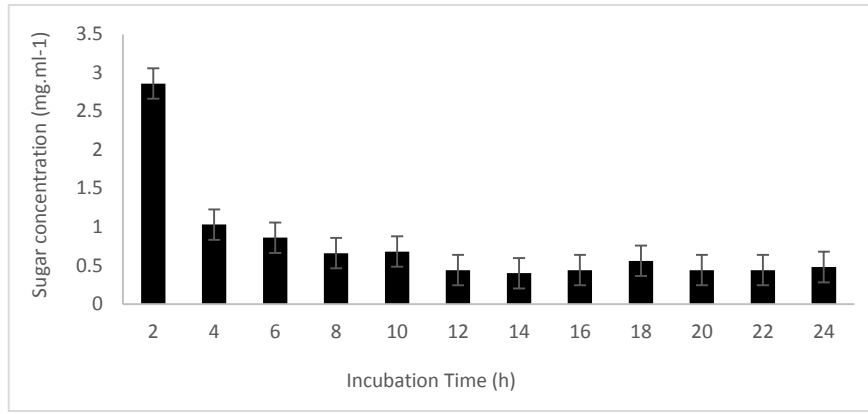

Fig. 1: The amount of sugar released during successive treatment of office paper with *T. viride* cellulase enzyme.

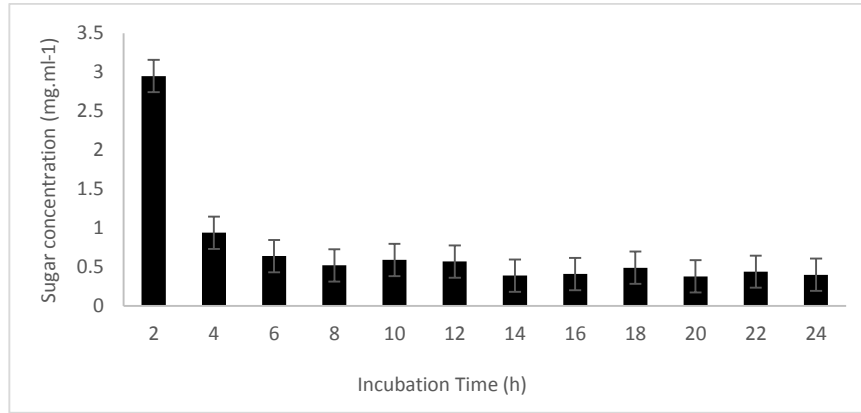

Fig. 2: The amount of sugar released during successive treatment of foolscap paper with *T. viride* cellulase enzyme.

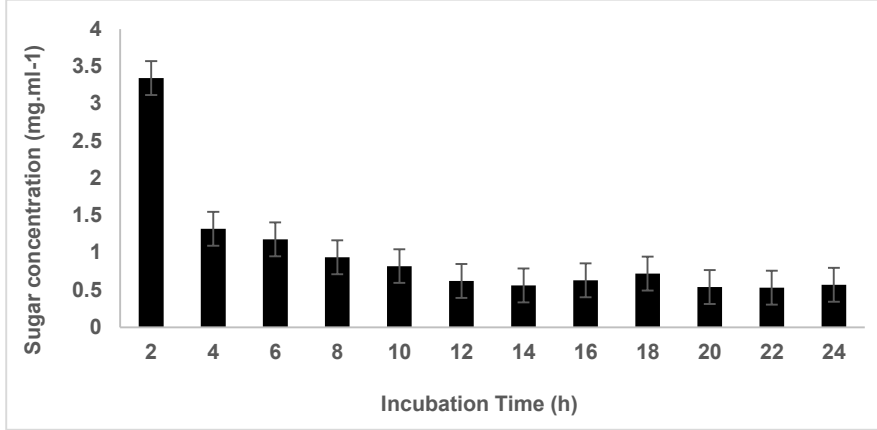

Fig. 3: The amount of sugar released during successive treatment of brown envelope paper with *T. viride* cellulase enzyme.

the first incubation period (1.5 mg.mL^{-1}) as well as during the second incubation period when sugar at a concentration of 1.4 mg.mL^{-1} was released. The amount of sugar released during the third incubation period decreased to a concentration of 0.6 mg.mL^{-1} which stayed relatively constant for the following two incubation periods. During incubation period number six (12 h) the sugar concentration decreased to an amount of 0.3 mg.mL^{-1} which increased to a concentration of 0.6 mg.mL^{-1} after 18 h of incubation and finally it decreased to 0.4 mg.mL^{-1} after 24 h of incubation. The rate of sugar released during the first 6 h of incubation was calculated at -0.15 mg.mL^{-1}.

When the cellulose content of Woolworths paper (Fig. 5) was bioconverted into sugars the amount of sugars released during the first two incubation periods was also relatively high at concentrations of 1.2 mg.mL^{-1} and 1.0 mg.mL^{-1}. This observation was almost similar to the sugar releasing pattern obtained during the degradation of newspaper (Fig. 4). During the third and fourth incubation period, the sugar concentration was lower at 0.6 mg.mL^{-1}, followed by a higher sugar concentration produced at 0.8 mg.mL^{-1} produced during the 5th incubation period, after 10 h of incubation. After the 12th hour incubation period a lower sugar concentration was produced at a concentration of 0.3 mg.mL^{-1} which varied between this value and 0.5 mg.mL^{-1} sugar concentration produced during the 18 h of incubation with a final sugar concentration of 0.4 mg.mL^{-1} released during the last incubation period after 24 h of successive incubation.

Fig. 6 reflects the sugar formation from Pick 'n Pay advertising paper during successive treatment with *T. viride* cellulase. The decline of sugar formation during the initial phase of saccharification was similar to the tendency observed during cellulase catalysed degradations of the other paper materials with values changing from 0.6 mg.mL^{-1} to 0.3 mg.mL^{-1} during the first three consecutive periods of saccharification. From the third period of incubation to the

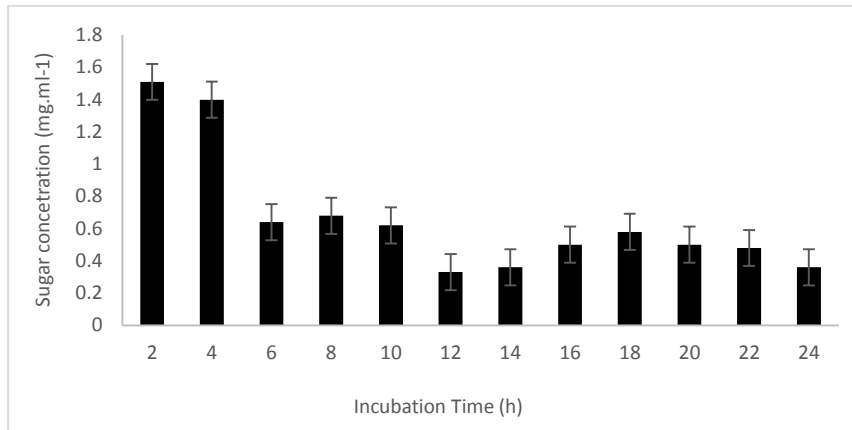

Fig. 4: The amount of sugar released during successive treatment of newspaper with *T. viride* cellulase enzyme.

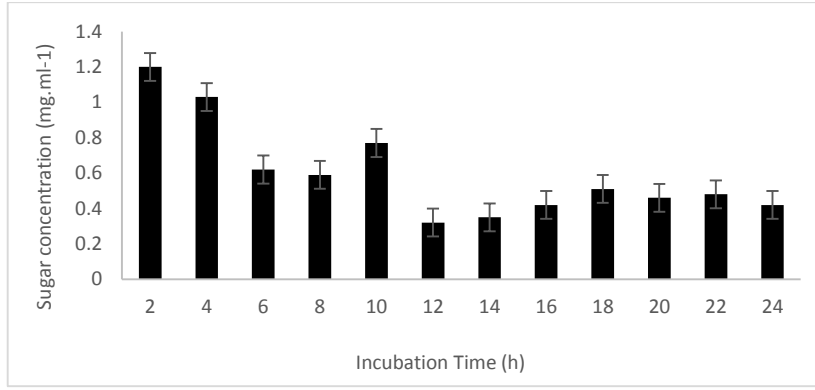

Fig. 5: The amount of sugar released during successive treatment of Woolworths paper with *T. viride* cellulase enzyme.

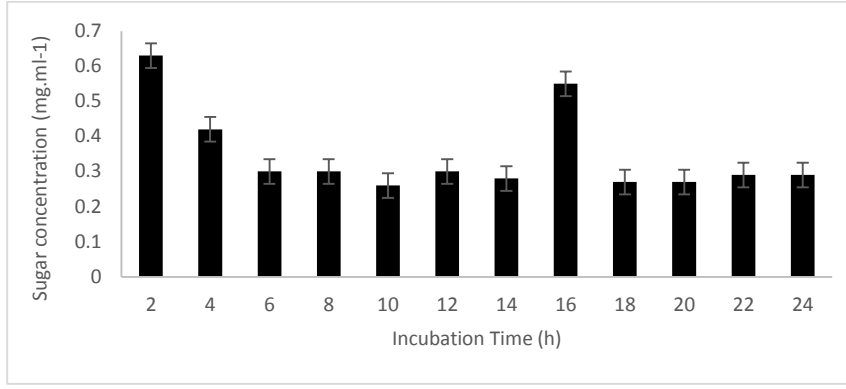

Fig. 6: The amount of sugar released during successive treatment of Pick 'n Pay paper with *T. viride* cellulase enzyme.

7th incubation period the amount of sugar produced stays constant at 0.3 mg.mL^{-1} with an increased amount of sugar produced during the 8th incubation period at a concentration of 0.6 mg.mL^{-1} while the decline in sugar production produced during the first three incubation period was calculated at -0.05 mg.mL^{-1}.h^{-1}. After the 8th incubation period, the sugars concentration produced during each incubation was almost identical at 0.3 mg.mL^{-1}.

The successive cellulase catalysed degradation of Pick 'n Pay advertising paper (Fig. 7) exhibited a sugar releasing pattern different to the patterns observed with other paper materials. Opposed to the other paper materials which

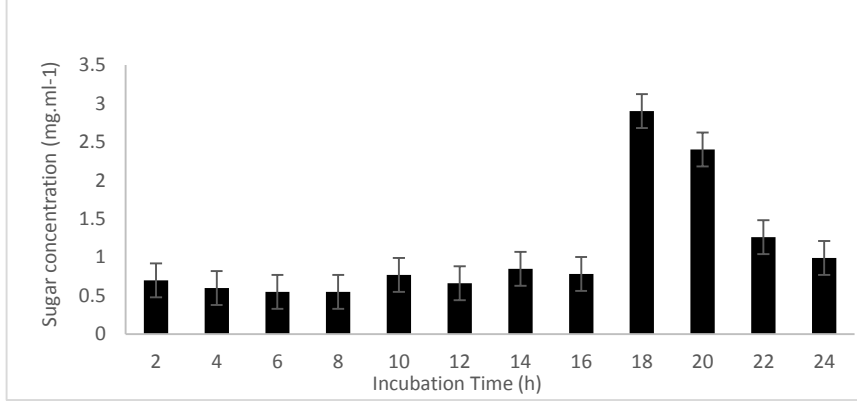

Fig. 7: The amount of sugar released during successive treatment of filter paper with *T. viride* cellulase enzyme.

resulted in maximum sugar production during the first two incubation periods, maximum sugar concentration released from Pick 'n Pay paper was observed during the ninth incubation period with the final incubation period producing more sugar than any of the first eight incubation periods. The amount of sugar produced during the first eight incubation periods varied between 0.44 $mg.mL^{-1}$ and 0.7 $mg.mL^{-1}$ while the highest sugar concentration of 2.9 $mg.mL^{-1}$ was obtained during the ninth incubation period.

From Table 1 it can be concluded that the highest total amount of sugar (13.1 mg) was released from filter paper during all 12 successive saccharification periods when degraded with *T. viride* cellulase. The second-highest amount of sugar was released from brown envelope paper at a mass of 11.5 mg, followed by office paper which degradation resulted in a mass of 9.0 mg sugar. The lowest mass of sugar production was released from Pick 'n Pay advertising paper which resulted in a mass of 4.2 mg. The average sugar concentration produced during the total degradation period follows the same tendency as the total masses of sugar released from various paper materials with the highest sugar concentration produced at a concentration of 1.09 $mg.mL^{-1}$ when filter paper was degraded and the lowest sugar concentration (0.35 $mg.mL^{-1}$) released from Pick 'n Pay advertising paper.

The percentage saccharification of the various paper materials is a way to compare the relative susceptibility of the paper materials to be degraded by *T. viride* cellulase. From the saccharification results presented in Table 1, it can be concluded that filter paper was the most effectively degraded when exposed to successive degradation followed by the newspaper, and foolscap paper. The paper material producing the least amount of sugar was Pick 'n Pay advertising paper resulting in 15 % degradation followed by brown envelope paper that was degraded to an extent of 17%. The observation that most of the paper materials produced a maximum amount of sugar during the first incubation period suggests that the amorphous section of cellulose (easily degradable) is more exposed to cellulase action (Hall et al. 2010, Beyene et al. 2017). After the first period of degradation, the relative amount of the crystalline section (difficult to degrade) has increased resulting in a lower degree of saccharification (Taherzadeh & Karimi 2008). The fact that Woolworths paper, Pick 'n Pay advertising paper and filter paper showed an increase in saccharification during the latter phases of degradation could be the result of the crystalline sections that were initially more exposed to the cellulase action with the amorphous cellulose becoming more available as the crystalline sections are hydrolysed.

The different sugar releasing patterns obtained during the cellulase catalysed bioconversion of seven different paper materials could be attributed to several factors such as the structural composition of the cellulase enzyme (Yang et al. 2011, Gandu et al. 2018), the chemical structure of the paper materials (Sahin & Arslan 2008) and additives, fillers and glaziers used as a part of the paper materials (Hubbe & Gill 2016).

With the annual global generation of solid waste reaching almost 20 billion tons and estimated amounts to be 27 billion tons by 2050, it is imperative that solid waste of which waste paper is a major component be considered as a possible feedstock rather than waste which has to be incinerated or be managed at dumping sites (Laurent et al. 2014). The waste

Table 1: Relative percentage saccharification of various paper materials when degraded with *T. viride* cellulase.

Paper material	Incubation period resulting in highest sugar concentration	Sugar concentration produced during incubation period resulting in maximum sugar concentration ($mg.mL^{-1}$)	Total sugar produced during 12 successive degradation periods (mg)	Average sugar concentration after 12 successive degradation periods ($mg.mL^{-1}$)	Mass of paper degraded (mg)	Percentage saccharification after 12 successive degradation periods (%)
Office paper	1	2.8	9.0	0.75	44	20
Foolscap paper	1	3.0	8.6	0.72	35	25
Brown Envelope Paper	1	3.3	11.5	0.95	66	17
Newspaper	1	1.5	8	0.66	28	28
Woolworths Advertising Paper	1	1.2	7.2	0.6	41	18
Pick 'n Pay Advertising Paper	1	0.6	4.25	0.35	28	15
Filter Paper	9	2.9	13.1	1.09	37	35

management change is already evident as the waste paper is investigated as a resource for the production of biomethane (Li et al. 2020, Takizana et al. 2019), nano-cellulose (Kumar et al. 2020, Putro et al. 2019), levulinic acid (Dutta et al. 2020) and bio-hydrogen (Poladyan et al. 2020). All these processes require the saccharification of the cellulose component of waste paper and thus it is one of the important observaitons of this study which illustrates the difference in sugar-producing profiles and sugar yields when bioconverted successively with fresh cellulase enzyme.

CONCLUSIONS

The increasing global population is producing more waste that needs to be managed to ensure a clean and healthy environment. Paper products are utilized by all global communities and it is a major component of solid waste with cellulose, a structural component of waste paper and glucose-based polymer also treated as waste as a result of traditional waste management procedures. Waste cellulose has the potential to be bio-converted into glucose a fermentable sugar through the catalytic action of cellulase, a hydrolytic enzyme. For the saccharification process to be more effective it is important that the waste bioconversion process is substrate specific as concluded from this investigation as each paper material exhibits a unique sugar releasing profile when bio-treated with cellulase enzymes. The successive treatment of cellulose relies on the continuous removal of glucose, a reaction product which limits the possibility of end-product inhibition and as a result the extent of the saccharification process. Results obtained from this investigation also suggests that different waste paper materials should be incubated separately with cellulase enzymes rather than a mixture of paper materials. It is also no guarantee that the degradation of a specific paper material will follow the same degradation pattern when exposed to other cellulase enzymes. The cellulase catalysed bioconversion of cellulose is an extremely complex procedure with a number of variables that should be optimized for maximally sugar production from the waste cellulose. Successive cellulase treatment of these waste materials is only a single hydrolytic factor that should be optimized for the effective degradation of waste cellulose materials.

REFERENCES

Alrumma, S.A. 2016. Enzymatic saccharification and fermentation of cellulosic date palm wastes to glucose and lactic acid. Braz. J. Microbiol., 4(1): 110-119.

Beyene, D., Chae, M., Dai, J., Danumah, C., Tosto, F., Demesa, A.G. and Bresler, D.A. 2017. Enzymatically-mediated co-production of cellulose nanocrystals and fermentable sugars. Crystals, 7(11): 322-328.

Canilha, L., Rodrigues, R.L.B., Antunes, F.A.F., Chandel, A.K., Milessi, T.S., Felipe, M.A. and Silverio DaSilva, S. 2013. Bioconversion of hemicellulose from sugarcane biomass into sustainable products. IntechOpen, 15-45.

Dutta, S., Yu, I.K.M., Tsang, D.C.W., Su, Z., Hu, C., Wu, K.C., Yip, A.C.K., Ok, Y.S. and Poon, C.S. 2020. Influence of green solvent on levulinic acid production from lignocellulosic paper waste. Bioresour. Technol., 298: 122544.

Gandu, M.L., Martin, C. and Jonsson, L.J. 2018. Analytical enzymatic saccharification of lignocellulosic biomass for conversion to biofuels and bio-based chemical. Energies, 11: 1-20.

Hall, M., Bansal, P., Lee, J.H., Realff, M.J. and Bommarius, A.S. 2010. Cellulose crystallinity-a key predictor of the enzymatic hydrolysis rate. FEBS J., 277: 1571-1582.

Hamelinck, C.N., Hooijdonk, G. and Faaij, A.P.C. 2005. Ethanol from lignocellulosic biomass: techno-economic performance in short-, middle- and long-term. Biomass and Bioenergy, 28: 384-410.

Hubbe, M.A. and Gill, R.A. 2016. Fillers for papermaking: A review of their properties, usage practices and their mechanistic role. Bioresources, 11(1): 2886-2963.

Jeoh, T., Wilson, D.B. and Walker, L.P., 2006. Effect of cellulase mole fraction and cellulose recalcitrance on synergism in cellulose hydrolysis and binding. Biotechnol. Prog., 22: 270-27.

Kim, E., Irwin, D.C., Walker, L.P. and Wilson D.B. 1998. Factorial optimization of a six-cellulase mixture. Biotechnol. Bioeng., 58: 494-501.

Kumar, V., Pathak, P. and Bhardwaj, N.K. 2020. Waste paper: An underutilized but promising source for nanocellulose mining. Waste Manage., 102: 208-303.

Laurent, A., Bakas, I., Clavreul, J., Bernstad, A., Niero, M., Gentil, M.Z. and Hauschild, T.H. 2014. Review of LCA studies of solid waste management system: Lessons learned and perspectives. Waste Manage., 34(3): 573-588.

Li, W., Khalid, F., Amin, F., Zhang, H., Dai, Z., Cheng, C. and Liu, G. 2020. Biomethane production characteristics, kinetic analysis, and energy potential of different paper wastes in aerobic digestion. Renew. Energy, In press.

Loelovich, M. 2014. Waste paper as a promising feedstock for production of biofuel. J. Sci. Res. Rep., 3(7): 905-917.

Mazzoli, R. 2012. Development of microorganisms for cellulose-biofuel consolidated bio-processings: Metabolic engineers' tricks. Computational and Structural. Biotechnol. J., 3(4): e201210007.

Miller, G.L. 1959. Use of dinitrosalicylic acid reagent for determination of reducing sugar. Anal. Chem., 31: 426-428.

Ndlovu, T.M. and Van Wyk, J.P.H. 2019. Relative saccharifiction of waste paper during successive treatment with garden snail (*Cornu aspersum*) cellulase. Sustain. Chem. Pharm., 11: 54-60.

Poladyan, A., Margaryan, L., Trchounian, K. and Trchounian, A. 2020. Biomass and biohydrogen production during dark fermentation of *Escherichia coli* using office paper waste and cardboard. Int. J. Hydrog. Energy, 45(1): 286-293.

Putro, J.N., Santoso, S.P., Soetaredja, F.E., Ismadji, S. and Ju, Y. 2019. Nanocrystalline cellulose from waste paper: Adsorbent for azo dyes removal. Environ. Nanotechnol. Monit. Manag., 12: Article 100260.

Rodriguez, C., Alaswad, A., Hassen, Z. and Olabi, A.G. 2017. Improvement of methane production from *P. canaliculata* through mechanical pretreatment. Renew. Energy, 119: 73-78.

Sahin, H.J. and Arslan, M.B. 2008. A study on physical and chemical properties of cellulose paper immersed in various solvent mixtures. Inter. J. Mol. Sci., 9(1): 78-88.

Saini, J.K., Saini, R. and Tewari, L. 2015. Lignocellulosic agriculture wastes as biomass feedstocks for second-generations bioethanol production: concepts and recent developments. 3 Biotech, 5: 337-353.

Seidl, P.R. and Goulart, A.K. 2016. Pretreatment processes for lignocellulosic biomass conversion to biofuels and bioproducts. Curr. Opin. Green Sustain. Chem., 2: 48-53.

Taherzadeh, M.J. and Karimi, K. 2008. Pretreatment of lignocellulosic wastes to improve ethanol and biogas production. Int. J. Mol. Sci., 9(9): 1621-1651.

Tahir, M., Hussain, T. and Behaylu, A. 2015. Scenario of present and future of solid waste generation in India: A case study of Delhi Mega City. J. Environ. Earth Sci., 5(8): 83-91.

Takizana, S., Baba, Y., Tada, C., Fuuda, Y and Nakai, Y. 2019. Preservation of rumen fluid for the pretreatment of waste paper to improve methane production. Waste Manage., 87: 672-678.

Van Wyk, J.P.H., Mogale, M.A. and Moroka, K.S. 1999. Bioconversion of waste paper materials to sugars: an application illustrating the environmental benefit of enzymes. Biochem. Educ., 27: 227-229.

Veluchamy, C., Raju, V.W. and Kalamdhad, A.S. 2017. Electrohydrolysis pretreatment for enhanced methane production from lignocellulose waste pulp and paper mill sludge and its kinetics. Biores. Technol., 252: 52-58.

Wu, C. and Cheng, C. 2005. A study of the hydrolysis of waste paper cellulose with a vertically hanging immobilized cellulase reactor and the reuse of the immobilized cellulase. J. Chin. Chem. Soc., 52: 85-95.

Yang, B., Dai, Z., Ding, S. and Wyman, C.E. 2011. Enzymatic hydrolysis of cellulosic biomass. Biofuels, 2(4): 421-450.

Nature Environment and Pollution Technology
An International Quarterly Scientific Journal

p-ISSN: 0972-6268
(Print copies up to 2016)
e-ISSN: 2395-3454

Vol. 20 | No.3 | pp. 1309-1313 | 2021

Original Research Paper

https://doi.org/10.46488/NEPT.2021.v20i03.043

Open Access Journal

Effect of Oxidation on the Formation of Disinfectant By-products of Low Molecular Weight Organic Matter

E. N. Hidayah*†, O. H. Cahyonugroho*, M. Mirwan*, R. B. Pachwarya and M. K. Asrori*****

*Department of Environmental Engineering, University of Pembangunan Nasional Veteran Jawa Timur, Surabaya, Indonesia

**Department of Chemistry, MNC, University of Delhi, New Delhi, India

***Department of Environmental Science, University of Pembangunan Nasional Veteran Jawa Timur, Surabaya, Indonesia

†Corresponding author: E.N. Hidayah; euisnh.tl@upnjatim.ac.id

Nat. Env. & Poll. Tech.
Website: www.neptjournal.com

Received: 14-09-2020
Revised: 07-12-2020
Accepted: 12-12-2020

Key Words:
Organic compounds
Total organic carbon
Oxidation
Disinfection by-products

ABSTRACT

Some natural organic compounds (NOC) such as aromatic compounds can trigger the formation of disinfection by-products (DBPs). In chlorination (disinfectant) process resultant water quality depletes. Some safe alternative oxidants are needed for cleaning water pollutants. $KMnO_4$ had shown better oxidation results, especially for reducing aromatic and non-aromatic organic compounds present in water. The aim of this study was to analyze the effect of $KMnO_4$ and $Ca(OCl)_2$ oxidants on the concentration of high and low molecular weight organic matter including aromatic compounds in the water sample. In this experiment, artificial organic compounds, namely sinapic acid (high molecular weight aromatic compound) and resorcinol (low molecular weight aromatic compound) were used to identify the characteristic of organic matter under different molecular weights. Sinapic acid and resorcinol were oxidized by using $KMnO_4$ and $Ca(OCl)_2$ with a minimum contact time of 60 minutes. Samples were analyzed for aromatic contents and total organic carbon (TOC) before and after completion of the experiment by using UV-Vis spectrophotometer at 254 nm wavelength (UV_{254}). It has been observed that both oxidants increased TOC concentration. $Ca(OCl)_2$ produces a higher percentage of organic matter degradation by-products (DBPs) such as chloroform ($CHCl_3$) a highly toxic compound than $KMnO_4$. Since $Ca(OCl)_2$ has a higher oxidation potential than $KMnO_4$. It has been observed that $KMnO_4$ is a safer oxidant than Ca(OCl)2 as potassium permanganate produces less amount of DBPs.

INTRODUCTION

Some natural organic matter (NOM) are present in water bodies in abundant amount. Generally, these organic compounds are a mixture of different kinds of organic matter. These organic compounds commonly originate from animals, plants, microorganisms and other dead biomes, and their degradation or oxidation products (Baghoth 2011). The presence of NOM contaminant in water causes many problems in the treatment processes, such as de-coloration, unpleasant odor removal, corrosion inhibition, coagulation process, oxidation, absorption, adsorption and membrane filtration process, and also on some oxidation of byproducts of disinfectants in water (Edzwald & Tobiason 2011). Generally, in water treatment processes, the disinfection reaction using chloride containing disinfectants is considered essential. When the NOM polluted water undergoes chlorination, some active chlorine compounds react with NOM to produce chlorinated disinfection by-products some of them are also toxic in nature like the generation of chloroform ($CHCl_3$). Some researchers have determined that higher levels of organic matter in water sources during the disinfection process also increases the number of carcinogenic compounds in the treated water (Bond et al. 2012). According to that information, it is necessary to think about the use of alternative oxidants or materials to eliminate NOM of water, such as (O_3) ozone, ClO_2, and $KMnO_4$ (Hidayah et al. 2017). Such Oxidation treatment improves water quality and reduces biological growth. Based on previous studies, it is stated that organic matter in raw water must be characterized for better understanding and its effects in water treatment (Sillanpaa et al. 2015). Therefore, synthetic organic materials (sinapic acid and resorcinol) is used for the experiment to represent organic matter, because of their similarity and properties to natural organic matter. In addition, of the above reasons, it has been known that the physical and chemical properties of these compounds are of paramount importance for different types of analyses. Therefore, characterization of changing of organic matter was easily identified during the experimental processes (Sillan-

paa et al. 2015). The synthetic organic materials having low molecular weights were selected for experimental purposes. It is a known fact that organic aromatic substances produce some carcinogenic byproducts when they react with improper oxidants (Bond et al. 2009). Such situation causes other issues in water treatment and byproduct has shown a harmful effect on the health of living things and environment (Hidayah et al. 2017). After going through many previous experimental results related to oxidative degradation of organic compounds and its by-products, this study was aimed to analyze the effect of $KMnO_4$ and $Ca(OCl)_2$ oxidants on the formation of disinfection by-products (DBPs) of sinapic acid and resorcinol under different sets of experimental conditions.

MATERIALS AND METHODS

Synthetic organic matters i.e. sinapic acid (molecular formula $C_{11}H_{12}O_5$, molecular weight 224.21 g/mol) 10 mg/L and resorcinol (molecular formula $C_6H_6O_2$, molecular weight 110.1 g/mol) 10 mg/L were used for experimental purposes, as shown in Fig. 1.

Initially, $KMnO_4$ oxidants were selected for experimental purpose, under different amounts of $KMnO_4$ oxidant 0.5; 1; 1.5; 2 mg/L and $Ca(OCl)_2$ oxidant 20; 30; 40; 50 mg/L during experiments. Synthetic organic compounds i.e. sinapic acid and resorcinol have been mixed with oxidants in a batch process pattern, all the samples were stirred for 60 minutes at 90 rpm. Periodically samples were taken from experimental setup to determine the concentration of organic matter in terms of TOC by UV-Visible spectrophotometer at 254 nm, and concentration of disinfection by-products i.e. trichloromethanes ($CHCl_3$) also known as (THMs). (Hidayah et al. 2018, APHA 2012).

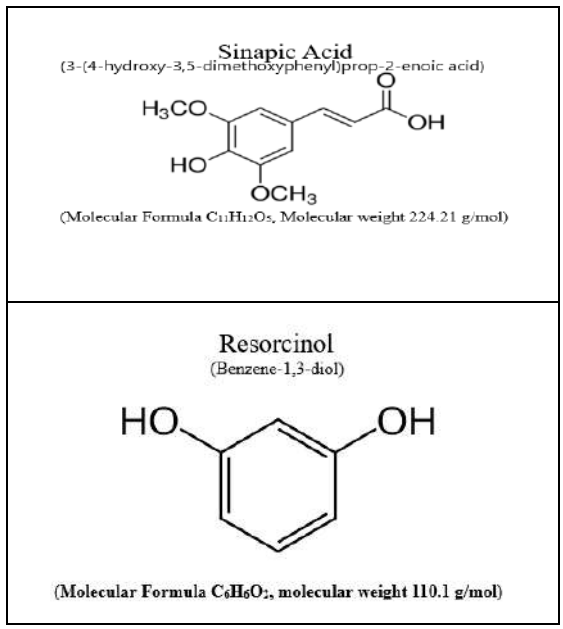

Fig. 1: Molecular formula sinapic acid and resorcinol.

RESULTS AND DISCUSSION

It is shown in Fig. 2 and Fig. 3, that 0.5 mg/L amount of $KMnO_4$ oxidant, increased TOC of degradation sample i.e. sinapic acid as the absorbance value decreased to 0.055 cm^{-1}. It indicated that aromatics organic compounds had degraded and non-aromatic compounds were present in more quantity resultant TOC of degradation sample of sinapic acid was incensed. Concentration of TOC in treated sample of resorcinol was increased as the absorbance value decreased to 0.008 cm^{-1}. it indicates that aromatic organic compounds were degraded. It is conjectured that the dominant compounds in resorcinol degradation sample when used 0.5 mg/L amount of $KMnO_4$ was non aromatic. Furthermore, this study has observed that 1.0 mg/L amount of $KMnO_4$ for oxidation of sinapic acid shown higher absorbance value and it was increased by 0.271 cm^{-1}. It has been conjectured with more quantity of aromatic compounds in treated sample when TOC was decreased. Meanwhile, this study found that absorbance value for resorcinol was also increased to 0.13 cm^{-1} when TOC decreased. It indicates the presence of aromatic compounds in treated samples of resorcinol as well as in the sinapic acid. When using 1.5 mg/L amounts of $KMnO_4$, sinapic acid and resorcinol both have shown a decrease in absorbance values i.e. 0.087 cm^{-1} and 0.016 cm^{-1}, respectively. This indicates the decrease of aromatic compounds in the treated sample. Lower absorbance UV absorbance at 254 nm means that after oxidation sinapic acid and resorcinol samples passes non aromatic compounds predominantly. When using 2 mg/L of $KMnO_4$ oxidant for sinapic acid and resorcinol, the absorbance value of the treated organic material sample was less than the untreated samples, it indicates that TOC increased in the treated samples and non-aromatic compounds were more dominant in the treated samples of sinapic acid and resorcinol then the untreated samples. When using 2 mg/L amount of permanganate for oxidation of sinapic acid and resorcinol the absorbance value (UV_{254}) of the treated organic material sample was less than the untreated samples, indicates more TOC with the domination of non-aromatic compounds in treated samples.

The effect of chlorine oxidant under dosage 20 mg/L of $Ca(OCl)_2$ for oxidation of sinapic acid indicated an absorption value of treated samples was 0.174 cm^{-1} less than the untreated samples. In addition, all the samples have been measured for UV-Visible spectrophotometer at 254 nm (UV_{254}). Decrease of absorbance value indicates that

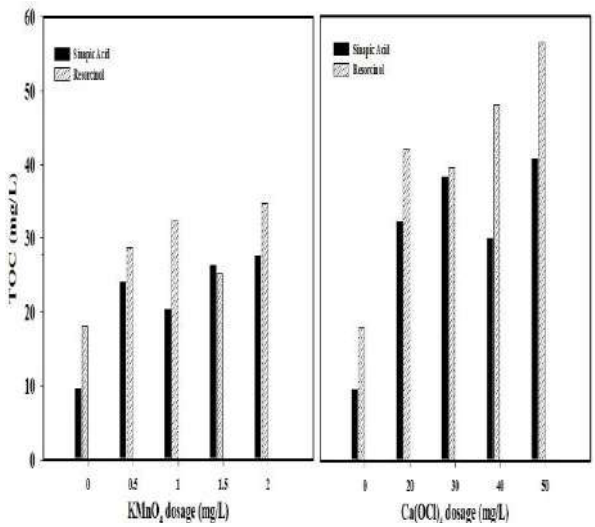

Fig. 2: Concentration of TOC in different low molecular weight under different dosage of oxidants.

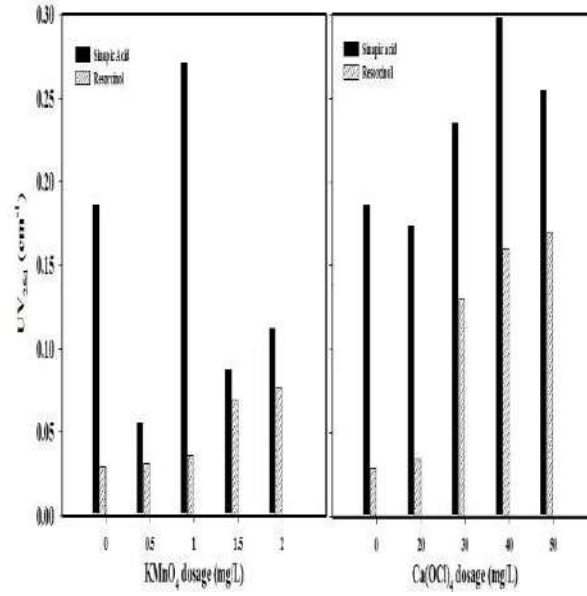

Fig. 3: Concentration of UV254 in different low molecular weight under different dosage of oxidants.

aromatic organic compounds are present in less quantity in treated samples as compared to the untreated samples. The results found that TOC increased, it indicates that the non-aromatic organic matter was present in more quantity in treated samples as compared to the untreated samples of sinapic acid.

Meanwhile, this study revealed that the treated sample of resorcinol shows a slight increase in the absorbance value i.e. 0.031 cm^{-1} higher than the untreated sample. It indicates the presence of aromatic organic matter in domination than the non-aromatic organic matter. This study also found less TOC value (treated sample) which indicates less amount of non-aromatic organic matter in the treated sample. Using 30 mg/L of $Ca(OCl)_2$ oxidant for sinapic acid, the result showed that TOC value was decreased, which indicates that quantity of non-aromatic matter was less in the treated sample as compared to the untreated sample. This study also observed TOC of the treated sample which was less than the untreated sample has shown that aromatic compounds are more dominant in the treated samples. When using 30 mg/L of $Ca(OCl)_2$ oxidant for resorcinol, the absorbance value (UV-254 nm) increased slightly by 0.036 cm^{-1} which indicates that the dominant compound was aromatic in the treated samples. The TOC value also increased slightly. Next, using 40 mg/L of $Ca(OCl)_2$ for sinapic acid has indicated of increase in absorbance value to 0.302 cm^{-1}, which means that the increase in organic carbon in with domination of aromatic matter, The increased TOC value also indicate higher organic matter. Using 40 mg/L of $Ca(OCl)_2$ for resorcinol, the absorbance value increased by 0.069 cm^{-1}, while the TOC value decreased, indicating that the aromatic organic matter was dominant than the non-aromatic organic matter. Furthermore, using 50 mg/L of $Ca(OCl)_2$ oxidant for sinapic acid, it has shown absorbance shifted toward lower value and absorbance decrease by 0.255 cm^{-1} but the TOC value increased, Both results indicated that the non-aromatic compounds were dominant over aromatic organic matter. TOC also increased due to the conversion of aromatic organic matter into non-aromatic organic matter. Then this study observed the effect of 50 mg/L of $Ca(OCl)_2$ on resorcinol, the absorbance value UV 254nm increased to 0.076 cm^{-1} and the TOC value also increased, it might be indicated that the aromatic organic matter was in domination over non-aromatic organic compounds. TOC vale also increased indicates that some aromatic organic matter was converted into simpler organic molecules.

Overall, Fig.2 shows the concentration of TOC for sinapic acid and resorcinol after oxidation under a variation amount of oxidants $KMnO_4$ and $Ca(OCl)_2$. Firstly, the effect of 0.5 mg/L amount of $KMnO_4$ oxidant on sinapic acid and resorcinol has been observed, and the results showed that both sinapic acid and resorcinol show higher TOC values i.e. 32.4 mg/L and 42 mg/L respectively. This study found that increasing the amount of oxidants ($KMnO_4$ and $Ca(OCl)_2$), the organic carbon values also increased such as changes in organic carbon value, observed in terms of organic carbon and aromatic organic carbon matter. These changes in higher organic carbon, TOC may be a result of the oxidation process which may have destroyed the organic layer of the surface of particles (Xie et al. 2013, Xie et al. 2016).

Secondly, this study has observed that TOC of resorcinol oxidation increased slightly higher than the sinapic acid oxidation, whether this study used $KMnO_4$ or $Ca(OCl)_2$ oxidations. From the above observations, it seems that the lower molecular weight of resorcinol may be one reason for its easier oxidation than organic matter having a higher molecular weight (Bond et al. 2012). Lower molecular weight organic matter influences the increase of organic matter. It may be due to an increase in the amount of degraded organic carbon.

Thirdly, $Ca(OCl)_2$ oxidant has a higher concentration of TOC than $KMnO_4$ under different amounts. It is a well-known fact that both $Ca(OCl)_2$ and $KMnO_4$ are considered strong oxidants. $Ca(OCl)_2$ has a higher reduction potential than $KMnO_4$. Further, it is also found that $Ca(OCl)_2$ oxidized more organic matter into organic by-products. Fig. 3 shows variations in the concentration of aromatic matter (UV-254 nm absorption) in treated samples of sinapic acid and resorcinol with different amounts of $KMnO_4$ and $Ca(OCl)_2$. It also shows similar changing trends with TOC concentration. Oxidation of aromatic and non-aromatic organic matter is generally a process of breaking down bigger organic molecules into smaller molecules by interaction and /or association with oxidants. The basic principle of oxidation by using $KMnO_4$ is the same as the oxidation process in disinfection. Basically, the oxidation aim was to remove the organic substances from the polluted water whether in pretreatment, or a post-treatment process to reduce the formation of organic by-products (DBPs) (Xie et al. 2016, Edzwald & Tobiason 2011).

Fig.4 shows the changes in concentration of trichloromethane or chloroform ($CHCl_3$). It has been observed that the concentration of $CHCl_3$ increased with the increased amount of oxidant. Chlorine or $Ca(OCl)_2$ oxidant contributes a higher percentage of chloroform ($CHCl_3$) concentration. This study revealed that increasing TOC was in accordance with increasing $CHCl_3$ concentration. These results clearly show that organic matter is a precursor for the formation of the disinfectant by-products (DBPs), in terms of $CHCl_3$ as shown in this study.

This study conjectures that different oxidants have different capacities to oxidize organic matter: to break the organic coating, to degrade aromatic and non-aromatic compounds, to degrade the organic carbon chain, and conversion of other organic matter. Previous studies had shown that increasing TOC concentration is in accordance with increasing $CHCl_3$ concentration (Hidayah et al. 2018). It has been also observed that the addition of chlorine oxidant into the treatment of samples gives a higher concentration of TOC, aromatic organic matter than permanganate, because chlorine has a higher electro volt value i.e. 1.482 V than permanganate 0.60 V (Xie et al. 2016). On the basis of different experiments, this study can say that the application of permanganate $KMnO_4$ as an oxidant is safer than chlorine $Ca(OCl)_2$.

CONCLUSION

This study concludes that $KMnO_4$ as an oxidant is safer than $Ca(OCl)_2$ oxidant. These oxidants are capable to convert aromatic organic compounds such as sinapic acid, resorcinol (experimental compounds), and other organic matter into lower molecular weight organic compounds. Degradation or oxidation of organic matter (aromatic and non-aromatic) was observed in terms of increasing the concentration of TOC. This study found the changing concentration of aromatic compounds, total organic compounds, and the formation of DBPs as indicated by the concentration of chloroform. This study conjectured that different oxidants have different capacities to oxidize organic matter, to break the organic coating, and to degrade aromatic organic molecules, the organic carbon chain. After long observation, this study concluded that permanganate ($KMnO_4$) oxidant is a much safer oxidant

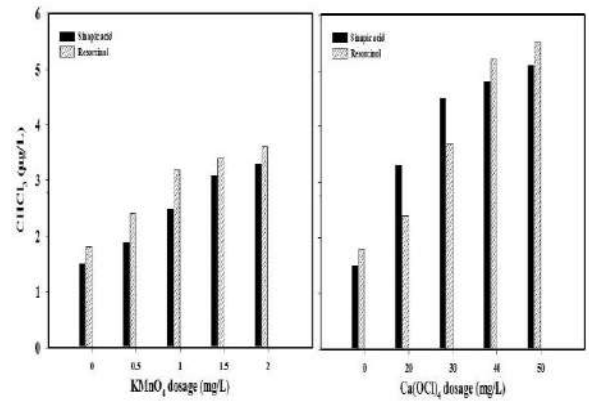

Fig.4: Concentration of $CHCl_3$ in different low molecular weight under different dosage of oxidants.

than chlorine ($Ca(OCl)_2$). $KMnO_4$ oxidant generates fewer amounts of disinfection by-products such as ($CHCl_3$) and many other DBPs.

ACKNOWLEDGEMENT

This study was a part of funding supported by advanced basic research grants from Research Institutions and Community Service, Universitas Pembangunan Nasional Veteran Jawa Timur. This research accordance with contract no. SPP/90/UN.63.8/LT/VII/2020.

REFERENCES

APHA, AWWA, WEF. 2012. Standard Methods for the Examination of Water and Wastewaters, 21th ed., American Public Health Association: Washington, D.C.

Baghoth, S.A., Sharma, S.K. and Amy, G.L. 2011. Tracking natural organic matter (NOM) in a drinking water treatment plant using fluorescence excitation-emission matrices and PARAFAC. Water Research, 45:797-809.

Bond, T., Henriet, O., Goslan, E.H., Parsons, S.A. and Jefferson, B. 2009. Disinfection by-product formation behavior of natural organic matter surrogates. Environmental Science and Technology, 43:5982-5989.

Bond, T., Templeton, M. R. and Graham, N. 2012. Precursors of nitrogenous disinfection by-products in drinking water: a critical review and analysis. Journal of Hazardous Materials, 235-236:1-16.

Edzwald, J.K. and Tobiason, J.E. (ed.) 2011. Chemical Principles, Source Water Composition, and Watershed Protection. In Water Quality & Treatment: A Handbook on Drinking Water. AWWA McGraw-Hill, New York, pp. 1-76.

Hidayah, E.N., Chou, Y. C., and Yeh, H. H. 2017. Comparison between HPSEC-OCD and F-EEMs for assessing DBPs formation in water. J. Environ. Sci. Health Part A., 52 (4): 391-402.

Hidayah, E.N., Agripina, A.T., Cahyonugroho, O.H. 2018. Effect of preoxidant on the chaning of low molecular weight of natural organic matter, International Seminar of Research Month, Science and Technology for People Empowerment, NST Proceeding, Volume 2018.

Sillanpää, M., Matilainen, A. and Lahtinen, T. (ed.) 2015. Characterization of NOM. In Natural Organic Matter in Water: Characterization and Treatment Method, Butterworth-Heinemann, Oxford, pp. 17–53.

Xie, P., Ma, J., Fang, J., Guan, Y., Yue, S., Li, X. and Chen, L. 2013. Comparison of permanganate preoxidation and preozonation on algae containing water: cell integrity, characteristics, and chlorinated disinfection byproduct formation. Environ. Sci. Technol, 47(24):14051–14061.

Xie, P., Chen, Y., Ma, J., Zhang, X., Zou, J. and Wang Z. 2016. A mini review of peroxidation to improve coagulation. Chemosphere, 155:550-563.

Nature Environment and Pollution Technology
An International Quarterly Scientific Journal

p-ISSN: 0972-6268
(Print copies up to 2016)
e-ISSN: 2395-3454

Vol. 20 | No.3 | pp. 1315-1321 | 2021

Original Research Paper

https://doi.org/10.46488/NEPT.2021.v20i03.044

Open Access Journal

Study of Change in Physico-Chemical Parameters by Treatment of Sludge from Common Effluent Treatment Plant (CETP) with Earthworms

S. Maheshwari†*, P. Kriplani*, A. S. Jethoo, P. Kumar** and M. Khwairakpam*****
*Department of Chemistry, Govt. Women Engineering College Ajmer-305002, Rajasthan, India
**Department of Civil Engineering, Malaviya National Institute of Technology, Jaipur-302017, Rajasthan, India
***Department of Civil Engineering, National Institute of Technology, Meghalaya-793003, India
Corresponding author: S. Maheshwari; seemamaheshwari@gweca.ac.in

Nat. Env. & Poll. Tech.
Website: www.neptjournal.com

Received: 22-10-2020
Revised: 20-11-2020
Accepted: 09-01-2021

Key Words:
Common effluent treatment plant sludge
Eudrilus eugeniae
Vermicompost
Cow dung
Sawdust
Total nitrogen
Phosphorus

ABSTRACT

One of the most vital problems of environmental protection concern is that of solid waste disposal. This problem continues to grow with the growth of population and the development of industries. The Common Effluent Treatment Plant (CETP) already establishes itself as a service to society at large, contributing towards a cleaner environment. However, the inappropriate disposal of CETP's hazardous sludge can cause serious environmental problems. The sludge if sent for landfilling may cause groundwater contamination, changing the soil fertility parameters as well. The research presented here is carried out to explore the ability of an epigeic earthworm *Eudrilus eugeniae* to transform the sludge produced from CETP into a value-added product i.e., vermicompost. In this study, six samples of feed mixture were used with different ratios of CETP sludge, cow dung, and sawdust. Physico-chemical parameters such as pH, Electrical Conductivity (EC), Volatile Solids (VS), Total Nitrogen (TN), Nitrate Nitrogen (NO_3^--N), Ammonium Nitrogen (NH_4^+-N) were characterized to analyze the quality of the compost formed. All these parameters are in the agreement with recommended standards of mature compost. The result shows that vermicomposting technique when used, epigeic earthworm *Eudrilus eugeniae* can work as a favorable alternative solution for the disposal of CETP sludge.

INTRODUCTION

Over the last few years, the problem of efficient disposal and management of organic solid wastes has become more rigorous due to the rapid increase in population, intensive agriculture, and industrialization. To maintain a cleaner environment, waste disposal has become an issue of vital importance. Due to rapid industrialization and urbanization, the consumption of water also increases resulting in the generation of a large quantity of wastewater (Suthar 2012, Tchobanoglous et al. 1993). The effluent treatment plants are good alternatives as they include the physical, chemical, and biological processes for the treatment of wastewater discharged from the industries and commercial complexes. Wastewater contains dissolved organic compounds which get suspended during primary and secondary treatment of wastewater generating sludge (Bantacut & Aulia 2019). In recent years, the methodology of sludge management has shifted from conventional methods such as incineration and landfill to the recent concept of sludge-conversion into nutrient-rich products (Maheshwari et al. 2019). Although various physical, chemical, and microbiological methods of disposal of organic solid waste are currently in use, these methods are time-consuming and costly. In this context, vermicomposting is an eco-friendly technology for the conversion of various kinds of organic waste into vermicompost. It is a biological process in which earthworms are introduced in the sludge to convert the organic wastes into humus-like material known as vermicompost. Epigeic earthworm species are able to consume different types of organic wastes which include sewage sludge, industrial sludge, animal dung, agricultural residues, household wastes, and industrial waste (Yadav & Garg 2009). According to a group of researchers (Dominguez & Edwards 1997, Saradha 1997), vermicomposting is mesophilic (10-32°C) and it involves the combined synergetic action of earthworm and microorganism for decomposition of waste and produces nutrient-rich compost. Vermicomposting of industrial sludge was carried out by decomposition of solid textile mill sludge (STMS) mixed with poultry droppings by using epigeic earthworm *Eisenia fetida*. (Kaushik & Garg 2004, Lee 1992, Neuhauser et al. 1998, Reinecke et al. 1992). A group of researchers (Edwards 1999, Edwards & Arancon 2004, Elvira et al. 1996) explained the bioconversion of solid paper-pulp mill sludge and primary sewage sludge with earthworms *E. andrei*. The results indicated that the loss of total carbohydrate was higher in the presence of earthworms (80%) than in their

absence (72%). Begum and Harikrishna (2010) studied the growth of *E. fetida* and decomposition of municipal sewage sludge for a period of 60 days (Begam & Harikrishna 2010, Bishop & Godfrey 1983, Canelles et al. 2002, Edward 1995). A six-month pilot-scale study was carried out on vermicomposting of sludge from paper mill using earthworm species *E. andrei*. The vermicompost obtained at the end of the experiment was rich in nutrients like nitrogen, phosphorus, potassium and had good water holding capacity, high humic acid content, and low levels of heavy metals. (Elvira et al. 1997, Garg & Kaushik 2005, Hemalatha 2012, Kalamdhad et al. 2012). Although some of the work has been explored on vermicomposting of sewage sludge and different industrial sludge like textile mill sludge, pulp, and paper mill sludge, food industry sludge, and distillery sludge using different earthworm species (Atiyeh et al. 2002, ROU 2007, Selladurai et al. 2009, Sinha et al. 2008, Yadav & Garg 2011). The study of vermicomposting of CETP sludge is still in infancy, so the purpose of the present work is the production of stabilized, matured compost by using CETP sludge and to evaluate physico-chemical and stability parameters of industrial solid waste.

MATERIALS AND METHODS

Earthworm species *Eudrilus eugeniae* was selected for this study because *E. eugeniae* is a major waste eater and biodegrading earthworm species. Earthworm species used in this study were collected from Morarka Organic Food Ltd. Jaipur Rajasthan. The bulking agent sawdust was collected from a woodshop and cow dung collected from the H-Quarters at MNIT Jaipur. CETP sludge was collected from CETP Bhiwadi District Alwar Rajasthan. (Fig. 1).

The experimental work was carried out with a different percentage of compost material i.e. CETP sludge, cow dung, and sawdust using earthworm species *E. eugeniae* (Fig. 2). The initial parameters of different ingredients for composting of sludge with sawdust and cow dung with different combinations are given in Table 1 and different percentages of compost material i.e. CETP sludge, cow dung, and sawdust is given in Table 2.

The objective of this study was to identify the most suitable combination of sludge, cow dung, and sawdust using earthworm species *E. eugeniae*. The experiment was conducted in a plastic container with a capacity of 20 L. 20 holes along the circumference and 15 holes (0.5 cm diameter) at the bottom of the container were drilled to provide aeration and drainage. Reactors containing different percentages of sludge, cow dung, and sawdust were kept at room temperature. Each reactor was inoculated with earthworm biomass of 100gm. The moisture content of feed in each reactor was maintained at 60-80%, throughout the study period by the sprinkling of an adequate quantity of water. Separate reactors were placed with the same conditions and combination of material but without earthworm to evaluate the efficiency of the process.

Sampling and Sample Analysis

About 150 g of homogenized wet samples of the feedstock was analyzed before the start of the experiment referred to as zero-day, then samples were analyzed after every six days interval. The zero-day refers to the substrate taken out before earthworm inoculation. Sample analysis was carried out at PHE Laboratory, civil engineering department MNIT Jaipur and Agricultural Research lab Durgapura Jaipur. The physico-chemical and biological parameters were analyzed, by the methods described in the standard methods for the examination of wastewater (APHA, AWWA & WEF 1999).

Fig. 1: CETP sludge storage site at CETP Bhiwadi.

Physico-Chemical Analysis

Various physico-chemical studies have been carried out such as pH, electrical conductivity (EC), volatile solids (VS), Total Nitrogen (TN), Nitrate nitrogen (NO_3^--N), Ammonium nitrogen (NH_4^+-N), etc. After the completion of the vermicomposting process, earthworm biomass was measured. The earthworms were separated from the compost by putting compost in sunlight for few minutes. The earthworms tend to move downwards away from the sunlight towards the bottom. When most of the earthworms move down, the upper compost free from earthworms was separated. Later on, a small part of compost with earthworm remained, which was separated by hand sorting method.

Vermireactors with Different Feed Mixture Percentage

R1 Vermicomposting of Sludge with Cow dung (CD) and Sawdust (SD) (80:20:00)

R2 Vermicomposting of Sludge with Cow dung (CD) and Sawdust (SD) (50:50:00)

R3 Vermicomposting of Sludge with Cow dung (CD) and Sawdust (SD) (50:25:25)

R4 Vermicomposting of Sludge with Cow dung (CD) and Sawdust (SD) (70:30:00)

Table 1: Initial Characteristics of Waste Material

Parameters	Sludge	Cow Dung	Saw Dust
pH	8.44	8.3	6.95
E.C.(mS/cm)	2.73	1.01	0.83
TKN(%)	1.22	1.56	0.89
NH_4-N(g/Kg)	0.092	0.158	0.041
NO_3-N(g/Kg)	0.877	0.332	0.121
TN(g/Kg)	13.08	15.93	9.02

R5 Vermicomposting of Sludge with Cow dung (CD) and Sawdust (SD) (40:40:20)

R6 Vermicomposting of Sludge with Cow dung (CD) and Sawdust (SD) (30:30:40)

Each Reactor contained a Control (i.e. CR)

RESULTS AND DISCUSSION

pH

The variations of pH in all the six vermireactors during the period of 24 days of vermicomposting are shown in Fig. 3 (with worms) and Fig. 4 (without worms). There is an initial increase in all vermireactors namely R1, R2, R3, R4, R5, R6 and decreased in the later phase of composting. The initial increase in pH means the participation of microbes in the degradation representing aerobic metabolism which produces the basic hydroxides and subsequent increase in pH in the initial phase of decomposition. In all the vermireactor initially, pH increased up to 6 days except R6 in which pH increased up to 12 days and later on starts decreasing. The reduction of pH in vermireactors was observed more than their controls. This could be because earthworm guts release

Table 2: Different percentage of compost material i.e. CETP sludge, cow dung, and sawdust (in brackets indicates the percentage content in initial feed mixer)

Vermireactors	CETP Sludge(kg)	Cow dung (Kg)	Saw dust (kg)
R1	1.2(80)	0.3(20)	0(0)
R2	0.75(50)	0.75(50)	0(0)
R3	0.75(50)	0.375(25)	0.375(25)
R4	1.05(70)	0.45(30)	0(0)
R5	0.60(40)	0.60(40)	0.30(20)
R6	0.525(35)	0.525(35)	0.45(30)

Fig. 2: Vermicompost reactors used in the experiment.

the neutral pH. The pH in vermireactor R2 was observed at 7.35 near-neutral pH as compared to all vermireactors and their controls (without worms).

Electrical Conductivity (EC)

Electrical conductivity is the ability to carry an electrical charge, a measure of the soluble salt content of vermicompost. EC value reflects the degree of salinity during composting, indicating its possible phytotoxicity effects on the growth of plants if applied to the soil. The variations of EC in different vermireactors during the period of 24 days of vermicomposting are illustrated in Fig. 5 (with worms) and Fig. 6 (without worms). Initially increase in EC was observed up to the 18th day with its subsequent decrease. The increase in EC is due to the degradation of organic matter, releasing minerals such as Ca, Mg, K, and P is available from. The decrease of EC in the later phase of composting is due to the precipitation of mineral salts. The highest EC was observed in vermireactor R2 among all the vermireactors. The augmentation in EC was more in vermireactors (with worms) than the control (without worms).

Total Nitrogen (TN)

Total nitrogen content was increased throughout the vermicomposting period as shown in Fig. 7 (with worms) and Fig. 8 (without worms). Initial total nitrogen values were 14.33 g.kg^{-1}, 18.44 g.kg^{-1}, 12.86 g.kg^{-1}, 14.35 g.kg^{-1}, 12.89 g.kg^{-1}, 11.47 g.kg^{-1} in vermireactors R1, R2, R3, R4, R5, R6 respectively. After 24 day of vermicomposting, total nitrogen content values were 25.34 g.kg^{-1}, 36.72 g.kg^{-1}, 24.12 g.kg^{-1}, 21.38 g.kg^{-1}, 22.75 g.kg^{-1}, 18.56 g.kg^{-1} in vermireactors R1, R2, R3, R4, R5 and R6 respectively. According to Bishop and Godfrey (1983), nitrogen-fixing bacteria might have also contributed to the increase in TN in the later stage of composting. It is suggested that along with N release from compost material, earthworms increase nitrogen levels by releasing mucus and by accumulating excretory products, body fluids, and other biological fluids rich in nitrogen. Decaying tissues of dead worms is yet another factor for TN to hike to a significant amount. The highest total nitrogen was observed in vermireactors R2 in 24 days of vermicomposting.

Ammonium Nitrogen (NH_4^+ N)

Ammonium concentration is an important indicator of compost stability and maturity. Mostly, ammonium nitrogen present during aerobic composting was derived from the rapid decomposition of waste. When ammonium concentration decreases and nitrate appears in composting material, it is considered ready to be used as compost. It has been noted that the absence or decrease in NH_4^+ N is an indicator of a high-quality composting process (Hirai et al. 1983).

The ammonium nitrogen concentrations decrease in both vermireactors with worms and without worms throughout the period of experimentation as shown in Fig. 9 and Fig. 10 respectively. The maximum decrease in ammonium nitrogen concentration was observed in vermireactor R4 from the initial level of 0.202 g.kg^{-1} to 0.0796 g.kg^{-1} and the minimum decrease was observed in vermireactor R1 from an initial level of 0.0693 g.kg^{-1} to 0.0336 g.kg^{-1}. The concentration of ammonium nitrogen decreases due to its conversion to nitrate nitrogen. Yadav and Garg (2009) reported that decreasing ammonium nitrogen concentration is due to Nitrate Nitrogen formation and volatilization as ammonia at high pH.

Nitrate Nitrogen (NO_3^--N)

During composting, nitrate nitrogen increases regularly due to the conversion of ammonium nitrogen into nitrate nitrogen

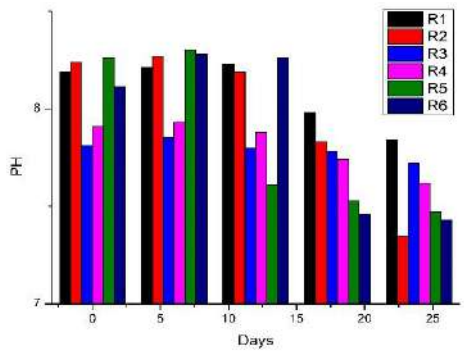

Fig. 3: Variation of pH in vermireactors (with worms).

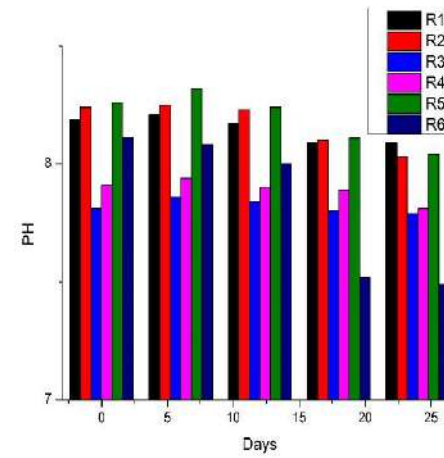

Fig. 4: Variation of pH in vermireactors (without worms).

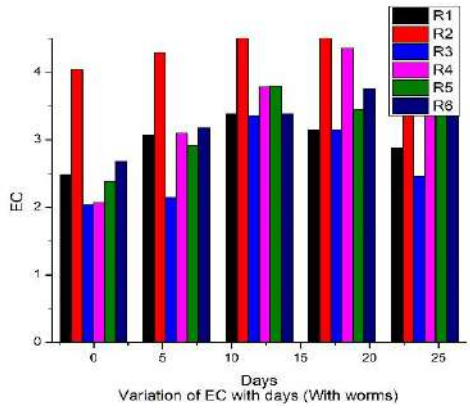

Fig. 5: Variation of electrical conductivity in vermireactors (with worms).

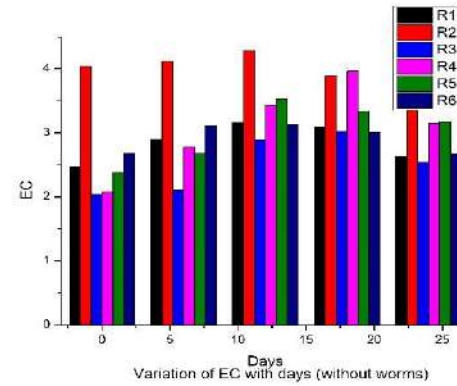

Fig. 6: Variation of electrical conductivity in vermireactors (without worms).

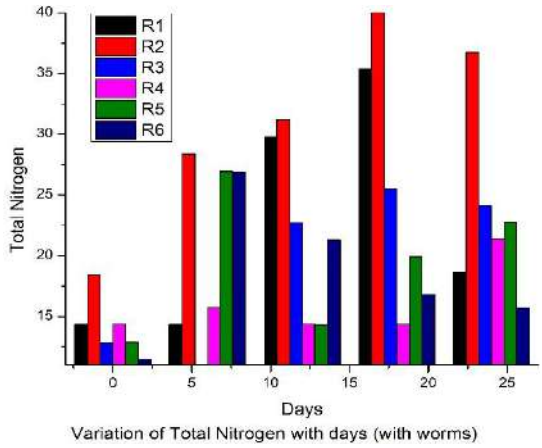

Fig. 7: Variation of TN in vermireactors (with worms).

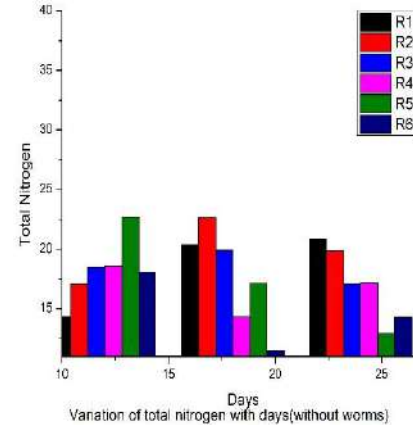

Fig. 8: Variation of TN in vermireactors (without worms).

and is a limiting factor in assessing compost maturity. The variation of nitrate nitrogen concentrations with and without worms along with the period of 24 days is shown in Fig. 11 and 12. Nitrate nitrogen increase in all vermireactors with an increase in the vermicomposting period. The highest nitrate nitrogen concentration was observed in R2 (0.5823 $g.kg^{-1}$) in 24 days of composting. So, it can be predicted that R2 showed better quality compost with the higher NO_3^--N content (Fig. 11).

Phosphorus

In this study, the available phosphorus was observed to increase as vermicomposting proceeds as shown in Fig. 13 (with worms) and Fig. 14 (without worms). An increase in phosphorus during vermicomposting was probably through mineralization and mobilization of phosphorous by the bacterial and fecal phosphatase activity of earthworms. Kaushik and Garg (2004) recorded a significant increase in total phosphorus and available-P after composting textile mill sludge blended with cow dung and agricultural residues for 11 weeks. Phosphorus content was observed to increase in all vermireactors as vermicomposting proceeds. The highest phosphorus was observed in vermireactor R2.

Earthworm Biomass

The overall earthworm biomass showed a decline in 24 days of vermicomposting of CETP sludge with cow dung and sawdust. The vermireactor R1, R2, R4 contain the mixture of sludge and cow dung while vermireactor R3, R5, R6 contain the mixture of sludge, cow dung, and sawdust. The maximum earthworm biomass reduction was observed in vermireactor R1 which contains 8020% of sludge and cow dung. Earthworm biomass decreased in feed mixtures as sawdust proportion increases. The minimum earthworm biomass reduction was observed in vermireactor R2 which contains 5050% of sludge and cow dung respectively. The vermireactors which contain a mixture of sludge, cow dung, and sawdust show a more reduction in earthworm biomass as

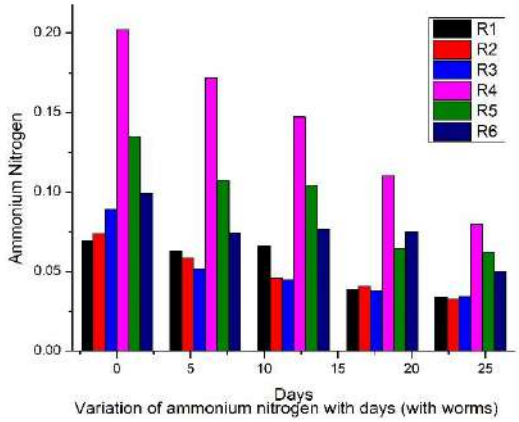

Fig. 9: Variation of NH_4^+-N in vermireactors (with worms).

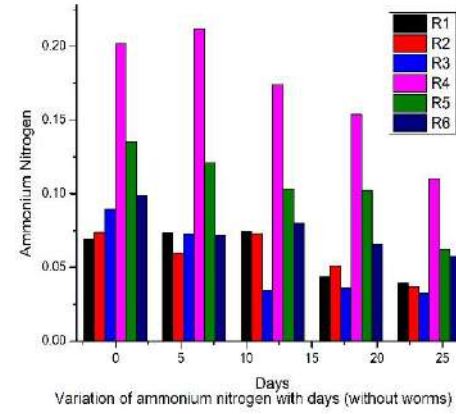

Fig. 10: Variation of NH_4^+-N in vermireactors (without worms).

compared to the vermireactors which contain the mixture of sludge and cow dung except for vermireactor R1.

CONCLUSIONS

The experimental results clearly indicate that vermicomposting may be used as a suitable technique to transform the sludge produced from a common effluent treatment plant. Physico-chemical analysis of compost of various parameters like pH, EC, total nitrogen, ammonium nitrogen, nitrate nitrogen, and phosphorus agreed with recommended standards. As ammonium concentration decreases and nitrate appears in

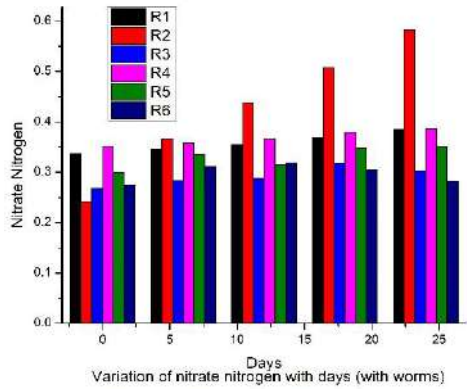

Fig. 11: Variation of NO_3^+-N in vermireactors (with worms).

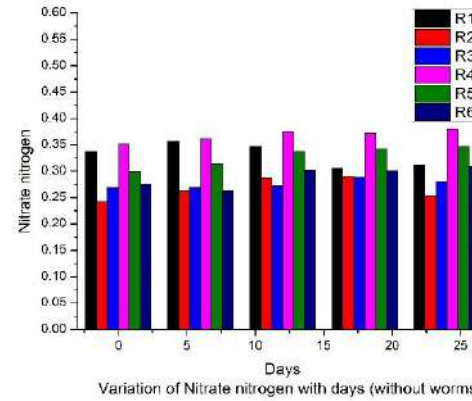

Fig. 12: Variation of NO_3^+-N in vermireactors (without worms).

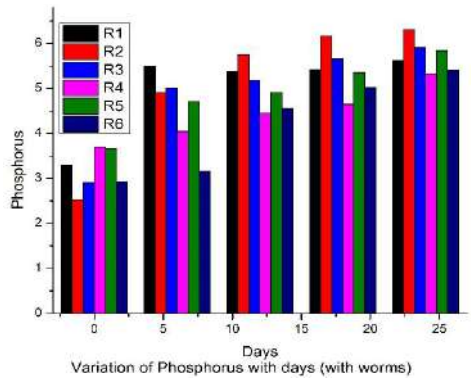

Fig. 13: Variation of phosphorus in vermireactors (with worms).

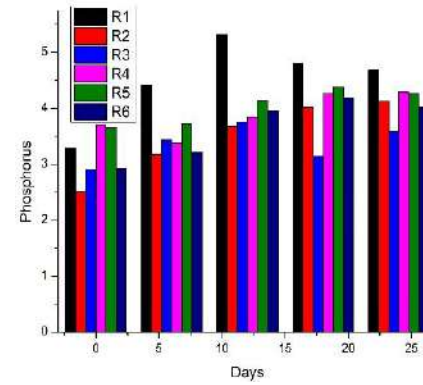

Fig. 14: Variation of phosphorus in vermireactors (without worms).

composting material, it is considered to be used as suitable compost. The vermicomposting of CETP sludge produced a good quality of compost with 1.14 % to 1.84 % total nitrogen and 0.0541% to 0.063% phosphorus content. The maximum total nitrogen and maximum phosphorus content were observed in vermireactor R2. The values of all the studied parameters were found higher in vermireactors with worms in comparison to vermireactors without worms. The earthworm biomass was observed to decrease in all vermireactors due to the hazardous nature of sludge. The minimum reduction was observed in vermireactor R2 which contains 50% sludge and 50% cow dung, and maximum reduction was observed in vermireactor R1 which contains 80 % sludge and 20 % cow dung. So, it is concluded that based on physico-chemical parameters, vermicomposting of sludge produced from CETP is a more efficient method than the traditional composting techniques.

ACKNOWLEDGMENT

The authors are thankful to Director Malaviya National Institute of Technology Jaipur India for providing necessary research facilities.

REFERENCES

APHA, AWWA, and WEF 1999. Standard Method for the Examination of Water and Waste Water. Washington DC, 20th edition

Atiyeh, R.M., Lee, S., Edwards, C.A., Arancon, N.Q. and Metzger, J.D. 2002.The influence of humic acids derived from earthworm-processed organic wastes on plant growth. Bioresour. Technol., 84(1): 7-14.

Bantacut, T. and Aulia, A.N. 2019. Assessment of chemical oxygen demand balance for energy harvesting in sugar mills wastewater treatment. Nat. Env. & Pol. Tech., 18(2): 413-423.

Begam, A. and Harikrishna 2010. Management of municipal sewage sludge by vermicomposting technique. Int. J. Chem. Technol. Res., 2(3): 1521-1525.

Bishop, P.L. and Godfrey, C. 1983. Nitrogen transformations during sludge composting. Biocycle, 24: 34-39.

Canelles, L.P., Olivares, F.L., Okorokova-Facanha, A.L. and Facanha, A.R. 2002. Humic acids isolated from earthworm compost enhance root elongation, lateral reemergence, and plasma membrane H^+ATPase activity in maize roots. Plant Physiol., 130: 1951-1957.

Dominguez, J. and Edwards, C.A. 1997. Effects of stocking rate and moisture content on the growth and maturation of *Eisenia andrei* (Oligochaeta) in pig manure. Soil Biol. Biochem., 29: 743-746.

Edwards, C.A. 1995. Historical overview of vermicomposting. Bio Cycle, 36(6): 56-58.

Edwards, C.A. 1999. Interview with Dr. Clive Edwards-part two. Casting Call, 4(2): 3-7.

Edwards, C.A. and Arancon, N.Q. 2004. Interactions among organic matter, earthworms, and microorganisms in promoting plant growth. In Magd, F. and Weil, R. (eds) Agro Ecosystems. CRC Press, Boca Raton, pp. 327-376.

Elvira, C., Goicoechea, M., Sampdro, L., Mato, S. and Nogales, R.1996. Bioconversion of solid paper-pulp mill sludge by earthworms. Bioresour. Technol., 75: 173-177.

Elvira, C. Sampedro, L., Benftez, E. and Nogales, R. 1997. Vermicomposting of sludges from the paper mill and dairy industries with *Eisenia andrei* a pilot-scale study. Bioresour. Technol. 63: 205-211.

Garg, V.K. and Kaushik, P. 2005. Vermistabilization of textile mill sludge spiked with poultry droppings by an epigeic earthworm *Eisenia fetida*. Bioresour. Technol., 96(9): 1063-1071.

Hirai, M. F., Chanyasak, V. and Kubota, H. 1983. A standard measurement for compost maturity. Biocycle, 24: 54-56.

Hemalatha, B. 2012. Vermicomposting of fruit waste and industrial sludge. Int. J. Adv. Eng. Technol., 3(2): 60-63.

Kalamdhad, A.S., Khwairakpam, M. and Kazmi, A.A. 2012. Drum composting of municipal solid waste. Environ. Technol., 33(3): 299-306.

Kaushik, P. and Garg, V.K. 2004. Dynamics of biological and chemical parameters during vermin-composting of solid textile mill sludge mixed with cow dung and agricultural residues. Bioresour. Technol., 94, 203-209.

Lee, K.E. 1992. Some trends opportunities in earthworm research or Darwin's children. The future of our discipline. Soil Biol. Biochem., 24: 1765-1771.

Maheshwari, S.M., Jethoo A.S., Vishvakarma, V.K., Khwairakpam, M. and Kriplani, P. 2019. Biodegradation of sludge produced from common effluent treatment plant (CETP) using drum composting technique. Nat. Environ. Pollut. Technol., 18(1): 231-236.

Neuhauser, E.F., Loehr, R.C. and Malecki, M.R. 1988. The potential of earthworms for managing sewage sludge. In: Edwards, C.A., and Neuhauser, E.F. (eds) Earthworms in Waste and Environmental Management. SPB Academic Publishing BV, The Hague, pp. 9-20.

Reinecke, A.J., Viljoen, S.A. and Saayman, R.J. 1992. The suitability of *Eudrilus eugeniae, Perionyx excavatus,* and *Eisenia fetida* (Oligochaeta) for vermicomposting in southern Africa in terms of their temperature requirements. Soil Biol. Biochem., 24(12): 1295-1307.

ROU, 2007. Literature Review of Worms in Waste Management: Recycled Organics Unit (Vol. 1. 2nd ed.). The University of New South Wales, Sydney, Australia.

Saradha, T. 1997. The culture of earthworms in the mixture of pond soil and leaf litter and analysis of vermifertilizer. J. Ecobiol., 9(3): 185-188.

Selladurai, G., Anbusaravanan, N., Prakash Shyam, K., Palanivel, K. and Kadalmani, K. 2009. Advances in Environ. Biol., 3(3): 278-284.

Sinha, R.K., Bharambe, G. and Chaudhari, U. 2008. Sewage treatment by Vermi filtration with the synchronous treatment of sludge by earthworms: A low-cost sustainable technology over conventional systems with potential for decentralization. The Environmentalist, 28: 409-420.

Suthar, S. 2009. Vermistabilization of municipal sewage sludge amended with sugarcane trash using epigeic *Esenia fetida* (Oligochaeta). J. Hazard. Mater., 163(1): 199-206

Tchobanoglous, G., Theisen, H. and Vigil, S. 1993. Integrated Solid Waste Management Engineering: Principles and Management Issues. McGraw Hill, Inc., New York.

Yadav, A. and Garg, V.K. 2009. Feasibility of nutrient recovery from industrial sludge by vermicomposting technology. J. Hazard. Mater. 168: 262-268.

Yadav, A. and Garg, V.K. 2011. Industrial waste and sludge management by vermicomposting. Rev. Environ. Sci. Biotechnol., 10(3): 243-276.

Nature Environment and Pollution Technology
An International Quarterly Scientific Journal

p-ISSN: 0972-6268
(Print copies up to 2016)
e-ISSN: 2395-3454

Vol. 20 | No.3 | pp. 1323-1329 | 2021

Original Research Paper

https://doi.org/10.46488/NEPT.2021.v20i03.045

Open Access Journal

Impact of Organic and Inorganic Fertilizers on Morphological and Biochemical Components of *Arachis hypogaea* L.

T. Azhaguthasan*, T. Ravimycin*† and K. Santhi**
*Department of Botany, Annamalai University, Annamalai Nagar, Chidambaram-608 002, Tamil Nadu, India
**Thiruvannamalai Arts and Science College, Thiruvannamalai, Tamil Nadu, India
†Corresponding author: T. Ravimycin; drmycin@gmail.com

Nat. Env. & Poll. Tech.
Website: www.neptjournal.com

Received: 29-12-2020
Revised: 26-02-2021
Accepted: 26-04-2021

Key Words:
Biochemical constituents
Fertilizers
Growth
Arachis hypogaea L.

ABSTRACT

The present investigation aims to study the comparative effect of different treatments of organic and inorganic fertilizers on the growth and biochemical constituents of groundnut (*Arachis hypogaea* L.). The plants were raised in the field with different treatments of fertilizers like arbuscular mycorrhizal fungi (AMF), *Azospirillum* (AZM), market waste compost (MWC), nitrogen (N), phosphorus (P) and potassium (K). The plant samples were collected after 15, 30, 60 and 90 days for the measurement of different growth parameters. The analysis of the morphological and biochemical parameters such as shoot and root length, fresh and dry weight, total leaf area, chlorophyll 'a' and 'b', total chlorophyll, amino acids, starch and total sugar was made at different days intervals. The effect of organic and inorganic fertilizers on growth parameters and biochemical constituents of leaves was significantly increased in all the treatments. In general, bio-fertilizer applications are to boost the effectiveness of Arbuscular Mycorrhizal Fungi (AMF), *Azospirillum* (AZM) and market waste compost (MWC) on nodulation and yield of groundnut. The organic fertilizers treated plants showed better performance than the inorganic fertilizers and control.

INTRODUCTION

Groundnut (*Arachis hypogaea* L.) is a leguminous plant and used for human consumption all over the world. It is the most significant oil crop and requires a suitable amount of plant nutrients at the correct instant for healthier yield and quality (Thayamini 2018). Consequently, the utilization of element fertilizers has concerned the insubstantial environmental balance of the soil, polluted groundwater, developed resistant races of pathogens and increased human healthiness risks. Chemical pollutants are exceedingly dispersed in the atmosphere and cause severe harm to human health, soil as well as the atmosphere (Ignacimuthu et al. 2007).

The residual toxicities of chemical fertilizers pretense the problem of environmental pollution and reduction of essential nutrients due to random use of inorganic fertilizers which cause a severe hazard to the sustainability of crop invention. Intended for constant groundnut production, the present farming demand integrated use of organic and inorganic fertilizers beside the bio-fertilizers. Arbuscular mycorrhizal fungi (AMF) are among the most general soil fungi and the mass of plant species has associations with AMF species. Therefore, it becomes essential to explore the most effective combination of inorganic fertilizers and bio-fertilizers for sustaining soil fertility and producing quality products. The bio-fertilizers, besides providing a good substrate for crop growth, facilitate the propagation of beneficial microbes in soil and also provide a residual effect for ensuing crops. These inoculants aid in gathering nutrient demands of crops through proper nitrogen fixation by increasing nodulation and solubilization of insoluble phosphorus and extend the nutrient absorption to inaccessible zones. In the present investigation, the effect of bio-fertilizers and inorganic fertilizers on the growth and biochemical components of groundnut have been studied.

MATERIALS AND METHODS

Experimental Site

The study was conducted as a field experiment at Botanical Garden, Department of Botany, Annamalai University, Tamil Nadu, India.

Cultivar

The seeds of groundnut (*Arachis hypogaea* L.) var. VRI 2 were procured from the Regional Research Station of Tamil Nadu Agricultural University, Virudhachalam, Cuddalore District, Tamil Nadu, India.

Methods

The experiment was conducted in randomized block design with five replication treatments. The treatments were

T1- Control, T2- Arbuscular Mycorrhizal Fungi (AMF), T3-*Azospirillum* (AZM), T4- Market waste compost (MWC), T5- AMF+AZM+MWC, T6- Nitrogen (N), T7- Phosphorus (P), T8- Potassium (K), and T9- N+P+K. The garden soil and selected groundnut seeds were sown in the field irrigated with normal tap water and maintained as the control. Various growth and biochemical parameters were recorded after 15, 30, 60 and 90th days.

Fertilizers

The AM Fungi (*Glomus fasciculatum*) and *Azospirillum* were collected from the Department of Microbiology, Tamil Nadu Agricultural University (TNAU), Coimbatore, Tamil Nadu, India. Raw organic materials like vegetable wastage enhance their suitability for application to the soil as a fertilizer resource, after having undergone composting.

Morphological and Biochemical Studies

The morphological studies were carried on the shoot and root length, fresh and dry weight and total leaf area. The following methods were used for the estimation of chlorophyll (Sadasivam & Manickam 1996), total free amino acids (Moore & Stein 1948), Starch (Summer & Somers 1949) and total sugar (Nelson 1944).

Statistical Studies

Statistical analysis of experimental results was carried out by SPSS version 16.0 (Two-way ANOVA). All the data were taken as a mean of five replications. The level of significance was calculated at $P \leq 0.05\%$.

RESULTS AND DISCUSSION

The effect of organic and inorganic fertilizers on the shoot and root length was observed and given in Figs. 1 and 2. Both the fertilizer treatments had shown a significant improvement on shoot and root length of groundnut. The highest shoot length was observed at (T5) treatment (68.3 cm/plant) followed by T9 (65.8 cm/plant) on the 90th day. A similar trend was noticed in root length of the groundnut on all the sampling days. In general, the application of bio-fertilizers treatments improves plant growth. Improvement of plant growth was significantly found by the application of both organic and inorganic fertilizers as source of mineral nutrition. Mineralization process of the organic substances releases the nutrient elements which leads to plant growth. Bio-fertilizers release nutrients more slowly but store them longer in the soil (Ayoola & Makinde et al. 2009). The nutrients from organic fertilizers support rapid root development (Baldi et al. 2010), which may have enhanced plant growth towards the end of plant life. Availability of organic substances, besides contributes to crop growth and yield directly by supplying nutrients and indirectly by modifying soil physical properties such as stability of aggregates and porosity that can improve the root growth rhizosphere and stimulate plant growth (Goss et al. 2013). Plant growth is influenced by nitrogen, phosphorus and potassium. Nitrogen as a component of chlorophyll, division and enlargement of cells in the apical meristem, the activity of the apical meristem generates the shoot growth that affects the increase of plant height.

The effect of organic and inorganic fertilizers on the fresh and dry weight is presented in Figs. 3 and 4. All the treated plants showed a stimulatory effect on the fresh and dry weight of groundnut over control. The highest fresh weight was observed at combined treatments of organic compost T5 (66.88 g/plant) followed by combined treatments of inorganic fertilizers T9 (54.76 g/plant). A similar trend was noticed in dry weight on the groundnut on all the interval days. Among the treatments, combined treatment was found to be more effective.

Under the application of both the fertilizers, the leaf area of the plant was increased with increasing treatment on all the sampling days. The leaf area was more in bio-fertilizer treatments as compared to inorganic fertilizer. The increased fresh and dry weights of plants could increase the chance for nutrient uptake throughout the highest exploitation of soil. Similar results found by Youssef et al. (2004) clearly indicate that the application of bio-fertilizers in *Calendula officinallis* and *Matricaria recutita* increased the plant growth and dry weight of shoot in the medicinal plants. The increase in leaf area could be due to the increase in the water content of the leaves and the presence of organic and inorganic nutrients.

The effect of bio-fertilizers and inorganic fertilizers treatments on parameters such as chlorophyll ‘a’ and ‘b’, total chlorophyll, total free amino acids, starch and total sugar content of leaves at different stages of the interval is represented in Figs. 6-11. Both the treatments had a significant effect on all the biochemical parameters and photosynthetic pigments when compared to the control plants. Chlorophyll ‘a’ was always higher than the chlorophyll ‘b’ in all the fertilizer treatments. Among the organic fertilizer treatments, the highest total chlorophyll content was observed in combined treatment T5 (2.04 mg/g fr.wt.) followed by T1, T2, T3 and T4 at 60 days. Moreover, fertilizers application, in addition, affects the accumulation of macro aggregate protected carbon and nitrogen. The application of only organic fertilizer, without the inorganic fertilizers, could not supply adequate nutrients that are responsible for chlorophyll synthesis. A high amount of total chlorophyll is necessary to sustain photosynthetic pigments and synthesize the enzymes resulting in increased growth and yield of groundnut plants (Ghosh et al. 2004). The addition of NPK nutrients can raise plant growth

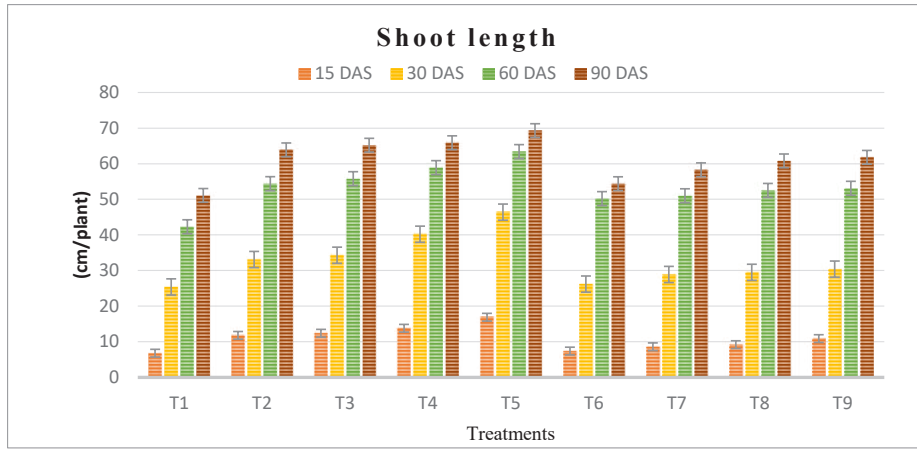

Fig. 1: The effect of organic and inorganic fertilizers on shoot length (cm/plant) of groundnut.

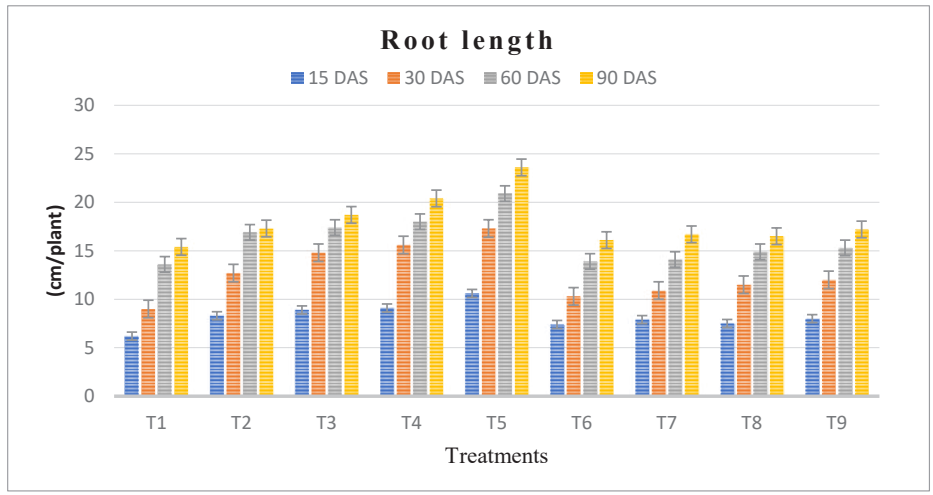

Fig. 2: The effect of organic and inorganic fertilizers on root length (cm/plant) of groundnut.

and production because these elements can stimulate roots, toughen plant stems and increase photosynthesis rates (Ayissa & Kebebe 2011). Similar, results were found in maize and Sorghum plants (Amujoyegbe et al. 2007).

A significant difference in total free amino acid content was observed in both the treatments when compared to the control. Among the organic fertilizer treatments, the highest amino acid content was observed in combined treatment T5 (8.86 mg/g fr.wt.) followed by T1, T2, T3 and T4 on the 60th day. While, among the inorganic fertilizer treatment, the combined treatment T9 showed the highest value when compared to individual treatments. Amino acid is the monomer of protein, the regular preserved food material insincere by plant system. It may be ascribed to increased nitrogen uptake of leaves due to the combined inoculation of bio-fertilizers. Since, bio-fertilizers support phytohormones manufacturing, which stimulates nutrient absorption as well as photosynthesis process, as a result of this amino acids content increases (Naser et al. 2016). Similar findings of the increasing trend in amino acids due to fertilizer application were reported in *Albizia lebbek* (Kumudha & Gomathinayagam 2007) and maize (Tejeda et al. 2008). In addition, amino acids may play an important role in plant metabolism and protein assimilation which is necessary for cell formation and consequently increase in fresh and dry matter (Nagwa et al. 2020).

The starch content in leaf of groundnut treated with organic and inorganic fertilizers also showed a significant difference. The highest starch content was observed in combined treatments on the 90th day. Among the organic fertilizer treatments, the highest sugar content was observed in combined treatment T5 (7.96 mg/g fr.wt.) followed by T1, T2, T3 and T4 on the 90th day. In both the treatments,

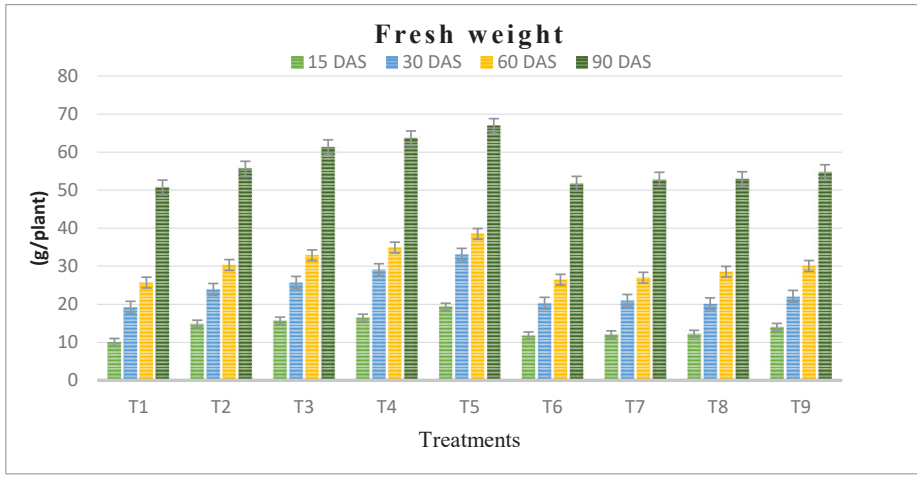

Fig. 3: The effect of organic and inorganic fertilizers on fresh weight (g/plant) of groundnut.

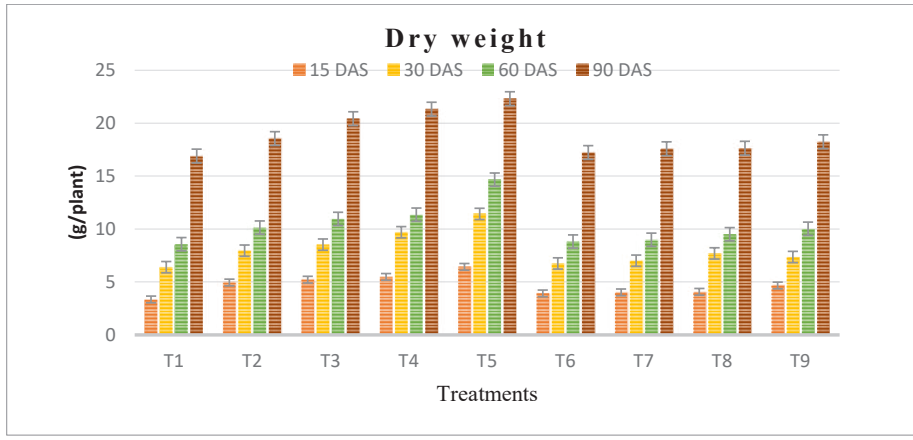

Fig. 4: The effect of organic and inorganic fertilizers on dry weight (g/plant) of groundnut.

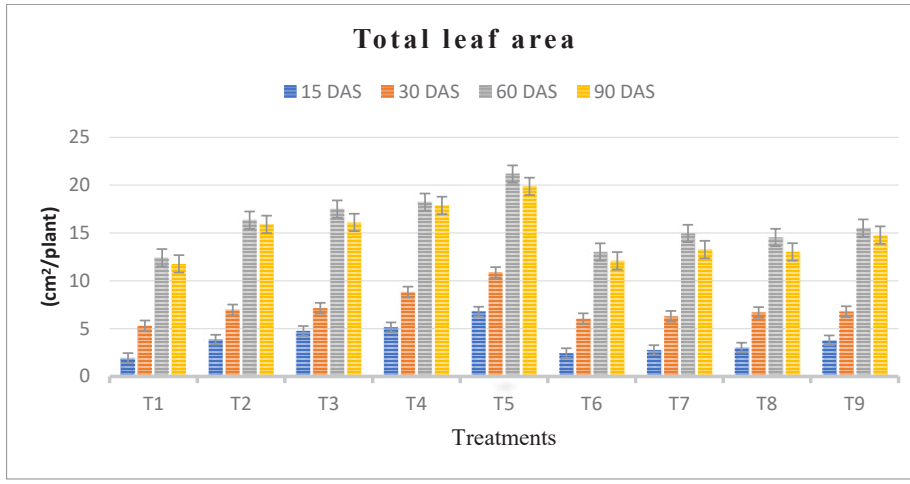

Fig. 5: The effect of organic and inorganic fertilizers on total leaf area (cm2/plant) of groundnut.

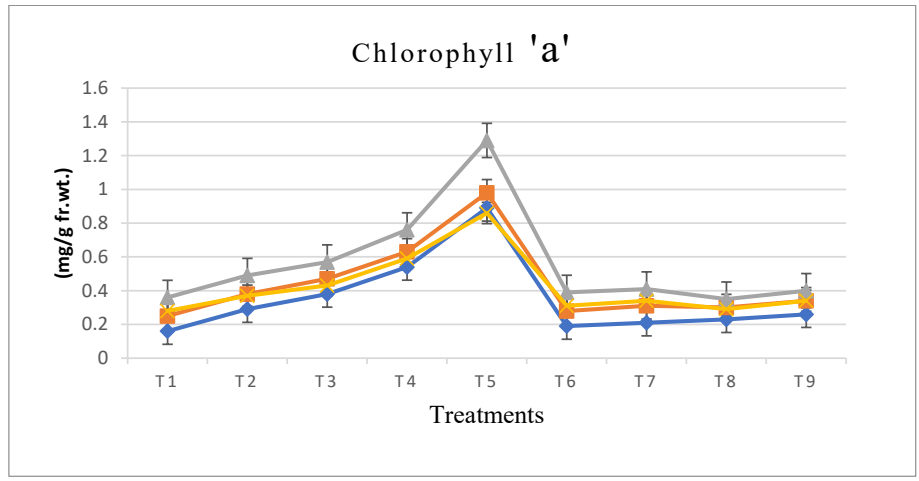

Fig. 6: The effect of organic and inorganic fertilizers on chlorophyll 'a' content (mg/g fr.wt.) of groundnut.

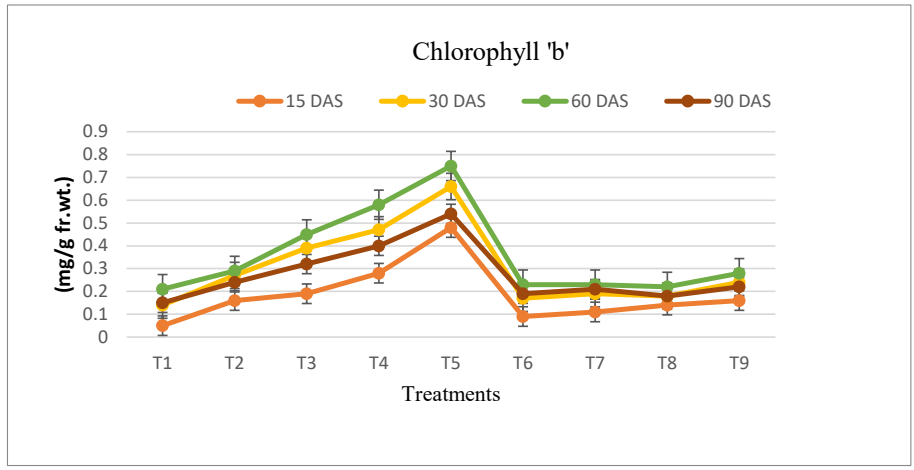

Fig. 7: The effect of organic and inorganic fertilizers on chlorophyll 'b' content (mg/g fr.wt.) of groundnut.

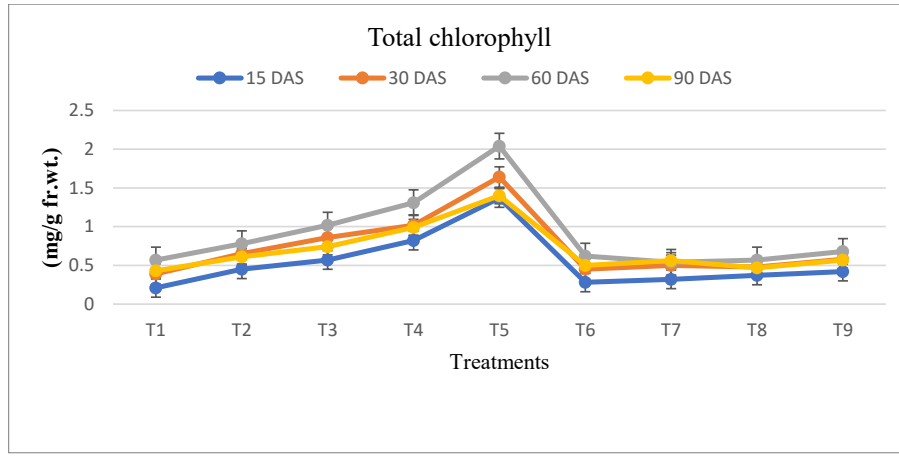

Fig. 8: The effect of organic and inorganic fertilizers on total chlorophyll contents (mg/g fr.wt.) of groundnut.

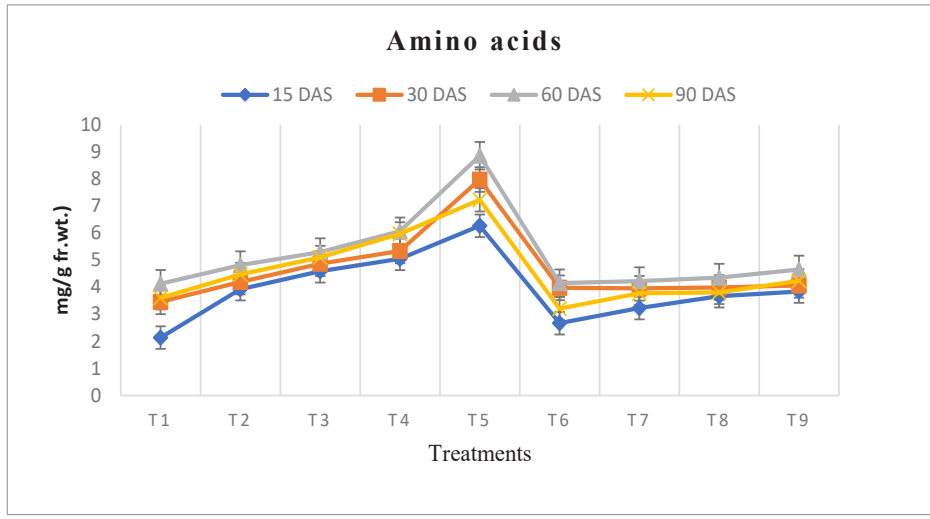

Fig. 9: The effect of organic and inorganic fertilizers on amino acid contents (mg/g fr.wt.) of groundnut.

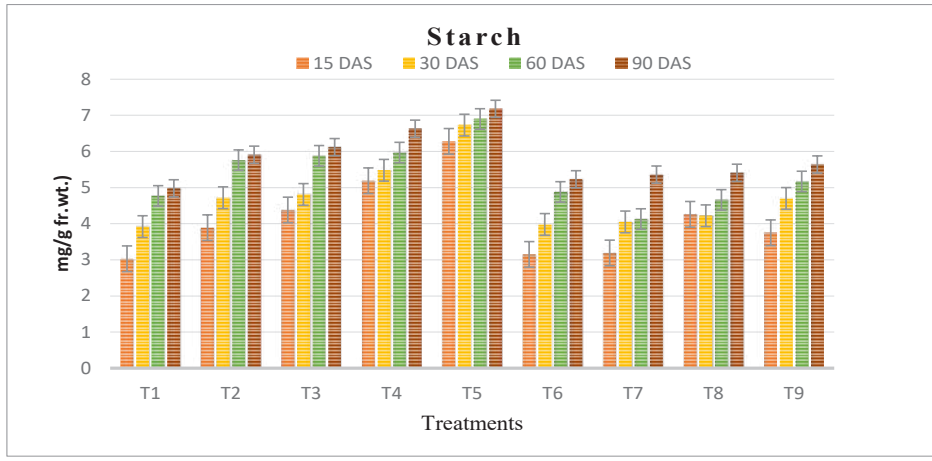

Fig. 10: The effect of organic and inorganic fertilizers on starch contents (mg/g fr.wt.) of groundnut.

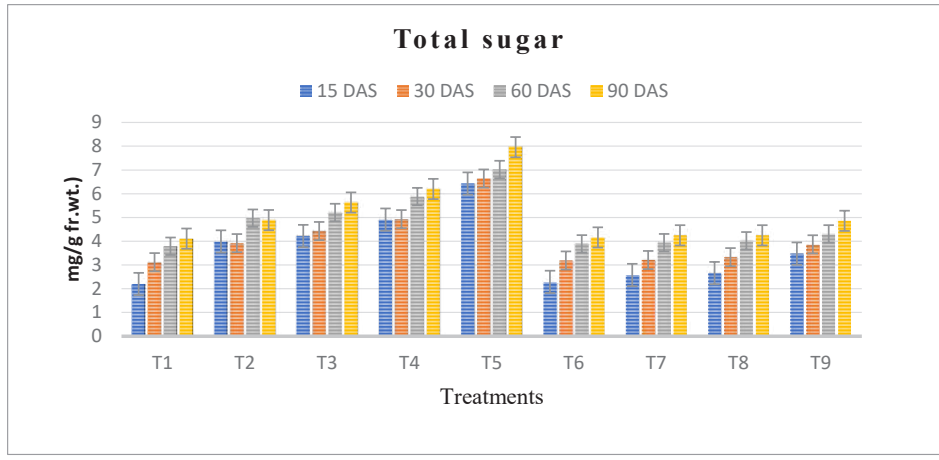

Fig. 11: The effect of organic and inorganic fertilizers on total sugar contents (mg/g fr.wt.) of groundnut.

combined treatments reported the highest evaluation, even though organic fertilizer treatment is found to be more efficient in inducing total sugar content. Carbohydrates are important energy constituents that are required for all the living organisms. The plant manufactures its organic substances during photosynthesis and breaks during respiration. The sugar content increase was higher in bio-fertilizer applied plots. The accumulation of the carbohydrates content due to various fertilizer applications conformed with the previous studies in different species such as potato (Mahendran & Kumar 1998), *Pisum sativum* (Nirmal et al. 2006) and *Albizia lebbek* (Kumudha & Gomathinayagam 2007).

SUMMARY AND CONCLUSION

The effect of organic and inorganic fertilizers on growth parameters and biochemical constituents of leaves was significantly increased in all the treatments. In general, bio-fertilizer applications are to boost the effectiveness of Arbuscular Mycorrhizal Fungi, *Azospirillum* and market waste compost on nodulation and yield of groundnut. The organic fertilizers treated plants showed better performance than the inorganic fertilizers and control. For sustainable groundnut production, recent farming demands an integrated use of organic and inorganic fertilizers along with bio-fertilizers. Hence, further study on the long-term application of bio-fertilizers, low-cost inputs on soil fertility, and groundnut production would be recommended.

ACKNOWLEDGMENT

The authors are thankful to Professor Dr. K.C. Ravindran, Head of the Department and Dr. V.Venkatesalu, Professor and Director (DARE), Department of Botany, Annamalai University for valuable suggestions during the investigation.

REFERENCES

Amujoyegbe, B. J., Opabode, J. T. and Olayinka, A. 2007. Effect of organic and inorganic fertilizer on yield and chlorophyll content of maize (*Zea mays* L.) and sorghum *Sorghum bicolour* (L.) Moench). African Journal of Biotechnology, 6(18): 69-73.

Ayissa, T. and Kebebe, F. 2011. Effect of nitrogenous fertilizer on the growth and yield of cotton (*Gossypium hirsutum* L.) varieties in Middle Awash, Ethiopia. Ethiopia Journal of the Drylands, 4: 248-258.

Ayoola, O.T. and Makinde, E.A. 2009. Maize growth, yield and soil nutrient changes with N-enriched organic fertilizers. African Journal of Food, Agriculture, Nutrition and Development, 9: 580-592.

Baldi, E., Toselli, M., Eiseenstat, D. M. and Marangoni, B. 2010. Organic fertilization leads to increased peach root production and lifespan. Tree Physiol., 30: 1373-82.

Ghosh, P. K., Ajay, Bandyopadhyay, K. K., Manna, M. C., Mandal, K. G., Misra, A. K. and Hati, K. M. 2004. Comparative effectiveness of cattle manure, poultry manure, phosphocompost and fertilizer-NPK on three cropping systems in vertisols of semi-arid tropics. I. Crop yields and system performance. Bioresource Technology, 95: 85-93.

Goss, M. J., Tubeileh, A. and Goorahoo, D. 2013. A review of the use of organic amendments and the risk to human health. Advances in Agronomy, 275-379.

Ignacimuthu, S. and Vendan, S.E. 2007. Botanical pesticides in insect pest management.Uttar Pradesh J. Zoo., 4(Suppl. 1): 141-154.

Kumudha, P. and Gomathinayagam, M. 2007. Studies on the effect of biofertilizers on germination of *Albizia lebbek* (L.) Benth. seeds. Adv. Plant Sci., 417-421.

Mahendran, P.P. and Kumar, N.I. 1998. Effect of biofertilizers and nitrogen on nutritional quality tuber yield and certain quality parameters of potato cv. Kufri Joti. South Indian Hort., 46: 97-98.

Moore, S. and Stein, W.H. 1948. Photometric method for use in the chromatography of amino acid. J. Bio. Chem., 176: 367-388.

Nagwa, M. K., Hassan, Neama, M., Marzouk, Zakaria, F. Fawzy and Said A. Saleh. 2020. Effect of bio-stimulants foliar applications on growth, yield, and product quality of two Cassava cultivars. Bulletin of the National Research Centre, 44:59.

Naser, H.M. et al. 2016. Effect of biofertilizers and putrescine amine on the physiological features and productivity of date palm (*Phoenix dactylifera* L.) grown on reclaimed-salinized soil. Trees, 30(4): 1149-1161.

Nelson, N. 1944. A photometric adaptation of the Somogyi's method for the determination of reducing sugar. Anal. Chem., 31: 426-428.

Nirmal, D., Kumar, A., Singh, R.K., Rai, A.K. and Rai, M. 2006. Effect of biofertilizers on quality of vegetable pea (*Pisum sativum* L.). Plant Arch., 6: 525-527.

Sadasivam, A. and Manickam, A. 1996. Biochemical Methods. New Age International Publishers, New Delhi, pp. 90-134.

Summer, J.B. and Somers, C.F. 1949. Laboratory Experiment in Biological Chemistry. 2nd New York: Academic Press, pp. 173.

Tejeda, M., Gonzalez, J.L., Garcia-Martinez, A.M. and Parrodo, J. 2008. Effects of different green manures on soil biological properties and maize yield. Bioresource Technol., 1758-1767.

Thayamini, H. Seran 2018. Effects of inorganic and organic nutrients combinedly used on yield and quality of groundnut (*Arachis hypogaea* L.), Bangladesh J. Sci. Ind. Res., 53(4): 289-296.

Youssef, A.A., Edri, A.E. and Gomma, A.M. 2004. A comparative study between some plant growth regulators and certain growth hormones producing microorganisms on growth and essential oil composition of *Salvia officinalis* L. Plant. Annl. Agric. Sci., 49: 299-31.

.

Nature Environment and Pollution Technology
An International Quarterly Scientific Journal

p-ISSN: 0972-6268
(Print copies up to 2016)
e-ISSN: 2395-3454

Vol. 20 | No.3 | pp. 1331-1337 | 2021

Original Research Paper

https://doi.org/10.46488/NEPT.2021.v20i03.046

Open Access Journal

Evaluation of Ecological Environmental Pollution in Green Building Construction

Shang Li
Institute of Architecture Engineering, Huanghuai University, Zhumadian 463000, China
Corresponding author: Shang Li; 115455561@qq.com

Nat. Env. & Poll. Tech.
Website: www.neptjournal.com

Received: 15-05-2021
Revised: 30-06-2021
Accepted: 02-07-2021

Key Words:
Green building
Construction process
Ecological environment
Pollution evaluation

ABSTRACT

The long-term extensive development mode of China's construction industry has resulted in the enormous consumption of energy resources, increasingly severe environmental pollution, and serious ecosystem degradation. Green construction is an essential route to implement the ecological civilization construction policy and achieve green building in China's construction industry. However, enormous environmental pollution has been generated because of a series of problems in China's green building construction, such as the lack of a scientific evaluation system for green building construction, loose field construction management, and weak awareness of environmental protection among constructors. Therefore, in this study, a pollution evaluation index system for green building construction was established from three aspects, namely, resource utilization, environmental load, and environmental management, to evaluate the class of ecological environmental pollution triggered by green building construction. Next, a model combining the analytic hierarchy process (AHP) and fuzzy comprehensive evaluation was built, followed by a case study. The results revealed that resource utilization was the main factor causing ecological environmental pollution in green building construction, accounting for 63.70%. Energy conservation and application of new pollution control technology were level III factors that should be given considerable attention. In the fuzzy comprehensive evaluation, the degree of membership of "good" was 0.4855, which was the maximum, indicating that the ecological environment of green building construction in this study was at "good" level, thereby indicating the environmental friendliness of green building construction. This study will be of positive reference values for identifying the ecological influencing factors of green building construction, reducing the waste of resources of green buildings, promoting green construction technologies, and innovating green construction management.

INTRODUCTION

With the development and promotion of industrialization, urbanization, and intelligence, industrial production is accompanied by a serious waste of resources and energy and environmental pollution, and building construction has generated the most direct and evident environmental impacts. As an important constituent part of the national economy, the construction industry is a significant industry boosting China's urbanization, but it is also a major cause of the environmental crisis. The construction industry, an important pillar of the national economy, has always been under the rapid development state in recent years. Despite being a pillar industry of the national economy, the construction industry is also characterized by enormous resource consumption and severe environmental pollution. As shown in Fig. 1, the total energy consumption of China's construction industry rapidly increased from 22,550,200 tons of standard coal in 2001 to 86,850,000 tons of standard coal in 2018, with an annual average growth rate of 16.77%. The resource and energy consumption and environmental pollution degree caused by building construction are serious because most construction units are still performing extensive construction operation, lacking the cognition and application of the theory of green building construction.

Green building construction refers to integrating environmental and resource protection into the construction, during which the conservation of energy, land, water resources, and building materials and environmental protection are achieved through scientific planning and management, and the resources are utilized to the greatest extent to reduce the waste of resources and mitigate the environmental pollution. The emergence of green building construction can not only improve the environmental protection problems and exert an evident effect on the social resource consumption in the construction industry but also relieve the pollution brought by the discharge of construction wastes during building construction, thereby reducing the pollution of the whole construction industry and promoting environmental protection. However, the layout of the construction site is disorderly; dust and noise pollution is serious, and the related standards of green building construction have not been completely met

in China's construction industry. Therefore, improving the reasonable ecological environmental pollution evaluation index system and evaluation and measurement methods for green building construction will be of guiding significance for construction units to practice green construction, save resources, protect the environment, and promote the sustainable development of the building construction industry.

EARLIER STUDIES

Green construction can achieve the enterprise goals with high efficiency, high standard, and high quality in construction projects, which can not only promote the development of a low-carbon economy but also maximize the socio-economic benefits. Hence, it has been widely applied in developed European and American countries. As for the evaluation of environmental benefits resulting from green building construction, Zhai et al. comparatively analyzed the heating, air conditioning, natural ventilation, and hot water supply systems of green buildings and traditional buildings in Shanghai. The results show that the integrated solar energy system of green buildings has high utilization efficiency, and it can reduce building energy consumption by approximately 30% (Zhai et al. 2008). Kim et al. evaluated and analyzed the green construction level in the construction phase from five angles, namely, energy consumption, material saving, utilization of water resources, environmental impact, and land utilization, analyzed the causes of the environmental pollution generated in each working procedure, and proposed the countermeasures and suggestions (Kim et al. 2011). Ghaffarian Hoseini et al. expounded the contemporary trend and application of green building and the influence of green building design on sustainable development. The results show that the sustainable energy source performance of green building has been transformed into a wise and feasible solution, thereby reducing carbon dioxide emissions and energy consumption of construction sectors (Ghaffarian Hoseini et al. 2013). Asdrubali et al. reported that the overall performance evaluation of green building was a complicated problem involving various aspects of building construction, energy sources, and environment and extended the monitoring of buildings in the Umbria area, Italy, and the results show that green building can reduce the environmental pollution caused by building energy consumption (Asdrubali et al. 2013). Sinha et al. stated the relationship between green building and sustainable development and discussed how the use of green building materials could mitigate the environmental pollution caused by building construction (Sinha et al. 2013). Chaudhary et al. analyzed the energy rating system of green buildings and explored the specific energy consumption and total energy consumption of typical buildings, and the results reveal that green construction can improve environmental pollution in comparison with the traditional concrete pouring-type buildings (Chaudhary et al. 2013). Parrish et al. constructed a green building evaluation index system based on a full life cycle and proposed the countermeasures in increasing the green construction level in each construction procedure (Parrish et al. 2014). Based on the evaluation factors of the green building evaluation system, Nilashi et al. combined the analytic hierarchy process (AHP) with the fuzzy logic method to evaluate the environmental performance of the green building, and the results show that this method system is a performance evaluation tool that is used to analyze the effects of various factors on the sustainable development of building construction (Nilashi et al. 2015). Al-Ghamdi et al. explored the application of the green building rating system from a system level, and the results indicated that the use of renewable energy systems resulted in an enormous economic burden on the field, but it can effectively improve the environmental benefits (Al-Ghamdi et al. 2016). Qin et al. evaluated the environmental risk factors of green buildings, and the study results showed the difference in risk importance among stakeholders, thereby providing a basis for different project participators to implement the corresponding risk management strategies according to their understanding of risk importance (Qin et al. 2016). Vidushini, S. et al. thought that the Singaporean construction industry consumed half of the energy sources in China and evaluated the four constituent parts of the Singapore Department Innovation System: technical system, market demand, doer interaction, and application of network and system framework. In addition, the results show that the further development of the Singaporean green building industry is hindered by the unwillingness of building users to change their habits, ineffective coordination among stakeholders, and mere innovation support of green buildings from the government (Vidushini et al. 2017). Hsieh et al. stated that more extensive green building construction could be promoted if the government sent stronger signal intensity to the green building industry (Hsieh et al. 2017). Wang et al. promoted a dynamic method to quantify the difference between expected and actual energy use in green building construction. The case study results show that the dynamic performance gaps among five buildings range from 3.0% to 53.5%, and the control performance degradation of the HVAC system may be the primary cause of the performance gap (Wang et al. 2020). Fu et al. analyzed the complicated relationship among the green behaviors of stakeholders and explored the driving paths of the green building industry based on the network analysis. The study results indicate that the development of the green building industry is important for implementing the green strategy and achieving the transformation and upgrading of the con-

struction industry (Fu et al. 2020). Razmjoo et al. believed that green building construction was of great significance for the development of the smart city; therefore, the government should achieve the coordinated development of society and the environment by implementing new green building energy policies (Razmjoo et al. 2021). Existing literature shows that although the concept of green building construction has been proposed differently in the globe and each country has its unique orientation, it is highly correlated with sustainable building, sustainable construction, green building, environment-friendly construction, and clean production, indicating that green construction is the technical embodiment of sustainable development of construction enterprises in the engineering construction link. In developed countries, particular attention is paid to "green building materials," where considerable research progress has been achieved to save material and energy sources, reduce the waste of materials during construction, mitigate the pollution of the construction site, lower the construction cost, and lengthen the service life of buildings. However, many challenges have been identified in the current green construction management in China, and the related policies and managerial supervision lack comprehensiveness and operability. Therefore, in this study, the AHP was combined with a fuzzy comprehensive evaluation to evaluate the class of environmental pollution caused by the construction of one green building and provide research ideas for future studies.

MODEL PROFILE AND INDEX SYSTEM

AHP-Fuzzy Comprehensive Evaluation Method

The AHP-fuzzy comprehensive evaluation method must determine the domain for the factors of the evaluation object, namely, M evaluation indexes.

$$u = \{u_1, u_2, \cdots\cdots, u_m\} \quad \ldots(1)$$

Next, the domain for the evaluation grade is determined using formula (2).

$$v = \{v_1, v_2, \cdots\cdots, v_m\} \quad \ldots(2)$$

Subsequently, the evaluation objects are quantified one by one from each factor $u_i\,(i = 1, 2, \cdots\cdots, n)$ to obtain the following fuzzy relation matrices:

$$R = \begin{bmatrix} R \mid u_1 \\ R \mid u_2 \\ \cdots \\ R \mid u_n \end{bmatrix} = \begin{bmatrix} r_{11} & r_{12} & \cdots & r_{1m} \\ r_{21} & r_{22} & \cdots & r_{2m} \\ \cdots & \cdots & \cdots & \cdots \\ r_{n1} & r_{n2} & \cdots & r_{nm} \end{bmatrix} \quad \ldots(3)$$

In matrix R, the factor in row i column j represents the membership of one evaluation object to the fuzzy subset of grade v_j from the factor u_i. The performance of an evaluation object from the aspect of one factor u_i is depicted through the fuzzy vector $(R \mid u_i) = (r_{i1}, r_{i2}, \cdots\cdots, r_{im})$, but it is mostly depicted by other evaluation methods using the actual value of one index. Thus, the weight vector of evaluation factors is determined. In the fuzzy comprehensive evaluation, the weight vector of evaluation factors is determined using formula (4):

$$Q = (q_1, q_2, \cdots\cdots, q_m) \quad \ldots(4)$$

In formula (4), the factor q_i in the weight vector Q is the membership of factor u_i to the fuzzy subset. In this study, the AHP was used to determine the relative importance of

Table 1: Evaluation index system of pollution induced by green building construction.

Level I index	Variable No.	Level II index
Resource utilization	V1	Construction waste recycling
	V2	Energy conservation
	V3	Use conditions of new energy resources
	V4	Application of new pollution control technology
Environmental load	V5	Atmospheric pollution
	V6	Noise pollution
	V7	Water pollution
	V8	Light pollution
	V9	Solid waste pollution
	V10	Soil pollution
Environmental management	V11	Qualification of green construction
	V12	Safety of green construction
	V13	Supervision of green construction
	V14	Green construction system

evaluation indexes, namely, $\sum_{i=1}^{n} q_i = 1$, $q_i \geq 0$, and $i = 1, 2, \cdots, n$. Next, Q was synthesized using R of each evaluation object to obtain fuzzy comprehensive evaluation results (vector B) of each evaluation object:

$$B = Q \times R = (q_1, q_2, \cdots\cdots, q_n) \begin{bmatrix} r_{11} & r_{12} & \cdots & r_{1m} \\ r_{21} & r_{22} & \cdots & r_{2m} \\ \cdots & \cdots & \cdots & \cdots \\ r_{n1} & r_{n2} & \cdots & r_{nm} \end{bmatrix} \quad \ldots(5)$$

Index System

Building construction is a complicated system with relatively complicated evaluation algorithms. The overall objectives of green building evaluation were generalized and classified to construct a scientific and reasonable green building evaluation index system. The green building construction index system was established and perfected on the basis of the concept of sustainable development, which specifically included environmental load, resource-saving, integrated management, and construction effect. Furthermore, the hierarchical evaluation model of this green building construction index system was optimized (Table 1).

THE CASE STUDY

Some of the green construction evaluation indexes that could be directly expressed by quantitative data could be accessed through questionnaire surveys, expert consultation, etc. Some quantitative indexes could be identified using specific values, such as power consumption, the recovery rate of construction water, waste discharge, and loss rate of building materials, which were primarily determined on the basis of the numerical values widely accepted by related national standards, specifications, and technical standards. The evaluation criteria for qualitative analysis of indexes could be formulated by discussion among experts and engineers. The evaluation index system was established by combining the evaluation theory of green buildings and green projects. In addition, the environmental protection and energy conservation indexes were screened out, and the AHP was used to measure the weights of 14 level II indexes (Table 2).

In this study, the evaluation result was divided into the following grades (excellent, good, ordinary, relatively poor, and poor). The statistical evaluation results were obtained through the questionnaire survey method. The number of experts was denoted as M. For example if N experts gave the evaluation grade Vi to this index, then the membership of this index to Vi could be calculated using the formula N/M. Similarly, the above-mentioned steps were repeated to obtain the membership matrix of this qualitative index. The membership of each index was obtained by calculating the frequency at different grades. The management of prefabricated green building construction in an economic development zone in Shandong Province, China, was implemented in this study. A total of 12 experts within the construction industry, six proprietor representatives, eight project managers, and 24 constructors were invited, and 50 questionnaires were given. The questionnaire survey results were organized and calculated, and the results are shown in Table 3.

According to formulas (1)-(5), the fuzzy evaluation matrix of level I indexes can be calculated as follows:

$$\begin{bmatrix} 0.1384 & 0.5883 & 0.1531 & 0.0721 & 0.0481 \\ 0.1853 & 0.4238 & 0.2949 & 0.0960 & 0.0000 \\ 0.2085 & 0.2569 & 0.1768 & 0.1957 & 0.1621 \end{bmatrix}$$

Table 2: Weights of environmental pollution factors during green building construction.

Weight of level I index	Weight of level II index	Total weight
0.6370	0.1141	0.0727
	0.4809	0.3063
	0.0691	0.0440
	0.3359	0.2140
	0.1817	0.0190
0.1047	0.1680	0.0176
	0.1984	0.0208
	0.0489	0.0051
	0.1534	0.0161
	0.2496	0.0261
0.2583	0.1330	0.0343
	0.4931	0.1274
	0.0708	0.0183
	0.3031	0.0783

Next, the fuzzy comprehensive evaluation vector was calculated as [0.1614 0.4855 01741 0.1065 0.0725]. The fuzzy comprehensive evaluation vector showed that the membership of "good" was 0.4855, which was the maximum. In this case study, the environmental pollution caused by green building construction was at "good" grade, being better than the ordinary traditional concrete pouring-type building construction, which verified the scientificity of green building construction. Green building construction can mitigate environmental pollution triggered by traditional construction primarily because personnel training was performed well in green construction, and constructors were regularly organized to accept the training regarding green and environmental protection. This project showed great performance in saving water, utilizing water resources, saving land, and protecting land resources. Water was saved, and the water use management system was formulated in strict accordance with the related standard. The standard requirements can be basically satisfied with regard to safety and civilized construction management, the health status of constructors, construction organization plan, occupational health, and safety training.

POLICY SUGGESTIONS

Constructing A Perfect Green Construction Organization Management System

Strengthening the cognition of green building management among employees and reinforcing the management of job responsibilities of managerial staff were necessary. Green building organization management focused on establishing a green construction management system. Managerial staff should implement a clear division of labor and arrange green construction managers and supervisors to ensure and promote the implementation of green projects. Transverse and longitudinal green construction and management organizations should be established, and the green construction responsibilities of each level and each department should be clearly defined. Moreover, job responsibilities should be carefully implemented; the list of job contents should be clarified, and the respective responsibilities should be fulfilled to boost green project construction. A systematic management system should be established to achieve systematic management from the aspects of personnel management, unit management, personal and unit information management, and job log management according to the features of construction enterprises and project construction.

Strengthening the Propaganda and Implementing Green Construction

Green construction can not only save energy resources and costs and reduce consumption but also effectively improve the core competitiveness of enterprises and elevate their management and technical levels. Strengthening green construction among employees is important to improve green construction management and implementation levels. Therefore, a regular training class should be set up. The material incentive method may be adopted to encourage employees to

Table 3: Membership of statistical survey results.

Level II index	Excellent	Good	Ordinary	Relatively poor	Poor
Construction waste recycling	0.2000	0.8000	0.0000	0.0000	0.0000
Energy conservation	0.0000	0.6000	0.1500	0.1500	0.1000
Use condition of new energy resources	0.7000	0.1000	0.2000	0.0000	0.0000
Application of new pollution control technology	0.2000	0.6000	0.2000	0.0000	0.0000
Atmospheric pollution	0.3000	0.5000	0.2000	0.0000	0.0000
Noise pollution	0.6000	0.1000	0.1000	0.2000	0.0000
Water pollution	0.0000	0.6000	0.4000	0.0000	0.0000
Light pollution	0.3000	0.5000	0.2000	0.0000	0.0000
Solid waste pollution	0.1000	0.8000	0.1000	0.0000	0.0000
Soil pollution	0.0000	0.2000	0.5500	0.2500	0.0000
Qualification of green construction	0.0000	0.4000	0.2000	0.4000	0.0000
Safety of green construction	0.3000	0.2000	0.2000	0.0000	0.3000
Supervision of green construction	0.0000	0.2000	0.3000	0.3000	0.2000
Green construction system	0.2000	0.3000	0.1000	0.4000	0.0000

deepen their understanding of green buildings, or outstanding employees can be dispatched to study green buildings, thereby improving their overall quality.

Enhancing the Technological Innovation of Green Construction

The development of different kinds of technologies is the foundation of green construction. The technologies related to green construction should be developing. Recycling of construction wastes after classification is an optimization scheme for material-saving measures. Water-saving measures should be formulated to recycle groundwater and rainwater according to the practical situation. The energy conservation plan and measures should be formulated. The land-saving measures for the temporarily planned land use should also be formulated. Furthermore, related environmental protection measures should be formulated. The application of new technologies could improve the technical level of green construction, for example, BIM technology, automatic computation technology of engineering quantities, and coding technology. The corresponding measures should be formulated to reinforce the supervision of each link and implement the full life cycle management, including project approval design, contractor selection, project progress, staged acceptance check, and overall acceptance check.

Constructing A Green Construction Evaluation System

The management team of the project department must apply the comprehensive quality management method to the respective goals to facilitate the work, refine and decompose the project green construction goals, and perform dynamic management, and work should be tracked and seamlessly managed. Moreover, the independent management of employees should be implemented through goal evaluation to improve their enthusiasm and initiative. Green construction projects should be evaluated on the basis of the following five aspects: environmental protection, water conservation and utilization of water resources, material saving and utilization of material resources, energy conservation and utilization, and conservation and protection of land resources.

CONCLUSIONS

The extensive development mode of China's construction industry led to enormous consumption of energy resources and increasingly severe environmental pollution. In this study, the evaluation theory of green buildings and green projects was combined to establish an evaluation index system, and an evaluation model was established using the AHP-fuzzy comprehensive evaluation method to measure the ecological environmental level of green buildings. The results showed that resource utilization was the primary factor for the ecological environmental pollution generated during green building construction, accounting for 63.70%. The fuzzy comprehensive evaluation results showed that the ecological environment of green building construction given in this case study was at "good" grade, which indicated the environmental friendliness of green building construction. Therefore, in-depth studies should be conducted from the aspects of ecological environmental monitoring of full life cycle through green building construction technology, innovation of green construction management methods, and comprehensive promotion of green construction management.

REFERENCES

Al-Ghamdi, S. G. and Bilec, M. M. 2016. On-site renewable energy and green buildings: a system-level analysis. Environmental Science & Technology, 50(9): 4606-4614.

Asdrubali, F., Uratti, C.B., Cotana, F., Baldinelli, G., Goretti, M., Moretti, E., Aldassarri, C.B., Belloni, E., Bianchi, F. and Rotili, A. 2013. Evaluation of green buildings' overall performance through in situ monitoring and simulations. Energies, 6(12): 6525-6547.

Chaudhary, T. and Piracha, A. 2013. Effective contribution of structural engineers to green buildings and sustainability. Canadian Journal of Civil Engineering, 40(1): 97-100.

Fu, Y., Dong, N., Ge, Q., Xiong, F. and Gong, C. 2020. Driving-paths of green buildings industry (GBI) from stakeholders' green behavior based on the network analysis. Journal of Cleaner Production, 273(18): 122883.

Ghaffarian Hoseini, A., Dahlan, N. D., Berardi, U., Ghaffarian Hoseini, A., Makaremi, N. and Ghaffarian Hoseini, M. 2013. Sustainable energy performances of green buildings: A review of current theories, implementations and challenges. Renewable and Sustainable Energy Reviews, 25: 1-17.

Hsieh, L. C. and Noonan, D. 2017. Strategic behavior in certifying green buildings: an inquiry of the non-building performance value. Environmental Management, 60(2): 231-242.

Kim, Y. D., Cha, H. S., Kim, K. R. and Shin, D. W. 2011. Evaluation method of green construction technologies using integrated lcc and lca analysis. Korean Journal of Construction Engineering and Management, 12(3).

Nilashi, M., Zakaria, R., Ibrahim, O., Majid, Abd., Zaimi.M., Zin, R.M., Chugtai, M.W., Abidin, N.I.Z., Sahamir, S.R. and Yakubu, D.A. 2015. A knowledge-based expert system for assessing the performance level of green buildings. Knowledge-Based Systems, 86(sep), 194-209.

Parrish, K. and Chester, M. 2014. Life-cycle assessment for construction of sustainable infrastructure. Practice Periodical on Structural Design and Construction, 19(1): 89-94.

Qin, X., Mo, Y. and Jing, L. 2016. Risk perceptions of the life-cycle of green buildings in china. Journal of Cleaner Production, 126(jul.10): 148-158.

Razmjoo, A., Nezhad, M. M., Kaigutha, L. G., Marzband, M., Mirjalili, S., Pazhoohesh, M., Memon, S., Ehyaei, M.A. and Piras, G. 2021. Investigating Smart City Development Based on Green Buildings, Electrical

Vehicles and Feasible Indicators. Sustainability, 13(14): 7808.
Sinha, A., Gupta, R. and Kutnar, A. 2013. Sustainable development and green buildings. Drvna Industrija, 64(1): 45-53.
Vidushini, S., Thomas, H. and Mansi, J. 2017. Green buildings in singapore; analyzing a frontrunner's sectoral innovation system. Sustainability, 9(6): 919.
Wang, D., Pang, X., Wang, W., Qi, Z. and Yin, R. 2020. Evaluation of the dynamic energy performance gap of green buildings: case studies in china. Building Simulation, 13(2).
Zhai, X. Q., Wang, R. Z., Dai, Y. J., Wu, J. Y. and Ma, Q. 2008. Experience on integration of solar thermal technologies with green buildings. Renewable Energy, 33(8): 1904-1910.

Nature Environment and Pollution Technology
An International Quarterly Scientific Journal

p-ISSN: 0972-6268
(Print copies up to 2016)
e-ISSN: 2395-3454

Vol. 20 | No.3 | pp. 1339-1345 | 2021

Original Research Paper

https://doi.org/10.46488/NEPT.2021.v20i03.047

Open Access Journal

Comparative Analysis of Municipal Solid Waste Management in Kochi and Indore

B. Paul and D. Paul†

Department of Energy and Environment, Symbiosis Institute of International Business, Symbiosis International (Deemed University), Pune-411057, Maharashtra, India

†Corresponding author: Dipen Paul; dipen.paul@siib.ac.in

Nat. Env. & Poll. Tech.
Website: www.neptjournal.com

Received: 24-09-2020
Revised: 15-10-2020
Accepted: 08-12-2020

Key Words:
Municipal solid waste
Solid waste management
Waste segregation

ABSTRACT

Conventionally, the general understanding of Municipal Solid Waste (MSW) management is collecting solid waste and its disposal through its developed channels or outside contracts. However, depending upon the situation and context, the definition of MSW varies between countries across the globe. For instance, in countries like Singapore and Japan, Municipal Solid Waste is defined as general waste. However, while categorizing the general waste, the industrial waste component is considered for Singapore and not for Japan. Similarly, different countries associate different definitions for MSW and it becomes a difficult challenge to suggest a single unified definition applicable for all countries. This paper aims to do a comparative analysis of Waste management in Tier-II cities of India, Kochi and Indore. Kochi is ranked 372nd and the latter 1st according to the latest Swachh Survekshan undertaken as part of the Swachh Bharat Abhiyan (Urban) by the Ministry of Housing and Urban Affairs. This paper highlights what the key elements missing out in the management of waste in Kochi from the reference perspective of Indore and identifying the measures Kochi needs to undertake to improve its ranking among the cleanest city in India are.

INTRODUCTION

In India, "Solid Wastes" are defined as solid or semi-solid domestic waste which is discarded after its primary use. The waste could be of any type depending upon the primary purpose of the product used. For example, sanitary waste from sanitary pads and napkins, commercial waste from food leftovers by restaurants, institutional waste, or industrial waste like concrete are all categorized as solid waste. Generally, these wastes are generated within the limits of local authorities and they are not categorized as a product or a by-product. The producer of the waste has no further use nor it is used for further production or consumption for it to be designated as a product. That is the reason why the generators decide to dispose of it. Waste generally includes materials generated during the life cycle of a product. Wastes are generated from the extraction of raw materials, processing of these raw materials into intermediates and final products, the consumption of final products, and other human activities excluding the residuals recycled or reused at the place of generation (MUD, GOI).

One of the core elements of a city's infrastructure is its solid waste management framework. As the city develops through increased urbanization, the demand for more human capital increases. These instances are a progressive part of any economic development and they have severe repercussions for the management of MSWs. More sophisticated management methods in MSW are required to reduce these repercussions which include activities that advocate socio-economic requirements (Sohkhlet & Nagargoje 2020). A poor solid waste management system may create serious negative environmental impacts. Reports say that almost 1.6 billion tonnes of carbon dioxide equivalent were generated from solid waste management across the globe, representing about 5% of total greenhouse gas (GHG) emissions. The current solid waste management practices across the globe are poor and the amount of damage these practices caused is massive. Not only do they cause harm to the macro-level functioning of the world's ecosystem but also the micro-level functioning of the world's ecosystem. Clogged drainage systems are breeding grounds for bacteria, leading to several diseases. On a global scale, approximately 37% of the waste generated is disposed of in a landfill of which only 8% is disposed of in sanitary landfills, and the remaining 33% is discarded in open fields and grounds in an unscientific manner. The global waste that is recovered through reuse, recycling, and composting is a mere 19% (Sohkhlet & Nagargoje 2020).

In India, the processes (collection, transportation, and disposal) involved in MSW management are very unscientific and chaotic. The dumping of wastes in and around the cities and towns has been increasing at an alarming rate without any proper control and landfills are found to be overflowing in

major cities which is a real challenge for the country (Gupta et al. 1998). These landfills are very difficult to reclaim due to the unscientific manner in which the waste is dumped and poses serious environmental implications such as groundwater pollution and global warming. In lots of landfills, the burning of waste without the use of incinerators and other scientific measures is prevalent and is increasing leading to air pollution in terms of increased total suspended particles and particulate matter emissions, which is equivalent to vehicular emissions at times. When it comes to the recycling of solid waste, it has mainly remained an informal sector with the absence of proper waste segregation practices and awareness programs to promote and highlight the importance of waste management (Luthra 2020). Except for a few cities, the majority of the country is yet to implement new technologies in the management of MSW. Nevertheless, the sector holds a huge economic boost for the country which mainly is due to the thriving demand for waste material and recycled products that could help the nation accelerate towards sustainable progress (Dolla & Laishram 2020).

In the context of this situation, we take two Indian cities, Kochi and Indore, which are both tier-II cities and part of the Smart Cities Mission undertaken by the Government of India. Since its inception, both the cities have been part of Swachh Survekshan and according to the results of the annual list of cleanest cities published in August 2020, Indore has emerged as India's cleanest city four years in a row, while Kochi was ranked 372, an improvement from 409 but below other regions from the state.

Dubbed as the "Queen of the Arabian Sea", Kochi is a metropolis located on the coast of Southern India in the state of Kerala bordering the Arabian Sea. Being gifted a beautiful natural harbor, it is one of the major port cities in India, falling near the international shipping lane. The city is often referred to as Ernakulam and is a part of the district of Ernakulam and the governing body of the city is the Kochi Municipal Corporation. The city is one of the most densely populated cities in southern India and as per the 2011 census, the population within the corporation limits stood at 677,381. Kochi holds the title of being the financial, commercial, and industrial capital of Kerala. Starting from being an important spice trading center from the 14th century onwards, the city has progressed rapidly and has the highest GDP as well as the highest GDP per capita in the state.

Located in the state of Madhya Pradesh, the city of Indore is the largest and most populated state and is often dubbed as the educational hub of central India as it houses both the Indian Institute of Management and the Indian Institute of Technology. The city is governed by the Indore Municipal Corporation and the body is often considered among the best Municipal Corporations across the country. Indore had a census-estimated 2011 population of 1,994,397 (municipal corporation) and 2,170,295 (urban agglomeration). The city is the financial capital of Madhya Pradesh, being a commercial center for goods and services and having a GDP of $14 billion as of 2011.

MATERIALS AND METHODS

Solid waste management has always been an important social and environmental issue in a country like India and its prominence has been gaining traction nowadays. The country has witnessed a substantial increase in solid waste generation and its impact is very much visible in the urban areas of the country. Over the years since India opened its doors after 1991, the country has undergone a massive change with rapid urbanization fuelled by rapid population growth, who have been adapting and changing their lifestyles with changing standard of living, adopting new food habits, etc. (Malviya et al. 2002). All these trends have increased the stress on MSW management which was already in a stressful state. Due to a lack of financial resources, an unacceptable choice of technology, and public apathy towards municipal solid waste, the sector is struggling a lot. Due to these factors, the country has a huge challenge and pressure to address this social and environmental issue which mostly falls into the hands of the Municipal authorities (Aich & Ghosh 2019).

Years ago, municipal waste was generally composed of biologically degradable matters since consumerism was low and the use of materials like plastic was very less. As a result, they did not create any serious problems for the communities as these were diverted for reuse or recycling through composting and later directly used as manure by the farming community (Ravi & Vishnudas 2016). After the increase in the use of plastics and other non-biodegradable materials for production and packaging purposes, the accumulation of these non-biodegradable materials in the total quantity of municipal waste increased. With uncontrolled waste management practices employed, these materials found their way into the suburban agricultural community which became increasingly harmful to the farmers and cultivators. There are various aspects while dealing with this challenge and among them, there are two major aspects, the technology applied and the general social mindset of the people. The social mindset of the general public is an important aspect of the management of MSW and addressing this challenge forms the basis for controlled management of the waste. In India, the general notion among the public is, it is the responsibility of the government to dispose of whatever waste they are generating across all the sectors. This approach towards this aspect is very alarming and at the same time very pa-

thetic. Only when society realizes that only they can manage this generated waste, the system becomes effective for the authorities and the environment. Municipal authorities must implement effective solid waste management which has to be executed ensuring that the adverse consequences on society are minimal. A centralized waste management system that is technologically driven has been developed and implemented in the developed industrial societies like Europe and North America (Ganesan 2017).

In India, Solid Waste Management (SWM) commensurates with the Solid Waste Management and Handling Rules, 2000 and 2016. The SWM rules 2000 voiced for a centralized waste management system where municipal governments were given the challenging task of playing a crucial role in the diversion of waste through the collection, processing, and final disposal of the solid. Due to various uncontrolled centralized waste management methodologies practiced by the municipal governments, the Solid Waste (Management and Handling) Rules, 2016 amendment was brought in as a deviation from its predecessor (SWM rules 2000) and the new rules prioritized the importance of source segregation and proper treatment of waste by improving the scope for recycling and reusing, thus focusing on the benefits that can be derived out of a circular economy. A study conducted by Rathore and Sarmah (2020) examined the economic, environmental, and social feasibility of circular economy in MSW management through a concept of converting collected organic MSW anaerobically into biogas and using that gas to generate electricity via a thermal power plant, thus reducing the overall dependency on coal-fired thermal power plants for power generation (Rathore & Sarmah 2020). The proposed system was found out to reduce the economic, social, and environmental burden on MSW management and was successfully implemented in the city of Bilaspur, India. While studies based on community-based efforts for sustainable integrated waste management have been carried for megacities, its entire potential needs further introspection in terms of final execution depending upon the individual social commitments of those communities (Colon & Fawcett 2006).

The state of Kerala witnessed a shift in its approach towards waste management from a centralized system to a decentralized system much before the amendment of SWM rules in 2016. The state produces approximately 3,410,243 MT of solid waste annually and the experience the state had with MSW has been important in changing the waste management rules of the country. A majority of the waste generated happens in the commercial capital of the state, Kochi and over the past years, the city has been struggling with its MSW.

The broad objective of this paper is to determine a technically and economically feasible solid waste management project for the city of Kochi which can be implemented in a phased manner by doing a comparative analysis with the city of Indore. The specific objectives of this paper:

- To compare the waste management in the Municipal Corporation of Kochi and Indore Municipal Corporation.
- Highlight the mechanism adopted by the two cities.
- Identify the challenges facing Kochi city and how the current measures implemented by Indore Municipal Corporation (IMC) can act as a solution for the city.

RESULTS AND DISCUSSION

Indore today generates over 1115 MT of garbage a day and all of the generated solid waste is collected at the source irrespective of being a residential or commercial establishment. The door-to-door waste collection services started in 2016 - in January as a pilot project. After a year, the city was collecting 100% waste through door-to-door services, and through its continuous efforts and collaborations with various residential and commercial units, they achieved 100% segregation of waste. None of this would have been possible without the efforts of the citizens of Indore who played a significant role in making the city neat and clean (Mokale 2019). Kochi has been growing at a rapid pace over the last decade and relentlessly pushing its borders cautioning the city planners. The number of high-rise apartments is among the highest in

Table 1: Projected population and total residential waste growth per day for Kochi and Indore.

Year	Kochi			Indore		
	Population	Per capita waste generated* (kg)	Total waste (Tons)	Population	Per capita waste generated* (kg)	Total waste (Tons)
2001	595575	0.518	308.51	1626297	0.321	522.04
2011	601574	0.518	311.62	2104658	0.321	675.6
2021	628645	0.518	325.64	2681831	0.321	860.87
2031	656934	0.518	340.29	2912701	0.321	934.98

*The per capita waste generated is assumed to be fixed concerning the 2012 CPCB value.

Table 2: Projected total increase per day in the share of different solid waste materials for Kochi and Indore in tonnes.

Solid Waste Material*	Kochi				Indore	
	2011	2011	2021	2031	2021	2031
Paper	2.52	5.47	6.97	7.57	2.64	2.76
Glass waste	1.37	2.97	3.79	4.11	1.43	1.5
Metal waste	1.99	4.32	5.51	5.98	2.08	2.18
Organic Waste	136.96	296.93	378.35	410.92	143.12	149.56
Plastic waste	1.93	4.19	5.34	5.8	2.02	2.11
Stones, ashes	130.29	282.47	359.93	390.92	136.15	142.28
Miscellaneous	36.55	79.25	100.98	109.67	38.2	39.92

*The percentage share of different solid materials is assumed to be fixed concerning the 2012 CPCB value

Indian cities, adding more waste. Due to poor maintenance of roads and drainage system along with poor management of MSW by the Municipal Corporation, the city will have to endure many challenges, and coming out of these issues will be capital intensive if it attains a metropolitan status (Ravi & Vishnudas 2018).

Population

While both the city's population is increasing based on the census studies, as per the analysis of the ecological footprint of waste generation in the residential areas of Kochi city, the city will be requiring an area equivalent to the current city size by 2050 if the present trend of MSW is followed upon.

Waste Collection, Disposal and Treatment

Table 2 represents the different types of solid waste generated and the approximate quantity of each type in 10 years. The values quantify the importance of segregation and the consequent smooth operation of the system.

Kochi

Approximately 47.5 residents of the city live in high-rise apartments while the remaining 52.5 percent have independent houses. The type of residence stems from the fact that most of the independent residence treat the waste generated at the premise itself, leaving the apartments to be completely dependent on the MSW services for waste treatment. The availability of land and the practice of unsustainable treatment measures lead to ineffective disposal of the waste. Therefore, the type of residence and the method of waste storage becomes crucial in implementing an efficient MSW.

The individual households mainly use three mechanisms for the treatment of waste:

- Household Treatment through composting or burning
- NGOs or Self-Help Group (Kudumbashree)
- Street Discard

The Kudumbashree and the Municipality have adopted door-to-door collection services for the households in Kochi covering both independent houses and high-rise apartments. Although the efficiency of Kudumbashree is applauded throughout the city, they only serve 15 wards of the total 71 wards present in Kochi City. The remaining wards are attended by the Municipal staff, whose unsatisfactory service delivery, households' unwillingness to pay the user charges associated with door-to-door waste collection, and the availability of land exacerbate the tendencies to adopt unsustainable practices such as street discard and burning.

Another major issue with the treatment of waste is the high proportion of non-segregated waste discarded on the streets. Even the municipal staff accept non-segregated waste from certain places. Those houses which chose to discard their waste on the streets usually use polythene bags to dispose of both biodegradable and non-biodegradable materials. The use of low-quality polyethylene bags affects the overall degradation process and efficient treatment. These wastes mix of non-segregated plastics, organic material, and plastics with non-recyclable quality eventually end up accumulating in the landfills (Sebastian, Kumar & Alappat 2019). Plastics are a real threat to the environment as well as to the effective management of MSW.

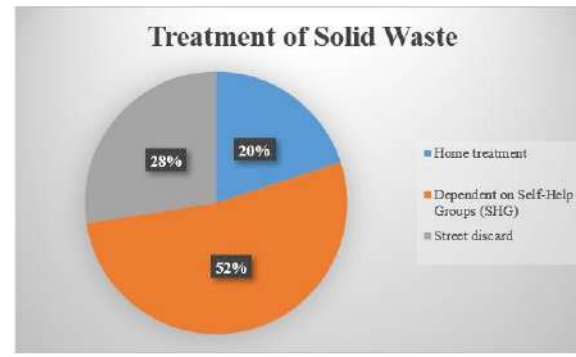

Fig. 1: Waste Treatment Methodology adopted by Kochi Households.

The city collects a total of 40% of the waste produced and is transported to the treatment plant. Along with the Kudumbashree self-help workers and municipal staff members, Kochi has almost 250 resident associations that assist the officials in the door-to-door collection process. The city houses 21 sanitation circles which act as secondary collection points where the waste is collected after the primary collection which is done with the help of Hand Carts, Wheel Barrows and Tractor Trailers. From the secondary collection centers, the waste is transported to the final treatment site using a fleet of 107 vehicles which includes tractor-trailers, tippers, and other trucks.

The Brahmapuram solid waste treatment plant was constructed in 2008 as part of the plans of the Kochi Corporation to establish an efficient MSW management to address the increasing waste issue. It was built after acquiring 33.3 acres of wetland and rehabilitating the residents in Brahmapuram. The facility was designed for basically two treatment processes. Windrow composting for the treatment of biodegradable waste using trommels and a Refuse Derived Fuel pelletizer for the storage and treatment of nonbiodegradable waste. The plant was equipped with vehicles for leachate suction. The remaining waste materials were landfilled in the adjacent marshland.

The plant fell into negative criticism within a year of its operations. Due to negligence in the technical planning of the plant and poor operations, the structures of the facility developed cracks due to the broken floor and subsequent sinking. The columns tilted and the tie beams fell out of alignment. The authorities failed to factor in structural requirements for construction on a marshland which led to the subsequent breakage. The consequence of the broken floor and the subsequent breakage was that windrow composting was no longer viable in the plant due to retention of high moisture content resulting in the inefficient operations of mechanized composting and eventual accumulation in the landfill.

Currently, only 10% of the waste reaching the facility is being treated and the remaining 90% of solid waste entering the facility is landfilled. The excess waste accumulation in the landfill adjacent to river Kadamprayar has resulted in excessive leachate percolation and water pollution. To make matters more concerning is the fact that one of the biggest fish markets in Kochi, the Chambakkara market, lies on the downstream path of the river. Given the nature of the plant, the environmental impact of the Brahmapuram waste treatment plant is massive. Kochi as a city has a long way to go in implementing effective MSW management and timing has not been this crucial as it is now.

Indore

Indore is divided into 85 wards which fall under 19 zones. Each ward has an average of 6000 households and numerous commercial establishments. The City specializes in collecting waste from all sources including residential, commercial, and industrial generators. Door-to-door collection service is implemented for household/apartment collection and bulk collection systems are used for semi bulk and bulk generators. With these systems in place, the city covers 100% of all the wards and ensures 100% collection from these wards.

The waste generators in Indore are classified as Domestic generators, Semi-Bulk Generators, and Bulk Generators based on the daily amount of waste generated. The generated waste is always segregated, and each classification segregates into different categories. Table 3 gives a detailed understanding of the classification of waste generators. The segregated waste generated by the domestic generators is collected by partitioned tippers known as Nigam trucks which have different chambers for different waste types. The chambers are fabricated in the ratio of 50:50, 60:40, and 85:15 depending upon the area and amount of the waste generated from the area. Each processing plant houses a computerized weighbridge which acts as the first point of interaction for the waste collection vehicles coming into the plant for offloading purposes. The vehicles are weighed upon entry and after offloading to determine the waste type. Upon completion, a receipt is generated and it is filed at the facility which contains all the information about the waste transported, the quantity, the type, source of waste, time, and vehicle details. All the dry wastes are transported to the Material Recovery Facilities (MRF) centers where they are offloaded for further segregation and processing. The wet waste from the GTS and Bulk generators are offloaded at the central composting plant for further processing. The domestic hazardous waste is offloaded at a separate facility after transferring from GTS in special biomedical vans. The domestic hazardous waste is transferred to the Common Biomedical Waste Facility (CBWTF) where it is incinerated.

Indore Municipal Corporation has to date constructed eight sophisticated ultra-modern Garbage Transfer stations to strengthen its secondary collection mechanism which overall brought in reduction to its cost of the secondary collection system and transportation system. Since the entire waste generated is processed, the corporation converted its

Table 3: Classification of waste generators in Indore.

Waste Generators	Amount/ Day	Segregation
Domestic	< 25 Kg	Wet, Dry, and Domestic Hazardous
Semi-Bulk Generators	25 - 100 Kg	Wet and Dry
Bulk Generators	> 50 Kg	Wet and Dry

Devguradia trenching site into a garden, demarcated it with a boundary wall, and planted 60,000 saplings. Once a dreadful place for the residents living close off, with constant fire and emission of foul smell, the achievement of Indore Municipal Corporation (IMC) is a benchmark for other Municipal Corporations to replicate and be a success story themselves.

The citizens of Indore were the true champions in making the entire system a grand success. Like any other Indian City, Indore too faced an existential crisis in dealing with its MSW. The steps adopted by the Information, Education, and Communication (IEC) played a crucial role in building the foundation for a Swachh Bharat Mission in Indore (Chauhan et al. 2020). IEC undertook the challenge of bringing about the behavior change required in the mindset of all the stakeholders, from citizens to the government authorities. They conducted a range of activities from cultural event promotions through street plays, wall paintings to mass communication strategy through content delivery via FM stations, social/ digital media campaigns, etc which brought out the much required behavioral change in all segments of the population, from residents to commercial establishment owners to industrial experts.

CONCLUSION

Indore is the cleanest city in India for four consequent years and that is not an easy milestone to achieve. Segregation is the base that has built a strong system in Indore which was brought in by creating a behavioural trait among the citizens through various awareness programs by the IEC. With the active participation of all the stakeholders and waste generators, Indore can process 100% of its waste. From being the most polluted city in Madhya Pradesh, the Madhya Pradesh Pollution Control Board (MPPCB) declared that the city's pollution levels have fallen by almost 50% to 80 micrograms per cubic meter which is very close to the safe limit set of 60 micrograms per cubic meter (Shrotriya & Smout 2010). The standards of the air quality index are determined by the Central Pollution Control Board. From the grappling efforts of IMC in its early years to its current status, the city of Indore is a shining example for other big cities that are struggling with waste management woes.

The MSW management in Kochi is a ticking time bomb and if the present trends of management are to be followed, by 2050 the city will be requiring an area equivalent to its corporation size to treat the waste generated by the city households. The unsustainability dilemma in the minds of residents towards waste treatment and disposal has been pointed out especially through their behavioral aspects of street discards and burning. The authorities should focus on replicating the activities undertaken by the IMC and IEC on the importance of creating a behavioural trait towards sustainable waste management among all its residents and stakeholders. Implementing a better efficient decentralized waste management by contracting the Kudumbashree workers and covering all the wards for the collection of waste that is properly segregated is important for Kochi to address its waste woes. Since a huge proportion of the residents have undertaken the home treatment of solid waste, the Corporation authorities should assist the households in establishing an effective household treatment facility by constructing biogas plants and creating markets where the residents can avail monetary benefits from the manure produced.

Landfilling is not an option of Kochi city given its geographical nature and polity. The government and authorities must focus on creating technical and engineering innovations to reclaim the existing landfill. The Brahmapuram plant needs a complete revamp by redesigning the entire structure with strong foundations to optimize the windrow compositing and mechanized compositing which results in the reclamation of landfills. Waste to energy power plant should be constructed on a priority basis which reduces the burden on landfilling while making sure the environmental impacts of the entire waste management are minimum. Finally, the authorities and policymakers must set out the overall strategies for implementing an effective MSW management body for the city of Kochi by making stringent laws and corrective actions wherever necessary.

REFERENCES

Aich, A. and Ghosh, S. K. 2020. Framework for auditing of municipal solid waste management system in India. In Solid Waste Policies and Strategies: Issues, Challenges and Case Studies (pp. 85-99). Springer, Singapore.

Chauhan, J., Gautam, V. K. and Mishra, P. N. 2020. To study information, education, and communication (IEC) campaign as a tool to spread awareness in understanding the support of 3R concept for waste minimization in Indore City as the cleanest city of India. In Solid Waste Policies and Strategies: Issues, Challenges and Case Studies (pp. 7-25). Springer, Singapore.

Colon, M. and Fawcett, B. 2006. Community-based household waste management: Lessons learnt from EXNORA's 'zero waste management 'scheme in two South Indian cities. Habitat International, 30(4): 916-931.

Dolla, T. and Laishram, B. 2020. Factors affecting public-private partnership preference in Indian municipal waste sector. International Journal of Construction Management, 20(6): 567-584

Ganesan, P. 2017. Landfill sites, solid waste management and people's resistance: A study of two municipal corporations in Kerala. International Journal of Environmental Studies, 74(6): 958-978.

Gupta, S., Mohan, K., Prasad, R., Gupta, S. and Kansal, A. 1998. Solid waste management in India: Options and opportunities. Resources, Conservation and Recycling, 24(2): 137-154.

Luthra, A. 2020. Efficiency in waste collection markets: Changing relationships between firms, informal workers, and the state in urban India. Environment and Planning A: Economy and Space, 52(7): 1375-1394.

M. Ramachandran, Vishal Fegade, N. Ganesh and Manoj Chaudhari, 2019. Municipal Waste Disposal Strategy by Fuzzy TOPSIS Method. International Journal of Engineering and Advanced Technology (IJEAT)

Malviya, R., Chaudhary, R. and Buddhi, D. 2002. Study on solid waste assessment and management-Indore city. Indian Journal of Environmental Protection, 22(8): 841-846.

Ministry of Urban Development (MUD), Government of India (GOI), MUNICIPAL Solid Waste Management, Part II: The Manual, 2016, Accessed on May 2020, http://swachhbharaturban.gov.in/writereaddata/Manual.pdf

Mokale, P. Smart waste management under smart city mission: Its implementation and ground realities. International Journal of Innovative Technology and Exploring Engineering, 5(12): 3095-3103

Rathore, P. and Sarmah, S. P. 2020. Economic, environmental and social optimization of solid waste management in the context of circular economy. Computers & Industrial Engineering, 145: 106510.

Ravi, A. and Vishnudas, S. 2018. Ecological footprint and waste footprint of Kochi City, India: A Combined Analysis. The Journal of Solid Waste Technology and Management, 44(4): 344-355.

Sebastian, R. M., Kumar, D. and Alappat, B. J. 2019. Easy estimation of mixed municipal solid waste characteristics from the component analysis. Journal of Environmental Engineering, 145(11): 1-11.

Shrotriya, V. and Smout, I. 2010. GHG emissions: an assessment at the municipal solid waste disposal site in Indore, India. International Journal of Environmental Technology and Management, 13(3-4): 362-371.

Sohkhlet, D. and Nagargoje, S. 2020. Municipal solid waste management: A comparative study between Sydney (Australia) and Pune (India). EDP Sciences, 170: 1-12.

Nature Environment and Pollution Technology
An International Quarterly Scientific Journal

p-ISSN: 0972-6268
(Print copies up to 2016)
e-ISSN: 2395-3454

Vol. 20 | No.3 | pp. 1347-1351 | 2021

Original Research Paper

https://doi.org/10.46488/NEPT.2021.v20i03.048

Open Access Journal

Spatio-Temporal Variability of Gamma Radiation Profile Along the Southern-Indian Coastline (Poompuhar to Nagapattinam Stretch)

T. Stalin Subbiah*, R. Mahesh*, P. Parthiban* and A. Das*†
*Centre for Environmental Engineering, PRIST Deemed to be University Thanjavur, Tamil Nadu, India
†Corresponding author: Ashutosh Das; scientists.crd@gmail.com

Nat. Env. & Poll. Tech.
Website: www.neptjournal.com

Received: 25-09-2020
Revised: 29-10-2020
Accepted: 08-12-2020

Key Words:
Natural radiation
Coastal radiation
Gamma dose
Beach sand

ABSTRACT

The present study is aimed at evaluating the radiation profile along the coast of the Poompuhar-Nagore range, which is known to be hydrodynamically active and is enriched with anthropogenic activities. The study of radiation on the coastal belt and evaluating their dynamics (magnitude and spatio-temporal variability) is crucial both for the coastal inhabitants as well as possible exploration of rare-earth minerals. The effective gamma radiation during the new moon along the coastal range varies between 0.9 to 3.55 $\mu sv.h^{-1}$, respectively. The annual equivalent dose is estimated up to gamma radiation of 0.26 to 2.80 $\mu sv.h^{-1}$. Generally, the concentrations of the gamma radiation measured are elevated in certain areas namely Chinnagudi, Kuttiyandiyur, and Chandrapadi. In particular, the gamma radioactivity is high at Chandrapadi and Chinnagudi during the new moon as it shows considerable amounts of radiation. There is a definite variation due to the moon phase on the gamma radiation profile of the area studied. Out of the eight coastal villages under study, about 60% of the coastal line shows high levels of gamma radiation during both new moon and full moon phases.

INTRODUCTION

Natural radioactivity is widespread in the Earth's environment, and it exists in various geological formations such as earth crust, rocks, soils, plants, water, sand, sediments, and air. The concentrations of natural radioactive materials depend primarily on geological conditions and vary by soil level of different geographical regions (Abinesh et al.2016). Beach sands are composed mainly of quartz, feldspar, and other minerals resistant to wave abrasion. They are mineral deposits formed by the combination of weathering, fragmentation, and degradation (Ching-Jiang et al.1993, Kanse et al. 2016, Lal 1991). Studies concerning the radiation hazards arising from the use of sand or soil showed that natural radiation is the largest contribution to external dose to the world population (Papadopoulos et al. 2014 & 2016). Ionizing radiations are a grave threat around the high background regions of the globe. The presence of monazite sand along the beaches among other factors has contributed to these dreaded radiations (Malathi et al. 2005, Mishra 1990, Monica et al. 2017, Singh et al. 2007). Predominant natural radiation affecting terrestrial systems and the most studied radio-nuclei is radon. Dynamics between terrestrial and cosmic processes on radiative distribution on various hydro-litho-climatic reasons are widely ventured, however, no integrated model has been developed so far (UNSCEAR 2000).

Study on dynamics of radiation in Indian coastline and their effect is scarce in peered-reviewed literature. India with its long coastline –supports a major fisherman population. Indian Rare Earth mining, exclusively located at coasts, is known to be enriched in monazite, garnet, and rutile (Ragel et al. 2008, Radhakrishna et al. 1993, Sivakumar et al. 2002). Risks associated with natural radiation due to coastal radiation is yet to be studied extensively. Hence, there is a need for the study of coastal radiation dynamics and delineation of radiation-risk prone zones.

The main objective of this study was to measure the gamma dose rates during the waxing phase along the coastal regions under study and thereby evaluation of the radiation profile vis-e-vis the altitude of the coastline of the study area (along and across the sea). Also evaluating the effect of the tide and regional topography on the radiation profile (stability and migration) to delineate the radiation-prone zone and identification of cause thereof by stratigraphic analysis.

STUDY AREA

The study area covers along the southern Indian coastline from Poompuhar to (Longitude 79°51'26.604" E to 79°51' 03.654" E) to Nagore (Latitude 11°08'23.94" N to 10°49' 26.892" N) comprising eight coastal villages namely Poompuhar, Chinnagudi, Kuttiyandiyur, Chandrapadi,

Kottucherrymedu, Karaikkal, Vadakkuvanjore, and Nagore, which covers a coastline stretch of about 40 km (Fig. 1). Each location is separated by a distance of four kilometers approximately.

The geology of the study area consists of alluvium, laterites, quartzites and biotite, hornblende-biotite, granite, and gneisses. The foliation and joints on these sand rocks control the course of the seashore, causing them to form a trellis drainage pattern, particularly to the south of the area. The sedimentary sand rock sequences are from cretaceous to recent; consist of grey sand intercalated with brown to dark grey clay.

MATERIALS AND METHODS

Selection of the Measurement Sites

The geo-coordinates of the locations were recorded (Latitudinal and Longitudinal position) using a handheld Global Positioning System (Standard GPS). Survey of coastal stretches along and across (every 5kms along the coast and 100 meters across) the coastline of the study area.

Gamma Absorbed Dose Measurements Using Portable Dosimeter

The ambient gamma absorbed dose rates were measured in the sampling locations using a GM counter-based dosimeter (Belvar- PKC-107). The gamma radiation levels were measured both inside and outside the dwellings at the surface of the ground. About 20 readings were taken at different points in each location.

Measurement of Radionuclide Activity Concentrations

A hand-held gamma radiation counter was used for profiling the dose rates along and across the coastline, before and after tidal cycles during the waxing phase (New moon, First Quarter & Full moon). The gamma radioactivity was recorded on beach sand samples by placing on the sand surface at all locations with a 10-meter interval (between each sampling point). The radiation measurements were recorded from the beach face that extends up to the berm, perpendicular to the shoreline (0 to 100 meters). The data was collected during the waxing phase i.e., periodically between the full moon and new moon phases. The recorded values were analyzed statistically. The average gamma radioactivity map and delineation of gamma radiation were prepared using the ARC-GIS Spatial Analyst tool (ArcGIS, Ver.10.3).

RESULTS AND DISCUSSION

Gamma Absorbed Dose Rates

The gamma absorbed dose rates along the coastal region under study measured using a portable dosimeter, are presented in Table 1. The overall gamma dose, measured using the dosimeter, varied in the range of 0.1 to 3.6 $\mu sv.h^{-1}$ with the mean value of 2.34 $\mu sv.h^{-1}$ (Fig. 2).

Comparison of Dose Measured Along the Stretch under Study

The highest activities were recorded along the Chinnankudi and Kutiyandiyur and Chandrapadi regions. The gamma-ray activity was directly related to the abundance of the pri-

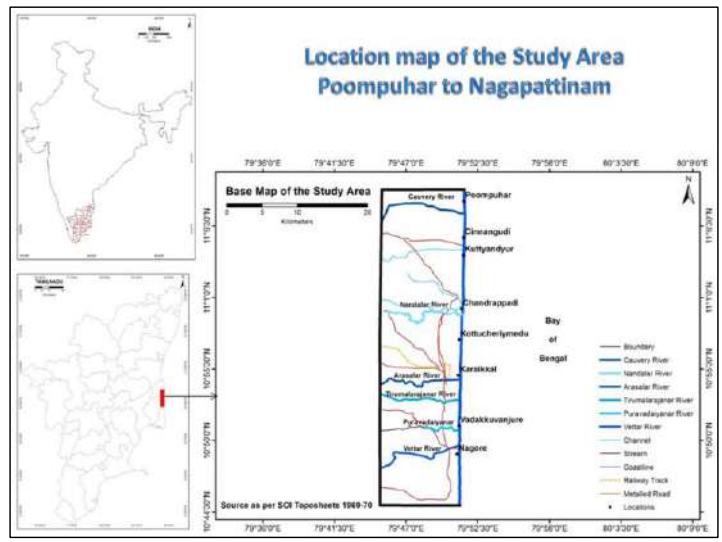

Fig. 1: Map of the study area.

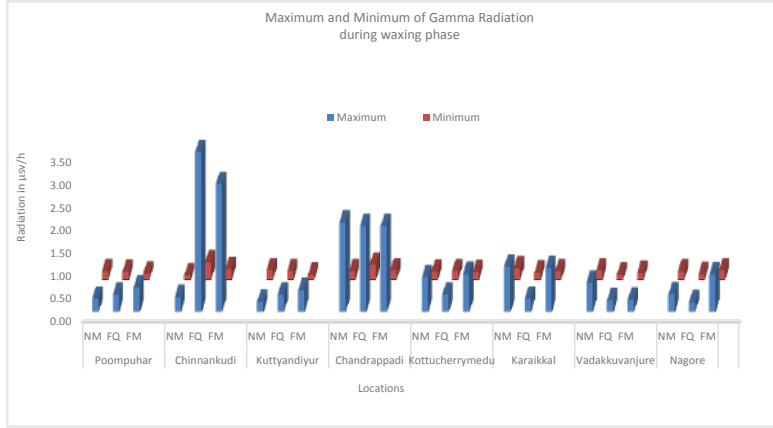

Fig. 2: Maximum and minimum gamma radiation during waxing phase.

mordial radionuclides in the area. The gamma values were the highest at Chinnankudi with 3.55 µsv.h^{-1}, followed by 1.72 µsv.h^{-1} at Chandrapadi (Table 1). It may be due to the fact that these two areas form strategic regions on either side of Chandrapadi with high amounts of radiations (i.e., Kuttiyandiyur and Kottucherimedu). Delineation of gamma dose rates at various locations during the period of study was analyzed with a spatial analyst tool. The values are found to be comparatively high in these regions (Fig. 3).

The calculated dose rates of gamma radiations of these regions indicate values as high as 3.55 µsv.h^{-1}. The comparably high values are certainly a major threat, affecting the region populated by the fishermen community. However, it is discomforting to know that still there are areas with thick mineral deposits, especially around the large fishermen population who defy any effort to remove the huge deposits, fearing erosion of their natural boundaries by the sea waves.

Table 1: Gamma radiation values during the period of study at all locations.

Horizontal Distance M	Poompuhar			Chinnangudi			Kuttyandiyur			Chanadrappadi		
	NM	FQ	FM	NM	FQ	FM	NM	FQ	FM	NM	FQ	FM
0	0.18	0.17	0.12	0.09	0.37	0.23	0.12	0.18	0.15	0.18	0.35	0.2
10	0.26	0.19	0.20	0.13	0.38	0.28	0.2	0.20	0.21	0.43	0.32	0.38
20	0.24	0.21	0.17	0.18	1.26	0.24	0.13	0.22	0.22	0.37	0.34	0.42
30	0.23	0.22	0.16	0.22	2.46	0.39	0.23	0.26	0.27	0.55	0.41	0.52
40	0.21	0.24	0.17	0.26	2.86	1.2	0.36	0.28	0.1	0.88	0.72	0.91
50	0.25	0.27	0.16	0.28	3.12	1.88	0.18	0.33	0.35	1.95	1.82	1.85
60	0.28	0.29	0.22	0.31	3.46	3.55	0.21	0.35	0.41	1.31	1.72	1.45

Horizontal Distance M	Kottucherrymedu			Karaikkal			Vadakkuvanjure			Nagore		
	NM	FQ	FM	NM	FQ	FM	NM	FQ	FM	NM	FQ	FM
0	0.17	0.18	0.16	0.2	0.15	0.4	0.2	0.1	0.14	0.18	0.12	0.2
10	0.17	0.20	0.21	0.3	0.32	0.3	0.59	0.14	0.12	0.23	0.20	0.25
20	0.32	0.22	0.33	0.3	0.18	0.4	0.42	0.16	0.14	0.25	0.11	0.28
30	0.19	0.26	0.45	0.2	0.2	0.2	0.32	0.15	0.14	0.35	0.15	0.39
40	0.71	0.28	0.66	0.4	0.17	0.2	0.63	0.19	0.26	0.29	0.22	0.45
50	0.34	0.33	0.73	0.3	0.21	0.2	0.42	0.21	0.17	0.34	0.18	0.59
60	0.75	0.35	0.75	0.4	0.2	0.2	0.37	0.23	0.16	0.38	0.19	0.67

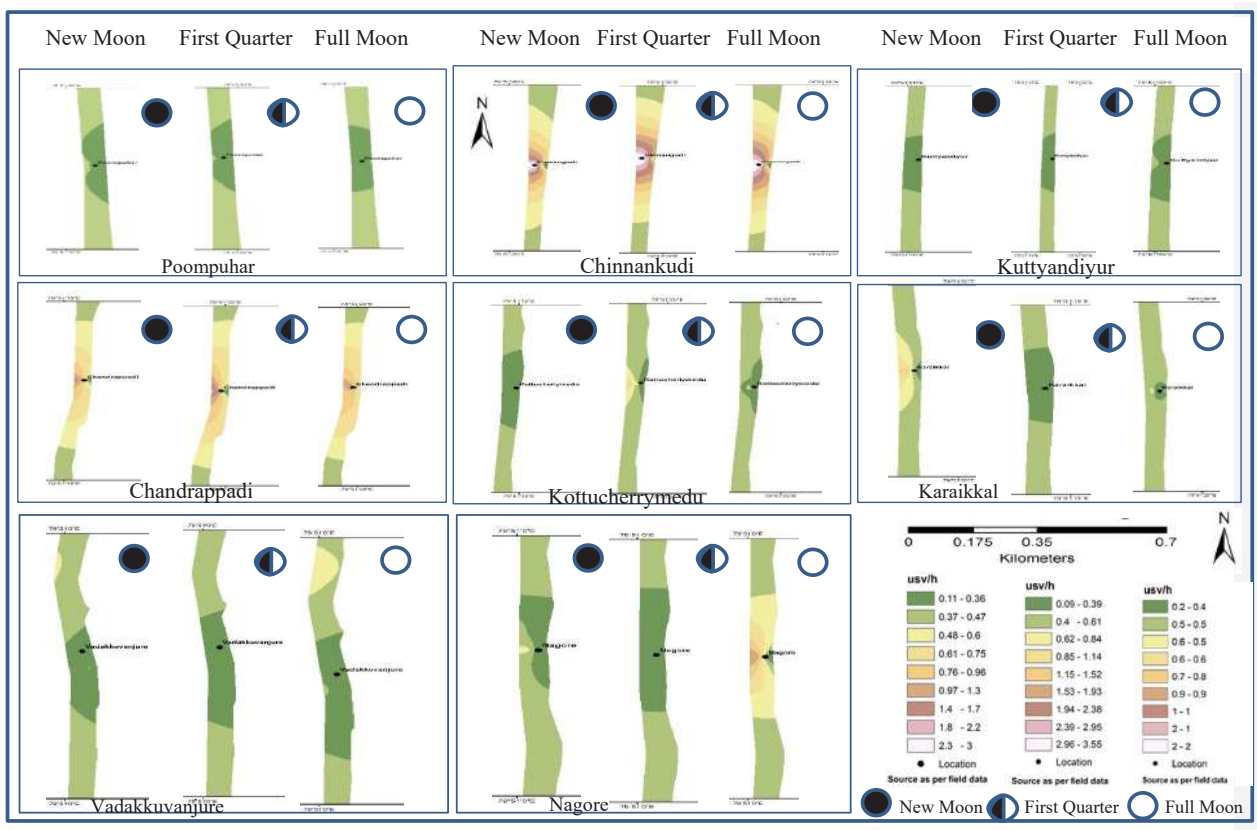

Fig. 3: Delineation of gamma dose rates at various locations during the period of study.

CONCLUSIONS

The effective gamma radiation during the new moon along the coastal range varies between 0.9 to 3.55 μsv.h^{-1}, respectively. The annual equivalent dose is estimated up to gamma radiation of 0.26 to 2.80 μsv.h^{-1}. Generally, the concentrations of the gamma radiation measured are elevated in certain areas namely Chinnagudi, Kuttiyandiyur, and Chandrapadi. In particular, the gamma radioactivity is high at Chandrapadi and Chinnagudi during the new moon as it shows considerable amounts of radiation.

There is a definite variation due to the moon phase on the gamma radiation profile of the area studied. Out of the eight coastal villages under study, about 60% of the coastal line shows high levels of gamma radiation during both new moon and full moon phases. It is obvious that gamma radiation variation mostly dependent on coastal hydro geomorphology and prevalent oceanic parameters.

REFERENCES

Abinesh, A. & Shanti G. 2016. Assessment of beach sand using gamma-ray spectrometer in Thiruvanathapuram District, Kerala of South India. Int. J. Technol. Eng., 5(3): 56.

Ching-Jiang, C., Pao-Shan,W. and Tich-Chichu, N. 1993. Evaluation of natural radiation in houses built with black schist. Health Phys., 64: 74-78.

Kanse, S.D., Sahoo, B.K., Gaware, J.J., Prajith, R. and Sapra, B.K. 2016. A study of thoron exhalation from monazite-rich beach sands of high background radiation areas of Kerala and Odisha, India. Environ. Earth Sci., 75: 1465.

Lal, D. 1991. Cosmic ray labeling of erosion surfaces: In situ nuclide production rates and erosion models. Earth Planet. Sci. Lett., 104: 424-439.

Malathi, J., Selvasekarapandian, S., Brahmanandhan, G. M., Khanna, D., Meenakshisundaram, V., and Mathiyarsu, R. 2005. Study of radionuclide distribution around Kudankulam nuclear power plant site (Agastheeswarram taluk of Kanyakumari district, India). Radiat. Prot. Dosim., 113(4): 415-420.

Mishra, U. C. 1990. High-level Natural Radiation Areas, Proceedings of the International Conference from 3-7 November 1990, Ramsar, Iran. IAEA Publication Series, IAEA, Vienna, pp. 29-36.

Monica, S., Visnu Prasad, A.K., Soniya, S.R. and Jojo, P.J.. 2017. Ambient gamma levels in the seaside regions of Alappuzha district, Kerala. Int. J. Pure Appl. Phys., 13(1): 179-187.

Papadopoulos, A., Christofides, G., Koroneos, A. and Stylianos, S. 2014. Natural radioactivity distribution and gamma radiation exposure of beach sands from Sithonia Peninsula, Central Europe. J. Geosci., 6(2): 229-242.

Papadopoulos, A., Koroneos, A., Christofides, G., Papadopoulou, L., Tzifas, I. and Stoulos, S. 2016. Assessment of gamma radiation exposure of beach sands in highly touristic areas associated with plutonic rocks of the Atticocycladic zone (Greece). J. Environ. Radioact., 162-163: 235-243.

Ragel, R.M.S. and Vetha, D.R. 2008. High background radiation sweeping along the southwest coast of Tamil Nadu, India. Curr. Sci., 94(10): 1250-1251.

Radhakrishna, A. P., Somashekarappa, H. M., Narayana, Y. and Siddappa, K. 1993. A new natural background radiation area on the southwest coast of India. Health Phys., 65(4): 390-395.

Singh, D., Shanker, V.N. and Neelakandan, V. P. Singh. 2007. Distribution of natural radioactivity and delineation of anomalous radioactive zones using in situ radiation observations in southern Tamil Nadu, India. J. Hazard. Mat., 141: 264-272.

Sivakumar, R., Selvasekarapandian, S., Muguntha Manikandan, N. and Raghunath, V.M. 2002. Natural indoor gamma background in Coonoor environment of South India. J. Radional. Nucl. Chem., 252(2): 413-419.

UNSCEAR 2000. Sources and Biological Effects of Ionizing Radiation. Annex B: Exposures from Natural Radiation Sources, New York.

Nature Environment and Pollution Technology
An International Quarterly Scientific Journal

p-ISSN: 0972-6268
(Print copies up to 2016)
e-ISSN: 2395-3454

Vol. 20 | No.3 | pp. 1353-1361 | 2021

Original Research Paper

https://doi.org/10.46488/NEPT.2021.v20i03.049

Open Access Journal

Analysis on Tourism Environmental Pollution and Tourism Economy-Ecological Environmental Coordination Degree: A Case Study from China

Zhong Wei Wang† and Huan Le Han
Yellow River Conservancy Technical Institute, Kaifeng 475004, Henan, China
†Corresponding author: Zhongwei WANG, Email: 94381557@qq.com

Nat. Env. & Poll. Tech.
Website: www.neptjournal.com

Received: 15-06-2021
Revised: 21-07-2021
Accepted: 01-08-2021

Key Words:
Tourism
Environmental pollution
Coordination degree
Shandong province

ABSTRACT

The rapid development of the tourism industry, range expansion, and intensity growth of human tourism activity have all caused intensifying ecological environmental problems while bringing considerable economic benefits. The ecological environment is currently faced with huge pressures due to the unreasonable tourism resource development, annual decrease in bearing capacity of the tourism environment, and excessive tourism consumption. To coordinate the relationship between tourism economic growth and ecological environment, this work carried out a case study based on Shandong Province, China. First, four aspects of environmental pollution caused by tourism were analyzed. Second, the tourism economy-ecological environmental coordination degree model and index system were established and then the coordination degree in Shandong Province from 2002 to 2019 was estimated. Results show that the tourism industry causes the following typical pollutions: water, soil, air, and noise. The coupling coordination degree (D) between the tourism economy and ecological environment in Shandong Province increased from 0.100 in 2002 to 0.995 in 2019, indicating the transition from serious imbalance to a high-quality coordination state. It is suggested to further promote tourism economy-ecological environment coordinated development by innovating the tourism-economy coupling development mode, creating the entire tourism industrial chain, increasing efforts in tourism reform, and exploring and implementing ecological compensation policies. Research conclusions have important significances to further study and explore the development status between the tourism industry and ecological environment and realize the coordinated development between the tourism industry and regional economy.

INTRODUCTION

The tourism industry has globally become the largest economic industry. With the rapid development of the global tourism economy and China's national economy, tourism has become one of the pillar industries to China's economic development. Recently, China has published many relevant policies to deepen reform in the opening of the tourism industry, accelerate its upgrading, optimize its structure, and support its development, facilitating its advancement into a strategic pillar industry of China's economic development and modernized service industry. However, with the development of the tourism industry, environmental problems caused by tourism economic activities have been a huge concern. Owing to unreasonable development and overload operation, tourism resource and ecological environment suffer excessive impacts, thus causing a series of environmental problems, including tourism-induced environmental pollutions (e.g., water, soil, noise, and waste pollutions), landscape hazards, and decreased biodiversity, among others.

Shandong Province, China is a province with high economic development and tourism development in Eastern China. It possesses a huge tourism industry scale and accepts numerous foreign and Chinese tourists. In Fig. 1, the foreign exchange earnings from tourism (million dollars) and reception of international tourists (million) increased each year from 2009 to 2019, with annual average growths of distribution at 9.33% and 3.03%, respectively. With the continuous growth of tourism income and tourists, the tourism industry has brought relatively serious environmental pollution. Given that the tourism industry in Shandong Province belongs to a typical resource and environment-dependent industry, the tourism activity scale in some regions disagrees with local environmental capacity. Hence, tourism resources are hazards, which are against the sustainable development in tourism regions in Shandong Province. Some tourism developers are only concerned with immediate interests and ignore environmental problems in the development process. Moreover, public consciousness of green tourism is weak, thus continuously increasing the carbon emissions of the entire tourism industry. The rapid development of the tourism industry not only promotes regional economic growth but also brings with it some environmental problems. The ecological environment of Shandong Province is vulnerable, and

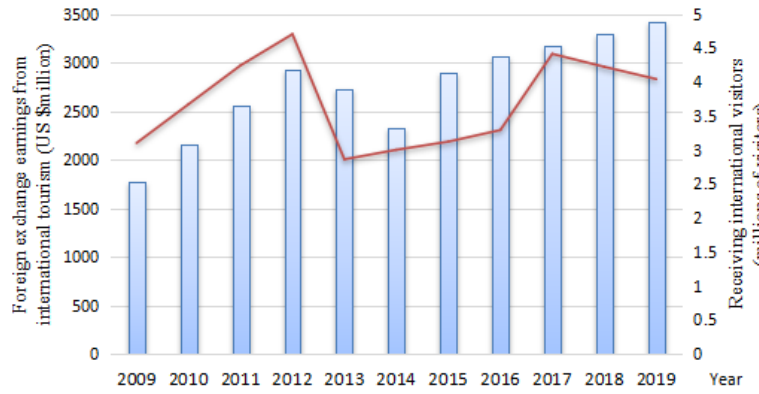

Fig. 1: Foreign exchange earnings from tourism and reception of international tourists during 2009-2019.

the effects of tourism activities on the ecological environment will be extremely obvious. Therefore, exploring the coupling relationship and mechanism between the tourism economy and ecological environment in Shandong Province, estimating the coupling development level of the two systems, and proposing suggestions for coordinated development are the necessary steps.

PAST STUDIES

Tourism-induced pollution hazards and the coordinated development between the tourism economy and ecological environment have become a hotspot in the sustainable development of the tourism industry. Since 1980, Chinese and foreign researchers have begun reporting many studies on environmental pollution and ecological safety problems in forest tourist attractions. In the aspect of tourism-induced pollution hazards: Greiner et al. studied the influences of environmental pollution on the optimization development of the tourism industry. Research results demonstrated that environmental pollution presents periodic effects on the tourism industry, and tourism activities decreased when heavy environmental pollution occurs (Greiner et al. 2001). Kocasoy et al. (2008) believed that the summer resort in the coastal regions discharges wastewater into the sea without any processing, thus worsening the water area in coastal regions. A case study based on two beaches in Turkey was carried out. Results showed that the direct discharge of wastewater in scenic areas into the marine environment without any processing led to serious seawater pollution. Jang et al. studied that abundant marine wastes were washed up to the beaches of Jiejie Island in Korea and influence the tourism industry of the island. This pollution event led the tourism industry to lose approximately 29-37 million dollars of revenue (Jang et al. 2014). Zhang et al. discussed the influences of the international tourism industry on China's energy consumption by replacing environmental pollution with CO_2 emission in the multi-variable framework based on the regional panel data from 1995 to 2011. Results demonstrated that the long-term effects of the tourism industry on CO_2 emission are a causal relationship (Zhang et al. 2016). Wilson et al. analyzed the influences of the tourism industry on the south of the Great Barrier Reef, and it was found to contribute to the litter level in the local areas. He found several tourism-sourced goods at places near the amenities, which led to waste pollution (Wilson et al. 2017). Ahmad et al. deemed that the rapid economic development in China and industrial transfer from East China to West China caused serious negative effects. According to research results, the tourism industry has negative impacts on the environments in Ningxia, Qinghai, Gansu, and Shanxi (Ahmad et al. 2018). Zeng et al. believed that unreasonable tourism development and huge energy consumption brought serious challenges to the urban environment in China. According to the results, the direct effects of tourism industrial development on the PM2.5 concentration presented an inverted U-shaped relation (Zeng et al. 2020). In the coordinated development between tourism economy and ecological environment, Huang et al. investigated the interactions between the tourism industry and mining industry in terms of economic contributions and spatial patterns in the biodiversity hotspot regions of Yunnan Province. It found that the tourism industry concentrates in underdeveloped regions, and it is an important industry to realize local economic development (Huang et al. 2011). Yuan et al. constructed the evaluation index system of the regional environment-tourism-economy coordinated development by using the pressure-state-response (PSR) model. Moreover, an empirical analysis on the coordinated development status between the environment and tourism economic system in western Hunan from 2001 to 2012 was carried out. Results showed that although the environment-tourism econom-

ic system in western Hunan has not reached a relatively high-efficiency index, the coupling degree among subsystems was not high (Yuan et al. 2014). Zheng et al. evaluated the comprehensive indexes and coordinated relationship between tourism economy and traffic system in 9 cities of the Pearl River Delta (PRD) by using the comprehensive evaluation model and coupling coordination model. Results showed that the tourism economy and traffic transportation in 9 cities of the PRD tended to form a coordinated development gradually, and the tourism economy in the central area of PRD was quicker than those in other regions (Zheng et al. 2016). Luo et al. carried out an expanded study on low-carbon tourist attractions and low-carbon tourism in Jiuzhaigou Valley by using the decarbonated development in the system of tourist attractions (DDSTA) index reference set and application set based on management entropy (Luo et al. 2017). Based on the sensitivity recovery pressure (SRP) framework, Kan et al. established the vulnerability evaluation system in the plateau tourist areas and provided a model that can be promoted to ecological vulnerability evaluation during tourism planning and development in high mountain regions (Kan et al. 2018). Lai et al. established the comprehensive evaluation index system of ecological environment, economy, and tourism industry, and calculated the coupling degree and coordination degree of 3 subsystems in 31 provinces in China from 2003 to 2017. Results showed that the mean coupling degree and mean coordination degree experienced a fluctuating upward trend from 2003-2017 (Lai et al. 2020). Yang et al. defined the restoration of urban tourism enterprises from the perspectives of social, economic, and ecological environments and constructed an evaluation index system of restoration power of urban tourism enterprises (Yang et al. 2021). Li et al. proposed the comprehensive evaluation index system of tourism development levels from the aspects of market scale, tourism economy, tourism resource, and tourism service. A coupling coordination degree model (CCDM) of tourism industry, urbanization, and ecological environment were built with panel data of Chongqing City from 2000 to 2017. As time goes on, the coupling coordination degree of the three systems increased progressively (Li et al. 2021). Burger et al. believed that the tourism industry can strengthen land protection on the landscape scale, thus protecting habitat and biodiversity (Burger et al. 2000). According to the existing literature review, Chinese and foreign scholars have achieved some research fruits on the relationship between the tourism industry and the regional economy. In China, studies focus on the transverse comparison between the tourism industry and regional economic development, but studies on longitudinal comparison and evolutional analysis have to be promoted. Moreover, the scientificity of the built comprehensive evaluation index system requires further discussion. Therefore, this study carried out a quantitative study on the coupling relation between tourism economy and ecological environment in Shandong Province, China, aiming to enrich the empirical range for studying tourism economy-ecological environment coordinated development. This study can provide some theoretical references to examine tourism in the study area and offer some policy suggestions to tourism economy-ecological environment coordinated development in Shandong Province.

TOURISM-INDUCED ENVIRONMENTAL POLLUTION HAZARDS

Water Pollution

Owing to tourism activities and sewage from the production and operation in the scenic areas, organic contents, mainly total nitrogen (TN) and total phosphorus (TP), increase significantly. In addition, substantial chemicals, such as cleansers and disinfectant fluid, are discharged into water bodies in scenic areas due to the affiliated industrial pollution discharge of tourism. Several pollutants continuously enter the water bodies of the scenic areas, thus causing water eutrophication and significantly increasing the microbial flora and suspended particles as well as reproductions of algae and fecal coliform. Boats and transport machines floating on the waters in the scenic areas are typically powered by diesel. The tail gas may cause water pollution, and poor maintenance of boat structures may cause diesel leakage which causes serious pollution to water bodies in scenic areas.

Soil Pollution

In tourism activities, the land surface surrounding arteries becomes bare due to the continuous stamping by tourists. Many problems result due to extensive loss of soil water, such as soil hardening, porosity reduction, permeability reduction, and increase in soil bulk density. The huge loss of soil water and increasing hardening degree weaken the adsorption of microelements in the soil surface layer and thus decrease organic contents and enzyme activity in the soil. Influenced by erosion of tourism lines, some regions have undergone serious soil degeneration. Construction of tourism attractions, tourist stamping, and unqualified garbage processing technology will also cause evident changes in the soil pH. Moreover, chemical reagents used by agricultural production near the tourism attractions, household wastes of tourists, and traffic tools can all increase the heavy metal contents in soils.

Air Pollution

The use of traffic tools, catering, hotel, and processing in

tourism attractions as well as harmful gases and substances represented by CO, SO_2, and Pb produced during the use of coal fuels in nearby factories can all worsen the air environment condition in the tourism attractions. Among them, SO_2 pollution which causes acidification of soils is the most serious. In the operation process of tourism attractions, garbage piling and fermentation caused by the poor disposal technology release considerable amounts of harmful gases, including methane and xylene. Suspended particles, such as flying dust and powder produced in the construction and development processes of tourist attractions as well as the smoke produced by relevant activities of affiliated industries in the scene, can all cause air pollution in the tourism scene.

Noise Pollution

The service process of tourism attractions produces excessive noise given that facilities and equipment such as roller coasters, boats, air conditioners, and machine rooms for tourism activities, consume substantial amounts of energy sources. Moreover, the power system and whistle of traffic tools, such as tour buses, sightseeing buses, self-driving cars, and trucks in the tourism attractions, from excessive noise. Tourist centers in the tourism attractions accumulate excessive noise due to the pronounced concentration or uproars of tourists. Different noises not only influence the tourism experiences of tourists but also affect the survival environment of animals and plants in the tourism attractions. The peak season of tourism activities in tourism attractions coincides with the season for animal and plant growth and development. Misconduct in the sightseeing process of tourists also brings notable impacts on the reproduction, migration, and other living habits of animals and may even cause their diseases and deaths.

MODEL INTRODUCTION AND INDEX SYSTEM

Coordination Degree Model

Estimation of coordination degree: Considering that two subsystems $S_j, j \in [1,k]$ of tourism economy and ecological environment are studied, the order parameter variables in the development process of these two subsystems are $e_j = (e_{j1}, e_{j2}, \cdots, e_{jn})$, where $n \geq 1, \beta_{ji} \leq e_{ji} \leq \alpha_{ji}, i \in [1,n]$. Without loss of generality, we suppose that the order degree of systems is positively related to the value of $e_{j1}, e_{j2}, \cdots, e_{jl}$ and is negatively related to the value of $e_{jl+1}, e_{jl+2}, \cdots, e_{jn}$. The tourism economy and ecological environmental system of Shandong Province include the Shandong tourism economic subsystem and Shandong ecological environmental subsystem. The order parameters in the development process of the tourism economic subsystem are $e_1 = (e_{11}, e_{12}, \cdots, e_{1n})$. According to the concept of order degree of the system, we defined the order degree of order parameter component e_{1j} of the tourism economic subsystem as:

$$u_1(e_{1i}) = \begin{cases} \dfrac{e_{1i} - \beta_{1i}}{\alpha_{1i} - \beta_{1i}} (i = 1,2,\cdots l) \\ \dfrac{\alpha_{1i} - e_{1i}}{\alpha_{1i} - \beta_{1i}} (i = l+1, l+2, \cdots n) \end{cases} \quad \ldots(1)$$

Where α_{1i} and β_{1i} are the maximum and minimum of index i of the tourism economic subsystem. According to this definition, we can know that $u_1(e_{1i}) \in [0,1]$ after normalization. The higher value indicates the greater contribution of e_{1i} to the order of tourism economic subsystem. In general, the total contributions of order parameters to the order degree of the tourism economic subsystem can be realized through the integrated approach of $u_1(e_{1i})$. First, the weights of different indexes have to be determined. To increase the scientificity of index weight, the classical CRITIC (CRiteria Importance Through Intercriteria Correlation) objective weighting method was applied. Diakoulaki D et al. proposed the CRITIC method (Diakoulaki et al. 1995):

$$\xi_j = \sigma_j \times \sum_{j=1}^{n} (1 - r_{ij}) (j = 1,2,3,\cdots,n) \quad \ldots(2)$$

where ξ_j is the influence degree of the evaluation index j on the system. σ_j is the standard deviation of the evaluation index j. r_{ij} is the correlation coefficient between evaluation indexes i and j. The higher numerical value of ξ_j indicates the greater influence degree of the evaluation index j on the system. Hence, the calculation formula of objective weight ω_j of the evaluation index j is

$$\omega_j = \frac{\xi_j}{\sum_{j=1}^{n} \xi_j} (j = 1,2,3,\cdots,n) \quad \ldots(3)$$

Where ω_j denotes the weight of different indexes. Apparently, the order degree of tourism economic subsystem is $u_1(e_1) \in [0,1]$. The higher value of $u_1(e_1)$ indicates the greater contributions of e_1 to the order degree of the system. Thus, the order degree of the tourism economic subsystem is higher; otherwise, it is lower. Suppose the order parameter in the development process of ecological environmental subsystem is $e_2 = (e_{21}, e_{22}, \cdots, e_{2i})$. Similarly, the order degree of the parameter component of ecological environmental subsystem e_{2i} can be obtained according to the calculation method of the order degree of tourism economic subsystem, which is $u_2(e_{2i})$: $u_2(e_{2i}) \in [0,1]$. Suppose the order degree of tourism economic subsystem is $u_1^0(e_1)$ and the order degree of ecological environmental subsystem is $u_1^1(e_1)$ at the initial moment t_0. When the system evolves to t_1, the order degree of tourism economic subsystem is $u_1^1(e_1)$, and the order

degree of ecological environmental subsystem is $u_2^1(e_2)$. If $u_1^1(e_1) \geq u_1^0(e_1), u_2^1(e_2) \geq u_2^0(e_2)$ are simultaneously proven, the tourism economy and ecological environment combined system is coordinately developed, and the coordination degree model is shown as follows.

$$c_2 = \left\{(u_1 \times u_2) / \left[(u_1 + u_2) \times (u_1 + u_2)\right]\right\}^{1/2} \quad \ldots(4)$$

Where c_2 represents the coupling degree of the combined system. u_1 and u_2 are order degrees of tourism economic subsystem and ecological environmental subsystem, respectively.

$$D = \sqrt{C \times T}, \; T = \alpha u_1 + \beta u_2 \quad \ldots(5)$$

where D is the coupling coordination degree of the combined system. T refers to the comprehensive evaluation index of tourism economy and ecological environment. α and β are coefficients for determining, which are generally determined as 0.5 and 0.5, respectively. Some differences exist in the mutual promotion degrees of subsystems in the combined system.

Grading of coordination degree: The coordination degree model involves the calculation of 3 indexes, namely, the coupling degree (C), coordination index (T), and coupling coordination (D). Finally, the coupling coordination degrees of different indexes are obtained through D and coordination grading standards. The coupling coordination degree originated from the capacity coupling coefficient model in physics. C value is calculated. The higher value indicates the greater interaction between the two subsystems. D value is equal to the product of C value and T value, and it ranges between 0–1. The higher value of D indicates the higher coordination degree between the two subsystems.

Index System

The tourism economy and ecological environment coupling evaluation index system shall involve tourism economic and ecological environmental development levels. Based on meeting the design principle of comprehensive, objective, operable, quantitative, and qualitative indexes, Table 1 shows an evaluation index system of tourism economy-ecological environmental coordination degree built preliminarily through a comprehensive analysis of definition connotations, influencing factors, and structural characteristics of tourism economy and ecological environment and by combining frequency analysis of evaluation indexes in existing studies. Additionally, the investigation period is from 2002 to 2019.

EMPIRICAL STUDY

According to the coupling evaluation model and formula, this study estimated and analyzed the tourism economy and ecological environment coupling development in Shandong Province. Fig. 2 shows the results. As seen from Fig. 2, the comprehensive evaluation level of the tourism economy in Shandong Province generally presents a fast growth trend, and the comprehensive evaluation level of the tourism economy significantly increases from 0.0002 in 2002 to 0.5908 in 2019. In this period, the economic growth rate was relatively high in Shandong Province. Accordingly, the growth rates of tourism income and resident income were in a high-level growing trend. Tourism plans, such as the "13th Five-year" Plan for Tourism Industrial Development of Shandong Province, were approved and implemented successively. These steps can all promote the sound and reasonable development of the tourism industry in Shandong Province. At the same time, Shandong Province was making considerable efforts to promote the integrated development of tourism, facilitating the transformation and upgrading of international tourism and guiding the "tourism +" mode, thus realizing rapid tourism economic growth in the province. From 2002 to 2019, the comprehensive evaluation level of the ecological

Table 1: Coupling coordination grading standards.

Interval of D	Coordination grade	Coupling coordination degree
(0.0–0.1)	1	Extreme imbalance
[0.1–0.2)	2	Serious imbalance
[0.2–0.3)	3	Moderate imbalance
[0.3–0.4)	4	Slight imbalance
[0.4–0.5)	5	Endangered imbalance
[0.5–0.6)	6	Poor balance
[0.6–0.7)	7	Primary balance
[0.7–0.8)	8	Moderate balance
[0.8–0.9)	9	Good balance
[0.9–1.0)	10	High-quality balance

environment in Shandong Province highly fluctuated and developed from 0.002 in 2002 to 0.8337 in 2019. Owing to the continuous development of the tourism economy, tourism activities cause a huge ecological environmental pressure, while the comprehensive evaluation level of the ecological environment remains low. Shandong Province successively issued environmental protection regulations in the process of international tourism destinations and comprehensive reform pilot zones of tourism by providing substantial capital funds to environmental protection control. These regulations somewhat promoted the improvement of the ecological environment. Government intensity policies and measures for pollution control and the industrial structure and resource configuration are optimized. Consequently, the comprehensive evaluation level of Shandong Province began to increase again.

As seen from Table 3, the D value increased from 0.100 in 2002 to 0.995 in 2019, indicating that tourism and ecology in Shandong Province have developed from extreme imbalance in 2002 to high-quality balance in 2019. Recently, China has issued many policy documents that support ecological protection and tourism industry integrated development. Shandong Province created a unique cultural experience, designed participated experiencing projects, and enriched the tourism product system by strengthening tourism development of cultural sites and relics using high-tech tools. Shandong Province built a group of high-quality resort areas, improved and created the national-level resort areas, and strengthened the dynamic management of provincial resort areas. Guided by building a good traditional cultural tourism base and a red cultural tourism base, the new advantages of cultural tourism in Shandong Province are created. Meanwhile, promoting and implementing the infrastructure construction of poverty alleviation pilots via tourism have begun. In Shandong Province, rural tourism resource points are enriching continuously, and tourism destinations available for tourists are increasing and thus effectively lowering the tourist density in key scenic areas and relieving ecological environmental pressure.

POLICY SUGGESTIONS

Innovate the Tourism Economic Coupling Development Mode and Relieve Ecological Pressure

The technology-dependent independent innovative tourism

Table 2: Evaluation index system of tourism economy and ecological environment coordination degree.

Indexes of tourism economic subsystem (Unit)	Indexes of ecological environmental subsystem (Unit)
Number of received inbound tourists staying overnight (people)	Daily handling capacity of urban sewage (10,000 m^3)
Number of days of received inbound tourists staying overnight and days (people/day)	Urban Greenland area (ha.)
Average stay of received inbound tourists (days)	Park area (ha.)
Number of star-rated hotels (hotels)	Cleaning area (10,000 m^2)
Labor productivity of total workers (1,000 yuan/people)	Amount of household waste clean-up (10,000 tons)
Per capita original value of fixed assets (1,000 yuan/people)	Wash rooms (rooms)
Revenues from 100 yuan of fixed assets (yuan)	Per capita green land area in parks (m^2)
Average occupancy rate of rooms (%)	Harmless handling capacity (tons/day)
Total number of travel agencies (agencies)	Natural reserve area (10,000 ha.)
Total number of tourism colleges (colleges)	Finished investment for industrial pollution control (100 million Yuan)

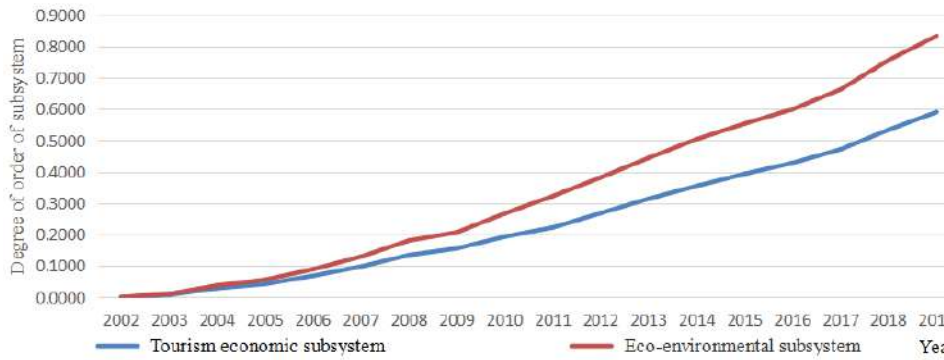

Fig. 2: Order degrees of tourism economic subsystem and ecological environmental subsystems.

economic coupling development mode is applied in core areas composed of regions with increasing coupling coordination, such as Weihai, Qingdao, and Yantai with highly developed infrastructure and traffic conditions and in the leading position of comprehensive potentials of the tourism industry. These areas shall use tourism industrial development as the bright spot of economic development under a new normal condition. As an important breakthrough that promotes local economic and social development, the tourism industry becomes one of the new dominant kinetic energies driving regional economic development. Finally, the coupling coordination development between the tourism industry and regional economy is realized. Further attention shall be paid to the environmental construction of industrial institutions and fundamental supports. The regulation effect of market mechanism and openness to foreign trade shall be increased. The internal growth potential of the tourism industry is improved by increasing the agglomeration effect and innovation ability. In addition, the market expansion potential of the entire industry is enhanced by guiding and mining market demand potentials. It is suggested to innovate the state of the tourism industry, increase industrial points, deviate industry chain, expand the industrial surface, and construct industrial clusters. New benefit modes are formed by deepening development.

Create the Entire Chain of Tourism Industry and Reduce Resource Waste

Establishing large-scale tourism groups through merge & acquisitions, creating a complete industrial chain, and increasing the levels of economic scale and range of the entire tourism industry. Centered at tourism demand, it shall strengthen mutual integration and permeation of the tourism industry and other industries to form an integrated development mode. With respect to integration mode, the tourism industry can be embedded into relevant industries, and these industries are endowed with tourism functions, thus realizing grafting between tourism industrial elements and other industries. The transboundary integration between tourism and various industries is promoted to drive the development of relevant industries. It gives birth to an infinite space for industrial development and facilitates tourism development in the entire region, thus increasing the coupling coordination degree between the tourism industry and regional economy to the coordination rising type. Different cities in Shandong Province shall focus on the construction and perfection of the basic elements of the tourism industry according to practical conditions. They can develop some new tourism products that are independent of tourism resources, such as festival travel and rural tourism, to expand the scope of the tourism industry and provide other practical pathways for tourism industrial development.

Table 3: Calculated results of coupling coordination degree.

Year	C value	T value	D value	Coupling coordination degree
2002	1	0.010	0.100	Extreme imbalance
2003	1	0.022	0.150	Extreme imbalance
2004	0.999	0.056	0.236	Moderate imbalance
2005	1	0.078	0.279	Moderate imbalance
2006	0.999	0.119	0.345	Slight imbalance
2007	1	0.167	0.409	Endangered imbalance
2008	1	0.228	0.477	Endangered imbalance
2009	1	0.261	0.511	Poor balance
2010	1	0.327	0.572	Poor balance
2011	1	0.384	0.620	Primary balance
2012	1	0.457	0.676	Primary balance
2013	1	0.532	0.729	Moderate balance
2014	1	0.601	0.775	Moderate balance
2015	1	0.662	0.814	Good balance
2016	1	0.718	0.847	Good balance
2017	1	0.791	0.889	Good balance
2018	1	0.898	0.948	High-quality balance
2019	1	0.990	0.995	High-quality balance

Increase Tourism Reform Strength and Advocate Green Tourism

Government at all levels, environmental protection and tourism department, tourism consumers, and relevant tourism enterprises in Shandong Province shall run through the philosophy of low-carbon environment-friendly tourism. Government and environmental protection sectors shall strengthen environmental monitoring and fulfil the environmental protection supervision. The government and tourism department shall make reasonable tourism plans, perform scenic area division and public tourism tool distribution among different scenic spots during the peak season of tourism, and relieve ecological pressure in the scenic spots. Tourism enterprises shall take the initiative in using environment-friendly materials and try to decrease waste-water and waste gas emissions in the production and management process. Tourists shall be aware of carrying bags and cups to reduce garbage production in the scenic areas. They shall try to choose environment-friendly public transport means and protect historical relics, landscape buildings, animals, and plants well during their travels. Scenic spots shall be far away from the pollution discharge enterprises, and the number of parking cars in the scenic areas shall be controlled strictly during the peak season of tourism. It shall advocate green transport means such as bikes, strengthen noise detection in cities, prohibit long-term whistles in scenic spots, and create a relaxed and quiet travelling environment. Scenic spots and mountain resorts shall be equipped with adequate garbage tins and environment-friendly washrooms, and all garbage shall undergo a harmless and timely disposal process.

Strengthen Publicity Education and Explore the Implementation of Ecological Compensation Policy

Owing to the rapid industrial development in modern times, many enterprises and masses excessively pursue economic benefits while maintaining weak consciousness of ecological environmental protection, thus resulting in forest degeneration and frequent occurrences of natural disasters and different degrees of damages to tourism ecological environment. Environmental protection and publicity require further strengthening. Government at all levels and environmental protection departments of Shandong Province can make publicity and education activities on environmental protection by using the Environmental Day and National Science Popularization Day and spread knowledge about ecological environmental protection via online We-media, radio programs, and TV shows to strengthen public consciousness regarding ecological environmental protection. The tourism department shall strengthen business ability training for environmental protection workers in the scenic spots. It should also encourage tour guides to spread tourism environmental protection knowledge when introducing the landscapes and advocate tourism enterprises to provide green and environment-friendly tourism products and services. Shandong Province shall explore the marketized ecological compensation mode of tourism and standardize the ecological resource market. An ecological compensation fund shall be set up. In particular, attention shall be paid to compensations for tourism ecological managers and local residents and relieving benefit imbalance among construction parties and ecological environmental protection.

CONCLUSIONS

Environmental problems become increasingly prominent due to behaviors such as the continuous booming of tourists, random piling of solid wastes, and excessive development of tourism resources. Scenic spots are faced with heavy water, soil, air, and noise pollutions. These environmental pollution problems in scenic spots not only seriously threaten ecological safety but also become key constraints against the sustainable development of the tourism industry. This study analyzes four aspects of tourism-induced environmental pollutions in Shandong Province, China. Moreover, it builds a tourism economy-ecological environment coordination degree model and an index system. It then estimates the tourism economic and ecological environment coordination degree of Shandong Province from 2002 to 2019. Results demonstrate that water, soil, air, and noise pollutions are four aspects of environmental pollutions caused by the tourism industry. The D value in Shandong Province increases from 0.100 in 2002 to 0.995 in 2019, indicating the successful transition from extreme imbalance to high-quality balance. Deepening studies on enriching the tourism industry and regional economic subsystems and subsequently exploring the temporal differences in coupling and coordination between the tourism industry and regional economy are recommended.

REFERENCES

Ahmad, F., Draz, M., Su, L., Ozturk, I. and Rauf, A. 2018. Tourism and environmental pollution: evidence from the one belt one road provinces of western China. Sustainability, 10(10).

Burger, J. 2000. Landscapes, tourism, and conservation. Science of the Total Environment, 249(1-3): 39-49.

Diakoulaki, D., Mavrotas, G. and Papayannakis, L. 1995. Determining objective weights in multiple criteria problems: The critic method. Computers & Operations Research, 22(7): 763-770.

Greiner, A., Feichtinger, G., Haunschmied, J. L., Kort, P. M. and Hartl, R. F. 2001. Optimal periodic development of a pollution generating tourism industry. European Journal of Operational Research, 134(3): 582-591.

Huang, G., Zhou, W. and Ali, S. 2011. Spatial patterns and economic contributions of mining and tourism in biodiversity hotspots: a case study in China. Ecological Economics, 70(8): 1492-1498.

Jang, Y. C., Hong, S., Lee, J., Lee, M. J. and Shim, W. J. 2014. Estimation of lost tourism revenue in Geoje island from the 2011 marine debris pollution event in South Korea. Marine Pollution Bulletin, 81(1): 49-54.

Kan, A. K., Li, G. Q., Yang, X., Zeng, Y. L., Tesren, L. and He, J. 2018. Ecological vulnerability analysis of Tibetan towns with tourism-based economy: a case study of the Bayi District. Journal of Mountain Science, 15(5): 1101-1114.

Kocasoy, G., Mutlu, H. and Alagöz, B. 2008. Prevention of marine environment pollution at the tourism regions by the application of a simple method for the domestic wastewater. Desalination, 226(1-3): 21-37.

Lai, Z., Ge, D., Xia, H., Yue, Y. and Wang, Z. 2020. Coupling coordination between environment, economy and tourism: a case study of china. PLOS ONE, 15 (2), e0228426.

Li, L., Yang, Q., Sun, C., Xie, X. and Zhang, F. 2021. Coupling coordinated evolution and forecast of tourism-urbanization-ecological environment: the case study of Chongqing, china. Mathematical Problems in Engineering, (3): 1-15.

Luo, Y., Wang, Z., Wang, J., Liao, Z. and Hu, M. 2017. Measuring decarbonated development of tourist attractions associated with ecological environment and tourism economy. Journal of Intelligent and Fuzzy Systems, 33(7): 1-10.

Wilson, S. P. and Verlis, K. M. 2017. The ugly face of tourism: marine debris pollution linked to visitation in the southern great barrier reef, Australia. Marine Pollution Bulletin, 117(1-2): 239.

Yang, X., Zhang, D., Liu, L., Niu, J., Zhang, X. and Wang, X. 2021. Development trajectory for the temporal and spatial evolution of the resilience of regional tourism environmental systems in 14 cities of Gansu province, china. Environmental Science and Pollution Research, 1-22.

Yuan, Y., Jin, M., Ren, J., Hu, M. and Ren, P. 2014. The dynamic coordinated development of a regional environment-tourism-economy system: a case study from western Hunan province, China. Sustainability, 6(8): 5231-5251.

Zeng, J., Wen, Y., Bi, C. and Feiock, R. 2021. Effect of tourism development on urban air pollution in china: the moderating role of tourism infrastructure. Journal of Cleaner Production, 280: 124397.

Zhang, L. and Gao, J. 2016. Exploring the effects of international tourism on china's economic growth, energy consumption and environmental pollution: evidence from a regional panel analysis. Renewable and Sustainable Energy Reviews, 53: 225-234.

Zheng, Q., Kuang, Y. and Huang, N. 2016. Coordinated development between urban tourism economy and transport in the Pearl river delta, China. Sustainability, 8(12): 1338-1338.

Nature Environment and Pollution Technology
An International Quarterly Scientific Journal

p-ISSN: 0972-6268
(Print copies up to 2016)
e-ISSN: 2395-3454

Vol. 20 | No.3 | pp. 1363-1368 | 2021

Original Research Paper

https://doi.org/10.46488/NEPT.2021.v20i03.050

Open Access Journal

Nitrate-Nitrogen ($N\text{-}NO_3^-$) in Ground Waters of Agricultural Zones in Tabasco, México; Risks for Aquatic Life and Human Health

I. Galaviz-Villa*†, C.A. Sosa-Villalobos*, N.L. Lagunes-Reyes*, C. Landeros-Sánchez, M.A. Castillo-Ferat*, A. García-Saldaña*, S. Partida Sedas*** and A. Cabal Prieto*****

*Tecnológico Nacional de México/Instituto Tecnológico de Boca del Río, Carretera Veracruz- Córdoba km 12 C.P. 94290. Boca del Río, Veracruz, México.

**Colegio de Posgraduados Campus Veracruz, Carr. Xalapa Veracruz km 88.5 carretera federal Xalapa-Veracruz, 91700 Ver. México.

***Tecnológico Nacional de México/ Instituto Tecnológico Superior de Huatusco, Av. 25 Poniente No.100, col. Reserva Territorial Huatusco, Veracruz, México, C.P. 94100.

†Corresponding author: I. Galaviz-Villa: itzelgalaviz@bdelrio.tecnm.mx

Nat. Env. & Poll. Tech.
Website: www.neptjournal.com

Received: 10-09-2020
Revised: 29-10-2020
Accepted: 08-12-2020

Key Words:
Agriculture
Animal husbandry
Leaching of N-compounds
Water pollution
Marine life protection

ABSTRACT

Nitrate nitrogen ($N\text{-}NO_3^-$), the most common pollutant in groundwater, is a result of the effect of diffuse sources of pollution like agriculture and animal husbandry intensive. The land use for these economic activities is very common in the Los Ríos sub-region in the state of Tabasco, Mexico, where the Los Ríos and Boca del Cerro aquifers are located. The aim of this research was to assess the concentrations of nitrate-nitrogen ($N\text{-}NO_3^-$) in groundwater, determine the quality in agreement with the maximum permissible limits established by national and international regulations, and the risks to the public health and aquatic life. The spatial distribution of $N\text{-}NO_3^-$ was determined using the inverse distance weighted (IDW) interpolation technique. The average nitrate-nitrogen concentration was 0.76 $mg.L^{-1}$, while the maximum concentration observed was 3.98 $mg.L^{1}$. This does not exceed the maximum permissible limit (MPL) established in the national and international normativity for drinking water. However, in 50% of the sampling sites, the concentrations of $N\text{-}NO_3^-$ exceed the MPL established in Mexico for the protection of the life of seawater. Relatively low concentrations of $N\text{-}NO_3^-$ have shown to be toxic to certain aquatic organisms, and the aquifers studied discharge a third of the water to the rivers in the area, which flow into the Laguna de Términos Campeche and the Gulf of Mexico. Laguna de Términos Campeche is one of the most diverse and rich environmental systems on earth, where numerous ecosystems converge such as coastal lagoons, wetlands, mangroves, seagrasses, and coral reefs.

INTRODUCTION

Groundwater is the largest reservoir of freshwater that is easily available to humans (Zaporozec 2002). In Mexico, 38.7% of the total volume of water granted for consumptive uses comes from groundwater (CONAGUA 2015). Among the pollutants that affect groundwater, nitrates are important because of their mobility, soluble nature, distribution area, and the risk they pose to human health and the ecosystem (Martínez et al. 2011). Nitrates are converted into nitrites by the action of certain bacteria in the esophagus. This conversion can also occur in other sites, including the small intestine and the colon (Ward et al. 2005). Nitrite is one of the most commonly reported agents causing methemoglobinemia (Basulto et al. 2014), a disease caused by the increase of methemoglobin in the blood. Its effects range from cyanosis (blue discoloration of the skin) to diarrhea, tachycardia, headache, fatigue, lipothymia, nausea, anorexia, and vomiting (Larios 2009). In addition, nitrate is a precursor in the formation of N-nitrous compounds such as nitrosamides and nitrosamines, which are gastric carcinogens produced by the combination of nitrites with amides and amines (Ward et al. 2005).

The enrichment of nutrients (phosphorus and nitrogen, as well as compounds of these elements) in marine and freshwater systems causes eutrophication (Karydis 2009), which affects algal blooms, anoxia, and death of aquatic organisms (Dokulil & Teubner 2010). In addition, the presence of nitrates in water represents a risk for living beings. As with humans, nitrate in aquatic organisms transformed into nitrite reduces the ability to transport oxygen in the blood (Camargo & Alonso 2007). These compounds can be found in groundwater as a result of natural and anthropogenic sources, among latter, agricultural activities represent a serious threat given that the use of fertilizers is not regulated and producers are often in the excessive application of them (Galaviz et al. 2011, Rodríguez et al. 2015).

In recent decades, extensive areas of forests, mangroves, popales, and tulares of the state of Tabasco have been disappearing to give way to a greater number of ejidos dedicated to agriculture and livestock (Munguía 2005). In the region of Tabasco Los Ríos, agriculture and livestock are the most important economic activity, and the use of land is, for the most part, dedicated to cultivated pastures (INEGI 2015). Added to this, in the municipalities that make up the study area, the fertilized surface shows a growth trend. From 2011 to 2016, the fertilized area in the municipalities of Balancán and Emiliano Zapata increased by 95% and 29%. In Tenosique, during the same period, the sown area decreased by 36%, although the fertilized surface increased by 2% (SIAP 2011, 2013, 2016).

Within this region, there are two aquifers, Los Ríos and Boca del Cerro, which are unconfined, with static levels ranging from 30 cm to 20 m and contain sulfated sodium, sodium bicarbonate, sodium chloride, and mixed waters (CONAGUA 2002a, 2002b). No historical data or background of similar studies conducted in these aquifers was found. Therefore, the objective of this study was to assess nitrate-nitrogen concentrations ($N\text{-}NO_3^-$) in groundwater of the Los Ríos and Boca del Cerro aquifers and compare them with national and international standards to determine if there is contamination that poses a risk to public health and aquatic life.

MATERIALS AND METHODS

The study area covered the municipalities of Tenosique, Balancán, Emiliano Zapata and Jonuta in the state of Tabasco, México in which the Los Ríos and Boca del Cerro aquifers lie (Fig. 1). The predominant climate is humid and warm with abundant rains in summer. The average annual temperature range is 26 to 28 °C and the annual rainfall is 1,500 to 2,500 mm (INEGI 2015, INIFAP 2016).

The information related to the use of soil, surface water, groundwater, and urban and rural localities was taken from the digital repository of the National Institute of Geography and Statistics for its interpretation, modification, and mapping in the geographic information system (GIS), QGIS, version 2.18.2 for Windows.

With the information provided by the State Water and Sanitation Commission (SWSC) from each municipality, the inventory of existing and active wells was carried out. Subsequently, the wells were identified through the GIS and the sampling sites were determined (Fig. 1).

The study was carried out from May to October 2017 in two sampling seasons - the dry season (May-June,) and the end of the rainy season (August-October). Thirty wells were

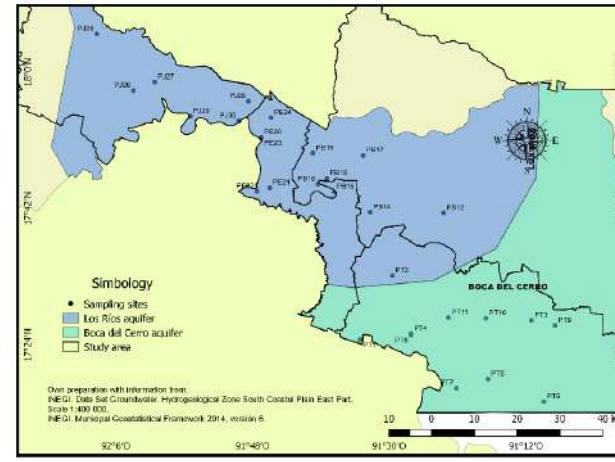

Fig. 1: Location of the aquifers Los Ríos and Boca del Cerro and groundwater sampling sites in the study area.

sampled, of which eleven are located in the municipality of Tenosique, eight in Balancán, five in Emiliano Zapata, and six in Jonuta. In situ measurements of temperature, electrical conductivity (EC), and hydrogen potential (pH) were made with HACH SENSION + MM 156 multisensor. The laboratory results were reported as nitrate-nitrogen ($N\text{-}NO_3^-$), and the laboratory analysis of the water samples was carried out by method 353.2 (automated colorimetry) of the EPA (1993).

The statistical analysis was carried out with the STATISTICA v.12 program. Kolmogorov-Smirnov normality tests and non-parametric analysis of variance were performed using the Kruskal-Wallis test to determine the existence of significant differences between the concentrations of $N\text{-}NO_3^-$ by land use. The $N\text{-}NO_3^-$ isoconcentration map was developed with the QGIS software, using the interpolation method of inverse distance weighting (IDW).

RESULTS AND DISCUSSION

Results

The maximum concentration of $N\text{-}NO_3$ in the low season was 3,979 $mg.L^{-1}$ and the minimum concentration was 0.0049 $mg.L^{-1}$. At the end of the rainy season, in 17 of the 30 sampling sites, the average concentration of $N\text{-}NO_3$ increased to 0.54 $mg.L^{-1}$, although the increase recorded in the sampling site corresponding to the population of Multé (Balancán) was 3.06 $mg.L^{-1}$. In eight sites, the decrease of $N\text{-}NO_3^-$ was on average 0.45 $mg.L^{-1}$, although the decrease recorded in the sampling site corresponding to the population of Chablé population was 2.07 $mg.L^{-1}$. In the remaining five sites, it was not possible to determine the difference in concentrations of $N\text{-}NO_3^-$, because in some seasons the result was less than the detection limit. In the rainy season, the maximum concentration registered

was 3,821mg.L^{-1} of N-NO_3^-, while the minimum was 0.0027 mg.L^{-1} of N-NO_3^-. The average concentration of N-NO_3 (0.872 mg.L^{-1}) was higher at the end of the rainy season than at the beginning of the rainy season. The averages of pH (7.3), EC (96.5), and temperature (29.4) showed high values in the dry season. The standard deviation of the concentrations of N-NO_3^- was higher in this season (Table 1).

DISCUSSION

The results obtained are explained by the temporary variability of N-NO_3^-, which in summer show minimum values (Graco et al. 2007) due to the biological demand of vegetation and crops (Nevárez & Flor 2014). The quartiles of the variable N-NO_3^- took the values of 0.028 (Q1) and 0.892 (Q3) in the dry season, and 0.032 (Q1) and 1.22 (Q3) in the rainy season. 50% of the observations were found between these values for each season (Table 1).

The Kolmogorov-Smirnov normality test with the Lilliefors correction ($d = 0.2672$, $p < 0.05$) indicated that the data of N-NO_3^- did not follow a normal distribution, which was confirmed by adjustment probability graphs (Fig. 2).

The result of the statistical analysis (Kruskal Wallis $H [2,24] = 2.467$, $p = 0.291$) showed that there was no statistically significant differences between the land use categories (grassland, agricultural and human settlement) when comparing the medians of their N-NO_3^- concentrations. Given that the proximity of the sources of contamination to the sampling sites is the variable most associated with the concentration of N-NO_3^- (Gallart 2008, Perdomo et al. 2001), it is probable that the results obtained are lower than the concentrations that could be found in areas dedicated to crops where nitrogenous fertilizers are applied (Estrada-Botello et al. 2002, Muñoz et al. 2004).

The spatio-temporal distribution of the concentrations of

Table 1: Descriptive statistics of the groundwater sampling of the Los Ríos and Boca del Cerro aquifers in the state of Tabasco, México.

STATISTICAL	N-NO_3^- (mg.L^{-1})		pH		C.E. (µS)		T (°C)	
	Dry season	Rainy season	Dry season	Rainy season	Dry season	Rainy season	Dry season	Rainy season
N	24.000	26.000	29.000	29.000	28.000	29.000	29.000	29.000
Mean	0.755	0.872	7.308	7.263	96.457	91.641	29.362	29.000
Median	0.232	0.313	7.350	7.260	85.600	78.300	29.600	29.200
Minimum	0.0049	0.003	6.050	6.070	30.900	28.130	26.300	26.730
Maximum	3.979	3.821	7.950	7.750	256.000	248.000	32.800	31.400
Q1	0.028	0.032	7.100	7.110	64.800	62.300	27.600	28.800
Q3	0.892	1.220	7.660	7.470	106.350	104.600	30.400	29.700
Variance	1.343	1.326	0.186	0.102	2879.37	2425.36	3.063	1.221
SD	1.159	1.151	0.431	0.319	53.660	49.248	1.750	1.105
SE	0.237	0.226	0.080	0.059	10.141	9.145	0.325	0.205

N= Number of observations, Q= Quartile, SD= Standard deviation, SE= Standard error

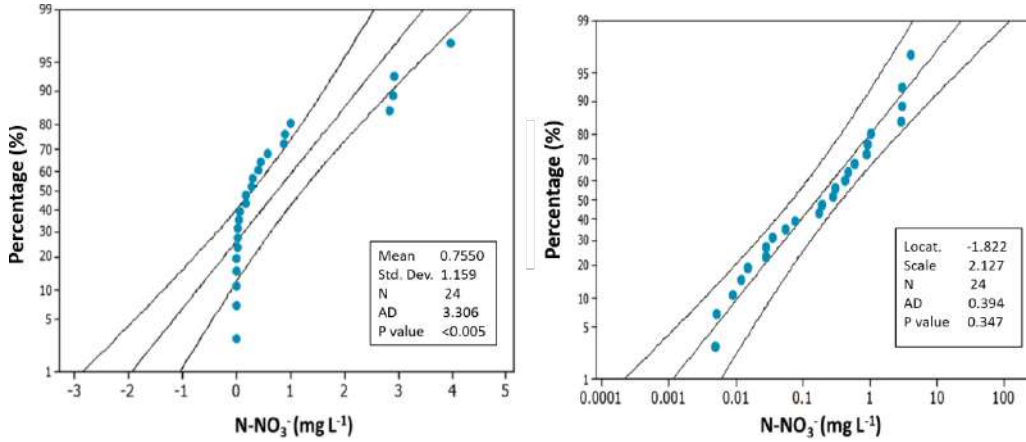

Fig. 2: Adjustment probability of the normal distribution (left) and normal logarithmic distribution (right).

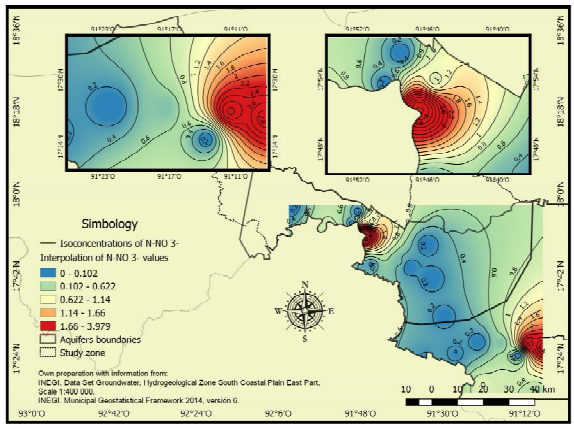

Fig. 3: Nitrate-nitrogen ($N\text{-}NO_3^-$) isoconcentrations in the study area during the dry season.

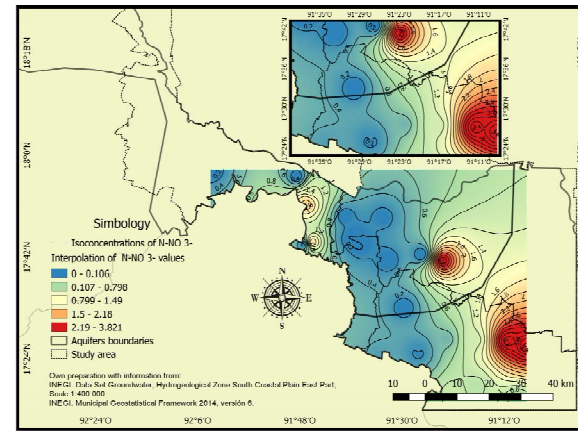

Fig. 4: Nitrate-nitrogen ($N\text{-}NO_3^-$) isoconcentrations in the study area during the rainy season.

$N\text{-}NO_3^-$ in groundwater showed slight differences. In the first season (dry season), two areas were detected indicating the sites with the highest concentrations of $N\text{-}NO_3^-$- one to the northwest of the municipality of Emiliano Zapata in the town Chablé and another north of Tenosique, in the towns of San Isidro and La Palma (Fig. 3). In the second sampling season (rainy season), concentrations were maintained high in the sites located in the municipality of Tenosique. However, in the Multé population of the municipality of Balancán the concentration of $N\text{-}NO_3^-$ increased (Fig. 4). This site showed the greatest variation from one sampling period to another.

The sampling sites with the highest concentrations of $N\text{-}NO_3$ are far from the sources of point pollution present in the area such as the Azsuremex-Tenosique sugar mill and the final disposal sites for urban solid waste. In these sampling sites, the use of the soil is for the cultivation of pastures (Fig. 5). Wells in Chablé are public-urban use, are more than 100 m deep, and are on the banks of the Usumacinta River. They are from the oldest wells, whose construction dates from the sixties. The uses in Tenosique belong to an ejido (San Isidro) and a Ranchería (La Palma), where the well water is destined for public-domestic use. Its depths are 80 m and 70 m, respectively.

These wells are the closest to the San Pedro River, being the town of La Palma on the banks of this river. The Multé well is on the banks of the Usumacinta River and less than 3 km from the San Pedro River. Its depth is 120 m and is the most recent of all, as it was built in 2014. The results obtained in these areas could be due to contributions from diffuse sources, due to the proximity of areas dedicated to irrigated agriculture (Chablé), and the proximity with the Usumacinta (Chablé, Multé) and San Pedro (San Isidro, La Palma) rivers. Because the wells near rivers obtain their recharge from these rivers and not from the aquifer that overrides them (Agudelo 2005), in this particular case, these rivers could transport nitrogenous compounds that eventually reach the referred aquifers.

The results of $N\text{-}NO_3^-$ obtained are below the maximum permissible limits (MPL) for drinking water established nationally and internationally in the official Mexican standard NOM-127-SSA-1994 (DOF 1994) and by the World Health Association (WHO 2011). First, a limit value of 10 $mg.L^{-1}$ (MPL) of $N\text{-}NO_3$ for water for human consumption, and second, a limit value of 50 $mg.L^{-1}$ of $N\text{-}NO_3^-$ equivalent to approximately 10 $mg.L^{-1}$ of $N\text{-}NO_3^-$.

The $N\text{-}NO_3$ concentrations found in this study were also compared with the Ecological Criteria for Water Quality (ECWQ) available in Mexico. The ECWQ establish different levels of concentration according to the minimum quality

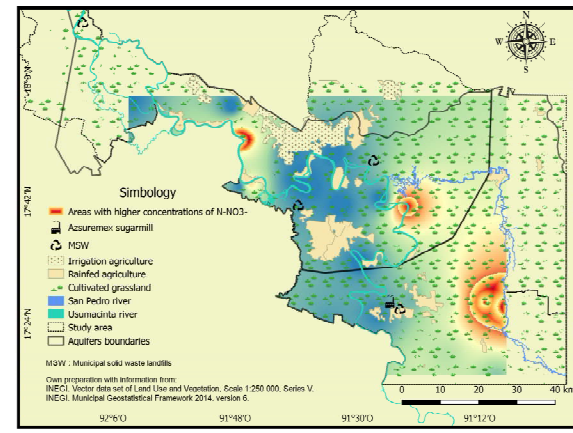

Fig. 5: Areas with higher concentrations of nitrate-nitrogen ($N\text{-}NO_3^-$) and sources of contamination in the study area.

required for the use of it as a source of drinking water (5 $mg.L^{-1}$ of $N\text{-}NO_3^-$), livestock use (90 $mg.L^{-1}$ of $N\text{-}NO_3^-$), and marine water life protection (0.04 $mg.L^{-1}$ of $N\text{-}NO_3^-$) (DOF 1989). The highest concentrations obtained in the present study are close to the established MPL for drinking water, and in 50% of the sampling sites, the concentrations of $N\text{-}NO_3^-$ exceed the MPL defined for the protection of the life of seawater. The latter is important because the aquifers studied discharge a third of the water to the rivers in the area, which flow into the Laguna de Términos and the Gulf of Mexico (CONAGUA 2002a; 2002b). Laguna de Términos is one of the most diverse and rich environmental systems on earth, where numerous ecosystems converge, such as coastal lagoons, wetlands, mangroves, seagrasses, and coral reefs. The Laguna de Términos stands out among the estuaries and coastal lagoons of Mexico due to its rich fauna, which is estimated at 122 species of ichthyofauna and 174 species of mollusks. Among the most valuable species is the pink shrimp, whose life cycle develops in this area (Toledo 2005).

According to Camargo and Alonso (2007), freshwater species are generally more susceptible to nitrate toxicity compared to marine species. Among the most vulnerable, the authors point to certain crustaceans, insect larvae, and fish. It has been shown, for example, that concentrations above 1.1 and 2.3 $mg.L^{-1}$ of $N\text{-}NO_3^-$ have adverse effects on salmonid fingerlings of the species *Oncorhynchus mykiss* and *Oncorhynchus tshawytscha*. Likewise, concentrations equal to 2.8, 4.4, and 4.5 $mg.L^{-1}$ of $N\text{-}NO_3^-$ are fatal for amphipods *Echinogammarus echinosetosus*, *Eulimnogammarus toletanus,* and trichoptera *Hydropsyche occidentalis*, in that order. Therefore, the $N\text{-}NO_3^-$concentrations in the aquifers studied may represent a risk to the ecosystem of the Laguna de Términos and the coastal zone of the Gulf of Mexico.

CONCLUSIONS

Nitrate-nitrogen ($N\text{-}NO_3$) concentrations in the Los Ríos and Boca del Cerro aquifers do not exceed the maximum permissible limits for drinking water established by NOM-127-SSA-1994 and by the World Health Association. Therefore, the water from the Los Ríos and Boca del Cerro aquifers does not represent an immediate risk to public health in terms of the nitrogen content of nitrates. However, the frequent consumption of water from these aquifers could eventually cause, in the long term, a significant accumulation of $N\text{-}NO_3^-$ and consequently, damage to public health. The concentrations of $N\text{-}NO_3^-$ exceed the MPL defined by the ECWQ for the protection of the life of seawater. Therefore, it is recommended to conduct studies in the discharge zones towards the Laguna de Términos and the coastal zone of the Gulf of Mexico, to determine if there is indeed damage to these aquatic ecosystems.

ACKNOWLEDGEMENTS

To the National Water Commission (CONAGUA) and to the National Council of Science and Technology (CONACYT) 2014-248265 Project "Evaluation of the effect of diffuse sources of pollution on the quality of the water of the Usumacinta River, in the state of Tabasco. To the Postgraduate College, Veracruz Campus; and the Boca del Río Technological Institute.

REFERENCES

Agudelo, C.L. 2005. Evaluación de las concentraciones altas de nitrato en el Manantial La Libertad y su relación con el campo de pozos La Valencia, Santo Domingo de Heredia, Costa Rica. Rev Geol América Central., 32: 84-85.

Basulto, J., Manera, M. and Baladia, E. 2014. Ingesta dietética de nitratos en bebés y niños españoles y riesgo de metahemoglobinemia. Pediatría Atención Primaria., 16(61): 65-69.

Camargo, J.A. and Alonso, A. 2007. Contaminación por nitrógeno inorgánico en los ecosistemas acuáticos: problemas medioambientales, criterios de calidad del agua, e implicaciones del cambio climático. Ecosistemas., Available at http://www.redalyc.org/articulo.oa?id=54016211

CONAGUA 2002a. Determinación de la disponibilidad de agua en el Acuífero Los Ríos, estado de Tabasco. Comisión Nacional del Agua. Available at https://www.gob.mx/cms/uploads/attachment/file/103376/DR_2707.pdf

CONAGUA 2002b. Determinación de la disponibilidad de agua en el Acuífero Boca del Cerro, estado de Tabasco. Comisión Nacional del Agua. Available at https://www.gob.mx/cms/uploads/attachment/file/103377/DR_2708.pdf

CONAGUA 2015. Estadísticas del agua en México. SEMARNAT. Available at http://www.conagua.gob.mx/CONAGUA07/Publicaciones/Publicaciones/EAM2015.pdf

DOF 1989. Diario Oficial de la Federación. Acuerdo por el que se establecen los Criterios Ecológicos de Calidad del Agua. Ciudad de México. Available at http://legismex.mty.itesm.mx/acu/acca001.pdf

DOF 1994. Diario Oficial de la Ferderación NOM-127-SSA1-1994 Salud ambiental, agua para uso y consumo humano-limites permisibles de calidad y tratamientos a que debe someterse el agua para su potabilizacion. Available at http://www.salud.gob.mx/unidades/cdi/nom/127ssa14.html

Dokulil, M.T. and Teubner, K. 2010. Eutrophication and climate change: Present situation and future scenarios. In Eutrophication: Causes, consequences, and control. Springer, Dordrecht., pp 1-16.

EPA 1993. Method 353.2 Revision 2.0 Determination of Nitrate-Nitrite Nitrogen by Automated Colorimetry. Available at https://www.epa.gov/sites/production/files/2015-08/documents/method_353-2_1993.pdf

Estrada-Botello, M., Nikolskii-Gavrilov, I., Gavi-Reyes, F., Etchevers-Barra, J. and Palacios-Vélez O. Balance de nitrógeno inorgánico en una parcela con drenaje subterráneo en el trópico húmedo. T Latinoameric., 20(2):189-198. Available at http://www.redalyc.org/revista.oa?id=573

Galaviz-Villa, I., Landeros-Sánchez, C., Castañeda-Chávez, M.R., Lango-Reynoso, F., Martínez-Dávila, J.P., Pérez-Vázquez, A. and Nikolskii-Gavrilov, I. 2011. Presence of nitrates and nitrites in water for human consumption and their impact on public health in sugarcane-producing areas. Trop and Subtrop Agroecosystems. Available at: http://www.revista.ccba.uady.mx/ojs/index.php/TSA/article/view/1273.

Gallart, J. 2008. Contaminación de Aguas Subterráneas: Nitratos y Coliformes. Available at http://ambientonline.es/Ediciones%20de%20Publicaciones/Premio%20Marcel%20Br%C3%BA%20i%20Turull%202008.pdf

Graco, M.I., Ledesma, J., Flores, G. and Girón, M. 2007. Nutrientes, oxígeno y procesos biogeoquímicos en el sistema de surgencias de la corriente de Humboldt frente a Perú. Rev Peruana Biol.,14(1):117-128.

INEGI 2015. Anuario estadístico y geográfico de Tabasco México: Instituto Nacional de Estadística y Geografía. Gobierno del Estado de Tabasco. Available at https://tabasco.gob.mx/sites/all/files/vol/ceieg.tabasco.gob.mx/fi/Anuario%20estad%C3%ADstico%20y%20geogr%C3%A1fico%20de%202015_0.pdf

INIFAP 2016. Datos históricos. Red de estaciones de INIFAP Tabasco. Available at http://www.inifap.gob.mx/SitePages/inifap2015/Transparencia/Contenido/Trans_Focalizada/Red_Estaciones/Red_Estaciones.aspx

Karydis, M. 2009. Eutrophication assessment of coastal waters based on indicators: a literature review. Global NEST, 11(4): 373-390.

Larios, L. 2009. Methemoglobinemia in children: Current situation. Rev Arch Médico de Camagüey, 13(3):1-9.

Martínez, F., Ojeda, D., Hernández, A., Martínez, J. and Quezada, G. 2011. El exceso de nitratos: Un problema actual en la agricultura. Synthesis., 11-16.

Munguía, A.S. 2005. Uso del suelo agropecuario y deforestación en Tabasco 1950-2000. Univ J Autónoma de Tabasco. México. p. 123.

Muñoz, H., Armienta, M., Vera, A. and Ceniceros, N. 2004. Nitrato en el agua subterránea del Valle de Huamantla, Tlaxcala, México. Rev Intern de Contaminación Ambiental., 20(3):91-97.

Nevárez, G. and Flor, F. 2014. Comportamiento de DBO 5, DQO, NH_4^+ y NO_3, mediante el diseño de un Humedal Artificial Subsuperficial para depurar aguas residuales de origen doméstico. La Técnica., 13:82-89.

Perdomo, C., Casanova, O. and Ciganda, V. 2001. Contaminación de aguas subterráneas con nitratos y coliformes en el litoral sudoeste del Uruguay. Agrociencia., 5(1):10-22.

Rodríguez, M.P., Rodríguez, J.G. and Viramontes, U.F. 2015. Desarrollo sustentable de los recursos naturales al disminuir riesgos de contaminación en actividades agropecuarias. CULCyT., p. 20.

SIAP 2011. Servicio de Información Agroalimentaria y Pesquera. Uso de tecnología y de servicios en el campo Cuadros Tabulares 2011. Estadística de Uso Tecnológico y de Servicios en la superficie agrícola. Available at https://www.gob.mx/cms/uploads/attachment/file/92646/Cuadros_tabulares_2011.compressed.pdf

SIAP 2013. Servicio de Información Agroalimentaria y Pesquera. Uso de tecnología y de servicios en el campo Cuadros Tabulares 2013. Estadística de Uso Tecnológico y de Servicios en la superficie agrícola. Available at https://www.gob.mx/cms/uploads/attachment/file/92737/Cuadros_tabulares_2013.compressed.pdf

SIAP 2016. Servicio de Información Agroalimentaria y Pesquera. Uso de tecnología y de servicios en el campo Cuadros Tabulares 2016. Estadística de Uso Tecnológico y de Servicios en la superficie agrícola. Available at https://www.gob.mx/cms/uploads/attachment/file/268251/Cuadros_tabulares_2016.pdf

Toledo, O.A. 2005. Marco conceptual: Caracterización ambiental del Golfo de México. In A. Botello, J. Rendón-von-Osten, G. Gold-Bouchot and C. Agraz-Hernández, Golfo de México, contaminación e impacto ambiental: Diagnóstico y tendencias, UNAM, Instituto Nacional de Ecología, México., pp 25-30.

Ward, M., deKok, T., Levallois, P., Brender, J., Gulis, G., Nolan, B. and VanDerslice, J. 2005. Workgroup Report: Drinking-Water Nitrate and Health Recent Findings and Research Needs. Environ. Health Perspect., 113(11): 1607-16014.

WHO. 2011. Guidelines for Drinking-water Quality. World Health Organization, Geneva., pp. 564.

Zaporozec, A. 2002. Groundwater Contamination Inventory, 2nd ed. UNESCO., pp. 265

Nature Environment and Pollution Technology
An International Quarterly Scientific Journal

p-ISSN: 0972-6268
(Print copies up to 2016)
e-ISSN: 2395-3454

Vol. 20 | No.3 | pp. 1369-1380 | 2021

Original Research Paper

https://doi.org/10.46488/NEPT.2021.v20i03.051

Open Access Journal

Microbial Reduction and Detoxification of Chromium from Tannery Effluent by Natural Inhabitants

Sawkat Ara Pinki*(**), Md. Reazul Karim*, Dipankar Dewanjee*, Habibur Rahman Bhuiyan*, H. M. Abdullah Al Masud* and Md. Imranul Hoq*†**

*Department of Microbiology, Faculty of Biological Sciences, University of Chittagong, Chattogram-4331, Bangladesh
**National University, Gazipur-1704, Bangladesh
***Industrial Microbiology Research Division, Bangladesh Council of Scientific and Industrial Research, Chattogram-4220, Bangladesh
†Corresponding Author: Md. Imranul Hoq; imran.mbio@cu.ac.bd

Nat. Env. & Poll. Tech.
Website: www.neptjournal.com

Received: 12-10-2020
Revised: 04-12-2020
Accepted: 08-12-2020

Key Words:
Industrial waste
Tannery effluent
Chromium
Hexavalent chromium
Detoxification
Bioremediation

ABSTRACT

Chromium (Cr), a chemical agent, has long been used extensively in leather tanning. Hexavalent chromium (Cr-VI) found in tannery effluent is highly toxic, carcinogenic and mutagenic to humans. Transformation of Cr-VI to its trivalent counterpart, Cr-III, is the basic process in its detoxification, and microbial transformation of Cr-VI to Cr-III has been one of the most widely studied forms of Cr bioremediation. This study aims to explore the ability of naturally occurring bacteria in reducing and detoxifying Cr in vitro and also from tannery effluent. Five efficient Cr reducing and detoxifying bacteria were isolated from tannery effluent, their morphological, cultural, physiological and biochemical characteristics investigated. They were identified as *Aeromonas eucrenophila*, *Bacillus megaterium*, *B. carboniphilus*, *B. licheniformis* and *B. subtilis*. Coincubation of the isolates with varying concentrations of potassium dichromate ($K_2Cr_2O_7$), a Cr salt, in minimum salts medium, pH 7 revealed notable reduction and detoxification of Cr within 24-72 h as determined by 1,5-diphenylcarbazide colorimetric method and atomic absorption spectrophotometry, respectively. The isolates exhibited substantial resistance or tolerance to 125 to 500 ppm $K_2Cr_2O_7$. Bacterial detoxification or reduction of was increasingly increased as the incubation period increased from 24 to 48 or 72 h and substrate concentration increased from 125 to 250 or 500 ppm. Most of the isolates exhibited increased reduction and detoxification at 37°C compared to that at 30°C or 45°C, and at pH 7 or 8 compared to that at pH 5 or 6. Furthermore, all the isolates exhibited highest detoxification or reduction when peptone was used as carbon source instead of glucose or ammonium acetate. In a chosen or optimized condition of 37°C temperature, pH 7, 125 ppm $K_2Cr_2O_7$ concentration and 48 h incubation period, most isolates exhibited 85-99% Cr reduction and detoxification from tannery effluent. It was, therefore, inferred that the isolates have potential as biological agent in reducing and detoxifying Cr from industrial effluent.

INTRODUCTION

Industrial pollution is a major factor to cause significant degradation to the environment around us. Since industrialization is continuously growing worldwide, in the present time, industrial wastes play the most common source of water pollution (Ogedengbe & Akinbile 2004). In a developing country like Bangladesh, solid waste or effluent from a tannery is directly discharged into water bodies or sewers without treatment (Verheijen et al. 1996; Favazzi 2002). Hence, tannery wastewater is thus found extremely polluted in terms of total dissolved solids (TDS), total suspended solids (TSS), biochemical oxygen demand (BOD), chemical oxygen demand (COD), heavy metals, etc. (Mondal et al. 2005). In Bangladesh, tanning industries are one of the main economic activities. Bangladesh now has 165 leather and footwear factories. Furthermore, it has 161 tanning industries that process rawhides into finished leather. The vast majority of these industries are located in and around Dhaka, whilst a very few are scattered all over the country (Gain & Moral 1999). A very recent study has expressed an estimation that a total of 232-ton solid waste and 20-million-liter wastewater are produced every day from these industries (Saha & Azam 2021). In the tanning industries, extensive use of Cr in the chrome tanning process results in the release of Cr that contaminates soil and water at production sites (Turick et al. 1996). The solid waste or wastewater discharged from the tanneries contains substantial amount of Cr (Franco et al. 2005). Cr is a highly toxic heavy metal and is known to be mutagenic, carcinogenic and teratogenic to humans, animals and plants. However, Cr exists in nature in various oxidation states ranging from divalent to hexavalent ones. Cr-III and Cr-VI are the most stable states, and the biological, toxicological and geochemical properties of them

vary remarkably. Cr-VI is known to be much more toxic than Cr-III for multiple reasons. In nature, Cr-III exists at a narrow range of concentration, and is an essential element because it regulates the metabolism of glucose in human body (Srinath et al. 2001). In contrast, Cr-VI is highly soluble in water, rapidly permeable through biological membranes, and prone to subsequently interact with intracellular proteins and nucleic acids. Cr-VI interacts with DNA quite indirectly, and exhibits genotoxicity via reactive intermediates produced during its intracellular reduction to Cr-III. The types of DNA damage caused by Cr-VI is thereby grouped into two major categories: oxidative DNA damage and Cr-III-DNA interaction (Sobol & Schiestl 2012). Even at very low concentration, Cr-VI is highly toxic and hazardous to human health. Other than Cr, the most commonly occurring heavy metals in tannery wastewater include lead, manganese, cadmium and copper. Occurrence of these toxic substances in surface water and soil leads to serious public health threat and significant risk to the ecological system (Sundar et al. 2010). The present study thus aims to investigate the ability of naturally occurring bacteria in reducing and detoxifying Cr at privileged nutritional and environmental conditions, and evaluate their potentiality as candidate agent of bioremediation of the heavy metal.

MATERIALS AND METHODS

Collection of Sample

Tannery effluent samples were collected in sterile plastic bottles from RIFF Leather Industries, Kalurghat Industrial Area, Chattogram, Bangladesh. They were immediately placed in an insulated box with frozen refrigerant packs in an insulated box and transported to the laboratory. Other than instant analysis, the samples were preserved at 4°C for further analysis.

Isolation of Bacteria from Tannery Effluent

The nutrient agar medium was used for the isolation of bacteria from the effluent, where the pH of the medium was adjusted to the pH of the sample. Pour plate and streak plate techniques were applied for the isolation, and well discrete identical single colonies were picked up and transferred into nutrient agar slants. In case no single colony appeared onto any plate, repeated streaking of the culture was carried out from plate to plate until at least one single colony was appeared. The slants were sealed in polyethylene bags and preserved in a refrigerator at 4°C as stock culture for further study. Subculturing at 2-week interval was maintained to keep the physiology and metabolic activity of the isolates unimpaired.

Cr Salt Used for *In Vitro* Investigation

Chemical name: Potassium dichromate
Chemical formula: $K_2Cr_2O_7$
Molecular weight: 294
Atomic weight: 52

Screening of Chromium (Cr) Reducing or Detoxifying Bacteria

The isolates possessing the ability to detoxify or reduce Cr in vitro were screened by incubating mid logarithmic growing cells of 106/mL density in varied concentrations of $K_2Cr_2O_7$ supplemented minimal salts medium (MSM) broth base, pH 7 for a substantial period of time (Bibi et al. 2012), and measuring the concentration of residual Cr-VI or total Cr, respectively, in the culture supernatant.

Measurement of Cr-VI Concentration

The concentration of residual Cr-VI in $K_2Cr_2O_7$ supplemented MSM culture supernatant following centrifugation at 4000 rpm for 5 min was measured by diphenylcarbazide colorimetric method (APHA 1998). In this method, 1,5-diphenylcarbazide (DPC) reagent was used as a colorimetric indicator, which reacted with Cr-VI in strongly acidic solution and resulted in the formation of magenta colored carbazone inner complex salt of a chromous ion (Cr-II). The absorbance of the color was measured at 540 nm in a spectrophotometer (Shimadzu UV-VIS 1800, Japan). In the course of the measurement, a calibration curve was prepared where the standard solution was diluted ranging the concentrations of 0.2-1 ppm by an interval of 0.2 ppm. The possible slight loss of Cr during digestion or other operations of the analysis was compensated by adding no inoculum to the standard solutions but following the same treatment to be applied to the sample. The calibration curve was constructed by plotting the blank-subtracted absorbance of the standard solutions versus respective concentration.

Measurement of Total Cr Concentration

The concentration of total Cr in $K_2Cr_2O_7$ supplemented MSM culture supernatant following centrifugation at 4000 rpm for 5 min was measured by atomic absorption spectrophotometry (APHA, WEF, AWWA 1992). In this method, the supernatant was mixed to double volume of concentrated HNO_3, and the mixture was heated to 100°C by a proper hollow cathode lamp of 10 mA current on a hot plate in an atomic absorption spectrophotometer (AAS) (Shimadzu AA-7000, Japan) to accomplish acid digestion until the final volume went down to initial supernatant volume. The extract was filtered through a Whatman 42 filter paper to remove any insoluble material, collected into a volumetric flask and diluted. The chrome

plating operation emitted total Cr, which was quantified by measuring the absorbance at 357.9 nm. In the course of the measurement, a calibration curve was prepared where the standard solution was diluted ranging the concentrations of 1-8 ppm by an interval of 2 ppm. The calibration curve was constructed by plotting the blank-subtracted absorbance of the standard solutions versus respective concentration.

Characterization of Cr Detoxifying or Reducing Bacteria

The bacterial isolates that possessed the ability to reduce or detoxify Cr following in vitro investigations were subjected to cultural, morphological, physiological and biochemical examinations. Cultural examinations include colony characteristics of the isolates onto nutrient agar plate, i.e., form, color, elevation, margin, surface and their growth pattern onto nutrient agar slant. Morphological examinations include Gram and acid-fast staining of the isolates and microscopic observation of their shape and arrangement. Physiological and biochemical examinations include motility, indole, Voges-Proskauer, methyl red, Simmons citrate, nitrate reduction, triple sugar iron, H_2S production, catalase, oxidase and urease tests.

Determination of Bacterial Resistance or Tolerance to Cr

Bacterial isolates exhibiting substantial ability to reduce or detoxify Cr were examined to determine their resistance or tolerance to Cr by a broth dilution method. In this method, mid logarithmic growing cells of 106 cells/mL density were incubated in brain heart infusion broth supplemented with varied concentration of $K_2Cr_2O_7$ for 24 hours at 37°C with agitation at 100 rpm. The turbidity of the broth, proportionate to bacterial growth, was measured at 600 nm in a UV-visible spectrophotometer (PG Instruments-UK, Model: T 80+ UV-VIS). The isolates that exhibited good to moderate growth at a significant concentration of Cr salt were considered as resistant or tolerant to Cr.

Determination of Minimum Inhibitory Concentration of Cr Against Bacterial Isolates

Minimum inhibitory concentration (MIC) of Cr against the isolates was determined by the broth dilution method described above. In this case, the minimum concentration of $K_2Cr_2O_7$ that prevented visible growth of an isolate was considered as MIC of Cr against that particular organism.

Determination of Minimum Bactericidal Concentration of Cr Against Bacterial Isolates

The broth culture of MIC test was applied as inoculum to determine minimal bactericidal concentration (MBC), where 100 µL of 18-h old culture was inoculated by pour plate method to nutrient agar plate. The plate was incubated at 37°C and the appearance or absence of growth was observed at 24 h. The minimum concentration that resulted in complete absence of growth onto the plate was considered as MBC.

Determination of Optimum Conditions for Bacterial Detoxification or Reduction of Cr

The efficiency of bacterial isolates in detoxifying or reducing Cr in vitro were investigated further as described above, whereas variety of conditions applied to determine the optimum ones that include $K_2Cr_2O_7$ concentration in MSM base, incubation period, reaction temperature, medium pH, and additional supplementation of the medium with glucose, peptone or ammonium acetate as carbon source. In every case, a number of pilot experiments were conducted to reveal closely fitted parameters.

Evaluation of Bacterial Detoxification or Reduction of Cr from Tannery Effluent in Optimized Conditions

Fresh tannery effluent sample was collected as described above and sterilized by filtration using 0.22 µ filter. The initial concentration of Cr-VI and total Cr in the effluent was determined as described above. The pH of the sample was adjusted to the optimum for each isolate, inoculated by mid logarithmic growing cells of 106 cells/mL density and incubated at optimized temperature for optimized time. The efficiency of the isolates was evaluated by measuring the residual Cr-VI or total Cr concentration as described above. The data were compared with that obtained under unoptimized conditions.

RESULTS

Cr Detoxifying or Reducing Ability of Bacterial Isolates from Tannery Effluent

A total of 16 pure cultures were isolated on nutrient agar slants from the nutrient agar plates following pour and streak plate inoculations of undiluted and diluted tannery effluent samples. The isolates were designated as E1-E16 and investigated for their ability to detoxify or reduce Cr within 24, 48 or 72 h in MSM base, pH 7 supplemented with 125, 250 or 500 ppm $K_2Cr_2O_7$ and incubated at 37°C. Interestingly, most of the isolates exhibited their ability to detoxify or reduce Cr in vitro at various time periods or Cr salt. However, both detoxification of Cr-VI and reduction of total Cr by the isolates designated as E3, E7, E9, E11 and E14 at 48 h and 250 ppm $K_2Cr_2O_7$ were remarkable, as plotted in Fig. 1. Hence, these five isolates were considered as potential Cr detoxifiers or reducers and chosen for further investigations.

Identification of Cr Detoxifying or Reducing Bacteria

The cultural, morphological, physiochemical and biochemical

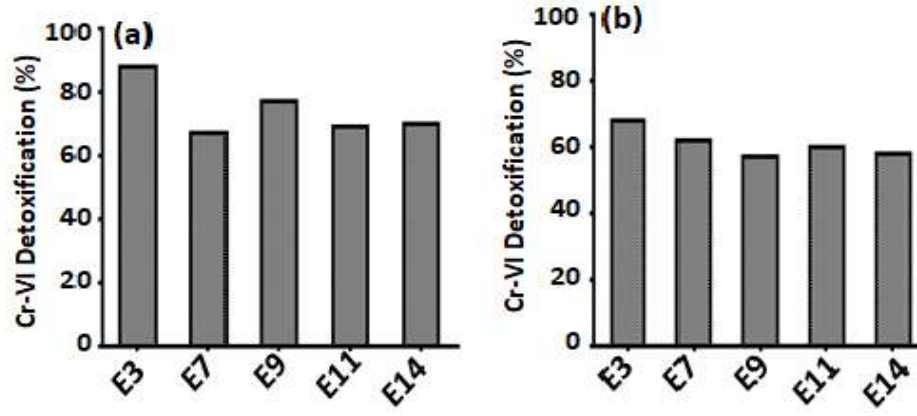

Fig. 1: Detoxification of Cr-VI and reduction of total Cr by selected isolates from tannery effluent. The experiments were conducted by inoculation of minimal salts medium base, pH 7 supplemented with 250 ppm of $K_2Cr_2O_7$ and incubation at 37°C for 48h followed by measurement of Cr-VI detoxification (a) by 1,5-diphenylcarbazide colorimetric method and reduction of total Cr (b) by atomic absorption spectrophotometry.

characteristics of the chosen 5 bacterial isolates that exhibited prominence in detoxifying or reducing Cr, as visualized in Table 1, were compared with the standard descriptions of wild bacteria according to Bergey's manual of determinative bacteriology, 8th (Buchanan & Gibbsons 1974) and 9th (Goodfeelow et al. 1994) editions. Comparative study revealed that the characteristics of the isolate designated as E3 closely resembled with that of *Aeromonas eucrenophila*. The isolate E3 was, therefore, identified as *Aeromonas eucrenophila*. Likewise, through comparative analysis, the isolate E7 was identified as *Bacillus megaterium*, E9 as *Bacillus carboniphilus*, E11 as *Bacillus licheniformis* and E14 as *Bacillus subtilis*.

Bacterial Resistance or Tolerance to Cr

In order to evaluate the candidacy of Cr detoxifying or reducing bacteria as biological agent, we examined their level of resistance or tolerance to Cr by culturing the isolates in brain heart infusion broth supplemented with various concentrations of $K_2Cr_2O_7$. The isolates exhibited diverse patterns of resistance or tolerance to Cr as revealed by their level of growth (Fig. 2). For example, the isolate *A. eucrenophila* exhibited tremendous resistance up to 125 ppm $K_2Cr_2O_7$ concentration, which dramatically reduced when the concentration increased to 250 ppm. On the other hand, the other isolates exhibited a dose dependent pattern of resistance with little fluctuations.

MIC and MBC of Cr Against Bacterial Isolates

The MIC of Cr against *A. eucrenophila* and *B. megaterium* was found 125 ppm, whereas against *B. carboniphilus*, *B. licheniformis* and *B. subtilis*, it was found 500 ppm. The MBC of Cr against all the isolates were found 2000 ppm (Table 2). Fig. 3 visualizes MBC values of *A. eucrenophila* and *B. carboniphilus*.

Concentration and Time Dependent Bacterial Detoxification or Reduction of Cr

The prevailing conditions with regard to Cr detoxification and reduction by the isolates were investigated in this study. The first attempt was made for Cr concentration and incubation period. Since the isolates exhibited substantial degree of resistance or tolerance to 125-500 ppm $K_2Cr_2O_7$ and also the MIC values of $K_2Cr_2O_7$ against the isolates ranged from 125-500 ppm at 24 h, we investigated the efficiency of the isolates at 125, 250 and 500 ppm $K_2Cr_2O_7$ at 24, 48 and 72 h. As illustrated in Figs. 4-8, most of the isolates were remarkably efficient in detoxifying or reducing Cr at all the concentrations applied. Notably, a 2-fold increase in concentration of $K_2Cr_2O_7$ from 125 to 250 did not cause massive variation in their efficiency. The same was observed when the concentration was increased from 250 to 500 ppm. In contrast, the efficiency of the isolates was significantly increased when the incubation period was increased from 24 to 48 h, or from 48 to 72 h at any concentration applied.

Temperature Dependent Bacterial Detoxification or Reduction of Cr

The effect of temperature on Cr detoxification or reduction by the bacterial isolates was evaluated at 30, 37 and 45°C while keeping the concentration of $K_2Cr_2O_7$ as 125 ppm and incubation period as 48 h. Most of the isolates appeared to exhibit maximum level of Cr detoxification or reduction at 37°C, and with few exceptions the efficiency of their detoxification or reduction was reduced when the temperature

Table 1: Cultural, morphological, physiological and biochemical characteristics of Cr detoxifying or reducing bacteria.

Characteristics	Observations				
	E3	E7	E9	E11	E14
Cultural					
Colony Form	Circular	irregular	irregular	circular	punctiform
Colony Color	Off-white	Off-white	Off-white	cream	cream
Colony Elevation	Raised	Flat	Flat	Flat	Convex
Colony Margin	Serrate	serrate	erose	entire	entire
Colony Surface	Smooth	smooth	smooth	smooth	smooth
Slant Character	Echinulate	Echinulate	Echinulate	Filiform	Filiform
Staining and Morphology					
Gram Staining	_	+	+	+	+
Acid Fast Staining	_	_	_	_	_
Shape	Short rod	Short rod	Short rod	Short rod	Short rod
Arrangement	Single	Single or pair	Single	Single	Single
Physiological and Biochemical tests					
Motility test	+	+	-	+	+
Indole	+	-	-	-	-
Voges-Proskauer	-	-	-	+	-
Methyl red	+	+	-	-	-
Simmons' citrate	-	+	-	-	+
Nitrate Reduction	+	+	-	+	+
Catalase	+	+	+	+	+
Oxidase	-	+	+	-	+
Urease	-	-	-	-	-
TSI	a/k	a/nc	a/k	a/k	a/a
H_2S production test	-	-	+	-	-

+, positive; -, negative; k/a, alkaline slant, acidic butt; a/nc, acidic slant, no change; a/a; acidic slant, acidic butt

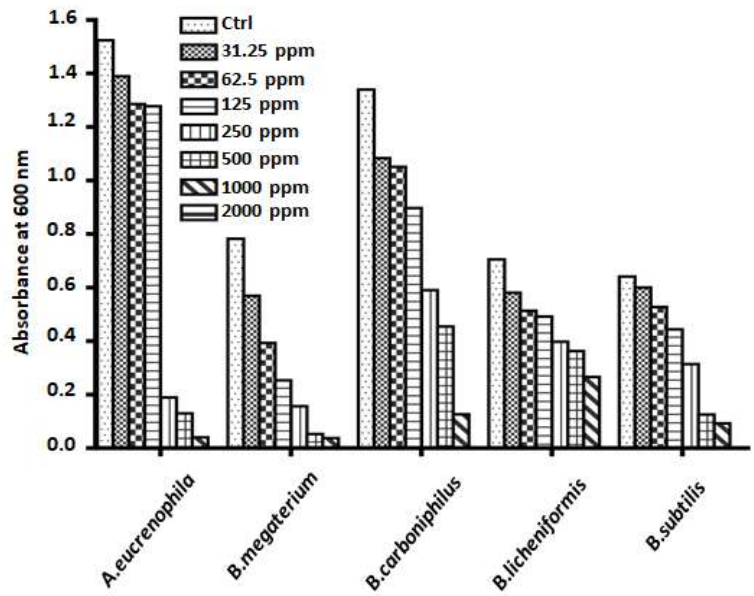

Fig. 2: Resistance or tolerance pattern of bacterial isolates from tannery effluent against Cr. The experiment was conducted by inoculation of brain heart infusion broth supplemented with 31.25, 62.5, 125, 250, 500, 1000, 2000 ppm of $K_2Cr_2O_7$ and incubation at 37° C for 24 h followed by the measurement of turbidity as bacterial growth at 600 nm in a UV-visible spectrophotometer.

Table 2: Growth of bacteria from broth dilution minimum inhibitory concentration (MIC) tests onto a nutrient agar plate

Bacteria	Concentration of $K_2Cr_20_7$ (ppm)		
	500	1000	2000
A. eucrenophila	++	+	_
B. megaterium	++	+	_
B. carboniphilus	+++	+	_
B. licheniformis	+++	++	_
B. subtilis	++	+	_

Note: Positive (+ = scanty, ++ = moderate, +++ = good), Negative (-)

was either increased to 45°C or decreased to 30°C (Fig. 9).

pH Dependent Bacterial Detoxification or Reduction of Cr

In order to figure out the favorable pH of the isolates in detoxifying or reducing Cr, we incubated the isolates in 125 ppm $K_2Cr_2O_7$ supplemented minimal salt medium base adjusted to pH 5, 6, 7 and 8 at 37°C for 48 h and examined their efficiency. In case of detoxification of Cr-VI, all the isolates exhibited maximum efficiency at

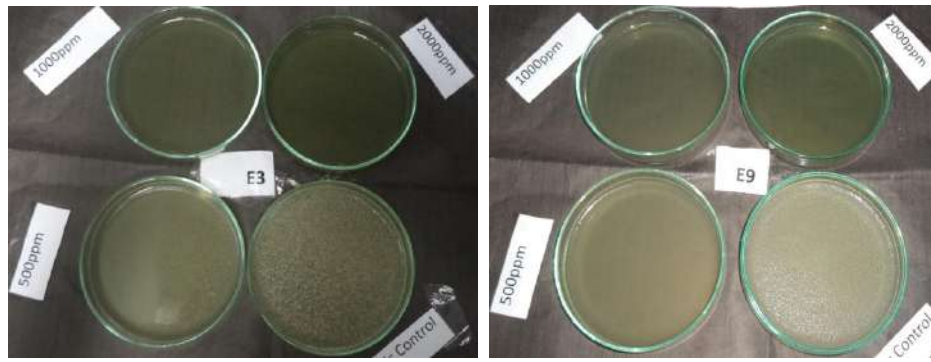

Fig. 3: Growth of (a) *A. eucrenophila* and (b) *B. carboniphilus* onto nutrient agar plate inoculated by overnight culture of brain heart infusion broth supplemented with varied concentration of $K_2Cr_2O_7$. The experiment was conducted by inoculation of nutrient agar plate by 18 h old culture of brain heart infusion broth supplemented with 500, 1000 and 2000 ppm of $K_2Cr_2O_7$ and incubation at 37° C for 24 h.

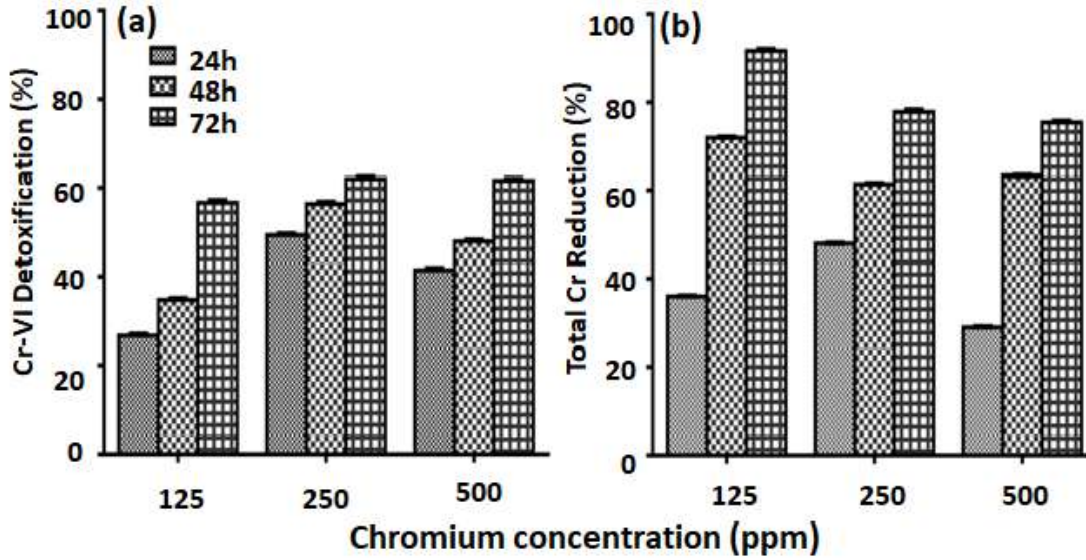

Fig. 4: Detoxification of Cr-VI and reduction of total Cr as $K_2Cr_2O_7$ by *A. eucrenophila*. The experiments were conducted by inoculation of minimal salts medium base, pH 7 supplemented with 125, 250 and 500 ppm of $K_2Cr_2O_7$ and incubation at 37°C for 24, 48 and 72 h followed by measurement of Cr-VI detoxification (a) by 1,5-diphenylcarbazide colorimetric method and reduction of total Cr (b) by atomic absorption spectrophotometry.

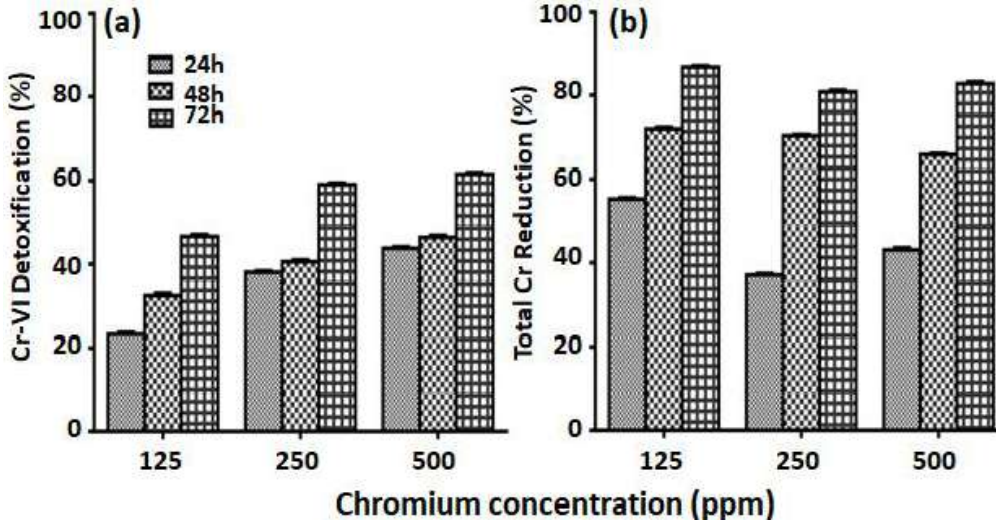

Fig. 5: Detoxification of Cr-VI and reduction of total Cr as $K_2Cr_2O_7$ by *B. megaterium*. The experiments were conducted by inoculation of minimal salts medium base, pH 7 supplemented with 125, 250 and 500 ppm of $K_2Cr_2O_7$ and incubation at 37°C for 24, 48 and 72 h followed by measurement of Cr-VI detoxification (a) by 1,5-diphenylcarbazide colorimetric method and reduction of total Cr (b) by atomic absorption spectrophotometry.

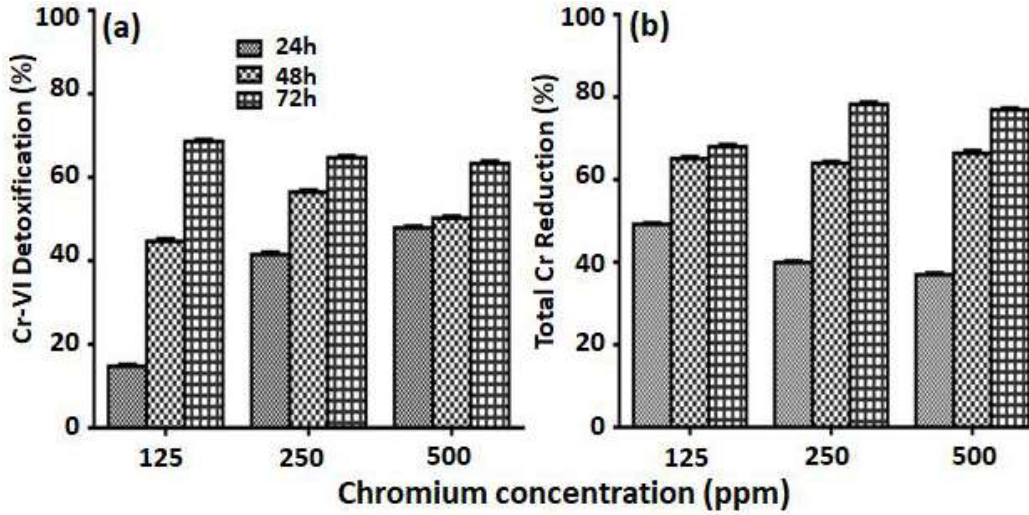

Fig. 6: Detoxification of Cr-VI and reduction of total Cr as $K_2Cr_2O_7$ by *B. carboniphilus*. The experiments were conducted by inoculation of minimal salts medium base, pH 7 supplemented with 125, 250 and 500 ppm of $K_2Cr_2O_7$ and incubation at 37°C for 24, 48 and 72 h followed by measurement of Cr-VI detoxification (a) by 1,5-diphenylcarbazide colorimetric method and reduction of total Cr (b) by atomic absorption spectrophotometry.

both pH 7 and 8 (Fig. 10a). The efficiency of detoxification was decreasingly decreased when the pH of medium was decreased to 6 or 5. On the other hand, 4 out of 5 isolates exhibited maximum reduction of total Cr at pH 7 (Fig. 10b). *B. subtilis* is the only exception that exhibited maximum efficiency of reduction at pH 8. Likewise, with lowering of pH to 6 or 5, the efficiency of reduction of decreasingly decreased.

Carbon Source Dependent Bacterial Detoxification or Reduction of Cr

The effect of carbon source or co-substrate on Cr detoxification or reduction by the bacterial isolates was evaluated by using glucose, peptone or ammonium acetate in the test medium while keeping the concentration of $K_2Cr_2O_7$ as 125 ppm, incubation period as 48 h and temperature at 37°C.

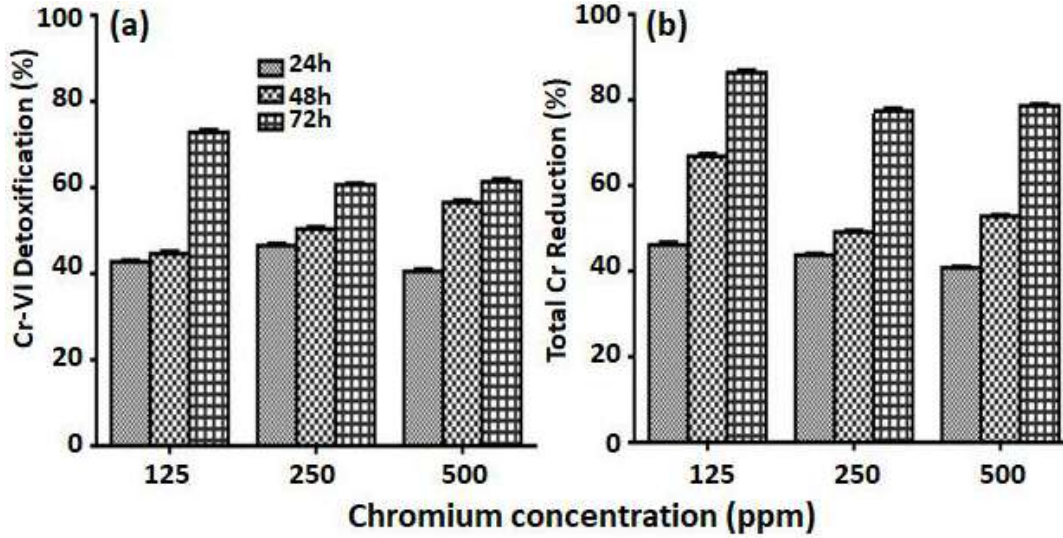

Fig. 7: Detoxification of Cr-VI and reduction of total Cr as $K_2Cr_2O_7$ by *B. licheniformis*. The experiments were conducted by inoculation of minimal salts medium base, pH 7 supplemented with 125, 250 and 500 ppm of $K_2Cr_2O_7$ and incubation at 37°C for 24, 48 and 72 h followed by measurement of Cr-VI detoxification (a) by 1,5-diphenylcarbazide colorimetric method and reduction of total Cr (b) by atomic absorption spectrophotometry.

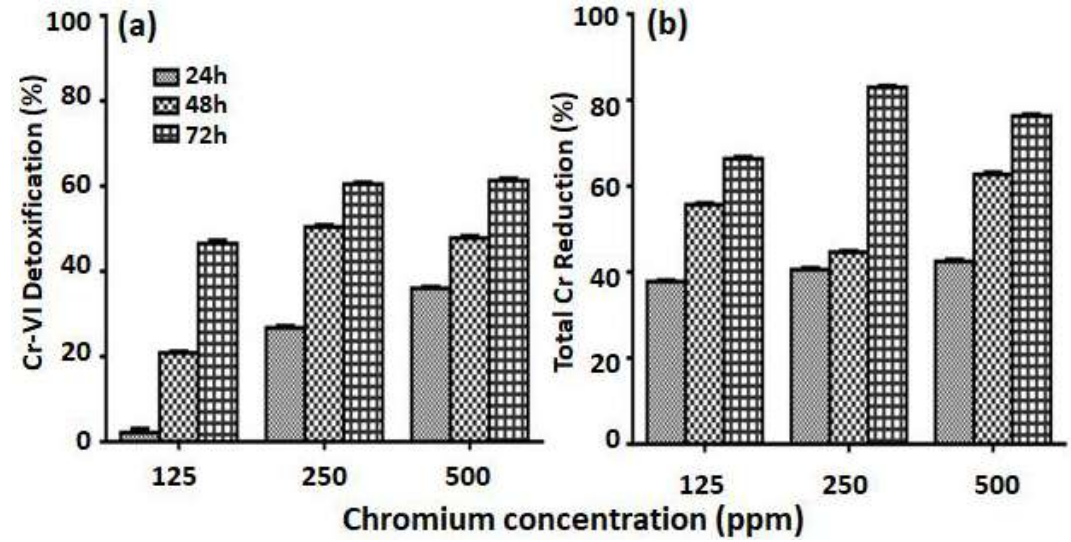

Fig. 8: Detoxification of Cr-VI and reduction of total Cr as $K_2Cr_2O_7$ by *B. subtilis*. The experiments were conducted by inoculation of minimal salts medium base, pH 7 supplemented with 125, 250 and 500 ppm of $K_2Cr_2O_7$ and incubation at 37°C for 24, 48 and 72 h followed by measurement of Cr-VI detoxification (a) by 1,5-diphenylcarbazide colorimetric method and reduction of total Cr (b) by atomic absorption spectrophotometry.

Notably, 4 among 5 isolates detoxified or reduced Cr much better in peptone rich medium compared to in glucose or ammonium acetate rich ones. The only exception lied for *B. megaterium*, which exhibited better detoxification of Cr-VI in ammonium acetate rich medium but reduction of total Cr in glucose rich medium (Fig. 11).

Potential of the Isolates in Detoxifying or Reducing Cr from Tannery Effluent

In order to evaluate the candidacy of the isolates in detoxifying or reducing Cr from tannery effluent, freshly collected sample was subjected to bacterial treatment in optimized conditions. Before inoculation, the sample was first sterilized by filtration to nullify the effect of existing microbial population. The pH of the effluent was adjusted to 7 while inoculated with *A. eicrenophila*, *B. megaterium*, *B. carboniphilus* or *B. licheniformis*. In case of *B. subtilis*, the pH was adjusted to 8. Co-incubation of effluent with bacterial isolates was performed at 37°C for 48 h. It is noteworthy that all the isolates exhibited significantly enhanced

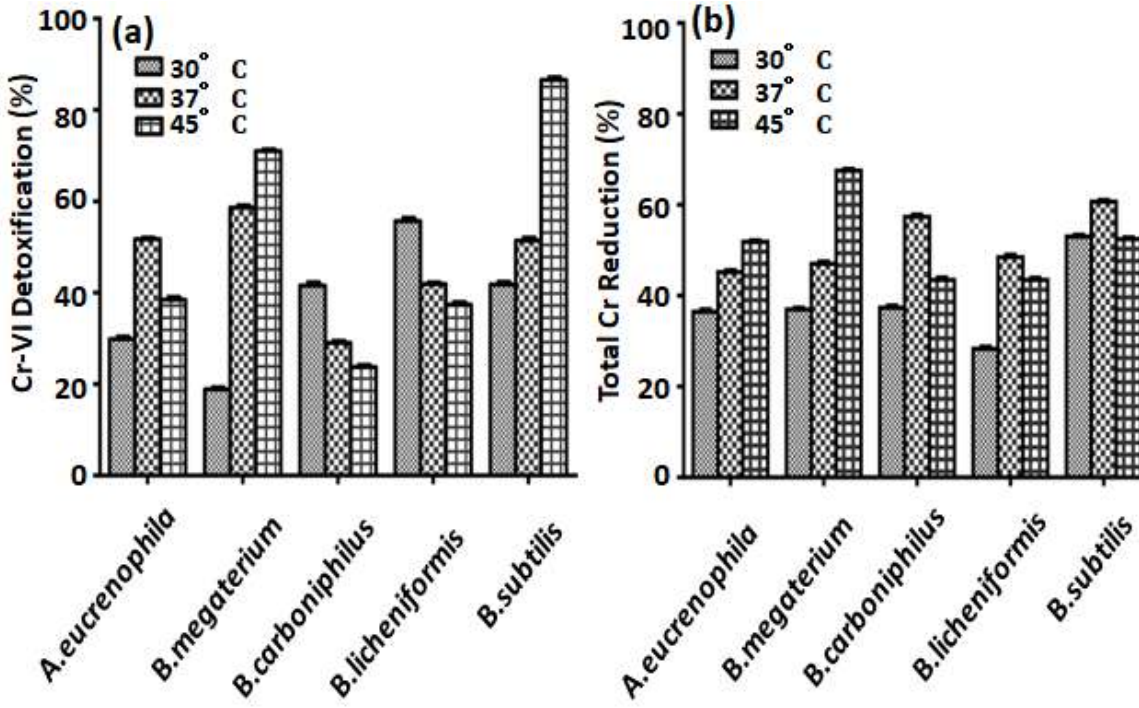

Fig. 9: Detoxification of Cr-VI and reduction of total Cr as $K_2Cr_2O_7$ by bacterial isolates at 30, 37 and 45°C. The experiments were conducted by inoculation of minimal salts medium base, pH 7 supplemented with 125 ppm of $K_2Cr_2O_7$ and incubation at 37, 37 or 45°C for 48 h followed by measurement of Cr-VI detoxification (a) by 1,5-diphenylcarbazide colorimetric method and reduction of total Cr (b) by atomic absorption spectrophotometry.

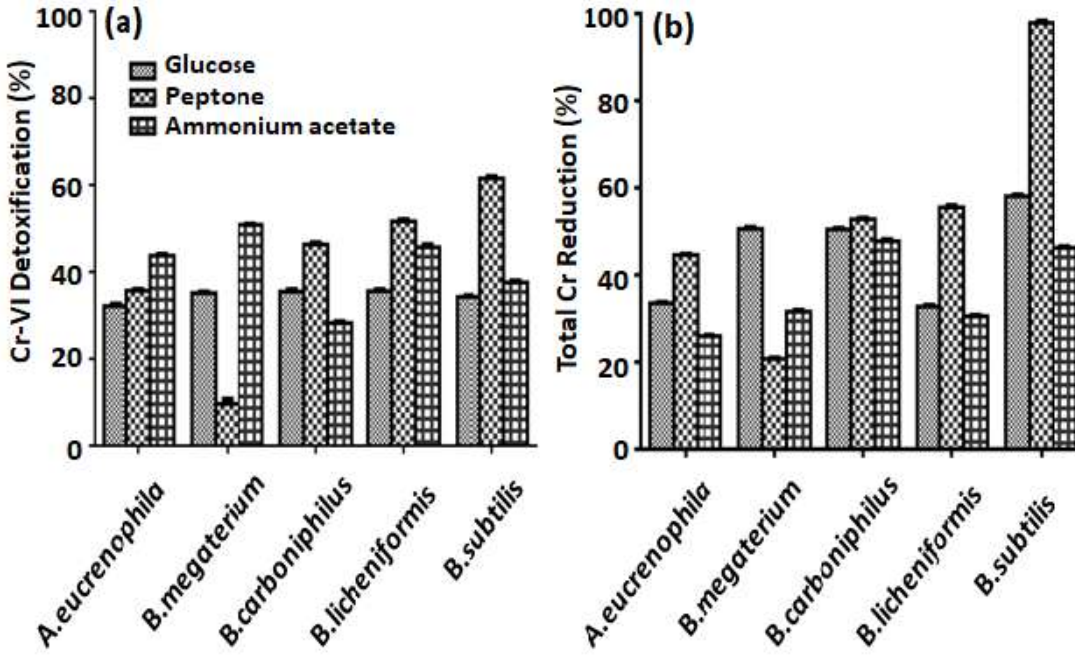

Fig. 10: Detoxification of Cr-VI and reduction of total Cr as $K_2Cr_2O_7$ by bacterial isolates at pH 5, 6 7 and 8. The experiments were conducted by inoculation of minimal salts medium base, pH 5, 6 7 or 8 supplemented with 125 ppm of $K_2Cr_2O_7$ and incubation at 37°C for 48 h followed by measurement of Cr-VI detoxification (a) by 1,5-diphenylcarbazide colorimetric method and reduction of total Cr (b) by atomic absorption spectrophotometry.

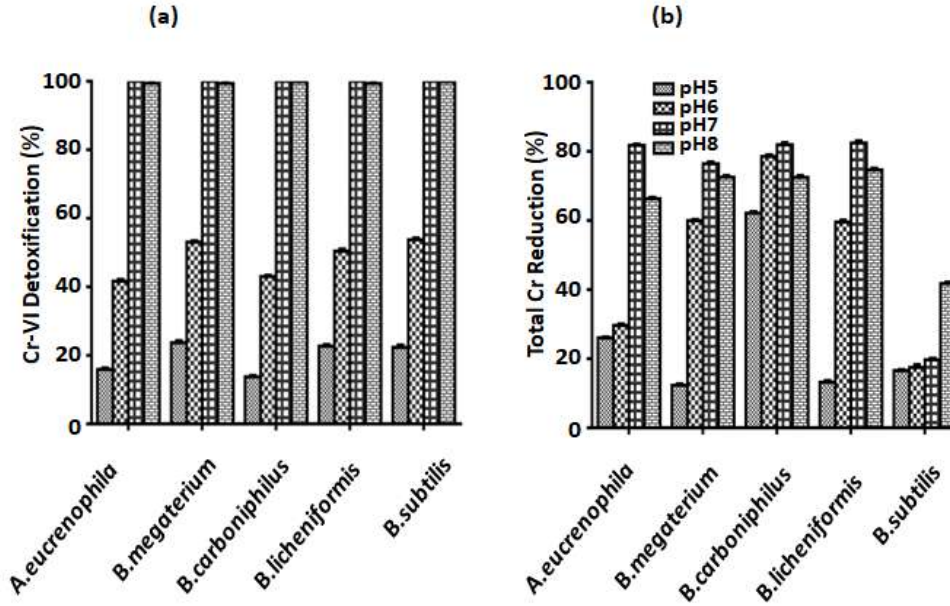

Fig. 11: Detoxification of Cr-VI and reduction of total Cr as $K_2Cr_2O_7$ by bacterial isolates using glucose, peptone or ammonium acetate as carbon source. The experiments were conducted by inoculation of minimal salts medium base, pH 7 supplemented with 125 ppm of $K_2Cr_2O_7$ and 400 ppm of glucose, peptone or ammonium acetate followed by incubation at 37°C for 48 h and measurement of Cr-VI detoxification (a) by 1,5-diphenylcarbazide colorimetric method and reduction of total Cr (b) by atomic absorption spectrophotometry.

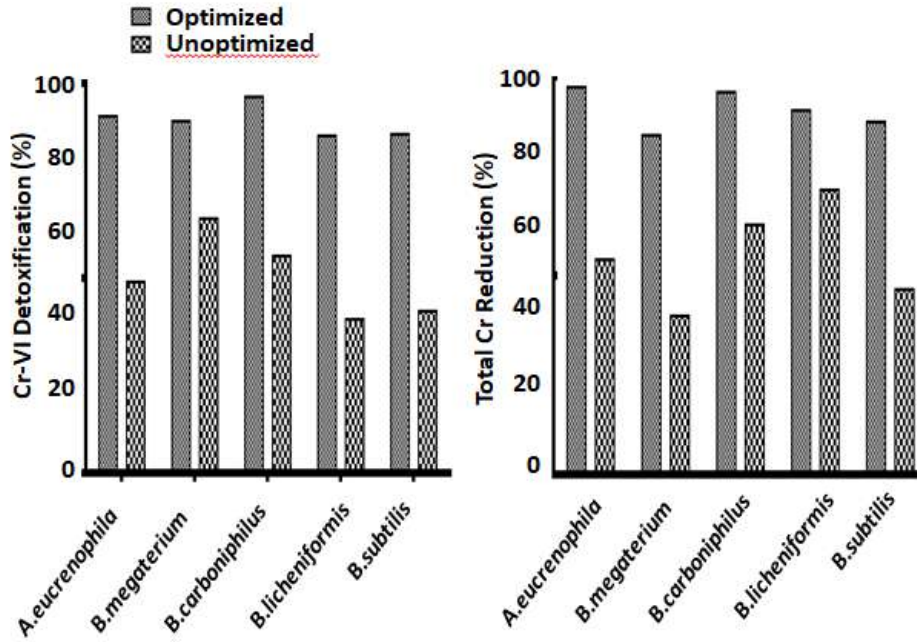

Fig. 12: Detoxification of Cr-VI and reduction of total Cr from tannery effluent by the isolates in optimized conditions. Freshly collected sample was preconditioned by filtration sterilization followed by pH adjustment to 7 for *A. eicrenophila*, *B. megaterium*, *B. carboniphilus* or *B. licheniformis*, and to 8 for *B. subtilis*. The treatment was conducted by inoculation of the preconditioned sample followed by incubation at 37°C for 48 h. Initial and final concentration of Cr-VI and total Cr in the effluent was measured (a) by 1,5-diphenylcarbazide colorimetric method and (b) by atomic absorption spectrophotometry, respectively. The rate of detoxification of Cr-VI and reduction of total Cr was calculated by subtracting final concentration from initial one, dividing by initial concentration, and multiplying by 100. The result was expressed as percent (%) of Cr-VI detoxification or total Cr reduction.

detoxification or reduction of Cr in optimized conditions compared to their unoptimized counterparts (Fig. 12).

DISCUSSION

The breakthrough towards the sustainable mitigation of overwhelming pollution caused by the tannery wastewater is installing an efficient, cost-effective, simple and environmentally friendly effluent treatment plant in each industry outlet. From time to time, diverse chemical and biological treatment systems, either independently, subsequently one after another, or in concert, have long been practiced as effective measures in dealing the hazardous effluents. Noticeably, the noble, operative and enduring abilities of naturally occurring bacteria to tolerate and reduce or detoxify heavy metals look the ever-expected and most reliable mean. This concept was the driving force in designing the present study to isolate, identify and optimize environmental conditions of natural bacteria to reduce or detoxify toxic Cr reside in tannery effluents.

The findings of this study reflect potential candidacy of indigenous and intrinsic bacteria of *Aeromonas* and *Bacillus* species in bioremediation of toxic Cr discharged into the wastewater from tanning industries. Our data clarify that an increased rate of detoxification or reduction was dependent on bacterial growth and exposure time. Our data also delineated the efficiency of the isolates was merely concentration dependent. Noticeably, the efficiency of the isolates increased when the incubation time was increased from 24 to 48 or 72 h. However, the elevated efficiency of most of the isolates over time was predominant up to 48 h. This observation also corresponds to the growth dependent efficiency of the isolates inferring the logarithmic phase of bacterial growth. It is likely that growth of bacteria and damage induced by Cr-VI are competing phenomena, where bacteria can adjust with the exposure of Cr-VI as long as the sources of metabolizable nutrients are available in the medium. Liu et al. (2006) explained the phenomenon as the bacteria required an increased incubation period for repair or adaptation when exposed to high level of Cr-VI in the medium. It has also been suggested that Cr-VI induced DNA damage can be repaired by the bacterial SOS function (Oh & Choi 1997). Growth dependent detoxification or reduction of Cr was also evidenced by Desai et al. (2008). Moreover, the efficiency of most of the isolates was found the utmost at 37°C compared to that observed at 30 or 45°C, which also corresponds to the growth dependent pattern of Cr detoxification or reduction. Reportedly, the optimal temperature of Cr-VI detoxification or total Cr reduction ranged between 25 and 37°C (Cheung & Gu 2007, Ibrahim et al. 2012). In this study, we also revealed detoxification or reduction of Cr to be influenced by pH. All the bacterial isolates exhibited their efficiency at neutral or higher pH. In contrast, the efficiency was reversed when the pH of the medium was lowered to 6 or 5. The efficiency of total Cr reduction but not of Cr-VI detoxification by *B. carboniphilus* was not much influenced by pH range tested. Bacterial detoxification of Cr-VI was reported to be significant at pH 6-8 (Wang et al. 1990) and insignificant at pH 5 or 9 (Bopp et al. 1983). Our data thus imply bacterial detoxification or reduction of Cr is enzyme mediated, since variation of pH affects the degree of ionization of most of the enzymes, thereby changes conformation of the proteins, and eventually the activity of the enzymes (Farrell & Ranallo 2000). The growth of the isolates as well as the efficiency of them in detoxifying or reducing Cr was found greatly influenced when glucose, peptone or ammonium acetate was additionally supplemented in the medium as a direct source of carbon or co-substrate. The co-substrate dependent bacterial efficiency lied on the property of any of the co-substrates as an electron donor for Cr detoxification or reduction. Our data clearly revealed the utmost detoxification or reduction of Cr by peptone as co-substrate compared to that by glucose or ammonium acetate. Being expensive, the potential of peptone to be used in an effluent treatment plant is considerably difficult. Ammonium acetate exhibited inconsistent pattern of potency as a co-substrate for the isolates investigated. Glucose, in contrast, exhibiting an optimum range of influence on bacterial detoxification or reduction of Cr, around 60%, seems reliable as a co-substrate. Horitsu et al. (1987) revealed the effect of glucose on the activity of Cr-VI reducing enzyme in *Pseudomonas ambigue* G-1, which was indeed exerted by completely protecting the enzyme from inactivation on dialysis but not by inducing the activity of the enzyme. Hence, glucose can be considered as co-substrate in Cr bioremediation because of its strong enzyme stabilizing ability.

The present study strongly configured that bacterial detoxification or reduction of Cr was highly dependent on exposure time and incubating temperature of the reaction as well as the pH of the medium. Negligible degree of detoxification or reduction was noticed in abiotic control at any time period, temperature and pH applied, indicating direct interaction of the bacteria in Cr-VI detoxification or total Cr reduction. When the optimized time, temperature and pH revealed by in vitro examinations were implemented in detoxifying or reducing Cr from tannery effluent, the efficiency of the isolates were found significantly increased. Hence, each of the bacterial isolates investigated in this study seems to possess potential as biological agent in Cr remediation from industrial effluent or contaminated soil or wastewater.

CONCLUSION

It is the pivotal findings of the present study that the naturally

occurring bacteria of tannery effluent, namely, *Aeromonas eucrenophila*, *Bacillus megaterium*, *B. carboniphilus*, *B. licheniformis* and *B. subtilis* exhibited identical efficiency of detoxifying or reducing Cr. The bacteria also exhibited significant level of resistance or tolerance to greatly increased concentration of Cr. It is noteworthy that the bacteria exerted maximum level of potency at 37°C and pH 7 following 48 h of incubation. These environmental or physicochemical parameters closely resemble to the most common or natural conditions of the biological reactor of an effluent treatment plant. Hence, the bacteria isolated, identified and investigated in details in this study possess tremendous potential to be used as biological agents in Cr bioremediation from tannery effluent or Cr contaminated soil or wastewater of industrial premises.

ACKNOWLEDGMENTS

The authors express our heartfelt gratitude to Dr. Mala Khan of Designated Reference Institute for Chemical Measurements, Bangladesh Council of Scientific and Industrial Research, Government of the People's Republic of Bangladesh for her generous support in providing laboratory facilities. The study was financed by the Research and Publication Cell of the University of Chittagong, Bangladesh.

REFERENCES

APHA 1998. Standard Methods for the Examination of Water and Wastewater, 20th ed. American Public Health Association, Washington DC, USA.

APHA, AWWA, WEF 1992. Standard Methods for the Examination of Water and Wastewater. American Public Health Association, American Water Works Association, Water Environmental Federation, Washington DC, USA.

Bibi, R., Arshad, M. and Asghar, H.N. 2012. Optimization of factors for accelerated biodegradation of reactive black-5 azo dye. International Journal of Agricultural Biology, 14: 353-359.

Bopp, L.H, Chakrabarty, A.M. and Ehrlich, H.L. 1983. Chromate resistance plasmid in *Pseudomonas fluorescens*. Journal of Bacteriology, 155: 1105-1109.

Buchanan, R.E. and Gibbons, N.E. 1974. Bergey's Manual of Determinative Bacteriology, 8th ed. Williams and Wilkins, Baltimore, USA.

Cheung, K.H. and Gu, J.D. 2007. Mechanism of hexavalent chromium detoxification by microorganisms and bioremediation application potential: A review. International Biodeterioration and Biodegradation, 59: 8-15.

Desai, C., Jain, K. and Madamwar, D. 2008, Evaluation of in vitro Cr(VI) reduction potential in cytosolic extracts of three indigenous *Bacillus* sp. isolated from Cr(VI) polluted industrial landfill. Bioresearch Technology, 99: 6059-6069.

Farrell, S.O. and Ranallo, R.T. 2000. Experiments in Biochemistry: A Hands-on Approach. Saunders College Publication, Orlando, FL, USA.

Favazzi, A. 2002. Study of the impact of the main policies and environment protection measures in Africa's leather industry. Principal: Assomac Servizi Srl for United Nations Industrial Development Organization.

Flora, S.D., Bagnasco, M., Serra, D. and Zanacchi, P. 1990. Genotoxicity of chromium compounds: A review. Mutation Research, 238: 99-172.

Franco, A.R., Calheiros, C.S.C., Pacheco, C.C., Marco, P.D., Manaia, C.M. and Castro, P.M.L. 2005. Isolation and characterization of polymeric galloyl-ester-degrading bacteria from a tannery discharge place. Microbial Ecology, 50: 550-555.

Gain, P. and Moral, S. 1999. Leather Industry: Environmental pollution and mitigation measures. Society for Environment and Human Development, Dhaka, Bangladesh.

Goodfeelow, G., Herrera, G., Garcia, M.T. and Pena, M. 1994. Bergey's manual of determinative bacteriology, 9th ed. Williams and Wilkins, London, UK.

Horitsu, H., Futo, S., Miyaazawa, Y., Ogai, S. and Kawai, K. 1987. Enzymatic reduction of hexavalent chromium by hexavalent chromium tolerant Pseudomonas ambigua G-1. Agricultural and Biological Chemistry, 47: 2417-2420.

Ibrahim, A.S.S., Elbadawi, B.Y., El-Tayeb, A.M. and Al-Salamah, A.A. 2012. Hexavalent chromium reduction by novel chromate resistant alkaliphilic Bacillus sp. strain KSUCr9a. African Journal of Biotechnology 11(16): 3832-3841.

Liu, Y.G., Xu, W.H., Zeng, G.M., Li, X. and Gao, H. 2006. Cr(VI) reduction by Bacillus sp. isolated from chromium landfill. Process Biochemistry, 41(9): 1981-1986.

Masood, F. and Malik, A. 2011. Hexavalent chromium reduction by Bacillus sp. strain FM1 isolated from heavy-metal contaminated soil. Bulletin of Environmental Contamination and Toxicology, 86: 114-119.

Mondal, N.C., Saxena, V.K. and Singh, V.S. 2005. Impact of pollution due to tanneries on groundwater regime. Current Science, 88(12): 25.

Ogedengbe, K. and Akinbile, C.O. 2004. Impact of industrial pollutants on quality of ground and surface waters at Oluyole industrial estate, Ibadan, Nigeria. Nigerian Journal Technological Development. 4(2): 139-144.

Oh, Y.S. and Choi, S.C. 1997. Reduction of hexavalent chromium by Pseudomonas aeruginosa HP014. Journal of Microbiology, 35: 25-29.

Opperman, D.J. and van Heerden, E. 2008. A membrane-associated protein with Cr(VI)-reducing activity from Thermus scotoductus SA-01. FEMS Microbiology Letter, 280(2): 2108.

Saha, B. and Azam, F.A.B. 2020. Probable ways of tannery's solid and liquid waste management in Bangladesh: An overview and review. Textile and Leather Review, 4(2): 76-95.

Sau, G.B., Chatterjee, S. and Mukherjee, S.K. 2010. Chromate reduction by cell free extract of Bacillus firmus KUCr1. Polish Journal of Microbiology, 59(3): 185-190.

Sobol, Z. and Schiestl, R.H. 2012. Intracellular and extracellular factors influencing Cr(VI) and Cr(III) genotoxicity. Environmental and Molecular Mutagenesis 53: 94-100.

Srinath, T., Khare, S. and Ramteke, P.W. 2001. Isolation of hexavalent chromium-reducing Cr tolerant facultative anaerobes from tannery effluent. Journal of General and Applied Microbiology, 47(6): 307-312.

Sundar, K., Vidya, R., Mukherjee, A. and Chandrasekaranc, N. 2010. High chromium tolerant bacterial strains from Palar river basin: Impact of tannery pollution. Research Journal of Environmental and Earth Sciences, 2(2): 112-117.

Turick, C.E., Apel, W.A. and Carmiol, N.S. 1996. Isolation of Cr(VI) reducing anaerobes from Cr contaminated and noncontaminated environments. Applied Microbiology and Biotechnology 44: 683-688

Verheijen, L.A.H.M., Wiersema, D. and Hulshoff Pol, L.W. 1996. Livestock and the environment finding a balance: Management of waste from animal product processing. J. De Wit International Agriculture Centre, Wageningen, The Netherlands.

Wang, P.C., Toda, K., Ohtake, H., Kusaka, I. and Yale, I. 1991. Membrane bound respiratory system of Enterobacter cloacaestrain HO1 grown anaerobically with chromate. FEMS Microbiology Letter, 76: 11-16.

... Continued from inner front cover

- The text of the manuscript should run into **Abstract, Introduction, Materials & Methods, Results, Discussion, Acknowledgement** (if any) and **References** or other suitable headings in case of reviews and theoretically oriented papers. However, short communication can be submitted in running with **Abstract and References.** The references should be in full with the title of the paper.
- The figures should preferably be made on a computer with high resolution and should be capable of withstanding a reasonable reduction with the legends provided separately outside the figures. Photographs may be black and white or colour.
- Tables should be typed separately bearing a short title, preferably in vertical form. They should be of a size, which could easily be accommodated in the page of the Journal.
- References in the text should be cited by the authors' surname and year. In case of more than one reference of the same author in the same year, add suffix a,b,c,.... to the year. For example: (Thomas 1969, Mass 1973a, 1973b, Madony et al. 1990, Abasi & Soni 1991).

List of References

The references cited in the text should be arranged alphabetically by authors' surname in the following manner: (Note: The titles of the papers should be in running 'sentence case', while the titles of the books, reports, theses, journals, etc. should be in 'title case' with all words starting with CAPITAL letter.)

Dutta, A. and Chaudhury, M. 1991. Removal of arsenic from groundwater by lime softening with powdered coal additive. J. Water Supply Res. Techno. Aqua., 40(1) : 25-29.

Hammer, D.A. (ed.) 1989. Constructed Wetlands for Wastewater Treatment-Municipal, Industrial and Agricultural. Lewis Publishers Inc., pp. 831.

Haynes, R. J. 1986. Surface mining and wetland reclamation. In: Harper, J. and Plass, B. (eds.) New Horizons for Mined Land Reclamation. Proceedings of a National Meeting of the American Society for Surface Reclamation, Princeton, W.V.

Submission of Papers

- The paper can be submitted by e-mail as an attachment in a single WORD file at **contact@neptjournal.com**
- The paper can also be submitted online in a single WORD file through the **online submission portal** of journal's website: **www.neptjournal.com**

Attention

1. Any change in the authors' affiliation may please be notified at the earliest.
2. Please make all the correspondence by e-mail, and authors should always quote the manuscript number.

Note: In order to speed up the publication, authors are requested to send the publication charges as soon as they get the 'initial acceptance' letter, and also correct the galley proof immediately after receipt. The galley proof must be checked with utmost care, as publishers owe no responsibility for mistakes. The papers will be put on priority for publication only after receiving the processing and publication charges.

Nature Environment and Pollution Technology

(Abbreviation: Nat. Env. Poll. Tech.)

(An International Quarterly Scientific Journal)

Published by

Technoscience Publications

A-504, Bliss Avenue, Opp. SKP Campus
Balewadi, Pune-411 045, Maharashtra, India

In association with

Technoscience Knowledge Communications

Mira Road, Mumbai, India

For further details of the Journal, please visit the website. All the papers published on a particular subject/topic or by any particular author in the journal can be searched and accessed by typing a keyword or name of the author in the 'Search' option on the Home page of the website. All the papers containing that keyword or author will be shown on the home page from where they can be directly downloaded.

www.neptjournal.com

©Technoscience Publications: The consent is hereby given that the copies of the articles published in this Journal can be made only for purely personal or internal use. The consent does not include copying for general distribution or sale of reprints.

Published for Proprietor, Printer and Publisher: Mrs. T. P. Goel, B-34, Dev Nagar, Tonk Road, Jaipur, Rajasthan, India; Editors: Dr. P. K. Goel (Chief Editor) and Prof. K. P. Sharma